UNIVERSAL
LIBRARY
OU_162081
UNIVERSAL
LIBRARY

539.76/In 61P 36090
International coference ...
Peaceful Uses of Atomic Energy.
Proceedings. Vol. 4. 1956.

OSMANIA UNIVERSITY LIBRARY

Call No. 539.76/In61P Accession No. 36090

Author International conference on peaceful Uses of Atomic Energy.

Title Proceedings. Vol.4. 1956

This book should be returned on or before the date last marked below.

PROCEEDINGS
OF THE
INTERNATIONAL CONFERENCE ON THE PEACEFUL USES OF ATOMIC ENERGY

Volume 4

CROSS SECTIONS IMPORTANT TO REACTOR DESIGN

Proceedings of the International Conference on the Peaceful Uses of Atomic Energy

Held in Geneva
8 August-20 August 1955

Volume 4
Cross Sections Important to Reactor Design

UNITED NATIONS
New York
1956

UNITED NATIONS PUBLICATION

Sales No. 1956.IX.1.Vol. 4

A/CONF.8/4

Price: U.S. $7.50; 54/- stg.; 32.00 Sw. frs.
(or equivalent in other currencies)

PREFACE

The Proceedings of the International Conference on the Peaceful Uses of Atomic Energy are published in a series of 16 volumes, as follows:

Volume Number	Title	Sessions Included
1	The World's Requirements for Energy; The Role of Nuclear Power	2, 3.2, 4.1, 4.2, 5, 24.2.
2	Physics; Research Reactors	6A, 7A, 8A, 9A, 10A.1.
3	Power Reactors	10A.2, 3.1, 11A, 12A, 13A, 14A.
4	Cross Sections Important to Reactor Design	15A, 16A, 17A, 18A.
5	Physics of Reactor Design	19A, 20A, 21A, 22A, 23A.
6	Geology of Uranium and Thorium	6B, 7B.
7	Nuclear Chemistry and the Effects of Irradiation	8B, 9B, 10B, 11B, 12B, 13B.
8	Production Technology of the Materials Used for Nuclear Energy	14B, 15B, 16B, 17B.
9	Reactor Technology and Chemical Processing	7.3, 18B, 19B, 20B, 21B, 22B, 23B.
10	Radioactive Isotopes and Nuclear Radiations in Medicine	7.2 (Med.), 8C, 9C, 10C.
11	Biological Effects of Radiation	6.1, 11C, 12C, 13C.1.
12	Radioactive Isotopes and Ionizing Radiations in Agriculture, Physiology and Biochemistry	7.2 (Agric.), 13C.2, 14C, 15C, 16C.
13	Legal, Administrative, Health and Safety Aspects of Large-Scale Use of Nuclear Energy	4.3, 6.2, 17C, 18C.
14	General Aspects of the Use of Radioactive Isotopes; Dosimetry	7.1, 19C, 20C.
15	Applications of Radioactive Isotopes and Fission Products in Research and Industry	21C, 22C, 23C.
16	Record of the Conference	1, 24.1, 24.3.

These volumes include all the papers submitted to the Geneva Conference, as edited by the Scientific Secretaries. The efforts of the Scientific Secretaries have been directed primarily towards scientific accuracy. Editing for style has been minimal in the interests of early publication. This may be noted especially in the English translations of certain papers submitted in French, Russian and Spanish. In a few instances, the titles of papers have been edited to reflect more accurately the content of those papers.

The editors principally responsible for the preparation of these volumes were: Robert A. Charpie, Donald J. Dewar, André Finkelstein, John Gaunt, Jacob A. Goedkoop, Elwyn O. Hughes, Leonard F. Lamerton, Aleksander Milojevic, Clifford Mosbacher, César A. Sastre, and Brian E. Urquhart.

The verbatim records of the Conference are included in the pertinent volumes. These verbatim records contain the author's corrections and, where necessary for scientific accuracy, the editing changes of the Scientific Secretaries, who have also been responsible for inserting slides, diagrams and sketches at appropriate points. In the record of each session, slides are numbered in numerical order through all presentations. Where the slide duplicates an illustration in the submitted paper, appropriate reference is made and the illustration does not appear in the record of the session.

Volume 16, "The Record of the Conference," includes the complete programme of the Conference, a numerical index of papers and an author's index, the list of delegates, the records of the opening and closing sessions and the complete texts of the evening lectures.

TABLE OF CONTENTS

Session 15A: Equipment and Techniques Used in Measuring Cross Sections Important to Reactor Design

			Page
P/576	Hughes	Velocity Selectors at Reactors	3
P/640	Mostovoi *et al.*	Mechanical Selectors at RTP (Slow)	12
P/641	Wladimirsky *et al.*	Mechanical Selectors at RTP (Fast)	22
P/421	Wiblin	Pulsed Sources	35
P/577	Cranberg	Fast Time-of-Flight Techniques	40
P/580	Bollinger	Neutron Detection	47
P/806	Higinbotham	Time-of-Flight Instrumentation	53
P/573	Taschek	Techniques for Cross Sections	62
P/767	Egelstaff	Pile Spectrometers at Harwell	70
P/574	Havens	Pulsed Accelerator Spectrometers	74
P/584	Thornton *et al.*	Cyclotrons for Neutron Spectrometry	87
P/578	Bonner	Accelerators for Neutron Spectrometry	92
P/582	Rosen	Spectrometry with Continuous Methods	97
P/596	Inghram *et al.*	Mass Spectrometric Methods	105
P/426	Rae	Capture in Reactor Materials	110
Record of Session			116

Session 16A: Equipment and Techniques (*concluded*): Cross Sections of Non-Fissionable Materials: Delayed Neutrons

P/356	Breton	Pile Oscillator	127
P/642	Bergman *et al.*	Slowing Down Time Spectrometer	135
P/832	Harvey	Fundamental Neutron Cross Sections	147
P/591	Bernstein, Smith	Cross Section of Xe^{135}	153
P/831	Keepin, Wimett	Delayed Neutrons	162
P/648	Girshfeld	Delayed Neutrons from U^{233}	171
Record of Session			177

Session 17A: Cross Sections of Fissionable Materials

P/422	Raffle, Price	Cross Sections Pu Isotopes	187
P/589	Leonard	Total and Fission Cross Sections Pu	193
P/586	Sailor	Slow Cross Sections U^{235}	199
P/423	Lynn, Pattenden	Slow Cross Sections U Isotopes	210
P/645	Adamchuk *et al.*	Heavy Nuclei Cross Sections	216
P/646	Nikitin *et al.*	Cross Sections of U^{233}, U^{235}, Pu^{239}	224
P/644	Kukavadse *et al.*	Pile Neutron Cross Sections of U^{233}	230
P/354	Auclair *et al.*	Slow Cross Sections Fissionable Nuclei	235
P/355	Szteinsznaider *et al.*	Fast Cross Sections Fissionable Nuclei	245
P/594	Diven	Measurement Fast Neutron Flux	251
P/424	Campbell, Lockey	Fission Cross Sections vs. Temperatures	258
Record of Session			262

Session 18A: Properties of Fissionable Materials (ν, η, α): Resonance Analysis *Page*

P/657 Spivak, Yerozolimsky .. Multiplication Factor, U and Pu 295
P/658 Alichanow *et al.* ..... Number of Fission Neutrons, U^{233}, U^{235} and Pu 301
P/660 Burgow ..... Number of Fission Neutrons Natural U 305
P/425 Egelstaff, Sanders .... Neutron Yields Fissile Nuclei..... 307
P/587 Palevsky ..... Capture to Fission, New Method 311
P/595 Kanne *et al.* ..... Capture to Fission, Intermediate Energy 315
P/585 Bethe ..... Analysis of Results 321
P/590 Hurwitz ..... Reactor Material Cross Sections 328
P/583 Melkonian ..... Analysis Low Energy Resonances 340
Record of Session 349

Session 15A

EQUIPMENT AND TECHNIQUES USED IN MEASURING CROSS SECTIONS IMPORTANT TO REACTOR DESIGN

LIST OF PAPERS

			Page
P/576	Neutron velocity selectors used at reactors	D. J. Hughes	3
P/640	A mechanical neutron velocity selector	V. I. Mostovoi *et al.*	12
P/641	A neutron selector with mechanical shutter	V. V. Vladimirski *et al.*	22
P/421	Neutron spectrometers based on pulsed sources	E. R. Wiblin	35
P/577	Time-of-flight techniques applied to fast neutron measurements	L. Cranberg	40
P/580	Recent advances in neutron detection	L. M. Bollinger	47
P/806	Time-of-flight instrumentation for neutron spectrometers	W. A. Higinbotham	53
P/573	Techniques for measuring elastic, non-elastic and transport neutron cross sections	R. F. Taschek	62
P/767	A review of pile neutron spectrometer work at Harwell	P. A. Egelstaff	70
P/574	Pulsed accelerator slow neutron velocity spectrometers	W. W. Havens, Jr.	74
P/584	Cyclotrons designed for precision fast-neutron cross-section measurements	R. L. Thornton *et al.*	87
P/578	Van de Graaff and Cockcroft-Walton accelerators for fast neutron cross-section measurements	T. W. Bonner	92
P/582	Techniques for measurement of neutron cross sections and energy spectra for sources which are continuous in energy and time	L. Rosen	97
P/596	Mass spectrometric methods for the determination of nuclear constants	M. G. Inghram *et al.*	105
P/426	A note on the analysis of neutron resonance data including examples taken from reactor materials	E. R. Rae	110

Neutron Velocity Selectors Used at Reactors

By D. J. Hughes,* USA

Although the present paper is concerned only with neutron velocity selectors used at reactors it is desirable to relate these particular instruments to others used for obtaining cross sections as functions of neutron energy. For slow neutrons, that is those of thermal and sub-thermal energies, reactors are the most important sources for no other methods can compete with the high intensities available from them. At the upper end of the energy range of interest to reactor design, however, the reactor velocity selectors are of little use. Their resolving power decreases rapidly with increasing neutron energy and neutrons produced in Van de Graaff accelerators are much more useful for cross-section measurements.

In the "high" energy or Mev region the Van de Graaff has been the most widely used instrument, while at "low" energy, below about 5 kev, crystal spectrometers and time-of-flight methods are applicable. Because of the nature of the instruments involved, the relative energy spread, $\Delta E/E$, decreases with energy in the former, and increases with energy in the latter region. As a result, the attainable energy resolution is the poorest ($\Delta E/E$ the largest) in a region between those appropriate for the two types of measurements. A few years ago the resolution was so poor ($\Delta E/E > 1$) in this intermediate region, which extended from about 1 to 20 kev, that a definite gap existed in the data on resonances as a function of energy. Recent improvements in techniques at both high and low energy have now closed this gap in the sense that at the energy of poorest resolution, about 5 kev, $\Delta E/E$ is now of the order of 0.1 and the region of the gap is covered with fair resolution by both methods. The way in which the reactor velocity selectors merge with the Van de Graaff instruments is well-illustrated by the curve for manganese (Fig. 1) taken from the neutron cross-section compilation, BNL–325.[18] The experimental points, identified by symbols, represent measurements with fast choppers at Argonne and Brookhaven, pulsed accelerators at Columbia and Knolls Atomic Power Laboratory (Schenectady), and the Van de Graaff at Argonne.

The closing of the gap hardly implies that anything significantly different from other energy regions will be found; rather the importance lies in the greater resolving power now available at both higher and lower energies. Thus the improvement shown in the various curves of BNL–325 relative to results available a few years ago, which reveals many additional resonances, is not so much in the region of the gap but in the higher and lower energies where the resolution is superior.

In both regions the instrumental task is one of producing neutrons of a narrow spread in energy at an adjustable energy, or selecting narrow energy bands from a source of wide initial energy spread. High neutron source intensity is essential because of the severe reduction in intensity resulting from monochromatization. For all but the lowest energy regions the improvement of neutron detectors is an important phase of the problem, for their efficiencies, usually discouragingly low, must be increased as much as possible to obtain practicable counting rates.

Below 10 kev there are at the present time two methods of neutron velocity selection or "neutron spectroscopy" in general use, one based on Bragg reflection of neutrons by single crystals and the other on time-of-flight measurements. The former method can be used only with reactors whereas the latter is applicable both to reactors and particle accelerators. The instruments used in these methods, crystal monochromators and time-of-flight velocity selectors respectively, have in common a neutron source produced by moderation of fast neutrons. This moderation, usually produced by elastic collisions with light nuclei, results in a neutron flux inversely proportional to energy, the "dE/E spectrum" so familiar in pile neutron physics. Furthermore, although the two techniques are based on entirely different methods of velocity selection, they both have resolutions (energy spreads, ΔE) that vary with energy in the same way ($\Delta E/E$ proportional to $E^{1/2}$). In other respects there are important differences; these determine the specific energy regions and cross sections best determined by instruments of the two types.

Concerning the time-of-flight instruments, the neutron source may be a pulsed accelerator such as a cyclotron or linear electron accelerator, or a mechanical shutter in a reactor beam ("chopper"). Many of the basic principles of operation are the same for the pulsed sources as the reactor velocity selectors. Examination of the compilation BNL–325, however,

* Brookhaven National Laboratory. Including instruments used at Argonne National Laboratory, Brookhaven National Laboratory, Oak Ridge National Laboratory, Phillips Petroleum Company (Arco) and General Electric Company (Hanford Works).

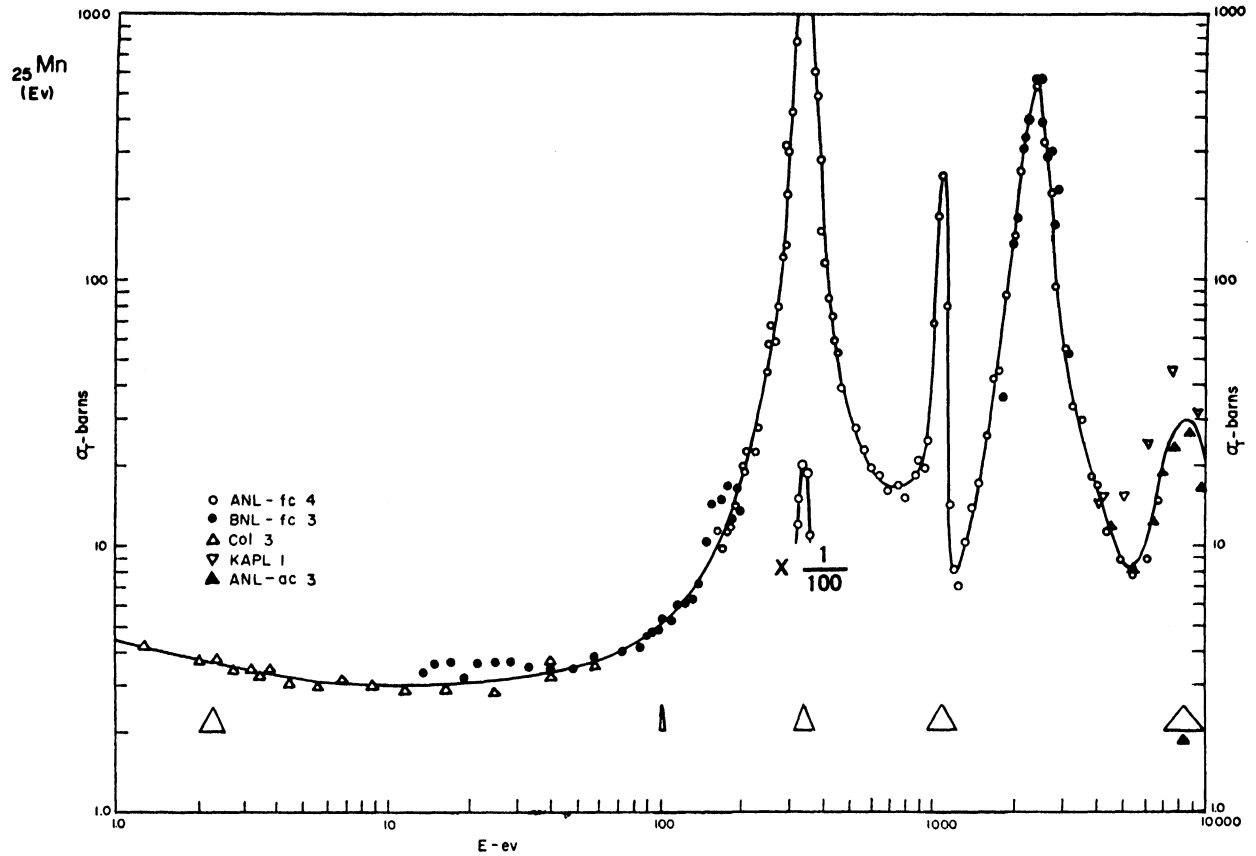

Figure 1. The total cross section of Mn, showing the "overlap" region between velocity selectors and Van de Graaff accelerators

shows that at the present time most of the measurements of neutron cross sections in the region below 10 kev, the region in which most resonances are found, have been made with velocity selectors used at reactors, that is, the crystal monochromators and neutron choppers. These reactor velocity selectors have been rather highly developed and it is doubtful if improvements of orders of magnitude can be made with them. The pulsed machines, on the other hand, although they have not produced nearly the volume of results obtained with the reactor instruments, seem to have the possibility of rather large improvements in resolution. An important advantage of the instruments used at reactors, however, is that many other experiments can be performed simultaneously at the reactor rather than one experiment occupying an entire machine.

Concerning the reactor velocity selectors, the crystal monochromators and choppers, these instruments are not really competitive for they complement each other, both in energy range covered and types of measurements, in a most desirable way. Both types of instruments are now to be found at many research reactors or are planned for use at such reactors. We shall see later how the crystal monochromators and choppers taken together cover the energy region from about 10^{-4} to 10^{4} ev, a 10^{8} range in energy.

During the last few years a tremendous amount of information has been gained on neutron cross sections in the resonance regions using these velocity selectors at reactors. The cross sections obtained, in particular the resonance parameters, have been of great value not only for their application to reactor physics but with respect to the basic nuclear theory as well. It has been possible to obtain detailed information concerning the radiation widths, neutron widths and spacings of hundreds of neutron resonances, each representing an energy level of the compound nucleus formed by neutron capture.

Comparison of the resonance structure of nuclei as presented in the recent compilation BNL–325 and the first edition of this compilation (AECU–2040) shows the apparent increasing complexity of resonance structure as resolution has improved. As an example the cross section of tin in the original compilation, the third supplement to the compilation, and the new BNL–325 are shown in Fig. 2. It is clear from this figure that careful interpretation is necessary at any particular stage in applying the results to theory to insure that all the resonances have been found in a given energy region. Fortunately, at the present time, enough information is available concerning the general characteristics of level parameters so that it is possible by objective means to determine if essentially all levels have been found in the energy region under investigation.

CRYSTAL MONOCHROMATORS

The crystal monochromator, or "spectrometer" as it is often described, requires a well-collimated high

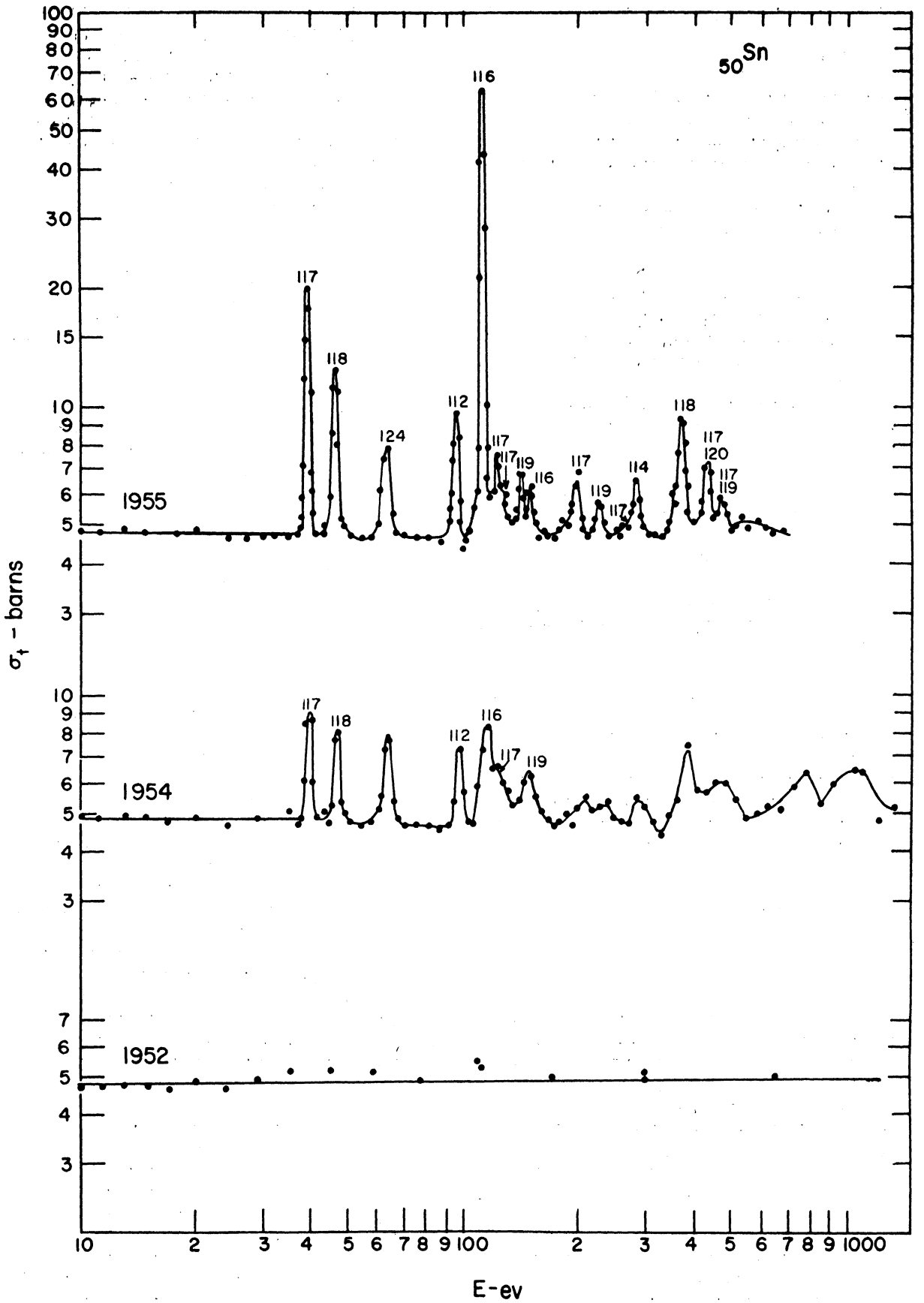

Figure 2. The total cross section of Sn as given in the compilation AECU-2040 (1952), its third supplement (1954), and BNL-325 (1955)

intensity neutron beam; thus a chain-reacting pile is necessary for its successful operation. In fact, as soon as pile neutron beams become available, crystal spectrometers were put in operation, at Argonne[1] and Oak Ridge[2] laboratories at about the same time. Others are now to be found at most reactors, at Chalk River,[3] Brookhaven,[4] Arco, Idaho,[5] Hanford, Washington,[6] Harwell,[7] Saclay, France,[8] and Kjeller, Norway.[9]

The beam of neutrons for a crystal spectrometer is formed by opening a hole through the shield of the pile and into the lattice, usually to a point as near the center of the pile as possible. At this point a high flux of neutrons in the "resonance" energy region, 1 ev to 100 kev, is found. The flux is distributed in energy according to the dE/E spectrum, thus with a magnitude that is the same in each energy decade (1 to 10 ev, 10 to 100 ev, etc.), this magnitude being 7×10^{11} cm^{-2} sec^{-1} in the Brookhaven pile for example.[10] The flux incident on the monochromating crystal, placed just outside the pile shield, is of course much less, being reduced enormously (a factor of 10^5 to 10^6) by the small solid angle subtended at the crystal by the source area (the base of the hole). The crystal is set at a small, adjustable angle to the incident collimated beam and the diffracted neutrons are detected by a counter, usually an enriched BF_3 proportional counter.

The neutron wavelength, λ, diffracted for a particular incident glancing angle, θ, is given by the Bragg formula

$$n\lambda = 2d \sin \theta \qquad (1)$$

where n is the order of the reflection (the reflectivity being the strongest for $n = 1$) and d the spacing of the lattice planes causing the particular reflection. As the incident beam is not strictly parallel there is a range of incident angles, $\Delta\theta$, and a corresponding range of reflected wavelengths given by

$$\Delta\lambda = \frac{2d}{n} \cos \theta \Delta\theta$$

or

$$\frac{\Delta\lambda}{\lambda} = \cot \theta \Delta\theta \qquad (2)$$

For a typical crystal, LiF, the value of d for the (111) planes is 2.32 Å, hence for neutrons of 1 ev energy, the glancing angle will be 3.5°. Whereas this value of θ is a practicable one, although small, θ becomes 0.35° for 100 ev neutrons, of the same order of magnitude as the angular collimation of the best monochromators in use today. Even for a collimation of 0.1° the conditions just described would imply an energy resolution $\Delta E/E$ ($\sim 2\Delta\lambda/\lambda$) of about 50 per cent at 100 ev.

The angular requirements just mentioned are important factors in reducing the range of utility of present crystal monochromators to energies well below 100 ev, in practice below about 20 ev. Another effect that restricts the instruments to low energy is the rapid decrease in reflected intensity with increasing energy. This decrease is a result not only of the decreasing incident flux ($1/E$) but of the reflectivity of the crystal itself, which varies as $1/E$. The resulting flux at the neutron detector drops off rapidly with energy, as $1/E^2$. The drop-off of the actual counting rate with energy is even more rapid because of the usual $1/E^{1/2}$ response of the detector itself. The general characteristics of crystal monochromators and their use at the pile is described by Hughes[10] and a description of a particularly high-resolution instrument at Brookhaven, which has an energy resolution of 0.4 per cent at 1 ev and 2.5 per cent at 50 ev (using the Be–$22\bar{4}2$ reflection), is given by Borst and Sailor.[4] Essentially the same monochromator is now in operation at Arco, Idaho.

CHOPPERS

There are two general classes of mechanical shutters or choppers usually called "slow" and "fast." These titles refer to the energy of the neutrons that are chopped rather than to the speed of the chopper itself, for both slow and fast choppers operate with rotational speeds of about 10,000 to 15,000 rpm.

Slow Choppers

A mechanical neutron "chopper" operating in the thermal region is the same in principle as the "fast chopper," but the "slow chopper" is of much simpler mechanical design. The slow chopper is of simple construction because the bursts produced are of the order of 20 instead of one microsecond and, in addition, the chopping of thermal neutrons can easily be accomplished with thin layers of cadmium instead of many inches of steel or plastic.

A slow chopper was used by Fermi at Argonne as early as 1943, and his design was incorporated into an apparatus built by Brill and Lichtenberger[11] at the same laboratory. A slow chopper of closely the same design is now in use[12] at the Harwell, England, pile. The Argonne chopper is a rotating cylinder made up of alternate cadmium (6 mil) and aluminum (30 mil) sheets, driven by an electric motor at speeds up to 180 rev/sec. A slow chopper of somewhat more advanced design is now being used at Brookhaven by Seidl *et al.*[13] The neutron channels of the rotating cylinder in this chopper are curved, with the result that neutrons of a particular velocity band only (the velocity depending on the rotational speed) are transmitted. The chopper thus produces bursts of neutrons (ranging from 10 to several hundred microseconds) and acts as a crude monochromator as well. Without monochromatization, the duty cycle of a chopper is low because sufficient time must elapse after a given burst to allow the slowest neutrons to pass the detector before the next burst can take place. With monochromatization limiting the velocity range passed to those velocities actually being detected in the various counting channels, the bursts can occur more frequently. In principle, the counter could be used continuously, one

partially monochromatized burst almost overlapping the next.

As the ideal conditions of no waiting time would require elaborately shaped channels different for each velocity range, the Brookhaven design is a compromise that allows a valuable increase in the duty cycle over straight channels, without reaching the perfect channel shape. In order to operate always at top rotational speed for good resolution, the curvature of the channels must vary with speed; in the Brookhaven equipment three interchangeable rotors of different curvature are used. The rotor, constructed of nickel screen coated with cadmium, is held inside a steel shell four inches in diameter and is operated by a dc motor at a top speed of 15,000 rpm. The neutron timing for twelve recording channels is done completely electronically, unlike the Argonne chopper (with its series of radial photocells), with the timing cycle triggered by a single photocell pulse coincident with the burst. Some typical results obtained with slow choppers will be discussed later.

Fast Choppers

In order to produce sharp bursts of neutrons for use at resonance energies, a shutter, necessarily heavy to stop neutrons of all energies, must open and close quickly, in about one microsecond. The large size and high speed of the "fast" chopper (i.e., a chopper for fast neutrons) make it a much more complicated device than the slow chopper for which thin cadmium sheets suffice to stop the slow neutron beam. Because of the limited energy range of the slow chopper (0–0.4 ev), very few neutron resonances can be studied with it.

The requirement of short burst length for the fast chopper leads to neutron beams of small area, hence low intensity; this latter tendency must be counteracted as much as possible to obtain a finite counting rate at the distant detector. These conflicting requirements result in a rather heavy, rapidly rotating shutter, containing shaped slits for the passage of neutrons, slits whose cross-sectional area is of the order of 0.01 in. by 1 in. As the slits in the moving shutter pass similar slits in a stationary collimator, neutron bursts of duration about 1 to 5 μsec, depending on the particular chopper, are produced.

The first fast chopper was used by Selove[14] at Argonne laboratory. It is essentially a steel cylinder of 4-in. diameter and 16-in. length, rotating about its long axis, which is horizontal, and containing machined slits along its length near the periphery. This chopper is normally operated at 10,000 rpm at which speed it produces 5 μsec bursts. The limitation in the shortness of burst arises from difficulties associated with the horizontal mounting on fixed bearings. The bursting strength of the rotor is not a limiting factor; it has been successfully spun to 40,000 rpm in spin tests (without bearings). Similar

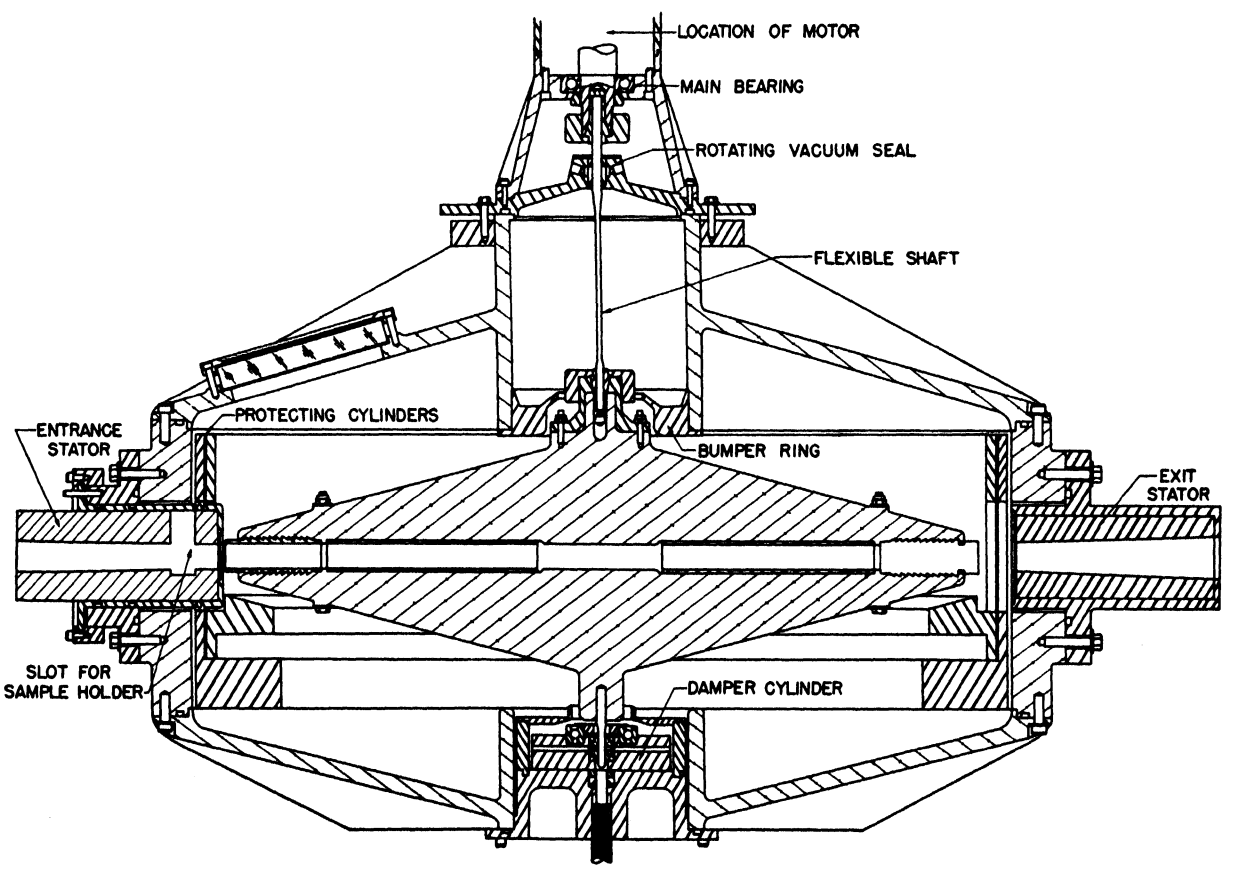

Figure 3. Diagram of the Brookhaven fast chopper

choppers, on horizontal axes with fixed bearings, are now in use at Oak Ridge[15] and Harwell,[16] which gives bursts about half the length of the Argonne machine. With the usual flight paths of about 10 meters, the resolutions are of the order of 0.5 μsec/m, when the other timing uncertainties are included (mainly channel time and detector delays).

An advanced chopper design is that of the Brookhaven machine (Seidl *et al.*[17]), Fig. 3, which has been in operation for about three years. The rotor is a horizontal disc, 30-in. in diameter, suspended by a thin flexible shaft in an evacuated chamber. The narrow slits for burst formation are machined in plastic pieces, which are held in the rotor between aluminum forgings. Designed to reach an ultimate speed of 15,000 rpm, at which a burst of 0.6 μsec would be attained, it has operated as high as 12,000 rpm. The first model built was operated for about two years at 6000 rpm with a burst length slightly over 1 μsec, and a second model is now in routine operation at 10,000 rpm. With a scintillation neutron detector and a flight path of 20 meters, the measured resolution function (including all timing uncertainties) has a width of 1.2 μsec, hence the resolution is 0.06 μsec/m under these conditions. The complexity of the resonance structure revealed by this instrument is shown in the curves to be discussed later.

A recently constructed fast chopper at Argonne laboratory has a drive system that is similar to that of the Brookhaven fast chopper, i.e., a high speed (15,000 rpm) electric motor directly coupled, through a flexible shaft, to the rotor, which turns about a vertical axis. The rotor is a 10-in. diameter monel disc with a 3-in. diameter uranium core. The rotor slits, which are perpendicular to the axis of rotation, are symmetrically shaped, being narrow at both ends. This feature produces a neutron burst width that is shorter by a factor of two than that obtained with the conventional slit system, although the angular aperture of the slits is reduced greatly. The slit system, designed primarily for measuring partial cross sections, consists of two groups of several slits each, crossing at right angles. Individual slit dimensions are 0.025 in. × 2.0 in., hence the total slit opening per burst is 2 cm^2 as compared with almost 0.15 cm^2 for the other fast choppers. The burst width is about 1.7μsec, giving a resolution of about 0.08 μsec/m with a 25-meter path or 0.035 μsec/m with a 60-meter path. Another rotor for the Argonne chopper, for use in transmission measurements, has not yet been completed. It will have only one group of parallel slits, each 0.015 in. wide, with an expected burst width about 1 μsec, giving a resolution of about 0.02 μsec/m with a 60-meter flight path.

COMPARISON OF CRYSTAL MONOCHROMATORS AND CHOPPERS

The results presented in the compilation BNL–325 are principally for total cross sections, which are obtained by transmission measurements. As only the relative counting rates are needed in determining the transmission, no knowledge of the absolute counter efficiency or of the neutron flux is needed. This fact, together with the high intensity available when only the transmitted beam is measured (in contrast to the scattered neutrons), is the reason for the relative simplicity and possibility of high accuracy (tenth per cent in some cases) in total-cross-section measurements. In spite of their greater difficulty, some partial cross sections, for scattering and reactions, have been measured and the results are to be seen in BNL–325.

For low energy neutrons, that is in the energy region below the Maxwell distribution, the slow chopper has been the most useful instrument at the reactor; the reflection of higher order neutrons tends to make the use of the crystal monochromator very difficult in the low energy regions. An illustration of the use of the slow chopper for these very low energy neutrons is given by Fig. 4, which shows the cross section of beryllium for neutrons below 1 ev. The points for the extremely cold neutrons, around 0.001 ev, were measured with the Brookhaven chopper and results are given for several sample temperatures, this work representing a study of the gain of energy from the lattice vibrations by the scattered neutrons. Above 0.2 ev the points labelled Col 13 represent measurements made with the Columbia pulsed cyclotron. The region around 0.02 ev was covered by measurements with the Argonne slow chopper; it is in this region that the rapid changes of cross section caused by Bragg reflections are seen.

The manner in which the slow chopper energy region fits into that covered by the crystal monochromators is exhibited in Fig. 5 for the cross section of normal uranium metal. Here the lowest energy points are those measured with the Brookhaven slow chopper and the slow chopper at Harwell is also represented. The other points in the figure marked Italy and Col were obtained with pulsed accelerators while Fr represents the French crystal spectrometer used with the pile at Saclay. A similar situation is illustrated in Fig. 6 for the separated isotope U^{235}. Here the lowest energy points are again those measured with the Brookhaven slow chopper. Those marked Han represent the crystal spectrometer results from the reactor at Hanford, Washington, and the remaining points were obtained with the Columbia pulsed cyclotron.

The region of usefulness of the crystal spectrometer extends only to the order of 10 ev because of the rapidly decreasing reflectivity of the crystal with energy; the intensity obtained with the fast chopper does not decrease with increasing energy and hence is a superior instrument for energies above 10 ev. The overlap region between the crystal monochromator and the fast chopper is illustrated by the curve for indium, Fig. 7. Here the resonance at 1.45 ev has been measured with the Brookhaven crystal spectrometer as well as the resonance at 3.8 ev. However, above this energy region the counting rate and resolution of the fast chopper is much better than that of

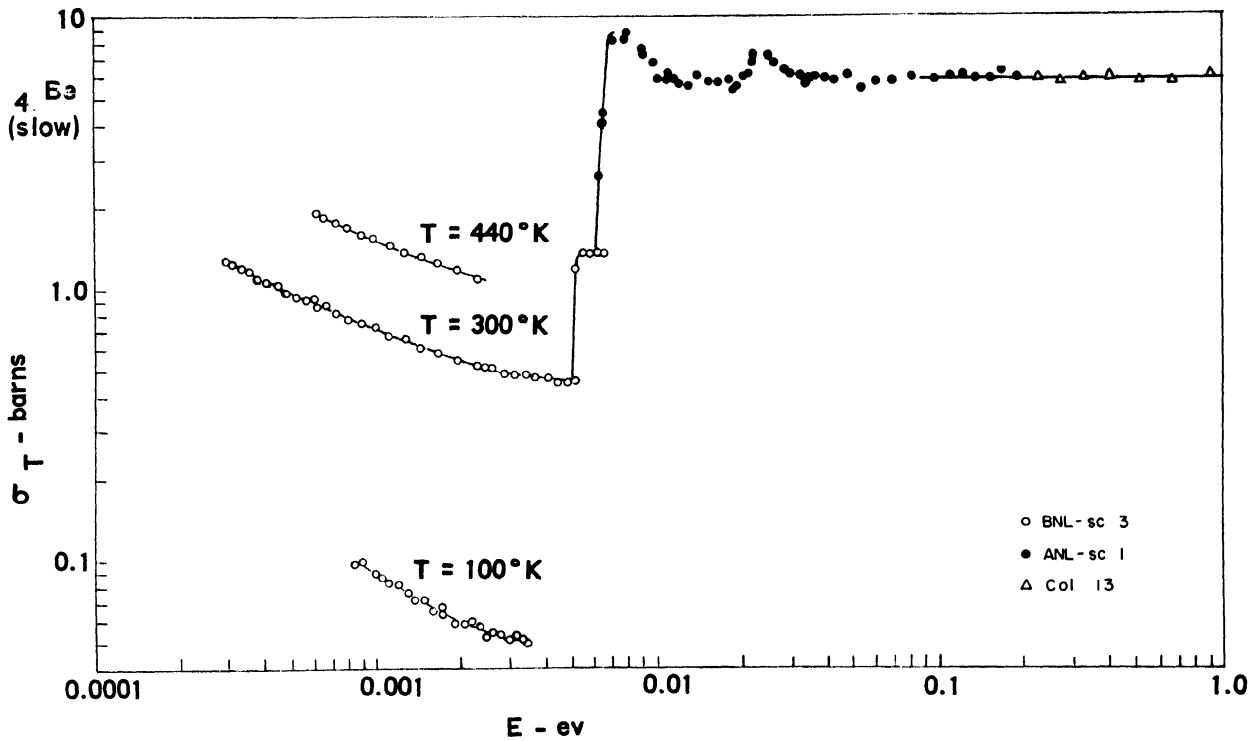

Figure 4. The cross section of Be for low energy neutrons, as measured with slow choppers and the pulsed cyclotron

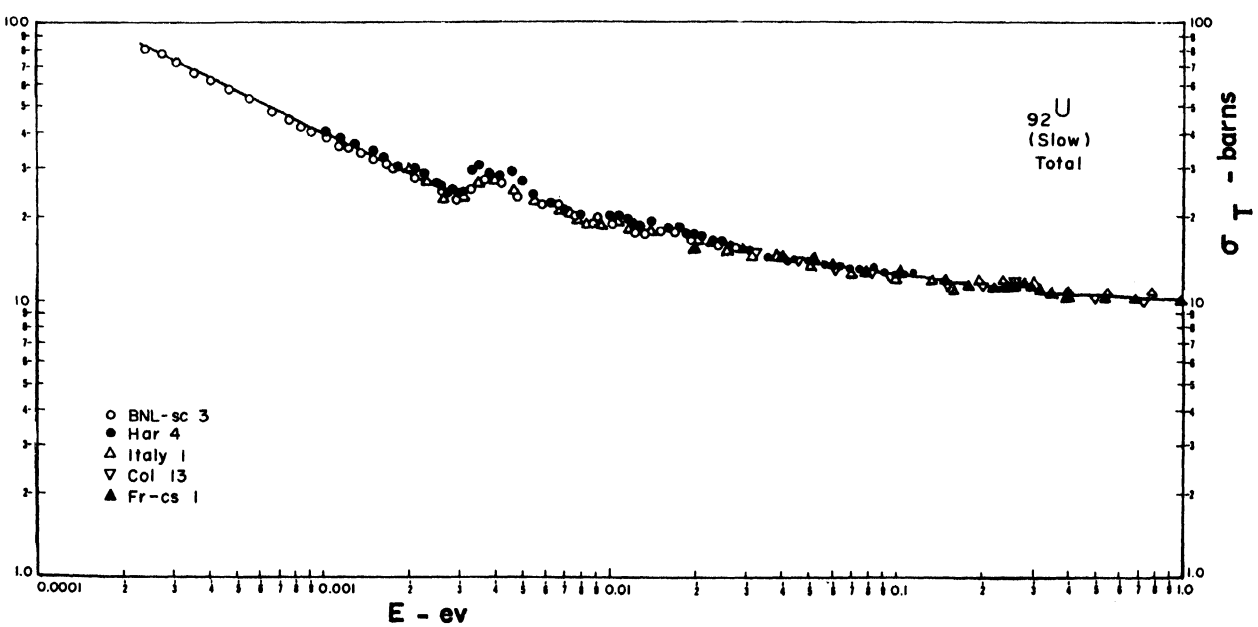

Figure 5. The cross section of U metal for slow neutrons, as measured by various selectors

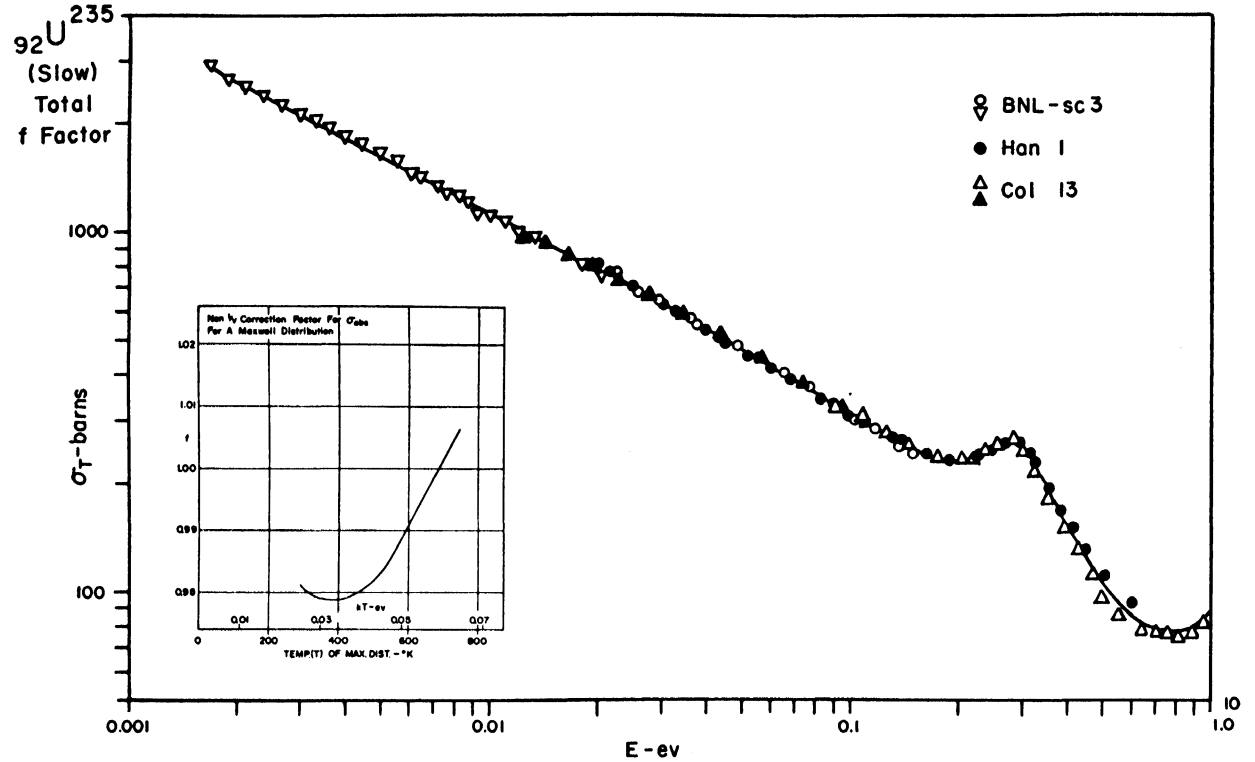

Figure 6. The cross section of U^{235} as measured by various velocity selectors

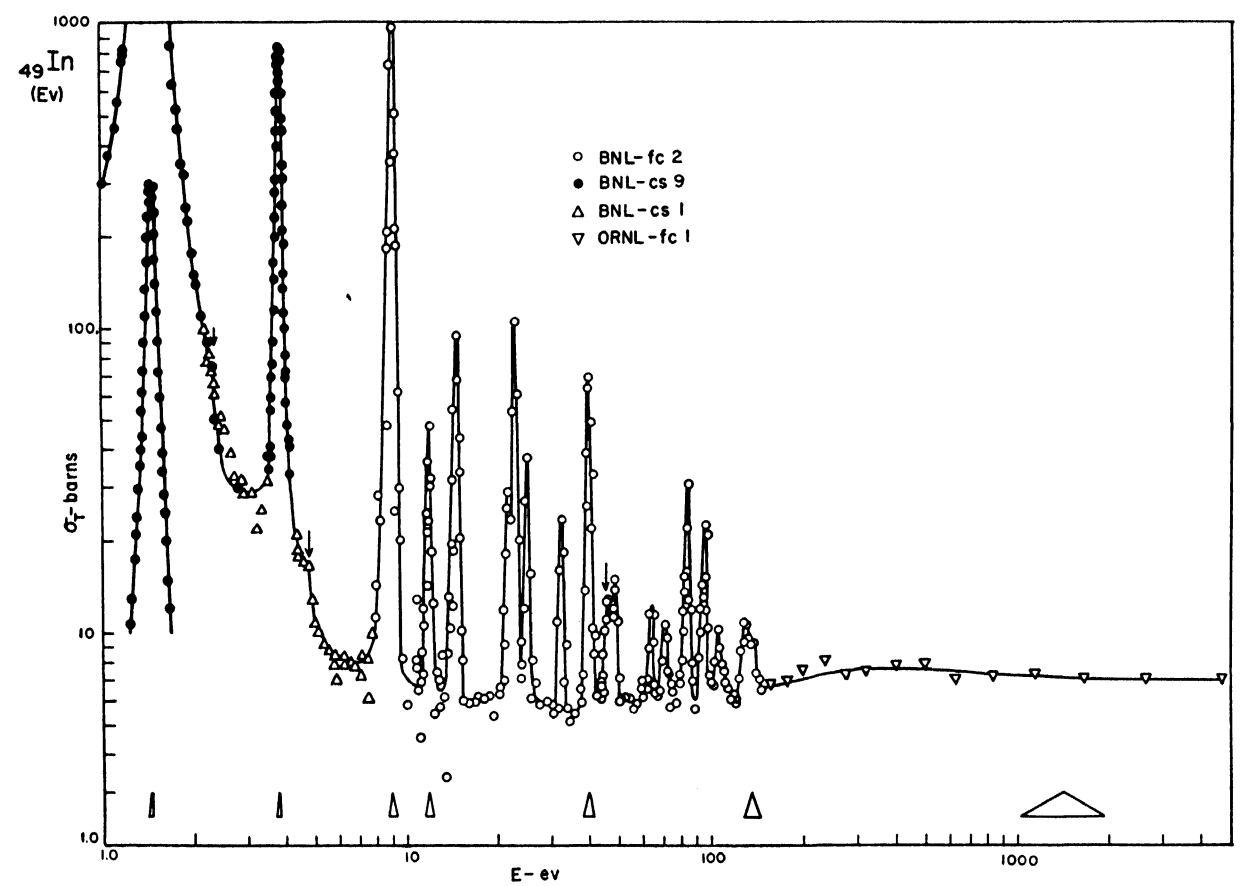

Figure 7. The cross section of In, illustrating the complementary relationship of the crystal spectrometer and fast chopper

the crystal monochromator so the resonances at higher energies have been measured with the fast chopper. For partial cross sections, however, the crystal monochromator has an important inherent advantage over time-of-flight instruments. As it produces a true monoenergetic beam, capture cross sections can be measured by activation, a procedure that is impossible with time-of-flight methods.

REFERENCES

1. Zinn, W. H., *Diffraction of neutrons by a single crystal,* Phys. Rev. *71,* 752 (1947).
2. Borst, L. B., Ulrich, A. J., Osborne, C. L. and Hasbrouck, R., *Neutron diffraction and nuclear resonance structure,* Phys. Rev. *70,* 557 (1946).
3. Brockhouse, B. N., *Resonance scattering of slow neutrons,* Can. J. Phys. *31,* 432 (1953).
4. Borst, L. B. and Sailor, V. L., *Neutron measurements with the Brookhaven crystal spectrometer,* Rev. Sci. Instr. *24,* 141 (1953).
5. Evans, J. E., private communication (1954).
6. Leonard, B. R., private communication (1954).
7. Egelstaff, P. A. and Taylor, B. T., *Slow neutron cross sections of zirconium and hafnium,* Nature, *167,* 896 (1951).
8. Netter, F., private communication (1954).
9. McReynolds, A. W. and Anderson, E., ***Thermal neutron resonance of Sm,*** Phys. Rev. *93,* 195 (1954).
10. Hughes, D. J., *Pile Neutrons Research,* p. 159 (Addison-Wesley Publishing Co., Inc., 1953).
11. Brill, T. and Lichtenberger, H. V., *Neutron cross section studies with the rotating shutter mechanism,* Phys. Rev. *72,* 585 (1947).
12. Egelstaff, P. A. and Taylor, B. T., *Slow neutron cross sections of molybdenum and bromine,* Nature *166,* 825 (1950).
13. Seidl, F. G. P., Palevsky, H., Randall, R. F. and Thorne, W., *Neutron time-of-flight velocity selector,* Phys. Rev. *82,* 345 (1951).
14. Selove, W., *The 5-ev neutron resonance in Ag,* Phys. Rev. *77,* 557 (1950); *A rotating-shutter time-of-flight spectrometer for the slow neutron resonance region,* Rev. Sci. Instr. *23,* 350 (1952).
15. Pawlicki, G. S. and Smith, E. C., *Preliminary investigations of neutron total cross sections with the Oak Ridge National Laboratory fast chopper,* Phys. Rev. *87,* 221 (1952).
16. Egelstaff, P. A., private communication (1954).
17. Seidl, F. G. P., Hughes, D. J., Palevsky, H., Levin, J. S., Kato, W. Y. and Sjöstrand, N. G., *"Fast chopper" time-of-flight measurement of neutron resonances,* Phys. Rev. *95,* 476 (1954).
18. Brookhaven National Laboratory Report 325, *Neutron Cross Sections* by Hughes, D. J. and Harvey, J. A. (Superintendent of Documents, Washington, D. C., 1955).

A Mechanical Neutron Velocity Selector

By V. I. Mostovoi, M. I. Pevzner, A. P. Tsitovich, USSR

Mechanical neutron velocity selectors make it possible to measure total cross sections and cross sections of reactions on monochromatic neutrons in a broad energy range.

On the reactor RTP there are two mechanical selectors, one of which has a flight path of 6.3 meters and is designed for taking measurements in the region between 0.005 and 100 ev. The maximum resolution of this selector is 0.8 μsec/m. The second mechanical selector, designed for investigations in the region between 10 to 10,000 ev, is a steel cylinder with lengthwise slits (see Fig. 1).

The selector is rotated by an air turbine with a speed of up to 20,000 rpm and produces neutron bursts of about 6 μsec duration. The flight path of this selector is 26.5 meters and the maximum resolution is 0.12 μsec/m.

The first of these two selectors is described in detail below.

The principal parts of a mechanical selector are a chopper, by means of which short neutron bursts are obtained, an electronic system, and detectors permitting registration of neutrons with a definite time of flight.

THE MECHANICAL CHOPPER AND ITS CHARACTERISTICS

The first mechanical selector to operate on a nuclear reactor beam was designed by Fermi, L. Marshall and T. Marshall.[1] To obtain neutron bursts, they used a rotating shutter with slits formed by cadmium plates. The operating range of the selector was limited to energies of less than 0.3 ev. The use of nickel plates instead of cadmium plates makes it possible to chop neutrons with energies considerably greater than 0.3 ev.

The neutron chopper of the mechanical selector we are describing consists of a set of alternating nickel and aluminum plates forming slits for the passage of the neutrons (Fig. 2). The aluminum plates were perforated to reduce neutron scattering. A stack of these plates with a cross section of 35 × 35 mm^2 is sandwiched between the two halves of a steel rotor 100 mm in diameter. The rotor is driven by a dc electric motor with a top speed of 16,000 rpm. The design of the rotor is shown in Fig. 2.

Two rotors were made, differing in slit width and the thickness of the nickel plates. A rotor with a set of nickel plates 0.5 mm thick forming slits 1 mm wide was used for measurements in the thermal-neutron region. In this case, the nickel plates were covered with an electrolytic, 0.1 mm thick cadmium layer. To take measurements in the epi-cadmium neutron energy region, a rotor was used with slits 0.5 mm wide with nickel plates 1.2 mm thick.

Calculations prove that for a rotor of 100 mm in diameter such a ratio between slit width and the thickness of the nickel plates produces an optimum effect-to-background ratio. The reduction of background was furthermore achieved by placing before the rotor a special collimator consisting of nickel plates 80 mm long. The thickness of the plates and the width of the slits of the collimator are exactly equal to the corresponding dimensions in the chopper.

The mechanical selector, a general view of which is given in Fig. 3, is mounted in the horizontal beam of the RTP. The boron-paraffin diaphragm system

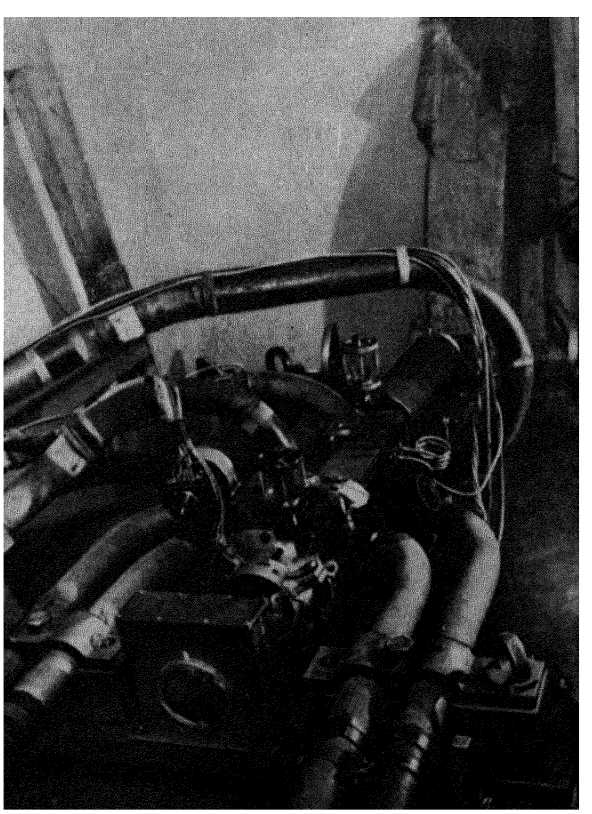

Figure 1

Original language: Russian.

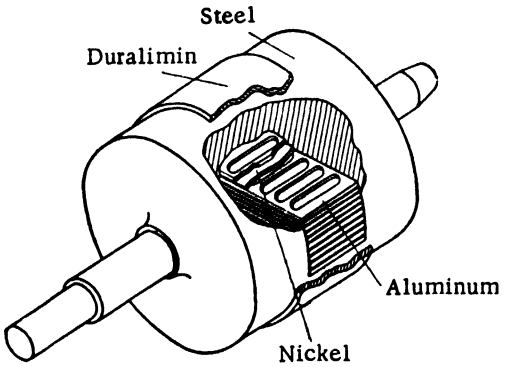

Figure 2

collimates the beam so that its diameter at incidence on the rotor is 34 mm. The beam travels a considerable part of its way from the apparatus to the detector in vacuum tubes so as to reduce neutron scattering by nitrogen nuclei. The integral neutron flux in the beam incident on the selector is 10^8 neutrons/cm²-sec with the reactor operating at nominal power. A measurement of the neutron spectrum showed that in this case the temperature of the Maxwell neutron distribution in the beam is equal to 640°K.

To carry out measurements of fission and total cross sections, a fission chamber and boron-filled counters, mounted in a special shield, were used as neutron detectors. The beam entered the counter shield through an aperture in a removable boron-paraffin plug. The flight path to the chamber was 605 cm and to the counter 630 cm.

A schematic view of the arrangement of the mechanical selector at the pile is shown in Fig. 4.

The fundamental parameters characterizing the selector are the resolving power, the background value and the value F, the definition of which will be given later (Equation 4).

Resolving power is usually defined as the ratio of the half-width of the spectral line to the flight path. The width of the spectral line and its shape depend on the duration and form of the neutron burst, the channel width and the detector length.* In the region of the high neutron energies the resolution is mainly determined by the duration of the neutron burst.

A detailed analysis of the passage of a parallel neutron beam through a revolving slit gives the following expression for the shape of the neutron burst, $J(v, t)$:

$$J(v,t) = 1 + \frac{2\omega B}{S}t; \quad -\frac{2R}{v} \geqslant t \geqslant -\frac{S}{2\omega R}$$

$$J(v,t) = 1 - \frac{\omega v}{4S}\left(t - \frac{2R}{v}\right)^2; \quad 0 \geqslant t \geqslant -\frac{2R}{v}$$

$$J(v,t) = 1 - \frac{\omega v}{4S}\left(t + \frac{2R}{v}\right)^2; \quad \frac{2R}{v} \geqslant t \geqslant 0$$

$$J(v,t) = 1 - \frac{2\omega R}{S}t; \quad \frac{S}{2\omega R} \geqslant t \geqslant \frac{2R}{v} \quad (1)$$

where S is the slit width, ω the rotor angular velocity, v the neutron velocity, and $2R$ the slit length.

The left-hand side of Fig. 5 shows the shape of a neutron burst for a neutron velocity $v > 4\omega R^2/S$ in which case the duration of the neutron burst does

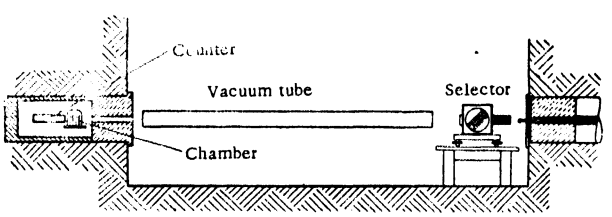

Figure 4. A schematic view of the arrangement of the mechanical selector on the beam

not depend on the neutron velocity and is given by $T_n = S/\omega R$. The right-hand side of the same figure shows the shape of a neutron burst for neutrons possessing a velocity $v < 4\omega R^2/S$. In this case the duration of the neutron burst depends upon the neutron velocity and is given by $T_n = 4\sqrt{S/\omega v} - (4R/v)$.

A knowledge of the form of the neutron burst makes it easy to calculate the half-width of the spectral line Δt. One finds the following approximate expressions for the half-width of the spectral line, on the assumption that the detector length is considerably less than the flight path:

$$\Delta t = \frac{2T_n + \tau}{4}; \quad T_n > \frac{5}{2}\tau$$

$$\Delta t = T_n + \tau - \sqrt{\tau\,(2T_n - \tau)}; \quad T_n < \frac{5}{2}\tau \quad (2)$$

where τ is the channel width.

The above expressions for neutron burst shape and duration were obtained for parallel beams. In ac-

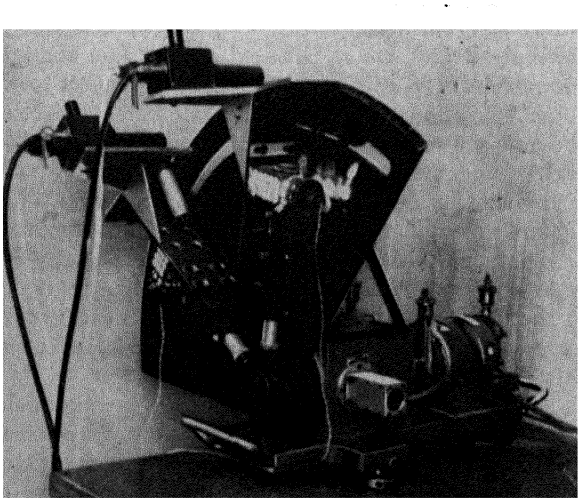

Figure 3

* The resolution is also influenced by the time of charge collection in the detector ("jitter") which should be taken into account when the channel width is short.

tuality, the beam has a certain divergency, which results in an increase in neutron burst duration. This increase in duration amounts to an effective widening of the slit.

Figure 6 gives the experimental transmission curve of the epi-cadmium neutron beam for a rotor with a slit width of 0.5 mm. As may be seen from this transmission curve, the angular width of the slit is equal to 40 ft, which corresponds to an effective linear slit width of 0.6 mm.

Assuming the effective slit width to be $S = 0.6$ mm, we obtain the following values for the neutron pulse duration at different rotor speeds:

rpm	16,000	12,000	8000	4000	2000
μsec	7	9	14	28	56

With neutron burst duration $T_n = 7$ μsec and the channel width $\tau = 4$ μsec, the maximum resolving power, without taking into consideration the finite detector length, then becomes $\Delta t/L = 0.8$ μsec/m.

The experimentally measured neutron spectrum differs from the spectrum of neutrons emerging from the reactor as the revolving rotor does not transmit neutrons of differing velocities equally. The ratio between the area under the neutron burst for neutrons with a velocity v, to this area for a neutron burst with an infinite velocity (Fig. 5, dotted line triangle), will be taken as the transmission of the rotor for neutrons with velocity v. From the expressions for the form of the neutron burst we may easily obtain the following expression for rotor transmission:

$$f(x) = 1 - \frac{8}{3}x^4; \quad 0 \leqslant x \leqslant 0.5$$

$$f(x) = \frac{16}{3}x(1-x)^2\left(1+\frac{x}{2}\right); \quad 0.5 \leqslant x \leqslant 1 \qquad (3)$$

where $x = R\sqrt{\omega/Sv}$.

Figure 7 shows the rotor transmission as a function of x. It should be noted that the above expression for rotor transmission differs somewhat from the expression given by Egelstaff in his recently published paper.[2]

For a given rotor velocity ω, neutrons possessing a velocity $v < v_{rp} = \omega R^2/S$ will not pass through the rotor since their time-of-flight through the rotor slits is more than the full slit overlap time. Thus, the modulated neutron beam has only neutrons with a velocity of more than v_{rp}. This circumstance enables us to prevent slow neutrons from previous neutron bursts from getting into the detector, provided the flight path L is less than $\pi R^2/S$.

In a given velocity range Δv, the number of neutrons that arrive to be recorded in the detector is much less than the number of neutrons in the same velocity range in the beam incident on the rotor. The ratio between these two numbers, F, is given by:

$$F = k \cdot \frac{S\tau}{2\pi R\,(T_n + \tau)} \cdot f(x) \cdot \frac{S}{S+d} \qquad (4)$$

where k is the neutron attenuation factor in the aluminum plates; d the thickness of the nickel plates, and $f(x)$ the transmission function in Equation 3.

For a selector with a rotor having a slit width of $S = 0.5$ mm, F is equal to 2×10^{-4} (for $f(x) = 1$).

The operating region of the rotor velocities is determined by the horizontal section of the transmission curve given in Fig. 7. Here, in the epi-cadmium neutron energy region, the transmission does not depend on the rotor speed. On the other hand, the background, due to rotor transmission with overlapping slits, increases in proportion to the rotor speed. Therefore it is highly essential to achieve a correct measurement of the background. It is evident that measuring the background by intercepting the beam, as was done by Fermi and his colleagues, is in this case unsuitable, in view of the absence of materials black to neutrons throughout the entire energy region being measured, and transparent for background neutrons.

Study of the spectral composition of the background shows us that it consists mainly of neutrons with an energy of more than 20 kev. This is due to the rapid drop in the nickel scattering cross sections at this energy. Thus the peak time-of-flight for background neutrons is 3 μsec, which is considerably less than the time-of-flight of neutrons being measured.

Therefore the background of a given energy channel will be determined basically by the rotor transmission at the moment the neutrons are recorded.

To determine the background it is enough to measure the counting rate with the rotor set in the appropriate position and multiply it by the ratio between the channel width and the measuring time. This method of background measurement, however, has certain shortcomings, for it requires an accurate knowledge of the channel width and does not allow changes in the power and spectral composition of the neutron beam.

We applied a method of simultaneously measuring both background and effect, which method is free of these shortcomings. It is based on the fact that the rotor transmission is symmetrical with respect to the "open" position, while the modulated neutron beam contains only neutrons above a certain velocity. The background measurement is taken before the arrival of the neutron burst, the time lead of the background channels being equal to the time-of-flight of the channels measuring the signal (see Fig. 8).

As the background is a slowly changing function of the angular position of the rotor, the background measurement is taken in a smaller number of channels (16), than the signal (64).

To produce the trigger-pulses, the following device was used: A double-faced, flat-parallel mirror was mounted on the rotor axis and two light sources and two photo-multipliers were installed on sectors (Fig. 3). Thus half a turn of the rotor produces two light-

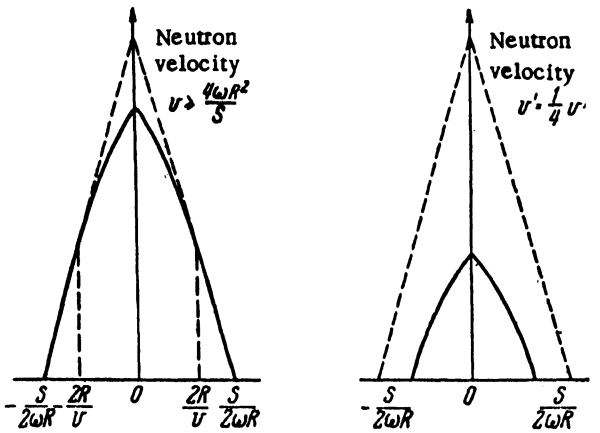

Figure 5

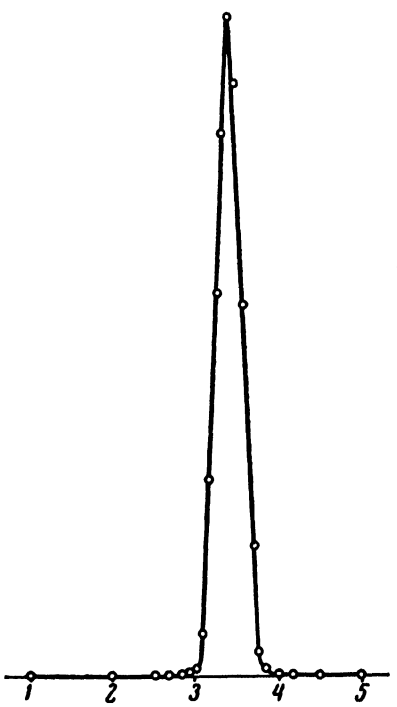

Figure 6

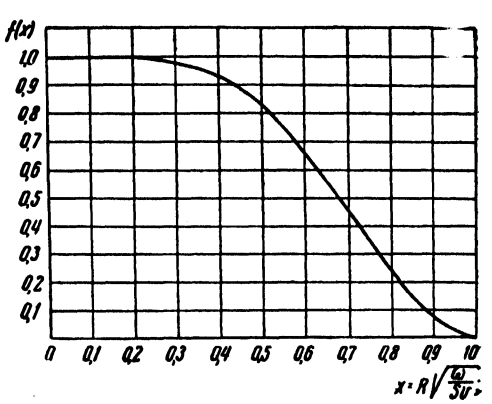

Figure 7

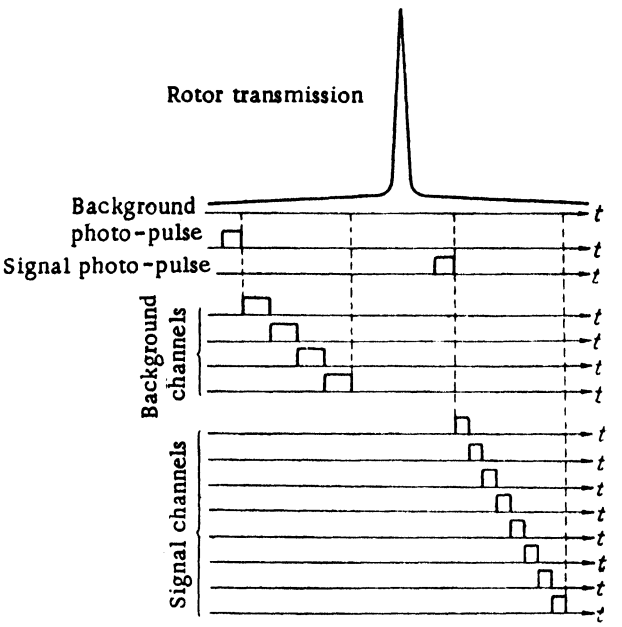

Figure 8

pulses, one of which is used to trigger the measuring channels and the other to trigger the background channels. The light sources may be moved along an angular scale with an accuracy of up to three minutes. This makes it possible to adjust the time relations between the commencement of the neutron pulse and the start of the signal and background channels. A number of tests were carried out to check background data obtained by the method described above. Amongst others, background measurements were done at indium and gold resonance energies by means of investigating the transmission of thick samples, as well as by comparing the results of these measurements with data obtained from static rotor background measurement.

ELECTRONIC CIRCUITS

The electronic circuits of the mechanical selector should perform the following tasks: (1) time selection of pulses from the counters and ionization chambers and recording them in individual channels, each of which corresponds to a definite neutron time-of-flight; (2) simultaneous measurement of background; and (3) the maintenance of a constant rotor speed of the chopper.

We used two types of time-analyzers. In the first, selection of the pulses is performed by means of electronic switching, with recording carried out by scaling circuits and mechanical counters. The second system uses a special electron-ray memory tube device for selection and recording.

Both systems are described in brief below.

Electronic Commutator Time-Analyzer

The block diagram of the electronic circuits is shown in Fig. 9. Let us see how the time-analyzer operates. It is triggered by photo-pulses obtained by

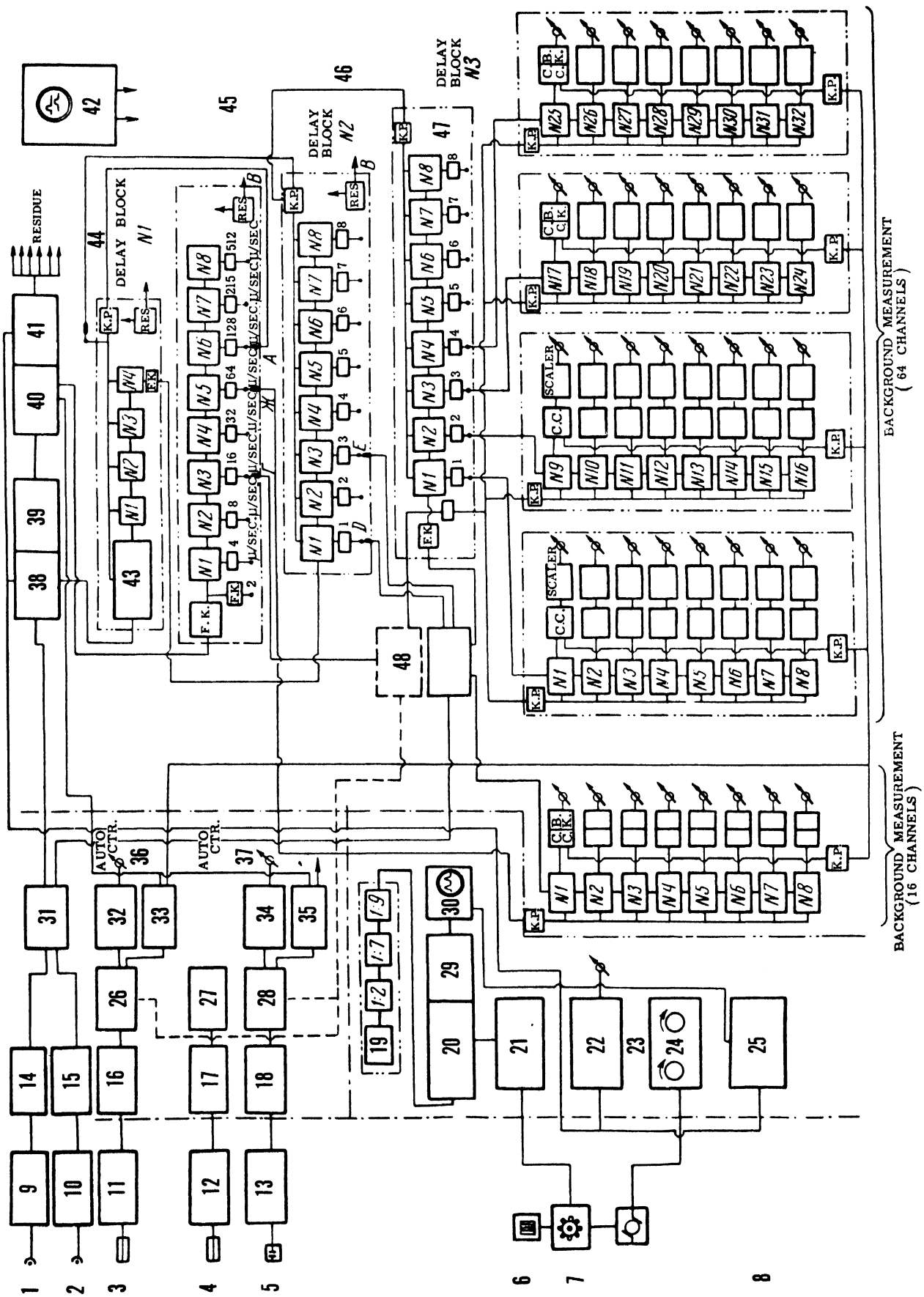
RESIDUE
DELAY BLOCK N1
DELAY BLOCK N2
DELAY BLOCK N3
AUTO CTR.
SCALER
C.C.
C.B.
C.K.
K.P.
RES.
F.K.
BACKGROUND MEASUREMENT (64 CHANNELS)
BACKGROUND MEASUREMENT (16 CHANNELS)

means of the above-mentioned optical system. In this system, the light sources with the photo-multipliers and mirrors are mounted so that one photo-pulse (photo-pulse No. 1, Fig. 10*b*) either coincides with or lags behind the neutron pulse, while the second (photo-pulse No. 2, Fig. 10*c*) leads the neutron pulse by a time determined by the conditions of the measurement.

These photo-pulses are used to start the measurement of signal and background, and also to control the timing circuits. To do the former, they are first differentiated (Fig. 10*d,e*) and then fed to the trigger circuits (Fig. 10*f,g*) which control the commutator. The (suitably delayed) commutator pulses (Fig. 10*m, o*) start operation of the signal and background counting channels, respectively.

To control the timing circuits, the photo-pulses are first mixed (Fig. 10*h*). The mixed signal controls the operation of the pulse oscillator, which produces oscillations of 0.5 Mc frequency throughout the entire period between the photo-pulses. These sinusoidal oscillations are converted to narrow pulses with a period of 2 μsec. (Fig. 10*j*), which are fed into a frequency divider. Pulses with periods of 4, 8, 16, 32, 64, 128, 256 μsec may be taken off from the output terminals of the divider. They define all the requisite time correlations in the analyzer (the position of the channels, width of the channels, etc.). There are three delay chains (No. 1, No. 2 and No. 3) for obtaining the necessary delays between the photo-pulses and the start of the signal and background measurements. Each chain consists of eight triggers (scaling steps) in series, so that each fires the next one. A pulse, lagging behind the leading pulse by a time $n\tau$, where τ is the time between two pulses in the series, can be obtained from the 12th stage of the delay system.

Similar trigger circuits control the coincidence circuits of the channels. The coincidence circuits accept detector pulses in consecutive and equal time intervals τ (Fig. 10*n,p*). The output of each coincidence circuit goes to a mechanical register. In order to conduct operations at high counting rates, 32 of the channels have scales of 16.

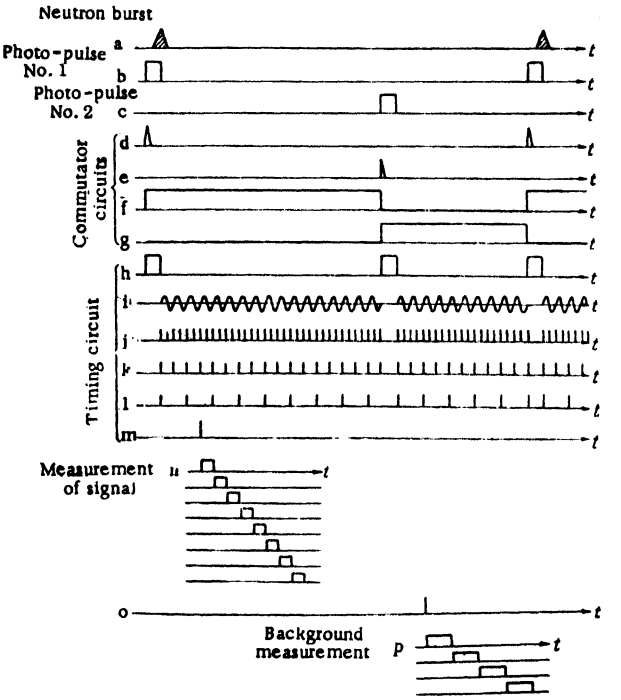

Figure 10

The system permits wide variation of channel delay and width, permitting series and parallel operation.

Of great importance in the time-analyzer are devices equalizing the channel width. In work with small channel widths (of 2 to 4 μsec), the time of the rise and fall of the control pulses is commensurate with their width as well as with the duration of the signals from the neutron detectors. In view of the fact that the recording circuits vary in sensitivity and resolution, a considerable spread appears in the effective channel widths.

Two methods have been used to eliminate this difficulty: pre-selection and phasing of the detector pulses. The first consists in excluding the pulses near the edges of each channel. Homogeneity in channel widths is thus ensured, but loss of a part of the neutron pulses is inevitable.

The second method proved more advantageous; it consists in moving the detector pulses to the middle of each channel. The principle of such an arrangement is explained in Fig. 11.

The detector pulses are fed to the input end of the memory cell (trigger or capacity). Periodic read out pulses, serving to reset the memory cells to their initial state, are likewise fed to the memory cell. Each detector pulse is memorized until the next read out pulse, after which it is transferred to the middle of the respective channel. Due to the fact that this phasing is the same for all the channels, the spread in the effective width is eliminated. In order to forestall a possible miscount under high counting rates, a special coincidence circuit is provided. The phasing device also improves operating conditions for the scaling circuit in each channel.

Figure 9. Block diagram of electronic circuits of mechanical neutron selector. (1) Photo-cell No. 1; (2) photo-cell No. 2; (3) counter; (4) counter; (5) chamber; (6) rotor; (7) audio frequency motor; (8) dc motor; (9) preamplifier No. 1; (10) preamplifier No. 2; (11) preamplifier; (12) preamplifier; (13) preamplifier; (14) amplifier of photo-pulse No. 1; (15) amplifier of photo-pulse No. 2; (16) linear amplifier; (17) linear amplifier; (18) linear amplifier; (19) crystal oscillator; (20) frequency divider; (21) invertor; (22) 1:200 scaler; (23) control of rotor speed; (24) coarse smooth; (25) tachometer; (25a) background channels (16); (25b) signal channels (64); (26) discriminator; (27) integral monitor; (28) discriminator; (29) saw-tooth oscillator; (30) electric tachometer; (31) mixer and trigger for commutator; (32) scaler 1:1024; (33) phasing circuit; (34) 1:64 scaler; (35) phasing circuit; (36) mechanical register; (37) mechanical register; (38) shaping of photo-pulse; (39) pulse oscillator; (40) pulse shaper; (41) reset pulse shaper; (42) oscilloscope; (43) coincidence circuit; (44) delay chain No. 1; (45) frequency divider; (46) delay chain No. 2; (47) delay chain No. 3; and (48) formation of preliminary pulse selection.

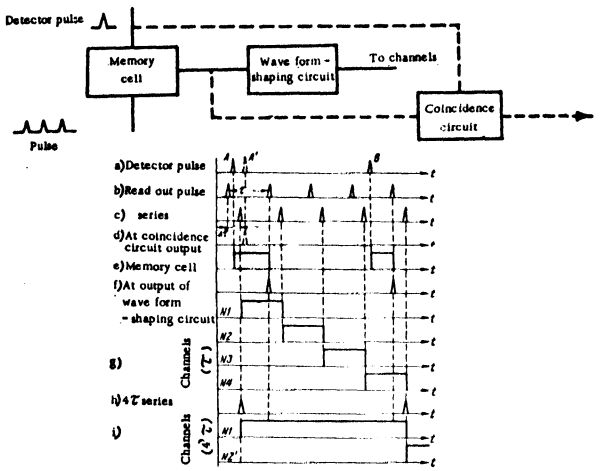

Figure 11

The uniformity of the channel widths is checked by means of a pulse generator, modulated in time by a saw-tooth voltage. This generator is synchronized with the photo-pulses, and signals for recording arrive in consecutive order in the channels of the time-analyzer. The delay between the photo-pulse and this signal is determined by the saw-tooth voltage, and, therefore, increases by a constant amount with each operation cycle. Such a generator makes it possible to check the uniformity of the channel widths with great accuracy within several minutes. A channel-width check is also made with the aid of satistically distributed pulses. Investigations have shown that the aforementioned methods reduce the spread in effective channel widths to 1%.

The rotor speed is maintained at a constant value by means of an audio frequency motor fed by a stable frequency.

This standard frequency is provided by a quartz-stabilized high frequency oscillator, the frequency of which (256 kc) is first reduced by three dividers to 2000 cycles. A further reduction in frequency is achieved by a binary scaling circuit. Oscillations of different frequencies are obtained from this circuit to govern the inverter that feeds the stator of the phonic wheel.

The rotor of the selector and the audio frequency motor are flexibly coupled to a dc motor whose speed may be continuously varied from 0 to 16,000 rpm.

A rough reading of the speed is obtained through an electronic tachometer, in which the rate of the photo-pulses is measured. Synchronization of rotor and the quartz oscillator can be checked by means of an oscilloscope. To determine accurately the number of revolutions and also to check the operation of the frequency divider, a 1:200 scaler is provided.

The electronic setup further includes linear amplifiers, discriminators and scaling circuits for recording the total numbers of counts from neutron pulses in the chamber and in the scintillation counter.

In order to ensure safety of personnel, the time-analyzer is situated 30 meters away from the mechanical selector. For that reason, right next to the chambers and the counters are preamplifiers which are linked to the main amplifiers by means of high-frequency cables. The amplifier for the proportional counters has an amplification factor of 10^4 and a pulse front rise time of 0.1 μsec. A linear amplifier with an amplification factor of 5×10^5 and a pulse front rise time of 0.05 μsec is used for the fission chamber.

All the electronic circuits are mounted on racks, which makes for convenient access to wiring and tubes. All are fed from electronically-stabilized rectifiers mounted in the lower part of the racks. A general view of the electronic setup is shown in Fig. 12.

Time-Analyzer with a Cathode-Ray Tube Memory Device

The time-analyzer we shall now proceed to describe enables us to reduce considerably the channel width and to make recordings directly on the cathode-ray tube screen.

The system consists of two closely connected units. The first unit does the time selection of the detector pulses, while the second records them. The time selection is effected by means of a memory device, the fundamental element of which is a double-beam oscillograph tube which has two independent electron guns and individual deflection circuits.†

One of the rays records the detector pulses on the tube screen. The second ray removes them again and transfers them into the respective channels of the recording device.

Let us examine the recording process (Fig. 13*a,b*).

The photo-pulse from the mechanical selector, triggers a circuit generating a pulse of duration t_m, delayed by t_t with respect to the triggering pulse. This signal controls a generator producing pulses which are used to form the horizontal step deflection potential. The time between the pulses determines the width of the channels of the analyzer. The detector pulses pass through the gate circuit only during the time t_m and then go to the steering grid. The beam is normally suppressed, but is, for 0.1 μsec, switched on by the detector signal. Due to the fact that a step voltage is applied to the horizontal plates, only strictly defined points are illuminated on the screen. Because of secondary emission from the screen, a charge is formed at each point hit by the beam.

Thus, the detector pulses are stored at definite points of the screen corresponding to definite neutron times-of-flight.

The sc recorded signals are subsequently read out to the respective channels of the recorder by the second ray (Fig. 13*c*). To control the second ray, a step voltage, with the same number of steps as during recording, but with the duration of the steps

† Certain problems of memory in cathode-ray tubes are discussed elsewhere.[3,4] The use of a single-ray tube for purposes of amplitude and time selection is also described elsewhere.[5,6]

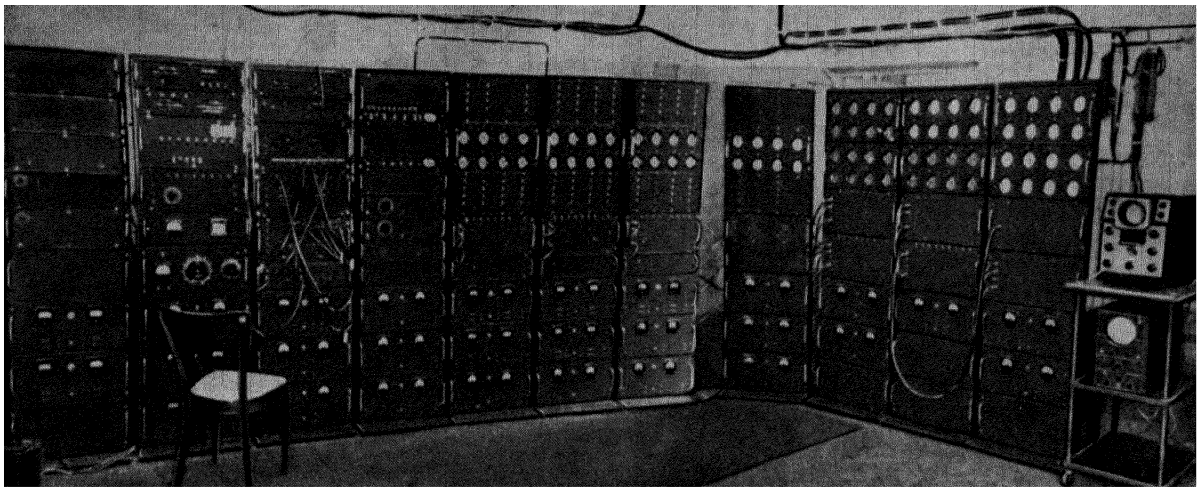

Figure 12

A

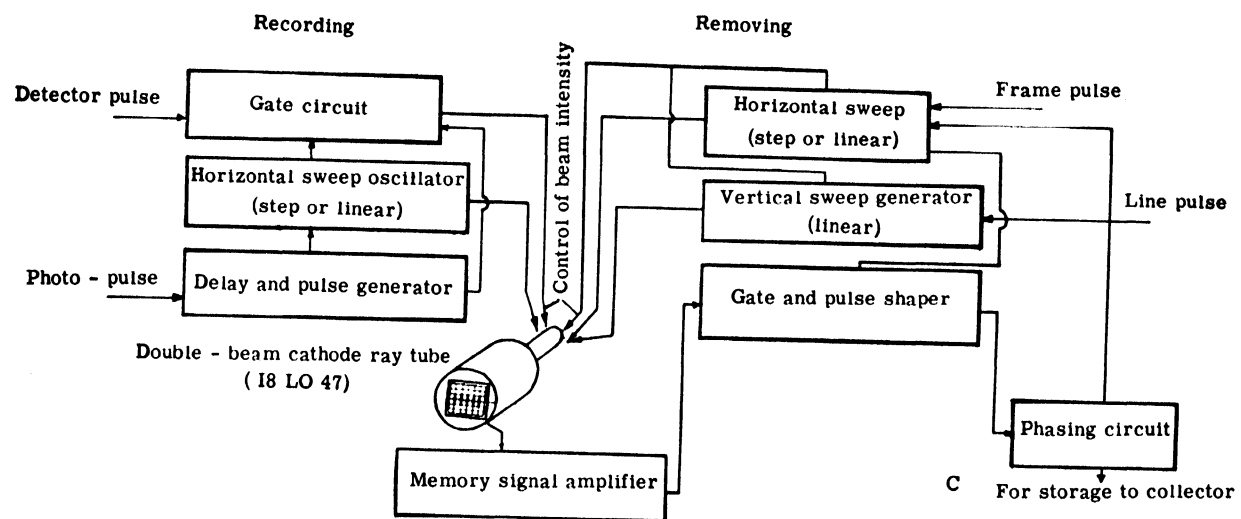

B

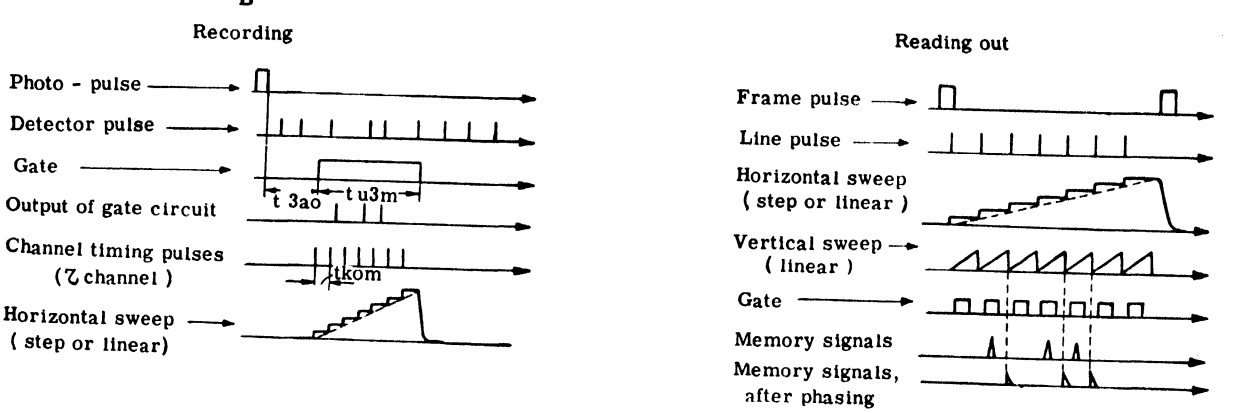

Figure 13

*

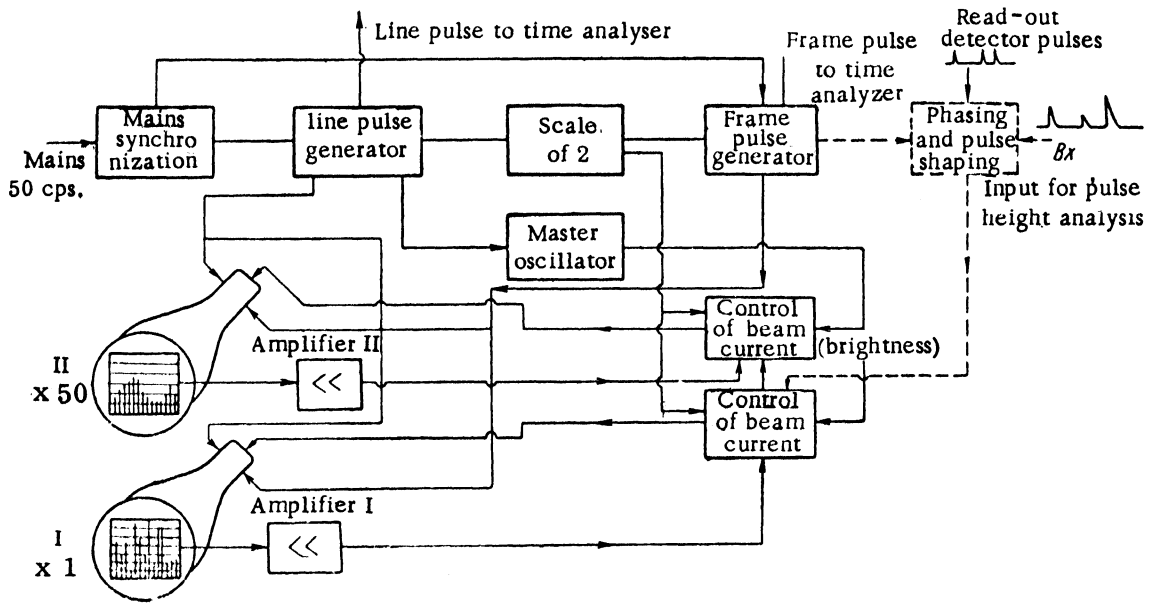

Figure 14

determined by the recording device, is applied to its horizontal deflecting plates. A saw-tooth voltage is applied to the vertical deflecting plates.

The entire system is so regulated that a removing ray passes through each point of the screen that has been illuminated by the recording ray. The removing ray is on all the time so that when it hits a point charged by the recording ray, a signal, henceforward called the memory signal, appears on the removing electrode, the metal grid in front of the tube screen.

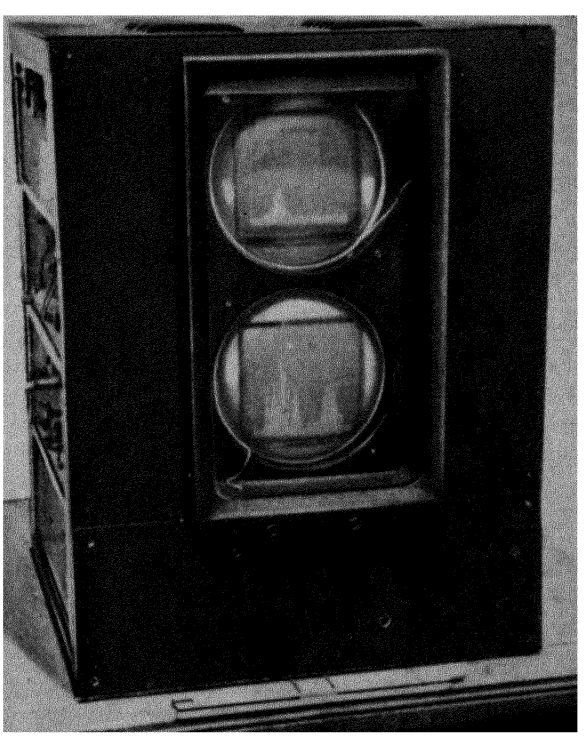

Figure 15

The current of the removing ray is sufficient for a complete removal of the charge in one passage. The memory signals are fed from the output end of the amplifier to a pulse shaper, a gate circuit and a phasing circuit, after which they are fed into the corresponding channels of the recording system.

The system we are describing also provides for operation with linear horizontal scanning instead of step scanning (see the dotted line in Fig. 13*b*). Such a scanning is more convenient in operating with small channel widths in so far as it does not require the formation of step oscillations. The uniformity of the channel widths in this case is also high, due to phasing, but additional graduation of the position of the channels is needed.

A very important characteristic of the system we are describing is the use of two independent rays for recording and for removing signals. This makes it possible to record and remove signals with different (non-synchronized) scanning frequencies, a point which is highly important for most time-analyzers. It is particularly important for the electronic apparatus of our mechanical selector, for in this case pulse recording is carried on throughout a considerable fraction of the operation cycle.

In order to make a device like this work correctly, the analyzer must not be overloaded, so that each channel receives for recording not more than one pulse per operating cycle.

Let us now make a brief examination of the recording device. The recording device displays a histogram of the pulses in the channels on a cathode-ray tube screen. To enable a sufficient number of pulses to be recorded in each channel, the recording device consists of two cathode-ray tubes operating as memory tubes (Fig. 14). The first (I) acts as scaler, and the second (II) as register.

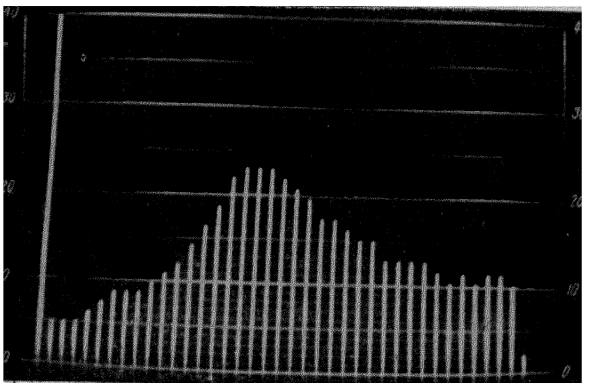

Figure 16

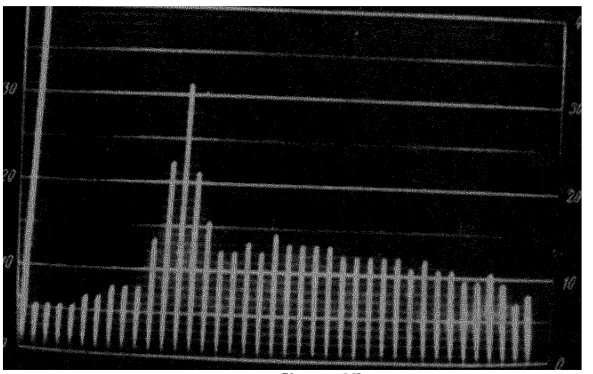

Figure 17

The principle of operation of the cathode-ray tube consists in that a "previous sweep" pulse controls the length of the signal on the steering grid and consequently the length over which each vertical sweep is illuminated. The "previous sweep" pulse, both here and in the scaler tube, is our name for the signal that appears on the removing electrode when the ray repeats its movement along the same vertical sweep, at the moment the ray reaches the point where it was switched off during its previous passage.

As this "previous sweep" pulse appears before the ray reaches the final point of the sweep, it can help us to remember the original length of the track (i.e. the luminous section of the sweep). The length of the tracks, each of which corresponds to a channel, is increased by a certain discrete value each time a signal arrives. Thus the number of recorded pulses in each channel is shown directly on the screen.

The cathode-ray tube scaling circuit is based on the same principles as the collector, except that now the ray returns to its initial state (the beginning of the line) each time a definite number of signals has been recorded, a signal then being fed to the respective register tube.

The sweep generators (line and frame) serve both the register and scaler tubes. To reduce the influence of ac backgrounds, the scanning oscillator frequency is synchronized to the line voltage. This decreases considerably the requirements for filtration of the power supply, wiring and tube screening. Such a solution somewhat restricts the operation speed (not more than 50 pulses per second should be taken by each channel) but nevertheless it has proved quite sufficient in solving numerous problems.

The frame scanning oscillator generates a step voltage with the same number of steps as the number of channels (lines). The period of the line oscillator is 250 μsec. Each line is traced twice by the way, which is necessary for the operation of the scaling circuit. The line scanning frequency is synchronized with a master oscillator which also controls the operation of the steering grid circuits. The period of its pulses is 5 μsec, and therefore up to 50 signals can be stored along each vertical sweep. Thus the capacity of each channel is 2500 pulses, and the capacity of the whole recording device 100,000 pulses.

The recorder we have described, a general view of which is given in Fig. 15, enables unintermittent observation of the data on the cathode-ray tube screen. A histogram of the spectrum is obtained directly on the collector tube screen, and retained for an unlimited period of time.

To illustrate the operation of the time-analyzer with this cathode-ray tube memory device, the photograph in Fig. 16 gives the results for the spectrum of neutrons from the experimental hole of the RTP. No pulses were fed to the first four channels. Measurements were taken with a flight path or three meters, the rotor speed being 4000 rpm. The rotor slit width was 1 mm and channel width 36 μsec.

To obtain the neutron density velocity distribution, the data obtained after subtracting the background and correcting for the transmission function must be multiplied by t^2 (t is the time-of-flight channel).

Figure 17 gives the results for a measurement of the fission of Pu^{239}. The flight path in this case was 3.35 meters. The well known resonance of Pu^{239} at 0.30 ev, is clearly seen.

The cathode-ray tube recorder described above has also been used to investigate amplitude spectra, for which purpose a supplementary circuit was built to convert pulse amplitude to pulse length. This amplitude analyzer proved convenient in studying isotopic composition of samples investigated on the selector.

Instances of measurings of the amplitude spectrum of alpha-particles are given elsewhere.[7]

REFERENCES

1. Fermi, E., Marshall, J. and Marshall, L., Phys. Rev. *72*, 193 (1947).
2. Egelstaff, P., Journ. Nucl. Energy, *1*, 57 (1954).
3. Katayev, S., *Television compendium*, A.U.R.C. (1935).
4. Williams, F. C., Kilborn, T., The Proc. of the Inst. of Electr. Eng, *96*, Part III, No. 40, 81 (1949).
5. Cunningham, J. A., Bulletin of the American Phys. Society, vol. 28, No. 3, 1953.
6. Bergman, A. A., *et al.*, P/642, *Neutron Spectrometer for Moderation of Neutrons in Lead*, Session 16A.1, Vol. 2, these Proceedings.
7. Adamchuk, Y. V., *et al.*, P/645, Session 17A, Vol. 2, these Proceedings.

A Neutron Selector with Mechanical Shutter

By V. V. Vladimirski, I. A. Radkewich, W. W. Sokolowsky, USSR

At present mainly two methods of energy measurement of the neutrons are used in neutron spectroscopy.

The first method is based on the spatial separation of neutrons by diffraction in crystals. In such spectrometers the reflection of the neutrons by crystals rapidly diminishes with increasing neutron energy, leading to serious losses in the luminosity of the apparatus. Besides this, with increasing neutron energy, the reflected beam gets nearer to the direct beam. This leads to serious difficulties in energy determination. Because of this, crystal spectrometers are used for neutron cross-section measurements only in the energy interval up to 10 ev.

The second method—the time-of-flight method—is based on the production of a time modulated neutron beam. The neutron velocity is determined by measuring the time needed to travel a given distance. The modulated neutron beam may be produced by modulating the ion source of an accelerator, or by mechanically interrupting a strong neutron beam emerging from a nuclear reactor.[1]

It is convenient to characterize the properties of the selector by its resolution $\Delta t/L$, where Δt is the uncertainty of the time-of-flight of the neutron, and L is the path length,* in units of μsec/m.

When the present work was begun (1950), the time-of-flight method was mainly used in conjunction with cyclotrons; the resolution power of such systems was 1.5 μsec/m[2,4]. The method of the mechanical interruption of the beam was not commonly used.

Fermi and Marshall[1] used a shutter, which was made of cadmium, which failed at high energies because of the rapid increase of its transparency with the energy of the neutrons. In 1950 we began to work on a new design of a mechanical shutter, where, instead of absorption, the scattering of the neutrons by the material of the rotor was used. In order to get a maximum scattering effect, it is necessary to collimate thoroughly before and after the shutter. The maximum neutron energy at which such a shutter may be used extends up to several hundreds kev as the total neutron cross section of elements of medium atomic weight (Fe, Ni, Cr) only slightly depends on the energy.

According to this idea a mechanical interrupter was designed and built and was installed at the research reactor at the end of 1952. The resolution of the instrument was $\sim$ 0.4 μsec/m with 5.5 m path length. By means of this instrument the cross sections of several elements were measured in the energy interval 5–1000 ev (the cross sections of Mn, U and U^{235} are shown in the present paper).

Simultaneously we worked on a new instrument with a greater resolution power, $\sim$ 0.07 μsec/m. At the beginning of 1955 the new spectrometer was put in action. This second spectrometer is described in the present report.

DESIGN OF THE NEUTRON SPECTROMETER

An over-all view of the neutron spectrometer is shown in Fig. 1.

The beam of neutrons emerging from the reactor passes through the collimator (2) located within the shield of the reactor (1), and falls on the first slit collimator (3) made of neutron absorbing material. A number of narrow neutron beams passes through the rotor (4). The rotor contains a system of slits that are an extension of the slits of the collimator. The interrupted neutron beam passes through the second slit collimator (6) which absorbs the neutrons scattered by the rotor over small angles. After travelling distance L the neutrons are registered by the detector (7).

The pulses from the detector are fed to the time-analyzer, which is put in action the moment the neutrons pass through the slits of the rotor. The time-analyzer is put in action by light starting-pulses.

Mechanical Interrupter (Chopper)

The mechanical interrupter (see Fig. 2) contains a rotor with 30 slits located perpendicularly to its

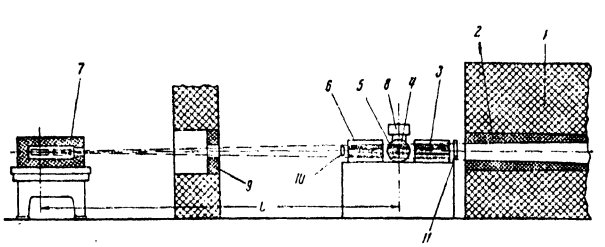

Figure 1. Diagram of neutron spectrometer: (1) shield of the reactor; (2) collimator channel; (3) first slit collimator; (4) rotor; (5) slits of the rotor; (6) second slit collimator; (7) neutron detector; (8) starting-pulse generator; (9) boron shielding; (10) sample; and (11) monitor

Original language: Russian.

* Δt the half width of the resolution curve depending on the duration of the neutron burst, channel-width, rise time of the counter-pulse, etc.,

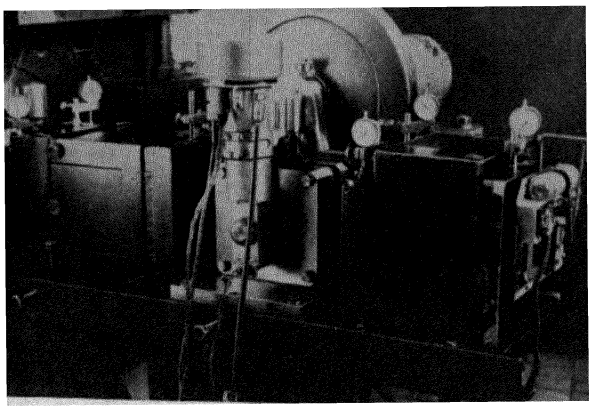

Figure 2. General view of the mechanical chopper

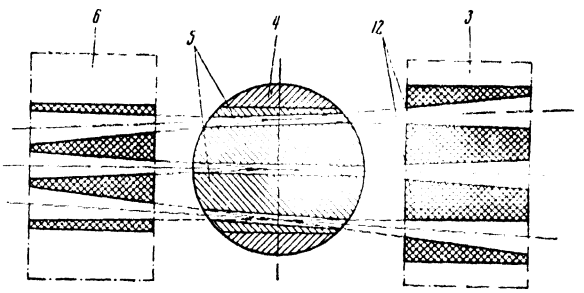

Figure 3. Sketch of mechanical shutter: (3) first slit collimator; (4) rotor; (5) plates of the rotor; (6) second slit collimator; and (12) collimator plates

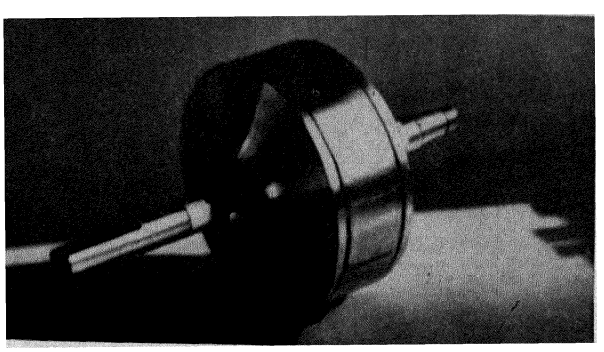

Figure 4. Rotor of the mechanical interrupter with a single set of straight slits

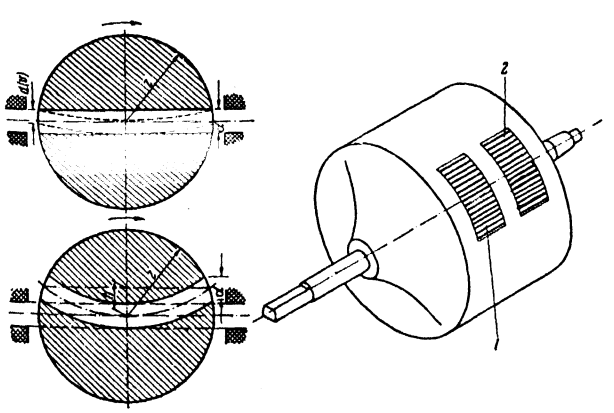

Figure 5. (1) Straight slits; and (2) curved slits

axes and two slit collimators located before and after the rotor along the direction of the neutron beam. A section of the mechanical interrupter is shown at Fig. 3 (the vertical dimensions are rather exaggerated).

The rotor (Fig. 4) is made of an alloy containing 70% Ni and 23% Cr. We chose this material because it possesses a high strength ($\sigma_B = 95$ kg/mm^2) and also a fairly large and constant scattering cross section ($\sigma = 18$ barns up to $\sim 10^4$ ev). The main data of the rotor are the following:

Diameter	150 mm
Slit width	0.2 × 24 mm
Distance between slits	2 mm
Number of slits	30
Weight with 2 slit system	16 kg
Rotating speed	24,000–30,000 rpm
Circumference velocity	119–230 m/sec

In order to diminish the detector area and simultaneously to increase the solid angle, i.e., the luminosity of the arrangement, the slit systems are made to converge at a distance of 18 m from the rotor. The rotor is driven by a 1-kw dc motor through a friction transmission with a 5:1 reduction. The speed of rotation of the rotor is controlled by hand and held constant within 1%. When the neutrons pass through the slits of the rotor, "cut-off" of neutrons occurs, which is the larger the smaller the energy of the neutrons. Neutrons having a velocity lower than

$$v = \frac{\omega r^2}{d}$$

where r is the radius of the rotor, ω the frequency of rotation, and d the slit width (see Fig. 5), will not pass through the rotor at all. For a rotor with the given dimensions and with a revolution speed of 24,000 rpm, neutrons having energies < 25 ev will be cut off. In order to have the possibility of performing measurements with energies lower than 25 ev, without reducing the revolution speed, i.e., without reducing the revolution of the instrument, the rotor has, in addition to the rectilinear slits a system of curvilinear slits (Fig. 5). The curvature of these slits, i.e., the sagitta h, is determined from the relation

$$h = \frac{\omega r^2}{v_0}$$

where v_0 is the velocity of the neutrons that pass without any cut off. The value of the sagitta is 0.4 mm, corresponding to an energy $\frac{1}{2}mv_0^2 = 6.5$ ev at 24,000 rpm or 2.3 ev at 14,400 rpm; with this speed the measurements of Ir and Sm were performed. As the values of h and d are of the same order of magnitude, there is no significant monochromatization of neutron beam. It was shown that it is possible to perform measurements with a resolution 0.3 μsec/m in the energy interval from 9 to 1.25 ev.

The stationary slit system (collimator) is made of wedge-like plates separated by aluminum spacers. The plates are pressed from boral ($B^{12}Al$), bonded

by bakelite. The collimators and the rotor were adjusted within 0.3 mm. Verification of the adjustment was made by photographing the beam at the end of the second slit collimator and at the location of the detector. The beam dimensions at a distance of 14 m from the rotor were 40 × 250 mm, in fair agreement with calculations. The small neutron beam area allowed the use of a small detector, which considerably diminished the background.

The starting pulse was obtained in the usual way. Light passing through special slit cut in the shaft of the rotor, falls on a photo-multiplier. The amplified pulse of the photo-multiplier serves as a starting-pulse for the time-analyzer.

Time Analyzer

Delayed coincidence circuits, where by means of a chain of triggers only the initial pulse is delayed, are rather inconvenient for use in multichannel time-analyzer, because of their intricacy and unwieldiness. For each coincidence circuit usually called "channel", it is necessary to have a separate trigger, and to form very long trigger-chains.

In 1950 we proposed a new principle of the multichannel time-analyzers, based on the arrangement of the coincidence circuits in a matrix. Such arrangements were described in 1953.[5] In such systems not only the starting pulse but also the neutron counter pulses are delayed. Each channel contains not a single trigger (which usually has 4–6 tubes), but $\sqrt{n}$ triggers, where n is the number of channels.

The first model of a 256-channel analyzer was put in action in summer 1951, a second model at the end of 1954.

The time-analyzer (Fig. 6) functions as follows. The starting-pulse starts a quartz-stabilized pulse oscillator, with period τ equal to the channel-width. The neutron pulse is fed to the distributing commutator, formed by a chain of l triggers, to the second input of which the pulses of the oscillator are fed. In each stage of the commutator the pulse is delayed by τ compared with the preceding stage. The commutator has l outputs with delays that are multiples of τ, from τ to $l\tau$.

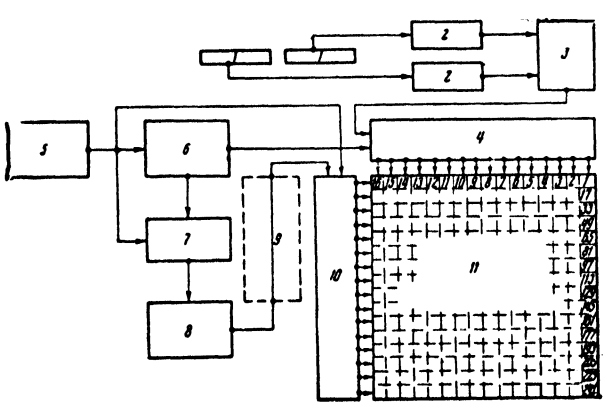

Figure 6. Block diagram of the time analyzer: (1) $B^{10}F_3$-counter; (2) amplifiers; (3) mixer with delay; (4) distributing commutator; (5) starting-pulse generator; (6) driving oscillator; (7) the gate; (8) scaling circuit; (9) phasing circuit and delay circuit; (10) driving commutator; and (11) coincidence circuit

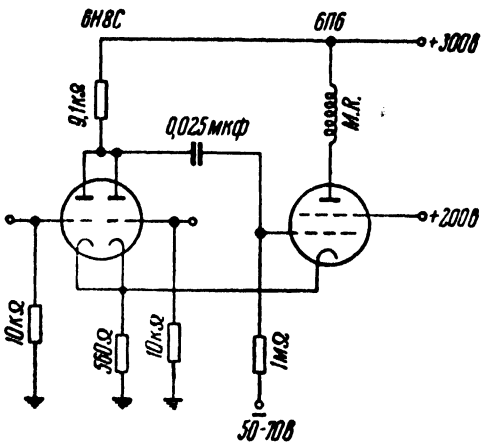

Figure 7. Coincidence circuit and output stage for the mechanical register

Simultaneously, a scaling circuit divides the frequency of the oscillator by l. The pulses with period $l\tau$ are fed to the chain of m triggers forming the second, slower commutator, which has m outputs with delays that are multiples of $l\tau$, from $l\tau$ to $ml\tau$. There are ml coincidence circuits forming a matrix of m lines and l rows. This allows one to register the coincidences of each of the outputs of the distributing commutator with any output of the second commutator. The coincidence circuit in row i and line k will register neutron pulses corresponding to a time-of-flight $(kl—i)\tau$, i.e., equal to the difference of the time delays in the commutators. As the pulses at the outputs of the commutators are in phase with the pulses of the driving oscillator, the length of all the channels is equal and the coincidence circuits need not meet any special requirements.

The coincidence circuits (see Fig. 7) operate directly on the mechanical counting relays and contain two tubes. The first, a double triode, selects the coincidences and serves as part of a univibrator. The second, a power-tetrode, drives the mechanical counting device and serves as the second part of the univibrator. The analyzer contains 16 lines and 16 rows, i.e., 256 channels. Each channel has one output to one of the two mechanical scaling devices, the changing over of which is performed by means of relays operated by a clock.

The adjusting of the quartz-pulse-oscillator presents certain difficulties and was made only in 1953.† Because of this, a considerable part of the measurements was performed with a continuously working quartz-oscillator. The resulting difference in phase between the oscillator and the starting pulse causes an additional uncertainty in the time-measurement.

In order to alter the channel-width, the pulses of the 1 Mc driving oscillator are fed to a scaling circuit which allows the channel-widths to be made equal to 1, 2 or 4 μsec. The neutrons are registered by two banks of $B^{10}F_3$ counters, located one after the other

† The circuit was designed by W. W. Okorokov.

along the beam. The pulses from each group are amplified by a separate amplifier, after which they are fed to a mixer, duly correcting for the difference in time-of-flight between the counters. This correction is different for different neutron velocities. After the mixer the pulses are fed to the time-analyzer. The counters had a length of 20 cm and diameter of 30 mm.

MEASUREMENTS

In addition to statistical errors, errors due to intensity fluctuation of the neutron beam or the neutron spectrum, of the rotation speed of the rotor, etc., are possible. As the measurements take a long time, these factors may lead to serious errors. In order to eliminate these errors, measurements with sample and without sample were alternated each 10–20 minutes. The interchanging was done automatically by means of a special circuit, actuated by a clock. The same circuit simultaneously actuated the changing-over of the mechanical counting devices of the time-analyzer and the monitor.

Estimation of the Resolution

We performed direct determinations of the resolution of the spectrometer by means of γ-quanta present in the neutron beam. The high tension at the neutron $B^{10}F_3$ counters, was elevated so that they would register γ-quanta. The starting-pulse was fixed with a certain advance relative to the moment of the opening of the shutter.

The dependence of the number of counts per channel on the time-of-flight gives directly the resolution function of the arrangement. This curve does not include, however, the error due to the finite length of the detector, which can be easily computed. Figure 8 gives the resolution-curve of the neutron spectrometer for two different modes of operation. Curve 1 was obtained with a channel width of 2 μsec, with an uncertainty in time scale of $\sim$ 1 μsec and a rotation speed of 12,800 rpm. Curve 2 was obtained with a channel width of 1 μsec, and the rotation speed equal to 22,000 rpm; the quartz generator was now triggered by the starting pulse. For comparison one of the best of the published resolution curves[6] is given in the same figure (curve 3).

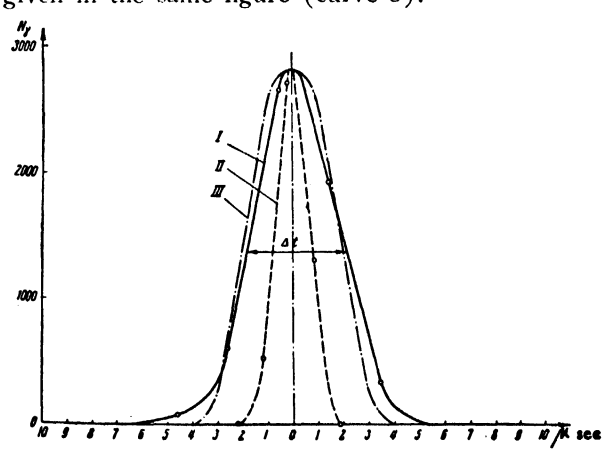

Figure 8. Resolution curves of the neutron spectrometer

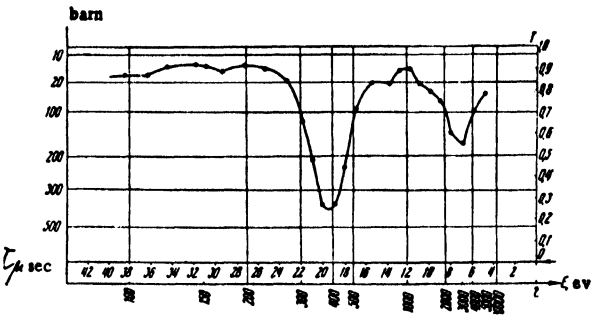

Figure 9. Transmission curve of sample Mn^{55}, $n = 3.6 \times 10^{21}$ atoms per cm^2, resolution 0.4 μsec cm^2

The time-of-flight uncertainty is usually taken to be the half-width of the resolution curve. The maximum resolution of our neutron spectrometer, with a 19 m path-length, then is 0.07 μsec per meter.

Estimation of the Background

The amount of background was determined by means of special channels of the time-analyzer, displaced relative to the other channel by a time-interval exceeding the time-of-flight of the slowest neutrons that are able to pass through the slits of the shutter. It was shown that the background was for 90% due to neutrons passing the closed shutter, and that these are mainly fast neutrons.

Because the transparency of the rotor is slightly higher near the open position than at the angles where the determination of the background was performed (30–40 degrees), special experiments were done in order to determine the excess of the actual background above the one measured. It turned out that the actual background was 30% higher than the background counted in the displaced channels. This correction was accounted for in the computations. It should be mentioned that the background was small, $\sim$ 15–18% of the total counting rate in the channel, so that there was no necessity to determine it more precisely.

Manganese

In order to examine the possibilities of the neutron spectrometer, measurements of the cross section of Mn were performed. We chose this element because the levels of Mn are far apart and measurements performed by means of other spectrometers had shown the existence of a strong resonance at 400 ev.

The manganese sample was 0.53 gm/cm^2 MnO_2, specially purified from Na. As manganese does not form oxides of stoichiometric composition, a chemical analysis was performed which gave the following results:

Mn: 63.21% O: 36.78%

Hence the sample contained 3.6×10^{21} atoms/cm^2.

The measurements were performed with a 5.3 m path length, a channel width of 1 sec and a resolution $\sim$ 0.4 μsec/m. Figure 9 shows the result as a function of energy. The statistical accuracy of the measurements is 8–10%. A resonance level at E_n = 360

± 30 ev and a broad resonance at $\sim$ 2600 ev, probably consisting of several levels, were observed. As the sample was thick ($\sigma_0 n \gg 1$), the area under the transparency curve makes it possible to determine the value of $\sigma_0\Gamma^2 = (1.5 \pm 0.7) \times 10^6$ ev^2 barn. Because of the low accuracy of the results, a more detailed analysis of the parameters was not undertaken.

Natural Uranium

The sample contained 28.89 gm/cm^2 of natural metallic uranium. With this sample two series of experiments were performed. In both cases the path length was 5.3 m.

First Series

In this experiment the channel width was 1 μsec, the speed of the shutter 22,000 rpm, and the number of channels 52. The resolution power, as measured by γ-rays, was 0.4 μsec/m. The counting rate was 15–20 counts per hour per channel with the background equal to 5 counts per hour per channel. The statistical accuracy of the cross-section determination was 10–12%. In the curve (Fig. 10) resonances exceeding the statistical errors are seen in the energy regions 70, 110 and 210 ev. As the widths of these resonances exceed the resolution, one may surmise that each of them consists of several levels.

Second Series

The channel width was 4 μsec, the speed of the shutter 14,000 rpm, the number of channels 52. The resolution power was 1.4 μsec/m, the statistical accuracy 4.5 to 10% (Fig. 11). The earlier published resonances at the energies 6.8; 21.6; 40.3 ev are seen, and the resonances obtained in the first series at energies of 70, 110 and 210 ev are confirmed.

From these two series of experiments it is possible to conclude that natural uranium, in addition to the resonances at 6.8 ev; 21.6, and 40.3 ev, the data on which had been published at the time of our measurements, possesses at least three groups of resonances in the energy regions of 70, 110 and 210 ev.‡

For the first three resonances the value of $\sigma_0\Gamma^2$ was determined.

1. $E_p = 6.8 \pm 0.5$ ev $\quad \sigma_0\Gamma^2 = 9.8 \pm 1.8$ barn-ev^2
2. $E_p = 21.6 \pm 2.0$ ev $\quad \sigma_0\Gamma^2 = 34 \pm 10$ barn-ev^2
3. $E_p = 40.3 \pm 4.6$ ev $\quad \sigma_0\Gamma^2 = 245 \pm 80$ barn-ev^2

The energies of the remaining levels may be listed as follows:

4. $E_p = 70 \pm 7$ ev
5. $E_p = 115 \pm 17$ ev
6. $E_p = 205 \pm 30$ ev

Uranium-235

The sample consisted of UO_2 powder. Chemical analysis showed that it contained 87.75% of uranium. The uranium contained 90.7% of the U^{235} isotope. The amount of pure U^{235} was 2.56 gm/cm^2.

With this sample three series of measurements were performed with resolving-power: ~0.4; 0.8 and

‡ The presence of these resonances is confirmed elsewhere.[8]

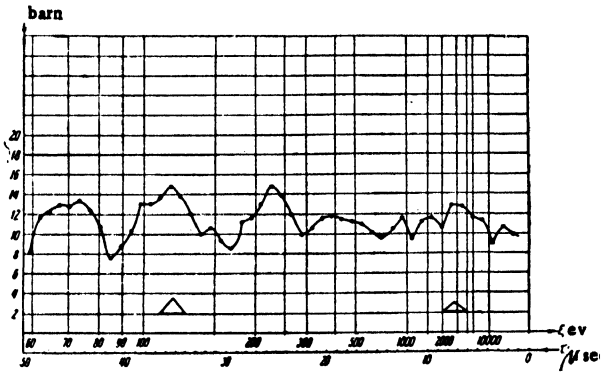

Figure 10. Total cross section of U as function of energy with n = 73.2×10^{21} atoms per cm^2 and resolution 0.4 μsec/m

1.3 μsec/m, with path length 5.6 m, and channe widths 1, 2 and 4 μsec. Figures 12 and 13 show th cross sections of U^{235} obtained in all the three serie

At present there are no published data on th cross section in the energy region investigated.[10] Th level at 6.2 ev is of special interest because there i a level near to it in U^{238}. As the sample containe up to 10% of U^{238}, one must allow the possibilit that the peak in the cross section at 6.2 ev is due t the presence of U^{238} in the sample. But quantitativ calculations showed that the curve cannot be ex plained by the presence of U^{238}. Besides the leve already mentioned, resonances at 8.6, 12, 13.5, 15.2 19, 22, 33.5, 49 and 97 ev were observed in a the measurements. As the experimental condition in all the experiments were different, one may cor sider the existence of these levels safely establishec

All results are in fair agreement with the dat obtained on the cyclotron, and on the other neutro selectors.[11,12,13]

Iodine

The measurements were carried out under th following conditions: (*a*) speed of the rotor, 12,80 rpm; (*b*) channel width, 2 μsec; (*c*) path lengtl 14.0 m; (*d*) calculated duration of neutron burs 2 μsec; (*e*) uncertainty of time-scale $\sim$ 1 μsec.

The resolution measured by γ-rays was 0.2 μsec/m.

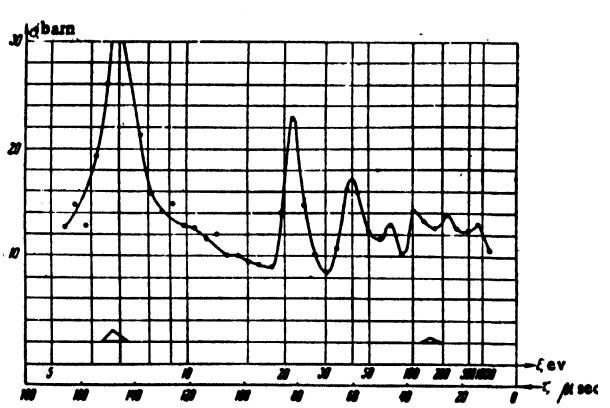

Figure 11. Total cross section of U as function of energy with n = 73.2×10^{21} atoms per cm^2 and resolution 1.4 μsec/m

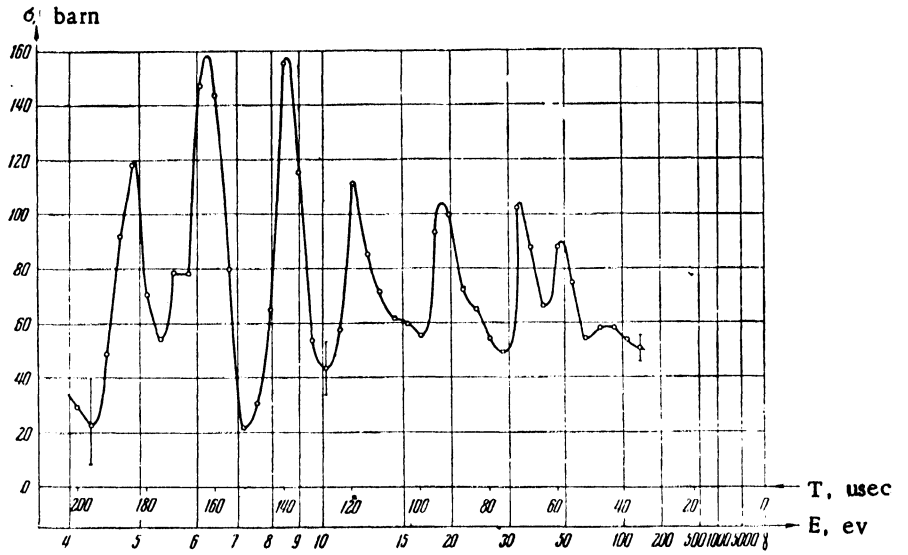

Figure 12. Total cross section of U^{235} as function of energy with $n = 6.56 \times 10^{21}$ atoms per cm^2 and resolution 1.4 μsec/m

The sample contained 3.94 gm/cm² or 18.55×10^{21} atoms/cm² of chemically pure iodine. It was placed in an aluminum container. During measurements without sample, an identical empty container was placed in the beam. The background amounted to 15–18% of the effect. The dependence of the total cross section of iodine on energy is shown in Fig. 14. Up to 20 ev no levels were observed; in the energy region from 20 to 100 ev, seven resolved levels, for which the energies and the values of $\sigma_0\Gamma^2$ were determined. $\sigma_0\Gamma^2$ was obtained by a method described elsewhere.[9] No corrections for the Doppler-effect were made.

Above 100 ev the levels were not fully resolved, and because of this were not analysed. The data on the first seven levels are given in the following table:

E_p, ev	$\sigma_0\Gamma^2$, barn-ev²
20.5 ± 0.4	9 ± 2
31.4 ± 0.6	70 ± 15
38.1 ± 0.9	155 ± 30
46.0 ± 1.2	78 ± 20
66 ± 2	27 ± 12
79 ± 3	97 ± 40
92 ± 4	50 ± 25

The total level density in the energy region $0 < E < 100$ ev for the two possible spin states of the compound nucleus, $I = 3$ and $I = 4$, is $1/14$ ev^{-1}.

The mean cross section in the energy region 300–10,000 ev is $\sigma = 7.5 \pm 0.2$ barns, three times bigger than the cross section in the energy region 10–20 ev.

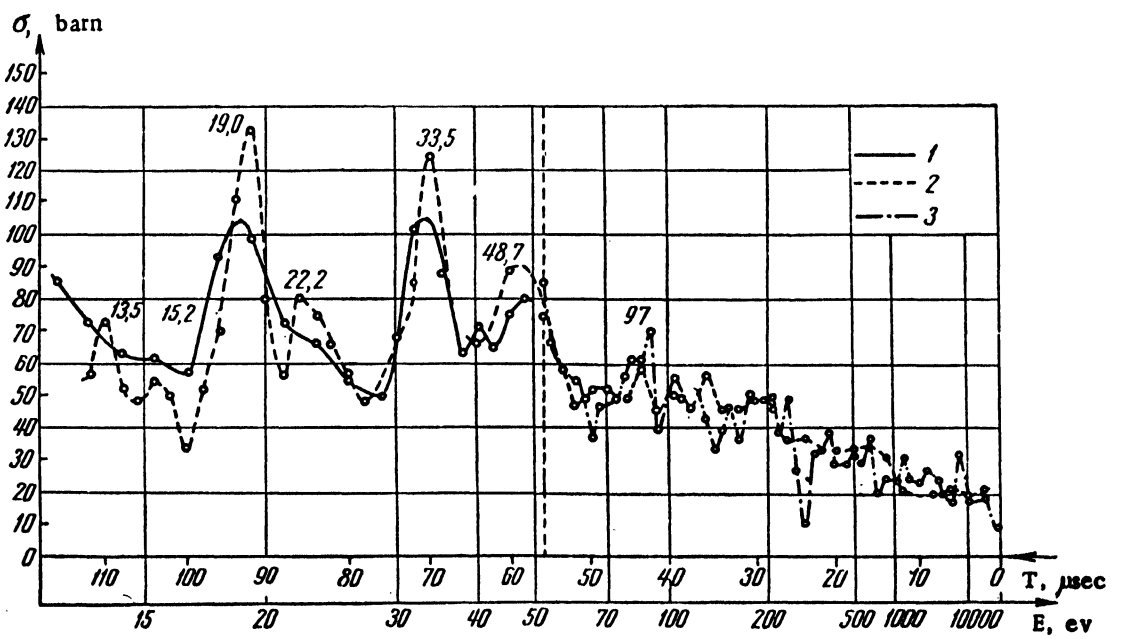

Figure 13. Total cross section of U^{235} as function of energy with $n = 6.56 \times 10^{22}$; (1) resolution 1.4 μsec/m; (2) resolution 0.8 μsec/m; and (3) resolution 0.4 μsec/m

($\sigma = 2.4 \pm 0.1$ barns). This, and the irregularity of the curve in this region, point to the presence of a great number of levels and possibly of separate groups of levels. But because of the insufficient accuracy it is not possible to make definite conclusions on the presence of these groups of levels.

The data obtained on iodine are in accordance with those published.[6] Because of a better resolution of the levels the values of $\sigma_0\Gamma^2$ obtained in our experiments have a higher accuracy.

Indium

The sample contained 9.87×10^{21} atoms/cm^2 of metallic indium. The measurements were carried out with path length 14 m and channel width 2 μsec. The resolution was 0.3 μsec/m. The results are shown in Fig. 15. In the curve a strong level at 8.9 ev and a number of weaker levels at 11.9, 14.5, 22.6, 24.9, 31, 48 and 84 ev are seen. The position of the first three levels is in accordance with the measurements carried out with the crystal spectrometer.[4]

Neodymium

The thin sample made from neodymium-oxide contained $n_{Nd} = 1.425 \times 10^{21}$ atoms/cm^2, $n_O = 2.14 \times 10^{21}$ atoms/cm^2. The experimental conditions were the same as in the case of indium. In the region from 5 to 35 ev an irregular spread of the experimental points is observed. Because of this, the cross sections given in Fig. 16 were obtained by summing the counts in adjacent channels. A number of strong levels is present above 40 ev. The strongest levels (or groups of levels) are observed at energies 42.8, 58.2, 158, 196, 375 and 1290 ev.

Praseodymium

The sample of praseodymium oxide had a thickness of $n_{Pr} = 1.33 \times 10^{21}$ atoms/cm^2, $n_O = 2.0 \times 10^{21}$ atoms/cm^2. The spectrum was obtained in the same way as that of indium and is given in Fig. 17. Up to 200 ev there are no maxima significantly exceeding the statistical error. Above 200 ev groups of levels are observed. The most distinct peaks are observed at 230, 375 and 1100 ev.

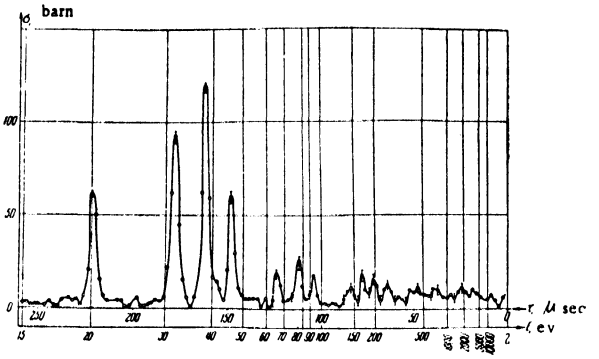

Figure 14. Total cross section of I^{127} as a function of energy with $n = 18.55 \times 10^{21}$ atoms per cm^2 and resolution 0.3 μsec/m

Palladium

Two samples of metallic palladium, 19.7×10^{21} atoms/cm^2 thick and 1.28×10^{21} atoms/cm^2 thin, were investigated. The spectra of both samples were investigated with the path length 18.9 m and channel width 2 sec. The driving oscillator was triggered by the starting pulse. The resolution power was 0.18 μsec/m. Figure 18 contains the results of the measurements with both samples. The cross-section curve in the resonances was drawn through the points for the thin sample, that between the resonances through the points for the thick sample. Peaks of the cross section are observed at energies 11.75, 13.0, 24.9, 32.6, 54.8, 89.8, 185, 278 and 940 ev. The resonances at 13, 25 and 33 ev have been observed earlier with a crystal spectrometer.[14]

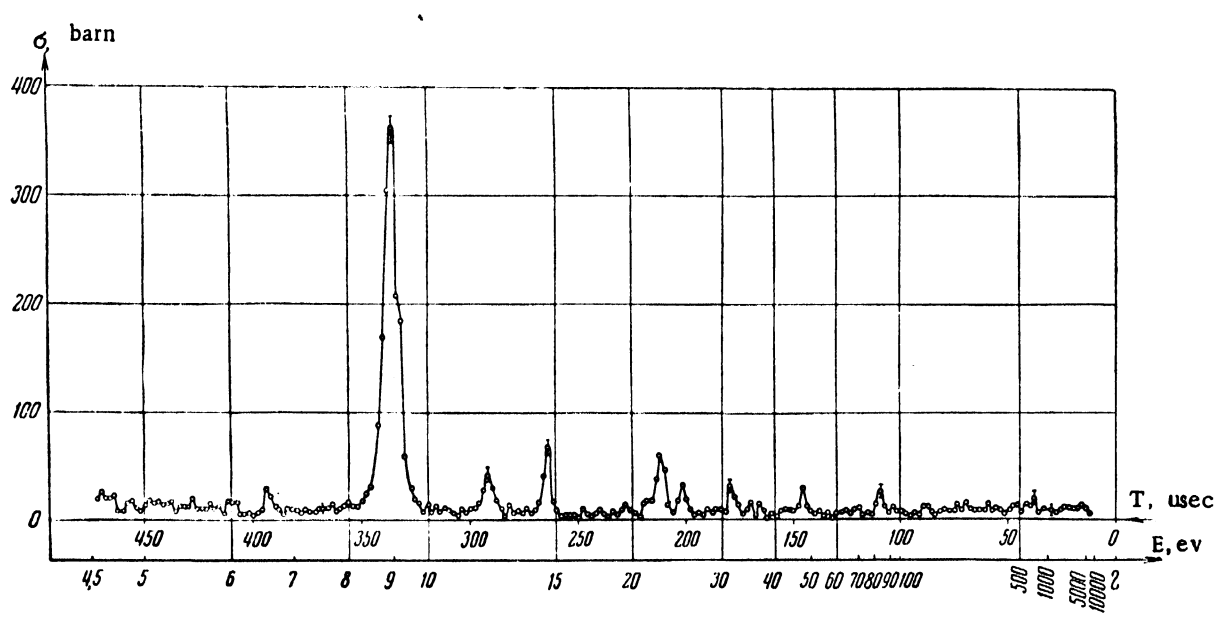

Figure 15. Total cross section of In as a function of energy with $n = 9.87 \times 10^{21}$ atoms per cm^2 and resolution 0.3 μsec/m

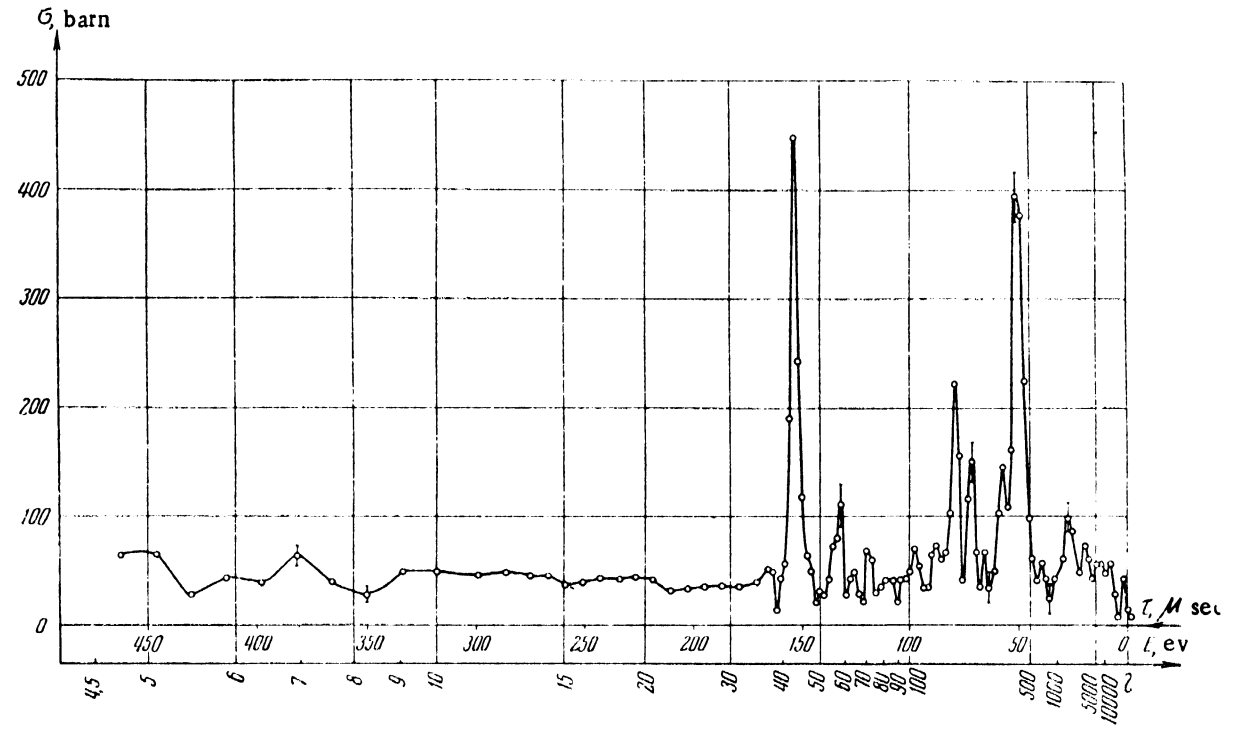

Figure 16. Total cross section of Nd as a function of energy with $n = 1.43 \times 10^{21}$ atoms per cm^2 and resolution 0.3 μsec/m

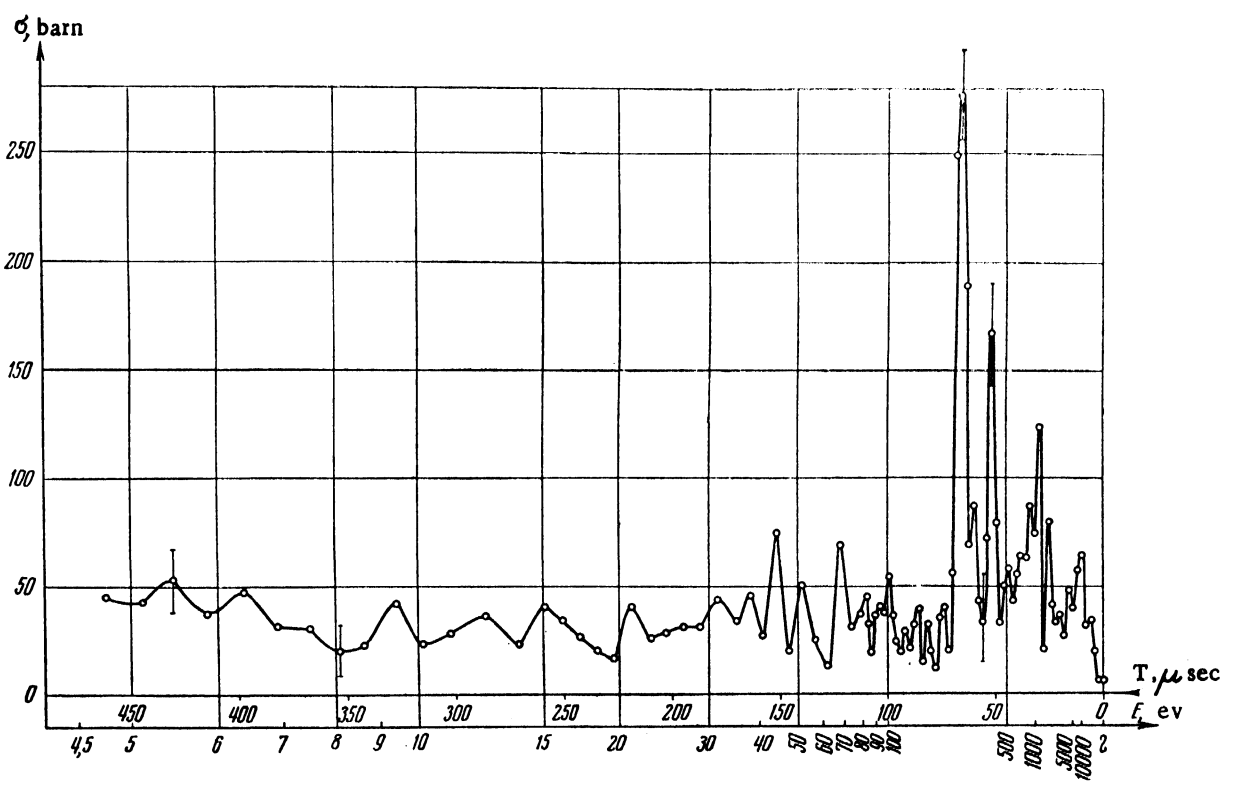

Figure 17. Total cross section of Pr^{141} as function of energy with $n = 1.31 \times 10^{21}$ atoms per cm^2 and resolution 0.3 μsec/m

Tantalum

Samples of tantalum sheets were investigated with path length 18.9 m. Two samples, with 10.0×10^{21} atoms/cm^2 (thick) and 1.39×10^{21} atoms/cm^2 (thin) were investigated with channel width 2 μsec and resolution 0.16 μsec/m; a third sample with a thickness of 2.78×10^{21} atoms/cm^2 was investigated with channel width 1 μsec and resolution 0.08 μsec/m. The results are given in Fig. 19. The first seven resonance levels 10.1, 13.6, 18.7, 20, 24, 35, 38.5 ev had been investigated earlier with smaller resolution-power[14]; the pairs 20 and 24, and also 35 and 38.5 ev not being resolved. In Fig. 19 weak levels at 30.0 and 63 ev are observed. Above 70 ev in the curve obtained with resolution 0.08 μsec/m, a series of narrowly spaced peaks is observed. Part of them coincides with the peaks obtained with a smaller resolution and doubtlessly corresponds to separate levels or groups of levels, but a more reliable interpretation of this part of the spectrum must await additional measurements with samples of different thicknesses and with a higher resolution.

Osmium

A thick sample of osmium, with $n = 9.74 \times 10^{21}$ atoms/cm^2, was investigated with resolution 0.3 μsec/m, path length 14 m and channel width 2 μsec. A thin osmium sample, containing 1.4×10^{21} atoms/cm^2, was studied with resolution power 0.16 μsec/m, path length 18.9 m, and channel width 2 μsec. Besides this, the thin sample was also investigated in the region below 7.5 ev with the curvilinear slit rotor. The statistical error in this last series was high and did not allow reliable data on the cross section to be obtained. There are indications for the existence of levels at energies 3.5, 4.5 and 5.2 ev. A strong level at 6.65 ev is confirmed by the measurements with the straight slits. Figure 20 contains the results obtained with the straight slits. By measurements with path length 14 m, two strong resonance levels at 6.67 and 8.88 ev were found. The following levels: 10.12, 12.25, 12.8, 18.8, 21.7, 28.5, 38.3, 44, 50.3, 75, 88, 110, 143, 215, 330 and 1000 ev, part of them not fully resolved, are present in both curves, with path lengths 14 and 18.9 m.

Iridium

A thick iridium sample, containing 13.53×10^{21} atoms/cm^2, was investigated with 14 m path length, channel width 2 μsec and resolving power 0.3 μsec/m. A thin sample, containing 1.67×10^{21} atoms/cm^2, was investigated with path length 18.9 m, channel width 2 μsec and resolution 0.16 μsec/m. The measurements with the thin sample were carried out with straight and with curved slits. The results obtained with the thick sample and straight slits are given in Fig. 21, those with the thin sample at low energies in Fig. 22. In the region 2.5–5 ev, the variations in the cross-sections lie within the limits of statistical error. Near 5 ev, a group of strong levels, not fully resolved, is observed.§ The peaks observed in two

§ Because of the non-uniformity of the thin sample the curve of Fig. 22 gives the right trend of the cross section with energy, but not its accurate absolute value.

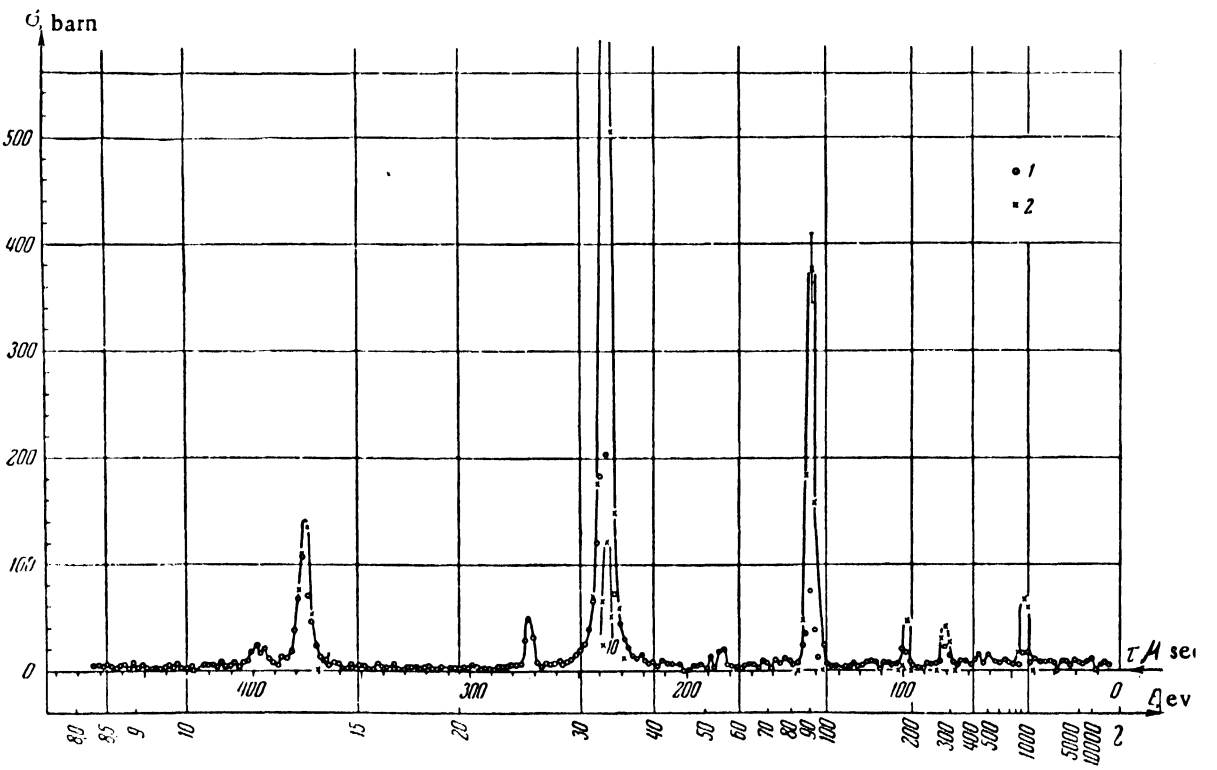

Figure 18. Total cross section of Pd as function of energy; resolution 0.18 μsec/m: (1) $n = 19.7 \times 10^{21}$ atoms per 1 cm^2, and (2) $n = 1.28 \times 10^{21}$ atoms per 1 cm^2

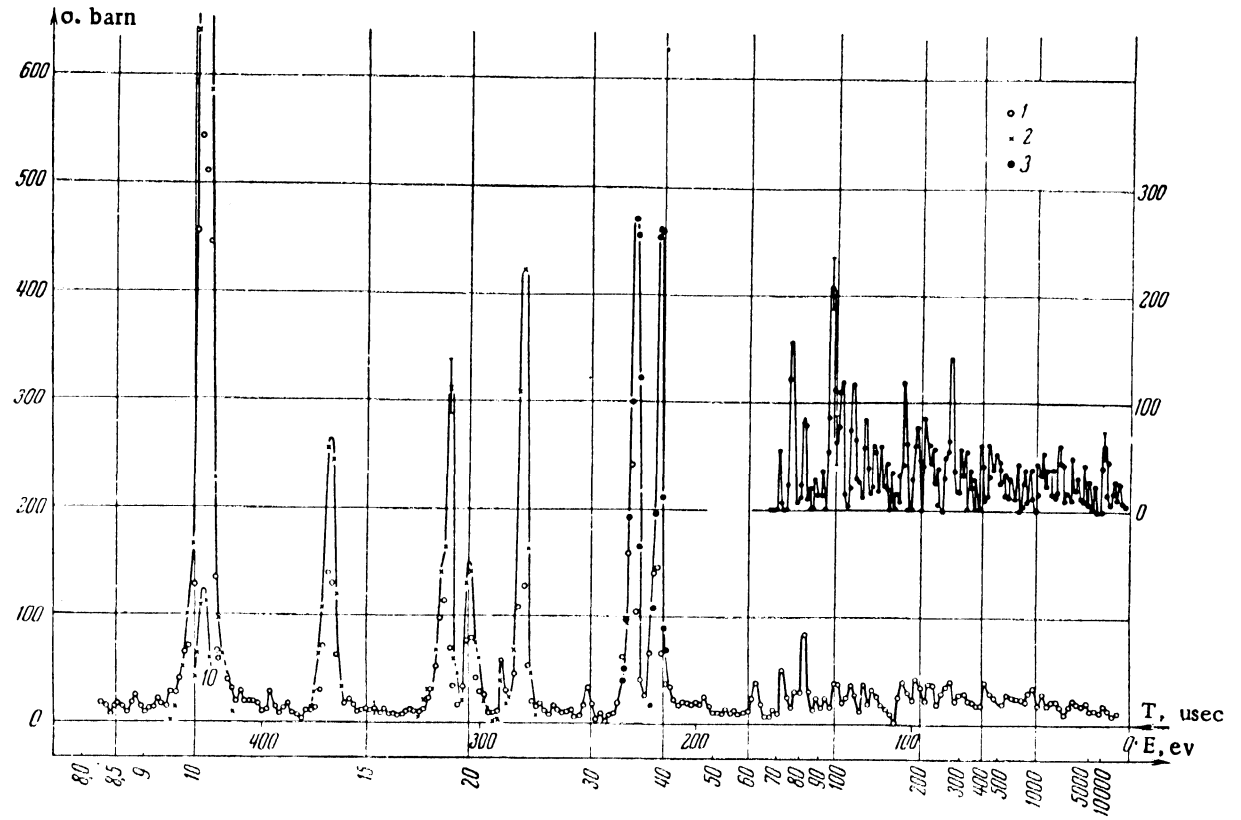

Figure 19. Total cross section of Ta^{181} as a function of energy: (1) $n = 9.98 \times 10^{21}$ atoms per cm^2 and resolution 0.18 μsec/m; (2) $n = 1.39 \times 10^{21}$ atoms per cm^2 and resolution 0.18 μsec/m; and (3) $n = 2.79 \times 10^{21}$ atoms per cm^2 and resolution 0.08 μsec/m

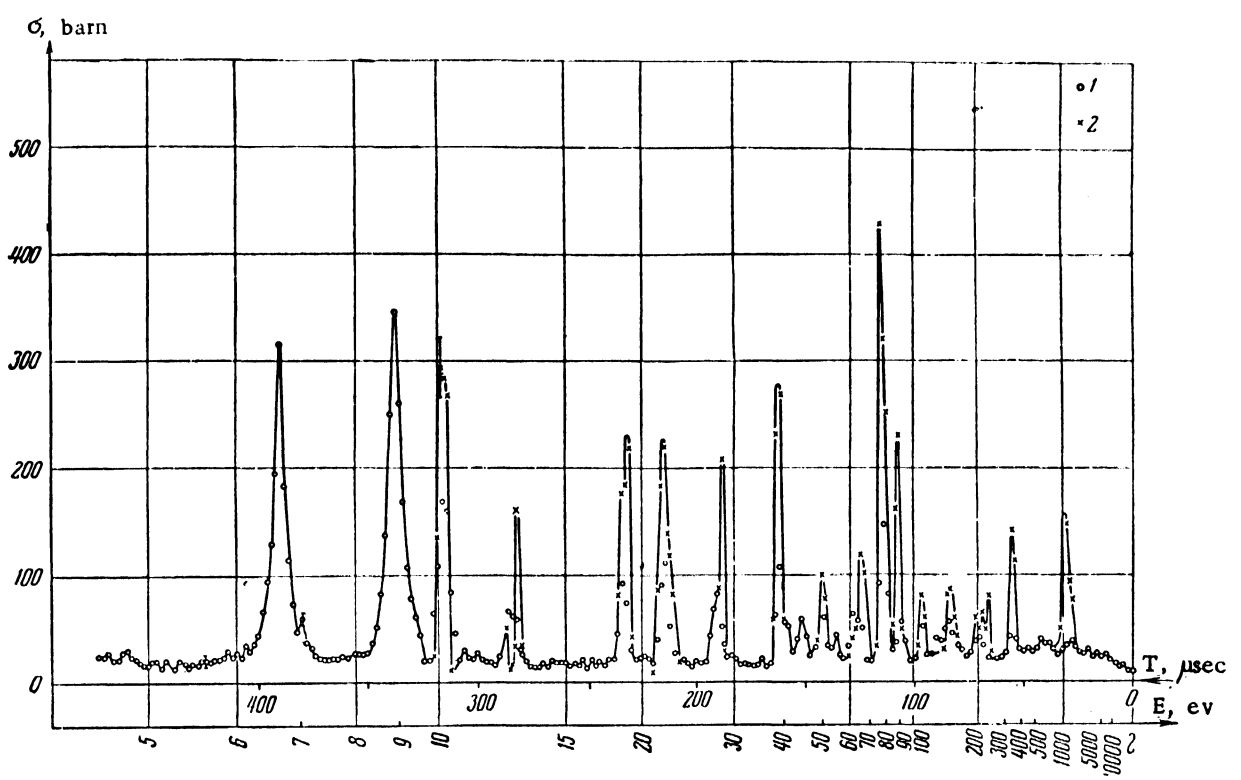

Figure 20. Total cross section of Os as a function of energy: (1) $n = 9.74 \times 10^{21}$ atoms per cm^2 and resolution 0.3 μsec/m; and (2) $n = 1.40 \times 10^{21}$ atoms per cm^2 and resolution 0.16 μsec/m

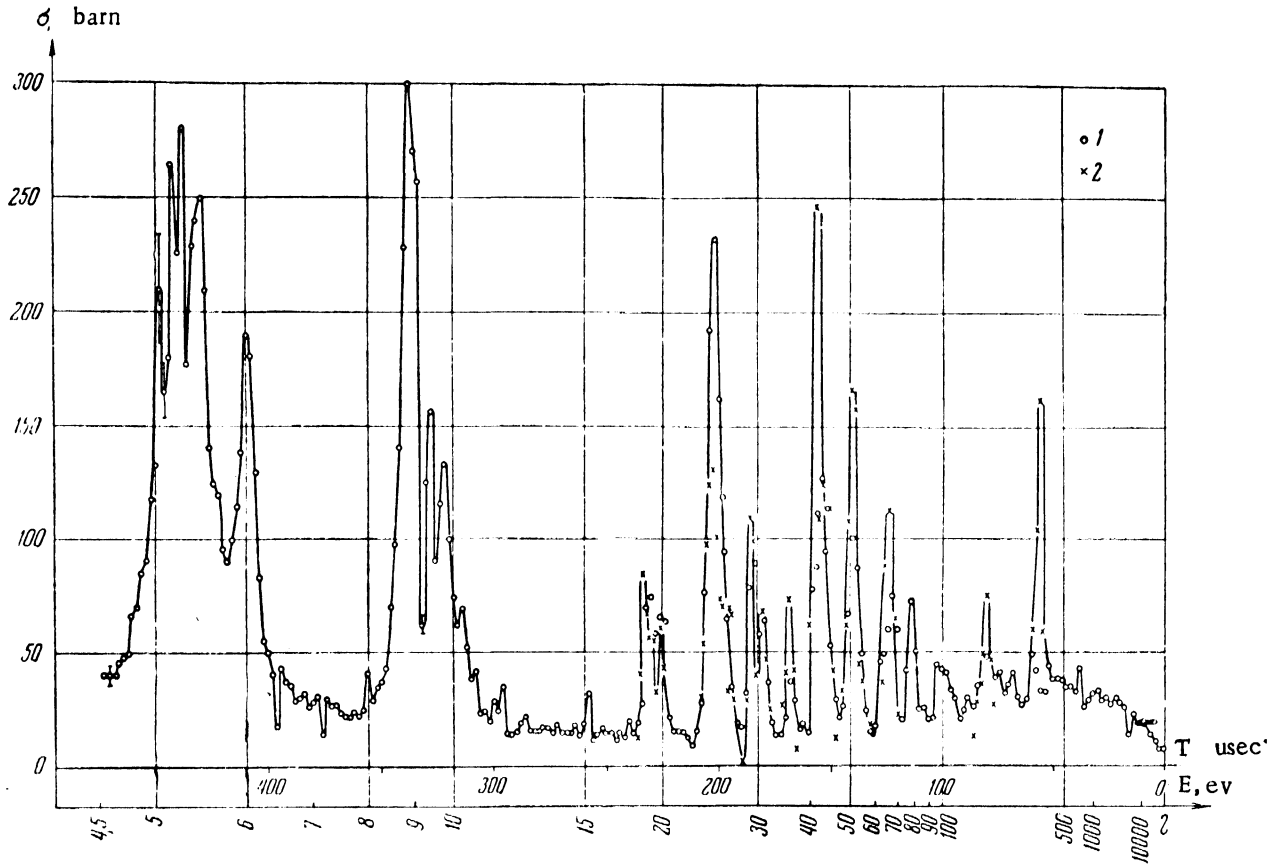

Figure 21. Total cross section of Ir as a function of energy: (1) $n = 13.53 \times 10^{21}$ atoms per cm^2 and resolution 0.3 μsec/m; and (2) $n = 1.67 \times 10^{21}$ atoms per cm^2 and resolution 0.3 μsec/m

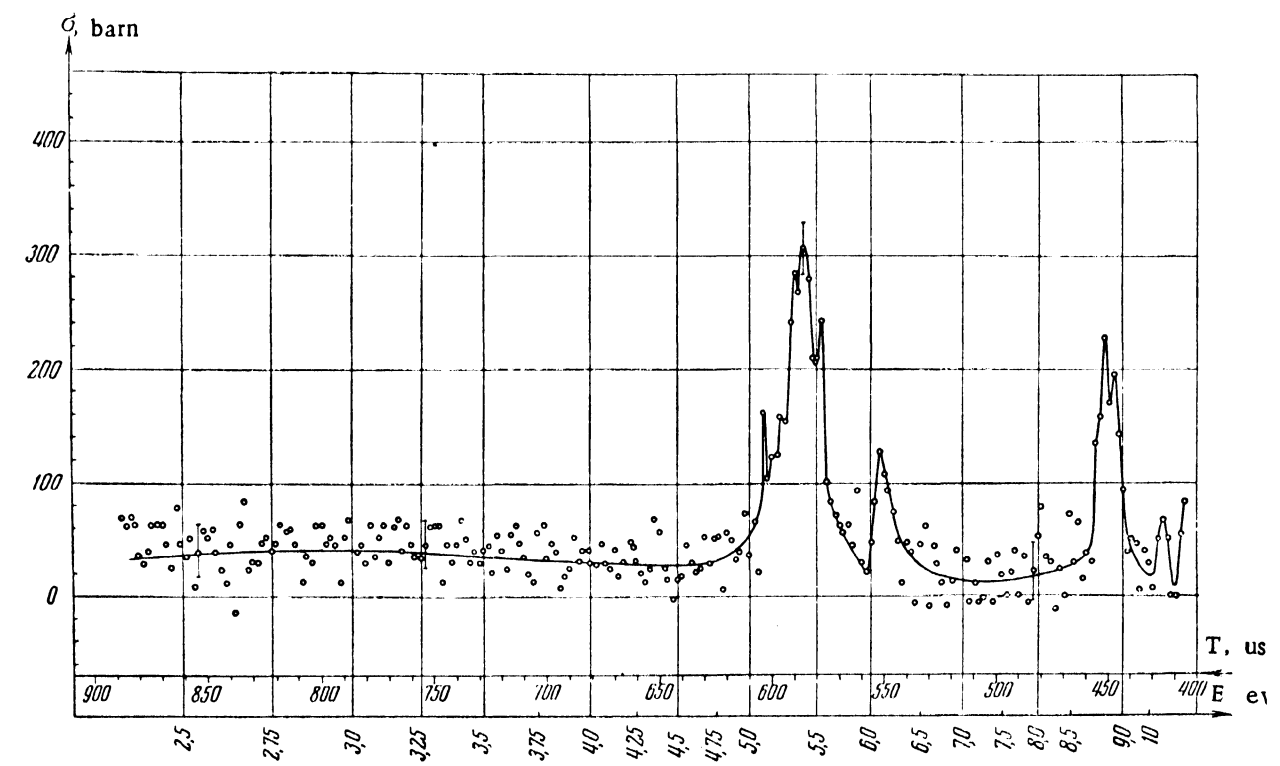

Figure 22. Total cross section of Ir as a function of energy with $n = 1.67 \times 10^{21}$ atoms per cm^2 and resolution 0.16 μsec/m

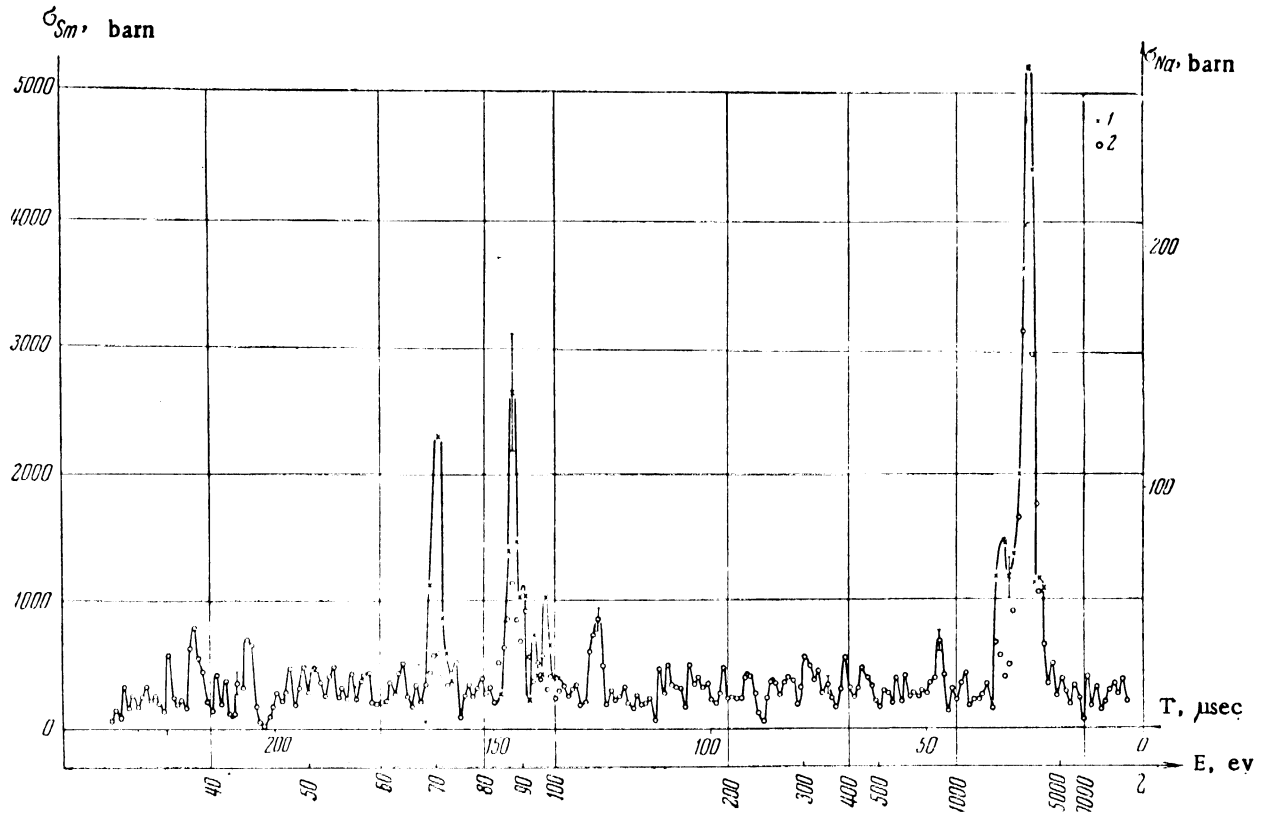

Figure 23. Total cross section of SM and Na^{23} as a function of energy at resolution 0.08 μsec/m: curve (1) 0.095×10^{21} atoms Sm per cm^2 and 1.83×10^{21} atoms Na per cm^2; curve (2) 0.35×10^{21} atoms Sm per cm^2 and 6.7×10^{21} atoms Na per cm^2

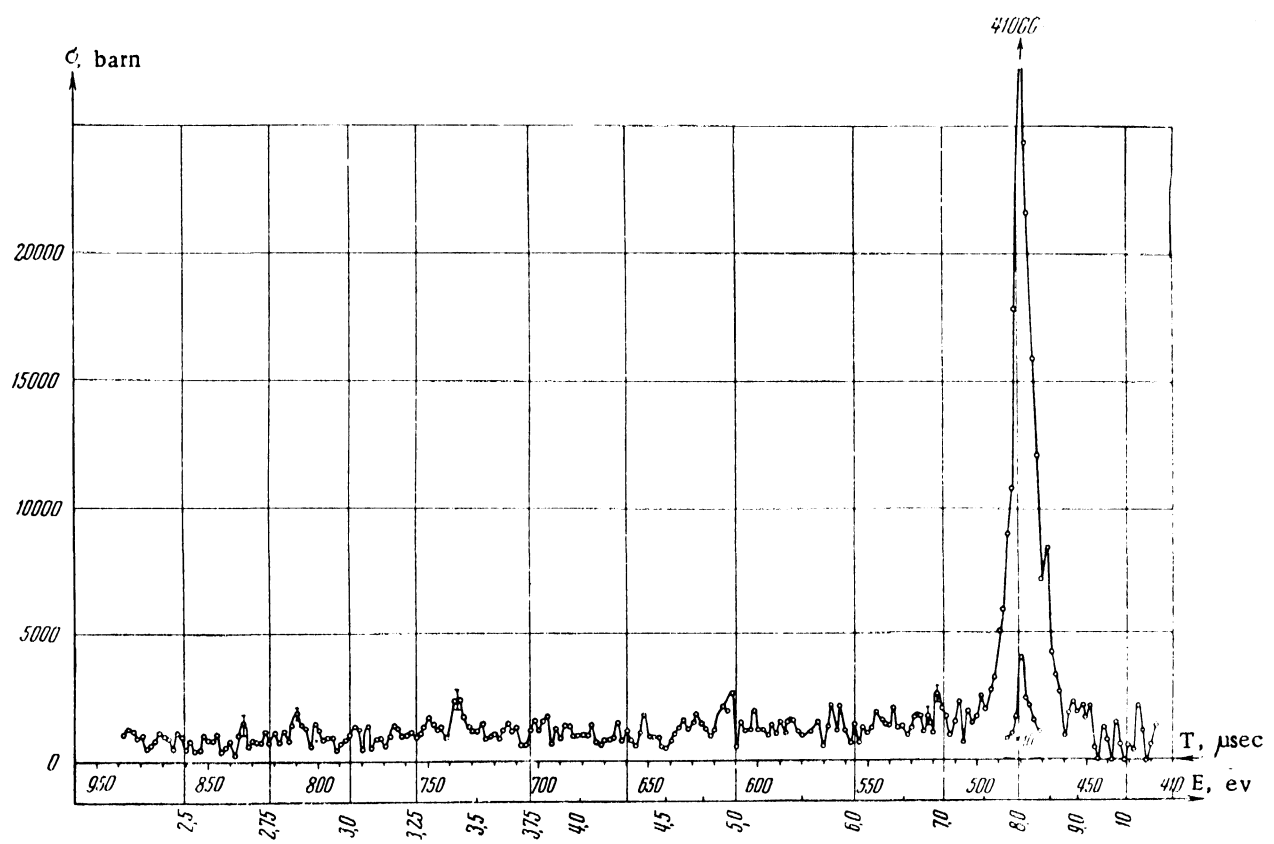

Figure 24. Total cross section Sm as a function of energy with $n = 0.095 \times 10^{21}$ and resolution 0.16 μsec/m

different measurements lie at energies 5.05, 5.19, 5.29, 5.84 and 6.03 ev. The dip between the peaks 5.19 and 5.29 ev is within the limits of statistical error. The next group of levels is located near 9 ev. The main peak lies at 9.1 ev. Two weaker levels have energies 9.4 and 9.8 ev. Further on, groups of partly resolved levels occur at 18.6, 19.8, 24.7, 29.2, 31.1, 35.7, 42 (probably double), 51, 66 and 80 ev. The shape of the cross section near 100 ev points to the presence of groups of unresolved levels. The position of these peaks is confirmed by the curve obtained with longer path and thinner sample.

Samarium

Samples containing samarium oxide with 0.095×10^{21} atoms/cm^2 (thin) and 0.35×10^{21} atoms/cm^2 (thick) were investigated. All measurements were carried out with path length 19 m. The measurements with the thick sample were carried out with resolving power 0.08 μsec/m (see Fig. 23). The thin sample was investigated in the energy region below 10 ev by means of the rotor with curved slits (Fig. 24).

The samarium sample was one that happened to be on hand, and, as is shown by the following chemical analysis, it contained only 10.2% pure samarium. The strong resonance at 3000 ev (see Fig. 23) could not be attributed to samarium as the cross-section value exceeded the quantum limit λ^2/π and was ascribed to Na. The presence of a large amount of Na in the sample was confirmed by chemical analysis: the sample contained 29.4% Na. Thus a study of neutron absorption spectra gives a semi-quantitative analysis of the sample. The mass-spectroscopic analysis of the sample showed the presence of not more than 2% neodymium with respect to samarium.

The very thin sample, investigated with the curved slits (see Fig. 24), yielded only the strongest level at 8.05 ± 0.07 ev, having a peak-cross section 41,000 barn. The known levels[14,15] at 3.41 and 4.93 ev were weakly visible. In the region 40–1000 ev, two strong levels at 70 and 86 ev, probably belonging to samarium were observed, but they can be identified accurately only in measurements with a pure sample. The level at 2970 ± 120 ev belongs to Na and is probably a complex level.

ACKNOWLEDGEMENTS

The authors want to express their appreciation to W. N. Bowina and S. S. Laptewa for doing the chemical analysis, and to G. M. Kukawadze for the performance of the mass-spectroscopical analysis.

REFERENCES

1. Fermi, E., Marshall, J. and Marshall, L., Phys. Rev., *72,* 193 (1947); Brill, T. and Lichtenberger, H. V., Phys. Rev., *72,* 585 (1947).
2. Rainwater, J. and Havens, W. W., Phys. Rev., *70,* 136, 154 (1946).
3. Rainwater, J., Havens, W. W., Wu, C. S. and Dunning, J. R., Phys. Rev. *71,* 65, 165, 174 (1947).
4. Havens, W. W. and Rainwater, J., Phys. Rev. *83,* 1123 (1951).
5. Gatti, E., Rev. Sci. Instr., *24,* 345 (1953).
6. Seidl, F. G. P., Hughes, O. J. *et al.,* Phys. Rev., *95,* 478, (1954).
7. Hellstrand, E. and Persson, R., Ark. fys., *6,* 57 (1953).
8. Bollinger, L. M., Dahlberg, D. A., Cote, R. E., Jackson, H. E. and Bull, Thomas, Bull. of A.P.S., *29,* 7, p. 8, (1954).
9. Melkonian, E., Havens, W. W. and Rainwater, J., Phys. Rev., *92,* 702, (1953).
10. Hubert, P., Vendryes, G. and Auclair, J. M., C. R., 238, 1873, (1954).
11. Nikitin, S. J., Galanina, N. D., Ignatyev, K. G., Okorokov, W. W. and Sukhoruchkin, S. I., P/646, Time-of-flight measurement of the total neutron cross-section of uranium-233, uranium-235 and plutonium-239, Session 17A, Vol. 4, these Proceedings.
12. Mostovoi, V. I., Pevzner, M. I. and Tsitovich, A. P., P/640, The Mechanical Neutron Velocity Selector, Session 15A, Vol. 4, these Proceedings.
13. Gerasimov, V. F. *et al.,* P/645, Fission and Total Cross Sections of Some Heavy Nuclides for Monochromatic Neutrons as Measured by a Mechanical Neutron Velocity Selector, Session 17A, Vol. 4, these Proceedings.
14. Neutron cross sections, (1952).
15. Sailor, V. L., Landon, H. H. and Foote, H. L., Phys. Rev., *96,* 1014, (1954).
16. Stephenson, R., Introduction to Nuclear Engineering, p. 59, McGraw-Hill Book Co., New York, (1954).

Neutron Spectrometers Based on Pulsed Sources

By E. R. Wiblin,* UK

This paper is primarily intended as a review of UK work in the field of neutron spectrometry by pulsed source time-of-flight techniques. It is, therefore, complementary to the papers[1] dealing with other similar neutron spectrometers and also to those describing instruments used in conjunction with piles.[2] The work is almost entirely confined to the intermediate, or resonance, region.

Several groups had, by 1949, made such measurements using some form of pulsed particle accelerator and a neutron emitting particle reaction. The intensities available and the measurement techniques were, however, inadequate at this time to allow good resolution work to be done at neutron energies higher than a few electron volts. There existed an operational need (quite apart from purely nuclear physics objectives) for data concerning the resonance region: very roughly from 1 ev to 100 kev. In the UK, the electron linear accelerator offered the possibility of a reliable, intense and cheap source of photoneutrons.

UK DEVELOPMENTS FROM 1949–1952

The developments outlined fall into a fairly logical pattern, although it must be admitted at once that this pattern has only become really clear as the work has progressed.

It was, initially, essential to gain experience in the technique of time-of-flight measurements of energy, as well as in counting methods suitable for use in the presence of a large gamma-ray "flash" at zero time. During this stage it was possible, incidentally, to make some total cross-section measurements rather better than those published at the time.

The neutron source for this series of experiments was a block of beryllium metal bombarded by bremsstrahlung from the original A.E.R.E. 3.2 Mev electron accelerator. An output of approximately 10^9 neutrons per sec, self-moderated in the target and emitted isotropically, was obtained. Proportional counters with enriched BF_3 gas were used and reasonable counting rates in the timing channels were obtained with a neutron flight path of about 10 m. The initial electron pulses and the timing channels were of 2 μsec duration and the resolution at energies above about 50 ev was the best in use at the time, as indicated in Table I. It was good enough for qualitative cross-section work and for evaluation of $\sigma_0\Gamma^2$ (the "strength" of a resonance) by area methods in cases where resonances were well separated.

Measurements made during this period have been reported[3,4] and the equipment fully described.[5]

The source intensity was inadequate for good fission cross-section work,[6] for the measurement of scattered neutrons and for the measurement of the yields of capture gamma rays from samples intercepting the neutrons. The lessons learned were plain: more neutrons were needed, narrower pulses and channels were desirable, and facilities for several parallel experiments must be built up if there was to be any economy in the use of the neutrons. Most important, electronic reliability is at a premium in this type of experiment, in which relatively large numbers of units are involved.

UK DEVELOPMENTS FROM 1952 TO 1955

The need for a greater neutron source strength was realised at an early stage and while experience was being gained with the 3.2 Mev accelerator, a new machine was designed[7] to give 15 Mev electrons and so to take advantage of high (γ,n) yields in heavy elements; in particular, in uranium. The eventual neutron source strength (about 10^{11} neutrons per sec—an increase of $\sim$ 100 over the earlier machine) was limited, in effect, only by the sole available source of rf power for the accelerator.

At the same time a new set of 100 timing channels was made[8] which, after an initial "work-up" period, have been most successful. Their design for use as either one set of 100 or two independent sets of 50 has been most useful in conjunction with the setting up of several flight paths and detector units.

It is profitable at this point to indicate how the use

Table I. The Energy Resolution of Some Neutron Spectrometers in 1949

	Resolution $\Delta E/E$ for comparable counting rates		
Neutron energy (ev)	*Harwell 3 Mev linear accelerator spectrometer*	*Columbia University cyclotron spectrometer*	*Argonne Lab. mechanical chopper spectrometer*
1	1/9	1/16	1/11
10	1/7.5	1/8	1/6
100	1/5	1/3	1/2.5
1000	1/2.5	1/1	>1

* A.E.R.E., Harwell. This paper is based on work carried out at Harwell by members of the Nuclear Physics Division with co-operation from the General Physics, Electronics, Metallurgy, Chemistry and Engineering Divisions, and from the Mullard Research Laboratory of Philips Electrical Ltd.

of the linear accelerator pulsed source spectrometer differs from other systems. One feature is that the full electron beam is extracted from the machine, allowing the target to be placed to suit the experiment, or experiments, in hand. Thus, for example, several different time-of-flight equipments may "look" at the same target from different directions —indicated, for the Harwell accelerator, in Fig. 1. It is quite easy to foresee a dozen such independent experiments proceeding; the limitation is commonly in electronics and availability of personnel!

Alternatively, the electron beam may be led down a long drift tube to a target placed inside a large immovable assembly such as, for example, a section of pile lattice. Time-of-flight equipment may then be used to examine neutron spectra in the assembly and several such measurements have been carried out successfully by this method.[9]

A most important feature has been the possibility of using gamma-sensitive detectors for capture gamma-ray studies or, indirectly, as neutron detectors.[10] The intensity of the gamma background, between pulses, due to the machine is effectively zero in spite of the intense initial "flash", in contrast to cyclotron and pile-beam spectrometers. Measurements of capture gamma-ray yields, in particular, are, therefore, possible in conditions of high resolution and the method has proved very powerful for, for example, surveying and locating the levels of a fresh element.[11,12] The experiment is "positive", as distinct from a transmission measurement, and good statistics are obtained in the resonances in a relatively short time. A typical yield curve is shown in Fig. 1.

The positive experiment can yield important information in the analysis of level parameters since it allows good measurements to be made with really thin ($n\sigma_0 \ll 1$) samples to be used, in contrast to transmission work. It is unfortunately not always easy to use the method since a knowledge of the variation in detector efficiency and capture gamma-ray spectra is necessary.[13,14]

Two disadvantages of the photoneutron pulsed source system may be noted. Firstly, the intense gamma flash presents a severe electronic problem in avoiding circuit paralysis at the shortest delays. This sets an upper limit to the energy coverage, but is compensated by the characteristics of a spectrometer used with a moderated source of neutrons. The channel counting rate can be shown to be proportional to $\sqrt{E}$ for the case of a detector of constant efficiency, which is closely approximated, at least up to 50 kev, by the boron scintillation detector of Rae and Bowey.[10] Thus, for a given source, higher energy measurements can be made with longer flight paths (and so with a reduction in gamma flash paralysis), while at the same time the maximum energy (or minimum time) limitation is less severe.

Secondly, relative to "chopper" spectrometers, the size of sample needed with present detectors is much larger and hence studies are, in general, restricted to materials of which at least gram quantities are available.

On the other hand very high resolution work is possible to quite high neutron energies and the information is obtained relatively quickly.

The most recent addition to the Harwell spectrometer is an electron injection modulator giving $\frac{1}{5}$ μsec electron pulses, and a set of "gates" of $\frac{1}{5}$ μsec channel width. These will extend the useful range of the spectrometer up to about 100 kev neutron energy for qualitative cross-section studies and allow resonance analysis to a few kev instead of a few 100 ev.

THE PRESENT SPECTROMETER

The plan layout, not to scale, is shown in Fig. 2, to which reference may be made in reading the following.

Source and Gates

The linear accelerator provides a pulsed source of electrons of about 14 Mev energy at a pulsed current of 25 ma. These are usually 400 pulses per second. The accelerator is a two-stage feedback machine fed by rf energy at a wavelength of 10 cm and a peak power level of 2 Mw. The electrons directly bombard an air-cooled, aluminium-clad, natural uranium target, and the neutrons emitted are moderated in paraffin wax to give a spectrum, which, from 1 ev upwards, approximates to a "slowing down" law.[2]

Accelerator and target are enclosed in a thick concrete shelter and the target may be viewed through ports from any of six detector positions situated at distances varying from 3 m to 55 m. Those paths longer than 7 m are contained in evacuated tubes to avoid air scattering, and individual collimation is provided.

For the investigation of lattice spectra as described above[9] the detectors in the "straight-ahead" flight paths (Fig. 2) are removed and an extension drift tube is used to bring the electron beam to a special target placed in the assembly, which is erected in this area outside the accelerator shelter. A special port and flight path (not shown in Fig. 2) are placed to view the assembly with a detector situated near the 11½ m station.

There are three sets of timing channels. One set of 100 can be used at either 2 μsec or 10 μsec duration and in either one group of 100 or two groups of 50 independently. This set is used for most low and medium energies in the region covered.

A second set of 40 gates is used exclusively for thermal work in connection with spectrum measurements and operates at durations between 100 and 400 μsec.

Both these equipments are conventional "repetitive unit" systems.

The third set of gates is for high energy work only and contains 70 channels of duration $\frac{1}{5}$ μsec. This equipment is of considerable technical interest and is due to ideas of Goulding, Kandiah, and Chambers.

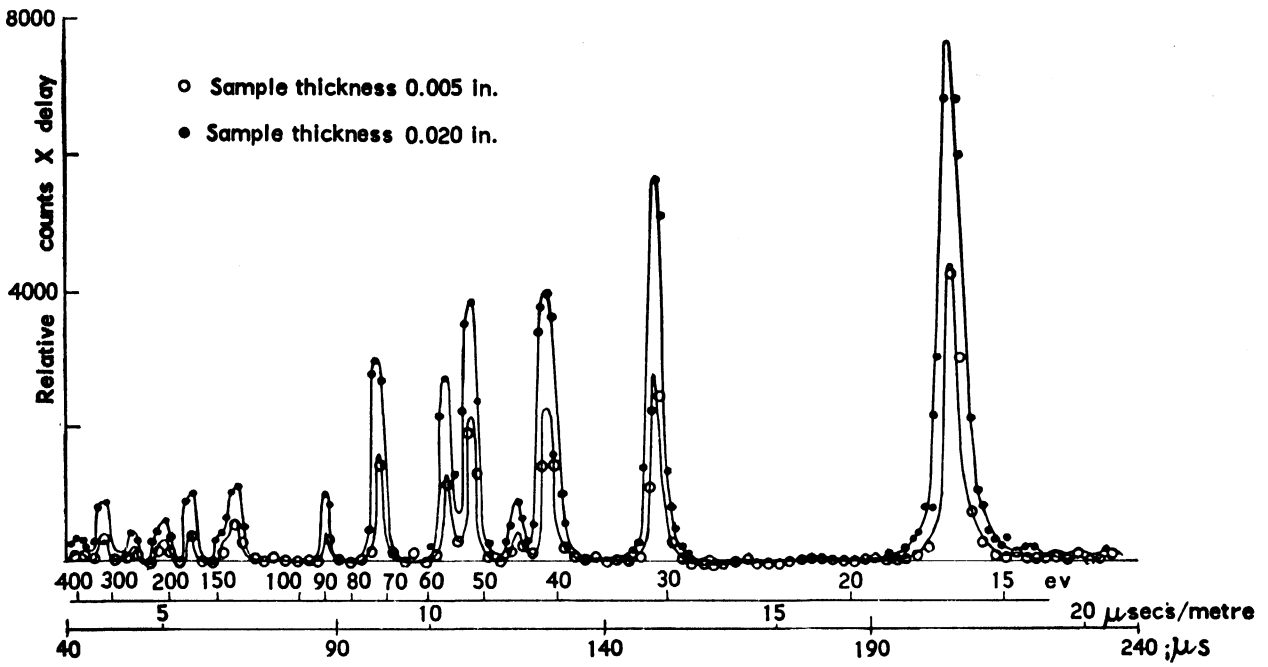

Figure 1. Yield curves of capture gamma rays for silver: circles, sample thickness 0.005 in., crosses, sample thickness 0.020 in.

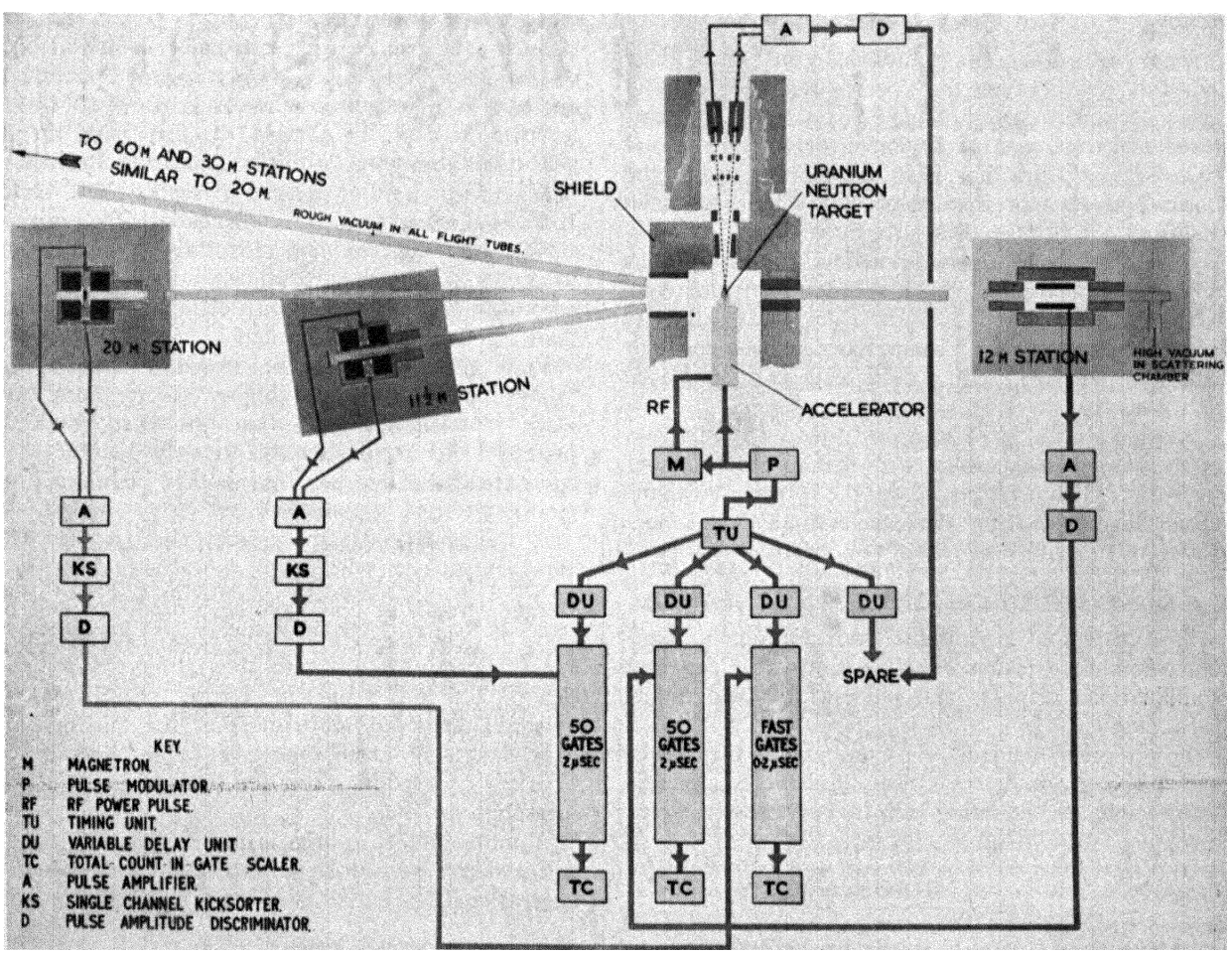

Figure 2. 15 Mev linear accelerator neutron spectrometer: (*M*) magnetron; (*P*) pulse modulator; (*RF*) rf power pulse; (*TU*) timing unit; (*DU*) variable delay unit; (*TC*) total-count-in-gate scaler; (*A*) pulse amplifier; (*KS*) single channel kicksorter; and (*D*) pulse amplitude discriminator

It consists of two units, one a conventional matrix arrangement of coincidence and count-registering channels which is, in effect, a series of 20 μsec gates. It is fed from a "time-expander" unit which changes the time-scale by a factor of 100 to yield an effective gate width of 0.2 μsec.

Signals from counters are circulated through a storage delay (20 μsec), preceded by a reference pulse derived from the accelerator trigger circuits (at a delay appropriate to the energy region to be examined). On emerging from the delay, the reference pulses are delayed by a further time ($\frac{1}{100}$ of the store delay; i.e., 0.2 μsec), while the signal pulses by-pass the extra delay. Circulation continues until the extra-delayed reference pulses coincide with the earliest (highest energy) signal pulses. At coincidence, a signal is passed on to the matrix analyser and the original circulating signal pulse is cancelled. Circulation continues until the next coincidence is achieved, and an output signal (due to the next lower energy neutron) is passed on to the matrix. This process continues until the end of a $2\frac{1}{4}$ msec cycle, (slightly less than the pulsed source cycle of 2.5 msec) when the system is cleared and recommences operation.

Detector Units

These are shown diagrammatically in Fig. 2. Four types of measurement have been attempted: of total cross section, of capture gamma-ray yield, of scattered neutrons, and of fission cross sections. Total cross-section work has been carried out using the boron-NaI detector at stations typified by that shown at 20 m. Capture studies have been carried out exclusively at the $11\frac{1}{2}$ m station and scattering work at the 12 m station. (This latter detector, consisting of an annular assembly of $B^{10}F_3$ counters shielded from the direct neutron beam, has also been used for transmission work, with a thick lead scatterer placed at its centre.)

Fission studies have been devoted to a comparison of the fission cross section with that of boron—using ionisation chambers placed in the (twin) straight-ahead direction from the accelerator, at distances between 3 m and 7 m.[6,14]

A SURVEY OF TYPICAL OPERATING CONDITIONS

It is profitable to examine the variation in counting rate and in resolution with energy for different combinations of gate- and pulse-widths and flight-path length.

For a given neutron yield rate from the source and for a given detector, the fundamental expression for channel counting rate is, very closely, given by

$$n = K \frac{N(\Delta t)^2 \sqrt{E}}{r^3}$$

where K is a constant, N is the peak neutron output rate of the machine, Δt is the gate width (assumed equal to pulse width), E is the neutron energy, r is the flight distance, providing that the detector efficiency is independent of energy.

Similarly, the resolution may be expressed in terms of the time and distance uncertainties

$$\frac{\Delta E}{E} = 2\left[\frac{2\Delta t}{t} + \frac{\Delta r}{r}\right]$$

where ΔE is the energy uncertainty at energy E corresponding to a time of flight t over a distance r, and $2\Delta t$ and Δr are, respectively, the uncertainties in the measurement of t and r.

In Fig. 3, the resolution referred to is half this quantity $\Delta E/E$, representing an approximation to the width at half height of the true resolution function.

If we fix N (for a given source) and Δr (for given target and detector) and set criteria for upper and lower limits to n depending on possible working counting rate† it is easy to construct a family of graphs for count rate and resolution. This has been carried out for the cases of $\Delta t = 0.2$ μsec or $\Delta t = 2$ μsec and for path lengths of 12, 21, 31 and 55 m.

The information is presented in condensed form in Fig. 3, which shows the energy coverage for resolutions of 1% or of 10% consistent with $1.0 < n < 20$ and also $0.1 < n < 1.0$.

Such a diagram can be extremely useful in planning a closely interlinked programme of experiments and also to indicate, for example, how great a benefit in coverage could be obtained by increasing the detector efficiency by a factor of as little as 3 or 4.

As things stand at present it is possible to obtain 10% resolution (which is adequate for descriptive cross-section curves and for "area" analysis of isolated resonances up to a few hundred ev) up to several hundred kilovolts with counting rates greater than 1 per minute in a channel.

For "area" analysis at greater energies, for "shape" analysis, or for higher energy descriptive work it is necessary to use the best resolution (~1%) and at present this is only possible, over any extended range, with rather low counting rates.

DEVELOPMENTS FOR THE FUTURE

One clear necessity is for a more efficient detector. Larger crystals of NaI have been used, but it is not easy to achieve an adequately low background at present, partly, at any rate, due to the trace quantities of active K^{40} present. Larger scintillators are essential, however, since most of the "inefficiency" of the present arrangement is purely geometrical. Work is proceeding along the lines of loaded liquid scintillators.

A more intense source is more expensive than a better detector—but is quite straight-forward engineering and has other uses. An accelerator is being

† The upper limit depends on the rate of arrival of signal pulses the gates can accept, and the lower limit on the counter background. "Overlap of pulses[2] is not considered since it is assumed that the pulse repetition cycle is chosen to avoid it.

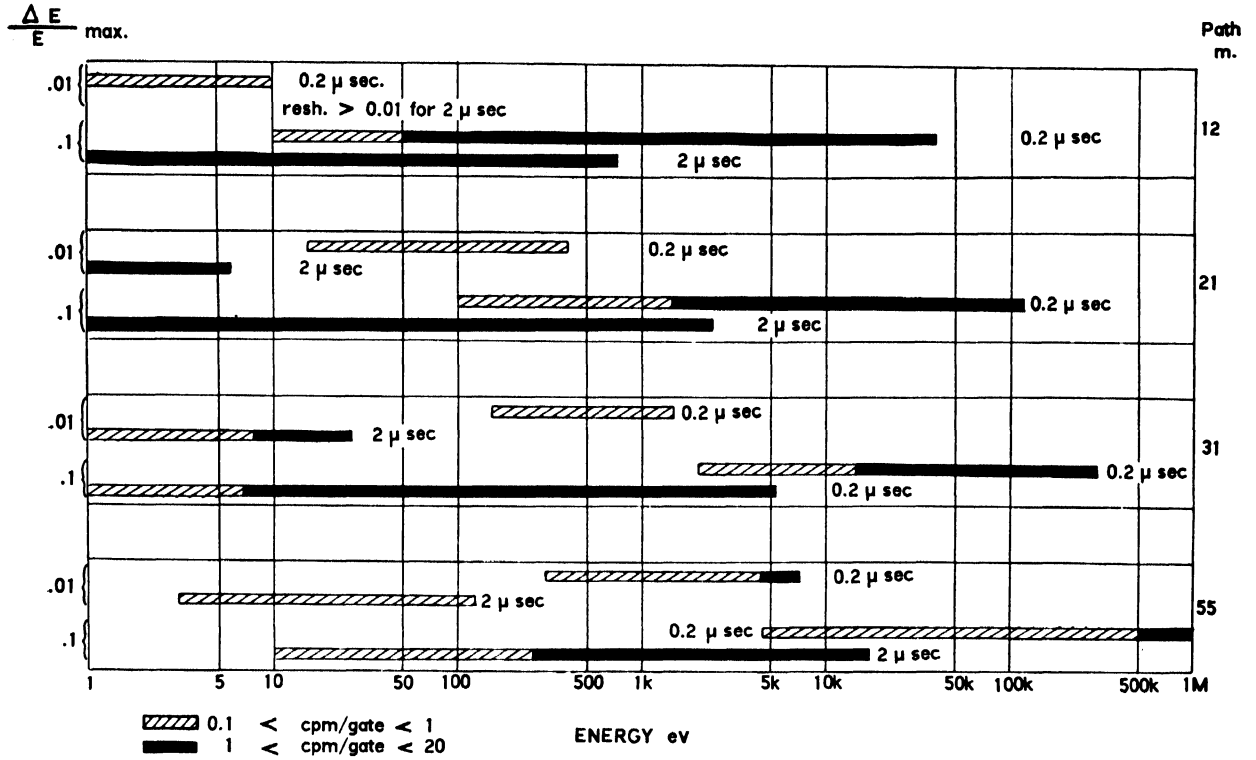

Figure 3. Experimental operation—15 Mev linear accelerator spectrometer

constructed to give a peak current of 1 ampere of 25 Mev electrons. This, it is estimated, will increase the source strength by about 200 times. If an increase in detector efficiency of a factor of 5 could be achieved, the effective overall gain of 1000 would allow, for the same counting rates, paths 10 times as long and resolutions 10 times improved. More profitably, in some cases, an increase of 5 times in path length would yield count rates increased by a factor of about 8.

As a third possibility, the conditions of Fig. 3 could be applied for very much smaller samples.

In order to accommodate thermal spectrum measurements (which imply low pulse repetition frequencies to avoid "overlap" of pulses) simultaneously with higher energy work (needing high repetition rates to give high count rates) it is proposed that a new electron output drift tube arrangement be made. In this a pulsed magnetic deflector is used to route 1 pulse in every 8 (for example) to the assembly target, leaving the remainder bombarding the main target. The effective repetition rates are then 50 and 350 respectively for a 400 pps total.

REFERENCES

1. Havens, W. W., Jr., P/574, *Pulsed Accelerator Slow Neutron Velocity Selectors,* Volume 4, Session 15A, these Proceedings.
2. Egelstaff, P. A., P/767, *A Review of Pile Neutron Spectrometer Work at Harwell,* Volume 4, Session 15A, these Proceedings.
   Hughes, D. J., P/576, *Neutron Velocity Selectors at Reactors,* Volume 4, Session 15A, these Proceedings.
3. Merrison, A. W. and Wiblin, E. R., *The Total Cross-Sections of Cobalt, Silver, Iodine, Aluminum, Nickel and Gallium between 1ev and 5 Kev.* Proc. Roy. Soc. A. *215,* 278 (1952).
4. Hodgson, E. R., Gallagher, J. F. and Bowey, E. M., *Neutron Total Cross-Sections.* Proc. Phys. Soc. A. LXV, 992 (1952).
5. Goulding, F. S., Hammerton, J. C., Kelliher, M. G., Merrison, A. W. and Wiblin, E. R., *The Development of a Neutron Spectrometer for the Intermediate Energies.* Proc. I.E.E. *101* Pt 1, 248 (1954).
6. Price, B. T. and Raffle, J. F., P/422, *Slow Neutron Cross-Sections of the Plutonium Isotopes,* Volume 14, Session 17A, these Proceedings.
7. Bareford, C. F. and Kelliher, M. G., *The 15 Mev Linear Electron Accelerator for Harwell,* Philips Tech. Rev. *15* No. 1, 1 (1953).
8. Trier, P. E., Hammerton, J. C. and Wolfendale, E., *A Time-of-Flight Neutron Spectrometer,* Philips Tech. Rev. *15 No. 2,* 325 (1954).
9. Unpublished work at A.E.R.E. by Sykes and Poole.
10. Rae, E. R. and Bowey, E. M., *A Scintillation Detector for Neutrons of Intermediate Energy,* Proc. Phys. Soc. A. LXVI. 1073 (1953).
11. Rae, E. R., *Gamma-Ray Yields from the Resonant Capture of Slow Neutrons,* Proc. of Glasgow Conf. on Nuclear Physics 1954.
12. Meservey, E., *Neutron Capture Cross-Sections by Capture Gamma Ray Counting,* Phys. Rev. *96,* 1006 (1954).
13. Rae, E. R., P/426, *A Note on the Analysis of Neutron Resonance Data. Including examples taken from reactor materials,* Volume 4, Session 15A, these Proceedings.
14. Lynn, J. E. and Pattenden, N. J., P/423, *Slow Neutron Cross-Sections of Uranium Isotopes,* Volume 4, Session 17A, these Proceedings.

Time-of-Flight Techniques Applied to Fast Neutron Measurements

By Lawrence Cranberg,* USA

Although velocity spectrometer technique is now well established for slow neutrons, the extension of this technique to higher energies is just developing. One reason for the delay is primarily technical. For fast neutrons, that is, the range 0.1 to 15 Mev, and path lengths of the order of magnitude of meters, the flight times to be measured are in the range 10^{-9} to 10^{-7} seconds. This is a range of times which, because of developments in photomultipliers, scintillators and amplifiers, has become accessible to measurement only in the last few years. It is significant also that in the fast neutron region monoenergetic neutrons are available from Van de Graaff, Cockcroft-Walton, and cyclotron accelerators. Consequently, in contrast to the situation for slow neutrons, measurements of total, elastic, and reaction cross sections may be made with relatively simple means because a velocity analysis of the neutron source is not required. Recently, however, interest has focused on the study of fast neutron spectra, particularly those resulting from inelastic neutron scattering, and it is primarily because of this problem that time-of-flight techniques are being developed concurrently at several laboratories. Interest in these spectra is motivated both by practical interest in reactor design and by the bearing of the results on nuclear theory.

A second application of the technique is to the study of neutron spectra resulting from reactions of charged particles with nuclei. The technique for studying these two sorts of problems is the same in principle. In practice the study of inelastic scattering is more difficult because the neutron flux to be detected is generally smaller, and because the problem of shielding the detector from the primary flux is a serious one. In what follows it will be assumed that inelastic neutron scattering is the measurement of primary interest.

If the neutron detector is also sensitive to gamma-rays, as is usually the case, a useful by-product of the application of time-of-flight technique to neutron spectroscopy is information on the gamma-rays. In particular, when only one level is strongly excited in the residual nucleus, the angular distribution for the gamma-ray accompanying the de-excitation of that level is obtained.

It will appear in what follows that the method also offers some practical advantages over present methods for measurement of the angular distribution of elastic scattering.

For fast-neutron spectra the photographic emulsion has thus far been the preferred method.[1] The slowness of this method, however, provides strong incentive for the development of electronic methods. Although only a few papers have appeared,[2,3,4] in which time-of-flight technique has been applied with positive results, progress is being made rapidly, and the present state of the technique will be illustrated primarily with data which has been hitherto unpublished.

In what follows under "General Considerations" will be given a discussion of the significant parameters of an experiment for measuring inelastic scattering of fast neutrons by time-of-flight. This is followed by a survey of methods of determining initial time, terminal time (detectors), and elapsed time. Details of the system in use at Los Alamos will then be given, together with illustrative results on inelastic scattering. Finally, the limitations of present techniques and desirable improvements will be discussed.

GENERAL CONSIDERATIONS

Without considering in detail all the design parameters of a time-of-flight system for measuring fast-neutron inelastic scattering, it is of interest to discuss a few which are of critical importance for the practicability and quality of the measurements. These are conveniently grouped under the heading of yield and resolution, although most of the design parameters affect both, generally in reciprocal ways.

Resolution

The relationship between the flight time and energy of a neutron, for a flight path D, measured in meters, is:

$$t = \frac{72.3\ D}{\sqrt{E}} \qquad (1)$$

where t is measured in millimicroseconds, hereafter abbreviated as mμsec, and E in Mev. Table I gives the energy spread for a flight path of one meter,

* Los Alamos Scientific Laboratory. Including instruments used at Brookhaven National Laboratory; Cornell University; Los Alamos Scientific Laboratory; and University of Michigan.

Table I

	E (Mev)				
Δt (mμsec)	*0.1*	*0.3*	*1.0*	*3.0*	*10.0*
1	0.00087	0.0045	0.028	0.14	0.87
2	0.0017	0.009	0.056	0.29	1.74
4	0.0035	0.018	0.11	0.58	3.5

corresponding to the given energy and given uncertainty in time Δt.

From Table I, it is clear that to obtain resolution at high energies the best time resolution is required. At the lower energies it turns out that time resolution is not important. In fact, the important quantity affecting the resolution at lower energies is the homogeneity in energy of the primary neutron flux. Thus, if the spread in energy of the primary neutron beam is ΔE, then the spread in energy of any neutron group excited by inelastic scattering will also be ΔE, if the yield curve for exciting the particular level does not vary appreciably over the interval. Thus the conditions for optimum resolution for high-energy groups (corresponding to the excitation of levels just above the ground state of the residual nucleus) are different from those for low-energy groups (high-lying levels).

For the lower end of the fast-neutron spectrum a thin target is required, and a short neutron flight path may be used, whereas for the higher end of the spectrum conditions are preferably reversed. These adjustments can, of course, be made. One must consider, however, that fast-neutron inelastic scattering is a virtually unexplored subject, experimentally. If one is to make measurements, at least in a survey, over the variables of primary neutron energy, scattering nuclide, and scattering angle, it is clear that a compromise is essential in which best accuracy and precision in particular situations are sacrificed for versatility. A compromise which has been found useful for many cases is described under the section "Los Alamos System."

Yield

The single most important factor determining the yield is the flux of primary, monoenergetic neutrons which is available. The method of determining the most suitable neutron source is as follows. From considerations of yield and monoenergetic purity, the source of primary neutrons is preferably one of the following three reactions, enumerated in order of ascending neutron energy for given energy of the bombarding particles: $T(p,n)He^3$, $D(D,n)He^3$, $T(D,n)He^4$. The yields of these reactions are well known.[5] It is necessary, however, for present purposes, to consider the yields of these reactions in relation to the energy spread associated with a given yield. This gives essentially a figure-of-merit for the source which takes into account the resolution attainable, where the spread in primary neutron energy is the factor limiting the resolution.

For concreteness, let it be assumed that the accelerator is a Van de Graaff machine, that a gas target is used with a window so thin and uniform that the straggling in energy of the accelerated particles striking the gas may be neglected. Then the spread in energy of the primary neutrons striking the scatterer is due only to the target thickness and the angle subtended by the scatterer at the target. Denoting the effect of target thickness by ΔE_t and that due to angle by ΔE_a, the following table (Table II) summarizes the yields and the energy spreads for each of the reactions listed. The target conditions assumed are: length, 3 cm; pressure, 60 cm of Hg at 0°C. The angle subtended by the scatterer at the target is assumed to be 15 degrees. The yield figure given is that for zero degrees.

From this table the following conclusions are of interest. Above 2 Mev neutron energy, the (p,n) reaction affords roughly constant yield for a given target thickness. By the criterion of yield per unit target thickness, conditions are nowhere more favorable than in this range of the (p,n) reaction, although they are almost as favorable in the 6 to 8 Mev range of neutron energy for the $D(D,n)He^3$ reaction. It seems reasonable, therefore, to consider these two source reactions and energy ranges as most promising for use with a Van de Graaff machine. In view of the large currents available from Cockcroft-Walton accelerators it is probable that neutron yields comparable with or better than those just considered can be obtained in practice at 14 Mev neutron energy by use of the reaction $T(D,n)He^4$ at 90 degrees.

INITIAL TIME

Information on initial time for neutrons resulting from inelastic scattering is usually inferred from the time at which the primary neutrons are produced in the target of a Van de Graaff, Cockcroft-Walton, or cyclotron accelerator. Account must be taken of the flight time of the primary neutron from target to scatterer and of many fixed delays in the electronics. In practice this is done by calibrating the time scale of the observed spectrum with reference to some known structure which is readily identifiable, such as the gamma-rays of inelastic scattering, the elastically scattered neutrons, or the inelastic neu-

Table II

Reaction	*Neutron energy (Mev)*	*Yield × 10⁻⁷ neutrons/ sterad/μcoulomb*	ΔE_t *(kev)*	ΔE_a *(kev)*
$T(p,n)He^3$	1	3.6	86	35
	2	7.6	60	56
	3	6.4	46	80
	4	4.7	39	105
$D(D,n)He^3$	4	1.6	290	52
	5	3.0	145	89
	6	3.9	110	125
	7	4.6	84	163
	8	5.1	69	202
$T(D,n)He^4$	16	3.5	400	65
	18	1.0	155	125
	20	1.0	93	185

trons from prominent levels which are well known from other studies. Thus, "initial time," in the sense in which the term is used here, is a time which differs by a fixed, determinable amount from the time at which the neutron of interest actually starts on its path. "Terminal time" is to be interpreted in a corresponding manner.

The phase-bunching in a cyclotron results in bursts of target current, usually of a few mμsec duration.[4] By applying radio-frequency voltage to a pair of electrostatic deflector plates at the output of a Van de Graaff or Cockcroft-Walton machine, bursts of target current of similar duration are readily produced. By detecting the target current directly, or by deriving a pulse from the dee or deflector voltage, indication is obtained of initial time. Another method utilizes the detection of the charged particle produced in coincidence with the neutron, as in $T(D,n)He^4$ reactions.[2] In a study of the neutron spectrum produced in fission, the fission fragments themselves were detected.[6] Also under development is the detection of the light pulse produced in a gas target by a beam of charged particles.[7] By any of these means there appears to be little difficulty in fixing initial time to a few mμsec or less.

TERMINAL TIME (DETECTORS)

The requirements to be met by the terminal time indicator are timing precision within a few mμsec, and an efficiency for the detection of neutrons which is known as a function of their energy, and is preferably flat over a wide range.

To meet the first requirement, the neutron detector is invariably a fast scintillator and photomultiplier. Various devices are contemplated as means of enabling the detector to encompass a large range of neutron energy. The simplest and most practical appears to be a scintillator loaded with hydrogenous material, coupled to a photomultiplier which is operated as close to its dark-noise level as is consistent with the tolerance for background. Liquids and plastics are favored because of their speed,[8] and the ease with which they may be fabricated in large forms. Detection efficiency as a function of energy is calculable in principle, but it appears to be preferable to determine the efficiency experimentally, by comparison with a long counter,[9] or counter telescope,[10] using monoenergetic neutrons. The results of calibrations carried out for two different biases against a long counter are shown in Fig. 1. The scintillator for which this result was obtained was a plastic† two inches in diameter by one inch thick, with roughened surfaces covered with Al_2O_3. The photomultiplier was an RCA 5819 selected from 50 for best signal-noise ratio. The bias corresponded to a counting rate due to tube dark-current of 2 counts per second.

A disadvantage of this type of detector is that there is a spread in size of output pulses down to the threshold level, and this occurs even for monoenergetic neutrons. This spread in sizes contributes to a spread in the times at which the time indicating device is fired. This spread is due to two causes: the first arises from statistical effects in the emission, transmission, and collection of scintillation photons,[11] and the second is due to the time spread associated with the photomultiplier.[12] From both causes the spread increases with decrease in the number of primary photons. This spread, as measured with a pulsed beam of monoenergetic neutrons, and the scintillator-detector arrangement described above, gives a width at half maximum of 10 mμsec for neutrons of 0.2 Mev energy, and 4.0 mμsec for neutrons of 0.35 Mev energy. These times were measured from photographs of a fast oscilloscope.[6] Fortunately the greater time spread is associated with longer flight times so that the effect, measured as a percentage of the flight time, does not increase rapidly with decreasing neutron energy.

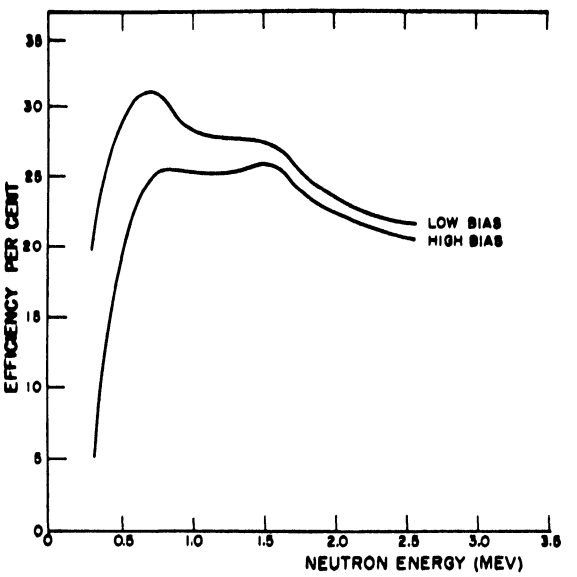

Figure 1. Detector efficiency as a function of energy for a plastic scintillator and selected RCA 5819 photomultiplier. The "low bias" corresponds to a counting rate of two per second due to photomultiplier dark current. The "high bias" corresponds to a bias 50 per cent higher, and a noise background of less than one per second

MEASUREMENT OF FLIGHT TIME

Numerous devices are in use or under consideration for measurement of transit times in the millimicrosecond range. These include delayed coincidence arrangements[13] with one or more channels, and a special version of this principle embodied in a device called a "chronotron." In a recent version[14] the chronotron consists of two delay lines cross-connected at ten equally-spaced intervals by voltage detectors. The initial and terminal time signals are each fed into one of these in such a manner that they proceed down the lines in opposite directions. That voltage indicator which detects the largest coincidence signal indicates the time separation of the signals.

† Plastic Scintillator "B" made by Pilot Chemical Co., Waltham, Mass., USA.

Another scheme of interest is one which converts the interval between two fast, timing pulses into a slow pulse whose height is proportional to the interval between them.[15] A pulse-height analyser then may be used to measure the pulse-height and hence the time-interval. The method of conversion is as follows. A fast discriminator‡ is triggered by one of the timing pulses, and the discriminator output pulse is used to start the charging of a capacitor at constant current. The charging is terminated by the pulse corresponding to terminal time. The resolution of one of these devices is such that when checked with fast pulses several volts or more above the discriminator threshold, almost all pulses fall within one channel whose width corresponds to 1.2 mμsec. For pulses of varying height which are only a volt or two above the discriminator threshold, there is a spread in time amounting to about 10 to 15 mμsec.

For applications in which the best precision of time measurement is justified, fast-coincidence technique,[13] or oscillographic recording[3] make it possible to measure to a fraction of a millimicrosecond.

LOS ALAMOS SYSTEM

The large Los Alamos Van de Graaff has been provided with a 40-watt radio-frequency oscillator operating at 3.7 Mc/sec, which supplies deflecting voltage to a pair of plates located at the place at which the beam emerges horizontally from the mass- and energy-analyzing magnet (Fig. 2). Application of this voltage to the plates results in reduction of the proton beam current on the target from a steady value of 20 microamperes, to an average value of 0.3 microamperes, corresponding to an estimated burst duration of 2 millimicroseconds, with two bursts per rf cycle. Monoenergetic neutrons of 2.5 Mev energy are produced in a tritium-filled gas target using the reaction $T(p,n)He^3$. For a target length of 3 cm, and a tritium pressure of 120 cm of Hg, the yield is 4.6×10^7 neutrons per second per steradian at zero degrees relative to the proton beam. The energy spread due to the target thickness is 100 kev and straggling in the 0.150 mil nickel foil window amounts to 60 kev.

Hollow cylinders are used as scatterers at zero degrees. Their axes are vertical and coincident with the axis of rotation of the detector and its shield. Their dimensions depend much on the element being studied, and on the amount of multiple scattering which is tolerable. The illustrative results given in Figs. 4 to 11 were usually taken with cylinders 5 cm long, 1.9 cm or 2.5 cm in outside diameter, and 0.95 cm inside diameter; whose centers were located 8.3 cm from the end of the target. The polyethylene scatterer was 5 cm long, 0.95 cm in outside diameter, and 0.64 cm in inside diameter.

The choice of a cylinder for the scatterer geometry

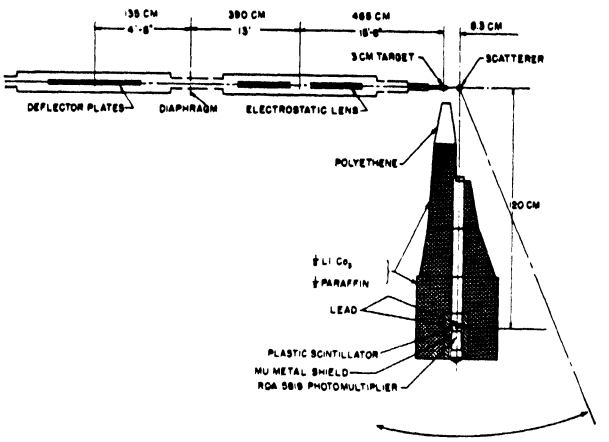

Figure 2. Schematic diagram of physical layout of apparatus for measuring the inelastic scattering of neutrons by time-of-flight

was motivated by considerations of rotational symmetry for angular measurements. It was made hollow rather than solid because of multiple-scattering considerations. For the polyethylene scatterer the small outside diameter results from the steep dependence on scattering angle of the energy of a neutron scattered from hydrogen. For the geometry given, the energy spread in scattering from hydrogen at a mean angle of 35 degrees is 15 per cent of the energy of the scattered neutron. At this angle the energy of the scattered neutron is 2/3 the energy of the incident neutron. The length of the scatterer enters into the energy resolution primarly through the angular dependence of the energy of the primary neutrons. This introduces an additional energy spread of 90 kev.

The detector is the two-inch diameter plastic for which the sensitivity curves are given in Fig. 1. It is set up 1.2 meters from the scatterer. Taking account of the solid angle subtended by the detector at the scatterer, and by the scatterer at the target, and of the efficiency of the detector, the counting rate to be expected in the detector, averaged over angle, is $4.0 \times 10^2 f$ per second. The quantity f is the fraction of neutrons incident on the scatterer which experiences a scattering.

In principle it should be possible to depend on the timing system to separate neutrons incident on the detector directly from the target, from those originating in the scatterer. Since, however, the primary neutron flux is 100 to 1000 times as great as the scattered flux, very stringent requirements would have to be imposed on the monoenergetic purity of the primary flux. It proves to be more practical to shield the detector against the primary flux. The arrangement is illustrated in Fig. 2. Lead of one to two inch thickness encloses the detector, and this shield is in turn enclosed in a six-inch thickness of a mixture of paraffin and lithium carbonate to moderate and capture neutrons. A polyethylene wedge shields the enclosure and the two-inch diameter hole which provides access to the detector through the shield. The axis of this two-inch hole is aligned to

‡ Designed by C. W. Johnstone, Los Alamos Scientific Laboratory. Design and construction of the converter unit are due to C. W. Johnstone, W. Weber, and J. L. McKibben, Los Alamos Scientific Laboratory.

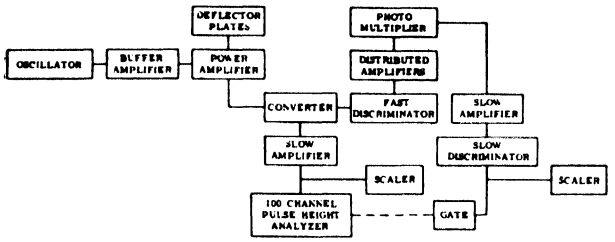

Figure 3. Block diagram of electronic apparatus for measuring the inelastic scattering of neutrons by time-of-flight

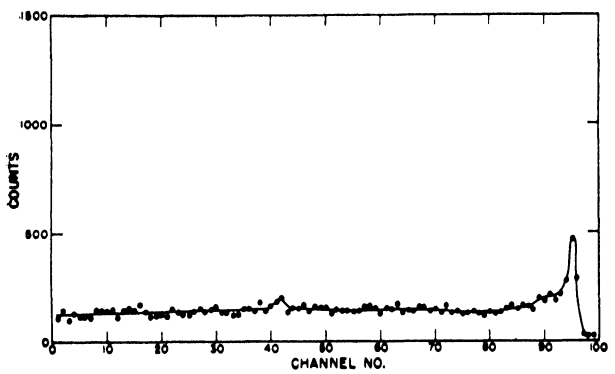

Figure 4. The time spectrum seen by the detector at 90°, with scatterer removed. The small peak in channel 42 is thought to be due to τ-rays originating in the target. The peak to the right is instrumental

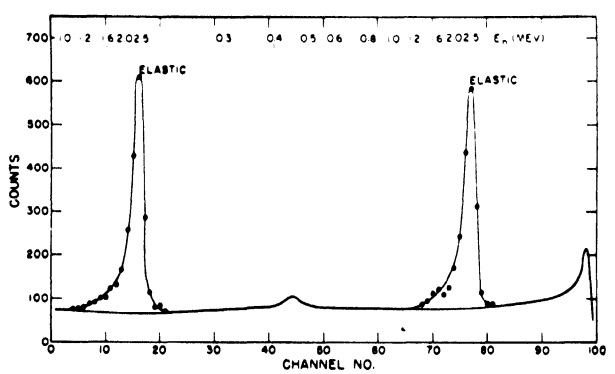

Figure 5. Carbon at 90°. The tailing of the elastic peaks on the lower energy side is partially instrumental and partially due to multiple scattering in the sample, with accompanying energy loss. The absence of structure other than that due to elastic scattering is consistent with the absence of known levels in carbon up to 4.4 Mev

intersect the scatterer axis. Without scatterer and with the primary flux given above, the counting rate in the detector, when it is in the 90 degree position, is 30 counts per second. Of these 6 are due to cosmic rays and noise in the photomultiplier, and the remainder are associated with the neutron flux. The arrangement is usable over the angular range from 20 to 150 degrees, but back angles are preferable because of more favorable background conditions.

A block diagram of the electronics arrangement is shown in Fig. 3. Time measurement is accomplished with a time-to-pulse-height converter of the type described earlier, together with a 100-channel pulse-height analyser. Initial-time pulses are derived once per cycle from the radio-frequency voltage. Since

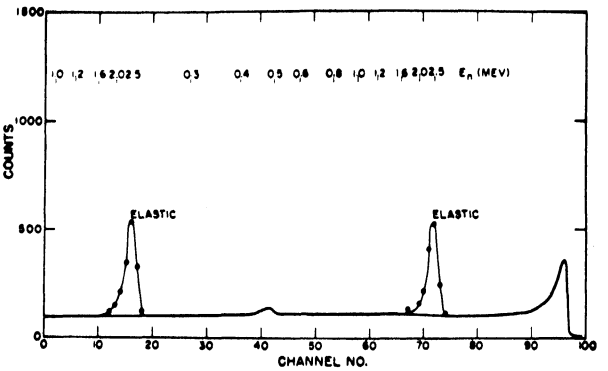

Figure 6. Calcium at 90°. The absence of structure other than the elastic peak is consistent with the fact that no levels are known in the 97 per cent isotope Ca^{40} up to 3.35 Mev. Known levels below 2.47 Mev energy in the other isotopes of calcium are not detectable

there are two neutron bursts per cycle this results in a double presentation of the data. A slow electronic system parallels the fast system and may be used to gate the pulse-height analyzer. This system is useful as a check on the effects of pulses near the threshold of the fast discriminator.

Figure 4 shows the time spectrum of the background at 90 degrees. The peak in the last few channels is entirely instrumental, arising from "start" pulses which are in coincidence with "stop" pulses. Each channel corresponds to an interval 2.3 millimicroseconds and time increases toward the left of the figures in a linear manner. Some illustrative spectra are shown, for the elements and angles indicated, in Figs. 5 to 11. Running times for each ranged from 5 to 10 minutes.

The absence of structure for the cases of calcium and carbon indicates that the wedge and shielding do not introduce spurious structure. The resolution over the spectra can be characterized as a width at half maximum of 4.6 millimicroseconds or 100 kev, whichever corresponds to the greater time. Cross sections may be derived from the energy sensitivity curve, together with a comparison with the scattering

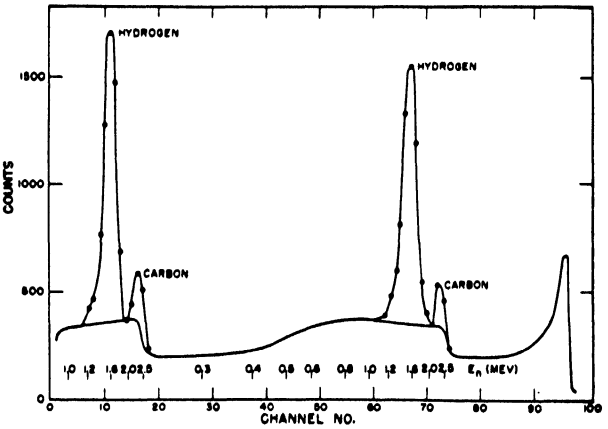

Figure 7. Polyethylene at 37°, showing the resolved peaks for the elastic scattering from hydrogen and carbon. At 37° the energy of the neutrons scattered from hydrogen coincides with the energy of neutrons scattered inelastically at 90° from 850 kev level in Fe^{56}

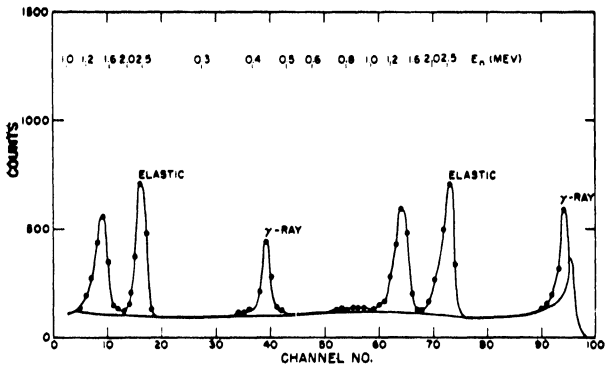

Figure 8. Titanium at 90°. The strong inelastic group corresponds to a level in titanium at 1.1 Mev. This and the subsequent spectra show clearly the gamma rays due to inelastic scattering

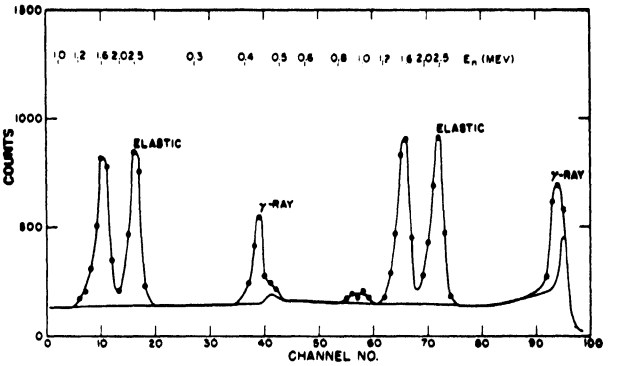

Figure 9. Iron at 90°. The well known strongly excited level at 850 kev in Fe^{56} is apparent as well as a weaker one at 1.4 Mev known to occur in Fe^{54}

from the hydrogen in polyethylene at a particular angle. The over-all accuracy of a cross section should be as good as the detector calibration, which is about 5 per cent, where signal-to-background ratio or resolution are not limiting factors. A rough figure for the minimum detectable cross section for a monoisotopic element is about 4 millibarns per steradian.

Because of the speed with which the data comes in, this system provides a useful method of measuring the angular distribution of elastic scattering. An attractive feature of this system for measuring the angular distribution of elastic scattering for light elements is that the corrections for variation of the energy of the scattered neutron with scattering angle are small because the energy sensitivity curve of the detector is fairly flat.

PRESENT LIMITATIONS AND FUTURE DEVELOPMENTS

Clearly, any increase in the yield of pulsed, monoenergetic, neutrons, or any decrease in the time spreads inherent in present detectors, can be turned to advantage in improving the range of usefulness of present systems. Also, improvements in designs and materials for shielding the detector from the primary flux would be of direct benefit.

Cyclotrons appear to be promising sources of large, pulsed fluxes, but it remains to be seen what can be done with the problem of shielding against the high background associated with these machines. A favorable prospect for improved fluxes with low background is associated with the development of a bunching system[16] for use in conjunction with a Van de Graaff or Cockcroft-Walton accelerator. Improvements suggested in the associated-particle method[2] also offer promise for the special case of 14 Mev and higher energy neutrons.

The prospects for improvements in scintillators and photomultipliers are less definite. Improvements in photomultipliers, particularly a reduction in the spread in transit time for given cathode area, are very desirable.

It will be noted that under the conditions described in the preceding section, increased flux will not improve the signal-background ratio, but only the counting rate. This is the case because the dominant

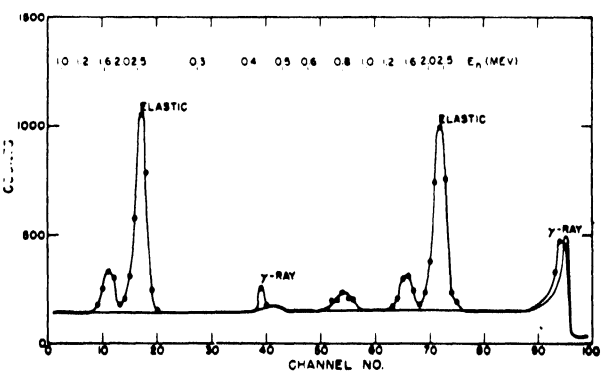

Figure 10. Bismuth at 135°. The levels excited are at 0.9 and 1.5 Mev, corresponding to known levels in Bi^{209}

background in the detector is associated with the primary neutron flux itself. Consequently, for a given scatterer the signal-to-background ratio can only be improved by improving the shielding. Thus far shielding design appears to be almost entirely an empirical matter, at least for this application. Calculations and further diagnostic testing with trial systems would be helpful.

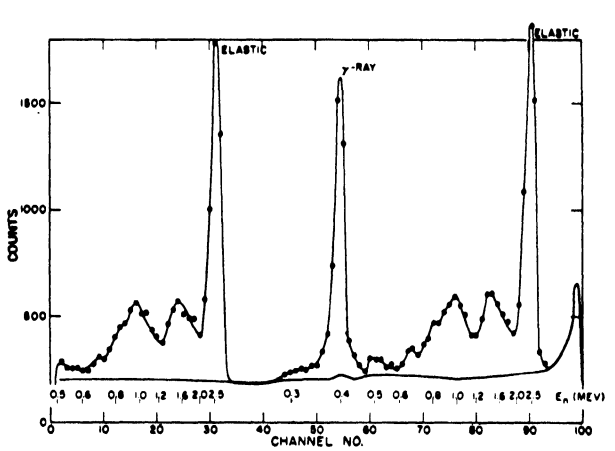

Figure 11. Copper at 90°. The levels excited strongly are at 1.0 and at 1.5 Mev. Weaker ones are at 1.7, 1.8 and 2.0 Mev. Assignments of these levels are not all clear primarily because of failure to resolve all the known levels in this energy range in the isotopes of copper. The displacement of the elastic peak in this figure compared to the other figures was made to reveal the left-hand cycle of data more completely

REFERENCES

1. Rosen, L., *Nuclear Emulsion Techniques for the Measurement of Neutron Energy Spectra*, Nucleonics *11*, No. 7, p. 32-38; No. 8, p. 38-44 (1953).
2. O'Neill, G. K., *Time-of-Flight Measurements on Inelastic Scattering of 14.8 Mev Neutrons*, Phys. Rev. *95*, 1234-1245 (1954).
3. Cranberg, L., Los Alamos Report No. 1654, *$Li^7(p,n)Be^7$ Reaction Study by Time-of-Flight*, April 1954.
4. Bloom, S. D., *A New Technique for Observing Cyclotron Phase-Grouping*, Paper I 7, Bull. of Am. Phys. Soc., Chicago Meeting, November 1954; Bloom, S. D., Muehlhause, C. O., Wegner, H. E., *Cyclotron Energy Measurement by Time-of-Flight*, Paper T-10, Bull. of Am. Phys. Soc., Washington Meeting, April 1955; Parkinson, W. C. and Grismore, R., University of Michigan, private communication.
5. A useful summary of pertinent data has been prepared for publication in Reviews of Modern Physics by Fowler, J. L., Oak Ridge National Laboratory, and Brolley, J. E., Jr., Los Alamos Scientific Laboratory.
6. Nereson, N., Cranberg, L., report in preparation.
7. Smith, R. V., Westinghouse Research Laboratory, private communication.
8. Swank, R. K. and Buck, W. L., *Decay Times of Some Organic Scintillators*, Rev. Sci. Inst. *26*, 1516 (1955).
9. Hanson, A. O. and McKibben, J. L., *A Detector Having Uniform Sensitivity from 10 kev to 3 Mev*, Phys. Rev. *72*, 673-677 (1947).
10. Diven, B. C., *Some Techniques for Measuring Fast Neutron Flux*, these proceedings.
11. Post, R. F. and Schiff, L. I., *Statistical Limitations on the Resolving Time of a Scintillation Counter*, Phys. Rev. *80*, 1113 (1950).
12. Smith, R. V., *Photomultiplier Transit Time Measurements*, Paper LA-11, Bull. Am. Phys. Soc., New York Meeting, January 1955.
13. Bell, R. E., Graham, R. L. and Petch, H. E., *Design and Use of Coincidence Circuit of Short Resolving Time*, Can. Jour. Phys. *30*, 35–53 (1952). Also Bell, R. E., *Nuclear Particle Detection (Fast Electronics)*, Annual Reviews of Nuclear Science *4*, 93-110 (1954).
14. O'Neill, G. K., *Direct Reading Analyzer for Short Time Intervals*, Rev. Sci. Inst., *26*, 285-290 (1955).
15. Moody, N. F., *Time Expansion for Millimicrosecond Pulse Intervals*, Electronic Engineering *24*, 289-294 (1952). Also Fraser, J. L., Chalk River Laboratory, private communication.
16. Mobley, R. C., *Proposed Method of Obtaining Short, Intense, Monoenergetic, Ion Pulses*, Phys. Rev. *88*, 360-361 (1952).

Recent Advances in Neutron Detection

By L. M. Bollinger,* USA

During the past few years there has been a considerable program in the United States for the improvement of the techniques of neutron detection. A large part of this effort has been directed at the development of counters to fill particular experimental needs. The present paper is concerned with a discussion of some of the systems that have recently been developed for use in neutron cross section measurements at energies less than a few Mev. Counters both for detecting neutrons, as such, and for investigating neutron-induced reactions are considered. When necessary to clarify problems of detection, experimental applications are also outlined.

DETECTION OF NEUTRONS

The rapid growth of the time-of-flight technique for measuring total neutron cross sections at low energies has required the development of slow neutron detectors having special characteristics. An ideal counter for this application should have a fast response time, a high counting efficiency, an insensitivity to γ-radiation and fast neutrons, and a large active surface area. None of the systems that are now in use has all of these desirable characteristics; in each case it has been necessary to sacrifice one or more property in order to emphasize another that is considered more important.

A detector that realizes an exceptionally high counting efficiency at the expense of a sensitivity to background radiations is the boron-loaded liquid scintillation counter[1,2] developed at Argonne for use with the fast neutron chopper.[3] The mode of operation of such a counter is as follows: A neutron enters the counting medium, consisting of a boron compound dissolved in a standard liquid scintillator. The neutron is moderated and is finally captured in a boron nucleus, which disintegrates according to one of the familiar reactions

$$n + B^{10} \begin{cases} \nearrow \; Li^7 + \alpha + 2.8 \text{ Mev} \\ \searrow \; Li^{7*} + \alpha + 2.3 \text{ Mev} \rightarrow Li^7 + \alpha + \gamma(0.48 \text{ Mev}) \end{cases}$$

of which the second reaction occurs with a 93 per cent probability for slow neutrons. An observation of the light produced by the ionizing particles released constitutes detection of the captured neutron.

The principal technical problems encountered in using a liquid detector of this kind are caused by the small magnitude of the light signal produced; the pulse given is equal to that from electrons having an energy of only 40 kev. The most serious difficulty attributable to the small signal is the broad pulse-height distribution obtained for slow neutrons, a distribution which makes discrimination against γ-rays and fast neutrons somewhat ineffective. A lesser problem is that the signal produced by slow neutrons is in the same pulse-height range as that caused by photomultiplier dark current noise.

A counter design which eliminates the latter of the above difficulties and minimizes the former is illustrated in Fig. 1. The counting solution used is 4 gm/liter of phenylbiphenylyloxadiazole and 20 mg/liter of POPOP (1, 4-bis-[2-(5-phenyloxazolyl)]-benzene) in equal parts of toluene and enriched methyl borate (70 per cent B^{10}). This solution is contained in a sheet steel vessel having the dimensions 14 by 18 by 2.5 cm. The interior surface of the vessel is coated with vitreous enamel, thus forming a good reflecting surface. The counting liquid is viewed by four Dumont 6292 photomultipliers which are selected for their good resolution and low noise. These tubes are paired by joining the anodes of those diagonally opposite, the signal from each pair being independently amplified. The gains of the photomultipliers are equalized by an adjustment of the voltage across each tube. The electronic system used requires a coincidence between the two amplifier outputs, thus eliminating noise counts, whereas counting of γ-ray background is minimized by requiring that the sum of amplifier outputs be in a given pulse-height range. Electronic difficulties caused by a high noise counting rate are reduced by cooling the counter to 10°C.

The operating characteristics of the counter shown in Fig. 1 and others of a similar design have been found to be very satisfactory for use in transmission measurements with the Argonne fast chopper. The pulse-height distribution obtained with slow neutrons is approximately triangular in shape, the full width at half maximum being about 65 per cent. The over-all counting efficiency ϵ of the system is given approximately by $\epsilon = 1.0\ E^{-0.13}$ for neutrons in the

* Argonne National Laboratory. Including work by H. Palevsky, Brookhaven National Laboratory; J. Ise, Jr., University of California Radiation Laboratory; J. E. Brolley, Los Alamos Scientific Laboratory; C. L. Cowan, Jr., Los Alamos Scientific Laboratory; B. C. Diven, Los Alamos Scientific Laboratory; and T. W. Bonner, The Rice Institute.

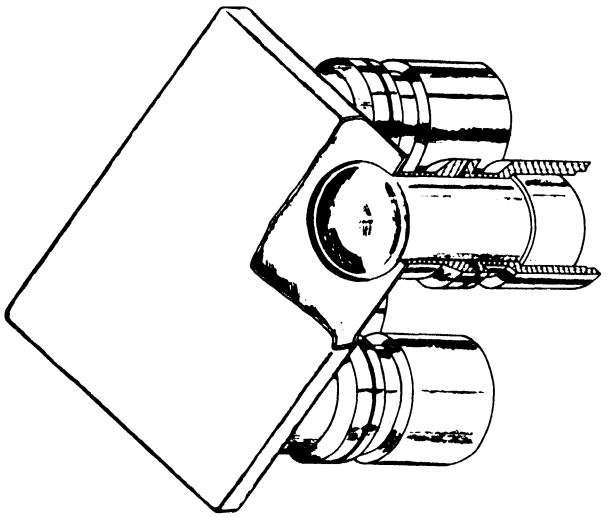

Figure 1. A boron-loaded liquid scintillation counter for neutron transmission measurements by the time-of-flight method

energy range $10 < E < 10{,}000$ ev; thus, it has an efficiency of about 40 per cent at 1 kev. The mean neutron capture time of the solution is about 0.6 μsec for a medium of infinite extent, and for the geometry used it is reduced to about 0.4 μsec at 1 kev. The background rate of the counter, when heavily shielded on all sides, is about 8 counts per second; an effort was made to minimize the counting of γ-radiation by making the counter thickness small. It should be emphasized that, for reasons of background, the boron-loaded liquid counter may be used in the straightforward way described above only when the source of neutrons is essentially free of γ-radiation; this condition can be achieved in some time-of-flight experiments because of the separation in time of γ-rays and neutrons.

Detector requirements for the Brookhaven fast chopper are similar to those of the Argonne chopper with the added complication, however, of a need to discriminate against a high γ-ray background. An insensitivity to γ-radiation has, of necessity, been achieved at the expense of counting efficiency; counting rates, on the other hand, have been maintained at a satisfactory level by developing two detection systems of exceptionally large surface area.[4] One of these systems makes use of the established method of neutron detection with BF_3 gas by containing an array of 128 proportional counters within a single pressure vessel. Individual counters within the array are 2.2 cm in diameter and 23 cm long; the wire cathode is 0.15 mm in diameter and the anode is made of steel tubing having a wall that is 0.25 mm thick.

The assembled system has a thickness, as seen by incident neutrons, of 9 cm and a sensitive area of 1600 cm^2. The pressure vessel containing the counter array is filled with enriched (96 per cent B^{10}) BF_3 gas to a pressure of 115 cm of Hg. The system is operated with cathodes at ground potential and 7000 volts on the anodes. For this voltage the gas amplification factor is of the order of 1000. A single amplifier is used for the entire array of counters.

The design expectations of the above gas counter have been fully realized. It has been in stable operation for many months with essentially no electrical difficulty. Careful selection of individual counters for the system caused all to have a similar pulse-height response, making the discrimination against counting of γ-rays effective. The counter "jitter time" (the maximum pulse collection time) is small, being only 0.4 μsec. The drawbacks of the system for time-of-flight measurements are those that are inherent in BF_3 gas counters. These defects are, first, an uncertainty as to the time of arrival of a slow neutron because of the counter thickness. If, on the other hand, the time uncertainty is reduced by making a thin detector, the counting efficiency becomes small; it is only 0.5 per cent at 1 kev for the Brookhaven gas counter.

In an effort to improve the efficiency and eliminate the time uncertainties of gas counters without sacrificing their insensitivity to γ-radiation, solid scintillation counters have also been developed for use in time-of-flight measurements at Brookhaven.[4] Intimate mixtures of 2 gm of enriched B_2O_3 and 1 gm of ZnS were fused together and formed into thin translucent scintillating discs having surface areas of 20 cm^2. Each disc was mounted on an RCA 5819 photomultiplier. The tube and scintillator were then placed in light-tight containers to form independent counting units. An array of 64 units of this kind operate in parallel to form a detection system of large surface area. The effective gain of each unit is controlled by adjusting the voltage difference between the cathode and first dynode. All units deliver their signals to a common amplifier.

The characteristics of the Brookhaven scintillation detector are significantly better than those of their gas counter for time-of-flight measurements. In particular, time uncertainties are negligibly small; the pulse rise time is less than 0.1 μsec and the neutron capture time is even less for the energies involved. The over-all detection efficiency is also somewhat improved, being about 1 per cent at 1 kev. At the present time, the efficiency cannot be significantly raised by increasing the thickness of the scintillating disc because of their low optical transmission. Again, because of lack of transparency, the counting rate vs bias curve obtained with these scintillators has no definite plateau. In spite of this drawback, γ-radiation is effectively avoided by using a relatively high bias, and stability in neutron detection efficiency is achieved by employing an especially steady high voltage supply.

The techniques that have been discussed above for counting slow neutrons are of little value in fast neutron detection but the criteria of excellence are similar; efficiency, speed of response and insensitivity to background radiations are desirable characteristics. Although there is no generally useful fast neutron

counter that incorporates all of these properties, the development of organic scintillators and scintillation techniques has made available a powerful tool for detection.

One ingenious application of organic scintillators has resulted in the development,[5] at The Rice Institute, of a detector of fast neutrons which is insensitive to γ-radiation and for which the detection efficiency is also strongly dependent on neutron energy. The construction of this counter and one of its applications are shown in Fig. 2. The counting medium consists of spheres of a plastic scintillator immersed in a non-hydrogenous, optically inert material (glass or trifluorochloroethylene liquid). The sphere diameter is chosen large enough so that, for a particular neutron energy, most recoil protons dissipate their energy within the scintillator; it must be small enough, however, to prevent the pulses of maximum size caused by γ-rays from being in the same pulse-height range as those due to the neutrons. Electrons due to γ-rays are prevented from traversing more than one scintillation sphere by the non-hydrogenous material separating them. Sphere diameters that have been used are 1.5, 2.5, 6, and 10 mm for neutrons having energies of 3.5, 4.5, 7.0, and 14 Mev, respectively.

The energy response of the plastic sphere counters is determined, to some extent, by the pulse height level at which pulses are accepted. For the application illustrated in Fig. 2, the measurement of elastic scattering cross sections, it is desirable to discriminate against the detection of neutrons having an energy lower than that for which the counter is designed. A selective response of this kind is obtained, for example, with the counter[6] adapted for 3.5-Mev neutrons, by accepting only those pulses that are greater than 85 per cent of the maximum pulse size obtained from 3.5-Mev neutrons. For this bias level, relative counting efficiencies are 100 per cent at 3.5 Mev, 29 per cent at 3.0 Mev, and 3 per cent at 2.7 Mev. Similar response curves are obtained for counters designed for other neutron energies.

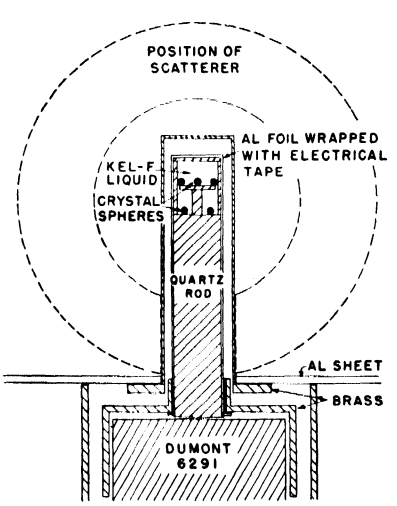

Figure 2. A typical plastic or crystal sphere scintillation detector of fast neutrons. In the application shown here, the counter is mounted within a scattering sample in the form of a spherical shell. The small size of the system may be judged by a comparison with the 4 cm diameter flat face of the photomultiplier

DETECTION OF NEUTRON-INDUCED REACTIONS

Our consideration of the counting systems described above has demonstrated the value of scintillation techniques for detection of neutrons. These techniques are an even more powerful tool for the study of nuclear reactions that involve neutrons.

The pioneer work[7,8] at Los Alamos on the construction of counters of very large size for detection of the neutrino has also resulted in the development of skills and techniques that are extremely valuable for counting neutrons in cross-section measurements. The most important of these is a method for detection and identification of a fast neutron entering a liquid counter by observation of a delayed coincidence between two pulses from the counter; the first pulse marks the time of production or arrival of the neutron, whereas the second is formed when it has been moderated and captured in some suitable material. When the boron-loaded liquid scintillator was first discovered at Argonne, it was suggested[2] that a delayed coincidence could be formed by a first pulse due to proton recoils and a second pulse caused by the capture of the neutron in B^{10}. The method achieved its full power, however, only with the use of a cadmium-loaded counting solution at Los Alamos;[7,8] the theory and use of these solutions for detection of fast neutrons is described in detail in reference 8.

In an important application of the method of delayed coincidence, several large liquid counters have been developed for the detection, with exceptionally high efficiency, of fission neutrons. One of these counters is used at the University of California Radiation Laboratory[9] for detection of neutrons emitted in spontaneous fission and another is used at Los Alamos[10] for both spontaneous and neutron-induced fission. The design of the counters used in these experiments is the same as that of the "large counter" described† in reference 8. The scintillating liquid is contained within a steel cylinder 72 cm in diameter and 76 cm long; a cylindrical opening 6.7 cm in diameter, within which samples are placed for investigation, passes entirely through the counter along its axis. The scintillation liquid used‡ is similar to that given in reference 8; the ratio of cadmium to hydrogen atoms in it is 0.003. The liquid is viewed by 90 Dumont 6292 and 1179 photomultipliers which are mounted flush with the 72-cm diameter cylindrical surface. The anodes of all 90 phototubes are connected in parallel, with the gain of each tube being controlled by adjusting the voltage across it.

† An illustration of the counter used at Los Alamos is given in a paper (P/592) by R. B. Leachman entitled *Determination of Fission Quantities of Importance to Reactors* in Volume 2, Session 7A, these Proceedings.

‡ The operational details given here are those of the Los Alamos group.

As a first application, the large counters are being used for a study of the multiplicity of neutron emission in nuclear fission; not only is the average number $\bar{\nu}$ of neutrons per fission measured but also the probability $P\nu$ for emission of a particular number ν. In these experiments a conventional gas ionization fission counter is placed in the center of the system. The detection of a count in this fission chamber is used to trigger the horizontal sweep of an oscilloscope, the vertical sweep being used to display the output of the liquid counter; each such event is recorded photographically. It consists, in general, of a prompt pulse followed by a system of delayed pulses; the prompt pulse is caused by fission γ-rays and recoil protons from fission neutrons, whereas each delayed pulse is due to γ-rays produced when a moderated neutron is captured in the cadmium of the counting solution. About 80 per cent of the neutrons are captured within 10 μsec. The number of delayed pulses recorded within 30 μsec gives a measure of the number of prompt fission neutrons produced.

A careful study§ has been made of the several efficiencies that are important for a complete understanding of results obtained with the above system. More than 99 per cent of the pulses from the gas-filled fission chamber are accompanied by a prompt pulse from the liquid counter. The efficiency for detection of a single neutron from fission of U^{235} was measured by comparing the known value of ν with the average number of delayed pulses observed per fission; the result obtained was an efficiency of 81.5 per cent. A Monte Carlo calculation shows that, for neutrons emitted by an isotropic source at the center of the detection system, the probability of neutron capture in cadmium is 99 per cent at 1 Mev, 94 per cent at 3.5 Mev, and 87 per cent at 5 Mev; about 96 per cent of fission neutrons are captured. The difference between the capture probability and the over-all efficiency may be accounted for by a failure, in a small fraction of events, to obtain capture pulses of adequate size; pulses smaller than approximately 2 Mev are rejected so as to keep the probability of observing a delayed pulse by chance sufficiently small. The very high background counting rates that are produced in large liquid detectors by cosmic radiation and local contamination constitute a definite problem for any application of the method of detecting fast neutrons by observing delayed coincidences.

Some of the general ideas that are discussed above were also applied in the development[11] of a complex system of liquid scintillation counters for use with the Argonne fast chopper in measurements of partial neutron cross sections. The important features of this system, which was designed for the efficient detection of slow neutron scattering, fission, and radiative capture events, are shown in Fig. 3. It consists of 6 boron-loaded liquid counters, of which 4 large "outer" counters surround the 2 smaller "inner" counters. The inner counters, in turn, are shaped so as to form a 5 by 15 cm open channel along the axis of the system. The sample to be investigated is mounted within this channel. The inner counters are filled with a scintillating solution composed of about 3.5 per cent B^{10} by weight, whereas the outer counters contain only 0.25 per cent. The signals from the 44 photomultipliers viewing the scintillation liquid are fed into 8 amplifiers, one amplifier being used for each outer counter and one for each end of an inner counter. The various systems of pulses obtained from the amplifiers, as discussed below, must be recognized and recorded electronically since accepted events are fed into a multichannel time-analyzer to be sorted into time channels.

The complexity of the detection system under discussion precludes a detailed discussion of its operating characteristics; general ideas will, therefore, be emphasized. The system was designed primarily for the measurement of slow neutron scattering cross-sections; it is also useful, however, for the detection of other neutron-induced reactions. Each reaction is identified by the distinctive system of pulses that it produces in the counter array. For the selection of a slow neutron scattered from the sample, a two-fold coincidence between pulses from an inner counter and from one and only one outer counter is required; moreover, both pulses must be within a specified range of pulse heights. This system of pulses is produced when the neutron is captured in the boron of the inner counter, with the ionizing

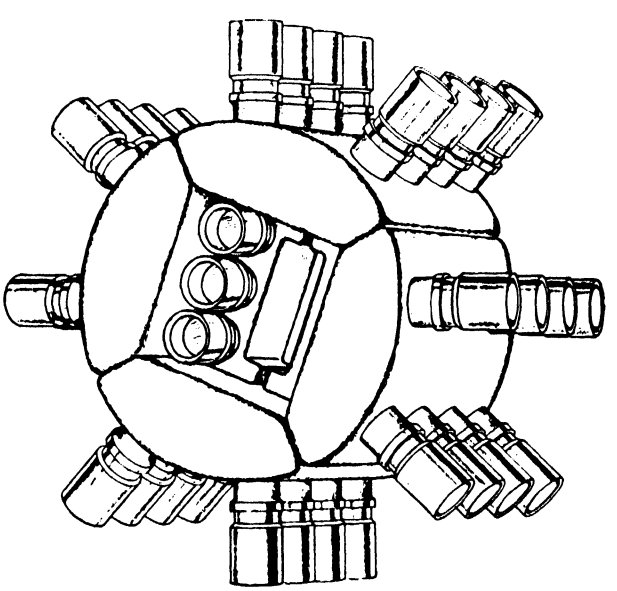

Figure 3. An array of 6 boron-loaded liquid scintillation counters for the measurement of partial cross sections of slow neutrons. The 4 outer counters form a system that is 51 cm in diameter and 51 cm long. The sample to be investigated is mounted (not shown) within the rectangular channel that passes between the 2 inner counters

§ Efficiencies measured at Los Alamos (reference 10) are quoted here.

particles that are formed being detected in an inner counter and the 480-kev γ-ray in an outer counter.

The unusual intricacy of the present scattering detector is necessitated by the requirements that it have a fast response time, a high counting efficiency, and an insensitivity to background radiations. The high boron concentration in the inner counter is required to obtain speed; for the counting solution used the mean neutron capture time is 0.6 μsec. Detection of the 480-kev γ-ray resulting from neutron capture in B^{10} is needed to discriminate against counting of γ-ray backgrounds, and the large size of the outer counters is needed to keep the over-all counting efficiency high; it is 25 per cent for 20-ev neutrons. In the study of non-fissionable materials the most bothersome background is that caused by the γ-rays produced by neutrons captured in the sample. For a typical sample material, cadmium, the detection efficiency for neutron capture is only 3 per cent of that for neutron scattering. The background due to capture γ-rays is, nevertheless, large for those cases where the cross section is almost entirely radiative capture. The scattering background caused by a sample of fissionable material has not yet been investigated experimentally but it is expected to be small.

When it is desired to detect fission events with the scattering detector, its general mode of operation is similar to that of the other large liquid detectors previously discussed. Typically, fission events may be selected by requiring any twofold coincidence followed by one or more delayed pulses; the initial coincidence is caused by γ-rays and recoil protons due to fission neutrons and the delayed pulse is given by the 480-kev γ-rays resulting from neutron capture in B^{10}. For the boron concentration used in the outer counter the mean neutron capture time is roughly 10 μsec; delayed pulses are, therefore, accepted for 10 μsec. The over-all efficiency for the observation of fission by detecting one or more capture neutrons is about 30 per cent; it could be greatly increased by replacing the boron by cadmium, but the detector could not then distinguish between scattering and capture events.

The development of the fission detector described above allows several important modifications in the techniques of fission cross-section measurements. First, using relatively thin samples, results are obtained that are comparable to those given by the conventional gas-filled chamber. The advantages of using the liquid detector are: (*a*) samples may be thicker than the extremely small value heretofore set by the range of fission fragments; (*b*) samples are easily changed; (*c*) the α activity of the sample does not limit the quantity of material that may be used, although γ-ray activity is bothersome, of course. A second, and perhaps more important, application of the detection system under consideration is for a direct measurement of σ_c/σ_f, the ratio of the radiative capture to fission cross sections, for neutrons of epicadmium energy. The basic ideas of the method were first used with the Brookhaven slow chopper.¶ In these measurements at sub-cadmium energies, the sample used is thick enough to absorb all incident neutrons, the resulting reaction being either radiative capture or fission; the effects of neutron scattering may be neglected. For this special case, the ratio of the incident neutron rate to the fission rate gives a direct measure of $1 + (\sigma_c/\sigma_f)$. In the more general case, some incident neutrons escape from the sample; hence the fraction of incident neutrons that are absorbed must be measured. This fraction is readily determined with the liquid scattering detector by counting the neutrons that are scattered out of the sample.

The other nuclear reaction induced by slow neutrons, radiative capture, is also efficiently detected by the large Argonne counter. The value of such a counter for cross-section measurements has not yet been demonstrated, however; possible changes of the spectrum and multiplicity of capture γ-rays could make the counting efficiency vary with neutron energy in an unknown way. Only if the counter is made large enough to detect radiative capture events with almost 100 per cent efficiency can this uncertainty be entirely eliminated. The present counter is not nearly large enough to achieve this objective.

One of the most recent advances in particle detection has been the discovery, at Argonne,[12] that noble gases may be used as detectors of ionizing radiations. The initial investigations of helium and argon gas showed that a large fraction of the scintillation produced is of too short a wave length to be transmitted through the glass envelope of an ordinary photomultiplier. Attempts to increase the wave length to the visible range by coating the counter with a plastic color shifter were successful, but the counting gas was rapidly poisoned by vapors from the plastic; cooling of the plastic to 0°C was found to eliminate the poisoning action. Further investigations showed that a small amount of nitrogen added to the counting gas also serves as an effective wave length shifter. The percentage of nitrogen required to obtain a maximum pulse height differs radically from one gas to another, being of the order of 10 ppm for helium and 10 per cent for argon. Scintillation pulses of large size have also been obtained without employing a color shifter by viewing the gas through a fluorite window with an EMI quartz window photomultiplier.

The investigation of gaseous scintillation counters has been continued at Los Alamos.[14] Krypton and xenon were studied and xenon was found to give a particularly large output pulse. For both of these gases the pulse height is increased by about a factor of two by cooling the system to 0°C.

The property of the gas scintillation counter that makes it particularly valuable is its short response time, which has been shown to be less than 10^{-8} sec.

¶ The Brookhaven work is described in a paper (P/587) by H. Palevsky entitled *Measurement of Capture of Fission Ratio of U^{235}, U^{233}, and Pu^{239} by a New Method*, Volume 4, Session 10A, these Proceedings.

The first applications of this property have been for measurements[15] of the fission cross section of Am^{241}. The effects of the high specific α activity of this material were avoided by clipping the output pulses to a width of only 2×10^{-9} sec. It seems certain that in the near future the noble gas scintillation counter will become a standard tool for study of the fission process.

The author wishes to express his appreciation to the many scientists who have, without exception, been most cooperative in supplying the unpublished information that was needed to assemble this paper.

REFERENCES

1. Muehlhause, C. O. and Thomas, G. E., *Slow Neutron Liquid Scintillation Detector* (abstract), Phys. Rev. *85*: 926 (1952).
2. Muehlhause, C. O. and Thomas, G. E., *Two Liquid Scintillation Neutron Detectors*, Nucleonics, *11*: 44, (1953).
3. Bollinger, L. M., Thomas, G. E. and Palmer, R. R., *Application of a Liquid Scintillation Neutron Detector to Time-of-Flight Spectroscopy* (abstract), Phys. Rev. *91*: 452 (1953).
4. Palevsky, H., Sjöstrand, N. G. and Hughes, D. J., *Neutron Detectors for the Brookhaven Fast Chopper* (abstract), Phys. Rev. *91*: 451 (1953).
5. McCrary, J. H., Taylor, H. L. and Bonner, T. W., *A Fast Neutron Counter with Energy Resolution* (abstract), Phys. Rev. *94*: 808 (1954).
6. Data of Taylor, Lonsjo and Bonner, private communication.
7. Cowan, C. L., Jr., Reines, F., Harrison, F. B., Anderson, E. C. and Hayes, F. N., *Large Liquid Scintillation Detectors* (abstract), Phys. Rev. *90*: 493 (1953).
8. Reines, F., Cowan, C. L., Jr., Harrison, F. B. and Carter, D. S., *Detection of Neutrons with a Large Liquid Scintillation Counter*, Rev. Sci. Instr. *25*: 1061 (1954).
9. Hicks, D. A., Ise, J., Jr. and Pyles, R. V., *Multiplicity of Neutrons from the Spontaneous Fission of Californium-252*, Phys. Rev. *97*: 564 (1955).
10. Diven, B. C., Martin, H. C., Taschek, R. F. and Terrel, J., *The Multiplicity of Fission Neutrons*, to be published.
11. Bollinger, L. M. and Thomas, G. E., private communication.
12. Palevsky, H., private communication.
13. Eggler, C. and Huddleston, C. M., *A Gaseous Scintillation Counter* (abstract), Phys. Rev. *95*: 600 (1954).
14. Boicourt, G. P. and Brolley, J. E., Jr., *Fast Detector for Fission Counting*, Rev. Sci. Instr. *25*: 1218 (1955).
15. Nobles, R. A., Henkel, R. L. and Smith, R. K., *Neutron Induced Fission Excitation Curve for Am^{241}*, Bull. Amer. Phys. Soc. *30*: No. 3, 16 (1955).

Time-of-Flight Instrumentation for Neutron Spectrometers

By W. A. Higinbotham,* USA

Neutron spectrometers are used to analyze the spectra or energy distribution of neutron beams in a manner similar to spectrographic analysis of beams of light. Some nuclear spectrometers make use of the diffraction from crystals and are analogous to the crystal spectrometers employed in analysis of visible and X-radiation. Other spectrometers determine the energy by measuring the time it takes each neutron to travel a certain distance. The energy is determined by the equations: energy = ½(mass)(velocity)^2 and velocity = (distance travelled)/(time-of-flight). The complete experimental equipment includes a means for modulating a neutron source so as to produce short pulses or "bursts" of neutrons, a neutron detector located at a distance from the pulsed neutron source, and electronic circuits for time analysis of the neutrons received at the detector. Such a neutron spectrometer is used to study the properties of various materials. First, the velocity spectrum of the source is recorded. Then a sample is placed in the neutron beam and the spectrum recorded again. The background counting rate is measured and subtracted from the recorded data. The transmission of the sample is computed point by point by dividing the counting rate with sample in the beam by the counting rate without sample. This paper will describe a number of recent developments in the electronic circuits used in the USA for measuring neutron time-of-flight.

At thermal energies, the velocities are low so that relatively simple circuits may be employed. The circuits which will be presented here are designed for use in the intermediate energy range and involve measurement of velocities from 10^3 to 10^7 meters per second over a distance of from 10 to 60 meters. The millimicrosecond techniques being developed for high energy time-of-flight analysis are described in a separate paper.

HISTORICAL

The first time-of-flight experiment was performed by Dunning, Pegram, Fink, Mitchell and Segre.[1] Slotted cadmium discs were rotated to interrupt or "chop" a collimated neutron beam from a RnBe source. Alvarez[2] modulated a cyclotron, and Fertel, Gibbs, Moon, Thomson, and Wynn-Williams[3] modulated a Cockcroft-Walton accelerator to produce pulses or "bursts" of neutrons. Baker and Bacher[4] pulse modulated the ion source of a cyclotron. Neutrons were produced when the accelerated deuterons hit a beryllium target. All detector pulses were recorded in one counter, for a reference, and by means of electronic switching the detector pulses which arrived in a selected time interval were recorded in a second counter. At this point I would like to define the phrase "time gate" to mean an electronically controlled switching circuit which permits signals (e.g., neutron detector pulses) to pass through when the time gate is "on" or "open" and which prevents such signal transfer when the time gate is "closed." In the circuit of Baker and Bacher a delay circuit was triggered at time zero, when the neutron "pulse" was formed. The delay circuit, adjustable from zero to 0.01 second, opened the time gate. The time gate was adjustable from 10 to 1000 microseconds.

As time went on these basic circuits were extended in a straightforward manner. More channels were added to speed up the taking of data. Shorter channel widths and longer distances from source to detector were employed to improve time resolution and to measure higher velocities.[5,6]

Circuits of this general type were built at Columbia University and Brookhaven National Laboratory in 1950 for use with modulated cyclotrons: Timing is obtained from a master oscillator which is started at time zero when the cyclotron beam hits the target. A delay signal is taken from a binary scaler which counts oscillator pulses. The delay signal starts a set of 32 contiguous time channels also synchronized by the oscillator. Two count recording circuits are associated with each of the 32 time channels for alternatively recording data with the sample "in" and "out" of the beam. Both the delay and the channel widths are variable from 1 to several thousand microseconds. Each of these systems uses about 500 radio tubes in the timing circuits. Power supplies and scaler-register circuits use nearly 500 more. For comparison, a 1000 channel analyzer circuit, using digital computer techniques, now under construction at the Argonne National Laboratory, uses about 200 tubes for timing, storage of counts and automatic printing of the accumulated data.

* Brookhaven National Laboratory, Upton, N. Y. Including work by L. M. Bollinger, Argonne National Laboratory; D. R. deBoisblanc, Phillips Petroleum Co.; M. H. Graham, Brookhaven National Laboratory; W. W. Havens, Columbia University; K. A. McCollom, Phillips Petroleum Co.; J. Rainwater, Columbia University; S. Rankowitz, Brookhaven National Laboratory; H. L. Schultz, Yale University; R. W. Schumann, Argonne National Laboratory; M. L. Yeater, Knolls Atomic Power Div., General Electric Co.

The time-of-flight circuits which follow were inspired by the pulse height analyzer circuits developed by Wilkinson[7] and Hutchinson and Scarrott.[8] They converted pulse height to time. Wilkinson's time measuring circuits were copied by Bollinger, Higinbotham, etc., as will be described in the next section. Digital computer storage circuits were first used by Hutchinson and Scarrott. A circuit by Schultz, described in a later section, is very similar to theirs.

It will not be possible to present the details of so many circuits in this article. Therefore the article will give a description of the different types of circuit and mention some of their interesting features. Circuit diagrams may be obtained from the designers of the several instruments.

MULTICHANNEL TIME-OF-FLIGHT ANALYZERS FOR LOW COUNTING RATES

The first modern analyzer circuit in this country was designed by Bollinger and Schumann at the Argonne National Laboratory for use with the "chopper" described by Selove.[6] In this case the counting rate is low so that the probability of detecting more than one pulse per neutron "burst" is considerably less than one. The analyzer is designed to measure the velocity of only one neutron per burst. In principle it works as follows: A light and photocell are arranged, as in Fig. 4, to provide a time zero pulse just as the neutron burst is formed. The T_0 pulse opens a "time gate" which permits pulses from a crystal oscillator to pass into a ring counter with 10 stable states. The counter activates each of ten terminals in succession. A second ring counter is triggered from the output of the first and controls a second set of ten terminals. The two sets of terminals are connected to a 10 by 10 array or matrix. A message register circuit is connected to each of the 100 intersections of the matrix. If a neutron is detected the time gate is closed and the ring counters stop, selecting one of the 100 register circuits.

Figure 1 is a block diagram of the Argonne analyzer. The photocell pulse turns on the bistable trigger circuit at time T_0. This opens electronic switch 3, permitting pulses from the 1 megacycle oscillator to pass through a binary scaler stage ($\div 2$) to the units ring counter. Prior to T_0, all stages of the ring counters are in the "off" state. If switch S_1 is closed, the T_0 pulse turns on the first stage of each ring counter. The units ring counter progresses at 2 microsecond intervals. Electronic switch 4 is normally closed so that the tens ring counter receives trigger pulses from the tenth stage of the units ring counter. The start of the counting period may be delayed from 0 to 2000 microseconds relative to T_0

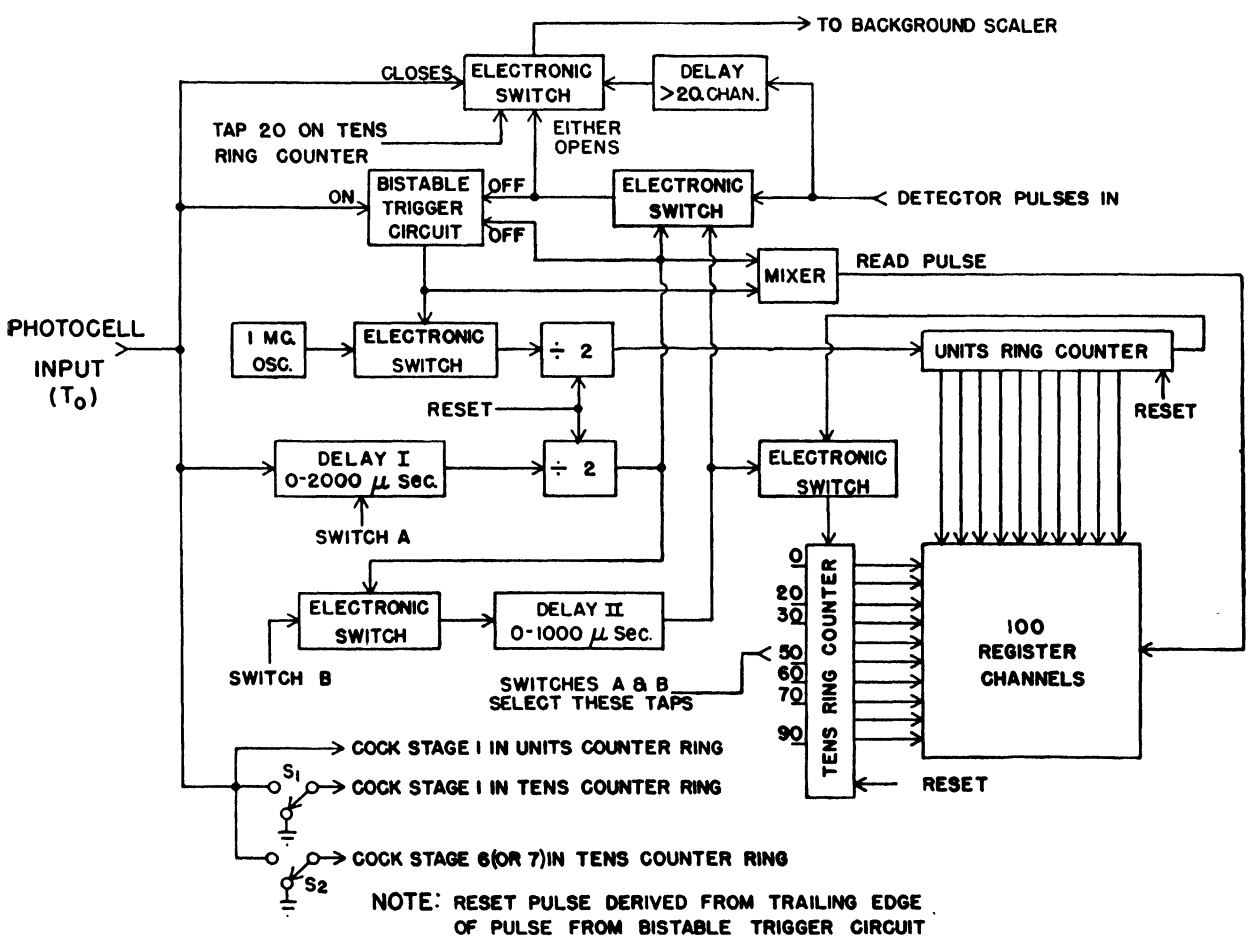

Figure 1. 100 channel analyzer, Argonne National Laboratory

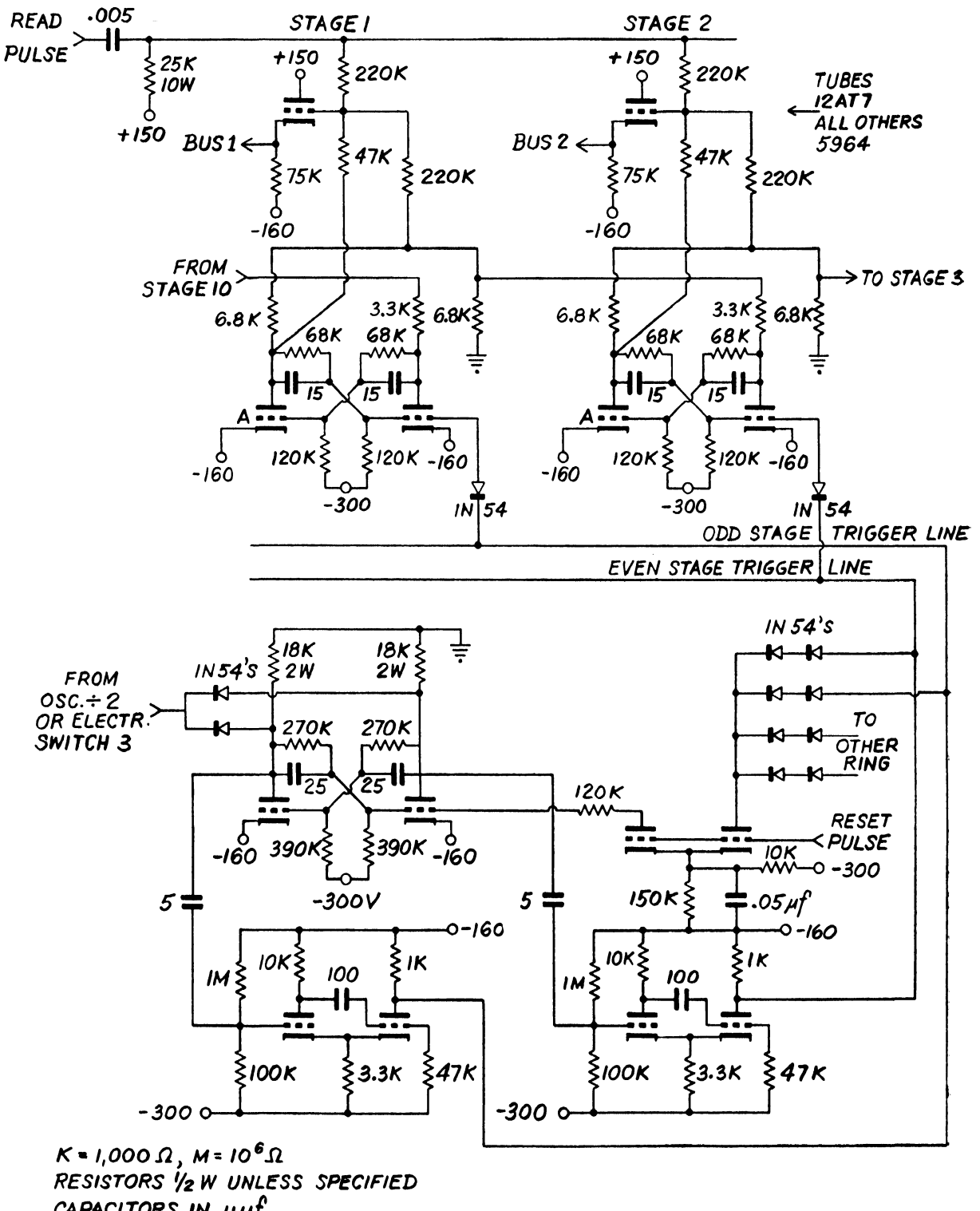

Figure 2. Ring counter circuit of Argonne analyzer

36090.

by delay I. At the end of the period set by delay I, pulses from one of the taps on the tens ring counter, selected by switch A, are permitted to trigger a binary scaler stage (÷2). This binary scaler stage exerts primary control of electronic switch 2. If a pulse is received from the detector after the binary scaler stage has been turned on, the bistable trigger circuit is turned off and electronic switch 3 is opened. Then the mixer circuit generates a "read" pulse which causes the matrix to record a count in the register channel selected by the matrix. After a short delay the ring counters, scalers, etc. are reset to their initial condition. If a pulse is not received from the detector within the 100 channel interval, a second pulse from the tens ring counter passes through switch A and delay I, and the binary scaler stage is turned off. When this occurs, the bistable trigger circuit is turned off; a "read" pulse is *not* generated; after a short delay all circuits are reset.

If both switches S_1 and S_2 are turned on, both stages 1 and 6 of the tens ring counter will be cocked by T_0. Then channels 1–50 and 51–100 record in parallel. Or a delay may be inserted between channels 1–50 and 51–100 as follows: The cycle selected by switch B starts delay II. Delay II opens electronic switches 2 and 4. At the end of delay II normal operation is resumed. It is also possible to use the two sets of channels alternatively by remote control of switches S_1 and S_2 and electronic switch 4 in order to record the spectrum without sample in the first 50 channels and the spectrum with sample in the beam in the last 50 channels.

Slow neutrons do not traverse the chopper slit so there is a time before T_0 when the detector count is due only to background or stray neutrons. All detector pulses pass through a delay circuit at the top of Fig. 2 to an electronic switch. It is closed at T_0 and opened at the end of an interval corresponding to twenty channels. (An alternate opening signal is provided in case the bistable trigger circuit is stopped before such an interval has elapsed.) The delayed pulses which pass through electronic switch 1 are the background counts which have occurred in a 20-channel interval just preceding T_0.

The 1 megacycle oscillator shown in Fig. 1 may be replaced by oscillators of lower frequencies so as to provide channels longer than 2 microseconds. Figure 2 shows part of a ring counter circuit. Each ring circuit consists of ten twin triode bistable elements. In the reset condition all left hand tubes are conducting. At T_0 one (or two) stages are inverted by a negative pulse at point A. Alternate stages of the ring counter are driven from a binary scaler stage as shown at the bottom of the figure. Matrix leads are driven through the triode tubes shown at the top. The "read" signal is added to the plate circuit signals in both ring counters. Each of the 100 recording circuits consists of a hot cathode gas tetrode and a mechanical message register. The grid of each gas triode connects to one lead from each of the two ring counters through two equal resistors.

The time-of-flight analyzer presently used with the fast chopper at Brookhaven National Laboratory is similar to the above. The analyzer, designed by Graham, Higinbotham and Rankowitz, is shown in Fig. 3. A pulse from a photomultiplier tube at time T_0 turns on the bistable trigger circuit and starts the "gated" 2 megacycle oscillator. The oscillator frequency may be divided as shown to give channel widths of 0.5 to 4 microseconds. Three ring counters are employed. The first two ring counters are used to define the 100 channels. The third ring is used to delay the start of the sensitive period by requiring that a detector pulse be in coincidence with one of the stages of the slow ring. The delay may also be varied in steps of 10 channels by starting the tens ring counter in different configurations. The tens ring counter is made up of 11 bistable elements, ten of which are connected to the matrix. The eleventh stage eliminates any ambiguity which might arise due to cumulative delay in the several counting circuits.

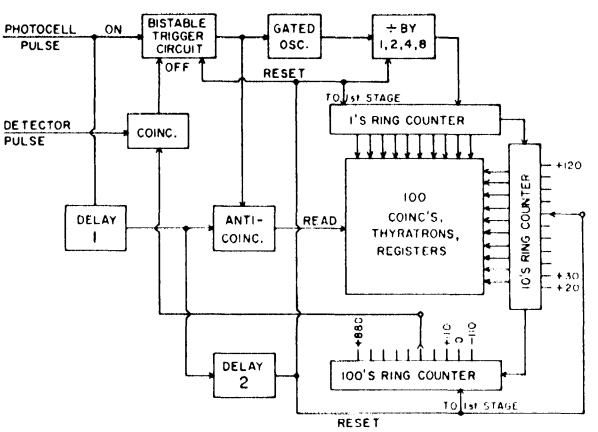

Figure 3. Brookhaven analyzer

The sum of the numbers adjacent to the switches on the 10's and 100's ring counters is the delay in units of a channel width to the start of the 100 channel recording interval. If a pulse is received from the detector within the selected interval, the bistable trigger circuit is turned off and the ring counters store the channel number. Delay I is manually set to follow the last channel of interest and to precede the next T_0 pulse. If a detector pulse has been received, the number stored in the ring counters is recorded. All circuits are reset by a pulse from delay 2. The frequency divider circuit and the units ring counter circuits are derived from the Chalk River scaler circuit.[8] The slower ring counter circuits are similar to those of Gatti[9] whose time-of-flight analyzer preceded ours. If we were to build such an analyzer today, we would use the Swedish Trochotron type MO-10 decade beam switching tubes[11] rather than ring counters.

MULTICHANNEL ANALYZERS FOR HIGHER COUNTING RATES

The analyzers described in this section are designed to record more than one pulse from the neu-

tron detector per burst of neutrons. As in the above, the start of the recording interval may be delayed from T_0. During the recording interval pulses from the detector are electronically switched into 100 or more consecutive count recording circuits. Considerably more is required of these circuits than of the circuits described above in regard to speed and accuracy of timing. The detected neutron pulses occur randomly in time. If the edges of the successive time gates are not infinitely steep, some counts may be lost between channels or counted in two adjacent channels. Poor timing might cause the channels to be unequal. The analyzers described in this section perform in a manner similar to the analyzers described briefly earlier. However, these circuits make use of a matrix in order to provide a large number of channels with a relatively small number of tubes.

The first analyzer of this type was designed by deBoisblanc and McCollum[12] of the Phillips Petroleum Co. for use with a fast chopper at the US Atomic Energy Commission's Reactor Test Station, Arco, Idaho. It is shown in Fig. 4. The shaded portion at the top left represents a face of the reactor. The chopper, with its four slits, is shown next to the reactor. The detectors are located 16 meters distant from the chopper. A light source and photomultiplier tube generate a pulse at T_0 which starts the variable delay. The variable delay is a commercially manufactured unit which uses a temperature regulated phantastron circuit and is stable to 1 part in 1000. The 100 adjacent counting channels start at the end of the delay period. The crystal oscillator has a frequency of 8 megacycles. The channel width selection unit contains binary frequency dividers to give channel widths of 0.5, 1.0, etc., microseconds. The electronic switch opens the gate circuit which permits pulses from the channel width unit to enter the units ring counter. The tenth stage of the units ring counter opens a gate permitting one pulse from the channel width unit to advance the tens ring counter one step. This insures that both ring counter circuits advance in phase.

After one complete cycle of 100 steps, the gate is shut off and all circuits are reset. The two sets of ten leads form a raster or matrix with 100 intersections. A triple coincidence circuit is located at each junction. The third input is from the detector pulse shifter. Each coincidence circuit in succession switches the pulses from the detector into a channel counting circuit. Each coincidence circuit consists of two germanium diodes and three resistors. Each counting circuit consists of a glow discharge decade counter tube, a hot cathode gas tetrode and a message register. The ring counter circuits are similar to the circuits shown in Fig. 2 but are designed for faster operation.

A detector pulse shifter circuit is used in order to ease the stringent timing requirements mentioned at the start of this section. Each pulse from the neutron detector-amplifier is delayed by an amount (not more than the duration of one channel) such that the corresponding pulse delivered to the coincidence circuits occurs in the middle of a channel interval. The circuit consists of a bistable trigger circuit. Pulses from the channel width unit, delayed by one-half channel interval, are connected to drive the trigger circuit in one direction. The amplifier lead is connected to drive it in the other direction. The normal

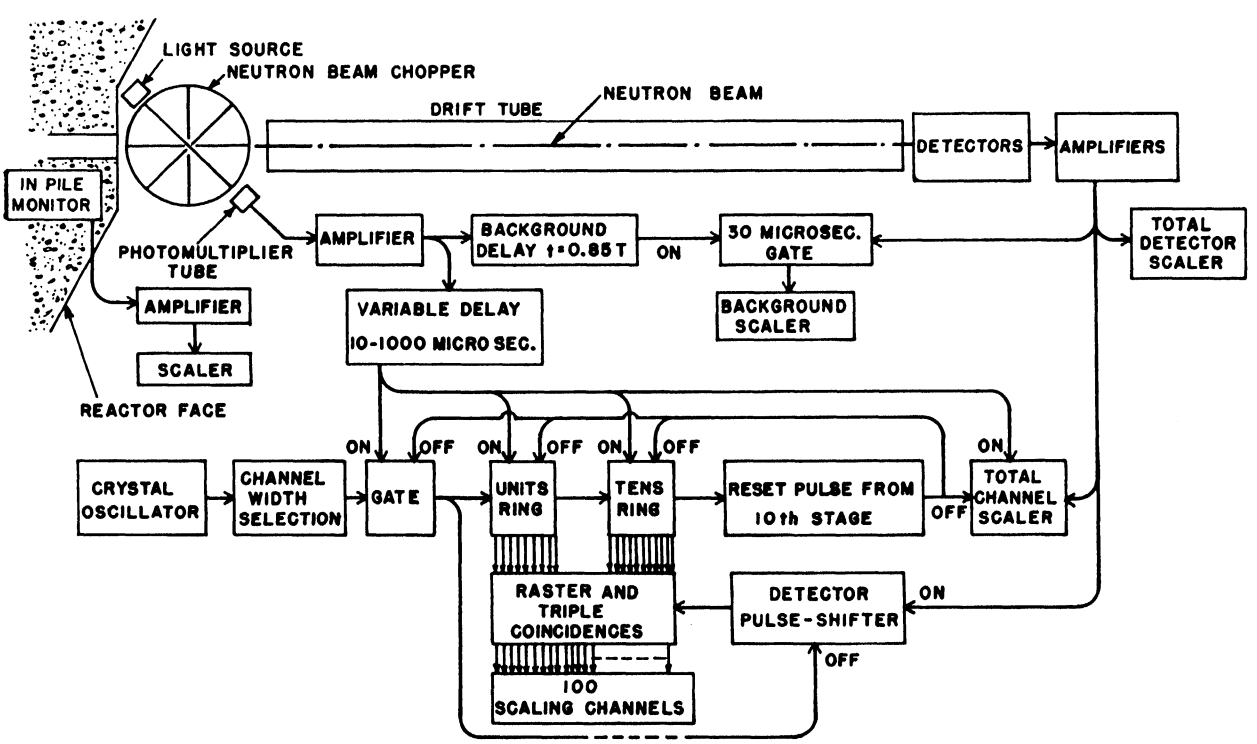

Figure 4. 100 channel analyzer, Phillips Petroleum Co.

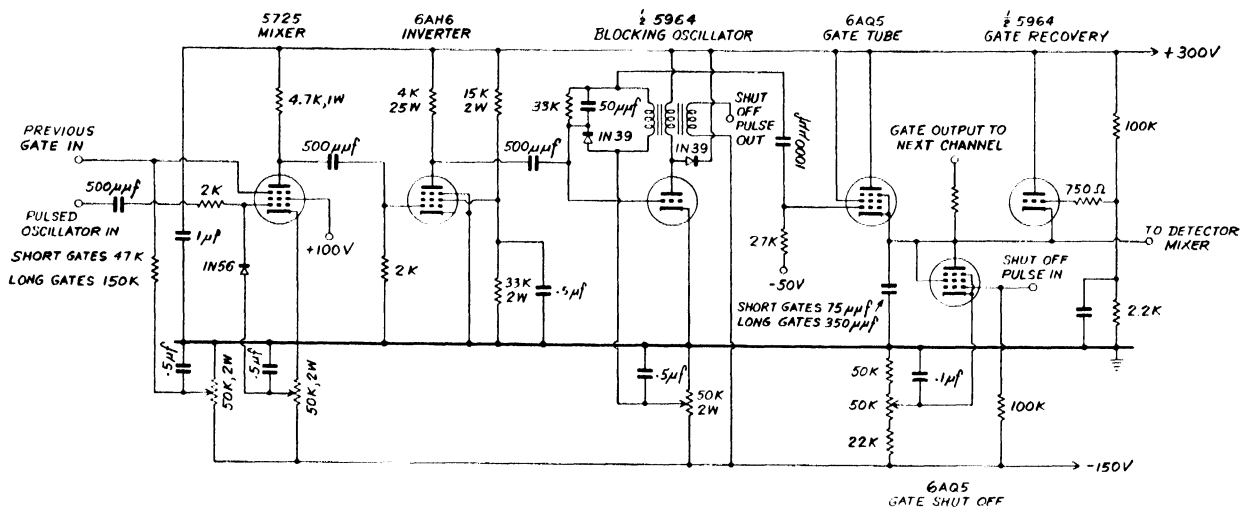

Figure 5. Ring counter circuit of General Electric Co. analyzer

state of the trigger circuit is determined by the pulses from the channel width unit. When a detector pulse is received, it throws the trigger circuit into the other state. The next pulse from the channel width unit throws the trigger circuit back to its normal state and a pulse is passed to the coincidence circuit. The figure shows circuits for recording the background counting rate and for recording all pulses received during the selected 100 channel interval.

Another analyzer of this general type has just been constructed at the Knolls Atomic Power Laboratory, General Electric Co., Schenectady, New York, by Yeater. The neutron bursts, in this case, are produced by a pulsed betatron. The betatron accelerates electrons to produce photons which, in turn, produce neutrons by the gamma-n reaction. It is similar in many respects to the Phillips Petroleum Co. instrument described above. The T_0 pulse is derived from a photomultiplier which is excited by photons when the betatron beam hits the target. A conventional delay circuit determines the start of the 100 channel counting interval. The channel timing is derived from a gated oscillator which is started at the end of the delay. Channel widths are 0.25 to 2.0 microseconds. The ring counter circuits, Fig. 5, make use of blocking oscillators to generate time gates with steep edges. Each ring counter circuit has ten of the elements shown in Fig. 5. At the start of the counting period the storage capacitor of the first stage is given a positive charge. The next channel timing pulse causes this capacitor to be discharged and the capacitor in the second stage is charged up, etc. The detector pulses are placed in coincidence with the gate output signal of all of the ring counter stages. The coincidence circuits contain a mixer tube, an inverter, and a blocking oscillator with components similar to those shown in Fig. 5. The outputs of the 20-coincidence circuits are arranged to form a ten by ten matrix. A coincidence circuit and a count recording circuit are connected to each of the 100 intersections of the matrix.

It is planned to obtain 200 channels of information by using the above circuits twice in succession. A second delay circuit will be triggered at the end of the first 100-channel interval. The second delay circuit will initiate a new cycle of operation. During the delay, the first set of 100 registers will be decoupled from the power supply and a second set of 100 registers will be connected to the register driving tubes. Diodes will be used in the register circuits to prevent interaction between the two sets of registers. The counting rate will be limited since each gas tetrode register driving tube may be fired only once per neutron burst.

The third analyzer of this type is being built by Rainwater at Columbia University. The T_0 signal will start a gated oscillator which provides stable timing pulses. The delay will be taken from counting circuits. After the delay, two 16-stage ring counter circuits will be driven to control a 16 × 16 matrix and provide 256 channels. Detector pulses will be "time shifted" as described above to align them with the center of the next channel. Channels will be 0.25, 0.5, 1.0, etc., microseconds in duration. Each coincidence-register drive circuit uses three triode tubes.

TIME-OF-FLIGHT ANALYZERS USING DIGITAL STORAGE TECHNIQUES

The first analyzer of this type was designed by Schultz at Yale University, New Haven, Conn. A mercury acoustic delay line was used as the storage or "memory" element. This has been rebuilt using a fused quartz acoustic delay line. The analyzers have been used with a microwave cavity linear electron accelerator which produces neutrons by the gamma-n reaction. This accelerator can be synchronized from the time-of-flight circuits. The Yale analyzer is shown in Fig. 6. The operation and circuits are very similar to those used by Hutchinson and Scarrot.[8] A master pulse is generated automatically to start operation of the circuits. The master pulse modulates

the 40-megacycle oscillator and causes an acoustic pulse to travel through the 1000-microsecond quartz delay line. The pulse is amplified and passed through a detector (or rectifier) circuit. It continues to recycle through the pass master pulse and reshaper units. The master pulse triggers a delay circuit which causes "channel marker" pulses and "clock" pulses to be generated for a time just less than 1000 microseconds. The master pulses pass through a frequency divider to trigger the linear accelerator.

A detector pulse is time shifted, as has been described, so as to arrive in synchronism with a 500-kilocycle channel pulse. The adder circuit causes a binary digit to be inserted in the corresponding channel. The binary digit continues to circulate through the quartz line, the amplifiers, the reshaper and adder circuits until another detector pulse is received in the same channel. Then the adder circuit adds one to the binary number stored in the channel interval. 2^{10} counts may be stored in each channel interval, since the binary digits have 0.2 microsecond spacing.

The information may be displayed on a cathode ray tube oscilloscope: The horizontal sweep circuit is triggered by the master pulse. A vertical sawtooth waveform, triggered by the channel pulses, is applied to the vertical deflection plates. And the "information out" terminal is connected to the control grid of the cathode ray tube. Schultz has designed an analogue printing circuit which also uses about 40 tubes: A delay circuit, triggered from the master pulse, is slowly varied from 0 to 1000 microseconds. It selects the first channel pulse for a number of cycles, then the second, and so on. While the delay selects one channel, in this manner, the digits stored in the selected channel operate gas tetrodes which control a set of relays. The relay contacts switch a set of resistors in such a manner as to generate a voltage proportional to the number in the channel.

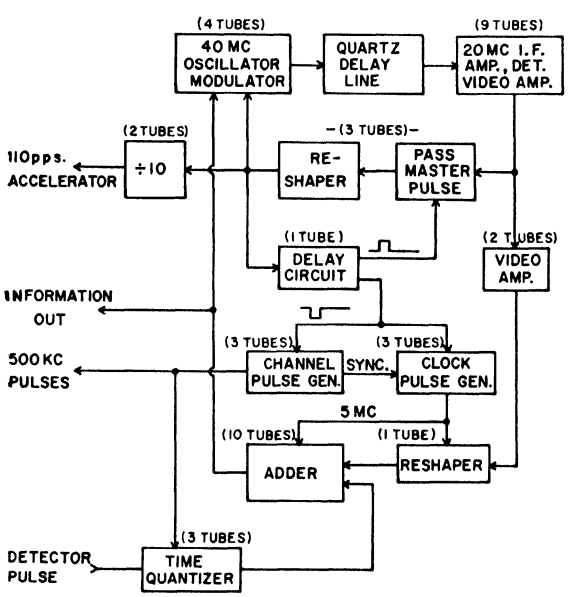

Figure 6. 500 channel analyzer with acoustic delay line storage

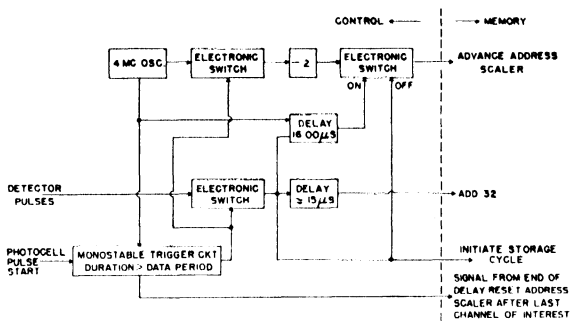

Figure 7. 1024 channel analyzer with magnetic core storage

The successive channel readings are plotted on a moving chart by a pen recorder.

In most cases it is not possible to trigger the neutron source from the analyzer circuits, so the quartz line method cannot be used. The remainder of the instruments to be described here may be triggered by a T_0 signal. Schumann has designed and is constructing an analyzer with 1024 channels which uses magnetic core storage. This will be used with a new "chopper" at the Argonne National Laboratory. Mr. Schumann and his associates have recently built a 256-channel pulse height analyzer using magnetic core storage. It uses the Wilkinson principle of converting pulse height to time. The time is measured by counting pulses from an oscillator. The number stored in the selected position is transferred to an arithmatic circuit. One is added to the number and it is transferred back into the magnetic core memory. The pulse height analyzer takes about 50 microseconds to record each pulse. It stores up to 2^{20} counts per channel. It includes a cathode ray tube display and has circuits for printing out the contents of the memory at the end of a run.

Schumann's analyzer is shown in Fig. 7. The T_0 pulse turns on the trigger circuit which is adjusted to turn itself off after the last channel of interest and before the next T_0 pulse arrives. The oscillator is a free-running crystal oscillator. The trigger circuit permits oscillator pulses to enter the divider circuit ($\div 2$). The output of the divider is 2 megacycles, which defines time channels of 0.5 microsecond duration (the divider may also be set to divide by 3, 4, 6, 8, etc., for wider channels). The channel pulses from the divider circuit pass through a second electronic switch, which is normally closed, to the "address scaler". The address scaler is a 10 stage binary scaler which is normally permitted to "count" 1024 channel pulses and is then shut off. When a detector pulse occurs, it passes through an electronic switch, controlled by the trigger circuit, and stops the address scaler by opening the electronic switch which follows the divider.

The address scaler remains in a state determined by the time when the detector pulse was received for 16 microseconds or 32-channel periods. During this time the binary number stored at the corresponding address or position in the magnetic core matrix is transferred to a set of trigger circuits; one is added

to the binary number and the new number is transferred back into the memory. 32 counts are added to the address scaler to compensate for the time it was off, and channel pulses from the divider are switched on again.

The magnetic cores are arranged in arrays 32 × 32. There are 16 such arrays, giving capacity for 2^{16} counts in each channel. The operation of magnetic core memories has been described in a number of places.[13,14] A combination of diode coincidence circuits and transformers are connected to the address scaler to direct the "read" and "write" signals with a small number of tubes.

The analyzer is arranged so that the channels may be separated into four sets of 256. There are circuits for recording the background counting rate in an interval 32 channels wide. The accumulated data may be presented in analogue form on a cathode ray tube display. At the end of an experiment the data will be automatically punched on teletype tape and plotted on a moving chart with a pen recorder. Fifty-eight tubes are used in the control and timing circuits; 104 tubes in the magnetic memory and arithmatic circuits; 40 tubes for the cathode ray tube display, the pen recorder and the teletype punch operations.

A similar analyzer is being constructed at Brookhaven National Laboratory, by Graham and Higinbotham. It will have 1024 channels. Channel widths will be 0.25, 0.5, 1.0, etc., microseconds. Storage on the face of cathode ray tubes[15] is used in place of the magnetic cores. The addition circuit makes use of SEAC diode switching logical elements.[16] Data in the memory will be displayed continuously on a cathode ray tube. At the end of the experiment, the data will be printed on a tape by means of a solenoid-operated adding machine.

Three laboratories are presently engaged in the cooperative design of an analyzer which will make use of a combination of cathode ray tube and magnetic drum storage. Havens, Columbia University, and Schultz, Yale University, will design the input and cathode ray tube circuits. Design of the magnetic drum and output devices is under the direction of Yeater, General Electric Co. The basic pattern of the instrument is shown in Fig. 8. The T_0 pulse will start a variable delay. Channels are defined by the 10 megacycle oscillator which starts after the delay. After 2048 cycles, the oscillator is turned off. While the oscillator is activated, neutron detector pulses are permitted to turn on the beam of the cathode ray tube. The beam of the cathode ray tube is moved in discontinuous steps by the divider and "stepping" circuits through 2048 discrete positions. Whatever detector pulses arrive during this "recording" period are stored on the face of the cathode ray tube.[14]

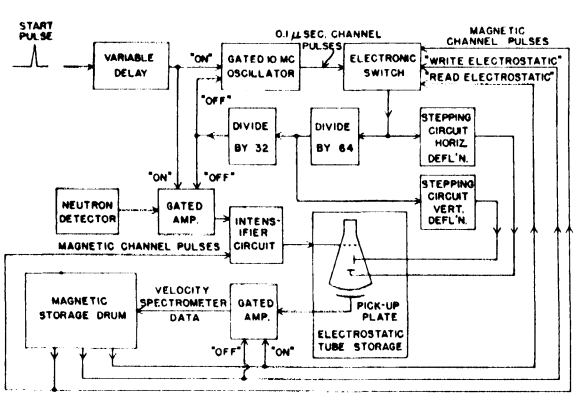

Figure 8. 2048 channel analyzer using cathode ray tube and magnetic drum storage

The speed of the magnetic storage drum is controlled so that it is in synchronism with the T_0 signals. After the detector pulses are recorded on the cathode ray tube the circuits are switched so that the detector pulses may be taken out of the cathode ray tube temporary storage and added to the numbers previously stored in corresponding channels on the magnetic storage drum.

The drum is provided with a "timing" track. Pulses from the timing track are fed to the dividers and stepping circuits so that the cathode ray tube beam is deflected through 2048 positions exactly as it was previously deflected by the oscillator. At each position the beam of the cathode ray tube is turned on (intensified). In this way, the stored counts cause pulses to appear at the pickup plate and all storage positions on the cathode ray tube are reset to the zero condition. Whenever a pulse occurs at the pickup plate, the number stored in the corresponding position on the drum is "read out." One is added to the number and the new number is "written" back onto the drum surface. Separate recording heads are used for the "read" and "write" operations.

There will be storage for 2^{13} counts in each of the 2048 time channels. Channel widths will be 0.1, 0.2, etc., microseconds duration. There will be a monitor display on a cathode ray tube. At the end of an experiment the stored data will be automatically punched on business machine cards.

REFERENCES

1. Dunning, J. R., Pegram, G. B., Fink, G. A., Mitchell, D. D., Segre, E., *Velocity of Slow Neutrons by Mechanical Velocity Selector,* Phys. Rev. *48,* 704 (1935).
2. Alvarez, L. W., *The Production of Collimated Beams of Monochromatic Neutrons in the Temperature Range 300°-10°K,* Phys. Rev. *54,* 609 (1938).
3. Fertel, G. E. F., Gibbs, D. F., Moon, P. B., Thomson, G. P. and Wynn-Williams, C. E., *Experiments with a Velocity-Spectrometer for Slow Neutrons,* Proc. Royal Soc., 175, 316 (1940).
4. Baker, C. P. and Bacher, R. F., *Experiments with a Slow Neutron Velocity Spectrometer,* Phys. Rev. *59,* 332 (1941).
5. Bacher, R. F., Baker, C. P., McDaniel, B. D., *Experiments with a Slow Neutron Velocity Spectrometer II,* Phys. Rev. *59,* 443 (1946).
6. Selove, W., *A Rotating-Shutter Time-of-Flight Spectrometer for the Slow-Neutron Resonance Region,* Rev. Sci. Instr. *23,* 350 (1952).
7. Wilkinson, D. H., *A Stable 99 Channel Pulse Amplitude Analyzer for Slow Counting,* Proc. Cambridge Philosophical Soc., 46, 508 (1950).

8. Hutchinson, G. W. and Scarrott, G. G., *A Precision Pulse Height Analyzer of Moderately High Speed,* Philosophical Magazine *42,* 792 (1951).

9. Moody, N. F., Howell, W. D., Battell, W. J., Taplin, R. H., *A Comprehensive Counting System for Nuclear Research,* Rev. Sci. Instr. *22,* 439 (1951).

10. Gatti, Emilio, *An Eighty-Channel Velocity Selector for Neutrons,* Rev. Sci. Instr. *24,* 345 (1953).

11. Manufactured by Haydn Brothers, Plainfield, New Jersey, USA.

12. deBoisblanc, D. R. and McCollom, K. A., *MTR Time-of-Flight Instrumentation,* Document No. IDO-16159, obtainable from the US Atomic Energy Commission, Office of Technical Services, Oak Ridge, Tenn.

13. Rajchman, J., *A Myriabit Magnetic Core Matrix Memory,* Proc. Inst. Radio Engr., 41, 1407 (1953); Radio Corp. of America Review *13,* 183 (1952).

14. Papian, W. N., *A Coincident-Current Magnetic Memory Cell for the Storage of Digital Information,* Proc. Inst. Radio Engr., 40, 475 (1952).

15. Williams, F. C., Kilburn, T., *A Storage System for Use with Binary-Digital Computing Machines,* Proc. I.E.E. (London), 96, Part II, 183 (1949); 96 Part III, 77, (1949); 97 Part IV, 453 (1950).

16. Greenwalt, S., Haueter, R. C., Alexander, S. N., *SEAC* (Standard Eastern Automatic Computer), Proc. I.R.E., 41, 1300 (1953). Elbour, R. D., Witt, R. P., *Dynamic Circuit Techniques Used in SEAC and DYSEAC,* Proc. I.R.E., 41, 1380 (1953).

Techniques for Measuring Elastic, Non-Elastic and Transport Neutron Cross Sections

By R. F. Taschek,* USA

The neutron balance and economy of a chain reacting system are strongly dependent on the elastic, inelastic and radiative capture cross sections of non-fissionable as well as fissionable materials contained in the system. The elastic and inelastic cross sections are primarily of interest for neutron energies above the kilovolt range (for inelastic scattering the first level in most nuclei is not lower than 20 kev or so) and into the Mev range, i.e., for the undegraded fission neutrons and for those degraded by a few collisions. The reason for this arises from the fact that above a few kilovolts the elastic and inelastic cross sections begin to have values which are competitive with processes such as radiative capture and fission in the thermal fissers which have decreased rapidly as the energy has gone up.

For elastic scattering, one is primarily interested in the differential cross sections (angular distributions) as a function of the incident neutron energy, at least so far as the heavier elements are concerned. A directly related quantity which determines the effect of neutrons being deflected through large angles (such as one desires in a reflector or moderator) is the "transport cross section" variously defined as

$$\sigma_{etr} = 2\pi \int_0^{\pi} \sigma_e(\theta)\ (1\text{-}\cos\theta)\ \sin\theta\ d\theta \qquad (1)$$

the elastic transport cross section, and

$$\sigma_{Tr} = \sigma_{in} + \sigma_{etr} \qquad (2)$$

the total transport cross section, which gives most weight to neutrons scattered at large angles.

For inelastic scattering the most desirable quantity to determine would, of course, be the energy dependence of the cross section for an incident neutron of energy E_n to be inelastically scattered to an energy E_n' at an angle θ, i.e., $\sigma(\theta, E_n, E_n')$. Any further information obtainable such as the spectrum of the gamma radiation following the inelastic scattering process is immediately of interest to those studying the shielding of reactors.

The following discussion will concern itself with counter methods and techniques which are being used to determine the angular distributions of elastically scattered neutrons and the so-called inverted sphere technique which has so far been most productive for measuring the total reaction or non-elastic cross sections for fast neutrons.

* Los Alamos Scientific Laboratory. Based on work done at Argonne National Laboratory; Bartol Research Foundation; Los Alamos Scientific Laboratory; Oak Ridge National Laboratory; The Rice Institute.

THE INVERTED SPHERE TECHNIQUE

As yet, a neutron spectrometer having resolution commensurate with all the requirements for reactor design above the tens of kilovolts incident neutron energy region does not exist. The closest approaches to solutions for the problem of measuring spectra presently exist in the photo-plate and time-of-flight methods discussed elsewhere.[1,2]

It has, however, been possible to measure reasonably accurately the total cross sections for all non-elastic processes by two methods,[3,4] one a sphere transmission, the other the difference between total and elastic scattering. This so-called "non-elastic cross section" is the sum of the cross sections for all processes except elastic scattering. At present the most used of these two techniques involves a measurement of the transmission of a thin spherical shell of the material in question with a counter having, ideally, a step function sensitivity near the incident neutron energy. If we postulate such a detector and a very thin shell of the nuclide for which the cross section is desired surrounding a spherically symmetric monoenergetic neutron source, then the cross section is given by

$$\sigma_{ne} = \frac{1}{tN} \ln \frac{1}{T}$$

where T is the observed transmission, N is the number of nuclei per cm^3, and t is the shell thickness. It has been assumed that the shell is thin enough so that multiple scattering of the neutrons is completely negligible and that there is no energy loss in elastic collisions. Under these idealized conditions the elastic scattering out of the detector is exactly compensated by the elastic scattering into the detector. The method is thus particularly powerful since the net effect observed is produced only by non-elastic collisions.

Actually, the first problem met is that the fast neutron sources likely to be of most use are highly asymmetrical in both intensity and energy; this is true of $Li^7(p,n)Be^7$, $T(p,n)He^3$, and $D(d,n)He^3$ which cover the neutron energy range from say 50 kev to 6 Mev,[5] i.e., the fission neutron range. The use of these sources internal to the sphere is thus

impossible. However, for the thin shell case, it is immediately obvious that the source and detector may be inverted with no effect on the transmission since all neutron paths are reversible. If this is done, the above-named sources may be used to measure the non-elastic cross sections for neutron energies which cover the fission neutron spectrum.

Let us assume henceforth that the detector is inside the sphere only. Then, since the neutron sources used are somewhat asymmetric even for small angles around the forward direction, it becomes desirable to make the angle subtended by the sphere small enough to minimize energy and intensity changes across the sphere. For the $T(p,n)He^3$ reaction a half angle of 3–4 degrees subtended by the sphere at source appears satisfactory. It is additionally necessary that the detector sensitivity be as nearly independent of angle of the incident neutrons as possible. Since it is also necessary to make the detector have a sensitivity approaching a step function, it is clear that this method of determining non-elastic cross sections is strongly conditioned by the quality of the neutron counter it is possible to make.

COUNTERS

The neutron detectors which have been used for the sphere experiments are hydrogen gas filled proportional counters, fission counters using those nuclides which have thresholds in their fast fission cross section, and specially designed organic scintillator counters. Each of these has its own advantages and disadvantages as discussed below. One of the first detectors to be used for experiments of this type was the spiral fission counter, as described in Rossi and Staub, containing as much as practicable of Np^{237}, U^{238}, and U^{236}. The fission cross sections of these materials rise reasonably steeply from practical thresholds although there are flat sections at some energies which may cause trouble.[6] The biggest difficulty with these counters is that they have inadequate sensitivities for the weak neutron sources listed above and thus require the transmission measurements to be made too close to the source to meet the small angle requirement mentioned above; also, the thresholds are fixed, which is generally undesirable if one wishes to make measurements as a function of energy. The thresholds of the various

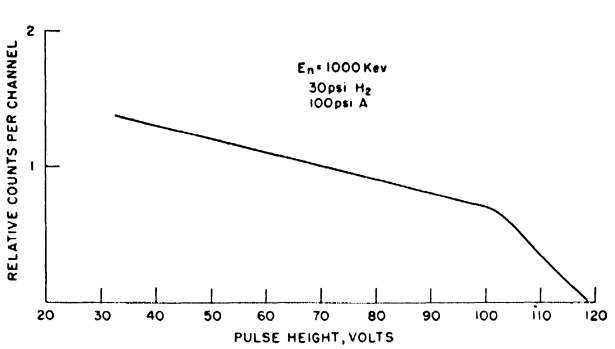

Figure 1. Pulse height distribution for 1 Mev neutrons incident on Allen proportional counter filled with 30 psi of H_2 and 100 psi of A

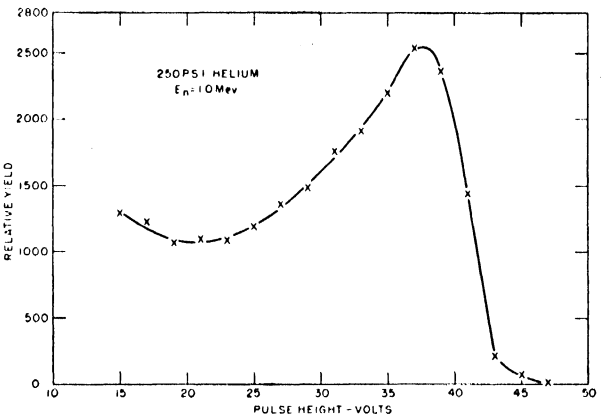

Figure 2. Pulse height distribution for 1 Mev neutrons incident on Allen proportional counter filled with 250 psi of He^4

nuclides now known to be useful go to only a little above 1 Mev, which limits the range of possible measurements to the low end of the fission neutron spectrum. Detector symmetry is fair to good. Measurements using such detectors have been made by Beyster and Carter[7] for incident fission neutron spectrum and by Ennis[8] for monoenergetic neutrons in the 1-Mev range.

The next obvious kind of counter to try is a gas-filled recoil detector. If the filling is hydrogen, an ideal counter gives a rectangular pulse height distribution; deuterium and helium which are also useful gases give pulse-height distributions which depend on the differential scattering cross sections at the energy in question. For real detectors, resolution, wall, gas impurity, and other effects distort the pulse-height distributions. In Figs. 1 and 2 are shown pulse-height distributions for H_2 + A and He respectively using the same counter.[9] At this energy, the advantage of He is obvious. By recording the pulse-height distribution on a multichannel pulse-height analyzer sensitivity curves are obtained for several energy thresholds at one time. Figure 3 shows sensitivity curves for deuterium and the fission cross section of U^{238} superimposed to show the relative resolution for different energies coming from, say, inelastic scattering. The fission cross section does not have the low energy cutoff one desires in a good threshold detector.

If it is desired to analyze pulse-height distributions in terms of complex neutron spectra by differentiation, hydrogen gives the most easily interpretable recoil spectrum, but it suffers from having a small stopping power which can, however, be partly overcome by adding a heavy gas such as A or Kr to the counter filling. The recoils from He^4 give a desirable pulse-height distribution near 1 Mev, but not for much lower or higher energies where the total cross section drops off rapidly and the angular distribution of He^4 loses much of its forward peaking. Deuterium above 500 kev gives a forward peaked recoil distribution which is desirable from the point of view of steep slope to the sensitivity curves; also wall effects at the same pressure are smaller using

deuterium rather than hydrogen, but below about 3.5 Mev the total cross section is lower. This last is not a complete disadvantage since it depends on what it is desired to emphasize.

In Fig. 4 is shown the counter developed and used by Allen[9] of Los Alamos Scientific Laboratory which exemplifies the problems met in using the sphere technique for obtaining non-elastic cross sections. This counter is used up to pressures of 300 psi with a ½ or 1 mil wire and up to 5 kv counter voltage to get sufficient gas multiplication, i.e., up to about 10. The hydrogen pulse-height distributions shown above indicate how good the counter is in regions where the wall effects are small. The angular sensitivity of the counter is flat between 10 degrees and 70 degrees, 70 degrees/0 degrees = 0.97 and 80 degrees/0 degrees = 0.90, where 0 degrees is perpendicular to the wire; it is not possible to make a measurement at 90 degrees. Other counters of a similar kind, but generally much larger, have been used by Beyster and Walt,[10,3] with both hydrogen and methane fillings. If a large range of recoil energies is to be looked at, the presence of carbon is usually undesirable because of the high energy of the forward carbon recoils. In all cases great care must be taken to minimize end effects in the counters. In the Allen counter this is done by a combination of field tubes and semiconducting plastic disks which help keep the field radial near the terminations of the wire.

The third type of counter in general use was developed by Bonner[11] and consists of several small spheres of plastic phosphor or stilbene embedded in oil (Kel-F liquid) of the same refractive index to facilitate the transmission of light produced by a

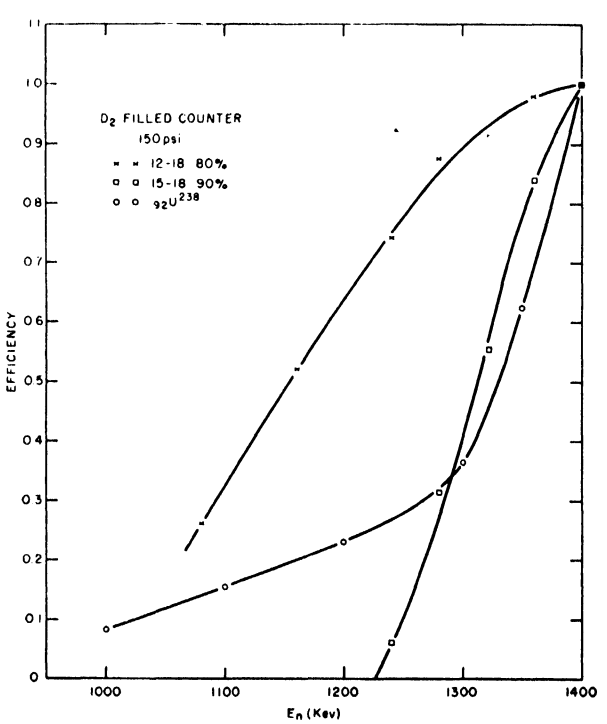

Figure 3. Comparison of efficiency curves for deuterium filled proportional counter with U^{238} filled spiral counter

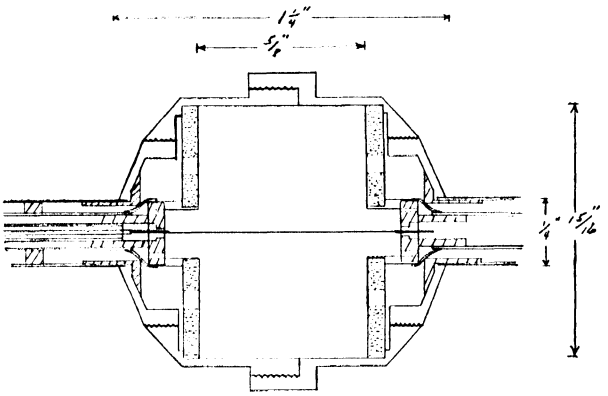

Figure 4. Small volume proportional counter developed by Allen: high pressure proportional recoil counter

proton recoil in the scintillator to a photomultiplier. A counter of this type used by Bonner *et al.* is shown in Fig. 5. The size of the balls used is optimized for each energy region and a pulse-height distribution is shown for this counter in Fig. 6 with the discrimination for gamma-ray background indicated. At high energies this type of detector seems to be the most favorable, its disadvantages being a relatively high gamma-ray sensitivity and a poor pulse-height response at low neutron energies. A typical efficiency curve is shown in Fig. 7.

MULTIPLE SCATTERING CORRECTIONS

Assuming that the experimental difficulties associated with neutron sources and detectors have been overcome, the actual determination of the non-elastic cross section from the sphere transmission measurements runs into another practical difficulty associated with multiple scattering of neutrons, which, in the ideal case, we assumed did not occur. We know reasonably well that at energies below about 20 kev there are no levels in any target nucleus which can cause true inelastic scattering; in this range most of the total cross section arises from approximately spherically symmetric elastic scattering plus a much smaller contribution from radiative capture. As the neutron energy increases into the Mev range, capture becomes very small, the average total cross section changes only slightly and inelastic scattering rises rapidly as the number of available levels increases. Now in the several Mev range where a large fraction of the total cross section is inelastic and the elastic becomes more strongly pronounced in the forward direction, the fractional contribution of second and further scattered neutrons from the elastic group to the observed transmission will not be large, but for low energies where nearly all of the total cross section is due to elastic scattering, appreciable corrections must be made to the transmissions to give the correct non-elastic cross sections. The effect of these corrections on cross sections is indicated by the following: The ordinary exponential transmission to terms in the thickness squared is

$$T = 1 - \sigma_{in} X + \tfrac{1}{2}\sigma_{in}^2 X^2 \qquad (4)$$

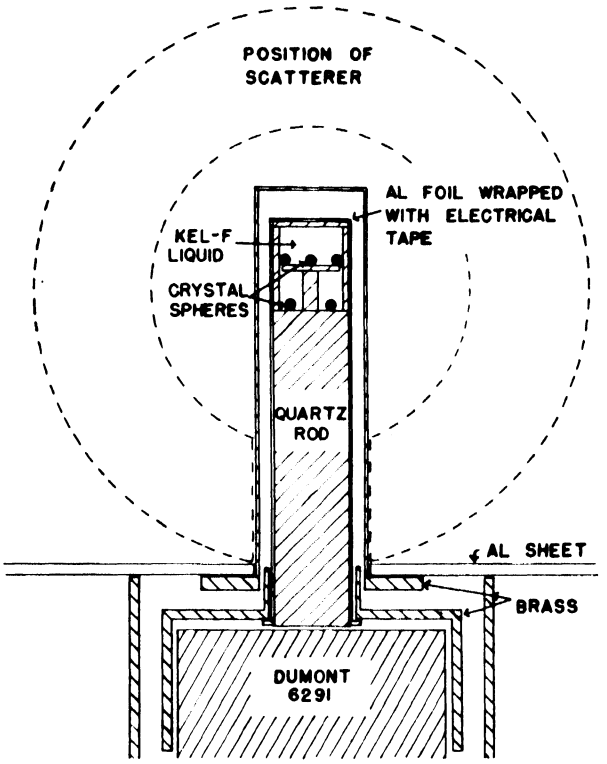

Figure 5. Ball scintillator counter developed by Bonner

whereas

$$T = 1 - \sigma_{in} X + \tfrac{1}{2}\sigma_{in} X^2 (\sigma_T - \sigma_{el} K) \quad (5)$$

is the correct formulation[12] if there is multiple scattering which is spherically symmetrical even though the shells may be considered thin. K is a geometrical constant $\geqslant 1\frac{1}{2}$. Clearly if $\sigma_{el}K \geqslant \sigma_T$, which is easily possible near the threshold for non-elastic effects, the transmission drops more nearly linearly than exponentially with X.

Bethe and Beyster[12] have derived an analytical formulation of the corrections to be made to observed transmissions in terms of the elastic transport cross section and escape probabilities for neutrons having made one or more collisions in shells which are definitely thick, i.e., one or two mean free paths.

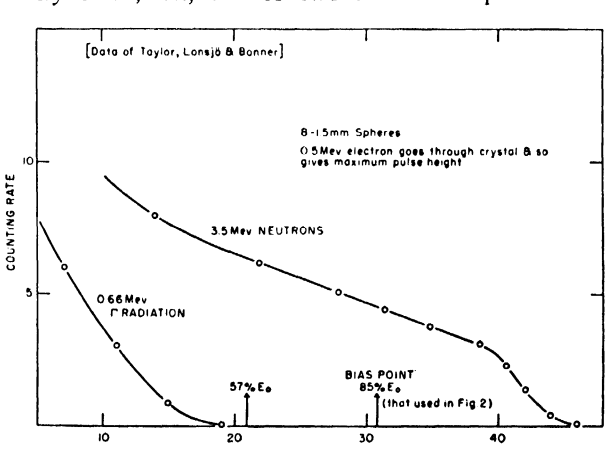

Figure 6. Pulse height distribution from Bonner counter for 3.5 Mev neutrons

At higher energies where the elastic scattering is definitely not spherically symmetric and for thicker shells, their more sophisticated analysis in terms of escape probabilities gives

$$1 - T = (1 - T_0)\frac{\sigma_{in}}{\sigma_{tr}} \left[1 + \frac{\sigma_{etr}}{\sigma_{tr}}(1 - P_1) + \frac{\sigma_{etr}^2 (1 - P_1)(1 - P_2)}{\sigma_{tr}(\sigma_{in} + \sigma_{etr} P_m)}\right] \quad (6)$$

where $T_0 = \exp(-N\sigma_{tr}t)$.

The P's are the escape probabilities and are machine calculated from the sphere geometries. P_m is the escape probability from the normal mode collision distribution in the shell and in fact a nearly correct answer is obtained from

$$1 - T = (1 - T_0)\frac{\sigma_{in}}{\sigma_{in} + \sigma_{el} P_m} \quad (7)$$

The multiple scattering effects have also been calculated by direct use of the Monte Carlo method and by a method developed by Bengt Carlson of Los Alamos Scientific Laboratory which fits experimentally determined elastic angular distributions with a four-point function instead of using the transport cross sections. In general the three methods give the same result.

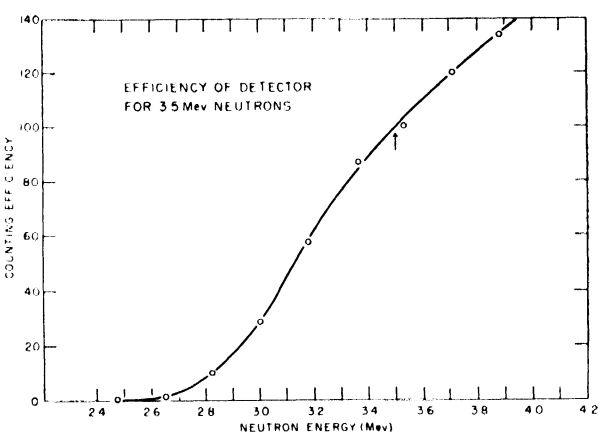

Figure 7. Efficiency curve for Bonner counter at 3.5 Mev

It is necessary, in addition, to make corrections for counter anisotropy, which may also be done by proper orientation of the counter during the experiment, for energy loss in elastic collisions with the lower weight nuclides, and for effects due to geometrical asymmetries from source to sphere. At high biases on the detector, the elastic scattering energy loss correction must be made for all nuclides and is the most important correction.

When these corrections are made a cross section for non-elastic scattering can be obtained which is probably accurate to about 5 per cent; the energy range for the cross section is defined by the shape of the particular detector sensitivity curve used. By use of several different detector sensitivities a crude idea can be obtained about the distribution in energy of the neutrons following an inelastic collision.

In the case of the fissionable materials a further complication arises from the ν neutrons from fission, some of which will have energies greater than the detector threshold. At the lower energies, i.e., up to about 2 Mev excellent experimental corrections can be made for the fission neutrons by first obtaining the counter pulse-height distribution with low energy primary neutrons only, which do not themselves produce observable pulses. This distribution can then be normalized to that portion of the distribution which sticks out beyond the cut-off pulse height for the fast primary neutrons. Thus the fission neutron effect can be subtracted out rather accurately. It is assumed, of course, that the spectrum of fission neutrons does not change appreciably in going from low to high incident neutron energy.

It is thus now possible to obtain the non-elastic cross sections over the whole range in which fast neutron sources are available for all the nuclides which can be obtained in sufficient quantity to make a spherical shell, i.e., if the shells are to be about one mean free path thick on the basis of the total cross section somewhere between 50 and 100 moles of the nuclide will be necessary for a shell having a 4 cm diameter cavity. This precludes the use of most separated isotopes immediately if there should be a desire for such data.

NEUTRON EXCITATION OF NUCLEAR ISOMERS

A method of obtaining inelastic scattering cross sections restricted to particular transitions is to observe the activation cross section for exciting a nuclear isomer with fast neutrons.[13] In this case measurements can be made on very small samples and even separated isotopes, but only a somewhat limited number of nuclides possess isomers. The cross section will generally be less than the total inelastic scattering cross section as measured by sphere transmission since only transitions to the isomeric state are observed, but in some cases, such as Au^{197m}, as much as half the total non-elastic cross section at the higher neutron energies arises from transitions to the 410 kev metastable state.

It is probable that the main advantage of using this method will be in trying to understand the details of low lying levels in the target nucleus for which sphere measurements are not likely to have adequate resolution. However, the method has not been fully explored as yet.

ANGULAR DISTRIBUTION OF ELASTIC SCATTERING

Since the forces of fast monoergic neutrons are approximately points and emit neutrons in all directions, the basic experimental problem to be considered in observing elastically scattered neutrons is to optimize the ratio of scattered neutrons to those coming directly from the source. This is generally done by interposing a moderating or shadow shield between source and detector. In addition, the detector is chosen to have a step function sensitivity near the primary neutron energy, since this will further discriminate against the direct source neutrons at back angles and against neutrons degraded in energy by the shield or by room scattering which is important in assuring that the spectrum of the scattered neutrons is known.

THE SCATTERING GEOMETRIES

Two classes of scattering geometries are in general use, each with its advantages and disadvantages. To have the scatterer in the form of a ring on whose axis lie the source and detector has the advantages of optimizing the amount of scattering material and simplifying the design and use of the shadow shield for the detector. In this case, the shadow shield may be entirely a heavy nuclide and produce its effect primarily by the scattering out of neutrons in the direct beam. A serious disadvantage of this method is that the angular range for obtaining the scattering is severely limited in the backward direction since here the detector must move closer to the source than the scatterer, which makes the shielding problem very difficult. This method[14] has been used by Little at the University of Texas, Coon at Los Alamos Scientific Laboratory, and by Whitehead and Snowdon at Bartol Research Foundation.

The other method[4] in common use at the Oak Ridge National Laboratory, University of Wisconsin, and the Los Alamos Scientific Laboratory by Johnson, Barschall, and Walt, respectively, utilizes small scattering samples around which the detector is rotated. Paraffin wedges are interposed between source and detector to optimize the scattered to background neutron ratio. Major advantages of this method are absence of effects due to source and counter asymmetries and changing distances. Although the geometry of this method is favorable for carrying out a large angular range of measurements, the detector is completely unshielded to room scattered neutrons and often has an unfavorable effect to background ratio. Figure 8 shows a typical geometry set up for measurements at 4 Mev by Walt of the Los Alamos Scientific Laboratory. The detector may be a hydrogen or He-filled recoil counter biased near the primary energy or it may be an organic scintillator for the higher energy measurements.

Since these measurements are not simply transmissions as for the non-elastic cross-section determinations, it is necessary to eliminate the product of the unknown counter sensitivity and the number of neu-

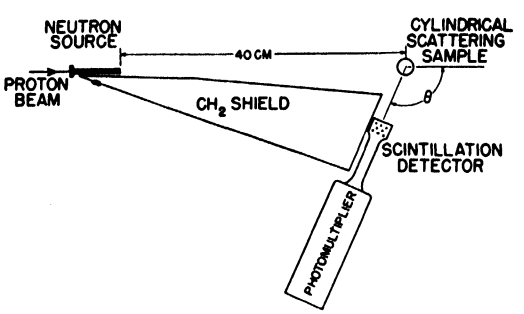

Figure 8. Geometrical arrangement for angular distribution of elastic scattering as used by Walt at 4 Mev

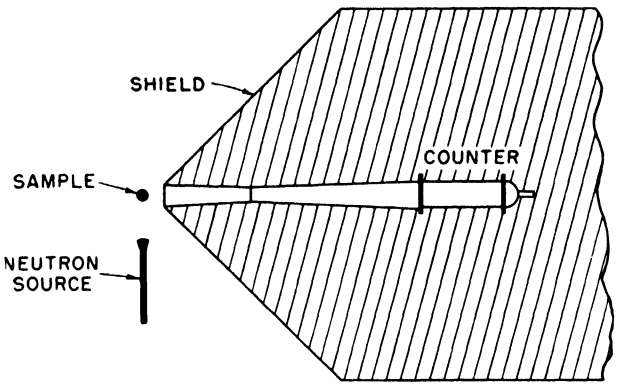

EXPERIMENTAL ARRANGEMENT

Figure 9. Use of shielded proportional counter for obtaining angular distributions of elastic scattering near 1 Mev

trons per cm^2 at the scatterer by making a measurement on the open beam. The uncorrected differential cross section is then given by

$$\sigma(\theta) = \frac{C(\theta) - B(\theta)}{D(0 \text{ degree})} \frac{r^2 d^2}{(r+d)^2} \times \frac{1}{N} \quad (8)$$

where $C(\theta)$ is the counting rate at θ with the sample in place, $B(\theta)$ the same with sample out and $D(0$ degrees$)$ is the open beam counting rate at 0 degrees; r and d are distances from target to scatterer and from scatterer to counter respectively while N is the total number of nuclei in the sample.

Figure 9 shows another method[4] used by Allen, Taschek, and Walton at the Los Alamos Scientific Laboratory. Here the counter, a high pressure hydrogen filled proportional counter is immersed in a shield and collimator tank filled with oil. In this shield the background in the counter from room scattered neutrons is very low and the collimation against the source neutrons is also good. Since the detector is far from the scatterer a high sensitivity is required, which is obtained in this case by operating the six-inch long proportional counter at pressures up to 30 atmospheres of H_2. A real advantage is gained with the counter shield in that the background is materially reduced and the time for obtaining good statistics is reduced. The collimator in the form shown is not quite properly designed since at small angles from the target, the moderating material on the side away from the target gives some in-scattering which could be reduced by a partition which would keep that portion of the collimator empty of oil.

In Fig. 10 are shown sensitivity curves for this counter compared with the equivalent curve if an Np^{237} spiral counter had been used. The pulse-height distribution obtained with this counter is not highly favorable since with the ½ mil wire used, diameter fluctuations as big as 10% were observed in a 15 cm length.

The angular resolutions which have been used in the paraffin wedge geometry are about ± 7.5 degrees Barschall and Walt, ± 4 degrees Walt and Beyster, and those used so far for the shielded counter are ± 3.0 degrees.

The scatterers are cylindrical for the bare counter geometry and can be rather long since all angles are accepted by the counter. In the shielded counter geometry, however, ¾-inch diameter spheres are used for scatterers due to the rather sharply defined collimator aperture. In both cases the scatterers are thick enough so that the incident beam is appreciably attenuated and this effect must be calculated and corrected for. It is also necessary to make a multiple scattering correction which is done analytically. Five cases have been checked by Monte Carlo runs to assure the validity of the analytic solution.

The elastic transport cross section is immediately obtainable from the observed angular distribution by applying Equation 1. Also important is the fact that rather good non-elastic cross sections are obtainable to subtracting the total elastic from the total cross section; the accuracies obtainable are not quite so good as for the sphere method, but if only small amounts of a nuclide are available it may well be possible to use this method and not the sphere method at all. The amounts of material necessary here are only ¼ to ⅓ moles, possibly even small enough to apply to separated isotopes.

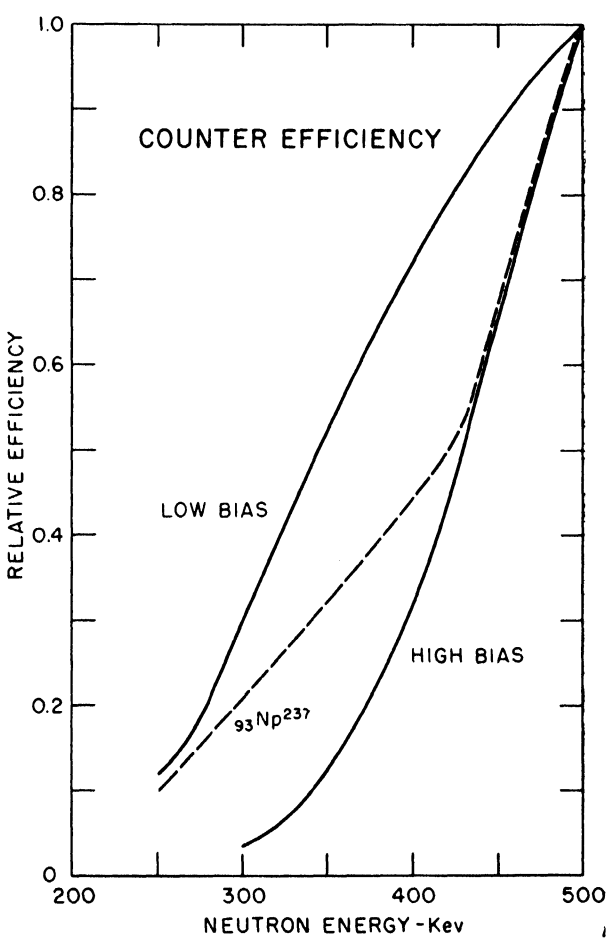

Figure 10. Efficiency of shielded counter at 500 kev compared with Np^{237} spiral counter

APPLICATION TO PILE NEUTRONS

The discussion so far has been concerned only with the use of monoenergetic neutron sources, but some early measurements were made at the Los Alamos Scientific Laboratory with the neutrons from a fast reactor and with the normal fission neutron spectrum. These measurements of both sphere scattering and angular distributions by Zabel and Jurney,[15] Beyster and Carter,[7] were feasible at an earlier time than those using monoenergetic neutron sources because of the high intensity of well collimated neutrons available from reactors. The detectors used in those experiments were fission in Np^{237}, U^{238}, and activation of Mg^{27} in the $Al^{27}(n,p)Mg^{27}$ reaction. No shielding was needed because of the initial collimation from the reactor. Clearly the cross sections measured are averages over the product of the neutron spectrum and the response of the particular detector used, i.e., these average cross sections are most applicable directly to reactor calculations, but have been superseded for many purposes by the measurements made as functions of neutron energy with monoenergetic sources.

NEUTRON SCATTERING ANGULAR ANALYZER

A rather unique device recently put into use by Langsdorf[16] at Argonne National Laboratory measures simultaneously at five angles the intensity of scattered neutrons independent of their energy. The cross section thus determined is

$$\sigma_t(\theta) = \sigma_{el}(\theta) + \sigma_{inel}(\theta) \qquad (9)$$

The experimental arrangement can best be described by referring to the following photographs, Figs. 11 and 12. The source collimator [$Li(p,n)Be^7$ is now used] forms a beam 6 in. × 16 in. high at a scatterer 9 in. wide by 18 in. long, which is thick enough to scatter about 10% of the incident neutrons at the usual 45 degree orientation to the beam. It is 5 feet from source to scatterer and 6 feet from scatterer to detector tank which gives 6 degree resolution at the 3 forward angles and 3 degrees for the two back angles. The pie-shaped shield tanks are oriented at angles of 22 degrees, 54 degrees, 92 degrees, 112 degrees and 144 degrees to the neutron beam and use borated water for shielding; they are 5 feet high, 5½ feet long, 20 inches wide at the front, and 5 feet wide at the back. The collimator hole is rectangular, 6 in. wide by 16 in. high by 36 in. to the internal detector cavity. This detector cavity is a vertical cylinder 21 in. high and contains 10 BF^3 counter tubes immersed in mineral oil. This gives 15% efficiency for neutrons incident on the assembly and the counter has quite a flat response in the Mev region. The arrangement has a very favorable background ratio, i.e., 5% to 10% at 90 degrees and 10% to 20% at 22 degrees the lowest angle. Another favorable aspect of the system is the elimination of various monitoring problems which arise for point-to-point measurements. This is particularly clear when one observes that typical data taking times are (for 16-hour days) 12 elements at 18 energies and 5 angles in 5 days.

Absolute detection efficiencies have been obtained with small Na-γ-D_2O neutron sources. Back scattering corrections must be made particularly for those neutrons which are scattered from the high intensity forward direction to the forward detectors and then into back angle counters where the number of neutrons may be very low due to asymmetry of elastic scattering.

The data from this method of detection should be analyzable into an inelastic angular distribution by using the elastic distributions from other experiments. Rapid data taking and a possibility of pushing errors down into the 2% to 4% region makes it a useful technique also for investigating angular distributions in resonances, and for more applied information such as albedo, transport, and transmission experiments.

The present status of counter measurements bearing on neutron scattering is the following: The total non-elastic (or reaction) cross sections are being accurately measured for most chemical elements as a function of neutron energy up to 14 Mev; the spectra

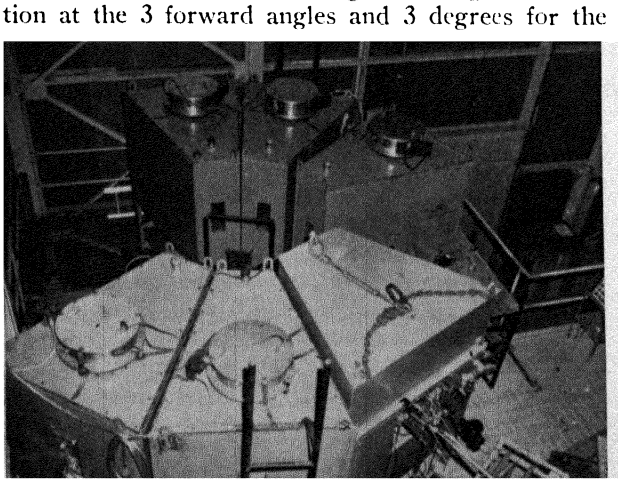

Figure 11. Photograph of arrangement used by Langsdorf to measure total elastic scattering showing neutron beam collimator

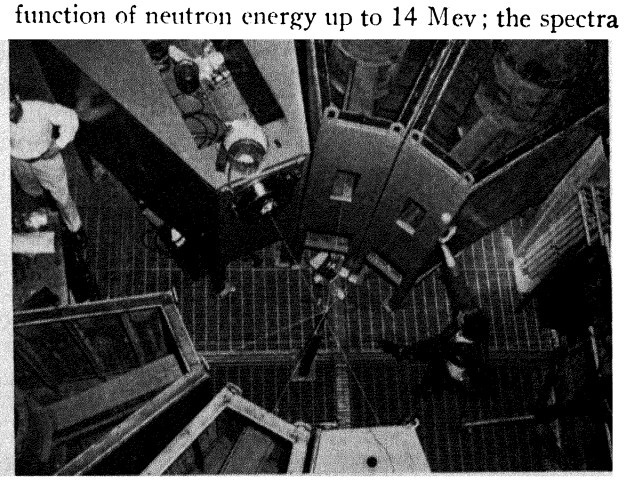

Figure 12. Photograph of arrangement used by Langsdorf to measure total elastic scattering showing location of detector banks

of the inelastically scattered neutrons are known only in those cases where one or a very few levels are excited, i.e., low energies and light nuclei except for 14 Mev neutrons; differential cross sections for elastically scattered neutrons are also being measured for most of the elements and a large number of energies; differential cross sections for inelastic scattering are not yet available, but may be determined from the Langsdorf counter measurements and possibly other techniques.

REFERENCES

1. Rosen, L., Los Alamos Scientific Laboratory, P/582, *Techniques for Measurement of Neutron Cross Sections and Energy Spectra for Sources which are Continuous in Energy and Time,* Volume 4, Session 15A, these Proceedings.
2. Cranberg, L., Los Alamos Scientific Laboratory, P/577, *Time-of-Flight Techniques Applied to Fast Neutron Measurements,* Volume 4, Session 15A, these Proceedings.
3. Gittings, Barschall and Everhart, *Inelastic Scattering of 14.5 Mev Neutrons by Lead,* Phys. Rev. 75: 1610, (1949); Phillips, Davis and Graves, *Inelastic Collision Cross Sections for 14-Mev Neutrons,* Phys. Rev. 88: 600 (1952); Beyster, Henkel and Nobles, *Inelastic Collision Cross Section at 1.0, 4.0 and 4.5 Mev Neutron Energies,* Phys. Rev. *97*: 563, (1955).
4. Walt, M. and Barschall, H. H., *Scattering of 1 Mev Neutrons by Intermediate and Heavy Elements,* Phys. Rev. *93*: 1062, (1954); Johnson, C. H. and Fowler, J. H., *Differential Cross Section for Elastic Scattering of Neutrons from N,* Phys. Rev. *95*: 637(A), (1954); Allen, Taschek and Walton, *0.5 and 1.0 Mev Differential Cross Sections for Elastic Scattering of Neutrons from Fissionable Elements,* Los Alamos Scientific Laboratory (unpublished).
5. Hanson, Taschek and Williams, *Monoergic Neutrons from Charged Particle Reactions,* Rev. Modern Phys. *21*: 635, (1949); Bonner, T. W., Rice Institute, P/578, *Van de Graaff and Cockcroft-Walton Accelerators for Fast Neutron Cross-Section Measurements,* Volume 4, Session 16A.1, these Proceedings.
6. Ennis, M. E. and Taschek, R. F., *Fission Cross Sections of U^{236}, U^{238} and Np^{237},* Los Alamos Scientific Laboratory (unpublished); Henkel, R. L., *Fission Excitation Curves for U^{236}, U^{238} and Np^{237},* Los Alamos Scientific Laboratory (private communication). See AECU 2040, *Neutron Cross Section Compilation.*
7. Carter, R. E. and Beyster, J. R., *Inelastic Collision Cross Sections for Fission Spectrum Neutrons,* Phys. Rev. *90*: 389(A), (1953).
8. Ennis, M. E., *Inelastic Collision Cross Sections of Fissionable Elements,* Los Alamos Scientific Laboratory (unpublished results).
9. Allen, R. C., *Sphere Measurements of Neutron Inelastic Collision Cross Sections,* Phys. Rev. *95*: 637(A), (1954).
10. Walt, M. and Beyster, J. R., Los Alamos Scientific Laboratory, (private communication).
11. McCrary, Taylor, and Bonner, *A Fast Neutron Counter with Energy Resolution,* Phys. Rev. *94*: 808(A), (1954), and Private Communication from Bonner, T. W.
12. Bethe, Beyster and Carter, *Inelastic Collision Cross Section Measurements for Fission Spectrum Neutrons,* Unpublished Los Alamos calculations.
13. Martin, Diven and Taschek, *Cross Sections for Production of In^{115m} and Au^{197m} by Inelastic Scattering of Neutrons,* Phys. Rev. *93*: 199, (1954); Ebel, A. A. and Goodman, C., *Inelastic Scattering of Neutrons by In^{115} and Au^{197},* Phys. Rev. *93*: 197, (1954); Stelson, P. H. and Campbell, E. C., *Cross Section for Excitation of Pb^{207m} by Inelastic Scattering of Neutrons,* Phys. Rev. *97*: 1222, (1955).
14. Little, Cadenhead, Leonard, Prud'homme, Vincent and Wills, *Angular Distribution of D(d,n) Neutrons Scattered from C, Al, S, Fe, Cd, Cu, W, and Pb,* Phys. Rev. *94*: 807(A), (1954); Whitehead, W. D. and Snowdon, S. C., *Angular Distribution of Neutrons Scattered from Aluminum, Iron and Lead,* Phys. Rev. *92*: 114, (1953); Coon, J. H. and Davis, R. W., *Elastic Scattering of 14 Mev Neutrons,* Phys. Rev. 94: 785(A), (1954) and private communications.
15. Jurney, E. T. and Zabel, C. W., *Scattering of Fast Neutrons,* Phys. Rev. *86*: 594(A), (1952).
16. Langsdorf, A. and Lane, R. O., *Angular Distributions of Scattering of Moderate Energy Neutrons,* Bull. Am. Phys. Soc., Vol. *30*, No. 3, Paper F 3 (1955) and private communications from Langsdorf, A.

A Review of Pile Neutron Spectrometer Work at Harwell

By P. A. Egelstaff,* UK

The study of the nuclear interaction of neutrons has, from the time of the discovery of the neutron till the availability of intense neutron beams from nuclear reactors, on the whole, been restricted to the high energy region of the order of 1 Mev neutron energy and to very low energies of a few electron volts and below. The simultaneous development of neutron bursts, energetically heterogeneous, either from pulsed neutron sources associated with accelerators or mechanically produced from the intense beams emerging from reactors has opened the energy region 10 to 10^5 ev. In addition, these developments and the use of intense monokinetic beams have transformed the field below 10 ev, and at the present moment both these fields are still changing and enlarging their scope very considerably. In this paper we shall review the current developments in the techniques and uses of neutron spectrometers based on the Harwell research reactors, but first we shall outline the theory of time-of-flight and crystal spectrometers in order to illustrate some of the considerations that arise in the design of these spectrometers.

TIME-OF-FLIGHT SPECTROMETERS

The general principle of the time-of-flight method is to form a neutron pulse of mean duration t_1, and allow a detector placed at a distance, r, from the source to record the events (capture, fission, scattering) in order of the time of arrival of the neutron inducing the process considered. In practice it is convenient to record into a sequence of "time channels" each of length t_2, opening after a given flight time.

The first precaution which must be taken is to avoid overlapping in time of the neutron pulses. Thus if V_1 and V_2 are the velocities of the fastest and slowest neutron in the pulse and p is the pulse repetition frequency, we must have:

$$\frac{r}{V_2} - \frac{1}{p} \leqslant \frac{r}{V} \leqslant \frac{r}{V_1} + \frac{1}{p} \qquad (1)$$

where V is the velocity of the neutrons we wish to detect. The counting rate is readily calculated[1] and is given by:

$$\frac{N(T) \cdot \Omega \cdot \epsilon V \cdot p t_1 t_2}{r} \qquad (2)$$

where $N(T)\,dT$ is the number density spectrum of neutrons in the source, $T = 1/V$, and Ω is the fractional solid angle subtended by the detector at the source and may depend upon collimators, and ϵ is the detector efficiency for neutrons of velocity V. The resolution is defined as the fractional uncertainty in the time-of-flight T, and is equal to the sum of the fractional uncertainties in time and distance, viz:

$$\frac{\Delta T}{T} = \frac{t_1 + t_2 + t_3}{Tr} + \frac{\Delta r}{r} \qquad (3)$$

The quantity t_3 includes timing uncertainties in the detector and the electronic equipment and can usually be made smaller than the $t_1 + t_2$, and Δr includes uncertainties in the points of origin and detection of the neutron.

It is usual to operate a time-of-flight spectrometer such that the best resolution for a given source strength and counting rate is obtained. This condition is satisfied for various circumstances as follows:

1. Because of the symmetry of t_1 and t_2 in Equations 2 and 3 they are made equal.
2. If $\Omega \propto 1/r^2$, then t_1 and t_2 are made as small as possible with proportional reduction of flight path.
3. If due to collimation $\Omega \propto 1/r$, then all values of t_1 and r give same result, so that any values are used.
4. If Ω is independent of r, then largest values of t_1 and r are used.
5. For the points (2) to (4) it is assumed that $\Delta r/r$ is small compared to the timing uncertainty, and that p is independent of t_1. When the former condition is not true it is best to keep the distance and timing uncertainties roughly equal. In the actual operation, as distinct from the design, of "choppers" the product pt, is constant, so that r could be increased as p is decreased.
6. For the slowing down spectrum (i.e., $N(T)$ constant) and $\epsilon \propto 1/V$ the counting rate is independent of velocity so that one flight path is used for the whole velocity spectrum.
7. For the slowing down spectrum and ϵ constant, the counting rate increases with V for fixed r, and thus the flight path should be increased as $V\Omega$.

At the present time many of these theoretical requirements are invalidated for practical reasons, thus there is a practical minimum to t_1 and t_2 of about 0.2 μsec and at that point t_3 may be important. There are also physical limitations on r, Δr and Ω, so that in many cases the design of a spectrometer may de-

* Atomic Energy Research Establishment, Harwell, Berks, England.

pend as much upon these factors as the theoretical ones.

CRYSTAL SPECTROMETERS

In the operation of the neutron crystal spectrometer a collimated beam of neutrons from a nuclear reactor is allowed to fall on a single crystal, and neutrons with wavelengths (λ) which satisfy the Bragg relationship:

$$\lambda = 2d \sin (\theta/2) \qquad (4)$$

are reflected. (d is the spacing of a given set of planes in the crystal and θ is the angle between the incident and reflected beams.) The resolution of the instrument depends upon the uncertainty in the angle θ, and this is equal to the sum of the divergence (α) of the collimated neutron beam and the mosaic spread (η) of the crystal. This uncertainty is independent of θ, and since in most practical cases $\sin \theta/2 \cong \theta/2$, the uncertainty ($\Delta\lambda$) in wavelength is a constant. A neutron's wavelength is directly proportional to its time-of-flight and therefore this relation is the same as the relation of Equation 3 for cases when $\Delta r/r$ is small.

The counting rate of the crystal spectrometer is proportional to:

$$\frac{N(\lambda)\Omega \cdot \epsilon \cdot R}{\lambda} \qquad (5)$$

with the previous notation. R is the reflectivity of the crystal and when extinction is negligible it is proportional to λ^2. This holds generally in the resonance region, so that for a slowing down spectrum and a detector efficiency proportional to λ (i.e., $1/V$) the counting rate varies as λ^2, in contrast to the constant counting rate of the time-of-flight spectrometer under these conditions. Also since α is proportional to Ω, it is desirable to make the mosaic spread less than α in order to obtain the best resolution for a given counting rate.

On the other hand when extinction is very great R is proportional to η. This holds usually for neutron wavelengths > 2 Å, so that for ϵ proportional to λ the counting rate is proportional to the density spectrum $N(\lambda)$. Moreover η and α are then symmetrical in the resolution and counting rate formulae (as with t_1 and t_2 for the time-of-flight spectrometer) so that it is best to make them equal in this case. The reflectivity R also contains the crystal structure factor, the thickness of the crystal and other factors and is discussed in detail by Bacon and Lowde.[2]

Again practical difficulties often decide the design of the spectrometer. Thus the mosaic spread of a crystal cannot be selected at will, neither can the spacing d. The thermal vibrations of the lattice lead to very weak reflections from the smallest interplanar spacings and preclude high resolution work. A beryllium crystal is found to be the best for resonance region studies, while crystals of Pb, Cu, CaF_2, etc., are satisfactory for work with thermal neutrons.

SPECTROMETER STUDIES AT HARWELL

For nuclear data studies at Harwell we have two crystal spectrometers, a "slow chopper" and a "fast chopper" in operation with the research reactor B.E.P.O. The total and fission cross sections of uranium and plutonium isotopes and the neutron yields per fission have been measured with these instruments, and we will describe briefly the manner in which they have been used for this work. It is assumed that the reader is familiar with the idea of a "chopper" as a device for artificially modulating the neutron beam from a reactor for time-of-flight measurements. A chopper usually consists of a disc or cylinder with a number of slits cut in it and is rotated in the neutron beam.

The Harwell slow chopper[1] provides a relatively large neutron beam (the cross-sectional area of which may be chosen arbitrarily in the range 1 to 50 cm^2) and consequently samples with relatively large area must be used. With abundant materials or rare materials with a large cross section this condition is easily satisfied, and thus measurements on most materials of interest are possible with this spectrometer. The total cross sections are determined from the attenuation of the neutron beam by a specimen, while fission cross sections are determined from the ratio of counts in a fission chamber to that in a boron foil ionisation chamber. The efficiency of the latter is determined relative to the activity induced in a gold foil in a separate experiment. The energy range covered by the slow chopper is about 10^{-3} to 0.2 ev, although the actual energy range covered in any experiment is fixed by the individual requirements.

The chopper is not so useful for neutron yield experiments because of the problem of the detection of fast neutrons from fission. Apart from the very low energy region ($< 5 \times 10^{-3}$ ev) the detector of a time-of-flight spectrometer must detect neutrons within a few micro-seconds of their arrival. Thus if we place a block of fissile material at the position normally occupied by the detector of the slow chopper and wish to detect the neutrons from fissions caused by slow neutrons of a given velocity, we cannot afford to moderate the fission neutrons before detecting them. This means that we must accept, in this type of experiment, the fairly low detection efficiencies of prompt fast neutron detectors.

In contrast, we can moderate the fission neutrons if the same experiment is carried out on the crystal spectrometer, since it provides a monokinetic neutron beam. Consequently the measurement of the number of neutrons from fission and the number of neutrons per neutron absorbed in fissile material have been studied at Harwell using a crystal spectrometer. In addition to this advantage the crystal spectrometer has a useful energy coverage for this type of experiment, since generally speaking one can cover the range from the thermal region to the lowest resonances (say 0.05 to 5 ev). Also total and fission cross-section measurements have been carried out on the crystal spectrometers using the same techniques

as for the slow chopper measurements. The combined slow chopper and crystal spectrometer data cover the thermal and epi-thermal neutron energy range of most interest in the design of thermal reactors.

In some cases the data obtained in the above manner is not complete because the size of the specimen is too small. This occurs in fission cross-section measurements because only a limited amount of material can be used in the fission chamber due to the need to limit the number of the "build-up" pulses from the natural radioactivity of the material. To some extent the latter difficulty can be overcome by using several amplifiers connected to different areas of the fission chamber, or by altering the technique to that of measuring the fission cross section through the detection of the fission neutrons. At the present time however it has been possible to complete the low energy fission cross-section work and also to extend it to higher energies through the use of the linear accelerator pulsed neutron source, so that we have not yet developed these techniques. On the other hand the need for the measurement of the total cross sections of small samples is met by the "fast chopper".

The term "fast chopper" is used to indicate that the chopper will work with neutrons with energies greater than about 0.5 ev. The Harwell "fast chopper" has been designed to operate over the neutron energy range 10^{-2} to 10^{5} ev, and use a neutron beam of cross-sectional area of $\frac{1}{8}$ cm^2. Consequently it is better called a "small beam chopper"; the small size of the neutron beam it uses arises simply because it is a "one slit per pulse" instrument. This is in contrast to the conventional "slow chopper" which allows many slits to open per neutron pulse. If the number of slits in the chopper is small then they can be shaped so that the detector can see the whole of the neutron source at the reactor centre, but if a large number of slits is used then the neutron beam will be severely collimated by the chopper.

For small sample work the specific neutron intensity at the sample must be high, thus the "small beam chopper" is useful for transmission measurements but not for fission or scattering cross-section measurements because its specific neutron intensity at the detector is very low. For those measurements it is better to design a large beam chopper which allows many slits to open per neutron pulse.

The Harwell "small beam chopper" has been used for the measurement of the total cross sections of uranium and plutonium isotopes over the thermal and intermediate energy ranges. However its usefulness as a small sample instrument is particularly apparent when working with highly radioactive materials. For example, the present programme on the chopper includes the measurement of the cross section of two samples of fission product caesium each of about 4 curies activity only.

THE FUTURE HARWELL PROGRAMME

At the completion of the current nuclear data programme on the uranium and plutonium isotopes, it will be necessary to consider the measurement of the cross sections as a function of neutron energy of transplutonic isotopes and of fission products. Many of these isotopes will be available only in very small quantities and will be highly radioactive. The problems therefore are ones of handling and preparation of the samples and of sample protection during the measurements. The spectrometers used in this field, in addition to being designed to work with small samples, must incorporate suitable features for dealing with these problems.

At Harwell the new research reactor (E.443) will greatly facilitate both the manufacture of sample material and the actual measurements. Three spectrometers are being designed for small sample work with this reactor, and we will describe briefly their construction.

First a Cauchois-type bent-crystal spectrometer, using a beryllium crystal bent to 1 m radius, and providing a neutron beam $1\frac{1}{2}$ in. $\times$ 0.1 in. at the detector is being built. This instrument will be used for fission and scattering cross-section measurements, and since the detector must be placed near the sample only moderate levels of activity can be tolerated. In this case the handling problems will not be difficult.

Secondly measurements of the total cross sections of high activity samples will be made with two choppers. Since the flux of thermal neutrons is so high and the resolution of the spectrometer in the thermal region need not be too high, it is better to design a small beam chopper specifically for the energy region below 1 ev. The samples for this chopper will be placed in tubes of 0.5 mm bore which will form part of the collimator. The chopper will be a single slit rotor with a slit width of about 1 mm so that the beam is collimated only by the sample tube. The sample has to be protected from the rotor in case of a rotor failure, and this is achieved by placing a steel can around the rotor which is free to rotate across the beam if touched by a disintegrating rotor. The detection limit on this equipment will be about 0.01 mm^2 macroscopic cross section. Thus if we are studying an isotope of atomic weight 150 and we have a 1 mg sample the detection limit will be 25 barns.

The third spectrometer is a fast chopper of new design. The "chopper" will consist of two single slit rotors which are placed in line in the neutron beam. A phase lag is introduced into the system so that a pulse transmitted by the first rotor is transmitted by the second rotor a time, t, later. Thus if the distance between the rotors is x, only neutrons with velocities in the neighbourhood of x/t can pass through both rotors. In this way one obtains a neutron pulse containing only a certain band of neutron velocities, and accurate selection of velocities within this band will be carried by the usual time-of-flight technique over a 100 m flight path. Thus we may allow a number of pulses to be travelling down the flight path at the same time since by appropriate choice of the velocity band width they will not overlap [see condition (1)], and consequently one obtains a high resolution with-

out a great loss in intensity. Additional advantages of this system compared to a single rotor are that the chopping speed is twice as fast, the background can be measured directly by reversing the rotors and the manufacture of the rotors is easier because they are smaller. The disadvantage is that the phase lag has to be controlled accurately.

The samples used with this spectrometer will be placed in an armour steel tube between the rotors, and again the rotors will be housed in rotatable steel cans. The whole will be placed in a concrete house so that samples of up to 1000 curies may be used.

REFERENCES

1. Egelstaff, P. A., *The Operation of a Thermal Neutron Time-of-flight Spectrometer,* J. Nuclear Energy *1,* 57 (1954).
2. Bacon, G. E. and Lowde, R. D., *Secondary Extinction and Neutron Crystallography,* Acta Cryst. *1,* 303 (1948).

Pulsed Accelerator Slow Neutron Velocity Spectrometers

By W. W. Havens, Jr.,* USA

All existing charged-particle accelerators used for slow neutron velocity spectrometry operate on the principle of producing short bursts of neutrons which are timed over a known distance to give neutron velocity and hence the energy. In some cases, the accelerator inherently produces bursts of charged particles, in others an external modulation is imposed. In all cases the charged-particle bursts strike suitable targets to produce short bursts of neutrons which are moderated in hydrogenous media to produce the desired slow neutrons.

The first pulsed accelerator neutron velocity selector was the 36-in. Berkeley cyclotron. Alvarez[1] modulated the output of the cyclotron by supplying the plate voltage of the oscillator with half wave rectified but unfiltered 60-cycle high voltage. Since the efficiency of the cyclotron decreases rapidly with decreasing dee voltage, most of the beam which was accelerated was confined to the time when the dee voltage was near the peak. By placing the detector at different distances from the paraffin surrounded target, the effects of neutrons of different velocities could be studied. This velocity spectrometer was limited to energies below 0.025 ev. The "on time" was 20 per cent of the cycle, which represents relatively poor resolution but eliminated the fast neutron background that had been one of the major limitations of the mechanical chopper built by Dunning, Pegram, Fink, Mitchell and Segre.[2]

Another pulsed neutron source was constructed by Fertel *et al.*[3] who modulated the ion source of a Cockcroft-Walton generator. The counts on a distant detector were recorded on an oscillograph as a function of the time after the neutron burst. The results obtained with this arrangement were not completely satisfactory because of the very low intensities obtained. Unfortunately, improvements in this accelerator were halted by conditions beyond the control of the experimenter.

Good results using a modulated Cockcroft-Walton accelerator were obtained by Manley, Haworth and Luebke[4] by deflecting the deuteron beam to strike a heavy ice target to produce very short neutron bursts. The timing circuits allowed for wide flexibility and several experiments were performed.

The method of modulating the ion source used by Fertel *et al.*[3] was applied to the Cornell cyclotron by Baker and Bacher.[5] Timed bursts of neutrons of 50 to 100 microseconds duration could be produced with a 2500-microsecond repeat time. Relatively good resolution was obtained and the first results on nuclear resonance levels using this type of spectrometer were reported. The apparatus was later rebuilt, expanded, and many further results published.[6] However, because of the low energy deuteron beam available with this cyclotron (1.5 Mev) the source strength was at least an order of magnitude less than that available with other accelerators and no results have been reported recently.

The operation of the Columbia 36-in. cyclotron and the Brookhaven 60-in. cyclotron slow-neutron-velocity spectrometers, which will be described in more detail later, is essentially the same as that of the Cornell spectrometer.

RESOLUTION AND COUNTING RATE

The design of a velocity spectrometer is affected by many factors, some of which depend on the experiments to be performed, while others depend on the type and characteristics of the accelerator with which the spectrometer is used. The advantages of pulsed accelerators for use as velocity spectrometers are (*a*) the accelerator is not producing neutrons while the neutrons are being counted so that the background is low; (*b*) the pulse of neutrons produced by the accelerator can be made extremely short because electromagnetic, rather than mechanical, changes are involved; (*c*) the production is restricted to a well-defined time interval.

Those properties of the neutron which are pertinent to velocity spectrometer design are listed in Table I.

The resolution of the apparatus depends on the duration of the neutron pulse, the moderation time, the duration of the detector modulation pulse, and the distance from moderator to detector. The resolution that can be obtained with any time-of-flight instrument is theoretically infinite since, in principle, the detector can be placed very far from the source. In practice, of course, the intensity available limits the resolution, since as the source detector distance increases, the intensity per burst at the detector decreases rapidly because of the increased distance and

* Columbia University. Including work by C. P. Baker, J. E. Draper, Brookhaven National Laboratory; L. J. Rainwater, L. Lidofsky, G. Grimm, Columbia University; E. R. Gaerttner, M. L. Yeater, General Electric Company; W. F. Good, E. C. Smith, J. H. Neiler, H. E. Banta, Oak Ridge National Laboratory; and H. L. Schultz, W. G. Wadey, Yale University.

Table I. Fundamental Relations Important in the Velocity Spectrometer Design

E	1 Mev	0.1 Mev	0.01 Mev	1000 ev	100 ev	10 ev	1 ev	0.1 ev	0.01 ev	0.001 ev
V in meters/second	1.38×10^7	4.38×10^6	1.38×10^6	4.38×10^5	1.38×10^5	4.38×10^4	1.38×10^4	4380	1384	438
Microseconds/meter	0.0723	0.229	0.723	2.29	7.23	22.9	72.3	229	723	2286
Collisions required to cascade from 7 Mev	2	4	7	9	11	14	16	18	21	23
Assumed mean free paths	4	1.3	0.8	0.7	0.7	0.7	0.7	0.4	0.2	0.2
Microseconds required to cascade from 7 Mev	0.005	0.01	0.03	0.06	0.2	0.7	2	4	9	20

because a slower repetition rate is needed to eliminate the overlap of neutrons from the previous bursts.

The moderation time depends on the energy of the neutrons as shown in Table I. This moderation time is always a small fraction of the time required for the neutron to travel one meter and can be considered equivalent to an uncertainty in the neutron path length of 2 to 3 cm for a 1- to 1000-ev neutron. The effective increase in path length for a paraffin source enclosed in a plywood box has been measured by the Columbia group[7] and found to be 3 cm, which is in good agreement with the results obtained from the theory of Groenewald and Groendijk.[8]

The counting rate per channel in a neutron velocity spectrometer is determined by the peak neutron intensity, the repetition rate of the accelerator, R, the time duration of the neutron burst, τ_s, the efficiency of the moderator, ϵ_m, the collimation, the source detector distance, d, the size of the detector, A, the time duration of the detector pulse, τ_d, and the efficiency of the detector. The efficiency of the moderator is usually governed by the geometry of the accelerator. For maximum efficiency, the moderator should be as close to the neutron source as possible.

When the area of the detector is small compared with the area of the neutron beam, the counting rate is given by the formula

$$N = \frac{k \cdot I \tau_s \tau_d A R}{d^2}$$

where the constant k includes the moderator, collimator and detector efficiencies, and all numerical factors.

For measurements above 0.5-ev neutron energy, the repetition rate of the accelerator, where it is at the disposal of the experimenter, is determined by the time-of-flight at which cadmium reduces the intensity to almost zero by resonance absorption so that overlap of successive cycles may be avoided. The peak of this resonance occurs at 175 microseconds per meter. This means that the time between bursts must be greater than about $150d$, or $R = 6700/d$, where d is in meters, when cadmium filtering is used. When the repetition rate of the accelerator is fixed, the path length that can be used must be equal to or less than that given by the above relationship.

To obtain a relationship between the counting rate and the resolution, we define the resolution, Δt, of an ideal velocity spectrometer as

$$\Delta t = \frac{\tau_s + \tau_d}{2d}$$

For many velocity spectrometers it is most efficient to use $\tau_s = \tau_d$, in which case we have

$$N = \text{const} \frac{(\Delta t)^2}{d}$$

where the constant now also includes the pertinent factors for a particular apparatus. This shows that there is a definite advantage to working at small distances. Of course, the other problems encountered become more difficult. As the distance decreases, the electronic circuits must be made faster and the background increases. Further, the resolution width is increased because of the uncertainty in the distance caused by the moderation of the neutrons and the position in the detector at which the neutron is detected.

In other velocity spectrometers, the burst time is negligible compared to the detector gate time. In this case

$$\Delta t = \frac{\tau d}{2d}$$

and the counting rate dependence on the resolution width and source detector distance is

$$N = \text{const} \frac{\Delta \tau}{d^2}$$

Here a much greater advantage is gained by using shorter distances.

If the beam is well-collimated so that the detector is always larger than the area of the beam, then the counting rate does not fall off as the inverse square of the distance. For the case in which the burst width is equal to the detector width, there is a definite advantage to using longer distances since $N \propto (\Delta \tau)^2 d$. In the case where the burst time is negligible, the counting rate is independent of distance. This means the distance to be used should be as large as is practical to minimize other problems.

The characteristics of the pulsed neutron velocity spectrometers now operating in the United States are given in Table II. In the last column the best resolution achieved, defined as $\Delta t = \frac{\tau_s + \tau_d}{2d}$, is given.

The resolution width of the apparatus is actually very difficult to determine since there are so many

Table II

	Particle accelerated	Particle energy in Mev.	Current in the pulse at target	Target	Peak neutron intensity in the burst	Source time duration τ_s	Detector time duration τ_d	No. of channels in time analyzer	Time between bursts in μ sec	Source detector distance d	Resolution attained with $\Delta t = \frac{\tau_s + \tau_d}{2d}$
Columbia University pulse transformer accelerator	H^2	0.40	10 ma	H^3 Zr	3×10^{12}	1 μ sec	0.5–512 μ sec	64	10^4–10^5	3	0.5
Columbia University 36-in. cyclotron	H^2	8	3 ma	Be	6×10^{13}	0.5–512 μ sec	0.5–512 μ sec	64	512–32,728	6	0.33
Brookhaven 60-in. cyclotron	H^2	21	1.2 ma	Be	3×10^{14}	1.2 μ sec	0.5–512 μ sec	64	512–32,728	4.3	0.2
Yale electron accelerator	e	5	40 ma	Be	3×10^{12}	0.1–2 μ sec	0.1–2 μ sec	500	10,000	5 or 15	0.4
General Electric betatron	e	100	30 ma	U	$> 10^{15}$	0.1 μ sec	0.2 μ sec	200	16,667	7 or 20	0.01
Columbia University synchrocyclotron	H^1	380	300 ma	W	$> 10^{17}$	0.05 μ sec	1–256 μ sec	256	16,667	35	0.014
Oak Ridge Van de Graaff	H^2	2.5	50 μa	Li	5×10^8	< 0.01 μ sec	< 0.01 μ sec	100	2	0.8	0.013

factors involved. A good measure of the resolution width is the ability of the apparatus to resolve two closely spaced levels. The results obtained with each of the velocity selectors with the best resolution achieved is given in the section on the particular apparatus.

For accelerator velocity spectrometers, the logical resolution width to give is the full width of the resolution function at the base. A complete discussion of these factors has been given in the literature.[9] Because other types of velocity selectors do not cut off as cleanly as those which depend on the modulation of charged particles, it has become customary to give the full width of the resolution function at half maximum. The full width at the base of the triangle for pulsed accelerator velocity spectrometers cannot be compared directly with the full width of the resolution curve at half maximum for the other type of velocity spectrometer. The resolution width is given in the last column of Table II. Although it is not exactly equal to the full width of the resolution curve at half maximum, it is a more reasonable basis for comparison between accelerator velocity spectrometers and other types.

NEUTRON SOURCE INTENSITY

The neutron intensity in the burst is determined from the energy and current of the charged-particle beam and the particular type of nuclear reaction used for the production of the neutrons. Since the neutron intensity is directly proportional to the current in the burst, this factor need not be considered further.

Very few data on the production of neutrons in thick targets as a function of the energy of the incident charged particle are available in the literature, since yield measurements are difficult to make and cannot be readily interpreted in terms of fundamental nuclear constants. In the energy region below a few Mev, the total neutron yield of a thick target can be determined from the cross section integrated over the energy spectrum of the particle as it is slowed down in the target. The dominant factors determining the yield are the ionization loss and the coulomb barrier. Since both the ionization loss and the coulomb barrier rise with increasing Z, light nuclei are favored. In practice, the only targets which need be considered for the production of neutrons by protons and deuterons below 50 Mev are deuterium and tritium, their compounds, and beryllium.

The total cross section for the production of neutrons in the $D(d,n)\mathrm{He}^3$ reaction[10] as a function of energy is given in Fig. 1. For low energy deuterons it is impractical to use a gas target because the thickness of the foil required to contain the gas degrades the energy of the charged particle beam by an amount which greatly decreases the neutron production. Most of the neutron work using this reaction has been done with heavy ice targets or deuterium adsorbed on a metal such as zirconium or tantalum. The production of neutrons as a function of the energy of the incident deuteron in a thick, heavy ice

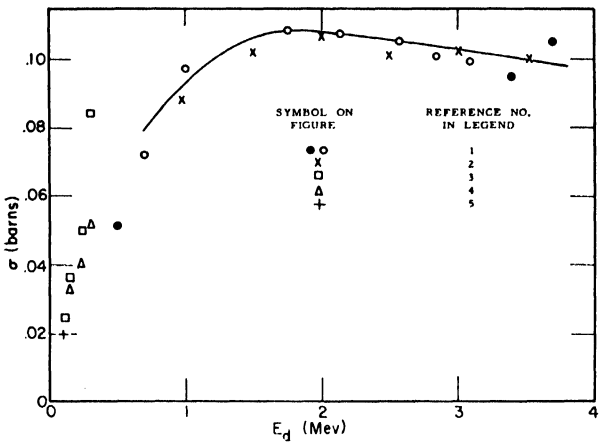

Figure 1. The total cross section vs energy for the $H^2(d,n)He^3$ reaction: (1) Hunter and Richards (H78); (2) Blair, Freier, Lampi, Sleator, and Williams, Phys. Rev., *74*, 1599 (1948); (3) Manley, Coon, and Graves, Phys. Rev., 70, 101(A) (1946); (4) Graves, Graves, Coon, and Manley, Phys. Rev. 70, 101(A) (1946); and (5) Bretscher, French, and Seidl, Phys. Rev., *73*, 815 (1948)

target as given by Hanson, Taschek and Williams is shown in Fig. 2 up to an energy of 1 Mev.

Above about 1.5 Mev the cross section does not change appreciably with energy, as can be seen from Fig. 1. If we assume that the cross section is constant, the calculation of the neutron production reduces to that of a target penetration problem. Since the energy loss is about proportional to $1/E$, the yield should be approximately proportional to E^2.

Actually, since the cross section decreases as the energy increases, and since the energy loss is a more complicated function than $1/E$, the yield should probably increase with energy somewhere between $E^{1.5}$ and E^2.

For very low energy particles, H^3 gas or H^3 adsorbed on zirconium serve as excellent targets for neutron production when bombarded with deuterons. The existence of the resonance at 124.3 kev with peak cross sections as high as 4 barns makes it possible to get extremely large numbers of neutrons at low bombarding energies. The cross-section curve for this reaction is shown in Fig. 3. The thick gas target yield for 600 kev deuterons is reported[10] as 5×10^8 neutrons per microcoulomb. The production of neutrons by 250 kev deuterons on deuterium and tritium-impregnated zirconium targets has been measured, by Coon *et al.*,[11] as a function of the number of microampere-hours bombarding the target with the results shown in Fig. 4.

For energies of heavy charged particles above a few Mev, beryllium is probably the best target to use because of its excellent mechanical properties. A thin sheet of beryllium is soldered to a large block of copper, which is water-cooled so that the target can withstand bombardment with several kilowatts of beam power without adverse effects. In the Columbia 36-in. cyclotron, a beryllium target prepared in such a manner has sustained up to 5 kw of beam power concentrated on an area less than 5 square millimeters.

Below about 1.8 Mev the neutron production in beryllium is fairly low because of the coulomb barrier. Above this energy, however, the cross section should be approximately constant and the yield should follow the $E^{1.5}$ to E^2 dependence. Smith and Kruger[12] report the yield of neutrons from 10 Mev deuterons on a thick beryllium target as 3.7×10^{10} neutrons per microcoulomb. Allen, Nechaj, Sun and Jennings[13] have measured the fast neutron yield at 15 Mev and report 1.9×10^{10} neutrons per microcoulomb. The discrepancy between these two numbers probably arises from the fact that in the 10 Mev measurements neutrons of all energies were counted, whereas for the 15 Mev deuterons the results apply only to those neutrons which are capable of exciting the $S^{32}(n,p)P^{32}$ reaction which was used as detector.

For protons and deuterons well above 50 Mev, the ionization loss gradually ceases to be the predominant factor in the yield since the energy lost by a nuclear collision approaches the energy lost by ionization. If we assume that about half of the energy of a proton goes into ionization and, on the average, half of the particles produced in a spallation reaction are neutrons, then from energy considerations alone about 40 to 50 Mev would be required per neutron produced. For 350–400 Mev protons several neutrons are produced per incident proton. Although no absolute measurements of the number of neutrons produced by high energy protons have been reported, rough measurements of the strength of the neutron source using the 400 Mev synchrocyclotron of Columbia University indicate more than one neutron is produced per proton.

The feasibility of using a high energy electron accelerator as a neutron velocity spectrometer was first pointed out by Cockcroft, Duckworth and Merrison.[14] These accelerators are naturally pulsed and have exceedingly high currents in the pulse. Using a 3.2 Mev electron linear accelerator which had a current pulse of 100 milliamperes and a pulse width of 2 microseconds, a lead target was bombarded to produce gamma rays. The gamma rays were used to produce the neutrons using the (γ,n) reaction in heavy water and beryllium. This arrangement gave a neutron intensity of 3×10^{12} neutrons per second

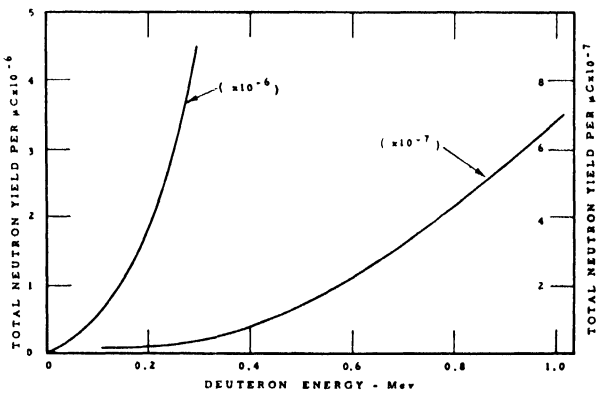

Figure 2. The total yield of neutrons from a thick ice target of D_2O as a function of the incident deuteron energy

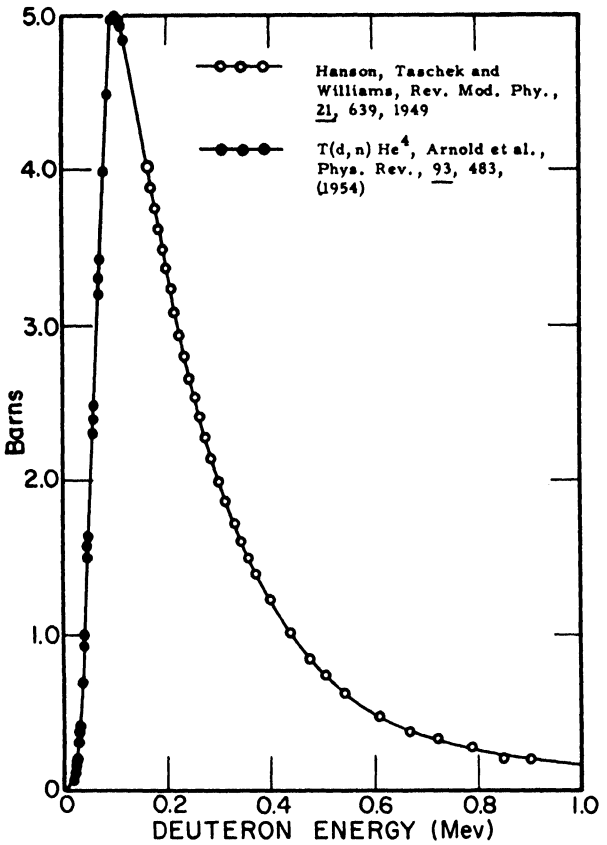

Figure 3. The total cross section for the T(*d*,*n*)He^4 reaction

in the burst. Using the new Harwell linear accelerator, Wiblin[15] reports that with an output energy of 13 Mev and a current pulse of 35 milliamperes the production during the burst is 10^{14} neutrons per second when the electrons strike a thick uranium target.

The existence of the giant (γ,n) resonances above 10 Mev in a large number of nuclei[16] means that almost any target can be used for the copious production of neutrons above this energy. Uranium seems to be best, since the (γ,n) resonance occurs at about 11 Mev[17] which is lower than most of the other (γ,n) resonances and in addition the $(\gamma,\text{fission})$ resonance exists which increases the neutron production.

The problem of determining the thick target yield from the total (γ,n) cross section as a function of the energy of the incident electron is difficult because of the uncertainty in the bremsstrahlung spectrum. Feld[18] has given a simple theory for this process which when applied to the data of Duffield and Huizenga gives the curve shown in Fig. 5 for the energy dependence of the yield per electron in a thick target.

The production of neutrons as a function of the energy of the incident electron in a thick uranium target has been measured by Baldwin, Gaerttner and Yeater[19] using the G. E. betatron with the results shown in Fig. 6. To determine the number of neutrons produced, they measured the activity induced in a rhodium foil surrounded by paraffin. The activity of the rhodium foil is plotted as a function of the energy of the incident electron.

Above about 25 Mev, where shower theory should hold for uranium, the neutron production is expected to increase linearly with energy as indicated by the dashed curve in Fig. 6. Above 80 Mev the deflector system in the G. E. betatron is not capable of deflecting all of the beam into the target and consequently the neutron production falls off. This fall-off is not a characteristic of the production process but is due to the character of the G. E. betatron.

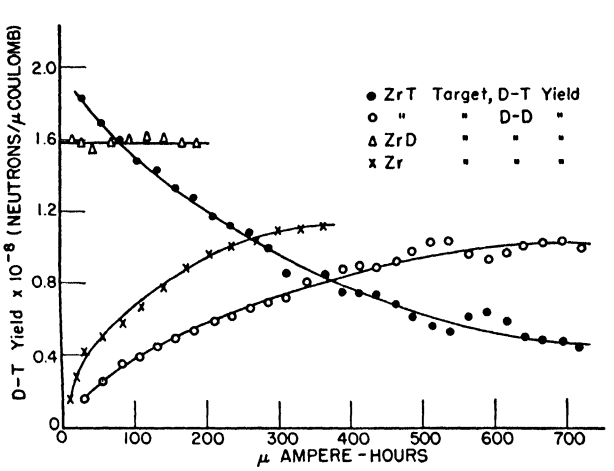

Figure 4. Neutron yield vs μa-hours for 250 kev deuterons

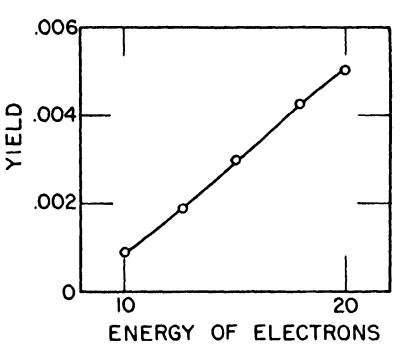

Figure 5. Neutron yield from uranium target bombarded by electrons

The positive curvature of the results obtained by the General Electric Company group should not be considered in disagreement with the results obtained from the calculations using Feld's theory and the results of Duffield and Huizenga, since there is very little overlap between the two curves.

It is gratifying to see that at least the order of magnitude of the neutron yield obtained by Wiblin at Harwell agrees with that obtained independently by Baldwin, Gaerttner and Yeater at the General Electric Company. The number of electrons in the burst in the G. E. betatron is of the same order of magnitude as the number of electrons in the burst in the Harwell linear accelerator. The neutron intensity of 10^{14} neutrons per second at 13 Mev would correspond

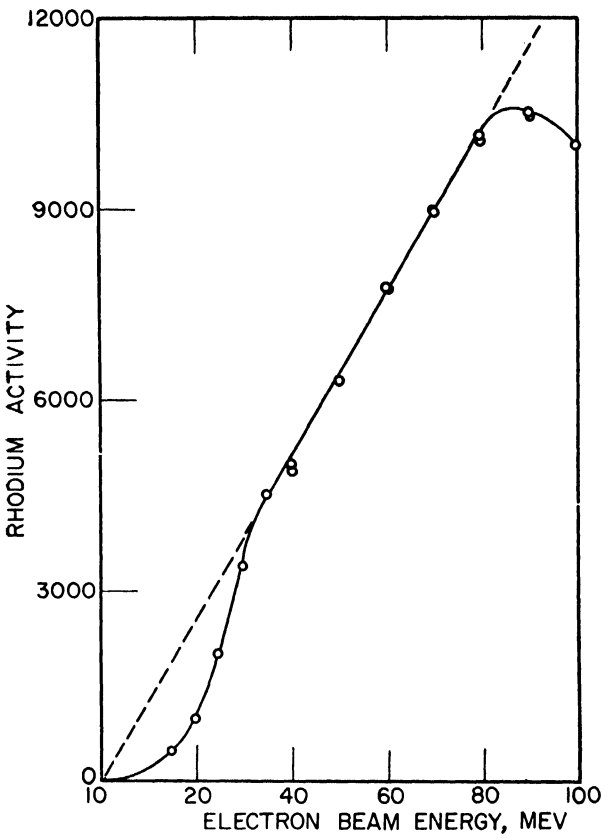

Figure 6. The activity of a rhodium foil in a standard paraffin geometry is plotted as a function of the energy of the electrons that strike a thick uranium target. This gives the neutron yield as a function of energy for a constant current in the accelerator

to a neutron intensity of about 3.5×10^{15} neutrons per second for the 80 Mev at which the G. E. betatron is operated. Since both groups measured average neutron intensity and calculated the neutron intensity from the pulse width and the repetition rate of the machine, the results are essentially in agreement.

NEUTRON DETECTION

In most of the early work with neutron velocity spectrometers, BF_3 proportional counters, and BF_3 ionization chambers were used as detectors. The advantages of the proportional counters over the ionization chamber are that the pulses are shorter and the electronic amplification required is less. The counter is, therefore, less sensitive to pickup. The ionization chamber, on the other hand, gives more uniform pulses, less drift, and can be run at higher pressure without requiring excessively high voltages for the size of the detector required.

Recently, the uncertainty in time response of the BF_3 proportional counter has become the limit on the spectrometer resolution. For a BF_3 counter, 5 cm in diameter and filled to a pressure of slightly less than one atmosphere, this uncertainty is about 2 microseconds. Since the time gates now used are considerably smaller than 2 microseconds, counters of this size can no longer be used. Recent developments in making banks of a large number (~100) of counters of small diameter (~ 5/8-in.) led to timing uncertainties as small as ~ 0.2 microsecond while maintaining the over-all counting volume. Ionization chambers, if constructed with care, have approximately 0.2 microsecond uncertainty in response. Thus, if time gates of ~ 0.2 microsecond or longer are employed, these detectors are useful and simple to operate.

Another disadvantage of BF_3 detectors is that a path length of ~ 10 cm along the beam is required to get reasonable detection efficiency. The resulting uncertainty of ~ 5 cm in flight path produces under some conditions the largest contributions to the resolution width.

Very fast detectors, which can also be made very short along the flight path, depend on detecting the gamma rays which result from neutron capture in a suitable absorber. Using organic scintillators to detect the gamma rays, the response time of the detector can be made less than 10^{-8} seconds. Since the gates used by velocity spectrometers in the low energy region are much longer than 10^{-8} seconds, this type of detector does not introduce any appreciable uncertainty in the timing. One difficulty with these detectors is that they are essentially gamma-ray detectors and special precautions must be taken to ensure that the gamma rays detected come only from the neutron absorber. Another difficulty is that the number of gamma rays emitted by the neutron absorber is usually a function of the energy. A thick boron absorber whose response is independent of energy can be used but since the energy of the gamma ray emitted is only 462 kev, this gamma ray is difficult to detect when any gamma-ray background exists.

A variation of the scintillation detector which can be very efficient for the detection of neutrons is a liquid scintillator containing boron or cadmium. The neutron is slowed down in the liquid and captured by the boron or cadmium. The gamma rays emitted are detected in the same liquid to give a high geometrical efficiency. The disadvantage of the detector is that its response time depends on the slowing down time of the neutron. The lifetime of the neutron in the solution can be made fairly low but since the probability of capture is an exponential decay the tail exists which extends to much longer times.

One fast detector which has been used successfully and is insensitive to gamma rays consists of a mixture of B_2O_3 with ZnS on the face of a photomultiplier. The α particle from the $B^{10}(n,\alpha)Li^7$ reaction causes a scintillation in the ZnS which is then detected by the photomultipliers. The response time of this detector depends on the response time of the ZnS, which is less than the time gates used by most velocity spectrometers at the present time.

PULSE TRANSFORMER ACCELERATOR

The pulse transformer accelerator is a small machine constructed at Columbia University to take advantage of the recent developments in high voltage

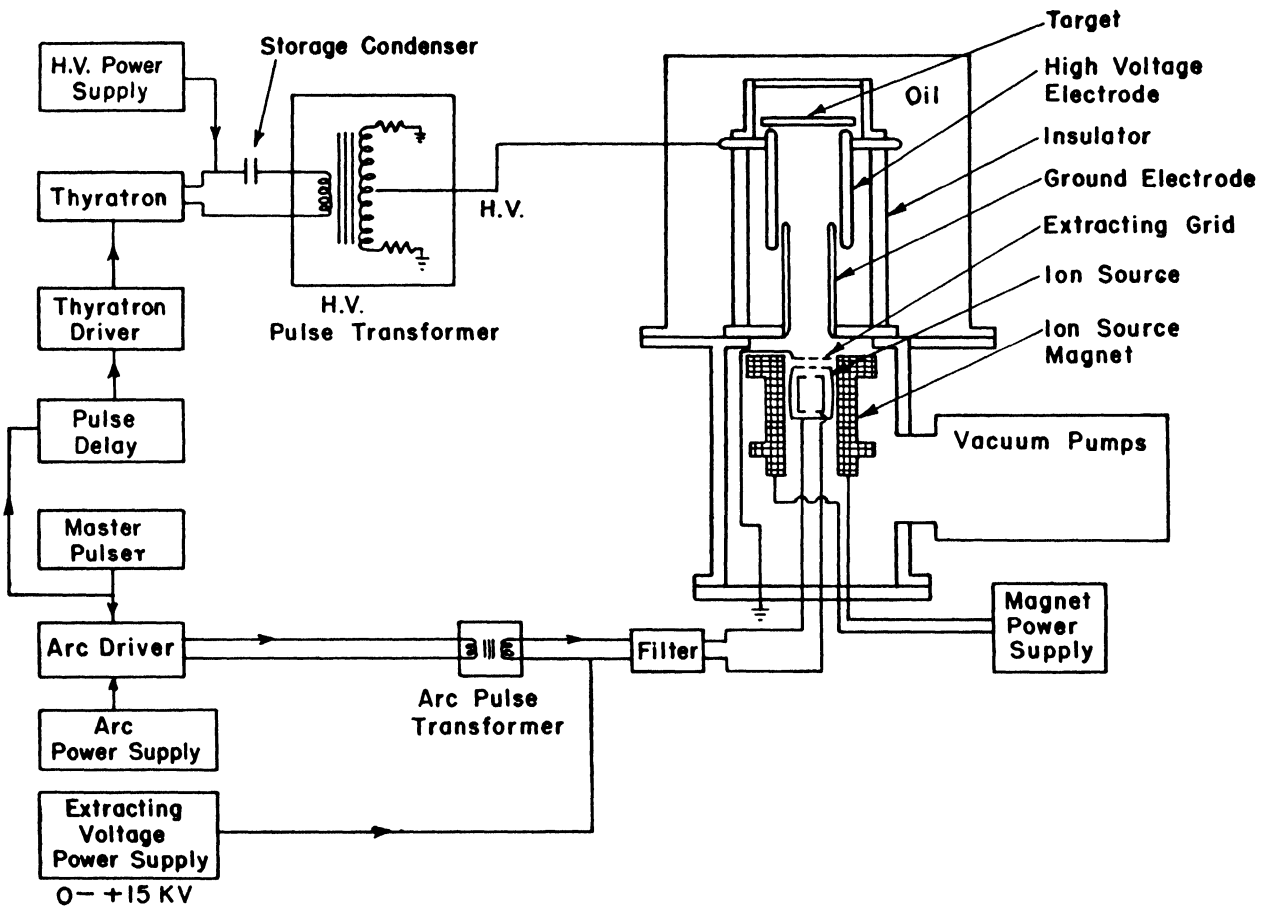

Figure 7. Block diagram of pulse transformer accelerator

pulse transformers. A voltage pulse up to 400 kev is applied to a single gap to accelerate deuterons which are introduced by a Phillips ion gauge arc source. The deuterons impinge on deuterium or tritium targets to produce a short, high intensity neutron pulse. The advantages of this device are simplicity and low cost of construction. The pulse transformer itself is capable of a peak power output of a few megawatts so that it is possible to accelerate large currents. A block diagram of the accelerator system is shown in Fig. 7.

In operation, a pulse from the master pulser triggers the arc driver turning on the ion source. The beam is extracted from the ion source by a dc voltage applied between an extraction grid and the exit cathode. The same pulse, suitably delayed, triggers the thyratron driver, discharging the storage condenser across the pulse transformer primary, thus applying a high voltage pulse between the ion source and target. A single gap accelerating tube structure separated by a Pyrex insulator has proved adequate in sustaining pulsed voltages as high as 350 kv.

At present, typical performances attained with the accelerator operated as a pulsed neutron source are: 350 kv high voltage peak, 1 microsecond pulse width, 50 pulses per second, 10^6 neutrons per pulse with deuterons on a Zr-D target.

One of the limits on the power output of the accelerator is set by the targets. Improved operation as indicated by increased neutron production has led very quickly to target destruction. The problem of a stable gas target usable with high beam power dissipation is not inherent in this machine but is particularly important here because the only reactions which will produce neutrons at the available accelerating voltages are those involving tritium or deuterium targets.

COLUMBIA 36-IN. AND BROOKHAVEN 60-IN. PULSED CYCLOTRON VELOCITY SPECTROMETERS

Both the Columbia 36-in. cyclotron velocity spectrometer and the Brookhaven 60-in. cyclotron velocity spectrometer operate the same way and can be discussed simultaneously. The geometry of the Columbia spectrometer is shown in Fig. 8; that for the Brookhaven spectrometer is shown in Fig. 9. The detailed operation of the Columbia velocity spectrometer has been described in several publications.[20]

The ion source of the Columbia 36-in. cyclotron is pulsed to produce a short burst of deuterons, which are then accelerated to strike a beryllium target and produce the fast neutrons. The cyclotron uses a hooded capillary arc source in which the hood is insulated from the rest of the arc source. For

velocity selector operation the hood is maintained at a positive potential of 2000 volts. This potential repels any positive ions in the capillary tube and prevents emission from plasma blown out of the lower part of the arc source. The arc is definitely off in its normal operating position. The arc is pulsed by applying about 500 volts between the filament and ground and removing the voltage applied to the hood. The pulse shape of the arc current is determined by looking at the voltage across a 5-ohm resistor in series with the arc.

For pulses of 4 microseconds duration or less, the arc pulse is not square even though the rise and fall time of the applied pulse is less than 0.1 microsecond. The arc current takes between 0.5 and 1 microsecond to rise to its full value. In practice it has been found that the intensity falls off very rapidly as the arc pulse width is reduced below 2 microseconds, and consequently shorter pulse widths are not used.

In the Columbia velocity spectrometer the energy of a resonance dip is determined from the source-detector path length and from the time interval between arc pulse and neutron detection. The timing of a detection interval after the arc modulation pulse is well known in terms of the basic timing circuits which are precise to approximately 0.1 microsecond. There is, however, a certain over-all delay time, t_d, of the system representing the time required to accelerate the deuterons, etc. This delay time is measured by placing in the beam a sample of paraffin

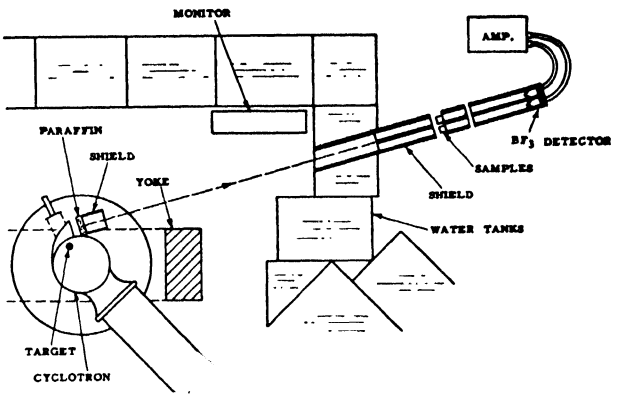

Figure 8. Geometry of the Columbia 36-inch cyclotron neutron velocity spectrometer

which has a transmission of about ½ for fast neutrons but is effectively opaque at low energies. The counting rate near zero time then gives the shape and delay of the fast neutron pulse striking the moderator and is an over-all check of the operation of the system. The position of energy levels is now checked by frequent measurements using the thick paraffin to determine t_d at the time of the measurements of the position of the resonance dip. The position of the dips for several elements which were previously investigated have been checked by this method with results that are consistent and in good agreement with those obtained at other velocity spectrometers.

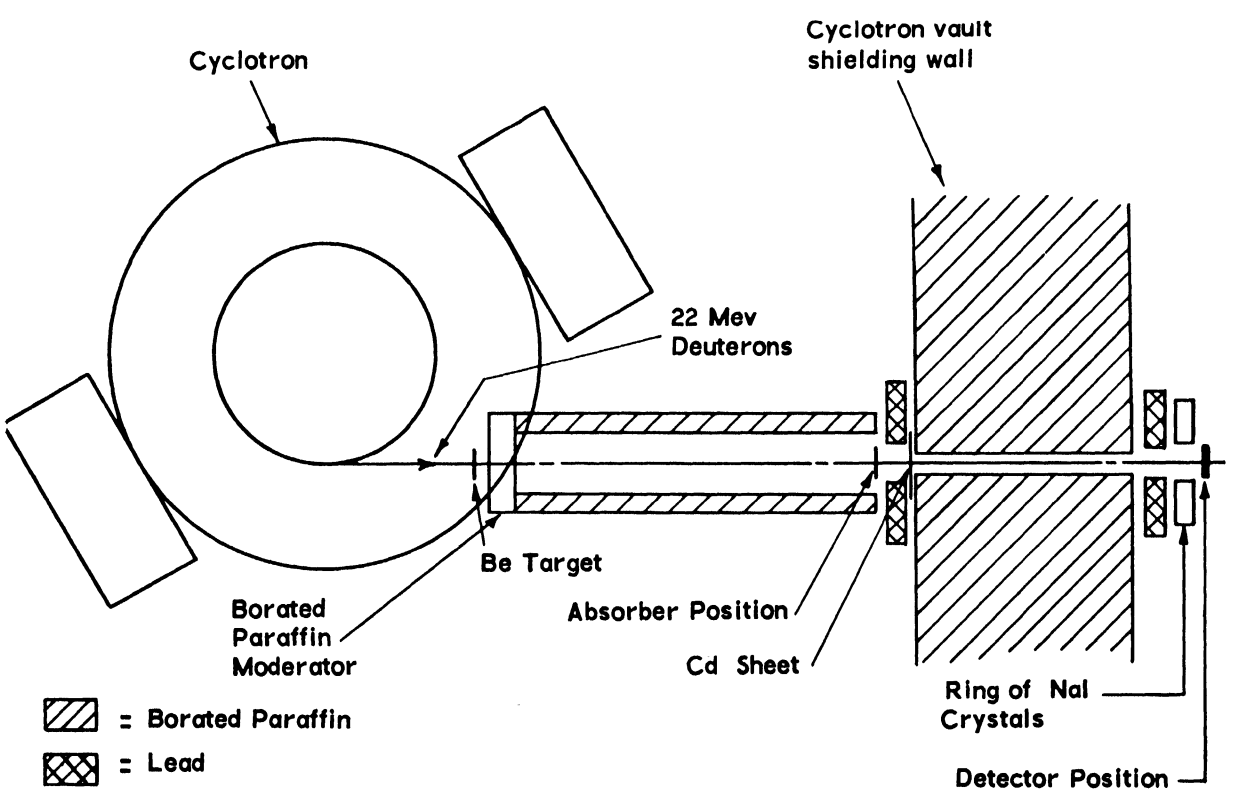

Figure 9. Geometry of the 60-inch Brookhaven cyclotron velocity spectrometer

In the Brookhaven cyclotron velocity spectrometer, the arc source is modulated by a thyratron which puts a 2000-volt pulse across the arc. The shape of the current pulse at the beryllium target after the deuterons are accelerated is examined with an oscilloscope. For the best resolution this pulse is approximately triangular in shape and has a full width at half maximum of 0.6 microsecond. The difficulties involved in measuring the delay time are avoided here by having the time analyzer triggered by the current pulse to the beryllium target.

For high resolution work the neutron intensity in the burst for a cyclotron can probably be increased by a factor of 20 both by pulsing the arc source and, when the beam reaches full energy, deflecting it into a target, in a period of time which is short compared to the arc-on time and the acceleration time of the machine. When the arc of a cyclotron is pulsed for a period of time which is short compared with the acceleration time, the beam will be between the radius r and $(r + dr)$ near the maximum radius. If the total beam between r and $(r + dr)$ can be deflected vertically into a target, the total number of particles contained in an arc pulse about 2 microseconds long can be deflected into the target in one revolution of the beam (< 0.1 microsecond). With this increase in source intensity, and because of the fact that with the ordinary cyclotron the repetition rate of the machine is at the disposal of the experimenter, the available counting rates obtainable might be higher than those obtained with an accelerator that has a considerably higher intensity in the burst but which is inherently a pulsed accelerator with its repetition rate fixed by its characteristics.

For poor and intermediate resolution work, the cyclotron can probably give the highest counting rate of any of the accelerators. Since the source on-time, detection time and repetition rate can be varied to fit the particular experiment, the number of neutrons obtained per second can approach the instantaneous production rate.

The Columbia 36-in. cyclotron velocity spectrometer uses a 6-meter path with a proportional counter detector 5 cm in diameter and 10 cm long filled to a pressure of 50 cm of BF_3. A number of results using this velocity spectrometer have been published. This spectrometer does not have the high resolution of some of the other velocity spectrometers and is not being used for high resolution work. The transmission of a sample of rhenium is shown in Fig. 10, which illustrates the best resolution that has been attained with this apparatus.

The Brookhaven 60-in. cyclotron velocity spectrometer uses a 4.3-meter flight path. The detector consists of a 2.5-in. circular disk of the sample viewed with six 3 cm diameter $\times$ 4 cm long cylindrical NaI crystals. In order to reduce background, fast coincidences (2×10^{-8} second) between any pairs of NaI crystals are required to feed a signal to the time-analyzer. Data are taken with a sample in the

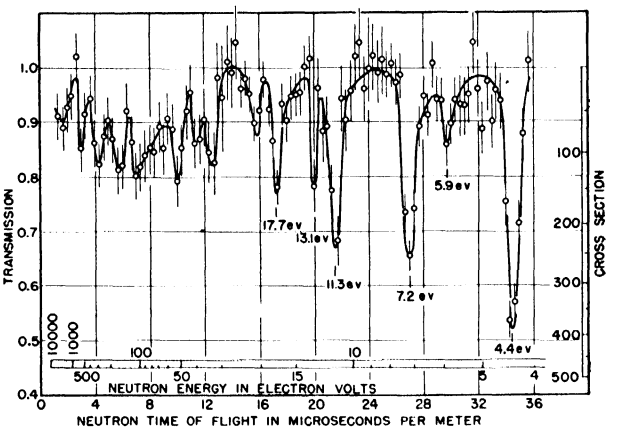

Figure 10. The slow neutron transmission of 0.518 gm/cm^2 of Re taken with the Columbia 36-inch cyclotron neutron velocity spectrometer

detector position alone and with a sample in both the detector position and in the absorber position as shown in Fig. 9. The data on a 0.012-in. thick sample of silver in the detector position taken in about two hours running time is shown in Fig. 11. The separation between the 51.80 and the 55.94 ev levels in silver is the best indication of the resolution of this spectrometer.

YALE ELECTRON LINEAR ACCELERATOR VELOCITY SPECTROMETER

The characteristics of the Yale linear accelerator have been described in the literature during the

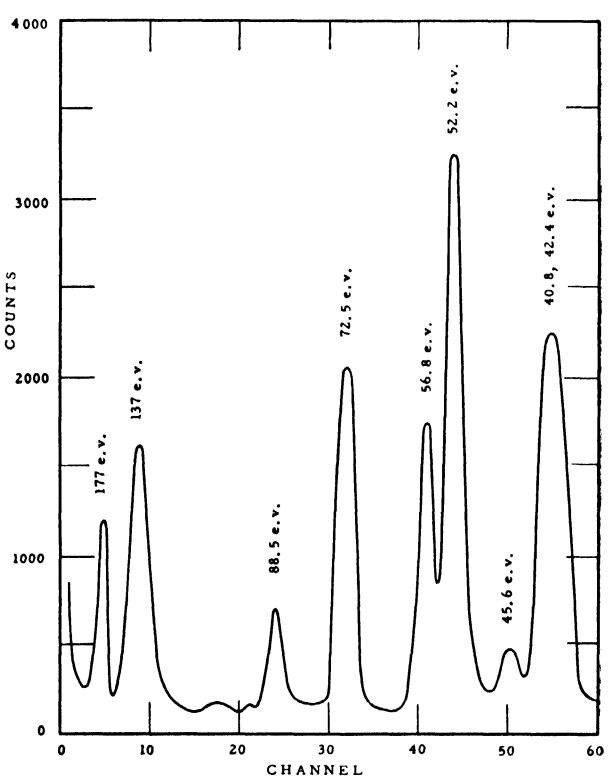

Figure 11. Results on silver with Brookhaven 60-inch cyclotron neutron velocity spectrometer using an (n, γ) detector

early stages of development.[21] The accelerator has been increased to 15 cavities for the acceleration of electrons instead of the 8 described in the literature. The design output energy of the machine is 15 Mev with a beam current of 100 ma.

The accelerator has been operating at 5 Mev with a beam current of about 30 milliamperes in a pulse 2 microseconds wide. The electron beam strikes a gold target. The bremsstrahlung from the gold produces neutrons in a beryllium block which is close to the gold target. With this arrangement the instantaneous neutron production is about 3×10^{12} neutrons per second.

The machine has just been modified to have an output energy of 10 Mev with a current of 100 ma. With this output the neutron production rate in the pulse should be about 10^{14} neutrons per second. The output power of the machine is now limited by the radio frequency power source.

The neutrons are moderated by a paraffin block and timed with a 500-channel quartz delay line time-analyzer with 2 microsecond channels. The analyzer governs the basic timing arrangement of the machine and triggers the electron gun at the proper time in the analyzer cycle. The number of channels is limited by the electrical length of the delay line. An additional cathode ray tube fast storage system is used in conjunction with the quartz delay line analyzer as a time expander to further divide any 5 or 10 microsecond interval into fifty parts to give detector gate widths as short as 0.1 microsecond. A diagram of the geometry of the velocity spectrometer system is shown in Fig. 12. The detector can be moved anywhere in the instrument room from 5 to 15 meters from the source. Because of intensity limitations, the detector has been used at the 5-meter position.

The detector is quite similar to that used with the Brookhaven 60-in. cyclotron velocity spectrometer. NaI crystals are used to detect the gamma rays emitted by the sample when a neutron is captured. The results of measurements on indium are shown in Fig. 13. The Yale results indicate the desirability of having a large number of channels in the time-analyzer. With the neutron intensity available, the time required to obtain data with a time-analyzer with a few channels would have been prohibitive, but with the 500 channels available, the time is no longer prohibitive.

GENERAL ELECTRIC BETATRON VELOCITY SPECTROMETER

The General Electric betatron has been described elsewhere in great detail.[22] Use of the machine as a neutron source required no significant development. The only changes required were to design a suitable target that could take maximum advantage of the photo neutron reaction and to add a more powerful deflector circuit that could deflect the electron beam into the target in a sufficiently short time. The use of this machine as a velocity selector has been described

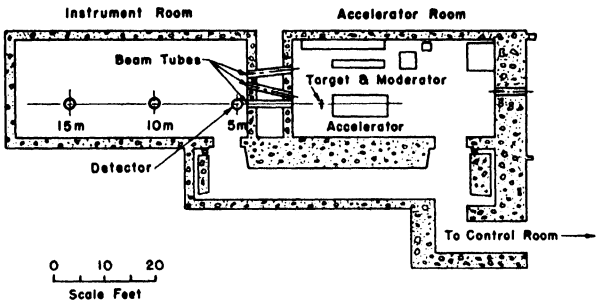

Figure 12. Geometrical arrangement of the Yale neutron velocity spectrometer system

in detail by Gaerttner, Yeater and Albert[23] and by Gaerttner, Yeater and McRoberts.[24]

The geometry of the system showing the betatron source, shielding, collimator and detector assembly are shown schematically in Fig. 14.

The neutron pulse is produced in the following manner. At the proper time in the acceleration cycle of the betatron, the deflector is operated to reduce the radius of the electron orbit, thus collapsing the beam inward into a ¾-in. cube of uranium which stops the electron beam and produces the neutrons. The neutrons are moderated by a polystyrene hemisphere which partially encloses the target.

The effective fast neutron pulse width is determined from the time required to collect the electrons on the target. For most of the results thus far obtained with this velocity selector, the electron collection time was 0.35 microsecond measured as the full width of the pulse at half maximum. The pulse is approximately gaussian in shape. Recent improvements in the betatron by Baldwin at the General Research Laboratories of the General Electric Company have reduced this collection time to 0.04 microsecond. With the collection time of 0.35 microsecond, the neutron intensity determined from the (γ, n) cross section of uranium and a knowledge of the number of electrons in the burst was calculated to be 3×10^{14} neutrons per second. This result has been confirmed experimentally to within a factor of

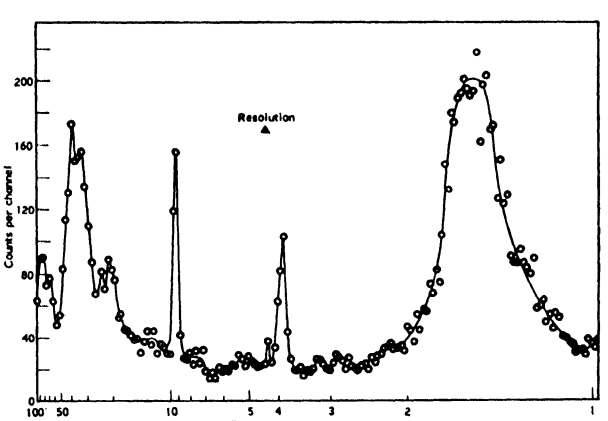

Figure 13. Observed capture spectrum with 0.1 gm/cm² indium using the Yale neutron velocity spectrometer with an (n, γ) detector

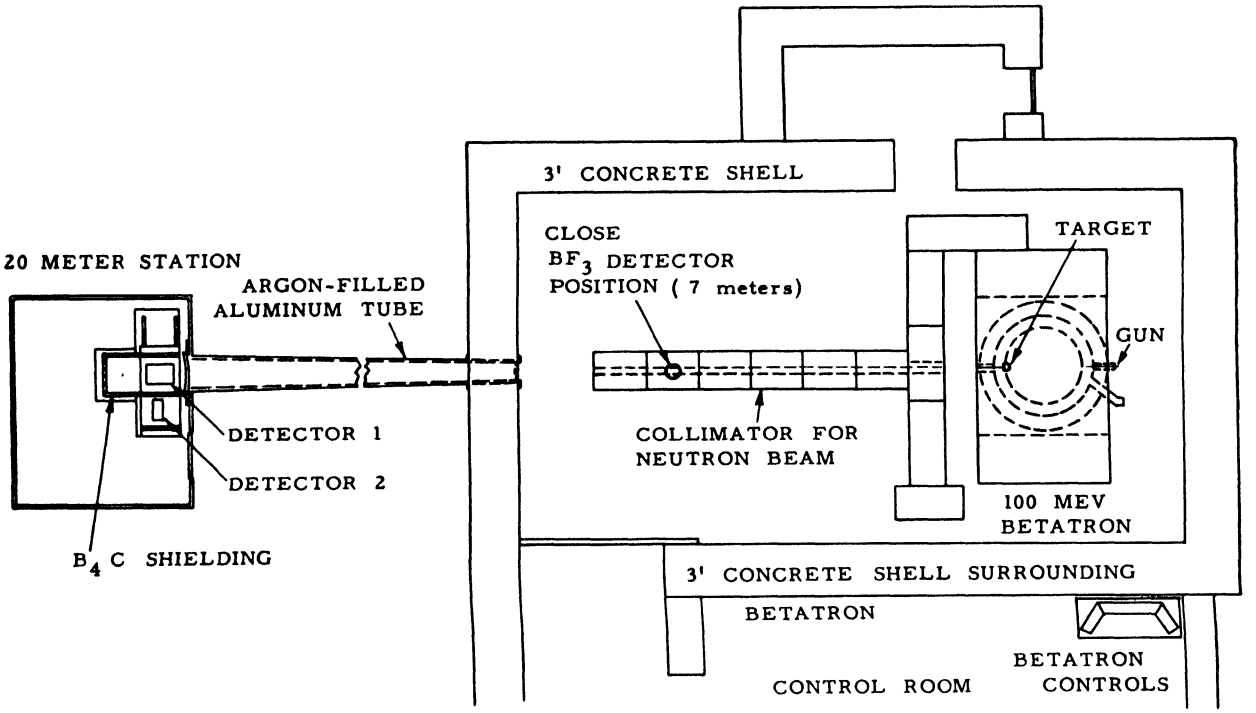

Figure 14. Geometry of the General Electric Company betatron neutron velocity spectrometer

2 by measuring the average neutron intensity. The neutron production rate of 10^{15} neutrons per second given in Table II is for the electron deflection time of 0.1 microsecond which is now used.

The inherent advantage of the betatron is well illustrated by the above considerations. Since the total beam is deflected into the target, the average neutron flux is independent of the burst width. This means that the instantaneous neutron intensity is inversely proportional to the burst width, which is a great advantage for high resolution.

A pulse of stray X-rays, coming from the betatron target simultaneously with the neutron burst, starts the time-analyzer. Two detector positions used are 6.9 meters and 19.6 meters from the source. At the 19.6 meter position a bank of 52 BF_3 proportional counters ¾ of an inch in diameter, with an active length of 12 inches, is used. The properties of these counters are described in a report by Fehr.[25]

The results obtained for the transmission of a 0.92 gm/cm^2 sample of Mn are shown in Fig. 15 taken with a resolution width of 0.02 microsecond per meter. The width of the curve indicates the resolution achieved.

A scintillation detector which has been described by Albert and Gaerttner[26] is used at the 7-meter position. This detector depends on the coincidence detection of gamma rays from neutron capture. The coincidence arrangement is used to discriminate against stray gamma-radiation. The detector consists of two annular containers, 6 inches long, 8 inches outside diameter, 4 inches inside diameter, filled with liquid scintillator. The two containers have their axis co-linear with the axis of the beam. The sample is placed between the two detectors to give good geometrical efficiency. Results on tantalum at the 7-meter position are shown in Fig. 16. Sharpness of the resonances is the best demonstration of the resolution.

COLUMBIA 400-MEV SYNCHROCYCLOTRON VELOCITY SPECTROMETER

The synchrocyclotron of Columbia University has been modified to permit its use as a rapidly pulsed high intensity neutron source for velocity spectrometer studies. Such studies do not interfere with the other experiments for which the accelerator is used.

The accelerator is operated as a sharply pulsed neutron source by deflecting the proton beam at the proper time. A pulse transformer, activated by the pulse from the frequency modulator, applies a voltage pulse of about 125,000 volts to two plates of an electrostatic deflector which are about 1 inch apart. The total beam is deflected vertically about 1 inch above the median plane so that it strikes a thick tungsten target which acts as the source of the fast neutrons. The neutrons are moderated by a nylon slab contained in an aluminum box just above the tungsten target. The vertical deflection takes place in one revolution of the beam, or in about 0.05 microsecond. This pulse width has been checked by using a fast neutron scintillation counter telescope. This telescope is arranged so that it responds to neutrons above 20 Mev and thus measures the pulse width of fast neutrons produced in the target.

In order to obtain the short burst, it was found necessary to use a beam collimator near the arc source of the cyclotron to remove protons having excessive vertical oscillations. The general neutron

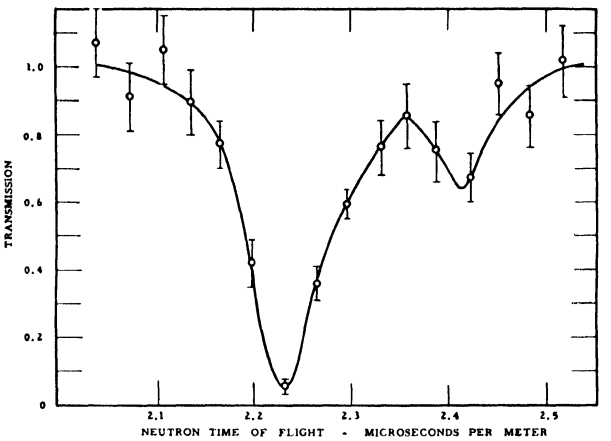

Figure 15. Neutron transmission of 0.92 gm/cm^2 manganese: B^{10} lined counters, 19.6 meter flight path. Results with the General Electric Company betatron velocity spectrometer using a boron detector

background was decreased by turning off the radio frequency accelerating voltage immediately after the beam had been deflected. It is interesting to note that the use of this radio frequency modulator improved the general operation of the cyclotron for other experiments, since it decreased the average power drain from the radio frequency source.

The instantaneous proton current has been determined from the cyclotron beam current measurements of the heating effect on a 1½-inch copper target. The average number of neutrons per proton, roughly calculated from the collision probability and the spallation cross section, is greater than 1, which gives a neutron intensity in excess of 10^{17} neutrons per second in the burst. The order of magnitude of this number has been confirmed experimentally by comparing the neutron counting rate obtained at the 36-in. cyclotron with that obtained at the 170-in. synchrocyclotron using a BF_3 counter in a standard paraffin geometry in each case.

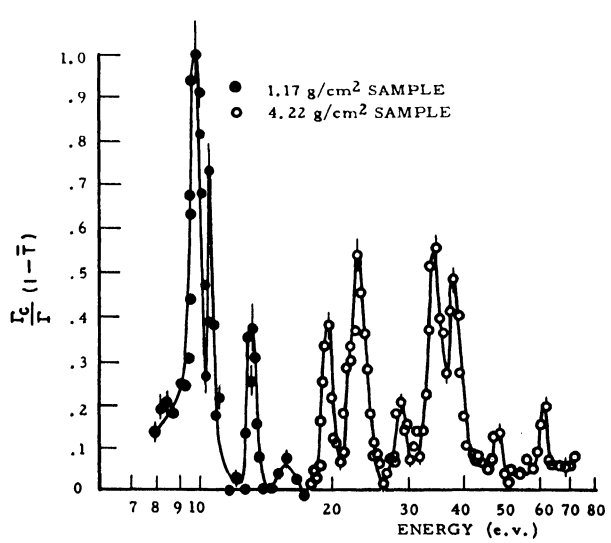

Figure 16. The results on tantalum using the General Electric Company betatron neutron velocity spectrometer with an (n, γ) detector

A schematic diagram of the geometry of this velocity spectrometer is shown in Fig. 17. The detectors used are large blocks of scintillating plastic which detect the gamma rays emitted after neutron capture. The results obtained with this velocity spectrometer on a sample of silver with $1/n = 1450$ barns/atom are shown in Fig. 18. The separation of the 40.38 ev and 41.56 ev levels is the best indication of the resolution of this instrument.

OAK RIDGE PULSED VAN DE GRAAFF ACCELERATOR

A new technique has recently been developed at Oak Ridge[27] to measure neutron cross sections in the kilovolt region using a 2.5 Mev Van de Graaff accelerator. Approximately monochromatic neutrons are produced by the $Li^7(p, n)Be^7$ reactions using a thick target to increase the intensity. The resolution does not depend on the energy spread of the neutron beam for a given angle with respect to the initial direction of the proton beam, as is usually the

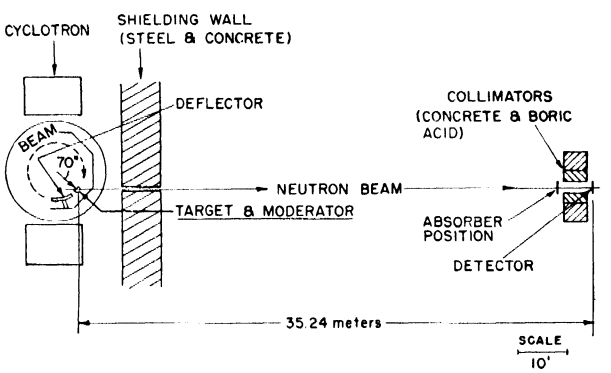

Figure 17. Geometry of Columbia synchrocyclotron neutron velocity spectrometer

case for neutron cross-section measurements with this type of machine. Good resolution is obtained by timing the neutrons over a measured path using newly developed ultrafast timing techniques.

The intensity of the neutron source is fairly low, but because no very low energy neutrons are produced, a high repetition rate can be used. Counting rates are obtained which compare favorably with those obtained with other neutron spectrometers in the energy range from 1 to 40 kev. Since, for bombarding energies of not more than 40 kev above threshold, the neutrons are emitted in the forward direction, the stray neutron background can be reduced considerably.

The neutron bursts are produced by using a device which deflects the proton beam of the Van de Graaff machine across a slit placed in front of the target assembly. The voltage applied to the deflector has a frequency of 0.5 megacycles. For machine energies of about 2 Mev the resultant beam pulses are 10^{-8} second or less in duration. The current pulses on the target are integrated by a device with a time constant of 5×10^{-9} second, amplified and limited for use as reference pulses. The time-

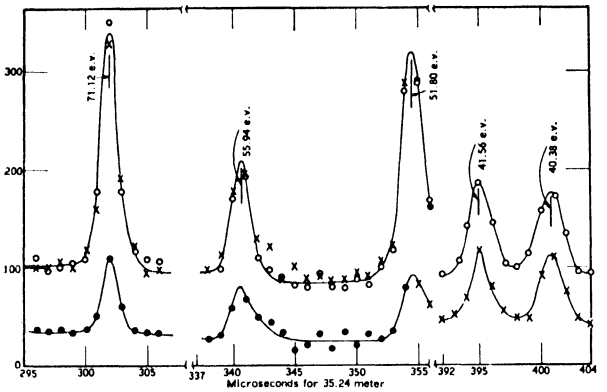

Figure 18. Results with Columbia synchrocyclotron neutron velocity spectrometer with an (n, γ) detector. Scintillation gamma-ray rate vs time of flight: ($1/n$) = 1450 barn/atom of normal silver at detector — 35.24 meter path

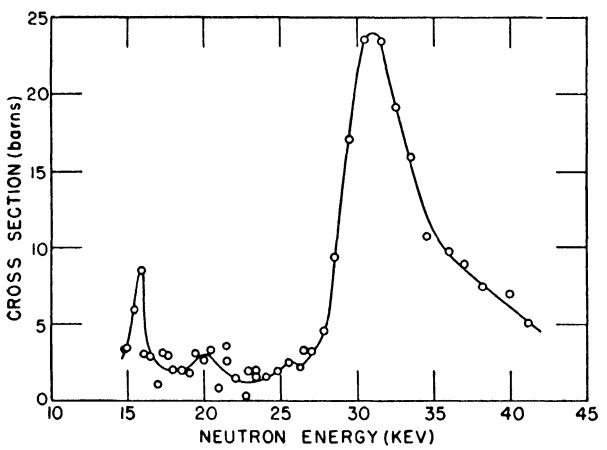

Figure 19. The cross section of iron using the Oak Ridge pulsed Van de Graaff accelerator and measuring the time of flight of the neutrons. The resolution used was 0.013 microseconds per meter

analyzer consists of a circuit in which the voltage rises linearly with time at the start of the neutron burst. Neutron pulses from the detector occurring at a particular time are converted to a voltage and an ordinary 100-channel pulse height analyzer is used to record the data.

For intermediate neutron energies the detector that has been used is a 4-inch diameter slab of boron-10 which contains 3.7 gm/cm^2. The gamma rays from the capture of the neutron in this slab are detected with NaI crystals. With the detector placed at 0.8 meter from the target, the resolution attained was 0.013 microsecond per meter. Results obtained with this velocity selector for measurements on the cross section of iron in the energy range 15 to 40 kev are shown in Fig. 19. The peak measured cross section for the 29-kev level is higher than that reported using other techniques. Additional levels, particularly the one at 15 kev, are also observed.

REFERENCES

1. Alvarez, L. W., *Phys. Rev.* 54, 609 (1938).
2. Dunning, J. R., Pegram, G. B., Fink, G. A., Mitchell, D. P. and Segre, E., *Phys. Rev.* 48, 704 (1935).
3. Fertel, G. E. F., Gibbs, D. F., Moon, P. B., Thomson, G. P., F. R. S., and Wynn-Williams, C. E., *Proc. Roy. Soc.* 175, 316 (1940).
4. Manley, J. H., Haworth, L. J. and Luebke, E. A., *Phys. Rev.* 61, 152 (1942); Manley, J. H., Haworth, L. J. and Luebke, E. A., *R.S.I.* 12, 587 (1941); Haworth, L. J., Manley, J. H. and Luebke, E. A., *R.S.I.* 12, 591 (1941).
5. Baker, C. P. and Bacher, R. F., *Phys. Rev.* 59, 332 (1941).
6. Bacher, R. F., Baker, C. P. and McDaniel, B. D., *Phys. Rev.* 69, 443 (1946); McDaniel, B. D., *Phys. Rev.* 70, 832 (1946); Jones, W. B., Jr., *Phys. Rev.* 72, 362 (1947); Jones, W. B., Jr., *Phys. Rev.* 74, 364 (1948).
7. Havens, W. W., Jr. and Rainwater, L. J., *Phys. Rev.* 83, 1123 (1951).
8. Groenewald, H. and Groendijik, H., *Physica* XIII, Nos. 1-3 (1947).
9. Rainwater, L. J. and Havens, W. W., Jr., *Phys. Rev.* 70, 136 (1946); Rainwater, L. J., Havens, W. W., Jr., Dunning, J. R. and Wu, C. S., *Phys. Rev.* 71, 65 (1947); Havens, W. W., Jr. and Rainwater, L. J., *Phys. Rev.* 83, 1123 (1951).
10. Hanson, A. O., Taschek, R. F. and Williams, J. H., *Rev. Mod. Phys.* 21, 635 (1949). Extensive work on the D(d,p)T, D(d,n)He^3, T(d,n)He^4, and He^3(d,p)He^4 cross sections below 120 kev has been done by Arnold, W. R., Phillips, J. A., Sawyer, G. A., Stovall, E. J., Jr. and Tuck, J. L., *Phys. Rev.* 93, 483 (1954).
11. Coon, J. H., Los Alamos Scientific Laboratory, private communication.
12. Smith, L. W. and Kruger, P. G., *Phys. Rev.* 83, 1137 (1951).
13. Allen, A. J., Nechaj, J. F., Sun, K.-H. and Jennings, B., *Phys. Rev.* 81, 536 (1951).
14. Cockcroft, J. D., Duckworth, J. C. and Merrison, E. R., *Nature* 163, 869 (1949).
15. Wiblin, E. R., Harwell, England, private communication.
16. Montalbetti, R., Katz, L. and Goldenberg, J., *Phys. Rev.* 91, 659 (1953).
17. Duffield, R. B. and Huizenga, J. R., *Phys. Rev.* 89, 1042 (1953).
18. Feld, B. T., *Nucleonics* 9, 51 (1951).
19. Baldwin, G. C., Gaerttner, E. R. and Yeater, M. L., Knolls Atomic Power Laboratory of the General Electric Company, private communication.
20. Rainwater, L. J. and Havens, W. W., Jr., *Phys. Rev.* 70, 136 (1946); Rainwater, L. J., Havens, W. W., Jr., Wu, C. S. and Dunning, J. R., *Phys. Rev.* 71, 67 (1947); Havens, W. W., Jr. and Rainwater, L. J., *Phys. Rev.* 83, 1123 (1951).
21. Schultz, H. L. and Wadey, W. G., *R.S.I.* 22, 383 (1951).
22. Westendorp, W. F. and Charlton, E. E., *J. App. Phys.* 16 (1945).
23. Gaerttner, E. R., Yeater, M. L. and Albert, R. D., Report KAPL 1084 of the General Electric Company (1954).
24. Gaerttner, E. R., Yeater, M. L. and McRoberts, W. J., Report KAPL 1108 of the General Electric Company (1954).
25. Fehr, E. *et al*, KAPL 1110 of the General Electric Company, *Fast BF_3 Counters for Velocity Selector Studies* (to be published).
26. Albert, R. D. and Gaerttner, E. R., Report KAPL 1083 of the General Electric Company (1954).
27. Good, W. F., Smith, E. C., Neiler, J. H. and Banta, H. E., private communications.

Cyclotrons Designed for Precision Fast-Neutron Cross-Section Measurements

By R. L. Thornton,* Keith Boyer,† and Jack M. Peterson,‡ USA

During the past twenty-five years, the constant-frequency cyclotron has demonstrated its value in many laboratories throughout the world. Its principal virtues have included substantial currents (ranging up to milliamperes) and moderate energies (up to about 20 Mev). These characteristics have been largely exploited in the study of nuclear properties, the production of unstable isotopes, and as a neutron source. In recent years the use of nuclear reactors has tended to make the latter two uses somewhat less important. Reactors, however, are not suitable for the production of monoenergetic neutrons, particularly in the high-energy region. Accordingly, particle accelerators are still invaluable for such purposes, and for such uses as the production of pulsed neutron sources for time-of-flight experiments.

Other characteristics of cyclotrons have, however, impaired their usefulness in fields in which homogeneity and variability of energy, freedom from background radiation, and critical beam trajectories with respect to the target are of particular importance. Such fields are those involving precision cross-section measurements of all kinds, production of monokinetic high-energy neutrons, investigation of resonance phenomena, and the like. In such investigations, the operating characteristics of cyclotrons have usually been less advantageous than those of linear accelerators such as the Van de Graaff and others. Since the maximum energy so far attained by these variable-energy dc accelerators is in the neighborhood of 6 Mev, it is obvious that a successful attempt to ameliorate these cyclotron limitations would permit an extension of such precision measurements as given above to a region of growing practical importance and of considerable physical interest.

A cyclotron designed with these aims in view should possess a number of special characteristics, both of the performance of the machine itself and also of the laboratory in which it is housed. The experiments under consideration are most conveniently performed using an external or deflected beam of the accelerated particles. Moreover, it is desirable to have available particle beams of the usual light isotopes, protons, deuterons, tritons, and helium ions. There is growing interest today in the acceleration of heavier ions such as those of carbon, nitrogen, and even heavier elements, and the possibility of using these should also be kept in mind. This external beam should be either continuously variable in energy, or variable in small easily controlled steps, from the peak energy available in the cyclotron to as low a value as is feasible. The latter figure should, of course, at least overlap the peak energies available from Van de Graaff generators. In addition to the feature of variability, there should be accurate determination of the energy at the values used, and the homogeneity of energy both in space (across the target dimensions) and in time should be compatible with the type of experiment to be performed. Currents of the order of microamperes or more of these ions should be focused on a target assembly of small dimensions (of the order of a few square centimeters or less) at such a distance from the cyclotron as to permit adequate shielding of the experimental equipment from the background radiation from the accelerator. Particularly for work involving neutrons, this target assembly should also be well removed from walls or other surfaces that can act as sources of scattered neutrons. Such of these requirements as involve target geometry are frequently difficult to achieve in existing cyclotron laboratories, and are most easily realized either by constructing a machine with these requirements in mind from the start, or by remodeling and relocating the cyclotron in a building designed with these aims in view. Modern developments in the field of particle focusing—in particular those using quadrupole magnetic fields—now make the focal requirements attainable, and ion currents now available—in the milliampere range—make it possible to achieve the somewhat contradictory goals of adequate target current and energy homogeneity.

Cyclotrons for precision cross-section measurements, whose designs were influenced by considerations such as those discussed above, have recently been installed at the Livermore laboratory of the University of California Radiation Laboratory and at the Los Alamos Scientific Laboratory. The remainder of this paper is devoted to a discussion of these machines as representative of present activity

* University of California Radiation Laboratory.
† Los Alamos Scientific Laboratory.
‡ University of California Radiation Laboratory, Livermore. Including work by C. J. Taylor, Ralph Stahl, Bob Smith and H. P. Hernandez, University of California Radiation Laboratory; T. Putnam, Los Alamos Scientific Laboratory.

in this field. No attempt is made to give much general engineering detail, since more complete descriptions will be published elsewhere. Attention is directed primarily to those aspects which make the cyclotrons suitable for these applications and to the manner in which these characteristics have been obtained. It is known that other laboratories in this country, and probably also abroad, are interested in similar devices. For example, a somewhat smaller machine at the University of Rochester has recently been reported.[1]

THE RADIATION LABORATORY 90-INCH CYCLOTRON

The 90-inch cyclotron installed at the Livermore laboratory is a new machine and was designed for the purpose of producing monoenergetic neutrons in the energy range from 2 to 30 Mev using the (p,T), (d,d), and (d,T) reactions. It will accelerate particles over these energy ranges:

Protons	2.6 Mev to 14.0 Mev
Deuterons	5.2 Mev to 12.5 Mev
Tritons	7.7 Mev to 8.3 Mev

Doubly charged helium ions can, of course, be accelerated under essentially similar conditions to twice the energies listed for deuterons. No experiments using heavier ions have yet been carried out. The corresponding frequency and the approximate magnetic field limits are 4.0 to 9.3 megacycles/sec and 2600 to 8600 oersteds.

The cyclotron is at one end of a large building, not originally designed for the purpose, and in the same area is located a 0.5-Mev Cockcroft-Walton accelerator. The two machines share a common control and particle-counting area. The cyclotron magnet, which is arranged with a horizontal field, is located in a pit 18 feet deep and the horizontal deflected beam passes through a concrete shielding wall 5 feet thick to the center of a 40-foot cubical experimental room. The cyclotron pit is roofed with movable concrete slabs 2.5 feet thick for radiation protection. All shielding is with concrete of normal composition.

The magnet yoke is based on a C-shaped cross section rather than the more usual H-section, and the magnetic field is horizontal. This permits vertical removal of the accelerator electrode assembly and the deflector system (see Fig. 1). As indicated earlier, the peak magnetic field has been limited to approximately 8500 oersteds. This was done to minimize the variation with the operating field of the radial and azimuthal field components. This in turn necessitates the large final orbit radius of 35 inches to attain the desired energies. The magnetic gap is 12 inches minimum, and 280,000 ampere turns are required to reach a field of 8500 oersteds. The magnet contains about 300 tons of steel and the oil-cooled coils containing 8.5 tons of copper are excited by a dc generator with current regulation to one part in fifteen thousand.

An unusual feature is the cam-shaped protuberance at the bottom of the magnet poles. The deflected ion beam undergoes sufficient radial deflection to enable it to emerge from the magnet at this point and hence normal to the fringing field of the magnet. This reduces the subsequent spreading of the beam, and by adjustment of the shape of the field at this region, some convergence can be produced. Azimuthal distortions in the magnetic field are introduced, however, which require careful correction. Because it was desired to use a single accelerating electrode—and, in consequence, sparking problems might be expected to limit the energy gain per revolution of the ions—a radial magnetic field gradient was adopted that amounts to only a 1% decrease in field from the center to the 35-inch radius. Shimming of the magnetic field was accomplished by machining the poles, and a field tolerance of 0.1% was adopted in these corrections. Minor variations, particularly in the azimuthal sense, can be produced in operation by energizing a series of pole-face windings. The windings near the center of the machine are circular; those at larger radii are quadrant-shaped, and they have a maximum effect of 0.2% at 8000 oersteds.

The arrangement of equipment in the vacuum chamber is shown in Fig. 1. The single accelerating electrode hangs from a quarter-wave resonant stem, and the whole assembly can be withdrawn vertically for repair or adjustment. For the higher frequency range (6.4 megacycles/sec and above), the electrical length of the stem is shortened by means of the grounding switch indicated. This switch must carry total rf currents of over 9000 amperes, or about 70 amperes for each linear inch of switch. The switch consists of a large number of ⅛-inch-wide fingers. Experience has indicated that switches of this type can safely handle about 300 amperes per inch. Continuous variation of resonant frequency in these two ranges is provided by motion of grounded liner panels which vary the electrode capacity to ground. The range of travel of these motor-driven panels is from contact to a maximum of three inches clearance. In operation a minimum of ¾ inch is usual. As smaller clearances correspond to lower-energy particles and hence to a lower electrode voltage, sparking problems are not strongly dependent on liner position. The

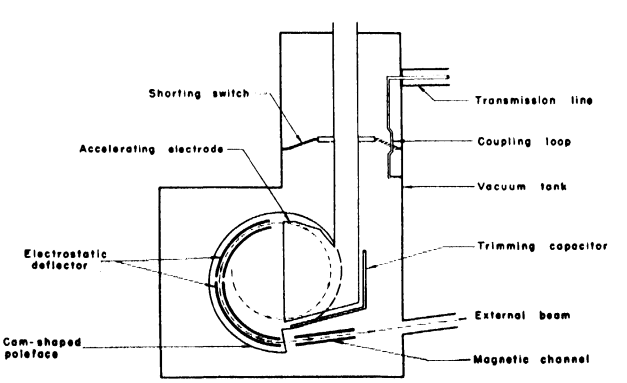

Figure 1. Vertical cross section of Livermore 90-in. cyclotron, schematic

shape of the electrode and its attachment to the stem were determined from model experiments, and result in a constant voltage to ground along the mouth of the electrode. A motor-driven capacitor at the rear of the electrode is automatically adjusted to keep the electrode system correctly resonant with the driving amplifier.

The radiofrequency system is designed to produce an electrode voltage in all ranges of twice the threshold value required to accelerate the ions. Accordingly the maximum peak voltage to ground is about 175 kilovolts and requires an exciting power of about 180 kw. It is a driven system beginning with a low-power crystal-controlled oscillator. One hundred crystals are used to cover the frequency range in 55-kc steps. The final amplifier, using an RCA A-2332 shielded grid triode, is designed to put out 380 kw at 79% efficiency. Grid neutralization of a form insensitive to frequency is used, and the grid inductance is a foreshortened parallel line and is tuned by motor-driven motion of the shorting plane. A servo system driving the trimmer capacity prevents temperature variations and other causes from detuning the resonator. Essentially the phase angle across the final amplifier is detected and supplies a signal to a servo amplifier which actuates the trimming capacitor. This system maintains the phase angle constant within 1 degree, thus keeping the resonator in almost perfect tune and permitting the inherent high efficiency of the amplifier and the frequency stability of the crystal-controlled oscillator to be utilized.

The final amplifier drives the resonator through a 50-ohm coaxial line which is electrically a half wave length at the highest frequency and which is loop-coupled at the resonator. In the low-frequency range a larger loop area is required than in the high-frequency range. This requirement was met by making the loop in the form of a 50-ohm parallel-plane transmission line which extends on both sides of the grounding switch. Thus, in switching from the low-frequency range to the high, the grounding switch serves not only to shorten the electrical length of the resonator but also to reduce the effective area of the coupling loop, the remainder of the loop structure above the grounding switch now becoming a part of the transmission line driving the resonator.

In order to break through the multipactoring region, electrode voltage is built up quickly. This is accomplished by pulsing on the screen voltage on a tube in the amplifier chain, all other voltages having been previously applied. In order to establish electrode voltage, the resonator must first be tuned to the signal frequency. This is done through the use of a small oscillator which applies a few volts to the electrode, enough for the control circuits to tune it to the correct frequency before application of the main power.

Automatic control of the power supplies to prevent damage through sparking or other failures is provided electronically by means of various "fault diverters." An electrode spark removes the driving power for a few seconds; a power arc (for example, in the output tube) results in immediate shorting of the power supply through an ignitron and in subsequent opening of the primary circuit. These provisions permit the use of a "stiff" power supply and result in improved electrode-voltage stability.

To minimize sparking problems resulting from surface contamination with organic films, mercury pumps are used with a total speed of 5000 liters per second. The design of these pumps and of the associated vacuum equipment is conventional, as is that of the ion source and other units not specifically described.

The electrostatic deflector system covers a total angle of about 150 degrees and is split into two separately adjustable sections. Adjustments may be made from the control console. The maximum field applied is 55 kv per centimeter with the maximum gap of 1.0 inch. The total radial deflection is 17 inches. After leaving the main magnetic field at the cam, the ion beam enters an iron channel which shields it from the stray field of the cyclotron magnet.

The geometry of the external beam is shown in Fig. 2. After leaving the cyclotron it enters a double-focusing magnet, which turns the beam and brings it to a focus at the middle of the five-foot shielding wall where a slit system is energy-selective. As the beam emerges on the other side of the wall, another (similar) magnet brings the beam to a focus at the neutron-producing target at the center of the experimental pit. The purpose of this steering arrangement is to minimize at the neutron target background radiations coming from the accelerator and from the energy-selective slits. For charged-particle work in another part of the experimental pit, the second steering magnet is turned off and then the first magnet is adjusted to focus the beam at the charged-particle target.

The cyclotron has now been operated for two months, but only with internal beams of protons. Beams up to 600 microamperes have been accelerated to full radius with no especial difficulty, at several frequencies corresponding to final proton energies ranging from 3 to 13 Mev. The machine operates easily and stably. The first beam was found within five minutes of the initial turn-on. An external beam has not yet been attempted; the deflector system is now being installed.

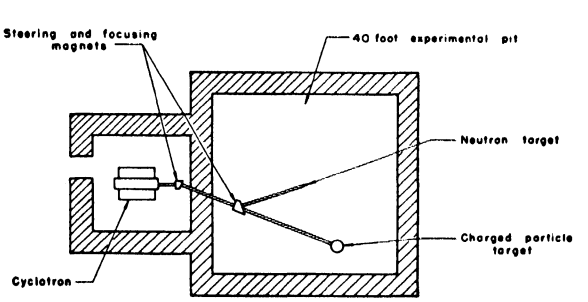

Figure 2. Plan view of 90-in. cyclotron external beam arrangement

THE LOS ALAMOS 42-INCH CYCLOTRON

This cyclotron was originally set up at Harvard University and, during the war years, was moved to the Los Alamos Scientific Laboratory. It has recently been extensively rebuilt and relocated in a new building. In its present form it is designed to accelerate ions in these energy ranges:

Protons	3.5 Mev to 9 Mev
Deuterons	7 Mev to 17.5 Mev
Tritons	10.5 Mev to 12 Mev

Doubly charged helium ions can also be used, the energies (for He^4) being double those indicated for the deuteron range. Some preliminary acceleration of quadruply charged carbon ions has also been accomplished. It is planned also to accelerate He^3 ions. The frequency and magnetic field ranges for the ions listed in the table are from 8.6 to 14 megacycles per second and from 5600 to 18,000 oersteds.

The cyclotron, which operates with the usual vertical field, is located in a concrete vault in a recently constructed research building. The shielding walls are four and five feet thick, and a removable ceiling of concrete blocks is four feet thick. The deflected ion beam (see Fig. 3) passes through one of the walls into an experimental vault with heavy concrete walls and a removable ceiling. This room is used for charged-particle work and for neutron work in which background is not a severe problem. It is planned to carry the beam a further 50 feet into an area having light steel walls and such that the minimum distance from the target to a scattering surface will be 20 feet. This low-background area will be used for neutron time-of-flight experiments and others in which low background is of paramount importance.

The magnet has a total weight of 100 tons; the pole diameter is 42 inches and the useful ion radius is 19 inches. The peak exciting power is 48 kw, and the magnet current is electronically stabilized to one part in 20,000. The useful magnet gap is about 5 inches. At all field values a radial gradient from center to the final radius corresponding to a 3.5% decrease is provided. In consequence of the wide field variations and the saturation effects at the higher values, this cannot be entirely accomplished by shaping the pole faces. Accordingly, the pole contours and Rose shim give the correct field shape at an intermediate field value. For higher and lower fields, the shape is corrected to the desired value by the use of edge-correcting coils inside the vacuum chamber, which can increase or decrease the field at the larger radii. These water-cooled coils consist of 5 turns top and bottom at a radius of approximately 18 inches, and carry a maximum current of ± 500 amperes. In addition to the radial field shape described above, an azimuthal field dependence modified from the type described by Thomas[2] is used. This consists of three iron sector plates inside the vacuum chamber, top and

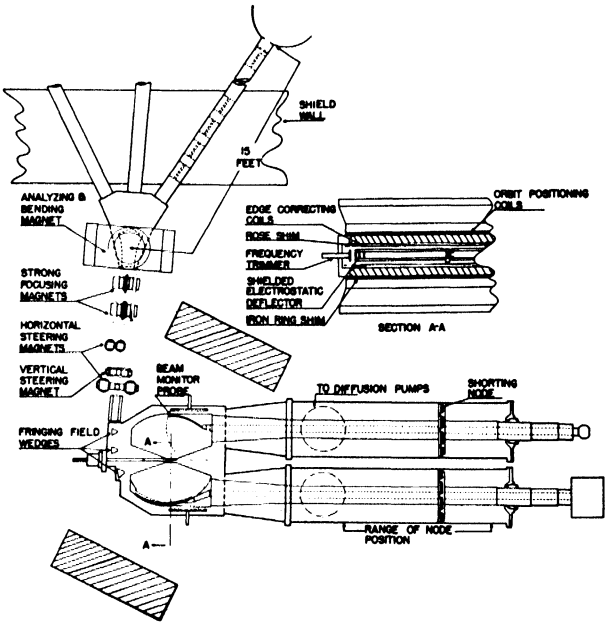

Figure 3. Schematic diagram of the Los Alamos cyclotron

bottom, and about 50 degrees wide. These shims produce a third harmonic field variation of ± 5% between 6- and 19-inch radii, and decreasing to zero from 6 inches to the center. The use of these shims has proved advantageous in providing additional axial stability and in centering the beam about the geometric center. Some reduction in the threshold electrode voltage is also achieved. Two orbit-centering coils are also provided to aid in centering the ion beam.

The arrangement of equipment in the vacuum chamber is shown in Fig. 3. Two accelerating electrodes are used and are supported by quarter-wave resonant stems in vacuum. Gross frequency changes are accomplished by changing the position of the shorting node, while intermediate values are obtained by varying the electrode capacity to ground. The 90 degree electrostatic deflector is mounted inside an electrode and hence is shielded from radio-frequency voltages; dc voltages up to 30 kilovolts are used. This low deflector voltage is due to the Thomas-type shims. One of the sectors is centered at the deflector entrance and this, in a cyclotron of this type, corresponds to maximum radial extension of the ions. The subsequent azimuthal reduction of field facilitates extraction and permits reduction of the deflecting field by a factor of 2.5.

The accelerating electrodes have an internal height of two inches and are supported by 8-inch-diameter aluminum tubes, copper-covered, and about 10 feet long. The movable shorting node may be actuated from outside the vacuum chamber and may be set at any desired position. The high-voltage lead and support for the deflector system is coaxial with one of the electrode supports, as can be seen in the figure.

The radiofrequency power is supplied by a self-excited oscillator using two 880 tubes in a push-pull

tuned-plate tuned-grid circuit. The maximum electrode potential to ground is 140 kilovolts. The oscillator is driven through the multipactoring region by a booster oscillator capacitively coupled to the grid circuit of the main oscillator. The booster oscillator is automatically biased off when the main oscillator is operating normally. The coupling loop to the electrode stems are 18 inches long and the amount of coupling is adjustable. The motor-driven trimmer capacitors automatically maintain equality of electrode voltage and constancy of frequency. The power supply is protected against overload by a constant current network.

The beam emerging from the deflector is focused horizontally and vertically by focusing wedges energized by the fringing field, and by the fringing field itself. A parallel beam about ⅜ inch in diameter is obtained at the entrance of the quadrupole focusing magnets. Two horizontal steering magnets and a vertical steering magnet align the beam along the geometric axis of the focusing and analyzing magnets. Energy analysis is obtained by placing slits before and after the analyzing magnet. The relative arrangement of these magnets is illustrated in Fig. 3. A second set of quadrupole strong-focusing magnets is planned to give a focus an additional 50 feet away for low-background neutron work, as was mentioned previously.

The ion source and oil diffusion pumps are essentially conventional in design. The pumping speed is about 5000 liters/sec for hydrogen. A separate, and smaller, mercury pumping system, together with a gas-recovery system, is provided for use with tritium and He^3.

Like the Livermore cyclotron, that at Los Alamos is still undergoing testing, particularly with regard to the external beam optics. Internal beams of more than two milliamperes of protons, deuterons, and helium ions have been obtained, and a deflection efficiency (measured at the entrance to the steering magnet) of about 10% has been established. No attempt has yet been made, however, to work with external beams greater than 100 microamperes. It is believed that the deflector efficiency can be substantially increased. The operation of the accelerator is very stable and reproducible. As the ions are accelerated from a radius of 4 inches to the final 19-inch orbit, the ion-beam intensity decreases by only about 12% which demonstrates the effectiveness of the axial focusing.

Grateful acknowledgement is made to many members of the laboratory staffs, both in California and at Los Alamos, for their contributions to the successful construction of these machines.

REFERENCES

1. Fulbright, H. W., Bromley, D. A. and Bruner, J. A., *An 8-Mev Variable-Energy Cyclotron,* Bull. Am. Phys. Soc. *30,* No. 3, 54 (1955).
2. Thomas, L. H., *The Paths of Ions in the Cyclotron:* I. *Orbits in the Magnetic Field,* Phys. Rev. *54,* 580 (1938); II. *Paths in the Combined Electric and Magnetic Fields,* Phys. Rev. *54,* 588 (1938).

Van de Graaff and Cockcroft-Walton Accelerators for Fast Neutron Cross-Section Measurements

By T. W. Bonner,* USA

The problem of measuring fast neutron cross sections with Van de Graaff and Cockcroft-Walton accelerators can be divided into three main categories. First, a nuclear reaction must be available which will supply neutrons of the required energy; furthermore, the cross section for the reaction must be large enough to give a usuable flux of neutrons. Second, an accurate control of the energy of the accelerated particles is necessary so that monoenergetic neutrons can be produced. Third, an installation of the accelerator in the laboratory must be provided which will (*a*) minimize the number of scattered neutrons which will reach the detector, and (*b*) reduce the number of neutrons from secondary sources that reach the detector.

LABORATORY INSTALLATION

Recently installed accelerators at Argonne National Laboratory, Bartol Research Foundation, Duke University, Los Alamos Scientific Laboratory, Oak Ridge National Laboratory, Rice Institute, and the University of Texas are in large rooms which reduce neutron scattering from the walls and ceilings. Scattering of neutrons from concrete floors can be very important, and, for this reason, present practice is to use thin metal floors made of iron or aluminum over a pit which is 2.5 m or more in depth. The target position is usually 7 to 10 m from the energy analyzer, which may be a secondary source of neutrons. With such large distances, an electrostatic alternate-gradient focusing lens is often used so that a beam of small diameter can be obtained at the target.

Most experiments are carried out using the atomic hydrogen beam. The molecular beam, especially in the case of deuterons, may produce a considerable number of neutrons when it strikes a metal surface. For this reason it is advisable to have the molecular beam hit either tantalum- or a gold-plated surface which can be easily removed for cleaning; this target spot should be periodically cleaned to remove carbon deposits and adsorbed deuterium. Reduction in the amount of secondary neutrons from the molecular beam is obtained by using radiofrequency ion sources[1] which give a very high ratio of the atomic to the molecular beam. Such ion sources have a lifetime of over 2000 hours of operation when used with ion beams of about 10 microamperes. They also operate with a very low gas consumption.

The accelerator should be shielded from the target position by heavy concrete walls which will absorb the X-radiation produced in the vacuum tube. In order to reduce the neutron flux to a safe level for operating personnel, control stations are placed a distance of $\geqslant$ 10 m from the target position and are shielded by concrete $\geqslant$ 70 cm in thickness.

ENERGY CONTROL

Cockcroft-Walton accelerators are generally used with thick targets and low bombarding energies so that accurate control of the energy of the accelerated particles is not a major problem. On the other hand, the control of the energy of the particles accelerated with a Van de Graaff is very important. Magnetic and electrostatic (energy) analyzers are each in wide use. High resolution electrostatic analyzers of the type developed by Warren, Powell, and Herb[2] are in use at Wisconsin, Argonne, and Duke. Electrostatic analyzers are also used at Los Alamos, Westinghouse and Johns Hopkins. Magnetic analyzers which deflect the beam through 90 degrees are used at Rice, Oak Ridge, Los Alamos and the University of Texas. The high potential is kept constant by a variable corona current which is controlled by the error signal from the analyzer; such a system is adequate although it does not give as fast control as a modulated beam of electrons in the acceleration tube.[3] Typical results[4] of the energy resolution and stability which can be obtained with magnetic analyzers are the following data of Banta, Johnson, and Judish at Oak Ridge: with a beam current at the target 25 microamperes they obtained an excitation curve for the 993 kev resonance in the reaction $A(p,\gamma)Mg$ which had a full width at half maximum intensity of 240 ev. This is an energy resolution of 0.024 per cent; similar resolution can be obtained with electrostatic analyzers.

NEUTRON SOURCES

Neutron sources may be classified as (1) those that are strictly monoenergetic and (2) those that are not monoenergetic but which give a great enough flux of neutrons of maximum energy to be useful in making cross-section measurements.

* Rice Institute. Instruments used by Argonne National Laboratory, Bartol Research Foundation, Brown University, Duke University, Johns Hopkins University, University of California (Livermore), Los Alamos Scientific Laboratory, Oak Ridge National Laboratory, Rice Institute, University of Texas, Westinghouse Research Laboratories, and University of Wisconsin.

Neutron Energy Range, 1–500 kev

$Li^7(p,n)Be^7$

The nuclear reaction that has proven most useful for experiments with low energy neutrons is $Li^7(p,n)Be^7$. The threshold for this reaction is 1.8811 ± .0005 Mev,[5] and is used as an energy calibration for analyzers. Neutrons from this reaction are monoenergetic up to a bombarding energy of 2.38 Mev which is the threshold for a second group of neutrons. Near the threshold this second group of neutrons is weak, being only about 1 per cent as intense as the higher energy group.[6] The relative intensity rises to about 10 per cent at a bombarding energy of 2.75 Mev[7] and remains at this level up to a proton energy of 5.4 Mev.[8]

The $Li(p,n)$ reaction makes a good neutron source because of its large cross section which has been accurately measured from threshold to 2.55 Mev.[9] Targets are made by evaporating Li from a furnace onto a thin tantalum backing mounted at the target position. Rotating targets are necessary in order to use proton currents of over 5 microamperes per cm^2. The design of Hemmendinger and Taschek at Los Alamos uses a rotation speed of one revolution per sec on a 2.5 cm diameter. The outside of the 0.0025 cm tantalum backing is cooled by a fine water spray. Under these conditions 30 microamperes of beam will produce a 30 per cent decrease in the neutron yield in 10 hours.

The Wisconsin group has used this source to measure the total neutron cross section in many elements.[10] More recently Hibdon, Langsdorf, and Holland[11] at Argonne have developed an improved technique for obtaining total cross sections with neutron energies from 1 to 100 kev. The background counting rate is reduced with a massive shield and

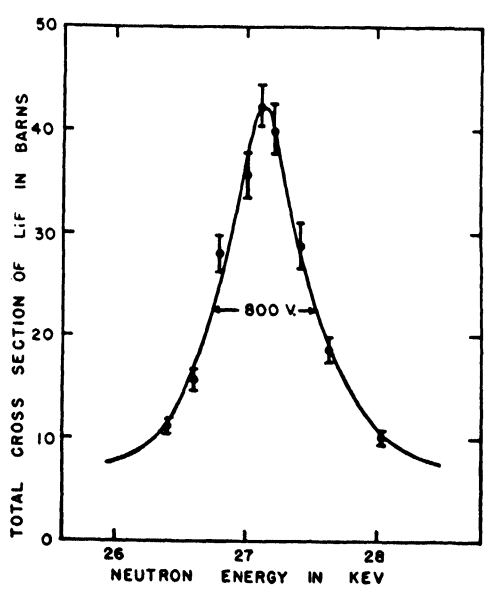

Figure 1. The total neutron scattering cross section in LiF as a function of neutron energy. Data obtained with neutrons at an angle of 120 ± 1 degrees to the direction of 2 Mev protons incident on a thin lithium target

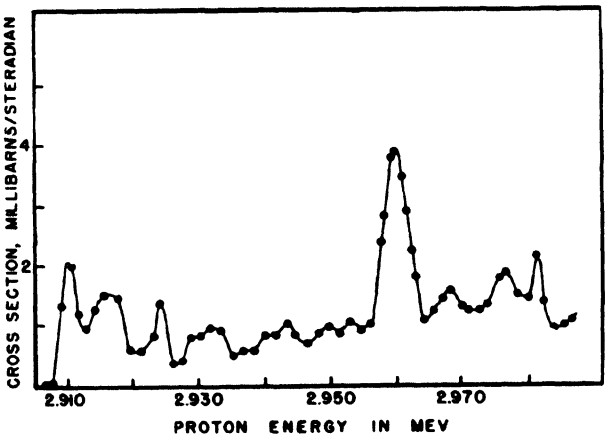

Figure 2. The differential cross section for production of neutrons at 0 degrees from the reaction $Sc^{45}(p,n)Ti^{45}$ measured in the laboratory system of coordinates. Data obtained with a target which was 3 kev thick

increased counting rates are obtained with an improved neutron detector made of a large group of boron trifluoride counters embedded in paraffin. With these improvements, thinner Li targets can be used and higher energy resolution can be obtained. Figure 1 shows the results of Mooring, Monahan, and Langsdorf[12] on the neutron total scattering cross section of a LiF sample showing the marked resonance in F^{19} at 27 kev. The experimental half-width is 800 volts which corresponds to an energy resolution of 3 per cent. Similar equipment is being used at Duke by Rohrer, Newson, Gibbons, and Cap.[13] They have observed resonances at neutron energies as low as 270 ev and obtain average neutron energy spreads of 1 kev at an energy of 10 kev and 3.3 kev at an energy of 100 kev. The fast choppers appear to have better resolution below about 5 kev. Improvements in the energy resolution of neutrons from Van de Graaff accelerators is theoretically possible and can be expected.

$Sc^{45}(p,n)Ti^{45}$, $V^{51}(p,n)Cr^{51}$, $Cu^{65}(p,n)Zn^{65}$, $Cu^{63}(p,n)Zn^{63}$

The $Li^7(p,n)Be^7$ reaction does not give monoenergetic neutrons at 0 degrees with energies less than 120 kev. Heavier elements will give lower energy monoenergetic neutrons at 0 degrees and therefore will be better sources of neutrons with energies less than 120 kev if they give comparable neutron fluxes. The (p,n) reactions in Sc^{45}, V^{51}, Cu^{65}, and Cu^{63} have been studied at Rice by Brugger, Bonner, Cook, and Marion using thin evaporated targets. The two reactions with the largest cross sections near threshold are $Sc^{45}(p,n)Ti^{45}$ and $Cu^{63}(p,n)Zn^{63}$. The cross section of the $Sc^{45}(p,n)$ reaction near the threshold is shown in Fig. 2. Pronounced resonances are observed with separations of about 3 to 5 kev. Experiments by Brugger, Bonner and Marion[14] give a threshold energy of 2.908 ± 0.004 Mev for the $Sc^{45}(p,n)Ti^{45}$ reaction, and indicate that the neutrons are monoenergetic up to a proton energy of 3.667 Mev where a second threshold is observed. The yield of kev neutrons at 0 degrees from this reaction is less

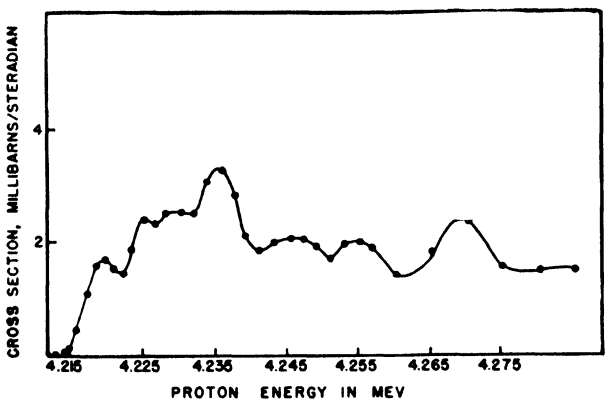

Figure 3. The differential cross section for production of neutrons at 0 degrees from the reaction $Cu^{63}(p,n)Zn^{63}$ measured in the laboratory system of coordinates. Data obtained with a CU^{63} target which was 4 kev thick

than that from the $Li(p,n)$ reaction at 120 degrees, but a larger solid angle can be used with the same spread in neutron energy. The theoretical minimum spread in neutron energy is limited by the Doppler effect due to the thermal motion of the struck target nucleus. The Doppler broadening from the $Li^7(p,n)$ reaction is considerably larger than that from the $Sc^{45}(p,n)$ reaction.

Figure 3 shows the cross section obtained by Brugger, Bonner and Marion[14] of the $Cu^{63}(p,n)Zn^{63}$ reaction with a thin evaporated target of Cu^{63} made with separated isotopes. Experiments with counters sensitive to threshold neutrons indicates that this reaction gives monoenergetic neutrons from a proton energy of 4.215 Mev, which is the reaction threshold, up to 4.410 Mev where a second group of neutrons appear.

At Oak Ridge, Banta, Johnson and Judish[4] have used $V^{51}(p,n)Cr^{51}$ reaction to study the fission and capture cross sections in heavy elements. The threshold for the $V^{51}(p,n)$ reaction is 1.56 Mev. Targets 2–5 kev thick were bombarded with 40 microamperes of protons and yielded a neutron flux of about 10^5 n/sec. Samples subtending a large solid angle were placed at 0 degrees to the proton beam. Experiments were carried out at the discrete energies of the resonances, at which neutrons with energies of 5, 11, 33, 39, 44, and 49 kev were produced.

Neutron Energy Range, 0.3 to 20 Mev

$H^3(p,n)He^3$

Monoenergetic neutrons in the energy range of 0.3 to 5 Mev are obtained from the reaction $H^3(p,n)He^3$. The cross section for this reaction has been studied at Los Alamos and Oak Ridge.[15] Figure 4 gives the measured cross sections at different laboratory angles. Targets can be in the form of gaseous tritium or tritium adsorbed in thin zirconium layers evaporated onto a wolfram or preferably a platinum backing. Gaseous targets give yields about 10 times those of the Zr-T targets for the same energy loss in the target. Aluminum foils which are 0.0005 cm thick are usually used to cover entrance holes which have a diameter of 0.4 cm. Currents up to 4 or 5 microamperes will not produce gas leaks in a good foil. The gas container should be made with thin walls and cooled by a jet of air. Better energy resolution can be obtained with Zr-T targets because of the inherent energy straggling (~20 kev) in the Al foil. γ-radiation is produced by proton bombardment of the Al foil and protons with energies more than 5.8 Mev produce neutrons from the reaction $Al^{27}(p,n)Si^{27}$.

$H^2(d,n)He^3$

Higher energy neutrons than are available from the $H^3(p,n)He^3$ reaction can be obtained from the $H^2(d,n)He^3$ reaction. The differential cross section for the emission of neutrons at 0 degrees, 10 degrees, 20 degrees, and 30 degrees is given in Fig. 5. Cross sections for this reaction have been measured by Hunter and Richards,[16] by Arnold, Phillips, Sawyer, Stovall and Tuck[17], and recently at deuteron energies above 1.75 Mev by Smith, Perry and Henkel[18] using stilbene crystal detectors, and by Smith and Perry[19] who counted proton recoils from a thin hydrogenous foil (neutron telescope). Gaseous deuterium targets are generally used for the reaction $H^2(d,n)He^3$ except at low bombarding energies. Aluminum foils give large neutron yields with deuteron bombardment, so nickel foils are substituted; foils with a thickness of from 0.00012 to 0.00025 cm are standard. Such foils will take currents of from 1 to 3 microamperes of deuterons with energies of from 1.5 to 5 Mev; some gas leakage is observed at currents that will not produce rupture of the foil. A different technique has been employed at Bartol where a 0.00013 cm nickel foil is supported on a fine grid which is 60 per cent open. With electrical scanning of the beam on the target, 30 microamperes of current is possible, without damage to the foil. Gas targets should not be longer than 2 or 3 cm because of the small angle scattering in the nickel foil. Neutron yields from the nickel foils become important with deuterons with energies above about 2 Mev; most of the neutrons have energies less than that from the $H^2(d,n)He^3$ reaction and so will not be counted with a biased neutron detector. Strong 4.5 Mev γ-radiation is produced in the deuteron bombardment

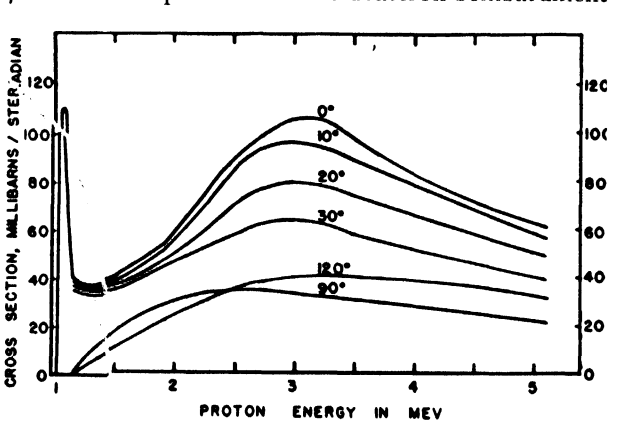

Figure 4. The differential cross section for neutrons from the reaction $H^3(p,n)He^3$ measured in the laboratory system of coordinates

of nickel. Low energy neutrons are also obtained from the C^{12} $(d,n)N^{13}$ reaction because of carbon contamination on the nickel foil and on the walls of the gas container. Neutrons and γ-radiation can also be produced in the material of the gas container itself. Such radiations are reduced if the walls of the container are gold plated or made of platinum.

Above 4.45 Mev low energy neutrons from the break-up of the deuteron are energetically possible but experiments of Henkel, Perry, and Smith[18] failed to detect an appreciable yield of these neutrons up to a deuteron energy of 7 Mev.

$H^3(d,n)He^4$

A large yield of 14 Mev neutrons is available from the $H^3(d,n)He^4$ reaction; a maximum total cross section of 5.0 barns is observed at a deuteron energy of 108 kev.[17,20] This reaction is frequently used with Cockcroft-Walton accelerators where neutron yields of 4×10^{10} neutrons per sec have been obtained at Los Alamos by Coon, Graves, Battat, and Davis[21] with a beam of 200 microamperes of 250 kev deuterons on a thick Zr-T target. With such large beam currents on a target with an area of 0.5 cm^2 the yield of neutrons decreases rapidly with bombarding time. Data of Coon, Graves, Battat, and Davis on the decrease in neutron yields are given in Fig. 6. Figure 6 also gives the yield of neutrons from a thick Zr-D target under similar conditions; such a target does not show a decrease in the yield with bombardment. With 125 kev deuterons the yield of neutrons is ½ as large as with 250 kev deuterons and the yield decreases with bombardment at twice the rate.

At deuteron energies from 0 to 4 Mev the $H^3(d,n)He^4$ reaction will give monoenergetic neutrons at 0 degree with energies from 14 to 21 Mev, and neutrons with energies down to 12 Mev at 157 degrees to the deuteron beam. The differential cross section for this reaction has recently been measured by Bame[22] at Los Alamos with a neutron telescope; these cross sections for the yield of neutrons at different laboratory angles are given in Fig. 7.

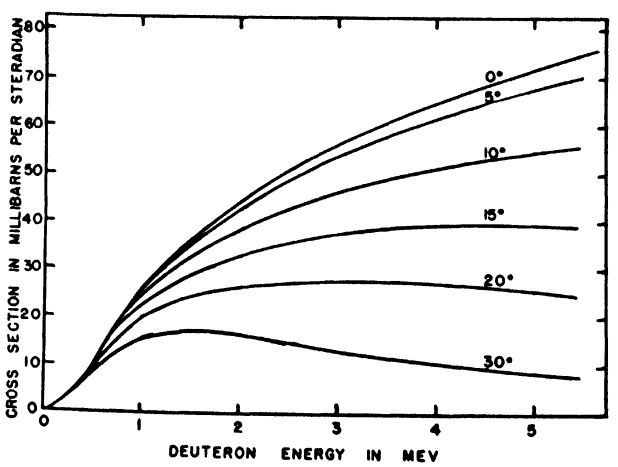

Figure 5. The differential cross section for neutrons from the reaction $H^2(d,n)He^3$ measured in the laboratory system of coordinates

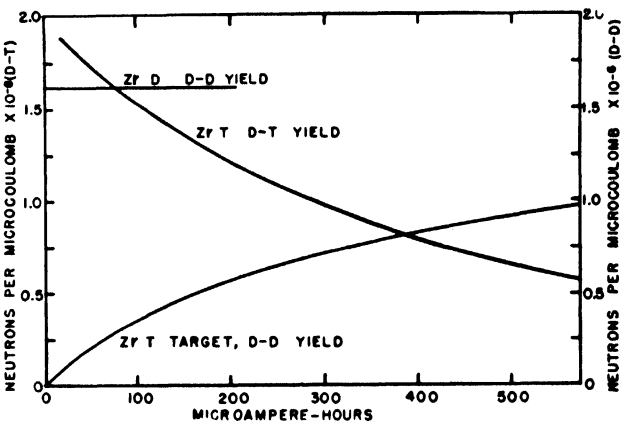

Figure 6. The yield of neutrons from the D-D and D-T reactions as a function of bombarding time

Henkel, Perry, and Smith[18] have recently found that deuterons with energies above 3.71 Mev produce low energy neutrons in the bombardment of tritium and have interpreted this as due to the break-up of the deuteron. The cross section for the emission of these low energy neutrons is about 35 mb per steradian at 0 degrees with deuterons of 6 Mev. At this deuteron energy, neutrons from the break-up of deuterium have a greater intensity than neutrons from the $H^3(d,n)He^4$ reaction.

The type of tritium targets used are similar to those discussed in the $H^3(p,n)He^3$ and $H^2(d,n)He^3$ reactions. At deuteron energies above 1 Mev, neutrons from the nickel foils used with gas targets give a considerable background of lower energy neutrons. Carbon contamination is also important. Zr-T targets may give a considerable background of lower energy neutrons because of deuteron reactions with nitrogen and oxygen which are often present in these targets in comparable quantities to that of tritium.

$C^{13}(\alpha,n)O^{16}$, $Be^9(\alpha,n)C^{12}$, $N^{14}(d,n)O^{15}$

Monoenergetic neutrons with energies up to 7 Mev can be produced in the reaction $C^{13}(\alpha,n)O^{16}$, with 5 Mev α-particles accelerated in a Van de Graaff. Good beams of singly-charged helium ions are obtained by introducing a small helium flow in a radio frequency ion source; less than 1 per cent as many doubly ionized helium ions are obtained.

Strong sources of neutrons with energy variable from 9 to 11 Mev, accompanied by neutrons with approximately 4.5 Mev less energy, are available from the reaction $Be^9(\alpha,n)C^{12}$. Neutron total cross sections and non-elastic cross sections in the energy range of 9 to 11 Mev can be made with a biased neutron detector using this source.

Neutrons with energies up to 8 Mev from the $N^{14}(d,n)O^{15}$ reaction have been used by Bastrom, Hudspeth, and Morgan[23] at Texas to measure the activation cross section in the reaction $F^{19}(n,\alpha)N^{16}$. This source is not monoenergetic but the neutron group of highest energy has approximately 5 Mev more energy than the second neutron group. The yield of 8 Mev neutrons from this reaction is much

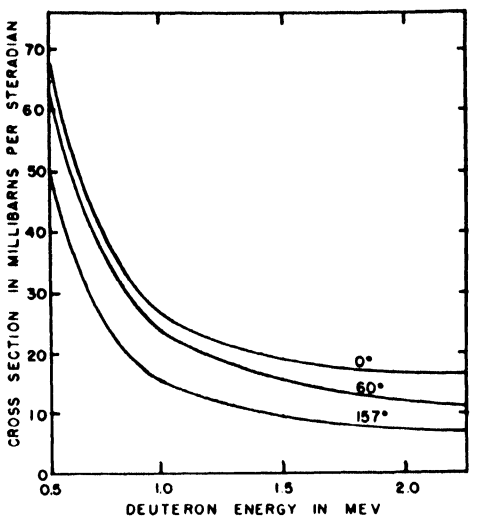

Figure 7. The differential cross section for neutrons from the reaction $H^3(d,n)He^4$ measured in the laboratory system of coordinates

less than can be obtained with the reaction $H^2(d,n)He^3$; however, higher neutron energies are obtained at a given bombarding energy from the $N^{14}(d,n)O^{15}$ reaction.

REFERENCES

1. Moak, C. D., Reese, H. and Good, W. M., *Design and operation Features of an R.F. Ion Source,* Phys. Rev. *83*: 232 (1951).
2. Warren, R. E., Powell, J. L. and Herb, R. G., *Electrostatic Analyzer for Selection of Homogeneous Ion Beam,* Rev. Sci. Instr. *18*: 559 (1947).
3. Bennett, W. E., Bonner, T. W., Mandeville, C. E. and Watt, B. E., *Resonances in the Disintegration of Fluorine by Protons,* Phys. Rev. *70*: 882 (1946).
4. Banta, H. E., Johnson, C. H. and Judish, J. P. (private communication).
5. Jones, K. W., Douglas, R. A., McEllistrem, M. T. and Richards, H. T., *Comparison of Nuclear and Gamma-ray Energy Scales,* Phys. Rev. *94*: 947 (1954).
6. Marion, J. B., Brugger, R. and Bonner, T. W. (to be published in Phys. Rev.)
7. Johnson, C. H. and Barshall, H. H., *Interaction of Fast Neutrons with Nitrogen,* Phys. Rev. *80*: 818 (1950); Hamermesh, B. and Hummel, J., *Neutron Groups from the Reaction Li7(p.n)Be7,* Phys. Rev. *78*: 73 (1950); Freier, G. C., Stratton, T. F. and Rosen, L., *The Excited Nuclear State of Be^7,* Phys. Rev. *79*: 721 (1950).
8. Cranberg, L. (private communication).
9. Taschek, R. and Hemmendinger, A., *Reaction Constants for $Li^7(p.n)Be^7$,* Phys. Rev. *74*: 373 (1948).
10. Barshall, H. H., Bockelman, C. K. and Seagondollar, L. W., *Total Cross Section of Fe, Ni, and Bi for Fast Neutrons,* Phys. Rev. *73*: 659 (1948); Bockelman, C. K., Peterson, R. F., Adair, R. K. and Barshall, H. H., *Total Cross Section Measurements for Fast Neutrons,* Phys. Rev. *76*: 277 (1949); Barshall, H. H., Bockelman, D. K., Peterson, R. E. and Adair, R. K., *Investigation of Nuclear Energy Levels in Lead,* Phys. Rev. *76*: 1146 (1949); Peterson, R. F., Adair, R. K. and Barshall, H. H., *Nuclear Energy Levels in Lead Isotopes,* Phys. Rev. *79*: 935 (1950); Miller, D. W., Adair, R. K., Bockelman, C. K. and Darden, S. E., *Total Cross Sections of Heavy Nuclei for Fast Neutrons,* Phys. Rev. *88*: 83 (1952).
11. Hibdon, C. T., Langsdorf, A. and Holland, R. E., *Neutron Transmission Cross Sections in the Kilovolt Region,* Phys. Rev. *85*: 595 (1953).
12. Moaring, F. P., Monahan, J. E. and Langsdorf, A., (private communication).
13. Gibbons, J. H. and Newson, H. W., *Neutron Resonances in Bi, Tl, and Pb,* Phys. Rev. *91*: 209 (1953); Rohrer, R. H., Newson, H. W., Gibbons, J. H. and Cap, P., *Activation of Al and Sc^{80} by p-Neutron Captures in the Kilovolt Region,* Phys. Rev. *95*: 302 (1954).
14. Brugger, R., Bonner, T. W. and Marion, J. B. (to be published in the Phys. Rev.).
15. Jarvis, G. A., Hemmendinger, A., Argo, H. V. and Taschek, R. E., *Reaction Constants for $T^3(p.n)He^3$,* Phys. Rev. *79*: 929 (1950); Willard, H. B., Blair, J. K. and Kington, J. D., *The Reactions $T(p.n)He^3$ and $T(p,\gamma)He^4$,* Phys. Rev. *90*: 865 (1953); Jarvis, G. A., (private communication). The published data of Jarvis, G. A., Hemmendinger, A. and Taschek, R. have been normalized to that of Jarvis by multiplying their cross section by 0.81. The data of Willard, H. B., Bair, J. K. and Kington, J. D., indicate about 20 per cent higher cross sections at 1.8 Mev than that of Jarvis.
16. Hunter, G. T. and Richards, H. T., *Yield and Angular Distribution of the D-D Neutrons,* Phys. Rev. *76*. 1445 (1949).
17. Arnold, W. R., Phillips, J. A., Sawyer, G. E., Stovall, E. S. and Tuck, J. L., *Cross Section for the Reactions $D(d,p)T$, $D(d,n)He^3$, $T(d,n)He^4$, and $He^3(d,p)He^4$ Below 120 kev,* Phys. Rev. *93*: 483 (1954).
18. Henkel, R. L., Perry, J. E. and Smith, R. K. (private communication).
19. Smith, R. K. and Perry, J. E. (private communication).
20. Conner, J. P., Bonner, T. W. and Smith, J. R., *A Study of the $H^3(d,n)He^4$ Reaction,* Phys. Rev. *88*: 468 (1952).
21. Coon, J. H., Graves, E. R., Battat, M. E. and Davis, R. W., (private communication).
22. Bame, S. J. (private communication).
23. Bastrom, N. A., Hudspeth, E. H. and Morgan, I. L. (private communication).

Techniques for Measurement of Neutron Cross Sections and Energy Spectra for Sources Which Are Continuous in Energy and Time

By L. Rosen,* USA

Total cross-section measurements with monoenergetic neutrons involve straightforward but very precise transmission determinations and are best carried out using electronic counter techniques. Crystal counters, in particular, are well suited to the attainment of good statistical accuracy at constant bias settings which may be quite close to that corresponding to the primary neutron energy.

In order to measure total neutron cross sections over energy regions which are not readily accessible to generators of monoenergetic neutrons, Nereson and Darden[1] have developed a method by means of which one may make use of a continuous spectrum. Basically the method involves the isolation of narrow energy bands from a continuous spectrum through the use of a detector which operates as a neutron spectrometer. Once isolated, each energy band may then be used as the neutron source for a standard good geometry transmission experiment.

Figure 1 shows a perspective cutaway view of the detector, which is operated directly in a collimated beam of neutrons. A thin hydrogenous layer at the front of the detector converts neutrons to proton recoils. After collimation the proton recoils pass first through a small proportional counter and then into a parallel plate, Frisch grid, ionization chamber which is operated as a neutron spectrometer in coincidence with the proportional counter. The spectrometer chamber is followed by a second ionization chamber with which it is operated in anti-coincidence. Whereas the purpose of the chambers in coincidence is merely to reduce background, the anti-coincidence arrangement is an integral part of the spectrometer. It permits one to discriminate against those proton recoils which are not stopped in the spectrometer chamber and hence do not produce, in this chamber, ionization commensurate with their energy. Variation of the gas pressure in the chamber, the use of deuterium as well as hydrogen as the radiator, and the use of absorbers in the path of the recoils give this instrument a great deal of flexibility in terms of the energy region accessible to it. The inherent energy resolution of the spectrometer, in terms of the width at half maximum for a group of 7-Mev monoenergetic neutrons, is approximately 8 per cent.

Using a fission spectrum as the primary neutron source, a large number of elements has been studied over the energy region 3–13 Mev. These experiments were performed under the conditions of $\sim$ 50 per cent transmission and 10 per cent energy spread. Although the energy resolution was inadequate to resolve narrow resonances, it was completely adequate for the objectives of the experiment. These were: (1) to obtain cross-section data for use in reactor design and shielding calculations and (2) to extend the existing information on cross-section trends as a function of atomic weight.

The results of the measurements are summarized in Figs. 2 and 3. Figure 2 is a photograph of a cardboard model constructed to show the trend of total cross section as a function of neutron energy. Although for the light elements, adjacent elements show little resemblance in cross-section characteristics, the heavy elements reveal marked similarities between neighboring elements. In particular it can be seen that the maximum, which occurs between 4 and 5 Mev at $A = 55$, shifts in a more or less regular manner to higher energies with increasing

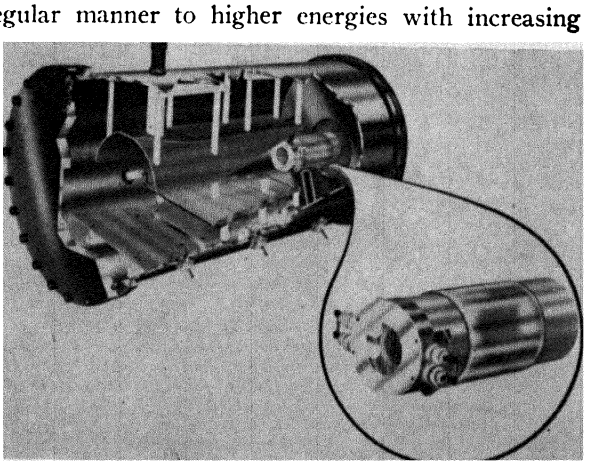

Figure 1. Cut-away view of ionization chamber (N. Nereson)

* Los Alamos Scientific Laboratory. Including work by A. Armstrong, S. Darden, G. Frye, J. Gammel, E. Graves, N. Nereson, L. Rosen and L. Stewart, Los Alamos Scientific Laboratory; G. J. Perlow, Argonne National Laboratory; W. M. Preston (now at Harvard University, Cambridge, Massachusetts) and P. H. Stelson, Massachusetts Institute of Technology; J. B. Weddell and B. Jennings, Westinghouse Research Laboratories.

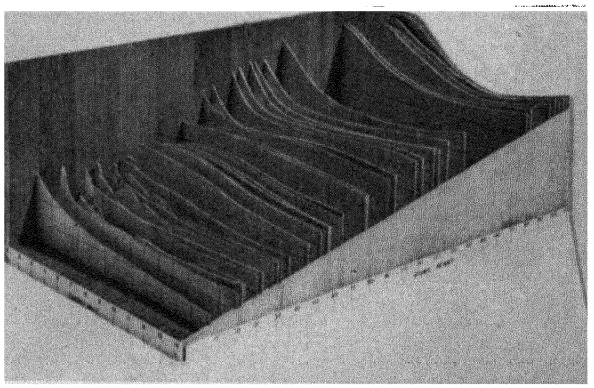

Figure 2. Cardboard model showing variation of average total cross section with energy and atomic weight. Each heavy line represents one barn (N. Nereson)

atomic weight. Likewise the minimum, which is first apparent at $A \cong 90$ also moves to higher energies with increasing atomic weight.

Where measurements with monoenergetic neutrons from accelerators have been made, they agree with the above results to within $\pm$ 10 per cent.

The lower energy limit of the above described method is approximately 3 Mev. This is the upper limit of interest for many problems of reactor design. In fact, the region of most interest in reactor design, exclusive of shielding problems, falls below 1 Mev. An electronic method capable of measuring neutron energy distributions from 50 kev to 1 Mev has recently been developed by Perlow. This spectrometer, shown schematically in Fig. 4, consists of two cylindrical proportional counters, side by side, with axes parallel. As in the case of Nereson's spectrometer, this spectrometer also utilizes collimated proton recoils, but they are produced in the counter gas rather than in an external radiator. Collimation is achieved by 400 holes, each 4.5 mm long, in a brass block separating the two counters. The collimation channels restrict the protons to within 28 degrees of a line parallel to the axes of the holes and normal to the counter axis.

Forward directed proton recoils generated in the gas of one counter pass into the other by way of the collimation channels. The counters are filled with methane to a pressure of a few cm Hg. A coincidence system selects the forward recoil protons whose energy is then given by the sum of the pulse heights from the two counters. The efficiency of this spectrometer is approximately 10^{-5} and the energy resolution ten per cent. Figure 5 shows a typical resolution function.

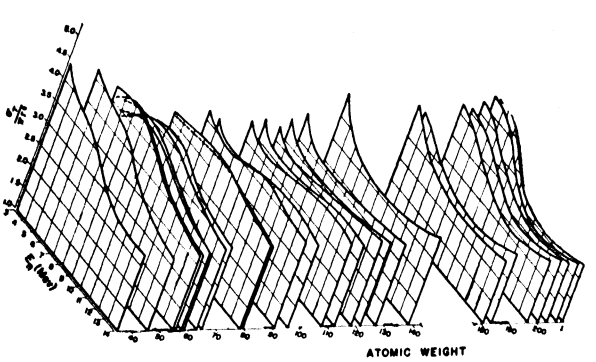

Figure 3. Neutron cross sections of elements heavier than chlorine (N. Nereson)

As of this writing, the most generally useful technique for neutron spectroscopy in the energy region 0.5–15 Mev is the nuclear emulsion technique.[2] In virtually all applications of nuclear emulsions to neutron spectroscopy, use is made of the trajectories of proton recoils to infer the energies of the incident neutrons. Basically the problem consists of measuring the range and orientation of the recoil protons. The precision with which these quantities are determined, together with the range straggling of the protons resulting from the nature of the slowing down process, determine the resolution of the method.

For neutrons of energy less than 15 Mev, 200–400 μ proton sensitive emulsions are quite adequate. These may be uniformly developed by a two-stage low temperature procedure. Before drying, the voids in the emulsion left by the removal of

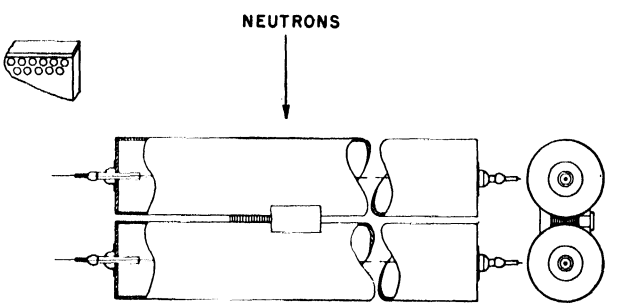

Figure 4. Schematic diagram of double proportional counter (G. J. Perlow)

unsensitized silver halides are filled with glycerine or resin in order to maintain the original thickness. This serves to avoid undue distortion as well as to ease the task of dip measurements. The plates may be conveniently scanned under a modified binocular microscope with special measuring stage and eyepiece protractor. Figure 6 pictures such an instrument. For each track which falls within given angular limits (usually 10–15 degrees) with respect to the incident neutron velocity vector, one records the projected length along the neutron velocity vector, the azimuthal angle with respect to this line and the vertical projection. These measurements, along with an appropriate range-energy table, are fed into an electronic computing machine which calculates the neutron energy corresponding to each proton recoil. Figure 7 illustrates the geometrical relationships before and after processing under conditions of normal shrinkage. By taking account of the hydrogen concentration in the emulsion, the probability for tracks leaving the emulsion, the solid angle of acceptance of proton recoils and the attenuation of the emulsion (where this is significant), one may arrive at the absolute number of neutrons/cm^2, as a function of energy,

incident on the emulsion. This factor of course enters directly into any calculation of the cross section for a given neutron-producing process. Where the cross section for a neutron scattering or emission process is to be obtained, it is not necessary to know either the hydrogen concentration of the emulsion or the absolute value of the solid angle of acceptance of proton recoils, provided that one uses emulsions to measure also the neutron flux incident on the scatterer. The energy resolution of this method is such that the ratio of the full width at half maximum to the neutron energy, for monoenergetic neutrons, is approximately 2.5 per cent at 14 Mev increasing to ~ 15 per cent at 1 Mev. Under controlled conditions of temperature and humidity the precision attainable in energy measurements is approximately 1 per cent for neutrons of energy greater than 5 Mev increasing to ~ 5 per cent at 1 Mev. The detection efficiency is such that for neutrons of 7 Mev, a neutron flux of 10^8 neutrons/cm^2 will produce, in 1 mm^2 of 200 μ emulsion, approximately 60 acceptable

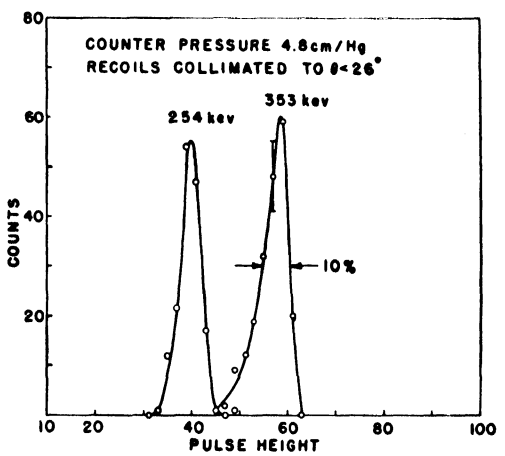

Figure 5. Resolution function for double proportional counter spectrometer (G. J. Perlow)

proton recoils which make an angle of less than 15 degrees with respect to the neutron direction and come to rest within the emulsion. Finally the accuracy with which one can determine the absolute neutron flux incident on the emulsion is ~ 10 per cent.

In order to illustrate the versatility of the method, we shall consider problems of the measurement of neutron spectra and/or neutron cross sections.

Since the spectrum of neutrons arising from thermal neutron induced fission of U^{235} is of fundamental importance to the design of reactors, we undertook to remeasure, as precisely as possible, this spectrum. Figure 8 illustrates the experimental arrangement. A beam of thermal neutrons from the Los Alamos slow neutron reactor is intercepted by a thin plate of U^{235}. Nuclear plates are arranged in good geometry with their axes passing through the center of the U^{235} plate. Background runs are made with a paraffin cone between the U^{235} and the neutron detectors. Over 10,000 proton recoil tracks were measured. In order to obtain adequate statistical

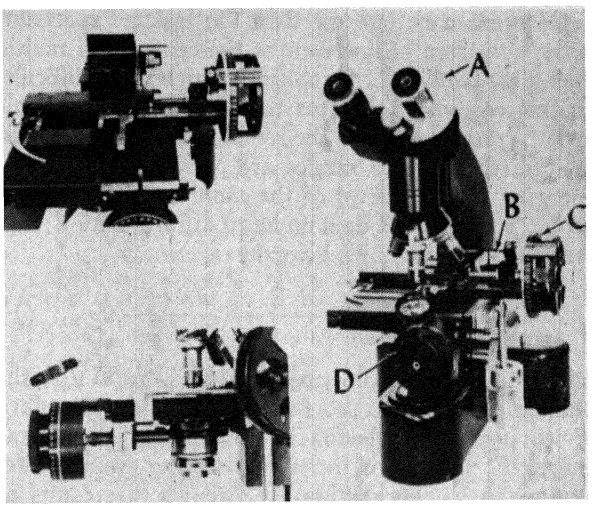

Figure 6. Leitz ortholox microscope as adapted for nuclear emulsion work

accuracy over the high energy portion of the spectrum, without measuring a prohibitively large number of low-energy recoils, much of the emulsion volume was scanned for high-energy proton recoils only. Figure 9 shows the results of the experiment. Over the region encompassed by these data (0.3–12 Mev) the fission spectrum is well represented by the relation $1.058 \times 10^3\ e^{-E/0.965} \sinh \sqrt{2.29E}$. It has also been shown by Nereson[3] using the same technique, that the Pu thermal neutron induced fission spectrum is quite similar to the U^{235} spectrum.

Concurrently with the above measurements an experiment was performed to determine the neutron leakage spectrum from a bare U^{235} critical assembly. Figure 10 shows the experimental geometry. The tower was for the purpose of avoiding difficulty from ground-scattered neutrons. Figure 11 is a comparison of the pure fission spectrum with the critical assembly leakage spectrum. The latter spectrum is seen to contain a considerable number of degraded neutrons, thus affording qualitative evidence for the preponderance of inelastic scattering over the "hardening" of the fission spectrum resulting from the variation of fission cross section with neutron energy.

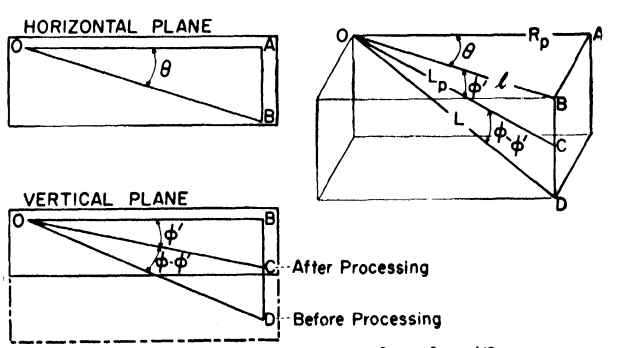

Figure 7. Orientation of track in unprocessed and processed emulsion

Of even more interest than the leakage spectrum is the spectrum of neutrons at the center of a multiplying assembly. This problem is much more difficult. In this case one measures the absolute range of all proton recoils within the emulsion, regardless of their direction. The ranges are converted to proton energies and the curve of the number of protons vs proton energy must then undergo differentiation; i.e., the neutron spectrum is given by

$$F(E) = \frac{A\,E}{n\,\sigma_{n-p}\,(E)}\,\frac{dN(E)}{dE} \qquad (1)$$

where A is the plate area analyzed, $N(E)$ is the number of protons (corrected for their probability of leaving the emulsion) in unit energy interval at energy E, and σ_{n-p} is the n–p scattering cross section at the same energy. Figure 12 shows the results of neutron spectrum measurements at the center of a fast reactor. Thus, the spectrum is much degraded from that of a pure fission spectrum, although the maximum occurs at about the same energy.

One of the most important unknowns in shielding studies is the differential cross section for neutron emission, with respect to energy of emitted neutrons, as a function of incident neutron energy. Such information is essentially lacking for almost all elements. Although neutrons of energy greater than 10 Mev are not prolific in the fission spectrum, their importance is far greater than their numbers would indicate due to their larger mean free paths and secondary reactions which they produce. Furthermore data obtained with high energy neutrons may

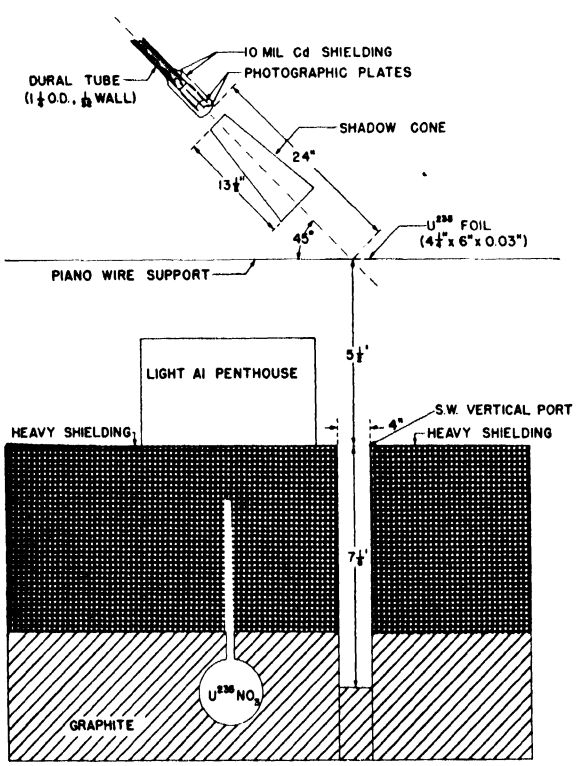

Figure 8. Schematic representation of the experimental arrangement for measuring the fission neutron spectrum of U^{235}

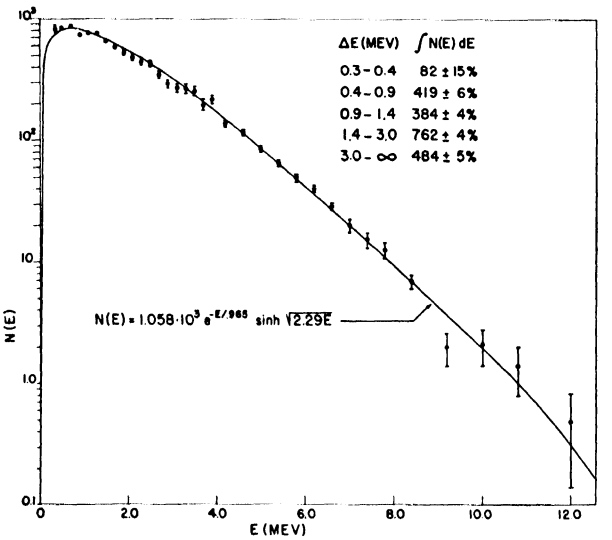

Figure 9. Fission neutron spectrum of U^{235}. Solid line represents best fit to the data using equation shown

be used to determine which nuclear interaction theories are in accord with experiment. These may then be considered more reliable for predicting neutron interaction cross sections for lower energy neutrons where data are not yet available.

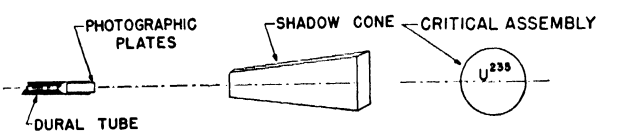

Figure 10. Schematic representation of the experimental arrangement for measuring the leakage spectrum from an untamped multiplying assembly of U^{235}

Nuclear emulsions have been used successfully to measure the absolute number of neutrons as a function of energy from the interactions of 14-Mev neutrons with various elements.[4] Figure 13 illustrates the experimental arrangement. This type of experiment is known as a "sphere" experiment.[4] An isotropic monoenergetic source is surrounded by a spherical shell of the material under investigation. The nuclear plate is arranged in good geometry with

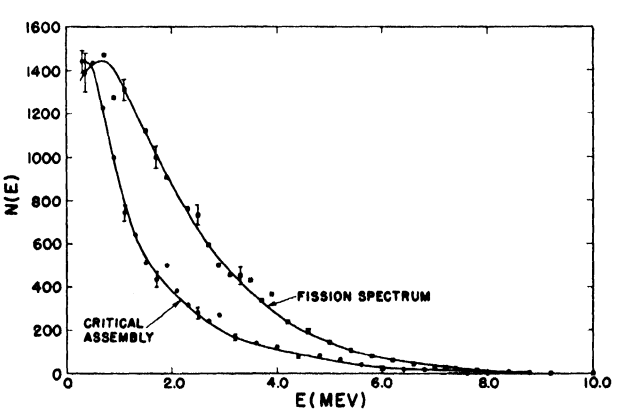

Figure 11. Critical assembly leakage and U^{235} fission spectrums. Here spectra are normalized on basis of their integrals

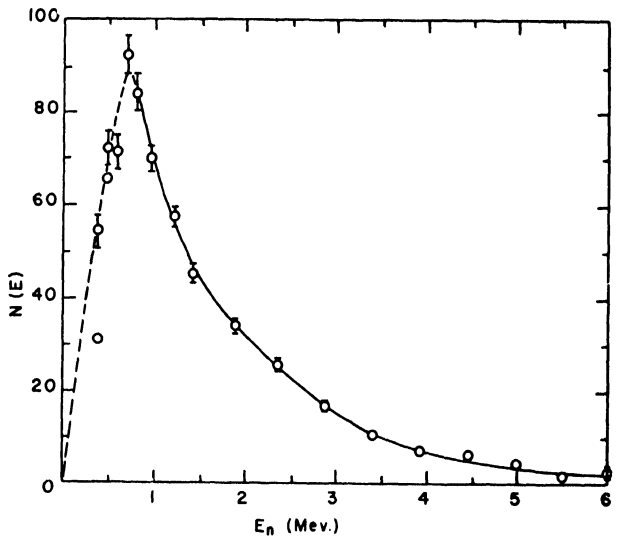

Figure 12. Neutron spectrum inside a fast reactor (N. Nereson)

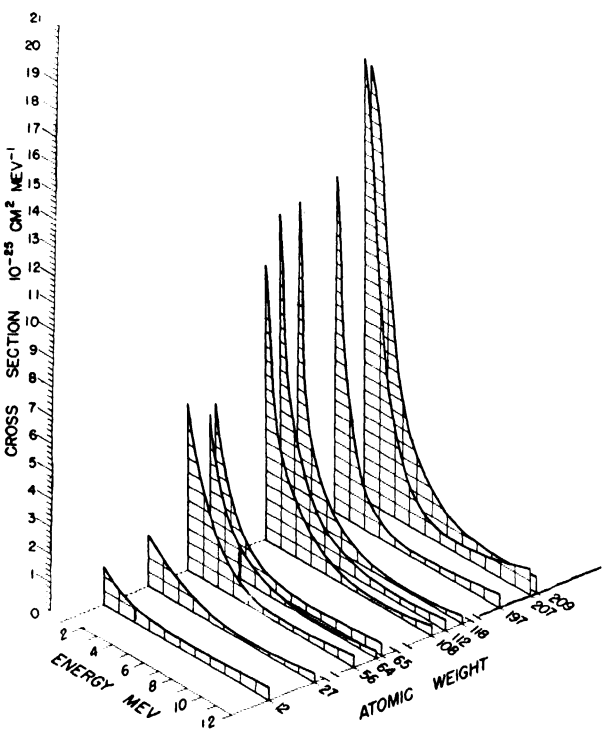

Figure 14. Neutron emission cross section vs energy of emitted neutrons for various elements bombarded by 14 Mev neutrons

respect to this sphere, which now becomes a secondary neutron source, with its axis coincident with one of the sphere radii. Figure 14 illustrates the results obtained for various elements. It might be remarked that the total cross section for emission of neutrons from non-elastic interactions is in every case consistent with recently published sphere multiplication measurements at 14 Mev.[5] With the possible exception of C^{12} very little structure can be seen due to the close spacing of the energy levels. Even in C^{12} a detailed spectrum reveals the 4.4-Mev level only poorly resolved due to center-of-mass motion. For elements above mass 50, the neutron spectrum falls

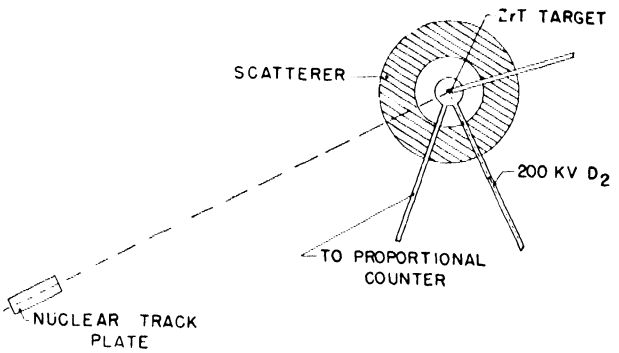

Figure 13. Schematic of experimental arrangement used in the interaction of 14 Mev neutrons with various elements

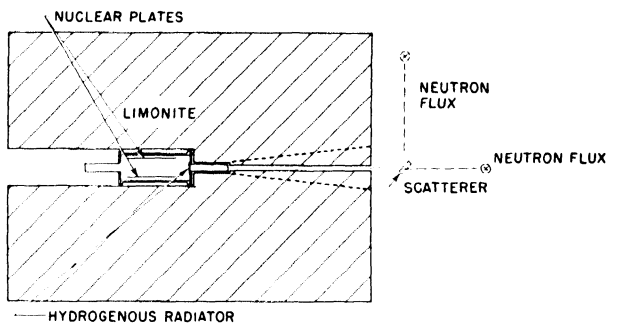

Figure 15. Neutron collimator

off exponentially up to ~ 4 Mev. This part of the spectrum is very much in accord with the statistical theory of nuclear reactions. However, this theory predicts less high-energy neutrons than one actually observes. We will return to this point later. For obvious reasons this type of experiment can only be performed with an isotropic primary neutron source.

Similar data may, however, be obtained with non-isotropic sources by making use of a neutron collimator. Figure 15 illustrates such a collimator. The construction and material of this collimator is a function of neutron energy. For neutrons of energy less than 5 Mev borated paraffin is quite adequate. For higher energies iron is extremely good on both a volume and weight basis. Where the primary source is continuous, a combination of iron and hydrogenous material is desirable. For example, a mix† of cement, limonite, and iron punchings has been successfully used. Figure 16 illustrates the efficacy of a limonite collimator for 14-Mev neutrons. The degraded neutrons are seen to represent less than 2 per cent of the main group.

The collimator may be used to look directly at a primary neutron source or to shield out the primary source and observe the secondary neutrons from the interaction of the primary neutrons with a scatterer. In the case illustrated the plates are used simply as detectors, an hydrogenous foil being used as the radiator. This arrangement is especially useful when one is attempting to detect neutrons in the presence of intense gamma radiation. This device was used to

† 1 part cement, 2 parts limonite, 4.4 parts scrap iron, and 0.3 parts water.

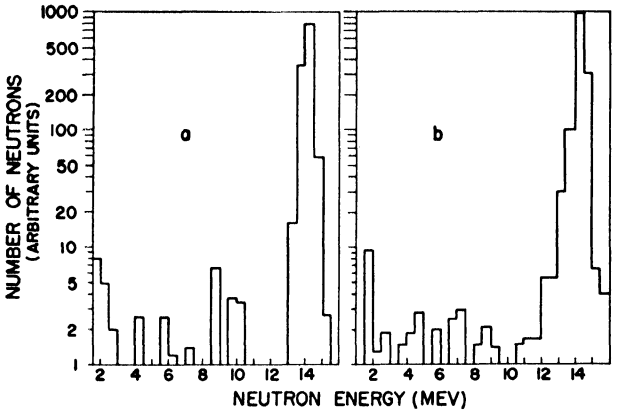

Figure 16. Neutron spectrum at the target: (*a*) is the spectrum obtained from proton recoils at 15 degrees; (*b*) is an average over fifteen angles from 15 to 40 degrees

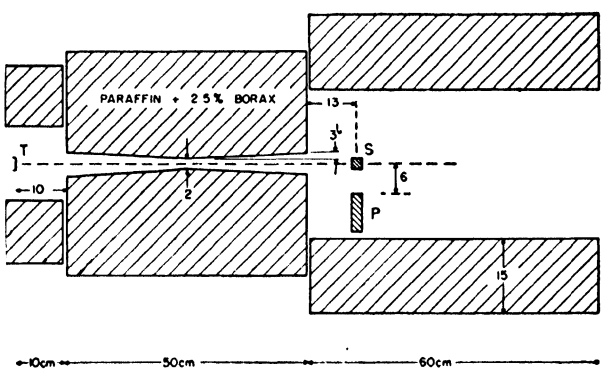

Figure 17. Experimental arrangement for inelastic scattering of fast neutrons (Stelson and Preston)

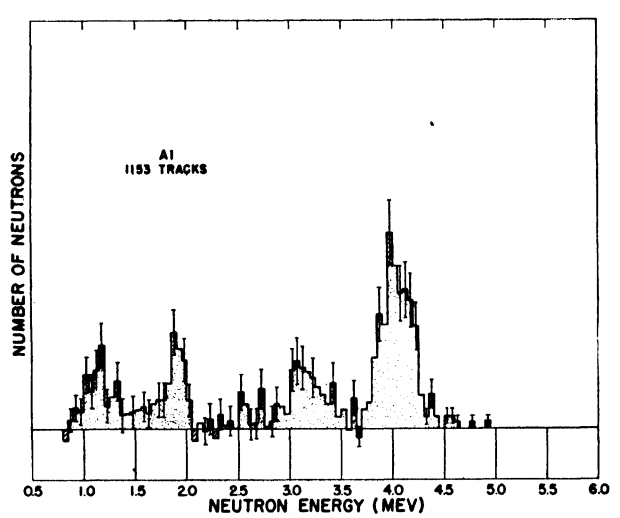

Figure 20. Inelastic scattering of 4.4 Mev neutrons by aluminum (Weddell and Jennings)

measure the total cross section of nitrogen as a function of neutron energy from 2–10 Mev. The neutron source was a fast reactor. The procedure consisted simply of measuring the neutron spectrum transmitted through a Dewar filled with liquid nitrogen and then repeating the measurement with the Dewar empty. The data thus obtained were in good agree-

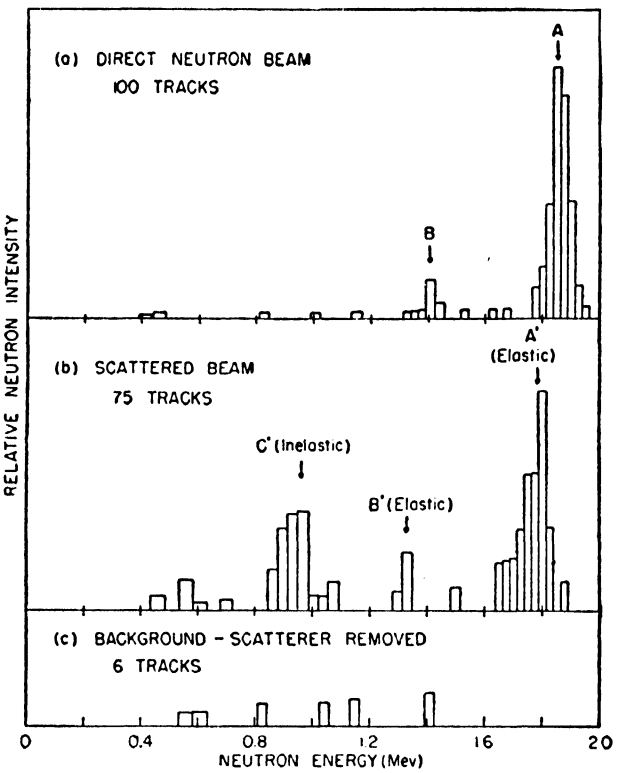

Figure 18. Histograms of relative neutron intensity vs neutron energy derived from recoil proton distributions in emulsions (Stelson and Preston)

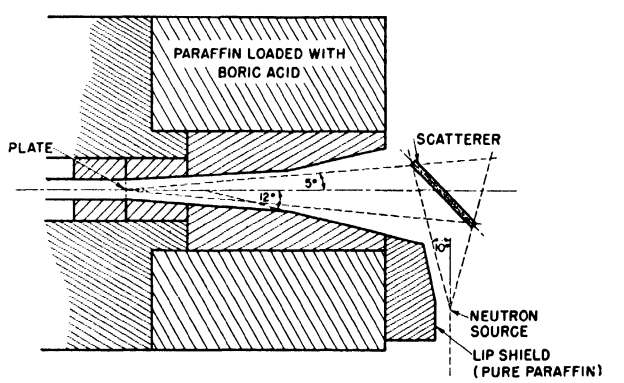

Figure 19. Neutron collimator (Weddell and Jennings)

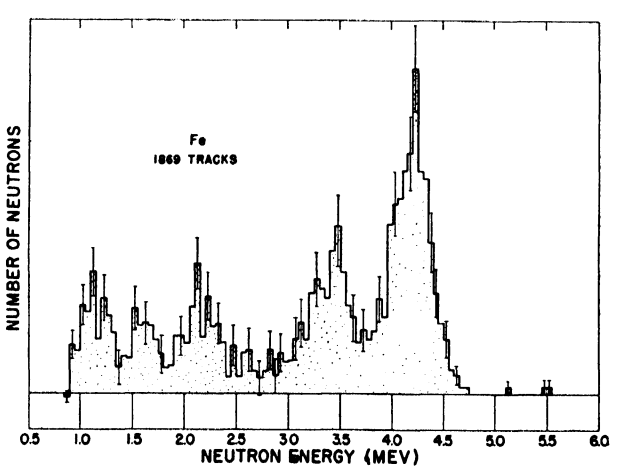

Figure 21. Inelastic scattering of 4.4 Mev neutrons by iron (Weddell and Jennings)

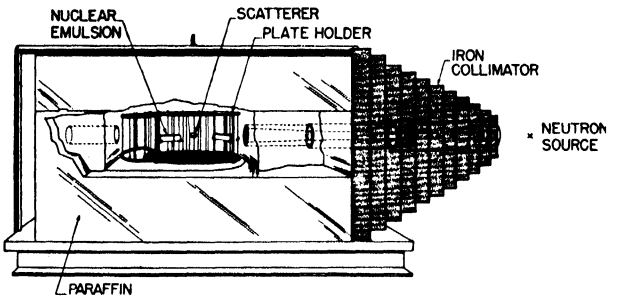

Figure 22. Neutron collimator for angular distribution measurements

ment with the more recent and more precise measurements of Nereson.[1] Similar arrangements have been used by Stelson and Preston and by Weddell and Jennings to measure elastic and inelastic neutron cross sections. In these experiments the nuclear plates are placed on the axis of the collimator and are used as both radiator and detector. Figure 17 pictures the collimator used by Stelson and Preston[6] to measure the elastic and inelastic scattering of 1.8-Mev neutrons from iron at 90 degrees with respect to the incident beam. Figure 18 shows their results.

Figure 19 shows the collimator used by Weddell and Jennings to study the elastic and inelastic scattering of 4.4-Mev neutrons from carbon, aluminum, calcium, iron, zirconium, and bismuth at 82 degrees ± 7 degrees with respect to the incident neutron beam direction. Some of their results are illustrated in Figs. 20 and 21. It should be pointed out that Stelson and Preston as well as Weddell and Jennings were successful in obtaining absolute cross sections. In the case of aluminum for example, Weddell and Jennings arrived at the following cross sections, in barns per steradian, for the various levels: elastic, 0.058 ± 0.012; (0.84 + 1.02), 0.023 ± .006; 2.21, 0.020 ± 0.005; 3.10, 0.012 ± 0.005.

By using a neutron collimator in a somewhat different way, it has been found possible to measure the differential cross section with respect to both energy and angle for the emission of neutrons when a scatterer is irradiated by a neutron beam. One proceeds as in the determination of a neutron spectrum with the exception that this spectrum is determined at various angles with respect to the incident neutron beam. Figure 22 is a schematic illustration of the experimental geometry. The detectors are arranged along the periphery of a circle whose center coincides with the center of the scatterer. The neutron collimator not only permits the irradiation of the scatterer by a narrow beam of neutrons, but also shields the detectors from the primary neutrons. One of the problems to which this method has been applied is the angular and energy distribution of neutrons from the bombardment of Bi by 14-Mev neutrons. Figure 23 illustrates the kind of data one obtains at each angle. The high-energy group is of course due to elastic scattering. It will be recalled that the energy distribution of the low energy neutrons suggests an evaporation process. If this be so their angular distribution should be iso-

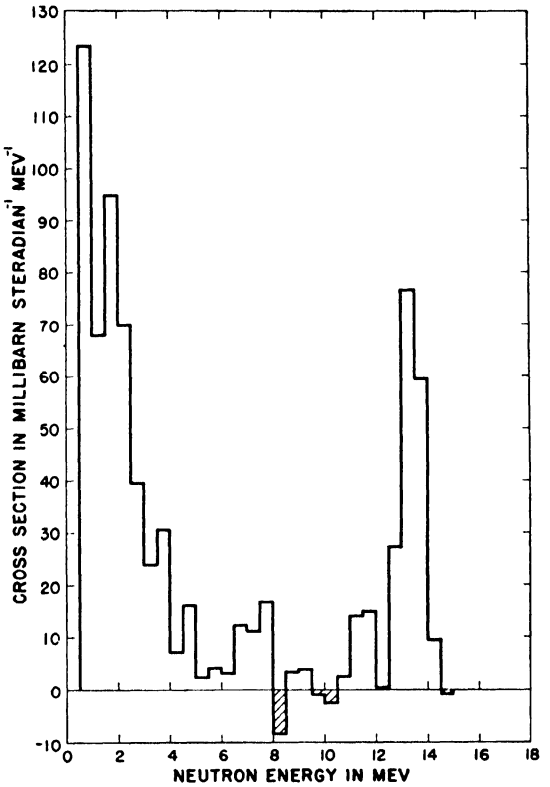

Figure 23. Neutron spectrum at 50 from 14 Mev neutrons on bismuth

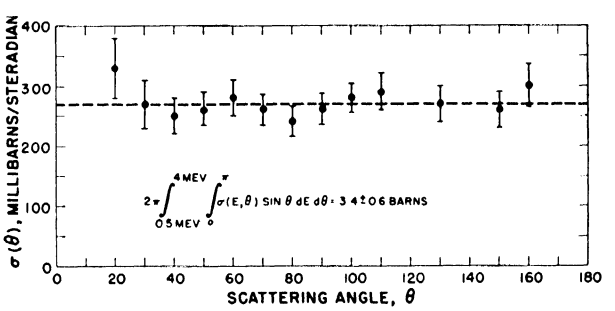

Figure 24. Cross section as a function of angle for the emission of 0.5 to 4 Mev neutrons from the interaction of 14 Mev neutrons with bismuth

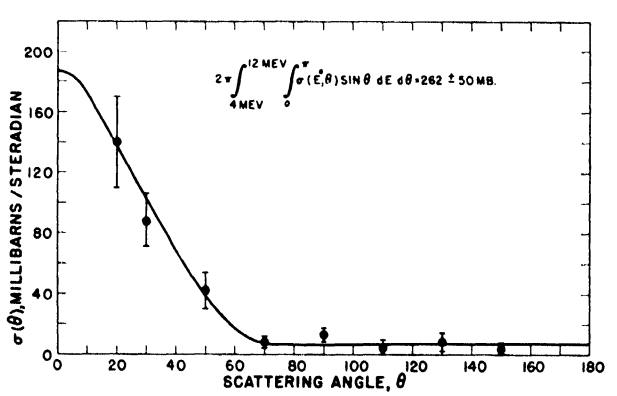

Figure 25. Cross section as a function of angle for the emission of 4 to 12 Mev neutrons from the interaction of 14 Mev neutrons with bismuth

tropic. Figure 24 shows that this is indeed the case. On the other hand the high-energy neutrons, although very few in number, are still more abundant than predicted by the statistical model. If they do not arise from an evaporation process the probability is strong that they will not only be anisotropic but also asymmetric. Figure 25 shows that this is certainly the case and indicates that these neutrons are probably the result of nucleon-nucleon encounters.

REFERENCES

1. Nereson, N. and Darden, S., *Average Neutron Total Cross Sections in the 3- to 12-Mev Region,* Phys. Rev. *89,* 775 (1953).
2. Rosen, L., *Nuclear Emulsion Techniques for the Measurement of Neutron Energy Spectra,* Nucleonics *11,* No. 7, 32 (1953); *11,* No. 8, 38 (1953).
3. Nereson, N., *Fission Neutron Spectrum of* Pu^{239}, Phys. Rev. *88,* 823 (1952).
4. Graves, E. R. and Rosen, L., *Distribution in Energy of the Neutrons from the Interaction of 14-Mev Neutrons with Some Elements,* Phys. Rev. *89,* 343 (1953).
5. Graves, E. R. and Davis, R. W., *Cross Sections for Nonelastic Interactions of 14-Mev Neutrons with Various Elements,* Phys. Rev. *97,* 1205 (1955).
6. Stelson, P. H. and Preston, W. M., *The Inelastic Scattering of Fast Neutrons from Iron,* Phys. Rev. *86,* 132 (1952).

Mass Spectroscopic Methods for the Determination of Nuclear Constants

By M. G. Inghram, D. C. Hess, R. J. Hayden and C. M. Stevens,* USA

Most methods for the determination of nuclear constants involve the observation of the transient particles, α, β, γ, π, etc., resulting from a nuclear reaction. In contrast the mass spectrometric method involves the observation of the product nuclides produced by that reaction. The nuclear constants are then calculable from the mass spectrometrically measured ratios of number of product to number of parent nuclides. If product and parent nuclides are isotopes of the same element, these ratios may be determined directly from mass spectrometric analysis. If they are nuclides of different elements, their ratios may be determined by mass spectrometric isotopic dilution analyses.[1]

Practical considerations of the mass spectrometric method show that in most reactions the resulting samples are so active or so small that mass spectrometers of high sensitivity must be employed. In order to improve the sensitivity of conventional mass spectrometers we have studied various methods for increasing ionization and detection efficiencies. To increase the ionization efficiency for metallic elements over that obtained with conventional gas sources, we have developed the Gehrcke and Reichenheim[2] surface ionization technique with special emphasis on the analysis of small samples.[3] For elements which ionize poorly from the simple surface ionization source, we have developed the multiple filament surface ionization source.[4] To obtain maximum detection sensitivity we have utilized an electron multiplier.[5,6] In order to improve accuracy when using surface ionization sources and electron multiplier detectors we have introduced the grid ratio recorder.[7] These improvements in technique have reduced the sample size necessary for heavy element analysis by a factor of 10^6 and have made possible many mass spectrometric determinations of nuclear properties of these heavy elements.

One of the constants of fundamental importance to reactor design is alpha (α), which is defined by the equation

$$\alpha = \sigma_c/\sigma_f \qquad (1)$$

where σ_c is the neutron capture cross section and σ_f is the fission cross section. Previously this quantity has been determined from independent measurements of the total neutron absorption cross section, σ_a, and of σ_f by means of the relationship

$$\alpha = (\sigma_a - \sigma_f)/\sigma_f \qquad (2)$$

A mass spectrometric determination of α depends, to a high approximation, only on the measurement of isotopic abundances before and after irradiation. A knowledge of absolute cross sections and neutron fluxes necessary for the determination of α by the earlier method is here necessary only to determine small correction terms. Thus, higher accuracy may be obtained.

An example of this type of measurement is the determination of α for U^{233} in a thermal reactor. This experiment was carried out jointly with Hagemann. If a mixture containing only U^{233} and U^{238} were irradiated, and if the absorption cross section of U^{234} and U^{238} are assumed negligible in comparison with that of U^{233}, α is given by the relation

$$\alpha^{233} = \frac{\left(\frac{N_{234}}{N_{238}}\right)_t}{\left(\frac{N_{233}}{N_{238}}\right)_o - \left(\frac{N_{233}}{N_{238}}\right)_t} \qquad (3)$$

N_a/N_b is the isotopic ratio of a to b and the subscripts o and t refer to before and after irradiation, respectively. When the above conditions are satisfied, α obviously depends only on mass spectrometrically determined quantities.

Since the cross sections of U^{234} and U^{238} are only small, not negligible, compared to that of U^{233}, a more extensive analysis is necessary. The equations which apply at any instant to a realizable uranium sample in a reactor are:

$$\frac{dN_{233}}{dt} = -\sigma_a{}^{233} N_{238}\Phi \qquad (4)$$

$$\frac{dN_{234}}{dt} = \sigma_c{}^{233} N_{238}\,\Phi - \sigma_a{}^{234} N_{234}\,\Phi \qquad (5)$$

$$\frac{dN_{235}}{dt} = \sigma_c{}^{234} N_{234}\,\Phi - \sigma_a{}^{235} N_{235}\,\Phi \qquad (6)$$

$$\frac{dN_{238}}{dt} = -\sigma_a{}^{238} N_{238}\,\Phi \qquad (7)$$

* Argonne National Laboratory. Including work by F. T. Hagemann, S. Untermyer, M. Levenson, E. Turk, S. Vogler, W. C. Redman, D. Okrent, R. Avery, P. R. Fields, W. M. Manning, G. L. Pyle, M. H. Studier, S. M. Fried, L. E. Glendenin, and E. P. Steinberg, Argonne National Laboratory.

Here the N's denote numbers of atoms and Φ is the neutron flux. The solution of this set of equations is

$$N_{233}(t) = N_{233}(0)\, e^{-\sigma_a^{233}\phi t} \tag{8}$$

$$N_{234}(t) = \frac{N_{233}(0)\sigma_c^{233}\,(e^{-\sigma_a^{233}\phi t} - e^{-\sigma_a^{234}\phi t})}{\sigma_a^{234} - \sigma_a^{233}} + N_{234}(o)e^{-\sigma_a^{234}\phi t} \tag{9}$$

$$N_{235}(t) = N_{233}(o)\,\sigma_c^{233}\,\sigma_c^{234}\left[\frac{e^{-\sigma_a^{233}\phi t}}{(\sigma^{234} - \sigma_a^{233})\,(\sigma_a^{235} - \sigma_a^{233})} - \frac{e^{-\sigma_a^{234}\phi t}}{(\sigma_a^{233} - \sigma_a^{234})\,(\sigma_a^{235} - \sigma_a^{234})} + \frac{e^{-\sigma_a^{235}\phi t}}{(\sigma_a^{233} - \sigma_a^{235})\,(\sigma_a^{234} - \sigma_a^{235})}\right] + \frac{N_{234}(o)\,\sigma_c^{234}\,(e^{-\sigma_a^{234}\phi t} - e^{-\sigma_a^{235}\phi t})}{\sigma_a^{235} - \sigma_a^{234}} + N_{235}(o)e^{-\sigma_a^{235}\phi t} \tag{10}$$

$$N_{238}(t) = N_{238}(o)e^{-\sigma_a^{238}\phi t} \tag{11}$$

To use this set of Equations 8, 9, and 10 are each divided through by Equation 11 to give three equations involving the three measured ratios. The first of these is used to determine the flux time (σ_a^{233} and σ_a^{238} are assumed known). The second and third both involve α and σ_a^{234} (since $\sigma_c^{233} = \sigma_a^{233}\,[\alpha/(1+\alpha)]$). Other cross sections are assumed known. Elimination of α between these two equations allows numerical calculation of σ_a^{234} and hence, of α. Correct estimation of the cross sections to use for the corrections was impossible because of lack of exact knowledge of the irradiation conditions. The assumption on which our calculation was based was that the flux distribution was Maxwellian, with $kT = 0.025$ ev. Thus σ_a^{233} was estimated at 499×10^{-24} cm^2 by dividing Haines' and Way's figure of 564×10^{-24} cm^2 for σ_a^{233} (0.025 ev) by 1.13 (as they suggest) to take into account the Maxwellian distribution. Likewise, σ_a^{235} and σ_f^{235} were taken as 560×10^{-24} cm^2 and 475×10^{-24} cm^2, respectively. These values were obtained by dividing Haines' and Way's figures by 1.15. In addition, σ_f^{234} was taken as 2×10^{-24} cm^2 and σ_a^{238} as 3×10^{-24} cm^2.

This set of equations, in contrast to Equation 3, apparently involves the cross sections and flux time very intimately. However, the numerical values which are put into Equation 9, the equation which essentially determines α, are such that the actual dependence of α on these terms is very slight. For example, an uncertainty of 10% in the flux time or in one of the cross sections would change α by only 0.05% of its value.

The experiment began with the preparation of the sample for irradiation. A solution of U^{233} ($U^{233}/U^{238} \cong 97/3$) was diluted with a solution of U^{238} to give a convenient U^{233}/U^{238} ratio of about 7/3. Depleted U^{238} ($U^{238}/U^{235} \cong 10^6$) was used in order to keep the U^{235} content to a minimum.

An aliquot of this solution containing 5 mg of U^{233} (7.1 mg total uranium) was spread over an area of 4 cm^2 in the center of a sheet of 0.015-in. thick aluminum foil. After evaporating the solution to dryness, the foil was heated for one hour at 500°C and the edges folded over the film of uranium oxide. The irradiation container consisted of an aluminum cylinder 1.36-in. in diameter and 4-in. long with a 2-in. tapered central hole fitted with a corresponding split tapered plug. The foil containing the sample was placed between the halves of the split taper and the plug pressed into the hole. The cylinder was capped and the assembly welded shut.

During the irradiation a neutron-flux monitor, consisting of a sample of Np^{237} mounted upon a 0.003-in. thick, chemically pure platinum foil, was placed in the split tapered plug next to the U^{233} sample. Specific alpha activity was used to determine the initial amount of Np^{237} and, after allowing sufficient time for decay of Np^{238}, the amount of Pu^{238} formed by the irradiation. Assuming Np^{237} has an effective cross section for reactor neutrons of 172×10^{-24} cm^2 and that Np^{237} and Pu^{238} have half-lives of 2.2×10^6-yr and 92-yr, respectively, the flux time of the irradiation was calculated to be 4.20×10^{20} neutrons/cm^2. In calculating this value correction for neutron capture by Np^{238} and Pu^{238} in the reactor was made.

After the irradiation the container was opened by cutting through the ends and pushing out the tapered plug. The aluminum foil, together with the uranium oxide, was dissolved in 3.5 ml of concentrated nitric acid and 0.5 ml of 10N hydrochloric acid and the solutions diluted to 50 ml with water. The uranium was separated from aluminum and fission products by extraction with ethyl ether after making the solution 10N in ammonium nitrate. The ether extract was washed with fresh 10N ammonium nitrate solution and the uranium re-extracted into water.

After extraction, the isotopic composition of the irradiated sample, as well as that of the original, unirradiated sample, was measured with a mass spectrometer equipped with a surface ionization source and electron multiplier detector. Nine separate loadings of filaments and 266 individual uranium spectra were measured. The mean results of these measurements are given in Table I. The uncertainties quoted are the precision indices of the separate determinations. In the calculation of the uncertainty in α, however, less exact knowledge of certain of these ratios was assumed. Because of possible nonlinearities in the collecting resistor beyond the accuracy of our measurements, and because of possible mass discrimina-

Table I. Isotopic Abundance Ratios

Sample	233/238	234/238	235/238
Original	2.395±0.005	0.00309±0.00008	0.00071±0.00004
Irradiated	1.872±0.004	0.04904±0.00013	0.00129±0.00003

tion in evaporation of ions from the filament, it was felt that the 233/238 ratios were not better than ¼ per cent and the 234/238 ratios not better than 1 per cent even when the precision index is better.

Utilizing the above data together with the earlier σ_a^{233} and σ_a^{238} cross sections in Equation 8 divided by Equation 11, a value of the flux time of 4.96×10^{20} neutrons/cm² was obtained. This is in rough agreement with that obtained by use of the Np. This agreement indicates that the value assumed for σ_a^{233} is not far off because the calculated flux time varies approximately inversely with this cross section. Thus, the absorption cross section of U^{234} was found to be $64 \pm 18 \times 10^{-24}$ cm², and the ratio of capture to fission cross sections of U^{233} is 0.0976 ± 0.0018. The error quoted takes into consideration the uncertainty in the flux time and in σ_a^{233} and is small because α^{233} is essentially determined by the product of these quantities, which is known much better than either. Using the value of 499×10^{-24} cm² for σ_a^{233} we obtained $\sigma_c^{233} = 44.4 \times 10^{-24}$ cm² and $\sigma_f^{233} = 455 \times 10^{-24}$ cm².

The variation of α with neutron energy is of fundamental importance in reactor design and of special importance in determining breeding gain of breeder reactors. In cooperation with Untermyer, Turk, Levenson and Vogler, Redman, Okrent and Avery, we have determined α for U^{235} and Pu^{239} in the EBR (Experimental Breeder Reactor). Alpha was studied as a function of position in that reactor. Since the average neutron energy is considerably higher at the center of this reactor than at the edge, the radial study gives information on the variation of α with neutron energy though the explicit relation between α and energy requires further correlation.

The previously described method for the determination of thermal α for U^{233} could not be used for the following reasons. First, the fast cross sections are small so that the change in isotopic ratio, i.e., the denominator of Equation 3, cannot be measured with sufficient accuracy for bombardments of reasonable length. Second, with fast fluxes all isotopes have comparable cross sections so that no isotope can be considered constant in amount during irradiation. For these reasons an alternative method for determining numbers of fissions was applied. The method used depended upon the equation

$$\left(\frac{N_f}{N_{235} + N_{236} + N_f}\right)_t = k\left(\frac{dn}{dt}\right)_{137} \qquad (12)$$

where N_f is the number of fissions which have occurred, $(dn/dt)_{137}$ is the counting rate, corrected for decay, in a standard counter of fission product cesium extracted from a standard weight of the irradiated sample. The constant k relates this counting rate to number of fissions; it is determined by counting the Cs^{137} in a sample previously irradiated in a fission chamber where the actual number of fissions was measured. The major error in this procedure involves the question of variations of fission yield of Cs^{137} as a function of neutron energy. Cs^{137} was chosen since it is at the peak of the fission yield curve and, hence, should be relatively insensitive to neutron energy. A check using a fast fission counter served to evaluate the magnitude of the error.

Using the above method for the determination of the number of fissions and the mass spectrometer for the determination of the number of captures, α for U^{235} is determined from the formula.

$$\alpha^{235} = \frac{\left(\frac{N_{236}}{N_{235} + N_{236} + N_f}\right)_t}{\left(\frac{N_f}{N_{235} + N_{236} + N_f}\right)_t} \qquad (13)$$

Since the bombardments actually used were so short, N_{236} and N_f were completely negligible in comparison to N_{235}. Combining Equations 12 and 13 gives

$$\alpha^{235} = \frac{\left(\frac{N_{236}}{N_{235}}\right)_t}{k\left(\frac{dn}{dt}\right)_{137}} \qquad (14)$$

Thus, the numerator is obtained directly from mass spectrometric measurements after irradiation and the denominator from the cesium fission product counting.

In the case of α for Pu^{239}, the plutonium analyzed was that formed from U^{238} by capture. Thus, Pu^{240} formed by capture in Pu^{239} was a second order effect. The method of determining the number of fissions by fission product counting as in the case of U^{235} was, therefore, not feasible because the fission products were derived from uranium and bore no simple relation to the number of fissions occurring in plutonium. The number of fissions was determined as follows. The relative fission rate of Pu^{239} as a function of position was determined by introducing Pu^{239} foils and counting gross fission products under standard conditions.

From a knowledge of the neutron flux distribution at the center of the reactor and the curves of fission cross section vs energy, the ratio of the fission cross sections $\sigma_f^{239}/\sigma_f^{235}$ was taken as 1.45 ± 0.10. Thus, the burn-up of Pu^{239} by fission at the center of the pile is calculated from the previously measured U^{235} as follows:

$$\text{Fission burn-up of } Pu^{239} = \frac{(\text{Fission burn-up of } U^{235}) \times 1.45}{2} \qquad (15)$$

The factor of two comes from the fact that the Pu^{239} was produced during the period of irradiation. Once this burn-up was known at the center of the pile, the Pu^{239} foils from the different positions served to give the fission burn-up at these other points. Any error in the $\sigma_f^{239}/\sigma_f^{235}$ ratio assumption introduces a systematic error in the values of α^{239} but does not alter the shape of the curve.

The samples were separated from fission products and other contaminants and, for mass spectrometric

Table II. α of U^{235}

Distance from center, cm	$\frac{U^{235}}{U^{238}} \times 10^5$	α
0	4.5±0.5	0.11±0.01
5.0	4.6±0.7	0.13±0.02
9.4	4.4±0.2	0.17±0.01

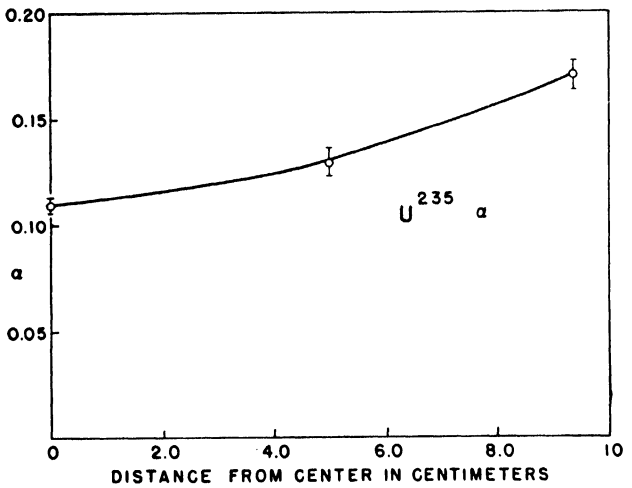

Figure 1. Variation of α for U^{235} in the EBR. Distance is measured from the center of the reactor along a horizontal line in the median plane of the reactor. Errors shown are only those arising from mass spectrometric determinations

analysis, were applied to one side filament of a multiple filament surface ionization source. The multiple filament source was necessary since it is a copious emitter of metallic ions whereas the single filament surface ionization source emits predominantly in the UO_2^+ position for uranium and in the PuO^+ position for plutonium. Since capture was very small in the samples measured, the O^{17} isotope would make measurement of the capture products impractical in the UO_2 or PuO positions.

The results of the measurements of α in different positions in the reactor are given in Table II and Fig. 1 for U^{235} and Table III and Fig. 2 for Pu^{239}. As is apparent from Figs. 1 and 2, in the EBR the variation of α with energy is important in the case of Pu^{239} and of considerably less importance in the case of U^{235}. The α for Pu^{239} could not be determined in the core because it was loaded predominantly with U^{238}. The first three points for plutonium were taken from the inner blanket and the last five from slices of a brick in the outer blanket.

This series of α determinations for the EBR was made on the materials initially loaded into the reactor. These materials were, in general, not of the right nature or position for best accuracy in the determination of α. Improved measurements will be made on samples loaded expressly for this purpose.

An important tool for the determination of nuclear properties, especially of the transuranic elements, has been the high flux time neutron irradiation. By this means significant changes in nuclide abundances are produced. Accurate mass spectrometric determination of these changes together with calculations therefrom lead to neutron absorption cross sections for the neutron energy spectrum used. Also, previously unknown nuclides may be formed and, hence, discovered in this manner.

Jointly with Fields, Manning, Pyle and Studier, a series of heavily irradiated plutonium samples were investigated. From the isotopic compositions observed, assuming $\sigma_a^{239} = 1150 \times 10^{-24}$ cm², $\sigma_c^{239} = 385 \times 10^{-24}$ cm², and $\sigma_f^{241} = 1100 \times 10^{-24}$ cm², the values for the cross section σ_a^{240} were found to vary between 500 and 600 $\times 10^{-24}$ cm² depending on the particular reactor used. The value for σ_c^{241} was studied in two reactors and found to vary between 310 and 360 $\times 10^{-24}$ cm². In the course of this work the isotope Pu^{242} was observed mass spectrometrically. This isotope was found independently a week earlier by the mass spectrometric group in Berkeley. In a second set of heavily irradiated plutonium samples studied jointly with Fried, Pyle, Fields, Diamond and Studier, the isotopes Pu^{244} (see footnote in reference 8), Cm^{246} and Cm^{247} (see footnote in reference 9) were discovered mass spectrometrically. A continued study of the heavily irradiated sample has been carried on.[8-13]

A further application of the mass spectrometer to the determination of nuclear constants is the determination of half-lives and branching ratios of radioactive decay. For example, the ratio of the half-lives

Table III. α of Pu^{239}

Distance from center, cm	$\frac{Pu^{240}}{Pu^{239}} \times 10^5$	α
11.1	1.1±0.2	0.06±0.01
15.4	1.0±0.1	0.09±0.01
17.6	0.9±0.2	0.11±0.02
23.9	3.2±0.2	0.14±0.01
26.5	2.8±0.3	0.16±0.02
29.8	3.5±0.4	0.24±0.02
34.1	6.8±0.7	0.44±0.04
37.6	23.0±1.6	0.44±0.03

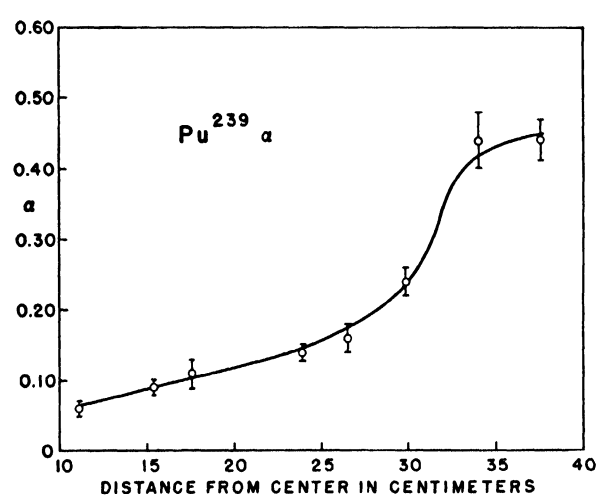

Figure 2. Variation of α for Pu^{239} in the EBR. Distance is measured from the center of the reactor in the median plane. Errors shown are only those arising from mass spectrometric determinations

of Pu^{239} to Pu^{240} was determined by measuring the relative amounts of uranium daughters U^{235} and U^{236} formed from a Pu^{239}-Pu^{240} sample containing a measured ratio of Pu^{239} to Pu^{240}.[14] Utilizing isotopic dilution techniques, it is possible to determine the amount of daughters produced from a given amount of parent and, thus, to determine half-lives absolutely. Branching ratios in radioactive decay can be obtained by diluting with two isotopes.

One further application of the mass spectrometer to the determination of nuclear constants lies in the field of fission yield measurements. The radiochemically determined fission yield curves published in 1946[15] showed two smooth peaks corresponding to light and heavy fission components. Mass spectrometric analysis by Macnamara, Collins, and Thode[16] showed that fission yields in the mass range around 134, as measured in xenon, did not lie on a smooth curve. Jointly with Glendenin and Steinberg we have made mass spectrometric fission yield investigations. In this work, the mirror peak in the fission yield curve corresponding to that found by Macnamara, *et al.*, as well as additional fine structure, was found in the region of mass 100.[17,18,19] Recent mass spectrometrically determined fission yields are on an absolute basis as a result of the use of the isotopic dilution technique.

REFERENCES

1. Inghram, M. G., *Stable Isotope Dilution as an Analytical Tool,* Ann. Rev. Nucl. Sci. *4*: 81 (1954).
2. Gehrcke, E. and Reichenheim, O., *Anode Rays,* Deutsch. Phys. Gesell. Verh. *8*: 559 (1906); *9*: 76 (1907); *9*: 200 (1907).
3. Inghram, M. G. and Hayden, R. J., *Handbook on Mass Spectroscopy,* National Academy of Sciences, National Research Council, Publication 311 (1954).
4. Inghram, M. G. and Chupka, W. A., *Surface Ionization Source Using Multiple Filaments,* Rev. Sci. Instr. *24*: 518 (1953).
5. Cohen, A. A., *The Isotopes of Cerium and Rhodium,* Phys. Rev. *63*: 219 (1943).
6. Inghram, M. G., Hayden, R. J. and Hess, D. C., *Electron Multipliers in Mass Spectroscopy,* Mass Spectroscopy in Physics Research, National Bureau of Standards Circular 522, 257 (1953).
7. Stevens, C. M. and Inghram, M. G., *Ratio Recording in Isotopic Analysis,* Rev. Sci. Instr. *24*: 987 (1953).
8. Studier, M. H., Fields, P. R., Sellers, P., Friedman, A. M., Stevens, C. M., Mech, J. F., Diamond, H., Sedlet, J. and Huizenga, J. R., *Plutonium-244 from Pile-Irradiated Plutonium,* Phys. Rev. *93*: 1433 (1954).
9. Stevens, C. M., Studier, M. H., Fields, P. R., Mech, J. F., Sellers, P. A., Friedman, A. M., Diamond, H. and Huizenga, J. R., *Curium Isotopes 246 and 247 from Pile-Irradiated Plutonium,* Phys. Rev. *94*: 975 (1954).
10. Studier, M. H., Fields, P. R., Diamond, H., Mech, J. F., Friedman, A. M., Sellers, P., Pyle, G., Stevens, C. M., Magnusson, L. B. and Huizenga, J. R., *Elements 99 and 100 from Pile-Irradiated Plutonium,* Phys. Rev. *93*: 1428 (1954).
11. Diamond, H., Magnusson, L. B., Mech, J. F., Stevens, C. M., Friedman, A. M., Studier, M. H., Fields, P. R. and Huizenga, J. R., *Identification of Californium Isotopes 249, 250, 251 and 252 from Pile-Irradiated Plutonium,* Phys. Rev. *94*: 1083 (1954).
12. Magnusson, L. B., Studier, M. H., Fields, P. R., Stevens, C. M., Mech, J. F., Friedman, A. M., Diamond, H. and Huizenga, J. R., *Berkelium and Californium Isotopes Produced in Neutron Irradiation of Plutonium,* Phys. Rev. *96*: 1576 (1954).
13. Bentley, W. C., Diamond, H., Fields, P. R., Friedman, A. M., Gindler, J. E., Hess, D. C., Huizenga, J. R., Inghram, M. G., Jaffey, A. H., Magnusson, L. B., Manning, W. M., Mech, J. F., Pyle, G. L., Sjoblom, R., Stevens, C. M. and Studier, M. H., *The Formation of Higher Isotopes and Higher Elements,* To be presented in Session S.4 of these proceedings.
14. Inghram, M. G., Hess, D. C., Fields, P. R. and Pyle, G. L., *Half-Life of Plutonium-240 by Determination of its Uranium-236 Daughter,* Phys. Rev. *83*: 1250 (1951).
15. Plutonium Project, *Nuclei Formed in Fission,* Rev. Mod. Phys. *18*: 513 (1946).
16. Macnamara, J., Collins, C. B. and Thode, H. G., *The Fission Yield of Xe^{133} and Fine Structure in the Mass Yield Curve,* Phys. Rev. *78*: 129 (1950).
17. Glendenin, L. E., Steinberg, E. P., Inghram, M. G. and Hess, D. C., *Nuclear Structure in Fission,* Phys. Rev. *84*: 860 (1951).
18. Steinberg, E. P., Glendenin, L. E., Inghram, M. G. and Hayden, R. J., *Fine Structure in U^{238} Fission,* Phys. Rev. *95*: 867 (1954).
19. Inghram, M. G., Hayden, R. J. and Hess, D. C., *U^{235} Fission Yields in the Rare Earth Region,* Phys. Rev. *79*: 271 (1950).

A Note on the Analysis of Neutron Resonance Data Including Examples Taken from Reactor Materials

By E. R. Rae,* UK

This paper is concerned with information about neutron cross sections in the energy region from a few to a few thousand electron volts, obtained with the Linear Electron Accelerator at Harwell, used as a pulsed source of neutrons for a time-of-flight spectrometer. This spectrometer is described in another paper by Wiblin.[1] In general the information is obtained from a number of different experiments. In one experiment, the fraction of incident neutrons transmitted by various samples of the material under investigation is measured as a function of neutron energy. In another, scattered neutrons are detected by a ring of BF_3 counters placed round the sample, and a yield curve is obtained as a function of neutron energy. In a third, a ring of sodium iodide crystals, suitably screened against neutrons, records the gamma-ray yield from neutron capture in the sample. Lastly, in the case of fissile materials, the fission yield is obtained by counting the output pulses from an ionisation chamber containing foils coated with thin films of the material under investigation.

Apart from measurements of potential scattering, which can be done directly, using very thick samples in a transmission experiment, the information generally required is a set of Breit-Wigner level parameters for the resonances occurring in the energy region investigated. In assigning these parameters, levels are normally considered to be adequately represented by the single-level Breit-Wigner formula, together with Bethe's theory[2] of Doppler broadening, corrected for crystal binding in the manner indicated by Lamb.[3] The methods of de-excitation of the compound nucleus are also normally assumed to consist of re-emission of a neutron, radiative capture and, where applicable, fission. In the energy region considered, inelastic scattering is ignored. If the resolution is good enough, then the information required can be obtained directly from the shape of the resonance curves observed with thin samples of the material, corrections being made for sample thickness, resolution and Doppler broadening of the resonance.[4,5,6] In most cases, however, the resolution available is not sufficiently good to enable such methods to be adopted. Under these circumstances, information can be obtained from the resonance areas, as indicated by Melkonian, Havens and Rainwater,[7] Seidl *et al.*[8] and others. Information can also be obtained from the minimum transmission (maximum yield) observed in a resonance,[5,6] provided the resolution function of the spectrometer is known, and from the interference observed between resonant and potential scattering.[9] Information from all these experiments is in the form of combinations of the Breit-Wigner parameters and may be listed as in Table I.

Experiments (*b*), (*c*) and (*d*) of column 1 of Table I cannot produce useful information from thick sample yields, because of the extreme difficulty of correcting for the effect of multiple collisions in the thick sample, which increases the probability of capture or fission at the expense of scattering. Samples of intermediate thickness may sometimes be used in experiments (*b*) and (*c*) under favourable circumstances where an approximate correction can be made for the effect of multiple processes. In the case of fission, however, there is the further complication of the necessity of keeping the samples thin enough to allow the escape of the fission fragments, and to avoid the presence of excessive numbers of α-particles. $\sigma_0\Gamma$, $\sigma_s\Gamma$ and $\sigma_a\Gamma$ are obtained as functions of Γ from the resonance areas using the curves of $A_E/\Gamma\cdot\sqrt{\pi}$ vs $n\sigma_0$ given by Seidl *et al.*[8]

Table I

Experiment	*Combination of parameters obtained*		
	*Thin sample** ($n\sigma_0 \ll 1$)	*Intermed. sample* ($n\sigma_0 \sim 1$)	*Thick sample* ($n\sigma_0 \gg 1$)
(*a*) Transmission	$\sigma_0\Gamma$	$\sigma_0\Gamma$ as function of Γ	$\sigma_0\Gamma^2$ / $\sigma_0\Gamma$ (from interference between resonant and potential scattering)
(*b*) Scattering	$\sigma_s\Gamma$	[$\sigma_s\Gamma$ as function of Γ]	-
(*c*) Capture	$\sigma_a\Gamma$	[$\sigma_a\Gamma$ as function of Γ]	-
(*d*) Fission	$\sigma_f\Gamma$	-	-

* Where n is the number of atoms/unit area of sample, σ_0 is total cross section at exact resonance, σ_a is cross section for process a at exact resonance, and Γ is total width of resonance at half maximum.

* A.E.R.E., Harwell. Work done by E. M. Bowey, J. E. Evans, J. E. Lynn and E. R. Rae.

Now a knowledge of any one of the combinations of parameters mentioned above, in fact defines a relationship between the level parameters of the resonance being investigated, for we can write

$$\sigma_0 = 4\pi\lambda^2 g\Gamma_n/\Gamma^2 \quad (1)$$

$$\sigma_a = 4\pi\lambda^2 g\Gamma_n\Gamma_a/\Gamma^2 \quad (2)$$

$$\therefore\ \sigma_0\Gamma = 4\pi\lambda^2 g\Gamma_n \quad (3)$$

$$\sigma_a\Gamma = 4\pi\lambda^2 g\Gamma_n\Gamma_a/\Gamma \quad (4)$$

and

$$\sigma_0\Gamma^2 = 4\pi\lambda^2 g\Gamma_n\Gamma \quad (5)$$

If we now consider for simplicity the case of a non-fissile substance; here we have only 4 parameters, Γ_n, Γ_a, Γ and g, of which 3 are independent. Let us take Γ_n, Γ and g. Then Equations 3, 4 and 5 become:

From Equation 3:

$$\Gamma_n = \frac{\sigma_0\Gamma}{4\pi\lambda^2 g} \quad (6)$$

From Equation 5:

$$\Gamma_n\Gamma = \frac{\sigma_0\Gamma^2}{4\pi\lambda^2 g} \quad (7)$$

Equation 4 minus scattering:

$$\Gamma_n^2/\Gamma = \frac{\sigma_a\Gamma}{4\pi\lambda^2 g} \quad (8)$$

And from Equation 4 minus capture:

$$\Gamma_n(1 - \Gamma_n/\Gamma) = \frac{\sigma_a\Gamma}{4\pi\lambda^2 g} \quad (9)$$

The spin factor g, for any resonance, can have in general two values. Let us call them g_1 and g_2. Then substituting $g - g_1$ in the above equation defines one set of relationships between Γ_n and Γ which can be represented graphically as shown in Fig. 1. Similarly $g = g_2$ gives a second set of curves. In principle one set of curves will be concurrent and the other will not, thus indicating the correct choice of g and so of the spin of the level concerned. Thereafter Γ_n and Γ can be obtained from the point of concurrence. In practice, the two values of g are usually too nearly identical to enable a spin determination to be made,

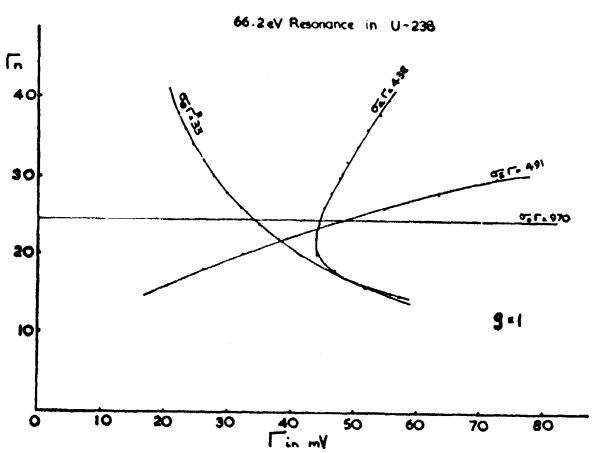

Figure 1. Γ_n vs Γ for 66 ev resonance in U^{238}

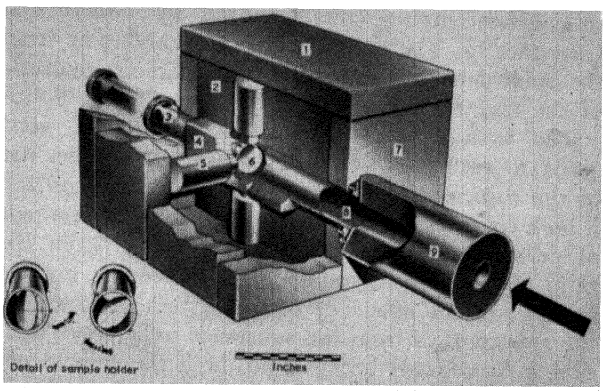

Figure 2. Photograph of apparatus for measuring τ-ray yields: (1) B_2O_3 shielding against neutrons from outside; (2) lead shielding; (3) sample holder in position; (4) wax and B_2O_3 protecting crystals from neutrons scattered by sample; (5) photo multiplier with sodium iodide crystals; (6) sample; (7) B_2O_3 shielding against neutrons from outside; (8) evacuated flight-path; and (9) part of neutron collimating system-filled with B_2O_3. Arrow shows neutron beam from linear accelerator

and in addition the curves do not exactly concur because of experimental errors. Nevertheless, in cases where g is indeterminate the value ½ can be used, and the point of best concurrence can be obtained using a method of least squares. This method of obtaining the parameters has the advantage that it can use information taken from a number of totally independent experiments, thus tending to reduce systematic errors, and further that the size of the area of concurrence gives an indication of the true errors of the results used, as distinct from purely statistical errors. At the present moment, a complete solution of this sort has only been evaluated[9] for a number of resonances in U^{238}, of which one set is shown in Fig. 1. The data used is rather old, having been obtained in 1953. The method, moreover, over-determines the result if total cross section, scattering and capture are all observed for more than one sample thickness. It can be shown that a similar method can be applied to the case of a fissile substance.

The remainder of this paper will be devoted to a brief description of the apparatus used at A.E.R.E. for the direct observation of capture cross sections from gamma-ray yields, and to presenting data obtained with this apparatus and from transmission experiments, on the elements niobium and sodium.

MEASUREMENT OF GAMMA-RAY YIELDS

Measurements of neutron capture cross sections with a time-of-flight spectrometer by observing gamma-ray yields have been carried out by Meservey[10,11] and by Albert and Gaerttner and coworkers.[12,13] The Harwell apparatus has been briefly described by the author[14] and Fig. 2 shows a diagram of this apparatus. The four crystals, which are situated 11.5 metres from the neutron source, are either connected in parallel, the output pulse-sizes required being selected by a single-channel pulse-height analyser, or else they are connected in two pairs, each pair being connected to an arm of a

coincidence circuit (method used by Albert and Gaerttner[12]). The output from the analyser or from the coincidence circuit is fed to the timing channels of the spectrometer. The 11.5 metre flightpath, together with timing channels of duration 2 μsec, gives a resolution of 0.17 μsec/metre. The use of the coincidence technique has the advantage that if both coincidences and the single counts in one pair of crystals are measured simultaneously, then the ratio of coincidence counts to single counts gives a measure of the efficiency of the system for counting the gamma rays from the substance under investigation.[12] As regards background, both the coincidence method, and the kicksorter method can yield a background of about 2% of the counts obtained with a "black sample" in the beam, but the latter requires a high value of bias, corresponding to an energy dissipation in the crystal of about 2 Mev.

To obtain a measurement of the apparent capture cross section of a resonance, ideally one would wish to be able to insert a sample which is black at that resonance, i.e. one which would absorb all neutrons over an energy interval greater than the resolution width of the spectrometer. While this is possible for low lying levels, it rapidly becomes impossible as the energy is raised, and in general for levels above 10 or 20 ev, the "black sample" count has to be deduced indirectly. Since the neutron spectrum is known, a knowledge of the "black sample" count for any one resonance in a substance would give the value for all other resonances, provided the efficiency of the gamma-ray detectors, expressed as counts/neutron captured, remained constant. The validity of this assumption has been discussed by Meservey[11] and also by Albert and Gaerttner.[12] Meservey was pessimistic, but experiments by the latter authors on tantalum indicated constancy to within 20%, and a considerable constancy in the case of silver. A measurement of the ratio of single counts to coincidences was recently made in Harwell for ten resonances in tantalum, and the result is shown in Fig. 3. The figures are consistent with a constant efficiency apart from the value for the weak resonance at 29.8 ev where the statistics were very poor. The results, in fact, suggest constancy to something better than 5%. A measurement of the same ratio for the first three levels in silver is shown in Table II.

Again it will be noted that the results are not inconsistent with a constant value for the efficiency, even though two different isotopes are involved. Some measurements were also made on U^{238}, involving the comparison between resonance areas observed by this method, and those observed for a similar sample by the transmission method. Here the pulse-

Table II

Resonance energy	*Isotope*	*Ratio of single counts/coincidences*
5.19 ev	109	17.3±0.4
16.4 ev	107	17.0±0.7
30.8 ev	109	19.1±1.6

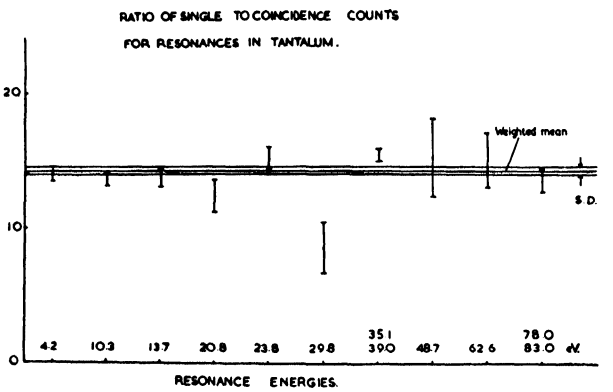

Figure 3. Diagram of ratios of single to coincidence counts for 10 resonances in tantalum

height analyser channel was set so that its sensitivity for counting scattered neutrons absorbed in the boron of the annular shield surrounding the sample, was equal to its sensitivity for counting gamma rays from the 6.7 ev resonance in U^{238}, both sensitivities being measured in counts/neutron interaction. In this way the gamma-ray yield curve corresponded exactly to a transmission curve for a similar sample, and the resonance areas could be compared directly. Once again the results were consistent with a constant gamma-ray efficiency for all the five resonances examined. Here, of course, the experiment was less direct, because of the effect of the scattered neutrons, but an estimated figure for the consistency of the efficiency would be better than 10%. It would seem, in fact, that no experiment performed so far, indicates any considerable variation in gamma-ray counting efficiency between resonances in the same isotope, and that it would therefore be reasonable to assume an uncertainty of the order of 5% to cover possible small variations. Once this assumption is made (and it can be checked qualitatively by a measure of the coincidences/singles ratio for the levels in any isotope being studied) then the interpretation of γ-ray yield curves is straightforward provided a resonance exists for which a "black sample" count can be obtained. Otherwise a reference count must be obtained from another substance which has a coincidence/singles ratio similar to that of the substance being studied. A correction is then applied for any small difference in gamma-ray efficiency on the assumption that it is due to different gamma-ray multiplicity.

EXPERIMENTAL RESULTS

Niobium

Two samples of metallic niobium obtained from A.E.A. Industrial Group were examined in the gamma-ray apparatus. These were of thickness 9.82 and 247 × 10^{20} atoms/cm² and will hereafter be referred to as the thin and intermediate samples. The samples were pure except for a trace of copper and about ½% of tantalum. Figure 4 shows the yield curve obtained (coincidence). The "black sample" count was obtained from tantalum which gives a

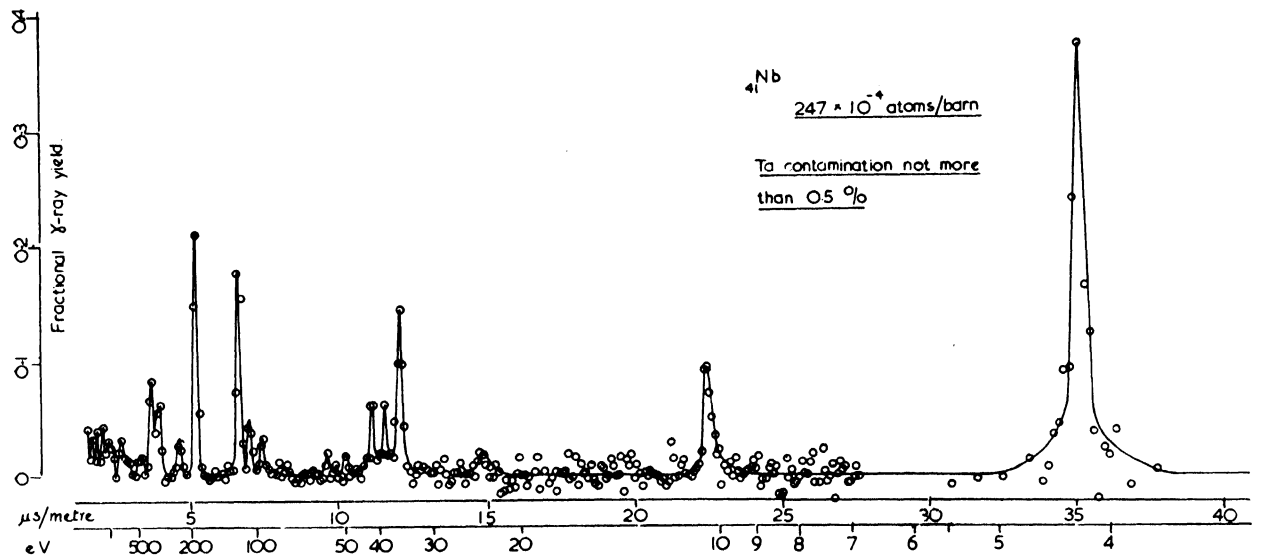

Figure 4. Gamma-ray yield curve for intermediate sample of niobium

similar coincidences/singles ratio to niobium, but which has a convenient resonance at 4.2 ev. Consistency between the coincidences/singles ratios of the levels observed in niobium was to within the statistical errors of these quantities. It will be observed from the yield curve that the presence of only ½% of tantalum accounts for most of the neutron capture at low energies. It is thus important, if niobium is to be used as a canning material, to produce it as free as possible from tantalum.

A third, thick, sample of metallic niobium (912×10^{20} atoms/cm^2) also obtained from A.E.A Industrial Group, was investigated in a transmission experiment. This was also done at 11.5 metres using the crystals with a boron sample as a neutron detector,[15] but with the electron pulse in the linear accelerator modulated to 0.3 sec, and with timing channels of a novel design giving a channel width of 0.2 sec. The new timing channels, which have been developed by Kandiah and Chambers at A.E.R.E. are briefly described in another paper.[1] They operate on the "time-expansion" principle which enables this high resolution to be obtained (~ 0.026 μsec/metre). Unfortunately the apparatus was still in a highly experimental state when used for this experiment, so the results obtained are put forward with some reserve. An observed total cross-section curve is shown in Fig. 5, based on a transmission curve in which adjacent points were averaged to improve statistics and to overcome the effect of certain electronic irregularities. This degraded the resolution somewhat to about 0.035 μsec/metre. Sufficient time was not available to do a proper series of counts with and without the sample in position. The cross-section curve is thus based only on runs with the sample in position, and is normalised to a potential scattering level of 6.2 barns as reported by the Argonne team.[16] The curve obtained confirms the existence of a number of small resonances shown in the points on the Argonne curve, but not drawn in. On the basis of the two capture runs and the total cross-section run, an analysis was carried out on the level at 195 ev. The thin sample run yields a value for $\sigma_a\Gamma$ of 191 ± 38 ev barns; the intermediate sample gives a value of $\sigma_a\Gamma$ as a function of Γ, and the thick sample gives $\sigma_0\Gamma$ as a function of Γ. These three results are combined in a Γ_n vs Γ diagram as shown in Fig. 6. Since the spin of niobium is 9/2, the value of g was taken as ½. It will be seen from the diagram that the three curves give two possible regions of concurrence, one giving a value of Γ of about 0.45 ev and the other 0.15. A study of the interference observed between potential and resonant scattering (Fig. 5), however, suggests the higher value to be the correct one, the interference analysis providing a value of Γ_n as indicated. The point of best concurrence of all the curves gives the following parameters:

$$\Gamma_n = 0.034 \pm 0.006 \text{ ev}$$

$$\Gamma = 0.37 \pm 0.06 \text{ ev}$$

$$\Gamma_a = \Gamma - \Gamma_n = 0.34 \pm 0.06 \text{ ev}$$

The capture cross section at resonance is thus 520 ± 140 barns.

Sodium

Four samples were investigated containing 0.00127, 0.00479, 0.0329 and 0.243×10^{24} atoms/cm^2. The two thinner samples were in the form of sodium nitrate, and the thicker ones of metallic sodium. The method of investigation was that of transmission over a flight-path of 31.8 metres, and using timing channels of 2 μsec duration (resolution 0.063 μsec/metre). Only the first resonance was examined and the corresponding neutron energy was found to be 2780 ± 60 ev. In this case the large width of the resonance (about 400 ev) permitted both an area analysis and the fitting of a Breit-Wigner resonance curve to the experimental points, despite

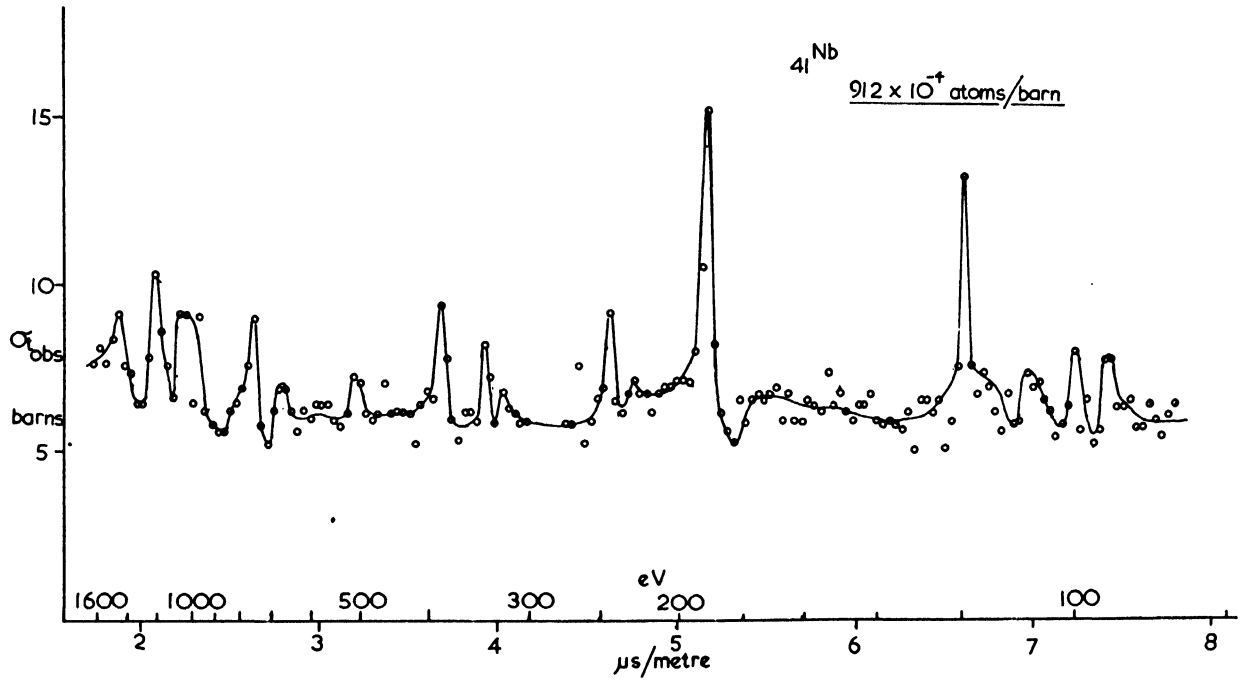

Figure 5. Observed total cross section of niobium

the high neutron energy involved. Let us consider first the area analysis. Here the following results were obtained:

Sample with 0.0329×10^{24} atoms/cm²

$$\sigma_0\Gamma^2 = (55 \pm 5) \times 10^6 \text{ ev}^2 \text{ barns}$$

Sample with 0.00479×10^{24} atoms/cm²

$$\sigma_0\Gamma^{3/2} = (32 \pm 4.5) \times 10^5 \text{ ev}^{3/2} \text{ barns}$$

$$[\sigma_0\Gamma = F(\Gamma) \propto \Gamma^{1/2}]$$

Sample with 0.00127×10^{24} atoms/cm²

$$\sigma_0\Gamma = (12.7 \pm 3.9) \times 10^4 \text{ ev barns}$$

If these equations are solved together in pairs they yield the following parameters:

$$\Gamma = 360 \pm 30 \text{ ev}$$

$$\sigma_0 = 400 \pm 150 \text{ barns}$$

The spin of Na^{23} is 3/2, and so the possible values of σ_0 are 352 and 587 barns, it being assumed that $\Gamma_n \gg \Gamma_a$. The measured parameters appear to favour the lower value for the cross section, and so to indicate the lower spin of 1 for the compound nucleus.

A Γ_n vs Γ plot for the three combinations of parameters determined experimentally is shown in Fig. 7 for the two possible spin states. The assumption that $\Gamma_n \gg \Gamma_a$ is represented by the straight lines at 45 degrees through the origins. Once again the lower spin value is favoured, though it is clear that the spread in the experimental results makes a clear decision difficult. If the lower spin value is correct, then since the curve corresponding to $\sigma_0\Gamma^2$ has the lowest error, it is clear that the best value of Γ is about 400 ± 20 ev.

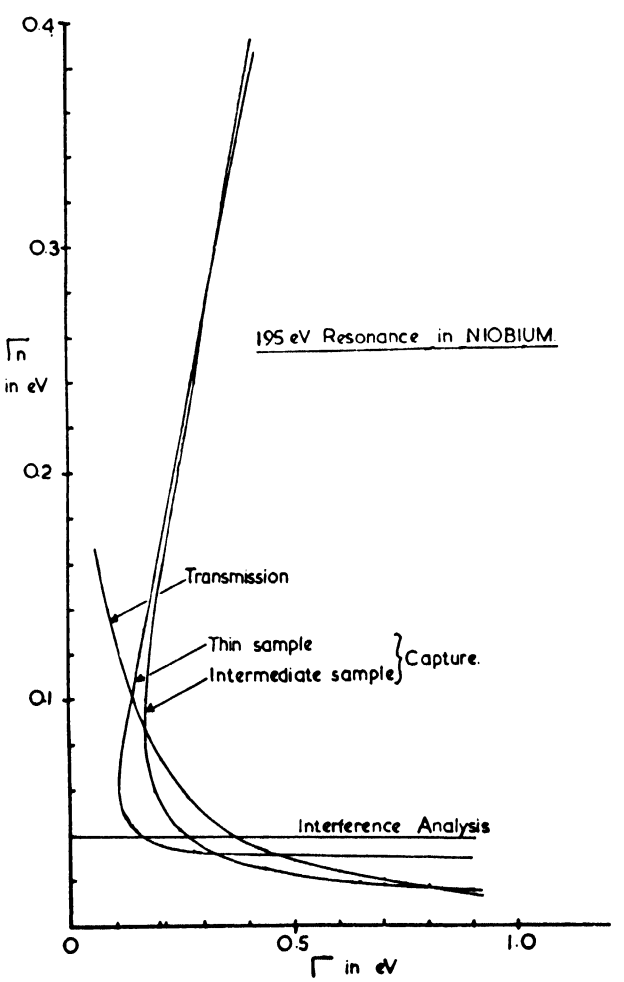

Figure 6. Γ_n vs Γ for 195 ev resonance in niobium

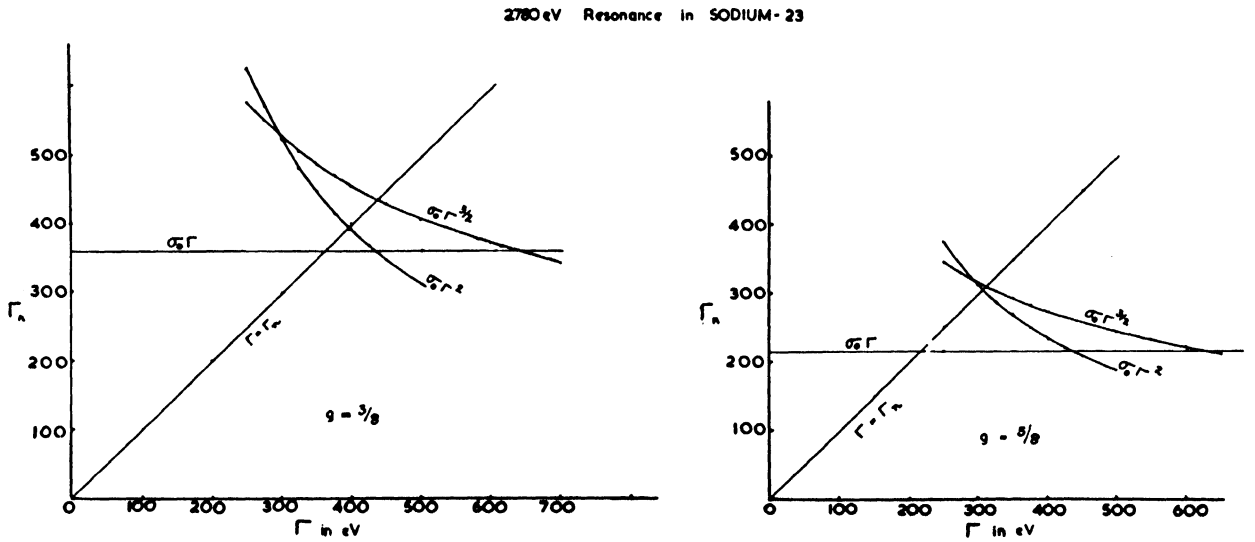

Figure 7. Γ_n vs Γ for 2780 ev resonance in sodium

ACKNOWLEDGEMENTS

I must express my gratitude to Miss E. M. Bowey and to Mr. J. E. Evans for their invaluable assistance in carrying out the series of experiments and in computing the results. I must also thank Mr. J. E. Lynn who provided the data on sodium, and Mr. E. R. Wiblin for many helpful discussions and for practical help with the experiments.

REFERENCES

1. Wiblin, E. R., P/421, "Neutron Spectrometers based on Pulsed Sources", this Volume.
2. Bethe, H. A., "Nuclear Physics B, Nuclear Dynamics, Theoretical", Rev. Mod. Phys. *9*, 140, 1937.
3. Lamb, W. E., "Capture of Neutrons by Atoms in a Crystal", Phys. Rev. *55*, 190, 1939.
4. Sailor, V. L., "The Parameters for the Slow Neutron Resonance in Rhodium", Phys. Rev. *91*, 53, 1953.
5. Melkonian, E. and Havens, W. W., Jr., "Calculation of the Effect of Finite Resolution on the Neutron Transmission Near Resonance", Bull. A.P.S., 29, 53, 1954.
6. Lynn, J. E. and Rae, E. R., "The Interpretation of Data Obtained with a Time-of-Flight Neutron Spectrometer in terms of Nuclear Resonance Parameters", Unpublished A.E.R.E. Committee Paper, 1954.
7. Melkonian, E., Havens, W. W., Jr., and Rainwater, L. J., "Slow Neutron Velocity Spectrometer Studies V", Phys. Rev. *92*, 702, 1953.
8. Seidl, F. G. P., Hughes, D. J., Palevsky, H., Levin, J. S., Kato, W. Y. and Sjostrand, N. G., "Fast Chopper Time-of-Flight Measurements of Neutron Resonances", Phys. Rev. *95*, 476, 1954.
9. Lynn, J. E. and Pattenden, N. J., P/423, "Slow Neutron Cross Sections of the Uranium Isotopes", Volume 4, Session 17A, these Proceedings.
10. Meservey, E., "Neutron Capture Cross Sections by (n,γ) Reactions", Columbia University Report CU 99, 100, 1952.
11. Meservey, E., "Neutron-Capture Cross-Sections by Capture-Gamma Counting", Phys. Rev. *96*, 1006, 1954.
12. Albert, R. D. and Gaerttner, E. R., "An (n,γ) Detector Designed for Use with a Velocity Selector for the Study of Low Energy Neutron Resonances", Knolls Atomic Power Lab., Report No. KAPL 1083, 1954.
13. Gaerttner, E. R., Yeater, M. L. and Albert, R. D., "A Study of Neutron Capture and Transmission with the KAPL Betatron Neutron Velocity Selector", Knolls Atomic Power Lab., Report No. KAPL 1084, 1954.
14. Rae, E. R., "Gamma-Ray Yields from the Resonant Capture of Slow Neutrons" Proc. Glasgow Conf. on Nuclear Phys., 1954.
15. Rae, E. R. and Bowey, E. M., "A Scintillation Detector for Neutrons of Intermediate Energy", Proc. Phys. Soc. A LXVI, 1073, 1953.
16. "Neutron Cross Sections", A.E.C. Document AECU-2040, Suppt. 3, 1954.

Record of Proceedings of Session 15A

TUESDAY MORNING, 16 AUGUST 1955

Chairman: Prof. E. Amaldi (Italy)
Vice-Chairman: Mr. C. Simane (Czechoslovakia)
Scientific Secretaries: Messrs. D. J. Littler and N. A. Dobrotin

PROGRAMME

P/576	Neutron velocity selectors used at reactors	D. J. Hughes
P/640	Mechanical neutron velocity selector	V. I. Mostovoi *et al.*
P/641	A neutron spectrometer with the mechanical interrupter	V. V. Vladimirski
	Discussion	
P/421	Neutron spectrometers based on pulsed sources	E. R. Wiblin
P/577	Time-of-flight techniques applied to fast neutron measurements	L. Cranberg
P/580	Recent advances in neutron detection	L. M. Bollinger
P/806	Time-of-flight instrumentation for neutron spectrometers	W. A. Higinbotham
	Discussion	
P/573	Techniques for measuring elastic, non-elastic, and transport cross sections	R. F. Taschek
	Discussion	

Mr. D. J. Hughes (USA) presented paper P/576.

Mr. V. I. Mostovoi (USSR) presented paper P/640. With regard to cathode-ray tube time analysis he added: At present a 512-channel time-analyzer is being developed. The preliminary memory circuit also uses a two-beam tube. For increased dependability and more complete utilization of the tube screen, a raster (grating) type is employed. To permit operating with channel widths of the order of 0.1 μsec a special form of sweep, in which "no time" is required for the return trace, is used. Recording of the signals is accomplished by a defocused beam, which simplifies the problem of maintaining coincidence of the rasters. Each raster consists of 256 points. An ultrasonic line similar to that used in the analyzer of Hutchinson and Scarott[10] is used in the recorder circuit. Two cathode-ray tubes are used to obtain 512 channels with a capacity of 2048 pulses.

Mr. V. V. Vladimirski (USSR) presented paper P/641. After having described the equipment he continued as follows: The total neutron cross-sections of a number of elements have been measured by means of this spectrometer. I shall not show the results obtained in measurements with a short base (about 5.5 metres), but instead will present the results of recent measurements on natural uranium which we did not have time to include in the printed paper. These results give a better indication of the actual resolving power of the instrument.

Slide 1 shows the spectrum of natural uranium in the energy range from 5.5 to 100 ev, measured with a flight path of 18.9 metres and a resulting resolution of 0.18 μsec/m. Determinations were made on two specimens: one, a thick one, having 62.5×10^{21} atoms per cm^2; the other, a thin specimen, having 2.33×10^{21} atoms per cm^2. Between the resonances the curve has been drawn through points for the thick specimen; in the resonances those for the thin specimen. The energy scale is not linear; the horizontal scale is linear in neutron flight times.

As will be noted from the slide, the principal levels of uranium at 6.70, 21.3 and 37.3 ev are clearly resolved. Accurate determination of the parameters is made difficult by the rather unsatisfactory selection of specimen thicknesses.

The spectrum of uranium for energies above 35 ev is shown in Slide 2. It is in good agreement with the data reported by the Harwell and Brookhaven Laboratories, except for the peak at 90 ev. This maximum requires further verification, for measurements on the thick specimen do not show an increase in absorption at 90 ev.

We have done two series of measurements (Slides 3 and 4) for thorium with a resolving power of 0.1 μsec/m: one for a specimen 37.1×10^{21} atoms per cm^2 thick, the other, for a specimen 2.42×10^{21} atoms per cm^2 thick.

The measurements cover two appreciably overlapping intervals: 18 to 200 ev and 35 ev to ∞. The results of the different measurements are in good agreement in the overlapping range, except for the twinning of the maximum in one of the figures; this is presumably due to one experimental point being in error. The data of the Argonne and Brookhaven Laboratories, published in the new edition of the Atlas of Neutron Cross Sections,

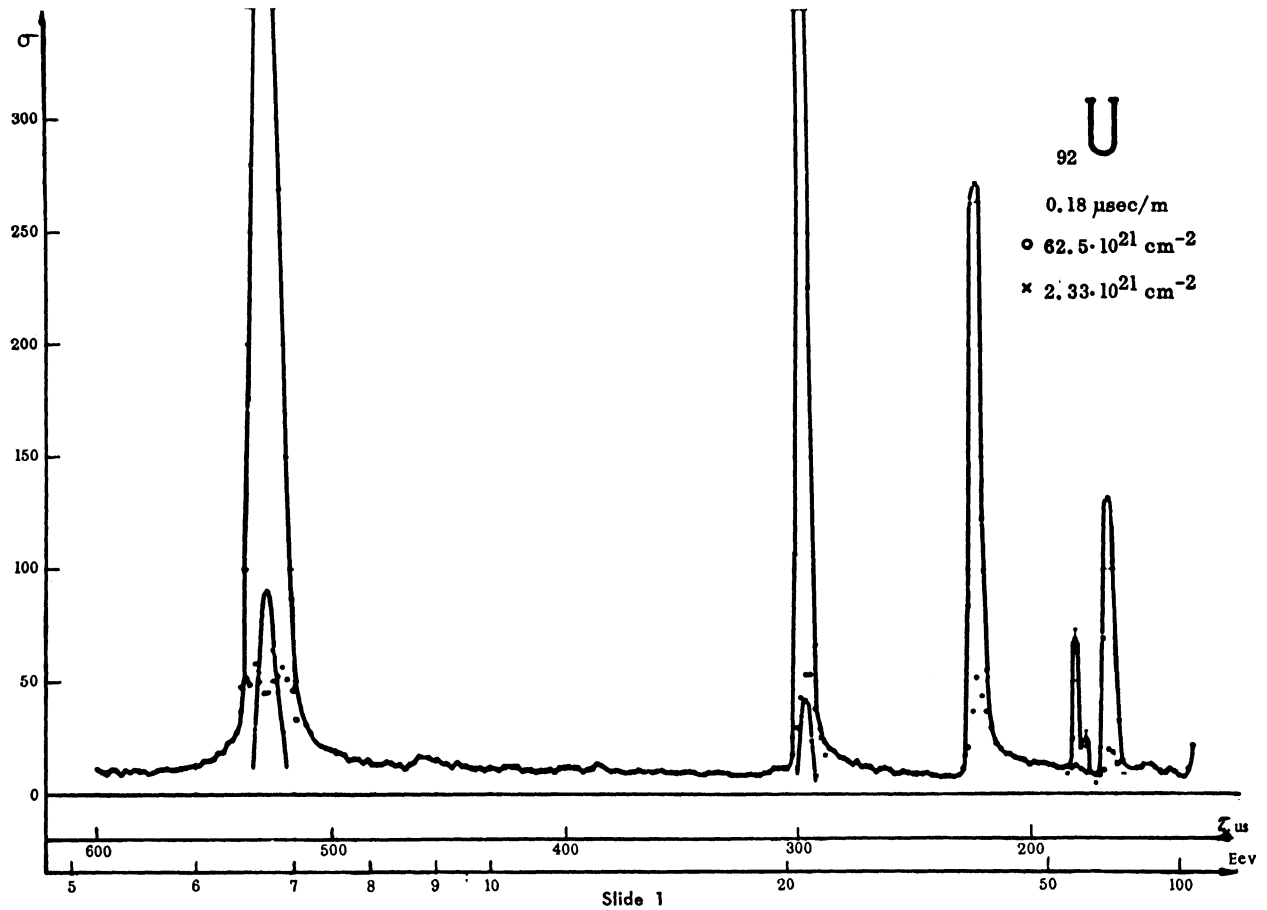

Slide 1

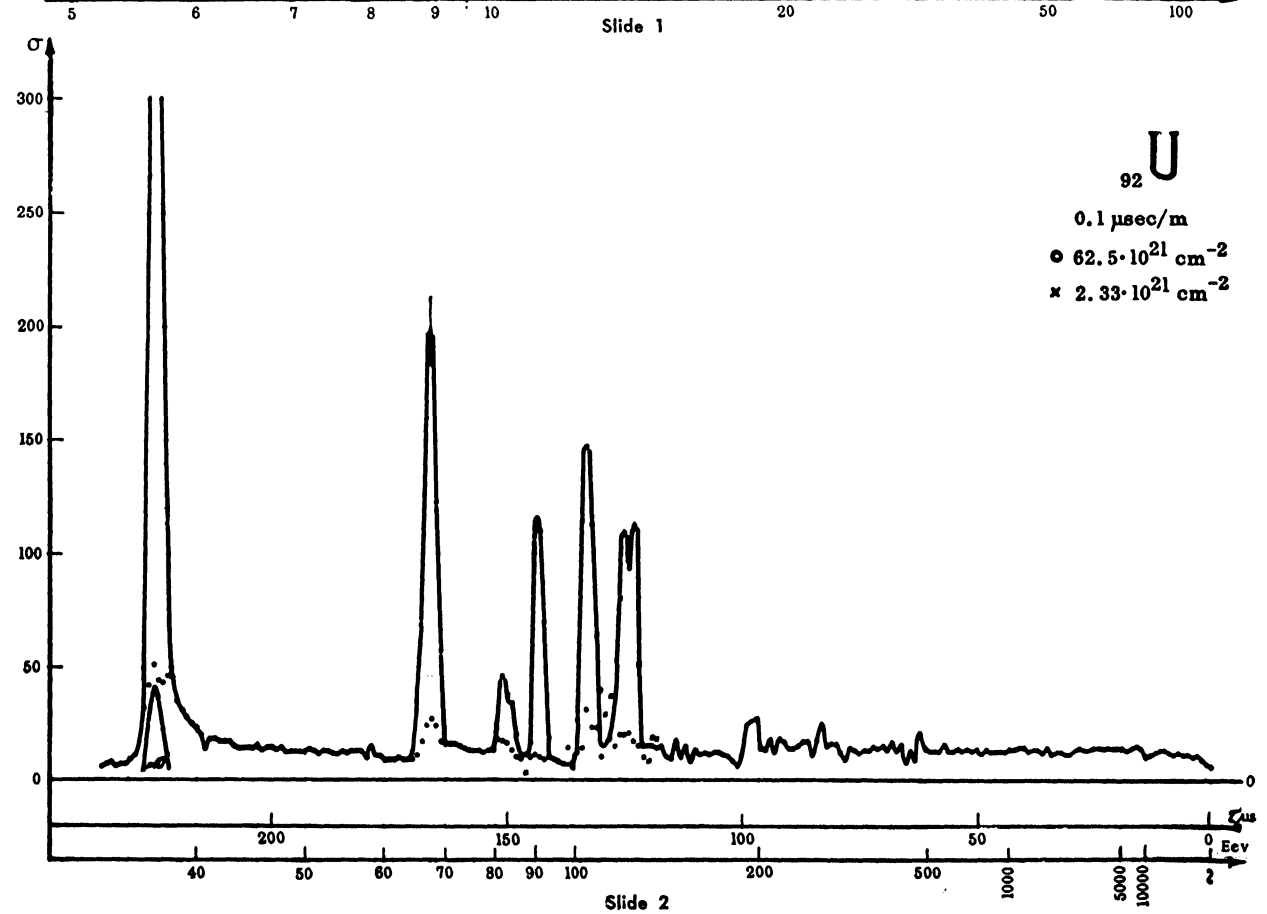

Slide 2

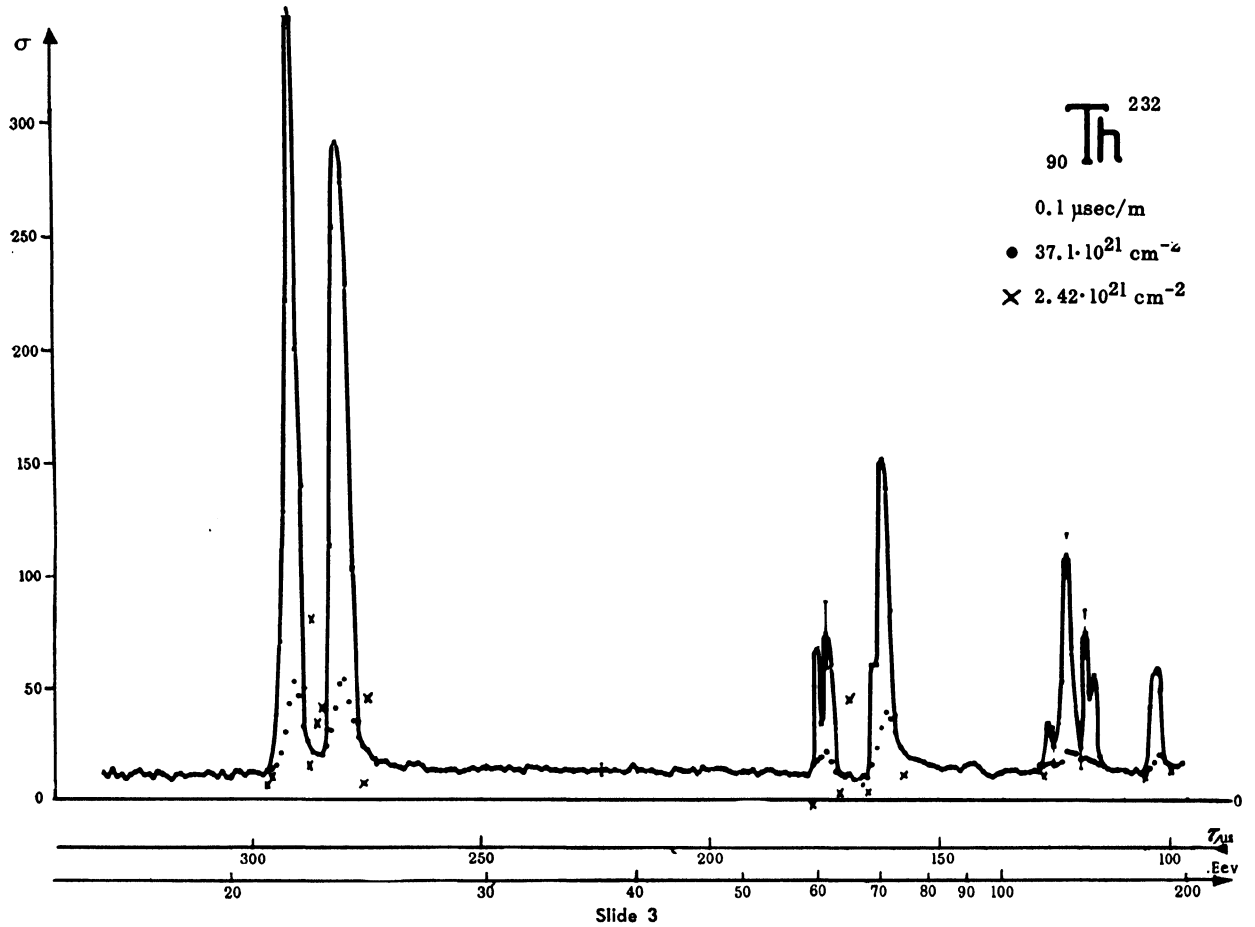

Slide 3

differ little from our results. The energy values corresponding to the main resonance peaks of thorium are 22.3, 23.9, 60.9 and 71.8 ev.

DISCUSSION OF P/576, P/640 AND P/641

Mr. F. L. Shapiro (USSR): Mr. Hughes in his report discussed a number of mutually complementary methods of using a reactor for the spectrometry of slow neutrons. I would like to describe briefly another possible way in which a reactor can be used for this purpose. In modern physical reactors the thermal neutron flux attains a value of 10^{14} neutrons/cm²/sec. The corresponding values of the neutron density and neutron gas pressure are 4×10^8 neutrons/cm³, and 10^{-8} mm Hg, respectively.

Advances in the technique of producing ion beams make it feasible to set up experiments in which the thermal neutron gas serves as the target subjected to bombardment.

Assume that we have an ion current $I = 1$ ma $= 6 \times 10^{15}$ ions/sec, flowing through a section of the neutron field 1 m in length. Let the neutron capture cross section or, more precisely, the activation cross section, σ, be 1 barn. Then the saturation activity will be

$$A = n\sigma_1 I = 4 \times 10^8 \times 10^{-24} \times 10^2 \times 6 \times 10^{15} = 240 \text{ disintegrations/sec}$$

This value is two to three orders greater than the minimum detectable activity.

By collecting the ions passing through the reactor and measuring the saturation activity as a function of the energy of the ion beam, we will, in effect, be determining the energy dependence of the neutron activation cross section of the atoms. Obviously, here the measured cross section refers to a neutron energy $E = mV_0^2/2$, where m is the mass of a neutron and V_0 is the ion velocity. This value will be M times smaller than the energy of the ion, where M is the mass number of the ion.

The resolving power of this method of neutron spectrometry is determined by the spread in the thermal neutron velocities. It will be given by

$$\frac{\Delta E}{E} = 2\sqrt{\frac{2kT}{E}}$$

where T is the absolute temperature of the neutron gas.

Some characteristics of the method are shown in the following table:

Neutron energy, kev	*0.1*	*1*	*10*
Ion energy, for M = 200, kev	*20*	*200*	*2000*
Resolving power			
At room temp. $T = 300°K$	4.5%	1.4% (0.016 μsec/m)	0.45% (1.6 × 10⁻³ μsec/m)
At $T = 20°K$	1.2%	0.36% (0.004 μsec/m)	0.12% (4.10⁻⁴ μsec/m)

At $T = 300°K$, $E = 10^3$ ev; $\Delta E/E = 1.4\%$ (0.016 μsec/m)

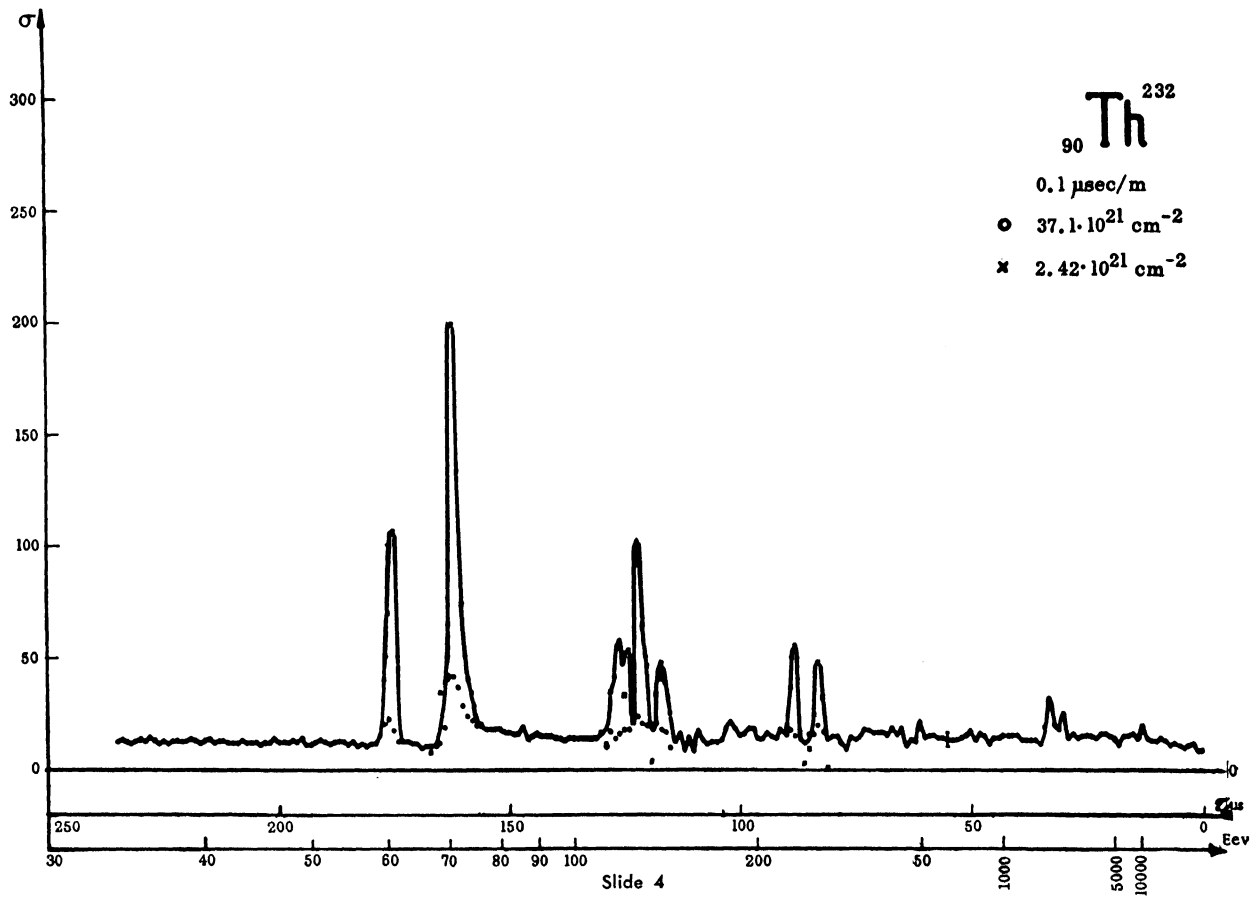

Slide 4

Cooling of the neutron gas improves the resolution. Thus, under the same conditions as above, but at $T = 20°K$, $\Delta E/E = 0.36\%$ (0.004 μsec/m).

The advantages of the method in question are the following: (1) good resolution in the region of hundreds and thousands of electron volts; (2) possibility of investigating separately the levels of each isotope in a natural mixture; (3) the fact that the activation cross section rather than the total cross section is measured; (4) the small amount of material required for the sample, which may permit making measurements with radioactive isotopes; and (5) elimination of the difficulties connected with the influence of the properties of the solid on the shape of the resonance line.

The shortcomings are the following: (1) the ion source and collector, which are located outside the reactor, require thorough shielding from scattered neutrons; (2) much more time is required for a complete series of measurements, since only one energy interval can be investigated at a time; (3) it is impossible to carry out measurements with isotopes forming stable or long-lived products as a result of neutron capture; and (4) the recoil in the emission of captured gamma-quanta makes focusing of the beam on the collector difficult.

Mr. Hughes (USA): This is an extremely interesting suggestion. There are quite a number of technical questions that I should like to discuss with Mr. Shapiro, but there is no time for that now.

However, the fact that so few neutrons come out of the reactor in a beam is a problem that has for a long time bothered all persons working with reactors. All of us have been trying to think of methods to get our equipment into the reactor, where the flux is so much higher. In a typical beam experiment, one neutron in a million is used in the apparatus. Hence, any suggestion that will increase the usable number of neutrons is very interesting. Of course, it is extremely difficult to operate any type of equipment inside the reactor itself. It is therefore a question of striking a balance between the loss of neutrons and the technical difficulty of putting the equipment into the reactor.

Mr. P. A. Egelstaff (UK): After the very interesting suggestion of Mr. Shapiro, I think I had better restrict my remarks to the lower energy region below, say, 20 kev. I should like to compare the chopper developments in the United Kingdom with those that have just been described in the USSR and the USA. In the United Kingdom we have a limited objective in our chopper work, that is, simply to measure the total cross section of small and particularly radioactive samples. As a result of this, we tend to call our choppers "small sample choppers," and we directed a great deal of attention to saving on the size of the sample. We have tried to develop for our new reactor a modified type of chopper. The particular advantages we claim for the system I want to describe are that it is capable of

giving an order of magnitude greater chopping speed than any existing chopper. In addition to that, with high resolution work we can do a preliminary velocity selection at the chopper, so that in fact we can fire a large number of neutron pulses down our flight tube simultaneously before detecting the first fications in design which we are incorporating.
one at the other end. In Slide 5, you see the modi-

The main features of this chopper are that we have tried to separate the functions of the chopper, namely that of stopping the neutron beam to eliminate your background and of modulating it. We have tried to divide those functions amongst two different chopping members. In this slide you see that we have a rotating collimator. This collimator contains the major part of the material that shuts off the neutron beam. It runs at a very low speed, 2×10^4 centimetres per second peripheral velocity, and has wide channels in it so that we get a very long broad neutron pulse. Then we have two small and light high-speed rotors. These are made from boron silicate glass fibres bonded with resin, because then we can make rods with high longitudinal strength but rather poor lateral strength. Two rods are made and then wrapped together with tape. In this way we make a rotor which consists of a single slit with sides around it. We have two of these rotors arranged so that their tips run in opposite directions. We believe that we can without difficulty get 1.2×10^5 centimetres per second tip speed on a single rotor, so that the chopping speed of the whole system will be twice that, 2.4×10^5. This is about five times faster than the present Brookhaven chopper which is the best that has been made so far. We shall do preliminary velocity selection in that small gap between the rotors, so that a part of the neutron spectrum only is allowed to travel down the flight path. The present rotor will have a half micro-second neutron pulse using a 0.050 slit width. With later rotors we hope to work down to a tenth micro-second neutron pulse, and then we hope to compete with the latest developments concerning pulsed sources.

Slide 6 shows the actual set-up that we plan to have in operation in a year's time. The collimator is shown with two high speed rotors, and a thousand curie sample placed between them. A biological shield is placed round the set-up. We use a 100-metre flight-path, and hope to use a neutron detector, rather optimistically, with an area of one square metre. The block diagram below shows the general lay-out that we propose to use covering the synchronization of the rotors to a standard oscillator, the gate system of a thousand channels, a memory, and the data being recorded on punched cards rather than directly on to registers.

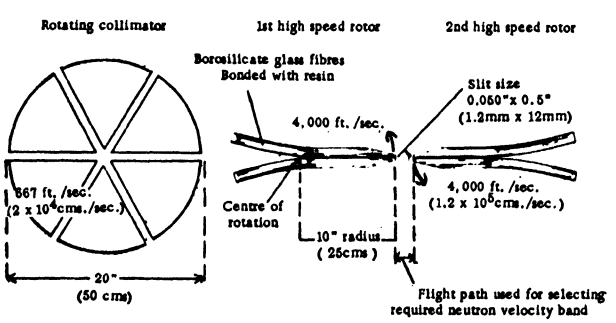

Slide 5. Plan view of superchopper. Notes: (1) the present rotors (1.2mm slit width) provide a 0.5 μsec neutron pulse, later rotors will be designed for shorter pulses down to 0.1 μsec; (2) the weight of one high speed rotor is approximately 3 lbs. (1.4 kg); and (3) the rotating collimator or a high speed rotor taken alone will pass neutrons from 0.5 ev to ∞

The CHAIRMAN: We have three more questions, the first by Mr. Havens of the United States in regard to Mr. Vladimirski's paper.

Mr. W. W. HAVENS (USA): What are the dimensions of the counter, and what is the pressure of BF_3 used in this detector? I should also like to know, with this detector information, what is the counting rate per microsecond per meter.

Mr. VLADIMIRSKI (USSR): The diameter of the counter is 30 mm; its length is 200 mm. We usually put two counters, connected to different groups, in one tank. For some measurements a large number of counters — up to 25 — is used; in such cases the total count may attain 500 an hour per microsecond of channel.

Mr. J. A. HARVEY (USA) (to Mr. Vladimirski): When you quote a resolution of 0.07 microseconds per meter, do you include the flight time of the counters which is important at the lower energies?

Mr. VLADIMIRSKI (USSR): No, this flight time is not included in the quoted figure.

However, simultaneously with the decrease in resolving power, due to the cutting off of the neutrons there is a reduction in the length of the burst, which one should take into account. The resolving power remains close to the upper limit.

Mr. J. E. SANDERS (UK): I should like to ask Mr. Mostovoi if he could give me more details of the fission chamber in which he manages to use 22 milligrammes of plutonium, since we have never obtained satisfactory operation using more than about 13 milligrammes of plutonium in a fission chamber.

Mr. MOSTOVOI (USSR): Essentially, this chamber is a double ionization chamber. The layer of fissile material is applied to a thin nylon support (0.3 microns). For better conductivity, this layer is then covered with silver or aluminum by evaporation in a vacuum. Each fission event occurring in this layer produces two fragments which fly off into the two halves of the chamber. The electrodes of both halves of the chamber are connected and the total ionizing pulse goes to the pre-amplifier. We utilize the ionization due to both fragments and thus increase the ratio of the ionization produced by the fragments, and the ionization due to the alpha particles. Furthermore, we make use of the initial part of the fragment trajectory, where the ionization density is appreciably higher, and the initial part of the alpha-particle path.

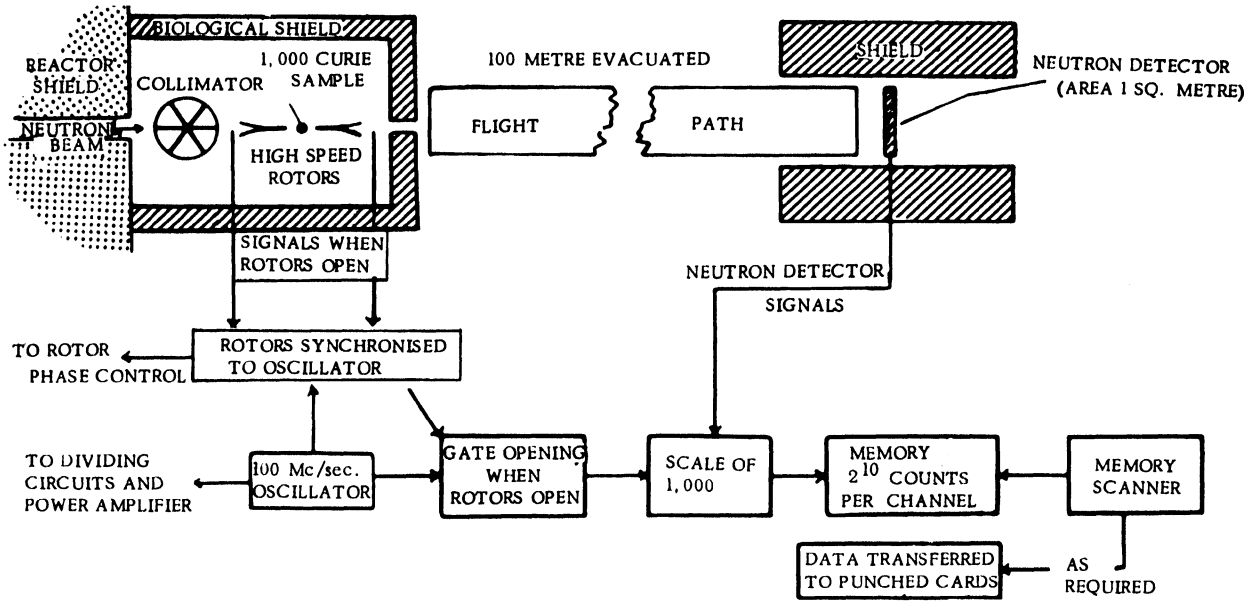

Slide 6. Layout of Harwell superchopper (at July 1955)

The distance between the electrodes is small—9 mm—and the pressure of the gas, which consists of argon with about 5 per cent CO_2, is 30 cm.

Mr. R. F. Taschek (USA): I should like to ask Mr. Mostovoi what is the rise time of the amplifiers used on this same plutonium counting chamber?

Mr. Mosotovoi (USSR): The rise time is 0.1 microseconds. However, as I pointed out, we were able to place a larger amount of plutonium in the chamber not by virtue of the short rise time of the ionization pulse, but thanks to the increase in the ratio between the ionization due to fragments and that due to alpha particles.

Mr. E. R. Wiblin (UK) presented paper P/421, preceding it with the following remarks: I wish to emphasize in the first place that, although this paper is presented by me alone, it represents the work of several people in several parts of the establishment at Harwell, and also of several people in the industry in the United Kingdom who have helped us in the building of apparatus. I should also like to acknowledge in the early part of the paper some information given to me by members of the United States delegation in making a comparison of the time-of-flight spectrometer based on pulsed sources with our own.

The paper in its written version does not cover a comparison of spectrometers from different places, but I have thought it a good idea to start this morning by spending a few minutes on making a comparison. I think I am correct in stating that historically the original pulsed-source spectrometer was operated on the Berkeley cyclotron by Alvarez in 1938. This used very long pulses, and only thermal neutron work was carried out.

In the United Kingdom the earliest results were obtained with a pulsed Cockcroft-Walton type HT set by a group under Sir George Thomson. A rather similar arrangement was used in the United States by Messrs. Manley, Hayworth and Luke in 1941, but in this case a swept beam technique was used instead of the pulsed ion source as in the United Kingdom system. Following this there were several successful applications of cyclotrons for pulsed neutron sources, notably at Cornell, which produced the first published time-of-flight resonance region data; but at Columbia under Professors Havens and Rainwater and their various associates was operated probably the most prolific machine in terms of results produced. This, again, used a pulsed ion source to produce a pulsed neutron source. A similar system is operated at Brookhaven and also much more recently with shorter pulses at Columbia a synchrocyclotron has been used. Some very refined results have been obtained and Professor Havens may have some comments to offer on this system.

The betatron has been applied to these techniques by the General Electric Company at the Knolls Atomic Power Laboratory and has produced, again, some very fine results. At the Oak Ridge Laboratory in the United States some high energy time-of-flight work has been carried out with a pulsed beam from a Van de Graaff machine. Very recently, at Columbia University again, a direct pulsed transformer operating a (d,d) source for neutrons has been used. We are now getting very close to the main part of what I want to say, which concerns principally pulsed source work using linear electron accelerators as the primary source of power. These have been used at Yale in the United States and at Harwell, which is particularly what I want to describe.

First I would like to make sure that we are talking the same language in relation to resolution. It may be expressed as follows:

$$\frac{\Delta E}{E} = 2\left[\frac{2\Delta t}{t} + \frac{\Delta r}{r}\right]$$

This is a well-known formula for the energy resolution in terms of the total time uncertainty $2\Delta t$, the time-of-flight t, the total uncertainty in distance measurement Δr and the distance r. Now consider an imaginary resolution function based upon the operation of two square pulses, one at the source and one at the detector gate, of a total base width of $2\Delta t$. Then width at half-height is Δt. In the table that follows this crude figure of merit is used to compare spectrometers. It is the total time uncertainty divided by 2, and this divided by the flight distance.

Pulsed Neutron Sources for Time-of-Flight Work

Machine	*Target*	*Neutrons/sec (pulse)*	$\Delta t/2d$
Columbia Cyclotron	Be	6×10^{13}	0.33
Brookhaven Cyclotron	Be	3×10^{14}	0.2
Col. Synchrocyclotron	W	$> 10^{17}$	0.014
GE Betatron	U	$> 10^{15}$	0.01
Oak Ridge VdeG	Li	5×10^{8}	0.013
Col. Pulse Transformer	D/T	5×10^{12}	0.5
Yale 5 Mev Lin Acc.	Au/Be	3×10^{12}	0.4–0.2
Harwell 3.2 Mev Lin Acc.	Pt/Be	2×10^{12}	0.2
Harwell 14 Mev Lin Acc.	U	4×10^{14}	0.15–0.004
Harwell 25 Mev Lin Acc.	U	$> 10^{16}$	< 0.001

There is another line to the table which is not shown because it is in the realms of projected activity in that it uses, with the accelerator, instead of the simple target for photo-emission from uranium, a near-critical assembly to multiply the output by a further factor. I now return to consideration of my paper, as briefly as I can, to discuss the present Harwell set-up.

Mr. L. CRANBERG (USA) presented paper P/577.

Mr. L. M. BOLLINGER (USA) presented paper P/580.

Mr. W. A. HIGINBOTHAM (USA) presented paper P/806.

DISCUSSION OF P/421, P/577, P/580 AND P/806

Mr. W. W. HAVENS (USA) made a comment which essentially consisted in reading the parts of P/574 dealing with the Columbia 400 Mev synchrocyclotron and the Oak Ridge pulsed Van de Graaff accelerator, and showing Figs. 17, 18 and 19 of that paper.

Mr. P. A. EGELSTAFF (UK): We have heard from Mr. Cranberg of the very beautiful work that has been done on time-of-flight measurements of neutron inelastic scattering. It is interesting to compare that method with the method used at Harwell using a helium-3 neutron spectrometer. This spectrometer was developed, at the suggestion of Mr. Bretscher, by Mr. Batchelor. In our spectrometer, which has the limitation, of course, that it is only useful in the range 100 kev to 1 Mev, we have a resolution of 3% and hope that this can be improved by purifying the gas used in the spectrometer somewhat further. The comparison I would like to make is that of resolution in the first place, and I would like to ask Mr. Cranberg if he could compare our resolution of 3% with that shown in his work; and also if a comparison can be made in the type of experiment for which the spectrometer can be used. For example, we have used the helium-3 spectrometer to measure the spectrum of delayed neutrons. In this example it is particularly useful, and this is a case where the time-of-flight technique cannot be used effectively.

Mr. CRANBERG (USA): I quite agree with Mr. Egelstaff that the methods are not competitive in all areas. However, I think it may be worth repeating that for angular distribution work the method I have described offers perhaps unique advantages. In terms of resolution, expressed as I believe Mr. Egelstaff has expressed it, as the percentage which the half-width is of the total, this is considerably better than in the work I have described so far. However, the focus of interest in the work I have described so far is not the achievement of optimum resolution, but rather development of a system which would be versatile and enable one to cover a large number of elements with good speed. If one attempted to optimize the parameters of the system to achieve the very best results I think that over certain parts of the energy range comparable results could be achieved with those which have been mentioned by Mr. Egelstaff.

Mr. B. P. ADYASSEVICH (USSR): In an investigation carried out by Bogdanov, Vlasov, Kalinin, Rybakov and Sidorov, a similar procedure in connexion with a cyclotron was applied to the study of neutron spectra formed in certain reactions with light nuclei. The ions were accelerated in the cyclotron in a narrow phase interval of the accelerating potential. The duration of the burst on the target was not over 5 μsec. The frequency of the accelerating voltage was 8.9 megacycles. The flight path was 3 metres. The neutrons were recorded by a fast scintillation counter (the scintillator was polystyrene with terphenyl). The resultant pulses of 3 μsec duration were fed into a coincidence circuit, to the other branch of which were applied pulse synchronised with the accelerating voltage of the cyclotron.

The instant of formation of neutrons was determined from the position of the peak of the gamma radiation from the target.

This procedure was used in investigating, at a zero angle, the spectra of neutrons formed by the bombardment of thin tritium and deuterium targets by deuterons with an energy of 14 Mev. In both cases, in addition to the principal groups of neutrons with an energy of 30 Mev (T,d), and 16 Mev (D,d), corresponding to the formation of He^4 and He^3 nuclei in the ground states, we found evidence of the presence of large groups of neutrons with lower energies. The intensity of these groups is several times greater than the intensity of the principal groups.

The presence of these groups testifies to the high probability of the deuteron splitting in such a way that the product nucleus formed simultaneously with the free neutron either will be in a highly excited

quasi-stationary state, or will split. For He^4, an excited state with a short lifetime is known from the $T(p,n)$ He^4 reaction. The energy of this state corresponds precisely to that of the measured group of neutrons. No analogous state for He^3 is known. However, in both cases the existence of the groups of slow neutrons can be explained without assuming the existence of quasi-stationary states of the final He^4 and He^3 nuclei. The question of the part played by the final states of these nuclei is of great interest and requires further investigation.

The data obtained indicate that non-monochromatic neutrons are formed in the $T(d,n)$ and $D(d,n)$ reactions when the energy of the deuterons is about 14 Mev.

Mr. CRANBERG (USA): I am very interested to hear these results, since they parallel some work which has recently been done at Los Alamos on the D-T reaction. I believe there is a letter to the editor en route which will probably appear in the *Physical Review* shortly. The application of time-of-flight techniques to target reactions is, of course, a very attractive one. I am very interested to hear of this work in the Soviet Union.

Mr. M. V. PASECHNIK (Ukrainian Soviet Socialist Republic): I think that Mr. Cranberg's report is one of the most interesting we have heard on the spectrometry of fast neutrons. I have several questions which I like to ask, but as our time is short, I will put them to Mr. Cranberg in private, if he has no objection.

Mr. CRANBERG (USA): I would be delighted.

Mr. P. HUBER (Switzerland): I would like to have some more information about the signal to noise ratio in a noble gas scintillation counter for a given alpha-particle energy.

Mr. BOLLINGER (USA): Without the question being phrased a little more accurately I am not sure I can give a good answer. Let me say I am not intimately familiar with the results, but in the curves I have seen, taken by Mr. Huddleston and others at Argonne, the photomultiplier noise is quite low, so that one could now, by using coincidence techniques, make photomultiplier noise entirely negligible. Even without the coincidence technique, for neutrons or particles of moderate energy, and particularly fission products, noise is not a problem.

Mr. WIBLIN (UK): I should like to make just one brief comment on Mr. Higinbotham's paper in order to describe the time expansion system used to produce the short 0.2 microsecond gates we have now in use at Harwell, Slide 7. I hope that this diagram will be reasonably clear. First of all, on the left, which I have marked *IG*, we have an input gate into which both signal pulses and a reference pulse are passed. These are circulated together through a 20 microsecond delay with a dividing or routing network at its end, which passes the reference pulse through an extra 0.2 microsecond delay. This is then returned together with the signal. The reference goes through the extra delay; the signal comes direct into a coincidence unit. Therefore, as the reference pulse circulates around this system, which is completed by an amplifier, it catches up with the delayed signal due to a neutron arriving later at the detector. This coincidence unit, in effect, registers the coincidence between a reference pulse and a neutron at some delay corresponding to the neutron energy. It then produces two things: an output signal to the register gates, which registers the arrival of a neutron of that energy; and, at the same time, a clearance pulse which goes back to the beginning, wipes out the signal due to that neutron, which is still circulating in this delay unit. The reference pulse then circulates a few more times through this $\frac{1}{5}$ microsecond extra delay until it catches up with the next neutron. Then the signal due to that neutron is passed out to the gates.

In this way, this expansion system provides a 100 to 1 time expansion ratio as between the full delay of 20 microseconds and the extra delay applied to the reference pulses of $\frac{1}{5}$ microsecond.

Mr. M. K. ROMANOVSKI (USSR): Mr. Higinbotham described a number of "memory" circuits and devices. I would like to know which of these he considers to be the best and most promising.

Mr. HIGINBOTHAM (USA): I am prejudiced, of course. The two circuits which I described at the end using the magnetic core or the cathode-ray tubes are almost identical. It is a question, then, of which will be cheaper, projecting this into the future. Either one of these can be extended to have more channels, and the width of the channel can be made narrower. One can build on this type of device almost without limit. On the other hand, I think that not everyone has a need for the most elaborate or most complicated machines. For example, where the quartz delay line technique can be used to trigger a pulse accelerator, it may be a cheaper and therefore a more useful device for many cases.

Mr. R. TASCHEK (USA) presented paper P/573.

DISCUSSION OF P/573

Mr. KAZACHKOVSKI (USSR): I would like to make two remarks on the methods of measurement in spherical geometry.

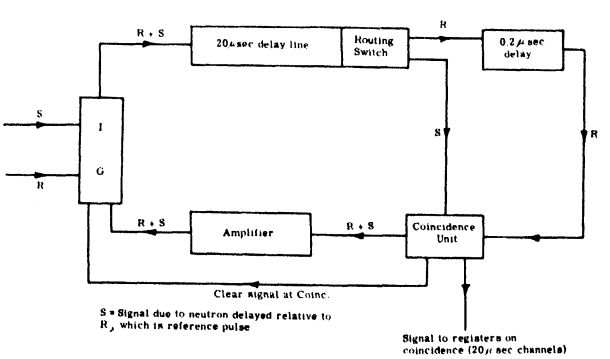

Slide 7. Time expander unit for 0.2 μsec gates

1. The equivalence of direct and inverse geometry holds not only for thin shells, as mentioned in this paper, but also for spheres of any radius. This can readily be proved in at least two different ways. Due to lack of time I will not elaborate on the proofs, but will limit myself to a few conclusions which may be of practical interest. Moreover, we are obviously not the only ones who know the equivalence of direct and inverse geometry.

In the case of measurements in inverse geometry, the distribution of the neutrons from a source within the solid angle occupied by the sphere must be cosinusoidal. For example, if the source is isotropic, it must be at a distance of more than four radii from the sphere. In this case the isotropic and sinusoidal distributions will be virtually identical.

Incidentally, an analogous situation obtains in direct spherical geometry for the transparent detectors usually employed. The latter must also be at least four radii distant from the source. Obviously a "black" detector can be located as near the source as desired.

2. I would like to propose a simpler method of taking into account multiple scattering in the sphere than the method described in the paper. It is based on the introduction of a new quantity: the mean length of the path travelled by the neutron prior to emerging from the sphere, $\bar{l}$.

The corresponding equation, derived by interpolation between the expressions for spheres of small and large radii, has the form:

$$\frac{\bar{l}}{R} = 0.71 + 0.50\ \frac{R}{\lambda} + 0.29\, e^{-0.46\, R/\lambda}$$

where R is the radius of the sphere and λ is the scattering mean free path of the neutron.

In the case of anisotropic scattering, instead of λ, one can use $\lambda + z$. In most cases the error involved will be negligible. The cross section is then computed according to the usual equation:

$$\sigma = -\frac{1}{N\bar{l}} \ln = T$$

where N is the number of nuclei per cubic centimetre and T is the ratio of the number of counts with the sphere to the number without the sphere.

The above equation can be used when the attenuation of the primary neutron beam is not too great. When T equals 0.8 or less, suitable corrections should be introduced for the self-absorption of neutrons with long trajectories inside the sphere.

Mr. TASCHEK (USA): I believe that that question requires more detailed examination. If, however, I have understood it correctly, I may say this: The effective path length, denoted here as $\bar{l}$, is a method which has also been used, I believe, by Barschall to make a correction of the same kind. We can, however, discuss this rather complicated question in more detail.

Mr. M. V. PASECHNIK (Ukrainian Soviet Socialist Republic): I would like to make one remark concerning the variation of the inelastic scattering σ in spherical geometry when scintillation counters are used.

Corrections must be made for the light-guide, which disturbs the spherical symmetry. The correction is particularly great in the case of heavy nuclei.

Mr. TASCHEK (USA): I believe that you are referring to the hole out of the bottom of the sphere. A correction is always made for that.

Session 16A

EQUIPMENT AND TECHNIQUES (*concluded*); CROSS SECTIONS OF NON-FISSIONABLE MATERIALS; DELAYED NEUTRONS

LIST OF PAPERS

			Page
P/356	Testing materials by the pile oscillation method in the Chatillon reactor	D. Breton	127
P/642	A neutron spectrometer based on measuring the slowing-down time of neutrons in lead	A. A. Bergman *et al.*	135
P/832	The determination and evaluation of fundamental thermal neutron cross sections	J. A. Harvey	147
P/591	The cross section of the fission product poison Xe^{135} as a function of energy	S. Bernstein and E. C. Smith	153
P/831	Delayed neutrons	G. R. Keepin and T. F. Wimett	162
P/648	The study of delayed neutrons emitted by uranium-233 as a result of irradiation by thermal neutrons	S. V. Girshfeld	171

Testing Materials by the Pile Oscillation Method in the Chatillon Reactor

By D. Breton,* France

The purpose of nuclear testing is the determination of the value of the materials destined to be used in reactors. The purpose of this, is to measure the capture cross section of these materials by comparing them, either to a calibrated sample of the same element, or to a material having a purportedly known cross section. Several methods may be used; those which appear to be most suitable use the disturbance caused in the operation of a reactor by the periodical insertion of a sample of the material to be studied. These methods, which are called oscillation methods, have received practical application in the US, Canada, England and France.

The method used in the US, Canada and England, consists of measuring the amplitude of modulation of the current produced in an ionization chamber placed in the reactor.

The method developed at Châtillon (France) is based on measuring the phase angle of the signal supplied by the ionization chamber.

This signal is due to the combining of a local signal with an over-all one, due to the effects of scattering and capture. Conversely, the former methods make use of only either of these signals, after elimination of the scattering effects.

GENERAL DESCRIPTION

A sample of graphite, parallelepiped in shape (99 × 95 × 190 mm), is given a reciprocating motion in a tangential channel of the reactor with a section of 100 × 100 mm. This graphite sample makes up the oscillator. A reference oscillator, called "standard oscillator," has been defined. Its weight is 2852 gm (density = 1.64), and its effective capture cross section is close to that of atomically pure graphite. The captures of samples geometrically identical to, and of nuclear quality different from, the standard, are compared. It is assumed that the effective scattering cross section of the various samples remains constant, and that their effective capture cross section is the only variable (as a consequence of the presence of impurities). The specific gravity of these samples need not be the same. The effective capture cross sections are determined with respect to that of boron (750 barns for 2200 m/sec neutrons).

Original language: French.

* Department of Reactor Studies of the Centre d'Energie Atomique (Atomic Energy Center).

Both extremities of the graphite sample are attached to a steel cable by means of a small aluminum cylinder. The capture effect of these fastenings is equivalent to that of the steel cable, which is supposed to continue inside the graphite block. One strand of this cable is fastened to the arm of a mechanical device which moves according to a sine law as a function of time, the other strand is held in tension by a counterweight (see Fig. 1). The channel in which the motion of the oscillator takes place does not contain any graphite at all. One end of the channel is blocked by a mobile lead and boron carbide guard, the other end normally is closed up by the concrete plugs which make up the protective device. A small hole has been drilled through these plugs, in order to let the cable through. The oscillator moves on an aluminum slide which is fastened to the bottom of the channel.

The detection device used is a boron trifluoride chamber placed as shown on Fig. 1. When the graphite block oscillates, the ionization chamber will deliver an alternating current of the same frequency as that of the motion, which is a function of the capture cross section of the graphite; on this, a direct current is superimposed, which is proportional to the working power of the reactor. The direct current component is filtered out, and the alternating current, after amplification, is injected into a harmonic analogical analyzer which determines the components, both in phase and in quadrature, of the fundamental of the ac component.

The standard used has a small hollow recess in its central part, which can receive bits of paper soaked in a titrated solution of boric acid. The addition of these, which thus carry known quantities of boron, increases the capture cross section of the standard graphite, and makes up the calibration of the method.

PRINCIPLE OF METHOD

Two phenomena will appear when the graphite sample is moving.

The number of neutrons captured or scattered by the sample varies as a function of the position which it occupies during its motion in the channel. The result is a variation of the reactivity Δk, which becomes apparent as a change in the reactor power. For a given graphite sample, Δk is a function of the capture cross section Σ_a, and of the scattering cross

section Σ_s, of the graphite, of the amplitude λ of the oscillation, and of the mean position of the oscillating sample r_0 in the channel. Since the dimensions of the oscillator cross section are very close to those of the channel, the effects due to graphite scattering are very conspicuous and show considerable predominance over those due to capture. In fact, it will be noted that, when the graphite block enters the reactor, its power will be increased. When some milligrams of boron are added to the graphite block, the power increase will be less than before. The neutrons, which but for the presence of the graphite block would have leaked out of the reactor, will be scattered, and there will be an additional opportunity of using them; the increase in the capture cross section of the graphite block will reduce this opportunity. Since neutron leakage plays a very important part, it will be necessary to cut all samples to be tested to the same section.

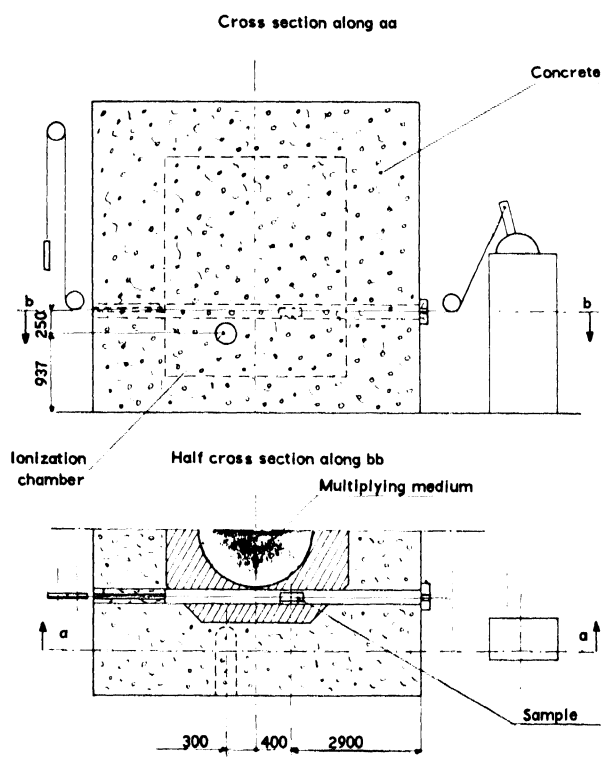

Figure 1. Cross section along aa; half cross section along bb

The variation in the reactivity which is due to the oscillation causes the power of the reactor to vary at all points, and the chamber detects a signal, called the over-all signal, which is out of phase by an angle ϕ with respect to the oscillating motion; ϕ is a function of the oscillation period, of the half-lives of the delayed neutrons, and of their abundance; this signal has been used, in particular, for the oscillation experiments carried out at Harwell by Colmer and others. In order to get rid of the effects due to scattering, these authors oscillated a graphite "train" in such a way that the channel in which this was done never was empty; when the graphite sample under study was moved to areas where the density gradient was zero, the reactivity variation then was only a function of the effective capture cross-section.

The motion of the graphite block in the channel affects the distribution of the surrounding neutrons. This would also happen if the reactor were a "static generator" of neutrons (for instance an Ra-Be source). It fades out very quickly away from the oscillator. As a consequence of its proximity, the ionization chamber used for the measurements detects this perturbation, which is a function of the capture and scattering cross sections of the oscillator, as well as of the oscillation amplitude λ and the mean position r_0 of the oscillator in the channel. The signal generated by this perturbation has to be, either in phase, or else in opposition, to oscillator motion.

Hoover and his group eliminated the effects due to scattering. The perturbation would then only be a function of the effective capture cross section of the oscillator. This signal has also been used in the oscillation experiments carried out at Châtillon.

The over-all signal and the local signal, combined in magnitude and phase, give a resultant R, the phase of which is shifted by an angle θ with respect to the oscillating motion. The current produced by the chamber will then be proportional to this resultant R. The harmonic analogue analyzer allows for the measuring of the amplitude and phase of this resultant, which is a function of Σ_a, Σ_s, λ and r_0.

Study of the Over-all Signal

If a reactivity variation $\Delta k = \Delta k_g e^{j\omega t}$ takes place in a reactor, the response of the reactor is such as to have the power vary according to the law:

$$dn = n_0 A \Delta k_g e^{j(\omega t + \phi)} \tag{1}$$

where dn is the variation of the neutron density measured at point r, n_0 is the neutron density measured at the same point, and A is the amplification coefficient of the reactor as defined by:

$$A = \left[\omega^2 \left(\tau + \Sigma_i \frac{\beta_i \tau_i}{1 + \omega^2 \tau_i^2} \right)^2 + \omega^4 \left(\Sigma_i \frac{\beta_i \tau_i^2}{1 + \omega^2 \tau_i^2} \right)^2 \right]^{\frac{-1}{2}} \tag{2}$$

ϕ is the phase shift in the reactor response, with regard to the variation of reactivity

$$\phi = \arctan \frac{\tau + \Sigma_i \dfrac{\beta_i \tau_i}{1 + \omega^2 \tau_i^2}}{\omega \Sigma_i \dfrac{\beta_i \tau_i^2}{1 + \omega^2 \tau_i^2}} \tag{3}$$

where $\omega = 2\pi/T$, T = oscillation period, $\lambda_i = 1/\tau_i$, half-life of delayed neutrons of the i species, β_i = percentage of delayed neutrons of the i species, and τ = life of the neutrons in the reactor.

Δk_g is a function of the capture and scattering cross sections of graphite, and proportional to the number, N, of graphite nuclei found in the sample:

$$\Delta k_g = N \Delta k_0$$

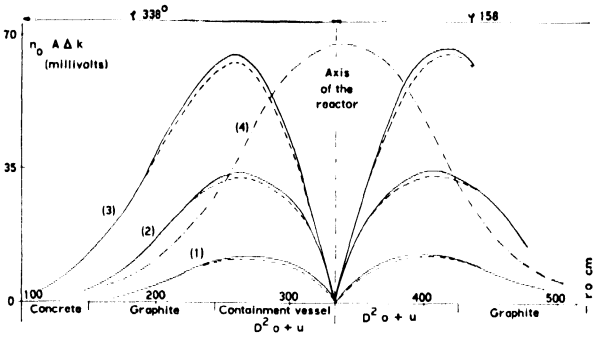

Figure 2. Variations of over-all signal amplitude as a function of r_0 (for $T = 4.5$ sec, power 400 watts); Curve No. 1: $\lambda = \pm$ 10 cm; Curve No. 2: $\lambda = \pm$ 30.5 cm; Curve No. 3: $\lambda = \pm$ 70 cm; (the dotted curves were obtained after 3 mg of boron had been added to the calibration sample); Curve No. 4: Neutron density in the channel (arbitrary ordinates); (the origin of the abscissae has been taken at the edge of the reactor protection)

Figure 2 shows the amplitude variations of the over-all signal (expressed in millivolts) produced by the standard oscillator which was first oscillated alone, then used with an addition of 3 mg of boron, as a function of its mean position r_0, and for three oscillation amplitudes. These curves were plotted with the help of an ionization chamber placed sufficiently far away from the oscillator not to detect the local signal produced by this oscillator. On the same diagram, phase ϕ also was plotted (ϕ is independent of the oscillation position). The time when the graphite is at midpoint was chosen as the origin. From this, it follows that ϕ undergoes a 180 degree variation when the mean oscillation point passes the center of the reactor.

Study of the Local Signal

The local signal has the form:

$$l = n_0 l_g e^{\,j(\omega t + \alpha)}$$

where $l_g = N\, l_0$ and l_0 is a function of Σ_a, λ and r_0. The proportionality between Δk_g, l_g and N is limited to the cases in which the sample is very much shorter than the channel. α is equal to zero when the local signal is in phase with the motion of the oscillator, and is equal to M when it is in opposition with said oscillator motion. The study of the variations of l_g, as a function of r_0 and λ, would require very rapid oscillation, so that the over-all signal could be made very weak as against the local signal. The mechanical set-up did not enable us directly to undertake this study.

Study of the Resultant Signal

The signals $dn = n_0 A \Delta k_g e^{\,j(\omega t + \phi)}$ and $n_0 l_g e^{\,j(\omega t + \alpha)}$ are two components that give a resultant R

$$R = n_0 N e^{j(\omega t)} (A \Delta k_0 e^{j\phi} + l_0 e^{j\alpha}) \qquad (4)$$

Their variation does not clearly follow a sine law; they contain a large percentage of harmonics. Since the harmonic analogue analyzer will detect only the fundamental, the other harmonics play no part in the measuring. The resultant is a vector which rotates at frequency ω. Its amplitude R is equal to:

$$n_0 N \left[A^2 \Delta k_0^{\,2} + l_0^{\,2} + 2A \Delta k_0\, l_0 \cos(\alpha - \varphi)\right]^{1/2} \qquad (5)$$

and its phase is defined by

$$\tan\theta = \frac{A \Delta k_0 \sin\varphi + l_0 \sin\alpha}{A \Delta k_0 \cos\varphi + l_0 \cos\alpha} \qquad (6)$$

θ depends, neither on the working power level of the reactor, nor on the number N of nuclei present in the oscillator.

Since the graphite blocks to be compared have been cut to the same measurements and θ is independent of N, this angle will be the same in the comparison of two blocks that are identical, as to capture, but of different specific gravities. This will be confirmed experimentally. Fig. 3 shows the value of angle θ as a function of the specific gravity of a given graphite block. The density variation has been brought about by drilling small holes ($\phi = 0.2$ cm) in the oscillating graphite block and filling them with the powder produced by the drilling; by using this procedure, it was possible to cause the apparent specific gravity to vary from 1.424 to 1.654. When the capture variations are limited to slight ones, such as in case of the comparison of two graphite samples, it will not be necessary to carry out a specific gravity correction.

Since the length of the oscillator (9 cm) is small with respect to the total length of the channel (510 cm), the specific location of the absorber, placed in the oscillator with a view to increasing its capture rate, will have no practical significance. This was verified experimentally, by means of an aluminum box having the same dimensions as the oscillator. This box, filled with graphite powder, oscillates in the channel, after which a few milligrams of boron are added at one point, and thereafter distributed all over the powder. It can then be ascertained that the phase and amplitude of the signal produced by

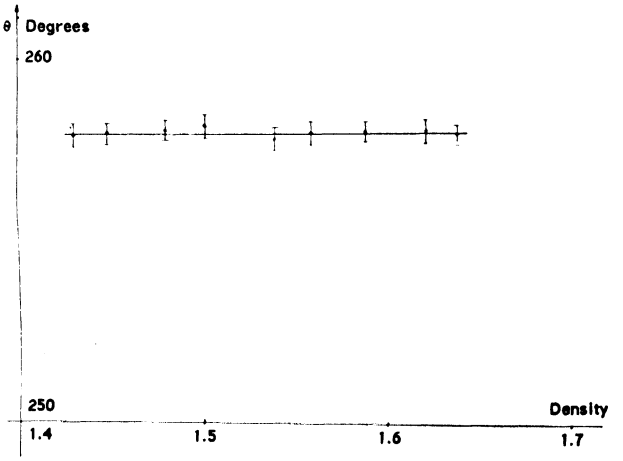

Figure 3. Variation of angle θ as a function of the apparent oscillator density in graphite (for $\lambda = \pm$ 30.5 cm; $r_0 = 289$ cm; $T = 4.5$ sec, reactor power 400 watts)

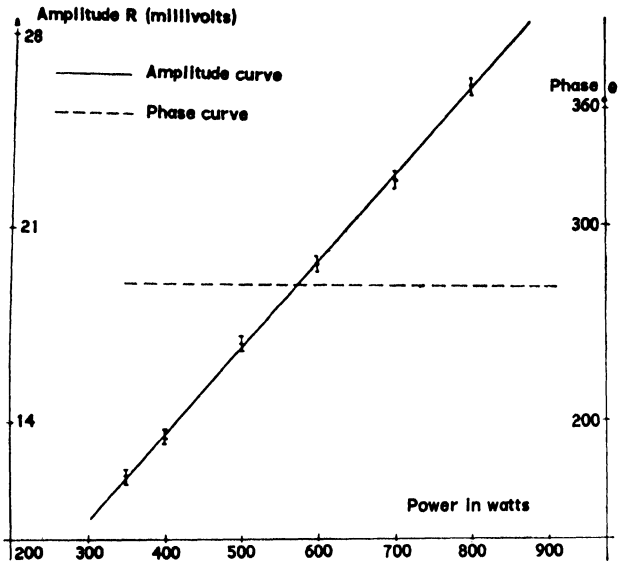

Figure 4. Variation of amplitude R and phase θ, of the resultant signal, as a function of reactor power (for $T = 4.5$ sec; $\lambda = \pm 30.5$ cm; $r_0 = 289$ cm)

the chamber remain the same but for the experimental errors, provided the amounts of boron added be kept small (10 mg). Equation 6 shows that angle θ does not depend on the working power level of the reactor, but that, conversely, the amplitude of resultant R is in direct proportion to it. Figure 4 shows the variations of θ and of R as a function of reactor power, for a mean oscillating position $r_0 = 289$ cm, an amplitude $\lambda = \pm 30.5$ cm and a half-life $T = 4.5$ seconds.

R and θ are functions of r_0, λ and T. Figure 5 shows these variations as a function of r_0 for $T = 4.5$ seconds and $\lambda = \pm 10$; ± 30.5; ± 70.5 cm.

Vectorial Representation

It is convenient to represent the local and over-all signals by vectors, which rotate at a frequency ω (Fig. 6).

Let $OA = n_0 N A \Delta k_0$ be the vector representing the over-all signal, the phase of which has been shifted

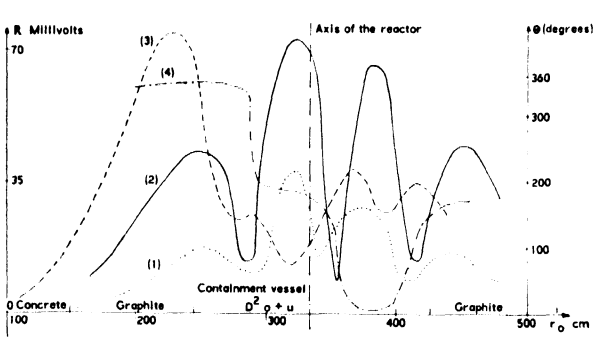

Figure 5. Amplitude variation of resultant R as a function of the mean oscillation position (for $T = 4.5$ sec, power 400 watts); Curve No. 1: $\lambda = \pm 10$ cm; Curve No. 2: $\lambda = \pm 30.5$ cm; Curve No. 3: $\lambda = \pm 70$ cm; Curve No. 4: $\theta = f(r_0)$ for $\lambda = \pm 30.5$ cm; (the origin of the abscissae has been taken at the edge of the reactor protection)

by an angle φ with respect to oscillator motion; $OB = n_0 N l_0$ be the vector which represents the local signal (B is to the right or left of O, according to whether the phase of the local signal is O or M); and OR be the resultant of the two vectors.

Since each vector is proportional to reactor power and the apparent density of the graphite, the power and density variations will distort the diagram homothetically.

When the over-all signal OA and resultant signal OR are both known, the resolution of triangle OAR will make it possible to determine the amplitude and phase of local signal OB. Figure 7 shows the amplitude and phase of the local signal as a function of r_0 for $T = 4.5$ seconds and $\lambda = \pm 10$ cm; ± 30.5; ± 70.5 cm.

No theory has been developed to account for the nature of these curves. It will be understood, however, that when the oscillator is far from the chamber, the neutrons that normally would have leaked out will be scattered by the oscillator, that a certain number of them will reach the chamber, and that the current produced by that chamber will increase. When the oscillator is placed close to a vertical plane which passes through the axis of the chamber, the neutrons which normally would have been captured

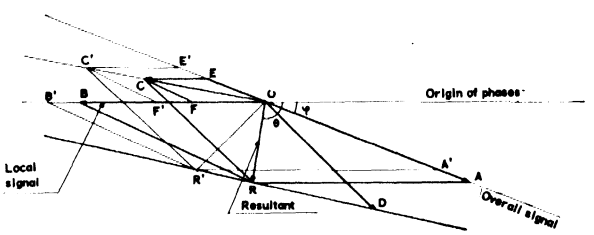

Figure 6

by the chamber are either captured or scattered by the oscillator, so that they no longer reach the chamber, and the current it produces decreases. An increase in the capture cross section of the oscillator increases the number of neutrons captured by the oscillator to the detriment of those that would be captured by the chamber, and causes the current developed to decrease still further. It will be noted that the local signal will practically zero when the oscillator moves in one or the other way from a point close to the axis of the chamber.†

The curves are not perfectly symmetrical, for the ionization chamber is not located in a plane of symmetry of the reactor block.

Study of the Variation of Angle θ as a Function of the Capture Cross Section of the Oscillator

When the capture cross section of the oscillator varies but slightly, it will be possible to write: Δk and l in the following forms:

† Actually, it is only the fundamental of the signal which is blotted out, but harmonic 2, conversely, is very much in evidence.

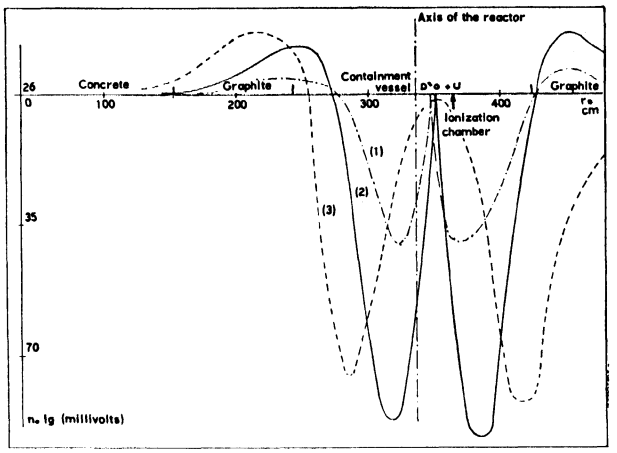

Figure 7. Variation of local signal amplitude as a function of r_0 (for $T = 4.5$ sec, power 400 watts); Curve No. 1: $\lambda = \pm 10$ cm; Curve No. 2: $\lambda = \pm 30.5$ cm; Curve No. 3: $\lambda = \pm 70$ cm; (Phase α of this signal is equal to 0 when the signal is located above the axis of the abscissae, equal to II when it is located below this axis)

$$\Delta k = \Delta k_{\epsilon=0} + \epsilon p \qquad (7)$$

$$l = l_{\epsilon=0} + \epsilon t \qquad (8)$$

where $\partial \epsilon = \Sigma_a' - \Sigma_a$, $p = \partial \Delta k / \partial \Sigma_a$, $t = \partial l / \partial \Sigma_a$, $\Delta k_{\epsilon=0} = \Delta k_g$, and $l_{\epsilon=0} = l_g$.

If Δk and l are so written out in Equation 5, the resultant R becomes

$$R^2 = n_0^2 \times [A^2 (\Delta k_g + \epsilon p)^2 + (l_g + \epsilon t)^2 + 2A (\Delta k_g + \epsilon p)(l_g + \epsilon t) \cos (\alpha - \varphi)] \qquad (9)$$

The curve $R = f(\epsilon)$ is a hyperbola. This is clearly shown on the vectorial diagram (Fig. 6); as capture increases, A will move to A', B to B' and R to R'. When capture by the oscillator varies, point R will move along straight line RR'. The amplitude of the vector OR' then will vary hyperbolically as a function of the abscissa of point R'. Figure 8 shows the variation of the amplitude of the resultant R as a function of the number of milligrams of boron added to the oscillator. This function takes on a different look according to parameters r_0, λ and T. It may happen that the hyperbola actually transforms itself into two straight lines, as shown on Fig. 9. For a capture variation ϵ, the variation in angle θ will be maximal for OR perpendicular to RR' (see Fig. 6). In this case

$$R^2 = n_0^2 \times \{[A^2 \Delta k_g^2 + l_g^2 + 2A \Delta k_g l_g \cos (\alpha - \varphi)] + \epsilon^2 [A^2 p^2 + t^2 + 2Apt \cos (\alpha - \varphi)]\} \qquad (10)$$

and

$$\tan \Delta\theta = \epsilon \left[\frac{A^2 p^2 + t^2 + 2Apt \cos (\alpha - \varphi)}{A^2 \Delta k_g^2 + l_g^2 + 2A \Delta k_g l_g \cos (\alpha - \varphi)}\right]^{1/2} \qquad (11)$$

The fact that the mathematical expressions for Δk and l as functions of r_0 and λ are unknown makes it difficult to determine the optimal measuring conditions, but it can be noted that the curve $\varphi = f(T)$‡ (curve 10) has a minimum at $T = 4.5$ seconds, and $\varphi = 22$ degrees; $\cos (\pi - \varphi)$ then is equal to -0.924.

It can then be seen that Equation 11 is close to its maximum when $\Delta k_g = l_g$ and $Ap = -t$. The angle θ is then equal to $-(\pi + \varphi)/2 = -101$ degrees.

‡ This curve was plotted from experimental results on the one hand, and from computation on the other, by taking for τ, βi and λi the values chosen by H. J. Lipkin.

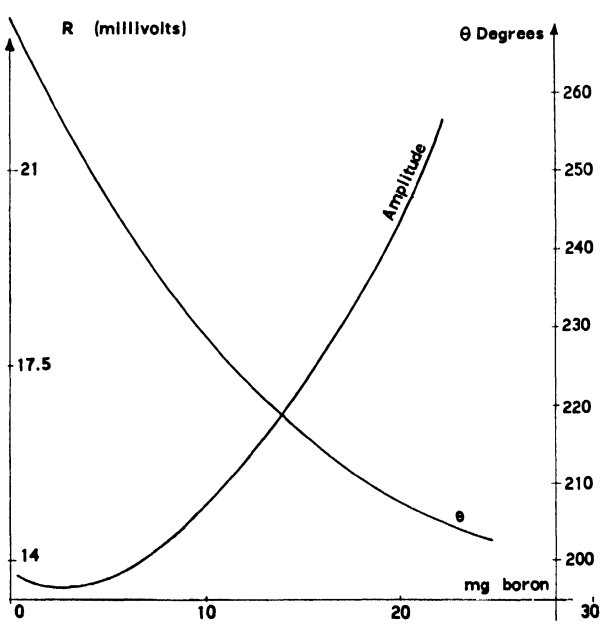

Figure 8. Variation of amplitude R and phase Θ of the resultant signal as a function of oscillator capture (for $\lambda = \pm 30.5$ cm; $r_0 = 289$ cm; $T = 4.5$ sec, reactor power 400 watts)

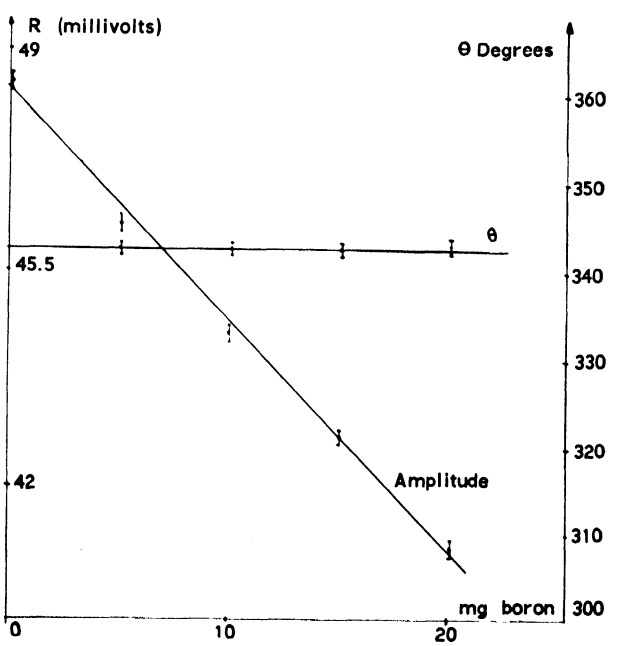

Figure 9. Variation of amplitude R and Θ of the resultant signal as a function of oscillator capture (for $\lambda = \pm 30.5$ cm; $r_0 = 240$ cm; $T = 4.5$ sec, power 400 watts

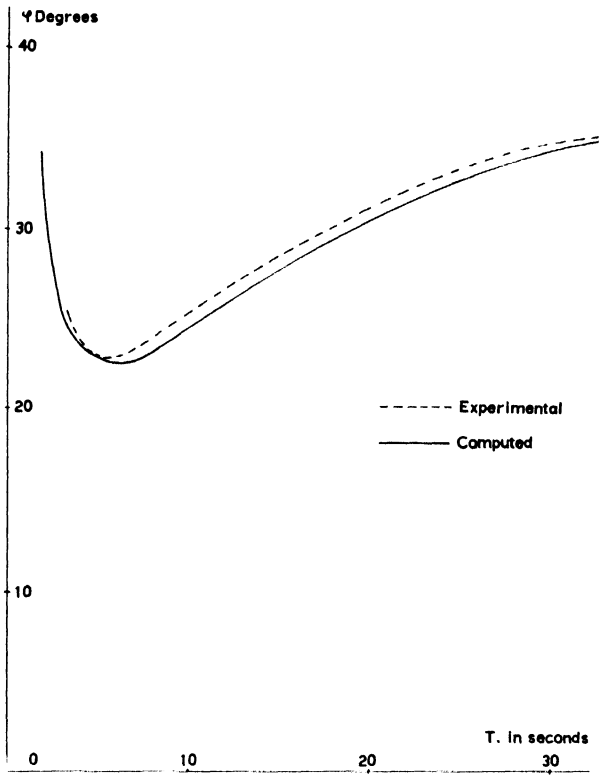

Figure 10. Phase shift of the over-all signal as a function of the frequency

Practically the optimal conditions are sought by setting an oscillation frequency of $T = 4.5$ seconds, an amplitude of $\lambda = \pm 30.5$ cm, and by moving the mean oscillation position r_0 until angle θ is close to -101 degrees. The curves of Fig. 5 show that there exist, in the channel, two positions for which the local and over-all signals are equal. One of them corresponds to $\theta = -101$ degrees, the other to $\theta = +79$ degrees; $(\pi - \varphi)/2$. For reasons of design the position was chosen nearest to the mechanical device which drives the oscillator, which is to say $r_0 = 289$ cm and $\theta = -101$ degrees. Under these conditions, Equation 11 can be written:

$$\tan \Delta\theta = \frac{\epsilon p\,(1 + \cos\varphi)^{1/2}}{\Delta k_g\,(1 - \cos\varphi)^{1/2}} \qquad (12)$$

or, since $\Delta\theta$ is small

$$\Delta\theta = \frac{\epsilon p\,(1 + \cos\varphi)^{1/2}}{\Delta k_g\,(1 - \cos\varphi)^{1/2}} \qquad (13)$$

Figure 8 shows that this actually is a linear function as long as the quantity of boron added does not exceed 10 mg.

Figure 2 shows the value of the over-all signal $n_0 A \Delta k_g$ for 0 and 3 mg, for $\lambda = \pm 30.5$ cm, $r_0 = 289$, and $T = 4.5$ seconds; the difference between these two values is equal to $n_0 A \epsilon p$. One will find: $n_0 A \Delta k_g = 29.15$ millivolts for the calibration block + 3 mg of boron, from which: $n_0 A \epsilon p = 1.65$ millivolt for 3 mg of boron. Under these conditions

$$\Delta\theta = \frac{1.65\,(1 + 0.924)^{1/2}}{30.8\,(1 - 0.924)^{1/2}}$$

$= 15$ degrees 3 minutes for 3 mg of boron.

It is found experimentally that adding 3 mg of boron to the calibration oscillator will bring about variation in angle θ, and that the amplitude of resultant R hardly varies at all (Fig. 7).

The vector diagram may be interpreted in the following way: The local and over-all signals each consists of two parts, the one due to scattering, the other due to capture by the oscillator. Let OE and OF be the parts of the over-all and local signals due to capture, and OC their resultant; OD will then be the resultant of the parts due to the scattering, since the amplitude of vector OR will vary but very little when the capture is increased. As a consequence, OR is at right angles to OC.

ELECTRONICS

The instrumentation is of the same type as that of Colmer, Wiblin and Woollen, at Harwell. It was designed and made by Pottier (Electrical Constructions, Saclay). Figure 11 shows a block diagram of the assembly. It consists, in the main, of a battery which cancels out, by opposition, the dc voltage present at the boundaries of the leakage resistance of the chamber, of a dc amplifier with considerable negative feedback, and of a harmonic analogue analyzer. This assembly makes up a highly accurate device, the purpose of which is to measure the amplitude and phase of the fundamental of the signal which is produced by the ionization chamber. This signal contains a great many harmonics, and will be written as follows:

$$\Sigma_n R_n \sin(n\omega t + \theta n)$$

The chamber produces a current proportional to $\Sigma_n R_n \sin(n\omega t + \theta_n)$ which is amplified by a dc amplifier having a gain of 50, and the harmonic analogue analyzer will carry out the following two mathematical operations:

$$\int_0^{\frac{2\pi k}{T}} \Sigma_n R_n \sin(n\omega t + \theta_n) \sin\omega t\, dt = \frac{kT}{2} R \cos\theta \qquad (14)$$

$$\int_0^{\frac{2\pi k}{T}} \Sigma_n R_n \sin(n\omega t + \theta_n) \cos\omega t\, dt = \frac{kT}{2} R \sin\theta \qquad (15)$$

The ratio between the values given by these two expressions will make it possible to compute angle θ. The square root of the sum of the squares is proportional to the amplitude of the fundamental given by the chamber.

When the reactor is not very well stabilized, the direct component of the current produced by the chamber is not completely zeroed; there will remain a small voltage which varies as a function of time, so that this current will then be equal to $\Sigma_n R_n \sin(n\omega t + \theta_n) + f(t)$. The result of the integration

carried out by this device will then depend on function $f(t)$. The only possible way in which this difficulty can be disposed of consists of stabilizing the reactor as well as possible, so that $f(t)$ be very low. A systematic study of this question has been made by Colmer and others. When the method is used for checking graphite samples, the direct voltage measured at the boundary of the leakage resistance of the chamber ($10^7\Omega$) amounts to 20 volts, and the amplitude of the signal amounts to $\pm 1 \times 10^{-2}$ volt.

Suitable devices and instruments also are provided for the automatic starting and stopping of the integrators. The signal produced by the chamber suffers many fluctuations, and it is indicated to integrate over a sufficiently long time in order to cancel them out to the furthest possible extent. In practice, one measurement is the result of 16 successive integrations ($k = 16$) and will therefore take about 80 seconds. This time will be considerably increased as a consequence of the need for stabilization of the reactor following introduction of an oscillator.

APPLICATION OF THIS METHOD TO THE COMPARISON OF THE CAPTURES BY TWO GRAPHITE SAMPLES

A mean position r_0, an amplitude λ and an oscillation period T shall be set, as explained above.

The standard or calibrating sample will first be oscillated alone, then with even larger amounts of boron. A curve then is plotted, which shows the value of the angle as a function of the number of milligrams of boron added to the calibrating sample. This is a linear curve, and it constitutes the calibration curve (Fig. 8). The calibration sample then is replaced by the graphite sample to be studied, and the value of θ is measured; by marking this value on the calibration curve, the capture difference between the two samples expressed in mg of boron can be derived.

The power level of the reactor, during these measurements, is 400 watts. It was chosen so as not to subject the experimenters to substantial doses of radiation at the time of the extraction of the sample. Moreover, it corresponds to the thermal equilibrium of the reactor when its cooling systems (D_2O pumps, blowers) are not in motion.

Precautions to Be Taken

All samples must be cut to the same measurements. Their width and height must be accurate within 0.2 mm; however, the length is less important, and any variation of less that 1 cm has practically no effect on the value of θ.

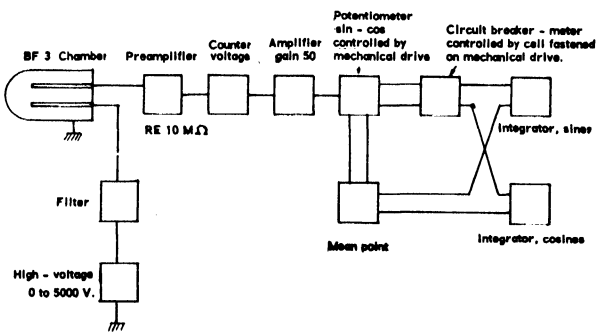

Figure 11. Block diagram

The power level of the reactor must be kept constant, within an accuracy of some 10^{-3}, while the measurements are being made. After the reactor has been working at 100 kw for 36 hours, it will be necessary to wait for six hours before measurements can be taken. It is essential that the temperature of the heavy water and of the uranium should remain constant, so as to avoid a slow power drift. Although angle θ is independent of the reactor's working power, it will nevertheless be necessary to stabilize the reactor well for the result of the measurements to be correct. However, the independence of θ as a function of the power is very useful in practice, since it will not be necessary, between two consecutive measurements, to stabilize the reactor at the same power, which often is a great advantage. A voltmeter allows for constant observation of the power variations of the reactor. Measuring will be started only when the reactor drift is very small.

The local and over-all signals depend on the distribution of the neutrons in the channel used for the oscillation. Use of the plates farthest from the channel for regulation is indicated. Their position should not be altered in the course of a measurement. The reactor is stabilized between two measurements.

Accuracy

When operating under favorable conditions of reactor power stability, it will be possible to determine the capture of a graphite sample with respect to the calibrating or standard sample with an accuracy of 0.03 mb. The accuracy is limited by the slow power drift of the reactor, and by the fluctuations of this power. Nevertheless, angle θ will suffer far smaller fluctuations than the amplitude of the resultant signal: the power fluctuations of the reactor will homothetically distort the diagram on Fig. 6, and the value of angle θ will not be altered. The values of θ and of R were measured 12 times consecutively, each measurement being the result of 16 successive integrations. The standard difference of R is equal to 0.0245 millivolt ($R = 1.28$ millivolt), whereas that of θ is 0 degrees, 4 minutes ($\theta = 269$ degrees, 16 minutes).

Since the reference standard is boron, it will be necessary to effect a correction when the impurities contained in the graphite do not follow a "$1/v$" law.

APPLICATION OF THE METHOD TO NUCLEAR PURITY CONTROL OF MATERIALS OTHER THAN CARBON

This method was used for the purpose of making comparisons between the captures by two lots of Be, as well as those of two lots of beryllium oxide. Use was made of a graphite block of the same dimensions as the standard one, provided with a recess in which the substance to be examined was placed. It is likewise possible to compare the captures of two lots of 180 gm of Be with an accuracy of $\pm$ 0.3 mm^2,

and of two lots of BeO weighing 1100 gm, with an accuracy of $\pm$ 0.4 mm^2.

Measurement of the Capture Cross Sections of Magnesium and Aluminum

The local and over-all signals both consist of two components, one due to capture, the other to scattering. Because of the device used, the scattering components are far more conspicuous than those due to capture. When a small quantity of a substance having a cross section which is not too large as compared to its capture cross section is added to the oscillating graphite sample, the local and over-all scattering signals will be subject to comparatively small variations, while those due to capture will be greatly altered (on the diagram, vector OD varies little, whereas OC varies far more). The variation of angle θ may then be ascribed, without any great error, to that of the capture cross section. By operating with a magnesium sample weighing 75 gm, it was found that its capture cross section was equal to 60 $\pm$ 3 mb.

CONCLUSIONS

This method has the advantage of allowing comparison of capture by two samples of highly scattering and sparsely capturing elements such as graphite, beryllium, and beryllium oxide, with a good accuracy and without any need for oscillating substantial amounts of these bodies. The method is a sufficiently rapid one, since the oscillation frequency is 4.5 seconds, and it is convenient, because it will not be necessary for the reactor power to be identical as one moves on from one measurement to the next. Finally, the method also allows for the determination of the effective capture cross section of elements such as magnesium or aluminum.

ACKNOWLEDGEMENTS

We wish to thank Professor J. Yvon, Head of the Department of Reactor Development, for the valuable advice that he gave us in the course of this work.

REFERENCES

1. Hoover, J. *et al., Measurement of neutron absorption cross section with a pile oscillator,* Physical Review, *74,* 8, 864-870 (1948).

2. Pomerance, H., *Thermal neutron capture cross sections,* Physical Review, *83,* 3, 641-645 (1951).

3. Pomerance, H., *Thermal neutron capture cross sections,* Physical Review, *88,* 2, 412-413 (1952).

4. Langsdorf, A., *Oscillatory method for measuring neutron cross sections by the effect on the reactivity of a chain reacting pile,* Physical Review, *74,* 1216-1217 (1948).

5. Weinberg, A. M. and Schweinler, H. C., *Theory of oscillating absorber in a chain reactor,* Physical Review, *74,* 8, 851-863 (1948) and A.E.C.D. 2044.

6. Littler, D. J., *The measurement of slow neutron absorption cross sections,* Atomics, *1, 7,* 189-195 (1950).

7. Colmer, F. C. W., Wiblin, E. R. and Woollen, W. B., *Fission balance tests in Gleep.* A.E.R.E. N/R 1163.

8. Colmer, F. C. W. and Littler, D. J., *Pile neutron absorption cross sections of some of the elements* (Letter), Proceedings of the Physical Society (G.B.) *63,* part 10, 370 A, 1175-1176 (1950).

9. Raievski, V. and Yvon, J., *La modulation du flux de neutrons dans le réflecteur d'une pile sous l'effet de l'absorption et de la diffusion,* Comptes rendus de l'Académie des Sciences (Fr) 231, 345-347 (1950).

10. Ertaud, A., Raievski, V. and Breton, D., *Méthode d'oscillation dans la pile appliquée à la comparaison d'échantillons de graphite,* Journal de Physique et le Radium, *12,* 784-788 (1951).

11. Lipkin, H. J., *Liaison de la réactivité de la pile Zoé modifiée avec la constante de temps d'une montée en puissance,* Note C.E.A. no. 49.

12. Pottier, J., *Un analyseur harmonique analogique,* Onde électrique (to be published in the autumn of 1955).

13. Brownrigg, W. G. L. and Littler, D. J., *Pile modulation and statistical fluctuations in Piles, A.E.R.E.* N/R. 476 (1950).

A Neutron Spectrometer Based on Measuring the Slowing-Down Time of Neutrons in Lead

By A. A. Bergman, A. I. Isacoff, I. D. Murin, F. L. Shapiro, I. V. Shtranikh, and M. V. Cazarnovsky, USSR

Neutrons slowed down by elastic collisions in a medium of mass number $M \gg 1$ gather into a comparatively narrow velocity group, which gradually shifts towards smaller values of velocity with increasing slowing-down time.

This fact was first noted by Feinberg in 1944; Lazareva and Feinberg[1] pointed out that it could be utilized in neutron spectrometry. Suppose that fast neutron bursts of short duration are periodically produced in a slowing-down medium; if a neutron detector is operated over a short time Δt delayed with respect to the burst by an interval t, then approximately monoenergetic neutrons will be selected, their energy being determined by the slowing-down time t.

An analysis by one author[2] showed that compared with the widely applied time-of-flight method, the sdt spectrometry method has two advantages:

1. A gain in intensity by 3–4 orders of magnitude can be obtained. Thus, a spectrometer can be constructed by using a comparatively simple neutron source, such as a low-voltage accelerator producing neutrons by the *d-t* reaction.

2. Neutron capture cross sections can be conveniently measured, while up to recent times only total cross-section measurements were carried out by the time-of-flight method.

The resolving power of the slowing-down-time (sdt) method in general is about 30% and does not strongly depend on the neutron energy. In spite of its limited resolving power the sdt method, by virtue of the above-mentioned merits, may be a valuable tool for investigation of the processes of radiative capture and of particle emission in the interval of neutron energies between 1 ev and ~ 10 kev.

The main features of the sdt method of neutron spectrometry are reviewed in the present paper and some results of its experimental investigation are likewise presented.*

PRINCIPAL FEATURES OF SLOWING-DOWN-TIME SPECTROMETRY

Slowing-Down Time

It can be shown that the mean velocity v of a neutron slowed down by elastic collisions with free nuclei in a homogeneous heavy medium is related to the slowing-down time by the formula

$$t = M\lambda \left(\frac{1}{v} - \frac{1}{v_0}\right) \tag{1}$$

where v_0 is the initial neutron velocity, M is the mass number of the moderator, and λ is the scattering mean free path (which is assumed to be independent of the neutron energy).

If the initial velocity is high, i.e., $v_0 \gg v$, the slowing-down time will practically be independent of the initial neutron velocity and will equal

$$t = \frac{M\lambda}{v} \tag{2}$$

According to Equation 2, the time required for neutrons to slow down to a velocity v is equal to the time it would take for a neutron of this velocity to traverse a certain distance $L = M\lambda$, which we shall call the effective flight path.

For lead $M = 207$, $\lambda = 2.9$ cm, $L = 6$ m. Thus, if a lead moderator is used the effective flight path is of the same order of magnitude as that encountered in the usual time-of-flight spectrometers in which this distance varies between 6 and 20 m.

Resolving Power

The resolving power of sdt spectrometers is determined by the neutron velocity spread about the mean value at the given moment. For $\bar{v} \ll v_0$ and $\lambda =$ constant, the velocity dispersion is (see Appendix and reference 3):

$$D = \frac{\overline{\Delta v^2}}{v^2} = \frac{2}{3M} + \frac{kT}{4E} \tag{3}$$

where $E = \frac{1}{2} mv^2$ is the mean neutron energy and T is the absolute temperature of the moderator. The first term in Equation 3 is principally due to fluctuations of the neutron path between two collisions and, to a smaller degree, to the statistical character of the energy losses in the scattering collisions. The second term accounts for the additional spread of the scattering energy loss which is due to the thermal motion of the atoms of the moderator.† At room temperature and $E > 3$ ev one has for lead

Original language: Russian.

* I. M. Frank continuously assisted us during the course of this work. At one of the stages of this investigation we were helped by A. V. Antonov.

† It is assumed in Equation 3 that $T \gg \theta$, where θ is the Debye temperature of the moderator.

$$\frac{\sqrt{\overline{\Delta v^2}}}{v} \cong 5.7\left(1+\frac{1}{E_{ev}}\right)\% \qquad (4)$$

The energy spread $\Delta E/E$ is twice as large. The neutron velocity distribution function has been calculated for heavy moderators by Kazarnovsky (see Appendix). For all practical purposes this distribution can be approximated by a Gaussian curve with a dispersion corresponding to $\sqrt{\overline{\Delta v^2}}$ as given by Equation 3. If the half-width of the curve be accepted as a measure of the spectrometer resolving power, then the theoretical value for the energy resolution will be

$$\frac{\delta E}{E} = 26\left(1+\frac{1}{E_{ev}}\right)\% \qquad (5)$$

For energies up to 1 kev the resolution of the time-of-flight method is better. However, on the one hand, capture cross-section measurements carried out even with a resolution of about 30% are undoubtedly useful, while on the other hand, there remains some possibility of improving the resolving power of the sdt spectrometers. One possible way of increasing the resolving power is to investigate the influence of resonance absorbers on the magnitude and form of the peaks in a resonance detector.

To illustrate this point we consider the following simple example. Suppose that the substance under investigation has two close resonance energy levels E_1 and E_2 ($E_1 > E_2$). A sample of the substance is placed at a distance r from the detector recording the neutron capture γ-rays produced in a second sample of the same substance. The first sample will absorb neutrons of energy E_1, thus reducing the density of neutrons of energy E_2 near the detector. Obviously the difference of the counting rates with and without the first sample depends on the distance r in the following manner

$$\Delta I \sim e^{-r^2/4\tau} \qquad (6)$$

where‡

$$\tau = \frac{M\lambda^2}{6}\ln\frac{E_1}{E_2} \qquad (7)$$

The difference between the levels E_1 and E_2 (even if it is much smaller than the width of the resolution curve) can be determined from the plot $\ln \Delta I = f(r^2)$. An analysis of this type should be possible at high neutron intensities.

In principle, methods in which use is made of the influence of resonance absorbers on the resonance detectors should yield a resolution of the order of the mean energy loss in a single collision, i.e., about 1% with respect to energy. Detailed investigation of these methods has not been carried out as yet, but it seems reasonable to assume that in certain cases their application may be profitable.

‡ In lead $M \gg 1$ and therefore the average logarithmic energy loss is assumed equal to $\xi = 2/M$.

Energy Limitations

Thermal motion of the moderator nuclei determines the lower energy limit of the sdt spectrometer; according to Equation 5 this energy is ~ 1 ev.

The upper energy limit of the sdt spectrometer is determined by the primary neutron spectrum and by the properties of the moderator. If the primary neutrons are mono-energetic and possess an energy E_0 which is less than the energy E_1 of the first excited state of the moderator nuclei, then spectrometry measurements will be possible up to the energy E_0. Moreover, as the energy is lowered the spectrum gradually widens out and (for λ = constant) it tends to the asymptotic width according to the equation (see Appendix and reference 3):

$$D = \frac{2}{3M}\left(1-\frac{E}{E_0}\right) \qquad (8)$$

If the initial neutron energy exceeds that of the first level, then, due to inelastic collisions, the neutrons will rapidly fill up the energy region between 0 and E_1; further slowing down will be caused by elastic collisions and will therefore be a slow process. As can be seen from Equation 1 the width of the energy distribution will also slowly decrease. This narrowing of the spectrum is due to a peculiar type of "focusing",[3] the essence of which is that for any given time interval fast neutrons travel over larger distances, that is, they experience more collisions, and are slowed down to a larger extent than slow neutrons. Unfortunately, this focusing property is comparatively weak and the asymptotic width[3] is reached only at small energies E, for which $E \ll E_1$.

With slowing down of the neutrons the dispersion of the velocity distribution tends to Equation 3 according to the law (for λ = constant)[3,4]

$$D = \frac{2}{3M}\left(1-\frac{E}{E_0}\right) + D_0\frac{E}{E_0} \qquad (9)$$

where D_0 and E_0 are the dispersion and mean energy of the "initial" neutron spectrum, that is, of the spectrum at the moment that slowing down by inelastic collisions ceases (it is assumed that the time of formation of this spectrum can be neglected).§

In lead[4] $E_1 = 0.57$ Mev and E_0 is of the order of 100 kev. No data on the dispersion of the "initial" distribution are available; it can be assumed that as to order of magnitude $D_0 \sim 0.3$. These estimates show that for $E = 1$ kev the spectrum width is larger by 40% than the asymptotic value; at $E = 10$ kev the spectrum becomes broader by more than three times. Thus the upper energy limit of the sdt spectrometer lies in the vicinity of 10 kev.

A possible way of studying the interesting energy region E 10 kev is to use some threshold reaction, e.g., $Li^7(p,n)$, $V(p,n)$, to obtain neutrons with a smaller energy than that of inelastically scattered neutrons.

§ To be more precise here $D_0 = \Delta\bar{x}_0^2/\bar{x}_0^2$, $E_0 = m/2\bar{x}_0^2$, where $x_0 = 1/v_0$ and v_0 is the neutron velocity. Averaging is carried out over the "initial" neutron spectrum.

Methods of Capture Cross-Section Measurements

An essential feature of the sdt method is that the counters can be surrounded on all sides by very thick absorbers, a circumstance that leads to an important feature of the method, namely: it now becomes possible to determine the capture cross section not only by transmission¶ measurements but also by counting capture γ-rays. The advantages of this latter method are as follows:

1. The efficiency of counting absorbed neutrons is independent of the energy; at $E \sim 10$ ev the efficiency is higher than that obtained with boron counters.

2. In the transmission method the unknown cross section is obtained as a small difference between two large quantities I_0 and I: $\delta \sim (I_0 - I)$.

Therefore, if small cross sections are measured, the stability of the recording apparatus must be very high. On the other hand, when capture γ-rays are recorded a quantity proportional to δ is directly measured and therefore, for equal accuracy of results, the stability requirements may be much lower. The small γ-ray background in the sdt spectrometer permits these advantages to be realized in a very simple manner, whereas in other types of spectrometers this cannot be accomplished because of the high γ-ray background. The fact that capture γ-ray counting has found application in the time-of-flight method[5] only in recent years can be explained by experimental difficulties due to the presence of a high γ-ray background.

Another possible way of investigating neutron capture by the sdt method is to study the influence on the neutron intensity of samples introduced into the moderator. If a sufficient amount of substance is available, total absorption cross sections can be measured in this way; the dependence of the absorption on the sample dimensions can also be investigated, including cases when absorption is small compared to scattering.

Intensity

Due to leakage the neutron density in the moderator decreases with increasing slowing-down-time, i.e., with decreasing neutron energy. According to the age theory, for a sufficiently large age τ, the slowing-down density in a rectangular prism of sides $2a$, $2b$, $2c$ can be expressed by the formula

$$q = \frac{Q}{abc} e^{-\omega\tau - \frac{t}{T}} \cos\frac{\pi x}{2a} \cos\frac{\pi y}{2b} \cos\frac{\pi z}{2c} \quad (10)$$

where

$$\omega = \frac{\pi^2}{4}\left(\frac{1}{a^2} + \frac{1}{b^2} + \frac{1}{c^2}\right)$$

and T is the mean neutron capture life in the moderator (it is assumed that T = constant, that is, the capture process follows the $1/V$ law), Q is the number of neutrons emitted per second, and τ is the age of a neutron of energy E:

$$\tau = \int_E^{E_0} \frac{M\lambda^2}{6} \frac{dE}{E} \quad (11)$$

Using Equation 1 it is easy to find the relation between τ and the slowing-down time t (for λ = constant):

$$\tau = \frac{M\lambda^2}{3} \ln\left(1 + \frac{t}{t_0}\right)$$

$$t_0 = \frac{M\lambda}{v_0} \quad (12)$$

Combining Equations 10 and 12 we find the following dependence of the slowing-down density on the slowing-down-time:

$$q \sim \left(\frac{t}{t_0} + 1\right)^{-\frac{M\lambda^2}{3}\omega} e^{-\frac{t}{T}} \cong \text{const}\ t^{-\alpha} e^{-\frac{t}{T}}$$

$$\alpha = \frac{M\lambda^2\omega}{3} \quad (13)$$

The number of neutrons recorded per unit time by a counter of efficiency $\sim 1/v$ is

$$I = qV\frac{\Delta t}{\theta} \quad (14)$$

where V is the counter volume, θ is the mean neutron lifetime in the counter gas, and Δt is the width of the recording channel.

In lead the mean neutron lifetime $T = 900$ μsec, while the time required for a neutron to be slowed down to an energy of 1 ev is $t \cong 400$ μsec.

Thus, in Equation 13 the first factor is of decisive importance. For a lead cube of 1.2 m side, $\alpha = 1$ and the slowing-down density is inversely proportional to the time; in this case the neutron flux is inversely proportional to the square of the time, i.e., it is proportional to the energy.

Thus the gain in intensity which the sdt spectrometry method offers increases with the measured energy.

EXPERIMENTAL ARRANGEMENT

Lead was chosen as the working medium for the sdt spectrometer; it is the easiest available of heavy elements and possesses a comparatively small neutron capture cross section. The first measurements were carried out with 1.3 × 1.3 × 1.3 m and 1.3 × 1.3 × 2 m stacks. Later on a block of dimensions 2 × 2 × 2.3 m (~ 110 tons of lead) was used. A sketch of the experimental arrangement is shown in Fig. 1. The neutron source was a zirconium-tritium target placed in the center of the lead block; the target was bombarded by a deutron beam accelerated up to 300 kv in an ion-accelerating tube of the usual type. The ion source (Penning type) was fed by voltage pulses

¶ If the measurements are carried out inside the moderator, transmission of the sample will depend on the capture cross section but not on the scattering cross section (in thin samples).

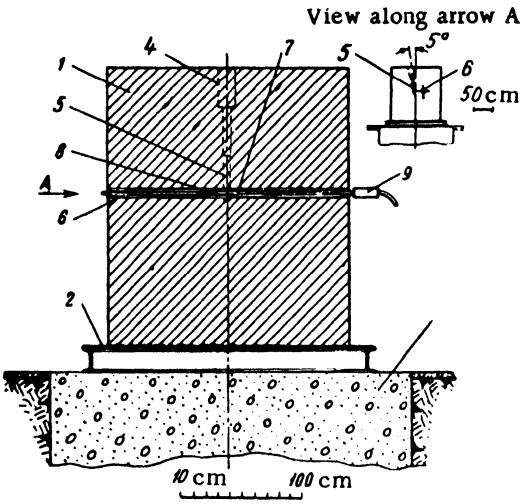

Figure 1. Sketch of experimental arrangement: (1) lead column; (2) steel frame; (3) concrete foundation; (4) channel for target tube; (5) target; (6) channel for counter and sample; (7) counter; (8) sample; and (9) preamplifier

of 1–3 μsec duration, the repetition frequency being 50–1250 cycles/sec. The duration of the ion pulse depended only weakly on the duration of the voltage pulse and was about 6 μsec. For further shortening of the neutron burst the deutron beam was deflected in an electric field between two plates mounted in the target assembly (Fig. 2) and fed by voltage pulses of short duration. This "electric shutter" reduced the duration of the beam striking the target to a value of 0.5 to 2 μsec. The current pulse in the ion source was about 10–20 amp; at currents of this magnitude the yield of atomic ions D^+ was as large as 85%. The pulse ion current incident on the target (diameter, 14 mm) was 3 ma, this corresponding to a neutron flux of $\sim 3 \times 10^{11}$ n/sec. The neutron yield was measured with proportional counters, which recorded the α-particles from the *d, t* reaction.

Neutrons slowed down in the lead were measured with proportional counters filled with BF_3 (natural boron), at a pressure of 60 cm Hg and also by ionization chambers coated with thin LiF or B_2O_3 layers and filled with argon. A glass-wall proportional counter of 3 cm diameter and $l = 11.5$ cm filled with a mixture of argon and isopentane at a pressure of 30 Hg was used to measure the neutron capture γ-rays. In most of the measurements the counters were arranged in a canal 55 mm in diameter cut out in the lead.

After amplification of the counter pulses their time delay (with respect to the neutron burst) was measured by means of a 50-channel analyzer[6] with a channel width of 2 μsec. An electronic memory device,[6] containing a common oscilloscope tube was incorporated in the analyzer and used to vary the channel width over a wide range. This device operated as follows. The electron beam, which is swept linearly, is suppressed until a pulse from the counter arrives; for each pulse arrival the beam opens and leaves a charged spot on the oscilloscope screen. After the first sweep, a second, scanning sweep follows. Its duration is 100 μsec and its trace on the screen is superimposed upon the recording trace. The electron ray is on during scanning and the memory signals are collected on the electrode mounted in front of the screen; the signals are then fed into the main analyzer for time analysis.

The scanning sweep also clears the screen for the next cycle.

By varying the recording sweep speed, any channel width lying between 0.1 and 100 μsec can be obtained.

In the present work the memory device was used for measurements with a channel width of 0.5 μsec. The system also included two additional channels, the width and position of which could be varied from 10 to 10,000 μsec. All time intervals were controlled by a quartz generator of 1 Mc frequency and were defined with high accuracy. At low amplification only large pulses from fast neutrons of 14 Mev energy were counted. These measurements were used to determine the position and width of the neutron burst.

MEASUREMENTS WITH Ag, Zn, Mn, Cd AND Cu

The time dependence of capture γ-rays intensity was measured for the elements listed above. Measurements were alternatively made with long, tube-shaped samples which were slipped over the counter or without these samples. The neutron capture γ-ray

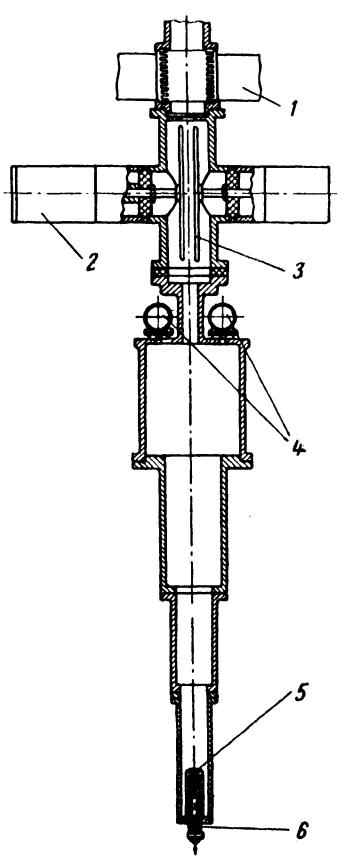

Figure 2. Target tube: (1) magnet for mass separation of ion beam; (2) pulse transformer; (3) deflectors (electric shutter); (4) alpha-counters; (5) target; and (6) target heater

intensity was assumed to be proportional to the difference of the counting rates obtained with and without the sample. This is not strictly true because the sample changes the background due to a (*a*) absorption in the sample of some of the γ-rays from the lead and (*b*) activation of the sample as a result of neutron capture (this gives an increase in the background). In the present measurements, however, the effect was usually much greater than the background and the samples were thin. Thus the first source of background variation could be neglected. Activation of the sample, and of the material of the counter and lead, and also the presence of a small number of thermal neutrons which remained from the preceding cycle all produced a weak background which slowly decreased over about 100 μsec. This background component was assumed to stay at the counting rate at the end of the operation cycle, i.e., directly before the burst. It was measured by means of an auxiliary channel which, for the usual cycle duration of 1600 μsec, recorded pulses arriving between 1500 and 1600 μsec after the burst.

The γ-ray intensity curve for Ag obtained with an Ag sample 0.1 mm thick in a stack of 130 × 130 × 200 cm is shown in Fig. 3.

The γ-ray intensity is very high at small slowing-down times; however, this does not at all mean an increase of the capture cross section but merely that the neutron flux is higher for small slowing-down-times.

The flux was determined from the boron counter measurements; in a wide energy range the counter efficiency is proportional to $1/v$ or, according to Equation 2, to time t.

The boron counting rate is then

$$I_B = C_1 F(t) t \qquad (15)$$

where $F(t)$ is the neutron flux, and C_1 a constant.

The γ-ray counting rate is given by

$$I_\gamma = C_2 F(t) \sigma_\gamma(t) \qquad (16)$$

where $\sigma_\gamma(t)$ is the capture cross section averaged over the neutron spectrum in the moderator at time t; C_2 is a constant.

Comparing Equations 15 and 16:

$$\sigma_\gamma = \frac{C_2}{C_1} \frac{I_\gamma}{I_B} t \qquad (17)$$

To find the absolute value of the capture cross section the coefficient C_2/C_1 must be known. This can be done, for example, by measuring the values of I_γ/I_B in the thermal energy range inasmuch as the thermal neutron capture cross section are known with high accuracy.**

** The efficiency of γ-counters with a thick cathode made of light materials is approximately proportional to the γ-photon energy; the efficiency of capture γ-ray counting is therefore proportional to the neutron binding energy and for any possible variation of the γ-spectrum from level to level of a given isotope it will only slightly change.

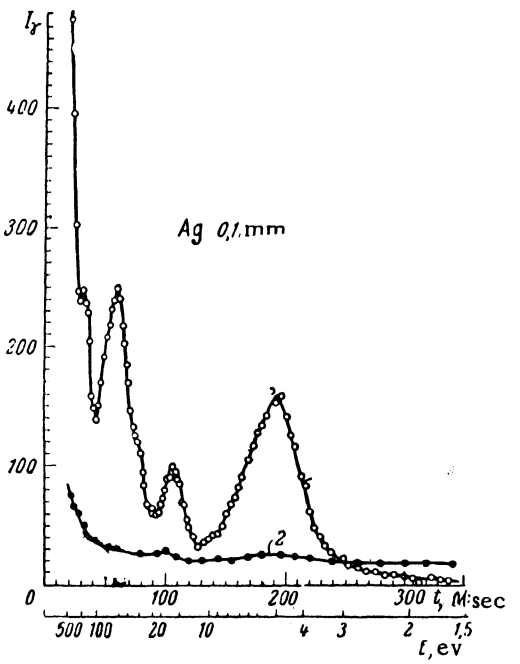

Figure 3. Capture gamma-ray intensity curve obtained from Ag sample 0.1 mm thick: block dimensions 1.3 × 1.3 × 2 m³; (1) effect; and (2) background

In the present investigation; however, we did not attempt to carry out absolute measurements of the cross sections and the work was confined to relative measurements of the energy dependence of the cross section, i.e., to measurements of $(I_\gamma/I_B)t$. It should be noted that Equation 17 is strictly valid only for thin samples; in the general case $(I_\gamma/I_B)t$ is not proportional to the cross section but to the probability of absorption of neutrons in the sample.

Most of our measurements performed up to the present apply to the energy region around 1000 ev and only a few measurements to the region $E \sim 5$ kev. Naturally, it is more difficult to work at $E >$ 1000 ev, i.e., at small slowing-down-times ($t < 14$ μsec) because (*a*) instrumental errors, such as those due to drift of the timing of the neutron burst, become more important and (*b*) the effect-to-background ratio becomes poorer as the effective capture cross section decreases with the energy, whereas at $E >$ 1 kev a large increase of the counter background is observed, the original of which is obscure.

In the following we present some results of measurements obtained for various substances.

Ag

The plot of $(I_\gamma/I_B)t$ for an Ag sample 0.1 mm thick is presented in Fig. 4 (block size 1.3 × 1.2 × 2 m) and in Fig. 5 (2 × 2 × 2.3 m). The energy dependence of the total cross section for silver has been repeatedly measured by the time-of-flight method. In the most recent work[7] the following levels have been mentioned: 5.22 ± 0.04 ev, 16.6 ± 0.15 ev, 31.1 ± 0.4 ev, 40.8 ev, 42.4 ev, etc.

In our measurements, levels 5.22 and 16.6 ev were completely separated. Level 31.1 ev could be

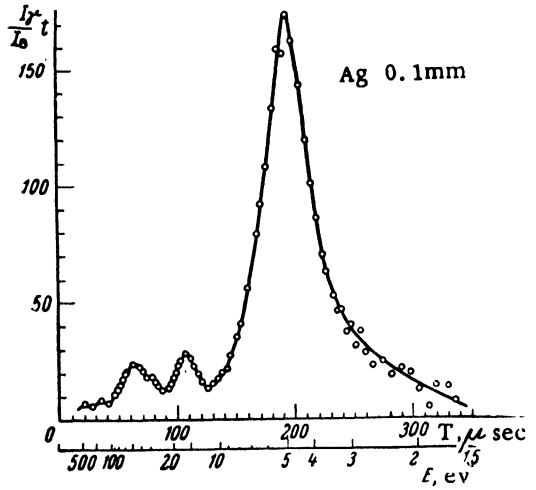

Figure 4. Neutron absorption probability curve for Ag sample 0.1 mm thick (arbitrary units): block dimensions 1.3 × 1.3 × 2 m³

established without doubt: all higher levels could not be separated and the curve peaks in the energy range above 31.1 ev merely reflect fluctuations in density and strength of the levels.

Transmission measurements were also carried out with silver, a boron proportional counter being employed as neutron detector. The sample was an Ag tube of 5.2 cm diameter, $l = 51$ cm and wall thickness 1 mm. The transmission curve for a 1.3 × 1.3 × 1.3 m prism is shown in Fig. 6. Minima of the transmission curve correspond to peaks in the capture cross-section curve (Figs. 4 and 5).

When the measurements are carried out inside the moderator, the apparent transmission (that is, the ratio of the counting rates with and without the sample) is lower than the true transmission because absorption of high energy neutrons by the sample during the preceding time intervals leads to a decrease of the neutron flux incident on the sample at

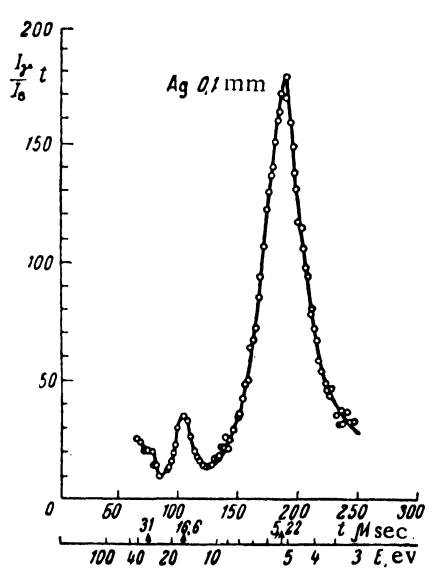

Figure 5. Neutron absorption probability curve for Ag sample 0.1 mm thick: block dimensions 2 × 2 × 2.3 m³

the given moment. This effect, which complicates analysis of the results, increases with increasing number of neutrons captured by the sample; it was already appreciable in experiments with samples 1 mm thick. Experiments with smaller samples of 0.1 mm thickness were therefore carried out. The area of the dip in the transmission curve at $E = 5.22$ ev satisfactorily agrees with the value expected from the level strength $\sigma_0\Gamma^2 = 377 \pm 25$ barns (ev)² found in reference 7.

Zn

According to the latest data[8] zinc possesses the following energy levels in the region $E < 10$ kev: 225, 455, 530, 1620, 2300, 2750 and 4600 ev. Zinc samples of 0.25 mm and 1 mm thickness were investigated in a lead block of 2 × 2 × 2.3 m dimensions. Three peaks were found, one of which corresponds to the 225 ev level, the second to two unresolved

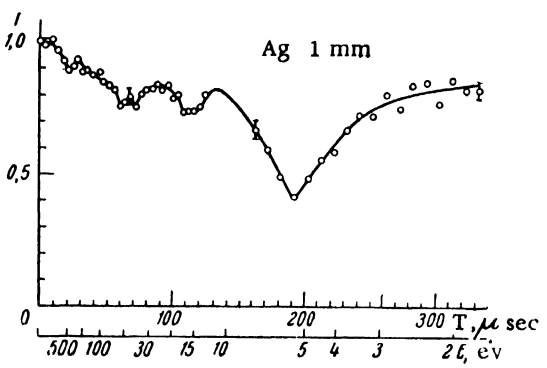

Figure 6. Transmission curve for Ag sample 1 mm thick: block dimensions 1.3 × 1.3 × 1.3 m³

levels 455 ev and 530 ev and the third to unresolved levels of $E > 1$ kev (Fig. 7). Under the conditions of the experiment (channel width 2 μsec and burst duration 2 μsec) these last levels could not be resolved. Measurements were not carried out under more suitable conditions.

Mn

The thickness of the MnO_2 sample was 0.14 gm/cm² of manganese. Besides the well-known first level of manganese[7] at $E = 346 \pm 11$ ev, a second level of $E = 1100$ ev discovered only recently[7,9] was also observed.

Cd

In preliminary experiments with a cadmium sample of 0.5 mm thickness two levels were found; the positions of these levels correspond to the two strongest of the cadmium levels (88.2 ev and 27.2 ev) mentioned in reference 10.

Cu

Copper levels at 2.5, 6 and 8 kev were reported in reference 11 in which monoenergetic neutrons from the $Li^7(p,n)$ reaction were used. Some ill-defined humps at $E < 10$ kev can be noticed in the copper cross-section curve obtained by the time-of-flight

method;[12] in particular there is a hump at $E \sim 700$ ev but no clear-cut peaks have been detected.

The intensity of γ-ray capture was determined for two copper samples of different origin; one sample was of the M-1 grade, that is, contained less than 0.1% of contaminations. The samples had the form of tubes of 3 or 4 mm wall thickness. One of the curves thus obtained is shown in Fig. 8. Besides the 2.5 kev level reported in reference 11, two other levels at $E \cong 250$ ev and $E \cong 700$ ev were observed.††

On the basis of the known levels Ag 5.22 ev and 16.6 ev, Zn 225 ev, Mn 346 ev and Cu 2.5 kev a graph t versus $E^{-1/2}$ was plotted. In accordance with Equation 1, this graph (Fig. 9) is found to be a straight line. This means that up to several kev the dependence of the lead scattering cross section on energy can be neglected. From the slope of the curve one finds that the spectrometer effective flight length $L = 5.94 \pm 0.06$ m, while the mean free path in lead is 2.87 cm and the scattering cross section 10.9 ± 0.2 b in accordance with the published

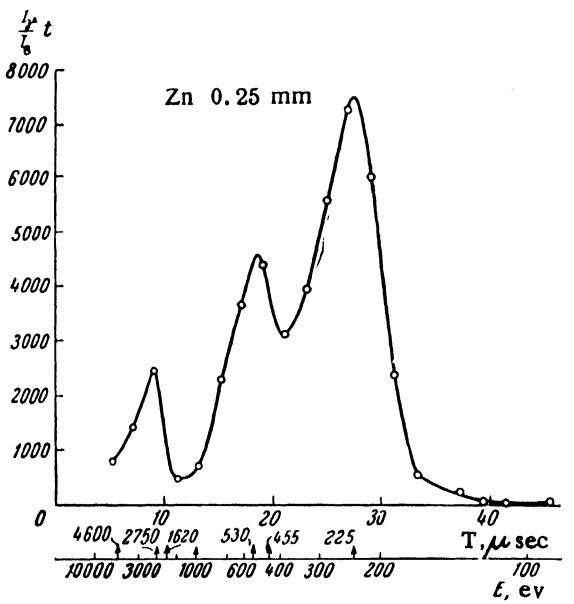

Figure 7. Neutron absorption probability curve for Zn sample 0.25 mm thick: block dimensions 2 × 2 × 2.3 m³

data. The positions on the energy scale of the two previously unreported copper levels mentioned above were also determined from the graph in Fig. 9.

INTENSITY. MEAN LIFE OF NEUTRONS IN LEAD

According to Equations 13 and 14, the neutron counting rate I in a boron counter and the slowing-down-time, t, are connected by the relation:

$$\ln I = -\alpha \ln t - \frac{t}{T} \qquad (18)$$

For comparison with experiment a knoweldge of the

†† The Atlas of Neutron Cross Sections, BNL 325, which we saw at the Geneva Conference, gives levels at $E = 240$ ev and $E = 600$ ev.

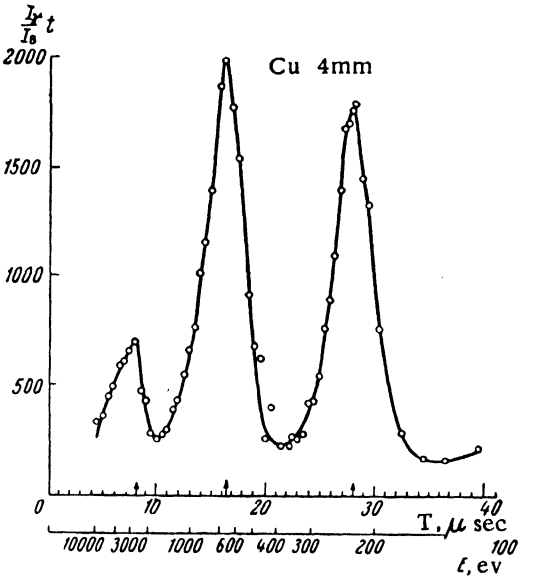

Figure 8. Neutron absorption probability curve for Cu sample 4 mm thick: block dimensions 2 × 2 × 2.3 m³

mean neutron lifetime in Pb is required. Values of the thermal neutron capture cross section in Pb vary between 0.16 b,[18] and 0.28 b,[14] and therefore it seemed desirable to measure the mean life directly; in these measurements a lead block of 2 × 2 × 2.3 m was used. From 1000 to 7000 μsec after the neutron burst the neutron density falls off exponentially. After correction for leakage of neutrons from the block, the neutron mean life was found to equal

$$T = 890 \pm 40 \ \mu\text{sec}$$

which corresponds to the following capture cross section for neutrons of 0.025 ev energy:

$$\sigma_c = 0.165 \pm 0.008 \text{ b}$$

The pile was made of CO-grade lead of 99.99% purity.

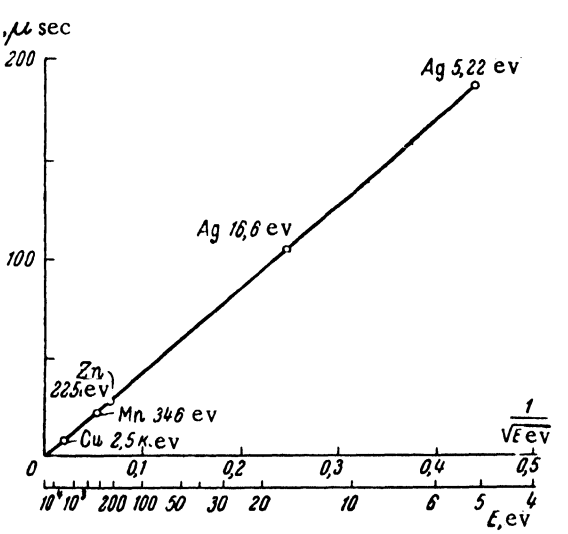

Figure 9. Plot of $t = f(E^{-1/2})$ (t = moderation time, E = mean energy of neutron at time t)

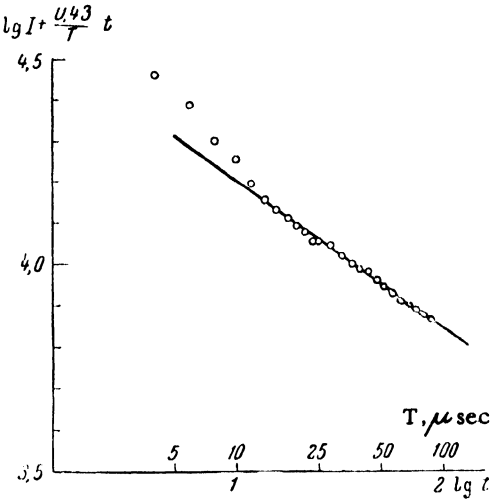

Figure 10. Dependence of neutron intensity I on moderation time

The value $T = 890$ μsec inserted into Equation 18 and the graph of $\ln I + t/T = f(\ln t)$ was plotted (Fig. 10). For $t > 10$ μsec ($E < 2$ kev) the points satisfactorily lie on a straight line with a slope corresponding to $\alpha = 0.36$. According to Equations 13 and 10 one should expect $\alpha \cong 0.35$ and thus the agreement is quite satisfactory. Deviations from linearity at $E > 2$ kev ($t < 10$ μsec) may be due to a number of factors: to the influence of higher harmonics of the neutron spatial distribution, to decrease of the scattering cross section in lead and finally to departure of the B^{10} (n, α) cross-section energy dependence from the $1/v$ law.

We shall next consider the absolute magnitude of the neutron flux in our experiments. For a slowing-down-time of 40 μsec ($E \sim 100$ ev) and a source intensity 10^8 n/sec, the counting rate in a boron counter of 2.9 cm diameter and 9.5 cm long was 250 cpm when the channel width was 2 μsec. This value agrees with Equations 10 and 14 if one takes into account that the source intensity should be doubled because almost every d–t neutron produces a $(n,2n)$ reaction in lead and if the age of 100 ev neutrons is set equal to $\tau \cong 4 \times 10^3$ cm^2. From the graph of the energy dependence of the total neutron cross section in lead[12] it can be found that an initial neutron energy $E_0 \sim 1$ Mev would correspond to this age. This seems to be a reasonable result, as the energy of the initial d–t neutrons is quickly lost in $(n,2n)$ and inelastic scattering processes in the lead.

In a time-of-flight spectrometer with a linear electron accelerator as neutron source[15], the slow neutron counting rate was 8 cpm for channel width 2 μsec, flight length 10 m and initial neutron intensity 10^9 n/sec. A counter 6.3 cm diameter and 50 cm long filled with enriched $B^{10}F_3$ at 600 mm Hg was used. Reducing these data to the counting efficiency, source intensity and effective flight length which we have in our experiments, a counting rate of 0.024 cpm would be found. At 100 ev and a flight length $L = 6$ m, a resolution of 30% can be obtained in the spectrometer used.[15] Reduction of the flight length to 3 m would increase the counting rate to 0.19 cpm. The values of 0.024 and 0.19 cpm should be compared to the value of 250 cpm observed in our experiments. It can be seen that in this case the sdt method offers an intensity gain of 3 or 4 orders of magnitude.

COMPARISON OF THE ENERGY DEPENDENCE OF THE CROSS SECTION FOR THE $Li^6(n,\alpha)$ AND $B^{10}(n,\alpha)$ REACTIONS

The time dependence of the counting rate in two identically constructed ionization chambers, one of which contained a 0.3 mg/cm^2 Li^6F layer, and the other a 0.5 mg/cm^2 B_2O_3 layer, was measured by alternately placing them at a given point within the lead block. Clearly, the ratio of the counting rates in the chambers should be equal to the ratio of the cross sections for the $Li^6(n, \alpha)$ and $B^{10}(n, \alpha)$ reactions. Results of the measurements are shown in Fig. 11. Between 20 ev and 5 kev the ratio of the cross sections of these reactions is constant to within 2%. This confirms and also extends to the higher energy region the results of Adamchuk, Yefimov and Pevzner who established the constancy of the cross section ratio for energies between 0.025 ev and 750 ev.

DISCUSSION OF THE RESULTS

The experimental results presented earlier show that the properties of the slowing-down-time lead spectrometer correspond to the theoretical predictions. Thus, the linear relation in Equation 1 between the slowing-down-time and the inverse velocity is observed experimentally, and within the limits of experimental errors (~ 2%), the effective flight path L agrees with the available data on the neutron scattering cross section in Pb. The time dependence of the slowing-down density in the lead block as well as the absolute value of this quantity also satisfactorily agree with predictions of age theory (Equations 13 and 14). The energy resolving power agrees with the value expected from theory (~ 30%), at any rate for energies $E \ll 100$ ev. This can be seen from the graph for the Ag capture cross section (Fig. 5): although the distance between levels 40.8 ev and 31.1 ev is 27% of the half-sum of these energies, the latter level is on the verge of

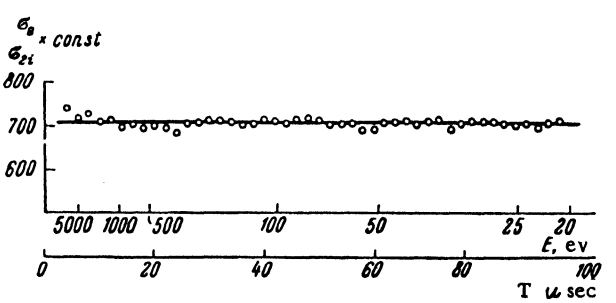

Figure 11. Energy dependence of cross sections of (n, α) reactions in B^{10} and Li^6 (in arbitrary units)

resolution. The form of the 5 ev Ag peak (Fig. 5) confirms this statement. The half-width of this peak is 40 μsec, whereas the expected value true width plus instrumental broadening is $\sim$ 36 μsec.

It should be noted that the first measurements which were carried out with a smaller column (1.3 $\times$ 1.3 $\times$ 2 m) yielded a higher value for the Ag peak width, 50 μsec (Fig. 4). In these measurements the counter was placed in a cavity of larger dimensions (7 $\times$ 7 cm^2) and the neutron burst lasted 6 μsec instead of the 2 μsec in the later experiments. Further estimates, however, show that this difference in peak width cannot be explained by these factors. It is conceivable that the larger peak width observed in the measurements with the small block was due to a broadening of the spectrum caused by contaminant neutrons reflected from the concrete foundation of the lead block or, especially, from the walls of the room which were shielded with water-filled tanks. The effect due to reflected neutrons should sharply decrease with increase of dimensions of the lead block; in the 2 $\times$ 2 $\times$ 2.3 m column it should not be appreciable.

Above 100 ev the resonance lines are broader than could be expected. Thus, the half-width of the 225 ev Zn peak is 6 μsec instead of 4.5 μsec. It is possible that part of the discrepancy is caused by an underestimate of instrumental peak broadening, the role of which should increase with the energy. On the other hand, it is quite possible that at $E > 100$ ev the large width of the initial energy spectrum has an appreciable effect. However, the resolving power of the spectrometer at $E > 100$ ev requires further investigation.

In the region $E \lesssim 1$ kev the γ-ray background in the block is relatively small and this enables one to measure absorption cross sections by recording capture γ-rays from comparatively thin samples. The thicknesses used by us, 0.1 mm Ag and 0.25 mm Zn, are by no means the limit. However, if one assumes that in Pb the $1/v$ law is valid, then the background is an order of magnitude higher than that due to the neutron capture γ-rays from Pb alone. The discrepancy is especially large for $E > 1$ kev. The additional background may be due to a number of causes: to neutron capture in the counter material or in Pb contaminants with densely spaced levels (e.g., Ag); to isomer levels excited by inelastically scattered primary neutrons; to resonance levels in one of the lead isotopes, etc. The quantity $I_\phi t/I_B$ (where I is the background γ-ray intensity) is not a monotonic function. A detailed analysis of the origin of the peaks has not been carried out.

The gamma-background problem deserves special study as further decrease of the background offers additional possibilities of the sdt method. One way of lowering the background is to shield the γ-counter from the mass of lead by using a substance that weakly absorbs neutrons, but strongly absorbs γ-rays. For this purpose an ideal material would be the doubly magic lead isotope Pb^{208}.

CONCLUSION

The present investigation has demonstrated the possibilities of using the lead sdt method for neutron spectrometry in the energy range from 1 ev to $\sim$ 10 kev. The main features of the method are: (*a*) effective flight path length $L = 6$ m; (*b*) in the energy range from several ev to hundreds of ev the energy resolution $\sim$ 30% and is poorer outside this region; (*c*) compared with the time-of-flight method it offers a gain in intensity of three or four orders of magnitude; and (*d*) the γ-background is small.

With regard to resolution the sdt method cannot compete with the time-of-flight method. It may be considered as a useful method complementary to the time-of-flight method as it permits one to measure the energy dependence of the total neutron absorption cross section and also to separately determine the cross sections for the reaction (n, γ) and for reactions in which charged-particles are emitted, even when these cross sections comprise only a small fraction of the total interaction cross section.

Application of the sdt method is demonstrated by results of measurement of the ratio of the effective cross sections for the reactions $Li^6(n, \alpha)$ and $B^{10}(n, \alpha)$, it was shown that this ratio is independent of energy for $E < 5$ kev. New results have also been obtained for copper: two hitherto unreported levels at $E \simeq 250$ ev and $E \simeq 700$ ev were detected.

APPENDIX: ENERGY DISTRIBUTION OF NEUTRONS OBTAINED FROM A PULSED SOURCE AND SLOWED DOWN IN A HEAVY MEDIUM

By M. V. Cazarnovsky

Neutron spectrometry based on measuring the slowing-down-time of neutrons in lead requires that the energy distribution of neutrons emitted by a pulsed source in a heavy medium be known with a sufficient degree of accuracy. This problem has been treated theoretically[16,17,18] on the following assumptions: (1) scattering of neutrons by nuclei of the moderator is elastic and spherically symmetrical in the center of mass system, (2) effects due to chemical binding or to thermal motion of the atoms of the moderator are negligible, (3) the mean free path λ is independent of energy, (4) neutron capture is negligible, (5) the energy is very small compared to the initial energy. On these assumptions Placzek[16] showed that the neutron velocity v and slowing-down-time t enter the energy distribution function only in the form of a dimensionless quantity‡‡

‡‡ The physical explanation of this fact is that after a sufficiently large number of collisions the distribution function becomes independent of the initial energy due to a peculiar velocity "focusing" of neutrons about the velocity $v = M\lambda/t$. The cause of this focusing can easily be understood from the following: the probability of a neutron experiencing a collision is proportional to v/λ; thus, if λ = constant neutrons moving with a high velocity will collide more often and slow down more rapidly than slowly moving neutrons. A same state of affairs will exist if λ decreases with increasing energy or increases slower than v. In the first case the focusing effect will be greater and in the second smaller, than in the case when λ = constant. If λ is proportional to the velocity, the focusing effect will be completely absent.

$x = vt/\lambda$; the positive moments of this function with respect to x were also determined by Placzek. Marshak[17] derived a function $F_0(x)$, the moments of which coincided with the exact values if the moment number n was large compared with the mass number M of the moderator atoms; this author also developed numerical methods for further approximations. von Dardel[18] slightly modified the method of choosing parameters for the function $F_0(x)$ and this appreciably increased the accuracy of the computations for $M = 2$. However, for moderator atoms of very large mass numbers ($M \gtrsim 100$) Marshak's (and also von Dardel's) method, on the one hand lead to very cumbersome calculations and, on the other hand, the reliability of the calculations cannot be judged by comparing the exact and approximate values of the moments as the neutron spectrum possesses a comparatively narrow maximum (dispersion $\sim M^{-1}$).

Thus, it was deemed necessary to find a less cumbersome and more reliable method for deriving the neutron energy distribution function. It was also necessary to investigate the role of various factors influencing the neutron spectrum in a real moderator (namely, dependence of the mean free path on energy; chemical binding and thermal motion of the moderator atoms; contaminants of other elements, in particular, hydrogen, etc.).

If the aforementioned assumptions are correct, the equation for the function expressing the collision frequency in a unit interval of parameter $u = \ln(E_0/E)$ will have the form:[17]

$$\frac{\lambda}{v}\frac{\partial\psi(u,t)}{\partial t} + \psi(u,t) = \int_{u-q_u}^{u} e^{-(u-u')}\psi(u',t)\frac{du'}{1-r^2} + \delta(u)\delta(t) \quad (1)$$

Following Placzek,[16] we seek the solution of this equation in the form

$$\psi(u,t) = \frac{1}{\epsilon t}n(z); \quad z = \frac{2\lambda}{\epsilon v t}; \quad \epsilon = 1 - r \quad (2)$$

where $n(z)$, as can easily be shown, is normalized to unity. Inserting Equation 2 into Equation 1 and eliminating $d[zn(z)]/dz$ by integrating over z we obtain after simple calculations:§§

$$n(z) = \frac{1}{\epsilon}\int_{(1-\epsilon)z}^{z} n(z')dz'\frac{2}{1-r^2}\left(\frac{z'}{z^3} - \frac{r^2}{z'z}\right) \quad (3)$$

We seek the solution of this equation in the form

$$n(z) = \exp\left\{\frac{1}{\epsilon}f_{-1}(z) + f_0(z) + \epsilon f_1(z) + \ldots\right\} \quad (4)$$

§§ It should be mentioned that the method presented here is applicable to quite a large class of problems of physical kinetics which reduce to similar integral (or, in the general case, to integro-differential) equations.

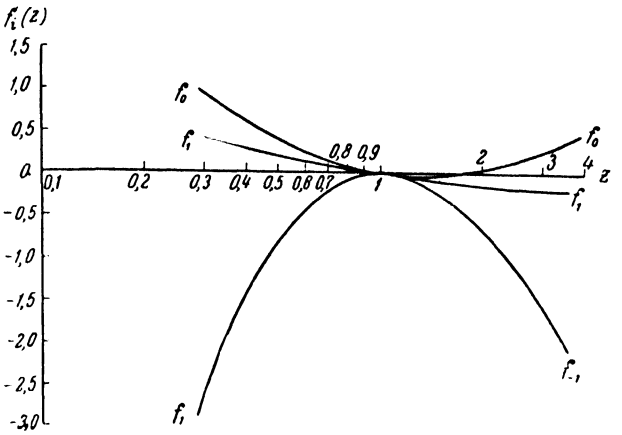

Figure 12. Graphs of the functions $f_i(z)$

Dividing Equation 3 by $n(z)$, inserting Equation 4 and introducing a new integration variable $x = (z - z')/\epsilon z$, we obtain

$$I(\epsilon) = \int_0^1 dx\,\frac{2}{1-r^2}\left[\frac{1-\epsilon x}{z} - \frac{r^2}{z(1-\epsilon x)}\right]\times \exp\left\{\frac{1}{\epsilon}f_{-1}[z(1-\epsilon x)] - \frac{1}{\epsilon}f_{-1}(z) + f_0[z(1-\epsilon x)] - f_0(z) + \epsilon f_1[z(1-\epsilon x)] - \epsilon f_1(z) + \ldots\right\} = 1 \quad (5)$$

Expanding $I(\epsilon)$ into a power series of ϵ, we obtain the following system of algebraic equations for the first few derivatives of the function $f_i(z)$:

$$I(0) \equiv \frac{2}{z}\int_0^1 dx(1-x)e^{-xz\frac{df_{-1}}{dz}} = 1$$

$$\left[\frac{\partial I_\epsilon}{\partial\epsilon}\right]_{\epsilon=0} \equiv \frac{2}{z}\int_0^1 dx(1-x)e^{-xz\frac{df_{-1}}{dz}} \times \left\{\frac{x}{2} + \frac{x^2z^2}{2}\frac{d^2f_{-1}}{dz^2} - zx\frac{df_0}{dz}\right\} = 0 \quad (6)$$

Hence the functions $f_i(z)$ can easily be expressed in parametric form

$$f_{-1}(z) \equiv \phi_{-1}(y) = -\int_0^y \left(2 - y'\frac{1-e^{-y'}}{e^{-y'}-1+y'}\right)dy'$$

$$f_0(z) \equiv \phi_0(y) = \frac{1}{2}\int_0^y \left(\frac{6}{y'} + 4y'\frac{e^{-y'}-4}{e^{-y'}-1+y'}\right)dy' - \frac{1}{2}\ln 3\left(\frac{2}{y} - \frac{1-e^{-y}}{e^{-y}-1+y}\right)$$

$$\ldots\ldots\ldots\ldots\ldots\ldots\ldots\ldots\ldots\ldots$$

$$z = \frac{2}{y^2}(e^{-y} - 1 + y) \quad (7)$$

The integration constants were chosen so that for $z = 1$ ($y = 0$), $f_{-1} = f_0 = 0$. By straightforward cal-

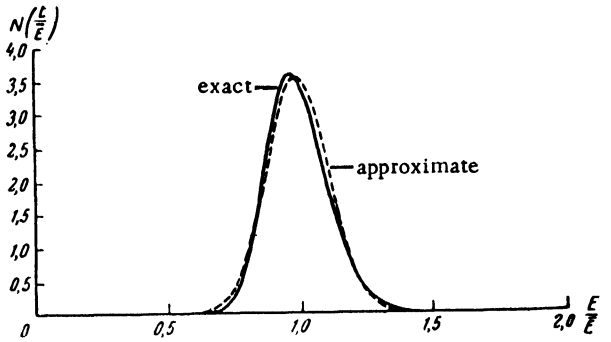

Figure 13. Neutron energy distribution in lead

culations it can be shown that for z close to unity

$$f_{-1} = -\frac{3}{2}(z-1)^2 + \ldots; \quad f_0 = -\frac{1}{4}(z-1) + \ldots$$

$$f_1 = -\frac{87}{320}(z-1) + \ldots$$

$$\text{For } z \to 0, f_{-1} \sim -\frac{2}{z}; \quad f_0 \sim \frac{3}{2}\ln\frac{2}{z}; \quad f_1 \sim -\frac{1}{4}\ln z$$

$$\text{For } z \to \infty, f_{-1} \sim -\frac{y^2}{2}; \quad f_0 \sim \frac{5}{2}|y|; f_1 \sim \frac{y^2}{24} \tag{8}$$

Graphs of the first three functions f_i are shown in Fig. 12. It is not difficult to see from Equations 4 and 8 that for most calculations of practical interest one may employ as a simple approximation to $n(z)$ the Gaussian function

$$n(z) = \sqrt{\frac{3M}{4\pi}}\, e^{-\frac{3M}{4}(z-1)^2} \tag{9}$$

and for the neutron energy distribution the function

$$N\left(\frac{E}{\bar{E}}\right) = \sqrt{\frac{3M}{16\pi}}\, e^{-\frac{3M}{16}\left(\frac{E}{\bar{E}}-1\right)^2} \tag{10}$$

where the "mean" energy $\bar{E} = mv^2/2$ (m = neutron mass) corresponds to $z(\bar{v}) = M + 1/\bar{v}t = 1$ (i.e., to the maximal $f_{-1}(z)$). Graphs of the exact¶¶ and approximate (Equation 10) neutron energy distribution functions are given in Fig. 13.

The neutron spectrum in a medium consisting of a mixture of heavy nuclei of various masses can be computed in a similar manner; the computation can also be applied if the mean free path is a proportional to a power of the velocity and capture takes place (but on the condition that the dependence of the capture mean free path is the same). For an arbitrary dependence of the mean free path on velocity, the approximate neutron energy distribution function can be represented by the expansion:

$$\psi(u,t) \cong (A/t)$$

$$\exp\left[-\frac{M+1}{2}\left\{\frac{1}{2}k(t)\left[\frac{v}{\bar{v}(t)}-1\right]^2 + \frac{1}{3}L(t)\left[\frac{v}{\bar{v}(t)}-1\right]^3 + \ldots\right\}\right] \tag{11}$$

closed analytical expressions being obtained for functions $v(t)$, $k(t)$ and $L(t)$. Generalization to account for capture does not raise any principal difficulties. Numerical calculations[19] show that in a real lead moderator these effects do not appreciably distort the neutron energy spectrum. The same may also be said of neutron diffusion (and escape from the moderator) in a sufficiently large Pb-cube[19] as used in neutron spectrometry.

Hydrogen contamination and thermal motion of the moderator atoms deserve special attention.

Admixtures of hydrogen lead to a slowly decreasing tail of slow neutrons in the spectrum, which is superimposed on the Gaussian term; if the amount of hydrogen admixture is very small the fraction which this term comprises will equal $1 - (\epsilon)^{\delta/\epsilon}$, where δ is the ratio of the total collision mean free path to that for collisions with hydrogen nuclei.

As Shapiro has shown on the basis of qualitative arguments, thermal motion of the moderator atoms may lead to considerable broadening of the energy distribution of neutron energies of the order of MkT, where k is Boltzmann's constant and T is the temperature of the medium. Rigorous calculations confirm this. In this case the dispersion of the neutron energy distribution function is given by Equation 3 in the paper.

REFERENCES

1. Lazareva, L. E., Feinberg, E. L.: Private communication (1950).
2. Shapiro, F. L.; Paper presented at a seminar (1950).
3. Shapiro, F. L.: Unpublished work.
4. Prescott, J. R., Proc. Phys. Soc., 67A, 540 (1954).
5. Albert, R. D., Yeater, M. L. and Gaertner, E. R., Bull. Am. Phys. Soc., *29*, No. 4, 56 (1954); Draper, J. E. and Baker, C. P., *ibid.*; Messervey, E., Phys. Rev., 1006 (1954).
6. Shtranikh, I. V.: Thesis (1954).
7. Seidl, F. G. P., Hughes, D. J., Palevski, H., Levin, I. S., Kato, W. J., Sjöstrand, N. G., Phys. Rev., *95*, 476 (1954).
8. Bollinger, L. M. and Dahlberg, D. A., Bull. Am. Phys. Soc., *29*, N 4, 57 (1954).
9. Bollinger, L. M., Palmer, R. R., Dahlberg, D. A., Bull. Am. Phys. Soc., *29*, N 4, 57 (1954).
10. Palmer, R. R. and Bollinger, L. M., Bull. Am. Phys. Soc., *28*, N 3, 25 (1953).
11. Marschak, H., Bull. Am. Phys. Soc., *29*, N 1, 37 (1954).

¶¶ It is easy to prove that the exact energy distribution unction is $N(E/\bar{E})d(E/\bar{E}) = n(z)\,dz$ and is the normalized probability that the neutron energy lies between $(E/\bar{E})$ and $[(E/\bar{E}) + d(E/\bar{E})]$.

12. Hughes, D. J., *et al., Neutron Cross Sections,* AECU 2040 (1952).
13. Harris, S. P., Muehlhause, C. O., Rasmussen, S., Schroeder, H. P., Thomas, G. E., Phys. Rev. *80,* 342 (1950).
14. Colmer, F. G., Littler, D. L., Proc. Phys. Soc., *63A,* 1175 (1950).
15. Merrison, A. and Wiblin, E. R., Proc. Roy. Soc., *215,* 278 (1952).
16. Placzek, G., Manhattan Project Report A-25 (quoted by Marshak[2]).
17. Marshak, R., Rev. Mod. Phys., *19,* 185 (1947).
18. Von Dardel, Phys. Rev., *94,* 12, 1272 (1954).
19. Cazarnovsky, M. V., Thesis (1955).

The Determination and Evaluation of Fundamental Thermal Neutron Cross Sections

By John A. Harvey,* USA

For many applications of slow neutrons involving cross sections of various materials, the use of a few accurately measured cross sections is of great value. These accurately measured cross sections can then be used to determine other cross sections by relative measurements, which can be performed more easily than absolute measurements. For example, absorption cross sections can be compared readily by means of a pile oscillator and hence the absorption cross section of the unknown can be determined if an accurately measured standard is available. These fundamental cross-section standards are also applied to measurements of neutron flux and to neutron source standardization. For example, the activation of a gold foil, the alpha counts of a boron counter, or the fission counts from a U^{235} fission counter allow us to make an accurate measurement of a neutron flux.

The requirements for useful fundamental standard cross section materials are: (1) that they have absorption cross sections which are much larger than their scattering cross sections, (2) that their absorption cross sections vary inversely as the velocity of the neutron or are almost $1/v$ in the thermal energy range, (3) that they are monoisotopic, and (4) that they are readily available and convenient to handle. Boron satisfies all these requirements except (3). Since there are small variations, about two per cent, in the relative abundance of its isotopes, it is necessary to stockpile a specific batch of material to use as a standard. Boron is also very useful to calibrate fluxes with a boron coated ionization chamber or a BF_3 gas-filled counter. The absorption cross section of gold departs slightly from a $1/v$ dependence but gold samples are so convenient to handle (thin foils of high purity) that gold is a valuable standard. For materials which depart from $1/v$, a correction factor, f must be applied to the 2200 m/s value in order to obtain the effective cross section when a Maxwell distribution of neutrons is used, such as in a pile oscillator. Gold also has the advantage that the absorption of a neutron produces an activity with a convenient half-life which is valuable as a standard for activation measurements. The absorption cross sections of boron and gold have been used as standards in all the pile measurements of absorption cross sections for elements and isotopes which are given in the Brookhaven neutron cross section compilation.[1] Most of the activation measurements in this compilation have used gold as the standard. The scattering cross section of U^{238} is several times the absorption cross section at 2200 m/sec, and thus does not satisfy requirement (1). However, since the absorption cross section of U^{238} is so fundamental to reactor design, accurate total cross-section measurements were made on it at very low energies as well as an accurate comparison to boron in the pile oscillator. Accurate total cross-section measurements were also made on U^{235} since its variation with energy in the thermal energy range is of fundamental importance to reactors. Its absorption cross section could not be obtained from a pile oscillator measurements since it produces neutrons in the fission process.

Early measurements on these standards nearly 10 years ago resulted in an absorption cross section of 710 b for normal boron, 93 b for gold, 2.6 b for U^{238} and 645 b for U^{235}. The 710 b value for boron was based on the value of 703 b by Fermi, Marshall, and Marshall,[2] 732 ± 9 b by Sutton *et al.*,[3] 743 ± 25 b by Rainwater and Havens[4] and 708 b by Bacher, Baker, and McDaniel.[5] In this early work various boron samples were used: BF_3 gas, B_4C, B_2O_3 dissolved in heavy water, and Pyrex glass. The present best US value for boron is 752 ± 3 b, which is about 6 per cent higher than the old value. This discrepancy cannot be ascribed to variations of the B^{10} content (which accounts for essentially all the absorption) since it varies by a maximum of only ± 2 per cent.[6] The scattering cross section of boron is small and cannot explain the discrepancy. Other possibilities are impurities in the boron compounds, such as water in the B_2O_3, and errors in the chemical analysis for the boron content of the samples. The 93 b value for gold was computed from the total cross section of 104 b measured at many laboratories by assuming a scattering of 11 b. The present best US value for the absorption cross section of gold is 98.7 ± 0.6 b. The reason for the discrepancy is that the scattering in the thermal energy region is considerably less than 11 b since the coherent scattering cross section is only 7.3 b and because of preferred

* Brookhaven National Laboratory. Including work by G. R. Ringo, S. Wexler, Argonne National Laboratory; R. S. Carter, D. J. Hughes, H. Palevsky, Brookhaven National Laboratory; W. W. Havens, Jr., M. Levin, and E. Melkonian, Columbia University; B. R. Leonard, Jr., General Electric (Hanford Works).

orientation and extinction effects. The absorption cross sections of 2.8 b for U^{238} and 645 b for U^{235} were obtained from unpublished measurements at Argonne and Los Alamos. The present US best values of 2.75 ± 0.04 b and 687 ± 4 b are considerably higher than the old values and no satisfactory explanations of the discrepancies are available.

EXPERIMENTAL METHOD

Absolute measurements of the absorption cross sections are very difficult to make since they bring in all the difficulties of absolute neutron flux determination and absolute alpha or beta counting. Thus, it is necessary to determine the precise values for absorption cross sections from total cross sections obtained by transmission measurements. This is possible in the thermal region when the absorption cross section is much larger than the scattering cross section. For example, the absorption cross section of normal boron at 2200 m/sec is nearly 200 times the scattering cross section of 4 b. Thus an error of 50 per cent in the scattering cross section introduces an error of only ¼ per cent in the absorption cross section. However, for a material like gold where the scattering cross section is about 10 per cent of the total cross section, the uncertainty in the scattering because of crystal interference effects is a serious limitation. The scattering in the thermal energy region is difficult to measure, and its calculation is uncertain because coherent Bragg scattering is reduced by extinction effects in the microcrystals and is modified by preferred orientation of the crystal gains. For U^{238} it is practically impossible to obtain the absorption from measurements of the total cross section since the scattering is several times the absorption at 2200 m/sec.

It is possible, however, to obtain the absorption cross section for gold and U^{238} from transmission measurements for very low energy neutrons because the scattering almost completely disappears in solids at these low energies. For neutrons with wavelengths longer than the crystal cutoff (twice the largest lattice spacing) the coherent cross section disappears and the remaining incoherent and inelastic scatterings are small compared to absorption. The cutoff wavelengths are about 5 Ångstroms and sufficient neutron intensity at longer wavelengths is available from reactors to make possible accurate transmission measurements with a slow chopper. In this long wavelength region the absorption cross section is almost $1/v$ and can be separated from the various types of incoherent scattering because of its velocity dependence and its independence of sample temperature. As the spin-dependent and isotopic incoherent scattering are constant with wavelength, whereas the inelastic scattering varies rapidly with temperature, these components can be identified. For a strictly $1/v$ absorber like boron the 2200 m/sec absorption cross section can be obtained directly from the absorption measured at these long wavelengths. For materials that are not $1/v$ in the thermal energy region small corrections (one per cent for gold and 0.4 per cent for U^{238} must be made to obtain the 2200 m/sec absorption cross sections.

The instruments that have been used for these accurate cross section measurements are slow choppers and crystal spectrometers at reactors and the pulsed cyclotron time-of-flight technique. These instruments have been described in detail by Hughes[7] and Havens, Jr.[8] Only features that are of specific importance to the measurements reported here will be outlined. The slow choppers at Argonne[2] and Brookhaven[9] have flight paths of several meters which result in an energy resolution of about five per cent. At Brookhaven the flight time is measured electronically, the standard being a one-megacycle oscillator. At Argonne the flight time is determined mechanically by the rotation of the chopper. The major uncertainty in the time-of-flight scale is the determination of the time at which the neutrons pass the shutter. This time is determined at Brookhaven by means of the graphite break at 6.70 Å and at Argonne by the beryllium break at 3.95 Å. The wavelength scales at both laboratories are accurate to 0.25 per cent. Samples are placed sufficiently far from the BF_3 detector that the in-scattering correction is negligible and close enough to avoid the small-angle scattering that takes place in fine grain materials, especially at long wavelengths. The counting rates are corrected for the dead time of the counting equipment. Background neutrons are determined by the insertion of a 0.010 in. sheet of cadmium in the neutron beam at the exit of the chopper. This thickness removes 99 per cent of the timed neutrons but does not affect the epi-cadmium neutrons that penetrate the chopper. The epi-cadmium neutron background is reduced as much as possible by adjusting the opening into the pile so that the cadmium ratio is a maximum. In addition, for the long wavelength measurements a beryllium filter is used which attenuates epi-cadmium neutrons greatly and decreases the low energy neutrons only slightly.

The crystal spectrometer at Hanford is similar to those instruments constructed at other laboratories. A beryllium crystal is used as a monochromator. The collimator is designed to give a high flux by using a relatively large beam and yet give sufficiently good resolution (~2 per cent in energy) in the energy range considered here. The energy calibration based on the beryllium crystal lattice parameters and the determination of the zero angle of diffraction results in an energy calibration good to a few tenths per cent up to 0.2 ev. Corrections for the second order diffraction are determined by using cadmium and gadolinium filters. Two neutron detectors are used, a boron chamber and a U^{235} fission detector.

The Columbia pulsed cyclotron time-of-flight neutron spectrometer has been described in detail in the literature.[4] In the energy range considered here the energy resolution and energy calibration is sufficiently good and does not introduce any error in the cross-section measurements. The change in detector effi-

ciency, determined by the filter technique described by Melkonian,[10] had been eliminated in the work reported here.

BORON

In the measurements on boron at Argonne and Brookhaven a solution of B_2O_3 in heavy water was used. The boron (mined in California) was in the form of boric acid powder and was from a batch stockpiled at Argonne for use as the US standard boron. The isotopic analysis of this boron was made with a mass spectograph at Oak Ridge and the fractional B^{10} content was 0.185, which is the same as that of the California boron measured at Oak Ridge to within ½ per cent. However, there is some question about the absolute accuracy of the isotopic determination. Thode *et al.*[6] have found 0.1871 for the B^{10} content in a careful absolute measurement and a range of ± ½ per cent in California boron.

The boric acid used in the Argonne and Brookhaven measurements was heated to drive off the water and converted into fused B_2O_3. When the material had reached a point where it no longer lost weight, it was checked by chemical analysis to see if it still contained any water. Several attempts were necessary before B_2O_3 was obtained that had less than 0.2 per cent (by weight) water. The boron content was determined before and after every transmission measurement made with each sample in order to detect any change in concentration. The chemical analysis was performed by saturating a given weight of solution with mannitol to increase its acidity, then titrating it with a standard alkali until it was neutralized. The amount of alkali used was an accurate measurement of the amount of B_2O_3 present. The boron content as determined by chemical analysis agreed to within 0.2 per cent with the calculated concentrations from the weight of B_2O_3 added to the D_2O.

The B_2O_3 was dissolved in D_2O rather than H_2O in order to avoid the large scattering cross section of the latter. To increase the concentration of the B_2O_3, the solution was heated to 40°C. The boron constituted about 60 per cent of the total cross section at 4 Ångstroms. The solutions were used in thin-walled aluminum holders, which allowed the thickness of the sample to be determined accurately. The amount of B_2O_3 in the samples was determined from the concentration, density, and thickness of the sample. Transmission measurements were made on the B_2O_3 + D_2O sample and a D_2O blank. A small correction had to be made to allow for the decrease in the density of the D_2O when the B_2O_3 was added and for the slight difference in the thicknesses of the holders. Several cycles of a D_2O blank, a D_2O background, a B_2O_3 + D_2O solution and a solution background run were made for each wavelength range.

At Brookhaven 5 wavelength ranges, each consisting of 12 channels, were run from 1.7 to 11 Ångstroms. At Argonne, measurements were made at only two neutron wavelengths, one near 3.95 Å and the other near 7.8 Å. The transmission was determined from the ratio of the counting rates after background had been subtracted. The total cross section of the B_2O_3 molecule was then corrected for scattering to obtain the absorption cross section per atom of boron. In the Argonne work, a value of 18 b per molecule of B_2O_3 was subtracted. The 18 b value is simply the sum of the scattering of the boron and oxygen. In the Brookhaven work, in order to allow for the coherent scattering of the boron and oxygen in the B_2O_3 molecule, a somewhat larger scattering was used based on a comparison of the scattering of the D_2O and B_2O_3. This scattering for the B_2O_3 molecule varied from 30 b at thermal to 40 b for measurements greater than 5 Å. At long wavelengths the scattering is only about one per cent of the total cross section.

The absorption cross section of boron divided by the neutron wavelength, λ, is plotted in Fig. 1. Many of the channels have been averaged in the Brookhaven data. A horizontal line can be drawn through the points which corresponds to a $1/v$ absorption cross section. The early work[3-5] had shown that the absorption cross section is $1/v$ up to one kev. The horizontal line at 418.3 b/Ångstrom corresponds to a 2200 m/sec absorption cross section of 752 b. The Brookhaven data give a value of 749 ± 4 b and the Argonne data 755 ± 3 b. The average of the two measurements is 752 ± 3 b.

A sample of boron glass was measured in the energy range 0.001 to 0.03 ev at Brookhaven[9] and from 0.01 to 1 ev at Columbia. The Pyrex glass sample had been analyzed by the Corning Glass Company, the composition was 13.35 ± 0.10 per cent B_2O_3 by weight, 80.15 per cent SiO_2, 4.5 per cent Na_2O, and two per cent Al_2O_3. These constituents gave rise to a scattering cross section of 46 b per atom of boron, assuming that the cross sections add. The low energy measurements at Brookhaven, when corrected for this scattering, gave a $1/v$ cross section corresponding to a 2200 m/sec value of 753 b. When corrected for the absorption of the constituents other than boron, a value of 752 ± 13 b was obtained. The 13 b error was based on the statistical fluctuations. However, because of the uncertainty in subtracting the scattering in this low energy region

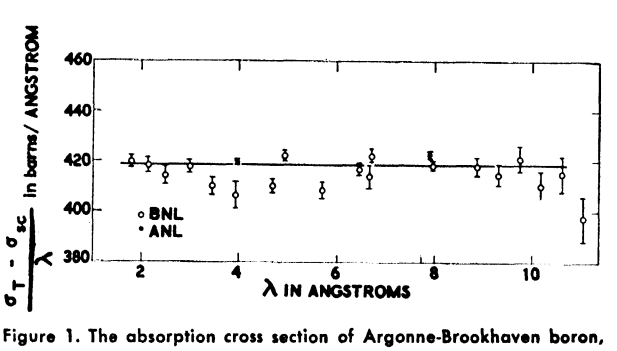

Figure 1. The absorption cross section of Argonne-Brookhaven boron, measured at Argonne and Brookhaven, divided by the neutron wavelength as a function of the neutron wavelength. The horizontal line corresponds to a 2200 m/sec absorption cross section of 752 b

and in the analysis of the boron content in the glass, further measurements were not made to reduce the statistical error. The higher energy measurements at Columbia gave a value of 750 ± 15 b. Again the 15 b error was mainly the statistical error. At these higher energies the sample was too thin for high statistical accuracy in the cross section. However, the agreement of the two measurements is good and agrees with the more accurate value of 752 ± 3 b.

The Argonne-Brookhaven boron has also been measured at Harwell and in Sweden. The Argonne-Brookhaven boron has been compared[11] to the Harwell boron by means of the pile oscillator at Harwell; a value of 771 ± 6 b for the Argonne-Brookhaven boron was obtained. In Sweden the Argonne-Brookhaven boron has been measured recently by von Dardel and Sjöstrand[12] by a modification of the earlier method of the measurement of the mean life of the neutron in a borax solution.[13,14] They obtained a value of 764 ± 3 b for the Argonne-Brookhaven boron. The three recent values 752 ± 3, 771 ± 6, and 764 ± 3, although they are in reasonable agreement and much higher than the old value of 710 are outside the errors quoted by the experimenters. It does not seem likely that the chemical analysis of the boron content in the samples could account for the discrepancy since good agreement was found when the same solution was analyzed by the Argonne, Harwell, and Swedish chemists. Also, the error in subtracting the scattering from the total cross section is small, since even if the scattering for the B_2O_3 molecule were assumed to be zero it would only raise the Argonne measurement to 758 b and the Brookhaven value to 755 b. Until further measurements are made we must conclude that the absorption cross section of the Argonne-Brookhaven boron lies between 750 and 765 b for 2200 m/sec neutrons.

GOLD

Transmission measurements were made[9] with the Brookhaven slow chopper on samples of rolled gold foils of purity greater than 99.9 per cent. Beyond the cutoff wavelength (4.7 Å) the total cross section is almost all absorption. The scattering cross section which consists of 0.3 b thermal inelastic scattering and 0.4 b spin incoherent scattering, is negligible compared to absorption. The data for the rolled gold samples for wavelengths greater than 4.7 Å are plotted in Fig. 2. In this figure the absorption cross section divided by λ is plotted as a function of λ. For wavelengths less than 4.7 Å it is necessary to subtract the coherent scattering. The lower curve in Fig. 2 shows the computed coherent scattering based on a coherent cross section of 7.3 ± 0.1 b and smeared out by the resolution of the chopper. When this scattering was subtracted from the total cross section for wavelengths less than 4.7 Å the points in the thermal region were several per cent below the solid curve in Fig. 2. This was because of preferred

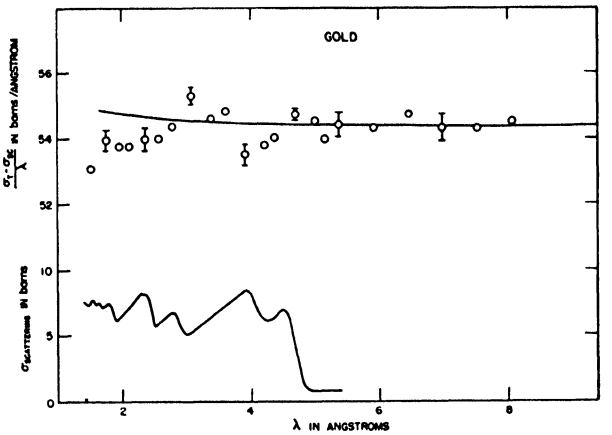

Figure 2. The absorption cross section of powdered gold for λ < 4.7 Å and rolled gold foil for λ > 4.7 Å, divided by λ as a function of λ. The shape of the line is computed from the parameters of the 4.9 ev resonance. The lower curve is the computed scattering

orientation and extinction effects in the rolled gold sample. A detailed examination of the total cross section revealed that the full value of the last coherent peak was not observed. Also changes in the total cross section were observed with the sample at an angle to the beam. Thus the scattering to subtract from the total in the thermal region was in doubt.

In order to investigate the cross section in the thermal region, samples of powdered gold were measured. There should be no preferred orientation or extinction effects in the powder. Because the sample thickness was difficult to measure it was determined by transmission measurements beyond the break and normalized to the rolled gold measurements. The results, $(\sigma_T - \sigma_{sc})/\lambda$, for wavelengths less than 4.7 Å are plotted in the upper half of Fig. 2. The points are somewhat low in the thermal region, possibly because of extinction effects. The shape of the solid curve is computed from the resonance parameters of the 4.9-ev resonance. Since this resonance accounts for nearly all the thermal cross section, it can readily be shown that

$$\sigma_{abs}/\lambda = K(1 + (0.0099\ E/0.0253))$$

The absolute value of k is determined from the long wavelength points and equals 54.3 b/Ångstrom. The absorption cross section at 2200 m/sec is then 98.7 ± 0.6 b. From recent measurements with long wavelength neutrons, Egelstaff[15] at Harwell has obtained a value of 98.4 ± 0.9 b. Since the absorption cross section of gold is not strictly $1/v$, the effective cross section in a Maxwell distribution is slightly different from the 2200 m/sec value. The f-factor from the energy dependence of the absorption cross section given above is 1.005. Thus when gold is taken as a standard for pile oscillator measurements, a value ½ per cent larger than the 2200 m/sec value should be used.

URANIUM-238

Since the scattering in the thermal region for U^{238} is several times the absorption, measurements had

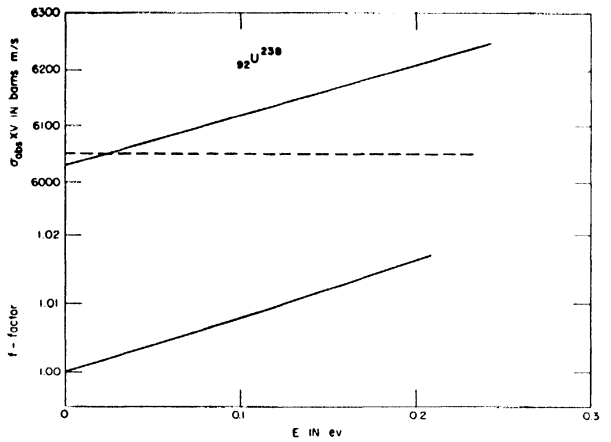

Figure 3. The upper curve is the absorption cross section of U^{238} multiplied by the neutron velocity as a function of neutron energy. The energy dependence is computed from resonance parameters and the absolute magnitude is determined from a total cross-section measurement for low energy neutrons and a pile oscillator measurement. The dotted line corresponds to a 2200 m/sec absorption cross section of 2.75 b. The lower curve is the computed f-factor for the absorption curve as a function of the energy of the neutron of most probable velocity in the Maxwell distribution

to be made at long wavelengths to determine the absorption. Total cross-section measurements were made on several samples of natural uranium with the Brookhaven slow chopper. The total cross section was corrected for the U^{235} contribution and the thermal inelastic cross section in uranium to obtain the absorption cross section of U^{238}. For these long wavelength neutrons the absorption cross section has a $1/v$ dependence. After correction for the slight departure of the absorption cross section from $1/v$ shown in Fig. 3, a 2200 m/sec value of 2.73 ± 0.07 b was obtained. The shape of the upper solid curve in Fig. 3 was computed from resonance parameters of the positive-energy resonances. The 6.7-ev resonance accounts for nearly 50 per cent of the thermal cross section and the other positive resonances account for another 30 per cent. The remaining 20 per cent is assigned to negative-energy resonances of the average size and the average spacing of the positive-energy resonances. The effect of these negative-energy resonances on the variation of the absorption cross section in the thermal range almost cancels the effect of the positive-energy resonance above the 6.7-ev one. Thus for U^{238} $\sigma_{abs} \times v = 6050(1 + (E - 0.0253)/269)$ b-m/sec. The f-factor (lower solid curve) computed from this absorption cross section is also given in Fig. 3 as a function of the energy of the neutron of most probable velocity in the Maxwell distribution.

The absorption cross section of U^{238} has also been measured relative to boron in the pile oscillator at Argonne; a depleted (30 ppm U^{235}) sample of U_3O_8 was used. The observed pile cross section of 3.15 ± 0.05 b must be corrected for the resonance absorption and the 30 ppm of U^{235} in the sample. After correction for the f-factor an absorption cross section of 2.71 ± 0.05 b for 2200 m/sec neutrons was obtained. Earlier work with the pile oscillator at Argonne resulted in a value of 2.85 b. We have taken the best value for the absorption cross section for 2200 m/sec neutrons to be 2.75 ± 0.04 b. Recently Egelstaff[16] at Harwell has reported a value of 2.8 ± 0.1 b, in good agreement with the US value. The dotted curve in Fig. 3 corresponds to a $1/v$ absorption cross section normalized to 2.75 b for 2200 m/sec neutrons.

URANIUM-235

The total cross section of U^{235} has been measured from 0.001 ev to 0.2 ev at Brookhaven,[17] Columbia, and Hanford. At each laboratory several samples of uranium metal enriched to various concentrations of U^{235} were measured. At Brookhaven, the low energy measurements were made with 0.050 in. samples enriched to about 5 and about 10 per cent in U^{235}; at Columbia enrichments of approximately 15 and 25 per cent were used. At all three laboratories measurements were made in the thermal region and up to 0.2 ev with different samples highly enriched in U^{235}. The total cross section of U^{235} was computed from the transmission with values of 2.75 b for the absorption cross section of U^{238}, 89 b for the absorption cross section of U^{234}, and 9 b for the scattering of both isotopes. The absorption cross section of U^{235} was obtained by subtracting a potential scattering of 9 b and an interference scattering from the large negative-energy resonance at −1.40 ev. This scattering tail drops from 4.7 b at zero neutron energy to 4.1 b at 0.2 ev. The results plotted as $(\sigma_T - \sigma_{sc}) \times v$ are shown in Fig. 4. The insert on Fig. 4 is the f-factor as a function of temperature from the solid curve on the $\sigma \times v$ plot. The data from the three laboratories and for the various enriched samples are in good agreement. The solid curve in Fig. 4 is the best line through the experimental points. The dotted curve at 1.511 barns m/μsec corresponds to an absorption cross section at 2200 m/sec of 687 b for U^{235}. An error of ± 4 b assigned to this value is based on the agreement of the results from the three laboratories. A value of 729 ± 15 b for the total cross section at 2200 m/s has recently been reported by Egelstaff[16] at Harwell. Subtracting a scattering of 13 b, gives an absorption cross section of 716 ± 15 b which is somewhat higher than the US value.

The absorption curve in Fig. 4 can be accounted for by contributions from the known positive energy resonance[18] and two negative-energy resonances. A large negative-energy resonance at −1.40 ev is necessary to explain the absorption cross section in the energy range above 0.2 ev. In the energy range below 0.1 ev it is necessary to place a second negative-energy resonance very close to zero energy. Although the positions of these two negative-energy resonances cannot be located very accurately, resonances at −1.40 ev and −0.02 ev do give a reasonable fit to the data. Fission cross section measurements normalized to 580 b at 2200 m/sec have been made at Hanford.[18] The 580 b

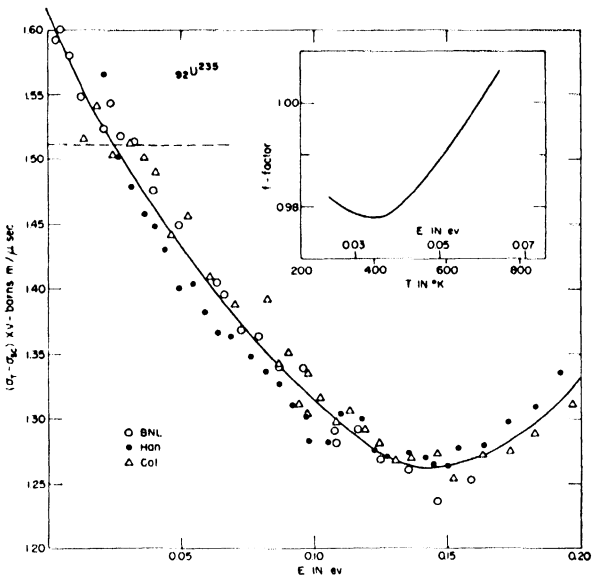

Figure 4. The absorption cross section of U^{235} measured at Brookhaven, Hanford, and Columbia multiplied by the neutron velocity as a function of neutron energy. The scattering cross section consists of a potential scattering of 9 barns and an interference scattering of about 4 barns which arises from the strong resonance at a negative energy at 1.4 ev. The dotted line corresponds to a 2200 m/sec absorption cross section of 687 barns. The insert shows the f-factor computed from the absorption curve as a function of the temperature T of the Maxwell neutron velocity distribution and the energy of the neutron of most probable velocity in the distribution

value is derived from an accurate measurement of $(1 + \alpha)$ of 1.183 by Inghram[19] at Argonne and the 2200 m/sec absorption value. Including these fission measurements and the η measurements presented by Palevsky,[20] the parameters for these negative-energy resonances are the following: For the -1.40 ev resonance, $g\Gamma_n^0 = 1.31 \times 10^{-3}$ ev, $\Gamma = 0.230$ ev, and $\alpha = 0.15$, which give $\Gamma\gamma = 0.030$ ev and $\Gamma_F = 0.200$ ev. Γ_n^0 is the neutron width of the level reduced to 1 ev. For positive-energy resonances $\Gamma_n^0 = \Gamma_n/\sqrt{E_0}$ in ev where E_0 is the resonance energy. For the small resonance at -0.02 ev, $g\Gamma_n^0 = 4.8 \times 10^{-7}$ ev, $\Gamma = 0.075$ ev and $\alpha = 0.7$, which give $\Gamma\gamma = 0.031$ ev and $\Gamma_F = 0.044$ ev. These parameters and those for the 0.3 ev level quoted by Sailor[8] give a computed $(1 + \alpha)$ curve which agrees very well with the data presented by Palevsky.[20]

CONCLUSION

The absorption cross sections of boron, gold, U^{238}, and U^{235} have been determined from careful total cross-section measurements at several laboratories in the United States. The absorption cross sections for 2200 m/sec neutrons are as follows: Argonne Brookhaven boron, 752 ± 3 b; gold, 98.7 ± 0.6 b; U^{238}, 2.75 ± 0.05 b; and U^{235}, 687 ± 4 b. The fission cross section of U^{235} for 2200 m/sec neutrons is 580 ± 5 b. A table of "best values" for the thermal cross sections of other elements and isotopes renormalized to these new standard values is given in the cross section compilation BNL-325.[1]

REFERENCES

1. Brookhaven National Laboratory Report 325, *Neutron Cross Sections* by Hughes, D. J. and Harvey, J. A., (Superintendent of Documents, Washington, D. C., 1955).
2. Fermi, E., Marshall, J. and Marshall, L., *A thermal neutron velocity selector and its application to the measurement of the cross section of boron,* Phys. Rev. *72,* 193 (1947).
3. Sutton, R. B., McDaniel, B. D., Anderson, E. E. and Lavatelli, L. S., *The capture cross section of boron for neutrons of energies from 0.01 ev to 1000 ev,* Phys. Rev. *71,* 272 (1947).
4. Rainwater, J. and Havens, W. W., Jr., *Neutron beam spectrometer studies of boron, cadmium, and the energy distribution from paraffin,* Phys. Rev. *70,* 136 (1946).
5. Bacher, R. F., Baker, C. P. and McDaniel, B. D., *Experiments with a slow neutron velocity spectrometer II,* Phys. Rev. *69,* 443 (1946).
6. Thode, H. G., Macnamara, J., Lossing, F. P. and Collins, C. B., *Natural variations in the isotopic content of boron and its chemical atomic weight,* J. Am. Chem. Soc. *70,* 3008 (1948).
7. Hughes, D. J., P/576, *Neutron velocity selectors used at reactors,* Volume 4, Session 15A, these Proceedings.
8. Havens, W. W., Jr., P/574, *Pulsed accelerator slow neutron velocity spectrometers,* Volume 4, Session 15A, these Proceedings.
9. Carter, R. S., Palevsky, H., Myers, V. W. and Hughes, D. J., *Thermal neutron absorption cross sections of boron and gold,* Phys. Rev. *92,* 716 (1953).
10. Melkonian, E., *A precise determination of the slow neutron cross section of the free proton,* Phys. Rev. *76,* 1744 (1949).
11. Green, A., Littler, D. J., Lockett, E. E., Small, V. G., Spurway, A. H. and Bowell, E., *The thermal neutron absorption cross section of boron,* J. Nuclear Energy *1,* 144 (1955).
12. von Dardel, G. and Sjöstrand, N. G., *The absorption cross section of boron for thermal neutrons,* (to be published).
13. von Dardel, G. and Waltner, A. W., *Determination of the neutron-protron capture cross section,* Phys. Rev. *91,* 1284 (1953).
14. Scott, F. R., Thomson, D. B. and Wright, W., *Thermal neutron capture cross sections of hydrogen, boron, and silver,* Phys. Rev. *95,* 582 (1954).
15. Egelstaff, P. A., *The operation of a thermal neutron time-of-flight spectrometer,* J. Nuclear Energy *1,* 57 (1954).
16. Egelstaff, P. A., *The neutron absorption cross sections of U^{238} and U^{235} at 2200 m/s,* J. Nuclear Energy *1,* 92 (1955).
17. Palevsky, H., Carter, R. S., Eisberg, R. M. and Hughes, D. J., *Neutron absorption cross section of U^{235} at 2200 m/s,* Phys. Rev. *94,* 1088 (1954).
18. Sailor, V. L., P/586, *The low energy cross sections of U^{235},* Volume 4, Session 17A, these Proceedings.
19. Inghram, M., P/596, *Mass spectrometric methods for determination of nuclear constants,* Volume 4, Session 16A, these Proceedings.
20. Palevsky, H., P/585, *Measurement of capture to fission ratio of U^{235}, U^{233}, and Pu^{239} by a new method,* Volume 4, Session 18A, these Proceedings.

The Cross Section of the Fission Product Poison Xe^{135} as a Function of Energy

By Seymour Bernstein and E. C. Smith,* USA

The cross section of Xe^{135} is of interest for both applied and fundamental reasons: (1) It is a fission-product poison of such large cross section that it affects markedly the operating characteristic of chain reactors. Knowledge of the cross section of Xe^{135} as a function of energy is useful in the design of nuclear chain reactors to be operated at various temperatures. (2) It is of interest from the point of view of nuclear structure, because it has one of the largest of known cross sections and lacks one neutron of being a closed neutron shell nuclide.

The existence of a fission product with a very large cross section was discovered very dramatically by Fermi and Wheeler in the start-up of the first Hanford reactor. From the dynamic behavior of the pile, they deduced that the cross section was about 4×10^{-18} cm^2, and was associated with a fission product of about 9 hours half-life. The value of the half-life suggested that the potent fission-product poison might be Xe^{135}. Following Fermi and Wheeler's observations, an intensive effort was made by several groups of workers at different reactors to repeat their measurement of the average cross section of Xe^{135} for pile neutrons by what is now often called the "danger coefficient method." Simultaneously with these efforts, several other groups measured the average cross section for isolated samples of Xe^{135} by the method of "negative activation." These measurements of the average cross section for not too well-defined neutron energy spectra were followed later by the complete neutron spectrometer measurements of the total cross section of isolated samples of Xe^{135} as a function of energy. In this report the principles of the danger coefficient and negative activation methods will be described briefly and some of the results mentioned. The major part of this report will be devoted to the velocity selector measurements of the total cross section as a function of energy.

DANGER COEFFICIENT METHOD

The basis of the danger coefficient measurements of absorption cross sections is that the introduction of a poison in a nuclear reactor will affect the multiplication constant, k, in a known fashion. Fission product poison affects k by changing the thermal utilization factor, f, by an amount which may be calculated by perturbation techniques.[1] If we introduce N_x atoms per cm^3 of absorber into a cell of the lattice, the effective k of the reactor is changed by an amount Δk which may be estimated to first order by

$$\frac{\Delta k}{k} = \frac{\Delta f}{f} W = f \frac{N_x \sigma_x}{N_u \sigma_u}$$

where f = thermal utilization factor, N_u = number of atoms of uranium per cm^3, σ_x, σ_u = absorption cross section of the poison and the uranium respectively, W = statistical weight of the cell. W is proportional to the square of the local flux.

Thus absorption cross sections may be measured by comparing the Δk obtained from the unknown with that obtained from a standard absorber when both are placed in a standard position in the reactor. This is the so-called "danger coefficient" method. The case of fission-product poisoning is complicated by the fact that the material is distributed throughout the fuel and that N_x depends on the time and previous reactor history. The time dependence may be expressed in the form

$$N_x = N_0 F(t)$$

where $F(t) = 1$ when $t = \infty$ and $N_0 = yN_u\sigma_f\varphi/(\lambda + \sigma_x\varphi)$ is the equilibrium concentration of xenon.

Here y = total chain yield of xenon-135, σ_f = fission cross section of uranium, ϕ = local neutron flux, λ = decay constant of Xe = 2.1×10^{-5} sec^{-1}, and $F(t)$ = function which expresses time dependence of xenon concentration. It depends on the flux in terms of the form $\lambda + \sigma\phi$, on previous power history of the reactor, and on the ratio of direct yield of Xe^{135} to "direct" yield of I^{135}. (Note: I^{135} is a daughter of 2-min Te^{135}, which we neglect.)

Thus for each cell,

$$\frac{\Delta k}{k} = y\,\sigma_x \frac{\sigma_f}{\sigma_u} f \frac{\phi}{\lambda + \sigma_x \phi} F(t) W$$

For the entire reactor we must then sum over all the cells and the total effect on the reactor is then

$$\frac{\Delta k}{k} = y\,\sigma_x \frac{\sigma_f}{\sigma_u} f F(t) \int_{Reactor} \frac{\phi W d V}{\lambda + \sigma_x \phi}$$

where the weights have normalized so that $\int W\, d\, V$

* Oak Ridge National Laboratory, Oak Ridge, Tennessee.

$= 1$. The analysis above neglects several factors, but the salient features of the measuring technique are indicated. Only the product $y\sigma_x$ may be obtained. The results depend on a number of measured parameters, for example, f, σ_f/σ_u, and ϕ. Xe effects depend on the local flux. The time dependence of the effect is known.

Ideally the experiment proceeds somewhat as follows: The relative flux distribution throughout the reactor is measured. The absolute flux is calibrated against pile power. The thermal utilization for the reactor must be known. The reactor is then run at high power for a reasonable fraction of the time necessary to saturate the Xe and then shut down. The Δk due to the xenon is then measured by observing the position of a calibrated control rod at which the reactor is just critical, or the pile period, or a combination of both. The reactor is run at quite low power to observe the control rod positions. Extraneous perturbations to the reactivity must be minimized, all sources of them must be monitored, and the proper corrections made. In particular the reactor should be maintained at constant temperature. This is a difficult task for certain types of reactors.

The first danger coefficient measurements of the xenon cross section were made simultaneously on the Oak Ridge graphite and the Argonne heavy water reactors. The measurements on the graphite reactor were made by Borst, Haydn Jones, Nordheim, Slotin, and Soodak. They obtained a value $\sigma_y = 0.16$ megabarns (1 megabarn $= 10^{-18}$ cm^2) initially. Improved conditions later gave a value of $\sigma_y = 0.18$ megabarns. The poisoning of the Argonne heavy water reactor (CP-3) was studied first by Morrison, Goett, May, and Zinn. The water in the tank was heated to maintain constant temperature. Their measurements resulted in a value for σ_y of 0.11 megabarns. Both values are subject to large errors.

A novel measurement was made in the Materials Testing Reactor by deBoisblanc and Nyer. They calibrated control rods in terms of silver poison distributed in the same manner as I^{135} concentration in a fuel element. Then they saturated an element at full power and followed the build-up and decay of the Xe poison in the element after the remainder of the reactor was loaded with new fuel. A value of $\sigma_y = 0.195 \pm 10$ per cent was thus obtained.

THE METHOD OF NEGATIVE ACTIVATION

The method of "negative activation" or "deactivation" was first used to measure the capture cross section of Xe^{135} by Elliot, Knight, Novey, and Shapiro in 1944. This method is based upon the fact that the activity of the Xe^{135} can be appreciably decreased by placing it in an intense neutron flux for an appropriate period of time. The activity of a radioisotope being destroyed by neutron capture is given by:

$$A = A_0 e^{-(\lambda + n v \sigma) t} \qquad (1)$$

where λ is the decay constant, nv is the neutron flux, σ is the capture cross section per atom, and t is the time. The experiment consists in comparing the activities of a sample of Xe^{135} before and after neutron bombardment with the activities over the same time interval of an identical Xe^{135} sample which has not been irradiated. The activity of the control sample is simply

$$A' = A_0 e^{-\lambda t} \qquad (2)$$

The Xe^{135} decays into 5×10^6 year Cs^{135} which does not contribute a measurable activity to the measurements. The Xe^{135} forms stable Xe^{136} on neutron capture. The activities of two initially identical Xe^{135} samples, after one of them has been irradiated in a reactor for t hours, may be compared in terms of the depletion, D.

$$D = \frac{A' - A}{A'} = 1 - e^{-n v \sigma t} \qquad (3)$$

The cross section can be determined from Equation 3, if nvt is known. The flux of neutrons, nv, to be used in Equation 3 is the arithmetic time average of the flux during the period of neutron bombardment of the sample.

Two independent determinations of σ were made by this method. The samples were exposed in the ORNL graphite reactor. The changes in the Xe^{135} activity caused by the neutron bombardment was 12 per cent in the first case and 28 per cent in the second. The thermal neutron flux was determined by absolute beta counting of a gold foil monitor. The values obtained for the capture cross section of Xe^{135} for the energy spectrum of neutrons of the graphite reactor were 1.3×10^{-18} cm^2 and 1.4×18^{-18} cm^2 for the two samples. The neutron spectrum in the reactor is approximately that of a Maxwell distribution corresponding to 520°K.

The method of "negative activation" was used also later by Pardue, Moak, Levy, Wollan, and Meiners at ORNL. In this effort coincidence counting was used. About 95 per cent of the Xe^{135} atoms decay via a 0.93 Mev beta-ray, followed by a partially converted 0.25 Mev gamma-ray. Coincidences between the Xe^{135} beta-rays and the conversion electrons were used to measure the relative amount of Xe^{135} present in the neutron irradiated and unirradiated sample. Coincidence counting was used rather than single beta counting in order to avoid possible interference from unforeseen contamination activities and also activity from the 5.4 day Xe^{133} activity. The Xe^{135} samples were irradiated in the ORNL graphite reactor. Neutron fluxes were measured using absolute beta counting from Au and Bi foils. An average value of 2.1×10^{-18} cm^2 was obtained for the cross section averaged over the ORNL graphite-reactor neutron-energy spectrum.

The method of negative activation or depletion was used also at the Metallurgical Laboratory in the period 1944–1945 by Freedman, Turkevich, Adams,

Sugarman, Raynor, and Stang, Jr. They exposed their samples in the "thimble" of the Metallurgical Laboratory heavy water reactor. The neutron-energy spectrum in this case is assumed to be approximately that of a Maxwell distribution corresponding to a temperature of 400°K. Gold and uranium foils were used in measuring the neutron flux. In the case of the gold foils, the absolute value of the flux was determined from the activity induced in the gold on neutron capture. In the case of the uranium foils, the flux was determined from the activity of the fission product 12.8 day Ba^{140} and the known fission yield. This group of workers gives 2.55×10^{-18} cm^2 as their best value of the cross section averaged over their heavy water 400°K neutron energy spectrum.

CRYSTAL SPECTROMETER MEASUREMENTS

The first successful measurements of the neutron cross section of Xe^{135} as a function of energy were made at Oak Ridge National Laboratory in the year 1948. This large-scale experiment was a cooperative effort of members of the Chemistry and Physics Division. Freed, Parker, Brosi, Hebert, DeWitt, Creek, Bogard, Ghormley, and Ruch were responsible for the chemical production of the sample. Brosi and Zeldes were responsible for the radioactive assay of the samples. Bernstein, Shapiro, Stanford, Dial, and Stephenson were responsible for the cross-section measurements.

In this work a focusing type single crystal spectrometer designed for transmission measurements of very small samples was used. Each sample was produced from 15 pounds of uranium metal which had been exposed to neutrons in the ORNL graphite reactor for 20 hours. The samples were in the form of PdI_2 and were contained in a sealed Pyrex capillary tubing. The largest initial strength of the samples was 10 curies of I^{135} activity corresponding to 12×10^{15} atoms of I^{135}. The daughter Xe^{135} grows from the I^{135} as a known function of the time reaching a maximum value of about 5×10^{15} atoms of Xe^{135} 11.3 hours after the I^{135} begins to decay. In the absolute calibration of the cross-section measurements absolute beta counting from pure I^{135} samples, and beta-gamma coincidence counting of pure Xe^{135} samples served as primary standards. The transmission of the sample was measured during the period of growth and decay of the Xe. The radioactive sample was placed inside the shield of the reactor. A thermal beam of neutrons from the reactor was allowed to pass longitudinally through the sample along the axis of the capillary tube onto a quartz crystal. The desired energies were selected from the incident continuous neutron-energy spectrum by use of the Bragg reflection law, $\lambda = 2d \sin \theta$. The total cross section in the energy interval from 0.015 ev to 0.20 ev was measured. A resonance in the cross section of Xe^{135} was discovered in the thermal energy region, which was described by the Breit-Wigner constants given below.

Experimental Arrangement

The entire experiment was designed on the basis of a sample only one square millimeter in cross-sectional area. Such a sample size was very small, indeed, even for the "intense" neutron beams available from the ORNL graphite reactor, the first chain reactor operating at appreciable power. A focusing type spectrometer of the type used for this work is well suited to the use of very small samples, since the sample may be placed at the position of the "point" source of neutrons and the detector at the "point" image. The design and operating characteristics of the spectrometer have been described before.[2]

A schematic diagram of the arrangement of the neutron beam collimator, sample, and detector is shown in Fig. 1. The point source was procured by means of the long hour-glass-like graphite collimator shown. The beam originates deep inside the pile where the neutron flux was about 10^{12} neutrons per cm^2 per second. The collimator converges uniformly from an initial cross section of 4 inches $\times$ 4 inches to a diameter of $\frac{3}{8}$ inch at the point S, four feet inside the outermost face of the pile shield. A 1.5 mm bore sealed Pyrex capillary tube containing the sample is placed at S so that its axis coincides with that of the collimator. The minimum cross-sectional area of the neutron beam is defined at the sample by the three-inch length of Pyrex capillary wall. After passing through the sample, the beam diverges again until it strikes the crystal, which focuses it on the detector slit.

The energy spectrum of the neutrons being emitted from the pile is roughly that of a Maxwell distribution corresponding to a temperature of 520°K. For the set of planes of the quartz crystal used, the energy of the Bragg reflected beam is given by:

$$E = \frac{1.136 \times 10^{-3}}{\sin^2 \theta} \qquad (4)$$

in which E is the neutron energy in electron volts, and θ is the glancing angle in degrees. The lower energy limit of usefulness of the instrument of about 0.02 ev was determined by the increasing amount of higher order reflection as the energy decreases. The upper energy limit of usefulness is determined by the rapid decrease in the number of neutrons in the Maxwell distribution at energies greater than the most probable energy.

Transmission measurements were made as a function of energy from 0.015 ev to 0.20 ev. In addition, the average total cross section for those neutrons having energies below the energy of the Cd cut-off was measured with the fission chamber in the direct beam in Fig. 1, by taking counts with and without cadmium surrounding the chamber.

The energy scale of the spectrometer was calibrated in terms of its angle readings by the following procedure. The transmission of BF_3 absorber was measured as a function of energy on both sides of

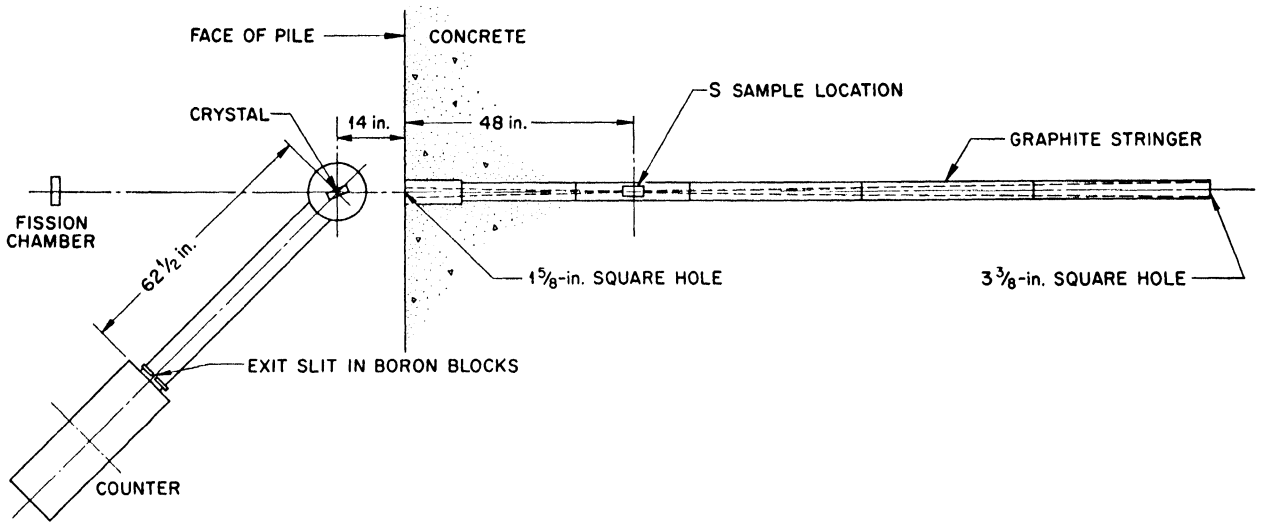

Figure 1. Schematic diagram of neutron beam collimator, sample, spectrometer, and detector

the direct beam. The reading of the spectrometer angle scale corresponding to zero scattering angle is then given by the average of two scale readings corresponding to equal values of the transmission measured on opposite sides of the direct beam.

Method of Analysis of the Data

The Xe^{135} grows from the I^{135} according to the relation:

$$N_2 = N_1^0 \frac{\lambda_1}{\lambda_2 - \lambda_1} (e^{-\lambda_1 t} - e^{-\lambda_2 t}) = N_1^0 f(t) \tag{5}$$

in which N_2 is the number of Xe atoms present at time t, N_1^0 is the number of I^{135} atoms present at time zero. There are no Xe atoms present at time zero. λ_1 and λ_2 are the transformation constants of I^{135} and Xe^{135} respectively. The transmission, T, of the sample is given by

$$T = T_1 e^{-N_1^0 f(t) \sigma_{Xe}} \tag{6}$$

in which T_1 is the transmission of the carrier material, and the exponential factor is the transmission of the Xe^{135}. Equation 6 can be written:

$$\ln T = \ln T_1 - N_1^0 f(t) \sigma_{Xe} \tag{7}$$

from which

$$\frac{d(\ln T)}{d(f(t))} = -N_1^0 \sigma_{Xe} \tag{8}$$

If the logarithm of the transmission is plotted as a function of $f(t)$, a straight line should be obtained whose slope is proportional to the product of the strength of the sample and the cross section of Xe^{135}. For a given sample the ratio of the slopes of the straight lines at the various energies gives the relative values of the cross sections at these energies. In calculating values of $f(t)$ the half-lives 6.7 hours for I^{135} and 9.2 hours for Xe^{135} were used.

Experimental Results

The transmission of the sample, of course, decreases as the amount of xenon increases. The growth and decay of the Xe is clearly shown by the data in Fig. 2, in which the transmission of one of the samples of Xe^{135} for Cd absorbable neutrons is plotted as a function of time. A plot of $d(\ln T)/df(t)$ for several values of the energy is shown in Fig. 3. The solid straight lines represent a least-squares fit to the data using Equation 7. The relative cross-sections per atom of Xe^{135} are given by the relative slopes of the lines.

A plot of the total cross section, σ, of Xe^{135} as a function of energy, E, is shown in Fig. 4. A plot of $\sigma\sqrt{E}$ vs E is shown in Fig. 5. In Fig. 4 and Fig. 5 the points represent the measured values. The solid curves represent a least-squares fit to the Breit-Wigner formula for the total cross section:

$$\sigma = g\, 4\pi\lambda\!\!\!^{-2} \frac{\Gamma_n \Gamma}{\Gamma^2 + 4(E - E_0)^2} \tag{9}$$

in which Γ_n is the neutron width, Γ is the total width, E_0 is the resonance energy, g is the statistical weight factor, $\lambda\!\!\!^{-}$ is the neutron wavelength divided by 2π, E is the neutron energy.

$$\Gamma_n = \left(\frac{E}{E_0}\right)^{\frac{1}{2}} \Gamma_n^0 \tag{10}$$

$$\Gamma = \Gamma_n + \Gamma_\gamma \tag{11}$$

$$g = \frac{2J + 1}{2(2I + 1)} \tag{12}$$

Γ_n^0 is the value of Γ_n at $E = E_0$; $\Gamma\gamma$ is the gamma-ray width of the level. I is the total angular momentum quantum number of the target nucleus; J is the total angular momentum quantum number of the compound nucleus. J has the two possible values, $I + \frac{1}{2}$ and $I - \frac{1}{2}$.

The spin[3] of Xe^{135} is very probably $\frac{3}{2}$. Therefore, g has the two possible values $\frac{3}{8}$ or $\frac{5}{8}$. The solid Breit-Wigner curves of Figs. 4 and 5 which repre-

sent the best least-squares fit to the data used the following values of the parameters.

$$g = 5/8$$
$$E_0 = 0.0849 \pm 0.0007$$
$$\Gamma_n^0 = 0.0186 \pm 0.0005$$
$$\Gamma\gamma = 0.09385 \pm 0.003189$$

The data could be fit almost equally well with the set of parameters:

$$g = 3/8$$
$$E_0 = 0.0851 \pm 0.0008$$
$$\Gamma_n^0 = 0.0310 \pm 0.0008$$
$$\Gamma\gamma = 0.0822 \pm 0.0031$$

The uncertainties given for the parameters are the standard errors.

Using a set of Breit-Wigner parameters, the capture cross section, σ_c, can be calculated from the formula:

$$\sigma_c = g\,4\pi\lambda^2 \frac{\Gamma_n\Gamma_\gamma}{\Gamma^2 + 4(E - E_0)^2} \qquad (13)$$

The scattering cross section, σ_s, is given by:

$$\sigma_s = g\,4\pi\lambda^2 \frac{\Gamma_n^2}{\Gamma^2 + 4(E - E_0)^2} \qquad (14)$$

The value obtained for the total cross section for Cd absorbable neutrons from the fission chamber

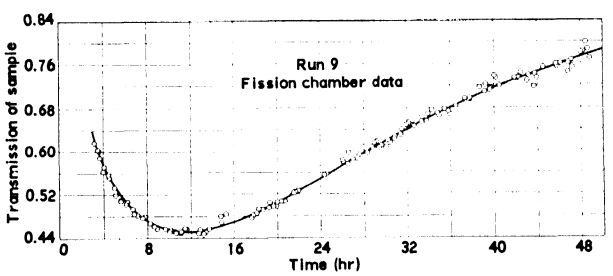

Figure 2. The transmission of one of the samples of Xe^{135} as a function of time

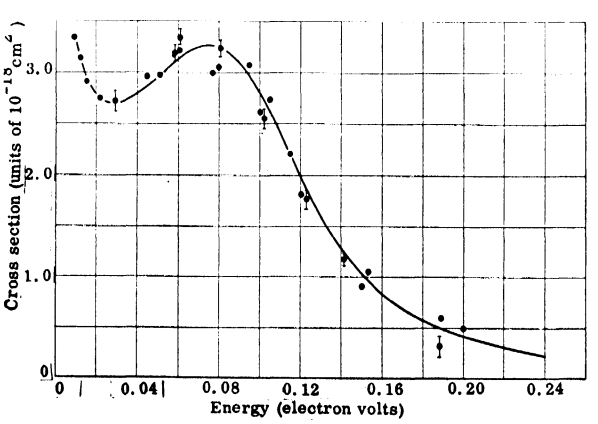

Figure 4. Total cross section of Xe^{135} vs energy

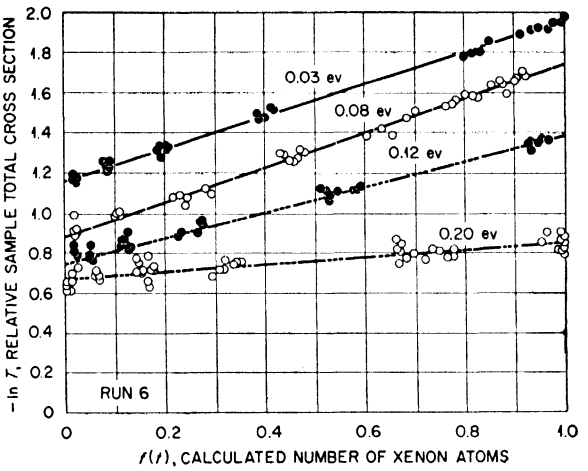

Figure 3. Logarithm of the transmission vs relative number of Xe^{135} atoms for several values of the energy. The relative cross sections per atom of Xe^{135} are given by the relative slopes of the lines

data is 2.6×10^{-18} cm^2. The average total cross section for a Maxwell distribution of 520°K can be calculated from Equation 9. The calculated average total cross section is 2.4×10^{-18} cm^2.

MEASUREMENTS WITH MECHANICAL VELOCITY SELECTOR

The total cross section of Xe^{135} was measured again in 1954 with a fast chopper neutron time-of-flight spectrometer. The participation of many people was necessary to bring the project to fruition. Parker, Martin, Lantaz, and Creek prepared the samples. Baldock and Sites made the mass spectrometer measurements for the sample strength analyses. Pawlicki, Smith, and Thurlow were responsible for the nuclear measurements. Arnette and Dismuke assisted with the necessary calculations.

Experimental Arrangement

The ORNL time-of-flight spectrometer used for these measurements is similar in principle to the

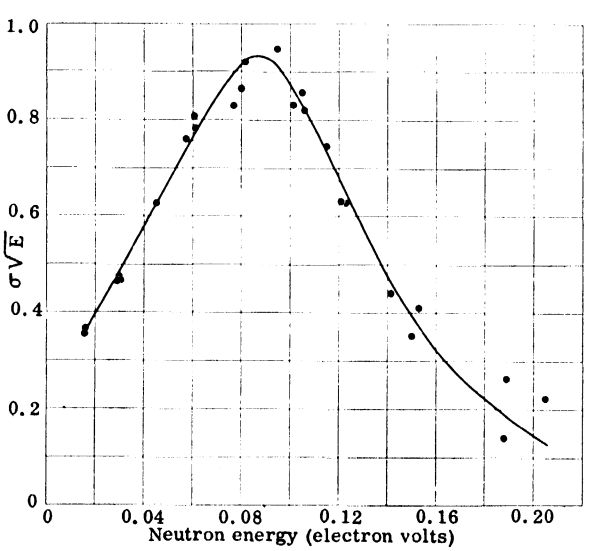

Figure 5. $\sigma\sqrt{E}$ vs E for Xe^{135}

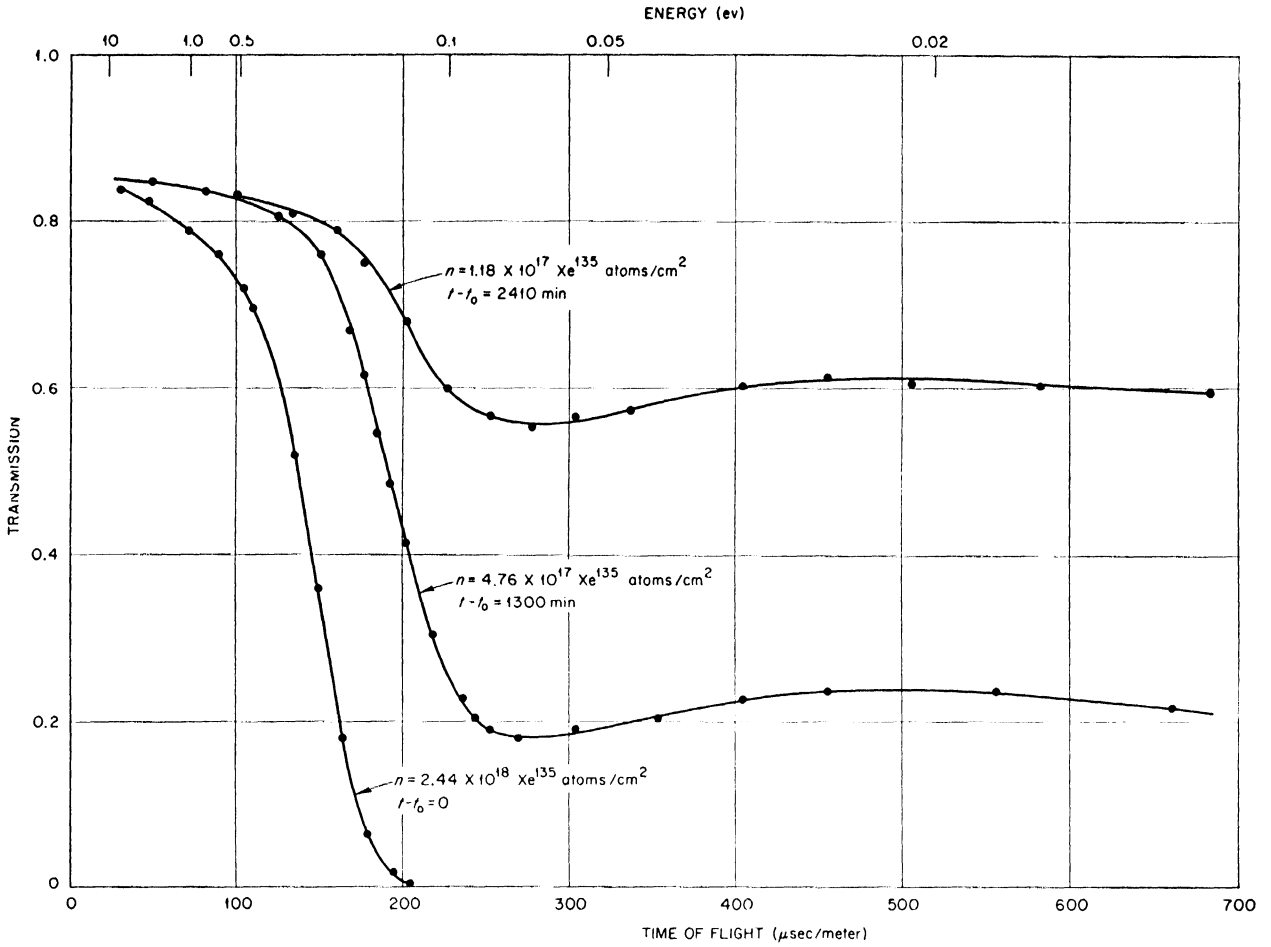

Figure 6. Transmission vs neutron time-of-flight

ones in use at the Argonne and Brookhaven National Laboratories.[4,5] It has been described in an unpublished report.[6] The rotor spins about a horizontal axis parallel to the neutron beam, which passes through only one of the twelve slots. Neutron burst widths from 4 microsec to 75 μsec are available. A flight path of 11.39 meters is provided. The detector is a boron triflouride ion chamber 30 cm long. Pulses in the detector are sorted in time by an 84-channel chain-gated analyzer with channel widths which may be varied from 3.5 μsec to 160 μsec. The resolution of the spectrometer is determined by uncertainties in the timing due to finite burst and channel widths, and to a finite detector length, but it was better than 5 per cent of the energy for these measurements. The energy range covered by the instrument is limited at the upper end of the neutron spectrum by the resolution and at the lower end by the very rapid decrease of intensity with energy of the Maxwellian distribution of the neutrons from the reactor. In this case no data were observed at neutron energies below 0.011 ev. Samples for total cross-section measurements are inserted in a slot in the collimator about 12 cm from the rotor. The beam area here permits samples of 1 cc volume with 0.30 cm^2 area in the beam. A manipulator is provided for remote handling of radioisotopes. All shielding for the xenon experiments was external to the reactor shield.

Samples Preparation and Analysis

Two samples of about 500 curies each were extracted from the off gases of the Homogeneous Reactor Experiment by adsorption on a charcoal trap. The xenon was reduced in volume and further purified by adsorption on successively smaller traps, and finally loaded into the same cells. A full description of the process is given elsewhere in these proceedings.[7]

The number of Xe^{135} atoms in a cell was determined after essentially all the 9.2-hour activity had decayed to its daughter, 2×10^6 yr cesium-^{135}. The cesium was extracted in an aqueous solution, and the concentration of cesium-135 was determined mass spectrometrically by dilutions with a standard cesium-133 solution. Sites made the mass analysis essential for these assays. The two cells contained 2.3×10^{18} and 2.85×10^{18} atoms of Xe^{135} per cm^2 at the time they were sealed.

Cross-Section Measurements

Transmissions of the sample were measured by comparing counting rates with the loaded sample

cell in the neutron beam with those obtained when the cell was removed from the beam. The transmission of a radioactive material is given by the expression

$$T = T_0 \int_{t-a}^{t+a} e^{-n_0 \sigma e^{-\lambda(t-t_0)}} dt \qquad (15)$$

$$\cong T_0 e^{-n_0 \sigma e^{-\lambda(t-t_0)}} \text{ if } \lambda a \ll 1 \qquad (16)$$

where T_0 = transmission of sample holder, λ = decay constant of Xe^{135} = 0.755 hour^{-1}, σ = total cross section of Xe^{135}, n_0 = number of Xe atoms per cm^2 at time t_0, t_0 = origin of time measurements, chosen here to be the time of the first sample in count, $2a$ = time interval during which a "sample in" measurement is taken, and t = clock time to the mid-point of the sample in counting interval.

In order to avoid corrections for sample decay during the course of a measurement, "sample in" counts were taken for 20-minute intervals, so a = 10 minutes and λa = 0.0126, which is quite small enough for the purpose.

If we take the natural logarithm of Equation 16 we obtain

$$-\ln T = -\ln T_0 + n_0 \sigma e^{-\lambda t} \qquad (17)$$

Thus a plot of $-\ln T$ as a function of $e^{-\lambda t}$ is a straight line with slope $n_0\sigma$ and intercept $-\ln T_0$. The data at each energy were fitted by the method of least squares to the straight line, Equation 17. Since about 1500 transmissions were measured for each of the two runs, the task of data reduction would have been formidable without the aid of the ORACLE, the Oak Ridge National Laboratory fast digital computer. Arnette was of invaluable assistance in programming the machine computations.

A graph of the transmission as a function of neutron time-of-flight (reciprocal velocity) appears in Fig. 6 for several times $t - t_0$. The data apply to the second of the samples received. At the time measurements began the transmission was less than $e^{-7} = 9 \times 10^{-4}$ for neutron energies less than 0.1 ev, so the lower energy cross-section measurements were made after the sample had decayed sufficiently. Transmission at energies greater than 0.5 ev are above 0.9 T_0, so cross-section measurements above this energy are limited in precision because the sample was too thin.

The cross section in the neighborhood of the 0.084 ev level was first examined in the region extending upward from 0.12 ev at a resolution of 3.3 μsec/meter (24 μsec burst and 28 μsec channels). After the xenon had decayed sufficiently the resolution was broadened to 15 μsec/meter (75 μsec burst and 96 μsec channels) and the cross section measured from 0.011 ev to 0.15 ev.

A plot of cross section as a function of energy appears in Fig. 7. The 96 μsec channel data also

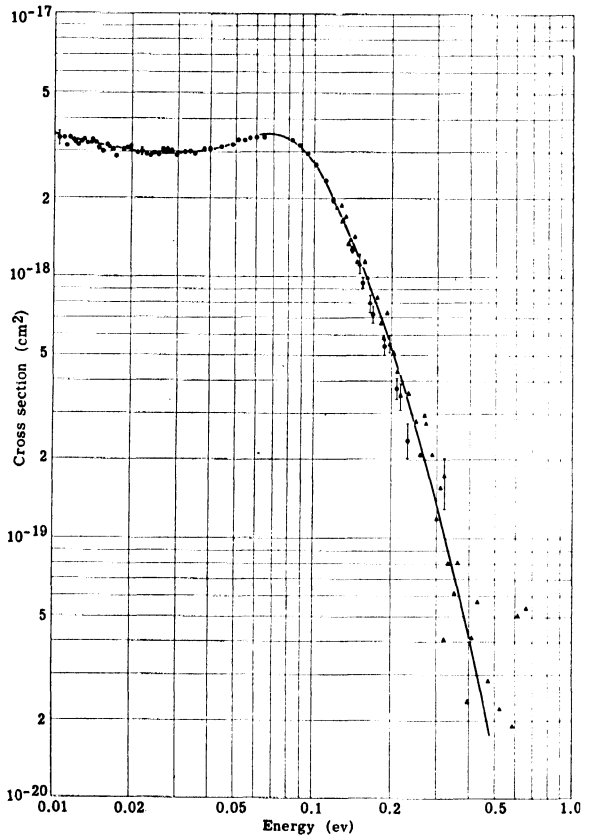

Figure 7. The total neutron cross section of Xe^{135} as a function of energy as measured with a fast chopper

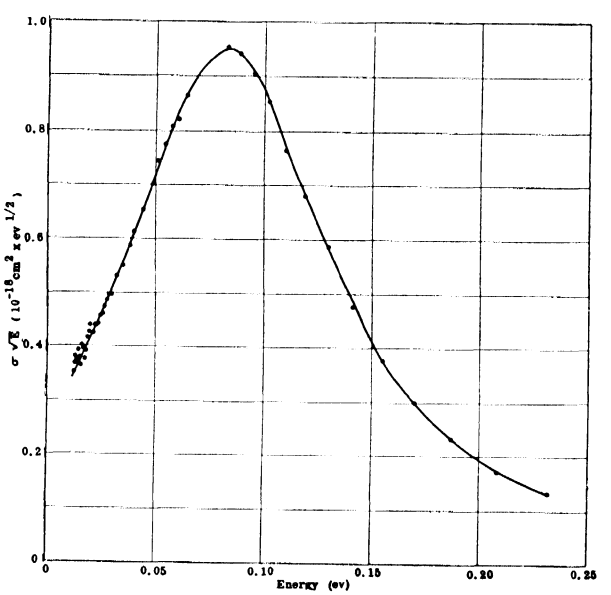

Figure 8. $\sigma\sqrt{E}$ vs E for the data of Figure 7

appear in a plot of cross section $\times$ (energy)$^{1/2}$ as a function of energy in Fig. 8, which shows more clearly some aspects of the level.

A preliminary fit to only 30 points of the data gives the following values for the parameters of the Breit-Wigner formula, Equation 9:

$$g\,\Gamma_n^0 = 0.011 \text{ ev}$$

$$\Gamma_0 = 0.10 \text{ ev} = \Gamma_n^0 + \Gamma_\gamma$$

$$E_0 = 0.084 \text{ ev}$$

Thus if $g = 3/8$, $\Gamma_n^0 = 0.030$ ev and $\Gamma_\lambda = 0.074$ ev and if $g = 5/8$, $\Gamma_n^0 = 0.018$ ev and $\Gamma_\lambda = 0.086$ ev, the reduced widths $\Gamma_n^0/\sqrt{E_0}$ are 105×10^{-3} ev and 63×10^{-3} ev for $g = 3/8$ and $5/8$ respectively.

The final result of a least-squares fit of all the data to the Breit-Wigner formula will be published as soon as it becomes available.

DEPENDENCE OF THE AVERAGE CROSS SECTION ON TEMPERATURE

The average cross section of Xe^{135} depends upon the shape of the neutron energy spectrum used in the measurement. Since the several measurements of the average cross section were made using reactors operating at different temperatures, the values obtained should reflect the effect of the differences in the neutron energy spectra.

The capture cross section as a function of energy can be computed from Equation 13 using one of the sets of Breit-Wigner constants given above. The average capture cross section for a given neutron energy spectrum can then be calculated. In Fig. 9 the average capture cross sections for Maxwell distribution spectra corresponding to various temperatures are shown by the solid curves. The average values of the capture cross section obtained by the method of negative activation, which were given above, can be compared directly to our calculated curves. In order to obtain a value of the average capture cross section from the danger coefficient data, quoted above, a value of the fission yield of Xe^{135} must be used. Recent measured values of this quantity range from 6 per cent to 7 per cent. For both of these methods, the values of the average capture cross section do not agree very well with the calculated values of Fig. 9, probably because of uncertainties in determinations of neutron flux, neutron energy spectrum, or fission yield.

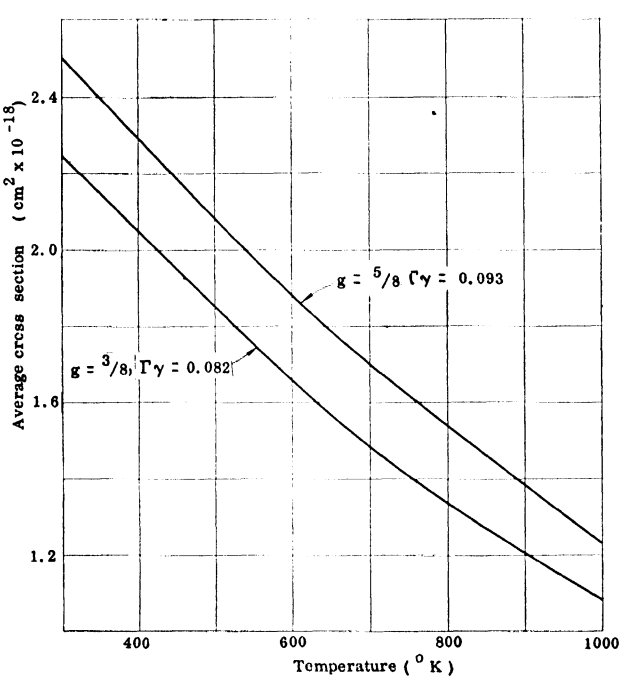

Figure 9. The average capture cross section of Xe^{135} as a function of the temperature of the Maxwell distribution neutron energy spectrum. The two curves are for the two values of Γ_γ derived from the crystal spectrometer data from the two values of g

ACKNOWLEDGEMENTS

The authors of this report are very grateful to Dr. A. Householder, N. Dismuke, R. Coveyou, and T. Arnette of the Oak Ridge National Laboratory for help in the statistical analysis of the data. They are also greatly indebted to the opening crew of the Homogeneous Reactor Experiment of Oak Ridge National Laboratory for their cooperation in the preparation of the Xe gas samples for the chopper work.

The major part of this report is devoted to measurements of the cross section as a function of energy. The first successful measurements of this kind were made at the Oak Ridge National Laboratory in 1948, using a crystal spectrometer. This large-scale experiment was a cooperative effort of the Chemistry and Physics Divisions. S. Freed, G. W. Parker, A. R. Brosi, G. M. Hebert, T. DeWitt, G. E. Creek, H. D. Bogard, J. A. Ghormley, and J. Ruch were responsible for the chemical production of the sample. A. R. Brosi and H. Zeldes were responsible for the radioactive assay of the samples. Seymour Bernstein, M. M. Shapiro, C. P. Stanford, J. B. Dial, and T. E. Stephenson were responsible for the cross-section measurements.

Measurements were repeated at ORNL in 1954, using a mechanical velocity selector and much stronger samples. G. W. Parker, W. J. Martin, P. M. Lantz, and G. E. Creek prepared the samples. R. Baldock and J. R. Sites made the mass analyses of the samples. E. C. Smith, G. S. Pawlicki, and P. E. F. Thurlow were responsible for the velocity selector measurements.

The early work on the average cross section for continuous neutron energy spectra of not too well-defined shape is described briefly. The work of the following groups is included.

1. N. Elliott, J. D. Knight, T. B. Novey and E. Shapiro of the Oak Ridge National Laboratory.

2. P. W. Levy, E. Meiners, C. D. Moak, L. A. Pardue and E. O. Wollan of the Oak Ridge National Laboratory.

3. R. M. Adams, M. S. Freedman, S. Raynor, L. B. Stang, Jr., N. Sugarman and A. Turkevich of the Argonne National Laboratory.

4. L. B. Borst, Haydn Jones, L. W. Nordheim, L. Slotin and H. Soodak of the Oak Ridge National Laboratory.

5. J. Goett, A. N. May, P. Morrison, and W. H. Zinn of the Argonne National Laboratory.

REFERENCES

1. Glasstone, S. and Edlund, M. C., "The Elements of Nuclear Reactor Theory", D. Van Nostrand Co. (1952).
2. Bernstein, S., Borst, L. B., Stanford, C. P., Stephenson, T. E. and Dial, J. B., Phys. Rev. *87,* 487 (1952).
3. Thulin, S., Phys. Rev. *94,* 734 (1954).
4. Selove, W., "A Rotating-Shutter Time-of-Flight Spectrometer for the Slow-Neutron Resonance Region", Rev. Sci. Instr. *23,* 350 (1952).
5. Seidl, F. G. P., Hughes, D. J., Palevsky, H., Kato, W. Y. and Sjöstrand, N. G., "Fast Chopper Time-of-Flight Measurement of Neutron Resonances", Phys. Rev. *95,* 476 (1954).
6. Pawlicki, G. S., "A Neutron Time-of-Flight Spectrometer", Report ORNL 1526, Office of Technical Services, Washington 25, D. C.
7. Parker, G. W., Lantz, P. M., Creek, G. E. and Martin, W. J., P/313, "Preparation of Kilocurie Quantities of Xe^{135}", Volume 14, Session 19C, these Proceedings.

Delayed Neutrons

By G. R. Keepin and T. F. Wimett,* USA

Six months after the discovery of nuclear fission, Bohr and Wheeler[1] suggested that neutrons could be emitted following fission if the β-decay of certain fission fragments produced nuclei with excitation energy greater than the neutron binding energy for such nuclei; the emission rate of these "delayed" neutrons would then be that of the preceding β-activity. Two year later—more than a year before achievement of the first self-sustaining chain reaction—Fermi pointed out† the importance of delayed neutrons in controlling the rate of fission. The role of delayed neutrons in reactor kinetics is now generally well-understood;[2,3]‡ their importance in reactor control has become a matter of practical experience in many laboratories.

RESUME OF PREVIOUS INVESTIGATIONS

The earliest detailed measurements on delayed neutron groups from U^{235} fission were made in 1942 by members of Fermi's group at the University of Chicago.[4] Five delayed neutron periods (half-lives) were found ranging from 0.4 sec to 56 sec. The two longer periods (22 and 56 sec) were attributed[5] to Br^{87} and I^{137} β-activity preceding neutron emission from excited states of Kr^{87} and Xe^{137}. In all observations on U^{235} prior to 1942, at most two groups of delayed neutrons had been reported.[6,7,8,9]

Since the war, rapid advances in reactor technology have stimulated further interest in the measurable properties of delayed neutrons. A summary of recent measurements on delayed neutrons from various fissionable materials is presented in Table VII. This tabulation includes the reported work (since 1947) on the "well-established" delayed neutron groups; i.e., those exhibiting periods between $\sim$ 0.1 second and $\sim$ 1 minute. The reported investigations on possible low-yield delayed neutron groups outside this range of periods do not lend themselves to tabular form; a separate discussion of these follows.

The first reported search for short delayed neutron periods was made by Gibbs and Thomson[8] with modulated (D, D) neutrons on U_3O_8. They found no delayed neutron periods of appreciable abundance between 10^{-3} and 10^{-1} second. In 1947, Hughes *et al.*[10] reported a new short delayed neutron period from U^{235} of half-life 50 milliseconds and abundance 0.033% of delayed neutrons. No periods between one and 50 milliseconds were found. These short-period activity studies were made with a thermal neutron shutter ("guillotine") to produce short irradiations at the Argonne heavy water pile. Later, de Hoffmann, Feld, and Stein[11] using the "dragon" assembly (Los Alamos) to obtain extremely short irradiations, reported "indications" of a short-period group of 4 millisecond half-life and abundance $\sim$ 2% of delayed neutrons.§ Brolley *et al.*[12] using a pulsed cyclotron beam to generate short neutron bursts found no U^{235} fission-product activity shorter than 0.43 sec half-life. Using a bare U^{235} critical assembly pulsed at intervals with an 11-Mev betatron, Bendt and Scott[13] have recently measured a short-period delayed neutron group of half-life 150 $\pm$ 41 milliseconds and abundance 2.7 $\pm$ 0.7 per cent of delayed neutrons. No shorter periods were found. They discuss the hypothesis that this group of delayed neutrons follows the decay of Li^9, the latter being formed as the light fragment in ternary fission.

The few measurements reported on long-lived delayed neutron groups are all recent, due in part to the extremely low relative yields of such neutrons, which implies the use of modern high-power reactors as fission sources. Three groups having half-lives of 3, 12, and 125 minutes and yields per fission of 5.8×10^{-8}, 5.6×10^{-10}, and 2.9×10^{-10}, respectively, have been reported[14] from studies with rhodium and indium foils irradiated within the uranium-bearing lattice of the Brookhaven reactor. The 3-minute period and abundance have been corroborated independently at Brookhaven.[15] Recent measurements by Kane, Kephart, and Hammel[16] on U^{235} foils irradiated in the Los Alamos Homogeneous Reactor ("SUPO") indicate a factor of ten lower abundance for the 125-minute period. These workers have suggested that the 2.8 Mev γ from Rb^{88} could be responsible for an apparent delayed neutron period of 125 minutes by photo-disintegration of deuterium in small quantities of hydrogenous material. Supporting

* Including work by R. Sher, L. R. Heintze, Brookhaven National Laboratory; G. R. Keepin, T. F. Wimett, P. G. Koontz, J. D. Orndoff, R. K. Zeigler, Los Alamos Scientific Laboratory.

† In a letter to Allison; October, 1941 (cf., reference 5).

‡ Scientists in many countries have contributed to an understanding of the time behavior of nuclear reactors; a review of the theoretical development has been given by Nordheim.[8]

§ Recent studies at Los Alamos on the contribution of room-return neutrons to detailed prompt burst shape indicate that this observed 4-millisecond period could be accounted for by neutrons scattered back to the dragon assembly from the surrounding walls and floor.

evidence is given by independent work at Oak Ridge,[17] Argonne,[18] and Chalk River[19] on photoneutron yields from U^{235} fission products in D_2O.

CURRENT MEASUREMENTS

The complex decay of delayed neutron activity is capable of most direct and accurate analysis when the irradiation time of the fissile material is (*a*) "instantaneous"; i.e., short compared to the shortest delayed neutron period, or (*b*) "infinite"; i.e., long compared to the longest delayed neutron period—also called "saturation irradiation" (cf., Appendix A). To ensure negligible neutron multiplication within the sample, one further requires a small amount (say a few grams) of fissile material to be irradiated; this, in turn, implies the use of extremely high-intensity irradiations to provide adequate counting statistics. The bare U^{235} metal assembly at Los Alamos ("Godiva" reactor) is well-suited to these requirements. With this assembly appropriately modified, both "instantaneous" irradiations (super-prompt-critical bursts of < 1 millisecond duration) and "infinite" irradiations (delayed-critical operation),¶ each consisting of $\sim 10^{16}$ fissions, have been used to emphasize the shorter and longer period contributions respectively. In addition the instantaneous irradiations provide an independent method of determining absolute total yield of delayed neutrons from the different fissile elements (cf., Appendix B).

A schematic diagram of the experimental arrangement is shown in Fig. 1. A pneumatic system transfers a 5-gm cylindrical sample of fissile material from the point of irradiation to a 4π-shielded counting geometry in ~ 0.05 seconds. A simple phototube arrangement ensures reproducible positioning of the sample within the center of the reactor during irradiation. For instantaneous irradiations, the integrated output of a scintillation detector is used to generate (at a preset radiation level) a "trigger" pulse which initiates sample transfer and counting. The shielding for the counting geometry consists essentially of a cylindrical tank of water, (6 feet in diameter and 6 feet high) saturated with boric acid. This was found to attenuate fission energy neutrons by a factor of $\sim 10^5$. Direct gamma-shielding is provided by an 8-inch lead shadow-shield between the reactor and detector. The reactor, sample transfer system, and detection equipment are remotely operated from a control room ¼-mile distant.

Two different detectors have been used. The first is a ZnS-boric acid scintillation counter[20] developed for this experiment with a neutron-to-gamma sensitivity ratio $> 10^4$ and energy response varying

¶ Prompt burst irradiations to enhance the contributions of short-period delayed neutrons were first employed by de Hoffmann, Feld, and Stein.[11]

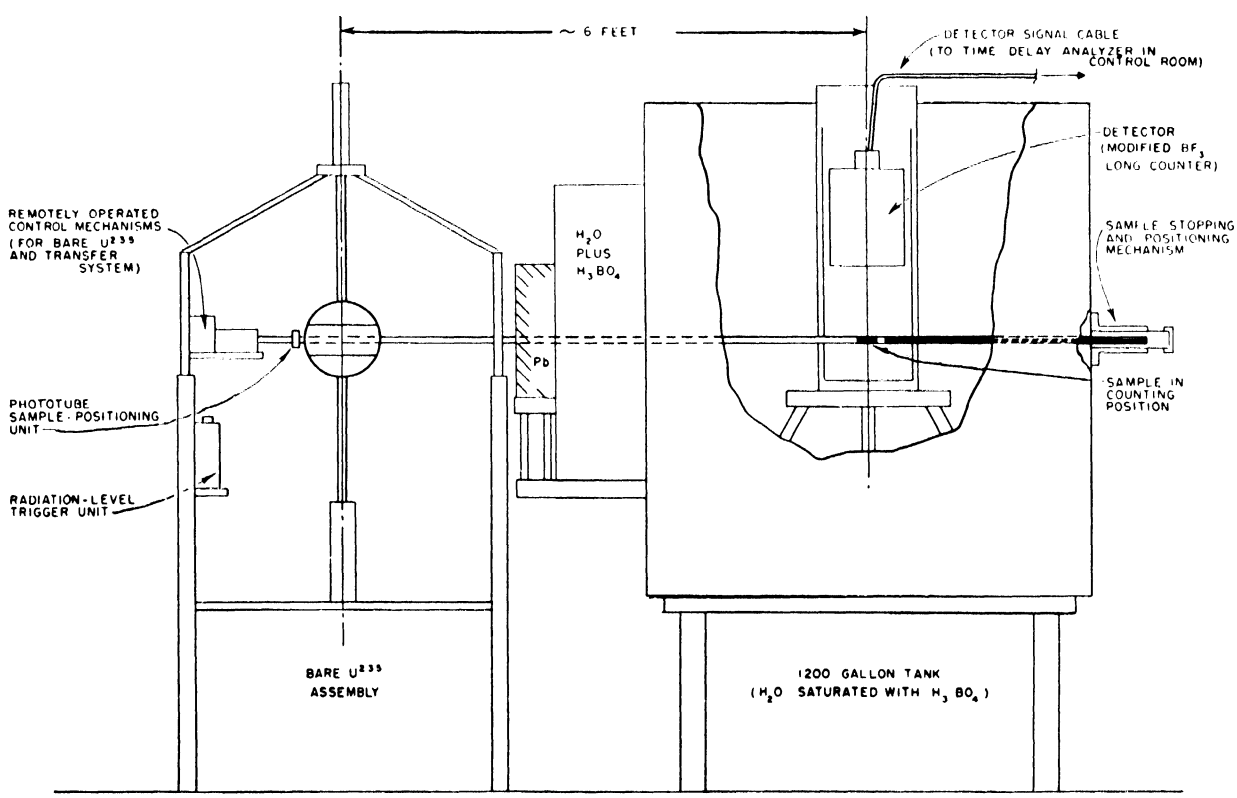

Figure 1. Schematic diagram of the experimental arrangement for delayed neutron studies at Los Alamos (control room is ¼ mile from assembly building)

Table I. Delayed Neutron Period and Relative Abundance Values for U^{235} — Los Alamos

Group index i	$\tau_{i\,1/2}$* (sec)	a_i/a†
1	54.3 ± 0.9	0.036 ± 0.006
2	21.7 ± 0.8	0.210 ± 0.019
3	5.87 ± 0.17	0.192 ± 0.027
4	2.18 ± 0.07	0.409 ± 0.022
5	0.46 ± 0.03	0.135 ± 0.008
6	0.126 ± 0.018	0.018 ± 0.004

* Calculated probable errors (from IBM-701 computer).
† $\Sigma a_i \equiv a \equiv$ total delayed neutrons per fission. Values reported include correction for detector response (BF_3 counter in modified "long" geometry).

Table II. Delayed Neutron Period and Relative Abundance Values for U^{238} — Los Alamos

Group index i	$\tau_{i\,1/2}$* (sec)	a_i/a†
1	53.0 ± 1.7	0.008 ± 0.003
2	22.0 ± 0.6	0.101 ± 0.040
3	5.30 ± 0.33	0.158 ± 0.050
4	2.00 ± 0.11	0.408 ± 0.033
5	0.51 ± 0.06	0.238 ± 0.025
6	0.18 ± 0.02	0.087 ± 0.010

* Calculated probable errors (from IBM-701 computer).
† Includes correction for detector response (BF_3 counter in modified "long" geometry).

roughly as $E_n^{-1/2}$ over the range of interest. The second detector is a ½-inch-diameter BF_3 counter in "long" geometry, modified** to give flat response within 5% from 23 kev to 1.2 Mev, which is believed to include the range of delayed neutron energies.[10,21,34] The number of source fissions (required for relative total-yield measurements) is determined by means of a U^{235} fission chamber which has been calibrated against radiochemical fission-yield determinations. The decay of delayed neutron activity is monitored by a multichannel recording time-delay analyzer[22] with 0.001-, 0.01-, 0.1-, 1-, and 10-sec channel-widths following in automatic sequence; the number of channels of each width is variable thus permitting selection of the most suitable channel-width distribution for a given decay curve. Provision is made for either photographic recording or direct print-out on electrosensitive paper. Using an iterative process, a least-squares fit to the counting data is made with an IBM-701 digital computer. The three longer periods (τ_1, τ_2, τ_3) and their abundance ratios are calculated from the infinite irradiation data; the four shorter periods (τ_3, τ_4, τ_5, τ_6) and their abundance ratios are calculated from the instantaneous irradiation data. The six relative abundances so obtained are then normalized to unity to give directly the fraction of delayed neutrons in each group. It is noteworthy that the 701 computer has recently been programmed (under the direction of Zeigler) to make a least-squares analysis on four periods and abundances simultaneously (8 × 8 matrix), thus eliminating all arbitrary time-division points except the one separating infinite and instantaneous data. Concurrently with the primary computation, standard deviations for both period and abundance values are calculated on the 701 computer (assuming normally distributed counting data). These calculated errors have indicated that the two longer periods are better determined from the infinite irradiation data, while τ_3 to τ_6 are better determined from the instantaneous data.

** The essential modification from the original long-counter geometry of Hanson and McKibben[23] is the addition of a shaped sleeve of boron plastic around the central BF_3 tube. The 5% error arises largely from uncertainty in calibration of the sources used: Sb-Be(E_n~0.025 Mev), Po-Li (E_n~0.4 Mev), Po-LiF(E_n~0.7 Mev), Mock Fission (E_n~1.5 Mev).

The period (half-life) and relative abundance values obtained to date for isotopically pure U^{235} ($E_n \simeq$ fission spectrum) are given in Table I.

Figure 2 shows the agreement between the experimental data for U^{235} and a curve calculated from the periods and abundances reported in Table I. Agreement of this kind was obtained for the delayed neutron decay curve of each fissionable isotope studied.

The period and abundance values obtained to date for isotopically pure U^{238} ($E_n \simeq$ fission spectrum) are presented in Table II.

Similar measurements were made on enriched uranium (~ 95% U^{235}); the resulting period and abundance values are given in Table III.

An independent check on the data of Table III is possible through the relation between reactor period and reactivity. This relation (the "inhour" equation of reference 3) may be expressed as

$$R = \frac{\tau_0}{T\gamma f} + \sum_{i=1}^{6} \frac{(a_i/a)\tau_i}{T + \tau_i}$$

where $R \times 10^2 \equiv$ reactivity in cents (100 cents ≡ reactivity interval between delayed and prompt critical), $\tau_0 \equiv$ prompt neutron (life-time ($\approx 10^{-8}$ seconds), $T \equiv$ reactor period (e-folding time), $\gamma \equiv$ average relative effectiveness of delayed neutrons compared to prompt neutrons, and $f \equiv$ delayed neutron fraction of total neutrons from fission. The inhour equation becomes most sensitive to short-period delayed neutron data in the region slightly below prompt critical. Measurements of period versus reactivity have been made in this region on the bare

Table III. Delayed Neutron Period and Relative Abundance Values for (~95%) Enriched Uranium — Los Alamos

Group index i	$\tau_{i\,1/2}$* (sec)	a_i/a* (Uncorrected)	a_i/a†
1	54.0 ± .9	.054 ± .007	.035 ± 20%
2	22.4 ± .5	.220 ± .022	.230 ± 20%
3	5.50 ± .08	.200 ± .012	.180 ± 20%
4	2.11 ± .03	.370 ± .009	.406 ± 20%
5	0.44 ± .02	.138 ± .005	.124 ± 20%
6	0.114 ± .010	.018 ± .003	.025 ± 20%

* Calculated probable errors (from IBM-701 computer).
† Includes preliminary correction for detector response (ZnS-boric acid scintillation detector.[20]

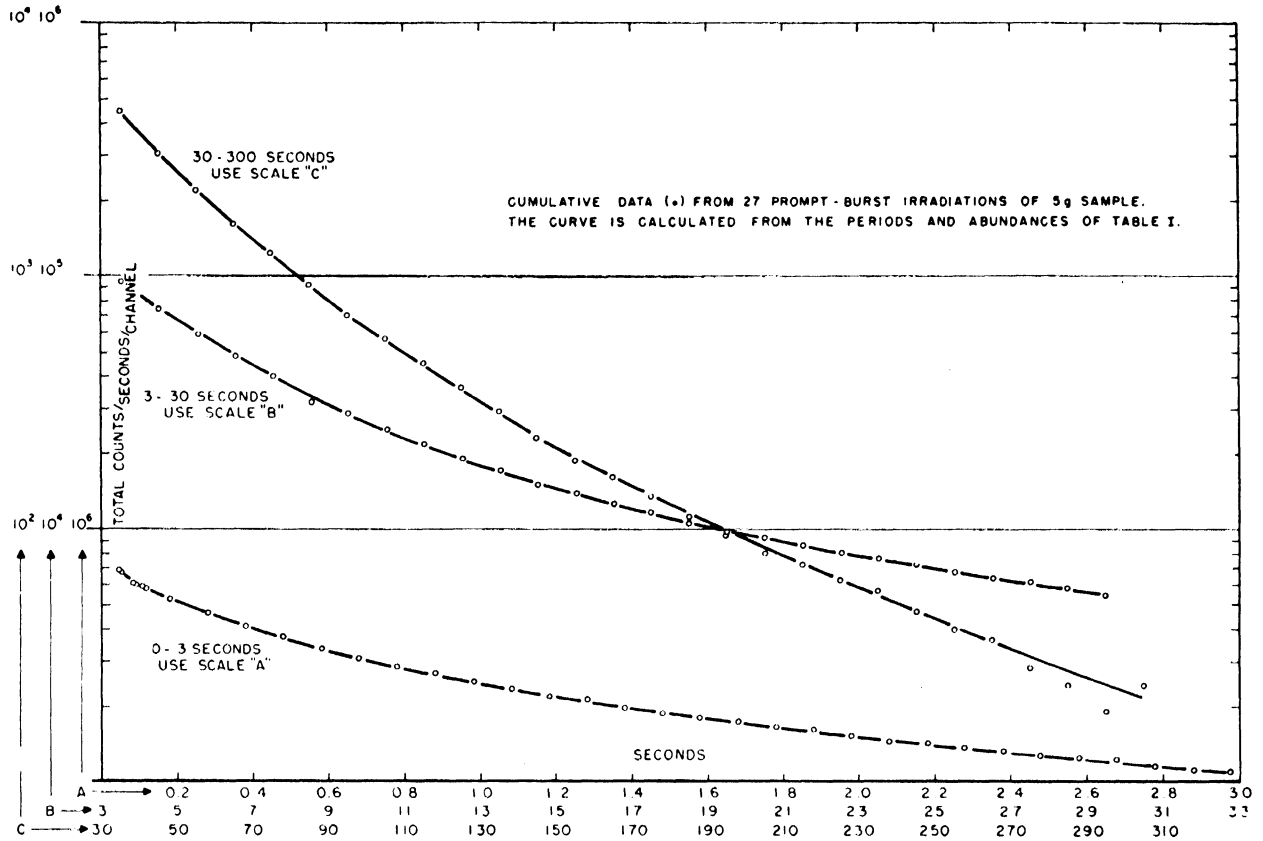

Figure 2. Delayed neutron decay following instantaneous irradiations of U^{235}

U^{235} reactor; Fig. 3 compares these measurements with the inhour equation using the U^{235} delayed neutron data of Hughes *et al.*[10] (Curve *A*) and of Table III above (Curve *B*). Further evidence in support of the sixth-group values of Table III is given by recent studies at Los Alamos on the detailed shape of super-prompt-critical radiation bursts from the bare U^{235} reactor.

Preliminary measurements have been made on the periods and abundances of delayed neutrons from the fission of Pu^{239} ($E_n \simeq$ fission spectrum). The results to date are given in Table IV.

Independent measurements on the delayed neutrons from U^{238} have been made by Sher and Heintze at Brookhaven. Samples of natural and depleted (1:10^5) uranium were irradiated in the Brookhaven National Laboratory pile. The detector was a BF_3 counter surrounded by paraffin, located at the terminus of a pneumatic transfer tube ("rabbit"). Short scaler-readout intervals ($\sim$ 0.2 sec) were accomplished by intermittent photography of the output scaler; i.e., the scaler was turned on and off at short time intervals and the interpolation lights photographed during the "off"-interval. The data analysis procedure was as follows: a least-squares fit was first made on irradiations of U^{235}, assuming the periods of Hughes *et al.*[10] The relative initial intensities obtained for U^{235} were then compared with the saturated abundance values reported by Hughes thus giving for each neutron group an empirical correction factor including the irradiation-time and counter-response corrections. These same factors were used to correct the observed initial intensities for U^{238} (obtained with identical counting geometry and irradiation time). The resulting yield-per-fission ratios for U^{238} (Table V) are appreciably larger than corresponding ratios from Table II.

Due to the relatively long transit time (1.5 sec) of the "rabbit," it was not possible to determine the shorter period contributions accurately.

Relative total yield measurements were also made at Brookhaven on U^{238} and U^{235} by means of a multiple-foil "sandwich." The "sandwich" made by interposing a thin foil of the fissile material between two polyethylene fission-fragment-catcher foils, was irradiated to saturation in the Brookhaven National Laboratory pile. Delayed neutron yield was then cal-

Table IV. Delayed Neutron Period and Relative Abundance Values for Pu^{239} — Los Alamos

Group index i	$\tau_{i\,1/2}$* (*sec*)	a_i/a_t†
1	53.7 ± 3.6	.037 ± .016
2	22.9 ± 1.1	.265 ± .037
3	6.11 ± 0.24	.193 ± .019
4	2.14 ± 0.06	.378 ± .013
5	0.40 ± 0.03	.120 ± .007
6	0.15 ± 0.05	.007 ± .004

* Calculated probable errors (from IBM-701 computer).
† Includes correction for detector response (BF_3 counter in modified "long" geometry).

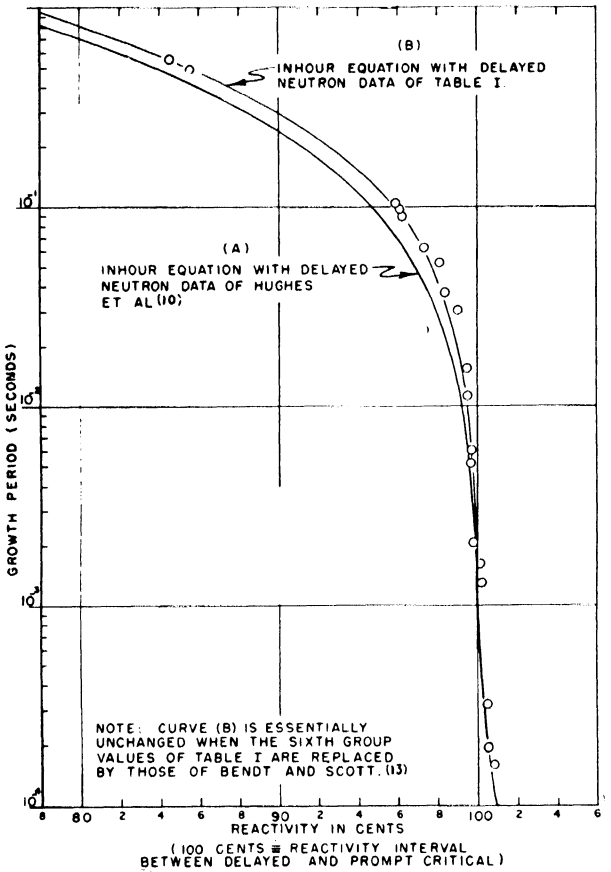

Figure 3. Period vs reactivity for the bare U^{235} assembly near prompt critical (points are from direct measurements (Los Alamos)). Note: curve (B) is essentially unchanged when the sixth group values of Table I are replaced by those of Bendt and Scott[13]

culated from the fissile foil counting data and normalized to number of fissions as determined from catcher-foil data. In this way the ratio of delayed neutron yield per fission in U^{238} to that in U^{235} was found to be 2.9 ± 0.3.

The absolute total yields of delayed neutrons per fission for five different fissile elements have been measured at Los Alamos (cf., Table VI) using the method outlined in Appendix B. The number of delayed neutrons is determined from neutron counting data following an instantaneous irradiation, and the number of fissions is determined by counting the 67-hr Mo^{99} (chemically separated) fission-fragment β-activity.

From measurements of mass increments between delayed and prompt critical for the bare U^{235} assembly (Godiva) and a bare Pu^{239} critical assembly (Jezebel), it has been determined that

$$\gamma_J f(Pu^{239})/\gamma_G f(U^{235}) = 0.32_4$$

where γ_J *and* γ_G are ratios of effectiveness of delayed neutrons to effectiveness of prompt neutrons for Jezebel and Godiva, respectively. The approximation $\gamma_J = \gamma_G = 1$, and the value $n/F(U^{235}) = 0.0173$ from Table VI gives

$$n/F(Pu^{239}) = 0.32_4 n/F(U^{235})\nu(Pu^{239})/\nu(U^{235}) = 0.0067$$

in agreement with the Pu^{239} yield given in Table VI. It will be noted that total delayed neutron yield decreases with atomic number while it increases with mass number for the uranium isotopes. This increase with mass number is due largely to greater relative abundances of the short-period groups, as for example in U^{238} compared to U^{235}.

A comparison of the existing results of delayed neutron measurements can be made by referring to Table VII. Substantial differences will be noted in the values reported by different authors for τ_3, τ_4, and τ_6 (U^{235}). However, the general agreement among period measurements (e.g., present values: Tables I through IV) for the various nuclides suggests the same delayed neutron precursors are produced in fission regardless of the fissioning nuclide. (Note that measured delayed neutron periods could be somewhat longer than radiochemically determined periods—i.e., β-activity of the chemically-separated precursor nuclide—due to cascade β-decay to the final neutron-emitting nuclide; the magnitude of this effect would, of course, depend on period values in the decay chain.)

It is generally accepted[35,36] that delayed neutron precursors should exhibit even neutron numbers slightly above the 50- or 82- stable shell configurations (i.e., the two "magic numbers" near the peaks of the fission yield curve). These precursors then decay by β-emission to excited states in odd-neutron-numbered nuclides which, being least tightly bound, have the greatest probability for neutron emission. All the known or hypothesized delayed neutron precursors support this assumption; viz., the chemically identified[5,30] Br^{87} 55 sec, I^{137} 22 sec, and Br^{89} (or Br^{91}) 5 sec activities and the hypothesized[30,33] Sb^{135} 2 sec and Sb^{137} (or As^{85}) 0.44 sec activities. Mass assignments for the latter isotopes were made from fission-fragment range measurements.

Table V. Delayed Neutron Yield Ratios for U^{238}—Brookhaven

$\frac{a_2}{a_1} = 15.9$	$\frac{a_4}{a_1} = 79.5$
$\frac{a_3}{a_1} = 28.6$	$\sum_1^4 a_i(238) / \sum_1^4 a_i(235) = 2.9$

Table VI. Absolute Total Yields of Delayed Neutrons—Los Alamos

Fissile isotope	U^{235}	U^{238}	Pu^{239}	U^{233}	Th^{232}
Absolute yield (Delayed neutrons per fission)	0.0173 ±0.0007	0.044 ±0.003	0.0067 ±0.0003	0.0078 ±0.0004	0.063 ±0.006

The available values of chemical fission yields for the different isotopes do not permit an accurate correlation with measured delayed neutron yields. Nevertheless it is useful to compare the yields of Table I with recent calculations[33] on delayed neutron emission probability. Starting with the original Bohr-Wheeler hypothesis and using Fermi β-decay theory, Pappas (loc. cit.) has computed the probability of delayed neutron emission as a function of a "charge stability" parameter, cf., Fig. 4. Emission probabilities calculated from the yield data of Table I are seen to be in general agreement with Pappas' theoretical curve. Although these results are certainly not definitive, present theory and experiment seem to be consistent.

Measurements on the delayed neutrons from fission of U^{235}, U^{238}, and Pu^{239} are continuing at Los Alamos with the experimental arrangement described above. Similar period and abundance measurements on U^{233}, Th^{232}, Th^{230}, Pu^{240}, Pa^{231}, and Am^{241} are also planned.

APPENDIX A. COMPARISON OF INSTANTANEOUS AND INFINITE IRRADIATIONS

The decay of delayed neutron activity following a saturation irradiation can be represented by:

$$\sum_{i=1}^{6} a_i e^{-\lambda_i t}$$

where a_i is the saturated abundance—and λ_i the decay constant—of the ith group. The summation includes the six "well-established" delayed neutron groups, excluding the (negligible) contribution of any long-period groups. Following an irradiation of total time T, the observed initial delayed neutron activity should be proportional to

$$\sum_{i=1}^{6} a_i(1 - e^{-\lambda_i T})$$

for a burst irradiation ($T \ll \lambda_i^{-1}$) we can make the approximation:

$$\sum_{i=1}^{6} a_i(1 - e^{-\lambda_i T}) \approx \sum_{i=1}^{6} a_i \lambda_i T$$

Thus the initial delayed neutron activity is proportional to $\sum a_i\lambda_i$ for an instantaneous irradiation, and proportional to $\sum a_i$ for an infinite irradiation. This effective weighting of initial activity by the factor λ_i following an instantaneous irradiation is clearly advantageous in studying the short-period delayed neutron groups.

APPENDIX B. DETERMINATION OF ABSOLUTE DELAYED NEUTRON YIELD FROM INSTANTANEOUS IRRADIATION DATA

The basic data for determining absolute yield is, (1) $\sum_{NC} \equiv$ total neutron counts following an instantaneous irradiation and (2) $F_s \equiv$ total fissions in the sample irradiated. F_s is determined by means of a fission-chamber monitor which has been calibrated against independent radiochemical fission-yield measurements. To take account of differing fission cross sections for the different sample materials, use is made of known relative fission cross-section values averaged over the source spectrum at the point of irradiation. For an instantaneous irradiation:

$$\sum_{NC} = F_s \epsilon \sum_{i=1}^{6} \int_0^{\infty} a_i \lambda_i e^{-\lambda_i t}\, dt = F_s \epsilon \sum_{i-1}^{6} a_i$$

where t is measured from the time of the burst, $\epsilon =$ absolute efficiency of (flat-response) detector in counts per source neutron, $a_i =$ abundance of ith group in delayed neutrons per fission, and $\sum a_i =$ absolute yield in total delayed neutrons per fission.

Absolute yield $= \sum a_i = \sum_{NC}/F_s\epsilon$

Since the initial counting rate following an infinite irradiation is proportional to $\sum a_i$, this may be used to check yield values as obtained above from the instantaneous irradiation data.

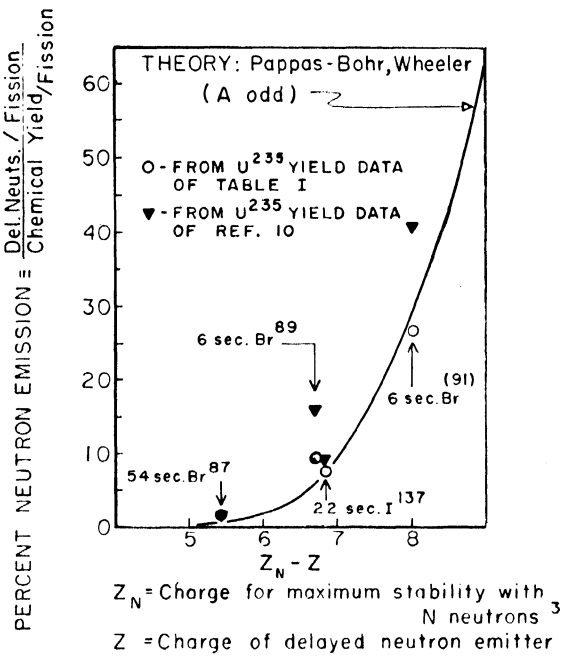

Figure 4. Probability of delayed neutron emission (U^{235}): Z_n = charge for maximum stability with N neutrons[33]; Z = charge of delayed neutron emitter

REFERENCES

1. Bohr, N. and Wheeler, J. A., *The Mechanism of Nuclear Fission,* Physical Review *56*: 426-50 (1939).
2. Anderson, H. L., Fermi, E., Wattenberg, A., Weil, G. L. and Zinn, W. H., *Method for Measuring Neutron-Absorption Cross Sections by the Effect on the Reactivity of a Chain-Reacting Pile,* Physical Review *72*: 16-23 (1947).
3. Nordheim, L. W., *Pile Kinetics,* MDDC-35 (1946); Physical Review *70*: 115 (1946).
4. Snell, A. H., Nedzel, V. A., Ibser, H. W., Levinger, J. S., Wilkinson, R. G. and Sampson, M. B., *The Decay Curve and the Intensity of the Delayed Neutrons, I,* Physical Review *72*: 541-4 (1947).

Table VII. Summary of Delayed Neutron Measurements*

These tables include the major work on delayed neutrons reported since 1947 with the exception of (1) mean energies of the delayed neutron groups (Refs. 10, 21, and 34); (2) the ultra-low yield delayed neutron groups (discussed in Part I of this paper); and (3) chemical identification of the β-unstable delayed neutron percursors (cf. Refs. 5, 30, and 33).

U^{235} (Enriched Uranium)

Group index i	E_n = thermal (Normal U_3O_8) Ref. 4 $\tau_{1/2}$	E_n = thermal (Normal U_3O_8) (U of C) a_i/a	E_n = thermal (Enriched U) Ref. 25 $\tau_{1/2}$	E_n = thermal (Enriched U) (ANL) a_i/a	E_n = thermal (UH^{10}~89% U^{235}) Ref. 10 $\tau_{1/2}$	E_n = thermal (UH^{10}~89% U^{235}) (ANL) a_i/a	E_n = slow (UH^{10}~73% U^{235}) Ref. 11 $\tau_{1/2}$	E_n = slow (UH^{10}~73% U^{235}) (LASL) a_i/a	E_n = fission spectrum (~95% U^{235}) Ref: this paper $\tau_{1/2}$	E_n = fission spectrum (~95% U^{235}) (LASL) a_i/a	E_n = fission spectrum (99.9% U^{235}) Ref: this paper $\tau_{1/2}$	E_n = fission spectrum (99.9% U^{235}) (LASL) a_i/a
1	56.0	0.045	55.0	0.035	55.6 ± 0.2	0.034 ± 0.009	55.4 ± 0.69	0.054	54.0 ± 0.9	0.035 ± 20%	54.3 ± 0.9	0.036 ± 0.006
2	23.0	0.319	22.47	0.240	22.0 ± 0.2	0.220 ± 0.023	22.4 ± 0.42	0.294	22.4 ± 0.5	0.230 ± 20%	21.7 ± 0.8	0.210 ± 0.019
3	4.4	0.350	4.43	0.327	4.51 ± 0.1	0.282 ± 0.017	5.5 ± 0.35	0.297	5.50 ± 0.08	0.180 ± 20%	5.87 ± 0.17	0.192 ± 0.027
4	1.8	0.159	1.13	0.398	1.52 ± 0.05	0.319 ± 0.017	1.7 ± 0.21	0.279	2.11 ± 0.03	0.406 ± 20%	2.18 ± 0.07	0.409 ± 0.022
5	0.4	0.127	–	–	0.43 ± 0.05	0.112 ± 0.011	0.36 ± 0.07	0.076	0.44 ± 0.02	0.124 ± 20%	0.46 ± 0.03	0.135 ± 0.008
6	–	–	–	–	0.05 ± 0.02	0.033	–	–	0.114 ± 0.010*b*	0.025 ± 20%‡	0.126 ± 0.018	0.018 ± 0.004
Absolute yield	0.010 ± 0.002 (*f*)		0.0078 (*f*)†			0.00755 (*f*)						0.0173 ± 0.0007 (*n*/*F*)

† Independent measurement; cf. declassified document CP-2317 (1944).
‡ Independent measurements of $\tau_6 = 0.150 \pm 0.041$ and $a_6/a = 0.027 \pm 0.007$ are reported in ref. 13.

U^{238}

Group index i	$E_{n\,max}$ = 14 Mev (99.3% + Cd) Ref. 29 (Westinghouse) $\tau_{1/2}$	$E_{n\,max}$ = 14 Mev (99.3% + Cd) Ref. 29 (Westinghouse) a_i/a	E_n = fission spectrum (>99.99%) Ref: this paper $\tau_{1/2}$§	E_n = fission spectrum (>99.99%) (BNL) a_i/a	E_n = fission spectrum (99.97%) Ref: this paper $\tau_{1/2}$§	E_n = fission spectrum (99.97%) (LASL) a_i/a
1	55.2	0.034	55.6	0.008	53.0 ± 1.7	0.008 ± 0.003
2	22.6	0.282	22.0	0.127	22.0 ± 0.6	0.101 ± 0.040
3	5.8	0.188	4.51	0.229	5.30 ± 0.33	0.158 ± 0.050
4	1.7	0.376	1.52	0.636	2.00 ± 0.11	0.408 ± 0.033
5	0.4	0.120	0.43	–	0.51 ± 0.06	0.238 ± 0.025
6	–	–	0.05	–	0.18 ± 0.02	0.087 ± 0.010
Absolute yield	0.08 ± 0.03 (*n*/*F*)		0.046¶ (*n*/*F*)		0.044 ± 0.003 (*n*/*F*)	

§ Assuming U^{235} periods of ref. 10.
¶ Based on n/F (U^{235}) = 0.016 for 4 periods.

U^{233}

Group index i	E_n = thermal Ref. 26 $\tau_{1/2}$**	E_n = thermal (ANL) a_i/a	E_n = fission spectrum Ref: this paper $\tau_{1/2}$	E_n = fission spectrum (LASL) a_i/a
1	55.6	0.075 ± 0.002		
2	22.0	0.238 ± 0.019		
3	4.51	0.350 ± 0.019		
4	1.52	0.254 ± 0.019		
5	0.43	0.083 ± 0.024		
6	0.05	–		
Absolute yield		0.0024†† (*f*)		0.0078 ± 0.0004 (*n*/*F*)

** Assuming U^{235} periods of ref. 10.
†† Based on $f(U^{235}) = 0.0073$ for 5 periods.

Table VII. Summary of Delayed Neutron Measurements (Continued)

Pu^{239}

Group index i	E_n = thermal		E_n = thermal		$E_{n\,max}$ = 0.6 Mev		$\bar{E}_n$ = fission spectrum		$\bar{E}_n$ = fission spectrum	
	Ref. 24	(LASL)	Ref. 25	(ANL)	Ref. 27 ***	(LASL)	Ref. 32	(Harwell)†††	Ref: this paper	(LASL)
	$\tau_{1/2}$	a_i/a	τ	a_i/a		a_i/a		a_i/a	τ	a_i/a
1	55.2	0.040	55.0 ± 0.27	0.030 ± 0.001	55.4	0.033	55.8 ± 0.5	0.025 ± 0.004	53.7 ± 3.6	0.037 ± 0.016
2	22.5	0.288	22.4 ± 0.33	0.294 ± 0.007	22.4	0.327	21.9 ± 0.4	0.229 ± 0.005	22.9 ± 1.1	0.265 ± 0.037
3	5.2	0.371	4.5 ± 0.13	0.322 ± 0.009	5.5	0.265	4.22 ± 0.15	0.341 ± 0.019	6.11 ± 0.24	0.193 ± 0.019
4	1.1	0.301	1.05 ± 0.04	0.354 ± 0.021	1.7	0.270	1.07 ± 0.06	0.405 ± 0.036	2.14 ± 0.06	0.378 ± 0.013
5	–	–	–	–	0.31	0.105	–	–	0.40 ± 0.03	0.120 ± 0.007
6	–	–	–	–	–	–	–	–	0.15 ± 0.05	0.007 ± 0.004
Absolute yield	$[0.0055(n/F)]$‡‡ $0.0030(f)$§§		$0.008(n/F)$¶¶		$0.0068 \pm 0.0004(n/F)$				$0.0067 \pm 0.0003(n/F)$	

‡‡ Independent measurement (ref. 31). Based on $n/F(U^{235}) = 0.019$ for 6 periods.
§§ Based on $f(U^{235}) = 0.00645$ for 4 periods.
¶¶ Based on $n/F(U^{235}) = 0.016$ for 4 periods.
*** Assuming periods of de Hoffmann (ref. 11) except τ_6.
††† Data for a Pu–U composite core ("Zephyr" reactor).

Th^{232}

Group index i	$E_{n\,max}$ = 24 Mev		$E_{n\,max}$ = 14 Mev		E_n = fission spectrum	
	Ref. 28	(Ohio State)	Ref. 29	(Westinghouse)	Ref: this paper‡‡‡	(LASL)
	$\tau_{1/2}$	a_i/a	$\tau_{1/2}$	a_i/a	$\tau_{1/2}$	a_i/a
1	55.6	0.041	56.0	0.136	54.0 ± 1.0	0.033 ± 0.003
2	22.0	0.146	20.0	0.318	22.0 ± 0.5	0.133 ± 0.015
3	4.5	0.292	4.4	0.303	6.2 ± 1.0	0.172 ± 0.050
4	1.51	0.266	1.4	0.191	2.1 ± 0.4	0.458 ± 0.055
5	–	–	0.41	0.052	0.52 ± 0.1	0.169 ± 0.025
6	0.13	0.255	–	–	0.18 ± 0.02	0.035 ± 0.010
Absolute yield			$0.08 \pm 0.03(n/F)$		$0.063 \pm 0.006(n/F)$	

‡‡‡ Preliminary data only.

* For each investigation, the following are tabulated: (1) $\bar{E}_n$, average energy of neutrons used to produce fission, (2) isotopic purity of fissile material, where indicated, (3) literature reference and laboratory where work was done, and (4) the half-lives and relative abundances of the delayed neutron groups. Half-lives, in seconds, are tabulated with probable errors, where indicated in the original paper. Relative abundances (corrected for detector response, where indicated) are given as a_i/a, the fraction of total delayed neutrons ($\Sigma a_i \equiv a$, total delayed neutrons emitted). Absolute total yields are given in the units of the original measurement; i.e., either as f, the delayed neutron fraction of total neutrons from fission, or as $n/F \equiv$ delayed neutrons per fission. (Note when n/F is measured, the dependence of yield on neutron energy thru ν (En) is eliminated; i.e., $f = (1/\nu)(n/F)$ where ν is the number of neutrons emitted per fission.) Unless otherwise stated, the yield reported in a given paper is based on the number of delayed neutron groups reported in that paper.

5. Snell, A. H., Levinger, J. S., Meiners, E. P. Jr., Sampson, M. B. and Wilkinson, R. G., *Studies of the Delayed Neutrons, II,* Physical Review *72*: 545-9 (1947).
6. Roberts, R. B., Meyer, R. C. and Wang, P., *Further Observations on the Splitting of Uranium and Thorium,* Physical Review *55*: 510-11 (1939); Roberts, R. B., Meyer, R. C., Hafstad, L. R. and Wang, P., *The Delayed Neutron Emission Which Accompanies Fission of Uranium and Thorium,* Physical Review *55*: 664 (1939).
7. Booth, E. T., Dunning, J. R. and Slack, F. G., *Delayed Neutron Emission From Uranium,* Physical Review *55*: 876 (1936).
8. Gibbs, D. F. and Thomson, G. P., *Possible Delay in Emission of Neutrons From Uranium,* Nature *144*: 202 (1939).
9. Brostrom, K. J., Koch, J. and Lauritsen, T., *Delayed Neutron Emission Accompanying Uranium Fission,* Nature *144*: 830 (1939).
10. Hughes, D. J., Dabbs, J., Cahn, A. and Hall, D., *Delayed Neutrons From Fission of* U^{235}, Physical Review *73*: 111-24 (1948).
11. de Hoffmann, F., Feld, B. T. and Stein, P. R., *Delayed Neutrons From* U^{235} *After Short Irradiation,* Physical Review *74*: 1330-7 (1948).
12. Brolley, J. E. Jr., Cooper, D. H., Hall, W. S., Livingston, M. S. and Schlacks, L. K., *A Search for Short Period Activities From* U^{235} *Fission Products,* Physical Review *83*: 990-3 (1951).
13. Bendt, P. J. and Scott, F. R., *Short-Period Delayed Neutrons From Fission,* Physical Review *97*: 744-53 (1955).
14. Kunstadter, J. W., Floyd, J. J. and Borst, L. B., *Long-Lived Delayed Neutrons From Fission,* Physical Review *91*: 594-6 (1953).
15. Sher, R. (Private Communication — 1955).
16. Kane, W. R., Kephart, J. F. and Hammel, J. E., *Search for a 125 Minute Delayed Neutron Activity,* (in press).
17. Bernstein, S., Preston, W. M., Wolfe, G. and Slattery, R. E., *Yield of Photoneutrons From* U^{235} *Fission Products in Heavy Water,* Physical Review *71*: 573-81 (1947).
18. Spatz, W. D., Hughes, D. J. and Cahn, A., *Photoneutrons Produced in* D_2O *and Be by Fission Product Gamma Rays,* MDDC-871 (1947); Physical Review *72*: 163 (1947).
19. Johns, M. and Sargent, B., *Photoneutrons in a Heavy Water Pile,* Canadian Journal of Physics *32*: 136-146 (1954).
20. Koontz, P. G., Keepin, G. R. and Ashley, J. E., *Zns(Ag) Phosphor Mixtures for Neutron Scintillation Counting,* Review of Scientific Instruments *26*: 352-6 (1955).
21. Burgey, M., Pardue, L. A., Willard, H. B. and Wollan, E. O., *Energies of the Delayed Neutrons From* U^{235} *Fission Products,* MDDC-16; Physical Review *70*: 104 (1946).
22. Koontz, P. G., Johnstone, C. W., Keepin, G. R. and Gallagher, J. D., *A New Recording Multichannel Time Delay Analyzer,* Bulletin American Physical Society *30*: 64 (1955); Review of Scientific Instruments *26*: 546-554 (1955).
23. Hanson, A. and McKibben, J., *A Neutron Detector Having Uniform Sensitivity From 10 kev to 3 Mev,* Physical Review *72*: 673-7 (1947).
24. de Hoffmann, F. and Feld, B. T., *Delayed Neutrons From* Pu^{239}, Physical Review *72*: 567-9 (1947).
25. Redman, W. and Saxon, D., *Delayed Neutrons in Plutonium and Uranium Fission,* Physical Review *72*: 570-5 (1947).
26. Cahn, A., Dabbs, J. and Hughes, D. J., *Delayed Neutrons From Fission of* U^{233}, Declassified document CP-3147 (1945).
27. Perry, R., (Private Communication — 1945).
28. Creveling, L. G., Hood, J. R. and Pool, M. L., *Delayed Neutrons From Thorium,* Physical Review *76*: 946-8 (1949).
29. Sun, K. H., Charpie, R. A., Pecjak, F. A., Jennings, B., Nechaj, J. F. and Allen, A. J., *Delayed Neutrons From* U^{238} *and* Th^{232} *Fission,* Physical Review *79*: 3-5 (1950).
30. Sugarman, N., *Short-Lived Halogen Fission Products,* Journal Chemical Physics *17*: 11-25 (1949); and Journal Chemical Physics *15*: 544 (1947).
31. Wilson, R. R., *Delayed Neutrons From* Pu^{239}, Physical Review *71*: 560 (1947).
32. Holmes, J., *Operational Features of Zephyr,* Journal of Nuclear Energy *1*: 47 (1954).
33. Pappas, A., *A Radiochemical Study of Fission Yields in the Region of Shell Perturbations and the Effect of Closed Shells in Fission,* (1953), Laboratory for Nuclear Science, Report No. 63, Massachusetts Institute of Technology.
34. Bonner, T. W., Bame, S. J. and Evans, J. E., *The Energy of the Delayed Neutrons From the Fission of* U^{235} (in press).
35. Mayer, M. G., *On Closed Shells in Nuclei,* Physical Review *74*: 235 (1948).
36. Coryell, C. D. and Sugarman, N., Paper No. 52, NNES Div. IV, 9 (1951).

The Study of Delayed Neutrons Emitted by Uranium-233 as a Result of Irradiation by Thermal Neutrons

By S. V. Girshfeld, USSR

ABSTRACT

It was shown that as irradiation of the sample with thermal neutrons ceases, U^{233} emits delayed neutrons. These neutrons were registered by a fast-neutron counter. An approximate decay curve of delayed neutrons in U^{233} was obtained and their yield, which was close to 0.25 per cent, was evaluated.

In the second part of the work, the samples of U^{233} and U^{235} were alternately activated near the wall of the reactor and were transferred to the fast-neutron counter by a pneumatic transfer to the method of tape pulse-notation. Four periods of delayed neutrons, known in the case of U^{235}, were detected in U^{233}. This made it possible to determine the yields of the respective groups of neutrons in U^{233} by comparison with the delayed neutron yields in U^{235}, which are known. For this purpose, a comparison was made of the number of delayed neutrons of each group emitted by the U^{233} sample with the number of neutrons of the same group from U^{325}; in addition a separate experiment was performed to compare the total fluxes of all secondary neutrons from U^{233} and U^{235} samples during radiation. The results obtained are given in Table I.

DETECTION OF DELAYED NEUTRONS IN U^{233} AND EVALUATION OF THEIR YIELD

Experimental Arrangement

Registration of delayed neutrons and fission neutrons was performed by a fast-neutron counter shown in Fig. 1, which figure also gives schematically the relative position of the boron-cadmium shutter (8), and the counter and uranium sample. The shutter is designated for quick stopping irradiation of the sample by thermal neutrons. The counter (1), filled with BF_3, was placed inside a paraffin block (2). On the outside, the block was shielded from thermal neutrons by a layer of cadmium (5) and a layer of boric acid (4).

The sample (12 gm of U^{233}) was inserted into a cylindrical depression (9) of the front wall of the set-up, thus being open to irradiation by neutrons of the thermal column only from one side, the front, if the boron-cadmium shutter is open.

The design of the shutter is shown schematically in Fig. 2. It consists of two halves hinged at (1). When lock (5) is released, the springs (2) pull the shutter-halves down, causing them to form a disc-shaped shield. This is the position of the shutter shown in Fig. 2. The thickness of the layer of boron carbide in the shutter is 15 mm.

The remote shutter control is through thin steel cables. The time constant of the shutter is 0.01 sec.

The signal from the neutron counter goes to the cathode follower (7), which is connected through a shielded cable to the amplifier (located in the hall), a discriminator and a scaler.

Procedure and Experimental Results

The experiments were conducted in the thermal column (see Fig. 3) with four graphite blocks between the fast-neutron counter and the reactor (the total length of the graphite was about 2.5 m).

The method of investigating delayed neutrons was as follows. First, with the shutter open, the counting rate of all secondary neutrons of the sample was measured. After this measurement, the grid of the first tube of the biased multivibrator of the scaler was grounded through a special contact circuit, as a result of which the scaler was stopped.

After that, the mechanical register at the output of the scaler was set to zero (this register is connected in series with the oscillograph recorder); and the recorder transport started. Following this, the shutter was thrown, with simultaneous starting of a stopwatch. At the moment the shutter closed the contact grounding the tube of the scaler was disconnected; so that the scaler was ready for registration of pulses from delayed neutrons. In addition, a current pulse was given to mark the time $t = 0$ (i.e., the moment the shutter closed, the end of irra-

Original language: Russian.

Table I

Period m (sec)	$T_5 = 55.3 \pm 0.9$	$T_4 = 22.2 \pm 0.2$	$T_3 = 4.5 \pm 0.04$	$T_2 = 1.5 \pm 0.07$	$T_1 = 0.43$
Yield in %	0.023 ± 0.0020	0.074 ± 0.0058	0.094 ± 0.0093	0.067 ± 0.0078	< 0.02

Total yield of delayed neutrons in U^{233}: 0.258%

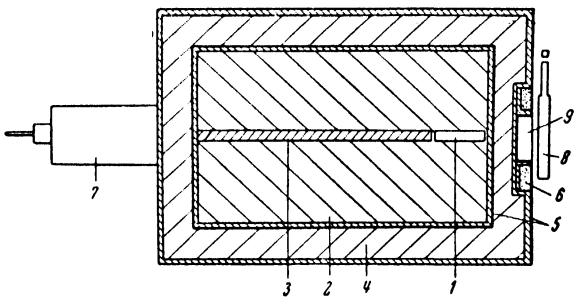

Figure 1. Diagram of fast neutron counter: (1) BF_3 counter; (2) paraffin; (3) paraffin; (4) boric acid; (5) cadmium; (6) boron carbide; (7) cathode follower; (8) shutter; and (9) room for sample

diation of the sample). A third pen was used to mark the time scale on the tape; its coil was given a sine frequency of 50 cycles. In 40 sec the counting rate had fallen to such an extent that registration on the tape had ceased, and the remaining pulses were registered by means of the stopwatch right up until the emission of delayed neutrons ceased.

A total of 23 such experiments were performed on the basis of which, after background corrections, an average curve for the time dependence of delayed neutrons was plotted. The total number of delayed neutrons registered in all 23 experiments was about 700, which was sufficient for certain qualitative conclusions.

Figure 4 shows the curve found for the delayed neutrons of U^{233}, and Fig. 5 shows the initial portion of this curve (up to $t = 1$ sec). The activation time

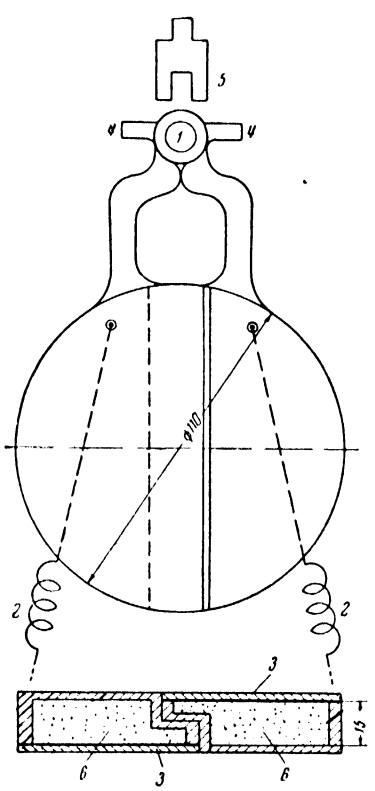

Figure 2. Neutron shutter: (1) hinge; (2) springs; (3) steel; (4) latches; (5) shutter lock; and (6) boron carbide

of the sample in these experiments was 10 minutes. This time is sufficient for establishing saturation flux of delayed neutrons.

From the curve in Fig. 5, we may draw the qualitative conclusion that among the groups of delayed neutrons from U^{233} there are few with periods of the order of hundredths and tenths of a second.

From the initial slope of the curve one sees that the counting rate of delayed neutrons at $t = 0$ equals 3 counts per second. The counting rate of all secondary neutrons in the case of open shutter, taking account of the resolution of the circuit (see below concerning the circuits resolution power), is 76,000

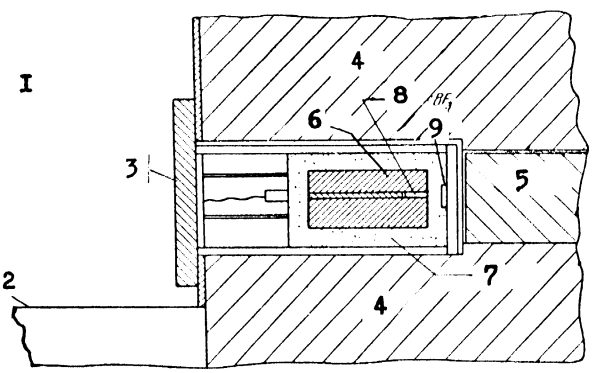

Figure 3. Position of fast-neutron counter in thermal column: (1) hall; (2) floor; (3) door of thermal column; (4) graphite; (5) graphite brick; (6) paraffin; (7) boron shield; (8) BF_3 counter; and (9) sample

counts per minute. Hence, the total yield of delayed neutrons is close to 0.25 per cent. This figure is approximate since the statistical accuracy of the results obtained in the thermal column is very low, and, also, strictly speaking, this delayed neutron flux cannot be compared with the stationary fission neutron flux because of the difference in their energy spectra.

MEASURING YIELDS OF DELAYED NEUTRONS IN U^{233} BY COMPARISON OF YIELDS IN U^{235}

Method

A more detailed investigation of the delayed neutrons of U^{233} was performed with the aid of the pneumatic transfer device. A small piece of U^{233} foil (58.9 mg) was fastened to a duralumin shuttle and was moved by compressed air to the reactor wall where it was activated during ten minutes, after which it was thrown out to the fast-neutron counter to obtain a delayed-neutron decay curve. Because of the high activation of the sample, the statistical accuracy of the decay curve was very high, and it was possible to analyse it into its partial exponentials and so to determine the delayed neutron periods. The experiment performed with a sample of U^{233} showed the presence of the same delayed neutron groups which are found in the case of U^{235} (with the exception of the group with period $T_1 = 0.43$ sec, which we could not detect). This made it possible to measure the yields of delayed neutrons in U^{233} through comparison with the known yields in U^{235}.

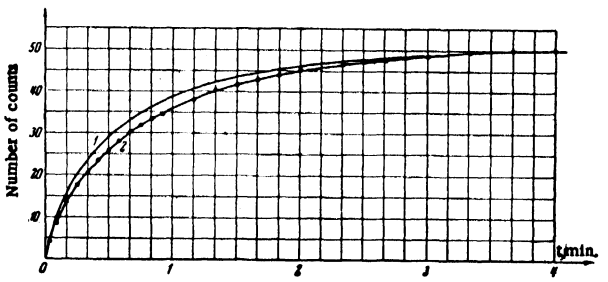

Figure 4. (1) $\phi(t)$, i.e., total counts curve calculated from data obtained on rabbit; and (2) experimental total count curve from delayed neutrons of U^{233} obtained in experiments in the thermal column

In explaining this procedure we shall use the following symbols.

Groups of delayed neutrons will be designated by the symbol i (i is 1, 2, 3, 4, 5 for groups with periods, respectively, of 0.43 sec, 1.4 sec, 4.6 sec, 22.2 sec, and 55.3 sec).

I is the maximum (saturated) number of all secondary neutrons emitted per second by the sample U^{233} in the case of long irradiation.

I_i is the delayed-neutron flux of group i, emitted per second by the same sample at the moment the long activation ceases.

$\alpha_i = 100 I_i/I$ is the yield in per cent of the ith group of delayed neutrons in U^{233}.

$\alpha = \sum_{i=2}^{5} \alpha_i$ is the total yield of delayed neutrons in U^{233}. Designating these same quantities for U^{235} by I', I_i', α_i and α', we obtain

$$\alpha_i = \alpha_i' \cdot \frac{I_i}{I_i'} \cdot \frac{I'}{I} \qquad (1)$$

For a determination of the yields α_i in U^{233} by comparing with the known yields of α_i' in U^{235} it is necessary to do the following:

1. To determine the ratio of the delayed-neutron fluxes of each group in U^{233} and U^{235} (I_i/I_i'). This may be done by analyzing the decay curves of delayed neutrons from U^{233} and from U^{235} in terms of exponentials extrapolating these to the end of activation ($t = 0$). Comparison of the fluxes with the aid of a fast-neutron counter is justified in this case, because fluxes of one and the same group of neutrons with one and the same energy spectrum are compared.

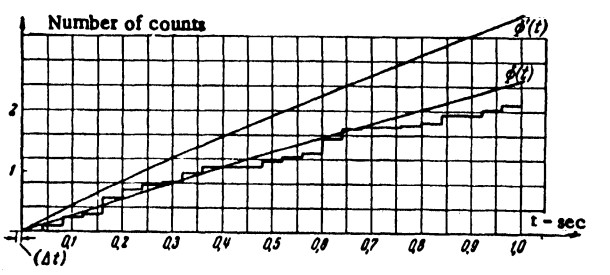

Figure 5. First part of total count curve up to $t = 1$ sec (steps)

2. To determine the ratio of the total fluxes of secondary neutrons from the samples during irradiation (I'/I).

COMPARISON OF TOTAL SECONDARY NEUTRON FLUXES FROM SAMPLES OF U^{233} AND U^{235} DURING IRRADIATION

To determine the ratio I'/I, the samples (58.9 mg of U^{233} and 33.2 mg of U^{235}) were alternately put in the center of the beam emerging through a channel in the reactor shield. A fast-neutron counter was placed to the side, as is shown in Fig. 6, to measure the fluxes of secondary neutrons from the samples.

The samples were placed in an envelope made of cigarette paper drawn over three fine wires mounted in a wide frame (Fig. 7). As a control experiment showed, the number of pulses from epi-cadmium neutrons of the beam scattered by the envelope and wires was negligibly small.

Epi-cadmium neutrons of the beam may also be scattered in the uranium sample itself, and then produce additional pulses. However, this effect is negligibly small in comparison with the effect of the fission neutrons, because the scattering cross section epi-cadmium neutrons by isotopes U^{233} and U^{235} is much less than the fission cross section for thermal neutrons, and, in addition, the number of epi-cadmium neutrons in the beam is small. The fact that

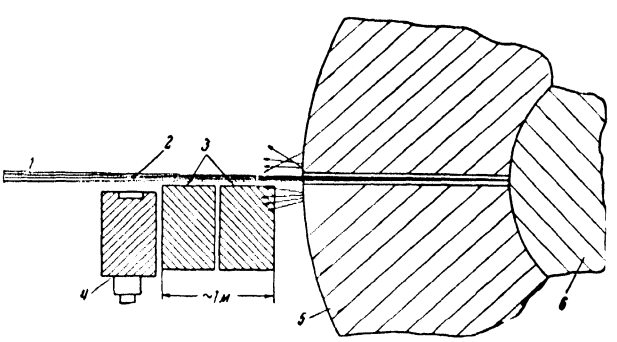

Figure 6. Fast neutron counter arrangement for measuring fission neutron flux: (1) beam; (2) sample; (3) graphite; (4) fast-neutron counter; (5) reactor shield; and (6) reactor

scattering of epi-cadmium neutrons by the samples may be disregarded was demonstrated by putting 286 mg of natural U_3O_8 powder in the envelope instead of the sample. The small rise in background, which was obtained in this case of an open beam, was entirely due to the fission of U^{235} in the natural uranium. The excess over background (a' and a), which appears when samples of uranium (U^{235} and U^{233}, respectively) are placed in the beam, is thus entirely due to the secondary neutrons emitted by the samples.

The ratio of the fluxes of secondary neutrons from samples, is, strictly speaking, not exactly equal to a'/a, because the fission neutrons from U^{235} and U^{233} have different energy spectra. However, the controlling experiment was done which showed that the

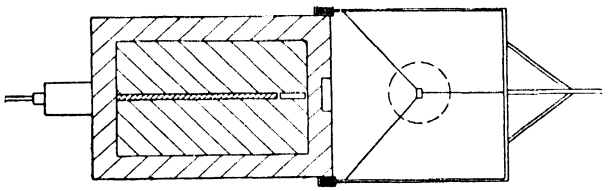

Figure 7. Device for introducing samples into the beam

difference in the efficiency of the fission neutron counter for U^{235} and U^{233} is small. In this experiment, additional blocks of paraffin and boric acid (see Fig. 8) the thickness of which was comparable to the thickness of the layer of paraffin and boric acid in the fast-neutron counter, were inserted between the counter and the sample. It turned out that the paraffin block decreased the neutron counting rate for U^{235} by a factor of 1.84 ± 0.04, and the neutron counting rate for U^{233} by a factor of 1.82 ± 0.03. The boron block, in the case of U^{235} gave a reduction of 1.49 ± 0.04, whereas in the case of U^{233} it was 1.50 ± 0.02. Thus, within the limits of error (1–2%), the decrease in the neutron-fission rate by an additional paraffin block was the same for both uranium isotopes, and the same was true for a boron block.

Hence it follows that the neutron-fission spectra from U^{235} and U^{233} may, for our problem, be considered the same, and that a comparison of the secondary neutron fluxes from two samples by the fast-neutron counter is justified.

As a result of the experiments in the beam, it was found that the ratio of fluxes of secondary neutrons from samples of U^{235} and U^{233} was $a'/a = 0.543 \pm 0.007$. However, the ratio of fluxes of secondary neutrons I'/I in Equation 1 during irradiation of the samples in the reactor is less than the ratio a'/a obtained in the external beam because of self-absorption of the primary neutrons in the samples. Self-absorption in the sample of U^{235} was greater because it had a thickness of 93.5 mg/cm², whereas the U^{233} sample had only 52.6 mg/cm². This circumstance is felt more during irradiation of the samples near the reactor core, where the flux of thermal neutrons is nearly isotropic, than in experiments in the external beam where the thermal neutrons impinge perpendicularly to the surface of the foil (in other words, in the case of isotropic irradiation the effective thickness of both samples increases, and the difference in self-absorption grows bigger). A simple geometrical calculation showed that in our case the ratio of

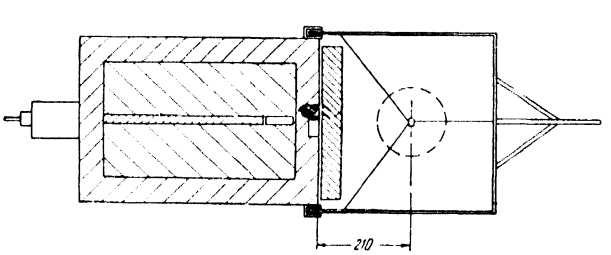

Figure 8. Same diagram as in Fig. 7 with an additional block made of paraffin or boric acid

fluxes I'/I in the case of irradiation in the isotropic flux of thermal neutrons near the reactor core is 0.93 of the ratio of fluxes a'/a obtained in the external beam. Thus $I'/I = 0.505$, and the yields of delayed neutrons in U^{233} will be found with the formula,

$$\alpha_i = 0.505\, \alpha_i' \frac{I_i}{I_i'} \qquad (2)$$

COMPARISON OF DELAYED-NEUTRON FLUXES FROM U^{233} AND U^{235}

The delayed-neutron decay curves from U^{233} and U^{235} were obtained with the aid of a rabbit. Two shuttles were alternately placed in the rabbit; one contained the U^{233} sample (58.9 mg), and the other the U^{235} sample (33.2 mg). The flight time of the shuttle was 0.4 sec. Delayed neutrons were recorded for three minutes, after that they were counted with a stopwatch.

For U^{233} eight total-count delayed neutron curves were obtained. These we shall call for the sake of brevity, integral curves. By averaging we obtained one integral curve for U^{233}. In a similar manner we obtained a mean integral curve for U^{235} from 8 integral curves. The total number of delayed neutrons registered for each sample is about 80,000.

The initial parts of the mean integral curves were corrected for the resolution of the circuits. The weights of the samples of U^{233} and U^{235} had been selected so that the initial counting rates were nearly the same. This reduces the error from inaccuracy in the determination of the resolution itself to a minimum. To determine the resolution, we obtained two integral curves from samples of U^{235} weighing 33.2 mg and 98.7 mg. The curve of the large sample was reduced to the weight of the small sample by dividing by 2.97 (=98.7/33.2). The discrepancy between these curves for large counting rates, made it possible to find the dependence of the resolution power on the real counting rate. The correction in the counting rate was -7% at the beginning of the curves. From $t = 20$ sec, corrections were insignificant. After the resolution correction, the mean integral curves were corrected for background and were analyzed.

Analysis was begun by obtaining the decay curves for both samples. For this purpose, the difference was found between the maximum ordinates of the mean integral curves for U^{233} and U^{235} (n_0 and n_0' respectively) and the ordinates n and n' of the same curves at time t, i.e., the following were found: $N(t) = n_0 - n(t)$ and $N'(t) = n_0' - n'(t)$. For U^{233} $N(t) = \sum_{i=2}^{5} \Phi_i(t)$, where $\Phi_i(t) = \Phi_{i0} \cdot 2^{-\frac{t}{T_i}}$, and for U^{235} $N'(t) = \sum_{i=1}^{5} \Phi_i'(t)$, where $\Phi_i'(t) = \Phi'_{i0} \cdot 2^{-\frac{t}{T_i}}$

$\Phi_i(t)$ is the average number of pulses from delayed neutrons of the ith group in the experiment with U^{233} registered in the time interval from t to ∞; $\Phi_i(t)$ is the same for U^{235}. The curves $N(t)$ and

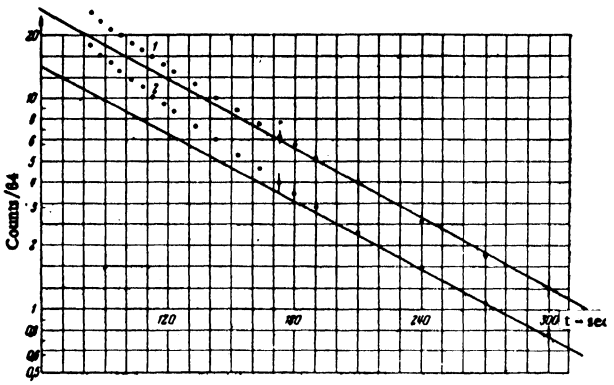

Figure 9. Selection of 55.7 sec period from experimental curves: (1) curve for U^{233} (58.9 mg); and (2) curve for U^{235} (33.2 mg)

$N'(t)$ were plotted in a semilogarithmic scale and analyzed according to the usual methods of analysis of the decay curves of a mixture of independent radioactive substances.

Figures 9, 10, 11, 12 shows exponentials Φ_5 and Φ_5', Φ_4 and Φ_4', Φ_3 and Φ_3', Φ_2 and Φ_2', from the decay curves. It was not possible to detect a period of $T_1 = 0.43$ sec in U^{233}.

By extrapolating each of the exponentials to $t = 0$, we find the values Φ_{i0} *and* Φ_{i0}'.

In order to determine the yields a_i we may set in Equation 2, $I_i/I_i' = \Phi_{i0}/\Phi_{i0}'$, which gives $\alpha_i = 0.505\ \alpha_i'\Phi_{i0}/\Phi_{i0}'$ by means of which we find the yields of delayed neutrons in U^{233}.

In order to determine the yields of neutrons with short periods more precisely, an experiment was carried out with short-time (three seconds) irradiation of samples near the reactor core. The integral curves were corrected for background and resolution. Although the exponents of periods $T_4 = 22.2$ sec and

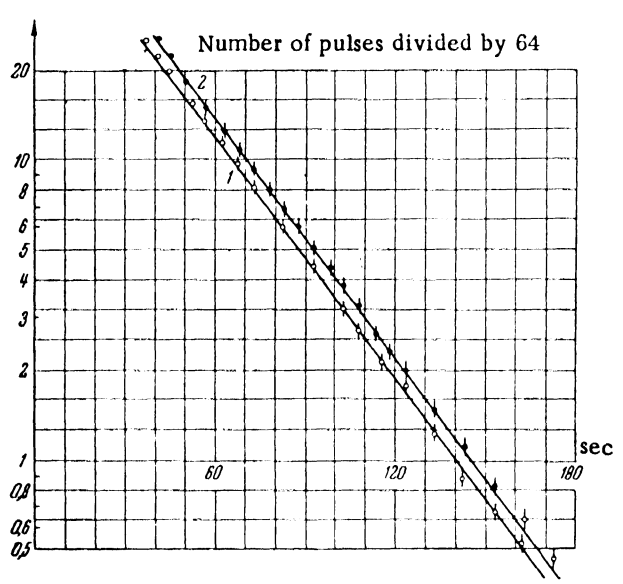

Figure 10. Selection of 22.3 sec period: (1) experimental curve for U^{233} (58.9 mg) minus the contribution of the 55.7 sec period; and (2) same for sample U^{235} (33.2 mg)

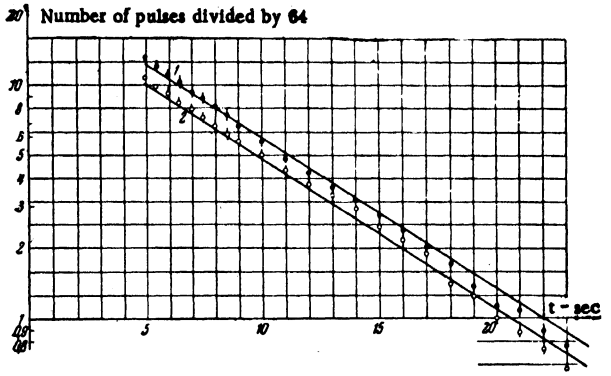

Figure 11. Selection of 4.7 sec period: (1) experimental curve for U^{235} (33.2 mg) minus the contributions of periods 55.7 sec and 22.3 sec; and (2) same for the sample of U^{233} (58.9 mg)

$T_5 = 55.3$ sec in these curves were but slightly dedectable, the curves were given a proper correction on the basis of the experiments with 10-min irradiation. The integral curves thus obtained, and due to neutrons of periods T_1, T_2 and T_3 were analyzed as described above, as a result of which more precise values for the ratios Φ_{i0}/Φ_{i0}' for the short periods T_2 and T_3 were obtained.

Table 2 gives results obtained as well as the yield values for U^{235} used in Equation 1. The total yield of delayed neutrons for U^{233} is 0.258 per cent.

If we disregard the difference in the efficiency of the fast-neutron counter with respect to instantaneous and delayed neutrons, then the total yield of delayed neutrons for U^{233} may be found from the data obtained in experiments in the thermal column (Fig. 5). In order to verify the initial counting rate of delayed neutrons use was made of the results of the experiments on the rabbit and the following function was plotted:

$$\Phi(t) = k[\Phi_{20} + \Phi_{30} + \Phi_{40} + \Phi_{50} - \Phi_{20} \cdot 2^{-t/T_2} - \Phi_{30} \cdot 2^{-t/T_3} - \Phi_{40} \cdot 2^{-t/T_4} - \Phi_{50} \cdot 2^{-t/T_5}]$$

also shown in Fig. 5. The coefficient k was chosen so as to obtain a fit at $t = 4$ min. $\Phi(t) = 50.5$ counts. The function $\Phi(t)$ follows very closely the step-curve in Fig. 5. This points to a fair agreement of the data obtained from the rabbit and those obtained

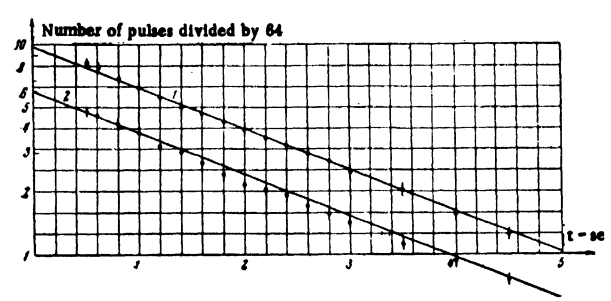

Figure 12. Selection of 1.5 sec period: (1) experimental curve for sample of U^{235} (33.2 mg), minus the contributions from periods of 55.7 sec, 22.3 sec, and 4.7 sec; and (2) same for the sample of U^{233} (58.9 mg)

Table II

Period (sec)	*55.3 ± 0.9*	*22.2 ± 0.2*	*4.5 ± 0.04*	*1.5 ± 0.07*	*0.43*
Yield for U^{233} (per cent)	0.023 ± 0.0020	0.074 ± 0.0058	0.094 ± 0.0093	0.067 ± 0.0078	< 0.02
Yield for U^{235} (per cent)	0.025 ± 0.0018	0.166 ± 0.0116	0.213 ± 0.020	0.241 ± 0.0212	0.085 ± 0.0101

in the thermal column. For comparison, the same plot gives the function $\Phi'(t)$ constructed on the basis of data obtained from the rabbit for U^{235}. The function $\Phi'(t)$ does not coincide with the step curve. If we determine the initial counting rate of delayed neutrons according to the curve $\Phi(t)$ and refer it to the counting rate of instantaneous neutrons (76,000 cpm), then the total yield in U^{233} is $\alpha = 0.22\%$.

CONCLUSION

1. Four groups of delayed neutrons, the periods and yields of which are given in Table 2, were observed in U^{233}. The periods proved the same as in the case of delayed neutrons from U^{235}, with the exception of $T_1 = 0.43$ sec which we did not succeed in detecting for U^{233}.

2. The total yield of delayed neutrons in the case of U^{233} is less than that of U^{235} and in U^{233} the long periods (in comparison with the short periods) are more abundant.

3. The relative yield of neutrons of period T_5 (if we take the yield of neutrons of period T_4 as unity), does not correspond to the relative yield of Br^{87} in U^{233} (if we take the yield of I^{137} as unity), as it should according to the scheme of the origin of delayed neutrons suggested by Snell *et al.*[2] The relative yield of neutrons of period T_5 was 1.5 times greater than expected from the relative yield of Br^{87} in U^{233}.

REFERENCES

1. Hughes, D. J., Dabbs, J., Cahn, A. and Hall, D., Phys. Rev. *73*: 111 (1948) Phys. Rev. *73*: 111 (1948).
2. Snell, A. H., Levinger, J. S., Meiners, E. P., Jr., Sampson, M. B. and Wilkinson, R. G., Phys. Rev. *72*: 545 (1947).

Record of Proceedings of Session 16A

TUESDAY AFTERNOON, 16 AUGUST 1955

Chairman: Mr. L. Janossy (Hungary)
Vice-Chairman: Mr. M. V. Pasechnik (Ukrainian SSR)
Scientific Secretaries: Messrs. N. A. Dobrotin and D. J. Littler

PROGRAMME

16A.1. Equipment and Techniques (concluded)

P/356 Testing materials by the pile oscillation method in the Châtillon reactor ..... D. Breton
DISCUSSION

P/642 A neutron spectrometer based on measuring the slowing-down time of neutrons in lead ..... A. A. Bergman *et al.*
DISCUSSION

16A.2. Cross Sections of Non-Fissionable Materials

P/832 The determination and evaluation of fundamental thermal neutron cross sections ..... J. A. Harvey
DISCUSSION

P/591 The cross section of the fission product poison Xe^{135} as a function of energy ..... S. Bernstein and E. C. Smith
DISCUSSION

16A.3. Delayed Neutrons

P/831 Delayed neutrons ..... G. R. Keepin and T. F. Wimett
DISCUSSION

Session 16A.1: Equipment and Techniques Used in Measuring Cross Sections Important to Reactor Design (concluded)

Mr. D. BRETON (France) presented paper P/356.

DISCUSSION OF P/356

Mr. J. A. HARVEY (USA): Is it possible to measure absolute cross sections or cross sections relative to boron for materials which have small absorption cross sections? If so, do you have any values for graphite or bismuth or beryllium?

Mr. BRETON (France): We did not measure the absolute cross section by this method. We only compared the capture cross section of two samples of graphite, or of two samples of beryllium or beryllium oxide.

Doubtless one could get some idea of the magnitude of the capture cross section of the materials, but the errors involved are too large for the result to be of any real value.

Mr. F. L. SHAPIRO (USSR) presented paper P/642.

DISCUSSION OF P/642

Mr. L. M. BOLLINGER (USA): Is it possible to determine parameters or to measure absolute cross sections by this new method?

Mr. SHAPIRO (USSR): Just as in other cases, when the resolving power is low the slowing down time method yields only certain combinations of the resonance level parameters. To obtain absolute values it is necessary to carry out a calibration by measurements with thermal neutrons or by comparison with the first level, if the parameters for it are known. As for the possible change in the gamma-ray spectrum from level to level, it is not important as long as the cathode of the gamma-counter is made of a light substance. In this case the efficiency of the counter is proportional to the energy of the gamma-quanta. Hence the effectiveness in registering the capture of a neutron is determined by the total energy of the gamma radiation, i.e., by the binding energy of the neutron, and is independent of how this energy is distributed among individual gamma quanta. The method I spoke about cannot compete as regards resolving power with the methods described by the speakers at this morning's meeting. However, the determination of capture cross-section values averaged over several levels is of a certain interest both from the practical point of view and for purposes of comparison with theory.

Mr. E. P. WIGNER (USA): I understood that you have evidence that the gamma rays which arise from the capture of the neutrons in different levels are different from level to level. Do you have such

evidence or did I misunderstand your statement?

Mr. SHAPIRO (USSR): I said that there may be differences in the gamma-ray spectra for different levels. While we have no experimental data regarding the gamma-ray spectra accompanying capture in any specific levels, it seems to me that such measurements would be of great interest, particularly in view of the fact—mentioned in Professor Bethe's paper*—that there are very appreciable variations in the neutron width from level to level.

Mr. H. BROOKS (USA): Would the author care to comment on the possibility of distinguishing capture and fission in this method and thus measuring capture-to-fission ratio of fissile materials?

Mr. SHAPIRO (USSR): Yes, capture can be distinguished from fission, for example, by recording the anticoincidence of gamma rays and fission fragments, i.e., the emission of gamma rays arising from capture. Such determinations can yield information on mean values. Inasmuch as the levels of uranium-235 are closely spaced, it is impossible to separate them by this method.

Session 16A.2: Cross Sections of Non-Fissionable Materials

Mr. J. A. HARVEY (USA) presented paper P/832.

DISCUSSION OF P/832

Mr. P. A. EGELSTAFF (UK): I should like simply to summarise some of the measurements that have been made at Harwell on the cross sections of gold and boron. I shall read out the actual measured values, with only very brief indications of the method used.

In the case of gold, using exactly the method that Mr. Harvey has described, we came to a value of 97.7 ± 0.9 barns, which is in agreement with the measurement Mr. Harvey has reported.

In the case of boron, we have made two transmission measurements for neutrons of 2200 m/sec, using our slow chopper. The first measurement was on a sample of B_2O_3 dissolved in D_2O. That gave a value of 774 ± 6. The second measurement was of a borax powder—it was rather a difficult measurement, but we believe we have successfully overcome the problems involved. That gave a value of 765 ± 9. We now quote our average value for the absorption cross section of boron at 2200 m/sec as 771 ± 5 b.

The Harwell boron standard has about 1½ per cent more boron-10 than the United States standard. In precise figures, 752 barns measured at Argonne and Brookhaven would be converted into 760 barns on our standard, which must be compared to the 771 we measured.

We have tackled this problem in another way. We have measured the ratio of boron to gold cross sections by two methods. The first method, using the thermal oscillator, has used silver as an intermediary, and gives the ratio of cross sections as 7.97 ± 0.08. The second method uses sodium as an intermediary, and here we measured the boron to sodium with a pile oscillator and sodium to gold by the activation method. We obtained boron over gold from this as 8.11 ± 0.13. Those two methods are in satisfactory agreement, so we quote the average value of the relation of boron to gold as 8.01 ± 0.06. I do not know if you can remember all these figures, but we now go back, and correcting all the boron measurements to the Harwell standard, compare the actual measured ratio with the ratio of the directly measured values of boron and gold, and we obtain the following results. For the Harwell gold and boron figures the ratio of direct values is 7.89 ± 0.08, which is in satisfactory agreement with the 8.01 ± 0.06. But the Brookhaven values give a ratio of 7.69 ± 0.05, which disagrees with the directly measured ratio of 8.01. I have no explanation at all for that discrepancy.

To conclude, there are two other experiments, which have not been done at Harwell, on neutron lifetime in a solution of boron. One was at Stockholm, which has been reported in the literature, and correcting their measurement to the Harwell boron standard gives a value of 775 ± 5 barns, which is in excellent agreement with our figure of 771. Then there is a recent measurement made at Oxford using again the neutron lifetime techniques but in a rather new way, and that gives 760 ± 3 barns for the Harwell boron. That result is in excellent agreement with the Brookhaven-Argonne value, and possibly in disagreement with our own value of 771. I think the only thing one can say here is that at least we have the satisfaction of knowing that the figure for the boron cross section in the neighbourhood of 765 would certainly be correct to about ¾ per cent.

Mr. HARVEY (USA): The only thing that I would want to stress is that one must remember that the Harwell boron is 1½ per cent higher than the Brookhaven, so it is a little misleading when you quote 771. I just wanted to point out to people that there

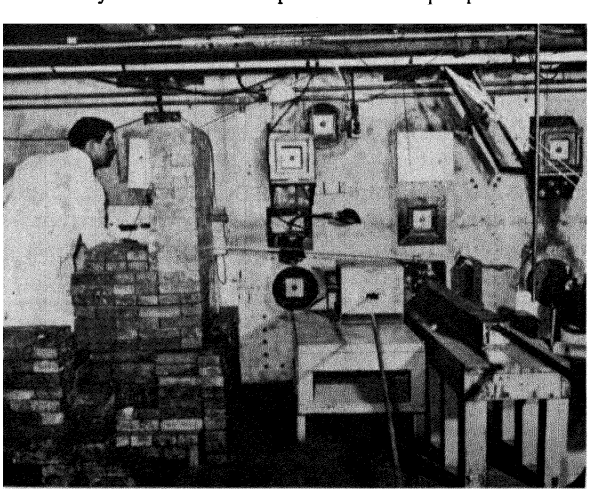

Slide 1

* P/585, Volume 4, Session 18A, these Proceedings.

is this difference in the boron. Your value of 771, on the Argonne-Brookhaven boron, would come down to about 760, so there is really not too much disagreement. I have the Harwell U^{238} value listed here and it is in very good agreement. The value reported was 2.8 ± 0.1, and that agrees very well with the Brookhaven measurement. The U^{235} will probably come up tomorrow, so I think we ought to leave it now.

Mr. J. E. SANDERS (UK): Could I ask Mr. Harvey how the capture cross section of U^{234} of 89 barns was measured?

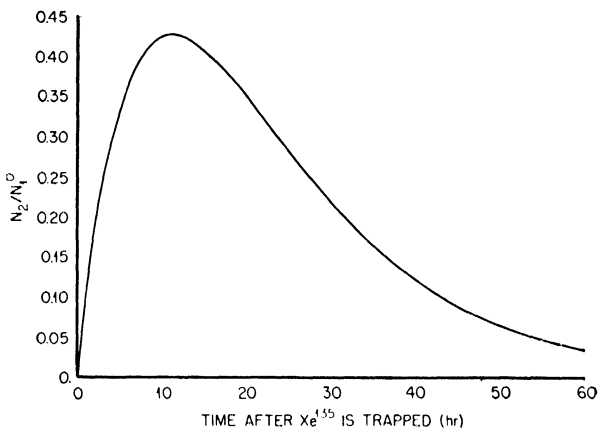

Slide 2

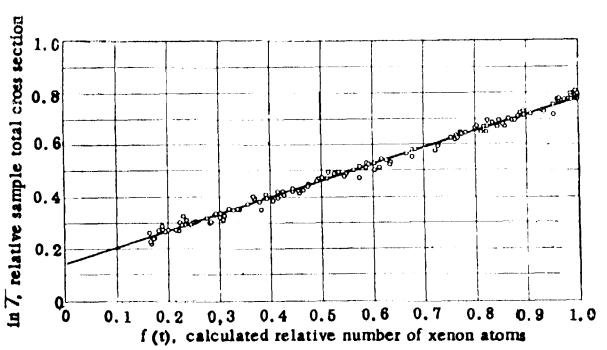

Slide 3. Fission chamber data

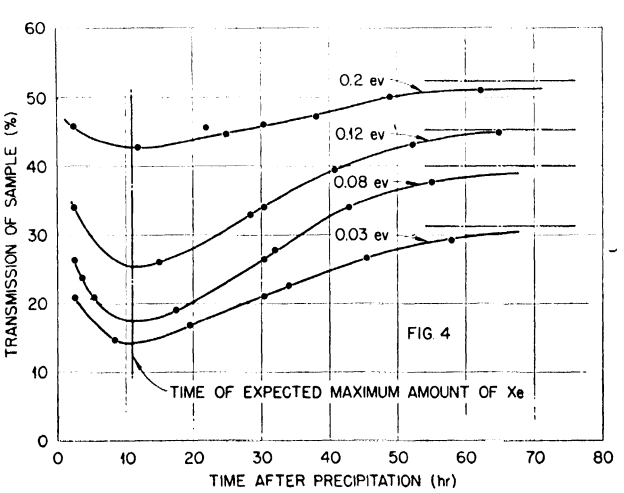

Slide 4

Mr. HARVEY (USA): I am sure that was a pile oscillator measurement at Oak Ridge. There are large quantities of high purity U^{234} available in the United States, so it would be quite a simple matter to measure it.

Mr. S. BERNSTEIN (USA) presented paper P/591. Those of his slides that are not in the paper are reproduced here with his comments:

Slide 1 is a photograph illustrating the method of handling the radioactive material. The man at the right behind the wall of lead bricks is inserting a xenon sample at the end of the long rod into the graphite stringer.

Slide 2 illustrates the growth and decay of the xenon-135 from the iodine-135.

Slide 3 is a plot of the logarithm of the transmission as a function of the number of xenon atoms again, for the thermal spectrum. It is a straight line whose slope is proportional to the cross section of xenon-135.

Slide 4 gives the transmission against time for the several energies 0.03 electron volts, 0.08, 0.12 and 0.20 electron volts, illustrating again a minimum for the measurement at each value of the energy and the approach to a maximum value as the xenon goes to zero.

DISCUSSION OF P/591

Mr. E. P. WIGNER (USA): Are there any signs of higher resonances that you have noticed?

Mr. BERNSTEIN (USA): As the work with the mechanical chopper went to much higher energies, perhaps up to a kilovolt, no resonances of energy higher than 0.08 electron volts were found. A resonance was found but it turned out to be in a stable isotope of xenon.

Mr. P. A. EGELSTAFF (UK): I trust you will forgive me for getting up again. I want to make a remark, under the heading of cross sections of non-fissile materials, on some measurements of capture cross sections of uranium-238 and thorium-232. These measurements were made by the activation technique, using our Van de Graaff machine as the neutron source, and are the work of Rose and Hanna.

Slide 5 shows the capture cross section of uranium-238 as a function of neutron energy from the region of about 30 or 40 kev to 1½ Mev or so. You will notice at about 1 Mev there is a sharp fall in the cross section. The value just before the drop off in cross section is about 0.1 barn which is of the same order as found in neighbouring heavy elements.

Slide 6 shows similar data obtained for thorium-232. Here we find a very sharp fall-away of the cross section in the neighbourhood of 800 kev. The actual value of the cross section is again 0.1 barn before it drops away. It is quite clear that this sharp fall-off in cross section at energies in the neighbourhood of 1 Mev is a very important feature from the point of view of capture in these materials in a fast reactor. Also, there is some interesting theoretical discussion on whether this fall-off in cross section,

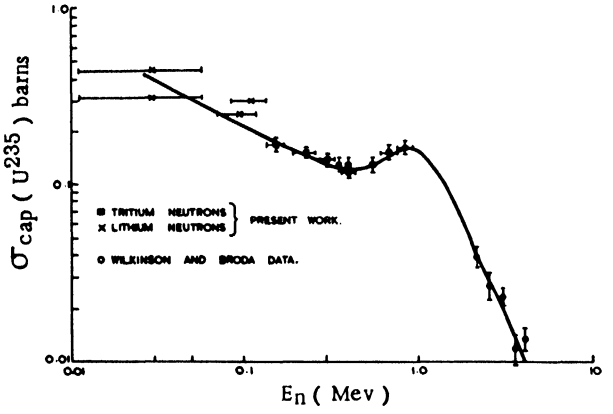

Slide 5. Cross section for the reaction U^{238} (n, γ) U^{239}

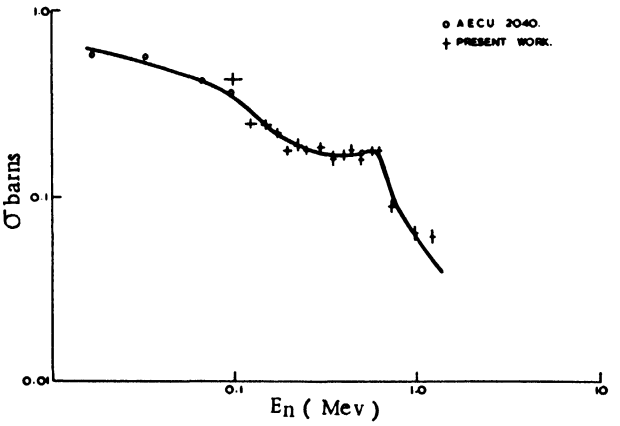

Slide 6. Cross section for the reaction Th^{232} (n, γ)

which we have found in these two isotopes, is associated with the beginning of inelastic scattering in these two materials.

Mr. D. OKRENT (USA): As I interpret Mr. Bernstein's results, at the end there seems to be a 10% uncertainty on what the cross section for xenon was, depending on which g value one should assign. Is this a correct interpretation?

Mr. BERNSTEIN (USA): Yes, it is. This comes about because what was measured was not the capture cross section but the total cross section. Then a capture cross section value was calculated and the result is that these values are different by 10%, depending on which value of g you use. The fitting of the formula to the total cross section as a function of energy was equally good for both values of the statistical weight.

Mr. OKRENT (USA): Is there no way of making a choice based on some of the other measurements, let us say the reactivity measurements that you mentioned earlier in your paper?

Mr. BERNSTEIN (USA): If those values were consistent or accurate enough, perhaps they might help. However, most of them were made many years ago and the answers differ very widely one from another—much more than they should because of the difference in temperature of the various piles. Even for the same pile, measurements might differ by perhaps a factor of 2. So that I think until there are better measurements of the capture cross section in some region of neutron energy, we just cannot choose between the two values of the statistical weight.

Mr. J. A. HARVEY (USA): Since Oak Ridge has the equipment for handling very active samples, I wonder if there are any measurements or plans for measurements on other fission products?

Mr. BERNSTEIN (USA): There are no plans at present for doing any more work with the xenon and I do not believe that there are any immediate plans for measuring the cross sections of other fission products as a function of energy.

Mr. A. G. WARD (Canada): In reply to the previous question, I should perhaps mention that I have seen a publication proof of a paper of Mr. Thode of MacMaster University in Canada. In this paper, he has measured the capture cross section of xenon-135 relative to boron by essentially mass spectrometer techniques, measuring the depletion of the caesium-135 isotope following high-flux irradiation. If my memory serves me right, his capture cross section value was 3.25 megabarns relative to a boron cross section of 755 barns, and the irradiation took place in the side reflector of the NRX pile where the spectrum should be predominantly thermal.

Mr. A. M. WEINBERG (USA): I should like to add just one remark to the remark Mr. Bernstein made. I believe it should be pointed out that part of the difficulty in determining the absolute cross section of xenon from power measurements is because what is really measured is the product of the fission yield and the cross section; and the fission yield is still a matter of some argument. There is uncertainty perhaps by something of the order of 5 per cent.

I should also like to raise a point in connection with Mr. Egelstaff's interesting curves. As far as I am aware, these represent some of the best measurements of capture cross sections in the high energy region. I was wondering if Mr. Egelstaff had tried to see whether the beginning portions of these curves are fitted by a $1/E$ dependence; it seemed to me that there was a break in the curve which could be interpreted as the setting in of the $1/E$ dependence of the capture cross section. I was wondering if Mr. Egelstaff has tried to fit the capture of uranium and thorium into this $1/\sqrt{E}$, followed by $1/E$ dependence.

Mr. EGELSTAFF (UK): I am afraid the simple answer is no. I am sorry but we have not yet tried that fit.

Mr. BERNSTEIN (USA): I might simply add the remark that we did try to take all the measured values of the average cross section for xenon-135 obtained by the negative activation method and by the fission method and compared them with the values calculated from my own measurements of the total cross section. However, the comparison was

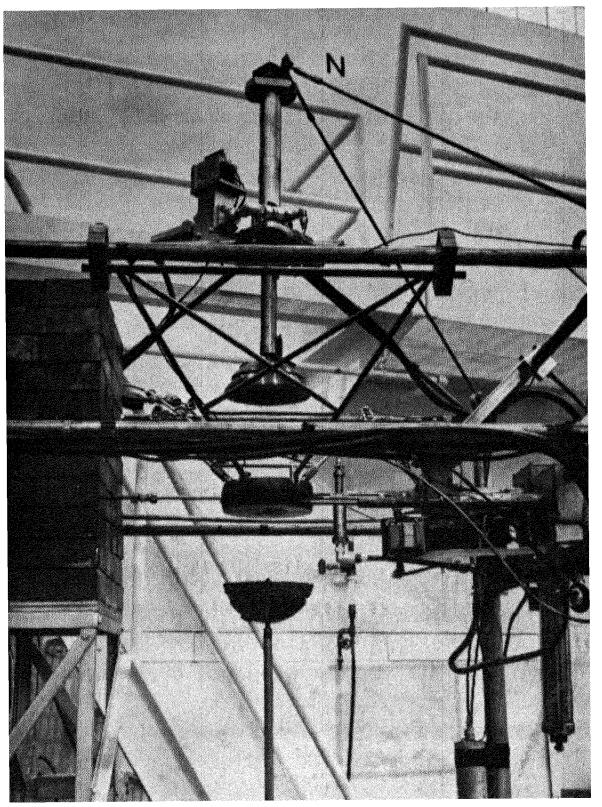

Slide 7

very poor indeed. I repeat that these measurements were made many years ago. They were extremely welcome and perhaps sufficiently accurate when they were made, but they do not compare favorably when they are placed in the proper position on the calculated plot of the capture cross section as a function of temperature of the Maxwell distribution.

Mr. WARD (Canada): In the present paper and also in one of the remarks just made, it was stated that the pile measurements measured essentially the product of the xenon cross section and the xenon yield. This is quite correct for a low-flux graphite pile. However, for the NRX pile at high power we measure much more closely the xenon yield alone.

Session 16A.3: Delayed Neutrons

Mr. G. R. KEEPIN (USA) presented paper P/831. In connection with the experiments on the bare U^{235} assembly at Los Alamos (Fig. 1 of the paper) he showed some further slides which are reproduced here with his comments:

Slide 7 shows a photograph of the bare U^{235} assembly at Los Alamos. The three portions of solid U^{235} metal can be seen. The top and bottom sections are brought together pneumatically. Fine adjustment of reactivity is accomplished by means of U^{235} control rods which are re-entrant into the center section. The phototube positioning unit is shown, and the transfer tube extends into the shielded tank on the left.

Slide 8 shows the entire assembly. Shown again are the three sections of the unreflected U^{235} assembly and the transfer tube which extends into the shielded counting geometry. The electronics associated with triggering and transfer of the material under study are shown, and the preamplifier and power supply for the fission chamber which monitors the total number of fissions. This entire room is a quarter mile from the control room, and all operations are conducted remotely.

Two different detectors have been used. The first is a ZnS-boric acid scintillation counter developed for this experiment with a neutron-to-gamma sensitivity ratio of about 10^4 and energy response varying as $E^{-\frac{1}{2}}$. The second detector is a counter in "long" geometry, modified to give flat response within 5 per cent from 23 kev to 1.2 Mev.

The decay of delayed neutron activity is monitored by a multi-channel recording time-delay analyzer with decade channel widths between 1 msec and 10 seconds following in automatic sequence; the number of channels of each width is variable thus permitting selection of the most suitable channel-width distribution for a given decay curve.

The analyzer, shown schematically in Slide 9, includes three basic units: (1) a four decade gated scaler with fast pulsed reset, (2) a 100 kc crystal-controlled interval timer and (3) a read-out coincidence circuit which duplicates the instantaneous reading of the gated scaler at intervals established by pulses from the timer unit. This duplicate reading is maintained for 0.5 msec during which time it is recorded either photographically or electrically.

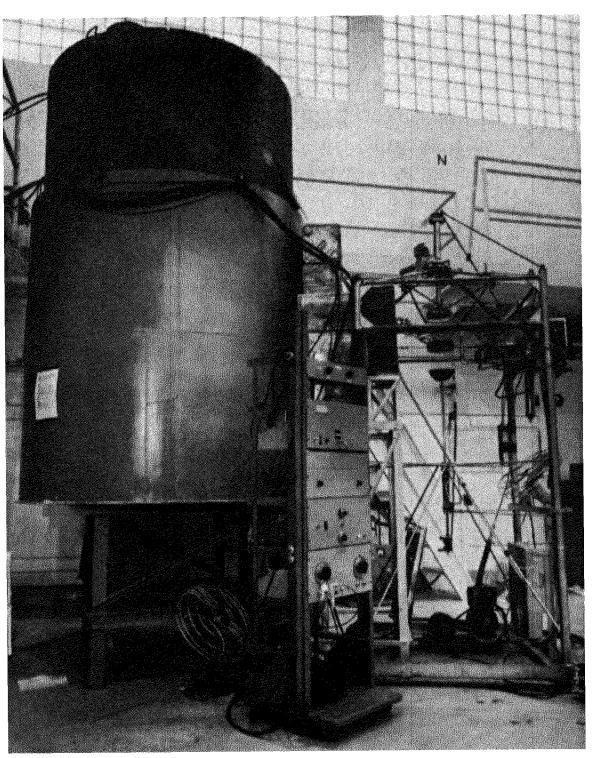

Slide 8

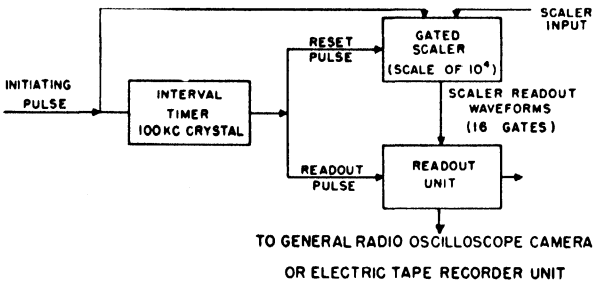

Slide 9

The timer pulse automatically resets the gated scaler after each read out, thus giving directly the differential number of counts per channel.

Slide 10 shows the recorder printing head in operation. The styli are driven by the discharge of a capacitor through an appropriate thyratron circuit.

Slide 11 shows the assembled analyzer including the timer unit. The thyratron driving unit is up at the top, and also the read-out unit, which contains 17 6A56 coincidence stages. This has proved to be a very useful instrument, where one must cover time scales from the millisecond region to the tens of seconds region, which is just what is required, of course, in delayed neutron analysis.

DISCUSSION OF P/831

Mr. J. E. SANDERS (UK): I should like to describe some experiments which are being carried out at Harwell by Batchelor and Hyder on the measurement of the energies of delayed neutrons from thermal fission of U^{235}. The measurement is being done using the helium-3 neutron spectrometer, which has already been described during this Conference.

Slide 12 shows the general experimental arrangement. A slug of natural uranium is irradiated in the thermal column of the BEPO reactor and is transferred by a pneumatic transfer tube after irradiation to a position, close to the helium-3 neutron spectrometer. The slug is separated from the spectrometer by a large mass of lead shielding to shield the counter from the very intense gamma radiation which is produced. Outside, we have a boric acid glass shield to prevent thermal neutrons scattered back from the walls of the laboratory from re-entering the counter. Here we have the head amplifier of the counter, for which the electronics is conventional. The counter feeds into a 30-channel pulse height analyser which is gated so that one records at times after irradiation adjusted to emphasize the particular delayed neutron periods. By analysing the height of the pulses from the helium-3 spectrometer, we can obtain the energies of the delayed neutron groups.

Slide 13 shows the energy spectrum of delayed neutrons of the 55-second period, that is the 55-second period according to Hughes, as a function of energy. We have the neutron energy in kilovolts along the horizontal axis, and the intensity plotted along the vertical axis. We see that there is indeed evidence for discrete neutron groups. The peak at the left-hand of the slide corresponds to an energy of 140 kev. There are obviously other delayed neutrons of high energy, but these we have so far not been able to resolve.

We see here, in Slide 14, the energy spectrum of the 22-second delayed neutron period for U^{235}, and in this case there is evidence of at least two energy groups. These energies are 360 kev and 470 kev, respectively, and again we have evidence of unresolved neutron groups further on.

I should just like to say that this work is in its early stages. One of the major difficulties is the shielding of the helium-3 counter from the intense gamma radiation which causes the resolution to be lower than the ideal resolution of the helium-3

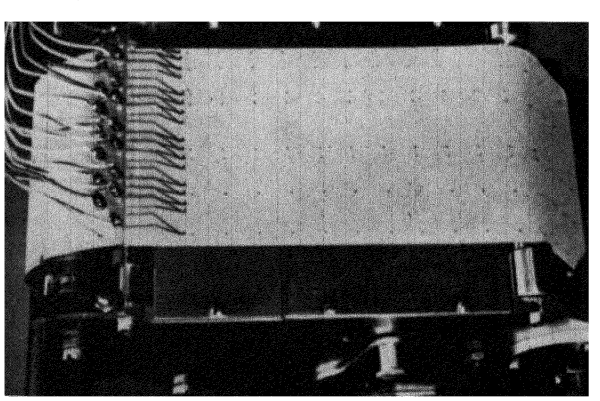

Slide 10

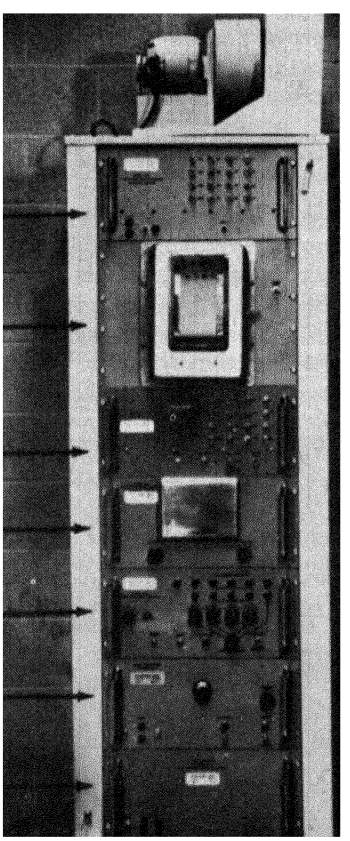

Slide 11

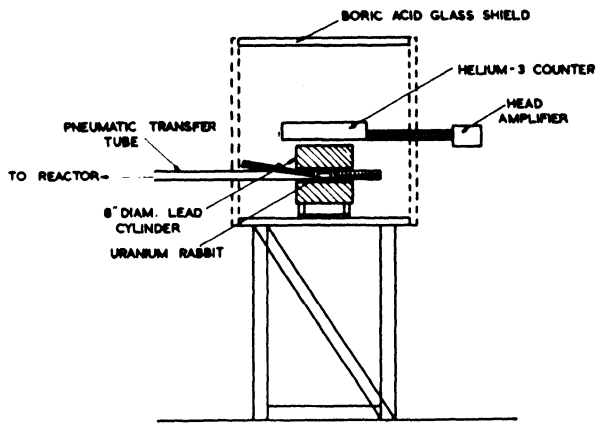

Slide 12. Experimental arrangement

counter, but I thought you might be interested to see these preliminary energy measurements.

There is one point about which Mr. Keepin has reminded me. He asked how these energy measurements compare with the energy measurements that were performed by Hughes in his original work. The average energy of the delayed neutron group measured by us is in quite reasonable agreement with the average energy as determined by diffusion measurements, and also with the measurements reported by Burgie using cloud chamber techniques.

Mr. S. KRASIK (USA): The curve which you showed for the period versus the reactivity was very convincing. Could you just say a few words to explain how the reactivity was determined absolutely?

Mr. KEEPIN (USA): The relation between reactivity and pile period is as follows:

$$R = \frac{\tau_0}{T\gamma f} + \sum_{i=1}^{6} \frac{(a_i/a)\tau_i}{T + \tau_i}$$

where $R \times 10^2 \equiv$ reactivity in cents (100 cents $\equiv$ reactivity interval between delayed and prompt critical), $\tau_0 \equiv$ prompt neutron lifetime ($\approx 10^{-8}$ seconds), $T \equiv$ reactor period (e-folding time), $\gamma \equiv$ average relative effectiveness of delayed neutrons compared to prompt neutrons, $f \equiv$ delayed neutron fraction of total neutrons from fission.

I might point out that γf corresponds to a measurement of the interval between delayed and prompt critical. You notice that at delayed critical T will be infinite, and therefore R will be zero. Now let us go to prompt critical. At that point the reactor period will be of the order of a millisecond, and hence the first term will still be negligible. This will be small compared with the shortest delayed neutron period, and therefore one obtains the summation of a_i/a which by definition normalizes to unity. So at prompt critical R equals 1. The interval in this parameter, R, is thus equal to one between delayed and prompt critical (this is essentially because we have divided through by γf). Regarding the experimental determination of this reactivity interval: delayed critical is of course the point of self-sustained reaction, or a constant level of power. Prompt critical is given by at least two methods with which you are undoubtedly familiar, and after determining the two fiducials—delayed and prompt critical—one divides this interval into one hundred parts and calls these "cents." Is that an answer to your question?

Mr. KRASIK (USA): I think I would be interested in hearing a little more explanation about the determination of prompt criticality.

Mr. KEEPIN (USA): I shall first mention an approximate method. If you plot period versus reactivity on any scale, you will find a point of inflection in the neighborhood of prompt critical. A more exact determination of prompt critical is possible by a measurement of the so-called alpha which is the reciprocal of the prompt neutron period. The measured (or extrapolated) value of reactivity at which α goes to zero is by definition prompt critical. Thus prompt critical is that reactivity at which the prompt neutrons alone can sustain a constant level ($\alpha \equiv 0$) without reactivity contributions from any delayed neutrons.

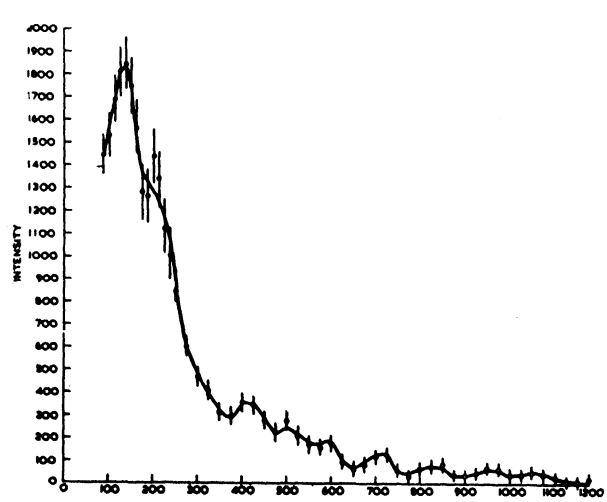

Slide 13. Delayed neutrons from U^{235} spectrum of the 55 sec period

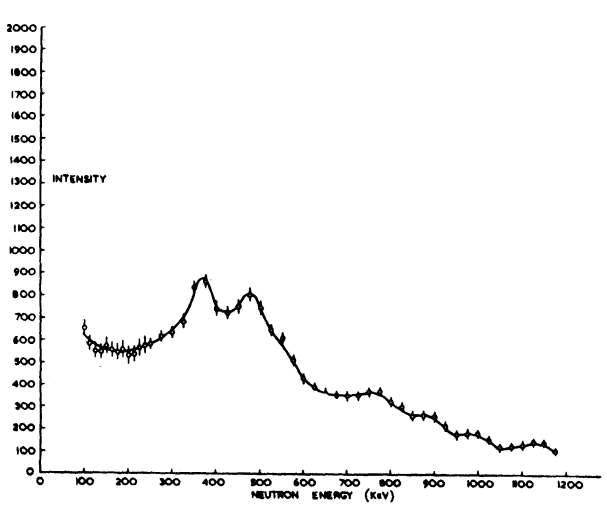

Slide 14. Delayed neutrons from U^{235} spectrum of the 22 sec period

Mr. E. R. COHEN (USA): I should like to ask about the effects of changing in the analysis the number of neutron groups that you use. Is the IBM code such that this number is available for adjustment, or must that be put in initially? If so, how does using 5, 6 or 7 change the results?

Mr. KEEPIN (USA): It is flexible in the sense that you can adjust it for 5, 6 or 7 periods. We have tried 5 but not 7 periods. For 5 it does not converge. The analysis is done by an iterative calculation which minimizes the difference between the observed data and the sum of the exponentials that one is trying to fit. The exponentials are expanded in a series of approximate (guessed) values and the first-order (linear) terms constitute a correction to these approximate values. The machine calculates a correction, applies it and prints out a corrected value. The final answer is obtained when these corrected values converge on a given number. With five periods it does not converge, that is it "hunts" or "wanders." With six periods it converges very well. Judging from the rapidity of convergence of the 701 for 6 periods we believe that a 7th period is not present in any significant abundance, but when time permits we shall investigate this more closely on the 701 computer.

Mr. SANDERS (UK): I wonder whether Mr. Keepin would care to give us his opinion on this remark: Is it always justified to assume that the decay of delayed neutron period follows a simple exponential law or, if it is the case that several beta decays precede the delayed neutron, might one have a more complex decay scheme which in turn would give different periods as the irradiation time was changed?

Mr. KEEPIN (USA): Actually, this observation is made in the written text of this paper. Following beta-decay cascade from the original fission fragment to the final delayed neutron precursor, (let us say bromine-87), there is not necessarily any reason why the measured delayed neutron period of the first group must agree with the beta-decay period. Note that the delayed neutron decay period could not be shortened; it could only be lengthened by this effect since it would hold up population of the delayed neutron precursor, Br^{87}. Thus a strict one-to-one correspondence need not be expected.

Session 17A

CROSS SECTIONS OF FISSIONABLE MATERIALS

LIST OF PAPERS

		Page
P/422	The cross sections of the plutonium isotopes ..... J. F. Raffle and B. T. Price	187
P/589	The total and fission cross section of plutonium ..... B. R. Leonard, Jr.	193
P/586	The low energy cross sections of U^{235} ..... V. L. Sailor	199
P/423	The slow neutron cross sections of the uranium isotopes ..... J. E. Lynn and N. J. Pattenden	210
P/645	Fission and total cross sections of some heavy nuclides for monochromatic neutrons as measured by a mechanical neutron velocity selector ..... Y. B. Adamchuk *et al.*	216
P/646	Time-of-flight measurement of the total neutron cross section of uranium-233, uranium-235 and plutonium-239 ..... S. J. Nikitin *et al.*	224
P/644	Determination of the absorption cross section and of the radiative capture cross section of uranium-233 for pile neutrons ..... G. M. Kukavadse *et al.*	230
P/354	Slow neutron cross sections of fissile nuclei ..... J. M. Auclair *et al.*	
P/355	Energy dependence of U^{233}, U^{235}, Pu^{239} fast neutron cross sections ..... D. Szteinsznaider *et al.*	
P/594	Some techniques for measurement of fast neutron flux ..... B. C. Diven	
P/424	Fission cross sections as a function of neutron temperature ..... C. G. Campbell and D. J. Lockey	

The Cross Sections of the Plutonium Isotopes

By J. F. Raffle and B. T. Price,* UK

PART I. FISSION CROSS SECTIONS

The Harwell programme of fission cross section measurements has been divided into (*a*) absolute measurements as 0.0253 ev, and (*b*) relative measurements covering as wide a range of neutron energies as possible, and relying on the absolute measurement for the determination of the scale of cross section. The convenience of this division lies in the different amounts of fissile material needed for the two kinds of measurement. For a reliable absolute determination one requires a fission chamber containing a very thin foil of fissile material, having a small self-absorption correction, and giving a good bias curve with a long plateau unaffected by alpha build-up pulses; an adequate counting rate can be obtained by working with low energy neutrons. On the other hand, measurements of the variation of fission cross section in the epithermal region generally have to make use of lower neutron fluxes, and the cross section itself is lower; so that any fission chambers used in such measurements must contain as much fissile material as possible.

Absolute Fission Cross Sections at 0.0253 ev (Raffle)

The fission cross section of plutonium-239 at 0.0253 ev was determined in terms of the gold cross section. Gold was chosen as the standard because, at the time the work was started, the American and British values for its cross section showed much better agreement than in the case of boron. Ideally, one would make the comparison in a monoenergetic beam of neutrons. However, the monoenergetic beams available at Harwell had too low an intensity for an irradiation of a gold foil to be satisfactory. The comparison was therefore carried out in two steps. The plutonium foil was first compared with a boron-10 foil in a time-of-flight spectrometer, and the boron-10 foil was then compared with a gold foil in a thermal neutron beam.

The plutonium-239 (containing 0.6% of plutonium-240) was laid down on an aluminium backing in the form of an oxide layer about 0.5 mg/cm^2 thick. The total number of atoms was determined by alpha-counting in a proportional counter of calculated efficiency, and also by comparison with other foils which had been both weighted and α-counted. The ionization chamber in which the foil was mounted was provided with "thin" windows for the entry and exit of the neutron beam, and was filled with a gas of high electron mobility. The collecting electrode was hemispherical, in order to give the best possible pulse distribution, and to reduce the effect of alpha build-up pulses to a minimum. The total number of fissions was determined by kick-sorting the pulses, and extrapolating distribution to zero pulse height.

A mechanical chopper with its associated time-of-flight equipment was used to select neutrons of energy 0.0253 ev from one of the BEPO beams. The plutonium chamber, and a rather similar gridded ionization chamber containing boron-10, were placed in the beam in turn, and the ratio of the counting rates determined. The rate of disintegration in the boron-10 chamber was then compared with the activity induced in gold foil when both were placed in a beam of thermal neutrons. The gold activity was measured by absolute β-γ coincidence counting, corrections being applied for the source geometry and the complexity of the gold decay scheme. Below about 0.5 ev the gold cross section follows $1/v$ law closely, so that only a small correction was required to convert the ratio of thermal cross sections to a ratio at 0.0253 ev.

The value of the fission cross section of plutonium-239 at 0.0253 ev was found to be 702 ± 20 barns, relative to a gold cross section at the same energy of 98.6 barns.

The determination of the absolute fission cross section of plutonium-241 was made with a sample of plutonium that had been irradiated in the Chalk River pile for 27 months, and which contained 27% plutonium-239, 51% plutonium-240, and 14% plutonium-241. It is possible to determine the fission cross section of plutonium-241 with such a mixed sample provided one assumes that it is the only other isotope present besides plutonium-239 which is appreciably thermally fissile. There is good evidence for this, both from systematics based on the binding energy of the ingoing neutron, and from other determinations of the isotopic fission cross sections.

The value found for the fission cross section of plutonium-241 at 0.0253 ev is 935 ± 40 barns.

Variation of Fission Cross Section with Neutron Energy (Price, Raffle, Richmond, Sanders)

The measurements of the variation of the fission cross section of plutonium-239 with neutron energy

* Work done by P. A. Egelstaff, D. B. Gayther, J. E. Lynn, K. P. Nicholson, N. J. Pattenden, B. T. Price, E. R. Rae, J. F. Raffle, R. Richmond, J. E. Sanders, and E. R. Wiblin.

made use of the neutron beams available from (*a*) the BEPO slow chopper neutron spectrometer (below 0.1 ev), (*b*) the BEPO single-crystal spectrometer (0.05 to 1 ev), and (*c*) the Harwell 15 Mev electron accelerator (above 0.25 ev).

These machines are discussed in papers by Egelstaff[1] and Wiblin.[2]

The fission cross section of plutonium-239 was compared with the (n,α) cross section of boron-10. The results for the low energy region below 0.1 ev are shown in Fig. 1. The portion of the curve between 0.1 ev and 1 ev, which was measured with a crystal spectrometer, relies for its absolute magnitude on an overlap with the chopper measurements. This overlapping was made difficult at energies around one quarter of the energy of the 0.3 ev resonance (i.e., $\approx$ 0.075 ev) owing to the very high efficiency with which the fission chamber detected the small proportion of second order neutrons present in the beam. The difficulty was overcome by removing the second order neutrons from the beam as far as possible with a filter of plutonium-239. The uncertainty in the overlap was estimated to be of the order of 2%. At other energies there was no difficulty in applying small corrections—amounting to a few per cent—to allow for the presence of second and third order neutrons in the crystal spectrometer beam. The time-of-flight measurements were, of course, free from this source of error.

The observed cross section at the resonance energy of 0.297 $\pm$ 0.01 ev was found to be 2910 barns, relative to a value of 702 barns at 2200 metres/second; the uncertainty in this cross section is $\sim$ 2% on account of the overlapping already mentioned, plus a further statistical error of $\pm$ 100 barns. This value is in reasonably good agreement with the value predicted from measurements of σ_{total}, ν(the number of neutrons per fission) and η(the number of neutrons produced per neutron absorbed).

In the energy region below 0.35 ev the results are fitted with an accuracy of about 2% by an analytical expression consisting of two single-level Breit-Wigner terms together with a $1/v$ term:

$$\sigma\sqrt{E} = 29.6\left[\frac{0.005}{E^2+0.005}\right]$$

$$33 + 2850\sqrt{0.297}\left[\frac{0.0026}{(E-0.297)^2+0.0026}\right]$$

Above 0.35 ev the agreement between this expression and the experimental results is less satisfactory, probably owing to the effect of resolution; but the expression reproduces the general trend of the results up to about 1 ev.

The parameters of the resonance at 0.297 ev deduced from this expression, and corrected for the effect of resolution and Doppler broadening, are

$$\Gamma = 0.098 \pm 0.003 \text{ ev}$$

$$\sigma_0 = 2940 \text{ barns}$$

This value of σ_0 is the contribution from the 0.297 ev resonance only.

The absolute scale of the linear accelerator measurement was obtained by an overlap with the crystal spectrometer results, the uncertainty in the normalization being 2½%.

The results at energies above 1 ev are shown in Fig. 2. It is known, from the total cross section measurements which will be described later, that the fission resonances at 11.2 and 15.1 ev are actually multiple. In the analysis given in Table I the compound nature of these resonances has been ignored. Although the data cannot properly be regarded as true resonance parameters, they are still of value for

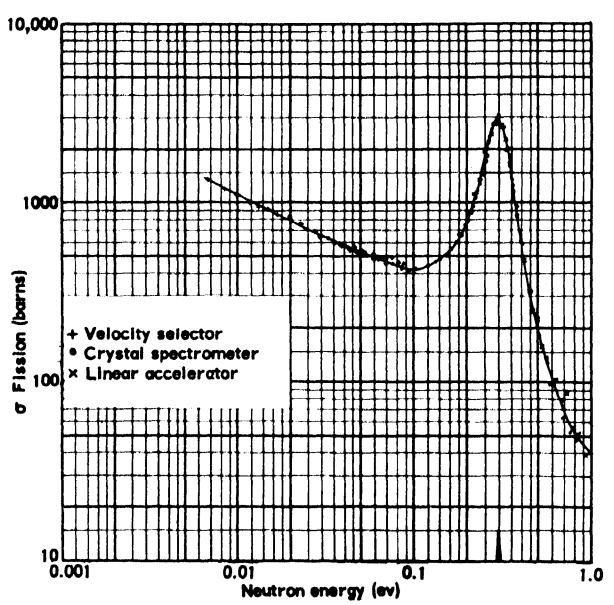

Figure 1. Values of the fission cross section of Pu^{239} (uncorrected for Doppler broadening)

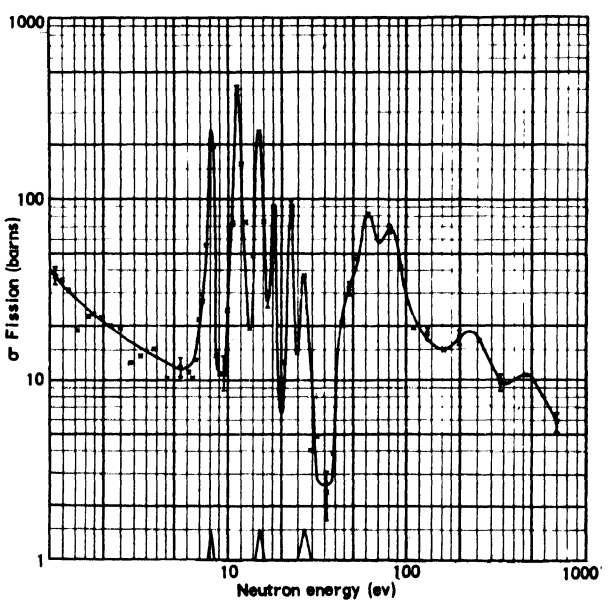

Figure 2. Values of the fission cross section of Pu^{239} (uncorrected for resolution or Doppler broadening)

Table I. Analysis of Fission Resonances in Plutonium-239

Resonance energy (ev) (fission observations)	*Resonance energies observed in total cross-section measurements (ev)*	*Estimated ($\Gamma\sigma_0$) fission (barns · ev)*
8.0 ± 0.2	7.85	72
11.2	11.0, 11.9	175
15.1	14.30, 14.75, 15.5	150
18.3	17.7	75
22.8	22.3	105
26.8	26.4	50

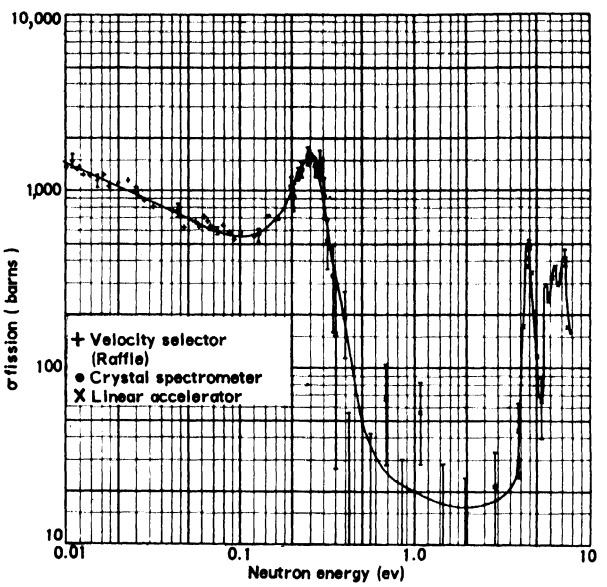

Figure 3. Values of the fission cross section of Pu^{241} (uncorrected for resolution or Doppler broadening)

determining $\alpha = (\sigma_{abs}/\sigma_{fiss}) - 1$ in the intermediate energy region.

The variation of the fission cross section of plutonium-241 was determined using a foil of the mixed plutonium isotopes of the same composition as was used for the absolute measurement. In the low energy region below 0.4 ev the cross section of the mixture was compared with the cross section of plutonium-239, but at higher energies it was found more convenient to use boron-10 as the material of known cross section. Measurements were otherwise similar to those already described.

After making a subtraction for the contribution of plutonium-239 the results shown in Fig. 3 were obtained. A resonance is found at an energy of 0.255 ± 0.02 ev, and there appear to be further resonances attributable to plutonium-241 at 4.45 ± 0.1 ev, 5.8, 6.3, 7.1, and possibly 10 ev. Except for the lowest resonance the precision of the measurements does not permit the determination of resonance parameters.

In the energy region below 0.3 ev the fission cross section of plutonium-241 is fitted to an accuracy of 2% by the expression:

$$\sigma\sqrt{E} = 111 + 1390\sqrt{0.255}\left[\frac{0.0028}{(E-0.255)^2 + 0.0028}\right]$$

Observed constants of the 0.255 ev resonance were

Full width at half maximum = 0.11 ± 0.02 ev
Height of resonance = 1390 barns
Cross section at 0.255 ev = 1600 barns

After correcting for resolution (1% correction) and Doppler broadening, the true constants of the resonance were found to be

$$\Gamma = 0.103 \pm 0.02 \text{ ev}$$

$$\sigma_0 = 1420 \pm 150 \text{ barns}$$

Above 0.3 ev the experimental values fall more rapidly with energy than those given by the above analytical expression. Although the experimental errors are admittedly very large it seems probable that a better fit might be obtained by the inclusion of a second low-energy resonance term, as in the case of plutonium-239.

PART II: TOTAL CROSS SECTIONS

The total neutron cross sections for the plutonium isotopes have been measured over the energy range 0.0015 ev to 100 ev. The same machines were used as for the fission cross-section determinations, and the cross sections were deduced from transmission measurements on samples of differing thickness and isotopic content. The majority of the resonances were analysed by studying the areas under thick and thin sample transmission curves. The observed variation of total cross section with neutron energy is shown in Figs. 4, 5 and 6, and a summary of the chief levels and their parameters is given in Table II. It is convenient to classify the results according to the machine used.

Slow Chopper Neutron Spectrometer (0.0015 ev—0.166 ev) (Pattenden)

The cross section plotted in Fig. 4 is the observed total cross section for material containing 1.2% of plutonium-240 and 0.08% of plutonium-241. Several samples of compressed plutonium oxide were used, and also a sample of plutonium metal. Most of the points plotted are, however, those obtained from two oxide samples containing 0.00033×10^{24} atoms/cm² and 0.0023×10^{24} atoms/cm². In order to avoid confusing the figure not all the experimental points are shown. In general the statistical errors on each point are less than 2%, but there may be a systematic error of up to 3% due to uncertainties in sample thickness.

The value of σ_{tot} for plutonium-239 at 0.0253 ev is 1050 ± 30 barns.

Crystal Spectrometer (0.03—5 ev) (Pattenden)

The curve shown in Fig. 4 is the observed total cross section for material containing 1.2% of plutonium-240 and 0.08% of plutonium-241, and the values are based chiefly on the two samples already mentioned. In addition, the observed values for an oxide sample of thickness 0.0029×10^{24} atoms/cm², and containing 7.53% of plutonium-240 and 0.79% of plutonium-241, are shown in the region of 1 ev.

Table II. Analysis of Total Cross Section Resonances in Plutonium-239 and Plutonium-240

	Resonance parameters		
E_0 *ev*	σ_0 *barns*	Γ *ev*	*Machine*
	Plutonium-239		
0.300	5310 ± 150*	0.100 ± 0.005	Crystal spectrometer
0.297 ± .002			Fast chopper
7.85	5000 + 700	0.067 ± 0.01	Fast chopper
7.85	8400 ± 2500	0.044 ± 0.007	Linear accelerator
7.80	–	–	Crystal spectrometer
10.95	3000 + 900	0.13 ± 0.04	Fast chopper
11.95	2000 ± 600	0.09 ± 0.03	Fast chopper
11.0	$\sigma_0\Gamma$~600 b-ev		Linear accelerator
11.9	$\sigma_0\Gamma$~400 b-ev		Linear accelerator
14.30	800	~0.07	Fast chopper
14.75	7000	~0.04	Fast chopper
14.6	unresolved		Linear accelerator
15.2	unresolved		Linear accelerator
15.5	unresolved		Fast chopper
17.75	~1200	~0.15	Fast chopper
17.7	1600	0.09 + 0.035	Linear accelerator
22.35	~4000	~0.06	Fast chopper
22.3	$\sigma_0\Gamma$~120 b-ev		Linear accelerator
26.4			Linear accelerator
32.5			Linear accelerator
	Plutonium-240		
1.058	(1.45 + 0.15) × 10^5	0.029 ± 0.003	Crystal spectrometer
1.057	(1.20 ± 0.2) × 10^5	0.028 ± 0.005	Fast chopper

* In this case the figure is the cross section at 0.30 ev corrected for resolution and Doppler broadening, and not σ_0 for the resonance.

The levels observed at 0.30 ev and 1.058 ev are assigned to plutonium-239 and plutonium-240 respectively. The observed peak cross section for the 0.30 ev level is 5120 barns, and this has been corrected for resolution and Doppler broadening to 5310 barns, assuming a Debye temperature of ~ 400°K for plutonium oxide. The total width of the resonance is 0.100 ev. The cross section is fitted by the following analytical expression containing two Breit-Wigner single level terms together with a $1/v$ term and a constant term.

$$\sigma_{tot} = 4 + \frac{1}{\sqrt{E}}\left[36 + 5197\sqrt{0.3}\left\{\frac{(0.10/2)^2}{(E-0.300)^2+(0.10/2)^2}\right\} + 43.31\left\{\frac{E+(0.11/2)^2}{(0.11/2)^2}\right\}\right]$$

Fast Chopper Neutron Spectrometer (Egelstaff, Gaythe, Nicholson) (a) 0.225—0.35 ev (b) 0.63—1.36 ev (c) 6.04—24.25 ev

Measurements have been made with this machine on both the 0.30 ev resonance and the 1.058 resonance using Pattenden's two samples. The 0.30 ev peak was explored in great detail with the thinner sample, fifty points being taken between 0.225 ev and 0.349 ev. The value of the resonance energy is given as 0.297 ± 0.002 ev. The measurements relied for the absolute value on a normalization with the crystal spectrometer results at the peak of the resonance. The thicker sample was used to measure the 1.058 ev resonance; the results were again normalized to the crystal spectrometer results, in this case at about 0.6 ev. This normalization was necessary because it was difficult to determine by any other means the number of plutonium atoms in the very small area of the sample that was exposed to the neutron beam. The assignment of the 1.058 ev resonance to plutonium-240 was confirmed by using another sample containing 8% of the isotope.

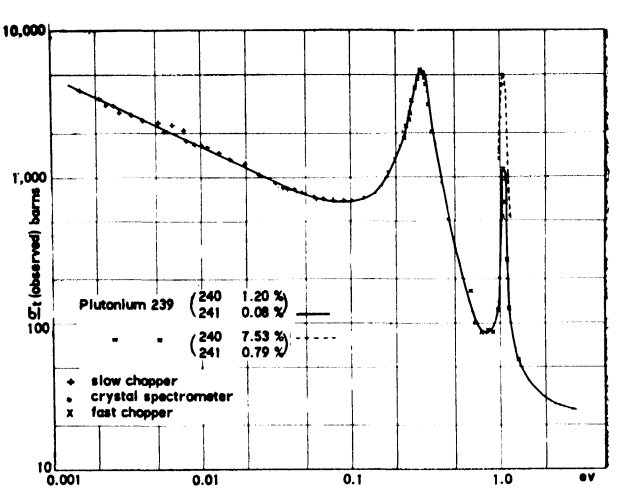

Figure 4

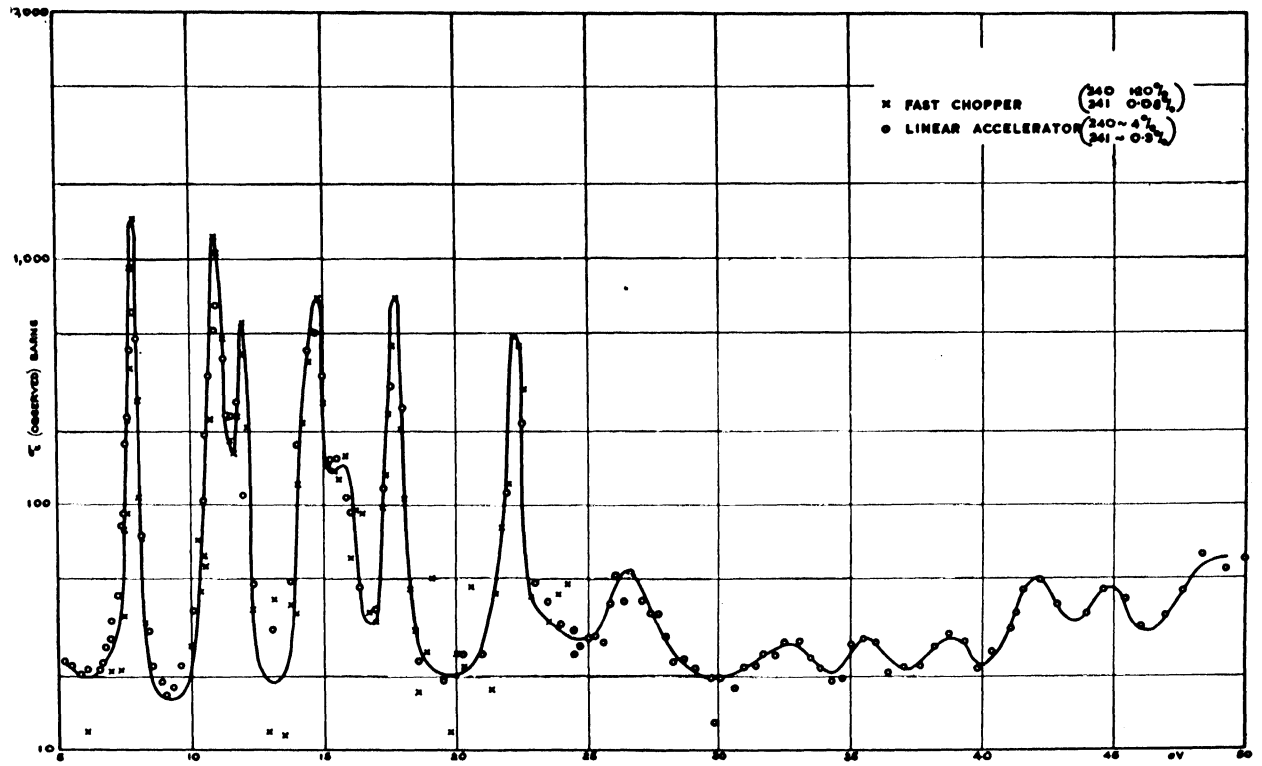

Figure 5

The calibrated thick sample was used to investigate the energy region from 5.5 ev to 25 ev, and resonances were observed at 7.85 ev, 10.95 ev, 11.95 ev, 14.3 ev, 14.75 ev, 17.75 ev and 22.35 ev (Fig. 5). The full width at half height of the resolution function in this energy range was 0.1–0.2 μsec/metre. The levels at about 15 ev are not fully resolved, but there could possibly be three distinct levels. The errors on the individual points shown in the figure are estimated to be about 12% at the peaks, and about 80% between resonances.

Linear Accelerator Neutron Spectrometer (*a*) 5-50 ev (Rae, Wilblin) (*b*) 40-90 ev (Lynn, Wiblin)

The observed total cross sections are plotted in Fig. 5. Two samples were used in the 5–50 ev range.

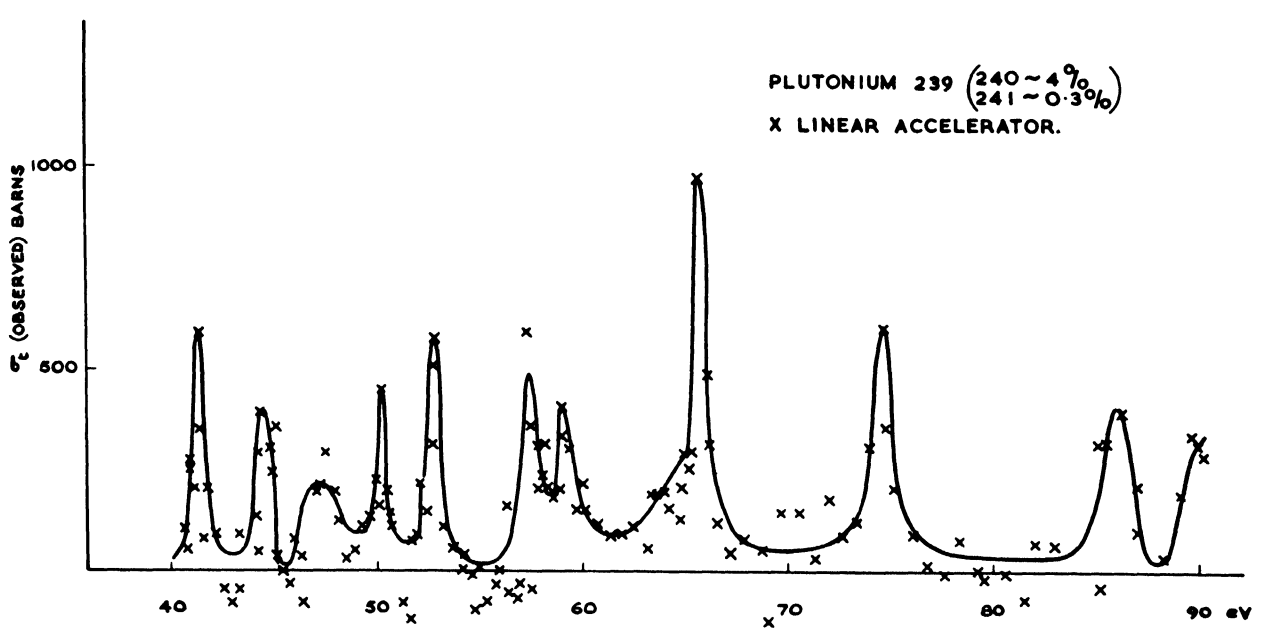

Figure 6

A sample of 3 in. diameter, containing 0.023×10^{24} atoms/cm^2 of plutonium metal, was used between resonances. The peaks were explored with a thinner 2 in. diameter sample of an aluminium-plutonium mixture containing 0.00122×10^{24} atoms/cm^2, with a plutonium-240 content of approximately 4%. The resolution was approximately 0.4 μsec/metre at 8 ev, 0.3 μsec/metre at 25 ev, and 0.2 μsec/metre from 25 ev upwards. The errors on the individual points are everywhere about 7%.

The values of observed total cross section from 40 to 90 ev (Fig. 6) were also obtained with a sample containing approximately 4% of plutonium-240. The resolution was about 0.5 sec/metre. The positions of the levels shown in Fig. 6 have been confirmed from other measurements on the yield of capture gamma rays, but the precision of the transmission measurements is insufficient to permit deductions regarding the values of the resonance parameters.

The results obtained with the various machines are compared in Table II.

REFERENCES

1. P/767, Volume 4, Session 15A, these Proceedings.
2. P/421, Volume 4, Session 15A, these Proceedings.

The Total and Fission Cross Section of Plutonium

By B. R. Leonard, Jr.,* USA

The neutron transmission and fission cross sections of plutonium-239 have been investigated by several research groups. The neutron spectrometers used have included modulated cyclotron and fast chopper time-of-flight spectrometers, crystal diffraction spectrometers, and Van de Graaff accelerators. Only those details of operation are discussed here which are of particular importance to the present measurements and the reader is referred to the available literature for a more complete discussion of these types of instruments.[1-4] Particular attention has been paid to the use of consistent expressions for the energy resolution of the different instruments used in these measurements. The resolution is expressed in the convention of the time-of-flight spectrometers as Δt in μsec/m (microseconds/meter) where $2\,\Delta t$ is the total uncertainty in timing divided by the flight distance. The quantity Δt is related to ΔE (ev), the full width at half maximum of the equivalent energy resolution triangle by $\Delta E/E = -0.028\,E^{1/2}\Delta t$.

The discussion of the plutonium cross section falls naturally into three energy regions: the thermal region extending to about five ev which is dominated by the resonance at about 0.3 ev, the resonance region from about 5 to 55 ev where most individual resonances have been resolved, and the higher energy region where only average cross sections have been obtained. The analysis of the cross sections presented has been based on the concept of non-interfering single-resonance levels which are characterized by the Breit-Wigner formulation[5]

$$\sigma(n,x) = \sqrt{\frac{E_0}{E}}\ \frac{\sigma_{x_0}\,\Gamma^2}{4\,(E-E_0)^2+\Gamma^2} \qquad (1)$$

where

$$\sigma_{x_0} = 4\pi\lambda^2 g\,\frac{\Gamma_n\,\Gamma_x}{\Gamma^2}$$

In the equations, the subscript zero refers to values at exact resonance, $2\pi\lambda$ is the neutron DeBroglie wavelength, Γ_n and Γ_x the partial widths for scattering and reaction x respectively, and Γ the total width is the sum of all the partial widths, and g the statistical weight factor. In the thermal region the resonant scattering contribution is small. Therefore the scattering interference effects have been neglected in the analysis and the scattering cross section has been assumed constant. In the resonance region assignments of the positions and of the strengths, $\sigma_0\,\Gamma^2$, of the observed levels have been made.

The discussion has been divided into separate sections on the total and fission cross-section measurements because of the large difference in methods involved in the two types of measurements.

THE TOTAL CROSS SECTION

The Thermal Region

Measurements of the total cross section of Pu^{239} have been obtained in the thermal neutron energy region by the use of modulated cyclotron neutron time-of-flight spectrometers. Early measurements were made by Anderson, Lavatelli, McDaniel, and Sutton at Los Alamos. A reasonably good determination of the shape of the total cross section was obtained from these measurements. However, the rather poor energy resolution and some uncertainty in timing limits the usefulness of a detailed analysis of these data. The value of the cross section at the peak of the 0.3 ev resonance, σ_{to}, which was obtained is of some interest since a thin sample ($n\sigma_{to} \simeq 1.25$) was available. A value of $\sigma_{to} = 5600 \pm 250$ barns (1 barn $= 10^{-24}$ cm^2) was obtained after a correction for resolution of about 6 per cent.

Transmission measurements in the thermal neutron energy region with improved resolution were carried out by Havens, Melkonian, Rainwater, and Levin with the Columbia University pulsed cyclotron neutron velocity spectrometer. The data obtained in these measurements are shown in Fig. 1 in the form $\sigma\sqrt{E}$ vs E for the energy region below 1 ev. Some of the Los Alamos data are also shown on this plot. In addition to the general features of the cross-section curve obtained in the Los Alamos measurements, the Columbia measurements show the existence of a level at 1.06 ev. By using samples of varying Pu isotopic composition it was found that the Pu^{240} isotope was responsible for this resonance.

Analysis of the Data

The total cross section in the thermal neutron energy region has been characterized by five over-

* General Electric Company, Hanford. Including work done by E. E. Anderson, Los Alamos Scientific Laboratory; L. M. Bollinger, R. E. Coté, Argonne National Laboratory; W. J. Friesen, Hanford; S. P. Harris, Argonne; W. W. Havens, Jr., Columbia University; C. T. Hibdon, A. S. Langsdorf, Jr., Argonne; L. S. Lavatelli, Los Alamos; J. M. LeBlanc, Argonne; B. R. Leonard, Jr., Hanford; M. Levin, Columbia; B. D. McDaniel, Los Alamos; E. Melkonian, L. J. Rainwater, Columbia; E. J. Seppi, Hanford; and R. B. Sutton, Los Alamos.

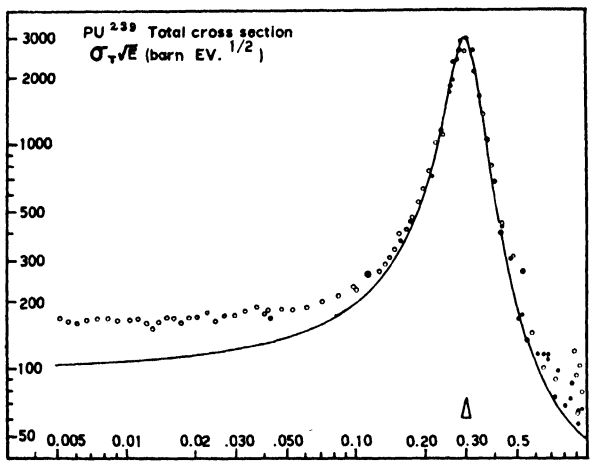

Figure 1. The total cross section of Pu^{239} in the thermal region. The open circles are Columbia University data corrected for the 1.06 ev resonance in Pu^{240}. The full circles are Los Alamos data. Both sets of data were obtained with modulated cyclotron neutron time-of-flight spectrometers. The solid curve is the Columbia University theoretical fit to the data without the term for the negative level

lapping effects. Besides the level at 1.06 ev attributed to Pu^{240} and the resonance at 0.3 ev there are a constant scattering cross section, a $1/v$ term due to distant levels, and one or more virtual levels at negative energy. In order to evaluate these effects separately, portions of the energy region were chosen in which one or two effects were dominant. The small contributions of the other effects could then be estimated from only approximate knowledge of their characteristics. When the several effects were evaluated in this manner, successive approximations were employed in order to obtain the final parameters.

The energy interval from 1.2 to 2 ev, which constitutes the high energy wing of the 1.06 ev level, has been used to determine $\sigma_{to}\Gamma^2$ for this level and the constant for the $1/v$ term. After the contributions of the other terms were subtracted from the experimental points the residual cross section, σ_{res}, was assumed to be given by

$$\sigma_{res}\sqrt{E} = \frac{\sigma_{to}\Gamma^2\sqrt{1.06}}{4(E - E_o)^2 + \Gamma^2} + k(\text{a constant}) \qquad (2)$$

In the energy interval considered $4(E - E_o)^2 \gg \Gamma^2$ and a plot of $\sigma_{res}\sqrt{E}$ vs $(E - 1.06)^{-2}$ was fit by a straight line. The measured slope of the line determines $\sigma_{to}\Gamma^2 \times \sqrt{1.06/4}$ for the 1.06 ev level, and the coefficient of the $E^{-1/2}$ term is equal to the intercept. The $1/v$ term was found to be given by $\sigma\sqrt{E} = 25$ barn-ev$^{1/2}$. A value of $\sigma_{to}\Gamma^2 = 4.28$ barn-ev^2 was found for the 1.06 ev level which corresponded to $\sigma_{to}\Gamma^2 = 292$ barn-ev^2 for the Pu^{240} isotope. Further information about the parameters of the 1.06 ev level was obtained by studying the shape of the level itself. For this purpose the thinnest sample and best resolution obtainable were employed. The transmission data obtained are shown in Fig. 2. Theoretical transmission curves were compared with these transmission data by integrating Breit-Wigner single-level curves over the resolution function of the apparatus. The effect of uncertainty in the resolution width was found to be small compared to the other uncertainties involved. The effect of varying $\sigma_{to}\Gamma^2$ and Γ was investigated simultaneously. The solid line shown on Fig. 2 is the resolution smeared transmission curve calculated for $\sigma_{to}\Gamma^2 = 330$ barn-ev^2, $\Gamma = 0.045$ ev and a resolution of $\Delta t = 1.33$ μsec/m. The best values obtained in this analysis are listed in Table I along with the estimated uncertainty of the fit.

The energy interval from about 2 to 6 ev has been used to determine the constant scattering term. After the contributions of the other terms were subtracted from the experimental points the residual cross section in this region was assumed to be given by

$$\sigma_{res} = \frac{k}{\sqrt{E}} + \sigma_{sc}\ (\text{constant}) \qquad (3)$$

A straight line fit was made to a plot of $\sigma_{res}\sqrt{E}$ vs $\sqrt{E}$. A value of 9 barns was obtained for the scattering cross section from the slope of the line, and the value of the intercept was consistent with the value previously determined for the coefficient of the $1/v$ term.

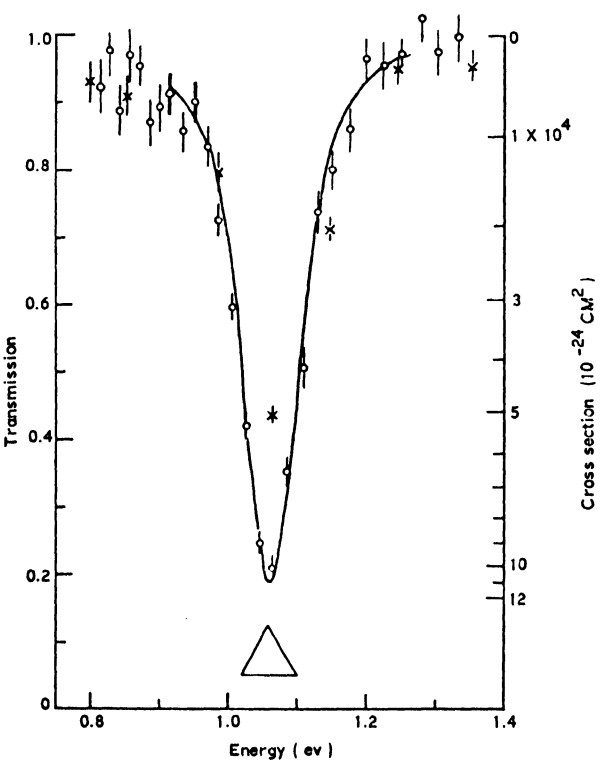

Figure 2. The 1.06 ev resonance in Pu^{240}. These transmission data were obtained with the Columbia University cyclotron neutron time-of-flight spectrometer. The open circles were taken with a resolution of 1.33 μsec/m, and the data represented by the crosses with about 3 μsec/m. The solid curve drawn is a resolution smeared transmission curve calculated for $\sigma_0\Gamma^2 = 330$ barn-ev^2, $\Gamma = 0.045$, and $\Delta t = 1.33$ μsec/m. The cross section scale refers to the Pu^{240} isotope

Table I. Resonance Parameters for the 1.06 ev Level in Pu^{240}

Shape Analysis	
$E_0 = 1.06 \pm 0.01$ ev	
$\Gamma \sim 0.042$ ev	$0.03 < \Gamma < 0.065$ ev
$\sigma_{to}\Gamma^2 \sim 350$ barn-ev^2	$250 < \sigma_{to}\Gamma^2 < 460$ barn-ev^2
$\sigma_{to} \sim 200{,}000$ barns	$60{,}000 < \sigma_{to} < 500{,}000$ barns
Wing Analysis	
$\sigma_{to}\Gamma^2_0 \sim 292$ barn-ev^2	

The resolution that was used at the 0.3 ev resonance was sufficiently good (3 μsec/m) that resolution effects on the resonance were unimportant. However a reliable measurement of the peak cross section could not be obtained because the thinnest sample available (0.479 gm/cm^2) was too thick to give a transmission significantly above zero at the resonance. The strength of the level was therefore determined from a study of the residual cross section in the wings of the resonance. Equation 1 can be rewritten for the residual cross section as

$$(\sigma_{res}\sqrt{E})^{-1} = (\sigma_{to}\Gamma^2\sqrt{E_0}/4)^{-1}\,[(\Gamma/2)^2+(E-E_0)^2] \tag{4}$$

A straight line fit was made to a plot of $(\sigma_{res}\sqrt{E})^{-1}$ vs $(E - 0.298)^2$. Then from Equation 4, the quantity $(\sigma_{to}\Gamma^2\sqrt{0.298}/4)^{-1}$ was determined from the measured slope of the line, and $(\sigma_{to}\sqrt{0.298})^{-1}$ from the intercept. The best values obtained for the parameters are shown in Table II with the parameters obtained in the Los Alamos measurements.

The Columbia University data which are plotted in Fig. 1 have been corrected for the contribution of the 1.06 ev resonance in Pu^{240}. The solid curve which is shown on this plot is the expression which has been so far derived for $\sigma\sqrt{E}$,

$$\sigma\sqrt{E} = 9\sqrt{E} + 25 + \frac{51.4\sqrt{0.298}}{4(E-0.298)^2 + (0.098)^2} \tag{5}$$

The large discrepancy between this curve and the experimental points at low neutron energies is the basis for the assumption of one or more virtual levels at negative energy. This excess cross section has been analyzed assuming a single level. The residual cross section has been plotted in the form $(\sigma_{res}\sqrt{E})^{-1/2}$ vs E. Assuming that $(E - E_0)^2 \gg (\Gamma/2)^2$, the slope of the straight line fit to this plot equals $(\sigma_0\Gamma^2\sqrt{E_0}/4)^{-1/2}$ and the intercept equals $E_0(\sigma_0\Gamma^2\sqrt{E_0}/4)^{1/2}$. The results of this analysis gave

Table II. Resonance Parameters for the 0.3 ev Resonance in Pu^{239}

	Columbia	*Los Alamos*
E_0	0.298 ev	0.295 ev
$\sigma_{to}\Gamma^2$	51.4 barn-ev^2	52.7 barn-ev^2 (derived)
Γ	0.098 ev	0.097 ev
σ_{to}	5360 barns	5600 ± 250 barns

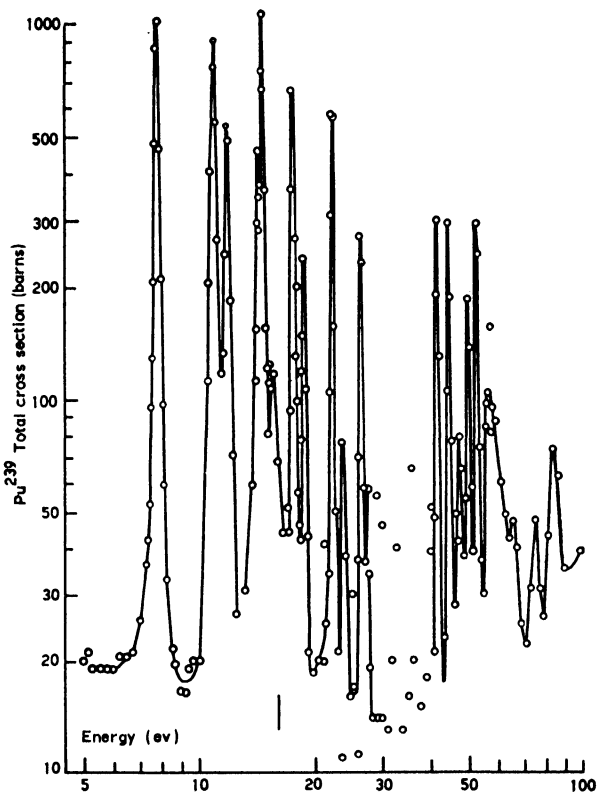

Figure 3. The total cross section of Pu^{239} in the resonance region. These data were obtained with the Argonne fast chopper with a resolution of 0.05 μsec/m. The data shown are uncorrected for resolution

$E_0 = -0.23$ ev and $\sigma_0\Gamma^2 = 27.5$ barn-ev^2 for the negative energy resonance parameters.

The Resonance Region

The total cross section of plutonium in the resonance region has recently been investigated by Bollinger, Coté, and LeBlanc with the Argonne fast chopper. The improved resolution now obtainable with this instrument of about 0.05 μsec/m has shown an increased resonance structure in this region. The data of these measurements are shown in Fig. 3. The points shown are the cross-section values calculated from the measured transmissions and are uncorrected for instrumental resolution or Doppler broadening. The smooth curve drawn through the points therefore does not represent a true cross section but is an aid in determining the positions of the resonance levels.

The prominent resonances below about 55 ev seem to have been resolved in these measurements. However weak resonances may not have been observed because of the close spacing of the levels. In the region of 29 to 40 ev where no strong resonances were observed there are possibilities of undetected weak resonances.

A preliminary investigation has been made to estimate the strengths of the observed levels below 30 ev from an area analysis of the transmission dips. The area method has been discussed extensively by Melkonian, Havens, and Rainwater.[1] If the cross section

responsible for the transmission dip is given by a Breit-Wigner single-level formula then the measured area, A_E, between the transmission curve and unity is given approximately by

$$A_E = \tfrac{1}{2}\pi n\sigma_0\Gamma \qquad n\sigma_0 \ll 1 \qquad (6)$$

$$A_E^2 = \pi n\sigma_0\Gamma^2 \qquad n\sigma_0 \gg 1 \qquad (7)$$

where $T = e^{-n\sigma}$, for the two limiting values of $n\sigma_0$. For the values of foil thickness used in the measurements the relation $n\sigma_0 \gg 1$ is true for most of the resonances. The measured areas then yield the approximate strengths, $\sigma_0\Gamma^2$, of the resonances. When the effect of Doppler broadening is considered the Equation 7 must be modified to include a factor $1/y$ which is dependent on the value of Γ for the resonance. This correction can be obtained from the curves of Seidl, *et al.*[2] For a very thick sample the dependence of $\sigma_0\Gamma^2$ on Γ is small and the average value of the directly measured Γ's obtained in the good resolution region is usually satisfactory. As the sample thickness decreases the dependence on Γ can become quite large. Most of the data of these measurements were taken with a sample thickness such that the dependence of $\sigma_0\Gamma^2$ on the value chosen for Γ was significant. Values of $\sigma_0\Gamma^2$ were therefore obtained for two different choices of level width, $\Gamma = 0.1$ ev and $\Gamma = 0.05$ ev. A very thick sample was also used for four of the resonances so that the dependence of $\sigma_0\Gamma^2$ on the assumed value of Γ was small. For three of these resonances better agreement of the values for $\sigma_0\Gamma^2$ obtained from the two sample thicknesses was obtained for $\Gamma = 0.05$ ev in contrast to the value of $\Gamma = 0.1$ ev for the 0.3 ev level. A summary of the positions and estimated strengths of the resonances observed from 5 to 30 ev is given in Table III. All these resonances are assumed to be in the Pu^{239} isotope.

Table III. A Summary of the Positions and Estimated Strengths of the Observed Resonances in the Total Cross Section of Pu^{239} from 5 to 30 ev.

E_0 (ev)	Sample thickness (atoms/barn 10^{24})	$\sigma_0\Gamma^2$ $\Gamma = 0.1$ ev	$\sigma_0\Gamma^2$ $\Gamma = 0.05$ ev
7.82	1.903	19	13
	35.32	10	10
11.0	1.903	34	28
11.9	1.903	15	10
14.3	1.903	9	4.5
14.7	1.903	19	13
15.3	1.903	(weak resonance - $\sigma_0\Gamma \simeq 24$, for $\Gamma = 0.1$ ev)	
17.6	1.903	18	11
	35.32	9	8
	35.32	12	11
18.7	1.903	(weak resonance - $\sigma_0\Gamma \simeq 41$, $\Gamma = 0.1$ ev)	
22.2	1.903	21	12
	35.32	10	9
(27.3) ?			
26.4	1.903	9	5
	35.32	9	8
(23.6) ?	35.32	(weak) ~ 0.4	

The Higher Energy Region

The recent Argonne fast chopper measurements cover the energy range up to 100 ev. Transmission dips which were observed at neutron energies of about 57 ev, 65 ev, 75 ev, and 85 ev are shown on the plot of Fig. 3. Earlier measurements by Bollinger and Harris at Argonne were extended to about 5000 ev. These data are shown on the plot of Fig. 4 with the smooth curve indicating the groups of resonance levels which were observed.

Transmission cross-section measurements of Pu^{239} have been made from 1.15 kev to 100 kev by Hibdon and Langsdorf at Argonne. The neutrons were produced by the $Li^7(p, n)Be^7$ reaction with the Argonne Van de Graaff generator. All the measurements were made by use of the neutrons observed at an angle of 120 degrees with respect to the incident proton beam. Thin Li targets about 1.3 kev thick were used in order to obtain good resolution. A large group of BF_3 counters embedded in paraffin and surrounded by a massive shield were used to reduce the background counting rates.[4] The high counting efficiency of this detector system made possible transmission measurements to neutron energies as low as 1.15 kev. The results of these measurements as shown on Fig. 4 show a steady drop in the total cross section from 18.5 barns at 1.15 kev to about 12 barns at 100 kev.

THE FISSION CROSS SECTION

The Thermal Region

Measurements of the variation of the Pu^{239} fission cross section relative to the $B^{10}(n, \alpha)Li^7$ cross section have been made by Leonard, Seppi, and Friesen at Hanford with a neutron crystal diffraction spectrometer. These measurements covered the range of incident neutron energies from 0.020 ev to 2.5 ev with an isolated point at 0.005 ev.

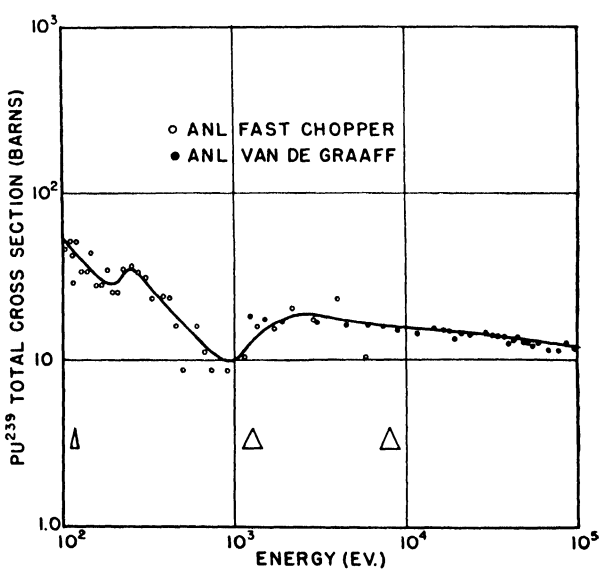

Figure 4. The total cross section of Pu^{239}. The open circles represent data obtained with the Argonne fast chopper. The full circles were obtained with $Li^7(p,n)Be^7$ neutrons from the Argonne Van de Graaff

The (10·1) and (10·3) reflections of a beryllium crystal monochromator were used to obtain suppression of higher order diffractions. Only first and second order diffractions were important above 0.02 ev because of favorable crystal structure factors. The data below 0.6 were obtained corrected for second order diffraction by the application of standard filter techniques. The (10·3) reflection was used above 0.1 ev and with a 0.31 degree angular collimation of the incident neutron beam gave an energy resolution of 2.75 μsec/m. The point at 0.005 ev was taken with a LiF (111) reflection with a powdered beryllium filter in the incident neutron beam to reduce the higher order diffracted neutrons.

The detector used was a double-chambered, argon-CO_2 filled, parallel-plate ionization chamber. The first chamber contained a foil with a thin deposit of boron enriched in B^{10}. The alpha-particle ionization pulses of the $B^{10}(n,\alpha)Li^7$ reaction were used to furnish an accurate $1/v$ comparison cross section. The second portion of the chamber was separated from the first with a thin aluminum window and contained a foil of about 0.1 mg/cm² deposit of Pu^{239} in the same neutron beam. A delay line clipper was used to reduce the alpha pile-up pulses and the fission fragment ionization pulses furnished the fission response. The total correction for neutron attenuation in the foils and gas of the chamber was less than 0.25 per cent for neutron energies greater than 0.02 ev. Both the boron and plutonium foils were prepared by high voltage sputtering techniques in order to assure good uniformity of thickness.

The background and order corrected ratio of fission to boron counting rate is proportional to $\sigma_f\sqrt{E}$. The absolute value of the fission cross section was not determined since the foil weights were not accurately known. The data were normalized to a value of $\sigma_f = 750$ barns for neutrons of 2200 m/sec velocity. This normalization is based on the value of σ_f (2200 m/sec) = 580 barns for U^{235}, and an average value of 1.405 for the absolute value of the ratio of Pu^{239} to U^{235} fission cross sections for the flux in a thermal column obtained by several investigators.

The data obtained for neutron energies below 1.0 ev are shown in the form $\sigma_f\sqrt{E}$ vs E on Fig. 5. The statistical deviations of the points below 0.3 ev are from 0.2 to 1.0 per cent and increase to about six per cent at 1.0 ev. The data shown are corrected in the region of the 0.3 ev resonance for instrumental resolution and Doppler effect. Both corrections are small; the maximum resolution correction was one per cent and the maximum Doppler correction was two per cent.

Analysis of the Data

Preliminary analysis indicated that a fit to the low-energy fission cross section could be made assuming two effects other than the 0.3 ev resonance. The first was a $1/v$ contribution from distant levels. The second was a residual cross section at lower energies indicating a contribution from nearby negative levels.

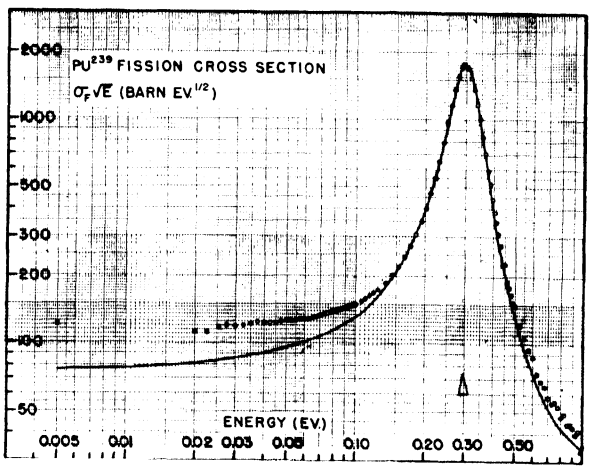

Figure 5. The fission cross section of Pu^{239} in the thermal region. These data were obtained with the Hanford neutron crystal diffraction spectrometer. The solid curve shows the fit of the Breit-Wigner single level to the 0.3 ev resonance plus a $1/v$ term. The excess cross section at low energies is attributed to negative levels

Each of these effects was evaluated in the energy interval in which it was the dominant one. Successive approximations were then applied to obtain the best parameters.

The residual cross section in the energy region from 1.2 to 2.5 ev showed no systematic deviation from $1/v$ within the precision of the data. These data were therefore averaged to obtain $\sigma_f\sqrt{E} = 25 \pm 5$ barn-ev$^{1/2}$ for the $1/v$ term. Most of the error assigned to this term arises from fluctuations in the data which may be due to the reflection of higher energy resonances in higher order diffractions.

The energy interval from 0.4 to 0.5 ev was used to determine $\sigma_{f0}\Gamma^2$ for the 0.3 ev resonance. The residual cross section was plotted as $(\sigma_{res}\sqrt{E})^{-1}$ vs $(E - E_0)^2$. From the slope of the straight line fit to this plot a value of $\sigma_{f0}\Gamma^2 = 37 \pm 5$ barn-ev² was determined.

The corrected data in the region of the resonance were used to obtain σ_{f0} and Γ directly from a shape analysis. A precise determination could not be obtained because of systematic deviations in the wings of the resonance. The nature of the discrepancy was such that the experimental values were lower than the Breit-Wigner curve around 0.15 ev and higher than the curve around 0.45 ev. The discrepancy was of the order of five per cent which was much larger than the statistical uncertainties of the points. In order to minimize this discrepancy it was found that the largest σ_{f0} and the smallest value of Γ commensurate with the estimated uncertainties of these parameters would give the best fit in the wings of the resonance. Chosen parameters are listed in Table IV.

The errors shown in Table IV are derived from the statistical uncertainties of the data and include an approximately equal contribution in E_0 and Γ due to an estimated uncertainty of 0.02 degrees in the calibrated zero of the spectrometer.

The 0.3 ev resonance parameters obtained from the shape analysis and the $1/v$ term were used to plot the solid curve of Fig. 5. The large discrepancy of this curve with the experimental points at low energies is the basis for the assumption of a negative level. This residual cross section was plotted in the form $(\sigma_f\sqrt{E})^{-1/2}$ vs E. Assuming that $(E - E_0)^2 \gg (\Gamma/2)^2$ the parameters $\sigma_0\Gamma^2 = 14.3$ barn-ev^2 and $E_0 = -0.19$ were obtained from the straight line fit to the data.

The Resonance Region

The variation of the Pu^{239} fission cross section with neutron energy has been measured by Anderson, *et al.*, at Los Alamos using a modulated cyclotron time-of-flight spectrometer. These measurements extended from thermal energies up to 500 ev. A detailed analysis of the thermal region has not been presented because of the rather poor resolution which was used in this region. The best resolution obtainable at the 0.3 ev resonance of 6.7 μsec/m caused a correction of about 10 per cent in the value of the peak cross section. Above 4 ev a resolution of about 1.67 μsec/m was used. Absolute cross-section measurements were not made in this experiment and these data have been normalized to agree with the low energy crystal spectrometer measurements in the vicinity of 0.5 ev.

Table IV. Resonance Parameters for the 0.3 ev Fission Resonance in Pu^{239}

Shape Analysis
$E_0 = 0.299 \pm 0.001$ ev
$\sigma_{f0} = 3190 \pm 50$ barns
$\Gamma = 0.102 \pm 0.004$ ev
$\sigma_{f0}\Gamma^2 = 33.2 \pm 3$ barn-ev^2 (derived)
Wing Analysis
$\sigma_{f0}\Gamma^2 = 37 \pm 5$ barn-ev^2

The detector used in these measurements consisted of a triple-chambered ionization chamber. The two end chambers each had two Pu^{239} fission foils with a thickness of about 0.3 mg/cm^2 in a double parallel-plate ionization chamber. The central chamber was filled with 3 cm Hg pressure of BF_3 counting gas and 60 cm Hg of argon. The BF_3 was used in the center chamber in order to obtain a response corresponding to the average spectrum, intensity, and flight path as seen by the two end fission chambers. Collimating grids were used in the fission chambers to discriminate against the most effective alpha pulses and delay line clippers were used to reduce the alpha pile-up rate. Data were obtained from the BF_3 and fission chambers in alternate runs so that the chamber was not moved from its position in the beam.

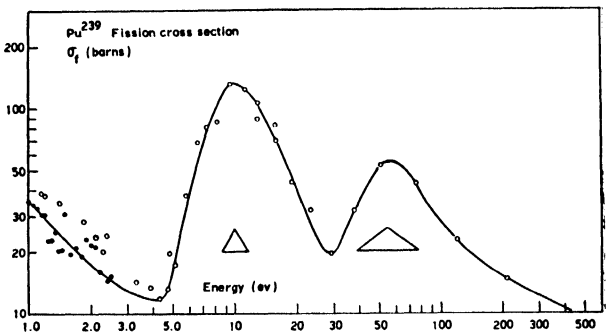

Figure 6. The fission cross section of Pu^{239} in the resonance region. The open circles represent data obtained with the Los Alamos cyclotron neutron time-of-flight spectrometer. The full circles are Hanford crystal spectrometer data. The Los Alamos data are normalized to the low energy data around 0.5 ev. Only groups of resonance levels were observed with this resolution

The data obtained above 1 ev are shown on the plot of σ_f vs E of Fig. 6, normalized to the low-energy data. The uncertainty of the background corrections in the low cross-section regions of this measurement is probably the cause of the disagreement with the crystal spectrometer data from 1 to 2.5 ev. With the resolution attainable in these measurements individual resonances were not resolvable. The broad peaks observed at about 10 and 55 ev correspond to the general grouping of resonance levels observed in the total cross-section measurements.

REFERENCES

1. Melkonian, E., Havens, W. W., Jr. and Rainwater, L. J., *Slow Neutron Velocity Spectrometer Studies, V. Re, Ta, Ru, Cr, Ga,* Phys. Rev. *92,* 702, (1953). This paper contains references to earlier work.
2. Seidl, F. G. P., Hughes, D. J., Palevsky, H., Levin, J. S., Kato, W. Y. and Sjöstrand, N. G., *"Fast Chopper" Time-Of-Flight Measurements of Neutron Resonances,* Phys. Rev. *95,* 476, (1954).
3. Borst, L. B. and Sailor, V. L., *Neutron Measurements with the Brookhaven Crystal Spectrometer,* Rev. Sci. Instr., *24,* 141 (1955).
4. Hibdon, C. T., Langsdorf, A. and Holland, R. E., *Neutron Transmission Cross Sections in the Kilovolt Region,* Phys. Rev. *85,* 595, (1954).
5. See for example: Blatt, J. M. and Weisskopf, V. F., *Theoretical Nuclear Physics,* John Wiley and Sons, N. Y., (1952).

The Low Energy Cross Sections of U^{235}

By V. L. Sailor,* USA

Until the present very little information about the cross section of U^{235} has appeared in the literature. The published data include values of the various thermal cross sections,[1-3] and three curves of the fission cross section as a function of energy.[4-6] Fission measurements made by Keller[4] indicated that the low energy cross section might differ from $1/v$. Independent measurements made at Kjeller, by Popović[5] and at Saclay by Hubert, Vendryes and Auclair[6] disclosed a resonance in the fission cross section at 0.29 ev. In addition, the shape of the cross-section curve[5,6] below $\sim$ 0.2 ev showed that a bound level ("negative energy" resonance) was present close to $E = 0$. The measurements of Hubert *et al.*[6] which extended over the energy range from 0.01 to $\sim$ 2.2 ev located additional resonances at 1.13 and $\sim$ 2.0 ev. Other than the above important results, all values of the U^{235} cross sections have remained unpublished.

It is the purpose of this paper to collect and summarize the results on the resonances in U^{235} which have been obtained in the United States. The earliest among these were extensive measurements made in 1944 at Los Alamos by McDaniels *et al.*[7] The cross section, as a function of energy, was measured over the energy range from 0.01 to 1000 ev. The measurements were made with the time-of-flight spectrometer formerly built and used at Cornell.[8] The main features of the total and fission cross sections were obtained from these data, although the instrument resolution was inadequate to resolve many of the resonances above $\sim$3 ev.

In 1947, a series of measurements with improved instrument resolution was undertaken at Columbia University[9-11] using the Columbia "Neutron Velocity Selector".[12] More recent studies have been made at Hanford,[13] at Knolls,[14] and at Brookhaven.[15-17] The results of these various studies are discussed in detail in the following sections.

THE RESONANCE SPECTRUM OF U^{235}

The cross section of U^{235} contains many weak and closely spaced resonances. The average spacing between resonances is only 0.7 $\pm$ 0.1 ev. Compared with isotopes of other heavy elements, the spacing in U^{235} is quite small and consequently, the resonance spectrum is unusually complicated. Further complications are introduced by the occurrence of fission. The results obtained at Columbia[9,10] have established that the same resonances appear in both the capture and fission cross sections. No exceptions to this have been found among the first fifteen resonances which lie in the region where instrument resolution was adequate; i.e., $E \lesssim 10$ ev. It should be noted, however, that the ratio of capture to fission is not the same for all resonances.

The Total Cross Section

The total cross-section measurements provide the most accurate information about the spectrum of resonances. These cross sections have been obtained from transmission measurements on samples enriched in U^{235}. It is important to note that the observed cross sections generally differ from the true cross sections especially near the peaks of the resonances. This discrepancy arises from the Doppler broadening and the finite instrument resolution. The discrepancy becomes greater at higher energy.

The total cross section below 0.6 ev is given in Fig. 1 These data were obtained with a crystal spectrometer by Leonard *et al.*[13] at Hanford. They

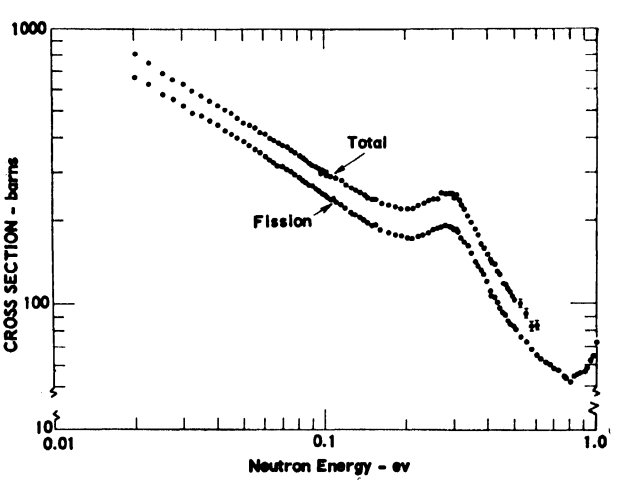

Figure 1. The total and fission cross section of U^{235} at energies below 1 ev. The fission curve has been normalized to 580 barns at $E = 0.0253$ ev. Uncertainties due to counting statistics are smaller than the diameter of the circles except in regions noted. These data were obtained with the Hanford crystal spectrometer[18]

* Brookhaven National Laboratory. Including work by W. W. Havens, Jr., M. Levin, E. Melkonian, V. Perez-Mendez, and L. J. Rainwater, Columbia University; E. R. Gaerttner, and M. L. Yeater, Knolls Atomic Power Laboratory of the General Electric Company; W. J. Friesen, B. R. Leonard, and E. J. Seppi, Hanford Atomic Products Operation of the General Electric Company; H. L. Foote, Jr., J. A. Harvey, D. J. Hughes, H. H. Landon, V. E. Pilcher, and V. L. Sailor, Brookhaven National Laboratory, Associated Universities, Inc.

are in good agreement with the results of Havens *et al.*[9] (not shown).

Recent measurements over the range from 0.1 to > 40 ev have been made with high resolution (0.15 to 0.20 μsec/m) with the fast chopper[15,18] and the crystal spectrometer[16,19] at Brookhaven. These data (Figs. 2–5) are the source of most of the resonance parameters listed in Table I. The data above 1000 ev were obtained with a Van de Graaff accelerator at Argonne by Hibdon and Langsdorf.[20]

The average spacing between resonances is derived from a histogram of the distance to the next level versus the level number (Fig. 6). This curve changes slope above 10 ev which indicates that instrument resolution was not adequate for separating all of the resonances above this energy. Above 40 ev (Fig. 5) the resonance structure gradually disappears due to inadequate instrument resolution. Variations in the cross section at higher energies represent fluctuations in the average strengths and spacings of levels.

The Fission Cross Section

The fission cross-section measurements of Perez-Mendez *et al.*[10] are presented in Figs. 7 and 8 (black dots). These data were obtained with a fission counter operated on the "Neutron Velocity Selector"[12] timing system. The fission counter was a pulse-ionization chamber having many sets of parallel plates coated with a thin, uniform deposit of enriched U^{235}. Pulses produced by the fission fragments were counted. The relative intensity of the neutron beam at each energy was obtained with a "thin" ($1/v$) BF_3 proportional counter.

Independent measurements at low energy (Fig. 1) made on a crystal spectrometer by Leonard *et al.*[13] agree reasonably well with the Columbia results. The method used by Leonard was similar to the above, except that the fission chamber and the boron counter were combined into one unit.

At much higher energy, the fission cross section (Fig. 8) has been measured on a time-of-flight spectrometer at Knolls by Yeater *et al.*[14] Although the instrument resolution used in these measurements was unusually good (0.05 μsec/m), the resonances lie too closely together to be resolved. Above ~ 500 ev, the Doppler broadening of the resonances becomes of the same order of magnitude as the average spacing, thus causing the resonances to merge. Therefore, the high energy data provide information about averages over many resonances but no information about individual resonances. The structure in the cross-section curve above 1000 ev is attributed to fluctuations in the average density and spacings of levels.

The fission cross sections obtained in all of the above measurements are not absolute. It is necessary to normalize the data to the value of the fission cross section at thermal (2200 m/sec). The value used in the normalization of all the data was $(\sigma_f)_{th} = (580 \pm 8) \times 10^{-24}$ cm². This was obtained by combining the thermal absorption cross section,[2] $\sigma_a = 687 \pm 7$, with the thermal value of $\alpha = \sigma_c/\sigma_f = 0.184 \pm 0.008$ determined by a mass spectrometer measurement.[21]

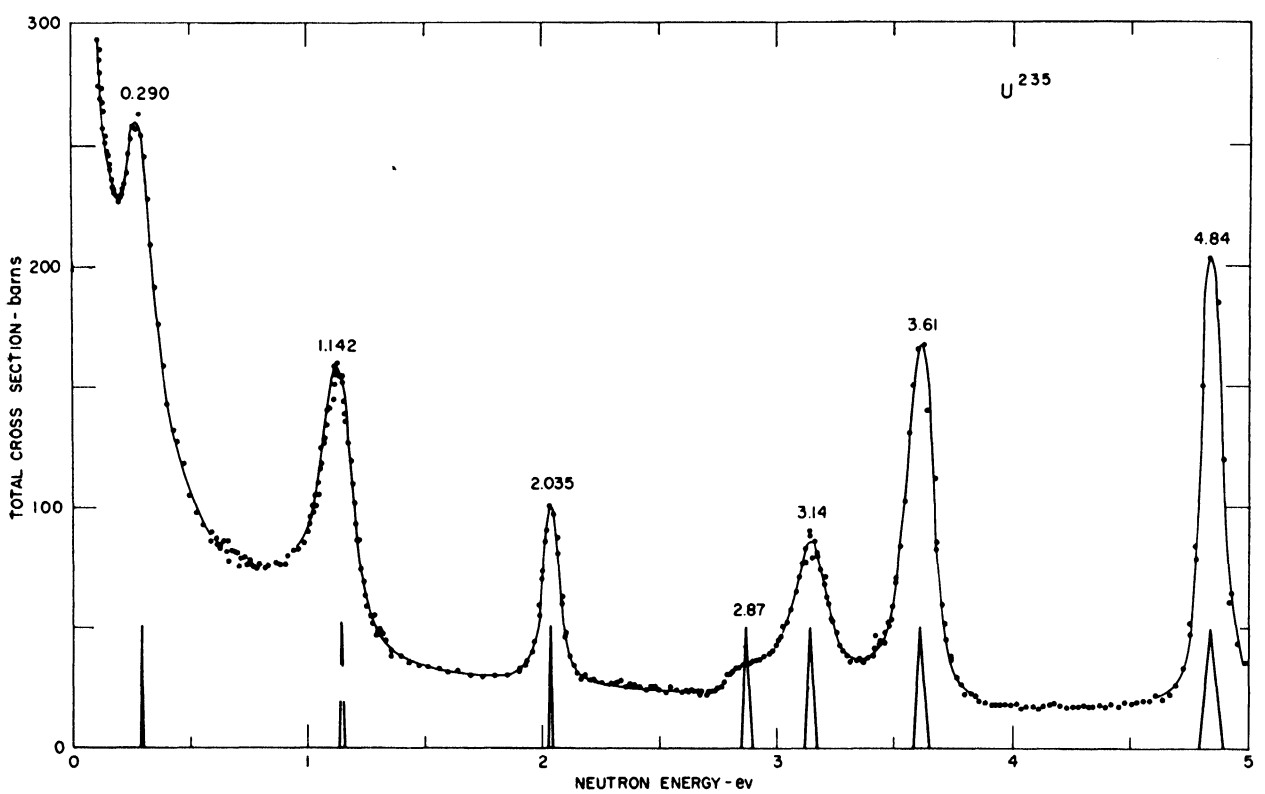

Figure 2. The total cross section of U^{235} below 5 ev. These data were taken at a resolution of 0.17 μsec/m with the Brookhaven crystal spectrometer[16]

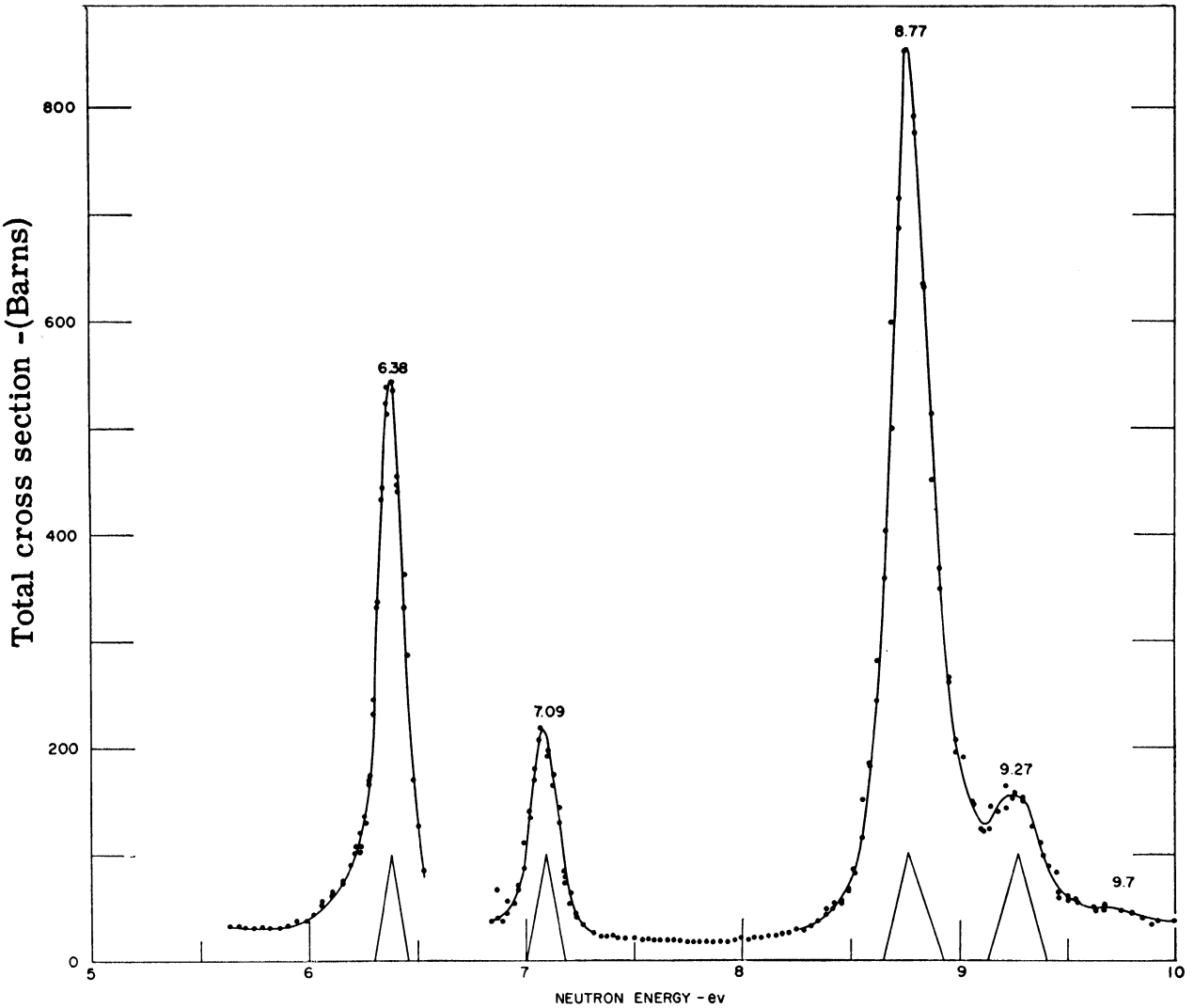

Figure 3. The total cross section of U^{235} from 5 to 10 ev. Resonances in U^{234} and U^{238} impurities in sample prevented observation in the region 5.0 to 5.6 ev and 6.5 to 6.8 ev. These data were obtained with the Brookhaven crystal spectrometer[16]

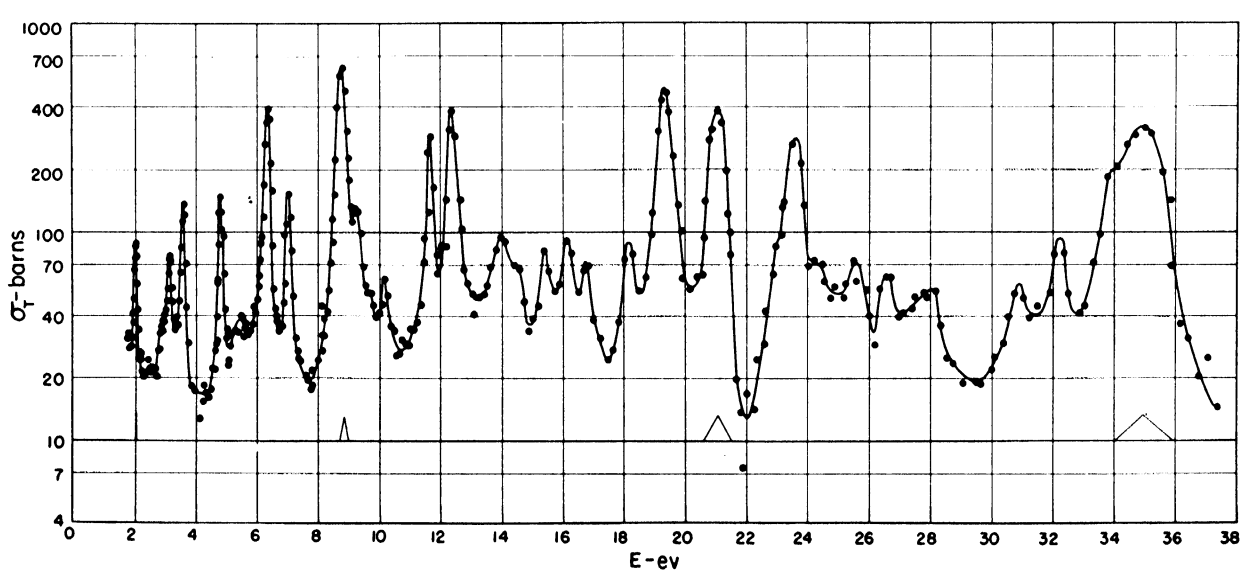

Figure 4. The total cross section of U^{235} over the range 2 to 40 ev. These measurements were made with the Brookhaven fast chopper.[15] Comparison with Figs. 2 and 3 shows that the measurements with time-of-flight and crystal spectrometers give good agreement

Table I. The Breit-Wigner Parameters for the Resonances in U^{235}

The values of $\alpha \equiv \sigma_c/\sigma_f$ for the 0.290 and 2.035 ev levels were obtained by combining fission and total cross section data. These lead to an average radiation width $\bar{\Gamma}\gamma = (29.5 \pm 6.0) \times 10^{-3}$ ev. All other entries in the table have been derived from total cross-section data and $\bar{\Gamma}\gamma$. The value of α listed is characteristic of the individual resonance at the center of the resonance. All partial widths are listed in units of millivolts where 1 mv $\equiv 10^{-3}$ ev. The number appearing under the entry in each case gives the estimated error in the corresponding digit immediately above.

Total parameters						*Fission parameters*			*Ref.*
E_0 (*ev*)	$\sigma_0\Gamma$ (*barn-ev*)	σ_0 (*barn*)	Γ (*mv*)	$2g\Gamma_n$ (*mv*)	$2g\Gamma_n^0$ (*mv*)	$\sigma_{f0}\Gamma$ (*barn-ev*)	Γ_f (*mv*)	α –	
−1.4	–	–	210	–	3.1	–	180	0.16*	†
2			30		3		20		
−0.02	–	–	75	–	0.00096	–	44	0.70	‡
0.290	13.9	109	128	0.0031	0.0058	10.8	98	0.29¶	†
5	5	5	5	2	3	4	5	4	
1.142	17.6	117	150	0.0154	0.0144	14.1	120	0.25	†
10	5	6	7	8	7	9	6	8	
2.035	5.0	114	44	0.0078	0.0055	1.5	14	2.3§	†
5	2	6	5	9	3	5	5	7	
2.86	1.8	20	90	0.004	0.002	1.2	60	0.5	‡
7	3	10	40	1	1	5	40	5	
3.140	13.0	76	170	0.031	0.018	10.7	140	0.21	†
5	1.3	8	20	3	2	1.2	70	7	
3.610	18.2	188	97	0.0505	0.0266	12.7	68	0.43	†
5	2	9	5	25	13	1.2	4	14	
4.84	16.7	350	48	0.0622	0.0282	6.4	19	1.6	†
3	1.7	35	5	30	15	1.6	7	6	
5.4									
2	8	–	–	0.04	0.017	–	–	–	‡, **
5.6	4			2	9				
2									
6.2	8	–	–	0.04	0.016	–	–	–	‡, **
2	4			2	8				
6.38	58.6	910	64	0.287	0.114	31.7	34.5	0.85	†
4	6.0	90	7	30	12	6.0	9.0	28	
7.09†	23	360	60	0.13	0.049	12	30	0.9	‡
5	2	130	20	1	5	3	20	5	
8.77†	160	1200	130	1.08	0.36	120	100	0.3	‡
8	13	400	30	9	3	15	30	2	
9.27†	20	–	–	0.14	0.046	–	–	–	‡
10	4			3	9				
9.5									
2	8	–	–	0.06	0.02	–	–	–	‡, **
9.8	4			3	1				
2									
10.2	11	–	–	0.09	0.027	–	–	–	‡
1	2			2	5				

The Scattering Cross Section

The scattering from U^{235} consists primarily of potential scattering. The scattering due to individual resonances can be computed from the resonance parameters. Such computations show that most of the resonances in U^{235} give scattering cross sections which are negligible relative to the absorption cross section (e.g., at $E = 1.14$ ev, the resonance scattering $\sigma_s - \sigma_p = 0.5 \times 10^{-3}$ barns, compared to $\sigma_c + \sigma_f \approx 150$ barns).

The ratio of the scattering to the total cross section has been measured at Columbia by Melkonian[11] using a method previously described.[22] The scattering cross section can be obtained from these data by combining with the total cross-section curves. A plot of Melkonian's scattering data is shown in Fig. 9. The relatively small value of the ratio σ_s/σ_t makes the measurements very difficult and accounts for the large uncertainty in the data. The average scattering cross section above 1 ev obtained from these data is $\bar{\sigma}_s = 11.3 \pm 1.0$ barns.

Using a crystal spectrometer at Brookhaven, Foote[17] has measured the scattering cross section at four energies. These values are listed in Table II.

The potential scattering cross section estimated from the nuclear radius (taken as $R = 1.47\ A^{1/3} \times 10^{-13}$ cm) is $\sigma_p = 10.3$ barns. The results of both Melkonian and Foote indicate $\sigma_s > \sigma_p$. A possible explanation for this in terms of the "negative energy" resonance is discussed in a later section.

Table I. The Breit-Wigner Parameters for the Resonances in U^{235} (*continued*)

Total parameters						Fission parameters			*Ref.*
E_0 (*ev*)	$\sigma_0\Gamma$ (*barn-ev*)	σ_0 (*barn*)	Γ (*mv*)	$2g\Gamma_n$ (*mv*)	$2g\Gamma_n^0$ (*mv*)	$\sigma_{f0}\Gamma$ (*barn-ev*)	Γ_f (*mv*)	a –	
11.7	70	900	80	0.63	0.19	44	50	0.6	‡
1	7	300	20	6	2	9	20	3	
12.5	160	2300	70	1.54	0.44	90	40	0.8	‡
1	12	800	20	12	3	20	20	5	
13.3	5	–	–	0.05	0.014	–	–	–	‡
3	3			3	9				
14.1	47	–	–	0.51	0.14	–	–	–	‡
2	12			13	4				
14.6	17	–	–	0.19	0.05	–	–	–	‡
3	5			6	2				
15.4	21	–	–	0.25	0.06	–	–	–	‡
2	4			5	2				
16.2	27	–	–	0.34	0.08	–	–	–	‡
2	7			8	2				
16.8	19	–	–	0.25	0.06	–	–	–	‡
2	6			8	2				
18.2	31	–	–	0.43	0.10	–	–	–	‡
2	8			11	3				
19.3	330	4100	80	4.9	1.11	190	50	0.7	‡
2	30	1200	20	5	10	30	20	4	
21.2	210	1800	120	3.4	0.74	160	90	0.3	‡
2	20	700	40	3	7	20	30	2	
23.0	17	–	–	0.3	0.06	–	–	–	‡
4	8			2	4				
23.7	110	600	170	2.0	0.40	90	140	0.21	‡
3	20	300	70	4	8	20	70	10	
24.6	28	–	–	0.5	0.11	–	–	–	‡
4	8			1	3				
25.7	39	–	–	0.8	0.15	–	–	–	‡
3	10			2	4				
26.8	31	–	–	0.64	0.12	–	–	–	‡
4	6			13	2				
28.0	42	–	–	0.9	0.17	–	–	–	‡
4	8			2	4				
31.2	45	–	–	1.1	0.20	–	–	–	‡
5	15			4	7				
32.4	76	–	–	1.9	0.33	–	–	–	‡
5	10			3	5				
33.9	180	–	–	5	0.8	–	–	–	‡
7	60			2	3				
35.3	360	2400	150	10	1.6	260	110	0.27	‡
6	60	900	50	2	3	50	50	13	

* Ref. 28
† Based on analysis by Sailor and Landon.
‡ Based on analysis by Harvey and Pilcher.
¶ Ref. 13.
§ Ref. 10.
** Evidence for existence of these resonances is inconclusive.

ANALYSIS OF THE RESONANCES

The Single-Level Formula

For a single isolated resonance the total cross section, σ_t, as a function of neutron energy, E, is given by the Breit-Wigner single-level formula:

$$\sigma_t = \sigma_c + \sigma_f + \sigma_s \tag{1}$$

The capture cross section may be written in the form:

$$\sigma_c = 4\pi\lambda\lambda_0 \frac{g\Gamma_n\Gamma_f}{4(E-E_0)^2+\Gamma^2}$$

$$= \sqrt{\frac{E_0}{E}} \frac{\sigma_{c0}\Gamma^2}{4(E-E_0)^2+\Gamma^2} \tag{1a}$$

The fission cross section as:

$$\sigma_f = 4\pi\lambda\lambda_0 \frac{g\Gamma_n\Gamma_f}{4(E-E_0)^2+\Gamma^2}$$

$$= \sqrt{\frac{E_0}{E}} \frac{\sigma_{f0}\Gamma^2}{4(E-E_0)^2+\Gamma^2} \tag{1b}$$

And the scattering cross section as:

$$\sigma_s = 4\pi\lambda_0^2 \frac{g\Gamma_n^2}{4(E-E_0)^2+\Gamma^2} + 16\pi\lambda_0 g\Gamma_n R \times \frac{E-E_0}{4(E-E_0)^2+\Gamma^2} + 4\pi R^2 = \frac{\sigma_{s0}\Gamma^2}{4(E-E_0)^2+\Gamma^2} + I\frac{E-E_0}{4(E-E_0)^2+\Gamma^2} + \sigma_p \tag{1c}$$

In the above equations, the subscript 0 refers to the value of the quantity at exact resonance, $2\pi\lambda$ is the neutron DeBroglie wavelength, and E is the neutron energy. The statistical weight factor is given by

$$g = \frac{1}{2}\left[1 \pm \frac{1}{2I+1}\right]$$

where I is the spin of the target nucleus. The total width, Γ, of the level is the sum of neutron width, Γ_n, the radiation width, Γ_γ, and the fission width, Γ_f. The effective nuclear radius is approximately $R = 1.47A^{1/3} \times 10^{-10}$ cm and the potential scattering cross section is given by $\sigma_p = 4\pi R^2$.

The above equation is strictly valid only for a resonance which is well isolated from its neighbors. However, only small errors are expected even when the formula is applied to closely spaced resonances as in the case of U^{235}. The total cross section resulting from many resonances would be given approximately as the sum of the Breit-Wigner contributions of the individual resonances:

$$\sigma_t = \Sigma_i \sigma_{ti} \qquad (2)$$

Evidence for measurable deviations in the case of U^{235} from Equation 2; i.e., interference between resonances, is discussed in a later section.

The quantities, E_0, g, Γ_n, Γ_γ and Γ_f completely define a resonance: if these parameters are known for each resonance and if the effective nuclear radius, R, is known, then the cross section can be accurately computed at any energy. The need for computations of this type for reactor design has made the accurate analysis of the resonances of considerable importance.

In addtion to the equations above, the following useful relationships should be noted:

$$\sigma_0\Gamma = 4\pi\lambda_0^2 g\Gamma_n \qquad (3)$$

$$\sigma_{f0}\Gamma = \sigma_0\Gamma_f \qquad (4)$$

$$\Gamma_f = \Gamma\,(\sigma_{f0}\Gamma)/(\sigma_0\Gamma) \qquad (5)$$

The reduced neutron width is defined as

$$\Gamma_n^0 \equiv \Gamma_n/\sqrt{E_0} \qquad (6)$$

The ratio of the capture to the fission cross section, $\alpha \equiv \sigma_c/\sigma_f$, becomes:

$$\alpha = \Gamma_\gamma/\Gamma_f \qquad (7)$$

at the center of a resonance. Also,

$$1 + \alpha = (\sigma_f + \sigma_\gamma) \approx \Gamma/\Gamma_f \qquad (8)$$

The total cross-section measurements provide values of E_0 (and λ_0), $g\Gamma_n$, and Γ. The remaining parameters can be derived only by combining the total cross section with one or more of the partial cross sections. Note, however, that experience with other isotopes indicates that Γ_γ varies by less than 20 per cent from resonance to resonance; hence if an accurate value of Γ_γ can be obtained for one or two resonances it can be used to compute Γ_f for cases where only Γ is known.

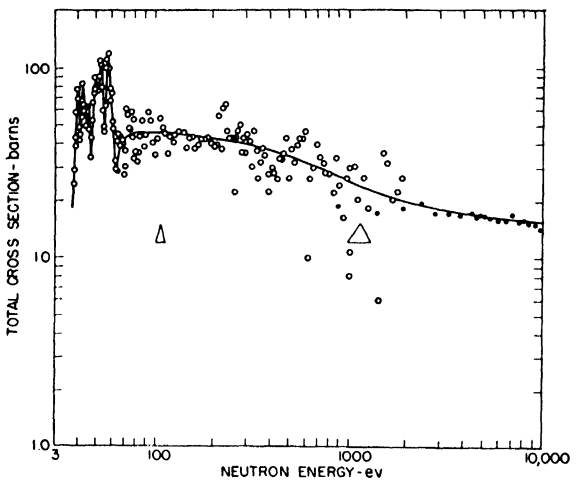

Figure 5. The total cross section of U^{235} above 40 ev. In this region the instrument resolution is inadequate for study of individual resonances. The open circles were obtained with the Brookhaven fast chopper[15] the black dots with the Argonne Van der Graaf accelerator[20]

The statistical weight factor, g, for each resonance can be obtained only by observing the resonance scattering. Unfortunately, in the case of U^{235}, resonance scattering cannot be directly observed because of its small magnitude relative to capture and fission. Thus, only the product, $g\Gamma_n$, can be obtained. For most purposes, however, the assumption that $g = 1/2$ is sufficiently accurate, since in U^{235} ($I = 7/2$) g can have only the values $7/16$ or $9/16$. With only small uncertainty, therefore, $\Gamma_n = 2g\Gamma_n$.

Methods for Analysis

Most of the U^{235} resonances up to 35 ev have been analyzed, although in some cases the parameters have very large uncertainties. Pilcher and Harvey have analyzed the Brookhaven fast chopper measurements[15] (2 to 35 ev) by the method of "area" analysis.[18,23] The Brookhaven crystal spectrometer data[16] (0.1 to 10 ev) were analyzed by the method of "shape" analysis.[24,25] Both types of analysis take ac-

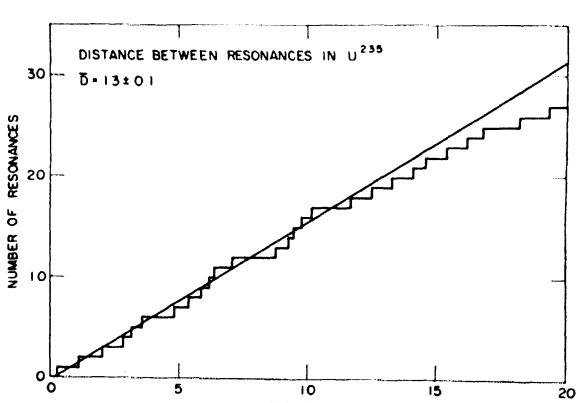

Figure 6. The spacing between resonances in U^{235}. The abscissae are the E_0 for each resonance; the ordinates are the total number of resonances with $E_0 > E$. The average spacing is given by the slope of the straight line. The apparent increase in level spacing above 10 ev arises from failure to observe all resonances, due to insufficient instrument resolution

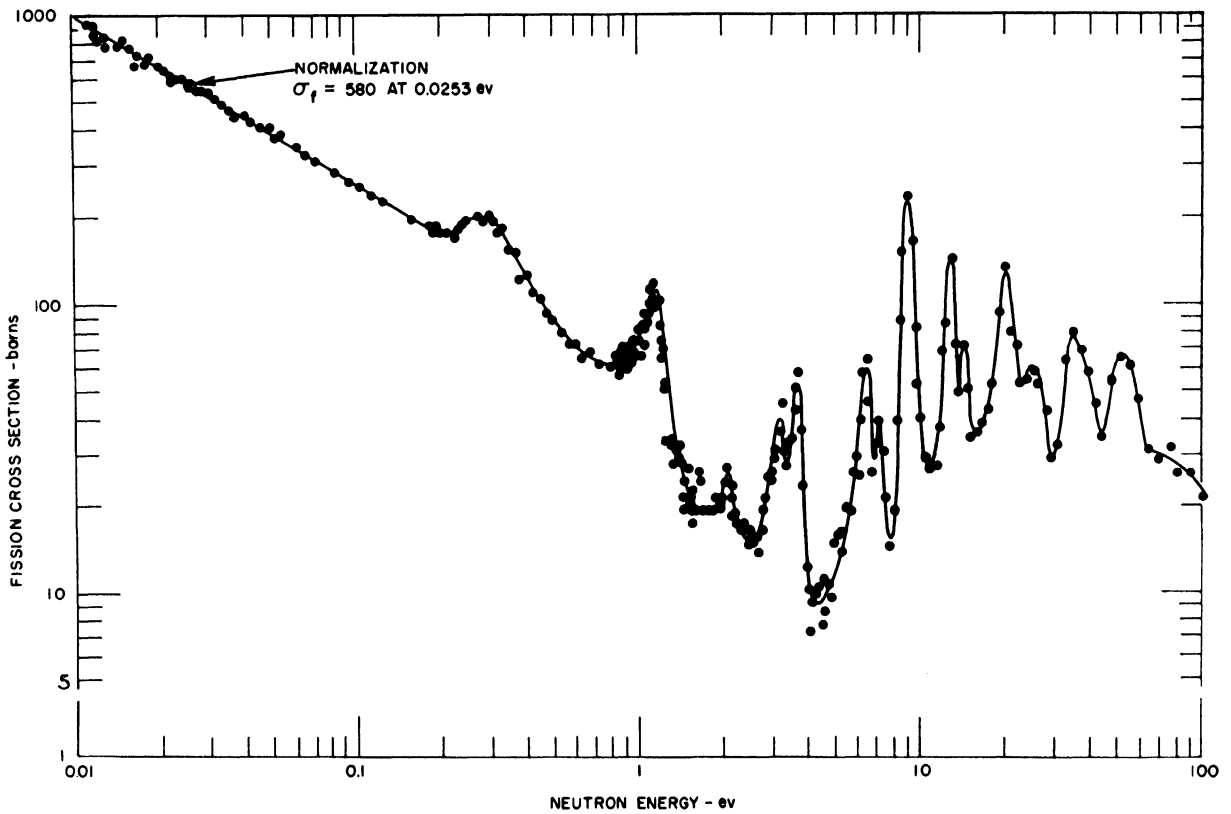

Figure 7. The fission cross section U^{235}. The curve has been normalized to 580 barns at 0.0253 ev. These measurements were made on the Columbia University "neutron velocity selector".[10] Within the limits of instrument resolution all resonances found in the total cross section appear also in the fission cross section

count of Doppler broadening. Corrections for instrument resolution have been made in the "shape" analysis, but these corrections are insignificant below 5 ev. The "area" method is independent of instrument resolution and is thus best suited for use above $\sim$ 10 ev.

The parameters obtained for the various resonances are listed in Table I. Values of E_0, $\sigma_0\Gamma$, Γ, σ_0, $2g\Gamma_n^0$ were obtained directly from the total cross-section curves. The entries containing $\sigma_{f0}\Gamma_f$, and α were obtained by combining the above parameters with the best value of the radiation width, $\Gamma_\gamma = (29.5 \pm 5.0) \times 10^{-3}$ ev. This procedure was necessary because of the large uncertainty in deriving $\sigma_{f0}\Gamma$ directly from the fission cross-section data.

DISCUSSION OF RESULTS

The Partial Widths and Level Spacings

The Reduced Neutron Widths

The values for $2g\ \Gamma_n^0$ ($\approx \Gamma_n^0$) listed in Table I show a distribution similar to that found in other isotopes.[26] The distribution curve for $2g\ \Gamma_n^0$ for the resonances below 10 ev is shown in Fig. 10. The distribution appears to be approximately exponential.

The Average Spacing per Spin State

The average level spacing per spin state, $\overline{D}$, would be approximately twice the average spacing, if we assume an equal number of levels in each spin state. Analysis of the data (Fig. 6) by Pilcher and Harvey gives $\overline{D} = 1.3 \pm 0.1$ ev.

The Ratio $\overline{\Gamma}_n^0/\overline{D}$

By combining the data in Fig. 6 with the data in Fig. 10 one obtains the ratio of the average reduced neutron width to the average spacing per spin state of $\overline{\Gamma}_n^0/\overline{D} = (1.0 \pm 0.2) \times 10^{-4}$. This is larger than

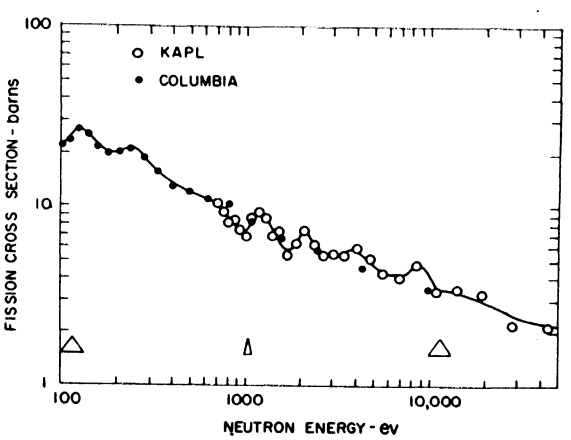

Figure 8. The fission cross section of U^{235} above 100 ev. In this energy region the resonances are too close together to be separated by the available instrument resolution; hence the cross sections are averages over groups of resonances. The black dots were obtained with the Columbia "neutron velocity selector",[10] and the open circles with the Knolls time-of-flight spectrometer[14]

is predicted by the nuclear model of Feshbach, Porter, and Weisskopf.[27]

The Radiation Width

A very important problem in the analysis is to obtain an accurate estimate of the radiation width, Γ_γ. Data for the 0.290 and the 2.035 ev resonances provide particularly good opportunities for calculating Γ_γ. Area analysis of Leonard's[13] total and fission data gives the value $(1 + \alpha) = 1.29 \pm 0.04$ for the 0.290 ev resonance. This combined with the "total" parameters gives $\Gamma_\gamma = (28.8 \pm 5.0) \times 10^{-3}$ ev.

The resonance at 2.035 is unusually narrow, having a total width of $\Gamma = 44 \times 10^{-3}$ ev which defines an upper limit for Γ_γ. Area analysis of the fission data[10] of this resonance gives $\sigma_{f_0} = 1.5 \pm 0.5$ barn ev. This result combined with the total data yields $\Gamma_\gamma = (30.8 \pm 8.0) \times 10^{-3}$ ev. The weighted average of the radiation width for these two cases is $\overline{\Gamma}_\gamma = (29.5 \pm 5.0) \times 10^{-3}$ ev.

The Fission Widths

The values of Γ_f obtained from the analysis show considerable variation from level to level but not as extreme as in the case of the Γ_n's. The average fission width based on the resonances below 10 ev is $\Gamma_f = (71 + 6) \times 10^{-3}$ ev.

The Effect of Bound Levels

Excited states in the compound nucleous which lie just below the neutron binding energy affect the cross section in the region of positive kinetic energy of the neutron. These bound states, commonly referred to as "negative energy" resonances show the characteristic Breit-Wigner shape in the "positive" energy region. Analysis of the data below 1.5 ev shows that the shape of the cross section can be explained in terms of two "negative energy" resonances. One resonance lies very close to $E = 0$ and exerts an appreciable influence only on the region below 0.1 ev. In an analysis of this region Harvey has obtained the parameters $E_0 = -0.02$ ev, $2g\Gamma_n^0 = 0.96 \times 10^{-6}$ ev, and $\Gamma = 0.075$ ev.

A least-squares fit of the background cross section over the range from 0.1 to 1.5 ev by Sailor has yielded parameters for the other resonance; these being $E_0 = -1.4 + 0.2$ ev, $2\,g\Gamma_n^0 = (3.1 \pm 0.6) \times 10^{-3}$ ev, and $\Gamma_f = (180 + 40) \times 10^{-3}$ ev. The Γ_f is based on a value of $\alpha = 0.16$ for this resonance. This value was obtained from the data of Palevsky *et al.*[28] after correcting for the influence of other resonances.

At first sight, the large Γ_n^0 obtained for the -1.4 ev level is disturbing since it is much larger than that of any of the "positive" energy resonances. However, this large value of Γ_n^0 is supported by recent scattering cross-section measurements by Foote.[17] Equation 1*c* can be used to compute the resonance scattering due to -1.4 ev level in the region from 0.1 to 1.5 ev. Values of the computed and measured scattering cross section compared in Table II are in good agreement, thus confirming

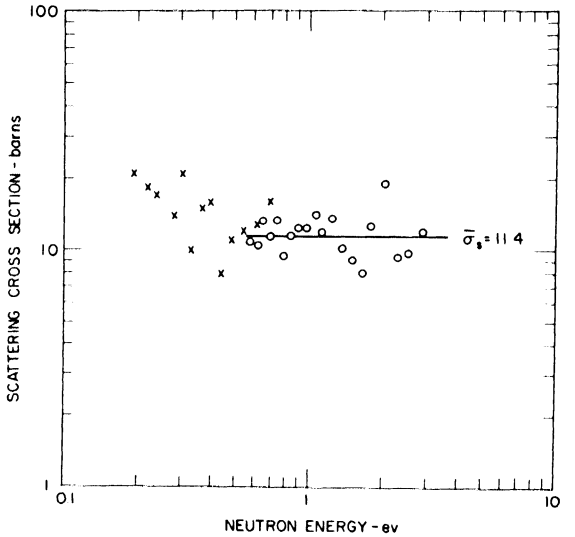

Figure 9. The scattering cross section of U^{235}. Scattering measurements in U^{235} are difficult because of the small amount of scattering relative to absorption. These measurements have been used only for obtaining the average scattering cross section above 0.6 ev; however, the data show an increase in σ_s below 1 ev due to the -1.4 ev level. These measurements were made with the Columbia "neutron velocity selector"[11]

the presence of an unusually strong level at the "negative energy".

Evidence for Interference between Resonances

When more than one resonance is present, Equation 2 is not strictly valid; i.e., the resultant cross section is not a simple sum of the single-level contributions of the individual resonances. The components of resonances which have identical reaction entrance and exit channels are expected to interfere with each other. Such interference effects have been observed in the case of the elastic scattering components; i.e., the (n,n) reaction. Here the condition of identity of entrance and exit channels is satisfied by resonances of the same g.

No experimental evidence has been found for interference between resonances in the capture component (i.e., the (n,γ) reaction). The absence of interference effects in (n,γ) reactions has been attributed to the large number of available exit channels for the gamma emission. Interference would occur in each exit channel but when many exit channels participate there would tend to be no net effect. This cancellation arises from the random signs of the channel amplitudes.

Until recently there has been no definite experimental evidence for interference between the fission components of resonance. Such interference would imply a unique exit channel for the (n,f) reaction.

It was previously noted by Havens *et al.*[9] that the cross section in the region from 0.4 to 1.0 ev could not be explained in terms of the sum of Breit-Wigner formulae for the 0.290 and the 1.142 ev resonances. The data at that time, however, were inadequate for detailed interpretation.

Table II. The Scattering Cross Section of U^{235}

The strong "negative energy" resonance at $E_0 = -1.4$ ev contributes appreciable resonance scattering in the energy region $0 < E < 2$ ev. Contributions from this level may be computed from the parameters in Table I using Equation 1c. The potential scattering is estimated to be $\sigma_p = 10.3$ barns from the nuclear radius. The total scattering is compared to the scattering cross section observed by Foote[17] at four energies. The other known resonances of U^{235} have negligible scattering contributions in this region.

	Contributions from the −1.4 ev level				
E	*Equation 1c (term 1)*	*Equation 1c (term 2)*	σ_p	*Total scattering*	*Observed scattering*
(*ev*)	(*barns*)	(*barns*)	(*barns*)	(*barns*)	(*barns*)
0.271	1.14	4.87	10.3	16.3	18.0 ± 2.0
0.756	0.69	3.77	10.3	14.8	14.7 ± 1.5
0.849	0.63	3.62	10.3	14.5	15.3 ± 1.5
1.458	0.39	2.85	10.3	13.5	13.5 ± 1.5

High resolution data obtained recently with the Brookhaven crystal spectrometer[16] has shown that most of the resonances below 10 ev in U^{235} exhibit definite asymmetry. This asymmetry cannot be attributed to characteristics of the spectrometer because the effect is not observed in other elements; e.g., Ag, Re, Ir, Au, etc. Furthermore, it should be noted that the resonance in U^{235} appearing at 2.035 ev is observed to be quite symmetrical. This resonance has a relatively small Γ_f. One must conclude therefore, that the asymmetries are truly characteristic of the U^{235} resonances.

Attempts have been made to explain the asymmetry in terms of weak unresolved resonances closely adjacent to the observed resonances. However, analysis of the data shows that the observed shapes of the resonances are not compatible with this explanation. Recently, Sailor has analyzed the data from 0.1 to 1.5 ev in terms of a many-level formula. The results of the analysis indicate that this interpretation gives an excellent fit to the data.

An approximation to the many-level formula has been given by Feshbach *et al.*[29] which is expected to be accurate to better than experimental precision.

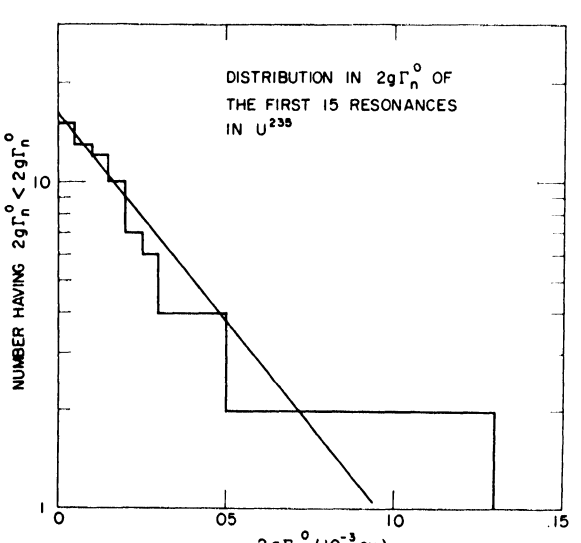

Figure 10. The distribution of neutron widths. Plotted as ordinate are the number of levels having widths less than the abscissa. The straight line would correspond to an exponential distribution

This equation yields a cross-product term for each pair of resonances which have the same value of g and the same exit channel. Cross terms between resonances i and j for the (n,f) process would be of the form:

$$\sigma_{ij} = 8\pi\lambda g \sqrt{\bar{x}_i \bar{x}_j}\; y_{ni}\, y_{nj}\, y_{fi}\, y_{fj} \frac{\left[(E - E_{0i})(E - E_{0j}) + \frac{\Gamma_i}{2}\frac{\Gamma_j}{2}\right]}{\left[(E - E_{0i})^2 + \left(\frac{\Gamma_i}{2}\right)^2\right]\left[(E - E_{0j})^2 + \left(\frac{\Gamma_j}{2}\right)^2\right]} \tag{9}$$

In addition, one obtains single-level terms (Equation 1*b*) for each resonance. The y_n and y_f are related to the neutron and fission widths as follows:

$$y_n = \pm\sqrt{\frac{\Gamma_n}{2}} \quad \text{and} \quad y_f = \pm\sqrt{\frac{\Gamma_f}{2}} \tag{10}$$

the signs being assumed random.

Preliminary fitting to the experimental curve was done in the region of the 1.142 ev resonance using an approximation to Equation 9 of the form

$$\sqrt{E}\,\sigma_{ij} = J \frac{(E - E_0)}{4(E - E_0)^2 + \Gamma^2} \tag{11}$$

where

$$J \equiv \frac{32\pi\lambda}{\sqrt{E}}\, g\sqrt{\bar{x}_i}\, y_{ni}\, y_{fi} \sum_{j\neq i} \frac{\sqrt{\bar{x}_j}\,(E - E_{0j})}{(E - E_{0j})^2 + \left(\frac{\Gamma}{2}\Gamma_j\right)^2} \tag{12}$$

and the term

$$\frac{\Gamma_i}{2} \sum_{j\neq i} \frac{\Gamma_j}{2}$$

was neglected. The approximation, J = constant, was used because program codes for Equation 11 were available for computing on a high speed digital computer. The results of the analysis are shown in Fig. 11(*a*) and 11(*b*). In the figure the data have been corrected for single-level contributions of the neighboring resonances (including the −4 ev level) and the potential scattering. The points are plotted

as $\sqrt{E}\,\sigma$. Figure 11(b) plotted on a magnified scale shows the difference between the observed cross section and the 1.142 ev single-level term (Equation 1). The derived interference term of the form (Equation 12) is designated as curve C. The value $J = -9.6 \pm 2.0$ barn-ev$^{3/2}$ was obtained, and gives the approximate magnitude of the interference over the range 0.6 to 1.5 ev.

If the parameters listed in Table I for the −1.4, 0.290, and 1.142 ev resonances are inserted in Equations 9 and 10, it is found that these three resonances would account for most of the interference in the range from 0.1 to 1.5 ev if they are of the same g. These results are shown as curve D in Fig. 11(b). In making this calculation it follows that the product $y_{nj}y_{fj}$ has the same sign for the −1.4 and the 0.290 ev resonances and opposite sign for the 1.142 ev resonance. These assignments are consistent with the observed asymmetry in the 0.290 ev level which is opposite to that of the 1.142 ev level.

The occurrence of interference would introduce only minor adjustments in most of the parameters listed in Table I. This is true because the interference terms are odd functions in $(E - E_0)$ and the methods of analysis would tend to cancel out the effects of the asymmetry. The interference effects would, however, have an important influence on the variation of η (or α) with energy. At present, the quantitative information is not adequate for computing this variation with the desired accuracy.

ACKNOWLEDGEMENTS

The preparation of this manuscript has been made possible by the many persons who generously contributed unpublished data. Drs. J. A. Harvey, W. W. Havens, Jr. and E. Melkonian have devoted much time to assist with many clarifying discussions.

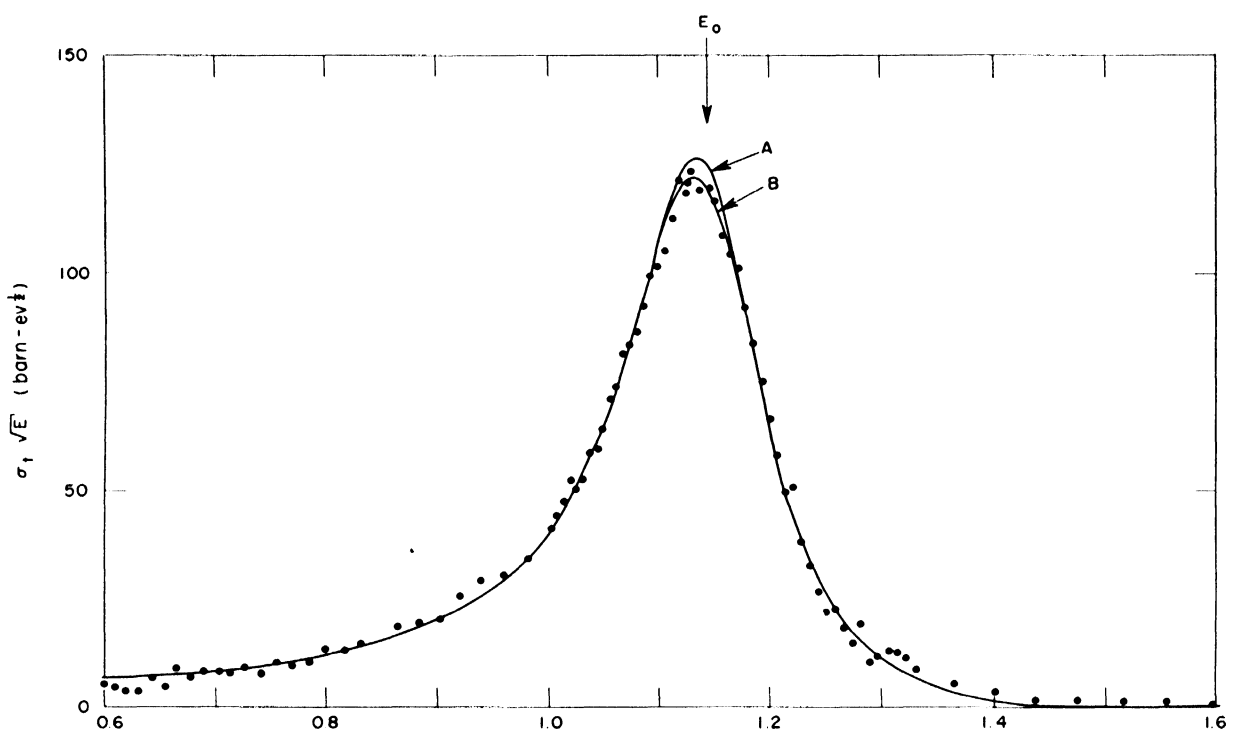

Figure 11a. The 1.142 ev resonance in U^{235}. The data have been plotted as $\sigma_t\sqrt{E}$ vs E, and the contributions of the -1.4 ev resonance and σ_p have been removed. The curve shown is the best fit to the data using a single-level formula plus an interference term. Curve B is the effect of Doppler broadening on curve A

REFERENCES

1. Office of Classification, USAEC TID-235; Can. J. Phys. *29*, 203 (1951) (Joint release by Canada, United Kingdom and United States).
2. Palevsky, Carter, Eisberg and Hughes, Phys. Rev. *94*, 1088 (1954).
3. Egelstaff, P. A., J. Nuc. Energy *1*, 92 (1954).
4. Keller, R., Arch. Sci. (Geneva) *6*, 280 (1953).
5. Popović, D., J. Nuc. Energy *1*, 3 (1954); Popović, D. and Rajsić, N., J. Nuc. Energy *1*, 170 (1954).
6. Hubert, Vendryes and Auclair, Compt. rend. *238*, 1873 (1954).
7. Anderson, Lavatelli, McDaniel and Sutton, Los Alamos Scientific Laboratory, University of California (unpublished, 1944).
8. Bacher, Baker and McDaniel, Phys. Rev. *69*, 443 (1946); McDaniel, B. D., Phys. Rev. *70* 832 (1946).
9. Havens, Rainwater, Wu, Dunning and Melkonian, Columbia University (unpublished, 1947-1950).
10. Perez-Mendez, Levin, Havens and Melkonian, Columbia University (unpublished, 1952-1953).
11. Melkonian, E., Columbia University (unpublished, 1954).
12. Rainwater, J. and Havens, W. W., Jr., Phys. Rev. *70*, 136 (1946); Havens, W. W., Jr. and Rainwater, J., Phys. Rev. *70*, 154 (1946).
13. Leonard, Seppi and Friesen, Hanford Atomic Products Operation, General Electric Company (unpublished, 1954).

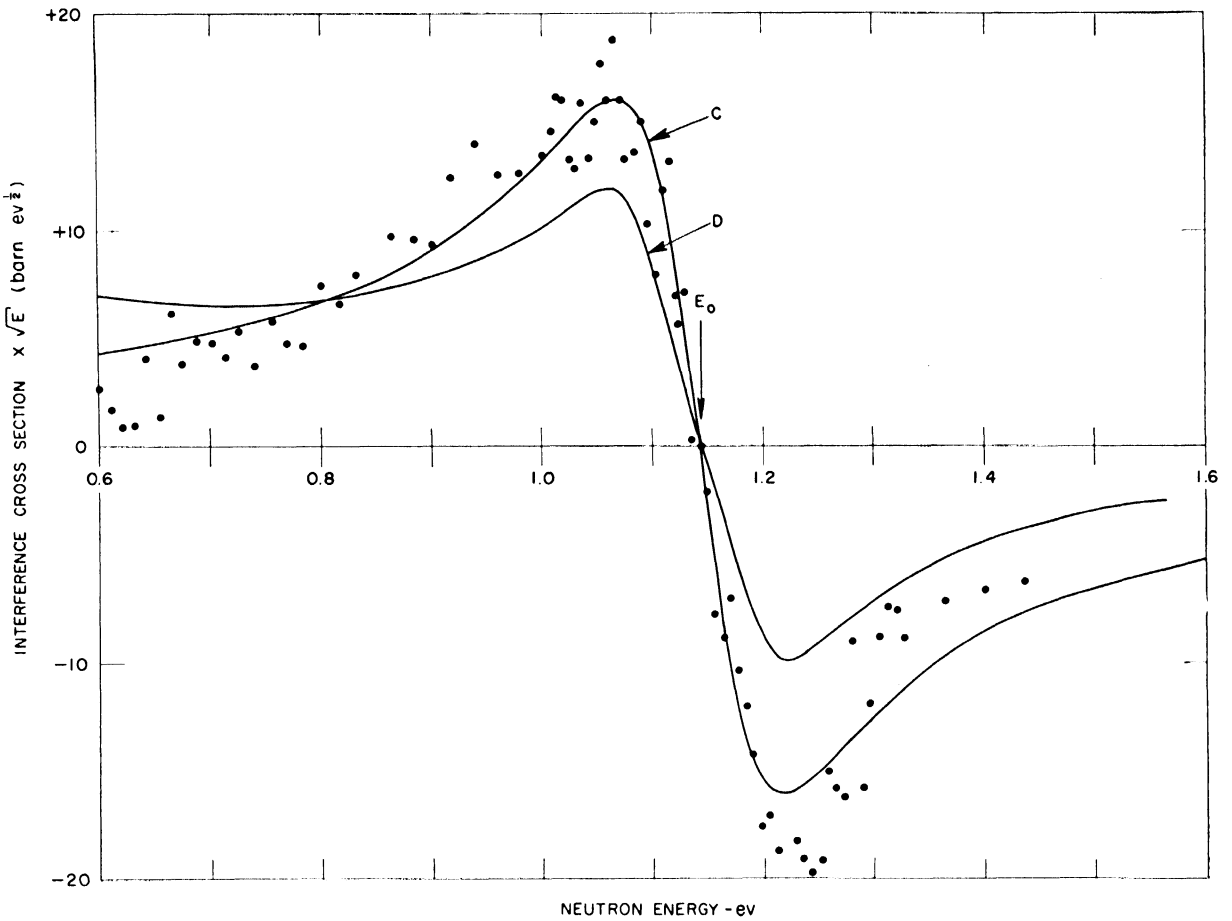

Figure 11b. The "interference term" of the 1.142 ev resonance. This curve offers one possible explanation of the asymmetry of the 1.142 ev resonance. The points are the difference between the observed cross section and the single-level formula contribution (Equation 1) derived from the analysis. Curve C is the derived interference term when Equation 11 is used in the fitting. Curve D is computed from Equation 9 assuming that the -1.4, 0.290, and 1.142 ev levels can interfere. The parameters in Table I furnish all values needed for the calculations except for an ambiguity in the sign of the terms

14. Yeater, Gaerttner and Kelly, Knolls Atomic Power Laboratory, General Electric Company (unpublished, 1954).
15. Pilcher, Harvey and Hughes, Brookhaven National Laboratory, Associated Universities, Inc. (unpublished, 1954).
16. Sailor, V. L. and Landon, H. H., Brookhaven National Laboratory, Associated Universities, Inc. (unpublished, 1955).
17. Foote, H. L., Jr., Brookhaven National Laboratory, Associated Universities, Inc. (unpublished, 1955).
18. Seidl, Hughes, Palevsky, Levin, Kato and Sjöstrand, Phys. Rev. *95,* 476 (1954).
19. Borst, L. B. and Sailor, V. L., Rev. Sci. Instr. *24,* 141 (1953).
20. Hibdon, C. T. and Langsdorf, A., Jr., Argonne National Laboratory, University of Chicago (unpublished, 1953).
21. Williams, D. and Yuster, P., Los Alamos Scientific Laboratory, University of California (unpublished, 1946).
22. Tittman, J. and Sheer, C., Phys. Rev. *83,* 746 (1951).
23. Melkonian, Havens and Rainwater, Phys, Rev. *92,* 702 (1953).
24. Wood, Landon and Sailor, Phys. Rev. *98,* 639 (1955).
25. Landon, H. H. and Sailor, V. L., Phys. Rev. *98,* (1955).
26. Harvey, Hughes, Carter and Pilcher, Phys. Rev. (in press).
27. Feshbach, Porter and Weisskopf, Phys. Rev. *96,* 448 (1954).
28. Palevsky, Eisberg, Hughes and Zimmerman, P/587, *Measurement of Capture to Fission Ratio of* U^{235}, U^{233}, *and* Pu^{239} *by a New Method,* Volume 4, Session 18A, these Proceedings.
29. See Equation A20 in appendix of ref. 27.

The Slow Neutron Cross Sections of the Uranium Isotopes

By J. E. Lynn and N. J. Pattenden,* UK

This paper reviews the various slow neutron cross-section measurements which have been carried out at A.E.R.E., Harwell, on uranium-233, uranium-235, uranium-238 and natural uranium. These include fission, total, radiative capture, scattering, absorption and activation measurements. The absorption and activation measurements refer to neutrons of velocity 2200 m/sec; the total and fission measurements are given as a variation of cross section with energy, covering a range in some cases from about 0.002 ev to about 800 ev. Some of the resonances observed have been analysed for peak cross section and width.

To cover the energy range 0.002 ev to about 0.15 ev, the B.E.P.O. thermal-neutron time-of-flight spectrometer[1] was used. Over the range 0.05 ev to about 5 ev, the B.E.P.O. single crystal neutron spectrometer[2] was used, employing the (220) planes of a crystal of calcium fluoride as the monochromator. Over the range 1 ev to about 800 ev, the 15 Mev linear accelerator neutron spectrometer[3] was used, producing bursts of photoneutrons from a uranium target, and velocity selecting the neutrons in each burst by a time-of-flight method.

Of the measurements reviewed in this paper, fission cross sections were measured by Price, Raffle, Richmond and Sanders. Total cross sections were measured by Egelstaff, Lynn, Pattenden and Taylor. Radiative capture and scattering cross-section measurements were by Rae and Collins respectively, and the absorption and activation cross-section measurements were by Small and Crocker respectively.

FISSION CROSS SECTIONS OF URANIUM-233 AND 235

These have been measured by two separate experiments. In one experiment the absolute value of the fission cross section at one energy (viz., 0.0253 ev) was determined. In the other experiment the variation of the fission cross section over a wide range of energy was measured. The result of the former could then be used to convert the latter into an absolute determination.

The techniques involved in both of these experiments are described in the companion paper[4] on plutonium. The isotopic composition of the uranium used (in the form of U_3O_8) in the measurements on each isotope is shown in Table 1.

* Atomic Energy Research Establishment, Harwell, Berks, England.

The absolute values of fission cross section for the two isotopes are shown in Table II. The pile beam results are the cross sections measured in a neutron beam scattered from a graphite block placed close to the centre of the Harwell graphite moderated thermal pile, B.E.P.O. The thermal beam results are cross sections measured in a neutron beam emerging from the graphite thermal column of B.E.P.O., at a temperature of 30°C. The error associated with each value is the sum of the probable errors in the flux determinations and the mass assessment.

The variation of fission cross section with energy has been measured from 0.01 ev to 25 ev for uranium-233, and from 0.005 ev to 150 ev for uranium-235. The observed values of $K\sigma_{fiss}$ for uranium-233 and uranium-235 are plotted against energy in Figs. 1 and 2 respectively. σ_{fiss} is the fission cross section, and K is the normalisation factor of such a value that $K\sigma_{fiss} = 1$ at 0.0253 ev energy. The individual points have a standard error which is usually less than 3 per cent. There is in addition a systematic error, applicable to the whole of the points forming a single run, which is at a maximum of about 4 per cent on the highest energy run in the case of both isotopes. Table 3 shows values of the energies of the observed resonances in uranium-235.

It will be noticed that there is a marked difference in the corrected heights of the resonances above and below 8 ev. These values are based on the assumption that each peak is a single resonance. If the peaks above 10 ev are actually due to unresolved groups of resonances, then the corrected peak cross-section values will be overestimates.

The observed cross section of uranium-235 shows a departure from a $1/v$ law in the thermal region that can be satisfactorily accounted for by assuming

Table I. Isotopic Composition of Fission Samples

	U^{233} content per cent	U^{234} content per cent	U^{235} content per cent	U^{238} content per cent
U^{233} sample	99.51	0.1	0.007	0.42 ± 0.05
U^{235} sample		0.4 ± 0.1	81.2 ± 0.1	18.4 ± 0.1

Table II. Absolute Fission Cross Sections

	$U^{238}\sigma_{fiss}$ barn	$U^{233}\sigma_{fiss}$ barn
Pile beam	556 ± 15	591 ± 18
Thermal beam	519 ± 15	623 ± 20
2200 m/sec	515 ± 15	638 ± 20

the existence of a resonance at 0.005 ev. The expression

$$K\sigma\sqrt{E} = \left[\frac{0.000807}{(E - 0.005)^2 + 0.003}\right] + 0.763$$

summarises the experimental data below 0.1 ev to an accuracy of better than 1 per cent. This expression is normalised to unity at 0.0250 ev. It implies that the width of the resonance is 0.11 ev. Although the figures quoted give the best fit, the limits on the value of resonance energy are about −0.01 ev to + 0.01 ev.

TOTAL CROSS SECTION OF URANIUM-233

The total cross sections of various samples containing uranium-233 have been measured by transmission methods. Three samples were made from oxide powder, of composition $U^{233}O_{2.05}$, with about 1 per cent of low cross-section impurity, and containing 5.78×10^{20}, 1.17×10^{21} and 6.66×10^{21} molecules/cm². Two samples were discs of uranium-233 metal, of thickness 4.774×10^{21} and 2.468×10^{22} atoms/cm². Impurities in the metal samples were principally thorium (0.1–0.5 per cent), uranium-234 (0.25–0.5 per cent) and uranium-238 (0.5–1.0 per cent); it was estimated that these would give a 1.4 per cent error to the thermal neutron cross section of uranium-233.

The measurements on the oxide samples have been corrected for oxygen cross section, using published values for the latter,[6] and the results are displayed in Figs. 3a and 3b. Sufficient counts were taken that the standard error on each point is about 2 per cent below 1 ev. Above 1 ev, the standard error is everywhere less than 8 per cent and averages about 5 per cent.

At 2200 metre/sec the total cross section is (610 ± 9) barns. Between 0.01 ev and 0.1 ev, the curve can be fitted to a $1/v$ line plus a constant (4.5 ± 2.5) barns. The first observable resonance is at 1.775 ev. Further resonances are observed at 2.30, 3.62, 4.76, 5.13, 6.04, 6.79, 9.38, 10.45, 12.8, 13.75, 15.6, 16.4, 19.0, 20.8, 22.3, 25.5, 28.5, 31.1, 32.1, 34.6, 37.1, 40.0, 40.8, 42.5, 49.1, 54.5, 56.7, 61.6, 65.0, 69.4, 75.1, 79.5, 82.6, 91.3, 98.1 ev. Below 30 ev the resolution width at half maximum of the resolution function varies from 0.8 μsec/metre at 1.78 ev to 0.22 μsec/metre at 21 ev, and above 30 ev was 0.1 μsec/metre.

Table III. Fission Resonances in Uranium-235, Normalised to 638 barns at 0.025 ev

Resonance energy ev	*Observed peak* σ_{fiss} *barns*	*Peak* σ_{fiss} *(barns) assuming*	
		(1) $\Gamma = 0.0$ *ev*	*(2)* $\Gamma = 0.15$ *ev*
0.30	204		
1.12	109	131	123
2.05			
3.1			
3.55	72.0	130	108
6.3	71	197	148
7.0	48.1	146	110
8.75	318	1230	890
12.2	137	750	520
13.9			
19.0	128	1160	830
24.8			
34	106	1900	1310
55			
72		Corrected for resolution	
90		and Doppler broadening.	

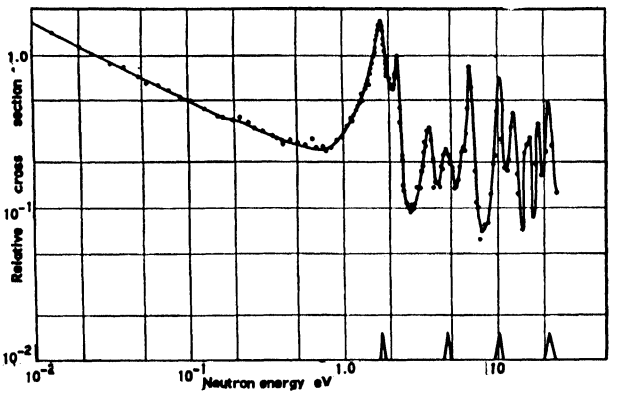

Figure 1. Relative fission cross section of uranium[233]

Attempts have been made to analyse the various data obtained for the 1.775 ev resonance. Area analysis[7] was applied to transmission curves from two of the samples measured by the crystal spectrometer. This gave the parameters peak cross section $\sigma_0 = (1650 \pm 350)$ barns, and width $\Gamma = (0.21 \pm 0.04)$ ev. However, a one-level Breit-Wigner curve having these parameters, with the addition of a term $88.5/\sqrt{E}$ barns to fit the thermal cross section, does not fit the observed points. The latter are substantially higher than the calculated line in the low energy wing of the resonance. An attempt was made to fit a single-level Breit-Wigner shape to the observed linear accelerator cross section, but no fit could be obtained for the same reason. The peak cross section observed by the linear accelerator was (890 ± 75) barns, with a resolution width of 0.08 ev; the peak cross section observed by the crystal spectrometer was (1050 ± 25) barns, with a reso-

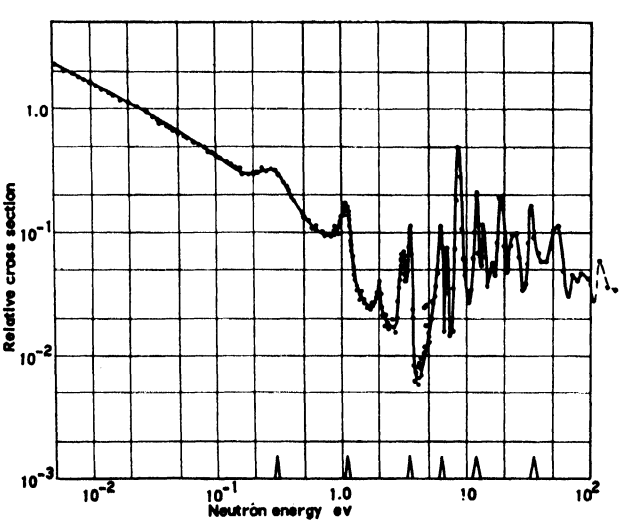

Figure 2. Relative fission cross section of uranium[235]

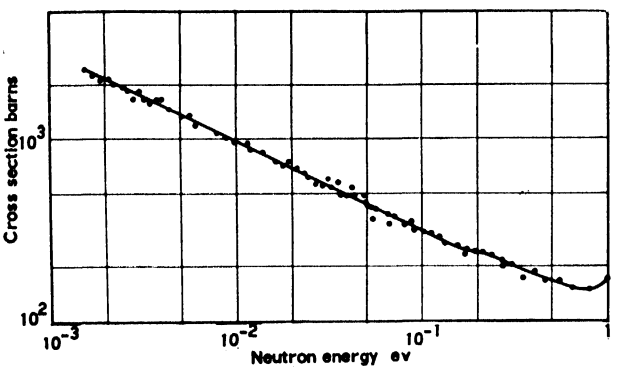

Figure 3a. Observed total cross section of uranium^{238}

lution width of 0.14 ev. This discrepancy is due to the difference in the sample thicknesses used, but it shows that the crystal spectrometer value is probably fairly close to the correct one (within perhaps 10%). Therefore the peak cross section obtained by area analysis is too large. The explanation for this is probably either that interference between the two lowest energy resonances produces an anomalous effect between 1.0 and 1.5 ev, or that another resonance is present, of energy between 1.0 and 1.5 ev, which is too small for a peak to be separated from the wing of the 1.775 ev resonance.

An attempt was also made to fit a one-level Breit-Wigner shape to the resonance at 3.62 ev, σ_0 and Γ being estimated from the observed shape (which should approximate to the real shape at this energy) to be 184 barns, and 0.34 ev. Again the attempted fit was too low on the low-energy side and too high on the high-energy side of the resonance. In view of the fact that single-level Breit-Wigner forms cannot be fitted to two at least of the first three resonances it was decided not to attempt analysis of the levels in the poorer resolution region.

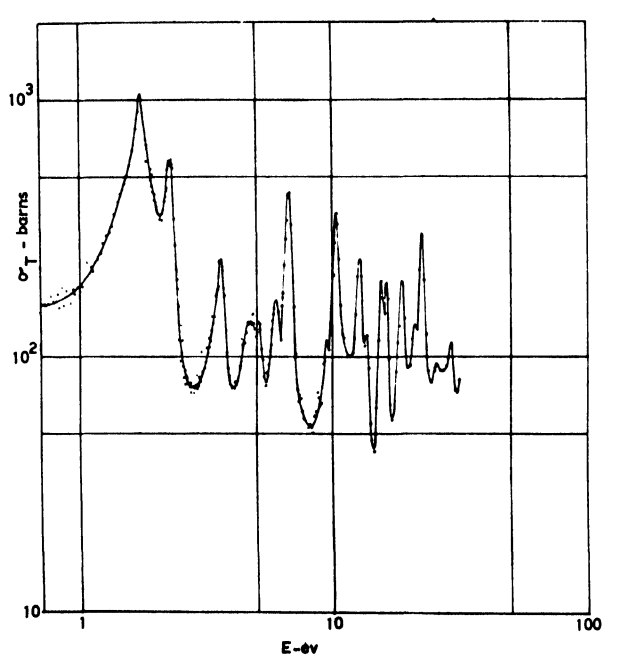

Figure 3b. U^{238}, the observed total cross section

TOTAL CROSS SECTION OF NATURAL URANIUM

The total cross section of a sample of natural uranium metal has been measured by transmission over a range of wavelengths from 0.013 Å to 9Å. The sample used was of thickness 2.295×10^{22} atoms per cm^2, and had a density of 18.8 gm/cm^2. The experimental results are shown plotted as points in Fig. 4a, on a time-of-flight scale. The statistical error on each point is about 2 per cent for the points at short times of flight. The fluctuations in cross section due to Bragg diffraction are clearly seen. The observed cross section at times of flight greater than 1320 sec/m is due to incoherent scattering, and absorption in the uranium-235 and -238. From the size of the steps in the cross section and the known crystal structure, the coherent scattering cross section of uranium-238 is estimated to be (9 ± 1) barns. From the observed cross section at shorter wavelengths (where coherent effects are unimportant), the total scattering cross section of uranium-238 is estimated to be (8.6 ± 0.2) barns. The full line drawn in Fig. 4a is the result of adding the calculated coherent scattering from several sets of planes to the absorption cross section, as a function of time of flight.

Table IV. Samples and Resolutions Used in Measurement of Natural Uranium Cross Section

Energy range (ev)	*Sample thickness (no. of atoms/cm^2)*	*Resolution (μ sec/metre)*
5–6.4	8.65×10^{22}	0.4
6.4–6.56	5.59×10^{21}	0.1
6.56–6.79	9.90×10^{20}	0.1
6.79–6.95	5.59×10^{21}	0.1
7.0–9.0	8.65×10^{22}	0.4
12.0–20.4	8.65×10^{22}	0.22
20.4–21.7	5.30×10^{20}	0.22
21.7–29.	8.65×10^{22}	0.22
29–240	1.50×10^{22}	0.1
240–800	1.50×10^{22}	0.035

The total cross section of natural uranium has been measured with the linear accelerator spectrometer[3] over the energy range 5 ev to 800 ev. The sample thicknesses and resolutions used are listed in Table 4. Since the object of most of this work was to obtain resonance parameters, there is a considerable scatter on the points between resonances in the observed cross-section curve (Fig. 4b). The standard deviation at 10 barns in the region of 5 ev to 29 ev is $\pm$ 1.0 barn, from 29 ev to 240 ev is $\pm$ 0.5 barn and from 240 ev to 800 ev is $\pm$ 2 barns. This last part of the curve has been normalised to 10 barns at 150 ev.

RESONANCE PARAMETERS OF URANIUM-238

Several resonances observed in the total cross-section curve of natural uranium are due to the predominant U^{238} isotope. The parameters of several of these resonances have been determined from the results of transmission experiments of the natural element in its metallic state. Table V gives details of the samples used.

Table VI shows the results of the analysis of the total cross-section experiments. The area method of analysis, employing in particular, the curves presented by Seidl *et al.*[7] and Melkonian, Havens and Rainwater,[8] has been used. A complete area analysis has been carried out in the case of the 6.67 ev resonance, $\sigma_0\Gamma^2$ and $\sigma_0\Gamma$ being measured. From these two values σ_0 and Γ and hence Γ_n and Γ_γ, the partial widths for elastic scattering and radiative capture respectively are determined.

Analysis employing interference between potential and resonance scattering has also been used. The full single-level Breit-Wigner formula may be written

$$\sigma(E) = \underbrace{\left[\frac{\sigma_0}{1+\left(\frac{E-E_0}{\frac{1}{2}\Gamma}\right)^2}\right]}_{\text{Resonance term}} + \underbrace{\left[\frac{2\sigma_0 ka}{1+\left(\frac{E-E_0}{\frac{1}{2}\Gamma}\right)^2}\cdot\frac{E-E_0}{\frac{1}{2}\Gamma}\right]}_{\text{Interference term}} + \underbrace{4\pi a^2}_{\substack{\text{Potential}\\ \text{scattering}}}$$

in the usual notation. The $\sqrt{E_0/E}$ factor is not included here because this analysis will apply only to resonances where the scattering is large, and where, in general, the region of study of the resonance will be confined within limits of $E - E_0$ small compared with E_0. The difference $\sigma(E) - \sigma(2E_0 - E)$ is now simply

$$\frac{2\sigma_0\Gamma ka}{|E-E_0|}$$

when $(E - E_0) \gg \frac{1}{2}\Gamma$ and from this fact $\sigma_0\Gamma$ may be determined in suitable cases. The analysis in practice consists of working out the observed cross-section curve in the region of the resonance and estimating the difference for a number of $|E - E_0|$ values which are then plotted against $1/|E - E_0|$. Resolution on the one hand and the closeness of neighbouring resonances on the other hand limit the range of $|E - E_0|$ values but these factors have not rendered too difficult the estimation of $\sigma_0\Gamma$ by this method for the 21.0, 36.8, 66.2 and 103.3 ev resonances. Another version of this method has been given by Levin.[9]

It is seen from the table that reasonably accurate values of Γ_n may be determined from total cross-section data (i.e., for zero-spin nuclei; in other cases $g\Gamma_n$ is estimated where $g = \frac{1}{2}[1 \pm 1/(2I + 1)]$ where I is the spin of the target nucleus). However, unless $\Gamma_\gamma \gg \Gamma_n$, it is not possible to get a good estimate of Γ_γ for it is found from the difference $\Gamma_\gamma = \Gamma - \Gamma_n$. From the point of view of reactor design it is necessary to know all three quantities for a particular resonance so that the radiative capture

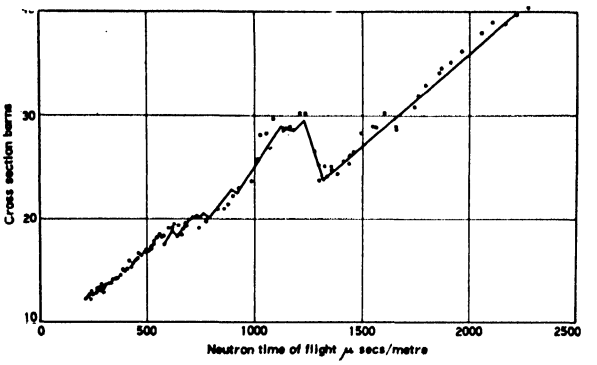

Figure 4a. Total cross section of natural uranium

cross section may be calculated. For this reason an attempt has been made to estimate Γ_γ by combining the results of the total, radiative capture and elastic scattering measurements made with the 15 Mev linear accelerator neutron spectrometer. The method of making the radiative capture measurements is described by Rae.[10]

The elastic scattering measurements have been made on a flight path of 12.3 metres by Collins. The samples are placed in the collimated neutron beam surrounded by an annular array of $B^{10}F_3$ proportional counters. A close-fitting shield of anhydrous boric oxide acts both as a trap for undetected scattered neutrons and as a shield which reduces the

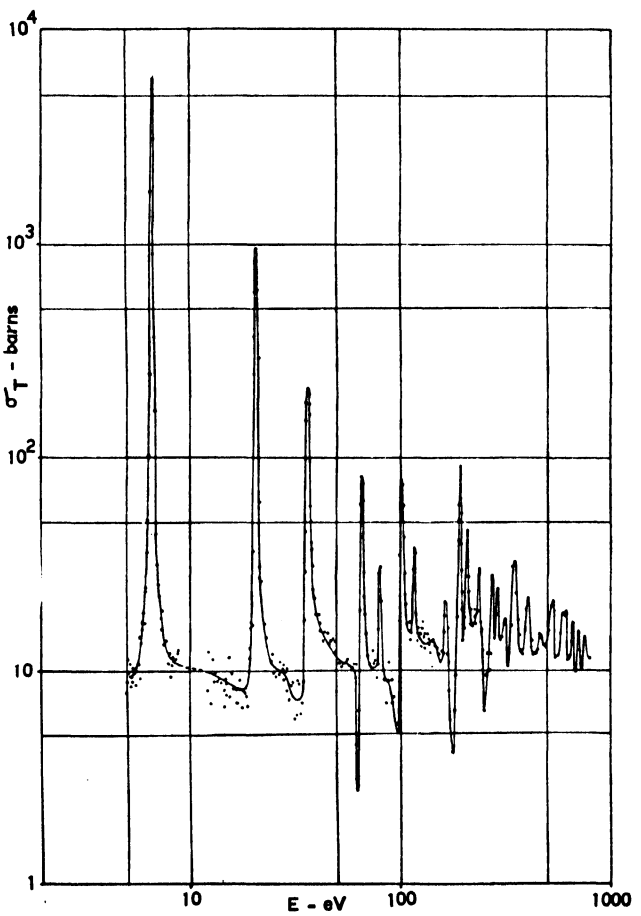

Figure 4b. The observed total cross section of U(natural)

Table V. Details of Samples Used in Obtaining Total Cross Section Data for Resonance Analysis

Resonance energy (ev)	*Sample thickness used for determining $\sigma_0\Gamma^2$ by "areas" (atoms/cm²)*	*Sample thickness used for determining $\sigma_0\Gamma^{3/2}$ by "areas" (atoms/cm²)*	*Sample thickness used for determining $\sigma_0\Gamma$ by "areas" (atoms/cm²)*	*Sample thickness used for determining $\sigma_0\Gamma$ by interference (atoms/cm²)*
6.67	5.59×10^{21}		9.90×10^{19}	
21.0	5.59×10^{21}	5.30×10^{20}		8.65×10^{22}
36.8	1.50×10^{22}			1.50×10^{22}
66.2	1.50×10^{22}			1.50×10^{22}
81.1			1.50×10^{22}	
103.3	1.50×10^{22}			1.50×10^{22}
117.5	1.50×10^{22}			
166			1.50×10^{22}	
191.5	1.50×10^{22}			

background to less than half a count per hour in a 2 μsec wide timing channel, the machine giving 400 bursts of neutrons per second. Under these conditions one per cent scattering of the beam gives rise to 10 counts per hour. The detector has been calibrated using lead, and all measurements are referred to the cross section of lead. Using this apparatus the fraction of the neutron beam scattered by a given sample may be obtained as a function of neutron energy. The measurements have been carried out using a number of samples of natural uranium, the two thinnest containing 1.02×10^{20} and 1.57×10^{20} atoms/cm². Rae employed a sample containing 1.66×10^{20} atoms/cm² in order to obtain the fraction of neutrons captured as a function of their energy. Both curves contain peaks due to the U^{238} resonances and the area under a given peak yields $\sigma_0\Gamma_n$ and $\sigma_0\Gamma_\gamma$ respectively as a function of Γ, using the curves given by Seidl *et al.*[7] This analysis ignores the effect of subsequent capture of scattered neutrons before these have emerged from the sample, which is extremely difficult to calculate. It is thought, however, that the effect may not be very large in the first few resonances in U^{238}. In these cases Γ is very small and the energy shift of the neutron upon scattering in the resonance would tend to shift the neutron right out of the resonance energy region. It was therefore decided to proceed with the resonance analysis assuming no loss of scattered neutrons by subsequent capture.

The method of analysis is described by Rae,[10] and the results are presented in Table VII. The analysis has only been carried as far as 118 ev. Resonances have been observed beyond this at 146, 166, 192, 210, 240, 275, 292, 320, 350, 410, 536, 595, 616, 670, 710 and 770 ev. Since the level spacing up to 220 ev averages 20 ev and appears surprisingly constant, it is certain that several of those above 220 ev are unresolved groups while others have been missed altogether.

TOTAL CROSS SECTION OF URANIUM-235

The total cross section of uranium-235 has been estimated over the energy range 0.006 ev to 0.6 ev, by comparing the observed total cross section of enriched uranium with the observed total cross section of natural uranium. The transmission of two samples of the enriched metal, of thickness 3.82×10^{21} and 1.70×10^{21} atoms per cm² were measured. The uranium contained (81.2 ± 0.1) per cent uranium-235. The results are plotted in Fig. 5. From these, the total cross section at 0.0253 ev is estimated to be (729 ± 15) barns. A resonance is observed at 0.30 ev, and is estimated to have a peak cross-section value of (120 ± 10) barns and a width of 0.14 ± 0.03) ev.

ACTIVATION AND ABSORPTION CROSS SECTIONS OF URANIUM-238

These results have been reported in J. Nuc. Energy *1*, 234 (1954) and J. Nuc. Energy (to be published, 1955). At 2200 metre/sec, the activation cross section was shown to be (2.75 ± 0.10) barns, and the absorption cross section was shown to be (2.76 ± 0.06) barns.

Table VI. Analysis of Total Cross Section Data on Natural Uranium
Resonance Parameters of U^{238} (b = barn; mv = 10^{-3} ev) *

E_0(ev)	$\sigma_0\Gamma^2$(b-cv²)	$\sigma_0\Gamma^{3/2}$(b-cv$^{3/2}$)	$\sigma_0\Gamma$(b-cv)	Γ(mv)	Γ_n(mv)	Γ_γ(mv)
6.67±0.04	15.4±1.4		585±123	26.5±8	1.5±0.3	25±8
21.0±0.3	39 ±7	195±17	960±200	40 ±18	7.8±1.6	32±20
36.8±0.15	125 ±22		1780±280	70 ±19	25±4	45±20
66.2±0.4	33 ±11		970±230	34 ±14	25±6	
81.1±0.5			58±17		1.8±0.6	
103.3±0.7	133 ±41		1800±380	74 ±31	71±15	
117.5±0.8	18		600±300		27±13	
166 ±2			130±60		8±4	
191.5±1.5	420 ±100				160 (assuming	
210 ±2					$\Gamma\gamma$ = 25 mv)	

* The errors stated are "limits of error", i.e., the standard deviation multiplied by 3, plus systematic errors.

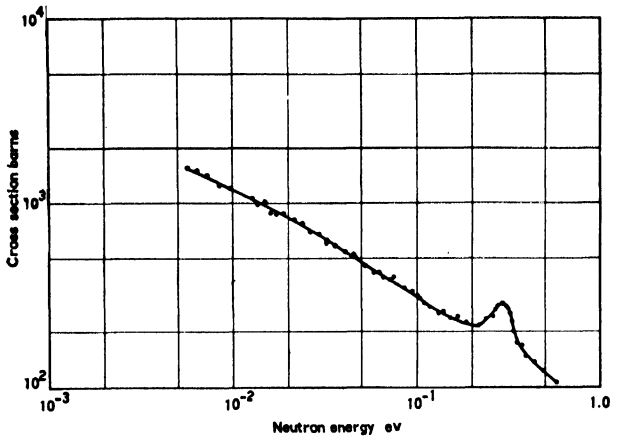

Figure 5. Observed total cross section of uranium^{235}

Table VII. Analysis of Total, Radiative Capture and Elastic Scattering Data on U^{238} Resonance Parameters

E_0 (*ev*)	Γ_n (*mv*)	Γ (*mv*)	$\Gamma\gamma=\Gamma-\Gamma_n$	*Reference*
6.67	1.4±0.1	27.5±1.5	26.1±1.5	a, c, e,
21.0	8.7±0.3	37.5±2.3	28.8±2.3	a, d, f
36.8	28.6±1.5	53.5±3.9	24.9±4.2	a, b, d, f
66.2	22.6±1.5	41.2±2.3	18.6±2.7	a, b, d, f
81.1	2	25		c, d,
103.3	67.5±3.0	83 ±4.5	15.5±5.4	a, b, d, f
117.5	23.2±1.5	36.8±4.5	13.6±4.8	a, c, d, f

a) $\sigma_0\Gamma^2$ from transmission (area analysis).
b) $\sigma_0\Gamma$ from transmission (interference analysis).
c) $\sigma_0\Gamma^2$ or $\sigma_0\Gamma$ as function of Γ from area analysis or minimum transmission of intermediate sample.[11]
d) $\sigma_0\Gamma\gamma$ from gamma-ray yield from thin sample.
e) σ_a and Γ from analysis of resonance areas of a number of samples.
f) $\sigma_0\Gamma_n$ from scattering yield from thin sample.

REFERENCES

1. Egelstaff, P. A., *The Operation of a Thermal Neutron Time of Flight Spectrometer,* Jour. Nuc. Energy. *1,* 57 (1954).
2. Taylor, B. T., *Measurement of the Neutron Spectrum at the Centre of the Harwell Pile,* A.E.R.E. Report. N/R 1005 (1952).
3. Wiblin, E. R., P/421, *Neutron Time-of-Flight Equipment based on Pulsed Sources,* Volume 4, Session 15A, these Proceedings.
4. Price, B. T. and Raffle, J. F., P/422, *The Slow Neutron Cross Sections of the Plutonium Isotopes,* Volume 4, Session 17A, these Proceedings.
5. Egelstaff, P. A. and Sanders, J. E., P/425, *Neutron Yields from Fissile Nuclei,* Volume 4, Session 18A, these Proceedings.
6. *Neutron Cross Sections,* U.S. A.E.C.U. 2040 (1953).
7. Seidl, F. G. P., Hughes, D. J., Palevsky, H., Levin, J. S., Kato, W. Y. and Sjöstrand, N. G., *"Fast chopper" Time-of-Flight Measurement of Neutron Resonances,* Phys. Rev. *95,* 476 (1954).
8. Melkonian, E., Havens, W. W., Jr. and Rainwater, L. J., *Slow Neutron Velocity Spectrometer Studies V,* Phys. Rev. *92,* 702 (1953).
9. Levin, J. S., to be published.
10. Rae, E. R., P/426, *A Note on the Analysis of Neutron Resonance Data including Examples taken from Reactor Materials,* Volume 4, Session 15A, these Proceedings.
11. Lynn, J. E. and Rae, E. R., *The Interpretation of Data Obtained with a Time-of-Flight Neutron Spectrometer in terms of Nuclear Resonance Parameters,* A.E.R.E. Committee Paper, NRDC 46.

Fission and Total Cross Sections of Some Heavy Nuclides for Monochromatic Neutrons as Measured by a Mechanical Neutron Velocity Selector

By Y. B. Adamchuk, V. F. Gerasimov, B. V. Yefimov, V. S. Zenkevich, V. I. Mostovoi, M. I. Pevzner, A. A. Chernyshov and A. P. Tsitovich, USSR

The peaceful uses of atomic energy require, besides solution of complex technical problems, extensive research in the neutron-physics properties of the elements used in nuclear reactors. It is particularly essential to investigate the interaction of monochromatic neutrons with fissionable elements for a deeper understanding of many problems connected with the operation of existing nuclear reactors and for their further improvement. Knowledge of cross sections for the interaction of monochromatic neutrons with the transuranium elements produced in nuclear reactors is important not only for an understanding of the processes occurring in the reactors but also for the use of transuranium elements as possibly more effective nuclear fuels.

Investigation of the dependence of the neutron cross sections of heavy fissionable materials on energy also yields valuable information for the theory of the structure and fission nuclei.

In the present paper experimental results are given of the study of the fission cross sections of U^{233}, U^{235}, Pu^{239}, Pu^{241}, and the total cross sections of Np^{237} and Am^{241} for monochromatic neutrons in the energy range 0.005–1000 ev.

APPARATUS

Our experiment was carried out with a mechanical selector described by Mostovoi, Pevzner and Tsitovich.[1] We shall therefore not dwell here on its structures and parameters but shall examine only the neutron detectors used.

Counters

Two types of proportional counters were used in the experiment. An end-window counter 20 cm long and 6 cm in diameter filled with BF_3 to a pressure of 150 mm was used for the measurement of thermal neutrons; and a group of 7 counters, each 20 cm long and 2 cm in diameter, filled with enriched BF_3 to a pressure of 600 mm, was used for epi-cadmium neutrons. All the counters were placed parallel to the beam.

Ionization Fission Chamber

Measurement of fission cross sections for monochromatic neutrons of substances with high alpha-activity is difficult because only a small amount of such substances can be used in the fission chamber. The limit to which the amount in the chamber can be increased, and, consequently, to which the chamber's efficiency may be raised, is prescribed by the alpha-particle pulse pile-up.

To increase the efficiency of the chamber, layers of the fissionable substance were deposited on films transparent for fission fragments. Thus, the ionization of both fragments was used in the chamber. This made it possible to increase the fission fragment to alpha-particle ionization ratio considerably. Besides that, only the initial parts of the fragment and alpha-particle paths were used in the chamber, which still further increased that ratio.

It will be noted that the elimination of pile-up by coincidence counting of the fragments yields less satisfactory results than by using the ionization sum of the two fragments.

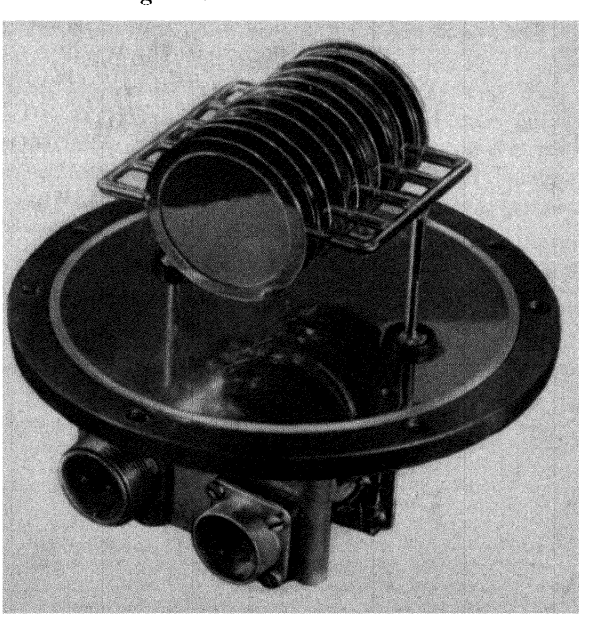

Figure 1

Original language: Russian.

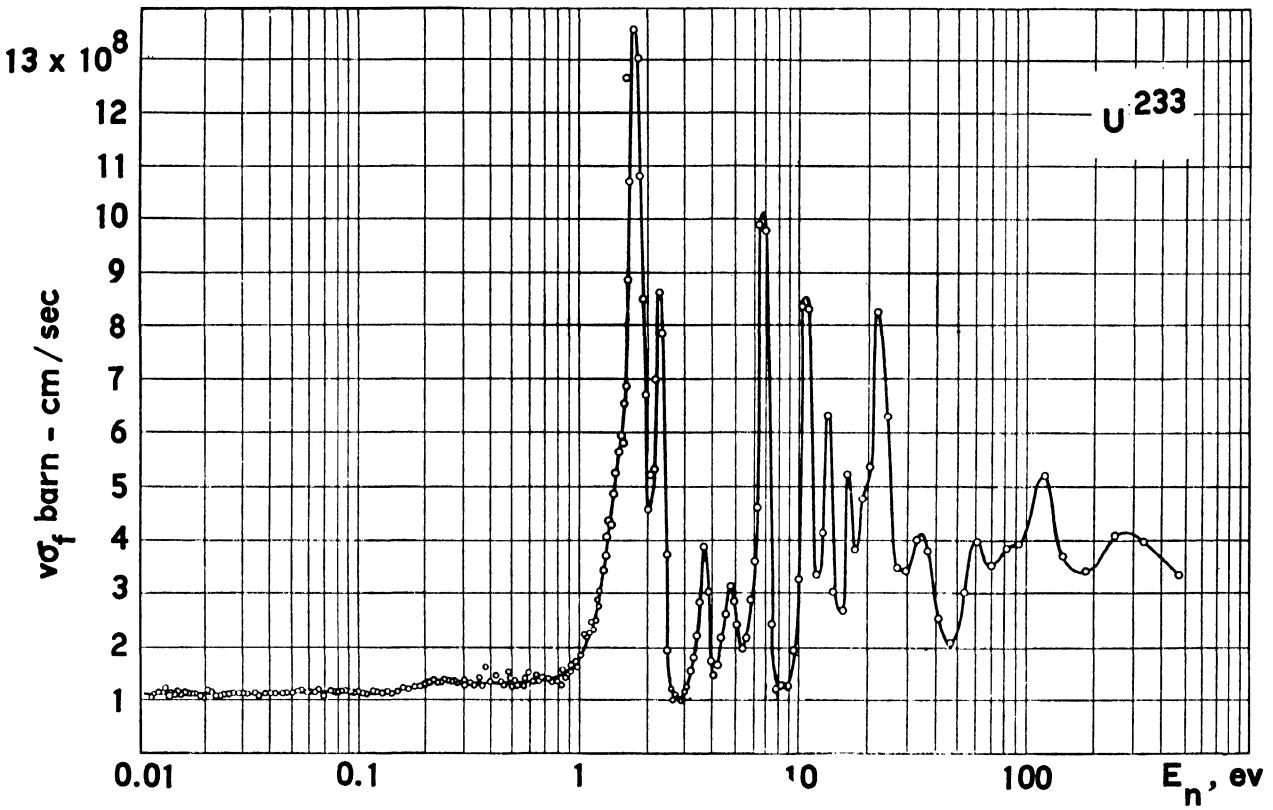

Figure 3

The fission substance layers, transparent for fission fragments, were prepared as follows: A nylon film 0.3 to 0.5 microns thick was placed on a brass ring with a 54 mm outer diameter and 42 mm inner diameter. On the film a suspension of a finely powdered oxide of the fissionable substance in amyl acetate was deposited, containing a small amount of nitrocellulose as a binder. The film with the oxide deposit was then covered with a thin vacuum-evaporated layer of aluminium or silver for electric conductivity.

The nylon film thus prepared is not durable, as it cannot stand strong alpha-radiation. Its lifetime depends on the specific alpha activity, the amount of the deposited substance, and the thickness of the film. Thus, for example, with a plutonium layer 0.5 mg/cm^2, the film lifetime is two to three months.

Usually five layers of the fissionable substance were placed in an 11-electrode ionization chamber shown in Fig. 1. The electrodes were spaced 0.9 cm apart, and the efficient length of the chamber for fission detection was 7.2 cm. The chamber was filled with chemically pure argon to a pressure of 40 to 70 cm (depending on the fissionable substance placed in the chamber), containing up to 10% CO_2. The bias curve of the chamber with 22 mg of Pu^{239} is given in Fig. 2. As may be seen on this bias curve, the efficiency of a plutonium chamber may be greatly increased by increasing the amount of the substance in it.

MEASUREMENT

Measurement Procedure and Some Control Experiments

The usual procedure of measuring fission cross sections consisted in simultaneously counting the number of pulses in the ionization fission chamber and the proportional BF_3 counter, connected to the two separate systems of the time-analyzer channels. Of the analyzer's 80 channels, 32 were used for measuring the effect in the fission chamber, 32 for measuring the effect in the proportional counter, and 16 for background measurement. The total counts (without time selection) in the fission chamber and in the proportional BF_3 counter were also measured. Performance stability of the apparatus was indicated by a constant ratio of these effects.

Since the flight paths to the chamber and to the counter in these measurements differed, the counting rates measured by simultaneous channels of both

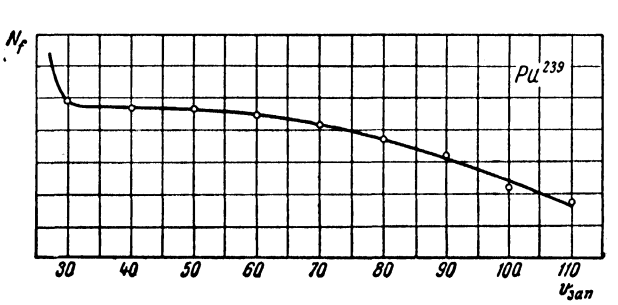

Figure 2

systems generally referred to different neutron energies. This difference was negligible in the $1/E$ spectral region, but it was essential and was taken into account in the thermal region. To remove this difference in the latter case, the measurements were carried out separately with the chamber and the counter, which were set at the same place on a flight path of 605 cm.

The ratio of the experimentally measured counting rate in the chamber to the corresponding counting rate in the proportional counter yields a value proportional to $v\sigma_f$, averaged over the spectral line selected by the mechanical selector, assuming that the counter's sensitivity varies with neutron velocity as $1/v$. Whenever necessary, allowance was made for the deviation of the counter sensitivity from the $1/v$ law.

By measuring with the mechanical selector we determined the energy dependence, of the relative fission cross section, which was then put on an absolute basis through the thermal cross section.

Selector resolution is taken to be equal to the width of the resolution function at half maximum. In the cross section graphs, the resolving power in different energy ranges is characterized by triangles with bases equal to the half-width.

Angular adjustment of the selector was performed as follows. The rotor was fixed at the point of highest neutron transmission and the mirror on the rotor axis was set so that the position of the reflected light beam with regard to the photomultiplier's slit corresponded to the front of the photopulses which starts the pulse oscillator of the time analyzer. By this arrangement the time difference between the neutron burst and the photopulse did not exceed the sum of the pulse front width (different for different rotation speeds) and the delay in the electronic circuits.

The selector was accurately calibrated for energy at various rotation speeds by measuring the location of the indium and gold resonance levels, and of the beryllium scattering cross-section cut-off.

These measurements were made separately with each of the two mirror surfaces to verify that these were exactly parallel. To test the accuracy of the mechanical selector as a whole the total cross sections of boron and Li^6 were measured first.

Fission Cross Sections of Uranium and Plutonium Isotopes

U^{233}

Figures 3 and 4 show the dependence of $v\sigma_f$ and σ_f on neutron energy measured with a chamber containing 50 mg of U^{233}. In plotting the curves it was assumed that the cross section at energy $E = 0.025$ ev was 510 barns.

As the curves show, the fission cross section does not drop below the $1/v$ curve drawn from the thermal region. The absolute value of U^{233} fission cross section in the thermal region cannot be explained by the levels in the 1.8 ev region only; an appreciable contribution is made by the negative level.

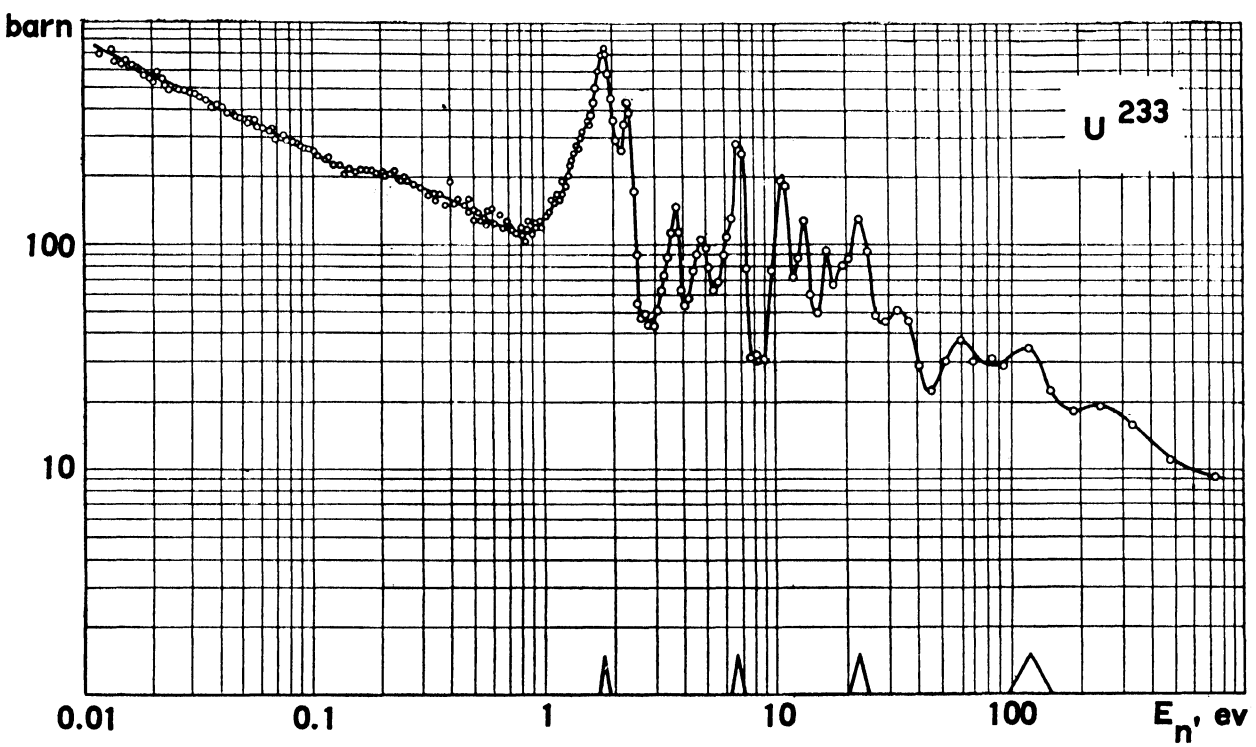

Figure 4

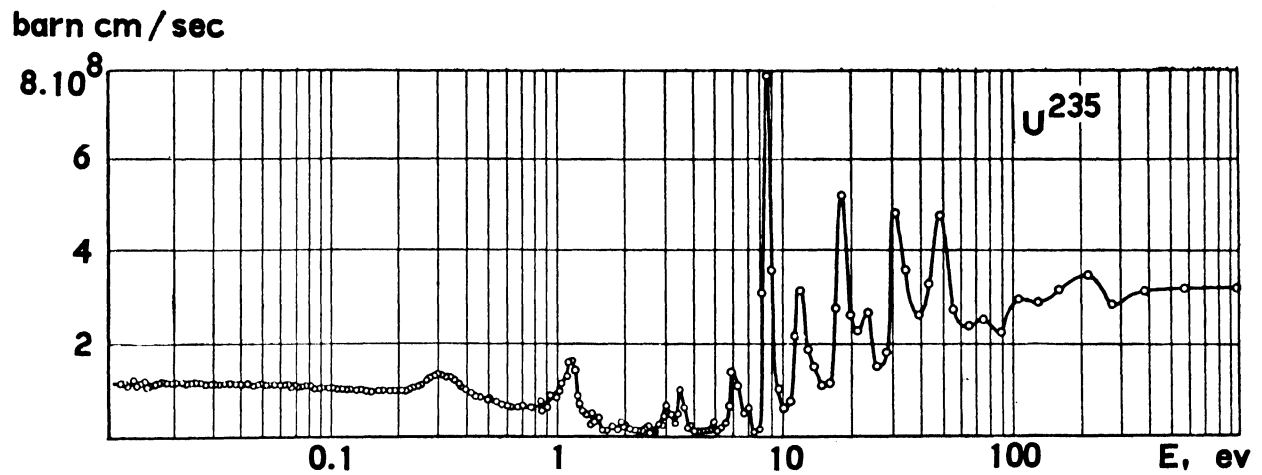

Figure 5

In the U^{233} fission cross section resonance peaks occur at energies 1.82, 2.3, 3.7, 4.8, 6.9, 10.7, 13.5, and 16 ev, and groups of unresolved resonance peaks at energies 22, 35, 60, and 120 ev. The resonance shape at energy 1.82 ev indicates the possible existence of a level with an approximate energy of 1.5 ev.

U^{235}

Figures 5 and 6 show the dependence of $v\sigma_f$ and σ_f on neutron energy measured by a chamber containing 70 mg of U^{235}. In plotting the curve it was assumed that the cross section at energy $E = 0.025$ ev was 540 barns.

The curves show that the cross section here obeys the $1/v$ law only up to an energy of 0.05 ev. In the energy region of 0.4 to 5 ev the fission cross section sharply decreases and on the average is below a $1/v$ curve drawn from the thermal region. In the

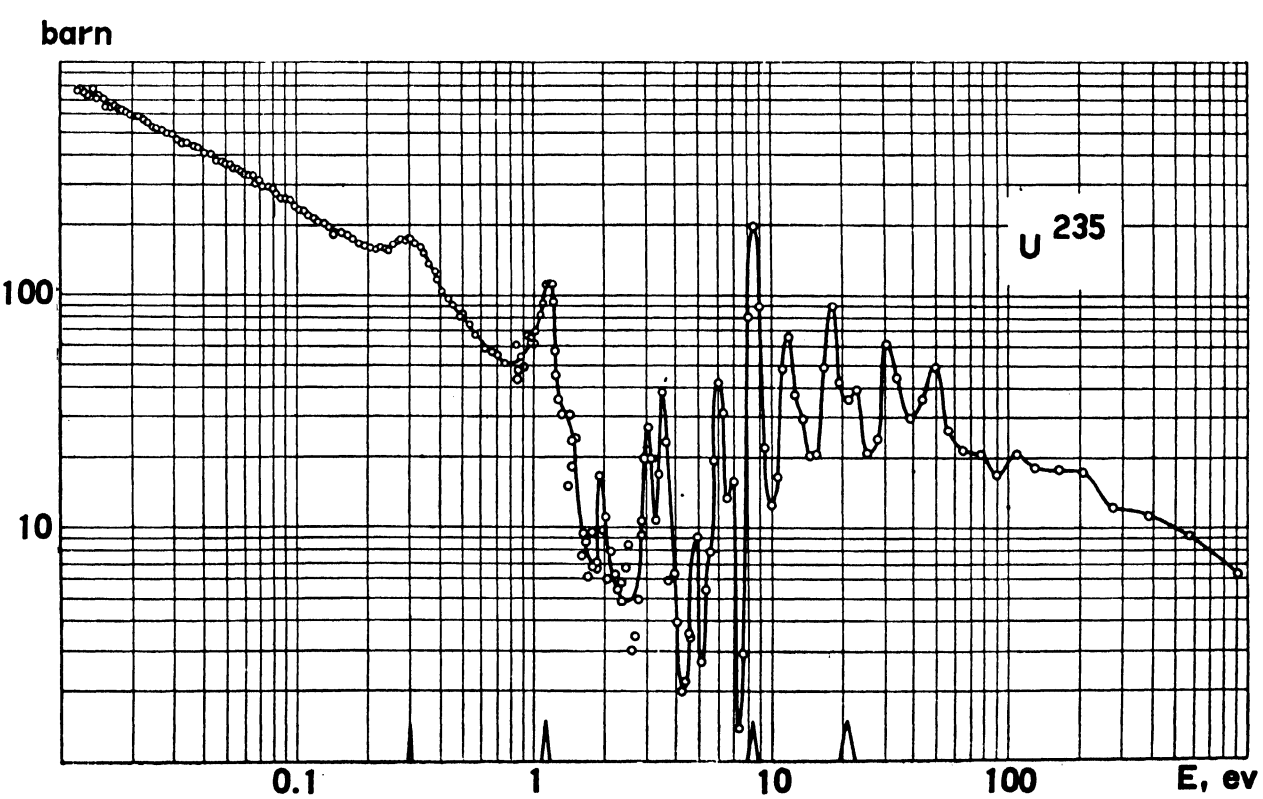

Figure 6

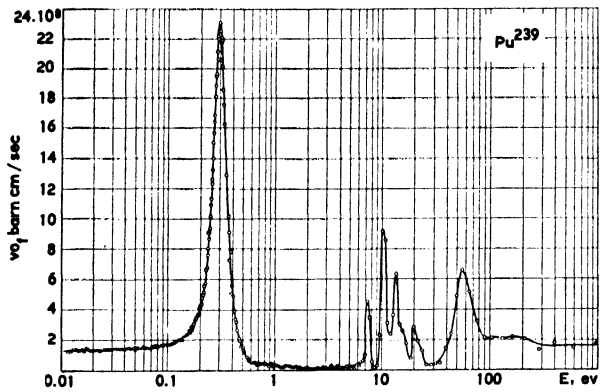

Figure 7

8 to 100 ev region, however, the energy cross section greatly increases and on the average is 3 times greater than that represented by the $1/v$ curve through the thermal region. In the fission cross section resonance peaks occur at energies 0.30, 1.13, 3.0, 3.5, 6.1, 8.4, 12.0, and 18.0 ev, and groups of unresolved resonance peaks at energies 31 and 50 ev. There may also be weak resonance peaks at energies 1.9, 4.8, 6.8, and 22 ev. The level at 0.3 ev and the next one are not sufficiently strong to explain the variation and the magnitude of the fission cross section in the thermal region. It must therefore be concluded that the negative level is also responsible for the value of the thermal cross section.

The results of the U^{235} fission cross-section measurements made by Hubert, Vendryes and Auclair, in France, with a crystal spectrometer in the region of 0.01 to 4 ev agree with our results, taking into account the resolution of both devices.[1] Popovic's recent measurements of U^{235} fission cross section in the region of 0.01 to 0.4 ev with a crystal spectrometer also agree well with our results.[2]

Pu^{239}

Measurements of Pu^{239} fission cross section were carried out by means of a chamber containing 22 mg of plutonium.

Figures 7 and 8 show the dependence of $v\sigma_f$ and σ_f on neutron energy measured with a chamber containing 22 mg of plutonium. In plotting the curve it was assumed that the cross section at energy $E = 0.025$ ev was 625 barns.

In the fission cross section resonance peaks occur at energies of 0.295, 7.4, 10.2, and 13.7 ev, and unresolved resonance peaks at energies of 20 and 55 ev.

The energy dependence and magnitude of the plutonium fission cross section in the thermal region can not be explained by the level at 0.295 ev or

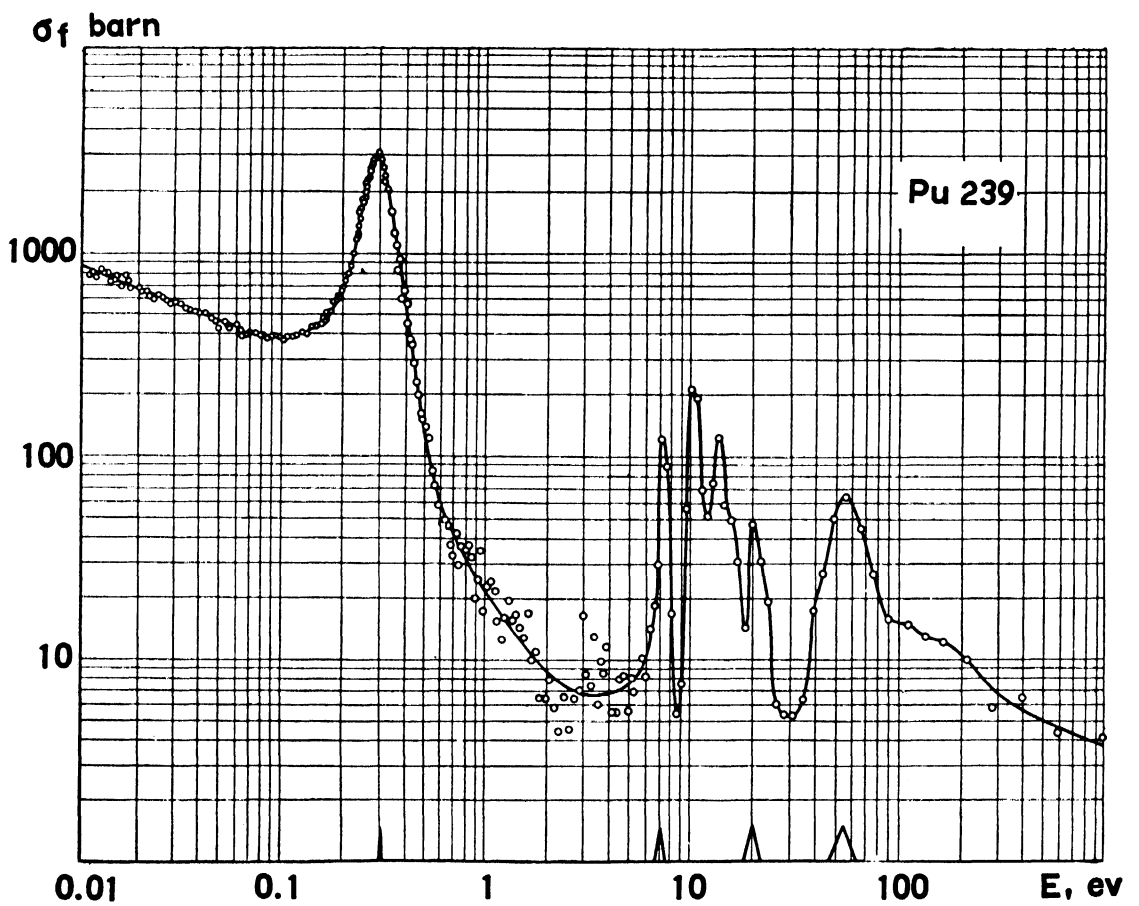

Figure 8

by the higher levels. For Pu as for U^{235}, we must assume the existence of a negative level.

Characteristic of the Pu fission cross section is the sharp drop in the region of 0.5 to 7 ev.

The resolving power is sufficiently high to determine the true parameters of the first level at 0.3 ev from the experimental curve. The best values are: $\sigma_0 = 2860$ barns $\Gamma = 0.095$ ev.* Correction of these results for the Doppler broadening of resonance, (which in the present case is equal to the Doppler broadening for the free plutonium atoms) gives a true width $\Gamma = 0.091$ ev and a true peak cross section $\sigma_0 = 2950$ barns.

The results obtained by Vendryes, Hubert and Auclair with a crystal spectrometer, and by Galula, Jacrot and Netter with a mechanical selector well agree with our findings.[3,4]

Pu^{241}

The fission cross-section measurement here was made with a 2 mg layer of plutonium, obtained by electromagnetic enrichment of a pile-irradiated plutonium sample.

The isotopic composition of the plutonium layer was determined by measuring its total alpha-activity, the number of spontaneous fissions, the differential alpha-particle spectra and its weight. The alpha-particle spectra were determined by a grid ionization chamber and amplitude analyser with electronic memory. The alpha-particle spectrum of the plutonium sample is shown in Fig. 9. These measurements showed the isotopic composition of the sample to be: Pu^{241}, 88.5%; Pu^{239}, 8.0%; Pu^{240}, 2.9%; and Am^{241}, 0.6%.

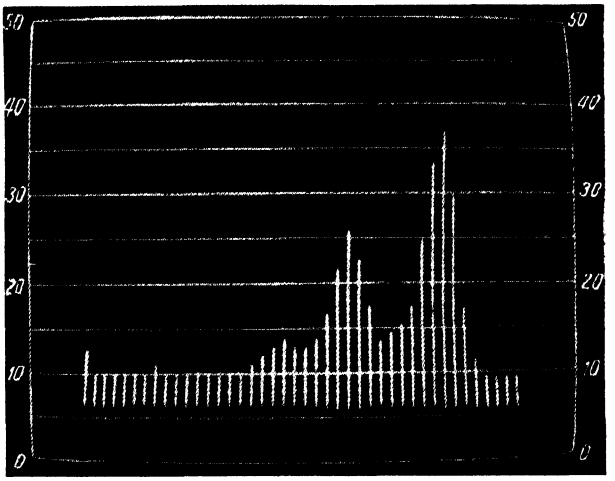

Figure 9

Figures 10 and 11 show the dependence of $\nu\sigma_f$ and σ_f on neutron energy determined for plutonium of this isotopic composition. In plotting the curves it was assumed that the cross section at energy $E = 0.025$ ev was 950 barns.

The Pu^{241} fission cross section energy dependence is similar to that of Pu^{239}. Pu^{239} has the same char-

* The experimental resonance peak cross section value is greater than σ_0 due to the contribution from the negative level.

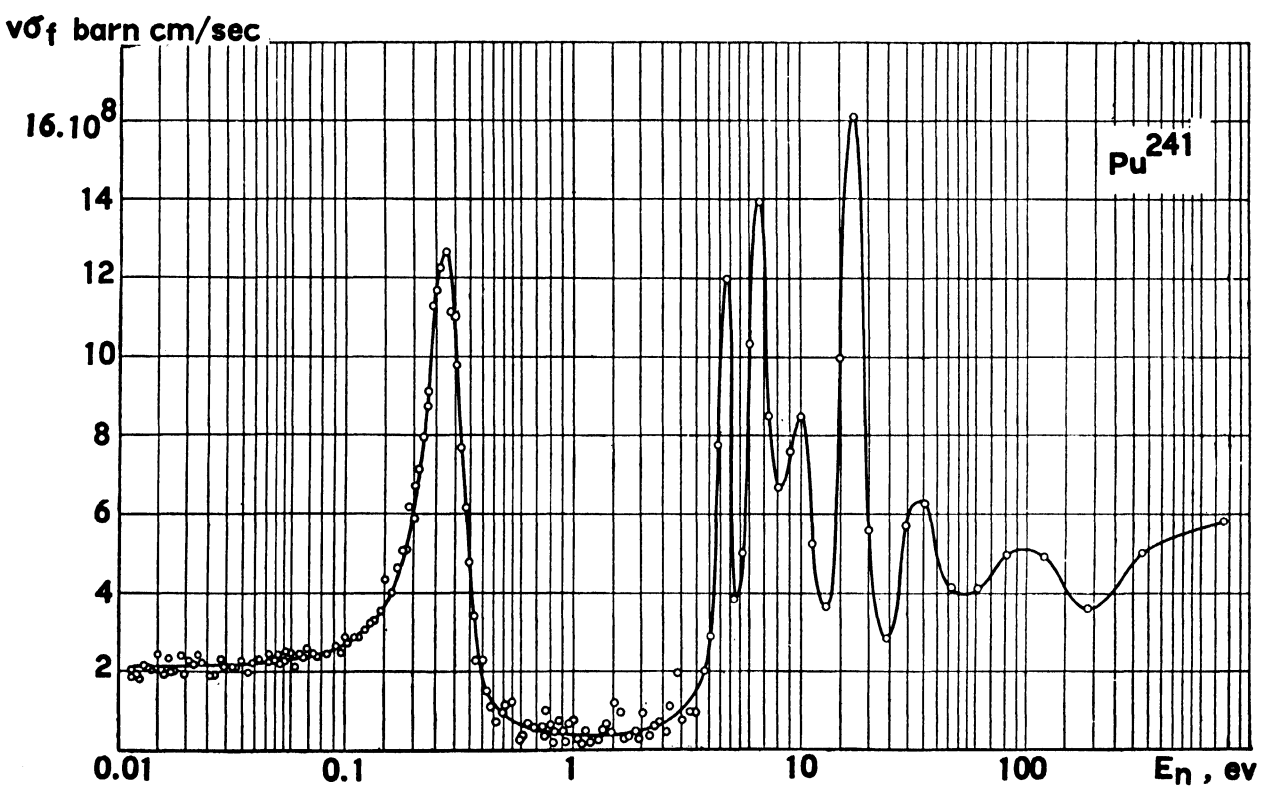

Figure 10

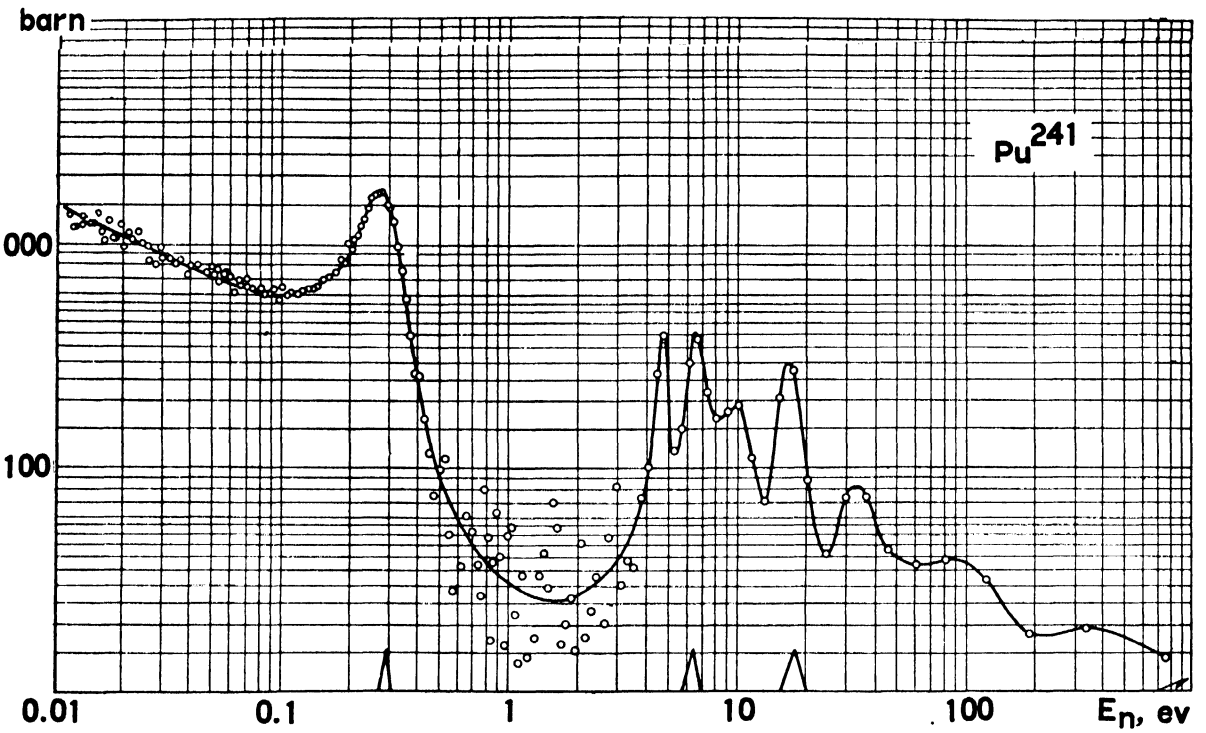

Figure 11

acteristic resonance peak at 0.995 ev as Pu^{241}, but with a different width, $\Gamma = 0.13$ ev, and a different peak cross section, $\sigma_0 = 1450$ barns. A detailed comparison of the other levels of Pu^{239} and Pu^{241} is complicated because the fission cross sections of Pu^{239} and Pu^{241} were evaluated at different resolving powers of the selector. There is, however, a great similarity between the arrangement of the Pu^{241} and Pu^{239} levels. This similarity cannot be explained by the presence of 8% of Pu^{239} in the investigated layer.

Total Cross Sections of Np^{237} and Am^{241}

The total cross section was determined by transmission measurements.

For Np^{237} the measurement was made on a sample containing 0.354 g/cm² of Np^{237} with a 0.02% admixture of Pu^{239}; and for Am^{241} on two samples,

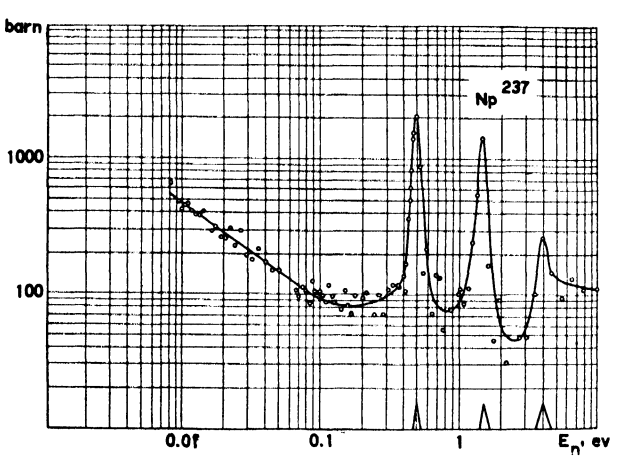

Figure 12

containing 0.521 g/cm and 0.0665 g/cm respectively of Am^{241}, with a 0.7% admixture of Pu^{239}.

The samples of Np^{237} and Am^{241} were prepared from powdered dioxides put in thin aluminum containers of 6 mm internal diameter. For measurement the containers were placed in a neutron beam with a 5 mm diameter, formed by paraffin-boron and nickel collimators.

The results of the Np^{237} measurements are given in Fig. 12. Resonance peaks have been observed at energies 0.5 ev, 1.5 ev, and 4 ev. The thermal region cross section deviates from the $1/v$ law, which suggests the presence of a near negative level.

The total cross section of Am^{241} is given in Fig. 13. Here resonance peaks were observed at energies 0.3, 0.53, 0.58, 1.26, and 1.9 ev, and groups of two or more unresolved resonance peaks at energies 2.4, 4, 5.5, 10, and 17 ev. The mean distance between the levels is thus less than 1.0 ev.

In the thermal region, the Am^{241} cross section approximately obeys the $1/v$ law.

A comparison of the total cross section of Am^{241} and the fission cross section of Pu^{239} shows that these nuclei have similar levels at energies 0.3 and 10 ev. The presence of 0.7% of Pu^{239} in the Am^{241} sample cannot explain the levels at 0.3 and 10 ev; it only slightly affects the total Am^{241} cross section in the 0.3 and 10 ev resonance regions.

CONCLUSION

It is of interest to compare the magnitude of the fission width Γ_f for various levels of the substances investigated by us, to see how it changes from level to level. The data presented here permits such a

comparison for the U^{233} group of levels at energy 1.8 ev, and for the two first levels of U^{235}, which have been investigated with a resolving power sufficient for this purpose.

Our analysis, based on the assumption that these levels do not interfere between themselves and with their neighbouring levels, leads to the conclusion that the fission width for the isotopes changes considerably from level to level. This divergence in the fission widths is apparently due to the level spin differences.

The influence of the spin of the excited nucleus on the fission probability indicates that the semi-classical concept of the fission process is not adequate.

Investigation of the fission cross sections of uranium and plutonium isotopes shows further that, within the experimental error, the first resonance levels for U^{235}, Pu^{239} and Pu^{241} are at the same neutron energy. It is possible that also U^{233} has a weak level at 0.3 ev, but this is covered up by a group of strong levels at 1.8 ev.

A first level at 0.3 ev was also observed in the total cross section of Am^{241}.

Thus, for at least four out of the five investigated nuclei which undergo fission with slow neutrons, the first level appears at the same energy. Considering the experimental error in determining the position of the levels, there is very little probability that this is accidental This result likewise cannot be explained by mutual contamination of the isotopes.

Measurements of total neutron cross sections of U^{233}, U^{235} and Pu^{239} have also been performed by Nikitin and coworkers with cyclotron time-of-flight equipment.[5]

The total neutron cross section of U^{235} has been measured by Vladimirski and coworkers with a mechanical selector.[6] The positions of the resonance peaks found in these measurements agree well with our results.

REFERENCES

1. Hubert, P., Vendryes, G. and Auclair, J. M., C.R., 238, 1873 (1954).
2. Popovic, Jour. Nuc. Energy, *1*, 3 (1954) ; *1*, 170 (1954).
3. Vendryes, G., Hubert, P. and Auclair, J. M., C.R., 239, 1034 (1954).
4. Galula, M., Jacrot, B. and Netter, F., C.R., 239, 1128 (1954).
5. Nikitin, S. J., *et al.*, P/646, Volume 4, Session 17A, these Proceedings.
6. Vladimirski, V. V., *et al.*, P/641, Volume 4, Session 15A, these Proceedings.
7. Mostovoi, V. I., *et al.*, P/640, Volume 4, Session 15A, these Proceedings.

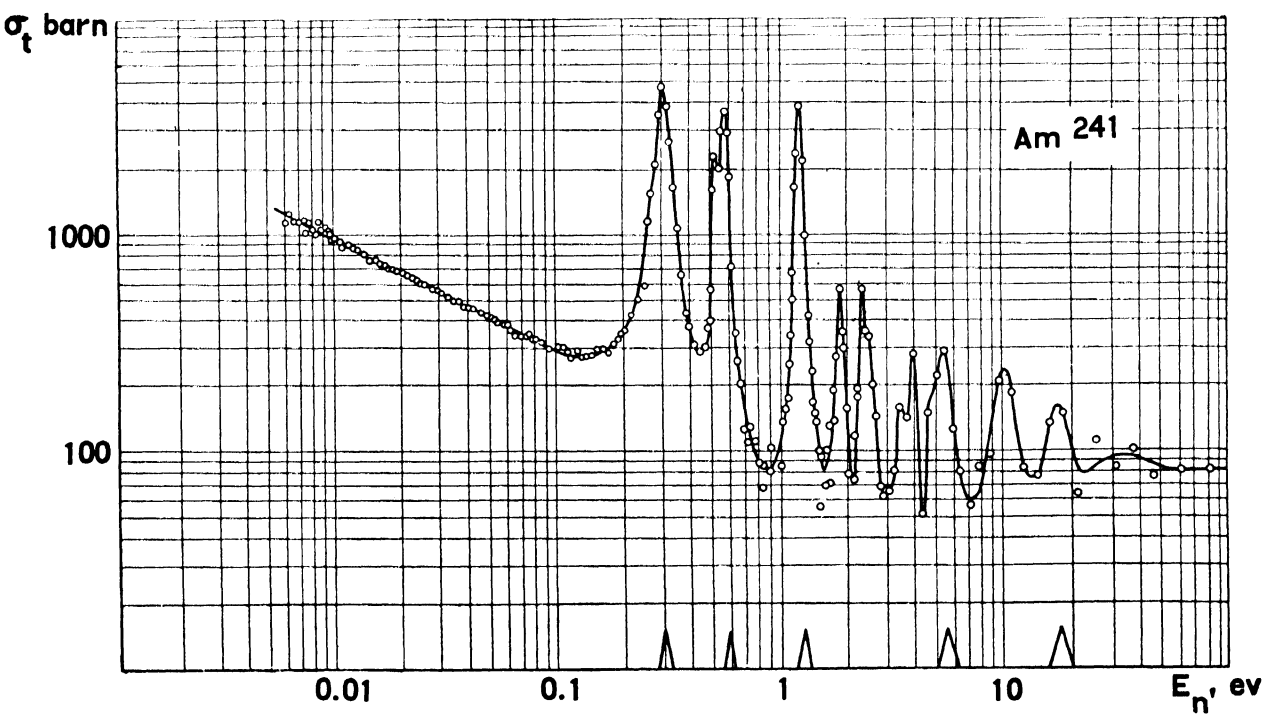

Figure 13

Time-of-Flight Measurement of the Total Neutron Cross Section of Uranium-233, Uranium-235 and Plutonium-239

By S. J. Nikitin, N. D. Galanina, K. G. Ignatiew, W. W. Okorokow and S. I. Suchorutchkin, USSR

In the study of the interaction of neutrons with matter the time-of-flight method is widely used. This method is successfully used in the energy region from ~ 0.001 to ~ 10,000 ev. In time-of-flight experiments the cyclotron,[1] the linear accelerator, the betatron and also the nuclear reactor, the beam of which is time-modulated in intensity, may serve as a source of neutrons.[2,3,8]

In the present paper a neutron selector with a pulsed cyclotron is described. Results of measurements of the energy dependence of the total neutron cross sections of heavy nuclei are given.

THE NEUTRON SELECTOR

Neutron Source and Collimation

A cyclotron with internal beryllium target served as the source of neutrons. In order to get a pulsed neutron beam, modulation of the ion arc of the source was used. The duration of the deuteron pulse, and correspondingly of the neutron pulse, could be varied from 4 to 32 μsec.

The neutrons were moderated in a paraffin layer 50×30×1 cm that was the actual neutron source.

From the moderator to the detector the neutrons travelled through a boron-paraffin collimator. The path-length was different, depending on the energy region investigated and equalled 127, 250, 310, 580 and 1600 cm. Figure 1 gives schematically the collimation arrangement and the location of the sample and the detector in the experiments with the path-length equal to 5.8 m.

Original language: Russian.

NEUTRON DETECTORS

In the experiments with path-length 5.8 and 16 m, proportional counters filled with BF_3, enriched in the B^{10} isotope, with a small admixture of argon were used.

In order to diminish uncertainty in path-length when using path-lengths of 1.27, 2.50 and 3.10 m, scintillation neutron counters, consisting of photomultipliers and ZnS(Ag) scintillators sintered in B_2O_3, were used.

Besides registering the neutrons passing the collimator, continuous control of the neutron-intensity given by the cyclotron was performed. For this purpose three monitoring neutron counters filled with BF_3 were placed near the cyclotron. All neutron intensity measurements were referred to the monitor count.

TIME-ANALYZER

Figure 2 shows the block-diagram of the recording part of the neutron selector. The interconnection of individual elements was as follows. A quartz pulse

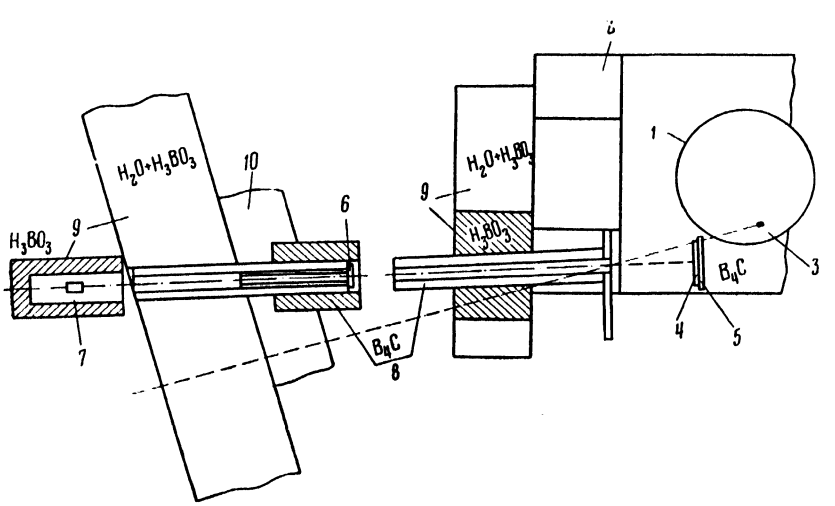

Figure 1. Collimation of the neutron beam (path length 5.8 m): (1) cyclotron chamber; (2) magnet yoke; (3) beryllium target; (4) moderator; (5) B_4C shield; (6) sample; (7) BF_3 counters; (8) B_4C collimator; (9) boric-acid shield; and (10) paraffin shield

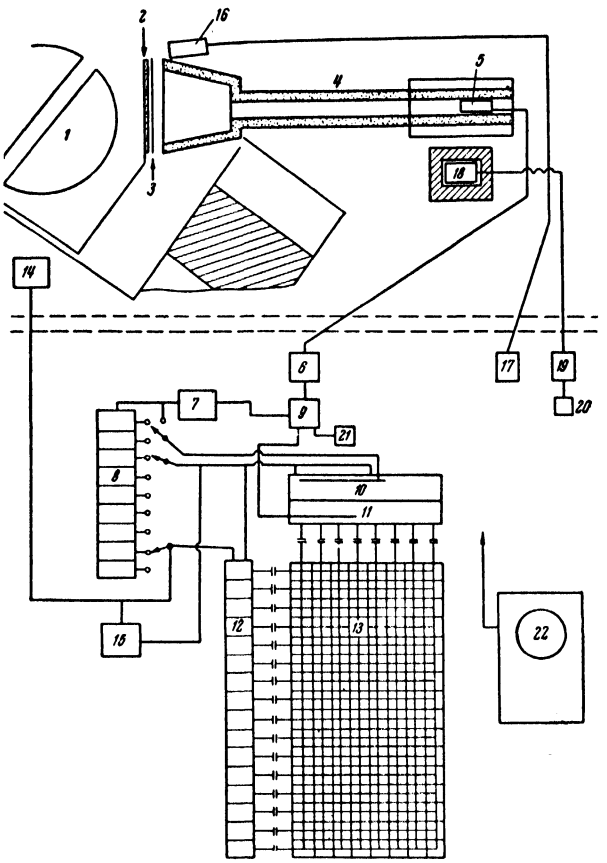

Figure 2. Block diagram of the neutron selector: (1) cyclotron; (2) B_4C filter; (3) moderator; (4) collimator (path-lengths 127, 250, 310 cm); (5) detector; (6) amplifier; (7) quartz oscillator; (8) timing system; (9) phasing circuit; (10) channel commutator; (11) coincidence circuits; (12) channel-group commutator; (13) registering cascades; (14) modulator of cyclotron source; (15) modulator of high-frequency oscillator; (16, 17) γ-detector and amplifier of the beam indicator; (18, 19, 20) monitor, a BF_3 counter with paraffin shield, amplifier and scaling circuit; (21) scaling circuit; and (22) oscilloscope

oscillator (7) with a period of 4 μsec drives the timing system (8) consisting of 10 binary scaling-circuits with a total scaling coefficient 2048. These circuits successively divide the oscillator frequency and give trains of square waves with periods 8, 16, 32 . . . 4096 sec. Pulses obtained by differentiating these waves are used to govern the individual units of the selector; the channel-commutator (10), the group-commutator (12) and the ion-source modulator. The channel-commutator and the group-commutator are open ring scaling-circuits, the first consisting of 8 stages, the second of 16 stages. The channel-commutator actuates successively the 8 main coincidence-circuits (11) over a time equal to the channel-width (adjustable from 4 to 32 μsec). The group-commutator successively connects the sixteen groups of channels to the main coincidence-circuits (11). Each group consists of 8 channels and covers the following time intervals (for a channel-width of 4 μsec): 0–32, 32–64, . . . 480–512 μsec. The neutron counter pulses (5) are fed to the pre-amplifier and the amplifier (6) and pass on to the discriminator and the phasing circuit (9) which standardizes its position relative to the starting time of the channel. From here the pulse is fed to the second input of the main coincidence-circuits. Depending on the time-of-flight the pulse is registered by the corresponding channel.

Each channel has two mechanical registers which are by turns connected to the output of the channel. This switching-over is done simultaneously with the displacement of the sample relative to the neutron beam. The exposure times with the sample in the beam and out of the beam are automatically determined by the monitor counter. In order to eliminate a low continuous component of the neutron intensity, the high-frequency oscillator of the cyclotron was modulated. The operation of the high-frequency oscillator-modulator was governed by the timing system (8).

CONTROL EXPERIMENTS

In order to obtain the experimental resolution curve the BF_3 counter, fairly well shielded from the scattered slow neutrons, was placed close by the moderator and its pulses were fed to the time-analyzer.

The curve obtained in this manner is shown in Fig. 3, from which it may be seen that it does not considerably differ from the ideal resolution curve, which in our case is an isosceles triangle with a base of $2\tau_{channel} = 8$ μsec ($\tau_{channel} = \tau_{arc}$).

The duration and the shape of deuteron pulses and the acceleration time of the deuterons was checked regularly by observing the shape and position of the γ-quanta burst coming from the target of the cyclotron. They were recorded by a scintillation counter with a large NaI (Tl) crystal.

The neutron flux getting to the counters from outside the collimator was determined in special control experiments. This flux amounted to $\sim 1\%$ of the neutron flux passing through the collimator and was taken into account when computing the cross sections.

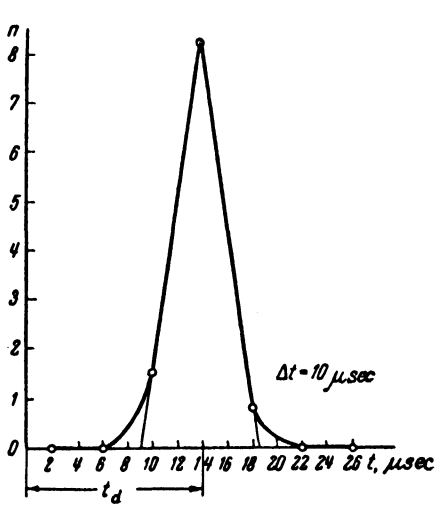

Figure 3. Resolution curve

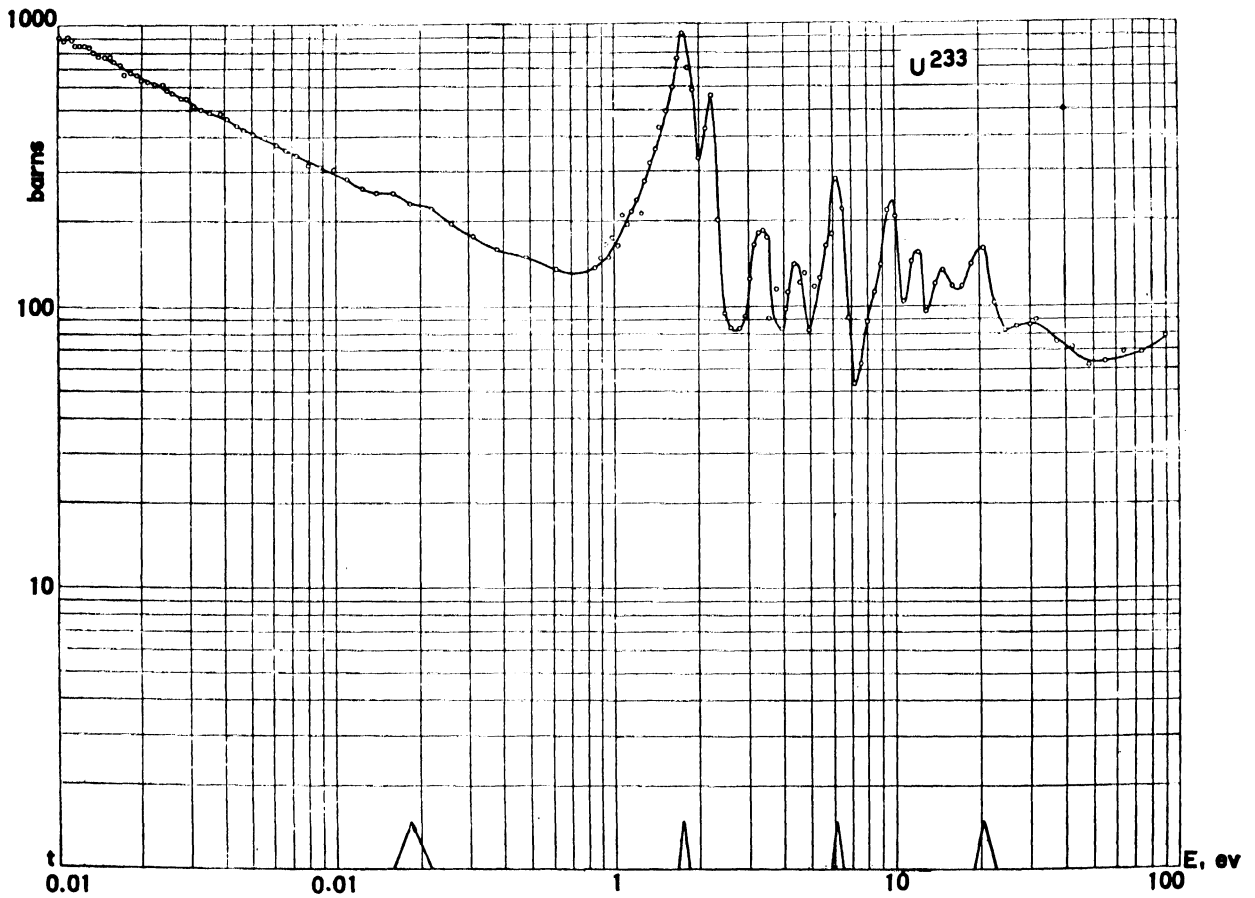

Figure 4. Total cross section of U^{233}

The study of the absorption of neutrons in boron may serve as a further check, as a slight admixture of background is enough to disturb the $1/v$ law, and this can easily be observed. Such measurements were carried out with all path-lengths and with boron absorbers of different thicknesses. In all these experiments the absorption of boron follows the $1/v$ law within the limits of the statistical error.

STUDY OF THE TOTAL CROSS SECTIONS OF HEAVY ELEMENTS

In order to get the total neutron cross sections, experiments with and without the sample in the neutron beam were performed. The value of the cross section was determined from the expressions,

$$\sigma = -\frac{1}{n} \ln T \qquad T = \frac{N(t)}{N_0(t)}$$

where n = the number of atoms per cm^2 in the sample studied, T = the transmission, $N_0(t)$ = the number of counts in the channel corresponding to the time-of-flight t with the sample out of the beam, $N(t)$ = the number of counts in the channel corresponding to the time-of-flight t with the sample in the beam.

EXPERIMENTAL CONDITIONS

The thicknesses of the samples used in the different experiments, the path-lengths and the channel-widths of the time-analyzer, are given in Table I.

The measurements carried out under different conditions overlap partly. The energy intervals from which the data were taken for Figs. 4–7 are also indicated in the table.

THE TOTAL CROSS SECTION OF U^{233}

The experimental results are given in Fig. 4. The thermal cross section (E_n = 0.025 ev) is 580 ± 20 barn.

Up to 0.3–0.4 ev the cross section is given by the $1/v$ law. At higher energies a slight irregularity of the energy-dependence is observed. Strong resonances are observed at energies: 1.7; 2.25; 3.4; 4.5; 6.25 ±

Table I

Sample	*Thickness gm/cm²*	*Energy interval, ev*	*Path-length, m*	*Width of channel and neutron pulse, μsec*
U^{233}	0.72	0.01–1.0	1.27	16
	1.2	1–3	5.8	8
	1.2	3–100	5.8	4
U^{235}	0.88	0.01–0.8	1.27	16
	0.88	0.8–3	2.5	4
	0.8	3–100	5.8	4
Pu^{239}	0.3	0.01–0.8	3.1	32
	0.3	0.8–1.5	3.1	4
	4.0	1.5–6	3.1	4
	1.07	6–100	5.8	4
	1.00	6–100	16	4

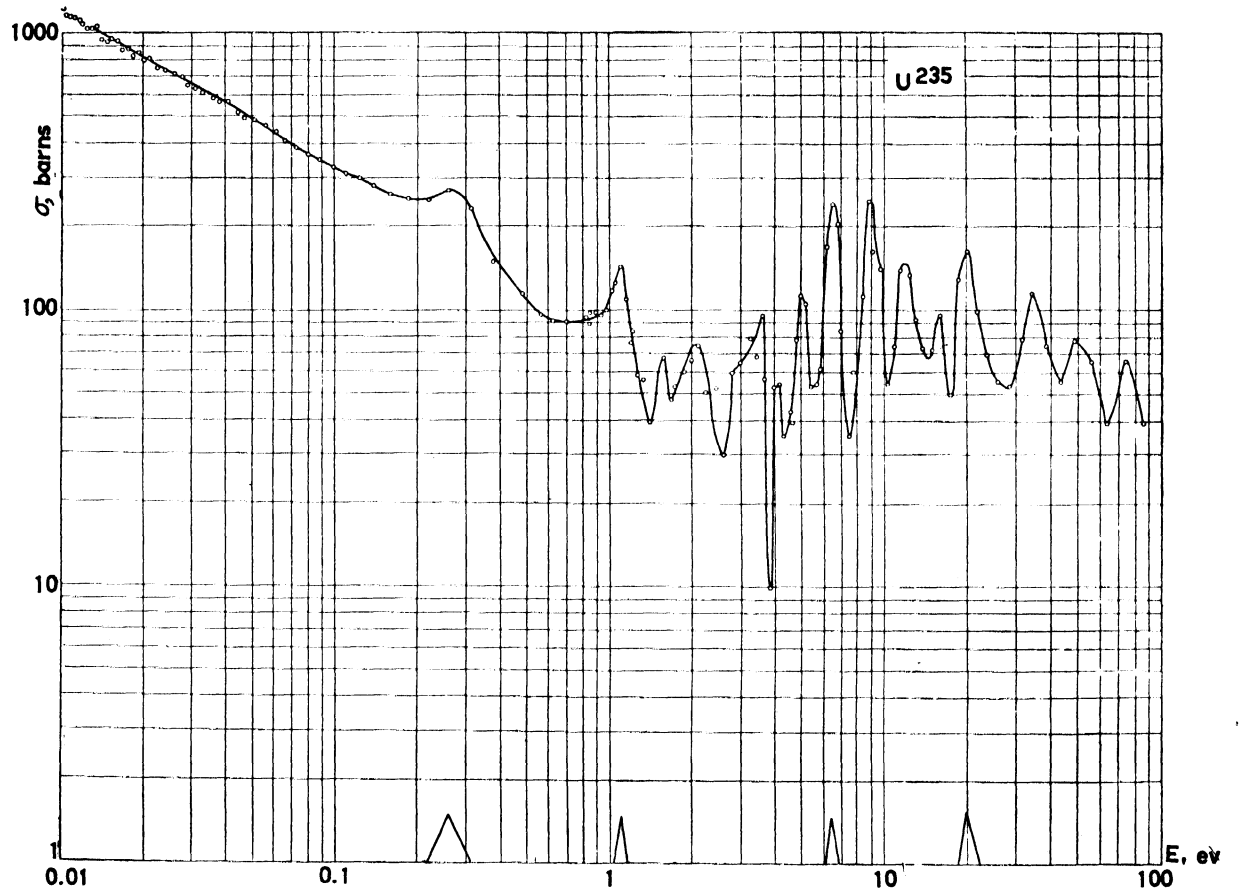

Figure 5. Total cross section of U^{235}

0.4; 10.0 ± 0.8; 12 ± 1.0; 15 ± 1.4 and 21 ± 2.2 ev. Some of these resonances are not fully resolved and are probably complex. The value $\sqrt{E}\cdot\sigma$ in the resonance region is on the average 3–4 times that in the thermal region.

THE TOTAL CROSS SECTION OF U^{235}

Figure 5 gives the dependence of the total cross section of U^{235} on energy. The results were corrected for the presence of U^{238} in the sample using the results of an isotopic analysis and data for the total cross section of U^{238} obtained with the same selector. The value of the thermal cross section was found to be 710 ± 20 barns, in accordance with the published data on the cross sections in this energy region.[4,5]

Resonances were observed at the neutron energies 0.3; 1.08; 2.0; 3.6; 5; 6.5; 8.7; 12; 16; 19.5 and 34 ev, and probably at 1.5 and 2.7 ev.

The higher resonances ($E_n > 5$ ev) were also observed with the mechanical neutron-selector.[3] In the energy interval 1.5–6 ev the experimental curve lies considerably lower than would correspond to the $1/v$ law extrapolated from the thermal region.

At energies $E_n > 6$ ev the value of $\sqrt{E}\cdot\sigma$, in the mean, exceeds that in the thermal region by 3–4 times.

THE TOTAL CROSS SECTION OF Pu^{239}

Figures 6 and 7 show the results of the measurements of the total cross section of Pu^{239}.

In the thermal region the cross section was 1040 ± 30 barns in accordance with other investigations.[6] The cross section is $1/v$ only in a narrow region near thermal. Resonances were observed at neutron energies: 0.295 ± 0.005; 8.1 ± 0.16; 11.3 ± 0.2; 12.3 ± 0.3; 15.1 ± 0.4; 18.3 ± 0.6; 22.8 ± 0.8 ev.

Preliminary calculations of the level strengths $\sigma_0\Gamma^2$ of these resonances lead to the following data: 40 ± 5; 12 ± 2.5; 29 ± 8; 9 ± 3; 69 ± 15; 24 ± 7; 13 ± 4 barn ev,[2] respectively. Besides this a number of unresolved resonances at energies 27.6; 43; 52; 59; 66; 84 and 96 ev were observed. As was shown,[8] the resonance level at 1 ev is due to an admixture of Pu^{240} in the sample.

CONCLUSION

Detailed investigation of the energy dependence of the cross sections of the heavy isotopes shows that the contribution of the near resonance-levels to the thermal region cross section, calculated from Breit-Wigner formula for a single level, does not account for the observed thermal region cross section.

In the energy region $E_n > 5$–6 ev all isotopes show groups of resonances which caused the average

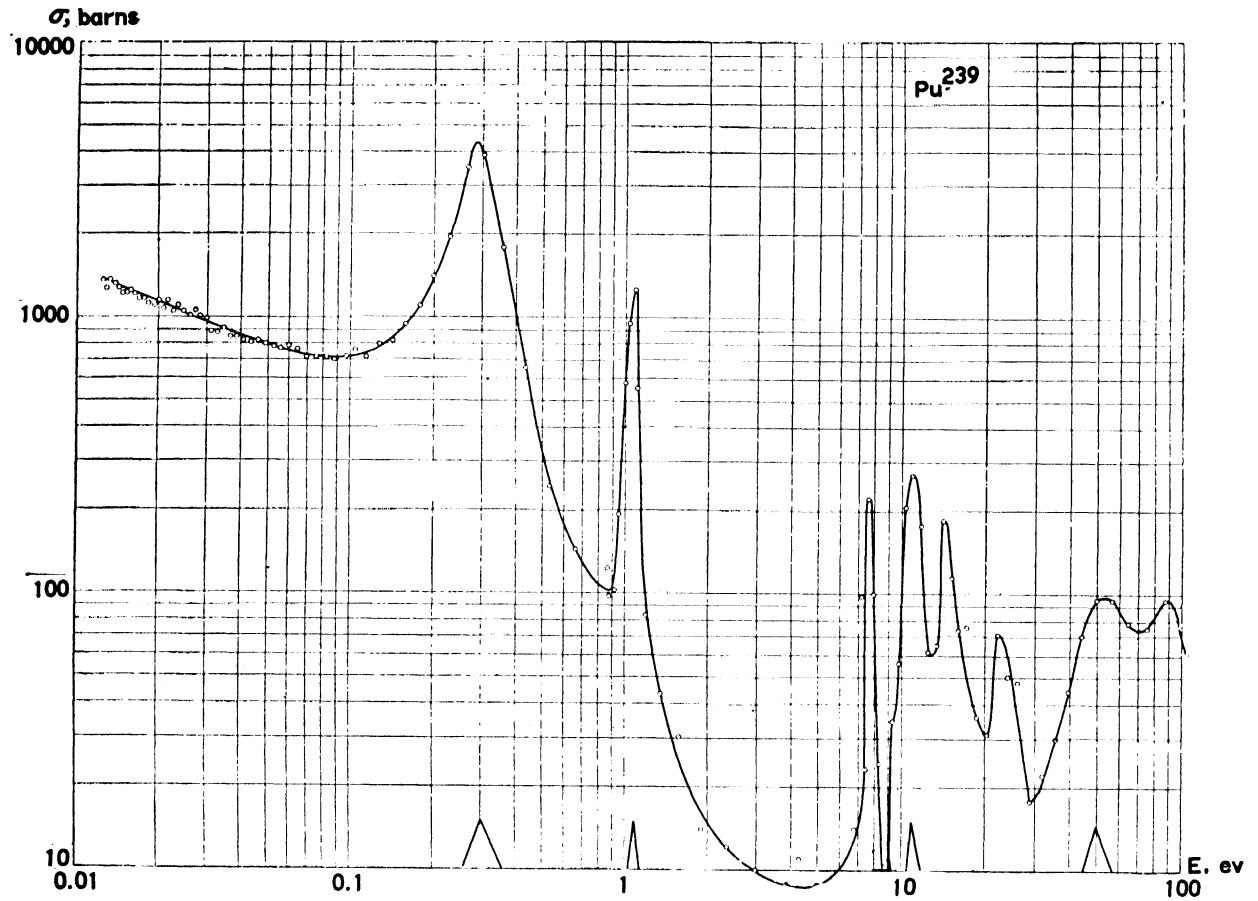

Figure 6. Total cross section of Pu^{239}

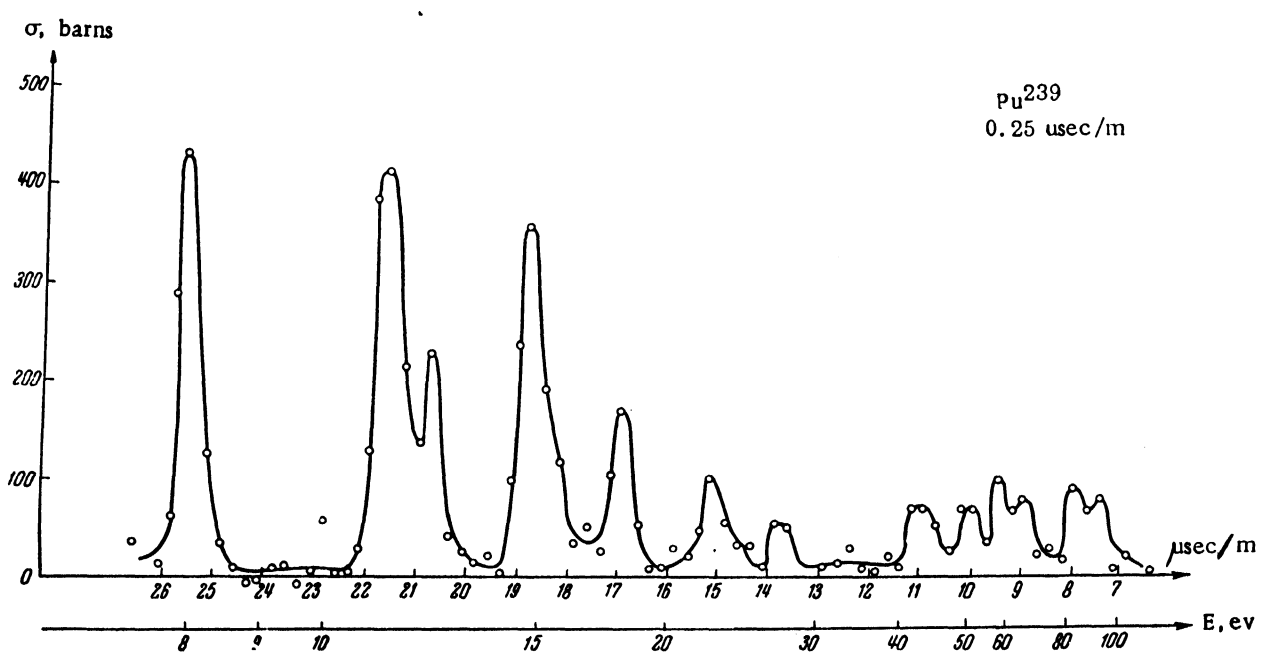

Figure 7. Total cross section of Pu^{239} in the energy interval 6–100 ev obtained with resolution 0.25 μsec/m

cross section to be 3 to 4 times larger than would correspond to the thermal region.

The energy dependence of the fission cross sections, measured with the same selector, shows mainly the same peculiarities as that of the total cross sections.

Those results are in agreement with the fission cross-section measurements carried out with the mechanical neutron selector.[7]

REFERENCES

1. Rainwater, L. J. and Havens, W. W., Phys. Rev., *70,* 136, 154 (1946); Rainwater, L. J., Havens, W. W., Wu, C. S. and Dunning, J. R., Phys. Rev., *71,* 65, 165, 174 (1947); Havens, W. W. and Rainwater, L. J., Phys. Rev., *83,* 1123 (1951).
2. Fermi, E., Marshall, J. and Marshall, L., Phys. Rev., *72,* 193 (1947); Seidl, F. G. P., Hughes, D. J. *et al.,* Phys. Rev., *95,* 478 (1954).
3. Vladimirski, V. V., Radkevich, I. A. and Sokolovsky, V. V., P/641, *A Mechanical Neutron Velocity Spectrometer,* Volume 4, Session 15A, these Proceedings.
4. Egelstaff, P., Journ. of Nuclear Energy, 1, No. 1 (1955).
5. Palevsky, H. *et al.,* Phys. Rev., *94,* 1088 (1954).
6. Canad. Journ. Phys., 30, 624 (1952).
7. Adamchuk, Y. B., Gerasimov, V. F., Yefimov, B. V., Zenkevich, V. S., Mostovoi, V. I., Pevzner, M. I., Chernyshov, A. A. and Tsitovich, A. P., P/645, *Fission and Total Cross Sections of Some Heavy Nuclides for Monochromatic Neutrons as Measured by a Mechanical Neutron Velocity Selector,* Volume 4, Session 17A, these Proceedings.
8. Mostovoi, V. I., Pevzner, M. I. and Tsitovich, A. P., P/640, *The Mechanical Neutron Velocity Selector,* Volume 4, Session 15A, these Proceedings.

Determination of the Absorption Cross Section and of the Radiative Capture Cross Section of Uranium-233 for Pile Neutrons

By G. M. Kukavadse, L. L. Goldin, M. P. Anikina and B. W. Ershler, USSR

When U^{233} is irradiated by neutrons, two competing processes take place: fission of U^{233} nuclei resulting in the production of fragments and a corresponding depletion or uranium, and radiative capture of neutrons converting U^{233} into U^{234}. For the purpose of measuring the cross sections of these reactions, foils made of U^{233} were irradiated for a long time in a nuclear reactor together with plates of metallic lithium, which served as an integral indicator of the neutron flux. The decrease in the amount of uranium was determined by the change of α-activity of the sample, by the amount of fission fragments produced and by the method of isotopic dilution. The amount of U^{234} was measured by mass spectrometric analysis of the irradiated uranium. An isotopic analysis of the irradiated lithium made it possible to calculate the integral neutron flux from the decrease in the concentration of Li^6 resulting from the reaction $Li^6(n, \alpha)H^3$.

PREPARATION AND IRRADIATION OF SAMPLES

The uranium samples were made of a foil 3.2×10^{-2} mm thick. The sample had the form of a plate 33×3 mm, and weighed 60.75 mg.

The lithium samples were made of metallic lithium. The areas of the uranium and lithium samples were equal. The lithium sample weighed 28 mg.

The samples were wrapped in 2.5×10^{-2} mm platinum foil and in a thin aluminium foil; they were then hermetically sealed in a lead envelope, and pressed into an aluminium container with lead spacer. The samples thus prepared were submerged in the water-filled channel of the nuclear reactor.

The design of the container is shown in Fig. 1.

TREATMENT OF THE SAMPLES AND QUANTITATIVE DETERMINATION OF U^{233} FISSION

After the containers had been opened, the lead packages were melted over a low-flame range, the aluminium foil was removed and the bright platinum envelope with uranium was entirely dissolved in cold aqua regia. The melted lead from the package, and the aluminium foil were tested, by activity, for the presence of fission fragments and uranium. The activity was less than 0.005 of the activity of the envelope with U^{233}. This activity was caused by activation of the lead. After eliminating the excess acid by evaporation in a water bath, the solution was transferred without loss to a measuring flask and diluted to a volume of 100 milliliters of 0.1N nitric acid. The amount of U^{233} in this solution was then found by the three methods described below.

U^{233} Determination by Means of the α-Activity of the Solution

0.050 milliliter of a standard solution, containing 0.482×10^{-4} mg of U^{233}, was placed on a thoroughly cleaned glass disc 1 cm in diameter and distributed evenly over an area of 0.2 cm^2. After drying, the activity was counted in a well-defined geometry on an α-counter. The following data for two such discs illustrate the reproducibility thus achieved:

	Number of pulses counted	*Time in minutes*	*Counts per minute*
Disc I	78,662	200	393.3
Disc II	35,757	90	397.3

It follows that the mean error in specific activity is of the order of 0.5%, and lies within the limits of statistical error.

The average value corrected for the background of 0.8 cpm is 394.5 ± 2.5 cpm.

Similar experiments were performed with the irradiated sample diluted 4×10^6 times in 0.1N HNO_3. The following values of the α-activity were found:

	Number of pulses counted	*Time in minutes*	*Counts per minute*
Disc I	28,484	275	103.6
Disc II	30,854	300	102.8

The average, corrected for background (1.5 cpm), was 101.8 ± 0.4 cpm.

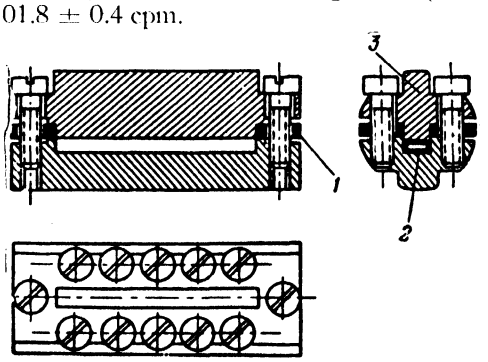

Figure 1. (1) Lead spacer; (2) lead envelope; and (3) aluminum envelope

Original language: Russian.

Taking into account the 2.08% U^{234} content, the specific activity of which is 0.64 of the specific activity of U^{233}, we find for the quantity of U^{233} in the sample 49.1 ± 0.3 mg.

U^{233} Determination in the Solution by the Isotopic Dilution Method

0.992 mg of natural uranium in the form of uranyl nitrate were added to a 1/50 part of the solution.

Mass spectrometric analysis of the mixture showed the peak ratio U^{233}/U^{238} equal to 1.008 ± 0.005, corresponding to an amount of U^{233} in the solution of 48.6 ± 0.25 mg.

Determination of the Amount of Split U^{233} from the Content of Cerium-140

By mass spectrometric method the isotopic content of the cerium, removed from the fission products with an yttrium carrier, and the isotopic content of cerium in a mixture consisting of 1/50 part of the solution and 0.0440 mg of natural cerium were determined.

In the fission fragments, the ratio cerium-140: cerium-142 was 1.01 ± 0.005 (Fig. 2, upper spectrogram), whereas in the case of the mixture with natural cerium it was 3.66 ± 0.07 (Fig. 2, lower spectrogram). From this, the content of Ce^{140} in the fission fragments was found to be 0.418 ± 0.016 mg. Taking the fission yield of this fragment according to Coryell and Sugarman[1] equal to 6.0%, we find 11.3 ± 0.4 mg for the amount of split U^{233}.

To the error of this result, however, one should add the error in the fission yield, which is not given in reference 1.

Thus the amount of split uranium determined by the various methods is:

From the α-activity:	11.65 ± 0.3 mg
From isotopic dilution:	12.15 ± 0.3 mg
From the yield of cerium-140 in the fission fragments:	11.3 ± 0.4 mg

The most precise results were those found from α-activity and isotopic dilution, and only they were used in the calculations. Their average is 11.9 ± 0.2 mg.

MASS SPECTROMETRIC ANALYSIS OF URANIUM

The mass spectrometric isotopic analysis of the samples of uranium was performed on a mass spectrometer with a sector (60 degrees) magnetic field. The chamber of the mass spectrometer is bent along an arc of 15 cm radius.

The ion source is of the thermionic type. A strip of 30–40 micron tungsten foil with a tungsten sponge mounted on it served as emitter.

The sample, in the form of an aqueous solution of uranyl nitrate, was dropped onto the tungsten sponge with a micro pipet.

The ion current was measured with a feed-back dc amplifier. The sensitivity of the amplifier, with an input resistance of 5×10^{11} ohms, was 0.25 millivolts per scale division. The peaks were registered by an automatic EPP–09 recorder.

UO_2^+ ions originated on the tungsten emitter as a result of surface ionization. For control, natural uranium was added to the sample of uranium-233 and 234 in a quantity giving equal peak height of U^{238} and U^{233}.

Near the high peaks of UO_2^+ corresponding to isotopes 238 and 233, small peaks are observed due to the ions $UO^{16}O^{17+}$ and $UO^{16}O^{18+}$ (Fig. 3). The heights of these peaks are 1/8000 and 1/250 of the height of the main peak, respectively.

As a result of the addition of natural uranium, there always appears a peak of U^{235} with a U^{235}/U^{238} peak ratio equal to 1/140.

The height of the peaks near U^{238} $O^{16}O^{16}$ was measured on all spectrograms and served as a check of the operation of the apparatus. In the five spectrograms used for the calculations the peak height ratios of $U^{238}O_2^{16}$ and $U^{238}O^{16}O^{18}$ were 260, 256, 246, 250 and 244. The peak heights due to $U^{235}O_2^{16+}$ and $U^{233}O^{16}O^{18}$ were also checked.

For the atomic ratio of U^{233} to U^{234} the following values were obtained: 46.3, 47.1, 48.5, 46.5 and 46.8, which gives the value 2.12 + 0.06% for N^{234}/N^{233}. The error slightly exceeds the statistical error.

MEASUREMENTS OF THE ISOTOPIC CONTENT OF LITHIUM

The isotopic content of the lithium was measured with a mass spectrometer. Lithium chloride was deposited on a nichromium-V strip. At a certain distance from the strip and parallel to it a tungsten filament heated by direct current was located. The strip was heated by the tungsten filament. Ionization of the atoms took place in collisions with the incandescent filament. This construction of the source ensured at a small evaporation speed a high degree of ionization of lithium.

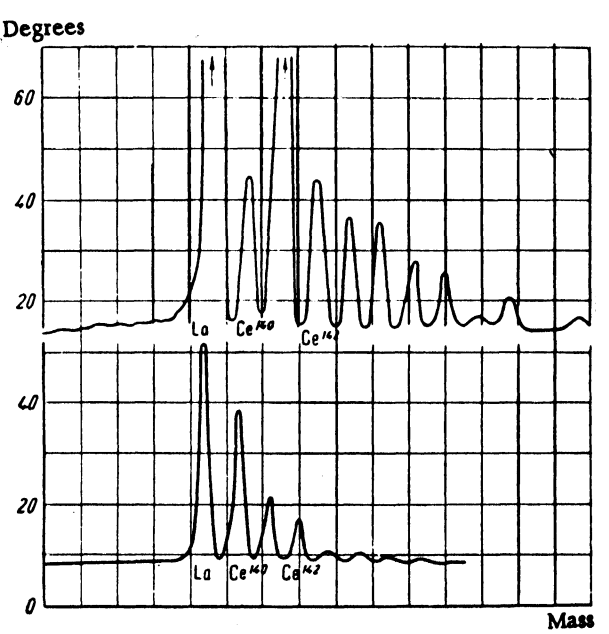

Figure 2. Mass spectrogram of natural cerium and of cerium in fission fragments

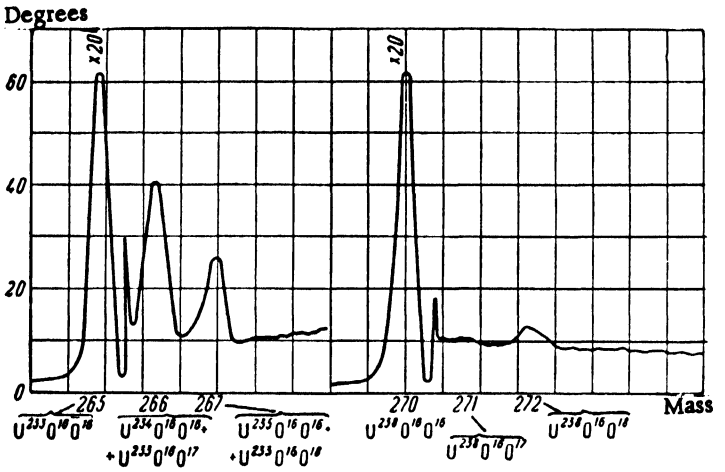

Figure 3. Mass spectrogram of uranium

Usually during measurement of the isotopic content of lithium a noticeable change in isotopic content is observed. At first the concentration of the light isotope Li^6 is too high, after some time it falls, showing, in case of proper operation conditions, a comparatively long plateau and, finally it falls sharply to zero. This phenomenon is due to the relatively large difference in the masses of Li^6 and Li^7, which causes a difference in evaporation speed. As will be shown elsewhere, in case of such a nonstationary process, the true concentration precisely equals that of the plateau.

Measurement of the isotopic concentration of natural lithium resulted in the value 12.36 ± 0.04 for the ratio of atomic concentrations of Li^7 and Li^6, in good agreement with the published data.

The ratio of concentrations for the irradiated lithium proved to be 16.66 ± 0.13.

Since the number of atoms of Li^7 does not change during irradiation, the ratio of the remaining atoms of Li^6 to their initial number is

$$\frac{N(t)}{N(0)} = 0.742 \pm 0.006$$

DISCUSSION OF RESULTS

Let us now calculate the ratio of cross sections of the radiative capture $\sigma_{n\gamma}$ to the absorption cross section σ_c for U^{233}.

Neglecting the decrease of U^{234} resulting from the absorption of neutrons (it is easy to see that taking account of this will change the result by a factor of the order of 0.998), then for this ratio we have:

$$\frac{\sigma_{n\gamma}}{\sigma_c} = \frac{N^{234}}{\Delta N^{233}}$$

$$= \frac{2.12 \times 10^{-2} \cdot 48.85}{11.9} = (8.7 \pm 0.3)\ \%$$

Neglecting the self-screening of the samples we obtain the following expression for the neutron absorption cross section of U^{233}:

$$\frac{\sigma_{cU}}{\sigma_{Li}} = \frac{\ln \frac{N_U(t)}{N_U(0)}}{\ln \frac{N_{Li}(t)}{N_{Li}(0)}} = 0.73$$

If we take account of self-shielding (see Appendix) we find:

$$\frac{\sigma_{cU}}{\sigma_{Li^6}} = 0.66 \pm 0.03$$

Taking $\sigma_{Li^6} = 930$ we find

$$\sigma_{cU} = 615 \pm 30 \text{ barn}$$

The work is being continued.

REFERENCE

1. Coryell and Sugarman, Fission Products, Book 2, Table V-2 (1951).

APPENDIX: DETERMINATION OF THE NEUTRON CROSS SECTIONS FROM THE "BURN-UP" DATA

In experiments on the determination of neutron cross sections from burn-up data it is usually necessary to work with relatively thick samples, in which self-shielding cannot be disregarded. The greatest accuracy is attained in those cases when a noticeable part of the nuclei that were present at the beginning decompose, i.e., when self-shielding cannot be considered constant during irradiation. We shall consider the case when the cross sections are calculated by comparing the amount of burn-up of the material being investigated with that of a reference substance.

Let us consider the case of a flat sample the thickness of which is many times less than its length and width. Let us assume that the cross sections of the investigated material and of the reference substance obey the $1/v$ law, so that

$$\sigma_\gamma = \frac{\sigma_1 v_1}{v} \qquad (1)$$

For a Maxwellian spectrum and an isotropic flux we find the number of neutrons crossing a unit area per second to be

$$\int_0^\infty dv v n_v \int_0^{\frac{\pi}{2}} d\theta \sin\theta\cos\theta \int_0^{2\pi} d\phi \qquad (2)$$

where n_v is given by the formula

$$n_v = n_0 \left(\frac{m}{2\pi kT}\right)^{3/2} v^2 e^{-\frac{mv^2}{2kT}} \qquad (3)$$

Here n_0, v, m, and T are density, velocity, mass, and temperature of the neutrons, respectively.

Let us introduce the mean square neutron velocity

$$v_0 = \sqrt{\frac{2kT}{m}} \qquad (4)$$

Integrating Equation 2, we find the flux falling on both sides of the plate equal to

$$\frac{n_0 v_0}{\sqrt{\pi}} \qquad (5)$$

It is easy to see that the number of neutrons crossing the plate is given by the expression

$$2\frac{2}{(\pi)^{3/2}} \pi n_0 \int_0^\infty dv \frac{v^3}{v_0^3} \int_0^{\frac{\pi}{2}} d\theta \sin\theta\cos\theta\, e^{-\left(\frac{v}{v_0}\right)^2} e^{-N\frac{\sigma_1 v_1}{v\cos\theta}} \qquad (6)$$

where N is the surface density of nuclei in the sample.

We introduce the following notation

$$u = \frac{v}{v_0} = v\sqrt{\frac{m}{2kT}} \qquad (7)$$

and

$$\alpha = N\frac{\sigma_1 v_1}{v_0} \qquad (8)$$

Comparing Equations 5 and 6 and using Equations 7 and 8, we find the number of absorbed neutrons equal to

$$\frac{n_0 v_0}{\sqrt{\pi}}\left[1 - J(\alpha)\right] \qquad (9)$$

where $J(\alpha)$ is given by the expression

$$J(\alpha) = 4\int_0^\infty du\, u^3 e^{-u^2} \int_0^1 dx x e^{-\frac{\alpha}{xu}} \qquad (10)$$

Since the number of absorbed neutrons is equal to the number of nuclei decomposed, we have

$$\frac{dN}{dt} = -\frac{n_0 v_0}{\sqrt{\pi}}\left[1 - J(\alpha)\right] \qquad (11)$$

and, using Equation 8 and integrating, we find

$$-\int_{\alpha(0)}^{\alpha(t)} \frac{d\alpha}{1 - J(\alpha)} = \frac{\sigma_1 n_0 v_1}{\sqrt{\pi}} t \qquad (12)$$

Equation 12 gives the exact solution of the problem, relating t and the duration of the irradiation.

In our case, where simultaneous irradiation of the material being investigated and of a reference substance is performed, Equation 12 holds for both. Writing Equation 12 for each of the substances I and II and noticing that with our assumptions $\sigma_I/\sigma_{II} = \sigma_{I,I}/\sigma_{I,II}$ does not depend on the neutron velocity v, we cancel $v_1 n_0 t/\sqrt{\pi}$ and find

$$\int_{\alpha_I(0)}^{\alpha_I(t)} \frac{d\alpha}{1 - J(\alpha)} = \frac{\sigma_I}{\sigma_{II}} \int_{\alpha_{II}(0)}^{\alpha_{II}(t)} \frac{d\alpha}{1 - J(\alpha)} \qquad (13)$$

For the most interesting case when self-absorption is not too large, it is more convenient to write Equation 13 in terms of a perturbation.

First consider the solution of the problem without self-absorption. In this case, of course,

$$\ln\frac{\alpha_I(t)}{\alpha_{II}(0)} = \frac{\sigma_I}{\sigma_{II}} \ln\frac{\alpha_{II}(t)}{\alpha_{II}(0)} \qquad (14)$$

In place of Equation 13 we write an identical equality

$$\ln\frac{\alpha_I(t)}{\alpha_I(0)} + \int_{\alpha_I(0)}^{\alpha_I(t)} d\alpha\left[\frac{\sqrt{\pi}}{1 - J(\alpha)} - \frac{1}{\alpha}\right] = \frac{\sigma_I}{\sigma_{II}} \ln\frac{\alpha_{II}(t)}{\alpha_{II}(0)} + \frac{\sigma_I}{\sigma_{II}} \int_{\alpha_{II}(0)}^{\alpha_{II}(t)} d\alpha\left[\frac{\sqrt{\pi}}{1 - J(\alpha)} - \frac{1}{\alpha}\right] \qquad (15)$$

Taking note of the fact that

$$4\int_0^\infty du\, u^3 e^{-u^2} \int_0^1 x dx = 1 \qquad (16)$$

and that

$$4\int_0^\infty du\, u^3 e^{-u^2} \int_0^1 x dx \left(\frac{\alpha}{xu}\right) = \alpha\sqrt{\pi} \qquad (17)$$

we can write Equation 15 in the form

$$\ln\frac{N_I(t)}{N_I(0)} - \frac{\sigma_I}{\sigma_{II}} \ln\frac{N_{II}(t)}{N_{II}(0)} = \frac{\sigma_I}{\sigma_{II}}\left\{K[\alpha_{II}(t)] - K[\alpha_{II}(0)]\right\} - K[\alpha_I(t)] + K[\alpha_I(0)] \qquad (18)$$

where

$$K(\alpha) = \int_{\alpha_1}^{\alpha} f(x) dx \qquad (19)$$

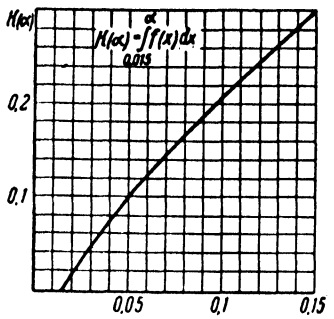

Figure 4. Graph of the function K(α)

$$f(\alpha) = \frac{\sqrt{\pi}}{1 - J(\alpha)} - \frac{1}{\alpha} = \frac{\frac{1}{\alpha}\int_0^\infty du\, u^3 e^{-u^2}\int_0^1 dx\, x\left\{e^{-\frac{\alpha}{xu}} - 1 - \frac{\alpha}{xu}\right\}}{\int_0^\infty du\, u^3 e^{-u^2}\int_0^1 dx\, x\,(1 - e^{-\frac{\alpha}{xu}})} \quad (20)$$

A graph of function K is given in Fig. 4, and the table below. Equation 18 is the exact solution of the problem.

CONCLUSIONS

The ratio of the cross sections of two simultaneously irradiated substances is determined by Equation 18, the function K being given by Equations 19 and 20, and being shown in Fig. 4. The values α entering into the formula are defined by Equation 8.

Function K (α)

α	K (α)	ΔK (α)
0.015	0	0.0169
0.020	0.0169	0.0153
0.025	0.0322	0.0146
0.030	0.0468	0.0135
0.035	0.0603	0.0132
0.040	0.0735	0.0128
0.045	0.0863	0.0122
0.050	0.0985	0.0120
0.055	0.1105	0.0115
0.060	0.1220	0.0115
0.065	0.1335	0.0110
0.070	0.1445	0.0110
0.075	0.1555	0.0107
0.080	0.1662	0.0106
0.085	0.1768	0.0102
0.090	0.1870	0.0103
0.095	0.1973	0.0100
0.100	0.2073	0.097
0.105	0.2170	0.095
0.110	0.2265	0.095
0.115	0.2360	0.093
0.120	0.2453	0.092
0.125	0.2545	0.090
0.130	0.2635	0.088
0.135	0.2723	0.087
0.140	0.281	0.085
0.145	0.2895	0.085
0.150	0.2980	

The problem should be solved by perturbation theory, considering the right-hand side small and substituting into it the solution found from the preceding approximation. The zero approximation is obtained if we set the right side equal to zero.

Slow Neutron Cross Sections of Fissile Nuclei

By J. M. Auclair,* M. Galula,† P. Hubert,* B. Jacrot,‡ R. Joly,* F. Netter,‡ and G. Vendryes,* France

The measurements described in this paper have the purpose of complementing our knowledge of certain heavy nuclei, which are very important in the study of nuclear reactors. These experiments have been made possible by the intense flux delivered by the Saclay reactor. The great variety of techniques used requires that the experiments be considered in three categories.

I. Study of the Variation of the Slow Neutron Cross Sections of Natural U, U^{233}, U^{235}, and Pu^{239} with Neutron Energy

EXPERIMENTAL TECHNIQUES

These measurements have been carried out with a time-of-flight spectrometer and a crystalline diffraction spectrometer set up at the outlet of two adjacent channels on the Saclay reactor. These channels, which were unobstructed all the way down to the tank, go into a region where the flux is approximately 2×10^{12} n/cm²/sec when the reactor operates at a power of 1000 kw.

The Time-of-Flight Spectrometer (F. Netter, M. Galula, B. Jacrot)

The measurements carried out with the time-of-flight spectrometer described elsewhere[1] consisted, in their essence, of a comparison of the spectral responses of two identical ionization chambers which contained a layer either of boron or of the fissionable material under consideration. The ratio between the counting rates of these chambers, corrected by a factor which allowed for self-absorption in the boron layer (a correction which is substantial only at very low energies) and for the thickness differences between the stainless steel sheets used as supports for the boron layer, is proportional to the product of the fission cross section by the mean velocity for the time-of-flight channel considered.

The resolving power always has been limited by the inadequacy of the counting rates. None of the measurements presented was carried out with the maximum resolving power of the equipment.

The base generally used is close to 7 meters. The resolution is represented: (*a*) at low energies (from 1.4×10^{-3} ev to approximately 10^{-1} ev) by a rectangle 28.5 μsec/m wide; (*b*) at medium energies—lower range—(from 10^{-1} ev) to some hundredths of ev) for U^{235} and Pu^{239} by a triangle, 5.7 μsec/m wide at half height; (*c*) at medium energies—upper range—(from 1 ev to 10^3 ev) for U^{233}, by a rectangle 8.5 μsec/m wide.

Crystal Spectrometer (J. M. Auclair, P. Hubert, R. Joly, G. Vendryes)

Let us go over the main features of the installation already described,[2] which is shown by Fig. 1 and the photograph in Fig. 2.

The steel collimator is 240 cm long, 8 cm high, and adjustable width from 0.15 to 2 cm. It is possible to set up anti-divergent slits by splitting the horizontal divergence of the beam into three.

Distance from crystal to detector is 250 cm.

Precision in the setting up of angles is ± 30 seconds of arc.

Crystals used are NaCl, transmission on plane [220]; LiF, reflection on plane [111] (supplied by the Conservatoire National des Arts et Métiers, Paris); and Be, transmission on planes [100] and [110] (supplied by Professor Kaufman, M.I.T., USA).

Detectors include BF_3 counter, for the transmission measurements, and multiple-layer fission chambers for measurements of the fission cross sections.

Study of the Variation in the Over-All Cross Section of Natural Uranium

This study was carried out with the help of a crystal spectrometer, by using an LiF monocrystal by reflection on plane [111], in order to reduce the number of neutrons which undergo a higher order Bragg reflection.

The curve obtained (Fig. 3) shows, at 0.29 and 1.2 ev, two small humps, the position and height of which agree with the fission resonances of U^{235}, such as was observed elsewhere.

Original language: French.

* Experimental Neutronics Division of the Commissariat à l'Energie Atomique.

† Centre National de la Recherche Scientifique and Nuclear Physics Division of the Commissariat à l'Energie Atomique.

‡ Nuclear Physics Division of the Commissariat à l'Energie Atomique.

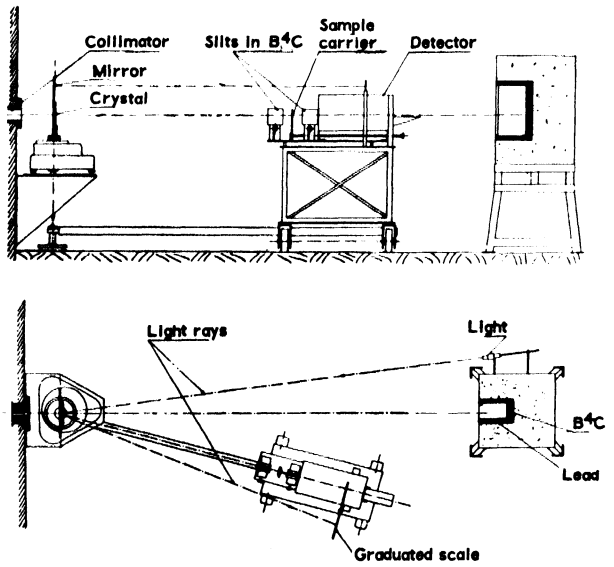

Figure 1. Crystal spectrometer

The general appearance of the curve was compared with that of a curve derived, by analysis, from the following assumptions:

1. The variation of the fission cross section of U^{235} is given by the measurements described below.
2. The σ_c/σ_f ratio of the capture cross section to the fission cross section of U^{235} remains constant when the neutron energy varies.
3. The capture cross section of U^{238} varies according to a $1/v$ law which is distorted to some extent, but in a calculable form, by the presence of the known resonances.
4. The diffusion cross section is constant.

It will be noted that, at the lower energies, the experimental curve shows slightly less increase than the computed curve. Since, on the other hand, the experimental points above 0.03 ev show a dispersion which can be accounted for by the crystalline structure of the sample, we believe that the difference between these two curves is due to effects pertaining to the crystal. We feel that it is not possible to lend very clear significance to the declassified value of 8.2 barns for the diffusion cross section applicable to 2200 m/sec neutrons. A comparison between the experimental and the computed curves seems to indicate that this cross section increases up to approximately 0.2 ev and reaches a constant value of 8.8 barns.

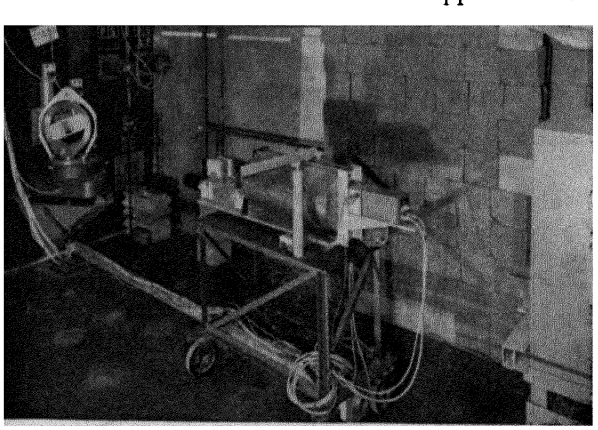

Figure 2. Crystal spectrometer

STUDY OF THE VARIATION OF THE FISSION CROSS SECTION OF U^{233}

The U^{233} used in this study was prepared at the Plutonium Division of the Commissariat à l'Energie Atomique, starting from irradiated thorium prepared in the Saclay reactor. A first source of 0.7 mg made it possible to carry out preliminary measurements in the thermal range, then, as larger quantities became available, the curve could be drawn with greater accuracy and prolonged. The work with a crystal spectrometer was carried out with a multi-layer chamber which contained approximately 25 mg of U^{233}, and the work with a time-of-flight spectrometer was carried out with a double chamber containing approximately 4 mg of the product.

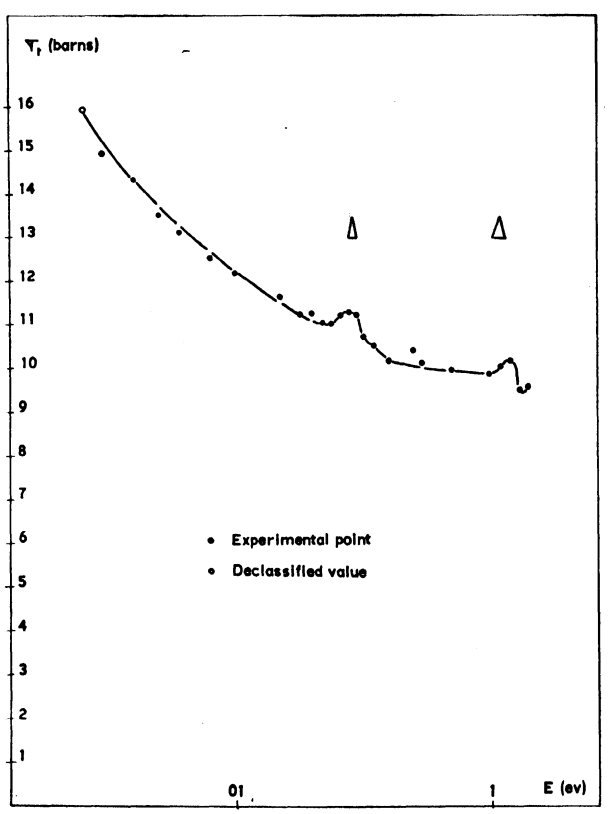

Figure 3. Total natural uranium cross section; crystal spectrometer

The results obtained were normalized for a value of 518×10^{-24} cm², for a speed of 2200 m/sec, which were measured independently (see further). They are shown on Fig. 4, on which the following features are to be noted:

The results obtained in the low energy range (Fig. 4*a*) are compatible with a $1/v$ law up to approximately 0.1 ev, without any possibility of ruling out the existence of a negative resonance, the con-

tribution of which to a possible variation of the product $\sigma_f v$ would not exceed 5 per cent.

In the region comprised between 0.2 and 6.0 ev, the measurements with a crystal spectrometer reveal several humps which may be ascribed to the presence, in the diffracted beam, of neutrons which have undergone Bragg reflections of the second or third order, the energy of which corresponds to resonances at 1.8 and 2.3 ev. We confirmed this viewpoint, by studying the effects of an absorbing cadmium screen on the beam of diffracted neutrons.

To obtain the curve in Fig. 4*b*, we use a more sensitive monitor (BF_3 counter) with the crystal spectrometer, but the efficiency of this counter as a function of energy is imperfectly known. Accordingly, the curve obtained must be viewed as provisional, but the position of the resonances observed is not markedly affected by this. Complementary measurements are under way.

The major peaks are located at 1.8 ± 0.02; 2.3 ± 0.02; 3.5; 5.1; 7 and 12 ev.

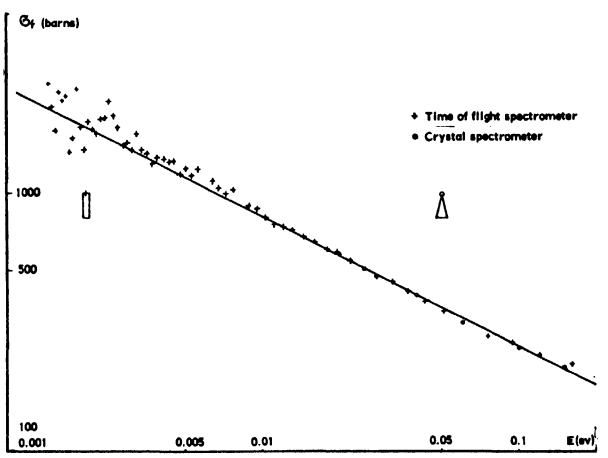

Figure 4a. Fission cross section for U^{238}

It is likely that some of these resonances are multiple, so that the asymmetrical aspect of the 7 ev peak is quite characteristic in this respect.

Above 10 ev, the separating power becomes very poor and the curve only shows a mean value (Fig. 4*c*).

STUDY OF THE VARIATION OF THE FISSION CROSS SECTION OF U^{235}

The measurements were carried out with a time-of-flight spectrometer, using an enriched uranium source, prepared with the electromagnetic separator of the Nuclear Physics Division of the Commissariat à l'Energie Atomique.[3]

The group using the crystal spectrometer began work with a multi-layer chamber which contained approximately 4 gm of natural uranium distributed over 166 layers. A marked improvement was achieved thereafter by using 80 mg of U^{235} enriched to 10% from another separator—the Amsterdam Philips.

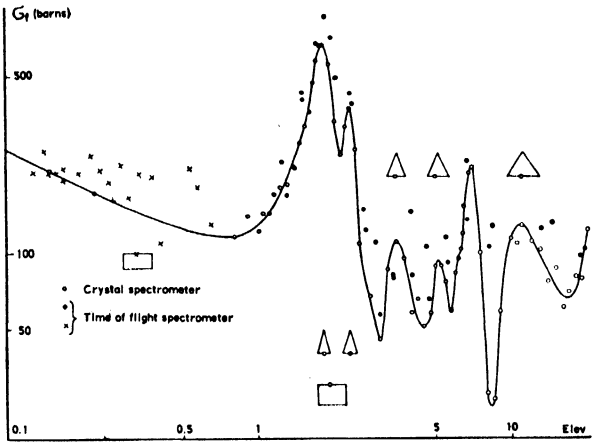

Figure 4b. Fission cross section for U^{238}

The results are shown in Figs. 8*a, b, d*. They reveal that there are several fission resonances. Curves are normalized to 580 barns for 2200 m/sec.

1. In the thermal region the cross section decreases faster than the reciprocal of the neutron speed. This suggests the existence of a resonance at a negative energy.

2. We found a series of resonances at the values: 0.29, 1.1, 3.4, 6.8, 9, and 14 ev.

However, the separating power used is not sufficient to support a claim that all the resonances present are resolved.

For the reason already mentioned in connection with the measurements made with a crystal spectrometer on U^{233}, the inadequate calibration of the monitor creates the same reservations.

STUDY OF THE VARIATION OF THE OVER-ALL CROSS SECTION Pu^{239}

The measurement was carried out by transmission on a plutonium oxide (PuO_2) sample containing approximately 0.5 gm of Pu^{239} and having a Pu^{240} content of less than 10^{-3}. The container used is shown on Fig. 6. It was specially designed to allow for the method of preparation of the source and the dangers inherent in plutonium.

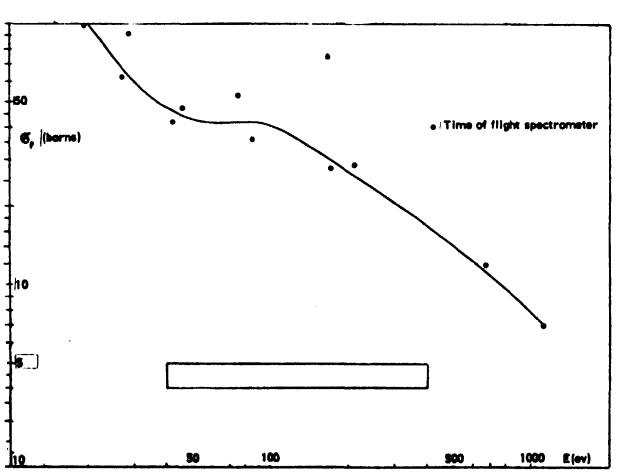

Figure 4c. Fission cross section of U^{238}

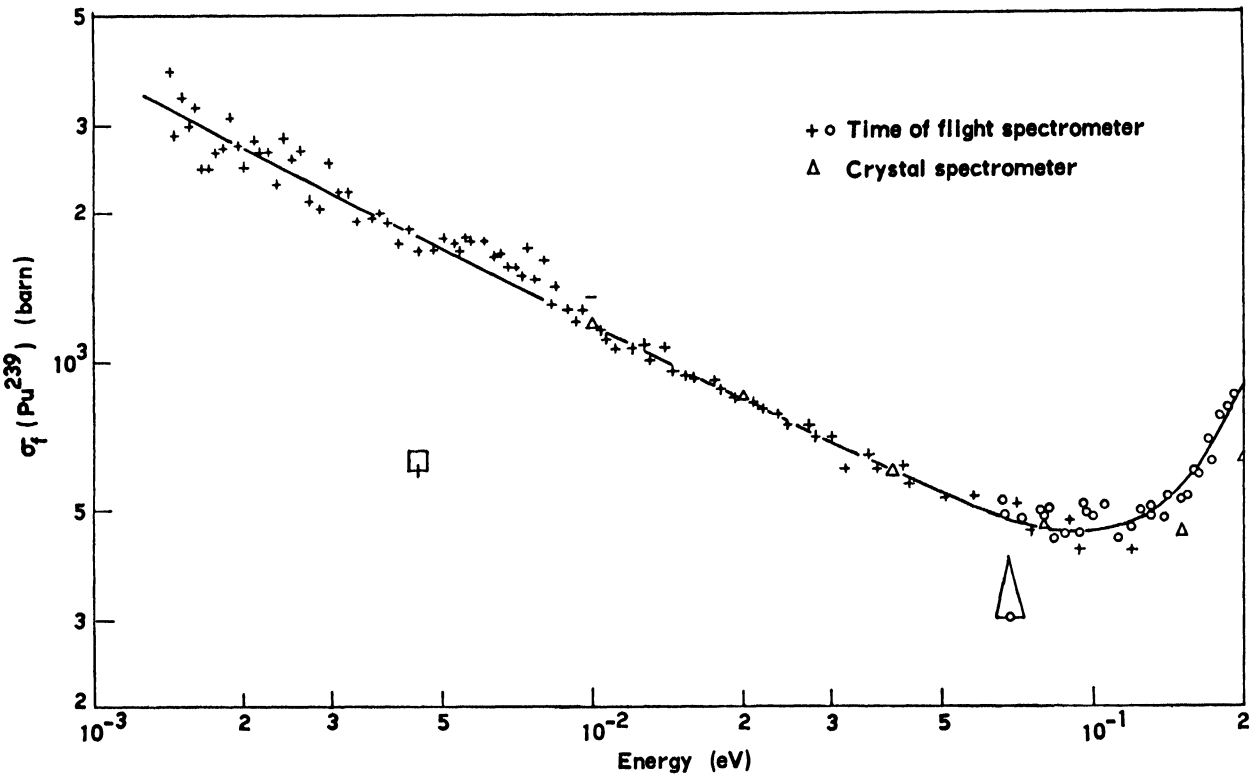

Figure 5a

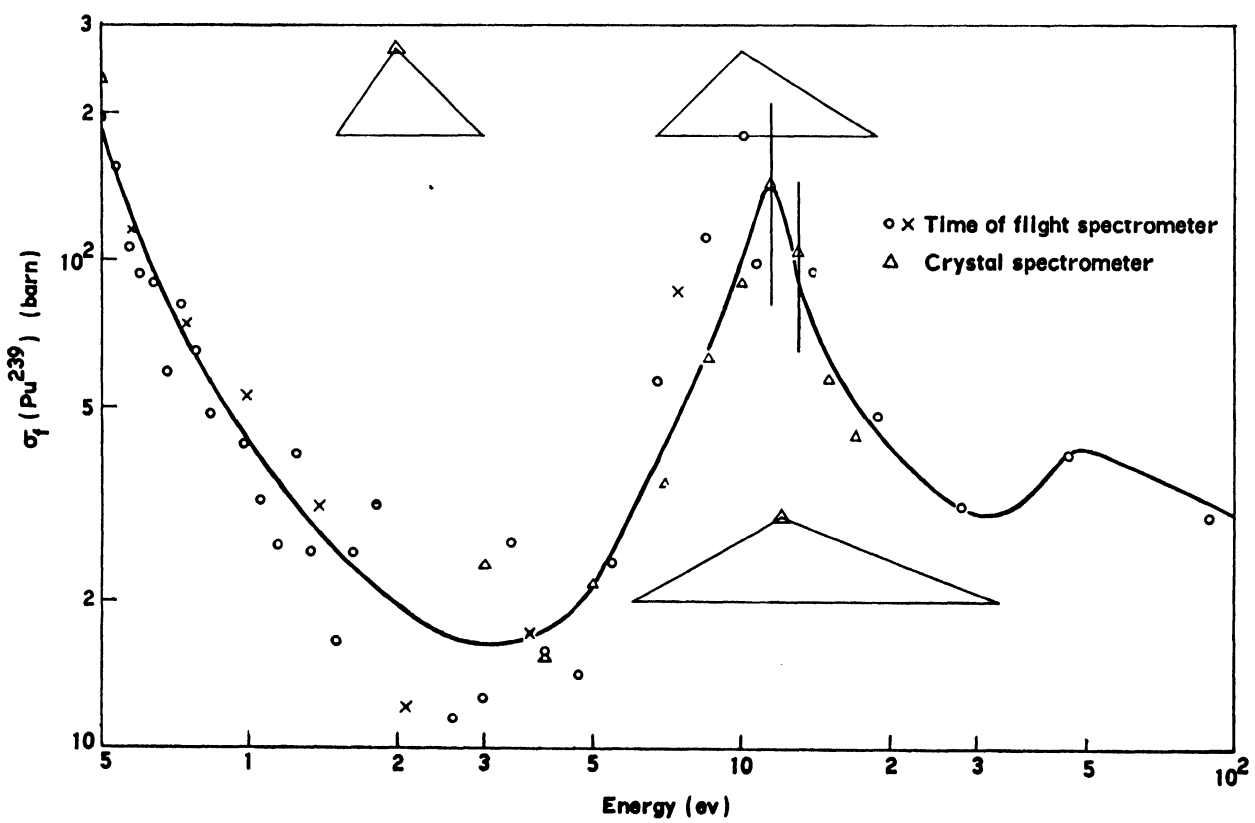

Figure 5b

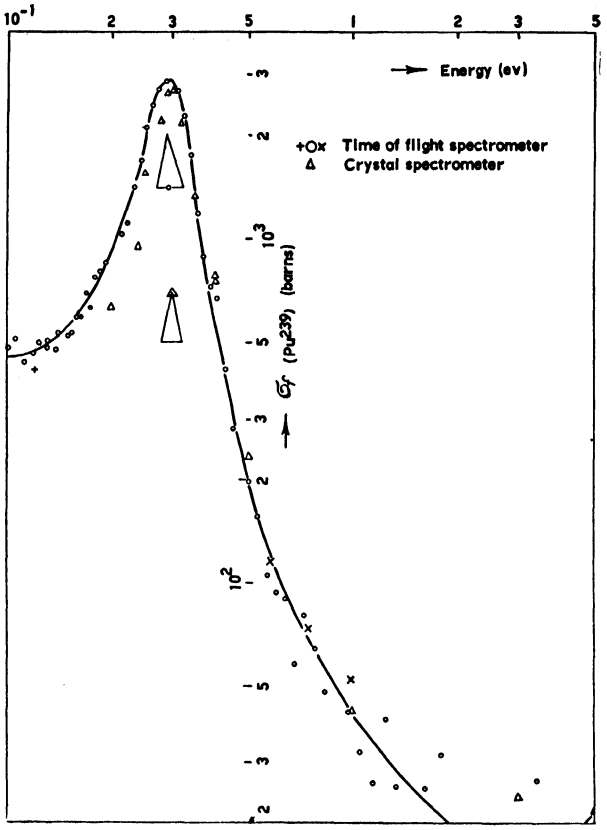

Figure 5c

We first used a container in which the sample used took the form of a compressed powder tablet 20 mm in diameter, so that transmission was adequate to make a study, in the thermal range, and up to approximately 0.5 ev. The plutonium was transferred to a container in which it offered an effective thickness approximately 2.2 times greater to the beam, making it possible to study the transmission at higher energies.

The samples were prepared at the Plutonium Division of the Commissariat à l'Energie Atomique by decantation and evaporation. Unfortunately, it has not as yet been possible to obtain very homogeneous thin screens, due to the parasitic phenomena which take place in the last phases of the evaporation (cracks, bubbles, etc.). An X-ray study of the layers revealed that the thick source was of adequate evenness, but this was not true in so far as the thin source was concerned, for which a part of the defects at least persists, after tamping down and tightening the piston.

As a consequence, in the range of large cross sections, namely from the low energies and up to approximately 0.4 ev, the rate of transmission observed might have been larger than the value it would have shown with a homogeneous screen. Accordingly, the curve obtained (Fig. 7), should be considered provisional, and serves only as an indication. We normalized it to the published value of 1065 barns for 2200 m/sec neutrons.

On the other hand, in the area of small cross sections, we were limited by the quantity of products available, which makes it necessary to close up the diaphragm and to work with a rate of transmission close to unit value.

The conclusions which now can be drawn from this study are the following:

Generally speaking, the curve which represents the variation of the over-all cross section σ_t has the same appearance as the curve which shows the fission cross section σ_f. It can be stated that the departure of the ratio σ_f/σ_t from its value for 0.025 ev remains lower than $\pm$ 20% in the realm of the energies lower than 0.5 ev. Beyond that, the measurements are too inaccurate for an indication to be given.

The separating power used, being better than during the measurement of σ_f, it became possible to reveal, among the group of resonances around 10 ev, three distinct lines located respectively at: 8, 11.5, and 15 ev.

STUDY OF THE VARIATION OF THE FISSION CROSS SECTION FOR Pu^{239}

The layers used were prepared by electrolysis and covered with a very thin film of a plastic material. Their Pu^{240} content was less than 10^{-3}. Each layer had a mass in the vicinity of 2.5 mg, over a surface of approximately 10 cm^2.

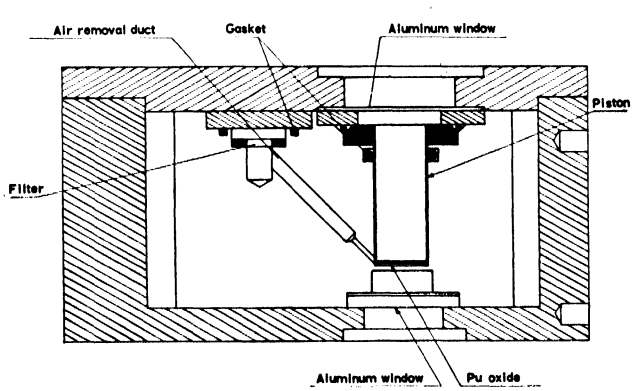

Figure 6. Container used to measure plutonium transmission

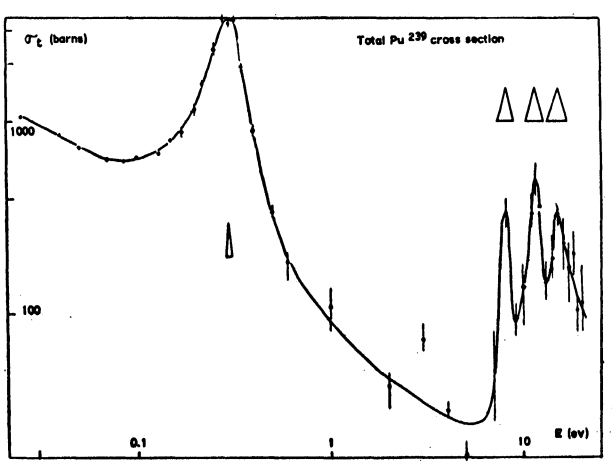

Figure 7. Total Pu^{239} cross section

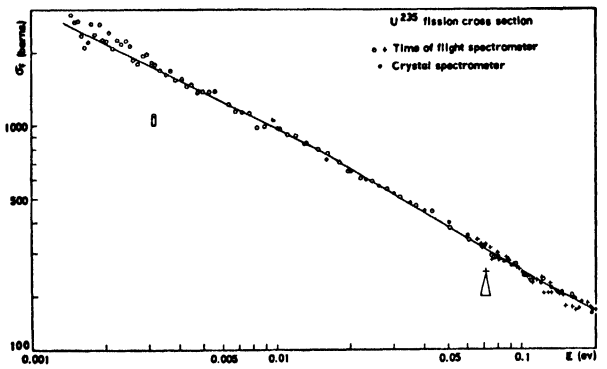

Figure 8a. U^{235} fission cross section

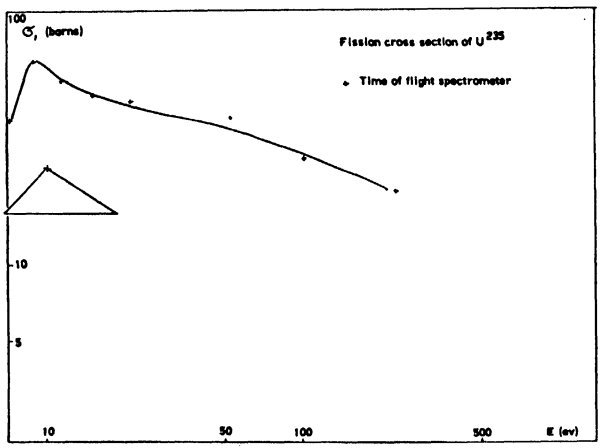

Figure 8b. Fission cross section of U^{235}

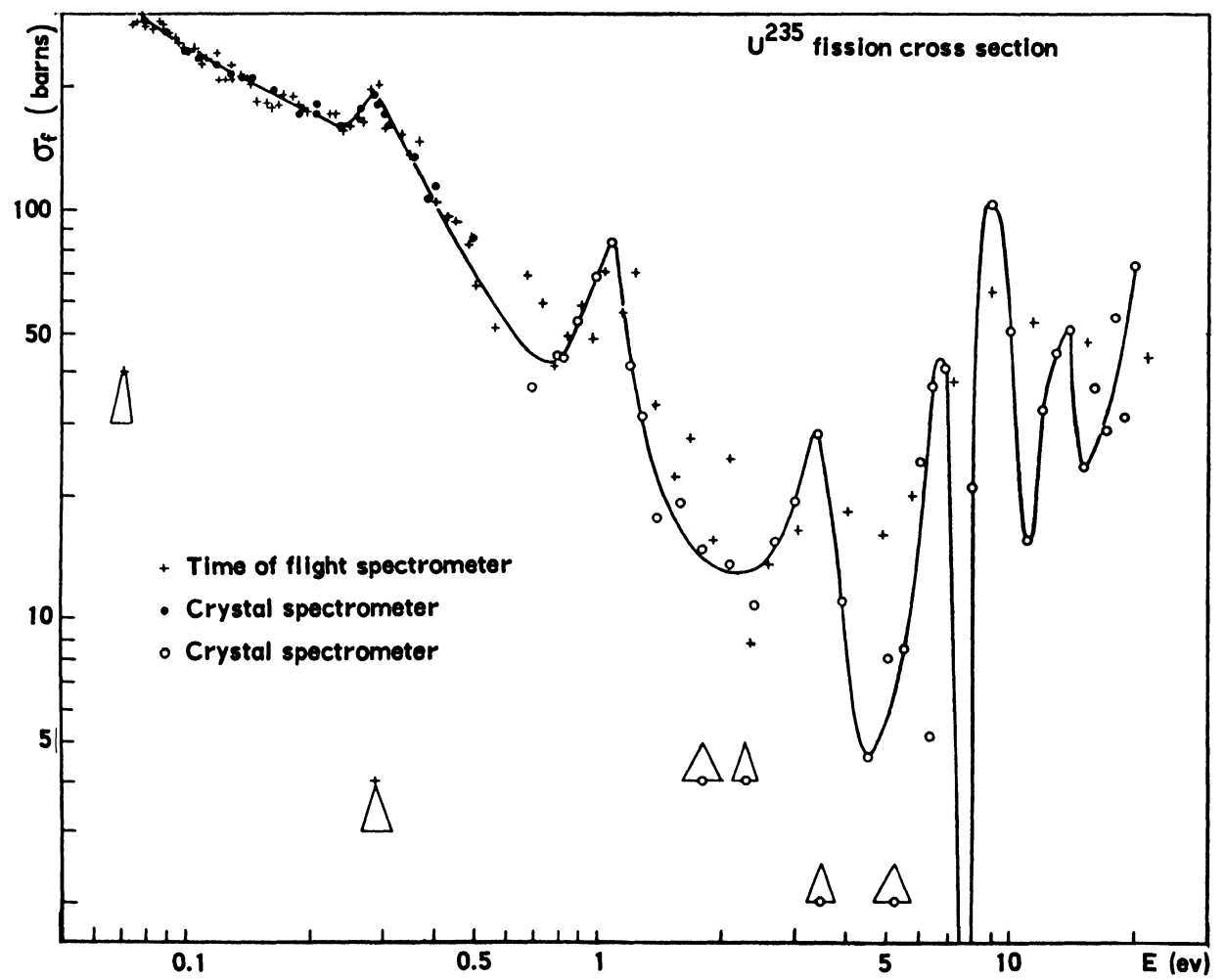

Figure 8c. Fission cross section of U^{235}

With the time-of-flight spectrometer, only one layer was used, while, for the measurements carried out with the crystal spectrometer, a 4-layer chamber was used.

For fission counting, we used, in both cases, the two megacycle amplifiers of the Commissariat à l'Energie Atomique operating with their minimum time constant (actually 3×10^{-7} sec), in order more readily to separate α accumulations.

The curves of Figs. 5*a*, *b*, *c* show the variation from 1.4×10^{-3} ev to 100 ev of the fission cross section of Pu^{239} as a function of neutron energy,

normalized to a value of 750 barns for a velocity of 2200 m/sec.

Thermal Range

The main feature of the results is the existence of a very marked resonance at a neutron energy $E_0 = 0.297 \pm 0.003$ ev.

The experimental width at the half-height of the resonance peak, measured with the time-of-flight spectrometer is $\Gamma = 0.10 \pm 0.01$ ev.

The curve obtained with the crystal spectrometer has a somewhat different form, which indicates, for the resonance, a width of 0.09 ± 0.01 ev.

This disagreement may not be accounted for by the effect of the separating power since, in both cases, the width of the resolution triangle at half-height is 0.025 ev, which corresponds to a negligible widening, and to a reduction of some 2% of the peak ordinate.

The Doppler effect is shown by a width of 0.011 ev, namely a correction which is negligible for the ordinate of the peak.

Allowing for the experimental value of the ordinate of the peak, the corrections indicated, and the statistical accuracy, the cross section at resonance is $\sigma_0 = 3000 \pm 150$ barns.

If it be desired to account for the curve by a Breit-Wigner one-level formula, it is necessary first to subtract the terms relative to the other resonances observed.

The contribution of the higher order resonances is a small term, for the large resonances found around 10 ev and above. This term is limited upwards by the value of the cross section at 1 ev.

On the other hand, the shape of the curve suggests the existence of a substantial negative resonance very close to the origin (likely $0 > E_0 > -0.5$ ev).

However, regardless of the parameters chosen for this negative resonance, the parameters tried out for the main resonance within the limits of the experimental data, and allowing for various corrections (for instance the energetic asymmetry of the resolution formula), there remains an irreducible discrepancy, with respect to a Breit-Wigner formula, in the area of the wings of the peak; in particular, the value of the cross section around 0.2 ev is too small when compared to that around 0.4 ev.

The measurements undertaken in order to find whether there was a very fine doublet at the 0.3 ev resonance were carried out with the time-of-flight spectrometer with a resolution represented by a rectangle having a width of some 10^{-2} ev, justifying the rejection of the hypothesis of a doublet to account for the shape of the curve.

Epithermal Range

Above a broad region in which the cross section is low, there is a peak at approximately 11.5 ev, which is the beginning of a wide zone of resonance, which is extensive and corresponds to the peak observed in the measurements of the over-all cross section.

The measurements on plutonium and U^{233} were made possible by the work carried out at the Plutonium Division under the direction of Regnaut.

The separation and purification of U^{233} were carried out by Chesné. The plutonium layers and the PuO_2 screen used for the transmission experiments were designed and prepared by Pinset, Prévot and Le Berquier.

II. Comparison of the Fission Cross Sections of U^{233} and Pu^{239} for Thermal Neutrons

(J. M. Auclair, P. Hubert, R. Joly)

PRINCIPLE OF THE MEASUREMENTS

The measurements consisted of a comparison of several U^{233} and Pu^{239} sources in a double fission chamber through which a neutron beam from the Saclay reactor was passed. The quantity of matter contained in each of these sources was thereafter measured by counting α-activity in a counter using a well-defined solid angle.

MEASUREMENTS OF THE FISSION RATE

The chamber used makes it possible simultaneously to count the fissions produced in two layers of the same dimensions, placed back-to-back. These layers, which have been prepared electrolytically at the Plutonium Division of the Commissariat à l'Energie Atomique have a superficial density of less than 25 $\mu g/cm^2$. The measurements were carried out by passing as uniform a neutron beam as possible through the chamber.

The pulses are amplified and counted by means of the standard electronic equipment of the Commissariat à l'Energie Atomique (2-megacycle amplifiers). We have observed that the discrimination plateau was excellent, making it possible to count the fissions with an efficiency of better than 0.995. Neutron absorption by the carriers is eliminated by turning the chamber around.

The proportion of fissions brought about by the non-thermal neutrons is measured by placing a cadmium leaf ahead of the chamber.

A correction was made in order to allow for the presence of 45 per cent of natural uranium in U^{233}.

MEASUREMENTS OF α-ACTIVITY

We used a proportional counter with a well-defined solid angle, which had the advantage of minimizing the effects due to back scattering and absorption, since only the particles which come out nearly normal to the plane of the source are let in the counting volume. In so far as the values admitted for these effects in the case of counting in a 2π

geometry with a somewhat greater source thickness[4] we felt that they were negligible.

The ratio of the disintegration half-lives α was taken to be equal to:

$$\frac{T_{Pu^{239}}}{T_{U^{238}}} = 0.150 \pm 0.001 \qquad (5)$$

We computed, from the times of irradiation used, that the measurements were not falsified by the presence of α-emitters U^{234}, Pu^{238} and Pu^{240} formed in the reactor by a secondary reaction. This result was verified, to the extent that it was possible to do so, by α-spectrometry.[6]

RESULTS

We used a total of two sources of U^{233} and four of Pu^{239}, which gave us eight different values of the ratio $\sigma_f U^{233}/\sigma_f Pu^{239}$ in a Maxwellian distribution. These values are shown in the following table:

Pu^{239} / U^{233}	*A*	*B*	*C*	*D*
1	0.632	0.655	0.629	0.627
2	0.623	0.657	0.625	0.623

It will be noted that the results are in agreement within the limit of the computed accuracy, with the exception of those in which the plutonium-*B* source comes into play.

The only possible explanation for this difference consists in assuming that plutonium penetrates into possible surface defects of the support. This would affect more the counting of the fission products which takes place in a 2π geometry, which agrees with the sign of the difference observed.

In so far as the aberrant source is very inhomogeneous, it appears justified to set it aside and to accept the mean value ($\sigma_f U^{233}/\sigma_f Pu^{239}$) for a Maxwellian spectrum = 0.626 ($\pm$ 1 per cent).

Knowing the value (σ_f Pu) 2200 m/sec = 750 $\pm$ 15 barns, the form of the neutron spectrum used[7] and the law of variation of the fission cross sections of U^{233} and Pu^{239} with neutron energy (see Part I), we can derive:

($\sigma_f U^{233}$) Maxwellian spectrum = 459 $\pm$ 14 barns

($\sigma_f U^{233}$) 2200 m/sec = 518 $\pm$ 16 barns

III. Measurement of the Mean Capture Cross Section of U^{236} for the Neutron Spectrum of a Reactor (J. M. Auclair, P. Hubert, R. Joly)

PRINCIPLE OF THE MEASUREMENTS

The absolute measurement of the β-activity of U^{237} formed by the reaction $U^{236}(n,\gamma)U^{237}$ in a sample of U^{236} irradiated in the Saclay reactor makes it possible to determine the capture cross section of U^{236} for a spectrum of reactor neutrons. The experiment was carried out in two stages:

First, U^{236} was accumulated in a sample of U^{235} enriched uranium, by lengthy irradiation at the center of the Saclay reactor. The measurement of the integrated flux to which the sample was subjected and the knowledge of the radiative capture cross section of U^{235} make it possible to compute the amount of U^{236} formed.

Second, following some decay of the U^{237} formed at equilibrium in the first part of the experiment, the sample mentioned before was irradiated at the center of the Saclay reactor for one week, and the total integrated flux received during this irradiation was measured. Then, after a separation of the fission products and Np^{239}, the amount of U^{237} formed during this second irradiation was determined by an absolute measurement of the β-activity with a 4π counter. This measurement was carried out with a source prepared from the irradiated sample which contained a known uranium quantity by counting the α-activity with a 4π counter operating as a proportional system. From these measurements, the average value of the cross sections for the $U^{236}(n,\gamma)U^{237}$ reaction for the neutron spectrum at the center of the Saclay reactor finally was derived.

A certain number of corrections are in order.

U^{237} is also produced by the $U^{238}(n,2n)U^{237}$ reaction. In order to allow for this, we also irradiated, during the second part of the experiment, a sample of U^{235}-depleted uranium. After separation of the fission products and of the neptunium, the absolute measurement of the β-activity of U^{237}, carried out as indicated before, makes it possible to evaluate the extent of the $(n,2n)$ reaction.

The separation of the fission products cannot be quantitative: it is necessary, therefore, to follow the decay of the U^{237} sources prepared from U^{235} enriched and depleted samples in order to allow for the residual fission products and, if need be, Np^{239}.

RESULTS

The total integrated fluxes to which the samples have been subjected during the two parts of the experiment were measured with the help of cobalt standards, the absolute activities of which were determined by the γ-γ coincidence method. For the activation cross section of Co^{59}, we took a value of 34.8 $\pm$ 2.0 barns at 2200 m/sec, with a $1/v$ variation law of this cross section and, for the half-life of Co^{60}, a value of 5.2 $\pm$ 0.1 years.

Where it came to computing the amount of U^{236} formed in the first part of the experiment, we took a value of 107 $\pm$ 5 barns for the absorption cross section of U^{235}, and, there again, computations were carried out assuming a $1/v$ variation of this cross section.

The corrections due to the fission products did not exceed 3%, none being needed for Np^{239}.

Our measurements give the following values:

(*a*) Ratio of $U^{238}(n,2n)U^{237}$ reactions to the $U^{238}(n,\gamma)U^{239}$ reaction in the neutron flux of the Saclay reactor: $3.1 \pm 0.8 \times 10^{-4}$.

(*b*) Average radiative capture cross section of U^{236} in the flux of the Saclay reactor: 24 ± 7 barns.

ACKNOWLEDGEMENT

We wish to thank Mme. Leresaux, of the Plutonium Division, who carried out the separation of Np and of the fission products of the uranium samples irradiated at a rate which made our measurements possible, as well as Messrs. Thommeret and Engelman, of the Measurements Division, who took charge of making the measurements on the cobalt sources used for the calibration of the fluxes.

Appendix: Measurement of the Fission Cross Section of U^{235} for 25 kev Neutrons (J. M. Auclair, P. Hubert, R. Joly)

The cross sections of U^{235} (fission) and of Au^{197} (activation) have been compared for 0.025 ev thermal neutrons from the Saclay reactor and 25 kev neutrons from an antimony-beryllium source. From this, the deduction can be made that the fission cross section of U^{235} for 25 kev neutrons is 5.4 ± 1 barns.

PRINCIPLE OF THE MEASUREMENTS

We compared, for thermal neutrons and for neutrons from an antimony-beryllium source:

1. The activity of the fission products emitted by a layer of natural uranium having a superficial density of 10 mg/cm², gathered on aluminum sheets 0.01 mm thick.

2. The activity induced by the neutrons in a gold leaf 0.01 mm thick.

OPERATING PROCEDURE

The uranium layer was prepared by painting it on the two sides of an aluminum sheet 0.1 mm thick, with dimensions of 50 mm × 100 mm. This layer was covered, by evaporation under vacuum, with a layer of 100 μg/cm² of aluminum, in order to avoid contamination of the aluminum sheets used for collecting the fission products.

The two sheets of aluminum used for this purpose also were 50 mm × 100 mm. They were placed in contact with the sheet which carried the uranium. For a measurement of their apparent activity, they were folded into 4 and piled up in the source carrier of a 4π type counter.

The uranium layer used was the same in both instances, so that it can be assumed that the efficiency of collection of the fission products does not vary. On the other hand, this method makes use of the whole of the fission products and minimizes the influence of a variation in the yield curve with the energy.

We simultaneously irradiated:

1. Two aluminum sheets identical to those used for the collection. They enabled us to arrive at the activity induced by the neutrons in aluminum and its impurities. This activity was very small (about 1% of the activity due to the fission products).

2. A gold leaf, the activity of which, as measured in a calibrated geometry, served as a reference.

The antimony-beryllium source (25 kev neutrons) is practically identical to that used by Hummel and Hammermersch.[1] The mean flux emitted by the source was, at the moment of the measurement, some 3.5×10^4 n/cm²/sec. In order to reduce the reflections and slowing down of neutrons by the adjacent materials, the source was suspended at the end of a wire, 6 meters from the ground.

The source of thermal neutrons was made up by the thermal column of the Saclay reactor. The flux, at the point where we used it, was of some 8.10^5 neutrons/cm²/sec.

All irradiations were carried out for 24 hours. The apparent activity of the fission products was measured under well defined conditions of time and chronology, between the first and fourth hour following the end of the irradiation.

RESULTS

The measurements were made difficult by the low counting rate of the fission products at 25 kev; it was some 10 counts per minute for a background of 40. For the thermal neutrons, this counting rate was some 20,000. The gold leaves had, in each of the two cases, a total apparent activity of some 300 counts per minute and 4×10^5 counts per minute.

The ratios of the counting rate of the fission products and the gold leaf were $(3.07 \pm 0.3) \times 10^{-2}$ and $(5.00 \pm 0.2) \times 10^{-2}$ respectively for irradiations at 25 kev and 0.025 ev.

If we take:

$$\sigma_f U^{235} \text{ at } 0.025 \text{ ev} = 580 \pm 8 \text{ barns}^9$$

$$\sigma_c Au^{197} \text{ at } 0.025 \text{ ev} = 98.7 \pm 0.6^{10}$$

we can derive from this that the ratio $\sigma_f U^{235}/\sigma_c Au^{197}$ at 25 kev, is 3.60 ± 0.4.

On the other hand, if we take the value published by Hummel and Hammermersch[8] for the capture cross section of gold for 25 kev neutrons namely 1.5 barns ± 15%, we can derive from this that

$$\sigma_f U^{235} \text{ at } 25 \text{ kev} = 5.4 \pm 1 \text{ barns.}$$

REFERENCES

1. Galula, M., Jacrot, B. and Netter, F., *Le spectromètre de vitesse à temps de vol pour neutrons lents du Centre*

d'Etudes Nucléaires de Saclay, J. Phys. Radium, *15,* 59-60S (1954).

2. Auclair, J. M., Hubert, P. and Vendryes, G., ***Etude des sections efficaces de fission de*** U^{233}, U^{235}, Pu^{239} ***pour les neutrons lents.*** J. of Nuclear Energy (1955) (sous presse).
3. Bernas, R., *Séparateur électromagnétique d'isotopes pour éléments légers et moyens,* J. Phys. Radium, *14,* 34 (1953).
4. Cotton, E., Lévêque, A. and Cohen, R., *Le problème de la numération des particules a en géométrie 50 pour 100,* J. Phys. Radium, *15,* 109 (1954).
5. Hollander, J. M., Perlman, L. and Seaborg, G. T., *Table of isotopes,* Revs. Mod. Phys., *25,* 469 (1953).
6. Measurements carried out at Saclay by M. Valladas.
7. Galula, M., Jacrot, B. and Netter, F., *Spectre des neutrons de la pile de Saclay,* J. Phys. Radium, *16,* 232 (1955).
8. Hummel, V. and Hammermersch, B., Phys. Rev. *67,* 82-1 (1951).
9. AECU 2040, 3rd supplement.
10. Carter, R. S., Palevsky, H., Myers, V. W. and Hughes, D. J., Phys. Rev. *716,* 92-3 (1953).

Energy Dependence of U^{233}, U^{235}, Pu^{239} Fast Neutron Cross Sections

By D. Szteinsznaider, V. Naggiar, and F. Netter,* France

SUMMARY

These measurements were carried out taking the value of the fission cross section of U^{238} as a reference. The neutrons were produced by the $Li^7(p,n)$ reaction in the Van de Graaff generator used at Saclay. The range studied extended from some tens of kev to 2000 kev. We found:

For Pu^{239}, $\sigma_f = 2.04 \pm 0.12$ barns; the cross section remains constant from 150 to 2000 kev.

For U^{235}, $\sigma_f = 1.15 \pm 0.15$ barns; the cross section remains constant from 700 to 1000 kev.

For U^{233}, $\sigma_f = 1.92 \pm 0.25$ barns, for 850 kev neutrons.

Principle of the Measurement

The fissionable material target, placed in an ionization chamber, is subjected to a flux of monokinetic neutrons. The number of fissions counted is given by:

$$F = a\, n\sigma\phi \qquad (1)$$

where a is the over-all efficiency of the fission chamber and electronic device, n is the number of nuclei per square centimeter of the fissionable substance, σ is the fission cross section, and ϕ is the neutron flux received by the target, assumed to be thin.

No direct determination of the absolute values of the fission cross sections was made. In order to obtain these figures, we compared (between 1500 and 2000 kev) the fission cross section of Pu^{239} with that of natural uranium, the value of which has been published.[1] The variation of the fission cross section of Pu^{239} as a function of energy, between 50 and 2000 kev, is taken by using (as a monitor) a long counter[2] the efficiency variation of which, at the low energies, has been measured with a recoil proton counter (see appendix). The variations of the cross sections with the energy of U^{235} and U^{233} are determined by direct comparison with Pu^{239} in the same neutron flux.

Experimental Set-up and Conditions

Calibration of the Van de Graaff accelerator is carried out by taking the threshold of $Li^7(p,n)$ at 1.882 Mev and the threshold of $C^{13}(p,n)$ at 3.236 Mev. The measurement of the magnetic field which determines the proton energy is carried out by a nuclear magnetic resonance method. The dispersion of the protons in energy is of some 0.5 per cent for a current of about 8 microamperes.

The lithium layer deposited by thermal evaporation on a tantalum carrier 0.3 mm thick makes up the bottom of a brass tube 30 mm in diameter, 20 cm long and 1 mm thick, having a wall thinned down to 0.5 mm on the target side. The electrical charges accumulated in the cylinder are measured by means of an integrator.

The 2 mg plutonium target contains approximately 1% of impurities, made up of uranium. The U^{235} enriched 20 mg uranium target is obtained by means of the isotope separator. The isotopic analysis indicates mass 238/mass 235 $= 6.72 \pm 0.10$.

The 0.7 mg U^{233} target contains approximately 50% natural U. We also used a 20 mg natural uranium target.

In the first series of measurements, each target was placed in an ionization chamber identical to two parallel plates one centimeter apart. In a second series of measurements, we used double chambers, with the same distance between the electrodes. The chambers are filled under two atmospheres of argon, which contains CO_2 under 2 cm Hg. In order to reduce the number of localized accumulations of the alpha-particles emitted by the plutonium, the amplifier uses a passing band of 3×10^{-7} sec, and the ionization chambers are so designed as to give a rapid increase in the pulses due to electronic accumulation, favored by an addition of CO_2, (on the other hand this gas contributes to decrease the drift of the chambers). The discriminating threshold is so adjusted as not to count alpha-particle accumulations. Reference is made to the alpha-counts and to the indications of a pulse generator, in order to control the chamber (very small) and electronic drifts. Figure 1 shows the geometry used in each series of measurements.

We used a relatively thick lithium layer (200 micrograms/cm^2) in order to obtain high counting rates, at the expense of energy resolution. In view of the thickness of the deposit, of the energy dispersion of the protons from the Van de Graaff accelerator, and of the opening of the neutron cone, the energy dispersion of the neutrons was $\pm$ 60 kev for 1600 kev, and $\pm$ 20 kev for 50 kev.

For neutrons with energies greater than 500 kev, we corrected the fission count due to the existence

Original language: French.

* Nuclear Physics Department of C.E.A.

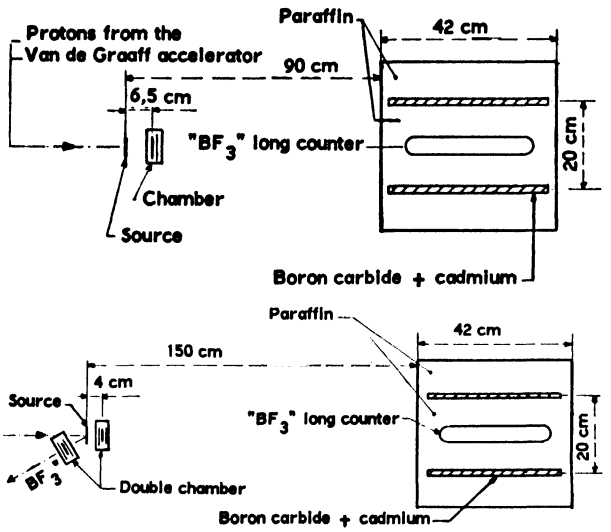

Figure 1.

of a group of neutrons corresponding to the excited condition of Be^{7}* at 435 kev.[3]

By varying the distance d, from the source of neutrons to the fissionable target, we noted that the variation in the fission count does not follow a $1/d^2$ law, namely that the fissionable target is not bombarded exclusively by neutrons coming directly from the source. In order again to find the experimental variation, it can be assumed that the fissionable target receives, in addition a certain number of scattered neutrons, which is constant with distance. It is thus computed that, at the distance for which the measurements of the first series were carried out, 9% of the fissions are due to scattered neutrons; in the second series, the use of a double chamber made it possible to get closer to the target, and under those conditions, the proportion was reduced to 5% (0 degrees). It was noted that, by surrounding the chamber with a cadmium sheet, the variation in the counted number of fissions was smaller than the statistical errors (2%).

RESULTS

Determination of the Fission Cross Section of Pu^{239} Referred to That of Natural Uranium

In order to place ourselves in such a position as to take the published fission cross section of natural uranium[1] as a reference, we determined the variation of the fission counts of a natural uranium target as a function of neutron energy between 800 and 2000 kev. using a "long counter" as a monitor. Our experimental curve (Fig. 2*a*, solid line) indicates the same variation as the published curve (Fig. 2*a*, dotted line) with an inflection point at the same energy. Between 1600 and 1800 kev, the two curves overlap with a precision greater than the statistical counting errors (1%).

The number of counted fissions F_{nat}, as standardized to the same number of neutrons, as detected with a "long counter," is proportional to the fission cross section if the efficiencies of the ionization chamber and "long counter" are independent of the energy. This hypothesis is justified, since the energy spectrum of the fission fragments[4] and their angular distribution[5] do not vary markedly as a function of the energy, from the thermal region up to 14 Mev. On the other hand, various workers[6] found that the efficiency of the "long counter" is constant within this energy range.

The comparison of the fissions of natural uranium and Pu^{239} targets, when placed in a double chamber gives, from Equation 1:

$$\frac{F_{Pu}}{F_{nat}} = \frac{(an)_{Pu}}{(an)_{nat}} \times \frac{\sigma_{Pu}}{\sigma_{nat}} \qquad (2)$$

The ratio of the effective numbers (an) is given by an experiment with thermal neutrons on the Saclay reactor, following measurement[7] of the ratio:

$$(\overline{\sigma_{Pu}}/\overline{\sigma_{nat}})_{therm} = 205.7 \pm 4$$

Taking, for the fission cross section of natural uranium, at 1600 kev, a value of 0.34 barns,[1] we find:

$$(\sigma_{Pu})_{1600\ kev} = 2.04 \pm 0.12 \text{ barns}$$

When computing the error, we allow for the errors in the ratio of the fission cross sections for thermal neutrons (2%), the statistical counting errors (2%), and those due to fissions caused by scattered neutrons.

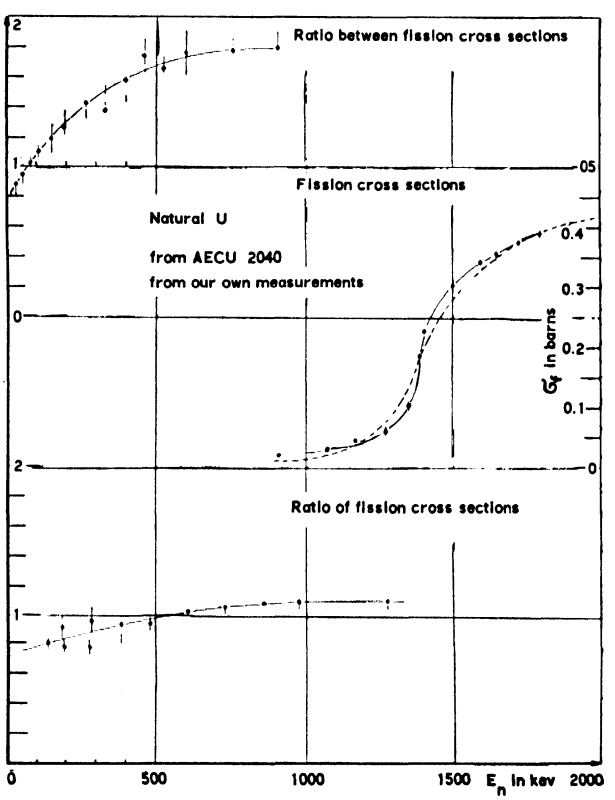

Figure 2. (a) center, Fission cross sections; (b) top, ratio between fission cross sections, Pu^{239}/U^{235}; and (c) bottom, ratio of fission cross sections, Pu^{239}/U^{238}

Variation of the Fission Cross Section of Pu^{239} as a Function of Neutron Energy

The variation of the fission cross section of Pu^{239} as a function of fast neutron energy (Fig. 3*a*) has been studied by using the "long counter" as a monitor. However, its efficiency no longer was constant at the low energies. We compared it, between 80 and 200 kev, to a recoil proton counter (see appendix). For the point located at 50 kev, the efficiency of the "long counter" was extrapolated. For energies above 200 kev, we assumed, in the tracing of the fission curve, that the efficiency of the "long counter" was constant. This hypothesis must be supported by appropriate experiments.

From this curve, it will be seen that the fission cross section of Pu^{239} was constant between 150 and 2000 kev, and it is interesting to use it as a reference material.

Computation of σ_{Pu}/σ_{U_5} and σ_{Pu}/σ_{U_3} Ratio

One uses, in a double chamber, either a Pu^{239} target or one of U^{235} enriched uranium, or again a Pu^{239} target and a U^{233} target. The ratio of the fission cross sections is given, as in Equation 2, by the ratio of the fission counts. The ratio of the effective numbers (an) is determined with thermal neutrons by taking

$$(\overline{\sigma_{Pu}}/\overline{\sigma_{U_5}})_{therm} = 1.47 \pm 0.3 \qquad (7)$$

and

$$(\overline{\sigma_{U_8}}/\overline{\sigma_{Pu}})_{therm} = 0.627 \pm 0.006 \qquad (8)$$

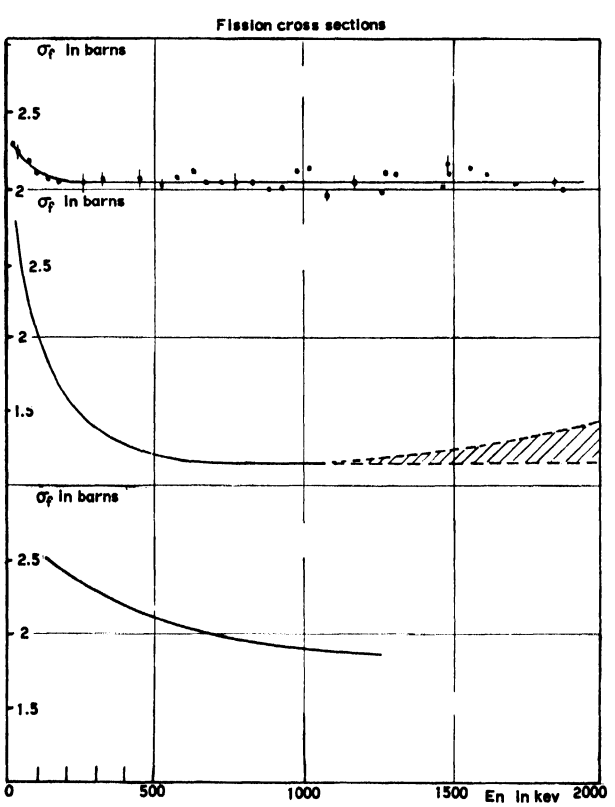

Figure 3. Fission cross sections; (a) top, Pu^{239}; (b) center, U^{235}; and (c) bottom, U^{233}

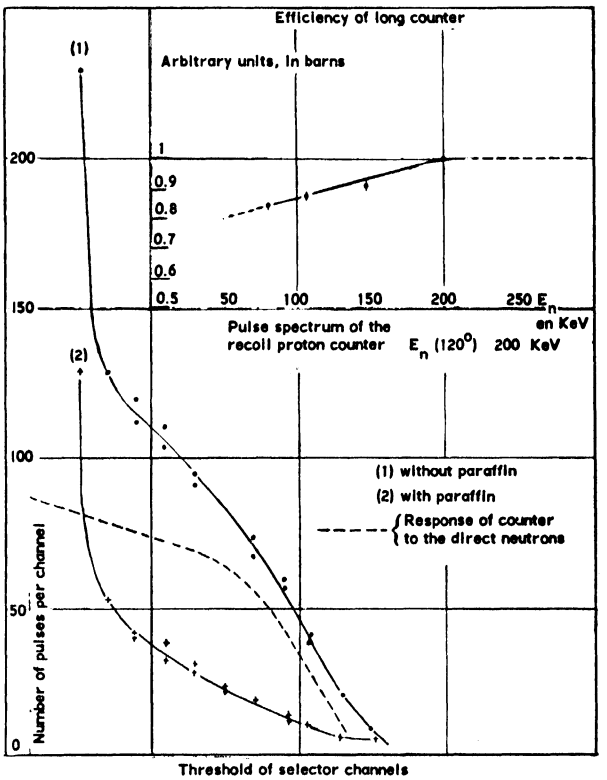

Figure 4. (a) bottom, Pulse spectrum of the recoil proton counter; and (b) top, efficiency of long counter

Figure 2*b* gives the variation of the ratio σ_{Pu}/σ_{U_5} as a function of the energy of fast neutrons, from 50 kev up to 1000 kev, fission threshold of U^{238}. We find:

$$\frac{\sigma_{Pu}}{\sigma_{U_5}} = 1.78 \pm 0.1, \text{ constant from 700 to 1000 kev}$$

Figure 2*c* gives the variation of the ratio σ_{Pu}/σ_{U_3} from 130 to 1250 kev. These results are corrected for the presence of natural U in the U^{233} target. In particular, we find:

$$\frac{\sigma_{Pu}}{\sigma_{U_3}} = 1.06 \pm 0.06 \text{ at } 850 \text{ kev}$$

In the energy range below 200 kev, the forward scattered neutrons no longer are monokinetic: there are two groups as long as the neutron cone is not fully opened. This effect is found, up to neutrons of 170 kev, for a 200 microgram/cm² target. In order to avoid this difficulty, we set ourselves up at 120 degrees with respect to the beam of protons. The size of the lithium and fission chambers then compels us to place the neutron source away from the latter, and therefore to increase the proportion of fissions due to scattered neutrons. On the other hand, the angular distribution of the neutrons is very anisotropic for the energies considered, with a forward preponderance, which further enhances the effect of the scattered neutrons. In order to establish a correlation between the measures carried out at 120 degrees with those made at 0 degrees, we

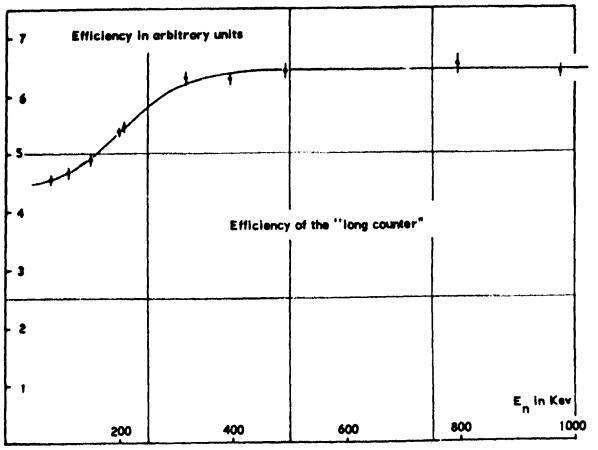

Figure 5. Efficiency of the "long counter"; efficiency in arbitrary units

measured the value of the ratio σ_{Pu}/σ_U at 200 kev for each geometry.

However, the measurements taken at 0 degrees give a ratio σ_{Pu}/σ_{U_5} which is smaller by 15% than that measured at 120 degrees. This discrepancy, unaccounted for, requires additional measurements.

Variation of the Fission Cross Sections of U^{235} and U^{233} as a Function of Neutron Energy

From the fission cross section of Pu^{239} and the σ_{Pu}/σ_U ratios as a function of energy, the curves pertaining to the fission cross sections of U^{235} and U^{233} can be derived (Figs. 3*b* and *c*).

For U^{235}, beyond the fission threshold of U^{238}, the cross section can be derived from a comparison of the fissions of the U^{235} enriched target and the U target, provided the isotopic abundance of each target be known. This region is indicated by the cross-hatchings which give the limits within which the fission cross section must vary.

As a conclusion, we find:

(σ_{Pu}) 150 at 2000 kev $= 2.04 \pm 0.12$ barns

(σ_{U_5}) 700 at 1000 kev $= 1.15 \pm .15$

(σ_{U_3}) 850 kev $= 1.92 \pm .25$

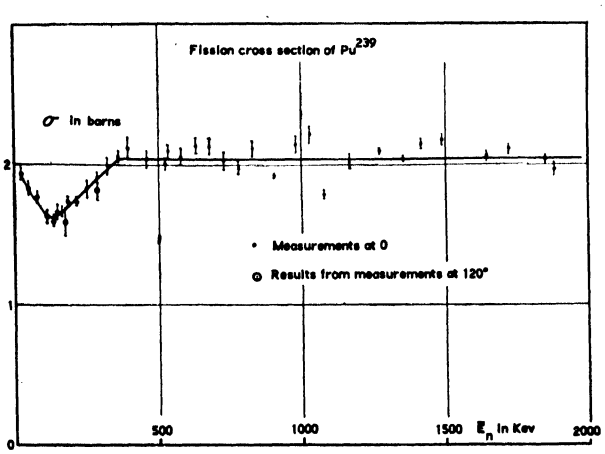

Figure 6. Fission cross section of Pu^{239}

We should like to remind the reader that these figures have been found by taking the fission cross section of natural U with respect to 1600 kev neutrons as a reference.

APPENDIX I

We used a recoil proton proportional counter identical to that described by Skyrme *et al.*[9] As indicated by these authors, the distribution of the pulses due to recoil protons is in good agreement with the theoretically computed distribution.

Figure 4*a* gives, as an example, the spectrum of the recoil protons, recorded with a 10-channel selector, for 200 kev neutrons (geometry 120 degrees), with and without a paraffin screen to stop the neutrons coming direct from the source, as well as for the corrective spectrum which derives from it.

Figure 4*b* shows variation in the efficiency of the "long counter", in the 80–200 kev range, taking, as a reference, the cross section of the neutron-proton diffusion.

APPENDIX II

"Long Counter" Efficiency

The comparison of the responses of the "long counter" and recoil proton counter was continued in the 200 to 500 kev range. The efficiency of the "long counter" as it was used is shown in Fig. 5 (revision of Fig. 4*b*). This efficiency is constant above 300 kev, but still varies from 200 to 300 kev. This determination is related to the value selected at each energy for the diffusion cross section of neutrons by protons. The values were taken from AECU 2040. Any modification of these values would show in all our results.

The Variation of Fission Cross Section of Pu^{239} with Neutron Energy

The efficiency of the cross section of Pu^{239} is roughly constant from 300 kev to 2000 kev.

This value is shown in Fig. 6 (revision of Fig. 3*a*). For neutron energies below 200 kev the results used are those which were obtained with a 120 degree angle.

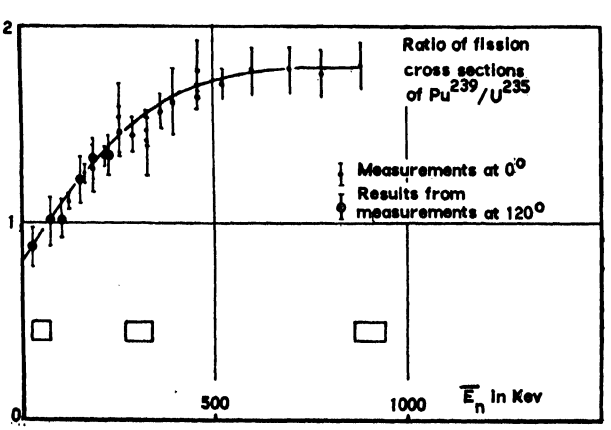

Figure 7. Ratio of fission cross sections of Pu^{239}/U^{235}

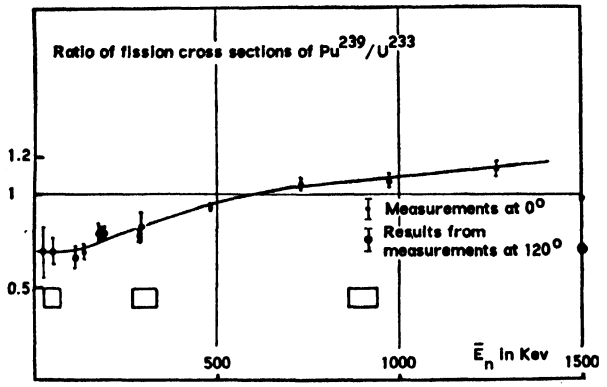

Figure 8. Ratio of fission cross sections of Pu^{239}/U^{233}

The contribution of scattered neutrons was studied as a function of the distance between the lithium target and the ionization chamber. The results, which are difficult to interpret, show that this contribution is important even at 0 degrees (around 10%).

Determination of σ_{Pu}/σ_{U_5} and σ_{Pu}/σ_{U_3}

We were able to show (Figs. 7 and 8—revisions of Figs. 2*b* and 2*c*) the effect of scattered neutrons by studying the variation of the fission counting rate with the distance between the lithium target and the double chamber (Fig. 9).

The corresponding imprecision, about 10%, will add another systematic error.

For neutrons with energies below 200 kev the results shown are those obtained at 120 degrees. The discrepancy between the points at 0 degrees and 120 degrees can be explained by scattered neutrons (at 120 degrees, the chamber is further from the lithium target and the ratio of scattered neutrons is higher).

The energy resolution and statistical precision on the experimental points are shown in the figures.

Variation of the Cross Sections of U^{235} and U^{233} with Neutron Energy

The cross section curves obtained with these corrected results are shown in Figs. 10 and 11 (revisions of Figs. 3*b* and 3*c*).

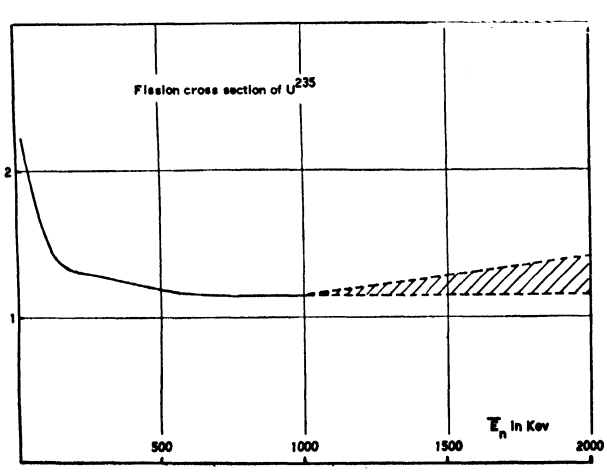

Figure 10. Fission cross section of U^{235}

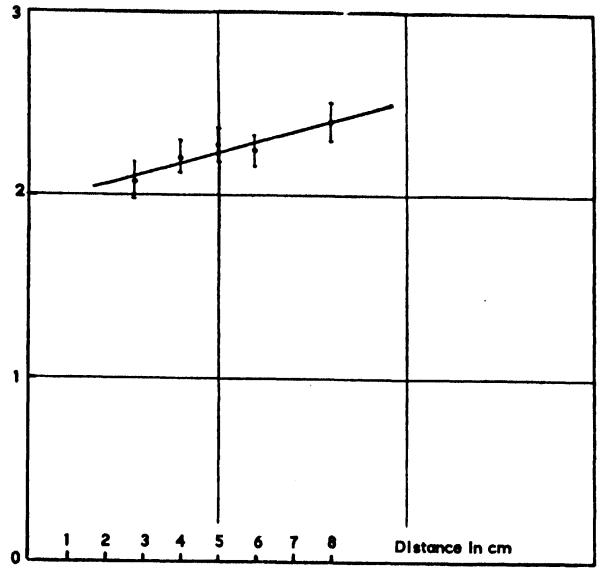

Figure 9. Variation of the ratio of fission counts Pu^{239}/U^{235} as a function of the distance from the neutron source

REFERENCES

1. Neutron Cross Sections, AECU 2040.
2. Hanson, A. O. and McKibben, J. L., *A Neutron detector having uniform sensitivity from 10 kev to 3 Mev,* Phys. Rev. 72: 673, (1947).
3. Feld, B. T., *Experimental Nuclear Physics,* 2: 380 (Segré edit.).
4. Friedland, S. S., *Energy Distribution of Fission Fragments of ^{235}U produced by 2.5 Mev and 14 Mev Neutrons,* Phys. Rev. 84: 75 (1951).
   Wahl, J. S., *Energy Distribution of Fragments from Fission of ^{235}U, ^{238}U and ^{239}Pu by fast Neutrons,* Phys. Rev. 95: 126 (1954).
5. Dickinson, W. C. and Brolley, J. E., Jr., *Angular Distribution of Fragments from Neutron-Induced Fission,* Phys. Rev. 90: 388 (1953).

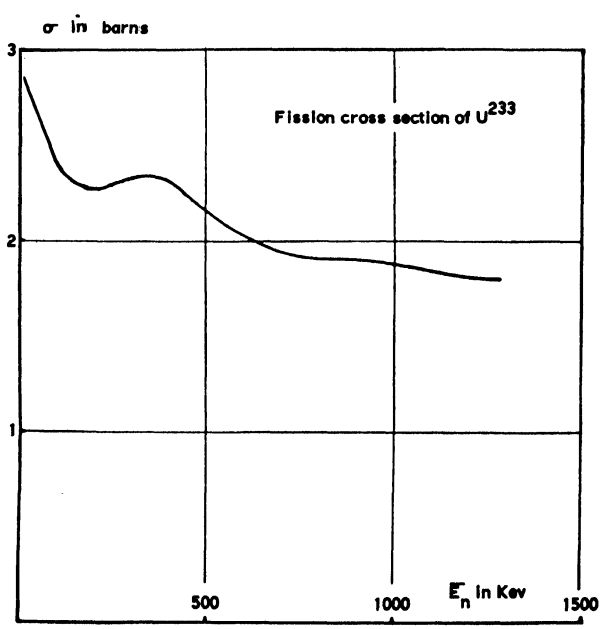

Figure 11. Fission cross section of U^{233}

Brolley, J. E., Jr., Dickinson, W. C. and Heukel, R. L., *The Angular Distribution of ^{235}U Fragments from Neutrons-Induced Fission as a Function of Incident Neutron Energy,* Bull. Am. Phys. Soc. 29 No. 4: 63 (1954).

6. Nobles, R. A. *et al., Response of the Long Counter,* Rev. Sci. Instr. 25: 334 (1954).

7. Lévêque, A., Cohen, R. and Cotton, E., *Mesure du rapport des sections efficaces de fission par neutrons thermiques de Pu^{239} et Unat,* J. Phys. Radium 15: 101 (1954).

8. Auclair, J. M. *et al., Comparaison des sections efficaces de fission pour les neutrons thermiques de ^{233}U et ^{239}Pu,* C.R. Acad. Sci. Paris (June 1955) to be published.

9. Skyrme, T. H. R., Tunnicliffe, P. R. and Ward, A. G., *A proportional Counter for Neutron Flux Measurements in the Energy Range 0.1 to 1 Mev,* Rev. Sci. Instr. 23: 204 (1952).

Some Techniques for Measurement of Fast Neutron Flux

By B. C. Diven,* USA

The measurement of cross sections for the interaction of neutrons with nuclei and for neutron-producing reactions often requires the absolute measurement of a neutron flux. Usually the accuracy of such cross-section measurements is limited by the uncertainties involved in the determination of the neutron flux. The many methods of flux determination are reviewed by Barschall, Rosen, Taschek, and Williams.[1] In the present paper, no attempt will be made to provide a comprehensive review of all methods of neutron flux measurements. Instead, there will be presented a discussion of a group of techniques commonly used in this laboratory which involve counters that are easily transportable from one neutron source to another. The methods described provide convenient means of flux determinations for neutrons having energies from a few tens of kilovolts to 20 Mev but do not represent the most accurate possible methods. For example, it should be possible to determine a flux of neutrons from the $T^3(D,n)He^4$ reaction more accurately by means of the associated particle method than by use of any detector discussed in this paper. Included in the discussion will be the use of two types of proton recoil counters and two types of long counters. The determination of the fission cross section of U^{235} in the energy range 250 kev to 3 Mev will also be described. This reaction serves as a useful secondary standard for flux determinations since its cross section is nearly constant over much of this energy range, and the use of a fission detector as a neutron monitor is fairly simple.

RECOIL PARTICLE METHOD

The recoil particle method of flux determination makes use of independently measured cross sections for elastic scattering of neutrons. This cross section can be measured accurately provided elastic scattering is the only reaction produced by neutrons in the nuclide, because then a transmission measurement to determine the total cross section gives the scattering cross section. Any method that determines the rate of production of recoil particles from neutron collisions in a known number of nuclei of such a substance will allow the incident flux of neutrons to be computed. Since the recoiling nuclei will have a distribution of energies extending down to zero energy, the total number of recoils can never be measured directly. In practice only one of the following is measured: (*a*) the rate of transfer of energy to recoils, (*b*) the number of recoiling nuclei whose energy exceeds a fixed value, or (*c*) the number scattered into a known solid angle. Method (*a*) involves measurement of the ionization current produced by recoils in an ionization chamber. This current, combined with the energy required to produce an ion pair, determines the rate of loss of energy by neutrons due to scattering. From the neutron energy and the angular distribution of scattered nuclei, the mean energy of scattered particles is determined. From the mean energy per recoil particle and the ionization current, the rate at which neutrons are passing through the detector can be calculated. This method has been discussed in detail by Rossi and Staub,[3] Bretscher and French,[4] and by Larsson.[5] Methods (*b*) and (*c*) are combined in the photographic plate work which is discussed elsewhere in these Proceedings.[6] Proportional or scintillation counters are very suitable for measuring the quantities mentioned in (*b*) or (*c*). One example each of methods (*b*) and (*c*) will be discussed here in some detail. All three methods require that the angular distribution of scattered nuclei be known in addition to the total cross section. The scattering substance usually chosen is hydrogen, for which the differential scattering cross section is accurately known up to 20 Mev and which has the further advantage in low energy work of giving the most energetic recoiling nuclei possible. The following formulas for *n,p* scattering have been fitted to experimental data by Gammel and Stewart[2] and provide a close fit to existing data up to 20 Mev.

$$\sigma_{total} = \frac{3\pi}{1.206E+(-1.8600+0.0941491E+0.000130658E^2)^2} + \frac{\pi}{1.206E+(0.4223+0.1300E)^2} \quad (1)$$

$$\sigma(\theta,E) = \sigma_{total} \cos\theta \left[\frac{1+2\left(\frac{E}{90}\right)^2 \cos^2 2\theta}{1+2/3\left(\frac{E}{90}\right)^2}\right] \quad (2)$$

* Los Alamos Scientific Laboratory. Including work by S. J. Bame, Jr., B. C. Diven, R. L. Henkel, G. A. Jarvis, J. E. Perry, Jr., and A. W. Schardt, Los Alamos Scientific Laboratory.

where E is the energy in Mev of the neutron in the laboratory system and θ is the scattering angle of the neutron in the laboratory system. The uncertainty in the total cross section probably is no greater than 1% up to 20 Mev. The differential cross section is approximately as accurate as the total up to 8 Mev. The uncertainty is about 1½% at 14 Mev and 2½ or 3% at 20 Mev.

Proton Recoil Detector for Low Energy Neutrons

A detector which has been used as a flux measuring device for monoergic neutrons with energies between 400 kev and 1.6 Mev consists of a proportional counter for observation of protons recoiling from a thin solid radiator. The observable part of the spectrum of pulse heights produced by these protons is measured. From this part of the spectrum, the total number of neutron-proton scatterings must be determined. The low energy part of the spectrum is obscured by pulses due to recoiling carbon atoms from the radiator and by pulses due to X- and γ-radiation. Since the pulse height produced by the recoil proton is determined by the proton energy and hence by the scattering angle of the neutron, the pulse-height spectrum is determined by the angular distribution of n,p scattering. For low energy neutrons the result is a rectangular pulse-height distribution in which there are equal numbers of pulses per unit pulse-height interval up to a maximum height beyond which there are no pulses. Then if all pulses above a height P are detected, the fraction of all pulses detected is $(P_m - P)/P_m$ where P_m is the maximum pulse height. Actually, the distribution is distorted by neutron energy spread and proton energy loss in the radiator. In practice the theoretical pulse-height distribution is deduced according to the methods given in Rossi and Staub,[3] as worked out by Case,[7] taking into account the thickness of the glycerol tristearate radiator, and the neutron energy spread. The theoretical curve is fitted to the experimental curve and the total number of proton recoils computed. Figure 1 is an example of the kind of fit which is obtained.

The detector is illustrated in Fig. 2. The proton recoil counter is 5 cm in diameter and has a counting volume 6 cm long, the length being fixed by use of field tubes as described by Cockcroft and Curran.[8] This counter is lined with a thin platinum cylinder which can be removed and carefully cleaned to minimize contamination by hydrogenous materials. The proton radiators consist of thin films (65 to 650 micrograms total weight) of glycerol tristearate deposited in a 2.6 cm diameter circle on a platinum disc. The glycerol tristearate is deposited by evaporation in a vacuum, the amount deposited being determined by weighing the platinum foils before and after deposition of the glycerol tristearate. Radiators of various thicknesses are used to check the consistency of weighing as well as the thickness corrections. Two 20-milligram samples of glycerol tristearate, evaporated by the same method as for radiator preparation, were analyzed for hydrogen content and found to have within a few tenths of a per cent of the theoretical amount of hydrogen by weight. The platinum foil is bent around the cylinder of the proportional counter, the radiator being placed over a hole in the cylinder and forming part of the wall of the counter. The counter is enclosed in a thin steel envelope which contains argon-carbon dioxide at a pressure which assures that all protons of interest are stopped in the gas. Since the counter is cylindrical, care must be taken that a proton at a large angle to the neutron beam will not strike the wall. A pressure of about 2 atmospheres is sufficient to achieve this result for 1 Mev neutron energy. The counter pressure must be low enough that pulses caused by X-rays from the accelerator do not become confused with the proton pulses. Because of these requirements the pressure is adjusted as required for different neutron energies. After amplification, pulses from the proton recoil counter are analyzed by a multichannel pulse-height analyzer.[9]

Several corrections and backgrounds must be determined in order to measure the flux. The effect of foil thickness and neutron energy spread has already been mentioned. The background due to recoil protons from hydrogen contamination of the counter gas and walls is measured by inserting a blank platinum foil in place of the proton radiator and making an exposure to the neutron beam. Such a background is shown in Fig. 1. The importance of this kind of background depends upon the amount of hydrogen on the radiator. At low neutron energies the radiator must be very thin and the ratio of number of protons from background to number from the radiator becomes large. This effect determines the lower limit of neutron energies at which this

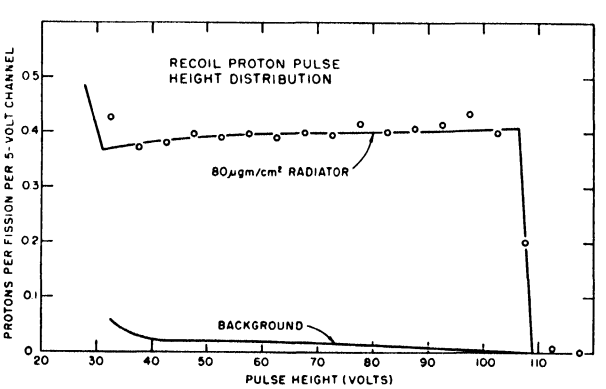

Figure 1. Distribution of pulse heights due to recoil protons from an 80 μg/cm^2 glycerol tristearate radiator when irradiated by 1 Mev neutrons. The detector is the proportional counter of Fig. 2. The circles are observed points with a channel width of 5 volts, background subtracted. The solid curve has the shape of the theoretical distribution of pulses from a radiator of this thickness and neutron energy spread of 0.030 Mev. Examination of the shape of the high energy cut off with narrower channels shows good agreement with the theoretical curve. The rise in the solid curve at low energies indicates the energies which can be obtained by recoiling carbon nuclei

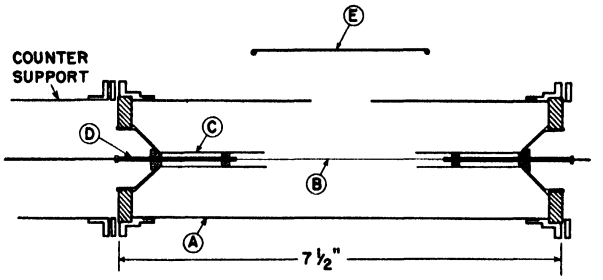

Figure 2. Double counter. Proportional counter for detection of recoil protons and ionization chamber for detection of fissions. *A* is the outer grounded cylinder of the proportional counter. *B* is the wire at positive high voltage, C are "field tubes" which are held at an appropriate intermediate potential to maintain uniform gas multiplication along the wire in the counting region and to shield the wire from ionization produced in the gas in the region outside of the counting region, *D* is a "guard ring" held at the same potential as the wire but insulated from it. The proton radiator of glycerol tristearate is coated on a metal foil and placed over the opening in the counter wall. *E* is the collecting electrode of the ionization chamber. The foil of fissionable material is placed back to back with the proton radiator, the cylinder of the proportional counter serving as the negative electrode of the ionization chamber

method of flux measurement is applicable. The size of the background can easily be reduced to the equivalent of 20 micrograms of radiator material, so that the minimum acceptable weight for a radiator is about 200 to 300 micrograms. This material is spread over 5 square centimeters and therefore amounts to about 50 micrograms per square centimeter. Corrections for energy loss in these radiators become large for neutron energies as low as 400 kev. In the case of 1.5 Mev neutrons all backgrounds and corrections can be kept smaller than 5%.

It must be remembered that because this is a biased detector, it is energy sensitive. Any neutrons less energetic than those of the primary beam will be detected with lower efficiency and cannot be detected at all if their energy is less than the minimum proton energy accepted. Also the counter is directional. Detection efficiency varies from a maximum for those neutrons striking perpendicularly to the plane of the radiator from one side to zero for those entering perpendicularly to the plane of the radiator from the other side. Hence the accuracy of the flux measurement will depend on the nature of the source of neutrons. For a point source with no background neutrons from odd directions and for which no energies other than a narrow range are present, it is possible to determine the flux with 2% accuracy. This will involve small corrections for the perturbation of the flux by the counter.

Counter Telescope for High Energy Neutrons

In the energy region above 3 Mev it is convenient to use a counter telescope[3,10,11] arrangement for measurement of neutron flux. In this device, only those recoil protons are chosen which emerge from a thin solid radiator in a direction close to that of the incident neutrons. One such instrument is shown in Fig. 3. Recoil protons are collimated by a system of apertures. As they traverse the two proportional counters, they lose a small amount of energy in each, giving rise to pulses in these counters. Finally most of the energy is lost in the crystal of the scintillator system. In order to reduce background due to neutron interactions in the crystal, a triple coincidence between the two proportional counters and the scintillator is required. Since recoil particles of nuclei which are present and which are heavier than protons have very short ranges, they cannot produce pulses in all three detectors. When a monoergic neutron flux is incident upon the radiator, the pulse-height spectrum from the scintillator due to recoil protons consists of a single sharp peak. An example of a pulse-height distribution of scintillator pulses in coincidence with proportional counter pulses from such a detctor is shown in Fig. 4. The width of the peak is accounted for by the combination of neutron energy spread, variation of proton energy due to radiator thickness, and range of scattering angles accepted. The small number of pulses below the main peak which remain after background has been subtracted can be attributed mostly to protons which are degraded in energy by penetration of the edges of the collimator system. It should be pointed out that this detector is a neutron energy spectrometer as well as a flux measuring device. In fact, it is possible, by use of this detector, to determine the flux of neutrons per unit energy interval from a polyergic source. Several such detectors are in use and differ considerably in details of design. If a large range of energies is to be covered, it is desirable to provide means of using radiators of differing thicknesses. In any case, a blank should be provided to allow observation of backgrounds due to hydrogen contamination of the detector. If the device is to be used strictly for measurement of monoergic fluxes, then a rather large scattering angle can be accepted, and a relatively thick radiator used, whereas in a counter intended for use as an energy spectrometer, the apertures should be so adjusted that acceptable protons are nearly in line with the direction of the neutrons in order that the proton energy should not differ greatly from the energy of the neutron which produced it; and the radiator should be sufficiently thin that the lowest energy protons of interest do not suffer a large energy loss.

It is possible to make a flux measurement of monoergic neutrons with this device with an accuracy of about 3%. Some quantities which effect the accuracy are discussed below.

1. The mass of the radiator can be determined very accurately in case of measurements with neutrons of energies of 3 or 4 Mev and higher since the radiator can then be quite thick.

2. The amount of hydrogen per gram of radiator material should be determined chemically, and such determinations should influence the choice of material for the radiator. The uncertainty in hydrogen content need be no greater than about one-half per cent.

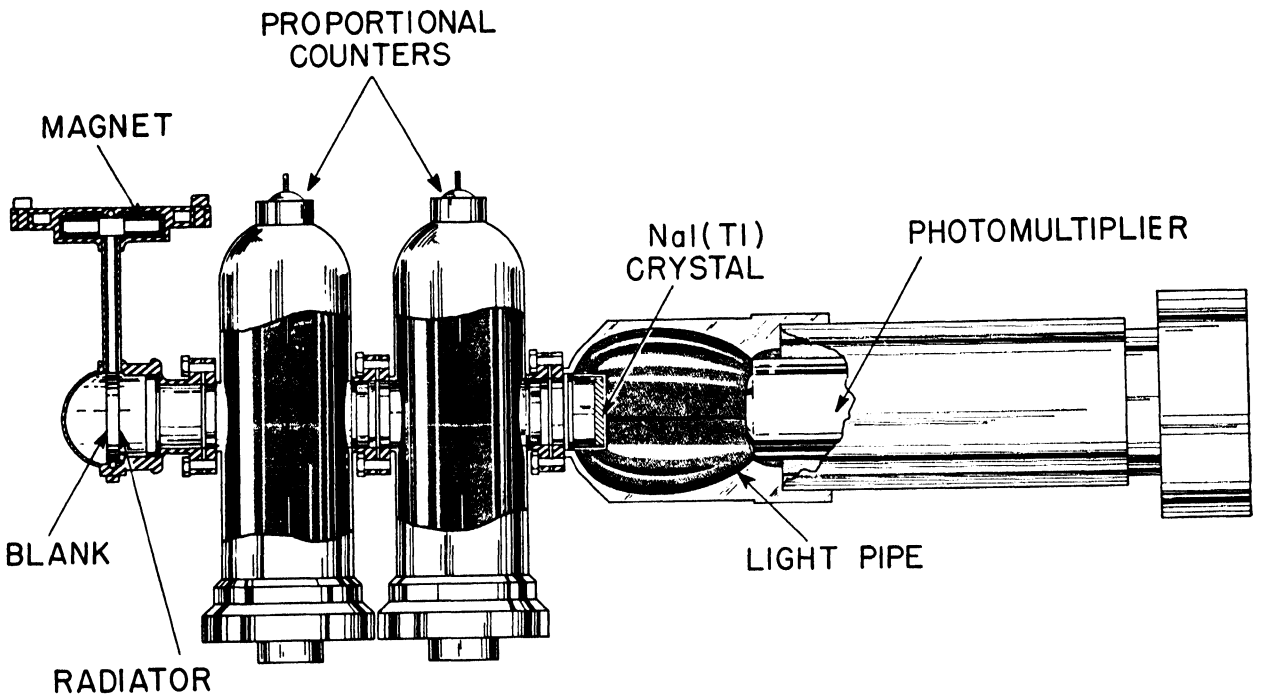

Figure 3. Counter telescope for flux measurements. Recoil protons from the radiator produce pulses in each proportional counter and in the scintillator. A triple coincidence of these pulses is required for an event to be recorded. An aperture in front of the scintillator crystal determines the fraction of all neutron scatterings in the radiator which is observed. Variations on this counter include provisions for the use of several radiator thicknesses, different scintillator crystals, gas counter in place of the scintillator and variations of apertures. The light pipe between the crystal and phototube is not essential

3. The accuracy with which the geometry of the system can be known depends on the details of the detector. In general, the larger the solid angle the more accurately it can be measured. Similar considerations hold for slit penetration problems. It may be possible to know the fraction of protons detected with an accuracy of one per cent. However, in view of the fact that n,p scattering is not spherically symmetric in the laboratory system, and the radiator is an extended source, the computation of the fraction detected of all recoil protons can be very tedious if a large range of scattering angles is accepted.

4. It is necessary to know the differential cross section for n,p scattering in order to obtain the neutron flux. This may be known with an accuracy of about 1% to 2% depending on the neutron energy.

5. In addition to the above considerations, several small corrections must be considered. The effects of scattering of the recoil protons in the radiator and in the gas of the proportional counters and scattering of neutrons by the detector itself, are examples. The first mentioned effect may be large at low neutron energies. These effects depend on the design of the detector and should be made as small as possible. Great care must be exercised to be sure that all recoil protons which enter the scintillator give a pulse. For instance, jitter in the relative time of the three counter pulses could result in loss of some recoil protons because of failure to achieve a triple coincidence. Very poor pulse-height resolution in any of the counters could result in loss of some events which should have been detected. In high neutron fluxes, chance coincidence problems can become serious. Care should be taken that α particles from the reaction of neutrons with carbon of the radiator are not mistaken for protons.

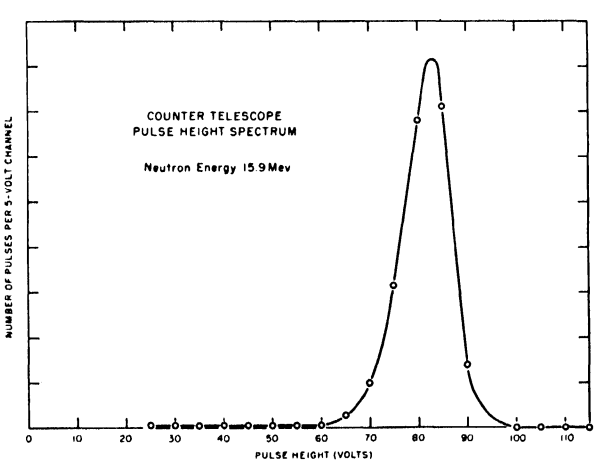

Figure 4. Pulse height spectrum from the scintillator of a detector similar to that shown in Fig. 3. These pulses are due to recoil protons from the radiator and are in coincidence with pulses in the two proportional counters. The width of the peak is accounted for by the thickness of radiator used and the range of accepted angles of recoil protons. In this example the maximum accepted angle between incoming neutron and recoil proton is 23 degrees. The radiator thickness is 50 milligrams per square centimeter

FISSION DETECTORS

The fission process provides a convenient secondary standard for neutron flux measurements. The U^{238} fission cross section is known with an accuracy of 3½ to 5 per cent in the energy region from 250 kev to 3 Mev. It is relatively simple to obtain other fission cross sections by determining their ratios to the U^{235} cross section. Although a fission counter is simple to build and use, considerable care must be exercised in order to measure a flux with such a detector. One must know (*a*) the amount of fissionable material and its composition, (*b*) the energy spectrum of neutrons, (*c*) the perturbation on the flux produced by the detector and (*d*) the fraction of fissions which are observed. Because of the large thermal fission cross section of U^{235}, if only a very small fraction of the flux is made up of low energy neutrons, these neutrons may account for a large fraction of the fissions. Enclosing such a counter with cadmium greatly reduces the effect of room-scattered neutrons which have thermal energies. In any case it is essential that backgrounds be very carefully investigated.

The general problems of determination of a cross section by comparison to U^{235} are quite similar to those encountered in the absolute determination of the U^{235} cross section by comparison to hydrogen. A description of this experiment will serve to indicate some of the general problems involved in this method. The U^{235} fission cross section was determined with the aid of the proton recoil flux measuring device described earlier. A method very similar to that described by Rossi and Staub (reference 3, page 165) was used. A double counter consisting of a fission chamber and a recoil chamber (see Fig. 2) was enclosed in a single case. The counter was surrounded with cadmium to reduce the background in the fission counter which was due to low energy room-scattered neutrons. The fissionable material and a thin layer of hydrogenous material were deposited on thin platinum foils which were placed back to back and comprised part of a grounded electrode common to the two counters. One great advantage of this system was that both materials were deposited as uniform layers of the same diameter and were separated from each other by only a few thousandths of a centimeter of platinum. The flux measurement by the proton recoil detector was then made at the same time and essentially in the same place as the observation of the fissions. Therefore, knowledge of the exact distance of the detectors from the neutron source and small angular misalignments were unimportant, and to some extent, effects of perturbations of the neutron flux due to the counter itself tended to cancel out. The fission counter was essentially a parallel-plate ionization chamber (actually the electrodes were sections of cylinders).

U^{235} foils consisted of 200 to 500 micrograms of U^{235} plated onto a 2.6 cm diameter circle on a platinum disc. The platinum foil containing the U^{235} was bent around the cylinder of the proportional counter so that the two foils were back to back and the deposits were centered one upon the other. In order to obtain an accurate measure of the amount of U^{235} on the fission foil used, a set of intercomparisons of several foils was made. Weights were determined by both quantitative electroplating and by actual weighting before and after deposition, care being taken in the latter case to convert the uranium completely to U_3O_8 by heat treatment in air to ensure a known composition. α-counting was used as a secondary method for comparison of the foils.

After amplification, pulses from the fission counter went into a discriminator and scaler. In order to determine the optimum bias setting for the discriminator, the pulse-height distribution produced by fission fragments was observed with an 18-channel pulse-height analyzer.[9]

The correction for the absorption of fission fragments in uranium could have been made according to the methods of Rossi and Staub[3] if the deposits had been perfectly uniform and flat. However, a study of the distribution in pulse height of the low energy "tail" of the fission pulse spectrum showed that there were more small pulses than could be accounted for by energy loss in a uniform, flat, layer of uranium. This effect was apparently due in part to roughness of the platinum surface. The correction of less than 2% which was applied involved extrapolation of the fission pulse-height spectrum to zero pulse height and then application of the absorption correction. The effect of counter scattering was determined by surrounding the counter with additonal layers of steel and cadmium and observing the change in the ratio of protons to fissions. The effect is about 1%.

Smaller corrections which were computed were the effect of foil scattering which increased the average path length of neutrons in the radiators, target scattering which provided some neutrons of low energy at the counter, and effect of center of mass motion of the fission fragments on the fraction of fissions detected.

From the knowledge of the amount of U^{235} on the fission foil, the amount of hydrogen in the proton radiator, the numbers of fissions and proton recoils which occurred during a run, and numerous backgrounds and corrections, the ratio of cross sections of U^{235} and H were computed.

The experiment may be thought of as having two parts. One part involved determination of the relative fission cross section as a function of energy, and the other part the determination of an absolute cross section at some energy. The experiment was broken up in this manner because, in order to find the absolute number of fissions from a foil, the uranium deposit on that foil must be quite thin compared to the range of fission fragments. This limits the counting rates available to about a thousand counts per hour. On the other hand, if the absolute cross section

is known at one energy, then a rather thick uranium layer may be used for counting fissions at other energies and the data can be normalized to the point taken with the thin layer. In determining the energy variation of the cross section, a foil containing about 5 milligrams of uranium was used, whereas for determining an absolute value, a foil containing about 360 micrograms was used. Fourteen points were taken at energies between 400 and 1600 kev. Several different thicknesses of proton radiators were used since the variation of maximum proton energy over that range is considerable. In this determination of relative cross section the various backgrounds and corrections listed in the previous paragraphs have little or no effect.

The final accuracy obtained in the absolute flux determination is believed to be about 2%. The uncertainty in the absolute fission cross section is about 3½% at 1¼ Mev. The relative values of the cross section as measured by this method at energies between 1 Mev and 1.6 Mev are probably accurate to about 2% and the values below 700 kev to about 5%. These measurements have been extended by use of a long counter to cover the region from 250 kev to 3 Mev. The results are shown in Fig. 5. The solid curve was obtained by using the long counter and is normalized to the value 1.27×10^{-24}cm^2 at 1.25 Mev as determined by the absolute measurement.

FLAT RESPONSE NEUTRON DETECTORS

A detector whose efficiency is independent of neutron energy is very useful as a means of comparing fluxes of different energies and for work with polyergic fluxes. One type of flat response detector which is commonly used consists of a proton recoil counter whose walls are coated with hydrogenous material and which is filled with a hydrogenous gas. A suitable combination of minimum acceptable pulse height, thickness of wall coating, and gas pressure allows one to obtain a flat response over a limited energy region. Fission counters are also flat over fairly extensive energy regions (see Section II) and have the advantage of providing large output pulses but have a relatively low efficiency. Such detectors have the advantage over some other flat response detectors such as long counters that the output pulses are coincident in time with the arrival of the neutron at the detector, thus, permitting the use of coincidence techniques.

One of the most versatile of the flat response detectors is the long counter of Hanson and McKibben.[12] This device consists of a $B^{10}(n,\alpha)$ gas proportional counter embedded in paraffin. By suitable adjustment of the geometry of boron counter and paraffin, a uniform sensitivity over a region of many Mev may be achieved. To some extent the flatness of response at high energies can be improved by sacrifice of flatness at low energies. Since individual long counters vary in details of construction, each should be calibrated individually. The use of natural neutron sources to determine the flatness of the detector was described by Hanson and McKibben.[12] It is also desirable to observe the response in more detail by use of monoergic fluxes. An absolute calibration can be made by means of any suitable flux measuring technique or by a calibrated natural neutron source. A very low energy calibration at 23 kev can be obtained by use of an Sb-Be photoneutron source; from 500 kev to several Mev a U^{235} fission counter is a convenient flux measuring device; a counter telescope can be used above 2 or 3 Mev and a point near 14 Mev can be taken by use of an associated particle monitor on a $T^3(D,n)He^4$ neutron source. Such measurements show that for each resonance in the total neutron cross section of carbon, there is a corresponding anomaly in the response of the long counter.[13] Figure 6 shows the response of one long counter as a function of neutron energy. The efficiency of this detector drops off about 10% at 25 kev and 30% at 14 Mev and 60% at 20 Mev. If a careful calibration is made, the long counter can be used to determine the absolute value of a flux with about 5% accuracy. If the relative response as a function of neutron energy is known, it is not necessary that the flux which is to be measured have the same energy spectrum as the flux in which the calibration was made.

The long counter is characterized by simplicity, reliability, and versatility. The equipment is so simple that the counter and associated electronic apparatus often operate continuously for a year or more with no repairs. It is insensitive to small changes of voltage on the BF_3 counter and to small amplifier gain shifts.

Since it is very difficult to measure a flux of neutrons with energies below a few hundred kilovolts, the long counter response cannot be measured easily between about 20 kev and 500 kev. A Monte Carlo calculation of the response of a long counter can be made provided the standard design is modified somewhat. The counter being considered in the laboratory uses simple cylindrical geometry and has the BF_3 detector shielded from thermalized neutrons

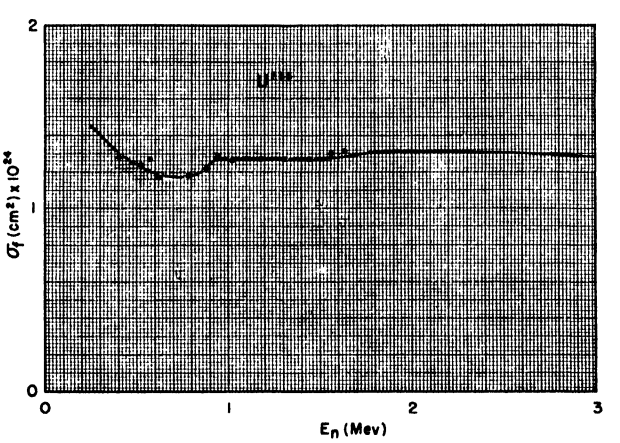

Figure 5. The fission cross section of U^{235}

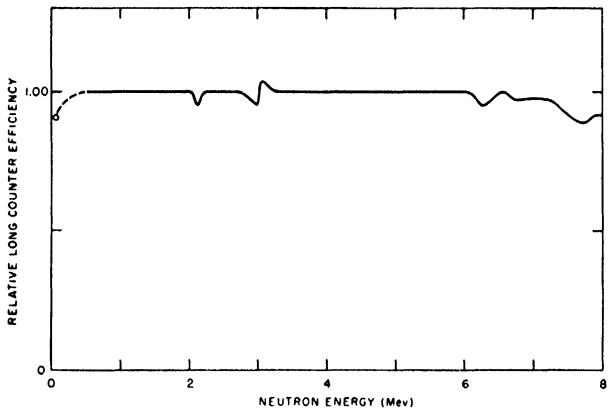

Figure 6. Response of a long counter. This curve shows the measured response of a particular long counter for neutrons of different energies. The measurements were made with calibrated neutron sources having different spectra and with monoergic neutrons monitored with proton recoil detectors

by means of a cadmium shield. By avoiding the necessity for calculations of the behavior of neutrons of energy low enough to be affected by the binding energy of hydrogen in paraffin, it is believed that the calculations will be quite precise. Relative efficiencies for energies between 20 kev and 1 Mev are being computed. As a check on the theoretical calculations of counter response, a hydrogen-filled proportional counter similar to that described by Skyrme, Tunnecliffe and Ward[14] may be used to calibrate the long counter in this energy region.

CONCLUSION

A group of counters has been described which provide means for measurement of neutron fluxes in the energy region between 20 kev and 20 Mev. The accuracy which can be readily achieved is about 5% above 500 kev and perhaps 10% below this energy. If very great care is taken it may be possible to measure a flux with about 2% accuracy using recoil proton detectors.

REFERENCES

1. Barschall, H. H., Rosen, L., Taschek, R. F. and Williams, J. H., *Measurement of Fast Neutron Flux,* Rev. Modern Phys. *24*: 1 (1952).
2. Private Communication, Leona Stewart, Los Alamos Scientific Laboratory (April 1955).
3. Rossi, B. B. and Staub, H. H., *Ionization Chambers and Counters,* McGraw-Hill Book Co., Inc., New York (1949).
4. Bretscher, E. and French, A. P., British Reports, BR-386 and BR-517.
5. Larsson, K. E., *The Use of the $^3T(d,n)^4He$ Reaction for a Comparison of Some Methods for the Absolute Measurement of a Fast Neutron Flux,* Ark. f. Fys. *9*: 293 (1955).
6. Rosen, L., P/582, *Techniques for Measurement of Neutron Cross Sections and Energy Spectra for Sources which are Continuous in Energy and Time,* Volume 4, Session 15A, these Proceedings.
7. Case, K. M., MDDC 92, Unpublished, Declassified Report, *Theory of Neutron Counters Using Proton Recoils from Paraffin.*
8. Cockcroft, A. L. and Curran, S. C., *The Elimination of the End Effects in Counters,* Rev. Sci. Inst. *22*: 37 (1951).
9. Johnstone, C. W., *A New Pulse-Analyzer Design,* Nucleonics *11*: 36, (1953).
10. Amaldi, E., Bocciarelli, D., Ferretti, B. and Trabacchi, G. C., *On Proton-Neutron Collisions II,* Ric. Sci. *13*: 502 (1942).
11. Kinsey, B. B., Cohen, S. G. and Dainty, J., *A Coincidence Method of Measuring a Fast Flux of Neutrons,* Proc. Camb. Phil. Soc. *44*: 96 (1948).
12. Hanson, A. O. and McKibben, J. L., *A Neutron Detector Having Uniform Sensitivity from 10 kev to 3 Mev,* Phys. Rev. *72*: 673 (1947).
13. Nobles, R. A., Day, R. B., Henkel, R. L., Jarvis, G. A., Kutarnia, R. P., McKibben, J. L., Perry, J. E., Jr. and Smith, R. K., *Response of the Long Counter,* Rev. Sci. Inst. *25*: 334 (1954).
14. Skyrme, T. H. R., Tunnecliffe, P. R. and Ward, A. G., *A Proportional Counter for Neutron Flux Measurements in the Energy Range 0.1 to 1 Rev,* Rev. Sci. Inst. *23*: 204 (1952).

Fission Cross Sections as a Function of Neutron Temperature

By C. G. Campbell,* and D. J. Lockey,† UK

It is convenient to describe the neutron energy spectrum in the core of a reactor by the sum of three components. The thermal component is assumed to follow a Maxwellian energy distribution, $M(E,T)$, which, when written in the form:

$$M(E,T) = \frac{E}{(kT)^2} e^{\frac{-E}{kT}} \qquad (1)$$

encloses a unit area. In this expression E is the neutron energy, T is the absolute neutron temperature, and k is Boltzmann's constant. The neutron temperature usually adopted is close to that of the moderator. The epithermal component is usually written as λ/E, in which λ is a constant, characteristic of the particular reactor, for neutron energies greater than 4 or 5 kT, but which abruptly becomes zero below this energy. The third component $S(E)$ is introduced to smooth into the Maxwellian distribution this abrupt lower limit to the epithermal component.

An effective cross section, $\sigma(eff)$, in the neutron spectrum of a reactor may now be defined, relative to the thermal component of the neutron flux:

$$\sigma(eff) = \frac{\int \left\{ M(E,T) + \frac{\lambda}{E} + S(E) \right\} \sigma(E) dE}{\int M(E,T) dE} \qquad (2)$$

The integrations cover the energy range from zero to fission energies, taken as ~ 2 mev.

In a similar way an effective cross section in a thermal neutron flux may be defined:

$$\sigma(eff, th) = \frac{\int M(E,T)\ \sigma(E) dE}{\int M(E,T) dE} \qquad (3)$$

Since λ is usually small, the value of Equation 2 will, to a considerable extent, be governed by that of Equation 3.

If the cross section, $\sigma(E)$, follows a $1/v$ law, then, as the temperature of the Maxwellian distribution is increased, the effective thermal cross section falls. If, on the other hand, $\sigma(E)$ has a strong resonance in the thermal region, then this behaviour is modified. In the case of the fission cross section of Pu^{239}, for example, with its strong resonance at 0.3 ev, calculations show that the effective thermal cross section increases significantly for neutron temperatures above 100°C. The bearing of this effect upon the temperature coefficient of reactivity increases with the Pu^{239} content of the reactor fuel.

Any detailed study of the fates of neutrons in a reactor core demands a knowledge of the temperature variation of all those effective cross sections involved. Amongst the more important of these are the fission cross sections of the fuel, and a series of experiments was therefore performed to give an independent integral check of the values calculated by using the current UK differential cross-sectional data. These experiments gave directly the variation with temperature of the effective thermal cross sections of Pu^{239}, U^{235} and U^{233}, relative to that of B^{10}.

PREDICTIONS BASED ON CURRENT CROSS-SECTION DATA

Integrations of the quantity shown in Equation 3 were performed numerically, using calculated Maxwellian distributions appropriate to twelve different temperatures in the range from 300°K to 700°K. These integrations were undertaken for Pu^{239}, U^{235} and a $1/v$ dependence.

The slow neutron fission cross sections adopted for Pu^{239} are those now reported by Raffle and Price:[1]

$$\sigma(E) = \frac{1}{\sqrt{E}} \left\{ \frac{4.79}{(E-0.30)^2 + \left(\frac{0.10}{2}\right)^2} + \frac{0.0785}{E^2 + \left(\frac{0.11}{2}\right)^2} + 30.0 \right\} \text{barns} \qquad (4)$$

This analytic form, which fits the experimental data very closely, consists of two Breit-Wigner single-level terms, together with a $1/v$ term.

For the thermal fission cross sections of U^{235}, Lynn and Pattenden's[2] expression was used:

$$\sigma(E) = \frac{1}{\sqrt{E}} \left\{ \frac{0.0819}{(E-0.005)^2 + 0.003} + 77.5 \right\} \text{barns}$$

This fits the experimental data below 0.1 ev to an accuracy of better than 1%.

Nuclear Doppler broadening of the energy levels involved in these expressions will make the cross sections dependent upon neutron temperature. Broadening of the 0.30 ev resonance in Pu^{239} will produce the greatest effect in those effective thermal cross

* A.E.R.E., Harwell.
† C. A. Parsons and Co., Newcastle.

sections considered, but even in this case a temperature increase of 400°C from room temperature produces a calculated increase in the effective cross section of less than 0.02%. Effects of Doppler broadening were therefore neglected.

The results of the numerical integrations are shown in Fig. 1 (and in the first four columns of Table 2 below). For the $1/v$ dependence, an arbitrary cross section of 1000 barns has been adopted at an energy of 0.0253 ev.

EXPERIMENTAL ARRANGEMENTS

Provided that the sensitivity of a fission chamber is independent of its temperature, a measurement of the effective thermal cross section at a temperature T of the fissile material within the chamber, relative to that of a $1/v$ detector, is given by the ratio of the counting rates of the chamber to that of a BF_3 filled proportional ionisation chamber, both chambers being situated in a large block of moderator maintained at the temperature T.

For our purposes it was convenient to choose graphite as the moderator. A cube of 3 ft side was built against the BEPO reactor, to receive neutrons from an experimental hole in the shield over a region of about 1 ft square. To the faces of the graphite, eight strip heaters were attached, each being of 1½ kw rating. Glass wool lagging was arranged on all faces of the cube. The graphite was maintained at selected temperatures up to 400°C by a thermostatic control of the heaters, the temperature being measured with iron-constantan thermocouples. That the block was at a uniform temperature throughout was checked by a survey with four thermocouples before making counter observations.

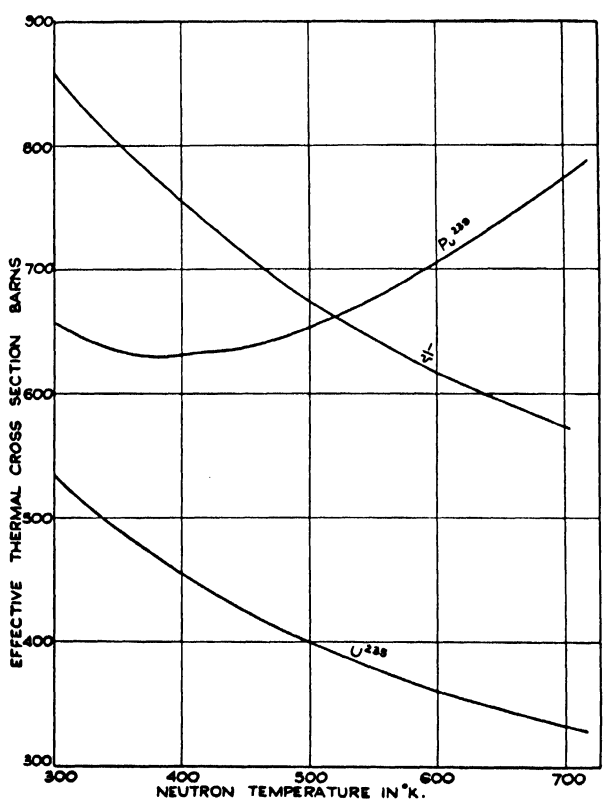

Figure 1

At the positions chosen for counting, which were near the centre of the graphite cube, the cadmium ratio, measured with an 0.004 in. thick indium foil was 380; the neutrons were therefore regarded as being completely thermalized. The neutron flux in these positions was $\sim 5 \times 10^5$ cm^{-2} sec^{-1}.

To make the counting observations independent of fluctuations in intensity of the incident neutron beam, in all the experiments the counting rates of three fission chambers, containing Pu^{239}, U^{235} and U^{233} respectively, were observed simultaneously with that of a BF_3 proportional chamber. This chamber, of 1 cm diameter was inserted to the centre of the cube in a 1¼ in. diameter aluminium tube, and was maintained at a constant temperature of $\sim$ 25°C by compressed air cooling introduced to the vicinity of the chamber through a ⅜ in. diameter aluminium tube. The air cooling had a negligible effect upon the uniformity of the graphite temperature.

To investigate experimentally any possible effects due to Doppler broadening of the resonances, three separate experiments were performed. At various temperatures up to 400°C the counting rates were observed with the fission chambers firstly air cooled to $\sim$ 25°C, and then at the graphite temperature. To detect any temperature dependence of the efficiency of the chambers, they were heated in a silica tube placed in the graphite block. A heater winding on the tube raised the chambers to any temperature within the range required without sensibly altering the graphite temperature, which was maintained at $\sim$ 25°C. The length of the chamber stem heated in this way was equal to the length heated by the graphite in the second experiment.

COUNTER DESIGN AND PERFORMANCE

A full description of the fission chambers has already been given.[3] Those used were constructed in a ¼ in. od nickel tube 3 ft in length. The sensitive length was 2 cm. A 0.192 in. id nickel cylinder, coated on the inside with the oxide of the fissionable material, formed the cathode. The thickness of metal in the deposit was $\sim$ 100 μg/cm^2 in the Pu chamber and $\sim$ 1 mg/cm^2 in both the U chambers. Self-screening of neutrons was thus negligibly small at all energies. The collector was a nickel sleeve of 0.134 in. diameter, which was quartz insulated from the chamber cathode. It was maintained at a potential of 300 volts by a 24 S.W.G. copper wire completely insulated from the 3 ft nickel stem by further quartz insulators. The filling gas was argon, at a pressure of 7½ atmospheres. An all-welded construction was adopted to allow operation up to $\sim$ 500°C.

Typical integral bias curves for the chambers are shown in Fig. 2. The plateaux of these characteristics were maintained at all temperatures up to 400°C, this being the highest temperature tested.

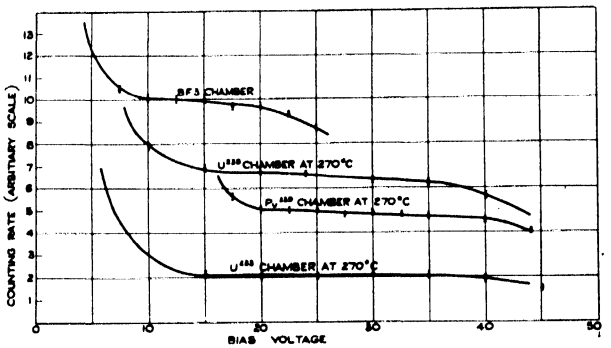

Figure 2. Chamber characteristics

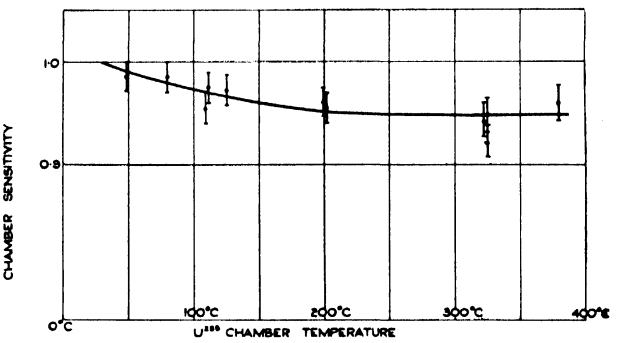

Figure 3. U^{235} chamber sensitivity

The BF_3 filled proportional chamber was constructed with a 1 cm od brass tube as its cathode. The sensitive length of this chamber was normally 2 in., but was restricted in this experiment to $\frac{1}{8}$ in. by a cadmium wrapping, to avoid excessively high counting rates. A 0.001 in. diameter anode was maintained at an operating potential of 1200 volts. The filling pressure was 40 cm Hg. A typical integral bias curve for this chamber is also shown in Fig. 2.

The output pulses from all the chambers were amplified $\sim 5 \times 10^5$ times before being fed to their discriminator and scaling circuits. It was found impracticable to maintain amplifier stability to better than 1 or 2 *dB* over the period of these experiments, and therefore the counting rate adopted in each test was that appropriate to the bias voltage mid-way between the noise (or α-particle) cut-off and the knee of the characteristic. This method was preferred to that of extrapolating the plateau to a zero bias voltage and then adopting this as the representative counting rate, since it is less dependent on the plateau slope.

DISCUSSION OF OBSERVATIONS

No significant dependence of the sensitivity of the Pu^{239} chamber upon its temperature was detected. With the graphite block at 25°C the results obtained, which have been normalised to unity at room temperature, are summarised in Table 1.

For the U^{235} chamber, however, a 6% reduction in sensitivity was observed for a 400°C increase in temperature. This behaviour was found repeatedly on heating and cooling the chamber. The variation of sensitivity with temperature is shown in Fig. 3.

With the chambers cooled Fig. 4 shows the ratios of the counting rates observed for Pu^{239} and U^{235} to that of the BF_3 chamber, as a function of graphite (or neutron) temperature. These results have been fitted by the method of least squares to the calculated ratios, normalised to unity at room temperature, and shown by the line drawn on the figure.

Table 1

Pu chamber temperature °C	$\frac{Pu}{BF_3}$ *counting rate*
25	1.000±0.015
112	0.997±0.017
323	1.000±0.023
325	0.999±0.016

Figure 5 presents in the same way the ratios obtained with the Pu^{239} and U^{235} chambers at the graphite temperature, along with the calculated ratios. Here the corrections for changes in the U^{235} chamber sensitivity have been applied to the U^{235}:BF_3 ratios.

The results obtained with the U^{233} chamber are not so complete as in the other cases, but are sufficient to show that the fission cross section is close to that of a $1/v$ detector at thermal energies. Some evidence was found to indicate that the U^{233}:BF_3 effective cross-sectional ratio increases by $\sim$ 5% as the temperature is raised to 400°C.

The agreement between the experimental results and those calculated from the current thermal cross-sectional data confirm that the data are correct, that Doppler broadening is negligibly small, and that it is valid to assume that neutrons in thermal equilibrium with a moderator assume a Maxwellian distribution characterised by the moderator temperature.

EXTENSION OF CALCULATIONS

Having confirmed the validity of the assumptions made to obtain the effective thermal cross sections, the calculations were extended to apply to reactor spectra by performing the integrations of Equation 2 with various values of λ at each neutron temperature. For these calculations λ was assumed to become zero at an energy of 5 kT. The term $S(E)$ adopted was assumed to increase linearly, starting from zero at 1 kT and reaching a value of $\lambda/5kT$ at an energy of 3 kT. A smooth connection of the equal ordinates at 3 and 5 kT was then adopted.

The following relation enables the required effective fission cross section to be determined for any λ-value and any neutron temperature:

$$\sigma(eff) = M(T) + \lambda C(T) \qquad (6)$$

Typical values of $M(T)$ and $C(T)$ for Pu^{239}, for U^{235} and for a $1/v$ cross-sectional dependence—normalised to a value of 1000 barns at 0.0253 ev—are given in Table 2.

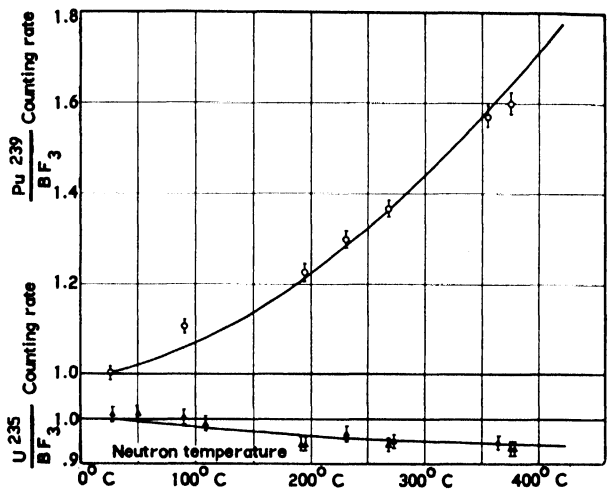

Figure 4. Chambers at 25°C

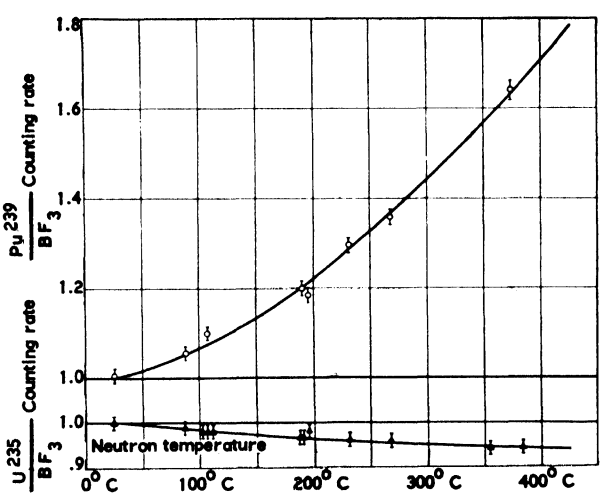

Figure 5. Pu^{239} and U^{235} chambers at graphite temperature

Table II

T, °K	Values of M(T)			Values of C(T)		
	Pu^{239}	U^{235}	1/v	Pu^{239}	U^{235}	1/v
300	657.3	534.5	857.7	2352	675.2	1180
325	646.6	511.7	825.1	2315	649.5	1133
350	634.6	488.7	803.3	2279	628.4	1092
375	630.9	470.2	777.6	2243	605.9	1055
400	631.6	454.1	755.0	2210	587.6	1022
425	633.1	438.6	733.0	2187	571.2	991
450	636.6	424.2	712.2	2151	556.9	963
475	644.5	411.4	694.0	2114	542.5	938
500	653.7	399.6	676.5	2096	529.9	914
550	675.8	377.8	644.2	2030	507.4	871
600	706.7	360.5	618.1	1980	489.8	834
700	773.3	331.3	572.6	1839	454.0	772

ACKNOWLEDGEMENTS

The authors wish to express their thanks to Mr. R. Aves who supplied the fission chambers; to Mr. P. G. Salmon who supplied the BF_3 chamber, and to the many other people who have helped from time to time in this work.

REFERENCES

1. Raffle, J. F. and Price, B. T., P/422, Volume 4, Session 17A, these Proceedings.
2. Lynn, J. E. and Pattenden, N. J., P/423, Volume 4, Session 17A, these Proceedings.
3. Aves, Barnes and MacKenzie, J. Nuclear Energy, *1*, 110 (1954).

Record of Proceedings of Session 17A

WEDNESDAY MORNING, 17 AUGUST 1955

Chairman: Mr. D. J. Hughes (USA)
Vice-Chairman: Mr. D. Popovic (Yugoslavia)
Scientific Secretaries: Messrs. J. Goedkoop and D. J. Littler

P/422 The cross sections of the plutonium isotopes ... J. F. Raffle and B. T. Price
P/589 The total and fission cross section of plutonium ..... B. R. Leonard
P/586 The low energy cross sections of U^{235} ..... V. L. Sailor
P/423 The slow neutron cross sections of the uranium isotopes ..... J. E. Lynn and N. J. Pattenden
P/645 Fission and total cross sections of some heavy nuclides for monochromatic neutrons as measured by a mechanical neutron velocity selector ..... Y. B. Adamchuk *et al.*
P/646 Time-of-flight measurement of the total neutron cross section of uranium-233, uranium-235 and plutonium-239 ..... S. J. Nikitin *et al.*
P/644 Determination of the absorption cross section and of the radiative capture cross section of uranium-233 for pile neutrons ..... G. M. Kukavadse *et al.*
P/354 Slow neutron cross sections of fissile nuclei ..... J. M. Auclair *et al.*
Discussion
P/355 Energy dependence of U^{233}, U^{235}, Pu^{239} fast neutron cross sections ..... D. Szteinsznaider *et al.*
P/594 Some techniques for measurement of fast neutron flux ..... B. C. Diven
Discussion

NOTE: The presentation of results in this session was ordered by topic rather than by paper. Thus some papers served as the basis for more than one presentation; also, a few presentations were based on papers not assigned to this session. Because of this, the complete verbatim record of the session is reproduced here.

Session 17A.1. Low-Energy Pu Cross Sections

The CHAIRMAN: This session is rather complicated because we have a lot of important results to present and the presentation is going to be done in a way designed to keep the material on a particular isotope in the same part of the program. This means that an individual paper will be given in bits. The first section will deal with plutonium but only parts of papers will be given; further parts of these same papers will later be given under U^{235} and U^{233}.

The first paper in this section is P/422 on the cross sections of the plutonium isotopes by Raffle and Price of the United Kingdom, and the paper will be given by Mr. Price.

Mr. B. T. PRICE (UK): The fission cross-section measurements that we have carried out at Harwell have been divided into two main groups of measurements—the absolute measurements at a standard energy of 0.0253 ev, and relative measurements which cover as wide a range of neutron energies as possible and which rely on the absolute measurements for the determination of the scale of the cross section. The absolute measurements consist of a determination of the fission cross section of plutonium-239 and plutonium-241 in terms of the gold cross section. We chose gold as the standard because at the time the work was started there was much better agreement between the values determined in America and Great Britain for the gold cross section than for the more normally used boron cross section. The measurement consisted of measuring the number of fissions in a plutonium chamber specially constructed so that this could be determined with high precision, and determining the activity of a gold foil by absolute counting. Ideally one would make the comparison in a monoenergetic beam of neutrons but because the beams available at Harwell at this standard energy of 2200 metres per second were not sufficiently intense for a good irradiation of a gold foil the measurement had to be carried out in two steps. The plutonium foil was first compared with an auxiliary boron-10 foil in a time-of-flight spectrometer and then this boron foil was later compared with a gold foil in a much more intense thermal

neutron beam. The gold cross section, you will remember, shows in the low-energy region a nearly $1/v$ variation with energy, so that only a small correction was necessary to convert the ratio observed in the thermal beam to the ratio at the standard energy. Raffle determined the fission cross section of plutonium-239 at the standard energy as 702 ± 20 barns, which is in very good agreement with some of the other measurements which will be reported today.

Slide 1 (Fig. 1 of P/422) shows the results obtained for plutonium-239 in the energy region below 1 ev. A large resonance exists at 0.3 ev. These measurements were carried out using three separate types of apparatus. In the energy region below 0.1 ev the apparatus used was a Fermi slow-neutron chopper. For the exploration of the peak a crystal spectrometer was used, and for a part of the peak and the higher energy region up towards 100 ev the 15 Mev linear reactor was the machine employed. Each of these measurements was in terms of arbitrary units and in order to obtain the scale in the region above 0.1 ev it was necessary to overlap the measurements of the different machines and to obtain the normalizing factor from the overlap.

One experimental trouble was observed in the crystal spectrometer measurements. The crystal spectrometer does not give a pure beam of monoenergetic neutrons, but the neutrons of the desired energy are contaminated with neutrons of energies 4 times and 9 times the required energy. At an energy of 0.075 ev, which is exactly a quarter of the energy of the 0.3 ev resonance, the plutonium fission chamber detects the unwanted neutrons with very high efficiency, whereas the boron chamber which was used as the comparison does not. The result of this, if you do nothing about it, is to produce a spurious wobble or peak in the fission cross-section curve at 0.075 ev. This caused quite a lot of trouble in our measurements and it was finally eliminated by passing the beam of neutrons through a plutonium-239 filter before it reached the detectors; the thickness of the filter was chosen so that it was very nearly black to 0.3 ev neutrons while being fairly transparent to 0.075 ev neutrons. In this way the correction was made manageable.

The cross-section curve can be represented by an analytical expression consisting of three terms, two of them being Breit-Wigner terms—the first associated with the resonance at 0.3 ev, and the second term with a resonance occurring at an energy around zero. This latter energy cannot be determined very precisely, but is not very different from zero. The third term is a $1/v$ term. The numbers are given in the paper.

This expression reproduces the experimental data with an accuracy of about 3 per cent over the region 0–0.35 ev and again the same expression holds from 0.6 ev up to about 1 ev. On the right-hand side of the peak the agreement is not very good, which is probably attributable to resolution effects in the

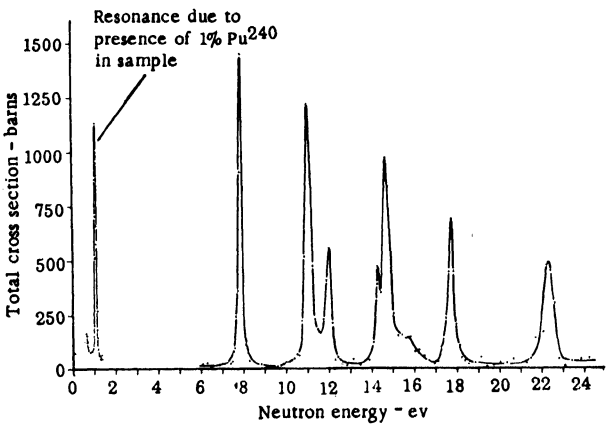

Slide 2. Total cross section of Pu^{239}

measurements.

I will not show a slide of the slow total cross-section measurements which look very similar, but I will say that, at the standard energy of 2200 m/sec, the total cross section has been determined as 1040 ± 30 barns.

At higher energies, a large number of resonances have been observed. Slide 2 shows the results up to 24 ev as determined by the fast chopper. All these resonances have been analysed, but above that energy we have not so far been able to assign resonance parameters to the resonances. I will come back later to the 1 ev resonance, which is in Pu^{240}.

Slide 3 (Fig. 6 of P/422) shows measurements which we have carried out up to 90 ev. So far it has not been possible to obtain a resonance parameter analysis of this data, but the measurements are to be improved in the near future.

In Table I on next page we have summarised the data obtained up to 24 ev on both the fission cross-section and on the total cross-section measurements. The first three columns show the energies of the resonances determined on the various machines for the total cross-section measurement. In the fourth column, the corresponding energies for the fission resonances are quoted; but these are of much lower precision than the other three columns, because in the high energy region it was necessary to work with a very short flight path in order to obtain a sufficient counting rate, and this reduced the accuracy with which the resonance energies could be determined.

In the next two columns we have shown $\sigma_0\Gamma$, the area of the resonance, both for the fission and the total cross-section resonances, and in the last column, by dividing one by the other, we show that within the admittedly not very great precision of some of these measurements, it appears as though the ratio between the fission and the total width does not stay constant. This point will be discussed at greater length by subsequent speakers.

So far I have concentrated on plutonium-239. Plutonium-241 is also thermally fissile, and we have determined the fission cross section at energies up to 10 ev, using a sample of plutonium which had

Table I. Slow Neutron Resonances of Pu^{239}

Resonance energy from total cross section			Resonance energy from fission cross section	σ_0 (fission) $\times \Gamma$ barns-ev	σ_0 (total) $\times \Gamma$ barns-ev	Γ (total) ev		$\frac{\Gamma \text{ (fission)}}{\Gamma \text{ (total)}}$
Fast chopper	Crystal spectrometer	Linear accelerator				Fast chopper	Linear accelerator	
–	Near zero	–	Near zero	–	–	–	–	0.69
0.297 ±0.002	0.300	–	0.297 ±0.010	288	520	0.10	–	0.55
7.85	7.80	7.85	8.0±0.2	72	360	0.067 ±0.010	0.044 ±0.007	0.20
10.95	–	11.0	11.2	140	500	0.13 ±0.04	–	0.28
11.95	–	11.9		35	300	0.09 ±0.03	–	0.12
14.3	–	14.6	15.1	150	60	~0.07	–	0.44
14.75	–				280	~0.04	–	
15.5	–	15.2			–	–	–	
17.75	–	17.7	18.3	75	160	~0.15	0.09 ±0.035	0.5
22.35	–	22.3	22.8	105	150	~0.06	–	0.7
–	–	26.4	26.8	~50	–	–	–	–

been irradiated in the Chalk River pile for a little over two years. See Slide 4 (Fig. 3 of P/422). This sample contained about two atoms of plutonium-239 for every atom of plutonium-241. It was a very mixed sample and it was necessary to subtract the effect of plutonium-239 in some way. This was done by comparing the apparent cross section of the mixture with the cross section of pure plutonium-239. Naturally, when we discovered the extraordinary coincidence that both isotopes have a very nearly identical form for their fission curve in this energy region, we had to make very sure that this really was the contribution from plutonium-241 and was not in some way a spurious contribution from the 239.

For plutonium-240, the data is quite difficult to collect. Plutonium-240 is an even-even nucleus and has, not unnaturally, widely spaced, very large resonances (Table II on this page). A resonance occurs at an energy of 1.05 ev and has a height of rather over 10^5 barns, the width being about 0.03 ev. No other resonance in plutonium-240 has been observed up to an energy of 24 ev, and one of our next tasks at Harwell is to find the next resonance. The thermal cross section of plutonium-240 is of the order of 200 barns, which is the kind of value one would expect if there were no important resonances below the resonance at about 1 ev.

Table II. Slow Neutron Resonances in Pu^{240} and Pu^{241}

	Resonance energy (ev)	Peak cross section (barns)	Width (ev)
Pu^{240}	1.054±0.005	$\sigma_0 = (1.35 \pm 0.15) \times 10^6$	0.029±0.003
Pu^{241}	0.255±0.020	σ_0 (fission) = 1420±50	0.103±0.02
	4.45±0.10		
	5.8		
	6.3		
	7.1		

Finally, by way of summary, we indicate in Table III on this page the cross sections of the various isotopes at the standard energy of 2200 m/sec.

I will not talk any more about what we have done because the details are available in our paper, but I would just indicate very briefly what still has to be done or what still can easily be done. The plutonium-239 work can be extended to an energy of about 100 ev with a good hope of being able to obtain the resonance parameters.

The fission cross-section measurements can also be greatly improved by using the method which is now being developed at Harwell by Farley for measuring effectively the product of the number of neutrons per fission and the fission cross section. If one makes the assumption that the number of neutrons per fission is constant, then by observing the fast neutrons ejected from a thin plate of plutonium one can get over many of the difficulties caused in ionization chamber design by the alpha-ray activity of plutonium. As regards plutonium-240, we hope to work with separated isotopes in the next year, and on plutonium-241 we are going to try and determine the total cross section very soon, using the same mixed sample of plutonium-239 and plutonium-241 which was used for the fission cross-section determination. If we may judge from the accuracy of the results obtainable on the fission cross section, we should perhaps be able to obtain an

Table III

Isotope	Fission cross section (barn)	Absorption cross section (barn)	Notes
Pu^{239}	702±20	1040±30	–
Pu^{240}	–	>170	Contribution from 1 ev resonance
Pu^{241}	935±40	–	–

accuracy on the total cross section in the low energy region of about 5 per cent.

The CHAIRMAN: According to the plan of this meeting, we will now have a series of short reports on plutonium only. These will actually be excerpts from various papers. The first of these short reports is an excerpt from paper P/645 of the Union of Soviet Socialist Republics. The report will be given by Mr. Gerasimov.

Mr. V. F. GERASIMOV (USSR): The measurements of the fission cross sections were made with a mechanical selector. The selector and the associated equipment used in the experiments have been described in detail in paper P/640 by V. I. Mostovoi. I have only a few words to say regarding the experimental procedure and the results obtained.

The variation of the fission cross section with the neutron energy was determined by simultaneously counting the pulses from an ionization fission chamber of special design and a boron counter by means of a double time analyzer. Since the flight paths to the chamber and to the counter were different, the events recorded by the two simultaneously operating channels of both systems referred, in general, to different neutron energies. This difference could be disregarded in the $1/E$ region of the spectrum, but it had to be allowed for in the region of the thermal spectrum. Consequently, measurements in that region were made alternately with the chamber and with the counter, which in this case were located at the same flight path distance, that of 605 cm.

The measurements of the fission cross section of Pu^{239} were made with a 22 mg sample of plutonium.

Slide 5 shows the dependence of the fission cross section on the energy; the curve values are normalized to a cross section of 625 barns at 0.0253 ev. It should be noted that in processing these data we were interested in the variation of the fission cross section rather than in its absolute value. Hence in normalizing the data we used this old and not necessarily accurate value for the cross section at an energy of 0.0253 ev.

The resonances observed in the cross section variation for Pu^{239} are marked in the graph.

Also shown are the parameters of the resonance level at 0.3 ev obtained from experimental data, taking into account the effect of the negative level and Doppler broadening.

Comparison of our fission cross-section data for Pu^{239} with the data from other laboratories shows good agreement up to an energy of 0.5 ev. In the region of the dip (0.5–6 ev) there is a certain divergence, possibly due to the lower accuracy of measurement in this region. At energies above 6 ev, there is probably some displacement of the energy scale where our observations are concerned.

The fission cross-section measurements for Pu^{241} were made with a layer of the material having a total weight of 2 mg. The isotopic composition of the prepared layer was determined from measurements of its total alpha-activity, rate of spontaneous fission, differential alpha-particle spectra and weight. The curve in Slide 6 shows the variation of the fission cross section with the neutron energy, for the material with the isotopic composition indicated on the slide. The curve was normalized to an assumed

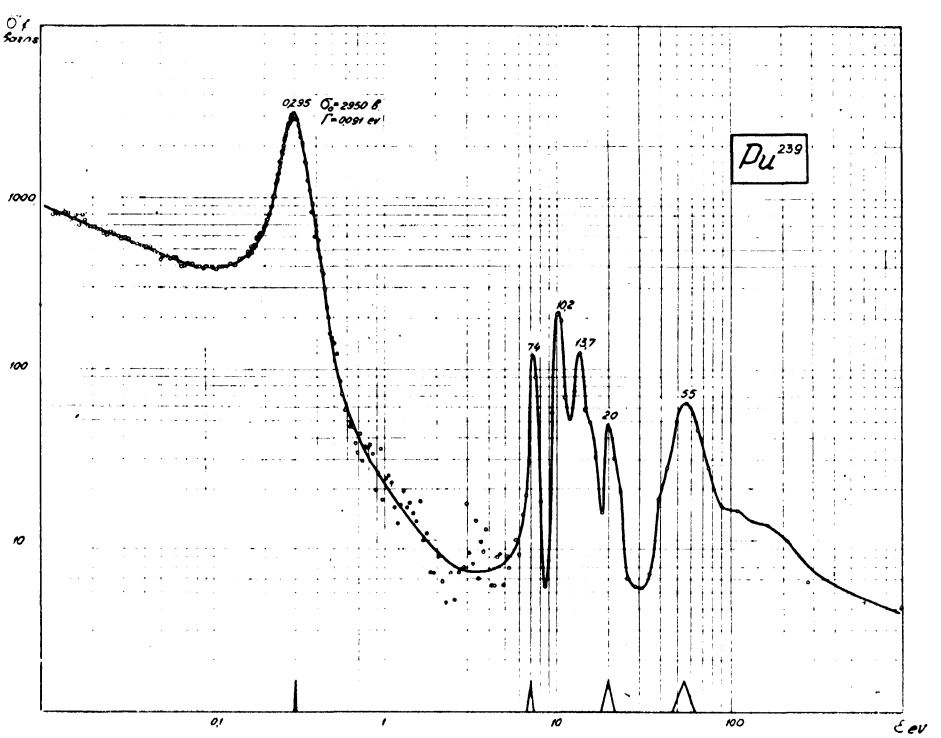

Slide 5

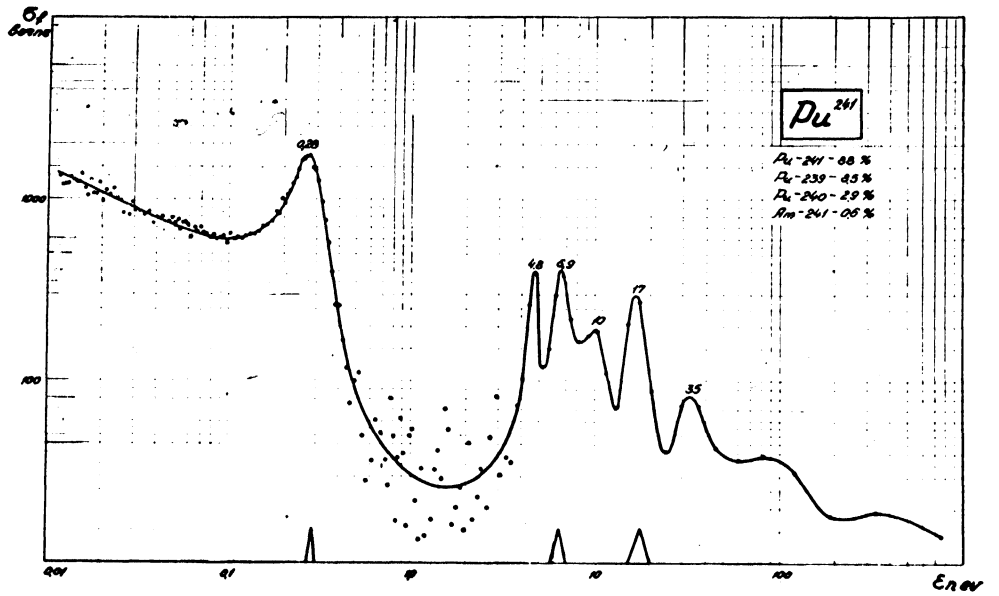

Slide 6

value of 950 barns at 0.0253 ev, based on averaging the values for the isotopes present in the sample of plutonium. These data show satisfactory agreement with the data obtained at Harwell.

In addition, the total cross section of Pu^{239} up to an energy of about 0.5 ev was determined by the transmission method. Metallic specimens of plutonium of different thicknesses were used for the measurements. The experimental results are shown in Slide 7. There is good agreement with the data of other laboratories.

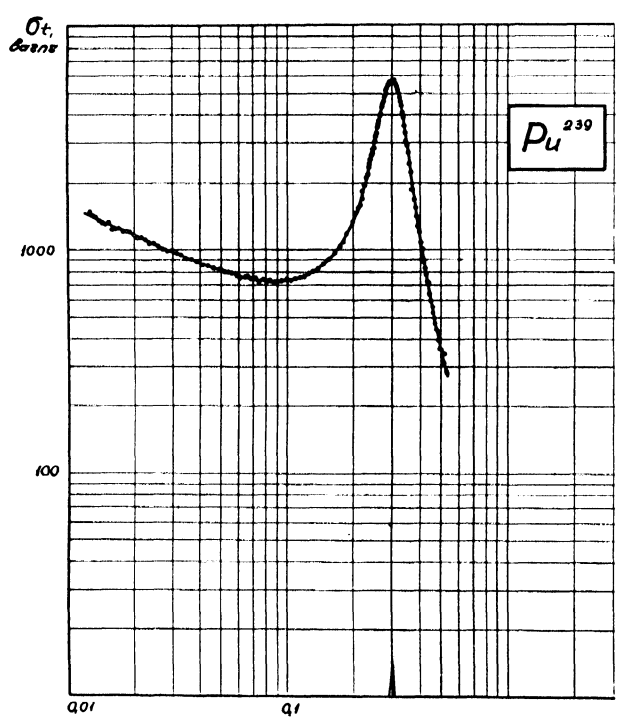

Slide 7

The CHAIRMAN: The next paper to be given is an excerpt from USSR paper P/646 on "Time-of-flight measurement of the total neutron cross section of uranium-233, uranium-235 and plutonium-239" by Mr. Nikitin and others, and will be presented by Mr. Sukhoruchkin.

Mr. S. I. SUKHORUCHKIN (USSR): I shall report on an investigation carried out by Nikitin, Galanina, Ignatiev, Okorokov and the present speaker. We studied the interaction of neutrons with heavy nuclei, using a neutron selector in combination with a pulse-operated cyclotron. We determined the total neutron cross section for a number of isotopes and the energy dependence of the number of secondary neutrons per captured slow neutron in uranium-233, uranium-235 and plutonium-239. The results of the latter part of the investigation were presented at a recent session of the Academy of Sciences of the USSR.

A block-diagram of the selector is shown in Slide 8 (Fig. 2 of P/645). The duration of the deuteron pulse on the internal beryllium target and, accordingly, of the neutron pulse, was varied from 4 to 32 microseconds. A boron-paraffin collimator [see Slide 9 (Fig. 1 of P/645)] was placed in the neutron path between the moderator and the detector. The length of this path—known as the flight path—was varied from 127 cm to 1600 cm, in accordance with the neutron energy region being investigated. In the case of the 1600 cm path, the neutrons were beamed through an evacuated tube, which prevented scattering by air. Enriched gas counters, as well as scintillation counters, were employed for recording the slow neutrons. The counter pulses were analyzed by means of a 128-channel matrix-type time analyzer.

The cross sections of plutonium-239 were measured in the neutron energy interval from 0.01 ev to

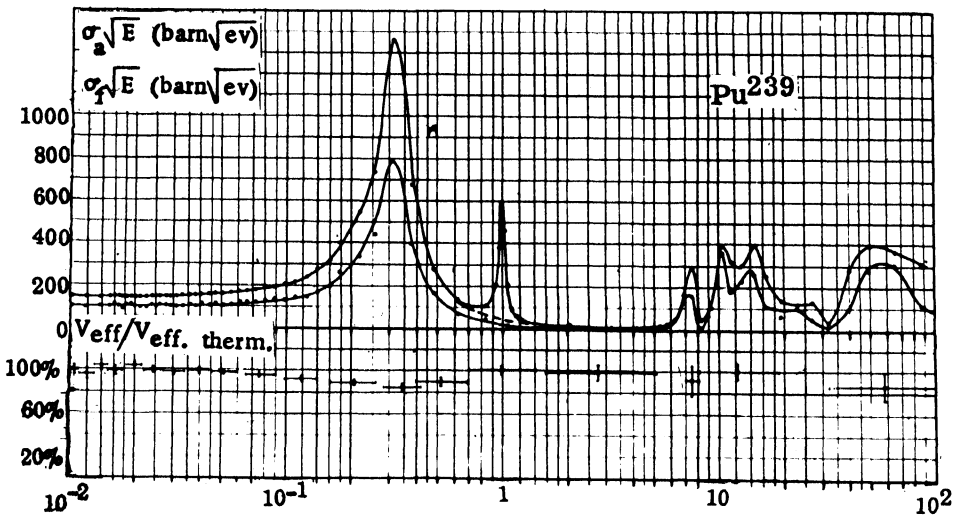

Slide 11

100 ev, as shown in Slide 10 (Fig. 6 of P/645). In the thermal energy region the cross section was found to be 1040 ± 30 barns, which is in agreement with data reported by other laboratories. In the thermal region there is an appreciable contribution from the negative level, which we may describe in terms of the following parameters: $E_0 \sim -1$ ev; $\sigma\Gamma^2 \sim 280$ barns-ev^2 and $\Gamma_f/\Gamma = 0.79$, on the basis of data on the variation of the absorption cross section and the variation of ν_{eff}. I should like to remark that the choice of parameters for the negative level based only on data for the absorption cross section, i.e., without regard to the data for ν_{eff}, does not seem to be altogether consistent.

A number of resonances were observed (Slide 11) in the absorption and fission cross sections of plutonium-239 at energies of about 0.3, 8, 11, 12, 15, 18 and 22 ev. Analysis of the first resonance level yields the following parameters: intensity $\sigma_0\Gamma^2 = 50$ barns-ev^2, width $\Gamma = 105$ mv and $\Gamma_f/\Gamma = 0.61$. The resonance at an energy of 1 ev is due to an admixture of plutonium-240 and is observed only in the capture cross-section curve.

Some additional data on the cross sections of plutonium-239 are to be found in reports presented at the session on the peaceful uses of atomic energy of the Academy of Sciences of the USSR. Questions connected with the energy dependence of ν_{eff} will be discussed at the next session (18A).

Recently we carried out some plutonium cross-section measurements with a longer flight path, about 15 meters. The resolving power was 0.25 μsec/m. Slide 12 shows the results obtained from the preliminary processing of the observed data.

The CHAIRMAN: We shall now hear an excerpt from paper P/354 from France, "Measurement of cross sections of fissile materials for slow neutrons" by Messrs. Berthelot and Vendryes, to be presented by Mr. Netter.

Mr. F. NETTER (France): Slow neutron cross sections of Pu^{239} have been measured at the Saclay pile by means of a crystal spectrometer (Auclair, Hubert, Joly and Vendryes) and by means of a time-of-flight spectrometer (Galula, Jacrot and Netter). Some features of the crystal spectrometer will be described in our contribution on uranium.

The time-of-flight spectrometer, described in paper P/357, has a mechanical chopper with an absorbing layer of boron which makes it possible to explore different energy regions without recourse to relative standards. This is particularly valuable for the 0.3 ev region in which instruments with a layer of cadmium are unable to operate. The resolution in the region of the first resonance of plutonium is about 6 μsec/m at half-height.

The variation of the total cross section of Pu^{239} with energy was determined by means of the crystal spectrometer, the transmission measurements being made on a specimen of plutonium dioxide containing about 0.5 grams of Pu^{239} and having a Pu^{240} content of less than 10^{-3}. The container used was specially designed to accommodate the samples and to minimize the dangers inherent in plutonium. Two thicknesses, differing by a factor of 2.2, were used for the specimen, depending on the energy region.

Because of the difficulties in preparing the thinnest layer, resulting in a lack of uniformity, the transmission at energies below 0.4 ev may have been overestimated. The results (P/354, Fig. 7) must therefore be considered tentative and only indicative of the probable values. The curve has been normalized to the published value of 1065 barns for 2200 m/sec neutrons. In the region of small cross sections we are limited by the amount of material at our disposal.

The following conclusions may be drawn from this study:

(*a*) In general, the curve for the variation of the total cross section σ_t has the same shape as the curve for the fission cross section σ_f.

(*b*) Due to the fact that the resolving power used in the total cross-section measurements was higher

than that for the fission cross-section measurements, we found that there are three distinct peaks situated at 8 ev, 11.5 ev and 15 ev in the group of resonances in the vicinity of 10 ev.

The deposits used in the ionization chambers for the study of the fission cross section of Pu^{239} were prepared by electrolysis and covered with a very thin layer of plastic. Their Pu^{240} content was less than 10^{-3}. Each deposit consisted of about 2.5 mg material spread over an area of approximately 10 cm^2.

The curves of Figs. 5*a*, *b* and *c* (P/354) show the variation of the fission cross section in the interval from 1.4×10^{-3} to 100 ev; the cross sections were normalized to a value of 750 barns for a velocity of 2200 m/sec.

Where the thermal region is concerned, the most important result of the investigation was that it showed the presence of a very sharp resonance at a neutron energy $E_0 = 0.297 \pm 0.003$ ev. The width of the resonance peak at half-height as measured by the time-of-flight spectrometer is about $\Gamma = 0.10 \pm 0.01$ ev.

From the experimentally determined height of the peak, the requisite corrections and the statistical accuracy, the cross sections σ_0 is estimated to be 3000 ± 150 barns. If it is desired to describe the curve by a Breit-Wigner single-level formula, one must first subtract the terms relating to the other resonances observed.

(*a*) The contribution of higher resonances is small because the important resonances occur at about 10 ev and higher. This term is bounded from above by the value of the cross section at 1 ev.

(*b*) On the other hand, the form of the curve indicates the existence of a strong negative-energy resonance near the origin (doubtless $0 \geqslant E_0 \geqslant -0.5$ ev). However, regardless of what parameters are selected for this negative-energy resonance or what parameters are tried for the principal resonance (within the limits imposed by the experimental data after corrections), there still remains a serious disagreement with the Breit-Wigner formula in the region along the wings of the peak. In particular, the cross section at 0.2 ev is too small compared to that at 0.4 ev. The observations were verified with a time-of-flight spectrometer having a resolution of 10^{-2} ev and there can be no question of a doublet.

In the epithermal region, after an interval in which the cross section is small, we find a peak at 11.5 ev marking the beginning of an extended resonance zone, in which the peaks observed in the total cross-section measurements are located.

The CHAIRMAN: The next is United States paper P/589 which actually represents all the work done in the United States on plutonium at several laboratories. The paper was written by Mr. Leonard and the excerpt will be presented by Mr. Gast.

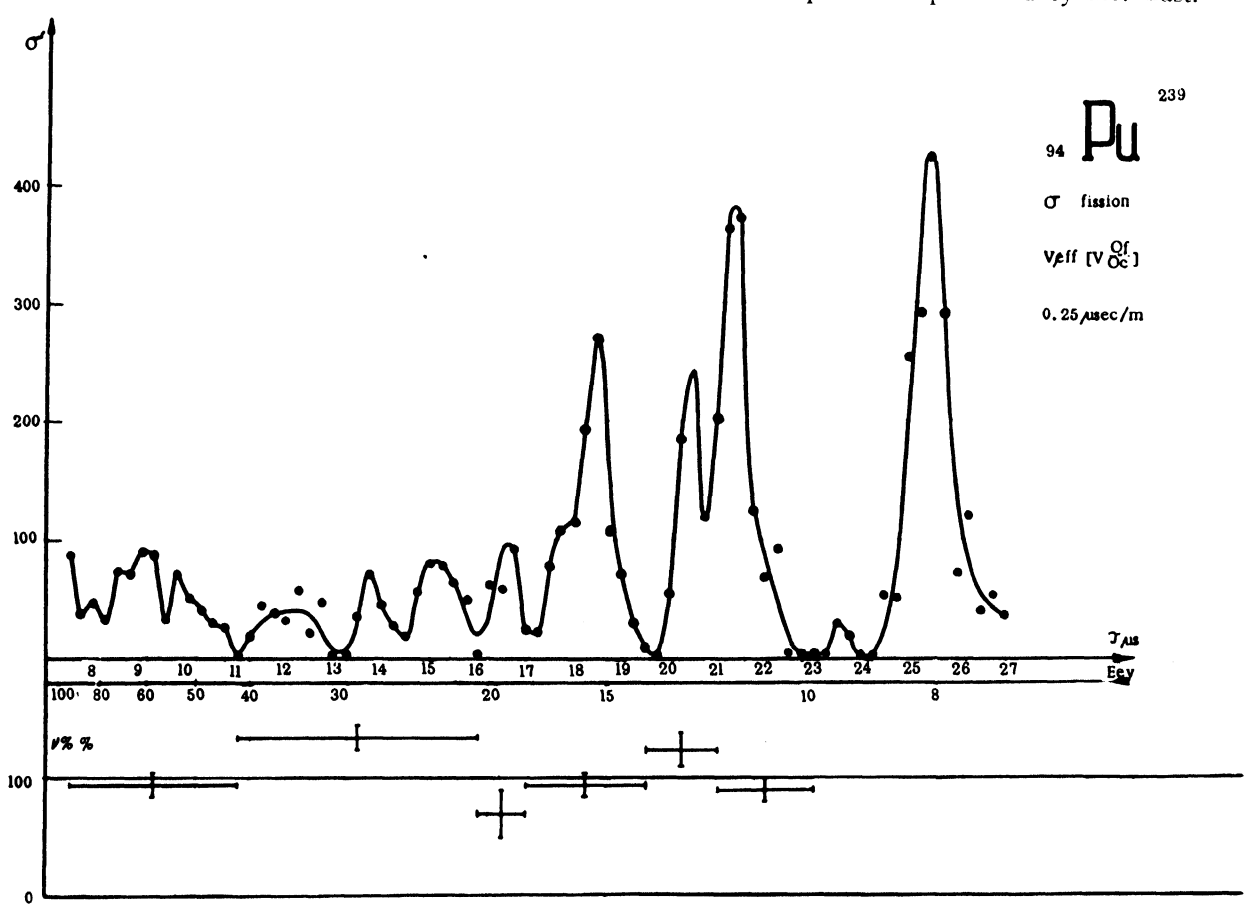

Slide 12

Mr. P. GAST (USA): I shall present a brief summary of the paper by Leonard which is itself a summary of the results obtained by many workers.

In the United States, the total cross section of plutonium-239 has been determined for energies up to 5 ev by transmission measurements using pulsed cyclotron neutron velocity selectors at Columbia University and the Los Alamos Laboratory. A value for σ_{total} of 1074 ± 15 barns has been established for 2200 m/sec neutrons. Other details of the measurements in this range are given in the published version of this paper. In the course of this work, some information was also obtained on the strong resonance of Pu^{240} at 1.06 ev.

Total cross-section measurements have been made in the energy region from 5 ev to 100 ev with the fast chopper time-of-flight spectrometer at the Argonne Laboratory and also with the pulsed cyclotron at Columbia.

The Argonne data are shown in Slide 13 (Fig. 3 of P/589). Resonances are shown at 7.8, 10.9, 11.9, 14.2, 14.6, 17.5, 22.2, 26.4 ev plus more resonances at higher energies. The resonance at 18.7 ev is due to tungsten in the target assembly. The resolution in these measurements was 0.2 microsecond/meter. An analysis of these data by Le Blanc at the Argonne Laboratory indicates that the levels at 11.9, 14.2, 17.5 and 22.2 ev have total widths of only about 0.03 ev. This width is of the same order of magnitude as the gamma width, 0.04 ev, in the low-level resonance at 0.3 ev.

Measurements have been made in the range from 1 to 6 kev with a Van de Graaff generator. The total cross section is found to decrease steadily from 19 barns to 12 barns over this energy range.

Fission cross-section measurements have been made from 0.020 to 2.5 ev with a neutron crystal diffraction spectrometer at the Hanford site. The fission rate of a thin plutonium foil was compared to the alpha counting rate of a thin boron foil. Both foils were mounted in a double-chambered parallel-plate ionization chamber in the same neutron beam. Since the foil weights were not known accurately, the results were normalized to a value of 750 barns at 2200 m/sec. The complete results are given in the published text of this paper. Analysis of the data for the fission cross section has been carried out in terms of the Breit-Wigner formula to obtain three terms:

1. A term $25E^{-1/2}$ barns due to higher levers.
2. A single level at negative energy.
3. The resonance parameters for the positive energy level were found to be $E_0 = 0.299$ ev, $\sigma_0 = 3190 \pm 50$ barns and a width of 0.102 ± 0.004 ev.

The variation of the fission cross section above 2.5 ev has been measured with a pulsed cyclotron at Los Alamos, but the results show much poorer resolution than the results obtained in the United Kingdom and in the USSR.

I should like to remark finally that the formulae derived for the low-energy total and fission cross sections are not in good agreement with the data in the wings of the 0.3 ev resonance indicating, possibly, some additional complications of structure, or interference between levels.

The CHAIRMAN: At this point, we have a short contribution based on P/641. that has been added to the program; it also, of course, is on plutonium isotopes. It is from the Union of Soviet Socialist Republics, giving mechanical velocity selector results, and will be presented by Mr. Vladimirski.

Mr. V. V. VLADIMIRSKI (USSR): Measurements of the total cross section of two specimens of metallic plutonium-239 with a small content of plutonium-240 were made on the spectrometer the design of which was described in Session 15A.

Measurements in the energy range from 7 to 25 ev were made with curved slits, a channel width of 1 μsec and a flight path of 19 m. The resolving power was about 0.08 μsec/m. Satisfactory results (Slide 14) were obtained for the following levels: 7.85, 10.95, 11.85, 14.46 (A single level is shown in the figure but detailed study of the experimental points showed that this is a double level.), 14.70, 15.40, 17.70, 18.50 (within the limits of the statistics), 22.35, 23.70 (within the limits of the statistics), and 26.36. The location of the levels is in good agreement with the data reported by the Argonne and Harwell laboratories. The final determinations of the intensity of the levels have not yet been made.

In the region above 30 ev (Slide 15) the total cross section was measured with straight slits, resolving power about 0.1 μsec/m. We obtained a more detailed spectrum than the Argonne Laboratory, but did not attain complete resolution of the levels.

The CHAIRMAN: This finishes the series of reports on plutonium but, according to the schedule, the discussion of these papers will not take place now. There will be discussion at the end of the presentations on U^{235} and U^{233}.

Session 17A.2. Low-Energy U^{235} Cross Sections

The CHAIRMAN: We will now proceed to the papers on U^{235}. The first paper will be P/586 from the United States—again, it represents the work of a number of laboratories—and it will be presented by Mr. Sailor.

Mr. V. L. SAILOR (USA): The purpose of this paper is to review and interpret the slow neutron cross sections of U^{235}. The paper, of course, contains results only from the United States. The data from other nations will be presented in the papers which immediately follow this one. Many persons have participated in these measurements. May I call your attention to the co-authors listed on the first page of the published paper. Because of lack of time it will not be possible to give recognition for individual contributions. You may refer to the bibliography contained in the paper for details about who did which measurement.

The cross section of U^{235} contains many weak and

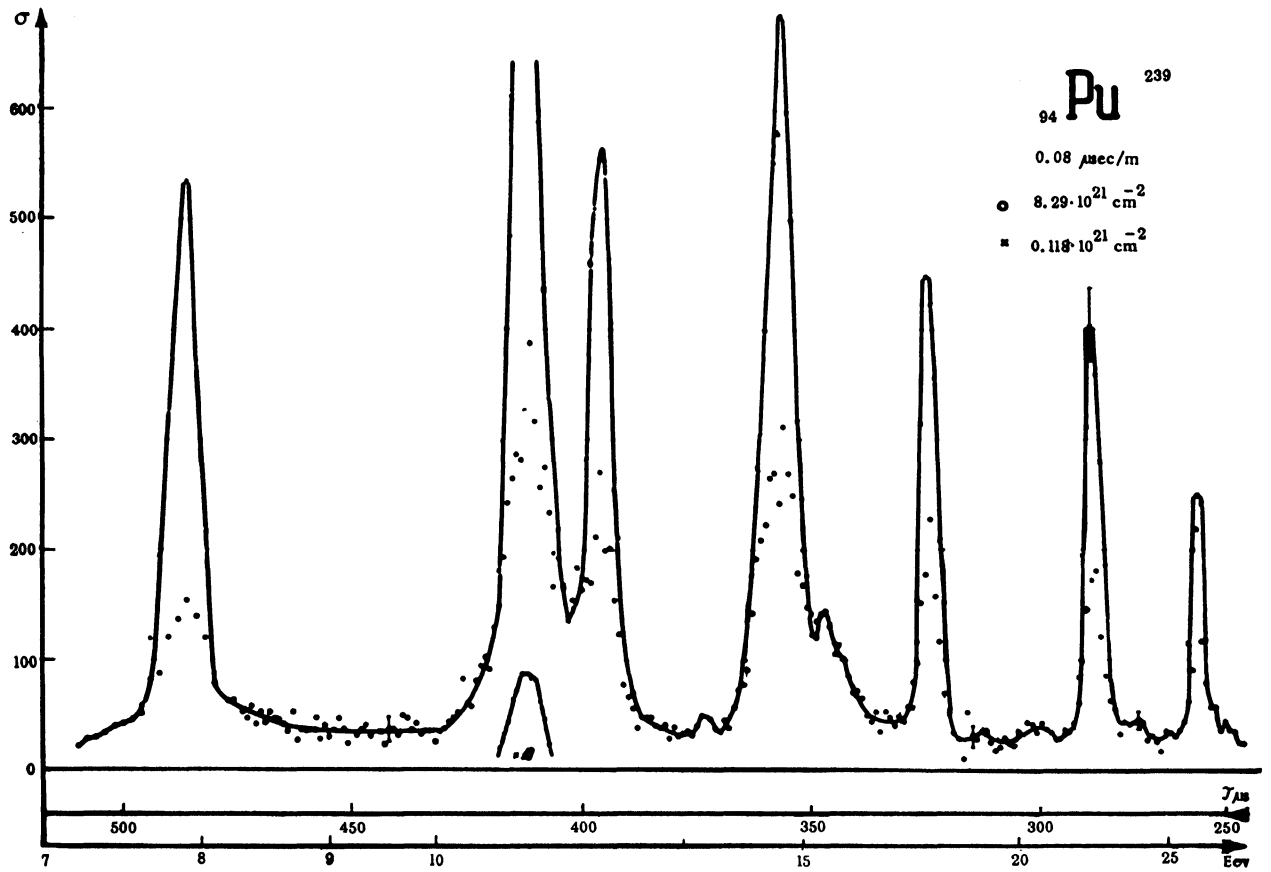

Slide 14

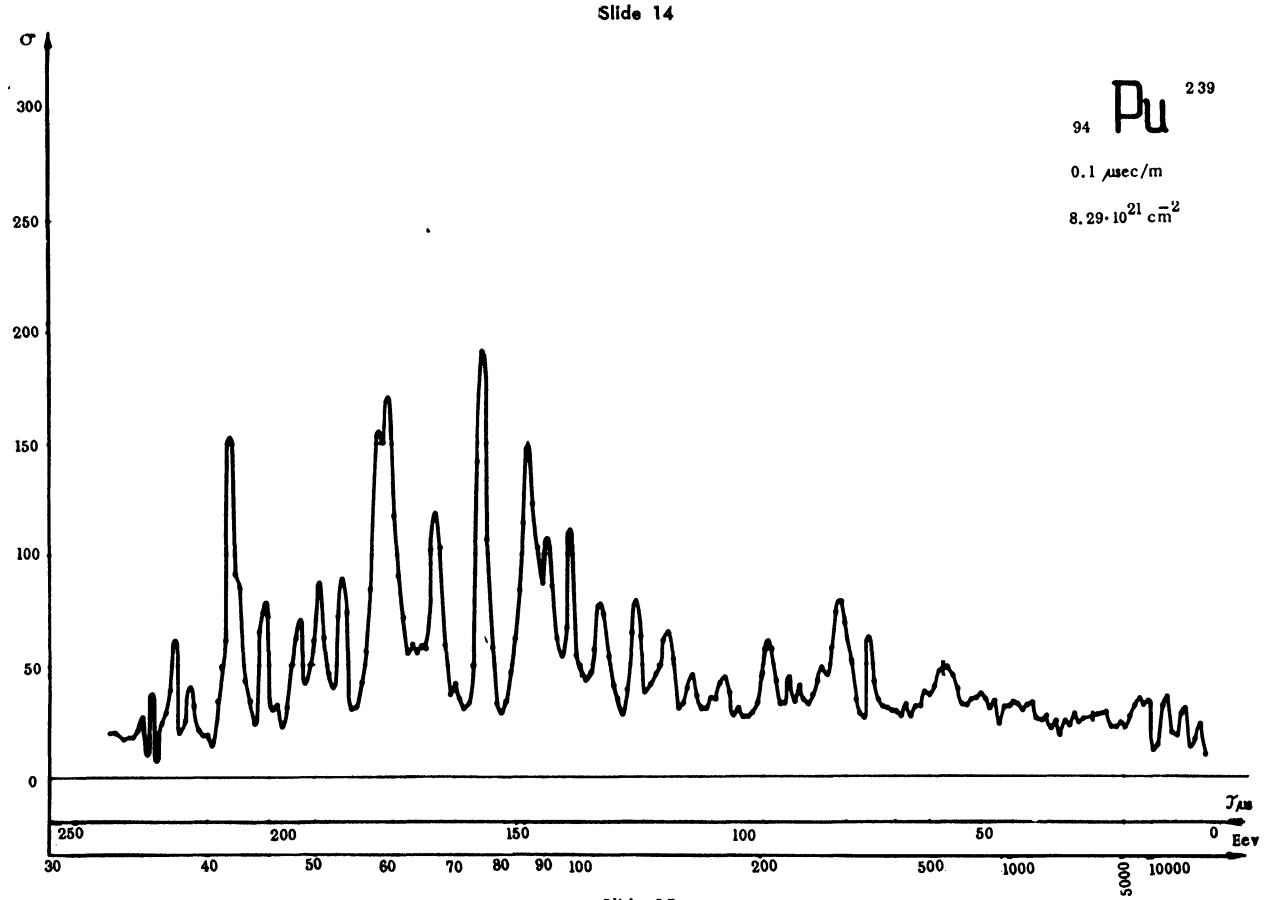

Slide 15

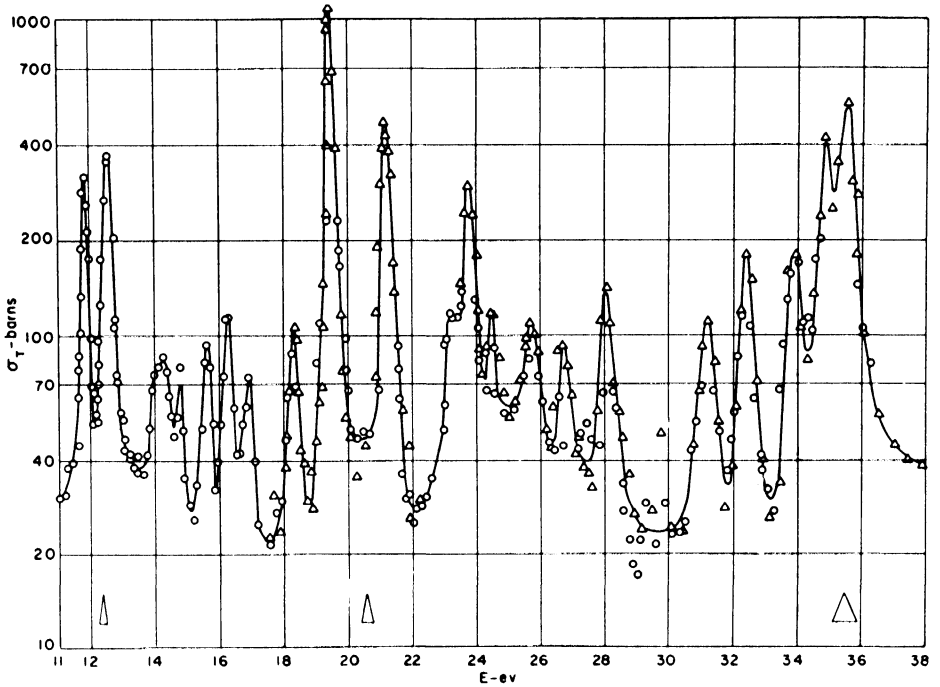

Slide 19

closely spaced resonances. The average spacing between levels is only 0.7 ev. Compared with isotopes of other heavy elements the spacing in U^{235} is quite small, and consequently, the resonance spectrum is unusually complicated. Further complications in the interpretation of the spectrum are introduced, of course, by the occurrence of fission. A quantitative understanding of such a complicated spectrum has been made possible only because of the great refinement which has occurred in measuring techniques during recent years. In particular, I refer to the great improvements which have been made in the resolution of spectrometers.

Let us first examine samples of available data and afterwards attempt to interpret the observed curves in terms of theoretical formulae. Because of the shortage of time only a small fraction of the available data can be shown.

The values of the total and fission cross sections at thermal energies have been very accurately determined in the United States. These results, however, were the subject of another paper, P/832, presented yesterday afternoon (Session 16A) by Mr. J. A. Harvey, so I will not repeat these results.

The first slide, Slide 16 (Fig. 1 of P/586) shows the total and fission cross sections at very low energies. These particular data were obtained with a crystal spectrometer at the General Electric Company Hanford Works. Similar curves have been obtained with many other instruments. A weak resonance at 0.3 ev is plainly evident. In addition, the curve at lower energies departs significantly from a $1/v$ dependence, indicating the presence of a nearby negative energy resonance or bound level.

Slide 17 (Fig. 2 of P/586) shows the total cross section up to 5 ev. These data were obtained with a crystal spectrometer at Brookhaven National Laboratory. I think the complexity of the uranium spectrum is evident from this curve. I would like to call your attention particularly to the first two levels and the region which lies between. We will discuss this region in greater detail later. The resonance at 2 ev proves highly useful because it provides one means of estimating the radiation width in U^{235}.

Slide 18 (Fig. 3 of P/586) shows the total cross section between 5 and 10 ev taken with the same crystal spectrometer. Resonances in U^{234} and U^{238} which were present in the sample prevented observation in the regions where data are not shown. We have obtained data with highly pure U^{235} samples to fill in those regions and some structure occurs between 5 and 6 ev. I am sorry I have no slide to show you of these data.

Slide 19 should be substituted for Fig. 4 of paper P/586. This gives the total cross section in the range from 11 to 38 ev. The circles on the slide were obtained with the Brookhaven fast chopper. The triangles which do not appear in the paper are data which were recently obtained by Fluharty and Simpson of the Phillips Petroleum Company in Idaho Falls, Idaho, using a fast chopper.

Between 40 and 100 ev, new data have recently been obtained with the Phillips Petroleum and the Brookhaven fast choppers which substantially improve the data in this region. Unfortunately, I have no prepared slide to show you of these results, but they appear in the addendum to the cross-section compilation BNL–325.

At energies above 100 ev, the existing spectrometers do not have sufficient resolution to resolve

completely the resonance structure and at about 500 ev the Doppler broadening of the resonances becomes large enough to cause the resonances to overlap. The cross section above 500 ev, therefore, appears to be a quasicontinuum. Variations in the cross section above this energy correspond to fluctuations in the average spacings and strengths of levels rather than to individual resonance structure.

Slide 20 (Fig. 7 of P/586) shows the fission cross section up to 100 ev. These data were obtained at Columbia University on the pulsed cyclotron. A close examination of this curve shows that all resonances which appear in the total cross section appear also in the fission cross section. This rule is true, at least up to 10 ev, the range over which instrument resolution permits a detailed comparison. It appears from these data that all resonances in U^{235} contain some fission and some capture. Note, however, that the ratio between capture and fission is not constant, but varies from resonance to resonance.

Measurements of the scattering cross section of U^{235} prove very difficult because of the small amount of scattering relative to capture and fission. In general, the resonances in U^{235} are too weak to give measurable amounts of resonance scattering, hence, the scattering cross section is due almost entirely to potential scattering. An important exception, which I will discuss more fully in a moment occurs below 1 ev where there is appreciable resonance scattering from a bound level.

Having seen these brief samples of data let us now turn our attention to the important question of interpretation of the data. The primary objective of the measurements is to obtain quantitative values of the various parameters which describe the resonance structure. These parameters have very important significance in nuclear physics, and of course can be used directly in important reactor calculations relating to reactor design. The ultimate test of the quality of the experimental data is the precision of the parameters that can be derived from the data.

In analyzing the resonance structure in U^{235}, it has been assumed that each resonance can be described by the Breit-Wigner single-level formula, and that the net cross section can be obtained by taking the sum of the contributions of all resonances. Now, of course, we know that the single-level formula is not strictly valid when applied to a complex resonance structure. However, the deviations are quite small, and at the end of my talk I shall discuss what evidence there is for deviations from the single-level formula in the case of the U^{235} spectrum.

For each resonance the total cross section is the sum of the partial cross section:

$$\sigma_{ti} = \sigma_{ci} + \sigma_{fi}$$

where scattering has been neglected. The form of the partial cross section is:

$$\sigma_{ci} = \left[4\pi\lambda\lambda_0 \frac{g\Gamma_n\Gamma_\gamma}{4(E - E_0)^2 + \Gamma^2} \right]_i$$

The net cross section would be the sum over all resonances plus potential scattering:

$$\sigma_t = \sigma_p + \sum_i \sigma_{ti}$$

For each resonance we seek the following set of parameters:

$$E_0(\lambda_0),\ g,\ \Gamma_n,\ \Gamma_\gamma,\ \Gamma_f$$

It turns out that for the present data g cannot be assigned but the product $g\Gamma_n$ is always obtained. However, $g \approx 1/2$, so this is not too serious a matter for most purposes. Of course, from the theoretical point of view it would be highly desirable to know the angular momentum associated with each resonance. Unfortunately, in the case of U^{235} none of the usual methods for measuring g appears to hold much promise.

The most accurate data available for analysis are the total cross-section data. This results from several basic experimental factors with which most of you are familiar. For this reason, most of the analysis of U^{235} has been carried out on total cross-section data, and the partial cross sections have been used only to supplement our information.

The parameters which can be obtained from the total cross section are E_0 (λ_0), $g\Gamma_n$ and Γ, where the total width is the sum of the partial widths. Note, however, that the neutron width is much smaller than either of the other two partial widths, and thus can be neglected in this sum. For this reason we can say that the fission width equals the total width minus the radiation width. Experience with other isotopes has shown that the radiation width is approximately a constant from resonance to resonance —fluctuations in this quantity are much less than 20 per cent. Therefore, if we can obtain an estimate of Γ_γ for U^{235}, we can, without much error, use the total cross-section data for calculating the fission widths.

There are two resonances in U^{235} for which the available data permit accurate estimates of Γ_γ: the resonance at 0.3 ev, for which one has very complete total and fission data; the 2 ev resonance has a very small fission component. The average Γ_γ obtained from these is $\overline{\Gamma_\gamma} = 29.5 \times 10^{-3}$ ev.

The total cross section curves were analyzed by two methods: (1) the "area" method, which is particularly useful at higher energies where instrument resolution is not too good, and (2) "shape" analysis, which can be used only in regions of very good instrument resolution, that is, below 10 ev. Both methods have been extensively described in the literature, and I shall not attempt to describe them here. The results obtained are summarized in Table I of the paper. The parameters in this table should not be considered as final values. They are in a constant state of improvement. Already some of the data on which these values were based is obsolete. Altogether some 40 resonances have been analyzed up to the present time. I am sure that during the

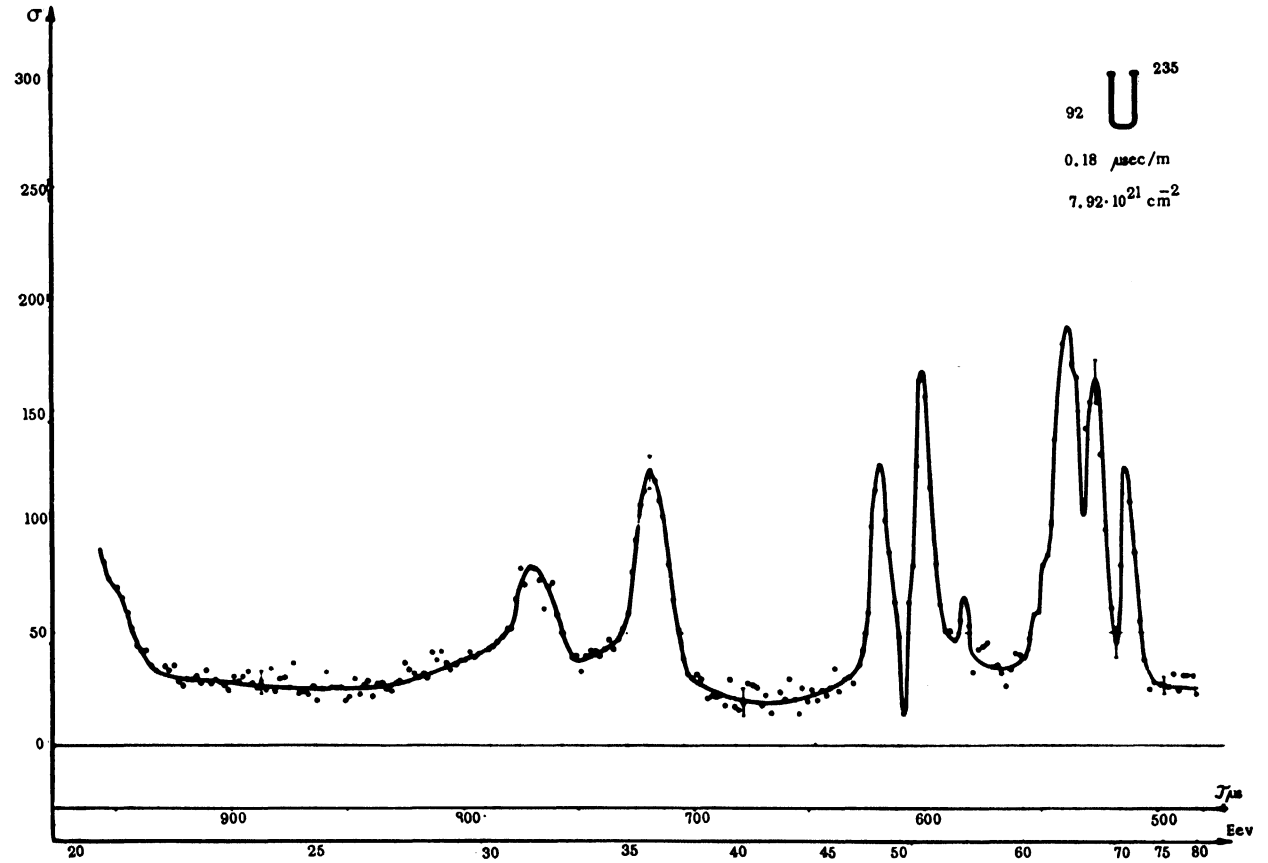

Slide 22

next year there will be substantial improvement in the precision of these parameters.

One of the most difficult regions in the cross section to understand is the region below 1 ev, as was previously pointed out to you. This, of course, is the region of greatest importance to reactor design.

Analysis of the region below 0.1 ev by J. A. Harvey and H. Palevsky of Brookhaven National Laboratory first demonstrated that the shape can only be explained by the presence of a weak negative resonance close to zero energy. This resonance has little influence outside the thermal region. Parameters for this resonance are listed in Table I of the paper P/586.

An additional negative resonance is needed to account for the magnitude and shape of the cross section between 0 and 2 or 3 ev. Careful curve-fitting yields parameters for this negative resonance which are listed in Table I. It is somewhat disturbing that the strength of this resonance turns out to be unusually large. It is stronger than any resonances observed in the positive energy region. The existence of this strong level, however, is supported by scattering measurements in the region 0.1 to 2 ev. A negative resonance having such a large reduced neutron width will give rise to appreciable resonance scattering in the positive energy region. Table II of the paper compares the observed scattering cross section to cross section calculated from the parameters of the negative resonance. Agreement is quite good. Some 20 points in addition to those listed in Table II have been measured and the agreement remains good.

One final curious feature about the cross section of U^{235} should be mentioned. At the start of the talk I mentioned that the region between the first two resonances was difficult to understand. The cross section appears to be too large in this region. Another fact relates to this—it was noted in the crystal spectrometer data that many of the U^{235} resonances did not have the proper symmetrical shape. The asymmetry could not be attributed to the instrument because resonances in other elements measured at the same time did not show this effect. Furthermore, the resonance at 2 ev which contains very little fission was quite symmetrical. It appears that the asymmetry is real and is associated with fission in U^{235}.

Efforts were made to explain the asymmetry by postulating weak unresolved resonances close by the observed peaks. Such an explanation, however, is incompatible with the observed shapes. Finally, an attempt was made to explain the asymmetry in terms of interference between levels, that is through the use of a many-level formula rather than a single-level formula. The addition of an interference term to the Breit-Wigner formula does indeed give a satisfactory fit to the data.

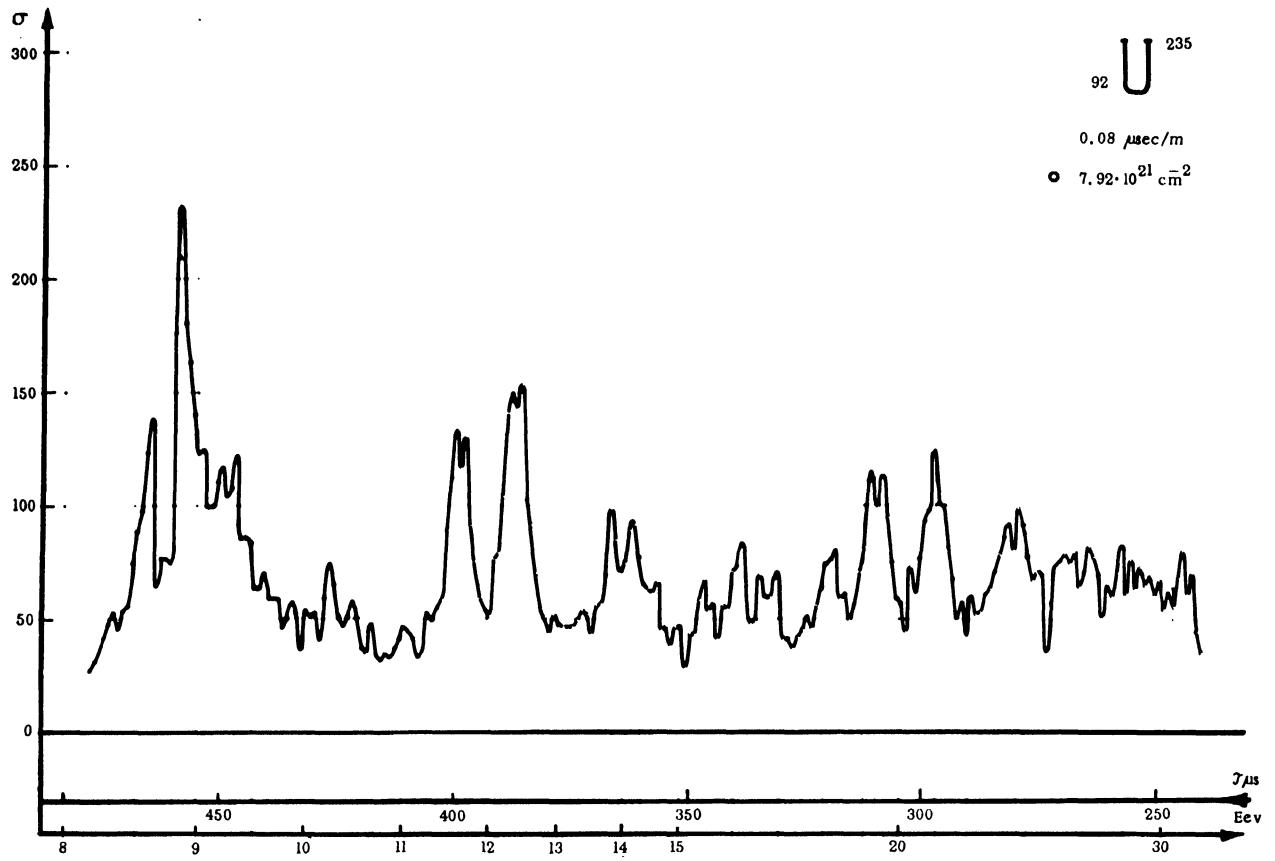

Slide 23

This is illustrated in Slide 21a (Fig. 11*a* of P/586) which shows the 1.14 ev resonance. The solid curve is the best fit obtained with a single-level formula plus an interference term. You are referred to the paper for details about the mathematical form of the interference which was used in the calculation. The magnitude of the interference term can better be seen in the next slide.

In Slide 22b (Fig. 11*b* of P/586) the single-level contribution has been subtracted away from the observed points. Curve *C* is the interference term used in the curve fitting. Curve *D* was computed from the many-level formula using the parameters in Table I and assuming that the −1.4, +0.29 and +1.14 ev levels are interfering. It is shown merely to illustrate that the magnitude of the asymmetry can be reasonably accounted for by interference.

Thus the shapes of several of the resonances in U^{235} make it appear quite likely that measurable departures from the single-level formula occur in the fission cross section, and that these departures arise from interference between resonances. Since this would have some theoretical significance it is important to obtain a more rigorous experimental test of this point. Such experiments are now being planned.

It should be noted that the presence of interference will introduce no large changes in the parameters of Table I of the paper.

The CHAIRMAN: Next Mr. Vladimirski will speak again on P/641.

Mr. V. V. VLADIMIRSKI (USSR): We investigated a specimen of uranium with an appreciable content of U^{234} and U^{238}. The total cross-section spectrum in the 2–8 ev region was determined with the instrument having a resolving power of 0.18 μsec/m. Curved slits were used. The results obtained (Slide 22) are in good agreement with those of other laboratories. The 5.2 ev level pertains to U^{234}; the 6.8 ev level to U^{238}. The 4.5–4.7 ev region is a convenient region for isotopic analysis of specimens with the aid of a neutron spectrometer.

In the 8–30 ev region (Slide 23) the specimen was studied using curved slits and a channel width of 1 μsec. Here we did not obtain complete resolution of all levels inasmuch as the spectrum of U^{235} is very complex.

In the region above 30 ev (Slide 24) the observed peaks probably represent groups of levels rather than individual levels.

If the admixture of U^{238} and the statistical errors are taken into account, our results in the region of high energies appear to be in agreement with the data of the Brookhaven and M. T. R. Laboratories.

The CHAIRMAN: The next short communication on the U^{235} low-energy cross sections is a USSR excerpt of P/645, given by Mr. Gerasimov.

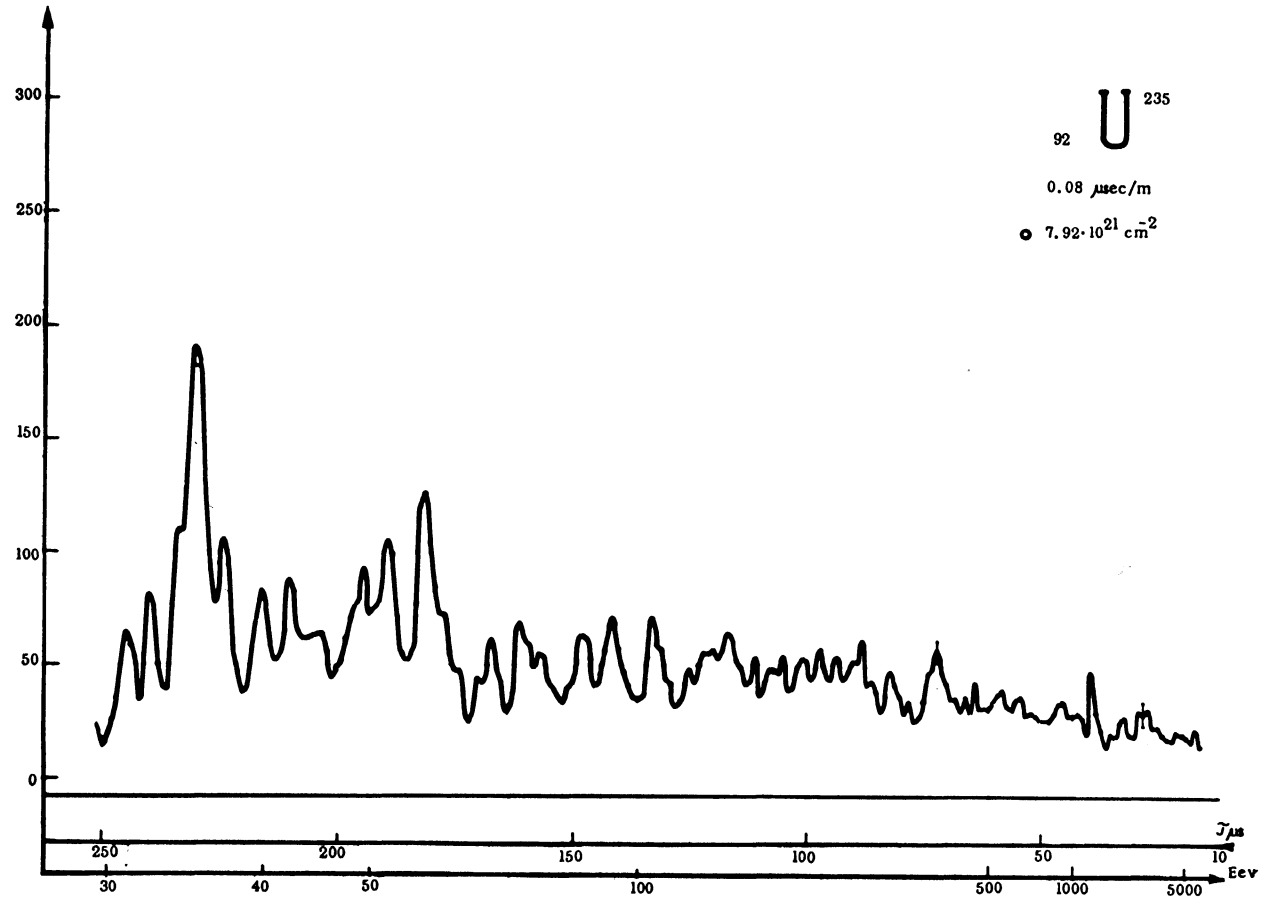

Slide 24

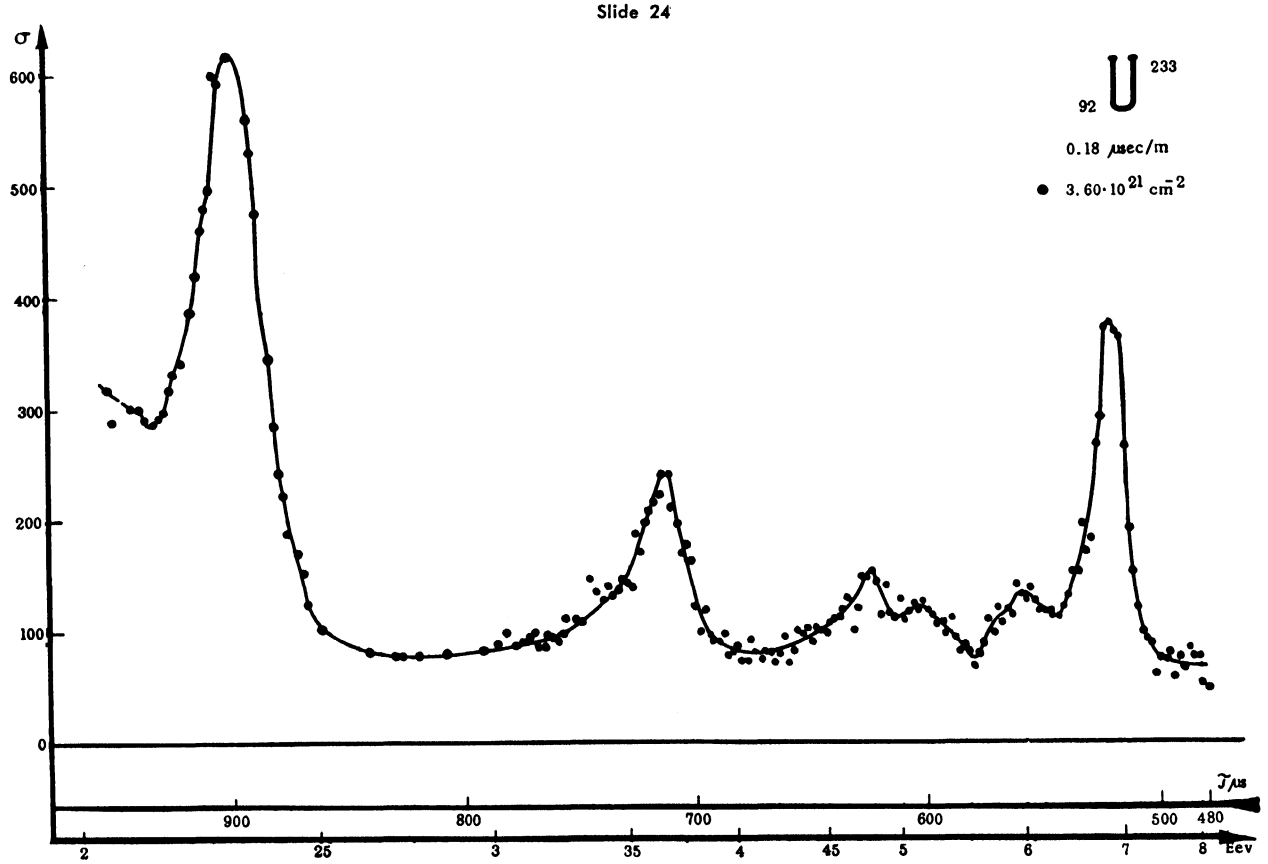

Slide 25

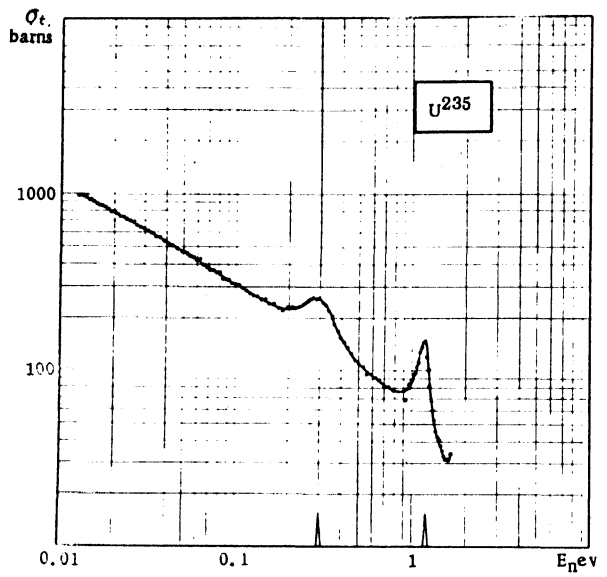

Slide 26

Mr. GERASIMOV (USSR): In my previous communication on the fission cross section of Pu^{239} I described the measurement procedure; hence I will now confine myself to an exposition of the results obtained.

Slide 25 shows the energy dependence of the fission cross section of uranium-235. The curve is normalized to a value of 540 barns at a neutron energy of 0.0253 ev. At energies from 1 to about 40 ev our values appear to be somewhat low in comparison with data from other laboratories. There also appears to be some displacement of the values along the energy scale. For the region above 40 ev our data are in satisfactory agreement with the results obtained in other laboratories.

In addition to measuring the fission cross sections we determined the total cross section of U^{235} by the transmission method up to an energy of about 1.5 ev. For our measurements we used specimens of metallic uranium of different thickness. The specimens were placed between the selector and the neutron detector. The neutron flight path was 6.3 meters. The data obtained are shown in Slide 26. They are in good agreement with results reported by other laboratories.

The CHAIRMAN: The next contribution on the low-energy cross sections of U^{235} is again from the USSR and represents work done with the pulsed cyclotron (P/646). It will be presented by Mr. Sukhoruchkin.

Mr. SUKHORUCHKIN (USSR): We measured the cross section of uranium-235 in the energy interval from 0.01 to 100 ev using a selector with a pulse-modulated cyclotron. The variation of the total cross section of U^{235} with the neutron energy is shown in Slide 27 (Fig. 5 of P/646). The results were corrected on the basis of the data on the isotopic composition and the total cross-section data for U^{238} obtained with the same selector. The cross section in the thermal region proved to be equal to 710 ± 20 barns, which is in agreement with values in the literature.

The cross section of U^{235} in the thermal region is determined by negative energy resonances. If we assume that there is a single negative (bound) level we obtain the following values for this level: $E_0 = -1$ ev, $\sigma_0\Gamma^2 = 450$ barn-ev^2 and $\Gamma_f/\Gamma = 0.83$. The magnitude of Γ_f/Γ for the nearest positive resonances proves to be smaller than that of the negative resonance. The drop in Γ_f/Γ between the 0.3 and 1 ev resonances is somewhat greater (about 15 per cent) according to our data than reported by Sailor *et al.* In the region of high energies U^{235} shows a large number of weak resonances (Slide 28); the average spacing between levels is only about 0.7 ev. The average value of the ν_{eff} for the 1.5–3.5 ev and 4–7 ev regions is about 55–65 per cent of that at thermal energies. For the 8–10 ev interval ν_{eff} increases to 90 per cent as compared with the value for the thermal region. The resonances with the low-

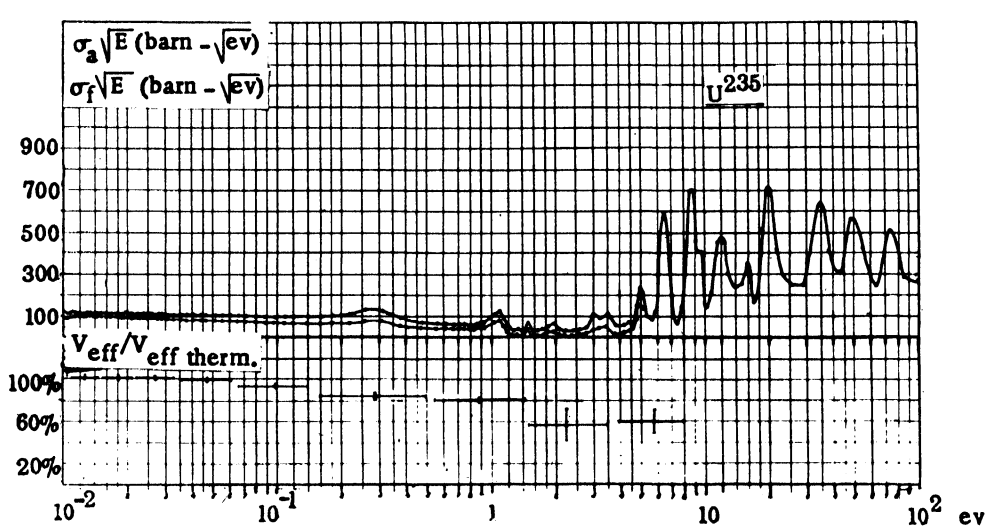

Slide 28

est value of Γ_f/Γ occur at $E_0 = 2.5$ and 6 ev. The results, which we have earlier reported at a session of the Academy of Sciences of the USSR, are in agreement with the data in the report by Sailor and his collaborators. The value of σ/E in the region above 6 ev is on the average 3–4 times greater than in the thermal region.

The CHAIRMAN: The next communication is again based on P/354 and deals with the fission cross section of U^{235}. This will be given by Mr. Vendryes.

Mr. G. VENDRYES (France): The investigations which have been carried out in France on U^{235} in the range of low energies were concerned primarily with measurements of the fission cross section. However, before presenting the results obtained along this line, I would like to show you a curve depicting the variation of the total cross section of natural uranium in the 0.03 to 1.4 ev energy range.

The curve in Slide 29 (Fig. 3 of P/354) was obtained with the Saclay crystal spectrometer, using a lithium-fluoride crystal as monochromator, by reflection from the [111] planes. The notable fact here is the presence of two small humps at 0.29 and 1.2 ev which correspond to the first two resonances of uranium-235.

Investigations of the fission cross section of U^{235} as a function of the neutron energy were carried out in parallel by Miss Galula, Mr. Jacrot and Mr. Netter using the time-of-flight spectrometer and by Mr. Auclair, Mr. Hubert, Mr. Joly and myself using the crystal spectrometer.

Here is a picture of the latter instrument which we purposely made of simple design [Slide 30 (Fig. 2 of P/354)].

Its principal features have already been described in paper P/354. Hence I will only note here that the resolving power generally used in the fission cross section studies is 6 microseconds per meter at energies below 1 ev and 1.5 microseconds per meter in the 1 to 20 ev range (width at half-height).

The detector for the measurements on U^{235} consists of a fission chamber containing a large number of thin deposits of natural or enriched uranium. A monitor containing boron, placed in the scattered beam, permits comparing the variation in the fission cross section with that for the reaction $B^{10}(n, \alpha)Li^7$.

The results obtained so far, which we consider purely tentative, are shown in the following curves:

As shown in Slide 31 (Fig. 8*a* of P/354), below 0.2 ev the cross section, normalized to an arbitrary value of 540 barns at 0.025 ev, decreases more rapidly than in inverse proportion to the velocity of the neutrons, which would indicate the existence of a negative resonance. To calculate the mean efficient cross section in the quasi-Maxwellian spectrum of the Saclay pile one should apply a factor of 0.98 to the value obtained on the assumption that the $1/v$ law is valid.

In the region extending to 20 ev, see Slide 32 (Fig. 8*b* of P/354), we have observed a series of resonances situated at 0.29 ± 0.01 ev, 1.1 ± 0.05 ev, 3.4 ev, 6.8 ev, 9 ev and 14 ev.

Since the resolving power we had to use did not permit of complete separation of these resonances, we did not think it worthwhile at the present stage of the investigation to attempt an analysis of these resonances.

In considering only the general shape of the curve we note a very pronounced drop in the mean fission cross section in the vicinity of 2 to 5 ev.

On the whole this curve is in good agreement with those given by other investigators within the limits of the resolving power. However, it seems to us that our curve is a little bit lower, and we attribute this to the difficulties we had with our boron monitor. For reasons having to do with the intensity we had to change our monitor for energies above 0.5 ev, so that here the agreement is not entirely satisfactory.

Above 10 ev the resolving power no longer permits separating the resonances. Nevertheless the results, Slide 33 (Fig. 8*c* of P/354), indicate an increase in the mean fission cross section to about double that obtained by extrapolation from the 0.025 ev point in inverse proportion to the neutron velocity.

The CHAIRMAN: The next paper, which is P/423 by Mr. Lynn and Mr. Pattenden, describes the work at Harwell on U^{235} cross sections, again the result of several instruments, will be presented by Mr. Egelstaff.

Mr. P. A. EGELSTAFF (UK): At this stage to show some more curves of the variation of total and fission cross sections as a function of neutron energy is really to demonstrate that the U^{235} nuclei found at Harwell are just the same as those found in other countries. Nevertheless, I will just show the curves for the sake of looking at them.

Slide 34 (Fig. 5 of P/423) shows the total cross section of U^{235} as a function of neutron energy in the region below 0.5 ev. It will be noted that it is identical with the curves you have already seen four times.

Slide 35 (Fig. 2 of P/423) shows the variation of fission cross section with neutron energy from the thermal region up to 100 ev. One can note that it has exactly the same character as the curves which have been seen. The actual values of the resonance energies and the product $\sigma_0 \times \Gamma$ for the levels seen can be found in the paper.

What I would like to do is to remark upon the absolute values of the total and fission cross sections at 2200 m/sec, because in the case of U^{235}, there are some discrepancies here between our values measured in the United Kingdom and the values which have been reported by the Union of Soviet Socialist Republics and United States of America. I will just summarize the measurements as I have taken them from the papers of various countries. If I make any errors in writing this down, I apologize to the people concerned because I am not quite certain whether

I have all the data from the USSR completely in focus. I may actually make the mistake of writing down only a part of USSR data.

The values are all for 2200 m/sec, and I shall write down these values as measured in the various countries. First the total absorption cross section, i.e., radiative capture plus fission.

In the United Kingdom we have the value as 716 ± 15, using the value of the scattering cross section reported in Sailor's paper. In the USSR the value, using the same value of scattering cross section, is 697 ± 20, and in the United States it is 687 ± 4 or 7. (There are two errors quoted in different papers, one of 4 and one of 7.)

I shall now turn to the fission cross section; the value determined in the United Kingdom is 638 ± 20. This value is obtained in exactly the way described by Mr. Price; a direct measurement of fission cross section. The USSR shows 570 ± 15 and the United States shows 580 ± 8. This error in the United States value is related to the error in the absorption cross section, and the 8 corresponds to the 7. If the 4 is correct, then that will have to be changed. These two measurements are actually by indirect methods, and our measurement is by a direct method, as described by Mr. Price.

The indirect method referred to makes use of the relationships

$$\eta = \frac{\nu}{1+\alpha}, \quad \alpha = \sigma_c/\sigma_f$$

So that if you measure various ones of these quantities, you can in fact actually deduce σ_f.

At Harwell we measured σ_f directly. The point here is that we find both total and fission to be somewhat greater than in other parts of the world, that is the absolute values.

I think possibly in the case of the absorption cross section the differences can be sorted out fairly easily by further measurements. The actual values do not differ too far, and a value in the neighbourhood of 700 represents a good average. But in the case of σ_{fiss} we have every reason to be confident in our own value, and we would make a plea for further direct measurements of the fission cross section in order to check whether there is any significance in this difference.

Session 17A.3. Low-Energy U^{233} Cross Sections

The CHAIRMAN: We shall now turn to U^{223}. Mr. Vladimirski will be the first speaker. He is presenting results from P/644 and P/641.

Mr. VLADIMIRSKI (USSR) presented paper P/644 as follows: I shall report on the work done by Goldin, Kukavadze, Ershler, and Anikina on the determination of the cross sections of U^{233}.

The ratio between the absorption and radiative capture cross section of U^{233} is of interest, since it determines the proportion of neutrons wasted in transforming uranium-233 into uranium-234. In practice it is most important to know this ratio for the reactor neutron spectrum. By irradiating in a reactor, it is possible to "burn up" the initial U^{233} and to operate with microscopic quantities of the daughter substances, which greatly increases the experimental accuracy.

The most direct method of measuring the ratio of the two cross sections is the following. In the irradiation of uranium, the fission reaction leads to a decrease in the amount of uranium, while radiative capture results in the transformation of uranium-233 into uranium-234. The sought ratio is therefore equal to the amount of uranium-234 formed, divided by the decrease in the amount of uranium as a result of irradiation. Like uranium-233, uranium-234 is an alpha emitter with a lifetime on the order of 10^5 years. The energies of the alpha-particles emitted by these isotopes are very near to each other and the alpha-spectra overlap. Consequently, an analysis of the alpha-spectra could not be used for isotopic determinations and mass spectroscopy had to be employed. Three different methods were used to determine the amount of fissioned uranium-233. First, we measured the decrease in the alpha-activity of the specimen. Second, we measured the amount of cerium-140 formed in the specimen as a result of fission. Finally, a mass-spectrograph was used to measure the amount of the remaining uranium.

The isotopic dilution method was used in two of these determinations: in measuring the amount of the remaining uranium-233 we added natural uranium, consisting mostly of the 238 isotope, and in measuring the amount of cerium-140 in the fission fragments we added natural cerium.

Slide 36 (Fig. 2 of P/644) shows a mass-spectrogram of the cerium in the fission fragments (top curve) and in the natural substance (bottom curve). In addition to the peaks associated with cerium, peaks for La and Nd appear in the spectrogram. The curves show the difference in the isotopic concentrations of cerium and indicate the potentialities of the mass-spectroscopy method.

Mass-spectrum analysis of uranium [Slide 37 (Fig. 3 of P/644)] is quite difficult, particularly when it is desired to measure concentrations of neighbouring isotopes one of which is present in large amounts while there is barely a trace of the other. In such cases, large errors may occur because of incomplete resolution of the peaks. With a view to avoiding such errors, we took advantage of the fact that in the case of uranium an incandescent filament emits primarily uranium dioxide ions. Where natural uranium is used in adjusting the mass-spectrometer, two clear maxima are seen near the peak for the ordinary dioxide. These are due to the fact that in addition to O^{16} there exist in nature two heavier oxygen isotopes: O^{17} and O^{18}. The instrument was considered to be properly adjusted only when the height of these maxima corresponded to the reference data for the isotopic concentration of oxygen.

Slide 38 (Fig. 3 of P/644) shows a mass-spectrogram of a specimen of the investigated uranium with the addition of a certain amount of natural uranium.

In addition to the ratio of the radiative capture and fission cross sections, the absolute magnitude of these cross sections was determined. To this end, a lithium monitor was irradiated, together with the uranium specimen. The total neutron flux was determined from the decrease in the isotopic concentration of Li^6 resulting from the (n, α) reaction. This decrease in the isotopic concentration of lithium was also determined by mass-spectrography.

Care must be exercised in computing the cross sections from the experimental data. In order to have enough material for mass-spectrometry, one must use specimens which cannot be regarded as thin for purposes of calculation. The self-shielding of the specimens does not remain constant during the course of the experiment, since an appreciable portion of the material is dissipated. Hence, as in many such experiments, we are faced with the problem of taking into account a quantity varying in time. The solution of this problem is given in the Appendix to the written report.

Let me describe the experiments in greater detail. The uranium specimens were in the form of foil 3.2×10^{-2} mm thick and weighed 60 mg. The lithium specimens, consisting of metallic lithium, weighed 28 mg. Before irradiation, the specimens were wrapped in platinum, enclosed in a soldered lead envelope and sealed in an aluminum container. The loss of uranium-233 during irradiation was 11.9 mg, i.e., about 20 per cent.

The mass-spectrometer had a thermo-ionic source. In the analysis of lithium, a two-filament source was used; the first filament served for the evaporation of lithium, the second, hotter filament, for its ionization.

The following experimental data were obtained:

$$\frac{\sigma_{n\gamma}}{\sigma_a} = (8.7 \pm 0.3)\%$$

$$\sigma_a = 615 \pm 30 \text{ barns}$$

The last figure was derived on the assumption that the cross section of Li^6 is 930 barns.

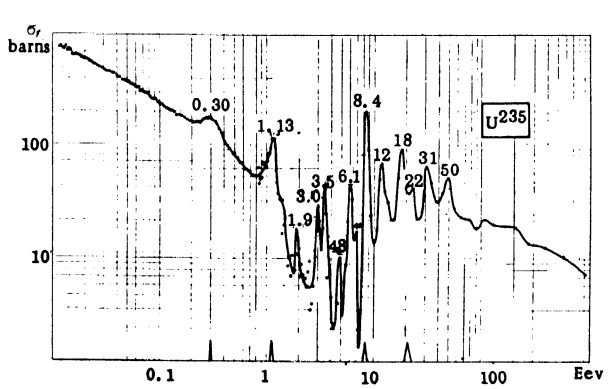

Slide 39

Mr. VLADIMIRSKI (USSR) then presented some further results in connection with P/641: Uranium-233 was investigated with straight slits in the energy range from 30 to 10,000 ev with a resolving power of 0.1 μsec/meter, and with curved slits in the energy range from 2 to 8 ev with a resolving power of 0.18 μsec/meter. The thickness of the specimen was 3.60×10^{21} atoms per cm^2.

The spectrum in the region of low energies (Slide 39) is in good agreement with the data of the Brookhaven Laboratory and the Harwell group and the measurements made by Nikitin *et al.*, presented at this Conference (in paper P/646). In the energy region above 30 ev we obtained a more complex structure of the spectrum (Slide 40) than is indicated by the Brookhaven measurements.

The CHAIRMAN: The next comment on this subject will be presented by Mr. Gerasimov of the USSR. It is from paper P/645.

Mr. GERASIMOV (USSR): The variation of the fission cross section of U^{233} with the neutron energy was measured using a chamber containing 50 mg of uranium-233. The results are shown in Slide 41. The data were normalized to a cross section of 510 barns at 0.0253 ev. As will be seen from the curve, the fission cross section for U^{233} never drops below the $1/v$ line extended from the thermal region.

The observed absolute value of the fission cross section in the thermal region cannot be explained by the levels in the 1.8 ev region. There must be an appreciable contribution in the thermal region from the level located to the left of zero energy. In addition to the levels apparent at 1.82, 2.3, 3.7, 4.8, 6.9, 10.7, 13.5 and 16 ev, there are groups of unresolved resonances at energies of 22, 35, 60 and 120 ev.

Detailed study of the shape of the peak at 1.82 ev indicates the existence of a level with an energy of around 1.5 ev.

Our results are in satisfactory agreement with those of the other laboratories.

The CHAIRMAN: The next comment on this subject will be given by Mr. Sukhoruchkin of the USSR. It is from paper P/646.

Mr. SUKHORUCHKIN (USSR): The fission and capture cross sections of U^{233} were measured in the energy range from 0.01 to 100 ev with a neutron selector used in conjunction with an intermittent beam cyclotron. I shall not show the capture and fission cross-section curves now (they will be presented in Session 18A), since our measurements were made primarily for the purpose of determining the variation of ν_{eff}, and shall confine myself to two conclusions, drawn from an analysis of these curves.

1. Uranium-233 is the only one of the isotopes considered here whose total cross section follows the $1/v$ law over a fairly wide energy range. According to our measurements the total cross section in the thermal region is 580 barns. The contribution to the thermal range of all the resonances we have succeeded in resolving is about 100 barns. Hence the

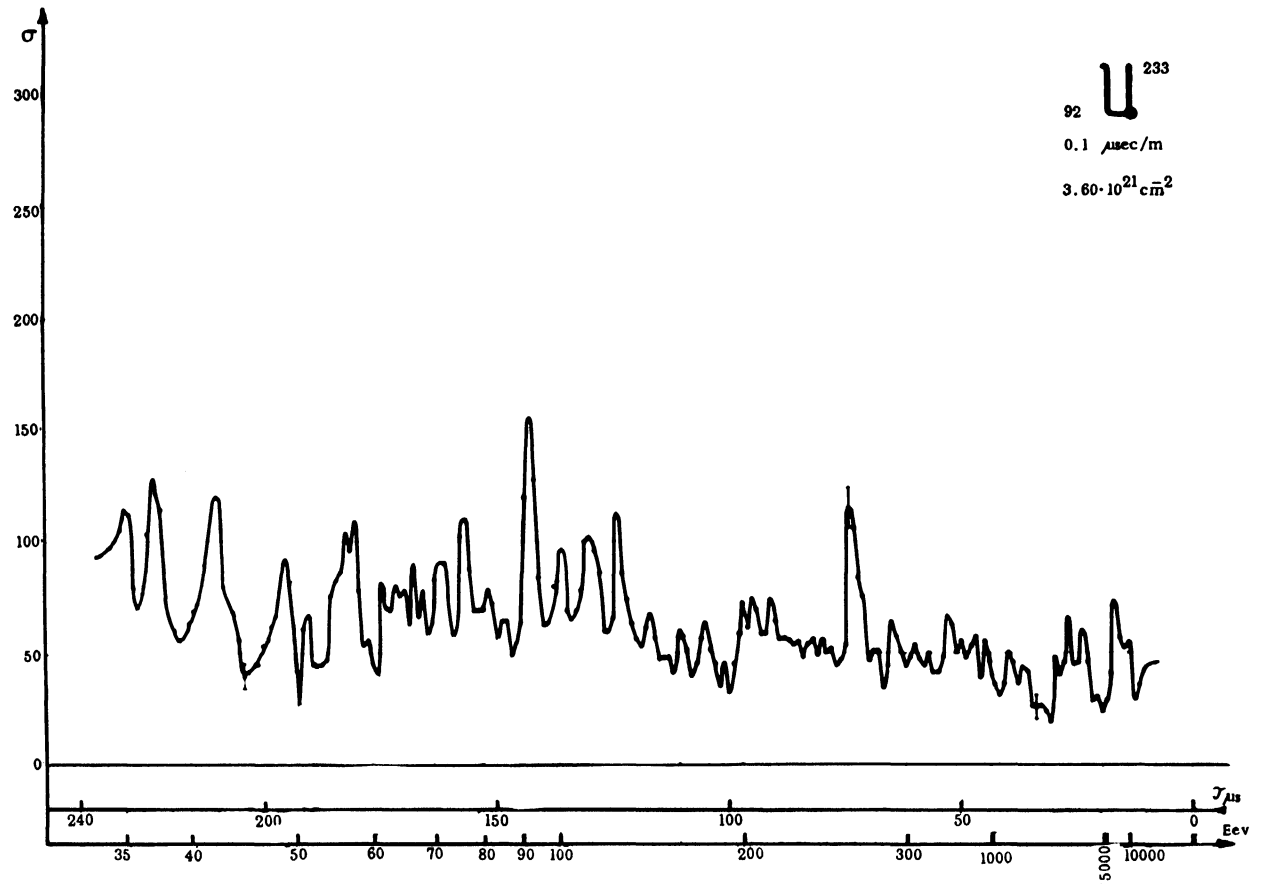

Slide 40

principal contribution is made by a very strong and far-lying negative-energy resonance, for which we determined the following parameters:

$|E_0| > 0.5$ ev; $\sigma_0\Gamma^2 \geqslant 100$ barn-ev^2; $\Gamma_f/\Gamma = 0.87$

Analysis of the group of resonance levels at 1.5–2 ev was carried out on the basis of the Breit-Wigner single level formula and led to the following results:

$E_0(ev)$	σ_0	$\Gamma_f(ev)$	$\Gamma\gamma(ev)$
1.45	175	0.37	0.03
1.75	1000	0.21	0.04
2.23	670	0.10	0.04

Inasmuch as the ratio Γ_f/Γ has virtually the same value for the negative level as for the 1.75 ev level, we can assume that the two levels have identical spins and that there is interference between them. It should be noted, however, that taking into account the interference should change the parameters of the first level only.

The CHAIRMAN: Now the U^{233} part of P/423 will be presented by Mr. Wiblin of the United Kingdom.

Mr. E. R. WIBLIN (UK): It seems that I have in fact a very pleasant task here in that the methods by which the measurements in the United Kingdom have been made have been described by Mr. Price and that the excellent agreement in some of the absolute cross sections has already been mentioned by Mr. Egelstaff for some of the U^{235} results. I can conclude this section of the United Kingdom results by pointing to some even closer agreement for U^{233}.

I am at a little disadvantage in completing Mr. Egelstaff's picture in that I have not available the United States results for these two values of the total absorption cross section and of the fission cross section.

Slide 42 (Fig. 3*a* of P/423) is the low-energy section curve for U^{233}, and again one can emphasize, as the last speaker did, the long region over which the $1/v$ law holds. I shall go back to that in one moment.

Slide 43 (Fig. 3*b* of P/423) shows the higher energy section from roughly 1 ev to 20 or 30 ev in the U^{233} total cross section.

Slide 44 (Fig. 1 of P/423) shows a composite curve for the relative fission cross section determined as Mr. Price described.

I would now just summarise the absolute thermal values which we have. Here, I can only cover, as I say, the United Kingdom and Soviet Union results.

Total absorption cross section of U^{233}: UK, 605 ± 10 barns; and USSR, 615 ± 30 barns.

Fission cross section: UK, 515 ± 15 barns; and USSR, 510 barns.*

* During the following discussion, Mr. Vladimirski (USSR) stated that the correct figure for USSR results would be 560 barns (paper P/644).

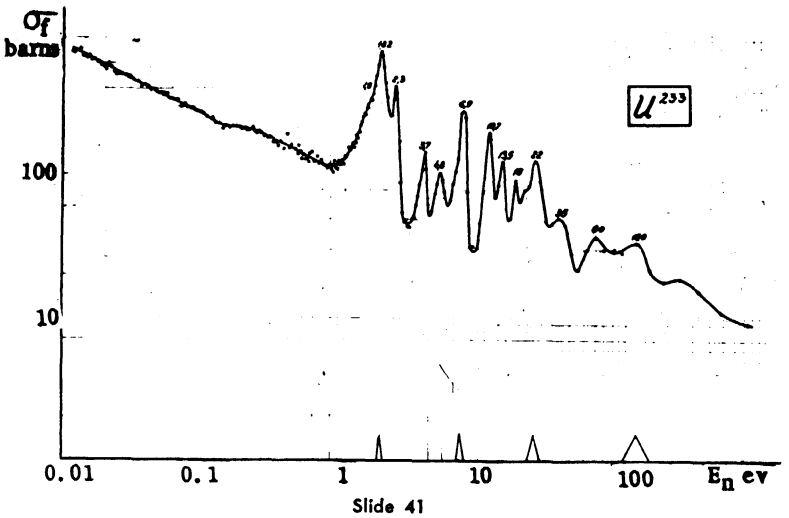

Slide 41

I think that was the correct figure.

I should emphasize that the USSR measurement is the indirect one and the UK the direct measurement.

The VICE-CHAIRMAN: The part of P/354 dealing with low energy U^{233} cross sections will now be presented by Mr. G. Vendryes (France).

Mr. VENDRYES (France): The investigations which have been carried out in France on uranium-233 in the region of low energies were concerned solely with measurements of the fission cross section. The work consisted of two parts: one, measuring the mean value of this cross section in the thermal neutron energy range and, two, determining the variation of the cross section as a function of neutron energy.

The first group of measurements, carried out by Mr. Auclair, Mr. Hubert and Mr. Joly, consisted of comparing the fission ratios of two layers of the same area, one of uranium-233, the other of plutonium-239, placed back-to-back in a double ionization chamber located in a beam of thermal neutrons from the Saclay pile. The quantity of deposit was determined by subsequent measurement of the alpha-activity in a proportional counter with a fixed solid angle. The neutron spectrum utilized was studied experimentally; it contains all the neutrons absorbed by a piece of cadmium foil 0.7 mm thick.

The ratio of the mean fission cross sections of the two nuclides was found to be 0.626 ± 0.010.

Using the mean cross section of plutonium calculated from the declassified value of 750 barns at 0.025 ev as reference, we deduced that the mean cross section of uranium-233 for this quasi-Maxwellian spectrum is 459 ± 14 barns.

The energy dependence of the fission cross section of uranium-233, like those of plutonium and uranium-235, was measured by means of a time-of-flight spectrometer and a crystal spectrometer and a crystal spectrometer with a beryllium monochromator. This investigation, in conjunction with the measurements described above, gave a value of 518 ± 16 barns at 0.025 ev.

The curves which I shall now show summarize the results to date, results which we still consider tentative.

Below approximately 0.2 ev, the variation of the fission cross section closely follows the $1/v$ law, represented in Slide 45 (Fig. 4*a* of P/354) by the solid line. Deviations from the law, if any, in this region do not exceed 5 per cent.

The curve in Slide 46 (Fig. 4*b* of P/354) from 0.2 to about 20 ev shows a series of resonances which could not be separated with the resolving power available. The resonances observed were situated at 1.8 ± 0.02. 2.3 ± 0.02, 3.5, 5.1, 7 and 12 ev.

Here too we have not yet attempted detailed analysis of these resonances. In this entire region, the mean fission cross section is 3 to 4 times greater than would be obtained by extending the $1/v$ line from 0.025 ev.

The same thing is true of the 20 to 1000 ev region, see Slide 47 (Fig. 4*c* of P/354). The measurements had to be made with a lower resolving power, which did not permit separation of the individual resonances.

DISCUSSION OF SESSIONS 17A.1, 17A.2, 17A.3

THE VICE-CHAIRMAN: We are now through with all the papers dealing with low-energy cross sections of fissionable materials, and the Chairman of the session, Mr. Hughes, is going to give a summary of all the results presented at this session.

THE CHAIRMAN: The situation this morning is certainly unusual, if not unique in science. We are comparing results on which we all have worked hard for some ten years and have worked independently. This morning we have asked the question, "How do our results compare?", and the answer—I feel sure you will agree—is "extremely well." I think, in fact, we can all feel a bit happy about the work we have done.

The best way for me to show, as Chairman, why we can feel happy about the situation is to compare the results from various countries. We have seen curves giving the results from one country at a time;

the obvious way to compare them is to look at results from all countries. I am enabled to do this actually because all of the workers have contributed so generously by sending curves to us several weeks in advance of the meeting. This has enabled us to put these results together, actually print them and get them into this large compilation which is being distributed here at Geneva. This* is the so-called "Blue Book," and this is an addendum to the Blue Book. I realize that there are not too many of these available, so what I will do now is show some slides which actually give the same information that is in this cross-section compilation. I want to repeat again that this is only possible because people were so extremely generous in sending us their curves in advance. From the first slide we can see how well results compare from the various countries.

Slide 48 gives the curve for U^{233}—the fission cross section of U^{233}. There is not time actually to describe which points go with which country. I merely want to illustrate the general fact that the points agree so well that in certain regions it is difficult to plot all the points. There of course is the question of the normalization of fission curves, but that is something that cannot be discussed at the present time because of the papers that will be presented in Session 18A which are vital to the question of normalization. However, the disagreements are not really very great in the normalization. One interesting point here which illustrates the value of combining independent results from various countries is the presence of an extremely weak resonance in the region of 0.2 ev. After discussion with various individuals, I have found that the experience in each country was the same. In each country, points were found in this region that were above the $1/v$ line. However, the points were above by such a small amount that it was thought to be experimental error. However, when the results of all countries are put together, there seems to be no doubt about it that there is an extremely weak resonance in this region. This means that in each country we do not need to work nearly as hard as we would otherwise. We have independent verification.

Slide 49 is the cross section of U^{233} in the ev region, and this is now the total cross-section. This represents work done, of course, by crystal spectrometers, fast choppers and mechanical velocity selectors. Here again, without going into detail, I am sure the general impression is quite clear, that the points land right on top of each other. In certain regions, where more effort has been put into the work the resolution might be slightly better. In some places points are shown for one country only. In one region the points happen to be best as run by a fast chopper —in other regions other instruments are better.

Slide 50 is the U^{235} curve. Again, in the low-energy region, and here the fission cross section. So again there is the question of normalization. In order to show these curves best for the purposes of the Geneva meeting, we have normalized them all to the same value. After this afternoon's session (18A), we will perhaps know a better normalizing value. But, again, the same fact emerges: the points land practically on top of each other. The agreement in shape is extremely good. This lower curve deals with something that will be discussed this afternoon, but let me just say one word about it which is, again, that the agreement is very good. This is the quantity $1 + \alpha$ which is the reciprocal of η. The line is $1 + \alpha$ obtained from the fission and from the total cross section.

The points are so-called direct measurements of η or $1 + \alpha$. You see the slow change in $1 + \alpha$ as the resonance, obtained both by the direct measurement and from the cross-section curves. Again the situation seems to be extremely good.

Slide 51 is U^{235} again in the ev region, and the total cross section. Here the resonance structure is so complex that it is impossible to show it in detail on this plot, so these inserts cover this particular energy region. It seems that as more and more work is done and as resolution improves, the resonance structure of U^{235} shows more and more complexity. The analyses of all these resonances—the computation of fission widths and radiation widths—are certainly something that will keep groups in several countries busy for a long time.

Slide 52 is the U^{235} fission cross section in the ev region. Here again there is the normalization question. We have used one normalization value. The points from various countries agreed very well in the location of resonances. There are some differences here which, we have found out in the last few days, are caused by a correction for scattering. This is partly our fault in plotting the data. We did not understand what correction had been made for scattering. This difference, therefore, will disappear.

Slide 53 is the cross section for Pu^{239} in the slow region and this is the total cross section. This curve shows such excellent agreement that it almost makes one feel emotional about this work which had been done in so many different countries. Incidentally, there is no normalization here, because, it is a total cross section. The agreement is so good we just could not plot the points in this energy region. It certainly illustrates the fact that even though we may not be able to talk to each other without wearing earphones, we certainly agree with each other when we measure the cross section of Pu^{239}.

Slide 54 is the fission cross section of Pu^{239}. Again the agreement is so good in this energy region that we could not plot all the points at the peak of the resonance. There is, of course, a question of normalisation, but we hope to settle that at this afternoon's meeting. Again, the $1 + \alpha$ curve is shown. Here there is some discrepancy between direct measurements and the computed curve. This again is a matter to be taken up this afternoon.

*Neutron Cross Sections, by D. J. Hughes and J. A. Harvey, U.S. Government Printing Office, 1955.

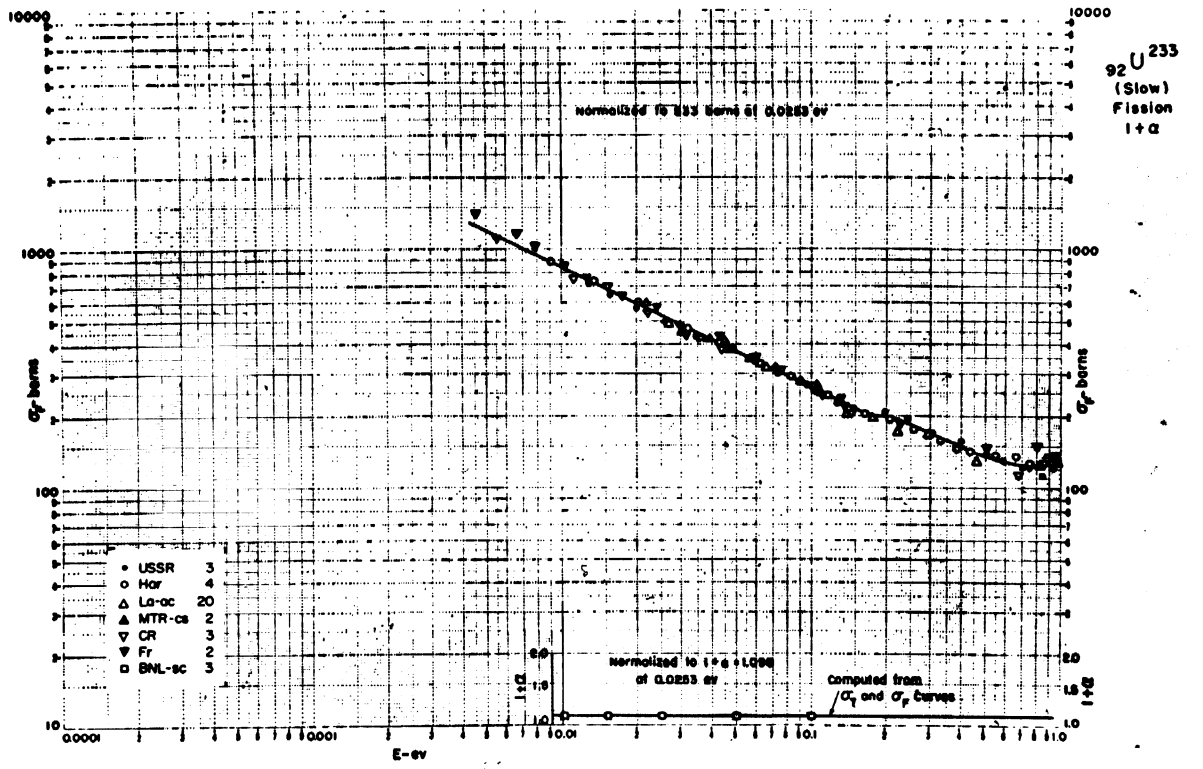

Slide 48

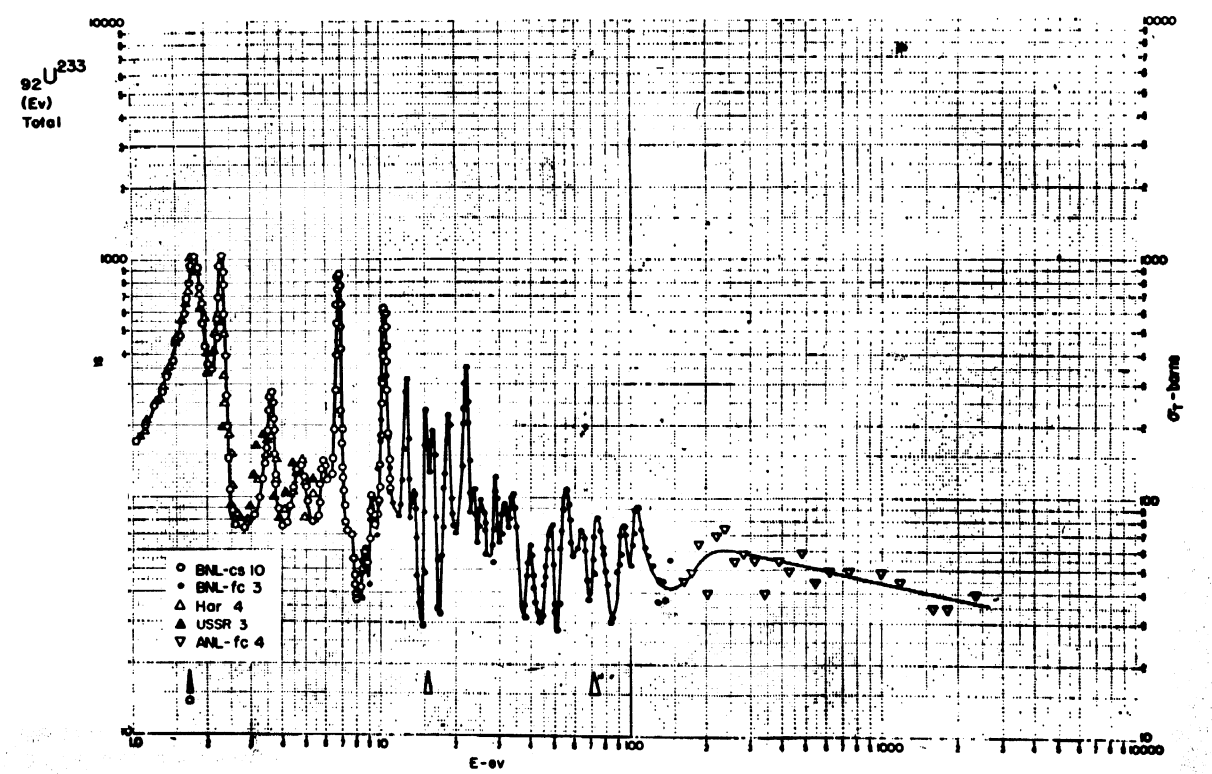

Slide 49

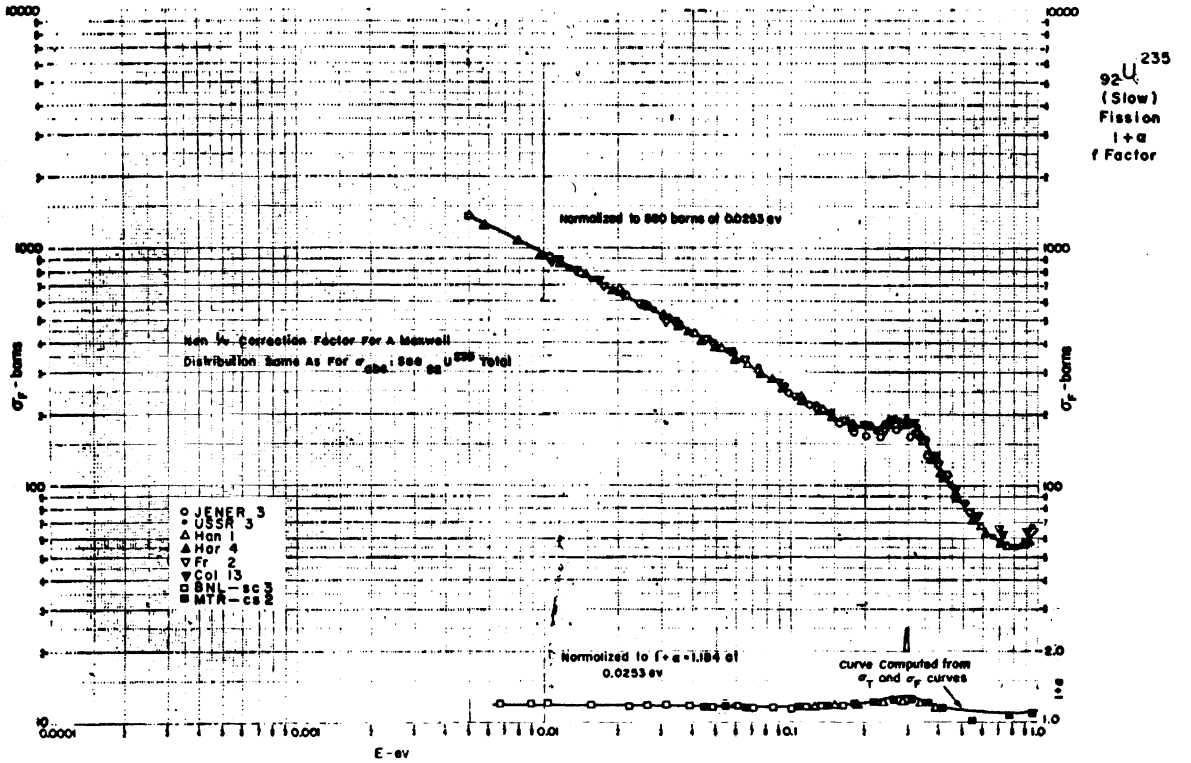

Slide 50

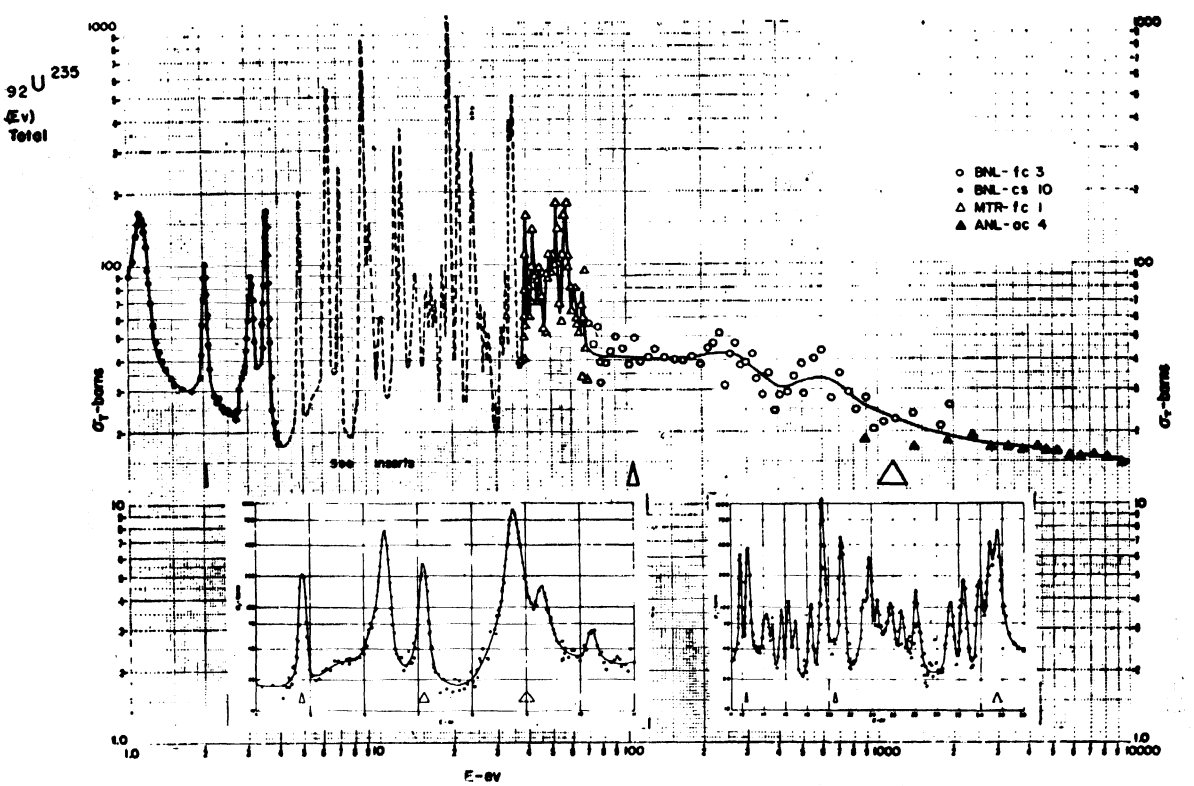

Slide 51

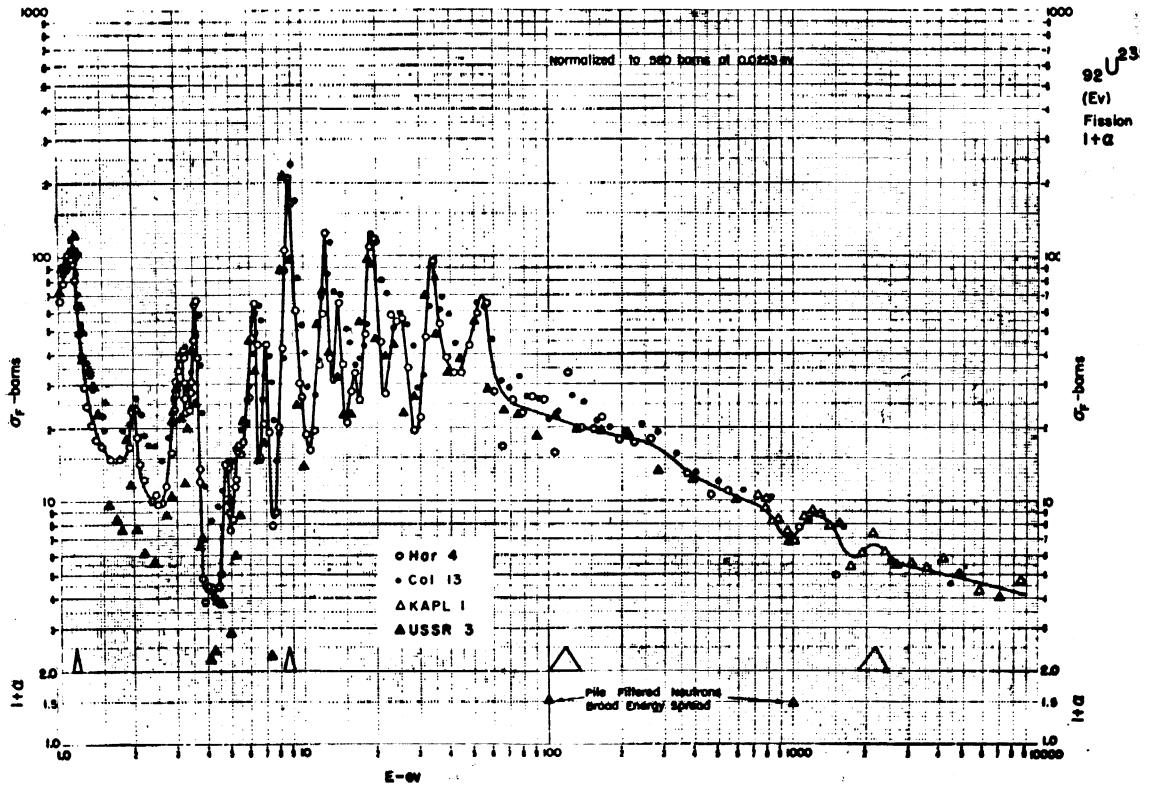

Slide 52

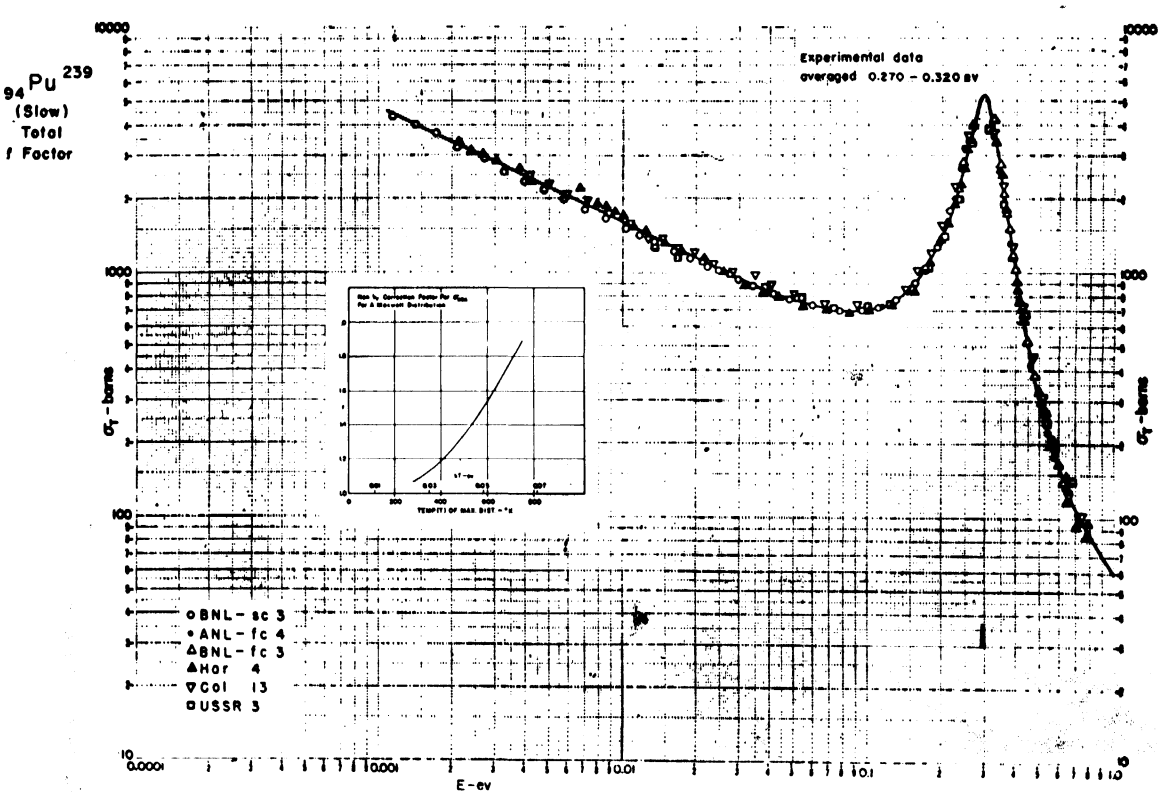

Slide 53

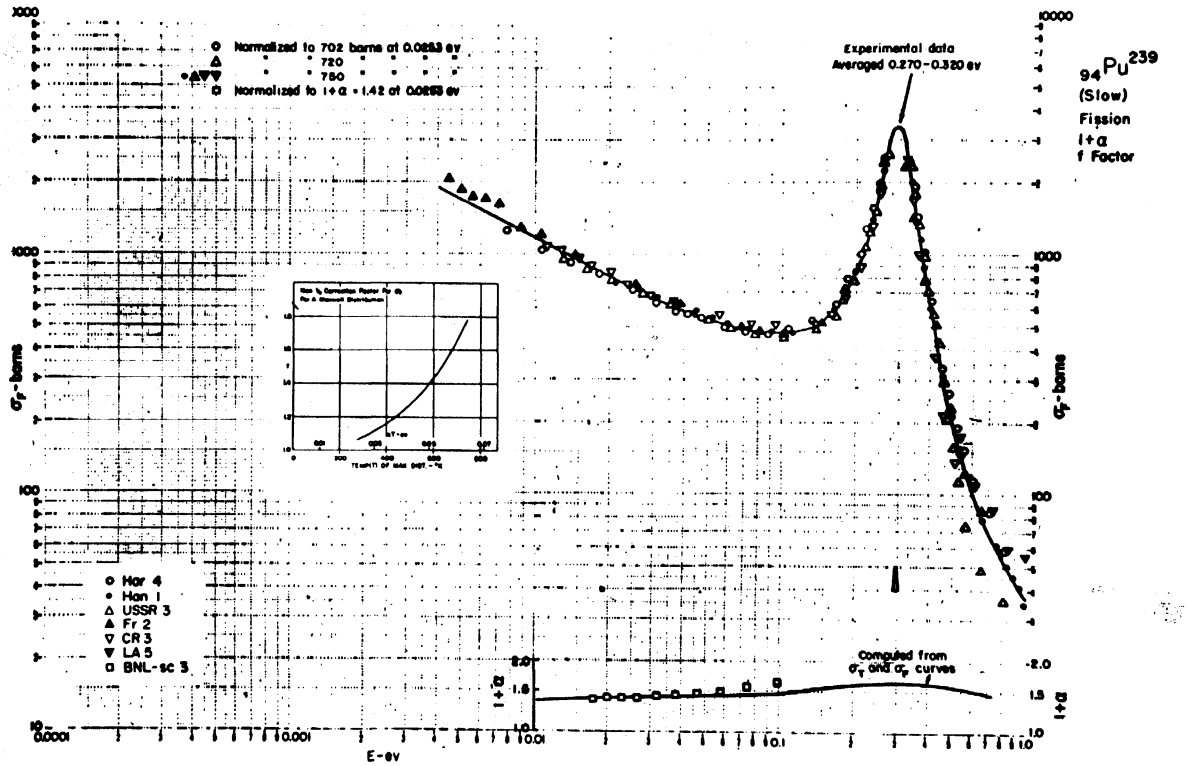

Slide 54

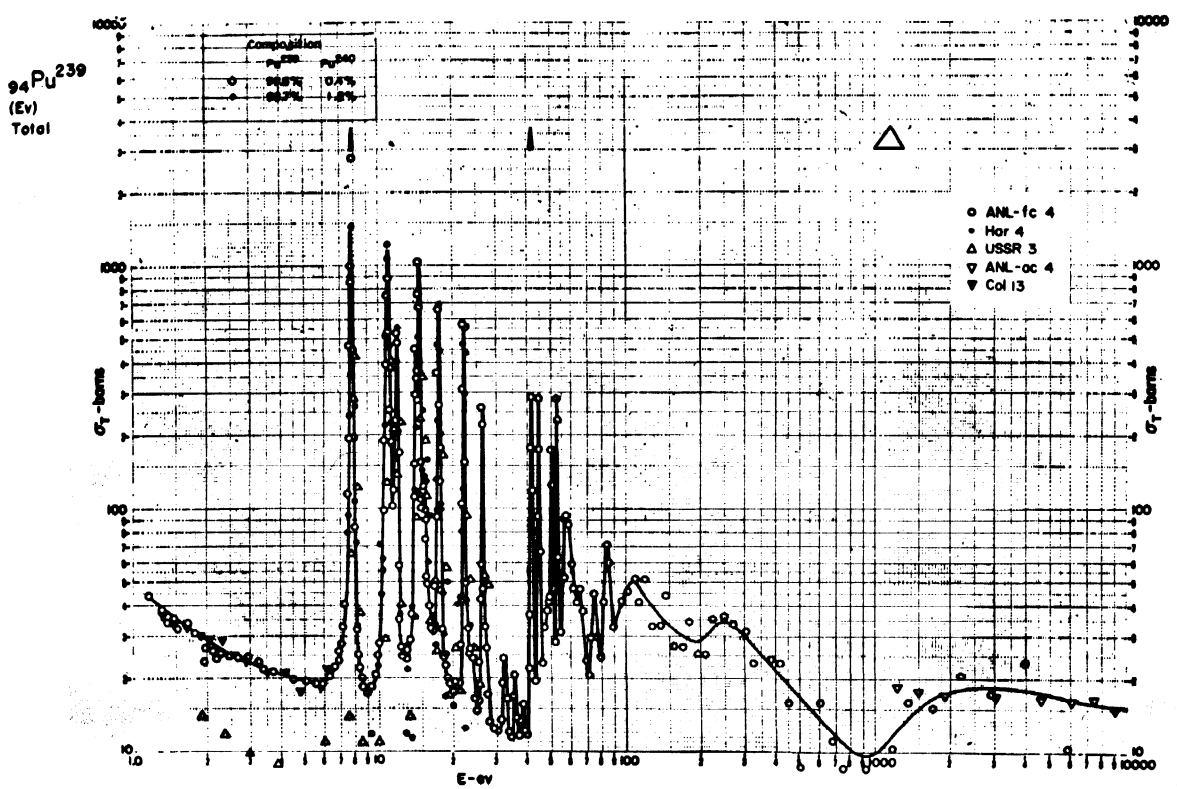

Slide 55

Slide 55 is the cross section of plutonium—the total cross section in the ev region—and here again the agreement of the points on this resonance illustrates the same fact, namely that the agreement which we have been able to obtain is extremely good.

You have heard something about the best values from each country for the fundamental cross sections, that is, the values at 2200 meters per second. We now have a set of best values from each country, and we hope that in the next day or two we may have sufficient discussions so that from these values there will emerge a set of the world's best values for the fundamental cross section.†

The VICE-CHAIRMAN: We shall now begin the discussion on all the papers which have been presented.

Mr. J. A. HARVEY (USA): Mr. Gerasimov, you mentioned in your paper that the Pu^{239} fission cross-section curve was normalized to 625 barns. We wonder how this cross-section value was derived. I believe that you referred to it as a preliminary value when you spoke this morning. I was wondering what is the present value which you would use?

Mr. GERASIMOV (USSR): The value of 625 barns for plutonium-239 was obtained not by us, but in another Soviet laboratory quite a long time ago. The value was obtained by comparing the fission cross section of plutonium-239 in the thermal region with the cross section of lithium. The value we now have is 720 barns.

Mr. H. PALEVSKY (USA): I was wondering, Mr. Price, how you reconcile the use of 4 barns for the scattering cross section of plutonium when $4\pi R^2$ will give you something of the order of 10 to 11 barns.

Mr. PRICE (UK): I believe that Mr. Egelstaff worked on this.

Mr. P. A. EGELSTAFF (UK): The point here is that the value of 4 barns is the best fit to the data in the region of about one-half to one or two ev. The potential scattering value which would be calculated, I agree, is substantially larger than this. We quoted this as an experimental value. You would normally assume that there is some interference phenomenon going on which would reduce the scattering cross section. I think that there is every reason to ask for direct measurements of the scattering cross section, rather than to infer scattering cross section, as we did, from total cross sections.

Mr. W. W. HAVENS, JR. (USA): Mr. Gerasimov, I just wanted to know what were the energy and currents of the cyclotron used for these measurements.

Mr. GERASIMOV (USSR): This question should really be addressed to Mr. Sukhoruchkin.

Mr. SUKHORUCHKIN (USSR): The energy of neutrons was about 12 Mev. As I am not a specialist in the cyclotron technique, I cannot reply as to the current used.

Mr. VLADIMIRSKI (USSR): Dr. Wiblin in his statement, referring to our results, cited the figure of 510 barns for the fission cross section of uranium-233. If I am not mistaken, a check will show that the correct figure for the cross section should be appreciably higher, namely, 560 barns. This is on the basis of the data in P/644 by Goldin *et al.*

Session 17A.4. High-Energy Cross Sections

Mr. M. A. BERTHELOT (France) presented paper P/355 as follows: The measurements I shall speak about were carried out at the Nuclear Studies Centre (Centre d'Etudes Nucléaires) of Saclay by a group consisting of Miss Szteinsznaider, Mr. V. Naggiar and Mr. F. Netter. They concerned the fission cross sections of Pu^{239}, U^{235} and U^{233} at neutron energies from 25 to 2000 kev.

The neutrons were obtained by the action of a beam of monoenergetic protons on a target consisting of a thin layer of lithium deposited by thermal evaporation on 0.3 mm thick tantalium foil. The proton beam was that produced by the Saclay Van de Graaff generator. The energy of the protons was determined within 0.3 per cent by a magnetic analyser for the intensity used, which was about 8 microamperes. The average energy was measured by means of the electric field of this analyser by the nuclear resonance method after calibration with reference to the thresholds of the following reactions: $Li^7(p,n)$ at 1.882 Mev and $C^{13}(p,n)$ at 3.236 Mev.

Taking into account the energy spectrum of the proton beam, the thickness of the lithium target and the angle of divergence of the neutron beams, the energy of the neutrons was determined within 60 kev for a mean energy of 1600 kev and within 20 kev for a mean energy of 50 kev. The spectral distribution curve roughly resembles a rectangle.

The intensity of the proton beams was measured by means of a Faraday trap and that of the neutron beams by means of a conventional long counter.

It was necessary to determine the variation of

† After the formal meeting, some of the participants met again and drafted the following statement:

INTERNATIONAL VALUES FOR THERMAL CROSS SECTIONS OF FISSIONABLE ISOTOPES

At Session 17A, Cross Sections of Fissionable Materials, of the International Conference on the Peaceful Uses of Atomic Energy, a large amount of recently declassified information was presented on the cross sections of the fissionable isotopes U^{233}, U^{235}, and Pu^{239}. In the low energy region, where extensive measurements were reported, excellent agreement was obtained for these isotopes, which are important in reactor design. At the suggestion of the Chairman, Dr. D. J. Hughes, the French, United Kingdom, Union of Soviet Socialist Republics and United States scientists met after the formal session to consider the thermal (2200 m/sec) absorption and fission cross sections of these isotopes. It was decided to prepare a set of world average values for these cross sections, which could be used as a means of coordinating reactor calculations based on them. The quoted errors of the world average values given here are based primarily on the spread in reported results and are sometimes larger than errors of specific quoted results.

	σ_{abs} (*barns*)	σ_{fiss} (*barns*)
U^{233}	593±8	524±8
U^{235}	698±10	590±15
Pu^{239}	1032±15	729±15

the sensitivity of the long counter with the neutron energy. To this end, we compared the count rates given by the long counter with those of a proportional counter (containing hydrogen at about 1 atmosphere pressure) giving the count of recoil protons. We then deduced the output curve for the long counter shown in Slide 56 (Fig. 4*b* of P/355) on the basis of the (n,p) scattering cross-section curve given in AECU 2040.

As you may see from this slide, the sensitivity of the long counter used remains constant to 400 kev and it decreases by about 30 per cent as we approach the region of the very slow neutrons.

Slide 57 (Fig. 1 of P/355) shows a schematic diagram of the experimental set-up. The fissile material under investigation is deposited in a thin layer on a flat metal sheet which serves as the high potential electrode of the parallel-electrode ionization chamber in which the fissions are counted.

In the first stage of the investigation, when we wanted to compare the cross sections of two different materials at the same neutron energy, we alternately used two identical ionization chambers. Later, and for most of the measurements, we used one double chamber, depositing the fissile materials to be compared on the two sides of the supporting foil and placing a collecting electrode opposite each side. We thus eliminated any uncertainties connected with the reproducibility of the neutron flux.

Usually the ionization chamber was located in front of the target serving as neutron source. However, when we wanted to make measurements with neutrons having very low energies the chamber was moved back at an angle of 120 degrees to the direction of the protons (as shown in the slide), in order to avoid the difficulties resulting from the fact that there are two groups of neutrons emanating forward when one operates in the low-energy range. The position of the chamber was changed at about 200 kev.

For the measurements on plutonium we used a source containing about 1 per cent of impurities of uranium. The target used in the measurements on uranium-235 was prepared in the Saclay electromagnetic isotope separator and contained 13 per cent U^{235}, the remainder being U^{238}.

The target used for the measurements on uranium-233 consisted of about 50 per cent of this isotope and 50 per cent of natural uranium. The principal cause of uncertainty in the experiments was the interference produced by scattered neutrons, striking the fissionable material target after pursuing a broken-line trajectory. A systematic study of the disturbance caused by these scattered neutrons is now under way, but has not yet been completed. In the light of the results to date, we do not think it will be necessary to make any appreciable corrections to the present data. I believe that in allowing for a possible systematic error of 10 per cent due to the scattered neutrons we are safe from unpleasant surprises.

All the measurements made were relative determinations. The values reported here are based on the value of 0.34 barns for the fission cross section of natural uranium at 1600 kev, taken from the American report, AECU 2040. Any change in this reference value will, of course, result in a proportional change in the data I shall present.

To justify the selection of this value as reference, we measured the energy dependence of the fission cross section of natural uranium. Slide 58 (Fig. 2*a* of P/355) shows the results of these measurements normalized to the curve of the AECU 2040 report in the 1600–1800 kev interval (dotted lines). We feel that the divergence between the two curves is insignificant.

The measurement program was the following:

1. Determination of the cross section of plutonium-239 in comparison with that of natural uranium at 1600 kev.

2. Determination of the relative variation in the cross section of plutonium-239 with the energy.

3 and 4. Measurement of the energy dependence of ratio between the cross sections of U^{235} and Pu^{239} and between the cross sections of U^{233} and Pu^{239}.

Let me review the parts in order; the first part concerned determination of the ratio of the fission cross sections of plutonium-239 and natural uranium at 1600 kev.

The measurements were made in the double ionization chamber, using two back-to-back targets: one of plutonium-239, the other of natural uranium. The sought ratio is found from the relationship

$$\frac{F_{Pu}}{F_{nat}} = \frac{(n\cdot a)_{Pu}\,\sigma_{Pu}}{(n\cdot a)_{nat}\,\sigma_{nat}}$$

That is, the number of fissions of the plutonium over the number of fissions of the natural uranium equals the quotient of the quantity $n\cdot a$ for plutonium divided by $n\cdot a$ for natural uranium, multiplied by the ratio of the cross sections.

In this expression n is the number of atoms per square centimeter of the target and a is the efficiency with which the ionization chamber detects fission events occurring in the target.

Hence we measured the ratio of the fissions of plutonium to the fissions of natural uranium at 1600 kev. If we know the ratio of the quantities $n\cdot a$, we can readily compute the ratio of the cross sections in question. The ratio $(n\cdot a)_{Pu}/(n\cdot a)_{nat}$ was determined by placing the same ionization chamber in the beam of thermal ions from the Saclay pile and applying the same relationship, this time to the thermal neutrons, using the ratio of the fission cross sections of plutonium-239 and natural uranium. This Lévêque, who found the ratio to be 205.7 ± 4. This ratio was obtained from an entirely independent experiment carried out by Cotton, Cohen and gave us the ratio of the quantities $n\cdot a$, used to compute the value of the cross section at 1600 kev:

$$\sigma_{Pu,\ 1600\ kev} = 2.04 \pm 0.12 \text{ barns}$$

The second part of the program had to do with the energy dependence of the fission cross section of Pu^{239}.

The variation in the fission count as the energy of the neutrons was reduced to about 25 kev was studied, the neutron beam being monitored by means of the long counter. The results are shown in Slide 59. It shows that the cross section remains constant at the just noted value of 2.04 ± 0.12 barns between 2000 and 350 kev. It will be seen that in the region of lower energies the fission cross section goes through a minimum of about 1.6 barns at an energy of approximately 125 kev.

Slide 60 (Fig. 3*a* of P/355) shows the results. It will be seen that the fission cross section remains virtually constant above 400 Kev and that it goes through a minimum at an energy of 125 kev; we determined this minimum value to be 1.6 barns.

The third part concerned measurements on uranium-235.

Slide 61 (Fig. 2*b* of P/355) shows the variation of the ratio $\sigma_{Pu^{239}}/\sigma_{U^{235}}$ with the neutron energy.

Slide 62 (Fig. 3*b* of P/355) shows the curve for the cross sections of U^{235} obtained on the basis of the last two curves. The hatched area indicates the uncertainty range in the region where the fission of uranium-238 intervenes. We have not made any accurate measurements in this region, but have only compared the count rate of a natural uranium fission source with that for the enriched source I mentioned previously.

As may be seen from the curve, the cross section remains virtually constant between 700 and 1000 kev, its value in this region being about 1.15 ± 0.15 barns.

The fourth and last part of the program concerned measurements on uranium-233. Here, again, we determined the variation of the ratio of the cross sections as a function of the energy. To this end we found the ratio of the quantities $n \cdot a$ for plutonium and for uranium-233 and in our calculations made use of the value of 0.627 ± 0.06 for the ratio in the thermal neutron region found as a result of the experiments described earlier at this session by Mr. Vendryes.

Slide 63 (Fig. 2*c* of P/355) shows the variation of the fission cross sections ratio σ_{Pu}/σ_{233} with the neutron energy.

Slide 64 (Fig. 3*c* of P/355) shows the cross sec- of uranium-233 as deduced from the values for plutonium I cited earlier. The absolute value was found to be 1.92 ± 0.25 barns at 850 kev.

Mr. B. C. Diven (USA) presented paper P/594 as follows: This paper describes several methods which are used especially for determining neutron flux during measurements of fast fission cross sections. Our procedure for the determination of the fast fission cross sections has been to make an absolute determination of the fission cross section of U^{235} at a few energies. This is done by a comparison to the *n,p* scattering cross section. Then we extend this measurement to other energies mostly by use of a carefully calibrated long counter. Then the cross sections for the other fissionable materials have been determined by measuring their ratios to the cross section for U^{235}, and also as an additional check, by extrapolating these cross sections by use of long counters.

The most difficult of these measurements was the absolute determination of one of the fission cross sections, which in our case was U^{235}. This was accomplished by comparing the rates at which fissions occur in a thin layer of fissionable material to the rate at which protons were scattered from a thin layer of hydrogenous material by neutrons from the same neutron beam. This method is almost identical, at least in principle, to that described in the book by Rossi and Staub.

Slide 65 (Fig. 2 of P/594) shows the counter which was used in this experiment. It is a double counter. The proton recoils are detected in the proportional counter region. Foils of the fissionable material and of the hydrogenous material are located in the proton recoil counter. The hydrogenous material faces in towards the center wire. The fissionable material is on a platinum foil which is placed back to back to the hydrogen radiator and faces a region which is an ionization chamber, the plate being the collecting electrode. Neutrons come in from above through the fissionable material onto the hydrogenous material, knocking protons into the proportional counter.

We have picked this particular method for determining the absolute cross section, using thin radiators of both materials, because they can be placed in essentially the same volume in space. The two materials are separated by only a few thousandths of a centimeter of platinum. This makes the problem of reproducing results much simpler than if we use a gas-filled counter which has considerable extension in space.

Slide 66 (Fig. 1 of P/594) shows the pulse-height distribution that we obtain in our proton recoil counter. A radiator which used 80 micrograms per square centimeter was about the weight that we used for most of this experiment. Shown in the slide is the number of protons per five volts pulse-height interval. Note that abscissa does not start at zero. The low-energy proton recoils are obscured by gamma rays and also by carbon atoms recoiling in the neutron beam.

We therefore only measured the upper part of its distribution and then must somehow determine the total number of neutron-proton scatterings which occurred. This is done by fitting the theoretical curve, taking into account the absorption of energy in the hydrogenous material. Such a curve is the solid line, which is fitted to the data that we actually obtained. In general the fits are very good. These are five-volt channel widths which do not show the true sharpness of the cut-off.

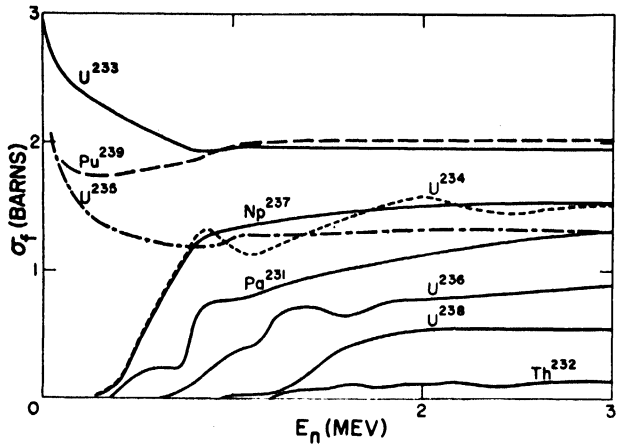

Slide 68

Slide 67 (Fig. 5 of P/594) shows the results we obtained for uranium-235. These numbers, of course, just come from the ratios of amounts of hydrogen and of uranium-235 and the ratios of counting rates plus a very large number of small corrections.

We believe that our best point is the one that we have worked hardest on at 1.25 Mev, for which we quote a value of 1.27 barns. We believe this is accurate to 3½ per cent.

The points shown on the curve were all taken with the proton recoil monitor, and in that sense are all absolute determinations. The solid line drawn through the points was determined primarily by a long counter extrapolation done independently by another group and normalized at 1.25 Mev. The shape of the cross section is determined by the long counter. It agrees very well with that determined by the proton recoil detector.

At low energy the results are not very good and I believe that the cross section in that region, below 700 kev should be considered to be good to about 7½ per cent. At high energy, let us say at above 1½ Mev, where the extrapolation was made entirely by long counter methods, about 5 per cent is the accuracy we like to quote. The cross sections for the other fissionable materials have been determined in several laboratories in the United States, mostly by counting fissions in a double chamber simultaneously from uranium-235 and from the other fissionable material.

Slide 68 shows a large number of fission cross sections which have been determined relative to U^{235}, and using those values these cross sections are obtained. These results are all in the cross-sections compilation which you can observe at your leisure. On the slide, however, you do see them all together so that you can see certain characteristics in common. Several of these cross sections, as I said, have been determined by various laboratories, and I believe that for those materials shown here, wherever we have been checked—for example, both at Oak Ridge and at Los Alamos—we have had very good agreement.

Slide 69 shows the fission cross section of neptunium-237 which has been carried to a higher energy. It is also shown in the compilation. There will be seen a very sharp rise in the neighborhood of 6 Mev.

Thorium-232 has very recently been carried up to 10 Mev with the large electrostatic generator at Los Alamos. The cross section, Slide 70, again shows a rise and then decreases above 8 Mev. Then there is an isolated point at 14 Mev. which indicates that the cross section is probably continuing to decrease somewhat in that region.

DISCUSSION OF SESSION 17A.4. (P/355 AND P/594)

The CHAIRMAN: This was the last scheduled paper for the session. We now have a few minutes for questions and discussion with regard to the last two papers.

The first question is to be asked of Mr. Berthelot

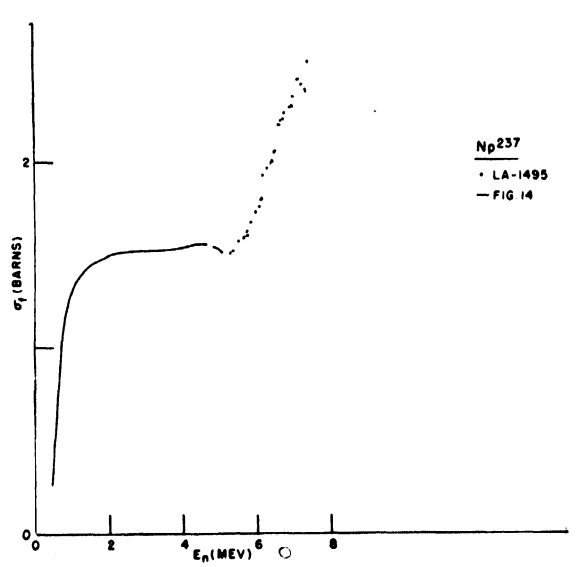

Slide 69

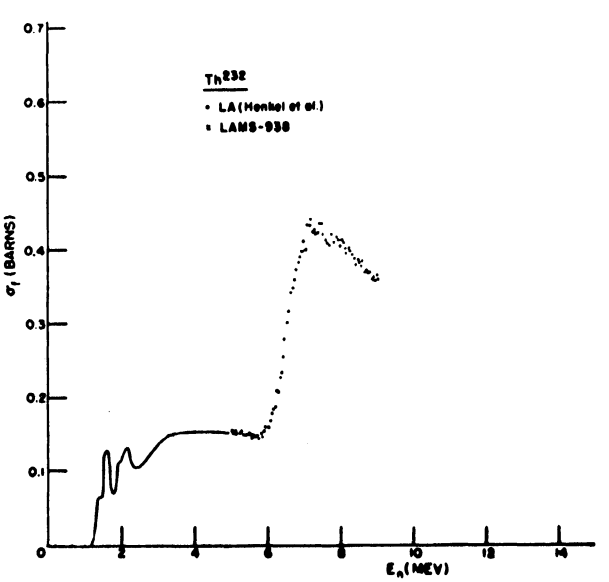

Slide 70

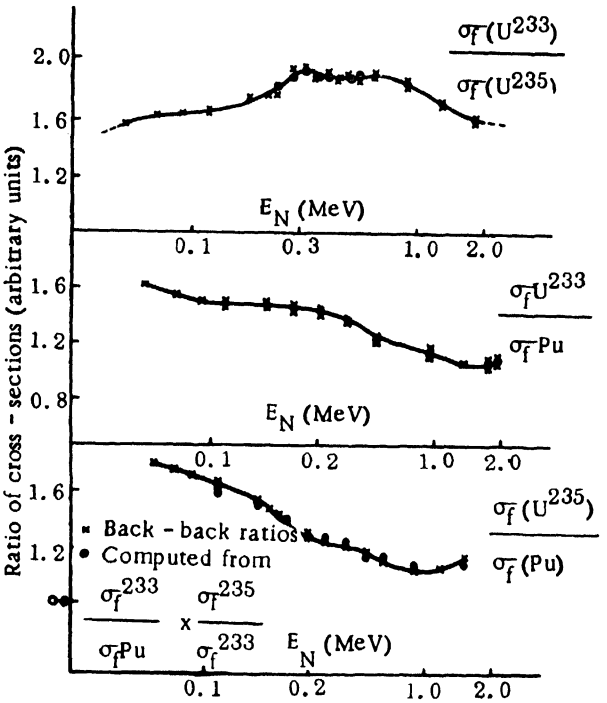

Slide 71. Fission cross section ratios: (variation with energy)

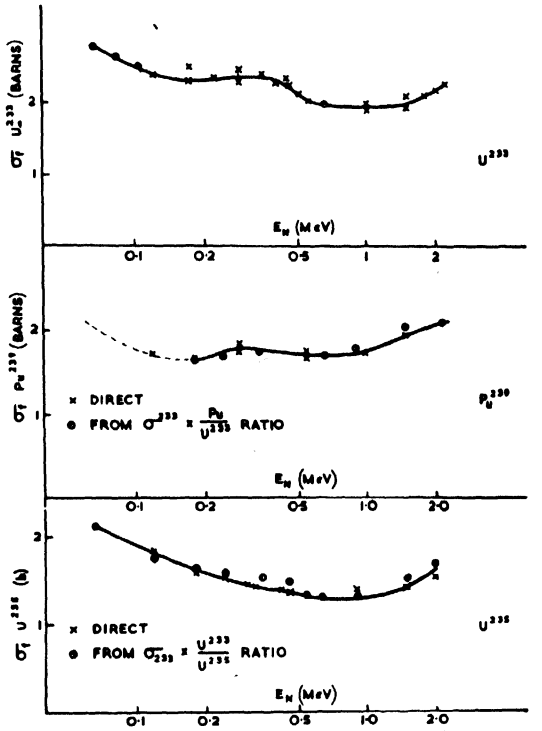

Slide 72. Fission cross sections

by Mr. M. S. Kodzodaev of the USSR. Since Mr. Kodzodaev is not present at this time, I shall read his question. He would like to have a little information about the measurements of ν_{eff} for U^{233}, U^{235} and Pu^{239}.

Mr. BERTHELOT (France): This has not been done.

Mr. EGELSTAFF (UK): I want to describe for a few minutes the results of several years of hard work by a team under the direction of W. D. Allen which has been working at Harwell on the measurement of the fission cross section of U^{233}, U^{235} and Pu^{239} in the region of 100 kev to 2 Mev. I will skip over all details of the measurements, but instead I will just indicate the various steps which Allen and his co-workers have taken.

In everything they have done they have tried to repeat every important step by two or more methods. They used the Van de Graaff machine as a neutron source, using a Li target for measurements below 625 kev and a tritium target for measurements above that. The flux measurement was done in two ways. First, they used a proportional counter. The performance of this counter was checked against the theory by running it at several pressures of hydrogen and several pressures of methane. Excellent agreement was found. They believe that the flux measurements made with the proportional counter were accurate to 2 or 3 per cent.

Flux measurements were also made with a long counter. The performance of the long counter as a function of neutron energy was checked with a number of neutron sources. It was found to be flat over a fairly large part of the range from 100 to 2000 kev, but at lower energies there was some falling away from the flatness similar to that shown in the diagram presented by Mr. Berthelot, although, in our case, the fall away was somewhat less than he reported.

The absolute calibration of flux was also checked; that is, the efficiency of the counter was checked with the Oxford photoneutron source. The Oxford group stated that they could measure the neutron flux from this source to 2 per cent. If we compare their flux measurement with that of our recoil counter, the agreement is within 1 per cent, which is actually better than the accuracy of the measurement.

The fission cross sections were done in two ways. First of all, the three ratios of plutonium, 233, 235 as functions of energy were measured with back-to-back fission chambers, and then the absolute value

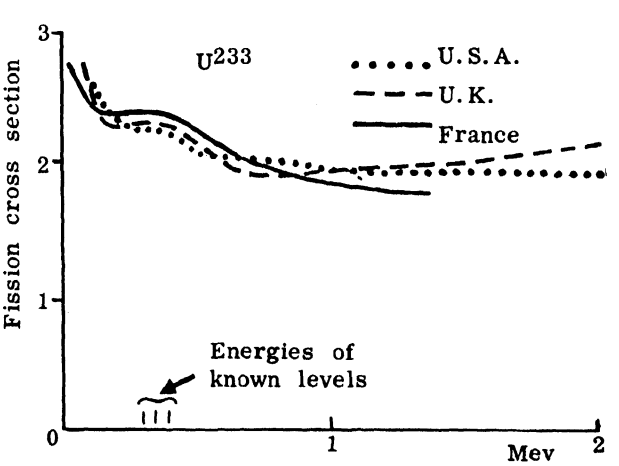

Slide 73

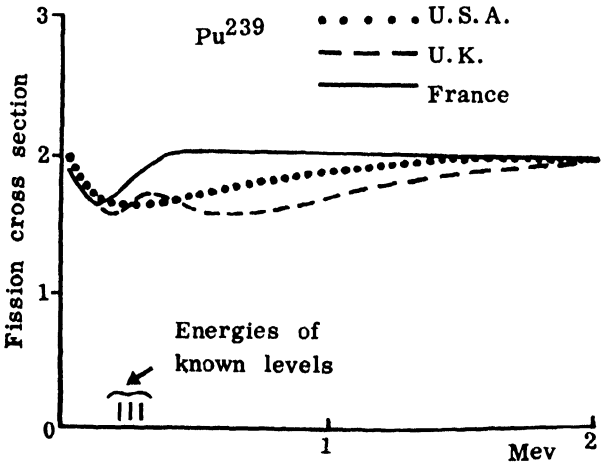

Slide 74

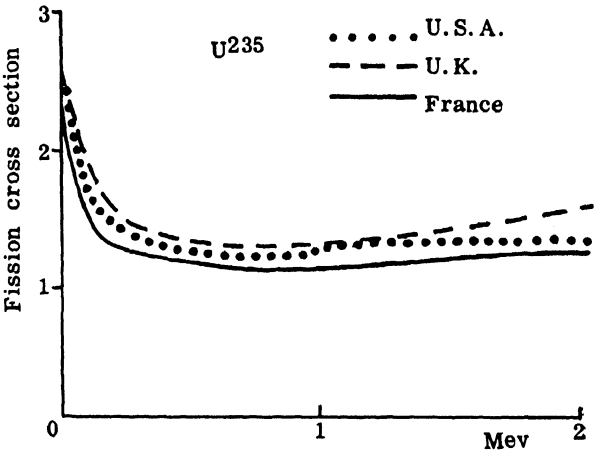

Slide 75

of each ratio was measured separately, and the variation with energy for each of the three isotopes also measured separately; so we have two values of the ratios of the three combinations. Thus we can work out the cross section of any element.

In addition, the absolute values of the fission cross sections at 600 kev and 1800 kev were measured for each of the three isotopes, and also the absolute ratio was measured at each of those points. Consequently, one can also work out the absolute value in two ways. All these cross sections agreed satisfactorily and we believe that the measurements which I am about to show are consistent and accurate to 3 or 4 per cent.

Slide 71 shows the ratios of the cross sections.

Slide 72 shows the absolute values of the cross sections, and it can be seen that the cross indicates the direct measurement; the circles indicate the same thing determined from the ratio measurements, and there is in every case reasonable agreement, although there may be some slight discrepancies.

To conclude, I should like to compare our data with that obtained in France and the United States. Through the co-operation of the workers in those countries I have been able to make a rough comparison of this data (Slides 73, 74, 75).

I have indicated the United States results with dots; the United Kingdom results with dashes, and the French results by a continuous line. Fairly good agreement can be seen, although some divergencies undoubtedly exist. For U^{235} the agreement is quite satisfactory; the displacement of the line is within the accuracy of the various measurements.

In the case of plutonium there is some disagreement, although only of the order of 5 to 10 per cent.

The contrast between the plutonium data and the other isotopes is that the plutonium data from the three countries are in excellent agreement from 1.5 to 2 Mev.

If I may just repeat the type of remarks Mr. Hughes made, I think that everybody in the high energy field can feel equally happy with those workers in the lower energy field in that good argeement has been found.

The CHAIRMAN: I have a written answer to a question which was asked previously by Mr. Havens. Mr. Sukhoruchkin gives this answer: The beam current was up to 1 milliampere.

Session 18A

PROPERTIES OF FISSIONABLE MATERIALS (ν, η, α): RESONANCE ANALYSIS

LIST OF PAPERS

		Page
P/657	Measurement of the neutron multiplication factor for thermal fission of uranium and plutonium ..... P. E. Spivak and B. G. Yerozolimsky	295
P/658	Number of fission neutrons per captured thermal neutron in U^{233}, U^{235} and Pu^{239} ..... A. J. Alichanov *et al.*	301
P/660	Number of fission neutrons per captured thermal neutron for natural uranium ..... N. A. Burgov	305
P/425	Neutron yields from fissile nuclei ..... P. A. Egelstaff and J. E. Sanders	307
P/587	Measurement of capture to fission ratio of U^{235}, U^{233}, and Pu^{239} by a new method ..... H. Palevsky	311
P/595	Capture-to-fission ratio of Pu^{239} and U^{235} for intermediate energy neutrons ..... W. R. Kanne *et al.*	315
P/585	Theoretical analysis of neutron resonances in fissile materials ..... H. A. Bethe	321
P/590	Status of information on reactor material cross sections ..... H. Hurwitz	328
P/583	Analysis of low energy neutron resonances ..... E. Melkonian	340

Measurement of the Neutron Multiplication Factor for Thermal Fission of Uranium and Plutonium

By P. E. Spivak and B. G. Yerozolimsky, USSR

To calculate a nuclear reactor it is highly important to know the number of the secondary fission neutrons emitted per one neutron captured by the nucleous of the fissile isotope. This quantity which we shall denote here ν_{eff}, can be expressed by $\nu_{eff} = \nu\ (\sigma_f/\sigma_c)$, where ν is the average number of secondary neutrons emitted per fission and σ_f and σ_c are the nuclear fission and capture cross sections, respectively.

Knowledge of the precise value of ν_{eff} is of particular importance for designing reactors to reproduce fissionable materials, as the reproduction factor directly depends on $\nu_{eff}-2$.

This paper gives the results we achieved in measuring the number of neutrons emitted per captured thermal neutron for isotopes U^{235}, U^{233} and Pu^{239}.

METHOD OF MEASUREMENT

The method of measuring ν_{eff} is based on comparing a sample of a fissionable material with a sample of a neutron absorbing substance (boron, for instance). The two samples are placed alternately in a large graphite column mounted on the top of an experimental uranium-graphite pile (Fig. 1).

A multilayer boron ionization chamber whose current is proportional to the thermal neutron density is placed in the graphite at some distance from the samples.

When the absorbing sample is introduced, the distribution of the thermal neutron flux in the graphite changes. The corresponding change of the current in the chamber ΔI_1 can be regarded as the effect of a thermal neutron sink whose intensity Q_1 is defined as the number of thermal neutrons captured by the nuclei of the sample per unit of time. Thus,

$$-I_1 = -k_1 Q_1 \qquad (1)$$

where k_1 is the ionization chamber efficiency of registering the thermal neutrons captured by the sample.

When the fissionable sample is introduced, the change in the thermal neutron flux and the resultant change in the boron chamber current ΔI_2 can be considered as the resultant of the thermal neutron sink of intensity Q_2 and the fast fission neutrons source of intensity $Q_2\nu_{eff}$ is the number of thermal neutrons captured by the fissionable sample per unit of time.

Consequently,

$$\Delta I_2 = -k_1 Q_2 + k_2 Q_2 \nu_{eff} \qquad (2)$$

where k_2 is the ionization chamber efficiency of registering the fission neutrons emitted by the sample.

After dividing Equation 2 by Equation 1 and introducing

$$x = \frac{\Delta I_2}{\Delta I_1} = (k\nu_{eff} - 1)\cdot y$$
$$y = \frac{Q_2}{Q_1} \qquad (3)$$
$$k = \frac{k_2}{k_1}$$

we get as the final result

$$\nu_{eff} = \left(\frac{1}{k}\ 1 - \frac{x}{y}\right) \qquad (4)$$

The effects of neutron scattering by the sample have not been taken into account in Equations 1 and 2 because the thermal neutron flux in the graphite at the position for the samples is practically isotropic, and therefore the neutron scattering by the sample does not change the chamber current. The absence of scattering effects can be verified by a sample of a non-absorbing neutron scattering material, such as graphite, for instance.

It follows from Equation 4 that to determine ν_{eff} it is necessary to find the values y and k besides measuring $x = \Delta I_2/\Delta I_1$.

The value $y = Q_2/Q_1$ represents the ratio between thermal neutron capture rates of the absorbing and fissile samples. Since both samples are put in the same place y is equal to the relation between the macroscopic effective capture cross sections of the samples (taking into account the self-screening effect of the nuclei. The macroscopic effective capture cross section value can be calculated from the weights of the samples and the tabulated nuclear capture cross sections. Such calculation, however, would yield too great an error in the final result. The value of y has therefore been determined in a separate experiment.

The factor k represents the difference between the ionization chamber efficiencies of registering the thermal neutrons as captured by the sample and the

Original language: Russian.

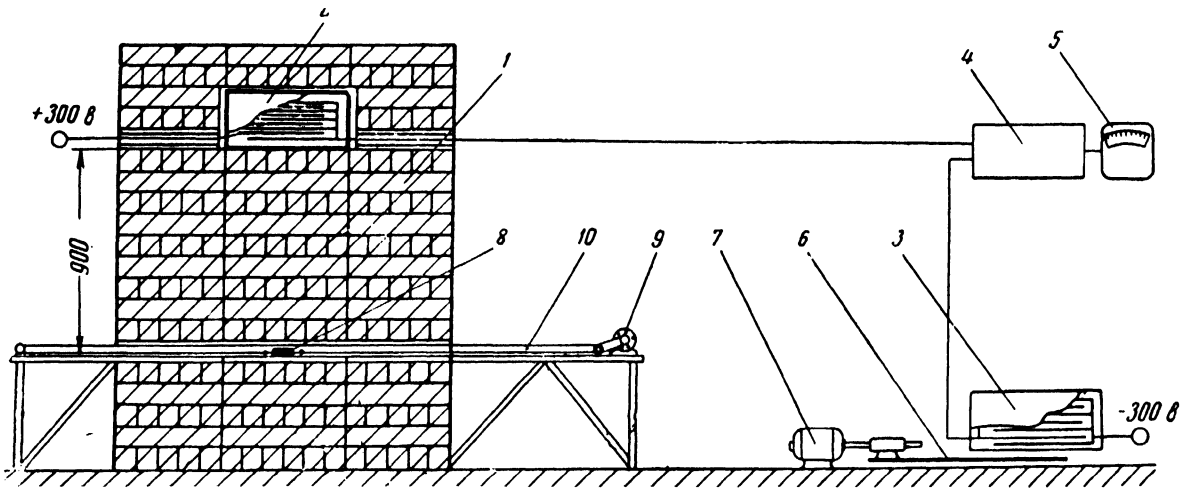

Figure 1. View of the experimental arrangement: (1) graphite column; (2) main boron ionization chamber; (3) auxiliary chamber; (4) amplifier; (5) output ammeter; (6) cadmium shutter; (7) remotely controlled selsyn; (8) sample; (9) motor for moving sample; and (10) steel wire

fast neutrons emitted by it. The value of this factor can be computed from the neutron slowing down and diffusion formulas, for the graphite column. In the present work, however, the value of this factor too has been determined experimentally.

The factor k differs from unity for three reasons:

1. The dimensions of the column are finite, which causes a leakage of neutrons varying with their energy.

2. The distance between the chamber and the samples in the graphite is finite, due to which a certain fraction of the fast neutrons emitted by the fissionable sample reaches the chamber before slowing down, thus lowering its efficiency.

3. The graphite absorbs more thermal neutrons than fast ones.

It is clear that the factor k would be exactly one when the diffusion medium were infinite, homogeneous and non-absorbing, and the distance between the chamber and the sample infinite.

In our case, the dimensions of the block and the distance between the chamber and the place for the samples were sufficiently large for k to be unaffected by further increase of these dimensions. The value of k was thus practically equal to the value for infinite dimensions k_∞.

Thus the method of determining k is as follows:

1. The dependence of $k\nu_{eff} = 1 - (x/y)$ for the fissionable sample on the specific absorption of the medium or on some other quantity proportional to this absorption (for instance, $1/L^2$, where L is the easily measured thermal neutron diffusion length) is investigated and plotted. The specific absorption can be increased above its inherent value by adding some kind of absorber to the graphite.

2. The obtained curve is extrapolated to the zero of the abscissa, corresponding to zero absorption of the medium, when, in accordance with the above, k_∞ and so in our case also, k is unity.

Thus we determine the value of ν_{eff} for our sample and the value of k for the column without extra absorption. The latter value can then be used for further measurements with other samples of fissionable isotopes.

Before passing to the experimental part of the work it should be noted that all the values to be measured for obtaining ν_{eff} namely x, y, k, are relative.

Equation 3 does not include any absolute parameters, such as neutron registration efficiency, neutron flux, capture cross section, etc. This circumstance constitutes the chief merit of the above method by which it is possible to obtain highly accurate data. The main difficulty in the measurements arose from the fact that the effects of the current changes ΔI in the chamber were small compared to the current I_0.

The distance between the chamber and the place for the samples is a very important parameter, the choice of which depends on the method of determining k. It has been shown by experiment that this distance must not be less than 80 cm. In our case the relative change of the current in the chamber due to the insertion of the samples was only

$$\frac{\Delta I}{I_0} \approx (1\text{–}2) \times 10^{-3}$$

For measuring such small effects with the necessary accuracy ($\pm$ 1%) the ionization chamber current was compensated by that of a second boron chamber mounted on the top of the pile at a sufficient distance from the column (Fig. 1).

Both chambers were connected to the input of a dc amplifier. In order to accurately regulate the compensation, the current in the auxiliary chamber could be gradually changed by a remotely controlled cadmium shutter, so that the ammeter connected to the output of the amplifier registered zero.

Table I. Samples

Sample number	Material	Compound	Weight, gm	Number of nuclei in sample	Degree of purity
1	Natural uranium	UO_2	144.8	3.23×10^{23}	Very pure
2	U^{235} (92.6% concentration)	U_3O_8	1.750	3.48×10^{21}	Admixture of Fe~1%
3	U^{233} (94.6% concentration)	U_3O_8	1.750	3.59×10^{21}	Admixtures $\leq 0.5\%$
4	Pu^{239} (99% concentration)	PuO_2	0.953	2.10×10^{21}	Admixture of La~0.5%
5	Boron	$Na_2B_4O_7 \cdot 10H_2O$	0.486	3.07×10^{21}	Chemically pure
6	Boron	H_3BO_3	0.302	2.95×10^{21}	Chemically pure
7	Boron	H_3BO_3	0.283	2.77×10^{21}	Chemically pure

THE EXPERIMENTAL ARRANGEMENT

The graphite column is a parallelepiped 180 × 180 centimeters at the base and 200-centimeters high mounted on the surface of the reflector of a uranium-graphite pile. The samples are automatically inserted in a 50 × 100 millimeter channel in the column, 50 centimeters from the bottom.

A large ionization chamber is installed in the graphite 90 centimeters from the channel. The chamber is a duraluminum box, not hermetically sealed, containing 40 rectangular 25 × 50 centimeter aluminum plates. The even numbered plates were interconnected in one group, and the odd ones in another. The plates are coated on both sides with a thin layer of amorphous boron. The total boron-coated area is 100,000 cm^2; and the total weight of the boron is 50 grams. One group of the plates is connected to a potential of 300 v, the other to the input of the dc amplifier by means of a cable with negligible electric leakage. The auxiliary chamber is identical to the main one.

The dc amplifier is a two-stage negative feedback unit with a current sensitivity about 10^{-10} amps per scale division of a 150-microampere ammeter.

The current in the main ionization chamber was 10^{-5} amp and was compensated with an accuracy of 10^{-10} amp.

Owing to the statistical fluctuations of the current in both chambers, the ammeter recording needle was not stationary. A ripple filter with a time constant of $T = 10$ sec was installed at the input of the amplifier whereby the amplitude of the needle fluctuations was reduced to an average of ± 1 scale division. The zero drift owing to slow changes in the neutron field of the pile caused by temperature changes, remained within the limit of 2–3 scale divisions per half hour. This effect could be easily eliminated by alternating measurements with and without sample. The fissionable and absorbing samples were contained in round aluminum boxes 3 mm thick, and 85 mm in diameter. After the samples were placed in the boxes and pressed, the lids were sealed. In order to fill the boxes uniformly the samples of U^{235}, U^{233} and Pu^{239}, as well as the boron compounds which were used as absorbers, were mixed with pure graphite powder. The samples of natural uranium were prepared from pure oxide. Table I gives data characterizing the used samples.

MEASURING THE RELATIVE ABSORPTION OF THE SAMPLES

It has been pointed out that to compute ν_{eff} from Equation 4 it is necessary to determine separately the ratio between the thermal neutron capture rates of the two compared samples.

For this purpose, a system of compensated ionization chambers, as described above, was used. The graphite column was disassembled up to the level of the channel. The main chamber was placed on a special support above the place for the samples (Fig. 2).

As we know, a boron chamber not surrounded by graphite is practically insensitive to fast fission neutrons directly entering the chamber. With a view to minimizing the effect of the fission neutrons which slow down in the graphite base of the column and enter the chamber as thermal neutrons, the whole surface of the base, with the exception of the aperture over the samples, was shielded by cadmium. By means of a Ra-α-Be neutron source of sufficient intensity it was proved that the measuring system was insensitive to fast neutrons within experimental error.

To eliminate the sample neutron scattering effects a special method was used. It can be briefly described as follows: a cadmium shutter (Fig. 3) was placed beneath the place for the samples to shut off a certain cone from the flux of neutrons passing through the sample towards the chamber. Neutron scattering in the sample causes an increase of the current in the part of the boron chamber screened by the cadmium shutter and a decrease in the remaining part of the chamber. The chamber and the cabmium shutter can be so placed as to completely balance both effects. This can be verified by samples which only scatter but do not appreciably absorb neutrons (graphite, magnesium, bismuth).

To decrease possible residual scattering effects, all the samples were prepared to have approximately equal macroscopic scattering cross sections, and when measurements were made without a sample, a box containing graphite of equivalent macroscopic scattering cross section was put in instead.

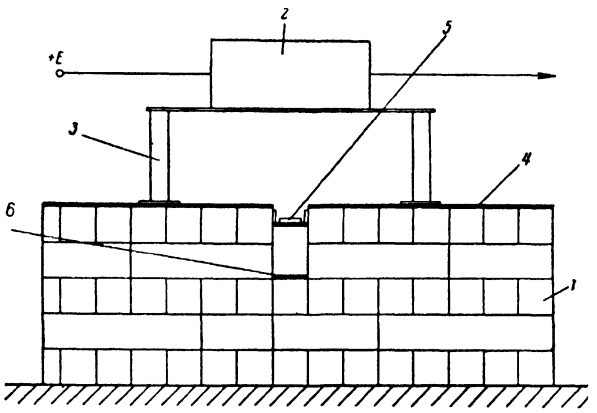

Figure 2. Arrangement for measuring relative absorption: (1) base of graphite column; (2) boron chamber; (3) support; (4) cadmium sheet; (5) sample; and (6) cadmium shield for compensation of scattering

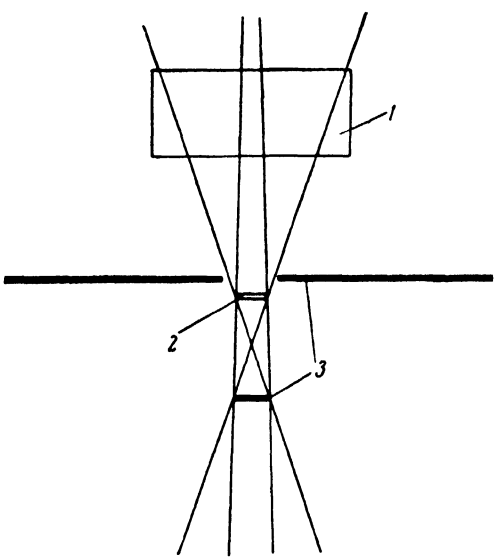

Figure 3. Principle of compensation for scattering: (1) chamber; (2) sample; and (3) cadmium

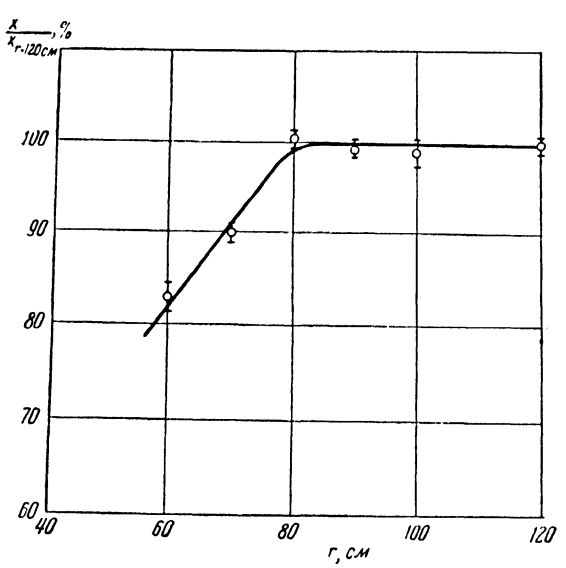

Figure 4. Dependence of the ratio $x = \Delta I_U/\Delta I_R$ on distance between sample and chamber

Control experiments have shown that the sensitiveness of the measuring system to neutron scattering was no more than $1/200$ of its sensitiveness to neutron absorption.

DETERMINATION OF THE FACTOR k

The factor k may be regarded as the ratio of the thermal neutron densities at distance r from sources of fast and thermal neutrons of equal intensity. The value of k for an infinite homogeneous medium equals

$$k = e^{\frac{L_f^2}{L^2}} \left(1 - \frac{L_f^2}{4\sqrt{\pi}} e^{-\frac{r^2}{4L_f^2} + \frac{r}{L} - \frac{L_f^2}{L^2}}\right) \quad (5)$$

This expression is valid provided $r \gg L_f$, where L_f is the slowing down length of the fast neutrons in the medium. The second term in brackets rapidly decreases with increase of distance. In the case of a graphite medium and fission neutrons ($L = 50$ cm, $L_f = 17.5$ cm) the value of the second term is less than 0.01 when $r \geqslant 75$ cm. According to Equation 5 the asymptomatic value $k = k_\infty$ is given by

$$k_\infty = e^{\frac{L_f^2}{L^2}} \quad (6)$$

which makes $k_\infty = 1.135$ for these values of L and L_f.

In order to determine experimentally the minimum distance for which the difference between k and k_∞ is sufficiently small, investigations have been carried out to find the dependence of the uranium-boron ratio $x = \Delta I_U/\Delta I_B$ on the distance r between the sample and the chamber. The curve in Fig. 4 shows the constancy of this ratio (and consequently of the factor k) at a distance of 70 to 75 cm and more, which is in complete agreement with the above considerations.

Similar measurements were made to determine the dependence of the value of x on the area of the column cross section. The minimum allowable value of the cross section was found to be 140×140 cm^2.

It has been mentioned earlier that the actual dimensions of the column exceeded these minimum values: the cross section of the column was 180×180 cm^2 and the distance $r = 90$ cm. These dimensions ensure that $k = k_\infty$ with sufficient accuracy.

To draw up an extrapolation diagram of the kv_{eff} dependence on the specific absorption of the column, the effects ΔI_U and ΔI_B had to be measured in the presence of aluminum sheets of different thickness placed between the layers of the graphite. So, too, was measured the thermal neutrons diffusion length in the column. This was done with a small boron absorber (the sink of the thermal neutrons) the effects of which were determined in a little boron chamber set at various distances from the absorber.

The experimental points in Fig. 5 represent the value of $kv_{eff} = 1 - (x/y)$ for the natural uranium sample, corresponding to the three values of $1/L^2$.

Table II. Summary of Results

No.	Investigated samples	Comparison sample	x	y	ν_{eff}
1	Natural uranium	Boron (no. 5)	−0.539±0.7%	0.995±0.9%	1.337±0.017
2	U^{235}	Boron (no. 6)	−1.392±0.5%	1.018±0.6%	2.065±0.025
3	U^{233}	Boron (no. 7)	−1.643±0.5%	1.008±0.6%	2.28 ±0.028
4	Pu^{239}	Boron (no. 7)	−1.352±0.5%	1.003±0.6%	2.035±0.025

The obtaining dependence of $k\nu_{eff}$ on $1/L^2$ practically does not deviate from a straight line, and a linear extrapolation to $1/L^2 = 0$ gives the value of $\nu_{eff} = 1.337 \pm 0.017$ for the natural uranium sample and, for k, in case of no extra absorption in the medium:

$$k = 1.155 \pm 0.01$$

which agrees with the value computed from Equation 6.

One may also draw an exponential curve as required by Equation 6 through the experimental points within the limits of indicated errors. The result of the extrapolation however, will change by not more than ± 0.5%, i.e., within the limits of the errors allowed for k.

It should be noted that the value of k in Equation 4 depends to a large extent on non-uniformity in the moderator near the sample. To eliminate any possible error, the central part of the column adjacent to the place for the samples was made up of specially selected graphite bricks tested for uniformity of their diffusion properties.

Moreover, the mass of the automatic device for moving the samples was reduced as much as possible.

Table III. Errors of Method

No.	Source of error	Error, per cent: For natural uranium	Error, per cent: For other isotopes
In measuring the value of x			
1.	Effect of neutron scattering in the sample	±0.08	±0.04
2.	Presence of absorbing materials near the samples (box, wire rope, non-uniformity in the graphite bricks)	0.05	0.05
In measuring the value of y			
3.	Effect of neutron scattering in the sample	±0.15	±0.05
4.	Effect of fast fission neutrons in chamber	±0.04	±0.03
In measuring the value of k			
5.	Uneven distribution of additional absorber in the block (aluminum sheets placed between layers of the graphite bricks)	±0.2	±0.2
6.	Finite dimensions of the detector in measuring the thermal neutron diffusion length	±0.2	±0.2
7.	Uncertainty of the extrapolation of the curve to zero (linear or exponential)	±0.5	±0.5

During measurement, there were inside the column only an aluminum box 0.3 mm thick, containing the sample, and a 1.5 mm steel-wire rope. It was shown experimentally that the correction due to these absorbers was about 0.4%.

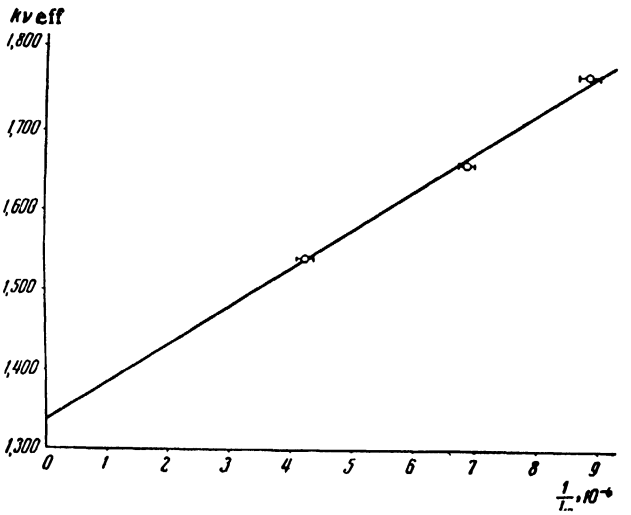

Figure 5. Extrapolation diagram $k\nu_{eff} = f(1/L^2)$

RESULTS OF THE MEASUREMENTS

Table II gives a complete summary of the results of the measurements carried out with the samples listed in Table I.

The values of ν_{eff} were computed from equation 4, k being assumed 1.155.

It should be noted that the results of measuring ν_{eff} for pure isotopes U^{235}, U^{233}, and Pu^{239} agree, within the experimental error, with the results of Alichanov, Vladimirski and Nikitin.[1] The value of ν_{eff} for natural uranium corresponds exactly with the result given by Burgov.[2]

From the data on the relative absorption of the samples given in Table II under y, together with the data on the number of nuclei in the samples as listed in Table I, it is possible to calculate the ratio of the capture cross sections of the isotopes under investigation to the boron cross section. This calculation yields the following ratios:

For natural uranium: 0.0095 ± 2%

For U^{235}: 0.86 ± 2%

For U^{233}: 0.78 ± 2%

For Pu^{239}: 1.325 ± 2%

Assuming that the capture cross sections of all these isotopes obey the $1/v$ law in the thermal neutron energy region, and taking the value of the boron capture cross section to be 755 barns at 1/40 ev, we obtain, accordingly, $\sigma_c = 7.15$ barns for natural uranium, $\sigma_c = 652$ barns for U^{235}, $\sigma_c = 587$ barns for U^{233} and $\sigma_c = 1000$ barns for Pu^{239}.

However, it should be borne in mind that the accuracy of the capture cross-section data depends on the accuracy of our knowledge of the number of the nuclei in the samples (Table I), i.e., on the errors made in determining the isotopic composition, the percentage of admixtures contained in the preparations, etc. What was said here about the capture cross sections does not apply to the chief contents of the present work, i.e., the results of measuring ν_{eff}, which do not depend on the number of the nuclei in the samples.

Table III gives a summary of all the methodical errors taken into account. The methods of determining or evaluating the principal corrections made in measuring x, y, and k have been considered. None of them exceeds 1 per cent.

The statistical errors in the measurements together with the apparatus inaccuracy amounted to $\pm$ 0.4% in measuring the value of x, $\pm$ 0.4% in measuring the value of y, and $\pm$ 0.8% in measuring the value of k.

The total statistical error in the value of ν_{eff} is 1 per cent.

The mean square value of the total methodical error computed from Table III is $\pm$ 0.6 per cent.

Thus the mean square value of the total error in the measurement of ν_{eff} is $\pm$ 1.2 per cent.

REFERENCES

1. Alichanov, A. I., Vladimirski, V. V. and Nikitin, S. J., P/658, *Number of Fission Neutrons per Captured Thermal Neutron in U^{233}, U^{235} and Pu^{239}*, Volume 4, Session 18A, these Proceedings.
2. Burgov, N. A., P/660, *Number of Fission Neutrons per Captured Thermal Neutron in Natural Uranium*, Volume 4, Session 18A, these Proceedings.

Number of Fission Neutrons per Captured Thermal Neutron in U^{233}, U^{235} and Pu^{239}

By A. J. Alichanov, V. V. Vladimirski and S. J. Nikitin, USSR

The measurement of the effective number of secondary neutrons, as $\nu_{eff} = \nu\sigma_f/\sigma_c$ (where ν is the number of secondary neutrons per one fission, σ_f the fission cross section and σ_c the total capture cross section, equal to the sum of the fission and radiation cross sections) leads to some difficulties.

The accurate determination of ν_{eff} from separate measurements of ν, σ_f and σ_c, is not expedient as it demands a lot of labour to get the precise values of these constants.

We have worked out a method of measuring ν_{eff} by observing the reactivity changes caused by the introduction into the reactor of a given amount of fissionable material. In order to get from the directly measured quantities to the value of ν_{eff}, it is necessary to determine in a separate experiment the ratio of the capture cross section of the fissionable material to that of boron for the thermal neutron spectrum.

Such measurements may be done with a high degree of accuracy without difficulty.

METHOD

The measurements of ν_{eff} were carried out on the heavy-water research reactor of the Academy of Science, USSR.[1] From the description of the reactor it may be seen that its control-system was specially designed for the measurements of reactivity changes. The precision drive of the control rods permits measuring small displacements accurate to within 0.1 mm. The control device possesses a high sensitivity, for example, the introduction of 1 mg of boron into the reactor (total cross section 4.10 cm) causes a displacement of the control rod of 1 mm. The method is based on this feature of the reactor.

The method is based on a comparison of the increase in reactivity, caused by the introduction into the reactor of a given amount of fissionable material, with the decrease in reactivity when a pure absorber (boron) is introduced. The changes in the reactivity were determined by the displacement of the control rod following the introduction of the samples. Thus it was possible to determine the amount of boron which, when introduced into the reactor, would compensate for the reactivity increase due to the introduction of the fissionable material.

If the total capture area of the fissionable material introduced equals $\sigma_1 N_1$ (N_1 is the number of fissionable nuclei, σ_1 the total capture cross section), and the captive area of boron compensating its positive reactivity is $\sigma_B N_B$, then ν_{eff} may be computed from the expression:

$$\nu_{eff} = \mu \left(1 + \frac{\sigma_B N_B}{\sigma_1 N_1}\right) \qquad (1)$$

The coefficient μ accounts for the different effect on the reactivity of the fast neutrons produced and of the slow neutrons absorbed.

For a reactor with a continuous lattice, the correction coefficient was computed by Galanin:

$$\mu = \frac{e^{\alpha^2\tau}}{\phi}\left(1 - 0.694\,\frac{a^2}{4\pi L^2}\,(1 + \kappa^2 L^2)\right)(1 - \epsilon) \qquad (2)$$

where for our reactor, $\phi = 0.903$, $k^2 = 8.0 \times 10^{-4}$ cm^2, $\tau = 150$ cm^2, $\alpha^2 = 81$ cm^2, and $L^2 = 6800$ cm^2. $\epsilon = 0.02$ is a small correction accounting for the uranium rods missing near the center of the reactor because of design considerations.

If all the fuel rods are in, the correction coefficient is found to be:

$$\mu = 1.222 \qquad (3)$$

Because of an uncertainty in the value of this coefficient and for the purpose of establishing the possible dependence of the effect on the neutron spectrum, the measurements were carried out with two essentially different uranium-rod arrangements. The first series of measurements was carried out with the lattice complete. In the second series a region free of uranium rods was left around the central experimental channel. The mean radius of this region, called the "thermal pit" was 35 cm.

For measurements inside this thermal pit the correction coefficient is much closer to unity; as the numerical calculations showed it was

$$\mu = 0.987 \qquad (4)$$

We also used another method for the determination of the correction coefficient for the thermal pit.

Let $N(r) = \overline{nv}$ be the spatial distribution of the thermal neutrons, normalized to unity at the centre of the reactor. When an absorber with a total cross section σ is placed at any point of the reactor, it absorbs $N(r)N_0\sigma$ neutrons per second, where N_0

Original language: Russian.

is the mean neutron flux at the centre of the reactor at a given power. The reactivity change $R(r)$, measured as the absorber cross section giving the same control-rod displacement when introduced at the centre of the reactor, is proportional to the number of neutrons absorbed and to the importance function $W(r)$, which expresses to what degree the negative source of neutrons due to an absorber placed at point r is weaker than a source of the same strength placed at the centre of the reactor. Normalizing the functions $R(r)$ and $W(r)$ to unity at the centre of the reactor we obtain:

$$R(r) = N(r)W(r) \qquad (5)$$

For a system with a uniform lattice throughout, except near the border one has, with fair accuracy,

$$W(r) = N(r) \qquad (6)$$

and thus the reactivity is proportional to the square of the density as would follow from elementary perturbation theory. As was shown by Kronrod, in a system with a pit, and in any system in the vicinity of the reflector, the course of the reactivity substantially differs from that of the square of the density. In this case the importance function may be computed as the ratio of the two quantities $R(r)$ and $N(r)$, both determined experimentally, provided the detectors and absorbers used do not themselves disturb the neutron density distribution appreciably.

For the lattice with a pit, $R(r)$ was measured by Burgov by moving a small boron absorber along the radius and the height of the reactor. He obtained the distribution of thermal neutrons from the activation of dysprosium detectors at different points of the reactor. The following integral was then calculated from these data:

$$J = \int \frac{e^{-\frac{r^2}{4\tau}}}{(4\pi\tau)^{3/2}} W(r)dv = 1.027 \qquad (7)$$

It indicates to what degree the effect of fast neutrons generated at the centre of the reactor and having (when moderated) a spatial distribution $e^{-r^2/4\tau}/(4\pi\tau)^{3/2}$, exceeds the effect of an equally strong source of slow neutrons at the centre of the reactor. Correcting by 0.5% for the resonance absorption, one obtains for μ:

$$\mu = \frac{1.005}{J} = 0.978 \qquad (8)$$

in good agreement with Equation 4.

Because of a considerable statistical inaccuracy in the experiments with dysprosium detectors, the error of this result may be 2%. Therefore in treating the experimental data we took for μ the value given by Equation 4, which is accurate to 0.5%.

The changes in reactivity caused by the introduction into the reactor of fissionable material and absorbers were determined as follows. Heavy-water solutions of the substances were put in the vertical experimental hole through the centre of the reactor to a depth corresponding to maximum neutron density. The reactor was operated at a power level of 20 watts kept constant within 0.3% by the automatic control device. The postion of the control rod before and after immersion was measured with an accuracy of 0.1 mm. The difference of the position-reading gives the value of the reactivity-change in units of control-rod displacement. Since in all measurements the lower end of the control rod was above the region of maximum neutron density, the rod efficiency increased when it got deeper into the reactor, and the calibrating curve (the dependence of rod displacement on the amount of boron introduced) was non-linear. As a result, the reactivity effect of the sample had to be determined by the method of least squares.

Because of the possibility of error in this procedure, we also used a compensation method. In this case boron was introduced directly in the solution of the sample being studied (U^{233}). It is obviously possible in this case to attain a zero reactivity effect and, hence, there is no need to use calibration curves.

The samples used were heavy-water solutions of boric acid, U^{233} oxalate, U^{235} oxalate and $Pu(SO_4)_2$. In the measurements six solutions were used. (Table 1).

The chemical analysis of the U^{233} and U^{235} samples showed an absence of tangible quantities of impurities with a large capture cross section as a result of which no corrections accounting for them were made. When evaluating the results obtained with Pu^{239}, corrections for the presence of hydrogen and sulfur were made. These were, respectively:

$$N_S\sigma_S = 0.73 \times 10^{-2}\ \text{cm}^2$$

$$N_H\sigma_H = 1.45 \times 10^{2}\ \text{cm}^2$$

Together these corrections correspond to an increase in the amount of boron in Equation 1 of 0.56 mg.

When determining the reactivity changes caused by the introduction of the samples into the reactor it is important to account for the action of the sample container. In order to determine this correction, calibrating measurements with all containers were performed. For this, the container was filled with pure heavy water, and the reactivity change due to its introduction in the reactor was determined. The effect of a container filled with heavy water on the reactivity is determined by two factors; the absorption of neutrons in the material of the container material and the increase of the amount of moderator in the reactor by introducing 300 cm³ of heavy water.

Table 1

No. of sample	*Isotope*	*Compound*	*Weight of isotope gm*	*Weight of boron gm*
1	U^{233}	$UO_2C_2O_4$	0.8865	–
2	U^{235}	$UO_2C_2O_4$	0.8886	–
4	U^{233}	$UO_2C_2O_4+B_2O_3$	0.7956	0.03965
9	Pu^{239}	$Pu(SO_4)_2$	0.9957	–
8	–	B_2O_3	–	0.0500
6	–	B_2O_3	–	0.1000

Table II

Sample No.	*1*	*2*	*4*	*9*
Reactivity effect of the container with solution	36.8	31.6	−6.8	48.0
Reactivity effect of the isotope	30.1	26.2	27.9	47.6
$1+\frac{\sigma_B N_B}{\sigma_1 N_1}$	1.97	1.74	2.00	1.71

Table IV

Sample No.	*1*	*2*	*4*	*9*
Reactivity effect of the container with solution	45.4	41.9	−0.1	66.9
Reactivity effect of the isotope	43.1	41.2	38.65	70.3
$1+\frac{\sigma_B N_B}{\sigma_1 N_1}$	–	2.16	2.395	2.03

These effects are of different sign and to a considerable extent compensate each other. The containers were calibrated before, during and after the experiments. In the case of the continuous lattice, the correction for the effect of the container amounted to 15% of the measured reactivity change; in the thermal pit it did not exceed 6%.

REACTIVITY MEASUREMENTS, DETERMINATION OF ν_{eff}

Table 2 contains the results of the reactivity measurements (expressed in mg of boron) for different samples, carried out with the complete lattice.

For calculating the values $|1 + (\sigma_B/\sigma_1)(N_B/N_1)|$ we took for the ratios of the capture cross section of U^{233}, U^{235} and P^{239} to that of the boron the values obtained in the experiments of Burgov, equal to 0.784, 0.914 and 1.517, respectively.

The last line gives the number of secondary neutrons not corrected for μ. The two measurements of $|1 + (\sigma_B/\sigma_1)(N_B/N_1)|$ in samples No. 1 and No. 4 differ by 1.5%. The measurement in sample No. 4 is the more precise one as it was obtained by compensation and did not require any extrapolation of the calibrating curve of the control rod. Because of this the value 2.00 was taken for $|1 + (\sigma_B/\sigma_1)(N_B/N_1)|$ of uranium-233.

If we now adopt the results obtained for U^{233} with sample No. 4, we get a new calibration of the control rod that does not require extrapolation of the calibration curves. In this case the calibration must be corrected so that the value of $|1 + (\sigma_B/\sigma_1)(N_B/N_1)|$ for uranium-233 measured with sample No. 1, becomes 2.00 as we obtained from the measurements with sample No. 4. From the thus corrected calibration curve the results for uranium-235 and plutonium were recalculated anew:

Isotope	U^{235}	Pu^{239}
$1+\frac{\sigma_B N_B}{\sigma_1 N_1}$	1.75	1.73

Taking as the most reliable data the mean value obtained by different methods, and accounting for the correction factor (4), we obtain the following average data with the complete lattice.

Table III

	U^{233}	U^{235}	Pu^{239}
$1+\frac{\sigma_B N_B}{\sigma_1 N_1}$	2.00	1.74	1.71
ν_{eff}	2.44	2.12	2.08

Table 4 contains the results of the reactivity measurements with different samples obtained in the thermal pit.

As may be seen from Table 4, the positive effect of U^{233} in sample No. 4 is fully compensated by the absorption in boron. Because of this, the measurements of ν_{eff} performed with sample No. 4 are practically free of errors resulting from control-rod calibration. Extrapolation of the calibration curve from samples No. 8 and No. 6 gives for sample No. 1 a very close but a less reliable result.

Because of this, in determining ν_{eff} for U^{235} and Pu^{239} use was made of the calibration based on samples No. 1 and No. 4; the positive effect of sample No. 1 was obtained from ν_{eff}, determined by means of sample No. 4, and the effects of sample No. 2 and No. 9 were then obtained by linear interpolation.

DISCUSSION

When comparing the results for the three metals in the complete lattice and in the pit lattice (Table 5) it is easily seen that the difference between the values of ν_{eff} obtained with these different rod-arrangements for U^{233} and Pu^{239} exceeds the limits of possible experimental errors.

In fact, the error in the coefficient μ for the two different rod-arrangements of the calibrating errors should lead (for all the isotopes) to practically the same difference between the values obtained with the two different rod-arrangements. The difference between the behaviour of U^{235} and that of the two other metals cannot be explained by the spread of the experimental values as the mean square error does not exceed 0.03. Probably, then, the difference is due to the differing energy dependence of the fission process for the investigated nuclei.

According to neutron velocity selector data, the capture and fission cross sections of U^{235} over a wide energy range are described by the $1/v$ law, whereas for U^{233} and Pu^{239} they sharply differ from the $1/v$ law at comparatively low neutron energies.

The number of epithermal neutrons in the pit lattice is much less than in the continuous lattice. On the whole we may consider the neutrons in the pit as being purely thermal. The epithermal neutrons in the case of the continuous lattice produce additional fission which leads to an increment of the reactivity effect. Actually, the method used is correct only in

Table V

Isotopes	U^{233}	U^{235}	Pu^{239}
With the pit	2.36	2.12	2.03*
Without pit	2.44	2.12	2.08
Difference	0.08	0	

* Corrected for the admixture of Pu^{240}.

the following two cases: if the fission and absorption spectra of the substance coincide with the absorption spectrum of boron, or if the neutron spectrum was the same when measuring the reactivity and when determining the cross section.

The cross section used for calculating the data had been obtained for a comparatively pure thermal spectrum. Therefore we must consider the data obtained with the pit as the correct data for U^{233} and plutonium. The agreement of the values obtained with for different neutron spectra in the case of U^{235} may serve as a good check of the method.

The accuracy of the results obtained may be estimated from the following considerations. The error in μ according to the estimation of Galanin does not exceed 0.5%. The error in a single reactivity measurement may amount to 0.2 mg B. As it is necessary to determine the reactivity effect of the solution, the container correction and the reactivity effect of the calibration solution, the accuracy in determining a reactivity effect of the order of 30–40 mg B will be about 1%. This corresponds to an error of about 0.5% in the final result. Allowing for possible errors in weight and purity determinations of the samples, we find in ν_{eff} an error equal to 1–1.5%.

Our results closely agree with the results of Spivak and Yerozolimsky, carried out by a different method.[2]

REFERENCES

1. Alichanov, A. I., Vladimirski, V. V., Nikitin, S. J., Galanin, A. D., Govrilov, S. A. and Burgov, N. A., P/623, *The Heavy Water Research Reactor*, Volume 2, Session 9A, these Proceedings.

2. Spivak, P. E. and Yerozolimsky, B. G., P/657, *Measurement of the Neutron Multiplication Factor for Thermal Fission of Uranium and Plutonium*, Volume 4, Session 18A, these Proceedings.

Number of Fission Neutrons per Captured Thermal Neutron for Natural Uranium

By N. A. Burgov, USSR

PROBLEM AND METHOD

The aim of the present investigation was the determination of the number of fission neutrons per captured thermal neutron for natural uranium. Henceforth this value will be denoted by η.

η and ν, the number of fission neutrons per fission, are connected by the relation:

$$\eta = \nu \frac{\sigma_f}{\sigma_f + \sigma_c}$$

Here σ_f is the fission cross section, and σ_c the radiative capture cross section. Both cross sections are taken per atom of natural uranium.

The increase in reactivity of a reactor when a uranium rod is inserted into it, was compensated by simultaneously introducing a heavy-water solution of a boron compound.

The experiments were performed on the heavy-water reactor of the Academy of Sciences, USSR. A thermal-neutron region, the so-called "thermal pit" was formed within the reactor, i.e., the centre of the reactor was emptied of uranium rods. The distance from the central experimental channel to the nearest remaining uranium rod was 28 cm.

The introduction of a point absorber into the reactor causes the following change in the multiplication factor:

$$\Delta k_c = -\,AV_c n_0(x) I_0(x) N_c \sigma_c \qquad (1)$$

where A is a constant, V_c is volume of the absorber, $n_0(x)$ is neutron density at the point where the absorber is introduced, N_c is number of absorber nuclei per cm^3, σ_c is effective absorption cross section for thermal neutrons of absorber nuclei. $I_0(x)$ is importance function.

If the neutron density at the position of the absorber obeys the equation

$$\Delta n_0(x) + \kappa^2 n_0(x) = 0$$

and κ^2 is constant throughout the volume of the reactor, then the importance function $I_0(x)$ is proportional to the neutron density.

When uranium is introduced, there will be a reduction of reactivity due to capture of thermal neutrons, and a simultaneous increase in reactivity as a result of the creation of fast neutrons

$$\Delta k_U = AV_U N_U n_0(x) I_0(x) [\eta\beta - 1] \sigma_{cU} \qquad (2)$$

N_U is the number of natural uranium nuclei, β a correction factor for taking care of the unequal effects on reactivity of the captured thermal neutrons and of the fast secondary neutrons.

If the absorber is not infinitely thin, then factors θ must be introduced which take care of the self-shielding of the internal layers.

In the case of compensation $\Delta k_c + \Delta k_U = 0$. Hence it follows that

$$\eta\beta = 1 + \frac{N_B \theta_B \sigma_{cB}}{N_U \theta_U \sigma_{cU}} \qquad (3)$$

if we introduce the weight of the boron and uranium used, P_B and P_U, then

$$\eta\beta = 1 + \frac{P_B \theta_B \sigma_{cB} A_U}{P_U \theta_U \sigma_{cU} A_B} \qquad (4)$$

MEASUREMENT AND RESULTS

1. The absorber consisted of a solution of borax ($Na_2B_4O_7 \cdot 10H_2O$) in heavy water. The water of crystallization in the borax was replaced by heavy water. A chemical analysis of the standard solution was carried out. 24.886 cm^3 of the standard solution contained 0.4530 gm of borax, with a boron content corresponding to 101.6% of the stoichiometric composition $Na_2B_4O_7 \cdot 10D_2O$.

The solution was placed in a quartz tube to form a column of approximately the same length as the uranium rod investigated.

The uranium rod was 4.9 mm in diameter and 8.14 cm long. It weighed 287.75 gm. The inside diameter of the quartz tube was 10 mm.

The uranium rod and the quartz tube with the solution were alternately introduced into the experimental channel, following which tube and rod were introduced together.

Table I gives the results of the measurements.

Analysing these measurements we find that:

(*a*) The introduction of the quartz tube with D_2O (without boron solution) is equivalent to the introduction of 1.31 ± 0.10 cm^3 of boron solution.

(*b*) The small change in height of the column of liquid (1–2 cm) affects but slightly the regulator reading.

Compensation is achieved by introducing

$$a = (22.82 \pm 0.2) \text{ cm}^3 \qquad (5)$$

Original language: Russian.

Table I

No.	Control rod reading with empty channel (mm)	Material placed in experimental channel	Height of liquid column (cm)	Volume of titrated solution (cm^3)	Control rod reading with sample introduced (mm)	Difference of control rod readings (mm)
1	66.1	Tube with D_2O	63	0	67.2	+ 1.1
2	66.1	Tube with D_2O	63	0	67.2	+ 1.1
3	149.8	Rod	–	–	109.0	−40.8
4	150.2	Rod	–	–	108.9	−41.5
5	150.0	Tube with D_2O	64	0.75	153.95	+ 3.95
6	150.0	Tube with D_2O	64.5	1.5	155.6	+ 5.6
7	150.2	Tube with D_2O	64.5	1.5	155.6	+ 5.35
8	150.4	Tube with D_2O	65	2.25	157.2	+ 6.8
9	150.5	Tube with D_2O	65	2.25	157.35	+ 6.85
10	150.5	Tube and Rod	65	2.25	114.6	−35.9
11	150.7	Tube and Rod	–	15	137.6	− 13.1
12	152.1	Tube and Rod	–	19.95	147.9	− 2.3
13	151.2	Tube and Rod	81.4	21.44	151.45	+ 0.25
14	151.4	Tube and Rod	81.4	21.44	151.38	+ 0.02
15	151.8	Tube and Rod	81.4	21.44	151.7	− 0.1
16	151.4	Tube and Rod	82.7	21.44	151.65	+ 0.25
17	151.4	Tube and Rod	82.7	21.44	151.7	+ 0.3
18	151.7	Tube and Rod	82.7	20.80	150.8	0.9
19	152.2	Tube and Rod	81.4	21.31	151.35	+ 0.15

of standard boron solution or, in terms of weight of boron

$$P_B = (47.6 \pm 0.4) \text{ mg of elementary boron} \qquad (5a)$$

CORRECTIONS, FINAL RESULTS AND DISCUSSION

For calculating the factors θ, which take account of self-shielding we used the following equation:

$$\theta = \frac{\frac{2L}{\rho} I_1\left(\frac{\rho}{L}\right)}{I_0\left(\frac{\rho}{L}\right)} \qquad (6)$$

where L is the diffusion length in the absorber, ρ is the rod radius, and I_0 and I_1 are modified Bessel functions. L_U is taken equal to 1.15 cm; L_B was calculated from

$$L_B^2 = \frac{1}{3}\lambda\lambda_{cB} \qquad (7)$$

$$\frac{1}{\lambda} = \frac{1}{\lambda_{cB}} + \frac{1}{\lambda_{tB}} \qquad (7a)$$

where λ_{tB} is the mean free transport path and λ_{cB} is the mean free path for capture. Then

$$\theta_u = 0.994 \qquad \theta = 0.998$$

The factor β was determined from the formula

$$\beta = \frac{\int_a^b I_0(x) n_0(x) \beta(x) dx}{\int_a^b I_0(x) n_0(x) dx} \qquad (8)$$

and

$$\beta(x) = \frac{\Phi'}{I_0(x)} \int I_0(x') \frac{1}{(4\pi\tau)^{3/2}} e^{-\frac{(\vec{r}-\vec{r}')^2}{4\tau}} dV \qquad (8a)$$

$I_0(x)$ was determined experimentally and was also numerically calculated.

β was then calculated by Galanin, who found

$$\beta = 1.013 \qquad (9)$$

In Equation 8a, Φ' is the neutron resonance escape probability both for the uranium rod itself, as well as for the rods located at a distance. It may be shown that Φ' is close to unity.

If (according to other measurements of the author) we take for the ratio $\sigma_{cU}/\sigma_{cB} = 1.025 \times 10^{-2}$; $A_U = 238.07$; $A_B = 10.82$, then the following final value is obtained

$$\eta = 1.341 \pm 0.006 \qquad (10)$$

This result is in agreement with the data obtained by Spivak and Yerozolimsky,[1] who obtained $\eta = 1.337 \pm 0.017$.

The results of the present experiments also agree with measurements of ν_{eff}^5 for the pure isotope U^{235} carried out by Alichanov, Vladimirski and Nikitin.[2]

If the value of ν_{eff}^5 for U^{235} found by these authors is used, then

$$\eta = \nu_{eff}^5 \frac{\sigma_{c5}}{\sigma_{cU}} \frac{N_5}{N_5 + N_8} = 1.35 \pm 0.03$$

where $N_5/(N_5 + N_8)$ is the concentration of U^{235} in natural uranium.

REFERENCES

1. Spivak, P. E. and Yerozolimsky, B. G., P/657, *"Measurement of the Neutron Multiplication Factor for Thermal Fission of Uranium and Plutonium,"* Volume 4, Session 18A, these Proceedings.
2. Alichanov, A. J., Vladimirski, V. V. and Nikitin, S. J., P/658, *"Number of Fission Neutrons per Captured Thermal Neutron in U^{233}, U^{235} and Pu^{239},"* Volume 4, Session 18A, these Proceedings.

Neutron Yields from Fissile Nuclei

By P. A. Egelstaff and J. E. Sanders,* UK

This paper summarizes measurements at Harwell on the three quantities $\bar{\nu}$, α and η for several fissile nuclides. The definitions are as follows:

$\bar{\nu}$ = average number of neutrons emitted per fission of the compound nucleus mass $A + 1$;

α = ratio of the radiative capture cross section to the fission cross section of the target nucleus mass A;

η = average number of neutrons emitted per neutron captured by the target nucleus mass A.

It is evident that: $\eta = \bar{\nu}/(1 + \alpha)$.

The first section of the paper describes measurements of $\bar{\nu}$ for thermal neutron induced fission of U^{233}, U^{235}, Pu^{239} and Pu^{241}.

The second section outlines the evaluation of α from cross-section data, including the variation of α with neutron energy.

Measurements of η for thermal neutrons and as a function of neutron energy are described in the third part of the paper.

The fourth section compares measured and derived values of η for U^{233}, U^{235} and Pu^{239}. Knowledge of η and its energy dependence is of fundamental importance for reactor calculations. In particular the number of neutrons available for capture in thorium or uranium-238 to produce fissile material is proportional to $\eta - 1$. In an ideal system with no neutron loss by capture or leakage "breeding" becomes possible when $\eta = 2$ (conversion factor = 1).

NEUTRON YIELDS PER FISSION

The average prompt neutron yields per fission ($\bar{\nu}$) have been measured for some uranium and plutonium isotopes by a direct fission-fragment and fission-neutron counting method. The fissions induced in a foil by a thermal neutron beam were counted in an ionisation chamber. The chamber was placed inside a paraffin-wax tunnel in which enriched BF_3 proportional counters were embedded, this serving as the neutron detector. The apparatus is shown in Fig. 1. In order to eliminate dependence on the absolute efficiency of the fission chamber the neutron detector was "gated" by square pulses triggered by fission pulses. The mean life of neutrons in the detector was about 155 μseconds and gate pulses up to a few milliseconds in length were employed. The neutron yield per fission is then simply proportional to the ratio of gated neutron counts to fission counts, after small corrections for "accidental" gate counts have been made. To obtain absolute values of $\bar{\nu}$, the neutron detector efficiency has to be known, while relative values merely involve counting rate ratios.

Relative $\bar{\nu}$ values for U^{233}, U^{235}, Pu^{239} and Pu^{241} have been measured by the above technique. For the Pu^{241} measurement a fission foil made from a highly irradiated plutonium sample was used and allowance made for the Pu^{239} contribution to the fission rate. All the measurements were made using a thermal beam from BEPO.

To obtain absolute values of the neutron yields the neutron detector was calibrated using natural uranium as a spontaneous fission source. The neutron yield was taken as $(1.59 \pm 0.09) \times 10^{-2}$ neutrons/sec-gm, measured in the GLEEP. The uranium in the form of a thin-walled cylinder was placed in the neutron detector in the position normally occupied by the fission chamber and the counting rate, and hence the detector efficiency, determined.

The results of the above work are given in Table I.

Table I

Nuclide	$\bar{\nu}$ *rel. to* U^{235}	$\bar{\nu}$
U^{233}	1.005 ± 0.016	2.45 ± 0.15
U^{235}	1.000	2.45 ± 0.15
Pu^{239}	1.168 ± 0.022	2.86 ± 0.18
Pu^{241}	1.217 ± 0.052	2.98 ± 0.21

Since a coincidence technique was employed the results refer to *prompt* neutron yields. Corrections for delayed neutrons are smaller than the uncertainties on our results.

Most of the error on the absolute values stems from the error on the neutron detector calibration and work is in progress to improve the calibration technique.

THE VARIATION OF α IN THE LOW-ENERGY REGION

The values of α in the low-energy region have been derived from the data on fission and absorption cross sections obtained on crystal and time-of-flight neutron spectrometers. In practice the ratio of the

* Work done by P. A. Egelstaff, D. B. Gayther, D. J. Littler, E. E. Lockett, J. E. Lynn, K. P. Nicholson, N. J. Pattenden, B. T. Price, J. F. Raffle, R. Richmond, J. E. Sanders and B. T. Taylor, Atomic Energy Research Establishment, Harwell, Berks, England.

absorption cross section to the fission cross section is first obtained from the measurements, and then α is found using the relation:

$$\alpha = \frac{\sigma_{Abs}}{\sigma_{Fiss}} - 1$$

Since differences in cross sections are involved which are rather small compared to the cross sections themselves, the values obtained for α have not a very high precision.

In order to avoid errors due to slight differences in energy scales and due to the use of different energies in the experimental points the cross-section data have to be smoothed before ratios can be taken.

In the case of U^{233} and U^{235} a simple smoothing technique was employed. Each measurement of the fission cross section was multiplied by the ratio of the absorption cross section to fission cross section at very low energy, deduced from the average of $\sigma\sqrt{E}$ over the lowest energy points where this product is approximately constant. The actual absorption cross section and the modified fission cross-section points were then plotted on the same cross section vs energy graph. Within the random fluctuations the two curves were found identical, indicating a constant cross-section ratio and hence a constant value of α.

Table II

	α Constant	
Nuclide	*Range*	*Precision*
U^{233}	0.005–2.1 ev	±20%
U^{235}	0.005–0.50 ev	±30%
Pu^{239}	0.002–0.50 ev	±11%

In the case of Pu^{239} a more exact smoothing method was used, involving the fit of an analytical expression to the cross-section data. This expression consisted of two Breit-Wigner terms and a $1/v$ component. A constant potential scattering cross section of 4 barns was taken as the best fit of the data above 2 ev. The resonance scattering can be shown to be quite negligible from the resonance parameters (as it can also in the case of U^{233} and U^{235}). The ratio of the absorption and fission cross sections fitted in this way was found constant over the range 0.002–0.50 ev. A constant value of α is thus

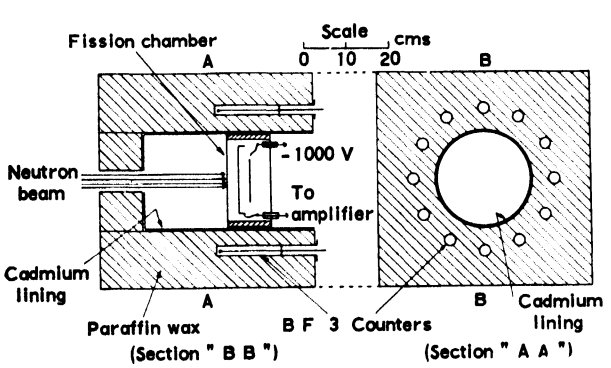

Figure 1. Arrangement of fission chamber and neutron counter for measuring neutron yield per fission.

indicated. The results of the calculations on U^{233}, U^{235} and Pu^{239} are summarized below (see Table II). The energy ranges above each include the first resonance of the nuclide in question.

Absolute values of α have been calculated from the cross-section data at a neutron velocity of 2200 m/sec. These values (Table III) will be expected to hold over energy ranges given above within the precision indicated there.

THE VARIATION OF α IN THE INTERMEDIATE ENERGY REGION

The variation of α in the intermediate energy region has been studied through the ratio of the fission and total widths of several resonances. The Harwell fission cross-section measurements yield values of $\sigma_f\Gamma$ for several levels (σ_f is the fission cross section at resonance, Γ is the total width), while the total cross sections measured with good resolution yield values of σ_γ and Γ for the same levels (σ_γ is the total cross section at resonance). Since the peak total cross section is equal to:

$$4\pi\lambda\!\!\!^{-2}\,\frac{g\Gamma_n}{\Gamma}$$

where Γ_n is the neutron width and g is a spin factor, the scattering width may be obtained within the uncertainty in g. All the scattering widths are found to be much less than the total widths so that this uncertainty is unimportant. Thus from this data we may obtain the values of the absorption width (Γ_a) and the fission width (Γ_f), and values of α and Γ for several levels are given in Table IV for the case of Pu^{239}.

The values of α, for the resonances above 0.3 ev, are more accurate than the values of Γ, and are uncertain by ± 30%.

In the case of U^{233} the above analysis is unreliable because levels are very broad, (~0.3 ev) and appear to overlap, so that the comparison technique used in the low-energy region was extended to 25 ev. From 2.1 to 25 ev it was found that α was equal to its value at 2200 m/sec to ± 40%. There are at least 16 levels between zero and 25 ev.

VALUES OF η FOR THERMAL NEUTRONS

The absolute value of η for U^{235} has been determined by the pile oscillation technique. The amplitude of the pile oscillations due to a sample of U^{235} in heavy nitric acid solution was measured as a function of U^{235} concentration. The slope at the origin of the amplitude vs concentration plot was compared with that of a similar plot for a standard boron solution. The ratio, R, of the slopes is then given by

$$R = \frac{\sigma_{235}}{\sigma_B}\,(W\eta - 1)$$

In this expression W is a weighting factor such that a fission neutron emitted by the sample is equivalent, as far as the pile reactivity is concerned, to W thermal neutrons ($W < 1$). σ_{235} and σ_B are the U^{235} and boron absorption cross sections referring to an interstitial lattice position. Basing these on the ab-

Table III

Nuclide	α *(2200 m/sec)*
U^{233}	0.18 ± 0.04
U^{235}	0.13 ± 0.04
Pu^{239}	0.48 ± 0.055

sorption cross sections at 2200 m/sec of 720 and 782 barns for U^{235} and boron respectively, it is found that η for U^{235} is 2.04 ± 0.04.

Although this value strictly applies to the pile neutron spectrum, it will in practice be very close to the value for thermal neutrons.

Relative values of η for thermal neutrons have been determined for U^{233}, U^{235} and Pu^{239}. Fission neutrons from "black" samples of fissile material irradiated by a narrow beam of thermal neutrons were detected by a long counter. Corrections were made for multiplication in the samples, and for scattering of the incident thermal neutrons and their absorption in the canning material. The relative η for thermal neutrons obtained are given in Table V, together with absolute values found by combining these ratios with the U^{235} data.

THE VARIATION OF η WITH ENERGY

The dependence of η on neutron energy in the low-energy region has been measured directly in order to check the predictions of the cross-section data discussed earlier.

Monoenergetic neutrons reflected out of a pile beam by the (200) planes of a KCl crystal pass through a boron foil $(1/v)$ monitor counter and then fall on a "black" disc of fissile material. The fission neutrons from this disc are counted by a ring of 16 BF_3 proportional counters embedded in a parffin-wax moderator. The experimental arrangement is shown in Fig. 2. Assuming that all neutrons striking the fissile sample are absorbed:

$$\eta = A \cdot \frac{N_n}{N_m} \cdot \frac{1}{\sqrt{E}}$$

where A is some constant, N_n and N_m are the fission neutron detector and monitor counting rates respectively, and E is the neutron energy. A small correction for scattering loss from the samples has to be made. In the range investigated this correction did not exceed 1%. Order contamination of the reflected beam was corrected for by the use of resonance absorbers.

The measurements on U^{233} extended over the range 0.025 ev to 1.80 ev (above which energy the sample ceased to be "black"). It was found that η was constant to within about ± 3% over this region which includes the first resonance energy. On the other hand for Pu^{239}, which was studied over the energy range 0.025 to 0.4 ev, the value of η in the neighbourhood of the 0.3 ev resonance was found to be 75 ± 5% of the value at 0.025 ev.

Table IV

Resonance energy E	α	Γ *ev*
0.30 ev	0.48	0.10
7.85	2.0	0.06
10.95	1.1	0.13
11.95	2.7	0.09
14.3	1.0	0.07
14.75		0.04
17.7	0.6	0.09

Table V

Nuclide	η *rel. to* U^{235}	η
U^{233}	1.069 ± 0.030	2.18 ± 0.08
U^{235}	1.000	2.04 ± 0.04
Pu^{239}	0.929 ± 0.30	1.90 ± 0.07

DISCUSSION OF RESULTS

Using the relation

$$\eta = \frac{\bar{\nu}}{1+\alpha}$$

we may deduce η from the $\bar{\nu}$ and α-data. Taking the relative $\bar{\nu}$ values, relative η values are found and given below (Table VI), together with the directly measured relative η. (Small corrections for delayed neutrons have been made.)

While the agreement between derived and measured values for Pu^{239}:U^{235} is satisfactory, the U^{233}:U^{235} ratio shows some disagreement, suggesting an unsuspected error in the nuclear data.

Absolute values of η derived from $\bar{\nu}$ and α, and also the directly measured values are given in Table VII.

If we take the direct measurements of η being the more exact data, it is clear that U^{233} is the most promising fuel for breeding in a thermal reactor. With $\eta = 2.18$ a conversion factor close to unity is expected.

The dependence of α on neutron energy gives the variation of η with neutron energy, provided $\bar{\nu}$ is assumed constant over the small range of excitation involved. (In fact for U^{235} the value of $\bar{\nu}$ has been measured over the range of 0.03–1.0 ev and found constant within ± 3%). The predictions of the α data for the η variation are presented in Table VIII together with the results of the direct measurements reported in a preceding section.

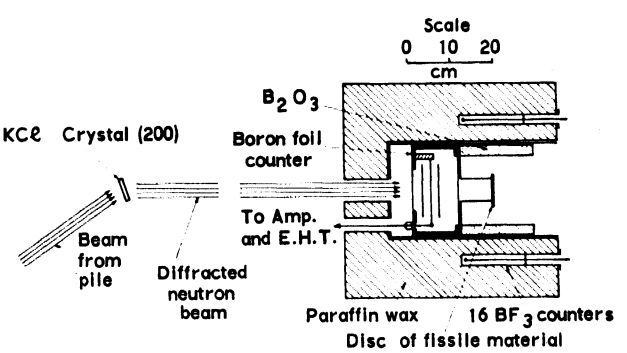

Figure 2. Experimental arrangement for measuring η as function of neutron energy

Table VI

Nuclide	η Relative (thermal)	
	From $\bar{\nu}$, α	Measured
U^{233}	0.960±0.044	1.069±0.030
U^{235}	1.000	1.000
Pu^{239}	0.888±0.051	0.929±0.030

Table VII

Nuclide	η Absolute (thermal)	
	From $\bar{\nu}$, α	Measured
U^{233}	2.10±0.14	2.18±0.08
U^{235}	2.19±0.15	2.04±0.04
Pu^{239}	1.94±0.15	1.90±0.07

Table VIII

Nuclide	η Variation			
	Predicted from α		Direct	
	Range, ev	Variation	Range, ev	Variation
U^{233}	0.005–2.1	Constant ± 4%	0.025–1.80	Constant ± 3%
U^{235}	0.005–0.50	Constant ± 4%	–	–
Pu^{239}	0.002–0.50	Constant ± 3.5%	0.025–0.4	η at 0.3 ev 75±5% of value at 0.025 ev

It will be seen that for U^{233} the predicted and directly measured η variation agree within the experimental errors: for Pu^{239} they do not. The discrepancy in the latter case is due either to a variation in $\bar{\nu}$ for Pu^{239}, or to unsuspected errors in the experiments, and further work is in hand to establish which explanation is correct.

It is interesting to consider the differences in α between the three nuclides. Using the value of α at low energies and the known total widths of the lowest levels of these three nuclides, the values of the fission (Γ_f) and radiative capture (Γ_γ) widths may be evaluated. These results are given in Table IX.

Table IX

Nuclide	Resonance energy	Γ_γ	Γ_f
U^{233}	1.78 ev	0.03 ev	0.18 ev
U^{235}	0.30	0.02	0.12
Pu^{239}	0.30	0.03	0.07

The values of Γ_γ show less variation than the values of Γ_f and are close to the known radiative capture widths of heavy nuclei. The variation of α between the three nuclei is largely due to a variation in Γ_f.

Table IV preceding, showing the values of α for several resonances in Pu^{239}, indicates that α is a sensitive function of neutron energy in the intermediate region. However the values of Γ are not sufficiently precise to establish whether the variation is due to a variation in Γ_f in all cases, although the difference in α between the 0.30 and 7.85 ev resonances is due to the difference in Γ_f for these levels. A variation of Γ_f from level to level shows that its value is closely related to a parameter other than the neutron binding energy.

The average value of η for Pu^{239} in the energy range 5 to 15 ev is about 1.2, so that to this extent Pu^{239} would be a poor fuel for low-energy intermediate systems. On the other hand for U^{233} over the energy range 0 to 25 ev, the value of η is close to $\bar{\nu}$ since α is small, and consequently it would appear to be a good fuel for intermediate systems.

CORRIGENDA, AUGUST 4, 1955

During the past two months further and improved cross section measurements on U^{235} and Pu^{239} have been made at Harwell. The results of these measurements have necessitated some modifications to the data on the variation of α with neutron energy. Tables II, IV, VIII and IX should be modified as shown below. In particular it will be seen that the discrepancy between the predicted and measured η variation for Pu^{239} discussed with Table VIII has now been largely resolved.

Table II: Replace by:

Nuclide	Variation of α
U^{233}	Constant ± 20% over range 0.005–2.1 ev
U^{235}	Value at 0.3 ev resonance 2.7 ± 1.0 times value at 0.025 ev
Pu^{239}	Value at 0.3 ev resonance 1.6 ± 0.2 times value at 0.025 ev

Table IV: α for the 0.30 ev Pu^{239} resonance should be 0.77 ± 0.10.

Table VIII: Replace by:

Nuclide	η variation	
	Predicted from α	Direct measurement
U^{233}	η constant ± 4% over range 0.005–2.1 ev	η constant ± 3% over range 0.025–1.8 ev
U^{235}	η at 0.3 ev is (84±8)% of value at 0.025 ev	
Pu^{239}	η at 0.3 ev is (84±5)% of value at 0.025 ev	η at 0.3 ev is (77±4)% of value at 0.025 ev

Table IX: Replace by:

Nuclide	Resonance energy, ev	Γ_γ ev	Γ_f ev
U^{233}	1.78	0.03	0.18
U^{235}	0.30	0.05	0.09
Pu^{239}	0.30	0.04	0.06

Measurement of Capture to Fission Ratio of U^{235}, U^{233} and Pu^{239} by a New Method

By H. Palevsky,* USA

The ratio of the capture to the fission cross section of reactor fuels near the thermal region is of fundamental importance in the understanding of the temperature characteristics of reactors. Actually the quantity directly needed for reactor application is not the ratio of capture to fission (α) but the number of neutrons produced per neutron absorbed (η). In recent years proposals for reactors using highly enriched fuels and for breeder reactors have pointed to the need for accurate experimental data for the η dependence on energy.

Three experimental methods for determining the change of η with energy have been used. The first method is based on observing the change in reactivity of existing reactors as a function of temperature. From these data the η variation is deduced by subtracting the other known factors which give rise to the total temperature effect. Such experiments are inherently limited in accuracy because the variations observed arise from the change in mean temperature of a Maxwellian distribution of neutrons, and because the η variation of the isotope of interest may contribute only a small part (~10 per cent) to the total observed effect.

The second method consists of obtaining η from two separate experimental measurements of the total and fission cross sections that are related to η by the following equation.

$$\eta = \frac{\nu\sigma_f}{\sigma_a} = \frac{\nu\sigma_f}{\sigma_f - \sigma_s} \qquad (1)$$

where ν is the number of neutrons released per fission, and σ_T, σ_f, σ_a, σ_s are the total, fission, absorption, and scattering cross sections respectively. In the slow neutron energy region σ_s is small compared to σ_T. The variation of σ_f/σ_a gives the variation in η since ν is constant for these energies. This method requires very accurate measurements of the change in two quantities σ_f and σ_a, because the ratio σ_f/σ_a changes by only a small amount. Furthermore, in the region of neutron resonances one needs to be sure that either the energy resolution is the same for both measurements or that the proper corrections are made for resolution. Because there was serious disagreement between results based on measurements of the first and second methods, it was obvious that some direct measurement of η was needed. As a result, the third method was devised and developed at Brookhaven several years ago.

DESCRIPTION OF η MEASUREMENT

In this experiment the variation of η is measured directly. Under exactly the same experimental conditions two measurements are made: (1) the emission rate of fission neutrons from a thick foil of fissionable material as the incident neutron energy is varied, and (2) the change, with energy, of the flux of neutrons incident upon the foil. Thus one obtains from the ratio of the two measurements the change with energy of η, the number of fission neutrons emitted per neutron absorbed. The fission neutrons are detected by means of a scintillation counter.[1] A thick uranium sample is used, so that nearly all the incident neutrons are absorbed, and a maximum counting rate is obtained in the scintillation detector. The incident flux is measured by a boron detector in the form of a BF_3 proportional counter which absorbs only a few per cent of the incident beam. The boron cross section, in the energy range of the measurements, varies as $1/v$,[2,3] and since the detector is "thin" the efficiency of the counter varies very nearly as the cross section.

To relate η to the measured counting rates assume the sample is black, then

$$\frac{C_U}{k_U\nu} = \nu\,\frac{\sigma_f}{\sigma_a}\cdot\frac{C_{BF_3}}{k_{BF_3}} = \eta\,\frac{C_{BF_3}}{k_{BF_3}} \qquad (2)$$

where C_U is the counting rate of the scintillation counter measuring the fission neutrons from the uranium, and C_{BF_3} is the counting rate in the BF_3 counter measuring the incident flux. k_U and k_{BF_3} are the efficiencies of the scintillation and BF_3 detectors, respectively. k_U is constant in the energy region of these measurements. k_{BF_3} will be proportional to $1/\sqrt{E_i}$, E_i is the incident neutron energy; therefore

$$\eta = \frac{k}{\sqrt{E_i}}\cdot\frac{C_U}{C_{BF_3}} \qquad (3)$$

where k is a constant independent of the neutron energy. In these experiments no attempt is made to make an absolute determination of η, what is meas-

*Brookhaven National Laboratory. Including work by R. M. Eisberg, D. J. Hughes, H. Palevsky, and R. L. Zimmerman, Brookhaven National Laboratory; W. J. Friesen, B. R. Leonard, and E. J. Seppi, General Electric Company (Hanford).

ured is the variation of η with energy. The data are normalized at $E = 0.0253$ ev to the values of η given in the Brookhaven cross-section compilation, BNL-325.[4]

In practice the sample is not quite black, and the absorption cross section is needed for computing the number of neutrons absorbed in the foil. However, since nearly all the incident neutrons are absorbed the experiment depends in an insensitive way on the absorption cross section. In treating the experimental small corrections are made for isotope impurities (1 to 3 per cent) departure of the BF_3 counter from $1/v$ law ($\sim$ 1 per cent) and for the internal scattering in the foil ($<$ 1 per cent).

The energy of the incident neutrons may be determined by a time-of-flight method as is done at the Brookhaven slow chopper or by means of a Bragg reflection, the method used at the Hanford crystal spectrometer.[5] The time-of-flight method lends itself more readily to the measurement of the *variation* of η, as the data for the entire energy interval of interest may be accumulated simultaneously in the timing channels. With the crystal spectrometer, data must be taken at each energy point by point.

FISSION NEUTRON DETECTOR

The fission neutrons are detected by means of proton recoils produced in a suspension of ZnS in lucite. This phosphor mixture is molded in the form of 2-in. diameter "buttons" approximately 1½ in. in length. One end has a slight spherical depression to give intimate contact with the face of the RCA 5819 photomultiplier. The buttons are made by heating a mixture of 70 grams of lucite molding powders and 4 grams of 40 μ ZnS-Ag to 120°C in a die under 2500 psi pressure.[1] A mechanically sturdy, nonhygroscopic cap is formed which can be easily handled for mounting onto the 5819.

The dimensions of the collimated neutron beam from the Brookhaven slow chopper are 1½ in. × 3½ in. Six 5819 photomultipliers are so located along the periphery of this area to surround the sample foil. The arrangement is shown in Fig. 1. The calculated fractional solid angle of the sample foil subtended by the six scintillation counters is 10 per cent.

The operating point for the scintillation counters is determined by a compromise to satisfy two criteria. First, the efficiency of the counter for fission neutrons should be as large as possible. Second, the sensitivity of the scintillation counter for γ-rays from the (n, γ) process in the fission foil must be so low that less than one per cent of the counts recorded are due to this process. From the work of Hornyak[6] and others at Brookhaven it was well established that the ZnS-lucite combination had low γ-ray efficiency; however, in order to be certain of the second criterion the following test was run. With the detector set up to perform the experiment, the fission foil is replaced by a foil of gold which is of a thickness calculated to produce approximately as many

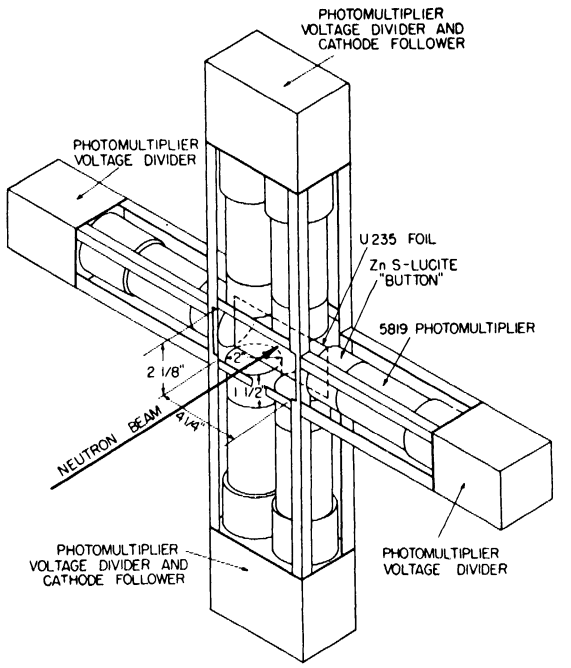

Figure 1. Schematic diagram of the fission neutron detector at the Brookhaven slow chopper

n,γ events as are produced in the foil of fissionable material. Then a combination of counter voltage, amplifier gain, and discriminator bias is found so that the counting rate is about 0.1 per cent of the counting rate when the fission foil was in place. The extra factor of $1/10$ is used because of the uncertainty about the number and energies of the γ's produced by (n,γ) reactions in gold and the particular isotope under investigation. Only a small loss of neutron efficiency results since the discriminator curve for γ-rays falls off much faster than the neutron curve.

Under the above operating condtions the over-all efficiency for counting fission neutrons from the U^{235} foil was approximately 10^{-3}, determined from a measure of the incident flux and the known fission cross section of U^{235}. Therefore, since the solid angle is 10 per cent, the efficiency of detection of fission neutrons incident upon the buttons is one per cent. The probability for a 1 Mev neutron to make a recoil proton, of any energy, in the traversal of the button is about $1/v$. Consequently only about $1/25$ of the recoil protons produce a large enough light pulse to be counted above the discriminator level.

RESULTS

By means of this direct method, measurements have been made with the Brookhaven slow chopper in the thermal region for U^{235}, U^{233} and Pu^{239}. At Hanford measurements with the crystal spectrometer have extended the data on U^{235} through the 0.3-volt resonance level.

U^{235}

Figure 2 shows the combined results of the experiments performed with U^{235} at Brookhaven and Hanford. The Brookhaven data are normalized to $\eta =$

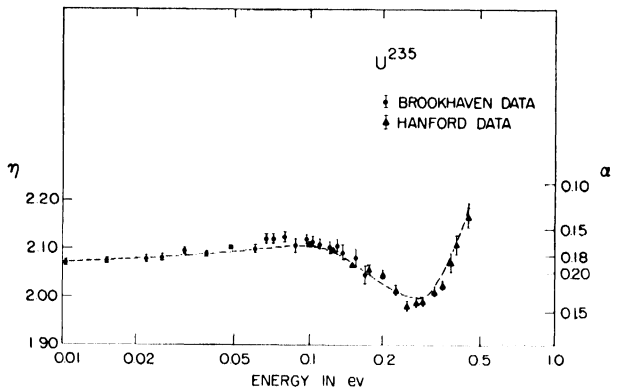

Figure 2. Energy dependence of η for U^{235} normalized to $\eta = 2.08$ at $E = 0.025$ ev. The dotted line is calculated from the ratio of the fission to absorption cross sections, given in BNL-325

2.08 at thermal ($E = 0.0253$ ev) the value quoted in the Brookhaven compilation.[4] The Hanford data are normalized to Brookhaven data in the energy region of 0.10 ev. The dashed line is computed from the ratio of σ_f/σ_a, from the cross-section data given in BNL-325. The agreement between the direct measurement and the variation of η computed from fission and total measurements is everywhere within one per cent. U^{235} is the only fissionable isotope at present where the total and fission cross sections are known with good enough accuracy so that such a comparison is meaningful. The observed η variation in U^{235} is a good example of the accuracy obtainable by this new method of measurement. The change in η in the thermal region is very small ($\sim$ 1 per cent from 0.01 to 0.1 ev). From the total and fission cross sections it is not possible to predict with certainty the sign of the slope of the η curve in the thermal region. The fact that the resonance parameters of the 0.29-ev level give an α greater than that measured at thermal by spectographic methods,[7] at first led one to believe that η would decrease with increasing energy in the thermal region. The results of the η measurements at Brookhaven showed the opposite to be true. This situation arises because contributions from at least two negative levels plus the contribution from the positive levels are required to fit the cross section of U^{235} in the thermal region. From the observed variation of η, and the total cross section, an estimate may be made of the α's of the negative levels.[8]

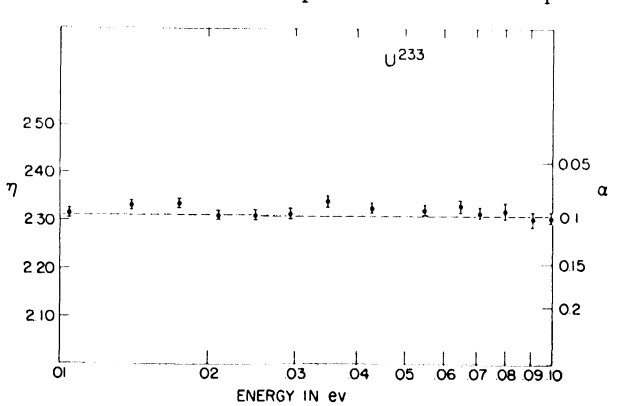

Figure 3. Energy dependence of η for U^{238} normalized to $\eta = 2.31$ at $E = 0.025$ ev. The dotted line is calculated from the ratio of the fission to absorption cross sections given in BNL-325

U^{233}

Figure 3 gives the results of the measurements to date on U^{233} normalized to $\eta = 2.31$ at $E = 0.0253$. η is seen to be constant within statistical error ($\sim$ 1 per cent) from 0.01 to 0.1 ev. The dotted line is computed from the curves drawn through the total and fission cross-section data in the Brookhaven cross-section compilation. The agreement between the two in this case is not meaningful as the statistical errors in the fission cross-section data would easily allow a $\pm$ 5 per cent variation in η over this energy interval.

Pu^{239}

Figure 4 shows the results of the measurements made with the plutonium in the energy interval 0.01 to 0.1 ev. The data are normalized to $\eta = 2.03$ at thermal. Here in marked contrast to U^{233} and U^{235} η is changing rapidly in the thermal region. The dotted line again is computed from fission and total cross-section data obtained from BNL-325. An examination of the statistical accuracy of the total and fission cross-section measurements and the errors of the η measurement indicates that the two measurements disagree by slightly more than the statistical errors. Here again, as in the case of U^{233}, it is seen that better cross-section data are needed if reliable comparisons to η measurements are to be attempted.

CONCLUSION

The direct measurement of η has several experimental features which allow for accurate interpretation of the data. The use of a thick sample makes the result insensitive to the absorption cross section and sample thickness. Furthermore, the corrections for scattering are reduced because in a "black" sample approximately 85 per cent of the neutrons scattered are re-absorbed. Because η varies much more slowly with energy than does either σ_a or σ_f this type of measurement does not require the good

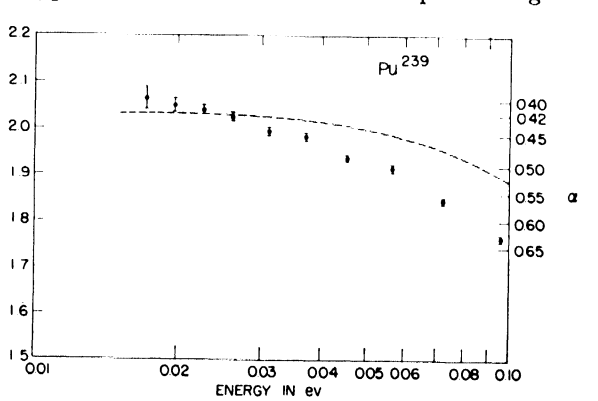

Figure 4. Energy dependence of η for Pu^{239} normalized to $\eta = 2.03$ at $E = 0.025$ ev. The dotted line is calculated from the ratio of the fission to absorption cross sections given in BNL-325

energy resolution that is needed for proper interpretation of total and fission cross-section data. Another advantage is that the same detector is used for all fissionable materials, one foil being substituted for another when a measurement on a different isotope is required. At the same time one is making η measurements, the total absorption cross section is also measured, as it is easily determined by transmission. It is then possible to determine accurately the fission cross section from the combination of σ_a and α.

REFERENCES

1. Higinbotham, W. and Handloser, J., *A high-sensitivity fast neutron survey meter,* Rev. Sci. Instr. *25,* 98 (1954).
2. Carter, R. S., Palevsky, H., Myers, V. W. and Hughes, D. J., *Thermal neutron absorption cross sections of boron and gold,* Phys. Rev. *92,* 716 (1953).
3. Egelstaff, P. A., *The operation of a thermal neutron time-of-flight spectrometer,* J. Nuclear Energy *1,* 57 (1954).
4. Brookhaven National Laboratory Report 325, *Neutron Cross Sections* by Hughes, D. J. and Harvey, J. A., (Superintendent of Documents, Washington, D. C., 1955).
5. For a survey of the methods used at reactors to determine neutron energies, see Hughes, D. J., *Pile Neutron Research,* Chapters IX and X, (Addison-Wesley Publishing Company, Inc., 1953).
6. Hornyak, W. F., *A fast neutron detector,* Rev. Sci. Instr. *23,* 264 (1952).
7. Inghram, M., P/596, *Mass spectrometric methods for determination of nuclear constants,* Volume 4, Session 16A.1, these Proceedings.
8. Harvey, J. A., P/832, *The determination and evaluation of fundamental thermal neutron cross sections,* Volume 4, Session 16A.2, these Proceedings.

Capture-to-Fission Ratio of Pu^{239} and U^{235} for Intermediate Energy Neutrons

By W. R. Kanne, H. B. Stewart, F. A. White,* USA

An experimental program to measure the capture-to-fission ratio (alpha) of Pu^{239} and U^{235} at various intermediate neutron energies was undertaken at the Knolls Atomic Power Laboratory in 1947 as a part of the Intermediate Power Breeder program. At that time the plutonium alpha was known to be high for thermal neutrons and in the 0.3 ev resonance, but it was important to investigate the possibility that alpha decreases for more energetic neutrons, so that breeding in some intermediate neutron spectrum might be feasible with relatively low critical mass reactors.

The initial method adopted was the exposure of thin samples of the fissionable materials, having adequate isotopic purity, to Hanford neutron flux filtered through appropriate shields. The amount of capture in the samples was measured by the change in isotopic composition, and the amount of fission was measured by quantitative fission product analysis. The change in Pu^{240} concentration was measured by its spontaneous fission, and U^{236} was measured by a mass spectrometer. Although laborious, the method chosen is direct.

Alternative methods based on standard measuring techniques to determine the Pu^{239} capture cross section require large amounts of plutonium and must overcome two difficulties. These are the scattering of neutrons and the production of fast neutrons by fission. By their nature these methods involve the measurement of small differences in large quantities, usually result in a measurement of $\nu-1-\alpha$ rather than α, and require the use of neutron detectors of special velocity sensitivity. Subsequent advances in technique have largely overcome these difficulties. Time-of-flight and sphere methods are in this category; these are now being used to explore the lower energy resonances. Although detailed comparisons have not been made, the results appear consistent with those reported here.

Granted that a method involving the measurement of a change in isotopic concentration in Pu was indicated, it was concluded at the time that spontaneous fission counting could produce reliable results more quickly and with less development than could mass spectrometer techniques. However, the development of a mass spectrometer of high isotopic discrimination in subsequent years would make this the more desirable method today.

Reactivity coefficient experiments in the intermediate neutron spectrum critical assembly (Preliminary Pile Assembly) were also conducted to determine the effective alpha, including self-shielding effects in resonances. Again these experiments involved the measurement of $\nu-1-\alpha$ essentially instead of α. Although the critical experiments were less sensitive than the isotopic measurements, they did provide a simple method for evaluating the effect of self-shielding on the effective value of alpha. Since the fuel in a potential power reactor would be strongly self-shielded, it was felt that these experiments might be very significant.

The results show that the plutonium alpha actually rises above the thermal neutron value and is not confined to a small number of strong resonances. But the comparison of the thick sample (reactivity coefficient) results with the thin sample (Pu^{240} spontaneous fission counting) results does show that the self-shielding effect of resonances is important.

It was concluded that the strong capture by Pu^{239} precludes the possibility of a practical intermediate breeder reactor.

Similarly, alpha for U^{235} was found to increase in the resonance region.

The values of alpha are summarized in Table I.

PLUTONIUM ALPHA EXPERIMENT

A neutron shield which eliminates thermal and 0.3 ev resonance neutrons reduces the fission rate in the sample exposed in a typical graphite-moderated reactor to the order of 1% of that in the total thermal pile flux. The change in isotopic concentration during a reasonable exposure (i.e., thermal nvt = 10^{20}) is of the order of 100 ppm, and the material in which this small change in isotopic concentration is to be

Table I. Capture-to-Fission Ratios for U^{235} and Pu^{239}

	Pu^{239}		U^{235}	
Median fission energy, ev	*Thin samples*	*Thick samples*	*Thin samples*	*Thick samples*
Thermal	0.42		0.17	
30	0.65			
100	0.81	0.45	0.52	0.35
1200	0.60		0.47	
2700		0.35		0.3
15,000	0.45		0.41	

* Knolls Atomic Power Laboratory.

measured should itself then have an initial Pu^{240} concentration of this order or less.

The early experiments were performed with 197 ppm Pu^{240} material. This was available from early reactor exposures of uranium in which the production of Pu^{239} and consequently Pu^{240} was low. Because of the high value of alpha for thermal neutrons, this material had to come from uranium in which the plutonium concentration was about 2 grams per ton. This indicates also the cost and the difficulty of the chemical processing problem for the procurement of special material with low initial Pu^{240} content.

Through the cooperation of the Hanford Works and the Argonne National Laboratory, a total of 72 mg of especially pure Pu were produced and separated in new facilities which avoided isotopic contamination. The uranium was shielded by cadmium during the irradiation to reduce Pu^{239} capture in comparison to production by resonance capture in U^{238}. Twenty-eight mg (from about 17.5 pounds of uranium exposed near the ends of a tube) had a Pu^{240} concentration of 48 ppm, and forty-four mg (from 17.5 pounds of uranium exposed at the center of the tube) had a Pu^{240} concentration of 145 ppm.

Three capsules containing samples of Pu, each in a special slug, were exposed for each part of the experiment. Two of these were isotopically pure material for the capture measurement, while the third was ordinary Pu available for fission product analysis. Each capsule contained 3 mg of PuO_2.

The capsules were made of 6 mm od pure platinum tubing, spun shut in hemispherical shape at one end. Leak tests assured that gaseous fission products were not lost from the capsule. Pu nitrate solution was evaporated to dryness in the capsule and ignited to the oxide. The open end was then crimped shut.

Two foils were prepared from each type of plutonium for the measurement of the background spontaneous fission rate. Similarly, one foil was prepared from the exposed material in each capsule in order to measure the increase in spontaneous fission rate. Each foil contained approximately 2 mg of Pu. Absorption curves of the emitted alpha-particles showed nearly all the particle ranges to be within ± 1 mm air equivalent of the mean range. Self-absorption is therefore sufficiently small. Pu weights determined by chemical aliquot, low geometry alpha-counting, and "fission weighing" agreed very closely. The latter method will be discussed later.

Three Pu foils obtained from the Los Alamos Laboratory were used to standardize the low geometry alpha-counter and the "fission weighing."

Shields designed to give neutron transmissions of ⅓ ("cut-off") at energies of 5, 30, 200, 1000 and 5000 ev were selected to discriminate between resonances and to investigate the trend in alpha. A survey of the capture cross sections of various materials indicated the following choice of shielding elements (Table II). The higher energy shields included cadmium to reduce heating in the boron.

Since the shields were cylindrical, an obliquity correction was applied to the transmission calculations to allow for the greater thickness of shield presented to neutrons not moving perpendicular to the shield axis. Figure 1 shows the spectrum of neutrons producing fissions in Pu samples, on the basis that the pile neutron flux varies logarithmically with energy in this region. The curves are normalized to equal area. These curves and similar ones for the higher energies were integrated to obtain the fraction of fission below various neutron energies given in Table III.

An unshielded (thermal) exposure was made to evaluate the techniques used in this experiment. The result, alpha = 0.42, is somewhat lower than previous measurements, which indicate a value between 0.50 and 0.55 when the resonance contribution is included. Since the probable error in each case is at least 10%, this result was considered as confirmation of the techniques.

Table II. Neutron Shields

Mean fission energy, ev	*"Cut-off" energy, ev*	*Material*	*Thickness*
30	5	0.176 ev capture resonance of cadmium	5 gm/cm²
		1.44 ev capture resonance of indium	3 gm/cm²
		0.635 and 1.35 ev capture resonance of iridium	0.5 gm/cm²
100	30	Ordinary boron	0.8 gm/cm²
1200	200	Boron enriched in isotope 10 because of size limitation and to reduce neutron scattering	0.5 gm/cm²
15,000	5000		1.7 gm/cm²

Table III. Neutron Fission Spectra

Energy	*"5 ev" shield*	*"30 ev"*	*"200 ev"*	*"1000 ev"*	*"5000 ev"*
5 ev	3.3%	1.1%	0		
32	53	27	2%		
200	80	62	23	4.8%	0.5%
1000	87	75	44	18.4	6.6
5000	91	82	66	44	28

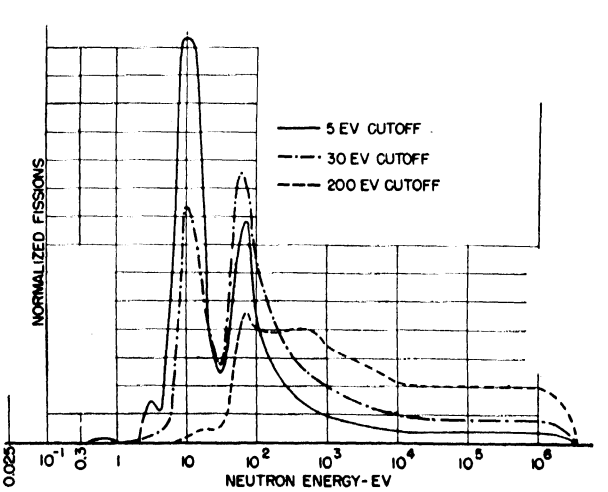

Figure 1. Normalized spectra of plutonium fissions

The total number of fissions was determined by chemical analysis of a number of fission products, primarily Ce^{144}, Sr^{89} and Zr^{95}. The probable error in the determination of fission for plutonium is approximately ± 20%, and for uranium is approximately ± 15%. The ratios of fission rates have somewhat lower probable errors (~ ± 10%) since fission yield and geometry errors largely cancel out. The largest uncertainty is in the fission yield data which are known to about ± 20%. Fission yields are unlikely to change with neutron energy in the kilovolt range by amounts comparable to the overall uncertainty.

The fission product analyses of the plutonium samples have been reviewed very critically because they enter directly into the final determination of alpha. In order to check further into the accuracy of the fission product analysis, the fission rate in a uranium monitor was measured. Uranium oxide is amenable to much simpler chemical treatment than exposed plutonium oxide, and the fission product yields are more reliable. Accordingly, a 100-mg sample of ordinary uranium was exposed in a separate sample slug between the two plutonium samples of the unshielded exposure. On the basis that the abundance of U^{235} is 0.71%, the observed fission cross-section ratio is

$$\frac{\sigma_f\,(Pu^{239})}{\sigma_f\,(U^{235})} = 1.6\ (\pm \text{ approximately } 20\%)$$

This is in very good agreement with the fission rate ratio expected from cross-section data.

The Pu^{240} concentration in the irradiated samples was determined by spontaneous fission counting. The experimental prerequisites include reliable ionization chambers, stable electronic circuitry, and proper shielding from cosmic-ray neutrons. In addition, it is necessary to have the resolving time of the circuitry sufficiently short such that milligram quantities of Pu can be assayed without having the alpha particles of the major isotope (Pu^{239}) pile up and yield pulses of sufficient amplitude to simulate spontaneous fission. It is desirable to count large samples of plutonium to decrease the counting time and to reduce errors from spurious counts.

The quantitative determination of the Pu^{239} sample weight was accomplished by exposing the sample foil (in the counter) to an unknown but reproducible thermal neutron flux. The number of induced fissions/minute was compared to those in standard foils of known Pu weight.

Table IV shows data obtained for representative samples of Pu. The final column (Table IV) gives the Pu^{240} concentration in parts per million of Pu^{239}. These numbers are based on a spontaneous fission rate of $1.66 \cdot 10^6$ f/gm-hr for Pu^{240}. An alpha pulse-height analysis showed that the concentration of Pu^{238} in these foils was sufficiently small so that its spontaneous fission had no effect on the results.

Table V is a summary of the data, listing the average values of all samples by both radiochemical and spontaneous fission assay. The amount of fission was determined by averaging results of the several fission products. The capture was computed by measuring the difference in Pu^{240} content between unirradiated and exposed material averaged for all samples.

Table IV. Typical Spontaneous Fission Data of Pu Foils

Experiment	*Pu wt (mg)*	*Pu^{240} fissions*	*Total hours*	*Pu^{240} ppm*
Background for 5, 30 ev	2.53	1924	2324	197 ± 5
Thermal	0.62	3082	936	3200 ± 60
5 ev	1.17	1953	2545	395 ± 9
30 ev	1.69	1441	1303	394 ± 10
Background for 200 ev	0.94	1606	7076	145 ± 4.9
200 ev	1.87	2183	3495	201 ± 7
Background for 5000 ev	2.47	1393	7082	48 ± 1.5
5000 ev	1.67	1008	4685	78 ± 2.1

The probable error in σ_c/σ_f values is approximately ± 15%, which arises mainly from the uncertainty in fission yields used in the fission determination.

The relative error is less than 10%.

URANIUM ALPHA EXPERIMENT

The most convenient tool for measuring the radiative capture of U^{235} is the mass spectrometer, and fission was determined by conventional radio-chemical analysis of Cs^{137} and Ce^{144}. These fission products give a reliable measure of fission for both U^{235} and Pu^{239}.

If the amount of U^{236} formed is less than 0.01% of the U^{235} in the sample, analysis in the conventional mass spectrometer is rather difficult. A serious limitation is the small angle elastic scattering of ions with residual gas molecules in the analyzer tube. It has been demonstrated at this Laboratory that about 10^{-4} of a beam of singly charged ions of mass M will be scattered to the mass $M \pm 1$ mass position in the image focal plane. This fraction holds roughly for available commercial instruments at an atomic mass of 200 and pressures of 10^{-7} mm Hg.

Accordingly, we have constructed a two-stage machine which allows but a single isotope at a time to pass through an intermediate slit. This scheme essentially reduces the effect of scattering by squaring the probability (about 10^{-4}) that an ion of mass 235 will arrive at the mass 236 mass position, since the probability is the same for each magnetic analyzer.

The positive ion beam is detected by a twenty-stage electron multiplier employed as a pulse amplifier. Thus, individual ions are counted and currents of 10^{-14} to 10^{-19} amperes may be measured. This detection of small currents by pulse-counting techniques makes possible the analysis of very small samples, and so avoids instrument contamination.

A prerequisite of paired magnetic-analyzers is the precise regulation of the magnetic fields. This is accomplished by means of nuclear magnetic resonance probes and associated equipment. The rf oscillators

Table V. Capture-to-Fission Valves (vs) Energy (Summary) for Pu^{239}

"Cut-off" energy	Shield	Median fission energy	Average fissions ppm	Average capture ppm	σ_c/σ_f
None	Cd-In-Ir	Pile spectrcm	7324	3104	0.42
5 ev	Boron + Cd	30 ev	690	448	0.65
30 ev	Boron + Cd	100 ev	242	197	0.81
200 ev	B^{10} enriched low density	1200 ev	94	56	0.60
5000 ev	Boron + Cd B^{10} enriched high density	15,000 ev	67	30	0.45

are tuned to the Lamour precessional frequency corresponding to the desired magnetic field. Thus the problem of field regulation is simplified from that of stable current regulation to that of the greater stability of rf oscillators.

Figure 2 demonstrates both the high abundance sensitivity (resolution of adjacent isotopes) and the current sensitivity of this instrument. A compilation of data analogous to that obtained for Pu, but with the capture being measured mass spectrometrically, is given in Table VI.

REACTIVITY ALPHA EXPERIMENT

It was indicated earlier that any method based on determining the neutron economy within an experimental reactor suffers because one measures essentially $\nu - 1 - \alpha$ rather than α. Although the accuracy of the neutron economy method is limited, the application of the results to reactor design is somewhat more direct. The α experiments which were done with the shielded capsules involved thin samples of plutonium and U^{235}, while the fissionable material in a power reactor would be significantly thicker. Due to the thicker sample in the power reactor, the self-shielding of the large resonances becomes an important factor. One cannot assume, furthermore, that the effect of self-shielding in the capture resonances would be comparable to that in the fission resonances. As a result, the value of α for thick samples of fissionable materials, in the environment of similar fissionable materials, might lead to a different value of α than expected from thin sample measurements.

The method which was used to measure α in the critical assemblies was suggested by Hurwitz, Jr., and is based on the theory of danger coefficient experiments developed by him. The experiments were conducted in the Preliminary Pile Assembly known as PPA-5 which was a mock-up of a potential intermediate neutron energy power breeder reactor. The reactor had a 33-to-1 beryllium-to-uranium ratio in the reactor core and was surrounded by a beryllium reflector. The core diameter was about 18 inches and the reflector thickness 1½ inches. The α experiments were done in two positions in the reactor core; at the center of the core and at the edge. The fission-distribution curves for these two positions in the reactor are indicated in Fig. 3. The curves were obtained from some multigroup calculations by Ehrlich of KAPL, and were adjusted to fit experimental data obtained from self-shielding measurements of some calibrated resonance absorbers. The curves indicate that 50% of the fissions occur below 130 ev at the edge of the core and below 2700 ev at the center. It is noted that the neutron flux at the edge of the core is somewhat similar to the spectrum of the 30 ev cut-off experiment. In this experiment 50% of the fissions in plutonium resulted from neutrons having energies below 90 ev.

If a poison, such as a gold foil, is placed in the core of the reactor, the pile reactivity will be decreased by an amount $\Delta k/k$. The reactivity change can be measured by the control-rod shift necessary to restore the pile to criticality after the poison is introduced. If the reactivity effects due to scattering and moderation are relatively small (as they are for strong absorbers), the reactivity change is proportional to the number of neutrons absorbed by the poison per number of fissions in the core, i.e.,

$$\frac{\Delta k}{k} = -\frac{\Delta a}{\Sigma f} F_L \qquad (1)$$

The proportionality constant, F_L, represents the

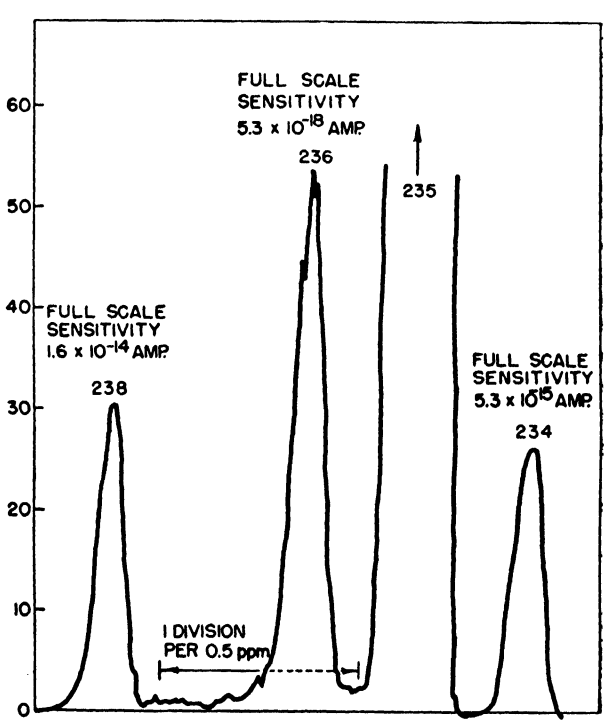

Figure 2. Spectrum of irradiated enriched uranium

Table VI. Summary of Ratio Chemical and Mass Spectrometric Data (U^{235})

"Cut off" energy	Median fission energy	Average fissions/mg U^{235}	Fissions ppm	Capture ppm	σ_c/σ_f
Unshielded (thermal)		7.32×10^{16}	28,590	4,797	0.174
Chalk River exposure					
30 ev	100 ev	1.66×10^{15}	648	340±34	0.525
30 ev	100 ev	1.70×10^{15}	664	340±23	0.512
200 ev	1200 ev	2.30×10^{14}	90	42±2	0.468
5000 ev	15,000 ev	1.64×10^{14}	64	26±2	0.406

value of the neutrons having an energy corresponding to the neutron absorption spectrum. If the reactivity is expressed in absolute units, the neutron value function can be interpreted as a geometric average of the fission probabilities for succeeding generations over an infinite number of generations. F_L has been called the iterated fission probability for low energy neutrons.

If fissionable material is introduced into the pile, there is a poisoning effect due to the absorption of neutrons, but, in addition, there is a beneficial effect on the pile reactivity due to the creation of new neutrons. The reactivity change due to the beneficial effect is proportional to the number of neutrons introduced into the pile per fission in the core. This is given by $\nu(\Delta f/\Sigma f)$. Since the escape probability for high energy neutrons, corresponding to the fission neutron spectrum, is larger than that for the absorption energy neutrons, the value of the high energy neutrons, F_H, will be somewhat smaller than F_L. The total reactivity change is given by

$$\frac{\Delta k}{k} = \nu \frac{\Delta f}{\Sigma f} F_H - \frac{\Delta a}{\Sigma f} F_L \qquad (2)$$

or

$$\frac{\Delta k}{k} = \frac{\Delta f}{\Sigma f}\left[\nu F_H - (1+\alpha)F_L\right] \qquad (3)$$

where $\Delta a = \Delta f(1+\alpha)$. Then

$$1+\alpha = \frac{1}{F_L}\left[\nu F_H - \left(\frac{\Delta k/k}{\Delta f/f}\right)\right] \qquad (4)$$

If F_H and F_L can be evaluated, then $1+\alpha$ can be determined for U^{235} or Pu by measuring both the reactivity change associated with the introduction of a fuel disk into the reactor, and the induced fission rate in the sample per fission rate in the entire reactor. The reactivity change is measured by compensating the addition of the fuel disk with a displacement of a calibrated control rod. The fission rate in the foil, Δf, is measured by counting the gamma activity induced in the foil, and the total fission rate Σf in the reactor core is determined by counting the activity of monitor fuel disks. The induced activity of the foils as a function of fission rate has been measured by exposing them to a calibrated thermal neutron flux.

Independent experiments must be performed to measure the values of F_L and F_H. The value of F_L is obtained by measuring the activation and danger coefficient of Au or Mn foils. From the beta activity of the calibrated foils and the gamma activity of monitor fuel disks $\Delta a/\Sigma f$ can be calculated.

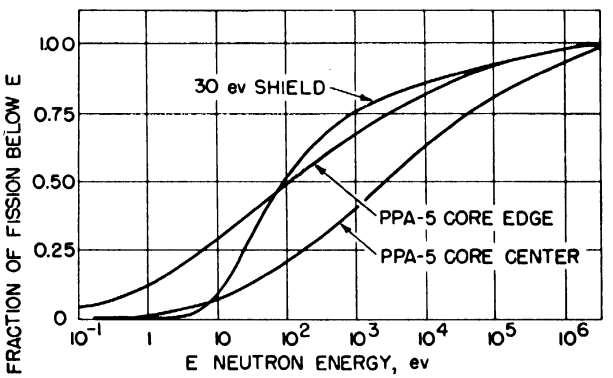

Figure 3. Energy distribution of the fissions in Pu for three types of neutron flux

In order to measure F_H, it is necessary to devise an experiment which will measure the beneficial effect of the fuel but not the absorption effect. To do this a fuel disk is enclosed in a pair of cylindrical cans made of cadmium and filled with paraffin. Some of the neutrons which enter the cadmium box are thermalized by the paraffin and ultimately absorbed by the fuel disk. It is noted that neutrons which are thermalized inside the cadmium box never escape to the rest of the reactor core, so that the disposition of thermal neutrons inside the box does not affect the over-all neutron absorption seen by the reactor core. By covering the fuel disk inside the paraffin with cadmium, the fission rate in this disk is changed, but the total number of neutrons absorbed by the box is not changed.

The difference in the activation of the fuel disk before and after it is covered by cadmium is a measure of Δf, and the difference in control rod settings is a measure of the reactivity change. From this information, plus the core fission rate as measured by monitor disks, the value of νF_H can be obtained.

Table VII indicates the accepted values for νF_H, F_L, and the reactivity coefficient per fission for U^{235} and Pu samples at the two positions in the reactor core. The values of α on the basis of these numbers are listed in the last column. For Pu it can be seen that α is about 0.35 at the center and 0.45 at the edge of the reactor core.

A study of Equation 4 using typical values for the various parameters indicates that the value of α is most critically affected by errors in F_H. A 5% uncertainty in F_H leads to a uncertainty in α of about 0.1, while 5% uncertainty in F_L or in $(\Delta k/k)/(\Delta f/\Sigma f)$ leads to an uncertainty in α of about 0.05.

Table VII. Accepted Values for νF_H, F_L, and the Reactivity Coefficient Per Fission for U^{235} and Pu at Two Positions in the Reactor Core

Fissionable material	*Position in core*	F_H	νF_L	$(\Delta k/k)/(\Delta f/\Sigma f)$	α
U^{235}	Center	1.39	0.79	0.35	0.3
U^{235}	Edge	0.94	0.55	0.19	0.35
Pu	Center	1.63	0.79	0.55	0.35
Pu	Edge	1.10	0.57	0.26	0.45

The probable uncertainty in the value of alpha associated with the entire experiment has been estimated as $\pm$ 0.10.

It is somewhat difficult to calibrate the control rod sensitivity and the value of Σf with good reliability. However, an inspection of Equation 4, together with the equations used to calibrate F_H and F_L, will show that uncertainties in the absolute control rod sensitivity and the absolute value of Σf will cancel, providing the same calibration data are used in all of the experiments.

The thickness of the foils used in the previously described experiments was 0.020 inch. The value of α was also measured at the edge of the core for Pu samples which were 0.060 inch thick. The value of α for this sample thickness was approximately 30% less than the measured α for a foil 0.020 inch thick. The self-shielding experiments, therefore, indicate that the capture resonances in Pu are sharper than the fission resonances. Self-shielding experiments with U^{235} indicated similar results.

The values of α which were measured in the shielded irradiation experiments were higher than those measured in the critical experiments. Since the fissionable samples used in the irradiation experiments had no significant self-shielding, the relative results of these experiments and the critical experiments are consistent if one assumes strong, narrow capture resonances and broad fission resonances in Pu and U^{235}.

ACKNOWLEDGEMENTS

It is a pleasure to acknowledge the theoretical contributions of H. Brooks which were made throughout the course of this work. The radiochemistry, a major effort in this experiment, was the work of L. P. Pepkowitz, R. P. Schuman and E. L. Shirley. Assistance was given on the mass spectrometer analyses by T. L. Collins. G. B. Gavin participated in the reactivity experiments.

Theoretical Analysis of Neutron Resonances in Fissile Materials

By H. A. Bethe,* USA

During the war the Los Alamos Scientific Laboratory made observations on the total and the fission cross section of U^{235} and Pu with a neutron velocity selector. The experiments showed very striking resonances in both cross sections.

The existence of well-separated resonances in fissile nuclei came as a surprise to most theoretical physicists. The very large cross section for fission in both U^{235} and Pu^{239} had led most of us to believe that the fission process must be extremely probable and must therefore be characterized by a very large fission width. Since the spacing between resonance levels was expected to be quite small, of the order of 1 ev or so, it had been expected that the various levels should overlap and that no separate resonances should be observed.

The first experiments confirmed the approximate estimates of the level spacing but gave sharp resonances of a width of the order of 0.1 to 0.2 ev. As we shall see, these results have essentially been confirmed by the more accurate work of recent years.

The small total level width was comparable to the then existing estimates of the radiation width of slow neutron levels. It was therefore conjectured that radiative capture might be of comparable magnitude as fission. Experiments done by Fermi and his collaborators in Chicago soon confirmed this: The total absorption cross section for thermal neutrons was about 20% greater than the fission cross section for the same neutrons measured at Los Alamos. The ratio of radiative capture to fission has come to be denoted by the letter α.

Further velocity selector measurements showed that α varied considerably from one resonance to another. Some resonances were found to have α as large as 1 or greater, the most notable of these, e.g., the 6-ev resonance of U^{235} has $\alpha = 2$. Of the greatest practical importance is the large resonance of Pu at 0.3 ev which has $\alpha = 0.6$.

The capture to fission ratio α is clearly of great importance for all nuclear reactors in which highly enriched fissionable material is used. Unless the neutrons are very rapidly decelerated through the resonance region, a considerable amount of parasitic absorption will occur if α is appreciable. The nuclides formed by this absorption, U^{236} and Pu^{240}, are not fissionable with slow neutrons and are useless.

The radiative capture is particularly detrimental for the performance of a breeder. The breeding ratio is ideally given by the quantity

$$\eta - 1 = \frac{\bar{\nu}}{1 + \alpha} - 1$$

This expression is valid if there is no absorption in any material except the fissile and the fertile material. In practice of course structural materials and coolants will greatly reduce the breeding ratio.

In U^{235} the value of ν, the number of neutrons emitted per fission, is about 2.5. If α is greater than 0.25, the breeding ratio will be less than 0.5, i.e., fissile material will be lost rather than bred. For Pu, with a value of ν of nearly 3.0, a value of α up to nearly 1 would still make breeding possible under ideal conditions, and a value of about 0.5 may be permissible when the structural absorption of neutrons is taken into account.

In 1946 it was realized that the value of α would be decisive for the performance of a breeder. Various experiments were initiated, particularly by the Knolls Atomic Power Laboratory at Schenectady, to determine this quantity as a function of neutron velocity. The initial hope was that the Pu level at 0.3 ev might be exceptional and that an increase of the neutron energy to a few tens or hundreds of ev would reduce α to something like its value for thermal neutrons, namely about 0.2. With such a value, a Pu breeder at intermediate energies would become feasible.

The most direct experiment consisted in irradiating a foil of Pu or U^{235} behind a B^{10} shield of appropriate thickness in the Hanford reactor. The B^{10} thickness was chosen to provide a broad neutron spectrum with a mean energy such as 100 ev or 1000 ev. The irradiated sample was taken out of the reactor and the number of fissions that had taken place was determined by measuring the activity of suitably chosen fission products. The radiative capture was determined by measuring the new isotope formed. In the case of Pu this was done by counting the spontaneous fissions in Pu^{240}; in the case of U, the amount of U^{236} formed was determined by a high resolution mass spectrograph. With the development

* Cornell University.

of the latter instrument, the second method turned out to be just as accurate as the first.

Both nuclides, U^{235} and Pu, showed a large value of between 0.4 and 0.8 at the energies investigated, i.e., from 30 to 10,000 ev. A less accurate experiment gave a slightly lower value, around 10 kev. These results removed the hope of designing an efficient breeder in this intermediate energy region, and thereby reduced the hope for a Pu breeder to the region of high energy, of 100 kev or more.

An experimental fast breeder reactor was constructed by the Argonne National Laboratory, and the value of α was measured in the flux provided by this reactor at various points. The flux is believed to have a peak around 200 kev near the center of the reactor. A value of α of about 0.15 for U^{235} was found at this point, with slightly higher values farther away from the center where the neutron energy is lower. This indicates that α decreases substantially at high energies which is in accord with theoretical expectation as will be discussed below. The results for Pu are similar. It therefore appears feasible to design a fast breeder working with Pu and having a good breeding ratio, or a fast converter using U^{235} as a fuel with a good conversion ratio.

VELOCITY SELECTOR RESULTS

U^{235} is probably the best investigated nuclide as far as low-energy resonances are concerned. Sixteen resonances have been observed between 0 and 10 ev and twenty-two between 10 and 36 ev. There is definite indication of further resonances at higher energies, and of a very strong resonance at negative energy. As we shall see in the discussion later on, a considerable number of resonances has probably been missed between 10 and 36 ev, and the total number up to 36 ev should probably be of the order of 60.

Very careful work has been done on obtaining the resonance parameters from high resolution velocity selector experiments. The main work on this subject has been done at Brookhaven National Laboratory by Hughes and collaborators; it is described elsewhere in this volume. The standard method used is to measure the transmission of two different thicknesses of U^{235}; the same method has been applied to many non-fissile materials. Two parameters of the resonance are thus obtained, namely the total width Γ and $2g\Gamma_n$ where g is the statistical weight,

$$g = \tfrac{1}{2}(1 \pm \frac{1}{2I+1})$$

where I is the spin of the target nucleus. It is in general not known whether the plus or the minus sign should be used for a particular resonance; therefore in practice g is put equal to $\frac{1}{2}$. In the energy region investigated the neutron width is always small, the largest being 10 mv (millivolts) for the 35 ev resonance. Therefore the total width may be regarded as

$$\Gamma = \Gamma_\gamma + \Gamma_F$$

where Γ_γ is the radiation, and Γ_F the fission width.

To determine Γ_γ and Γ_F separately it is best to measure the fission cross section in addition to the total cross section. The relation is as follows

$$\sigma_F = \frac{\Gamma_F}{\Gamma_\gamma + \Gamma_F}\,(\sigma_{tot} - \sigma_{sc})$$

where σ_{sc} is the scattering cross section. It may in general be put equal to the potential scattering which is about 10 barns and is rather unimportant in the energy region in question.

Unfortunately the experiments on the fission cross section cannot easily be done with as good resolution as those on total cross section because the fission detectors which have to be used are much less sensitive than the B^{10} detectors which are commonly used for transmission measurements. Therefore in the fission measurements only the lowest resonances, up to about 6 ev, could be fully resolved. For all resonances above 10 ev no resolution has been possible so that several resonances appear merged into a single peak. Fission cross-section measurements with a velocity selector have been done particularly at Columbia University and at Harwell. At energies below about 1 ev slow chopper measurements have been made with various piles.

When the fission and total cross section are compared for the low-energy resonances in U^{235}, one finds great variation in the fission width from one level to another but no perceptible variation of the radiation width Γ_γ. This is in agreement with results obtained on a large number of non-fissile nuclides by the Brookhaven group. They have found that quite generally the radiation width is very nearly constant from level to level for any particular nuclide. Landon and Sailor have studied two nuclides with particular care and have found variations in Γ_γ up to about 20%, but they conclude that only the most accurate measurements will reveal variations in Γ_γ.

It is reasonable that this should be so because radiation can lead from the compound nucleus to many thousands of levels of lower energy. Therefore radiative capture actually corresponds to a large number of different channels, and it would be most surprising if the widths of all these channels varied in the same direction simultaneously from level to level. The only thing which we can reasonably expect is that the radiation width may be different for the two possible values of the compound level, $j = I \pm \frac{1}{2}$. Empirically it seems that even this variation is not appreciable.

On the basis of this argument the Brookhaven group have assumed that the radiation width stays constant also for the levels above 6 ev for which it cannot be determined by direct experiment. The value assumed for the radiation width was 30 mv. Then the total width determines the fission width and $\alpha = \Gamma_\gamma/\Gamma_F$. The value of the fission width varies between about 20 and 140 mv.

The assignment of radiation and fission width can then be tested with the help of the unresolved fission cross-section measurements. For this purpose we

Table I. The Fission Integral, $\int \sigma_f dE$, for U^{235} in Various Regions of the Spectrum, in barn-ev

Energy region	*7.8–10.8*	*10.8–15.7*	*15.7–23*	*23–29.5*	*29.5–38*	*38–46*	*46–62*
From resonance parameters*	240	315	640	280	750	230†	670†
From fission measurements	240	300	460	325	550	290	820
Average of σ_f in region	80	61	55	50	58	41	51
$\sigma_f \sqrt{E}$	240	220	245	255	340	270	375

* Deduced from transmission measurements; summary paper by L. Sailor *et al.*, P/586, Volume 4, Session 17A, these Proceedings. † Value of α assumed to be ½.

grouped together various rather large energy intervals. In each interval we calculated the expected value of $\int \sigma_F dE$ from the resonance parameters which had been deduced from the transmission experiments. Alternately we obtained the same quantity by integrating the fission cross section observed at Columbia over the energy region in question. No attempt was made to analyse the fission cross section into resonances, nor was any background subtracted from the measured fission cross section. This amounts to attributing the observed fissions in a given interval, let us say 15.7 to 23 ev, to the resonances occurring in that interval which is likely to be a good assumption.

The result is shown in Table I. The agreement between the two values of $\int \sigma_F dE$ is seen to be quite good. This justifies the assumptions made by Brookhaven about Γ_γ and Γ_F. For all resonances for which these quantities had not been obtained by Brookhaven we assumed $\alpha = ½$. The same assumption was made for the energy region from 38 to 62 ev where the transmission data have not been analysed into separate resonances.

In Table I we have also given the average fission cross section in each of the intervals which is seen to be between 40 and 80 barns. In addition, we have given the quantity $\sigma_F \sqrt{E}$ which should be constant when averages are taken over several resonances, according to the continuum theory of nuclear reactions. It is seen to be reasonably constant and should not be exactly constant because not many resonances are in each interval.

This information is extended to lower and higher energies in Table II. At lower energies the quantity $\sigma_F \sqrt{E}$ is seen to be considerably less than in the energy region covered by Table I. This is true of the thermal value which is only about 90 instead of $250\sqrt{\text{ev}}$-barns, and even more so in the region of a few ev where this quantity goes down to about 20. Indeed it was already noticed in the early Los Alamos experiments that the fission cross section has a "hole" in the region of a few ev.

This hole is of considerable practical importance for reactor design. As neutrons are slowed down toward thermal energy they must cross the energy region of a few ev. In this region they will not cause many fissions but they will be strongly absorbed by many structural materials which may be in the reactor. Therefore it is desirable to have the neutrons traverse this region rapidly in order to minimize losses of neutrons by a parasitic capture.

In the energy region from 60 ev to 700 ev the measured value of $\sigma_F \sqrt{E}$ is essentially constant. Between 700 and 3000 ev there are two pronounced maxima and minima, presumably due to an accumulation of levels. Such fluctuations above 3 kev can no longer be observed because of lack of resolution.† The quantity $\sigma_F \sqrt{E}$ rises gradually with energy in this region. This rise, especially between 20 and 200 kev, is probably largely due to the inset of contributions from neutrons of orbital momentum 1. This effect is contained for instance in the curve by Blatt and Weisskopf, page 348, which gives the cross section for formation of the compound nucleus.

If we assume the average measured value of 0.5 for α, the reaction cross section is given approximately by $\sigma_r = \sigma_F(1 + \alpha) = 400/\sqrt{E}$ in the energy region from about 8 to 3000 ev. This is precisely the value which is predicted by the theory of the black nucleus if the depth of the nuclear potential is chosen to be 42 Mev, following the assumption of Feshbach, Porter and Weisskopf, Phys. Rev. *96*, 448 (1954). This would mean that the 1-particle

† Very recently the KAPL group have observed maxima and minima in this high energy region.

Table II. Average Fission Cross Section of U^{235}

E	(*ev*)		*0*	*1.5–6*	*7.8–10.8*	*70*	*100*	*200*	*400*	*700*
$\sigma_f \sqrt{E}$	($\sqrt{\text{ev}}$-barn)		97	21	240	240	245	275	270	275
E	(kev)	1.0	1.25	1.75	2.2	3	5	10	20	50
$\sigma_f \sqrt{E}$		230	320	240	340	305	340	370	400	470
E	(kev)	100	200							
$\sigma_f \sqrt{E}$		570	670							

resonances predicted by the "cloudy crystal ball" model of Feshbach *et al.* do not have any influence for this value of the atomic weight. Recent modified calculation by Weisskopf *et al.* seem to be compatible with this result whereas in the paper of Feshbach *et al.* a lower value of $\sigma_r\sqrt{E}$ was predicted for U^{235}.

The same quantity can also be deduced directly from the resonance parameters. The Brookhaven group have found from their parameters that the average value of the neutron width up to 36 ev is given by $g\Gamma_{n0}/D = 1.0 \times 10^{-4}$. This corresponds exactly to $\sigma_r\sqrt{E} = 400$. By contrast $\sigma_\gamma\sqrt{E}$ for U^{238} is only about 50 in the region around 1 kev. This is due to strong competition from elastic scattering, due to large neutron width for this nuclide.

The low-energy data from velocity selectors require for their explanation the assumption of a resonance at negative energy. This is true for all the three common fissile nuclei, U^{233}, U^{235} and Pu^{239}. For U^{235}, Sailor has determined the parameters of this resonance and obtained

$$E_0 = -1.4 \text{ ev}$$
$$2g\Gamma_{n0} = 3.1 \text{ mv}$$
$$\Gamma_F = 180 \text{ mv}$$

This neutron width is exceptionally large, the largest otherwise observed being 1.6 mv. It is conceivable that there are two strong resonances at negative energy close together. The fact that there is a very large neutron width has been directly confirmed by measuring the elastic scattering in the region from 0.1 to 1 ev which was found large and in accord with the assumed Γ_{n0}. The negative energy resonance accounts for practically all of the fission cross section at 0 neutron energy. At this energy the observed $\sigma_F\sqrt{E}$ 96 of which the negative resonance contributes 92 $\sqrt{\text{ev}}$-barns.

We have already discussed the fluctuation of the fission width. Further data on this parameter are given in Table III. It is reasonable that the fission width should fluctuate between levels because fission is essentially only one mode of possible disintegration of the compound nucleus. From the data in Table III, it appears that the fission width is about uniformly distributed between 0 and a maximum of about 180 mv. However since this quantity is known for only 16 levels, conclusions about the statistics are uncertain.

The widest distribution is shown by the reduced neutron width, $2g\Gamma_{n0}$. Table III gives the values of this parameter for some of the most important individual resonances. Table IV gives the distribution of $2g\Gamma_{n0}$ among various size classes. Since there are many resonances of small size, the classes have been chosen accordingly.

The fourth and fifth column of Table IV give separately the observed number of levels in each class in the interval up to 10 ev, and from 10 to 36 ev. It is evident that up to 10 ev there are many levels in the two lowest classes whereas from 10 to 36 very few were found in these classes. It is very likely that the smallest resonances have been missed in the upper energy interval. This is also confirmed by the fact that the total number of observed levels, 22, in the upper energy interval is not proportionately higher than the number of levels in the lower interval, 16. We have therefore assumed that small resonances have been missed in the upper energy level, and have given in column 6 of Table IV an estimate of the actual number of levels of each class in the interval from 10 to 36 ev. This estimate has been made in such a way that the total number of levels in the upper interval is 2.6 times greater than that in the lower interval. All extra levels have been attributed to the two lowest classes.

In column 7 of Table IV we have added the numbers of levels in the two energy intervals. In class G, over 3 mv, we have included the negative energy resonance. In column 8 we have given the cumulative number of resonances, i.e., all those which belong to the given class or higher ones.

Harvey, Hughes, Carter and Pilcher have already noticed that the reduced neutron widths for nonfissile elements fluctuate widely. They have proposed that the distribution be described by a formula

$$e^{-y}dy \qquad (1)$$

where y is the ratio of Γ_{n0} to its average value. We believe that this formula, while qualitatively correct, does not do justice to the large number of very narrow levels or to the considerable number of levels which have many times the average width. For instance, for U^{235} the Brookhaven data give $\Gamma_{n0Av} = 0.125$ mv. The two observed levels at 19 and 35 ev have therefore respectively 9 and 13 times the average width, and the negative energy level is even wider. This contradicts the assumed distribution of Harvey *et al.*

Since there is no theory of the statistical distribution of reduced neutron width, we feel free to assume a purely empirical formula for it, designed merely to fit the data. In order to account both for the small and large widths we propose the distribution

$$e^{-x}dx \qquad (2)$$

Table III. Information on Low-Energy Levels of U^{235}

E_0 ev	Γ_f mv	a	$2g\Gamma_{n0}$ mv
−1.4	180	0.16	3.1
0.29	98	0.29	0.0058
1.14	120	0.25	0.0144
2.03	14	2.3	0.0055
2.86	60	0.5	0.002
3.14	130	0.23	0.014
3.61	68	0.43	0.027
4.85	26	1.13	0.028
6.4	16	1.9	0.13
8.8	100	0.3	0.36
11.7	50	0.6	0.19
12.5	40	0.8	0.44
19.3	45	0.7	1.11
21.2	90	0.3	0.74
23.7	140	0.21	0.40
35.3	110	0.27	1.6

where x is proportional to the square root of the neutron width, or precisely

$$x = \sqrt{2\Gamma_{n0}/\Gamma_{n0Av}}$$

This formula fits the observed distribution very well as is shown in column 9 of Table IV. It seems that even our formula gives somewhat too few levels of very large neutron width for U^{235}, but for some other elements the deviation is slightly the other way. We consider it the best empirical fit so far suggested.

Recent investigations by Hughes and Harvey (Letter to Editor, Phys. Rev.) show that Equation 2 gives too many wide levels for all nuclei investigated, except U^{235}. The best fit to *all* available evidence, including U^{235}, may be the Equation proposed by Thomas, viz.,

$$\frac{dx}{\sqrt{\pi}}\, e^{\frac{-x^2}{4}} \qquad (2a)$$

This also has some slight theoretical foundation, being a Gaussian distribution of the matrix element for neutron emission. Hughes' Equation 1, when written in terms of x, becomes

$$x dx\, e^{\frac{-x^2}{2}} \qquad (2b)$$

In column 10 of Table IV we list the fraction of the average cross section which is contributed by levels in each class when an average is taken over very many levels. It is seen that the main contribution comes from classes C to F which contribute about equal amounts, i.e., from Γ_{n0} between 1/16 and 3 mv. Very weak and very strong levels contribute very little if our formula is correct. Column 2 gives the ranges of the variable x corresponding to each class.

THEORETICAL CONCLUSIONS FROM THE DISTRIBUTION OF NEUTRON WIDTHS

If we accept the distribution of neutron widths of Equation 2, we may calculate the expected average cross sections for various processes averaged over many levels. The easiest case is that of radiative capture by a non-fissile element. In this case the capture cross section is given by

$$\sigma_{\gamma Av} = 2\pi^2\lambda^2 \left(\frac{g\Gamma_n\,\Gamma_\gamma}{\Gamma_n + \Gamma_\gamma}\right)_{Av} = \tfrac{1}{2}\,\sigma_r \int \frac{x^2 z^2}{z^2 + x^2}\, e^{-x} dx \qquad (3)$$

The integral can be evaluated and yields

$$\sigma_{\gamma Av} = \sigma_r\, \tfrac{1}{2}\, z^2 f(z) \qquad (4)$$

where σ_r is the reaction cross section and

$$f(z) = 1\text{-}z(\sin z\, Ci\, z - \cos z\, si\, z) = 1 - ReH(iz) \qquad (5)$$

where the notation in Jahnke-Emdes table of functions has been used, and where

$$\sqrt{2\Gamma_\gamma/\Gamma_{nAv}} \qquad (6)$$

A table of the function f is given in Table V.

Table V also gives the expected ratio of the capture cross section to that for formation of the compound nucleus, σ_r. In the last line of the table is given the ratio of the actual $\sigma_{\gamma Av}$ to the value which would be obtained if all neutron widths were the same and were equal to Γ_{nAv}

$$\sigma_{\gamma elem} = \sigma_r\Gamma_\gamma/(\Gamma_{nAv} + \Gamma_\gamma) \qquad (7)$$

This quantity is called in Table V the "elementary" capture cross section.

It is seen that the actual capture cross section is much less than the elementary cross section. The reason is that the levels with large neutron width which have a large cross section for formation of the compound nucleus, also suffer from severe competition of elastic scattering because their neutron width is comparable with the radiation width.

As a consequence we must expect that for a given formation probability of the compound nucleus, the average capture cross section is much lower for those nuclides which have a large neutron width, i.e., large level spacing. An example is U^{238}. The average over the seven lowest energy resonances, up to about 100 ev, gives $\Gamma_{n0Av} = 2.6$ mv. At 1 kev neutron energy this will give $\Gamma_{nAv} = 82$ mv. The radiation width, again deduced from the low-energy levels, is 30 mv, the same as for U^{235}. For these values of the parameters, Table V indicates that the elementary cross section is reduced to about 60%, yielding $\sigma_\gamma = 0.6 \cdot (30/112)\sigma_r$. Assuming the reaction cross section to be $400/\sqrt{E}$, the capture cross section becomes $64/\sqrt{E}$. This agrees reasonably well with observation and explains the relatively small capture cross section of U^{238} in terms of its large level spacing.

Table IV. Statistical Distribution of Neutron Widths in U^{235}

	1	2	3	4	5	6	7	8	9	10
Class	$2g\Gamma_{n0}$ (mv)	x	< 0	0–10	10–36 ev	10–36 corr.	Total	Total $> E_1$	From Eq. 2	Contr. to σ %
A	up to 1/64	0–0.5	1	5	1	13	18	58	58	1.3
B	1/64 to 1/16	0.5–1	–	8	4	13	21	40	35	6.7
C	1/16 to 1/4	1–2		1	9	9	10	19	21	24.4
D	1/4 to 9/16	2–3		1	3	3	4	9	8	25.3
E	9/16 to 1	3–4		0	2	2	2	5	3	18.4
F	1 to 3	4–7		0	2	2	2	3	1	21.0
G	over 3	> 7	1	0	0	0	1	1	0.06	2.9

Table V. Ratio of Capture to Compound Cross Section if the Statistical Distribution of Γ_n is Given by Equation 2

$\Gamma_{n\,Av}/\Gamma_\gamma$	0.005	0.02	0.04	0.08	0.125	0.25	0.5	
f	0.0048	0.018	0.033	0.065	0.082	0.137	0.202	
$\sigma_{\gamma\,Av}/\sigma_r$	0.97	0.90	0.83	0.72	0.66	0.55	0.404	
$\sigma_{\gamma\,Av}/\sigma_{\gamma elem}$	0.975	0.92	0.86	0.78	0.74	0.69	0.606	
$\Gamma_{n\,Av}/\Gamma_\gamma$	1	2	4	8	22.2	50	100	
f	0.295	0.378	0.476	0.570	0.697	0.773	0.871	1
$\sigma_{\gamma\,Av}/\sigma_r$	0.295	0.189	0.119	0.071	0.0314	0.0155	0.0087	0
$\sigma_{\gamma\,Av}/\sigma_{\gamma elem}$	0.590	0.567	.0595	0.641	0.728	0.788	0.880	1

Generally, in the intermediate energy range from about 100 ev to 100 kev, the capture will be substantially less for those nuclides which have large level spacing. It is well known that this continues to be true at higher energies at which the capture cross section is directly proportional to Γ_γ/D. This rule is important for the selection of structural materials to be used in reactors especially when neutron economy is important.

It is well known that the lighter elements, e.g., those around Fe, have large level spacing and therefore do not absorb strongly. For any given range of mass numbers, the nuclides of even A give generally larger level spacing in the compound nucleus formed by slow neutron capture than those of odd A. This rule was first recognized by Hurwitz and Bethe, and has since been confirmed by many experiments especially at Brookhaven. One reason for the smaller level spacing for odd A is that the compound nucleus is apt to have higher excitation energy. Another reason is that there exist in this case two level systems in the compound nucleus, with $j = I \pm \frac{1}{2}$ whereas if we start from even A, the compound nucleus has only one level system of $j = \frac{1}{2}$. This makes the average spacing for odd A half as large as for even A, under otherwise equal conditions.

Experimentally the first indication of the difference in neutron capture between nuclei of odd and even A for neutron energies of a few kev was obtained by Dessauer *et al.* at the Knolls Atomic Power Laboratory in 1949. The laboratory had a critical assembly with a neutron spectrum having a maximum at about 3 kev, and danger coefficients of various elements were measured in this spectrum. It was found that odd-Z elements usually had more capture than their even-Z neighbors. Activation measurements showed that the even-A isotopes of the even-Z elements were responsible for the reduced capture. A ratio of 5 in the capture cross section between odd and even A was estimated from these experiments, with no perceptible differencee between odd-neutron number and odd-proton number.

Even more striking effects have been observed for "magic" nuclei. The average capture cross section of such nuclei for neutrons of several hundred kev is reduced by a factor of about 50 compared to their non-magic neighbors. Hughes and collaborators have found that the level spacing and the neutron width for magic nuclei is correspondingly enhanced. They point out that the difference in neutron binding energy between this case and the normal case is not large enough to explain this large ratio although it tends in the right direction.

A spectacular example of neutron capture leading to a magic nucleus is the nuclide Xe^{135}. Its first resonance, at 0.08 ev, has a cross section of 3.4 million barns and $2_g\Gamma_{n_0} = 83$ mv, an exceedingly large value. It must be expected that this isotope has very large level spacing so that it will presumably not give any appreciable capture above its first resonance. The importance of the first resonance for the operation of thermal reactors is well known.

Turning now to fissionable isotopes, we shall first discuss the situation at low energy where the neutron width is negligible compared to radiation and fission width. We have already mentioned that the fission width does not seem to show as wide a distribution as the neutron width. Indeed if it did we could use Table V to compute the average fission width divided by the radiation width. It is easily seen that the ratio $\sigma_F/(\sigma_F + \sigma_\gamma)$ would be given by f if the distribution (2) were valid for fission width. In order to explain the observed ratio $1/(1+\alpha) = \frac{2}{3}$ we would have to assume an average fission width about twenty times the radiation width, according to Table V. This result is clearly incompatible with the observed fission widths.

We have therefore made simply the following crude assumption. We assume that there are two classes of fission levels, one of $\Gamma_F = 30$ mv and the other of $\Gamma_F = 150$ mv. In the first class, α will have the value 1, in the second class, 0.2. We further assume that there are equally many levels in either class; this leads then to the correct average value of α at low energies, 0.5.

At high energies experiment shows that α decreases. Let us accept 0.15 as the observed value of α at 200 kev. The most natural explanation is to assume that the fission width increases strongly from 0 to 200 kev. This is in fact to be expected since the fission process is very sensitive to the available energy. One evidence for this sensitivity is the rapid increase of the fission cross section of Np^{237} above its threshold. It is therefore not at all unreasonable to assume that the fission width of U^{235} increases by a factor of 3 between 0 and 200 kev. Such an increase would make $\alpha = \frac{1}{3}$ for the first class of fission levels, and $\alpha = \frac{1}{15}$ for the second class, giving an average of about 0.15.

There may be a further reduction in α due to the competition of the neutron width which at 200 kev has become reasonably large. However this effect is only about 20% as we shall see presently. Therefore the increase of the fission width from 0 to 200 kev may be as little as a factor of 2 but presumably not less.

We shall now try to calculate the sum of fission and capture cross section assuming the same distribution of neutron width at 200 kev as at 0 energy. The neutron width is $\Gamma_{n_0}\sqrt{E}$ so that using the average value $\Gamma_{n_0} = 0.125$ mv, we get for the average of the actual neutron width about 55 mv. This value is assumed to hold for all contributing orbital momenta which is of course a crude assumption.

For the first set of levels the fission width will be 90 mv assuming a factor 3 between 0 and 200 kev, and fission plus radiation width 120 mv. The ratio $\Gamma_{nAv}/(\Gamma_F + \Gamma_\gamma)$ is therefore about 0.45, leading to $(\sigma_F + \sigma_\gamma)/\sigma_r \approx 0.42$. For the second set of levels, $\Gamma_F = 450$, $\Gamma_F + \Gamma_\gamma = 480$ mv and $\Gamma_{nAv}/(\Gamma_F + \Gamma_\gamma) = 0.11$. For this set of levels then Table V gives $(\sigma_F + \sigma_\gamma)/\sigma_r = 0.68$. Since the two classes of levels are assumed to occur with equal frequency, the average between these two results has to be taken so that fission plus capture should be about 55% of the cross section of the compound nucleus.

Now according to the curve in Blatt and Weisskopf, page 348, the reaction cross section at this energy should be about $1.2\ \pi R^2$. Assuming $R = 1.4 \times 10^{-13}A^{1/3}$, this gives a reaction cross section of 2.8 barns of which 55% is 1.55. The observed fission cross section is 1.5, leading to fission plus capture of 1.72 barns. The agreement is reasonably satisfactory. It would be improved by assuming a somewhat lower neutron width which might actually be demanded for the neutrons of $l = 1$.

The same calculation yields for α a value of 0.135, about 15% lower than the elementary value obtained by neglecting the neutron width.

We have thus seen that the fluctuation of the neutron width and of the fission width from level to level permits a rather detailed account of the behavior of the average cross sections with energy, in addition to being compatible with the direct evidence from the velocity selector work. Moreover, we have seen that the average neutron width observed for U^{235} is in good accord with that expected from a black nucleus.

Status of Information on Reactor Material Cross Sections

By Henry Hurwitz, Jr.,* USA

It is difficult for those of us now engaged in the design of nuclear reactors to fully appreciate the vast increase in knowledge of reactor material neutron cross sections which has occurred in the past fifteen years. Although even now there remain areas in which additional cross-section information is needed, these areas of uncertainty are indeed minor compared to those which confronted the reactor physicists in the early 1940's. Because of the limited cross-section information which was available to them, the designers of the early reactors had to proceed cautiously, testing each aspect of the design with extensive experiments, and being always alert to the danger of an impurity with unknown cross section, or an unexpected resonance. Now, although it is still desirable to corroborate nuclear design calculations with critical experiments before final construction of a reactor, we may be confident that calculations based on the currently available cross-section information will give a good description of the essential features of the reactor behavior.

The most striking testimony of the expansion of our knowledge of neutron interactions is furnished by the cross-section compilation prepared by the Brookhaven Compilation Group.[1] This collection, which includes the results from work in many laboratories in many countries, provides a sound foundation for theoretical calculations on all types of reactors. But despite the broad range of information which it contains, the Brookhaven compilation does not represent the sum total of all of the information on reactor material cross sections which is at our disposal. It was not possible, for example, to include in complete detail all the available information on neutron angular distributions resulting from elastic scattering, or neutron energy spectra resulting from inelastic scattering. It was also not feasible to include the substantial quantity of cross-section information which is implicit in integral quantities such as resonance integrals, critical experiment reactivity coefficients, and neutron migration distances.

The rapid expansion in neutron cross-section information has been due in no small measure to the reactor development program itself. Not only have the reactor programs in the various countries of the world provided stimulation for the measurement of neutron cross sections, but also the reactors have shown themselves to be valuable tools in making these measurements. First, neutron beams from high flux reactors have been effectively used in crystal spectrometers and velocity selectors.[2] Secondly, reactivity coefficient and pile oscillator experiments performed in the reactors themselves have been particularly fruitful in providing information about capture cross sections. Thirdly, the intense flux of neutrons in high-power reactors has greatly increased the range of activation cross sections which can be measured. Thus the capture cross sections of many short-lived artificial isotopes are now known. Finally, the measurement of integral quantities such as critical mass, lattice parameters, and reactor neutron spectra have furnished useful checks on the over-all consistency of the cross-section data. The development of facilities for separating isotopes in substantial quantities has also contributed greatly to our cross-section knowledge by making possible the investigation of the nuclear properties of individual isotopes.

Historically, differential experiments with directed beams of monoenergetic neutrons and experiments of the integral type have played a complementary role. The differential experiments have in general provided the more accurate cross sections, but the integral experiments, when properly performed and analyzed, have often anticipated the results of the differential cross-section measurements. Furthermore, studies of integral quantities such as resonance escape, and neutron migration distances have enabled successful reactor designs to be achieved without a detailed knowledge of the cross sections of the various reactor materials.

It is to be expected that measurements of integral quantities will continue to play an important role in reactor design. Nevertheless, the high state of development of cross-section measurement techniques and calculational methods is making it possible to design reactors from the fundamental cross-section data without the use of semi-empirical interpretations of integral measurements. It is, for example, now possible to use the time-of-flight data on individual U^{238} resonances to calculate the resonance integral for infinite dilution as accurately as it can be measured.[3] Furthermore, studies at the New York University Institute of Mathematical Science indicate that it is now feasible to use Monte Carlo techniques in conjunction with the data on the individual resonances, to study the detailed dependence of the effective resonance integral on rod size and lattice spacing.[4]

* Knolls Atomic Power Laboratory.

In situations where strong self-shielding of the uranium resonances occurs, however, an accurate calculation of the resonance integral requires knowledge of the uranium resonance parameters above the present limit of about 500 ev.

CAPTURE CROSS SECTIONS OF REACTOR MATERIALS

The capture cross sections of reactor materials have an importance to reactor development which is second only to the fission cross sections themselves. In the thermal energy range these capture cross sections cannot be predicted from nuclear theory since they depend on the chance location of the resonance closest to zero incident neutron energy. Fortunately, there are many techniques for the measurement of thermal cross sections so that our knowledge in this area is satisfactory. The most accurately known thermal cross section is that of the boron (n,α) reaction which is commonly used as a standard. As discussed in detail by Harvey,[5] the present best value is 755 ± 4 barns at a neutron velocity of 2200 meters per second.

Pile oscillator measurements have been a prolific source of information on the thermal cross sections and resonance integrals of many materials which are important to reactor development either because of their use in reactor components or because they appear as impurities or as fission products. The sensitivity of pile oscillators have been continually improved so that at present there are several installations which can detect a sample cross section of 10^{-3} cm^2 (corresponding to 0.02 milligrams of natural boron).[6] The high sensitivity is particularly useful in measuring the cross sections of separated isotopes which are available only in small quantities.

A pile oscillator measurement of particular importance is that of the carbon neutron capture cross section. This cross section has been difficult to obtain because of its small size, and because neutron capture in C^{12} leads to a stable isotope. A pile oscillator measurement at the Argonne National Laboratory with highly purified graphite[1] has now yielded the value 3.2 millibarns for the carbon capture cross section, which is some 30% smaller than the earlier value 4.5 millibarns.

The pile oscillator measurements of the zirconium thermal capture cross section have also been of great practical significance. The full potential of zirconium as a non-poisonous reactor structural material for use at moderately high temperatures was not initially recognized because of the presence of hafnium impurity in the zirconium samples which were originally measured. The fact that the neutron numbers in the natural zirconium isotopes are magic or near magic gave a hint that the zirconium capture cross-section should be smaller than initially observed. This conjecture has been proved correct by subsequent measurements of the natural zirconium capture cross section with high purity samples at Argonne, Harwell, and Oak Ridge.[1] These measurements have converged on a value of 0.18 barns.

The extensive measurements of thermal neutron cross sections have made possible reasonably good estimates of fission product poisoning in thermal reactors. The results of a recent attempt to calculate thermal neutron fission product poisoning from the measured yields and cross sections of the various isotopes are shown in Figure 1.[7] The curves show upper and lower limits for the ratio of total fission product cross section to fission cross section as a function of the fraction, B, of original U^{235} nuclei which have been fissioned. The curves extend to burn-ups greater than unity since it was assumed in the study that U^{235} was continuously added to replace the atoms destroyed. Fission products were assumed not to be removed except by neutron absorption. The contribution to fission product poisoning by isotopes formed by neutron absorption in the original fission products was taken into account. The contribution of Xe^{135} was not included. The U^{235} fission cross section was taken as 580 barns.

Important contributions to the uncertainties in these results arise from Sm^{151} and Tc^{99}. The Sm^{151} cross section is known only from mass spectrographic analysis of fission product samples and is estimated to be between 2000 and 9000 barns.[8] Recent Oak Ridge studies indicate that the Tc^{99} cross-section is not greater than 100 barns.[1] The remainder of the uncertainty results mainly from several fission products for which the cross section is known only to be less than about 15 barns.

The correct fission product poisoning is probably close to the dotted line in Fig. 1. The initial shape of this line corresponds to a fission product cross section of 80 barns per fission (excluding Sm^{149} and Xe^{135}). At a burn-up of 10% the effective fission product cross section has dropped to 65 barns per fission (including Sm^{149} but not Xe^{135}) due to saturation of the products with large cross sections. At a burn-up of unity the effective fission product cross section has dropped to about 50 barns per fission (again including Sm^{149} but not Xe^{135}). Since the

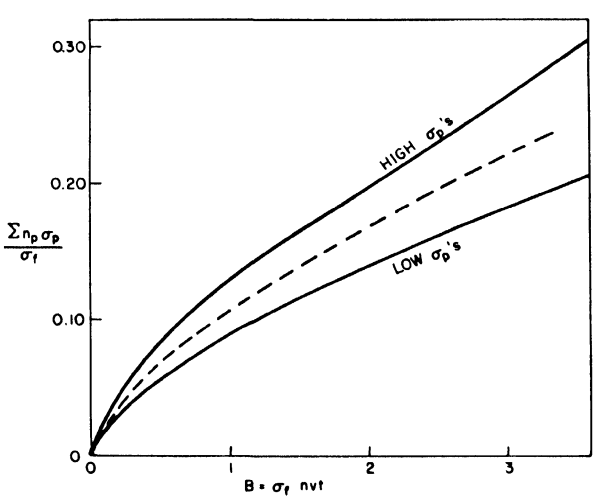

Figure 1. Ratio of thermal neutron fission product cross section to fission cross section as a function of burnup (excluding Xe^{135})

uncertainty in these figures is of the order ± 30%, there is a need for further improvements in the information of fission product thermal neutron cross sections.

Of even greater importance to the problems of long term reactivity variations and neutron economy than fission product effects are the properties of the transuranic isotopes produced in the reactors. Much of the information concerning the cross sections of these isotopes has been derived from radiochemical analysis of highly irradiated samples of U^{235} and Pu^{239}. Pile oscillator, and reactivity coefficient measurements with highly irradiated samples of fissionable material have also been of value in determining the properties of the transuranic elements. The bearing of the results of these investigations on the long term reactivity variation problem is discussed by Spinrad.[9]

A cross section of particular importance to the thorium breeding cycle is the thermal neutron capture cross section of Pa^{233}. This isotope has a 27-day half-life so that there is an appreciable probability that when it is formed in a high flux reactor by neutron capture in Th^{232} it will capture an additional neutron and become Pa^{234} before it can decay into U^{233}. Since U^{234}, which results from the beta decay of Pa^{234}, is not fissionable by thermal neutrons, a neutron capture by Pa^{233} costs a fissionable nucleus as well as a neutron. The capture cross section of Pa^{233} is difficult to measure because of its short half-life. The present best value is derived from recent measurements in the Materials Testing Reactor. These measurements give a thermal capture cross section of 66 ± 7 barns and a resonance integral of 680 ± 100 barns for the formation of both of the Pa^{234} isomers.[1] In addition to the direct relation of capture cross sections to reactivity and neutron economy, the capture cross sections of certain isotopes are important because of their bearing on the radioactivity which is produced in various parts of the reactor and the associated problem of reactor accessibility for repairs. An interesting example of this nature is provided by Ta^{182} which is formed by neutron capture in the naturally occurring isotope Ta^{181} which may be present as an impurity with niobium in stainless steel. Ta^{183} has a half-life of 111 days and emits hard gamma rays. If Ta^{182} captures a neutron, it becomes Ta^{183} with a half-life of only 6 days. Because of its short half-life, the Ta^{183} decays relatively rapidly after reactor shutdown and so does not constitute a serious obstacle to reactor accessibility. The second order reaction leading to Ta^{183} would be unimportant from the practical standpoint were it not for the fact that the capture cross section of Ta^{182} is apparently very large. Recent measurements have shown the thermal neutron capture cross section of Ta^{182} to be 47,000 ± 5000 barns.[33] This cross section is large enough to appreciably reduce the seriousness of the tantalum activity problem in reactor structural materials by limiting the accumulation of Ta^{182}.

RESONANCE CROSS SECTIONS

One of the facts which recent studies of long term reactivity variations and reactor temperature coefficients have emphasized is that even in thermal reactors the deviation of cross sections from the $1/v$ law near thermal energies must be carefully considered if accurate design information is to be obtained. Since many of the important nuclei have resonances close to zero energy, the ratios of effective thermal neutron cross sections change considerably from one reactor to another. Such variations are difficult to unravel by studying the observed behavior of the various reactors themselves. It is, therefore, fortunate that it is proving possible to measure the energy variation of the cross sections even of unstable nuclides.

Perhaps the most noteworthy example of cross-section measurements of unstable nuclei is the study of the Xe^{135} resonance at the Oak Ridge National Laboratory.[10] This investigation has shown that the energy variation of the Xe^{135} cross section can be described by the Breit-Wigner resonance formula with $E_0 = 0.086$ ev, $\Gamma = 0.11$ ev, and $\sigma_0 = 3.4 \times 10^6$ barns.

Another low-lying resonance of an artificial isotope which has great practical importance occurs in Pu^{240}. This isotope is produced in considerable quantity in thermal reactors containing plutonium because of the high thermal radiative-capture cross section of Pu^{239}. A measurement performed with the Columbia University time-of-flight spectrometer gave the following parameters for the lowest resonance of Pu^{240}: $E_0 = 1.06 \pm 0.02$ ev, $\sigma_0 = 1.7 \pm 0.9 \times 10^5$ barns, and $\Gamma = 0.045 \pm 0.015$ ev. Further measurements of the energy dependence of the Pu^{240} cross section are in progress at several laboratories.

The great quantity of experimental data which has been collected on neutron cross sections of the stable isotopes in the resonance range is of practical value to reactor development from two standpoints. First, the information may be directly applied to a number of reactor design problems relating to migration of intermediate energy neutrons, resonance absorption effects, temperature coefficients due to Doppler broadening of resonances, and control rod effectiveness. Secondly, the experimental information is essential to the development of nuclear theories which in turn make possible the prediction of cross sections which have not yet been measured. The status of current nuclear theories, and the role which these theories play in predicting cross sections of importance to reactors, are discussed in detail by Weisskopf.[12]

As a result of the concurrent improvement in resolution of time-of-flight neutron spectrometers and electrostatic devices for producing monoenergetic neutrons beams it is now possible to cover the entire energy range of interest to reactors with "good resolution" in the sense that the spread in energy is small compared to the energy itself. The resolution of 0.01 microseconds per meter which is ap-

proached by time-of-flight instruments in several laboratories provides an energy resolution of about one-third an ev at 100 ev, and 300 ev at 10 kev. Since the energy spread of neutron beams produced by electrostatic accelerators which are now in operation is less than one kev, these machines provide "good resolution" above a few kev. The overlap of the time-of-flight and electrostatic accelerator results is well illustrated by the information on the total cross section of manganese[1] in which the same resonances in the energy region between one and ten kev show up in both the time-of-flight and electrostatic accelerator data.

This, of course, does not imply that all resonances in the reactor energy range can be resolved or even separated. Indeed, for energies above 10 kev, resonances can be separated only for nuclei with atomic mass below about 100, and for certain of the magic nuclei (e.g., the lead isotopes). Fortunately, techniques are available for obtaining information about the properties of individual resonances which are separated, but not resolved and about the statistical distribution of resonance parameters when the resonances are not even separated. These techniques, which include transmission measurements with foils of various thickness and self-indication measurements in which the neutron detector is the same substance as the target being studied, are discussed by Melkonian.[13] Measurements of this type have in many cases been facilitated by the availability of separated isotopes. This allows individual resonances to be assigned to the proper isotope and thereby removes the uncertainty in resonance parameters which exists when the concentration of the isotope giving rise to the resonance is not known.

The major statistical features of nuclear resonances which are apparent from the substantial quantity of resonance data which has been collected may be summarized as follows.[14] The resonance spacing decreases with increasing atomic weight as would be expected from the statistical nuclear model. For nuclei of atomic weight below $A = 25$ the spacings, which are obtained primarily from experiments with neutrons from electrostatic accelerators, are measured in hundreds of kev. Between $A = 25$ and $A = 50$ the spacings drop to the order of 10 to 100 kev for even A and less than 10 kev for odd A. At $A = 100$, the spacings have dropped to the order of 100 ev. From $A = 100$ to the heaviest isotopes the spacing undergoes a further decrease to about 20 ev for the even-A isotopes and about one ev for the odd-A isotopes. Thus, Th^{232} and U^{238} have level spacings of about 20 ev whereas U^{233}, U^{235}, and Pu^{239} have spacings of the order of one volt.[15] The reduction in spacing with increasing A is less rapid in the region above $A = 100$ since the effect of the increase in number of particles in the nucleus is in part compensated by the decrease in the binding energy of the incident neutron from about 8 Mev at $A = 100$ to 5 Mev at $A = 238$.

Exceptions to the general trend of level spacings occur when the number of neutrons or protons is equal to one of the magic numbers (particularly 50, 82 and 126). For such target nuclei the spacing is exceptionally large, the effect being more pronounced when the neutron number is magic than when the proton number is magic. For example, Pb^{206} and Pb^{207}, for which the proton number is magic, are believed to have spacings of the order of 10 kev. Pb^{208}, which is doubly magic, has a resonance spacing of several hundred kev, which is large enough to allow individual resonances to be seen in the one Mev region.[1] The even isotopes of zirconium, which have neutron numbers at or just above 50, have been observed to have spacings of the order of 1 kev which is at least twenty times larger than the spacing in neighboring non-magic nuclei. The isotopes of tin ($Z = 50$) have spacings of about 100 ev, whereas the indium isotopes ($Z = 49$) have spacings less than 10 ev.

Concurrent with the decrease in resonance spacing with increasing atomic weight is a decrease in Γ_n and Γ_r, the neutron and radiation resonance widths. The radiation widths, which are of the order of one kev for levels in the lightest nuclei, fall to a few ev at $A = 25$, somewhat less than one ev at $A = 50$, and less than 0.1 ev for A of 100. Above $A = 100$, the radiation widths decrease less rapidly. In the uranium isotopes the radiation width is approximately 0.03 ev.

The radiation widths of resonances in a single isotope appear not to vary by more than 20 per cent. This is not true for the neutron widths which, in addition to having a secular variation as the square root of the energy, also have strong fluctuations from one resonance to another. In studying the trend of neutron widths with atomic number it is therefore appropriate to speak in terms of the reduced neutron width, Γ_n^0, which is the actual width divided by the square root of the energy in ev. The decrease in reduced neutron widths with increasing A is more rapid than the decrease in radiation widths. This has the important practical consequence that in the lighter elements the neutron width in general exceeds the radiation width so that the resonances lead to neutron scattering whereas for heavy elements the reverse is true so that the resonances lead primarily to neutron capture. The ratio Γ_n^0/D of the average reduced neutron width to level spacing, D, of levels of a given spin and parity is a measure of the average formation probability the compound nucleus. On the basis of early theories this ratio should be approximately constant. The more recent cloudy-crystal ball nuclear model,[12] on the other hand, predicts a maximum in this ratio for an atomic number in the neighborhood of 150. On the basis of the experimental resonance data, Γ_n^0/D is large in the region of the theoretical maximum, although the observed peak is not as large as the theory would indicate. The peak in Γ_n^0/D is reflected in the strong absorption of the rare-earth elements, which is of practical importance to reactors not only in relation to loss of

neutrons by impurity and fission product absorption but also because of its possible application to the design of control rods.

The greater fluctuations in reduced neutron widths as compared to radiation widths is believed to be related to the fact that, whereas a compound nucleus can decay by gamma ray emission into several possible final states, the re-emission of a neutron leaves the target nucleus in its ground state when the incident neutron energy is below the inelastic scattering threshold. Thus the smoothing effect of averaging nuclear transition probabilities over several final states, which is present in decay by gamma emission, is absent when the decay takes place by neutron emission. On the basis of recent neutron width studies,[14] it appears that the distribution of reduced neutron widths† is approximately exponential, i.e., that the number of reduced widths in the range $d\Gamma_n^0$ is proportional to $(\exp C\Gamma_n^0)d\Gamma_n^0$ where C is a constant characteristic of the particular nucleus. The experimental data does not exclude a similar distribution which has been suggested on theoretical grounds,[16] namely $(\Gamma_n^0)^{-1/2}$ $(\exp C\Gamma_n^0)$ $\times$ $d\Gamma_n^0$. Still a third distribution has been suggested to better describe the high frequency of levels with unusually large neutron widths.[15] This distribution corresponds to an exponential distribution of $(\Gamma_n^0)^{1/2}$ rather than Γ_n^0.

The large fluctuations in reduced neutron widths have the practical consequence of reducing the average capture cross section below that which would exist with the same average value of Γ_n^0/D but no fluctuations. This is because in resonances which have particularly large values of Γ_n^0 the compound nucleus has a better chance of decaying by re-emission of a neutron. Thus, although the contribution to total cross section of strong resonances is large, the contribution to the capture cross section is not correspondingly large. Indeed, if Γ_n is large compared to Γ_γ the contribution of an s-resonance to the integral over energy of the capture cross section approaches the limiting value $2\pi^2\lambda^2 g\Gamma_\gamma$ where g is the statistical weight of the level.

A complication in the direct application of velocity selector information to reactor problems is that, whereas the velocity selector experiments in general measure total cross sections, the capture cross sections are more important for reactors. Transmission experiments utilizing targets of two different thicknesses, or self-indication techniques can provide values of $g\Gamma_n$ and the total width, Γ.[13] If Γ is large compared to Γ_n the capture cross section integrated over the resonance, is proportional to $g\,\Gamma_n$ but otherwise there is an additional factor $\Gamma_n/\Gamma = (|\Gamma - \Gamma_n|/\Gamma)$. If the spin of the target nucleus is zero so that g is unity the factor is in principle determined, although if Γ_n is larger than Γ_γ there may be considerable uncertainty in its value. When the spin of the target is not zero, there is an inherent uncertainty in g which may be resolved from the transmission measurements alone only if Γ_n is large compared to Γ_γ and if $g\Gamma_n$ and Γ can be measured with sufficient accuracy to distinguish between the two possible spin values. Additional information on the ratio of scattering to capture in low energy resonances is available from direct observation of the scattered neutrons.[17] In addition to helping to specify the spin state of the compound nucleus, these scattering measurements provide consistency checks of the accuracy of the experimentally determined resonance parameters.

In practice, the fact that Γ_γ is apparently almost constant for a particular isotope is of great help in determining the capture cross sections. Indeed, if the distribution of Γ_n^0, the value of Γ_γ and the level spacing for a nucleus can be obtained from the study of the low energy levels, the average capture cross section variation with energy can be reliably extrapolated to energies far above those at which the individual resonances can be studied.

A somewhat more direct method of obtaining information concerning capture cross sections consists of time-of-flight measurements in which the capture gamma rays emitted by the targets are detected. If the capture gamma rays' multiplicity is independent of energy for a particular nucleus the ratio of capture cross section is a function of energy to thermal capture cross section can be obtained. Capture gamma measurements of Ta^{181} at the Knolls Atomic Power Laboratory yield resonance parameters which are consistent with those obtained in the transmission measurements so that at least in this case the multiplicity of gamma rays appears to be fairly constant.[18] It therefore appears that capture gamma measurements should be of considerable help in the investigation of capture cross sections in the high intermediate-energy region where the radiation width is small compared to the neutron width, or where individual resonances are not resolved. Self-indication measurements using capture gamma-ray detectors are especially useful in providing information on peak resonance cross sections, and their applicability is not contingent on the assumption of constant gamma multiplicity.

Both because the time-of-flight measurements are time consuming and expensive, and because of the inherent limitation of the time-of-flight measurements at high energies, there is still great value in the measurements of average capture cross sections by other techniques. The two most important techniques are measurement of reactivity effects in chain reacting systems (i.e., reactivity coefficient, or pile oscillator experiments) and activation experiments which are applicable when neutron capture leads to a radioactive nuclide.

Pile oscillator and activation measurements in a thermal neutron reactor can be used to obtain resonance integrals if the sample is located inside a cadmium shield.[19,6] Such experiments give information

† The experimental information actually refers to the distribution of $2g\,\Gamma^0$ since the statistical weight, g, is undetermined for most resonances in nuclei of odd mass.

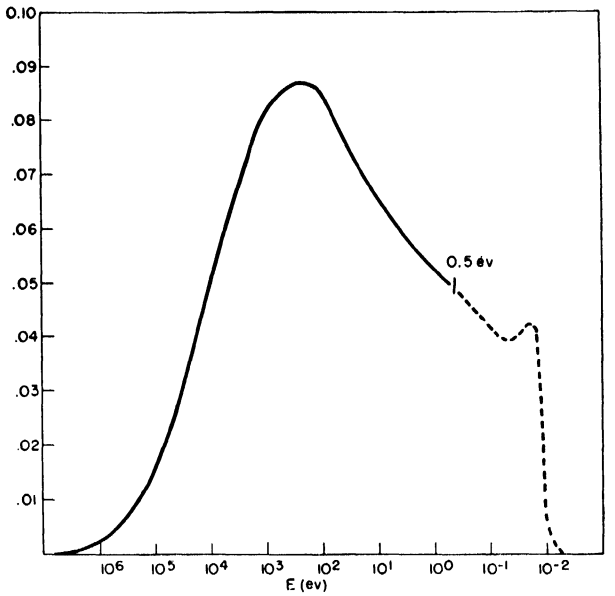

Figure 2. Estimated relative contribution to reactivity coefficient of capture in a 1/v absorber per logarithmic energy range in PPA-5

mainly about the low energy resonances. Information about the higher energy resonances may be obtained by reactivity coefficient measurements in intermediate assemblies as discussed by Snyder.[20] For elements in which the capture cross section is not too small, the reduction in reactivity due to placing a sample of the element at the center of a chain reacting assembly is proportional to the integral over energy of the product of the absorption cross section of the element, the neutron flux per unit energy range, and the adjoint function (i.e., the value of a neutron to the chain reaction as a function of energy). The neutron spectrum in the assembly (KAPL–PPA–5) in which the experiments reported by Snyder were performed is characterized by Fig. 2, which shows the estimated absorptions per unit logarithmic energy as a function of energy weighted by the neutron value at the corresponding energy for a $1/v$ absorber. It is apparent that about one-half of the reactivity coefficient comes from absorptions above 100 ev. The relative reactivity coefficients per mole of the elements which were measured is shown in Fig. 4. (On the scale of Fig. 4 the reactivity coefficient of natural boron is —24 cents/mole.)

A series of activation experiments has been performed at the Knolls Atomic Power Laboratory in a somewhat higher spectrum by Dearnley, Soisson and Yunker. The neutron spectrum existing in a beryllium block irradiated by 2 Mev X-rays was used in these irradiations. The neutron spectrum in the block is estimated to be of the form

$$n\,v\,dE = E^{0.4}\,dE/E$$

The samples were located inside shields of various combinations of absorbers to eliminate the low energy neutrons. One of the shields employed was the "200 ev" boron shield used in the alpha experiments described by Kanne and Stewart.[21] This was a boron shield having a transmission of $1/e$ at 200 ev. The estimated absorptions per unit logarithmic energy range of a $1/v$ absorber in the neutron spectrum inside the shield is shown in Fig. 3. The ratio of the activation cross section of the isotopes exposed in the shield to the U^{235} fission cross section in the same spectrum is shown in Fig. 5. For comparison, the activation cross sections in a fission neutron spectrum as given by Hughes, Garth, and Levin is shown in Fig. 6.[22]

A notable feature of both the activation and reactivity coefficient measurements is the low value of the capture cross sections for nuclides with magic numbers of neutrons ($N = 50, 82, 126$) and a similar, but less pronounced, effect for nuclides with magic numbers of protons ($Z = 50, 82$).

It also appears, particularly from the reactivity coefficient, that the capture cross sections of even Z elements are systematically smaller than for odd Z elements. In fact, the reactivity coefficient results would be consistent with the assumption that most of the capture cross section of even Z elements is contributed by the isotopes with odd neutron number. Although it would be possible to ascribe some of these effects to systematic variations in the average of Γ_n^0/D, it is more satisfactory from the standpoint of current nuclear theories to assume $\overline{\Gamma_n^0/D}$ is constant and to ascribe the effects instead to variation in D. In the region where neutron widths are small compared to radiation width, the average capture cross sections are independent of D for constant $\overline{\Gamma_n^0/D}$. In the intermediate and high energy range, however, Γ_n is not small compared to Γ_γ so that the average capture cross section should decrease monotomatically

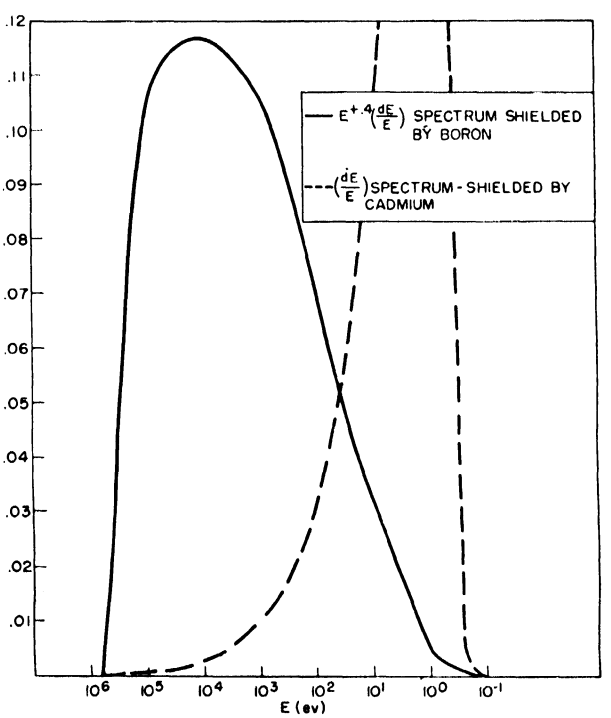

Figure 3. Estimated absorption per logarithmic energy range for a 1/v absorber irradiated in "200 ev" boron shield

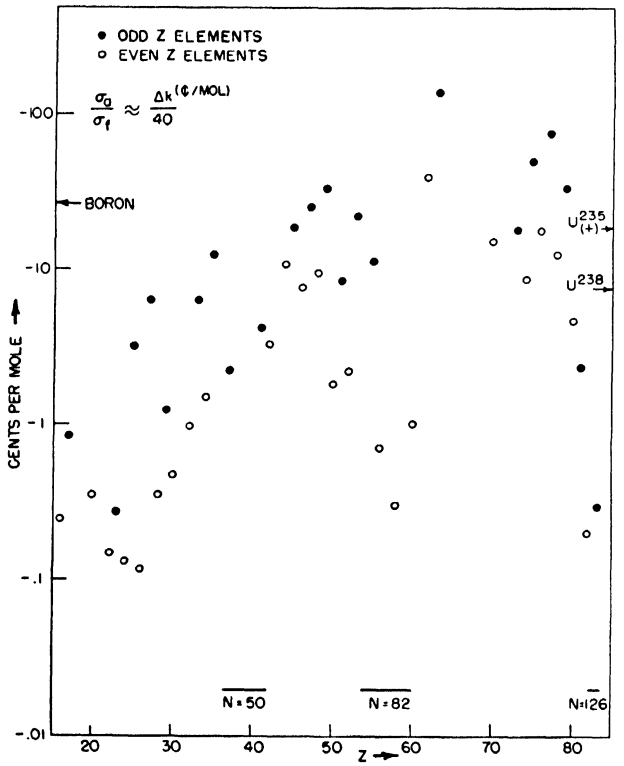

Figure 4. Central reactivity coefficients in PPA-5 (estimated scattering corrections applied)

with increasing D. As observed above, the dependence of capture cross sections on D in the intermediate energy range is accentuated by the fluctuations in Γ_n.

The observed capture cross sections are not consistent with the assumption that level spacing depends only on the excitation of the compound nucleus above its ground state since this assumption would predict high cross sections for even Z-odd N nuclei and low cross sections for even Z-even N nuclei and odd Z-even N nuclei. Furthermore, it would not predict abnormally low capture cross sections for magic-Z nuclei. To explain the reactivity coefficient data an alternate assumption has been proposed[21,23] that level spacings depend on excitation of the compound nucleus above a characteristic "fictitious" ground state which is a smooth function of Z and N and does not reflect the odd-even and shell structure variations in the actual ground state. This assumption predicts small capture cross sections for even Z-even N targets, and large cross sections for even Z-odd N and odd Z-even N targets. Still larger cross sections would be predicted for odd Z-odd N nuclei. This viewpoint would predict comparably small capture cross sections for magic Z and magic N nuclei. (Actually the latter are observed to be smaller.) Possible effects of the spin, J, of the compound nucleus on level spacings have also been suggested.[26] The actual dependence of D on J is not clear since, although a purely statistical nuclear model would give D inversely proportioned to $2J + 1$, pairing energy effects favor low J and hence would tend to increase D for large J. The inability of spin effects alone to explain odd-even alternations in level spacing is apparent from the fact that although odd Z-even N targets and even Z-odd N targets lead to compound nuclei of similar J, the resonance spacing for odd Z-even N targets is, if anything, smaller than that for even Z-odd N targets[14] whereas, the binding energy of the incident neutron is considerably larger in the latter case.

Aside from the theoretical interest in determining variations of level spacing and capture cross section due to odd-even and shell effects, there is clearly great practical importance in obtaining a more complete experimental and theoretical understanding of the situation. The interpretation of reactivity coefficient and activation measurements of the type discussed above in terms of the increasing quantity of differential resonance data which is becoming available should provide a useful check of the consistency of the entire picture.

A particularly important aspect of neutron capture data is its bearing on the practical question of breeding gain in fast reactors. Because of inelastic scattering of reactor materials it is anticipated that in a high-power breeder reactor an appreciable fraction of the neutrons will be degraded to intermediate energies where the neutron capture can be important. The direct activation and reactivity coefficient capture cross-section measurements are not completely satisfactory in providing the desired capture cross-section information needed for reactor design since the former are limited almost entirely to nuclei with even neutron number, and the latter are inaccurate in fast neutron assemblies since in such assemblies inelastic scattering and moderation effects on re-

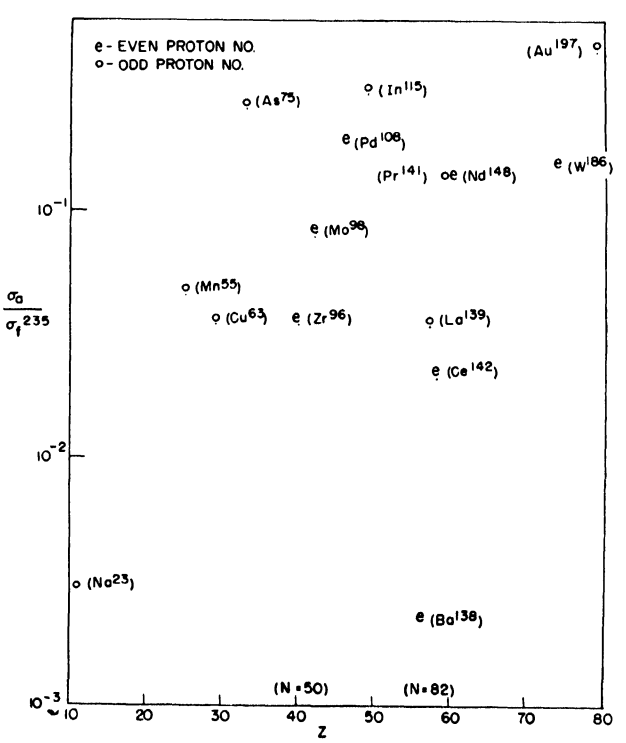

Figure 5. Activation measurements in "200 ev" shield

activity tend to mask the capture effects. Hence, the theoretical extrapolation of experimental information obtained in the accessible energy ranges will continue to play an important role in reactor design.

Before leaving the subject of capture cross sections it is of interest to compare the fission product poisoning effects in thermal, intermediate, and fast reactors. It is estimated from the reactivity coefficient surveys that in an intermediate assembly of the KAPL–PPA–5 type the ratio of the capture cross section of an average pair of fission products to the U^{235} fission cross section is between 0.3 and 0.5. On the basis of the activation measurements, the cross section per fission product pair for fission neutrons is about 110 millibarns if the unmeasured even Z-odd N isotopes are assumed to have cross sections three times as large as the neighboring even Z-even N nuclei. If the even Z-odd N cross sections are assumed the same as the neighboring odd Z-even N nuclei the cross section is 80 millibarns. Nuclei with proton or neutron numbers equal to 50 and 82 are always assumed to have small cross sections.)

It is noteworthy that on the basis of present information fission product poisoning appears to be more serious for intermediate reactors than for either fast or thermal reactors. This is so because in thermal reactors the fission products with exceptionally large cross sections are burned out rapidly so that the effective fission product cross section at burn-ups of practical interest is much smaller than the sum over all fission products of cross section times yield. In the region of several hundred kev both the neutron capture and fission processes must compete with neutron re-emission after the compound nucleus has been formed. Because the fission widths, Γ_f, are much larger than the radiation widths, the fission process competes more favorably with neutron re-emission than does radiative capture.‡ In the low intermediate energy region neither burnout of the high-cross-section products nor competition with scattering is important so that the ratio of fission product capture cross sections to the fission cross section is large.

TRANSPORT AND INELASTIC SCATTERING CROSS SECTIONS

Transport and inelastic scattering, although they do not influence neutron economy as directly as do the capture cross sections, are of equal practical importance because of their bearing on reactor size and neutron spectrum. Indeed, some structural materials may have a greater adverse effect on breeding ratio by virtue of their inelastic scattering, which degrades neutrons below the U^{238} fission threshold or to an energy where radiation capture is serious, than by virtue of their direct contribution to neutron capture.

In the low energy region where the neutron wavelength is large compared to nuclear dimensions, the transport scattering cross section, σ_{tr} [i.e., $\sigma_s(1 - \cos\theta) + \sigma_c$] may be obtained directly from the total cross section since the scattering is isotopic in the center of mass system. Although the scattering is not in general isotopic above 0.1 Mev, the transport cross section has in the past frequently been estimated from the total cross sections which are more accessible experimentally. In recent years, however, extensive and reliable measurements of scattering angular distributions as a function of energy have become available[27] so that transport cross sections may be calculated directly from the experimental data. The transport cross sections are in general found to be substantially smaller than the total scattering cross section because of the preponderance of smaller angle scattering.

The experimental situation is particularly favorable for the light elements where the spin and parity of individual resonances can be identified from the angular distribution data. This then allows the scattering angular distributions to be re-synthesized theoretically and extended to energies for which detailed measurements have not been made.[28] For intermediate and heavy nuclei such a procedure is not feasible so that reliance must be placed on experimental measurements in the Mev energy range in which the angular distributions from the individual resonances are not resolved, or upon theoretical calculations of the gross features of the scattering averaged over many resonances.

When the neutron mean free path fluctuates rapidly with energy as is the case in the 1 Mev range for nuclei of intermediate and heavy atomic weight, the quantity most pertinent to neutron transport effects is the average of the square of the neutron mean free path. This quantity is not directly obtainable from transmission measurements when the resonances are unresolved. It is, however, possible to obtain information relating to the fluctuation in total cross section by transmission self-indication measurements as has been discussed by Monahan and Langsdorf.[27] The fluctuation problem may also be studied theoretically in terms of the statistical distribution of resonance parameters and spacings as deduced from time-of-flight measurements at low energy. This was done in the analysis of Doppler effect temperature coefficients in fast reactors.[28]

The advances in techniques for performing reactor calculations have placed greater demands on the accuracy of the experimental transport cross-section measurements. Procedures for handling reactor problems in more than one spatial dimension and for treating deviations from the diffusion approximation by use of the automatic digital computing machines

‡ The fluctuations in neutron width help to explain the fact that the capture cross sections of non-fissionable nuclei in the intermediate energy region are in general much smaller than the U^{235} fission cross section even though the average of Γ_n^0/D for non-fissionable nuclei is the same or larger than for U^{235}. The neutron width fluctuations allow resonance scattering to compete strongly with resonance capture even in energy regions where the average neutron width is smaller than the radiation width.

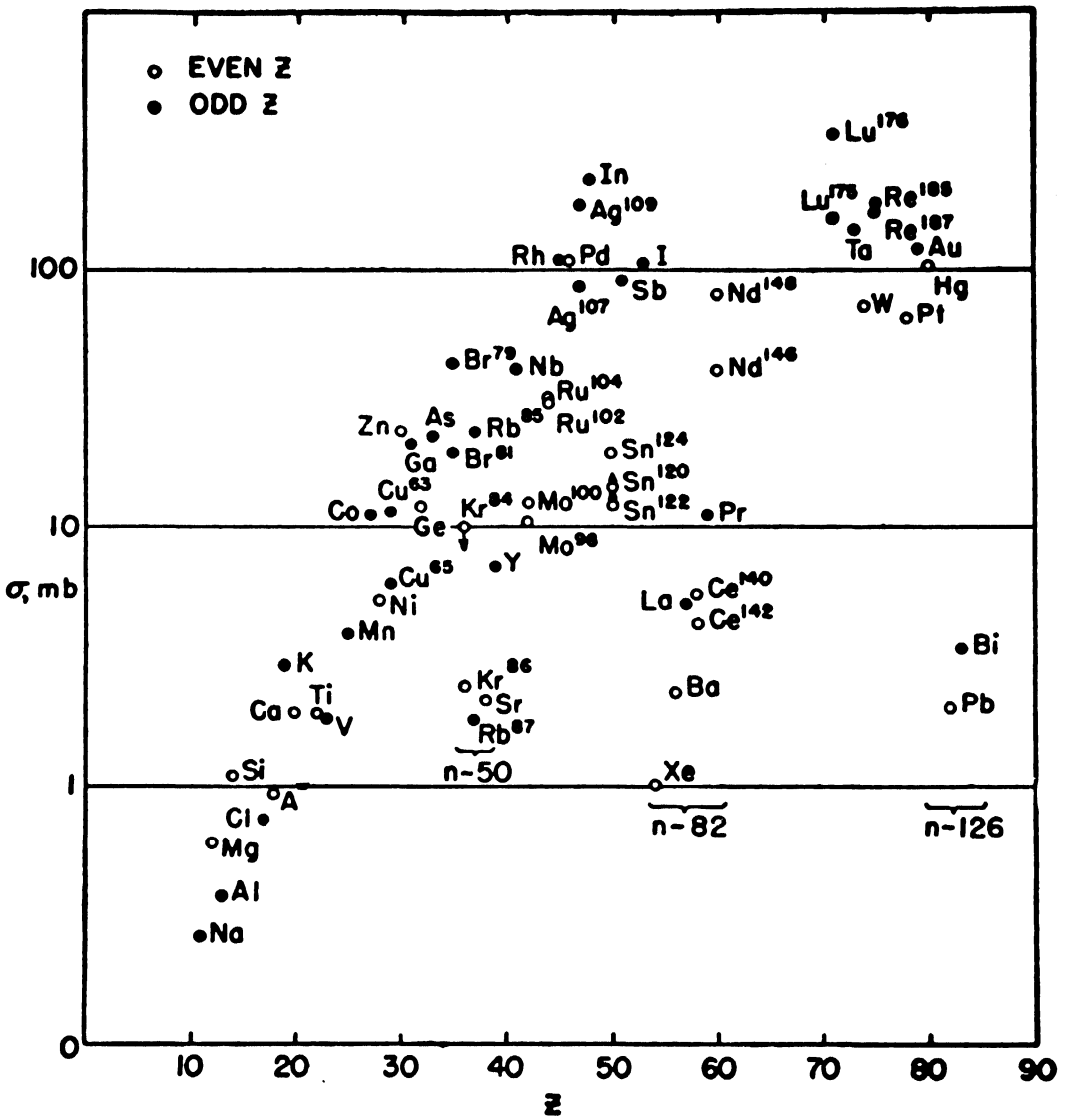

Figure 6. Cross sections in millibarns as a function of atomic number for fission neutron spectrum (from Hughes, Garth and Levin, Phys. Rev. 91, 1423 (1953))

have made it feasible to seek an accuracy of considerably better than five per cent in reactivity calculations for highly enriched assemblies in which leakage is important.[29] If approximately one-third of the neutrons leak from the core, a calculation of reactivity to two per cent requires a calculation of the leakage to about four per cent. This in turn requires a knowledge of transport cross sections in the high energy region where most of the leakage occurs to about two per cent. (In thermal reactors the significant quantity for calculating leakage is the age which is proportional to $1/(\xi\,\sigma_s\sigma_{tr})$. The average logarithmic energy loss per collision, ξ, depends on scattering angular distribution in essentially the same manner as does the transport cross section, σ_{tr}, so that the percentage error in leakage is twice that in the transport cross section.) At the present time the uncertainty in transport cross sections for fast neutrons is at least five per cent so that there is practical justification for attempting measurements to reduce the error still further.

Uncertainty in inelastic scattering in many cases is a more serious source of error in reactor calculations than uncertainties in the transport cross sections themselves. An evaluation of the effect of inelastic scattering on neutron leakage requires a knowledge of the spectrum of inelastically scattered neutrons as well as the total cross section. This is illustrated by Fig. 7 which shows the estimated importance of a neutron to the chain reaction (i.e., the adjoint function) as a function of its energy for three typical reactor types: a small, water moderated reactor containing highly enriched fissionable material (such as the Material Testing Reactor), a beryllium moderated reactor similar to the KAPL PPA-5, and a large plutonium-oxide power breeder reactor with a core containing six moles of U^{238} per mole of Pu^{239}. In the latter reactor, whose properties were

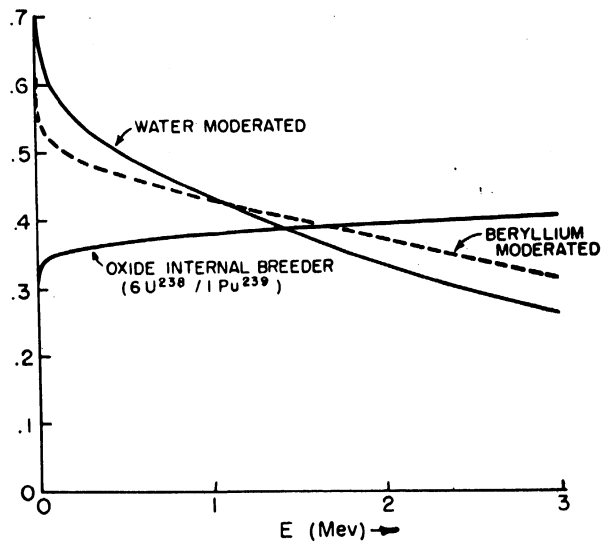

Figure 7. Neutron importance

calculated by Sampson and Luebke of the Knolls Atomic Power Laboratory, the neutron importance decreases with decreasing neutron energy due to radiative capture in the U^{238}. It should be noted that in all three cases the neutron importance changes rapidly in the region below one Mev.

Figures 8 and 9 illustrate the importance of neutron spectrum to the breeding ratio. In Fig. 8 the estimated multiplication of neutrons due to fast fissions in U^{238} (i.e., the "fast effect") is shown as a function of the energy at which a neutron is inserted into the core of the plutonium fast breeder mentioned above. (The dotted line represents the fission neutron spectrum.) Figure 9 shows the present information on the variation of the capture-to-fission ratio (alpha) of Pu^{239} with energy.

Because of the high U^{238} fission threshold, neutrons which have been inelastically scattered have little chance of producing fast fissions, hence the total inelastic cross section rather than the spectrum of the inelastically scattered neutrons is most important in determining fast fissions. (A similar situation prevails in shielding problems since the neutron penetration after inelastic scattering is much smaller than before the scattering so that the neutron removal cross sections depend primarily on the total inelastic cross section.) The situation is quite different in regard to the increase in neutron radiative capture in the fissionable material as a result of inelastic scattering. As is evident from Fig. 9 the rise in capture-to-fission ratio is most rapid at low energy so that in this connection a small cross section for inelastic scattering to a low energy may be more serious than a larger cross section for inelastic scattering with small energy loss. Furthermore the spectrum of neutrons inelastically scattered to the region of one or two hundred kev should be proportional to the square root of the final neutron energy for heavy nuclei so that this low energy part of the spectrum could be important.

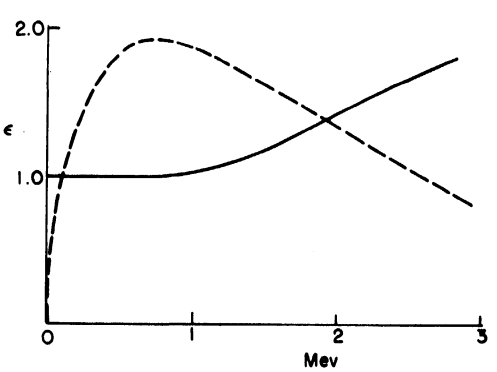

Figure 8. Trend of fast effect

Present information on total inelastic cross sections is reasonably satisfactory since most of the important inelastic cross sections are known to within about a tenth of a barn at several incident neutron energies.[25] The total inelastic cross section in general rises with increasing atomic weight except that the magic nuclei have abnormally small inelastic cross sections for fission neutrons due to the small number of low-lying excited states of the compound nucleus. For higher incident neutron energies the difference between magic and non-magic nuclei becomes less

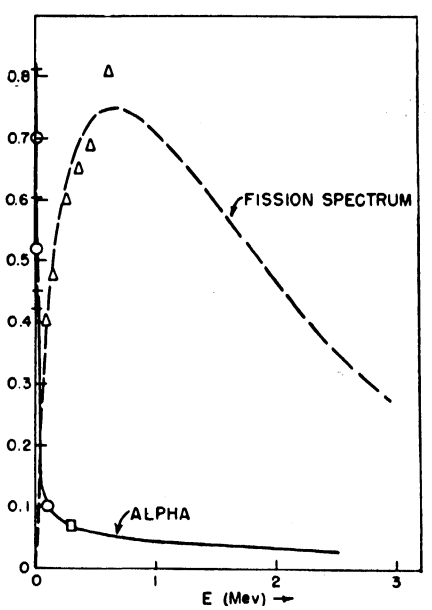

Figure 9. Alpha of Pu^{239}

pronounced. For example, the zirconium inelastic cross section in the 4 Mev range is slower than that of neighboring non-magic nuclei, but not as low as that of lighter elements such as iron.

Although the high energy part of the spectrum of inelastically scattered neutrons has been explored in some detail, the low energy part is poorly known because of the problem of detecting proton recoils from low energy neutrons. In general the experimental data show a less marked softening of the scattered neutron spectrum as the incident neutron energy is reduced from 14 Mev to the fission spectrum energy region than might be expected from a statisti-

cal nuclear model.[30] If it can be shown by further experiments that the probability of inelastic scattering of fission spectrum neutrons to the hundred kev energy region is indeed small, the problem of designing fast breeder reactors will be considerably simplified.

Much of the present work on the measurement of differential spectra of inelastically scattered neutrons is directed toward providing a detailed description of the scattering in terms of the excitation of the individual levels of the target nucleus.[31] This procedure is feasible for target nuclei which either have low mass or are magic so that the number of relevant excited states is small. The important structural materials zirconium and iron fall into this category. Measurements of the gamma rays resulting from inelastic scattering are of particular value in determining the energies and excitation functions of the various states of the target nucleus.[33]

As further differential spectrum data are obtained by the methods which are now available for studying inelastic scattering,[25,33] the reactor calculations will lean less heavily on the threshold detector measurements with heterogeneous neutron sources[30] which have proved so useful in the past. This exemplifies the trend which is characteristic of the entire field of neutron cross section analysis for reactor application in which advances in experimental techniques are making possible a continued increase in the detail and accuracy with which the properties of reactors can be predicted.

REFERENCES

1. Hughes, D. J. and Harvey, J. A., *Neutron Cross Sections,* Brookhaven Report BNL-325 (1955).
2. Hughes, D. J., P/576, *Neutron Velocity Selectors Used at Reactors,* Volume 4, Session 15A, these Proceedings. Wollan, E. O. and Shull, C. G., P/579, *Neutron Diffraction Research in the United States,* Volume 2, Session 6A, these Proceedings.
3. Maklin, R. L. and Pomerance, H. S., P/833, *Resonance Capture Integrals,* Volume 4, Session 20A, these Proceedings.
4. Richtmyer, R. D., *Monte Carlo Study of Resonance Escape in Hexagonal Lattices,* Institute of Mathematical Sciences, New York University Report NYO-6479 (1955) (unpublished).
5. Harvey, J. A., P/832, *The Determination and Evaluation of Fundamental Thermal Neutron Cross Sections,* Volume 4, Session 16A, these Proceedings.
6. Pomerance, H., *Thermal Neutron Cross Sections,* Physical Review *83,* 641 (1951); Langsdorf, A., *The Thermal Neutron Reactor as an Instrument for Measuring Neutron Cross Sections,* Argonne National Laboratory Report ANL-4342 (1949) (unpublished).
7. Sampson, Robb, Stehn and Davidson, *Poisoning in Thermal Reactors Due to Stable Fission Products,* Knolls Atomic Power Laboratory Report KAPL-1226 (1954) (unpublished).
8. Inghram, Haydn and Hess, *U^{235} Fission Yields in the Rare Earth Region,* Physical Review *79,* 271 (1950).
9. Spinrad, Carter and Eggler, P/835, *Reactivity Changes and Reactivity Lifetimes of Fixed Fuel Elements in Thermal Reactors,* Volume 4, Session 20A, these Proceedings.
10. Bernstein, S. and Smith, E. C., P/591, *Summary of Cross Section Measurements of the Fission Product Poison, Xe^{135},* Volume 4, Session 16A, these Proceedings.
11. Havens, W. W., Jr. *et al.* (private communication).
12. Weisskopf, V. F., P/830, *The Theoretical Prediction of Neutron Cross Sections of Nonfissionable Elements for Energies up to 10 Mev,* Volume 2, Session 6A, these Proceedings.
13. Melkonian, E., P/583, *Analysis of Low Energy Neutron Resonances,* Volume 4, Session 18A, these Proceedings.
14. Harvey, Hughes, Carter and Pilcher, *Spacings and Widths of Nuclear Energy Levels,* Physical Review *98,* (June 1, 1955).
15. Bethe, H. A., P/585, *Analysis of the Velocity Selector Results of Fissile Materials,* Volume 4, Session 18A, these Proceedings.
16. Porter, C. E. and Thomas, R. G. (private communication).
17. Sheer, C. and Moore, J., *Measurement of Scattering Cross Sections for Low-Energy Neutron Resonances,* Physical Review *98,* 565 (1955).
18. Albert, Yeater and Gaerttner, *Neutron Capture Measurements with the GE Betatron Velocity Selector,* Physical Review *95,* 644 (1954); Gaerttner, Yeater and Albert, *A Study of Neutron Capture with the KAPL Betatron Neutron Velocity Selector,* Knolls Atomic Power Laboratory Report KAPL-1084 (1954) (unpublished).
19. Harris, Muehlhause and Thomas, *Low Energy Neutron Resonance Scattering and Absorption,* Physical Review *79,* 11 (1950).
20. Snyder, T. M., P/602, *The Critical Assembly—A Nuclear Design Tool,* Volume 4, Session 21A, these Proceedings.
21. Kanne, Stewart and White, P/595, *Capture-to-Fission Ratio of Pu^{239} and U^{235} for Intermediate Energy Neutrons,* Volume 4, Session 18A, these Proceedings.
22. Hughes, Garth and Levin, *Fast Neutron Cross Sections and Nuclear Level Density,* Physical Review *91,* 1423 (1953).
23. Hurwitz, H., Jr. and Bethe, H. A., *Neutron Capture Cross Sections and Level Density,* Physical Review *81,* 898 (L) (1951).
24. Lang, J. M. B. and Le Couteur, K. J., *Statistics of Nuclear Levels,* Proceedings of the Physical Society *A67,* 586 (1954).
25. Taschek, R. F., P/573, *Elastic, Non-Elastic and Transport Neutron Cross Sections,* Volume 4, Session 15A, these Proceedings.
    Cranberg, L., P/577, *Time-of-Flight Techniques Applied to Fast Neutron Measurements,* Volume 4, Session 15A, these Proceedings.
    Walt, M., P/588, *Angular Distributions and Non-Elastic Neutron Scattering,* Volume 2, Session 6A, these Proceedings.
26. Willard, Bair and Kington, *Elastic Scattering Angular Distributions of Fast Neutrons on Light Nuclei,* Physical Review *98,* 669 (1955); Baldinger, Huber and Proctor, *Streuung von Schnellen Neutronen an O^{16},* Helvetica Physica Acta *25,* 142 (1952); Goldstein, H., *Fast Neutron Data for Oxygen,* Nuclear Development Associates, Inc., NDA Memo 15C-15 (1953) (unpublished).
27. Monahan, J. E. and Langsdorf, A., Jr., *An Analysis of Neutron Self-Indication Transmission Cross Sections,* Bulletin of the American Physical Society, Vol. *30,* No. *1,* 8 (1955).
28. Goertzel, G., P/613, *An Estimation of Doppler Effect in Intermediate and Fast Neutron Reactors,* Volume 4, Session 23A, these Proceedings.

29. Hurwitz, H., Jr., P/608, *Comparison of Theory and Experiment for Intermediate Spectrum Assemblies,* Volume 4, Session 23A, these Proceedings.

30. Carter, R. E. and Beyster, J. R., *Inelastic Collision Cross Sections for Fission Spectrum Neutrons,* Physical Review *90,* 389 (1953); Beyster, Henkel and Nobles, *Inelastic Collision Cross Sections at 1.0-, 4.0-, and 4.5-Mev Neutron Energies,* Physical Review *97,* 563 (1955); Walt, M. and Beyster, J. R., *Interaction of 4.1-Mev Neutrons with Nuclei,* Physical Review 98, 677 (1955); Graves, E. R. and Rosen, L., *Distribution in Energy of the Neutrons from the Interaction of 14-Mev Neutrons with Some Elements,* Physical Review *89,* 343 (1953).

31. Feld, B. T., *On the Inelastic Scattering of Fast Neutrons,* Physical Review *75,* 1115 (1949); Hauser, W. and Feshbach, H., *The Inelastic Scattering of Neutrons,* Physical Review *87,* 366 (1952); Griffith, G. L., *Gamma Radiation from Neutron Inelastic Scattering,* Physical Review *98,* 579 (1955); Jennings, Weddell, Alexeff and Hellens, *Scattering of 4.4-Mev Neutrons by Iron and Carbon,* Physical Review *98,* 582 (1955); Lind, D. A. and Van Loef, J. J., *Analysis of Inelastic Neutron Scattering Data for Mn, Fe, and I,* Bulletin of the American Physical Society, Vol. *30,* No. *3,* 21 (1955).

32. Mateosian, E., *Neutron Capture Cross Section of* Ta^{182}, Physical Review *97,* 1023 (1955).

33. Day, R. B., P/581, *Gamma Rays from Neutron Inelastic Scattering,* Volume 2, Session 6A, these Proceedings.

Analysis of Low-Energy Neutron Resonances

By Edward Melkonian,* USA

The study of the low-energy neutron cross sections by transmission measurements as well as by scattering, radiation capture, and fission has shown a resonance structure. This has been attributed to the existence of energy levels in the compound nucleus which is one neutron heavier than the target nucleus. It is expected that eventually there will be a theory of nuclear structure which will explain the positions and characteristics of these levels. In the meanwhile, it is the aim of experiment and analysis to locate and study all accessible levels to provide data for developing such a theory. In addition, it is very useful in designing nuclear reactors to know all the nuclear properties of the materials which enter into the construction of reactors. The field of low-energy neutron spectroscopy can examine with relatively high resolution those levels which are just above the binding energy ($\sim$ 8 Mev) of the nucleus formed from the target nucleus with the addition of one neutron. It is the aim of analysis to deduce from measurements those quantities which describe the nuclear properties even when the experiments are imperfect (e.g., poor resolution, poor statistics, background) and distorted by non-nuclear effects (e.g., Doppler-broadening).

To carry out these functions it is necessary to adopt a theory of nuclear resonance. With few exceptions, all of the methods of analysis of low energy neutron resonances are based on the assumption that the one-level Breit-Wigner formula is valid. In the few favorable cases where a direct match of the experimental data to the Breit-Wigner formula could be made, excellent agreement has been obtained. However, the energy range covered was only a few level widths about the resonance energy. Some work has also been done on the more general many-level formula which shows deviations from the Breit-Wigner formulation far from a level, but applications have been tried in a few individual cases only.

The one-level Breit-Wigner equations for the various processes are

$$\sigma_c = \sigma_0 \cdot \frac{\Gamma_\gamma}{\Gamma} \cdot \left(\frac{E_0}{E}\right)^{1/2} \cdot \frac{1}{1+X^2} \qquad (1)$$

$$\sigma_s = \sigma_p + \sigma_0 \cdot \frac{\Gamma_n}{\Gamma} \cdot \frac{\left(1 + 2\frac{R}{\lambda\!\!\!^{-}_0} \cdot \frac{\Gamma}{\Gamma_n} \cdot X\right)}{1+X^2} \qquad (2)$$

$$\sigma_f = \sigma_0 \cdot \frac{\Gamma_f}{\Gamma} \cdot \left(\frac{E_0}{E}\right)^{1/2} \cdot \frac{1}{1+X^2} \qquad (3)$$

$$\sigma_0 = 4\pi \lambda\!\!\!^{-}_0{}^2 \, g \, \frac{\Gamma_n}{\Gamma} \qquad (4)$$

and the total cross section is

$$\sigma = \sigma_c + \sigma_s + \sigma_f \qquad (5)$$

where

$$X = \frac{E - E_0}{\Gamma/2},$$

$$g = \tfrac{1}{2}\left(1 \pm \frac{1}{2i+1}\right), \text{ and } \Gamma = \Gamma_\gamma + \Gamma_n \, \Gamma_f;$$

E = energy of incident neutron, E_0 = energy at exact resonance, σ_0 = the total cross section at resonance, σ_p = the potential scattering cross section, i = the spin of the target nucleus, $2\pi\lambda_0$ = the wavelength of the neutron at E_0, R = the effective radius for potential scattering of the isotope and spin state responsible for the resonance, Γ = the width of the resonance at half-maximum, and Γ_n, Γ_γ and Γ_f are the partial widths for neutron emission, γ-ray emission, and fission, respectively.

Since these formulae apply properly only in the center of mass system, the Doppler-broadening arising from the thermal motion of the nuclei must be taken into account.[1] The Doppler-broadened resonance cross section for negligible resonance scattering, and $E_0 \geq 0.5$ ev is given by

$$\sigma = \sigma_0 \left(\frac{E_0}{E}\right)^{1/2} \psi(\beta, X) \qquad (6)$$

where

$$\psi(\beta, X) = \frac{1}{\sqrt{\pi}\beta} \int_{-\infty}^{\infty} \frac{1}{1+y^2} \, e^{-\frac{(x-y)^2}{\beta^2}} \, dy \qquad (7)$$

$$X = \frac{E - E_0}{\Gamma/2}, \; y = \frac{E' - E_0}{\Gamma/2}, \; \beta = \frac{2\Delta}{\Gamma}$$

and

$$\Delta = 2\,(m E_0 K T/M)^{1/2} \qquad (8)$$

* Including work by L. Bollinger, Argonne National Laboratory; J. A. Harvey, D. J. Hughes and V. Sailor, Brookhaven National Laboratory; W. W. Havens, Jr., E. Melkonian and L. J. Rainwater, Columbia University; E. R. Gaerttner, G. M. Roe and M. Yeater, General Electric Company.

where m = the mass of the neutron, M = the mass of the nucleus, k = the gas constant, and T = the temperature of the sample. Lamb[2] has shown that if the specimen is a solid, these equations are valid only when $(\Delta + \Gamma) \gg 2k\theta$, where θ is the Debye temperature of the sample. If this condition is met it is possible to account for lattice binding by substituting for the real temperature T an effective temperature T_{eff} as defined by Lamb.

Other dimensionless parameters used in the literature in place of β are

$$\xi = \frac{\Gamma}{\Delta} = \frac{2}{\beta}; t = \left(\frac{\Delta}{\Gamma}\right)^2 = \frac{1}{4}\beta^2$$

Figure 1 shows the function $\psi(\beta, X)$ for a few values of β. Extensive tables of this function have been published.[3]

In actual experiments, the observed shape of a resonance is further broadened by imperfect instrumental resolution. Since this varies considerably with energy, the techniques of analysis depend to a large extent upon the degree of resolution. We start with cases where the resolution is almost perfect, and proceed to cases of poorer resolution. Since most work on neutron resonances has been done by making transmission measurements, most of the discussion centers about this.

ESSENTIALLY PERFECT RESOLUTION

Where the shape of an observed level is not distorted by imperfect resolution, the cross section may be calculated exactly from the formula

$$T \equiv \text{transmission} = e^{-n\sigma} \qquad (9)$$

where n = number of nuclei/cm^2 in the path of the beam. The full Breit-Wigner formula for the total cross section, $\sigma = \sigma_e + \sigma_s + \sigma_f$, is retained, if necessary, and the Breit-Wigner parameters obtained by a detailed curve fit to the cross section. The greatest stress is placed upon the wings, the region in the neighborhood of the peak, or the area under the cross-section curve depending upon the

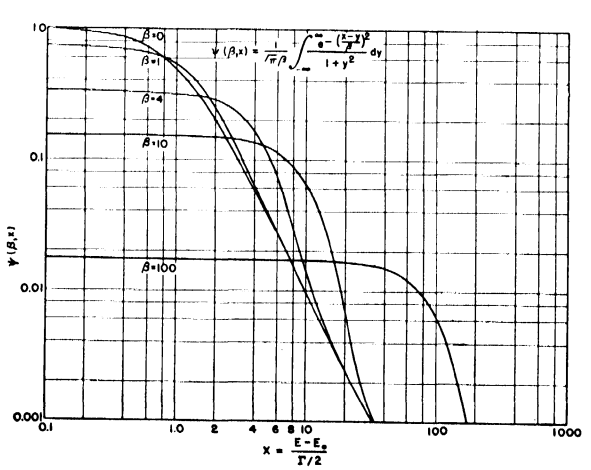

Figure 1

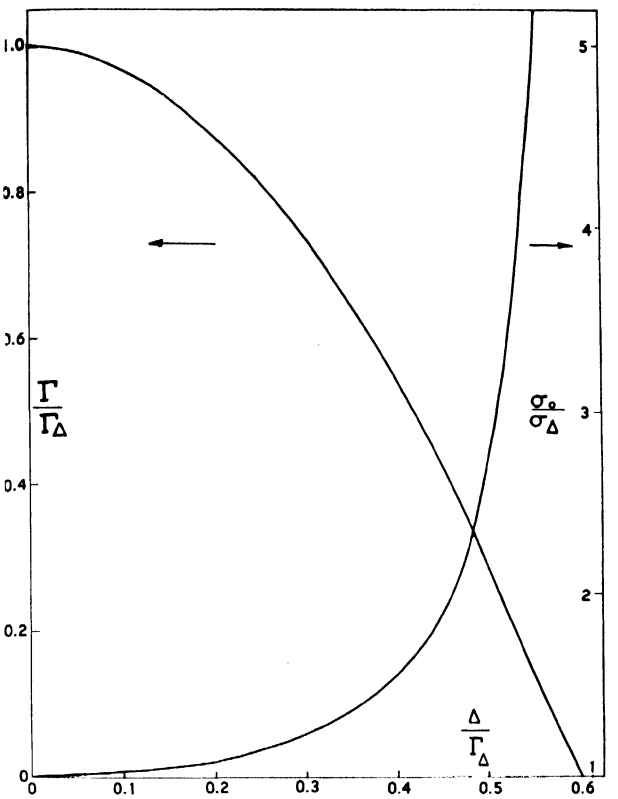

Figure 2. Graph for determining σ_0 and Γ, given the Doppler width Δ and the measured values of $\sigma\Delta$, the peak height, and Γ_Δ, the full width at half maximum, of the Doppler-broadened resonance

experimental accuracy and the reliability of accounting for contributions from other levels. Under the best conditions, all of the parameters may be obtained from a transmission measurement. However, the total cross-section formula is so insensitive to the statistical weight factor g that scattering measurements are usually necessary to determine g.

Even with perfect instrumental resolution, the peak cross section and level width cannot be read off directly because of the broadening effect of the thermal motion. Several procedures are available to deduce the true parameters.

I. The observed peak cross section, σ_Δ, and the observed width, Γ_Δ, are read off the graph. The parameters σ_0 and Γ are determined from Fig. 2 where Γ/Γ_Δ and σ_0/σ plotted in terms of Δ/Γ_Δ. (This method is useful where resonance scattering is negligible, and $E_0/E \approx 1$).[4]

II. The Breit-Wigner formula with Doppler-broadening is expanded about a curve obtained from approximate values of the parameters. This gives a large number of equations linear in the corrections to σ_0 and Γ. These are solved by the method of least squares, usually with the aid of high speed calculating machines.[5]

III. The Breit-Wigner formula without Doppler-broadening is fitted as in II to the experimental curve (to about 2Γ away from E_0) by the method

of least squares. The resulting parameters are interpreted as σ_Δ and Γ_Δ, and Fig. 2 is used to get σ and Γ. This method must be used with caution since the assumption is made that the Doppler-broadened Breit-Wigner curve has the same shape near resonance as the Breit-Wigner curve for the center of mass system, with σ_0 and Γ replaced by σ_Δ and Γ_Δ, respectively. For cases of small Doppler-broadening where this method has been most useful, this procedure probably introduces negligible error, but each case must be tested separately.

IV. The area under the cross section curve gives $\sigma_0\Gamma$ independent of the Doppler effect, and may be taken as one constant in the curve fit.

MODERATELY GOOD RESOLUTION

Where the resolution width is of the order of or less than the level width, curve fitting methods may still be employed but with some modifications. However, curve fitting now depends upon how well the size and shape of the resolution function are known. Since the calculated cross section is no longer significant, one must work directly with the observed transmission.

I. The resolved curve may be deduced from the experimental curve by inverting the effect of resolution smearing. In particular, a Taylor expansion may be made and inverted. However, second and higher order derivatives of the experimental curve appear and a reliable evaluation of these is usually difficult. Having obtained the resolved curves, the above procedures may be employed.[4]

II. The Breit-Wigner formula with Doppler-broadening and with resolution smearing is expanded about the same function evaluated for approximate values of the parameters. Least-squares fitting is then used to obtain the corrections to the parameters used initially.[5]

III. Trial values of the parameters may be used to calculate a simulated experimental transmission curve with Doppler and resolution effects included. By plotting on the same graph as the data, a comparison is made, adjusted trial values taken, and the process repeated until a set of parameters gives a best fit. For the case of negligible resonance scattering, but with the $\sqrt{E_0/E}$ included, tables have been prepared which make the required calculations easier. High speed calculators are also helpful in the solution of this problem.[6]

For the case $E_0/E \approx 1$, a master set of transmission curves for various degrees of resolution can be prepared, and the experimental curve compared with these until one is found which gives the best fit. Such curves, of which Fig. 3 is a sample, have been calculated for a range of values of $n\sigma_0$ from 0 to 10, and for a triangular resolution function having widths up to ten times Γ. The best procedure here is to get first a relationship between σ_0 and Γ from an area measurement by methods to be discussed later. Then for each trial value of $n\sigma_0$, Γ is deduced from the area relationship, and the data plotted on the curve for the assumed value of $n\sigma_0$. This is done for a variety of choices of $n\sigma_0$ until one is found which gives a best fit for the resolution used. Correction for the Doppler effect is not inherent in this method. Approximate correction can be made by interpreting the parameters from the best fit as σ_Δ and Γ_Δ, and using Fig. 2 to get σ_0 and Γ.

IV. Frequently the resolution is good enough so that the entire curve except for the region within a few Γ's of the resonance energy is resolved. Under these conditions, a curve fit may be made to the "wings" of the cross-section curve to yield useful combinations of parameters.

Sometimes particular combinations of parameters may be plotted so as to give a straight line whose constants may be determined graphically or by a least-squares fit. For example, for the case of a predominantly capture resonance, the Breit-Wigner formula can be written as

$$\sigma - \frac{\sigma_0\,\Gamma\,R}{\lambda_0\,(E-E_0)} = \frac{\sigma_0\,\Gamma^2}{4(E-E_0)^2}\left(\frac{E_0}{E}\right)^{1/2} + \sigma_P \tag{10}$$

in the wings of the resonance. The second term of the left-hand side is small for this case, and may be estimated with sufficient accuracy. A plot of the left-hand side against $[1/(E-E_0)^2]\sqrt{E_0/E}$ for the wing data, which are free from resolution and Doppler-broadening, results in a straight line whose intercept gives σ_p and whose slope gives $\sigma_0\Gamma^2/4$.[11]

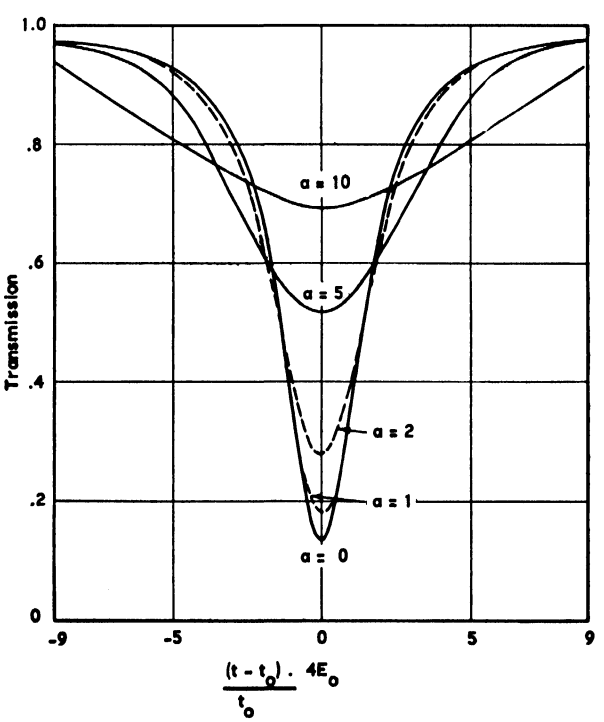

Figure 3. Effect of triangular resolution function on the Breit Wigner transmission for $n\sigma_0 = 2_0$ $a = 2\Delta\ E/\Gamma =$ full width at half maximum of resolution triangle in units of $\Gamma/2$

Under conditions of good resolution, many variations of these methods may be used, and each measurement frequently calls for a slightly different procedure.

POOR RESOLUTION, BUT LEVELS ISOLATED

Where a transmission dip is well enough resolved as a single level, but not well enough so that curve-fitting methods may be applied, area methods are usually used.[4,6,7,8] Again, meaningful values of the cross section cannot be calculated in the vicinity of a resonance, and all of the analysis is performed directly on the observed transmission curves. The basis of the area method is that the area above the transmission dip of a resonance is independent of the shape and magnitude of the resolution used provided certain conditions are met.

In applying the area method to predominantly absorption resonances the following simplifying conditions are usually adopted: (1) the interference term between potential and resonance scattering is neglected, and (2) $\Gamma/E_0 \ll 1$, so that $(E_0/E)^{1/2} \approx 1$ over the level. The Breit-Wigner formula then becomes

$$\sigma = \sigma_{const} + \sigma_r$$

$$\sigma_r = \sigma_0 \left\{1 + [2(E - E_0)/\Gamma]^2\right\}^{-1} \qquad (11)$$

$$T = (T_{const}) \cdot (T_r) = e^{-n\sigma_{const}} \cdot e^{-n\sigma_r}$$

where σ_r denotes the resonance cross section.

If σ_{const} is evaluated in some way, the experimental transmission curve may be divided by T_{const} to give T_r (experimental). For a strong resonance and a thin sample, $T_{const} \approx 1$ and the correction may be neglected. The "areas" A_E and A_t are defined as

$$A_E = \int_{-\infty}^{\infty} (1 - T_r) dE \qquad (12)$$

if an energy abscissa is used, and

$$A_t = \int_{-\infty}^{\infty} (1 - T_r)\, d\,t \qquad (13)$$

if a time-of-flight abscissa is used. With $\Gamma/E_0 \ll 1$

$$A_t = \left(\frac{t_0}{2\,E_0}\right) \cdot A_E \qquad (14)$$

is a good approximation and will be used in the following analysis. Subsequent developments will be in terms of A_E since simpler expressions are obtained. However, A_t is generally measured when time-of-flight techniques are used, and Equation 14 must be used to obtain A_E.

For an extremely thick sample ($n\sigma_0 \gg 1$) or an extremely thin sample ($n\sigma_0 \ll 1$), the integral for A_E can be evaluated analytically, giving, respectively,

$$A_E^2 = \pi\, n\, \sigma_0\, \Gamma^2 \qquad (n\sigma_0 \gg 1) \qquad (15)$$

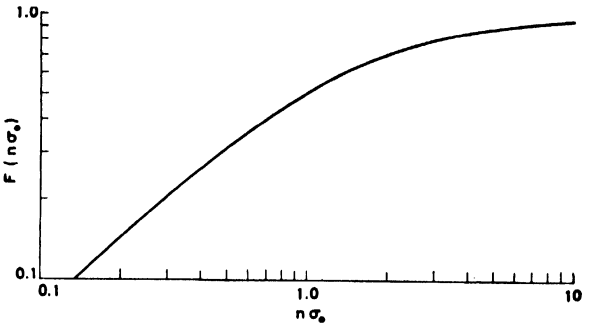

Figure 4. For $n\sigma_0 < 0.14$, $F(n\sigma_0) = (1/4)\, n\sigma_0\, (1-1/2 n\sigma_0)$ to 0.2 per cent. For $n\sigma_0 > 10$, $F(n\sigma_0) = 1-1/2\, n\sigma_0$ to 0.2 per cent

$$A_E = \frac{1}{2}\, \pi\, n\, \sigma_0\, \Gamma \qquad (n\sigma \ll 1) \qquad (16)$$

For intermediate values of $n\sigma_0$, the integral for A_E can be evaluated in terms of the Bessel function of imaginary argument[9]

$$A_E = \frac{1}{2}\, \pi n \sigma_0 \Gamma \left[e^{-n\sigma_0/2}\right] [I_0(n\sigma_0/2) + I_1(n\sigma_0/2)] \qquad (17)$$

or numerical methods may be used. It is convenient to define and use a function

$$F(n\sigma_0) = \frac{4\,E_0^2\,A_t^2}{\pi n \sigma_0 \Gamma^2\, t_0^2} = \frac{A_E^2}{\pi n \sigma_0 \Gamma^2} \qquad (18)$$

which is shown in Fig. 4.

If now the expression for $F(n\sigma_0)$ be solved for Γ, we have

$$\Gamma = A_E/[\pi n \sigma_0\, F(n\sigma_0)]^{1/2} \qquad (19)$$

which is an explicit relationship between Γ and σ_0 provided A_E and n are known. If measurements are available on a second sample of sufficiently different thickness, a second relationship between Γ and σ_0 is obtained. The simultaneous solution of the two equations gives the values of σ_0 and Γ.

The usefulness of this method of analysis is usually limited by the accuracy of the area determination. The least accurate part of this determination, in many cases, is the evaluation of the contribution to the area of the "wings" of the curve. The uncertainties arise partially because of the difficulty of determining the area accurately of a small effect over a large energy range, and partially from the presence of other uncertain contributions to the cross section, e.g., uncertainty in evaluating T_{const} and overlapping of nearby levels of other isotopes and spin states. These difficulties can be minimized by using the following procedure for the treatment of the wing area. First, only the portion of the wings which seems reliable is included in the central area to give a partial area A_E' or A_t'. This is used to obtain the first approximate values of σ_0 and Γ'. Using these values, the area under the portion of the wings not included is calculated and added to the original area to give the next approximation A_E'' or A_t'' and,

hence, new values of σ_0 and Γ. This process is repeated until succeeding values do not change.

The successive approximation feature of the method just described can be eliminated in the following manner. Let the wings of the experimental transmission curve be cut off symmetrically about the resonance energy (or time-of-flight) at points such that T_r is 0.9 or greater. Under these conditions, if the instrumental resolution function does not itself have wings that partially smear the resonance over a wider region, the experimental curves and the actual T_r curves will nearly coincide in the wings. Then the Breit-Wigner relation may be used for T_r beyond the cut-off points. Using only the first term in the expansion of $(1 - T)$ far from resonance, the calculated wing area which was omitted is $n\sigma_0 \Gamma^2/2\epsilon$, where $E_0 \pm \epsilon$ are the energies at which the curve was cut off. Then,

$$A_E = A_E' + n\sigma_0 \Gamma^2/2\epsilon \qquad (20)$$

where A_E' denotes the partial area from

$$E = E_0 - \epsilon \text{ to } E = E_0 + \epsilon$$

Using the previous expression for A_E, a solution for Γ is obtained in the form:

$$\Gamma = \frac{A_E'}{[\pi n\sigma_0 F(n\sigma_0)]^{1/2}} \cdot \frac{2}{1 + [1 - \alpha/F(n\sigma_0)]^{1/2}} \qquad (21)$$

where $\alpha = 2A_E'/\pi\epsilon$.

This expression gives Γ in terms of the measured (partial) area A_E' and the value of σ_0. If two sample thickness are used, a curve of Γ vs σ_0 is plotted for each sample, and the values of σ_0 and Γ determined from the intersection. To simplify these calculations, a plot of Γ/A_E' vs α for various values of $n\sigma_0$ is given in Fig. 5. The case $\alpha = 0$ reduces to the earlier problem where the wings have not been cut off.

If the width of the level, Γ, is large compared to the Doppler width, the above area analysis can be applied directly. However, if this is not the case, the cross section near resonance is given by Equation 6 with $(E_0/E) = 1$. The calculated area above the transmission dip will now be larger than that obtained when the Doppler width is neglected.

When the Doppler effect is included, the area above the transmission curve is given by the formula

$$[A_E]_D = \frac{1}{2}\Gamma \int_{-\infty}^{\infty} [1 - e^{-n\sigma_0 \psi(\beta, X)}]\, dx \qquad (22)$$

This integration has not been carried out analytically so that series expansions and numerical methods have had to be used.

$[A_E]_D$ is shown plotted in Fig. 6 in the form of a correction to the area without the Doppler-broadening,

$$D \equiv \frac{[A_E]_D - A_E}{A_E} \qquad (23)$$

For the limiting case, $\beta \to \infty$

$$D \to \left\{ (\pi n\sigma_0 \Gamma/2A_E) - 1 \right\} \qquad (24)$$

One can readily understand the qualitative behavior of the Doppler correction, $D = ([A_E]_D - A_E)/A_E$, in the limiting cases of a very thin sample and a very thick sample for given β. If the sample is very thin ($n\sigma_0 \ll 1$), the exponential in Equation 22 can be expanded and, in the first approximation, we obtain

$$[A_E]_{D\ thin} = \frac{1}{2}\Gamma \int_{-\infty}^{\infty} n\sigma_0 \psi(\beta, x)\, dx \qquad (25)$$

which equals $\pi n\sigma_0\Gamma/2$ and is exactly the same expression we would obtain if the Doppler effect were not present, giving $D = 0$. If the sample is extremely thick ($n\sigma_0 \gg 1$), the transmission of the sample will be effectively zero several level widths

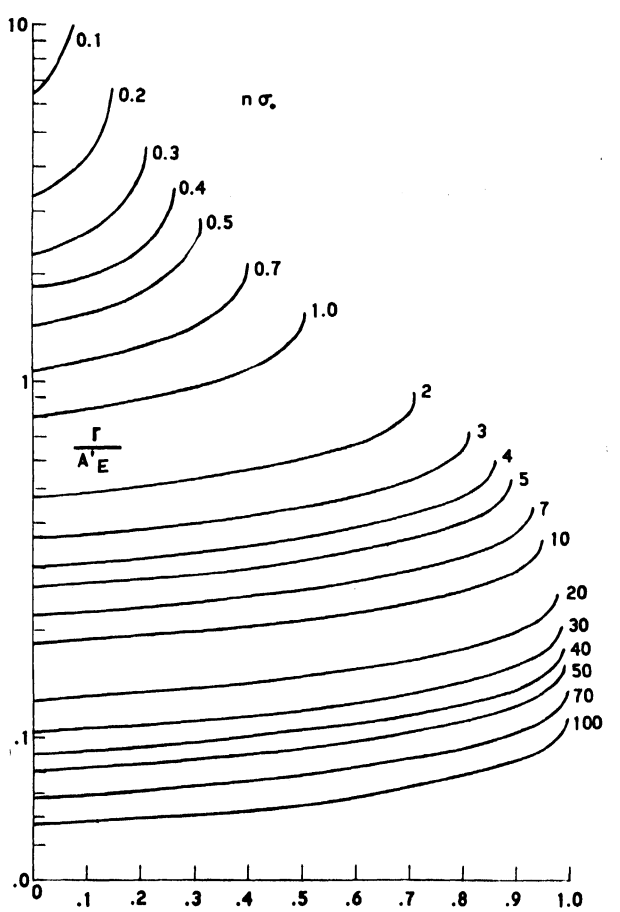

Figure 5. (Γ/A_E') = as a function of $n\sigma_0$, and $\alpha = 2A_E'/\pi\epsilon$, where $E \pm \epsilon$ are the cut-off points, (when measurements are made on a time-of-flight basis, $A_E' = 2(E_0/t_0)A\tau'$, and $\alpha = (2A\tau'/\pi\tau)$, where $t_0 \pm \tau$ are the cut-off points)

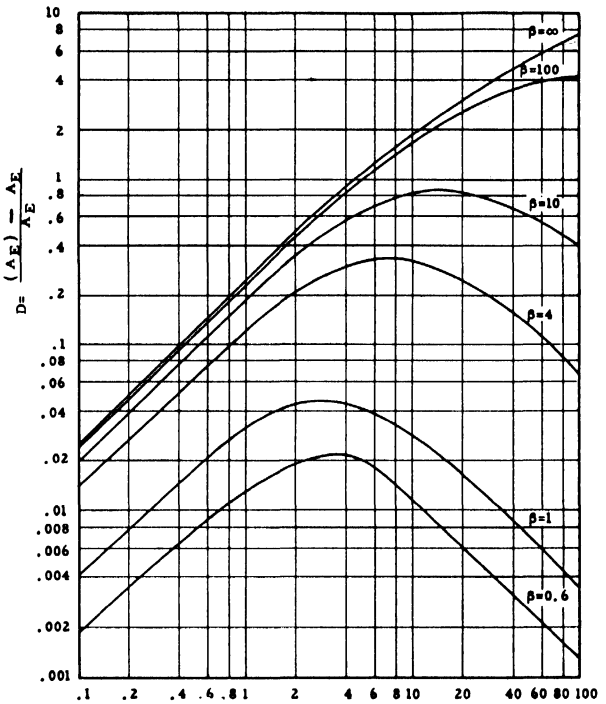

Figure 6. Effect of Doppler broadening upon area above transmission dip. $\beta = 2\Delta/\Gamma$

away from the center of the level, where the Doppler effect makes the greatest difference in cross section. Further out, where the transmission rises above zero, the Breit-Wigner formula is only slightly affected by the Doppler-broadening, so that the area above the transmission curve is only slightly increased. For a given β, these effects become less and less as $n\sigma_0$ becomes greater, so that the Doppler correction approaches zero, in the limit.

The most convenient procedure to use in correcting for Doppler-broadening is to use the plot of Fig. 7 where $(1 + D)$ is plotted against (Γ/A_E') $(A_E'_D/2\Delta)$. The procedure is to select a value of $n\sigma_0$, read Γ/A_E' from Fig. 5 for the calculated value of α, calculate $(\Gamma/A_E') \cdot (A_{ED}/2\Delta)$, and read off $(1 + D)$ from Fig. 7, for the foregoing value of $n\sigma_0$. The initial value of α is then divided by $(1 + D)^2$, and the procedure is repeated until succeeding values of $(1 + D)$ do not change. Then $\Gamma = (\Gamma/A_E')\ A_{ED}'/(1 + D)$. By taking a series of values of $n\sigma_0$, Γ vs σ_0 is obtained. Measurement on a second sample allows determination of σ_0 and Γ separately. Note that Fig. 5 is still correct when the Doppler effect is introduced, with A_E' replaced by $A_{ED}'/(1 + D)$ as the ordinate and in the equation for α, and ϵ by $\epsilon\ (1 + D)$.

An alternative procedure is to treat the wing area omitted as a correction, and to use the graph of Fig. 8.[4] Knowledge of A, Δ, and n gives for each chosen value of Γ a unique value of σ_0. If this is done for two different sample thicknesses, the value of σ_0 and Γ are determined from the intersection of the σ vs Γ curves. Since the value of the area A initially obtained excludes the portion of the wings for values of the energy outside the interval $(E_0 - \epsilon)$ to $(E_0 + \epsilon)$, the area neglected, $n\sigma_0\Gamma^2/2\epsilon$, must be added after each evaluation of σ_0 and Γ until the values of σ_0 and Γ no longer change significantly.

Another procedure leads to a simple graphical solution for the case of several samples without requiring the plotting of σ_0 vs Γ curves.[10] This method is based upon Fig. 9, where A/Δ is plotted against $n\sigma_0(\Gamma/\Delta)$, for various values of Δ/Γ, on log-log paper. All of these quantities are dimensionless and the input data, A/Δ, do not involve unknown parameters. In use, points are plotted for each of two samples at the correct ordinates, A/Δ, and a distance apart horizontally corresponding to the ratio of the sample thicknesses. If these two points are moved horizontally, this will fit only one of the curves, whose Δ/Γ value then gives Γ directly, and whose abscissa gives σ_0. The actual plotting and sliding of points has been done most easily by placing a sheet of glass cloth over the curves, and against a straight edge so that the points plotted on it slide horizontally. If the experimental errors in A are also plotted it is very simple to obtain the resultant errors in Γ and σ_0 by a slight shift of the sheet carrying the plotted points. If more than two sample thicknesses have been used, they are all plotted and

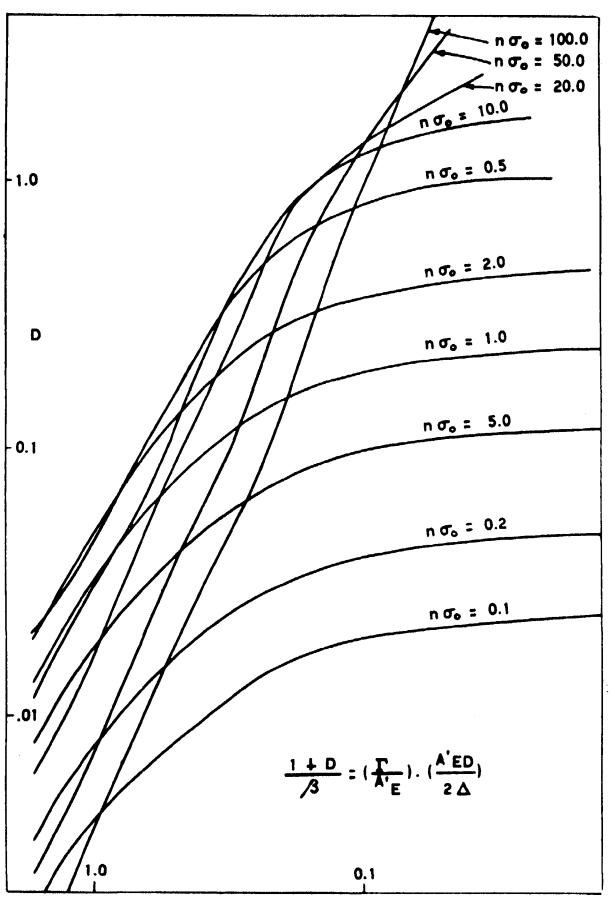

Figure 7. Graph used to correct for Doppler effect

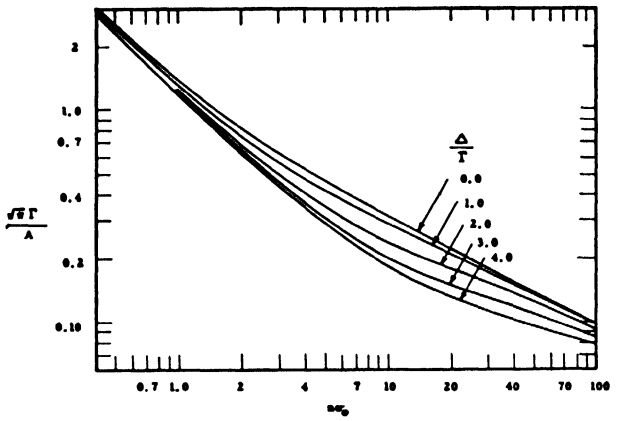

Figure 8. Graph for calculating σ_0 in terms of Γ, given A, Δ, and n

the procedure is to find the single curve that best fits all the points, just as for the case of two samples.

The wing correction is not inherent in this method, and a wing contribution, $n\sigma_0\Gamma^2/2\epsilon$ consistent with the final parameters must be added to the experimentally determined area.

When data on only one sample thickness are available in the application of any of the area methods of analysis, σ_0 and Γ cannot be evaluated separately without further information. Recent data have shown that Γ_γ is a slowly varying function of the atomic weight to a fair approximation. Approximate evaluation of σ_0 can then be made by assuming for Γ the values of Γ_γ appropriate for the atomic weight of the element under investigation. If the level contains an appreciable amount of scattering, Γ_n can be calculated from the first approximation value of σ_0 by means of Equation 4 and added to Γ_γ to give a better value of Γ. Successive approximations lead to a consistent set of values of σ_0 and Γ for the assumed value of Γ_γ.

It is important to note that even though transmission measurements give immediate results relative to total cross-section values only, information about scattering is obtained from Equation 4. Thus, when both σ_0 and Γ have been obtained, Γ_n and Γ_γ are determined. (The value of g must either be deduced by scattering measurements, taken as unity for $i = 0$, or assumed to be $\frac{1}{2}$ otherwise.) When fission is present, additional measurements or information are needed for a complete separation of the various reactions.

When the conditions for the method of area analysis do not apply, it is still possible to apply a similar method in special cases.[11] The above development of the area method does not apply to asymmetric resonances, e.g., when resonance scattering predominates, or when a very thick sample is used, particularly at lower energies. The basic idea of the method, that the area above the experimental transmission curve must be equal to the area above a calculated curve if the correct resonance parameters are used, is still valid. The procedure, then, is to compare the experimental area with calculated areas based on various choices of parameters until agreement is reached. This method has been applied to the case of scattering resonances when the Doppler effect can be neglected.[11]

MEASUREMENTS WITH SAMPLE AT DETECTOR POSITION

In recent years measurements with the element under investigation at the detector position have become fairly common. Advantages are that the uncertainty in collection time usually associated with BF_3 detectors is almost completely eliminated, and that the physical length of the detector is reduced considerably, both effects leading to increased resolution. Two types of measurements are considered, one in which the capture gamma rays are studied as a function of energy, and another in which this arrangement is considered as a detector, and transmission measurements made with another sample of the same element.

Sample at Detector Position Only

This gives very good resolution, and is best for separating closely spaced levels. However, interpretation in terms of level parameters is somewhat difficult since the efficiency of gamma-ray detection cannot be determined directly. One procedure is to include, among the various thicknesses of samples used, one which is sufficiently thick so as to show a maximum counting rate for several points near the resonance peak. If this sample is not so thick in terms of gm/cm² as to reduce the transmission of the gamma rays, this maximum counting rate may be used to determine the over-all efficiency of detection. The resulting curve is very much like $(1 - T)$ and may be handled as in the case of ordinary transmission.

When the ratio Γ_n/Γ is not small, a correction must be made for those neutrons which are captured after one or more scatterings in the detector.[12] The

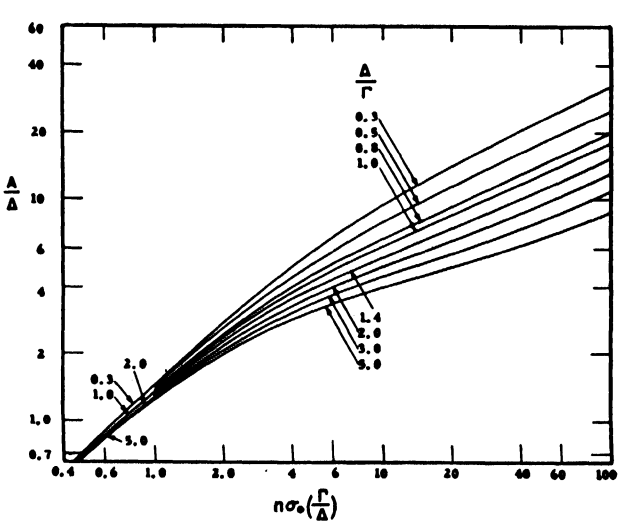

Figure 9. Curves used in obtaining resonance parameters from measured areas of transmission dips

calculation of the required correction is made difficult by the fact that the neutron energy, and hence the cross section, change after each collision. If we consider only the effect of a single scattering, it is possible to get a simple result in the limiting case of a detector which is effectively black at the peak of the resonance, but not black in the tails of the resonance. An approximate correction for the effect of multiple scattering may then be made by comparing this single scattering calculation for a resonance absorber with the known results for single scattering and multiple scattering in a non-resonance absorber.

For single scattering effects only, the ratio of neutrons captured after one scattering, to those captured in the first collision, is given by (Γ_n/Γ) $T(W)$ where $W = 4\ m\ E_0/\sqrt{M\ n\sigma_0\Gamma^2}$ and $T(W)$ is plotted in Fig. 10.

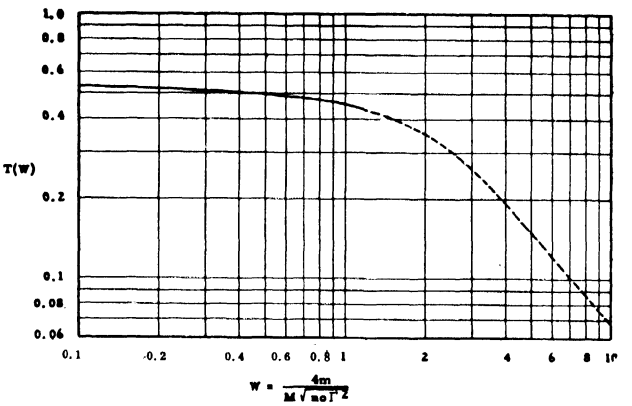

Figure 10. Graph of $T(W)$ which is used in correcting for neutron capture after single scattering in resonance detector

Sample at Detector and Transmission Positions

Here the previously mentioned advantages of using the element under study at the detector position are retained, and at the same time calibration difficulties are circumvented by making transmission measurements. If n_D and n_T refer to the number of atoms/cm^2 in the samples at detector and transmission positions, respectively, the self-indication cross section is defined as

$$\sigma_{si} = \frac{\int_{-\infty}^{\infty} (1 - e^{-n_D\sigma_0\psi(\beta, X)})\ e^{-n_T\sigma_0\psi(\beta, X)}\,dx}{\int_{-\infty}^{\infty} (1 - e^{-n_D\sigma_0\psi(\beta, X)})\,dx} \tag{26}$$

$$= \frac{\int_{-\infty}^{\infty} (1 - e^{-(n_D+n_T)\sigma_0\psi})\,dx - \int_{-\infty}^{\infty} (1 - e^{-n_T\sigma_0\psi})\,dx}{\int_{-\infty}^{\infty} (1 - e^{-n_D\sigma_0\psi})\,dx}$$

(Note that σ_{si} is dimensionless and hence not a cross section.) The three integrals which enter into the second form of σ_{si} are exactly the same integrals which have been dealt with in the ordinary transmission measurements with detectors having slow variation of efficiency with energy. An additional parameter, n_D/n_T, has now to be considered.

Figures 11 and 12 show graphs of σ_{si} for $\beta = 0$ and $\beta = 10$, as samples of the more extensive calculations which have been made. Wing corrections are not included, the assumption being made instead that the areas are measured as far from the resonances energy as necessary or that self-consistent corrections will be made. These curves are useful in deciding upon the various thicknesses of samples needed for a specific measurement, and for evaluating the results. The method of making corrections for multiple scattering in the detector sample has not been worked out in general for the case of transmission measurements. For thin samples and not too large Γ_n/Γ, the correction is expected to be negligible. The graphs imply that more sensitive results are obtained if the detector sample is made thin relative to the transmission sample. This is balanced by the fact that as the detector samples get thinner a lower counting rate is obtained, and a poorer signal to background may result. The optimum choice of n_D/n_T has not been established. A reasonable choice seems to be to take equally thick detector and transmission samples.

In some cases, however, the two samples cannot be made of equal thickness. An example is the case of a fission detector in which the fission material (e.g., U^{235}) is deposited on plates and the fission fragments counted. Because of the short range of fission fragments, the layers must be thin, so that a

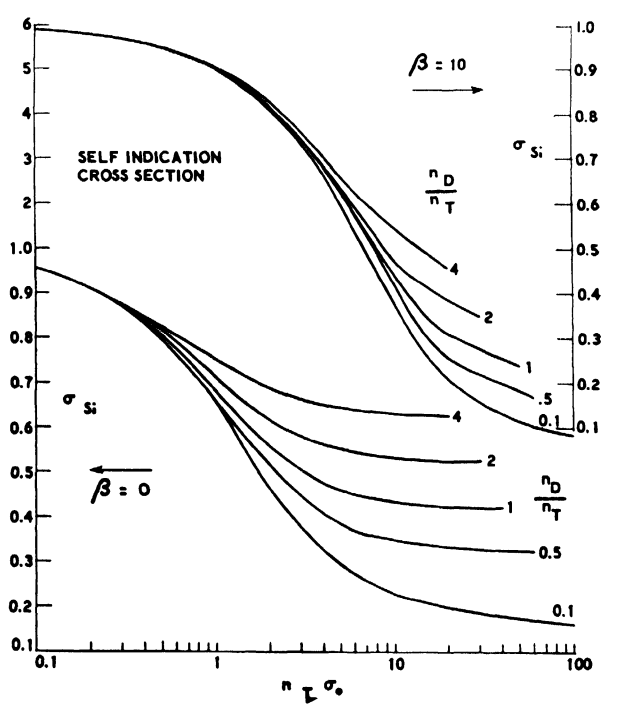

Figure 11. (Below), Figure 12. (Above)

detector of reasonable size has a thickness at resonance of $n\sigma_0 \sim 0.05$. However, this detector may be used in transmission on samples having large values of $n\sigma_0$.

For the case of equal-sample thickness at detector and transmission positions, extensive calculations have been performed to take into account the use of the area within a small energy interval about the resonance energy for the case of a rectangular resolution function. Graphs have been prepared giving σ_Δ/σ_E in terms of $2\epsilon/\Delta$ for various values of Δ/Γ and the observed self-indication cross section, where again the areas between $(E_0 - \epsilon)$ and $(E_0 + \epsilon)$ are included. By suitable interpolation, σ_Δ can be calculated for each assumed value of Γ. When applied to the data on silver taken on the Columbia 400 Mev synchrocyclotron neutron velocity spectrometer, it is found that the values of σ_Δ obtained depend only slightly upon the choice of Γ. The value of σ_0 for each assumed value of Γ can then be obtained from a graph of σ_0/σ_Δ in terms of Δ/Γ. To get the values of σ_0 and Γ separately, it is necessary to combine these results with a measurement of a different combination of parameters, e.g., $\sigma_0\Gamma^2$ or $\sigma_0\Gamma$.

REFERENCES

1. Bethe, H. and Placzek, G., Phys. Rev. *51,* 462 (1937); Bethe, H., Rev. Mod. Phys. *9,* 140 (1937).
2. Lamb, Jr., W. E., Phys. Rev. *55,* 190 (1939).
3. Rose, M. E., Miranker, W., Leak, P., Rosenthal, L. and Hendrickson, J. K., *A Table of the Integral* $\psi\ (x, t) = \frac{1}{2\sqrt{\pi t}} \cdot \int_{-\infty}^{\infty} \exp\left[\frac{(x-y)^2}{4t}\right] \cdot \frac{1}{1+y^2}\, dy$ Westinghouse Atomic Power Division, Report WAPD-SR-506; Vols. I and II, October, 1954.
4. Seidl, F. G. P., Hughes, D. J., Palevsky, H., Levin, J. S., Kato, W. Y. and Sjöstrand, N. G., Phys. Rev. *95,* 476 (1954).
5. Sailor, V. L., Phys. Rev. *91,* 53 (1953).
6. Havens, Jr., W. W. and Rainwater, L. J., Phys Rev. *70,* 154 (1946).
7. Melkonian, E., Havens, Jr., W. W. and Rainwater, L. J., Phys. Rev. *92,* 702 (1953).
8. Havens, Jr., W. W. and Rainwater, L. J., Phys. Rev. *83,* 1123 (1951).
9. Ladenburg, R. and Reiche, F., Ann. Physik *42,* 181 (1913).
10. Hughes, D. J., *A Method for Rapid Analysis of Neutron Resonances,* (to be published), (1955).
11. Palmer, R. R. and Bollinger, L. M., *Neutron Cross Section Measurements of Antimony, Gallium, Cadmium, and Mercury* (to be published).
12. Roe, G. M., *Correction for Scattering in an* (n, γ) *Detector* (Private Communication).

Record of Proceedings of Session 18A

WEDNESDAY AFTERNOON, 17 AUGUST 1955

Chairman: Prof. P. Scherrer (Switzerland)
Vice-Chairman: Prof. M. D. da Souza Santos (Brazil)
Scientific Secretaries: Messrs. I. Ulehla and D. J. Littler

PROGRAMME

P/657 Measurement of the neutron multiplication factor for thermal fission of uranium and plutonium ..... P. E. Spivak and B. G. Yerozolimsky

P/658 Number of fission neutrons per captured thermal neutron in U^{233}, U^{235} and Pu^{239} ..... A. J. Alichanov *et al.*

P/660 Number of fission neutrons per captured thermal neutron for natural uranium ..... N. A. Burgov

P/425 Neutron yields from fissile nuclei ..... P. A. Egelstaff and J. E. Sanders

P/587 Measurement of capture to fission ratio of U^{235}, U^{233}, and Pu^{239} by a new method ..... H. Palevsky

P/595 Capture-to-fission ratio of Pu^{239} and U^{235} for intermediate energy neutrons ..... W. R. Kanne *et al.*

DISCUSSION

P/585 Theoretical analysis of neutron resonances in fissile materials ..... H. A. Bethe

P/590 Status of information on reactor material cross sections ..... H. Hurwitz

DISCUSSION

Mr. M. S. KOZODAEV (USSR) presented paper P/657.

Mr. V. V. VLADIMIRSKI (USSR) presented papers P/658 and P/660. He stated the final result of the latter paper as follows: An additional correction on the order of 0.5 per cent for the multiplication of fast neutrons in the uranium rod should be applied to the results. This was not done in the printed text of Burgov's paper P/660, so that the values given for the number of fission neutrons are somewhat too high. The necessary correction was introduced by Burgov after a preliminary discussion of his contribution in Moscow. Hence, the new final figure obtained by Burgov for the number of fission neutrons for a natural mixture of uranium isotopes:

$$\eta = 1.334 \pm 0.006$$

is in good agreement with the results obtained by Spivak and Yerozolimsky:

$$\eta = 1.337 \pm 0.017$$

The value of η for a natural mixture of uranium isotopes, computed from the data obtained by Alichanov, Vladimirski and Nikitin for the number of fission neutrons from uranium-235, is:

$$\eta = 1.35$$

Lastly, we have the value given by a group of workers of the Physical Institute of the Academy of Sciences, as reported at the July session of the Academy in Moscow:

$$\eta = 1.31 \pm 0.25$$

Mr. J. E. SANDERS (UK) presented paper P/425. As his presentation differed at several points from the original (and later corrected) paper, it is reproduced here, except for the introduction:

In order to find absolute values for $\bar{\nu}$ we have measured the efficiency of the neutron detector using natural uranium as a standard fission neutron source. The results of these experiments are shown in Slide 1 (Table I of P/425) where we list both the relative values of $\bar{\nu}$ for U^{233} and U^{235}, Pu^{239} and Pu^{241}, and also the absolute values of $\bar{\nu}$ depending upon the calibration with natural uranium. It is seen that there is a general trend of increasing $\bar{\nu}$ with increasing mass number of the fissioning nuclide. Such a tendency is also shown by published data on spontaneous fission.

By using a monochromatic neutron beam instead of the thermal beam from the reactor we have shown that in the case of U^{235} the number of neutrons per fission is independent of neutron energy over a range from 0.03 ev to 1.1 ev. Using a modified version of this apparatus with fast neutrons provided by a lithium (p,n) neutron source, the value of $\bar{\nu}$ at 800

kev incident neutron energy has been compared with the value at thermal energy.

We find that with 800 kev neutron energy the number of neutrons per fission is 1 per cent greater than the number of neutrons per fission at thermal energies, whereas for the range from 0.03 to 1.1 ev again we find that $\bar{\nu}$ is independent of energy within the limits of accuracy in our measurements. That range, you will remember, covers two resonances in the slow neutron cross section of U^{235}.

The values of α—the ratio of radiative capture to fission cross section—have been deduced from our measurements of absorption cross section and fission cross section, and you have heard full descriptions of these methods in this morning's session (17A). The values of α obtained in this way are necessarily rather inexact because they involve the differences in cross sections rather than the values themselves. Using the cross sections at neutron velocity of 2200 m/sec, the alpha values found for three nuclides are shown in Slide 2 (Table III of P/425).

Similarly, using the energy dependencies of the cross sections measured on the various neutron spectrometers we can find values of α in the first positive resonance of the nuclides, and these are shown in Table I on this page, where we give the value of α at the first resonance compared to the value of α at 0.025 ev. You will see there that in U^{235} and Pu^{239} the value of alpha in the resonance is appreciably greater than the value at thermal energies. In the case of U^{233} the value of alpha is the same, within our limits of experimental accuracy.

Combining the α values with the value of the total width of the resonances, we are able to deduce the partial widths for gamma-radiation and for fission in these three nuclides. These are shown in Table II (a correction of Table IX of P/425). Here we give Γ_γ and Γ_f for the three resonances, and you will note that while Γ_γ stays approximately constant the value of the fission width varies considerably between the three nuclides. This phenomenon has been remarked upon by other contributors to this Conference.

Resonance analysis has been used in the intermediate energy region to obtain α for resonances in this region. The cross sections have been measured by the Harwell fast chopper and by the Harwell linear accelerator.

I would like to show now values of α for resonances in Pu^{239}. In Slide 3 (Table IV of P/425) we give values of α and the values of the total width of several resonances in Pu^{239}, and you will notice that in general the value of α in these resonances is appreciably greater than the value of α at thermal

Table I. α in Neutron Resonances

Nuclide	*Resonance energy*	$\frac{\alpha\ (resonance)}{\alpha\ (0.025\ ev)}$
U^{233}	1.80 ev	1.0 ± 0.3
U^{235}	0.30 ev	2.7 ± 1.0
Pu^{239}	0.30 ev	1.6 ± 0.2

Table II. Resonance Widths

Nuclide	*Resonance, ev*	Γ_γ *ev*	Γ_f *ev*
U^{233}	1.78	0.03	0.18
U^{235}	0.30	0.05	0.09
Pu^{239}	0.30	0.04	0.06

energies, which is 0.48. In the case of U^{233} a similar analysis shows that in this nuclide α, as far as we can tell, is constant in the various resonances up to at least 25 ev—that is, over a region including at least 16 resonances in this nuclide. This behavior is markedly in contrast to the variation of α shown by plutonium-239.

Values of η, the number of fission neutrons emitted per thermal neutrons captured have been measured for uranium-233 and uranium-235, using the pile oscillator technique in the Gleep reactor at Harwell. The amplitudes of the pile power oscillations, when samples of the fissile material and samples of a standard boron solution are oscillated in the pile, are compared, and, knowing the absorption cross sections and the pile constants determining the leakage of fast neutrons from the reactor, and absolute value of η can be found.

We have done this, as I said, for uranium-233 and uranium-235. In addition we have compared values of η for uranium-233, uranium-235 and plutonium-239 by placing "black" totally absorbing samples of these nuclides in a thermal neutron beam and counting the fission neutrons emitted by means of a long counter. This gives a relative value of η.

We have not attempted so far to make absolute measurements by this technique. If we combine the absolute values measured on the pile oscillator with these relative values, we arrive at the following values of η (Table III on next page) applicable to a thermal spectrum of neutrons.

I will ask you to note that these values are slightly different from those which we have put in our paper, since we have just received the details of some recent measurements done at Harwell. We had the measured values measured by the techniques I have just described in the right-hand column. In the second column we have listed the values of η calculated from the relation $\eta = \bar{\nu}/(1 + \alpha)$.

I have described the measurement of these quantities in the first two sections of the paper, and it is seen that within the rather broad experimental errors on the indirect values of η there is reasonably good agreement between the derived values and the values measured by the direct method.

Now the value of η for Pu^{239} is rather lower than other values reported, but the values for U^{233} and U^{235} show very good agreement with the results that have just been reported by Vladimirski and Kozodaev.

The variation of η with neutron energy, which is an important bit of information for reactor design, can be predicted from the variation of α with neutron energy assuming that η is constant over the small energy range involved. In order to check the predic-

Table III. η for Thermal Spectrum

Isotope	η *from* $\bar{\nu}$, α	η *measured*
U^{233}	2.10±0.14	2.23±0.05
U^{235}	2.19±0.15	2.06±0.04
Pu^{239}	1.94±0.15	1.91±0.07

tions of this method, a direct technique has also been employed and the principle is shown in the Slides I shall show now:

The monochromatic beam is produced by diffraction at a potassium chloride crystal. It passes through a thin boron $1/v$ counter, then on to a sample of the fissile material being investigated. This sample is thick enough to completely absorb all neutrons falling upon it. The fission neutrons emitted by the sample are counted by the BF_3 counters imbedded in a paraffin-wax block. It is quite easy to see, I think, that by comparing the counting rates in the BF_3 counters with those in the boron flux monitor [Slide 4 (Fig. 2 of P/425)] the value of η can be easily obtained. The energy is determined by the angle at which the crystal is set.

This technique has been employed for uranium-233 and plutonium-239.

In Table IV on this page we present values of η in the first resonance of these nuclides compared with the η value at 0.025 ev. These are the values measured utilizing the technique I have just described.

We have not done any measurements on U^{235} so far. Here we have values derived from the α values in the resonances which I showed earlier in this talk, and it is to be seen that in the case of U^{233} and plutonium-239, where we have also made the direct measurements, the data seem to agree fairly well.

Slide 5 shows the actual measured variation in the case of U^{233}. The points are measured by the technique I have just described for getting η as a function of energy, while the cross-section data, that is, the data on α, predict that η should lie within the lines shown, and it will be seen that there is reason-

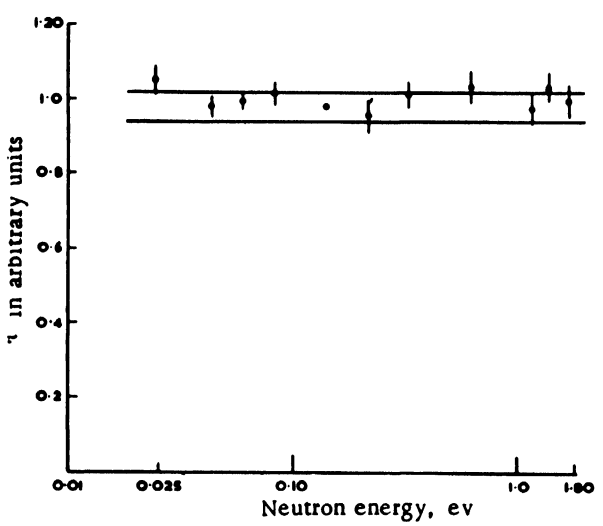

Slide 5. η U^{235} as function of neutron energy. Cross-section data predicts η should lie within lines shown

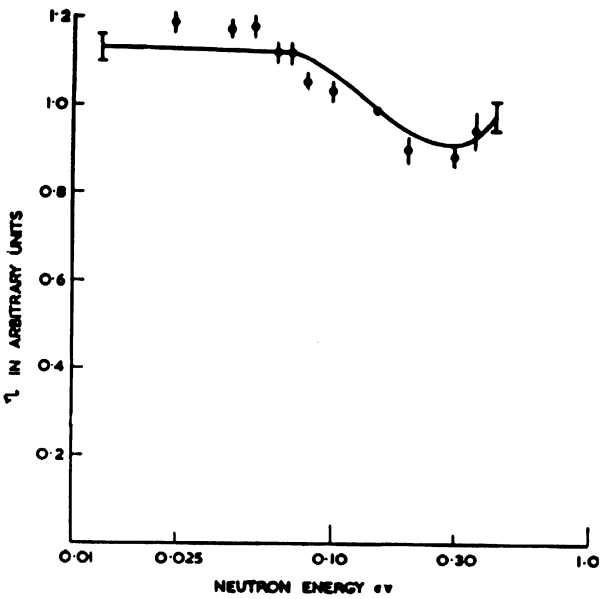

Slide 6. η Pu^{239} as function of neutron energy; curve obtained from ratio of fission to absorption cross section

able agreement between the direct measurement of η as a function of energy and the predictions of the cross-section measurements.

Slide 6 shows the same sort of picture for plutonium-239. Again the points are those measured by the direct method and the continuous curve is predicted from the measurements of the absorption and the fission cross section. In this case the directly measured value appears to have significantly more variation than the predictions of the cross-section values, although the difference is not far outside the experimental errors in our measurements.

A possible though rather unlikely cause of this discrepancy might be that $\bar{\nu}$ should vary from thermal up into the first resonance of plutonium-239. But I think that this is rather an exotic explanation of the discrepancy and the difference probably lies in some unknown experimental error in our measurements.

In conclusion, we would like to remark that in general, as we have seen, there is good agreement between the directly measured values of η and its energy dependence and the values derived from the cross-section data, although more information is required in the intermediate energy region.

The high thermal value of η for uranium-233, together with the fact that this η value appears to be constant, at least up to an energy of 25 ev, since we have seen that α is constant up to this energy, sug-

Table IV. η in Neutron Resonances

Nuclide	*Resonance Energy*	$\frac{\eta\ (resonance)}{\eta\ (0.025\ ev)}$ *Measured*	$\frac{\eta\ (resonance)}{\eta\ (0.025\ ev)}$ *From* α
U^{233}	1.80 ev	1.00±0.04	1.00±0.06
U^{235}	0.30 ev		0.84±0.08
Pu^{239}	0.30 ev	0.77±0.04	0.84±0.05

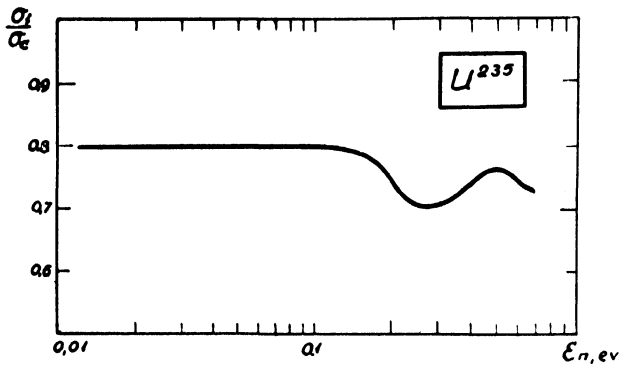

Slide 7

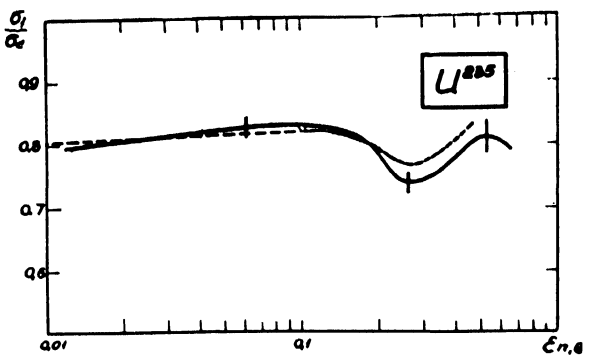

Slide 8. Dotted curve obtained by H. Palevsky (USA)

gests that from the purely nuclear point of view the thorium-uranium-233 system is a favourable one for the breeding of nuclear fuel.

Mr. H. Palevsky (USA) presented paper P/587.

Mr. W. R. Kanne (USA) presented paper P/596.

DISCUSSION OF PAPERS P/657, P/658, P/660, P/425, P/587 AND P/596

Mr. V. I. Mostovoi (USSR): In connection with the papers by Mr. Palevsky (P/587) and Mr. Sanders (P/425) I would like to mention the results of some measurements of the fission to capture cross-section ratio of uranium-235 and plutonium-239 in the 0.01–0.7 ev region recently made in the Soviet Union.

The fission to capture cross-section ratio, σ_f/σ_c was determined by the method of separate measurement of the fission cross section and of the total cross section. The results of such cross-section measurements are given in the reports presented at this Conference.

The capture cross section was determined from the total cross section by subtracting only the potential scattering which was obtained equal to 8.2 barns for U^{235}, U^{238} and Pu^{239}.

The fission to capture cross-section ratio for U^{235} is shown in Slide 7.

The energy dependence of this ratio is in qualitative agreement with the data given in Mr. Palevsky's report.

However, we obtained a more appreciable decrease in the value of σ_f/σ_c in the region of the 0.3 ev resonance. This difference may be explained by the fact that we did not take resonance scattering into account. In fact, as noted in Mr. Sailor's* paper, the negative energy level at $E_0 = -1.4$ ev introduces considerable resonance scattering in the 0–2 ev energy interval. Measurements made by Foote† indicate that the scattering cross section in the vicinity of the 0.3 ev resonance is almost two times greater than the value of the potential scattering assumed by us.

If the data on resonance scattering in U^{235} quoted in the paper by Mr. Sailor are taken into account, the curve for the energy dependence of the fission to capture cross-section ratio will have the form shown in Slide 8.

The dotted line in the figure represents data from Mr. Palevsky's report. It will be seen that there is satisfactory agreement within the limits of experimental error.

Slide 9 shows the fission to capture cross-section ratio curve for plutonium-239. The variation of this ratio with the energy in the 0.01–0.1 ev energy interval is in good agreement with the data (obtained by a similar method) in Mr. Palevsky's paper.

In his paper, it was mentioned that the variation of the ratio of the capture to fission cross sections σ_f/σ_c with the energy differs from the variation of the average number of neutrons produced per neutron captured $\eta = \nu\,\sigma_f/\sigma_c$. It might be assumed that this difference is due to the variation from level to level in the average number of neutrons emitted per fission. However, the results of measurements made in the USSR by Nikitin and his colleagues show a variation of σ_f/σ_c with the energy that is in agreement, within the limits of experimental error, with the variation of the cross-section ratio determined in the present investigation, all the way up to 0.34 ev.

Moreover, direct determinations of the ratio of ν in the 0.15–0.5 ev interval to ν in the thermal region, made by Kalashnikov, Lebedev, Mikaelian and Pevzner indicate that this ratio remains constant within 1.5 per cent.

We have learned in private conversations that similar experiments have been carried out in the United States and Great Britain.

Mr. M. S. Kozodaev (USSR): I would like to make a brief report on the work carried out by P. E. Spivak, B. G. Yerozolimsky, G. D. Dorofeev, V. N. Lavrenchik, I. E. Kutikov and Iu. P. Dobrynin for the purpose of determining the number of neutrons (ν_{eff}) emitted by the isotopes U^{233}, U^{235} and Pu^{239} per neutron capture when the material is bombarded by neutrons in the 30 kev to 1 Mev energy interval, i.e., in the energy range comprising the main part of the neutron spectrum of non-moderated reactors.

Photoneutrons obtained from the Sb^{124} + Be (30 kev), Ga^{72} + D_2O (140 kev), Na^{24} + D_2O (260 kev) Na^{24} + Be (900 kev) reactions were

* P/586, in Session 17A, this volume.
† P/555, Session 18B.1, Vol. 9, these Proceedings.

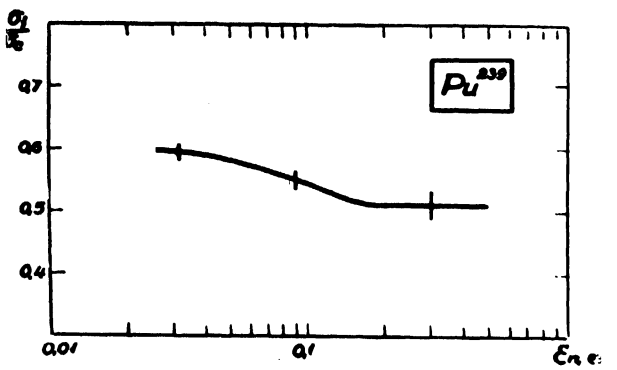

Slide 9

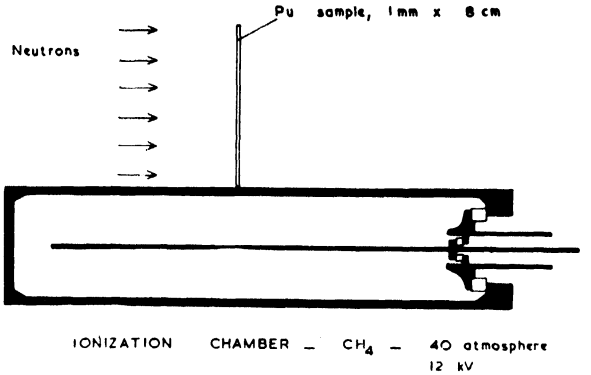

Slide 10

used in this investigation. The method for determining ν_{eff} was based on measuring the absorption and production of neutrons in the fissile isotope specimen. The measurements were carried out by means of two indicator systems with a different sensitivity to photoneutrons from the source and to neutrons of the fission spectrum.

This method permits reducing the determination of the absolute values of ν_{eff} to measurement of relative values only, a procedure which makes it possible to carry out the measurements to a high degree of accuracy.

The set-up consisted of a graphite column with a cavity housing the photoneutron source and the specimen. Two sets of boron counters were mounted in the graphite at different distances from the cavity and connected to two recording systems. This set-up was used for determinations of the *absolute* value of ν_{eff} in the neutron energy interval of 30 to 260 kev. For measuring ν_{eff} in the region of higher energies, a cylindrical ionization chamber with layers of U^{238} was used for detecting the fission neutrons. This second set-up was used to determine the *relative* variation of ν_{eff} with energy in the 30 to 900-kev interval.

The measurements showed that the value of ν_{eff} for all the investigated isotopes increases with the energy of the primary neutrons, as may be seen from the table below:

	30 kev	*900 kev*
U^{238}	2.25 ± 0.07	2.60 ± 0.13
U^{235}	1.86 ± 0.04	2.28 ± 0.08
Pu^{239}	2.01 ± 0.05	2.52 ± 0.12

The greatest increase over the 30 kev to 1 Mev energy interval is observed in the case of Pu^{239}. The observed variation of ν_{eff} is in agreement with the qualitative predictions of statistical theory, according to which the radiative-capture cross section of neutrons in this energy range must decrease faster with increasing energy than the fission cross section.

Mr. R. F. Taschek (USA): I simply have a question to ask of Mr. Sanders: what is the value and the accuracy of the sensitivity of the neutron detector which was used in the determination of $\bar{\nu}$?

Mr. Sanders (UK): The counter used for the measurement of $\bar{\nu}$ contained 16 BF_3 counters in paraffin wax and had a sensitivity to fission neutrons of 1.05 per cent. This efficiency is known to an accuracy of about $\pm$ 5 per cent. This inaccuracy accounts for most of the uncertainty on our values of $\bar{\nu}$.

Mr. F. J. M. Farley (New Zealand): I should like to report on a method which is now being used at Harwell to study the variation of η and the fission cross section in the intermediate energy region. The method uses a fast neutron counter and is rather similar to the method of Palevsky. The object is to study the neutron yield from fissile samples with a fast neutron detector of rapid response. The experiments are done in conjunction with the Harwell linear accelerator.

In Slide 10, you see the neutrons come from the left. There is a plutonium sample, 1 mm thick, 8 cm in diameter, and alongside it there is a fast neutron counter. This is an ionization chamber filled with methane, CH_4, to a pressure of 40 atmospheres with a collector to which 12 kev is applied. The collection time is 2 microseconds, and the over-all efficiency for detecting fissions in the sample, including the solid angle factor, is about 1 per cent.

If the sample is thin, the neutron yield gives a measure of $\nu \cdot \sigma_f$. For thicker samples, η can be determined by comparing the fast neutron yield with the number of slow neutrons stopped in the sample as indicated by a subsidiary transmission experiment.

At the top of Slide 11 you see a hypothetical transmission experiment. The area of the dip is the area A, which is compared with the neutron yield plotted against the same parameter, giving the area B. Then the value η will be proportional to B/A. A correction is necessary for the scattering in the sample. The method is to be calibrated by using a thermal neutron beam, for which η is known. The type of results which this method can yield is illustrated by Slide 12.

This shows the neutron yield curve for a 1 mm plutonium sample. You see here a rather detailed picture of a neutron yield. First, there are the familiar resonances in the low-energy region, but a little more detail is shown than in some curves which we saw this morning. We see a shoulder on the 10.8 ev resonance. The figures at the top give the energy in ev of the resonance. We see some resolution of the structure in the region beyond 50

ev. These peaks going out to 460 ev will probably correspond to the peaks on the total cross section in this region shown this morning by Vladimirski.‡

The experiments are not yet complete, and values of η have not yet been calculated. However, one may observe that the heights of the peaks shown in this curve are in the same order as the heights of the peaks in the total cross-section curves. This suggests, just as a rough approximation, that η does not vary very much from resonance to resonance.

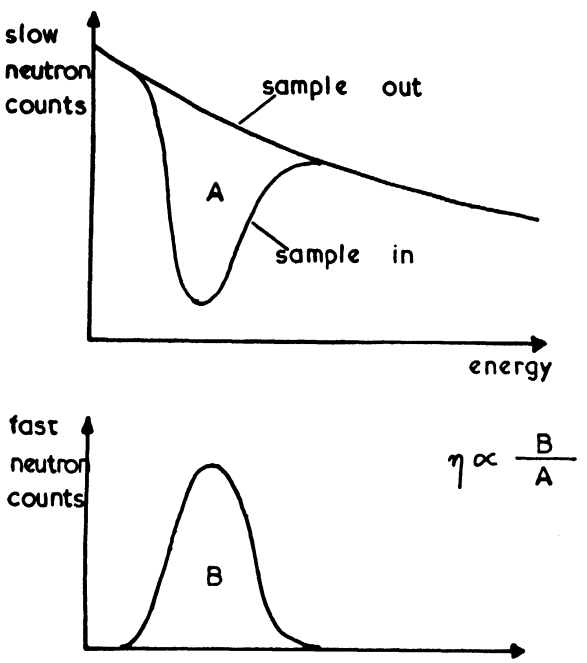

Slide 11

Mr. S. I. Sukhoruchkin (USSR): We used a neutron selector with a pulsed beam cyclotron for determining the dependence of the number of secondary electrons (ν_{eff}) on the energy of the incident neutrons. The number of fission events was determined from the number of secondary neutrons emitted from the specimen bombarded with slow neutrons. Both effects—absorption and fission—were measured simultaneously by two 64-channel time-analyzers; the ratio of the fission effect to the differential absorption effect in each of the measuring channels, taking into account the neutron velocities, gave a direct indication of the value of ν_{eff}.

The method is applicable in any energy region inasmuch as the principal obstacle to comparison of the absorption cross section with the fission cross section measured by the chamber, i.e., the self-shielding effect in a specimen of finite thickness, is absent. The use of a cyclotron as an intermittent source of slow neutrons is highly expedient with this method, since by virtue of the modulation of the ion source and high-frequency oscillator the background is reduced to that due to spontaneous fission.

‡ Session 17A.

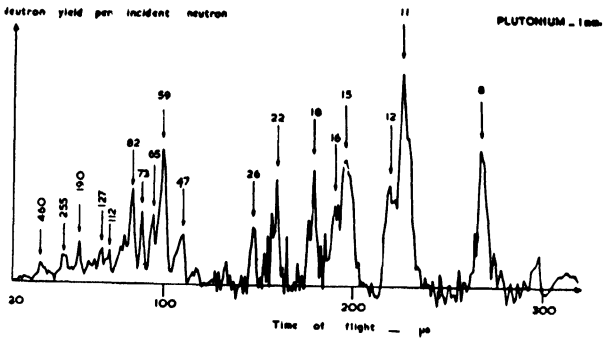

Slide 12

This method can also be used with other neutron sources, particularly when investigating substances with a high alpha-activity such as plutonium-239.

The experimental results are shown in Slides 12, 13 and 14, where in addition to ν_{eff} we give the values of $\sigma_f\sqrt{E}$ and $\sigma_c\sqrt{E}$ obtained in the course of the same measurements. It follows from the cited data that U^{233} is the only isotope for which ν_{eff} averaged over a wide energy spectrum is not lower than in the thermal region.

Kirpichnikov and Okorokov used the same method for carrying out measurements of ν_{eff} with a flight path of 16 metres and a resolving power of 0.25 μsec/m. The preliminary results obtained by these investigators indicate that the radiation width of plutonium-239 may also vary. This is evident in the case of the levels at 8 ev, 11 ev and 12 ev. It follows from the results of several cross-section measurements carried out by us and measurements carried out by Vladimirski, Sokolovski and Radkevich with a neutron chopper that the levels at 8 ev and 12 ev are 1.5–2 times narrower than the level at 11 ev; at the same time the value of ν_{eff} increases both in going from 8 ev to 1 ev and from 11 ev to 12 ev. We plan to carry out a detailed investigation of the resonance region of plutonium-239, bearing in mind that the spin dependences of this isotope may be exceptionally pronounced since the initial nucleus has a spin ½. It must be borne in mind that in our investigations and analyses we have assumed the value of ν (the number of neutrons per fission event) to be constant, i.e., invariable from level to level. The validity of this assumption must still be verified.

Mr. A. D. Callihan (USA): In view of the values of η for U^{233} which have been discussed this afternoon, I would like to comment on an experiment which is scheduled for presentation tomorrow afternoon,§ but because it is more appropriate here we would like to mention it now. This is an experiment done in the United States in which the critical concentrations in spheres were compared, when made critical first with aqueous solution of U^{233} and second with U^{235}. Such measurements have been made at the 25°C in spheres of two sizes. On the assumption that the leakage spectrum is the same for the

§ P/834 in session 20A3, Vol. 5, these Proceedings.

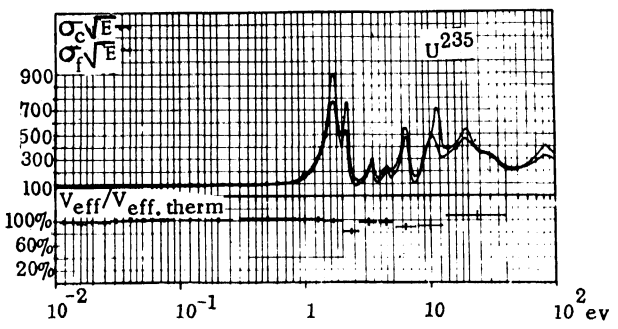

Slide 13

two solutions in a particular sphere, from a comparison of these concentrations one can make a comparison of the values of η for the two isotopes.

We have noted in Slide 16 (Figs 14 and 15 of P/834) the results of our experiment in two spheres, one with a diameter of 26.4 cm and the other with a diameter of 32.0 cm. The hydrogen to U^{233} or U^{235}, as the case might be, atomic ratio at critical in a water reflected aqueous solution of the fissile material, is noted for the two spheres. If one assumes a value of η for U^{235} to be 2.08 $\pm$ 0.02, then from the ratio arising from a comparison of the concentrations one obtains 2.32 for η for U^{233}.

Mr. HIGOTSBERGER (Austria): I am referring to Mr. Kanne's paper P/595 on measurements with a mass spectroscope, and I think I remember having seen a sensitivity figure of 5.3×10^{-18} amp. I would like to ask Mr. Kanne what amounts of statistical fluctuations at this sensitivity have been observed and how the fluctuations have been eliminated.

Mr. KANNE (USA): The curve showing the peaks indicates the statistical variations that might be observed so far as any one run of data is concerned. These data are taken by electron multiplier-counters, counting the ion beams, and consequently the statistics of these counts are still quite good.

Mr. H. A. BETHE (USA) presented paper P/585.

Mr. H. HURWITZ (USA) presented paper P/590.

DISCUSSION OF PAPERS P/585 AND P/590

Mr. MOSTOVOI (USSR): What can you say about the distribution of spacing between levels for a given mean spacing for one and the same nucleus? Is its relationship to the mean spacing purely haphazard?

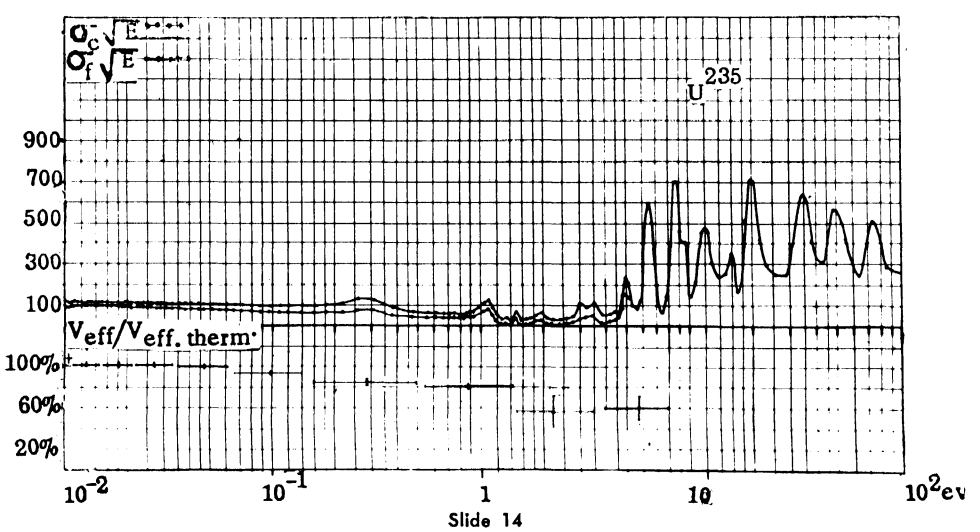

Slide 14

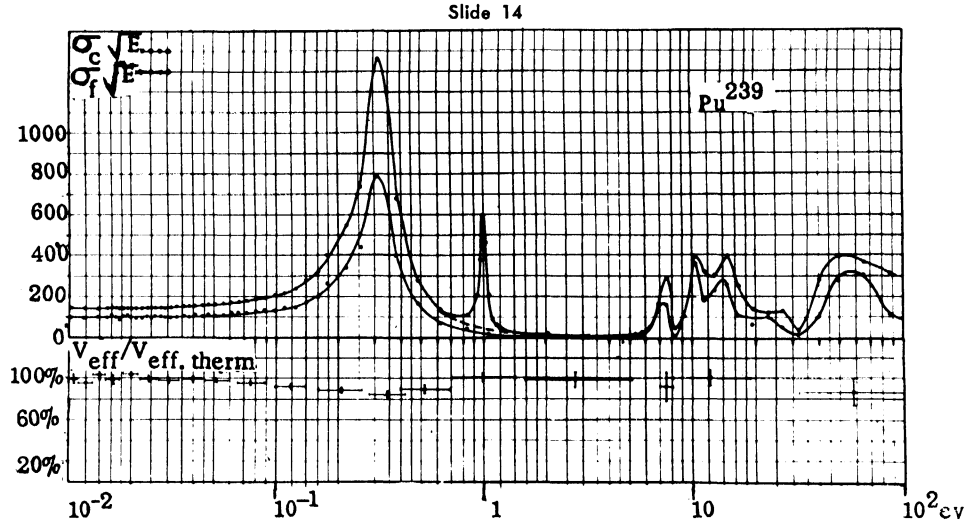

Slide 15

At the RPT Laboratory in the USSR, in the study of the cross sections of fissionable nuclei for monochromatic neutrons it was found that the first resonance level for U^{235}, Pu^{239}, Pu^{241} and Am^{241} occurs almost at one and the same energy (0.29 ± 0.01 ev). It is possible that there is also a weak level for U^{233} at the same energy. The same results for uranium and plutonium isotopes have been obtained in the United States, the United Kingdom, France and Norway.

It is highly improbable that the occurrence of the levels for so many nuclei within an interval of 0.02 ev is fortuitous.

What comments could you make on this subject?

Mr. BETHE (USA): As regards the first question, concerning the distribution of energy levels when you know the average spacings, quite a number of experiments were conducted at Brookhaven Laboratory, but the analysis is far from complete. I think that the data so far are compatible with the assumption of a random distribution, but at one time it seemed that very close spacings were less likely than would be expected from a random distribution. If the distribution were random, that would mean that a spacing x would occur with a probablity to exp $(-x)$. It seemed at one time as if the distribution looked more like x exp$(-x)$, as if every second level was left out, which of course is not reasonable. I think that this requires much more analysis than has been given to it so far. I have been struck rather often by the high frequency of the closeness between very strong levels, and I consider this to be accidental, although I have no explanation.

As regards the second question, I should consider the appearance of three or four levels at 0.3 ev as purely accidental. Similar accidents have happened many times in nuclear physics. The number of levels is tremendous. I think that there is no reason to believe that the kinetic energy zero of a neutron should have any particular significance. Also, if you look at the various levels at 0.3 ev, they look entirely different. The one in plutonium is very big; the one in uranium-235 is moderate; the one in uranium-233 is hardly detectable. I think one should regard these as perfectly normal levels which just happen to come at the same energy.

Mr. E. R. WIBLIN (UK): I think that perhaps it is rather under false pretences to describe this as a comment on Mr. Bethe's paper as such. It is rather a comment to illustrate an adaptation of technique to help in the combining of the results of several different types of cross-section measurements to evaluate resonance parameters, in particular, Γ, Γ_n, and possibly the spin factor g. I should just make the remark that perhaps delegates will find a more full description in paper P/426, from the United Kingdom by Mr. Rae.

I should like to write down rather quickly the four modifications or rearrangements of the single-level resonance formula at resonance for four types of cross-section measurement from a thin sample transmission as follows:

$$\frac{\sigma_0\Gamma}{4\pi\lambda^2_g} = \Gamma_n \qquad \frac{\sigma_s\Gamma}{4\pi\lambda^2_g} = \Gamma_n^2/\Gamma$$

$$\frac{\sigma_n\Gamma^2}{4\pi\lambda^2_g} = \Gamma_n \cdot \Gamma \qquad \frac{\sigma_a\Gamma}{4\pi\lambda^2_g} = \Gamma_n\left(1 - \frac{\Gamma_n}{\Gamma}\right)$$

The measured quantities are at the top line in the left-hand fraction in each case. It is quite easy to see from those four equations that one can in fact plot curves relating to Γ_n and Γ for the four types of measurements.

I am sorry that in this session devoted very thoroughly to fissile materials I have only an illustrative slide for this purpose relating to silver. As is so often the case, silver has been used as an object to try out one's technique.

Two diagrams have breen prepared (Slide 17) in which the horizontal line comes from the thin sample transmission ($\sigma_0\Gamma$ curve); the other three correspond to the other measurements.

In this case we have a choice of two possible g values. The one on the right-hand side, $g = 3/4$ is clearly the chosen value, rather than $g = 1/4$. The curve further serves to emphasize, if this is needed, the value of the scattering measurement, since it gives far the best cut or intersection with the other experimental curves in determining the values of Γ_n and Γ.

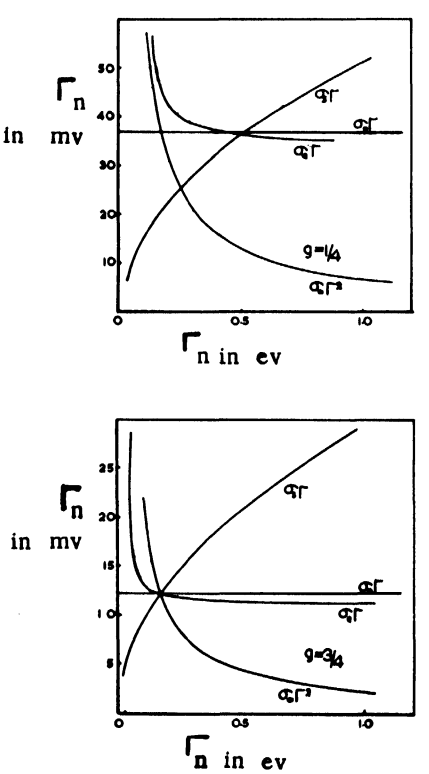

Slide 17. 5 — 22 — ev resonance in silver

Mr. F. L. SHAPIRO (USSR): I would like to ask Mr. Bethe whether he could explain in the light of different nuclear models how two states of the same nucleus, characterized by neutron widths several orders of magnitude apart, differ. Can this difference be made manifest in any other way other than already established by experiments?

Mr. BETHE (USA): I think that it would be very surprising if the nuclear levels had the same width, since the neutron emission is only one channel. It would be very surprising if there were the same channel width for all energy levels of the nucleus. I do not think that this has much to do with any other properties of the nucleus. It is a property referring just to the one mode of disintegration by the emission of a neutron.

Mr. SHAPIRO (USSR): If we have a light nucleus in which neutron scattering is the basic process, there is presumably only one channel. In this case, should variation of the neutron widths from level to level be observed? Wherein does the difference lie between levels with different neutron widths?

Mr. BETHE (USA): I would still expect a large fluctuation in width. I suppose that one might appeal, for instance, to the intermediate nuclear model which Mr. Wigner developed recently as a basis of the clouded crystal ball model. According to this intermediate model, a given state of the compound nucleus may contain a larger or smaller fraction of one-particle states in which a neutron is separated from the residual nucleus in the ground state. The fraction of this concentrated state in which the residual nucleus is in the ground state varies more or less accidentally from one compound level to another. In addition, of course, it has an over-all variation which corresponds to the one-particle resonances. You would find very similar things in atomic states also. When you look at the various atomic states, you would see, let us say, that one atomic state contains the ground state of the parent atom with one electron less, and the next one contains a highly excited state.

M. V. RAIEVSKI (France): I would like to ask a question relating to paper P/590.

In this paper, Mr. Hurwitz gives an absolute value for the capture cross section of graphite, determined with the Argonne pile oscillator. Could Mr. Hurwitz give us some details of the procedure that was followed? If this figure was obtained by comparison with a standard, could he tell us how the standard itself was measured?

Mr. HURWITZ (USA): I am sorry that I do not have many details of this experiment. It is my understanding, however, that there was a comparison of small samples of different purities, and then a measurement of diffusion length with the sample of the less pure type which could then be used as calibration in the pile oscillator measurements. However, I am not sure that this is exactly the method that was used.

Mr. A. M. WEINBERG (USA): I am wondering if Professor Bethe could comment on the remarkable constancy of α in U^{233} over the first 20 volts?

Mr. BETHE (USA): I really do not know, but I would suggest that α is very small in U^{233}, that the fission width is very large, and that there may be fluctuations of perhaps 5 per cent which have not been seen. I would therefore think that probably you would have to measure much more accurately in this case where α is so very small for all levels. The remarkable thing, of course, is that the fission width for U^{233} is so much bigger than for anything else.

PEACEFUL USES OF ATOMIC ENERGY:

Proceedings of the International Conference in Geneva, August 1955.

The following is a complete listing of the sixteen volumes which comprise this publication, together with the main subjects covered by each volume.

VOLUME 1

The World's Requirements for Energy: The Role of Nuclear Power

World Energy Needs
Capital Investment Required for Nuclear Energy
The Role of Thorium
The Role of Nuclear Power in the Next 50 Years
Education and Training of Personnel in Nuclear Energy
Economics of Nuclear Power

VOLUME 2

Physics, Research Reactors

Special Topics in Nuclear Physics
Fission Physics
Research Reactors
Research Reactors and Descriptions

VOLUME 3

Power Reactors

Experience with Nuclear Power Plants
Fuel Cycles
Design of Reactors for Power Production
Power Reactors, Prototypes

VOLUME 4

Cross Sections Important to Reactor Design

Equipment and Techniques Used in Measuring Cross Sections Important to Reactor Design
Cross Sections of Non-Fissionable Materials: Delayed Neutrons
Cross Sections of Fissionable Materials
Properties of Fissionable Materials

VOLUME 5

Physics of Reactor Design

Integral Measurements
Resonance Integrals
Fission Product Poisoning
Criticality in Solutions
Zero Energy and Exponential Experiments
Zero Energy Experiments on Fast Reactors and Reactor Kinetics
Reactor Theory

VOLUME 6

Geology of Uranium and Thorium

Occurrence of Uranium and Thorium
Prospecting for Uranium and Thorium

VOLUME 7

Nuclear Chemistry and the Effects of Irradiation

The Fission Process
Facilities for Handling Highly Radioactive Materials
Chemistry of Fission Products
Heavy Element Chemistry
Effects of Radiation on Reactor Materials
Effects of Radiation on Liquids
Effects of Radiation on Solids

VOLUME 8

Production Technology of the Materials Used for Nuclear Energy

Treatment of Uranium and Thorium Ores and Ore Concentrates
Production of Metallic Uranium and Thorium
Analytical Methods in Raw Material Production
Production Technology of Special Materials

VOLUME 9

Reactor Technology and Chemical Processing

Waste Disposal Problems
Metallurgy of Thorium, Uranium and their Alloys
Fabrication of Fuel Elements
Liquid Metal Technology
Chemical Aspects of Nuclear Reactors
Chemical Processing of Irradiated Fuel Elements
Waste Treatment and Disposal
Separation and Storage of Fission Products

VOLUME 10

Radioactive Isotopes and Nuclear Radiations in Medicine

Isotopes in Medicine and Biology
Therapy
Diagnosis and Studies of Disease

VOLUME 11

Biological Effects of Radiation

Modes of Radiation Injury and Radiation Hazards
Mechanisms of Radiation Injury
Protection and Recovery
Genetic Effects
Human Implications

VOLUME 12

Radioactive Isotopes and Ionizing Radiations in Agriculture, Physiology, and Biochemistry

Isotopes in Agriculture
Radiation-induced Genetic Changes and Crop Improvement
Tracer Studies in Agriculture
Animal Physiology
Plant Biochemistry
General Biochemistry

VOLUME 13

Legal, Administrative, Health and Safety Aspects of Large-Scale Use of Nuclear Energy

Legal and Administrative Problems
Reactor Safety and Location of Power Reactors
Safety Standards and Health Aspects of Large-Scale Use of Atomic Energy

VOLUME 14

General Aspects of the Use of Radioactive Isotopes: Dosimetry

Isotopes in Technology and Industry
General Uses, Production and Handling of Radioactive Isotopes
Dosimetry

VOLUME 15

Applications of Radioactive Isotopes and Fission Products in Research and Industry

Radioactive Isotopes in Research
Radioactive Isotopes in Control and Technology
Fission Products and their Applications

VOLUME 16

Record of the Conference

Opening of the Conference and the Presidential Address
International Co-operation in the Peaceful Uses of Atomic Energy
Closing Presidential Address
Evening Lectures
Author Index and Paper Index